frontiers | Research Topics

Biomarkers and immunotherapy of hepatic-biliary-pancreatic cancers

Edited by
Yunfei Xu, Hongda Liu, Xuesong Gu and Zheng Gong

Published in
Frontiers in Immunology
Frontiers in Oncology

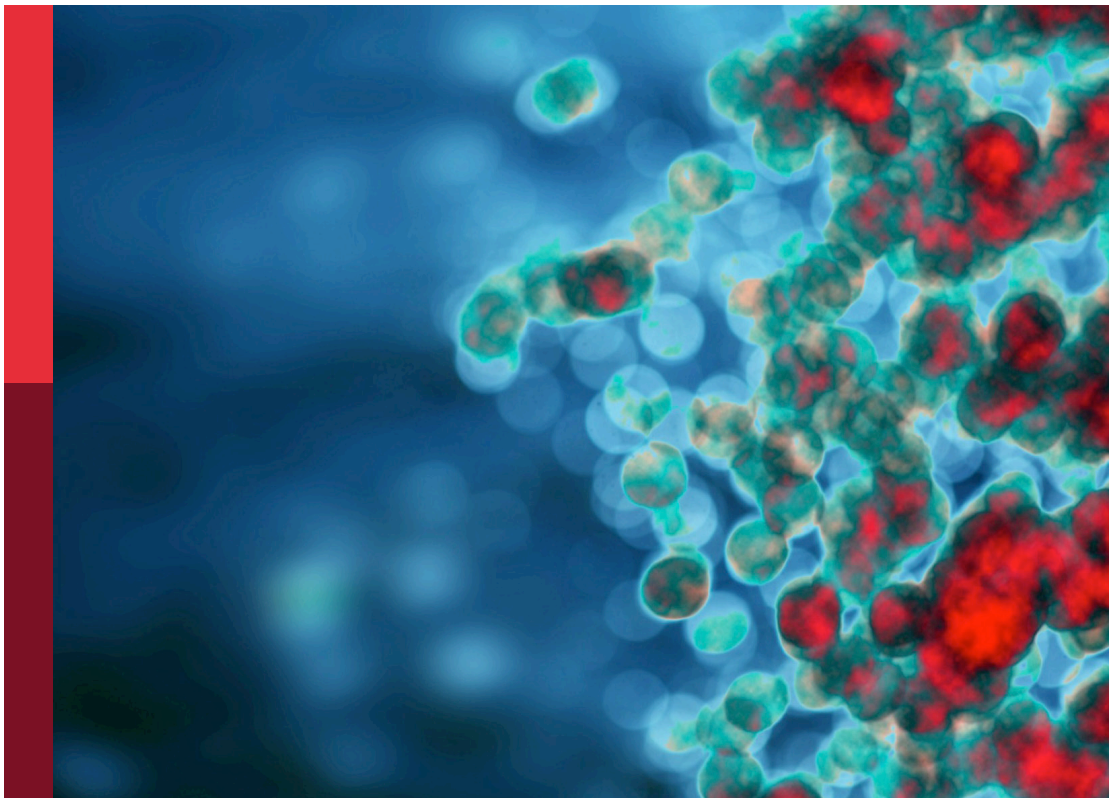

ISSN 1664-8714
ISBN 978-2-8325-3890-6
DOI 10.3389/978-2-8325-3890-6

About Frontiers

Frontiers is more than just an open access publisher of scholarly articles: it is a pioneering approach to the world of academia, radically improving the way scholarly research is managed. The grand vision of Frontiers is a world where all people have an equal opportunity to seek, share and generate knowledge. Frontiers provides immediate and permanent online open access to all its publications, but this alone is not enough to realize our grand goals.

Frontiers journal series

The Frontiers journal series is a multi-tier and interdisciplinary set of open-access, online journals, promising a paradigm shift from the current review, selection and dissemination processes in academic publishing. All Frontiers journals are driven by researchers for researchers; therefore, they constitute a service to the scholarly community. At the same time, the *Frontiers journal series* operates on a revolutionary invention, the tiered publishing system, initially addressing specific communities of scholars, and gradually climbing up to broader public understanding, thus serving the interests of the lay society, too.

Dedication to quality

Each Frontiers article is a landmark of the highest quality, thanks to genuinely collaborative interactions between authors and review editors, who include some of the world's best academicians. Research must be certified by peers before entering a stream of knowledge that may eventually reach the public - and shape society; therefore, Frontiers only applies the most rigorous and unbiased reviews. Frontiers revolutionizes research publishing by freely delivering the most outstanding research, evaluated with no bias from both the academic and social point of view. By applying the most advanced information technologies, Frontiers is catapulting scholarly publishing into a new generation.

What are Frontiers Research Topics?

Frontiers Research Topics are very popular trademarks of the *Frontiers journals series*: they are collections of at least ten articles, all centered on a particular subject. With their unique mix of varied contributions from Original Research to Review Articles, Frontiers Research Topics unify the most influential researchers, the latest key findings and historical advances in a hot research area.

Find out more on how to host your own Frontiers Research Topic or contribute to one as an author by contacting the Frontiers editorial office: frontiersin.org/about/contact

Biomarkers and immunotherapy of hepatic-biliary-pancreatic cancers

Topic editors

Yunfei Xu — Shandong University, China

Hongda Liu — Nanjing Medical University, China

Xuesong Gu — Beth Israel Deaconess Medical Center, Harvard Medical School, United States

Zheng Gong — Jackson Laboratory, United States

Citation

Xu, Y., Liu, H., Gu, X., Gong, Z., eds. (2023). *Biomarkers and immunotherapy of hepatic-biliary-pancreatic cancers*. Lausanne: Frontiers Media SA.

doi: 10.3389/978-2-8325-3890-6

Table of contents

frontiers | Frontiers in Oncology

TYPE Editorial
PUBLISHED 23 October 2023
DOI 10.3389/fonc.2023.1301416

OPEN ACCESS

EDITED AND REVIEWED BY
Peter Brossart,
University of Bonn, Germany

*CORRESPONDENCE
Hongda Liu
liuhongda@jsph.org.cn

RECEIVED 24 September 2023
ACCEPTED 16 October 2023
PUBLISHED 23 October 2023

CITATION
Qian Y, Jia W and Liu H (2023) Editorial: Biomarkers and immunotherapy of hepatic-biliary-pancreatic cancers. *Front. Oncol.* 13:1301416. doi: 10.3389/fonc.2023.1301416

Editorial: Biomarkers and immunotherapy of hepatic-biliary-pancreatic cancers

Yawei Qian[1], Wenyu Jia[2] and Hongda Liu[1]*

[1]Department of General Surgery, The First Affiliated Hospital of Nanjing Medical University, Nanjing, China, [2]Department of Endocrinology, Qingdao Municipal Hospital, Qingdao, Shandong, China

KEYWORDS

hepatic-biliary-pancreatic cancers, biomarker, therapeutic strategy, drug resistance and metastasis, clinical studies

Editorial on the Research Topic
Biomarkers and immunotherapy of hepatic-biliary-pancreatic cancers

1 Introduction

Hepatic-Biliary-Pancreatic (HBP) cancers represent a formidable challenge within the broader spectrum of gastrointestinal malignancies (1). These cancers encompass a complex array of diseases affecting the liver, bile ducts, and pancreas. Incidence rates for HBP cancers have been on the rise, a concerning trend attributed to various factors, including changes in dietary patterns and exposure to environmental pollutants (2). The treatment landscape for HBP cancers, much like other gastrointestinal malignancies, comprises a multifaceted approach that encompasses surgical interventions, chemotherapy, radiotherapy, and the more recent addition of immunotherapy (3–5).

Despite substantial strides in cancer research and treatment modalities, HBP cancers continue to pose significant hurdles. These challenges manifest as recurrent tumors, metastasis to distant organs, and the development of drug resistance, all of which can thwart the prospects of complete recovery (6). The burgeoning field of oncology is witnessing a transformation fueled by innovative research technologies. Genomics, high-throughput sequencing, proteomics, metabolomics, immunotherapy, nanotechnology, liquid biopsy, robotic surgery, artificial intelligence, organoids, and microbiome analysis are among the cutting-edge tools being rapidly integrated into clinical and biomedical research.

These avant-garde approaches have yielded a treasure trove of information that is reshaping our comprehension of HBP cancers. The insights gleaned from these novel techniques have cast new illumination on existing theories, prompting a reevaluation of established paradigms and doctrines. Such breakthroughs have the potential to chart novel pathways of understanding, ultimately leading to more precise and efficacious treatments with fewer adverse events for patients. By keeping abreast of the latest research findings, clinicians and researchers can identify emerging diagnostic and prognostic factors, biomarkers, and risk factors that hold the promise of improving our grasp of the

molecular underpinnings of cancer initiation, progression, recurrence, and drug resistance (7).

Furthermore, the exploration of targeted anti-cancer agents represents a pivotal avenue for enhancing the traditional armamentarium of chemotherapy and radiotherapy in combating HBP cancers (8). These efforts are pivotal in advancing the field and offer renewed hope for patients grappling with these formidable diseases. As reported in the Research Topic of Biomarkers and Immunotherapy of Hepatic-Biliary-Pancreatic Cancers, we can anticipate significant strides in the diagnosis, prognosis, and ultimately the survival of patients affected by these intricate malignancies. In sum, the confluence of cutting-edge research methodologies and unwavering dedication to improving patient outcomes promises a brighter future in the fight against Hepatic-Biliary-Pancreatic cancers.

2 Hepatocellular carcinoma

HCC, also known as primary liver cancer, is a formidable malignancy originating from hepatocytes, the primary functional cells within the liver. Its incidence has seen a steady rise in recent decades, contributing to its status as a significant global health concern (9). HCC is predominantly associated with chronic liver diseases, including hepatitis B and C infections, excessive alcohol consumption, non-alcoholic fatty liver disease (NAFLD), and metabolic disorders, particularly cirrhosis (10). Interestingly, in patients with Budd-Chiari syndrome (BCS), the risk factors for developing HCC were examined by (Li K. et al.). Among 113 BCS patients studied, 10.6% (12/113) were diagnosed with HCC. Those who had BCS-associated HCC tended to be older and had elevated serum AST and total bilirubin levels. HCC nodules in these patients were typically found in the right posterior lobe and showed irregular and heterogeneous enhancement during the arterial phase with washout during the delayed phase on CT imaging. The study suggests that BCS patients with IVC block and hepatic venous outflow tract stricture may be at higher risk for HCC development.

The aggressive nature of HCC, coupled with its often late-stage diagnosis, has limited therapeutic options, making it a formidable challenge for healthcare professionals. However, recent advancements in genomics and molecular biology have illuminated the underlying mechanisms of HCC and hold the promise of improved patient outcomes. Zhu Z. et al. reported that high expression of polycomb repressive complex 2 component, PHF19, was correlated with poor prognosis of HCC. PHF19 expression related to tumor mutational burden and immune infiltrates, notably myeloid-derived suppressor cells and Th2 CD4 + T cells. Enrichment analyses linked PHF19 to cell cycle, DNA replication, and immune processes, thus highlighting PHF19 as an epigenetic regulator affecting cancer progression and immune infiltration, with potential clinical implications. Huang et al. investigated the role of Actin-related protein 2/3 complex subunit 5 (ARPC5) in various cancers. ARPC5 was found to be upregulated in most cancer types and associated with worse prognosis in certain cancers. It exhibited low tissue and cell specificity in normal tissues and was linked to tumor microenvironment scores, immune cell infiltration, and immune-related genes in many cancers. Additionally, ARPC5 was positively correlated with factors like TMB, MSI, and RNA modification genes in specific cancers. In their experimental analyses, ARPC5 was found to promote proliferation, migration, and invasion in HCC. Yu et al. examined the role of Complement Factor H-related 4 (CFHR4) in HCC, which was significantly reduced in HCC tissues and was associated with various clinicopathological factors. Functional analysis revealed its potential involvement in several biological pathways, including carcinogenesis and metabolic pathways. CFHR4 expression correlated with immune cell infiltration, affecting various immune cell types. High CFHR4 expression was linked to better survival outcomes in HCC patients. The study also constructed potential CFHR4-related regulatory networks. Xiang et al. found that spermine synthase (SMS), involved in polyamine biosynthesis, is overexpressed in HCC. SMS overexpression in HCC patients is unrelated to hepatitis virus infection and is associated with poor prognosis. High SMS levels are linked to decreased survival rates and limited effectiveness of immune checkpoint blockade (ICB), therefore may impact HCC development by affecting various immune-related pathways. Liu Y. et al. investigated the role of CEP192 in HCC and found that its expression increased with tumor stage and was linked to poor clinical features, recurrence, and higher mortality. CEP192 played a role in the proliferation and self-renewal of hepatic progenitor-like cells, and silencing it inhibited cell proliferation. CEP192 was also associated with immunosuppressive elements in the tumor microenvironment, suggesting it could predict responses to immune checkpoint inhibitors. Cai L. et al. reported that transmembrane protein 88 (TMEM88) plays a role in the canonical Wnt signaling pathway. Their study analyzed TMEM88 expression in HCC, revealing a negative correlation with tumor stage and grade. High TMEM88 levels predicted better overall and disease-specific survival. TMEM88 overexpression reduced HCC cell proliferation *in vitro* and suppressed HCC progression in a mouse model. Interestingly, Ai et al. developed a bioinformatics pipeline that accurately estimates the number of infiltrating immune cells and bacteria in tumor and normal tissues. Using this pipeline on liver cancer samples, they identified specific bacteria and immune cell types that differ between healthy and diseased tissue, achieving an 84% accuracy in distinguishing them. This tool can help researchers better understand the interactions between immune cells, bacteria, and cancer cells.

In addition to single prognostic biomarkers, a large proportion of studies are now focusing on establishing prognostic model using multiple molecules. Zhang H. et al. identified four distinct tumor microenvironment (TME) subtypes (C1, C2, C3, C4) based on immune, stem, and stromal cell compositions. C1 and C2 exhibited an immune-active TME, while C3 and C4 displayed an immune-insensitive TME. Patients in the C3 subtype had notably worse prognoses, demonstrating the potential for personalized treatment approaches in HCC based on TME subtypes. Liver zonation, characterized by distinct functions across the radial axis of the liver lobule, can impact the development of liver cancer, as reported by (Zhang T. et al.). Their study identified hepatocyte-specific zonation markers and used them to classify HCC into three

clusters: non-zonational-like, central-like, and portal-like. Each cluster exhibited different clinical characteristics, immune infiltration, and prognosis. Chen J. et al. identified 16 differentially expressed genes (DEGs) related to liver cancer immunotherapy using machine learning. A CombinedScore based on these DEGs predicted patient response to immunotherapy. Patients with a low CombinedScore were likely to respond better. Metabolism pathways were more active in patients with a high CombinedScore. The CombinedScore was associated with immune cell levels, immune checkpoint expression, and genomic features. Specifically, CDCA7 was identified as a potential therapeutic target and was linked to macrophage polarization and T cell activity. Sun et al. identified two major subtypes of HCC based on the expression of Golgi apparatus-related genes (GARGs). The high-risk subtype (C1) had lower survival rates and poorer response to immunotherapy, along with characteristics indicating immune escape and TP53 mutations. A risk assessment profile based on GARGs was developed, helping predict prognosis and immunotherapy response in HCC patients. Additionally, the study found that interfering with the expression of the BSG gene restricted the proliferation and migration of HCC cells, suggesting it may be associated with poor HCC prognosis. Luo et al. focused on the role of cancer-associated fibroblasts (CAFs) in its progression. The researchers gathered data from various databases and used single-cell transcriptome analysis and ligand-receptor interaction analysis to identify CAF-related genes. They then developed an artificial neural network (ANN) model based on 12 prognostic CAF-related genes, creating a CAF activation score (CAS). Functional and immune analyses showed that high-CAS samples had more active cell crosstalk and immune activity. Mutational analysis revealed differentially mutated genes between high- and low-CAS samples. Clinical analysis resulted in a prognostic nomogram for HCC patients. A novel risk score (RS) based on CD4+ Tconv-related long non-coding RNAs (lncRNAs) was developed for HCC patients by (Zhu L. et al.). Their RS, consisting of six lncRNAs (AC012073.1, AL031985.3, LINC01060, MKLN1-AS, MSC-AS1, and TMCC1-AS1), demonstrated good predictive ability for overall survival (OS) in HCC patients and various clinical subgroups. Patients in the high-risk group exhibited an immune response phenotype characterized by high infiltration of macrophages and CAFs and low infiltration of natural killer (NK) cells. Furthermore, the low-risk group showed favorable responses to immune checkpoint inhibitors. Song et al. delved into the impact of DNA methylation regulators (DMRegs) on HCC. Their data clusters modifications based on DMRegs expression, genetics, and transcription in HCC samples. These alterations correlate with clinicopathological traits, prognosis, and immune cell infiltration patterns. The results introduces a DMRegs-related gene score (DMRegs_score) as a prognostic indicator, showing high scores are linked to poor outcomes. The DMRegs_score also shows promise in predicting drug sensitivity. Liu P. et al. also focused on HCC and the role of methylcytosine (m5C) regulators in predicting clinical responses to immunotherapy. Researchers analyzed data from 371 HCC patients and identified six differentially expressed genes (DEGs) to construct a prognostic risk model and two diagnostic models. The prognostic risk model effectively predicted patient outcomes, and the high-risk group showed a worse prognosis. Additionally, the high-m5C score group was predicted to be less responsive to immunotherapy but more sensitive to chemotherapy and potential targeted drugs. Overall, these insights offer potential for refining prognosis of HCC.

Furthermore, several strategies to help distinguish the potential efficiency of immune therapy were reported. Yuan G. et al. examined the significance of liver stiffness (LS) measured by shear wave elastography (SWE) in advanced HCC patients treated with PD-1 inhibitors and lenvatinib. A LS value of 19.53 kPa at baseline was identified as the optimal cutoff for predicting treatment efficacy. A nomogram combining baseline tumor LS and albumin-bilirubin grade was developed to predict treatment outcomes. High stiffness tumors were associated with metabolic pathways, while low stiffness tumors were related to DNA damage repair. Patients with high stiffness tumors had lower immune cell infiltration, suggesting potential drug candidates to enhance immunotherapy efficacy. Xu et al. developed a novel prognostic predictor for (PD-1 inhibitor therapy in HCC patients, independent of Child-Pugh grade. The study analyzed data from HCC patients who received PD-1 inhibitors and introduced a novel ALG grade based on serum ALP and GGT levels before treatment initiation. The results showed that patients with Child–Pugh grade A and ALG grade 3 at baseline had worse outcomes. From the gene level, chromosome 11q13 amplification (Amp11q13) was identified as a common variation in HCC patients. Yan et al. reported those with Amp11q13 tended to have higher levels of Des-γ-carboxy-prothrombin (DCP), more tumors, and were more likely to have portal vein tumor thrombosis (PVTT). In patients treated with PD-1 inhibitors, Amp11q13 was associated with a higher risk of progression, shorter progression-free survival (PFS), and a potential link to hyperprogressive disease (HPD). Liu C. et al. also identified predictive biomarkers for the effectiveness of combination therapy involving anti-angiogenic drugs and PD-1 antibodies in HCC patients. They collected data from 40 advanced HCC patients undergoing this combination therapy and found that high levels of CD3+CD4+CD279+ and CD3+CD8+CD45RO+CD62L+ T lymphocytes, as well as a high tumor mutational burden (TMB), were associated with a positive treatment response. Conversely, high levels of CD3+CD4+CD28+ T lymphocytes were linked to a poorer response. Specific gene mutations, such as TP53 and ARID1A, also correlated with non-response, while amplification mutations in 11q13-CCND1, FGF3, FGF4, and FGF19 were observed in a patient with hyperprogression. Interestingly, in a meta-analysis by Zongli Zhang et al., which focusing on HCC patients treated with immune checkpoint inhibitors (ICIs), the impact of antibiotic use on treatment outcomes was assessed. The analysis included six retrospective studies with 1056 patients, of which 33.33% received antibiotics. The results indicated that antibiotic use did not significantly affect OS or progression-free survival (PFS) in HCC patients treated with ICIs. Furthermore, antibiotics did not have a significant impact on objective response rate (ORR) or disease control rate (DCR). Therefore, their evidence suggests that antibiotics do not substantially alter the therapeutic efficacy of ICIs in HCC patients. A prognostic model was developed for unresectable HCC patients treated with a combination of ICIs

and tyrosine kinase inhibitors (TKIs) by (Li X. et al.). Their model incorporates seven clinical parameters, including ECOG PS, TACE, EHM, PLR, ALT, AFP, and Child-Pugh score, which can help predict the efficacy of the combination regimen in unresectable HCC patients. Guo et al. established a prognostic model called the PIMET score for unresectable hepatocellular carcinoma (uHCC) patients receiving lenvatinib monotherapy or lenvatinib plus immune checkpoint inhibitors (ICI). The model includes metastasis and protein induced by vitamin K absence or antagonist-II (PIVKA-II) as risk factors. Patients were stratified into PIMET-low, PIMET-int, and PIMET-high groups. The PIMET score effectively predicted OS and treatment responses, distinguishing patients who benefit from the combination of lenvatinib and ICI. Taken together, stiffness tumors, ALG grade, clinical parameters (such as ECOG PS, TACE, EHM, PLR, ALT, AFP, and Child-Pugh score), Amp11q13, and mutations of certain genes (in 11q13-CCND1, FGF3, FGF4, and FGF19) could serve as potential predictive biomarkers for HCC patients undergoing immune therapy.

Several retrospective or prospective clinical studies were conducted regarding the treatment of HCC. For example, Xie et al. reported that combining ICIs with molecular targeted agents (MTAs) after lenvatinib progression in advanced hepatocellular carcinoma (aHCC) showed promising anticancer effects and safety. PFS and post-progression survival (PPS) were notably extended. No significant differences in efficacy were observed between ICI+Lenva and ICI+Others groups. Prolonged PPS was associated with Child–Pugh grade A, AFP < 400 IU/ml, and concomitant locoregional treatment. Adverse events were manageable. Wang K. et al. reviewed local ablative therapy in HCC. Radiofrequency ablation (RFA) is a primary treatment for early-stage HCC, but other techniques like microwave ablation, cryoablation, irreversible electroporation, and phototherapy are under investigation. Combining immunotherapy with ablation is a promising strategy, as ablative therapy can trigger local and systemic immune responses. Their review summarizes the current status of ablation and immunotherapy for HCC, explores the immune effects of ablation, and discusses combination strategies, including those involving biomedical materials. Combination therapies are attracting more and more attentions. Zeng et al.'s retrospective study aimed to compare the efficacy and safety of ICI plus bevacizumab (BEV) versus ICI plus receptor tyrosine kinase inhibitor (TKI) as first-line treatments for uHCC. The study included 94 patients and assessed PFS, OS, objective response rate (ORR), and disease control rate (DCR). While the median OS and PFS did not significantly differ between the two groups, the incidence of adverse events varied. Palmar-plantar erythrodysesthesia syndrome was more common in the ICI+TKI group, while upper gastrointestinal bleeding occurred primarily in the ICI+BEV group. Cai M. et al. compared the effectiveness and safety of two treatment approaches for advanced HCC. One group received transarterial chemoembolization combined with lenvatinib plus a PD-1 inhibitor (TACE-L-P), while the other received TACE combined with lenvatinib (TACE-L). Results showed that TACE-L-P led to longer overall survival (16.9 vs. 12.1 months), extended progression-free survival (7.3 vs. 4.0 months), and higher response rates. TACE-L-P was particularly beneficial for patients with extrahepatic metastasis or more than three tumors. Adverse events were similar between the two groups, therefore supporting TACE-L-P as a promising treatment for advanced HCC, especially in specific patient subgroups. Combining intensity-modulated radiotherapy (IMRT) with atezolizumab and bevacizumab (atezo/bev) in HCC patients with extrahepatic portal vein tumor thrombus (ePVTT) was also studied in a prospective multicenter research by (Wang et al.). The treatment demonstrated a promising objective response rate (76.6%) and a median overall survival of 9.8 months. There was no significant correlation found between tumor mutational burden (TMB) and treatment outcomes. The most common treatment-related adverse events were manageable, with no treatment-related deaths reported. Their approach appears to be a valuable option for HCC patients with ePVTT, although further research is needed for confirmation.

3 Bile duct cancer and gallbladder cancer

Cholangiocarcinoma represents a rare yet highly aggressive malignancy that emerges from the epithelial cells lining the bile ducts, responsible for transporting bile from the liver to the small intestine (11). This cancer is categorized into two primary forms: intrahepatic and extrahepatic cholangiocarcinoma, distinguished by their anatomical locations. Intrahepatic cholangiocarcinoma originates within the liver, while extrahepatic cholangiocarcinoma manifests outside the liver, typically within the bile ducts. Cholangiocarcinoma's challenging clinical landscape arises from its elusive early symptoms, often leading to advanced-stage diagnoses with limited therapeutic options. However, contemporary research has been dedicated to unraveling its molecular underpinnings and identifying potential therapeutic targets, offering renewed optimism for the management of this intricate malignancy. Advances in precision medicine and immunotherapy have opened new avenues for developing more effective treatment modalities (12).

Li Y. et al. reviewed the function of bile, which directly contacts biliary tract tumors, contains complex components closely linked to BTC development. The bile components hold potential as biomarkers for BTCs. Furthermore, emerging evidence suggests that bile components play a role in regulating immune responses. Their review also explores the relationship between bile components and BTCs, their biomarker potential, and their immunoregulatory effects, highlighting their promising applications in BTC diagnosis and treatment.

As for the BTC treatment, Zhang Y. et al. reported that patients with advanced cholangiocarcinoma receiving PD-1 inhibitor combination therapy, experiencing immune-related adverse events (irAEs) was associated with better disease control, longer OS, and extended progression-free survival (PFS). These findings suggest that irAEs may serve as a positive predictor for treatment efficacy in this context. IrAEs were identified as independent prognostic factors for both OS and PFS, highlighting their potential as a valuable clinical indicator. Yang X. et al. found that

for patients with unresectable intrahepatic cholangiocarcinoma (iCCA), DEB-TACE+ICIs demonstrated superior outcomes compared to gemcitabine+cisplatin chemotherapy. DEB-TACE +ICIs led to higher objective response rates, extended PFS, and prolonged OS. Independent risk factors for worse PFS and OS included chemotherapy, tumor size >5cm, and multiple tumors. The incidence of treatment-related adverse events was comparable between groups. Therefore, they concluded that DEB-TACE+ICIs was a more effective and well-tolerated treatment approach for unresectable iCCA patients compared to chemotherapy. Zhang W. et al. showed that combining lenvatinib, pembrolizumab, and GP chemotherapy is promising for a patient with initially unresectable ICC. After six cycles of treatment, the tumors shrank, and tumor marker levels normalized. The patient underwent successful liver resection with no signs of recurrence or metastasis after 15 months. Jiang et al. conducted a meta-analysis involving advanced BTC patients, the effectiveness and safety of anti-PD1/PDL1 therapy were evaluated. The combination of anti-PD1/PDL1 with anti-CTLA4 and chemotherapy demonstrated the best outcomes, with a median PFS of 12.4 months, median OS of 16.0 months, a 45.1% ORR, and a 95.0% DCR. Anti-PD1/PDL1 monotherapy had the lowest efficacy but a safer profile. Overall, anti-PD1/PDL1 therapies showed promising efficacy and could be considered an alternative for aBTC treatment, despite some associated toxicities, particularly in the first-line setting. Another meta-analysis by Xian et al. aimed to assess the prognostic value of PD-L1 expression in ICC patients. Ten trials involving 1944 cases were analyzed. The low-PD-L1 group had significantly better OS, recurrence-free survival (RFS), and time to relapse compared to the high-PD-L1 group. Additionally, high PD1 levels were associated with poorer OS and RFS. Multivariate analysis confirmed PD-L1 and PD1 as independent predictors for OS and RFS. These findings suggest that PD-L1/PD1 expression can serve as valuable prognostic and predictive biomarkers in ICC and potential therapeutic targets. However, the adverse effect should not be ignored. For example, Zhu S. et al. reported a 48-year-old male ICC case with non-bacterial cystitis as an immune-related adverse event (irAE) following treatment with PD-1 and PD-L1 antibodies. In that case, psoriasis worsened, and urinary discomfort recurred, leading to treatment discontinuation and surgery. After chemotherapy with atezolizumab, urinary discomfort reappeared. Urine cultures showed no bacteria, and cystoscopy biopsy indicated non-bacterial bladder inflammation. This highlights a rare case of immunotherapy-induced non-bacterial urinary tract inflammation. On the other hand, Wang Y. et al. reviewed the antiangiogenic therapy in controlling BTC progression. Understanding the molecular basis of angiogenesis in BTCs is crucial for treatment strategies and patient selection. This review summarizes recent advances in antiangiogenic approaches for BTCs, emphasizing molecular mechanisms and clinical trial outcomes. The potential future of antiangiogenic therapy in BTCs is also discussed, offering insights into this challenging malignancy's management.

Gallbladder cancer is a rare cancer which are mostly reported as case reports (13, 14). Wu et al. reported that, in the context of uncertain ICI benefits in gallbladder cancer, a 45-year-old female with multiple abdominal lymph node metastases received camrelizumab combined with paclitaxel and gemcitabine (AG) to shrink the tumor before surgery. Postoperatively, her quality of life improved. Camrelizumab + AG presents a potential treatment for gallbladder cancer with such metastases but requires confirmation through clinical trials. Another case by Zhang Y. et al. reports successful treatment of advanced gallbladder cancer with high PD-L1 expression or high tumor mutation burden (TMB-H) using a combination of tislelizumab and S-1. Most patients experienced effective tumor control, while one had immune-related pneumonia (irP) resolved with therapy and surgery. Despite tumor control resuming after surgery, recurrent irP led to discontinuation and tumor progression. The findings suggest that combining anti-PD-1 antibodies with S-1 is a safe and effective treatment for GBC, particularly for biomarker-positive cases, offering a novel approach to advanced GBC therapy.

4 Pancreatic cancers

Pancreatic cancer is a formidable and often fatal malignancy that originates in the pancreas, a crucial organ with both endocrine and exocrine functions. Pancreatic ductal adenocarcinoma (PDAC) represents the most prevalent histological subtype, responsible for the majority of pancreatic cancer cases. Characterized by rapid progression, early metastasis, and resistance to conventional therapies, pancreatic cancer has long posed a significant clinical challenge (15). Recent research efforts have expanded our comprehension of the intricate molecular alterations and the complex tumor microenvironment driving its pathogenesis (16). Advances in early detection methods, targeted therapies, and immunotherapies have emerged as promising avenues for combating pancreatic cancer, offering renewed hope for improved patient outcomes (17).

Zhang Y. et al. explored the clinical and functional significance of F-box only proteins (FBXOs) in PDAC. They identified six FBXOs (FBXO1, FBXO20, FBXO22, FBXO28, FBXO32, and FBXO45) that were significantly upregulated in PDAC tissues, correlating with adverse patient prognosis and clinicopathological features. Promoter methylation influenced FBXO expression, and genetic alterations and mutations in these FBXOs affected patient outcomes. Additionally, the study revealed associations between FBXOs and immune infiltrations, including B cells, T cells, NK cells, macrophages, and dendritic cells, suggesting their role in the immune response. Functional analysis implicated these FBXOs in various signaling pathways, making them potential diagnostic and therapeutic targets for PDAC. Similarly, Sijde et al. investigated the role of circulating cytokines in predicting treatment response and overall survival in PDAC patients undergoing FOLFIRINOX chemotherapy. High levels of IL-1RA after one cycle of chemotherapy are associated with reduced tumor progression during treatment. Additionally, serum concentrations of IL-7, IL-18, and MIP-1β after one cycle of FOLFIRINOX correlate with overall survival. These findings suggest that specific cytokines and immune cells play crucial roles in chemotherapy response and PDAC progression, potentially paving the way for cytokine-based

treatments in the future. Eckhoff et al. showed that in patients with intraductal papillary mucinous neoplasm (IPMN) and PDAC, the activity of peripheral blood monocytes, specifically TNF expression upon R848 stimulation, inversely correlates with disease progression. Patients with low-grade IPMN and stage 1 PDAC exhibit higher TNF expression compared to those with high-grade IPMN and stage 2/3 PDAC, indicating innate immune reprogramming as IPMNs progress to invasive cancer. Additionally, sera from IPMN and PDAC patients contribute to the suppression of TNF induction in healthy donor monocytes, suggesting the involvement of soluble mediators in this process. Yuan H. et al. focused on 5-methylcytosine (m5C) modification in long non-coding RNAs (lncRNAs) and its implications in PDAC. Utilizing clinical data and genetic transcriptome information from the TCGA database, the researchers conducted bioinformatic analyses to establish an m5C-related lncRNA prognostic risk model for PDAC patients. This model effectively distinguished between PDAC and normal tissues and accurately predicted survival outcomes for PDAC patients. Zhuang et al. aimed to develop a prognostic classifier to assess hypoxia status and related molecular characteristics in PDAC. They classified PDAC into three clusters based on 16 known hypoxia-related genes and identified nine differentially expressed genes to construct an HIF-1 score system. This system effectively predicted patient survival outcomes and demonstrated superior predictive ability compared to previous hypoxia signatures. Furthermore, the study explored the oncogenic pathways and immune cell infiltration status associated with different HIF-1 scores, highlighting the potential for combination treatment strategies for highly hypoxic and immunosuppressive PDAC tumors. Su et al. also aimed to develop an immune-related gene prognostic risk index (IRGPRI) for pancreatic adenocarcinoma (PAAD) and explore its implications. Using the TCGA and GEO datasets, 16 immune-related hub genes were identified to construct the IRGPRI. Low IRGPRI was associated with favorable outcomes, immune-related pathways, and higher benefit from ICIs. High IRGPRI correlated with cancer-related pathways, less favorable outcomes, and lower benefit from ICIs. Chen X. et al. believe that the extracellular matrix (ECM) is crucial in the tumor microenvironment, affecting cancer cell behavior. Therefore their study explored ECM-related genes (ECMGs) in PAAD and pan-cancer contexts. Seven ECMGs were identified as PAAD hub genes, associated with tumor stage and prognosis. ECM-based subtypes showed distinct features in oncogene/tumor suppressor gene expression, the immune environment, and chemotherapy sensitivity. A prognostic panel, combining ECM-related mRNAs and lncRNAs, was developed and validated for accurate PAAD prognosis prediction.

5 Pan-cancer

Pan-cancer analyses, especially in-depth reviews, are critical for a comprehensive understanding of certain tumor-related biomarkers (18, 19). For example, Zhao et al. reviewed the Structural Maintenance of Chromosome 4 (SMC4), a member of the ATPase family involved in various cellular processes such as chromosome organization, DNA repair, and genome transcription. This review delves into the multifaceted functions of SMC4, including its role in cell division, RNA splicing, DNA metabolism, and the immune response. The focus is on its relevance in cancer, where high SMC4 expression is consistently associated with poorer overall survival. By analyzing data from various sources, this review suggests that SMC4 could serve as a valuable prognostic marker and potential therapeutic target in cancer. MicroRNAs (miRNAs) have gained significant attention in cancer research due to their pivotal role in tumorigenesis. Lu et al. reviewed the role of miR-608 as a tumor suppressor, which had been found to be downregulated, particularly in solid tumors. Extensive *in vivo* and *in vitro* experiments have verified its tumor-inhibiting properties. MiR-608 exerts its influence on various biological processes, including cell proliferation, invasion, migration, and apoptosis, by targeting transmembrane proteins and modulating key signaling pathways. This review summarizes miR-608's expression profile, biological functions, and underlying mechanisms, underscoring its potential as a diagnostic, prognostic biomarker, and therapeutic target in cancer. Another review by Wang J. et al. focused on immunotherapy, especially ICI, which is entering a new era of precision medicine. Clinical benefits of ICI in digestive system cancers are limited, and it often comes with side effects and high costs. To address this, the development of biomarkers for predicting immunotherapy effectiveness is crucial. They reviewed various potential biomarkers, including microsatellite mismatch repair, tumor mutation burden, specific mutated genes or pathways, PD-L1 expression, immune-related adverse reactions, blood biomarkers, and patient-related factors in predicting immunotherapy efficacy against digestive system cancers. The establishment of dynamic personalized prediction models based on multiple biomarkers holds promise for future research in this field.

Ti et al. examined squamous cell carcinomas (SCCs) from different sites to investigate the relationship between tumor mutation burden (TMB) and prognosis and immune cell infiltration in SCCs. TMB had varying effects on prognosis in different SCCs; it was associated with better prognosis in lung and cervical SCCs but worse prognosis in head and neck and esophageal SCCs. Older age, smoking history, earlier stage, and no lymphatic invasion were linked to higher TMB. Immune-related genes and immune cell proportions also varied between high and low TMB groups, thus provides insights for immunotherapy biomarkers in SCCs. In HPB malignancies, various T cell types with immune checkpoint receptors exist. Wan et al. reported that HCC shows a favorable presence of tissue resident memory T cells that respond well to immune checkpoint therapies. In contrast, pancreatic ductal adenocarcinoma (PDA) has terminally differentiated T cells with less potential for activation, regardless of chemotherapy. Combining checkpoint therapies may benefit HCC, while alternative approaches are needed for CCA and PDA. Shen et al. conducted a phase II clinical trial for advanced solid tumors resistant to standard treatments, in which a combination therapy was evaluated. Patients received targeted radiotherapy followed by liposomal irinotecan, camrelizumab, and anti-angiogenic drugs. Among 52 evaluated patients, there was a

34.6% objective response rate and an 82.7% disease control rate. Median progression-free survival was 5.3 months, and overall survival was not reached during the study period. Taken together, although treatment-related adverse events were common, the combination therapy showed promising anti-tumor activity and good tolerability in diverse advanced solid tumors.

As genomics technology continues to progress, it opens up new avenues for medical research and patient care. The analysis of gene expression profiles, coupled with the integration of patients' clinical information, medical imaging, and laboratory data, holds the potential to revolutionize the field. Emerging bioinformatics techniques, such as machine learning algorithms, promise to play a pivotal role in this transformation, enabling the creation of predictive models that are both highly accurate and robust. These models, in turn, will serve as invaluable tools in guiding medical decision-making. This wave of research endeavors is poised to focus on the development of personalized therapeutic drugs and treatment strategies, which aim to enhance treatment efficacy while minimizing unnecessary risks to patients. A deeper exploration of the intricate mechanisms underlying immunotherapies and chemotherapies will pave the way for the identification of novel therapeutic targets and innovative combination treatment approaches. Collectively, these advances are steering the medical field towards a future characterized by personalized treatment and intelligent medical care. This progressive trajectory promises to provide patients with increasingly precise and effective healthcare services, ultimately improving their overall well-being.

Author contributions

YQ: Writing – original draft. WJ: Writing – review & editing. HL: Writing – review & editing.

Acknowledgments

Expressing profound gratitude, we acknowledge all the authors, reviewers, and editors whose invaluable contributions have enriched this Research Topic.

Conflict of interest

The authors declare that the research was conducted in the absence of any commercial or financial relationships that could be construed as a potential conflict of interest.

Publisher's note

References

1. Zhang J, Xiao J, Wang Y, Zheng X, Cui J, Wang C. A universal co-expression gene network and prognostic model for hepatic–biliary–pancreatic cancers identified by integrative analyses. *FEBS Open Bio* (2022) 12(11):2006–24. doi: 10.1002/2211-5463.13478

2. Soerjomataram I, Bray F. Planning for tomorrow: global cancer incidence and the role of prevention 2020–2070. *Nat Rev Clin Oncol* (2021) 18(10):663–72. doi: 10.1038/s41571-021-00514-z

3. Anwanwan D, Singh SK, Singh S, Saikam V, Singh R. Challenges in liver cancer and possible treatment approaches. *Biochim Biophys Acta (BBA)-Reviews Cancer* (2020) 1873(1):188314. doi: 10.1016/j.bbcan.2019.188314

4. Huguet JM, Lobo M, Labrador JM, Boix C, Albert C, Ferrer-Barceló L, et al. Diagnostic-therapeutic management of bile duct cancer. *World J Clin Cases* (2019) 7 (14):1732. doi: 10.12998/wjcc.v7.i14.1732

5. Werner J, Combs SE, Springfeld C, Hartwig W, Hackert T, Büchler MW. Advanced-stage pancreatic cancer: therapy options. *Nat Rev Clin Oncol* (2013) 10 (6):323–33. doi: 10.1038/nrclinonc.2013.66

6. Wang S, Li Y, Xing C, Ding C, Zhang H, Chen L, et al. Tumor microenvironment in chemoresistance, metastasis and immunotherapy of pancreatic cancer. *Am J Cancer Res* (2020) 10(7):1937.

7. Li K-S, Zhu X-D, Liu H-D, Zhang S-Z, Li X-L, Xiao N, et al. NT5DC2 promotes tumor cell proliferation by stabilizing EGFR in hepatocellular carcinoma. *Cell Death Dis* (2020) 11(5):335. doi: 10.1038/s41419-020-2549-2

8. Petrowsky H, Fritsch R, Guckenberger M, De Oliveira ML, Dutkowski P, Clavien P-A. Modern therapeutic approaches for the treatment of Malignant liver tumours. *Nat Rev Gastroenterol Hepatol* (2020) 17(12):755–72. doi: 10.1038/s41575-020-0314-8

9. Rumgay H, Ferlay J, de Martel C, Georges D, Ibrahim AS, Zheng R, et al. Global, regional and national burden of primary liver cancer by subtype. *Eur J Cancer* (2022) 161:108–18. doi: 10.1016/j.ejca.2021.11.023

10. Li X, Ramadori P, Pfister D, Seehawer M, Zender L, Heikenwalder M. The immunological and metabolic landscape in primary and metastatic liver cancer. *Nat Rev Cancer* (2021) 21(9):541–57. doi: 10.1038/s41568-021-00383-9

11. Brindley PJ, Bachini M, Ilyas SI, Khan SA, Loukas A, Sirica AE, et al. Cholangiocarcinoma. *Nat Rev Dis Primers* (2021) 7(1):65. doi: 10.1038/s41572-021-00300-2

12. Banales JM, Marin JJ, Lamarca A, Rodrigues PM, Khan SA, Roberts LR, et al. Cholangiocarcinoma 2020: the next horizon in mechanisms and management. *Nat Rev Gastroenterol Hepatol* (2020) 17(9):557–88. doi: 10.1038/s41575-020-0310-z

13. Juengpanich S, Li S, Yang T, Xie T, Chen J, Shan Y, et al. Pre-activated nanoparticles with persistent luminescence for deep tumor photodynamic therapy in gallbladder cancer. *Nat Commun* (2023) 14(1):5699. doi: 10.1038/s41467-023-41389-1

14. Jia Z-Y, Zhu Y-D, Wu X-S, Yang J-X, Wu W-G, Wang X-A, et al. Improved long-term outcomes after innovative preoperative evaluation and conception of precise surgery for gallbladder cancer. *Cancer Med* (2023) 12(18):18861–71. doi: 10.1002/cam4.6513

15. Spiers L, Gray M, Lyon P, Sivakumar S, Bekkali N, Scott S, et al. Clinical trial protocol for PanDox: a phase I study of targeted chemotherapy delivery to non-resectable primary pancreatic tumours using thermosensitive liposomal doxorubicin (ThermoDox®) and focused ultrasound. *BMC Cancer* (2023) 23(1):896. doi: 10.1186/s12885-023-11228-z

16. Karamitopoulou E. Emerging prognostic and predictive factors in pancreatic cancer. *Modern Pathol* (2023) 36(11):100328. doi: 10.1016/j.modpat.2023.100328

17. Casarcia N, Rogers P, Guld E, Iyer S, Li Y, Burcher JT, et al. Phytochemicals for the prevention and treatment of pancreatic cancer: Current progress and future prospects. *Br J Pharmacol* (2023). doi: 10.1111/bph.16249

18. Kaubryte J, Lai AG. Pan-cancer prognostic genetic mutations and clinicopathological factors associated with survival outcomes: a systematic review. *NPJ Precis Oncol* (2022) 6(1):27. doi: 10.1038/s41698-022-00269-5

19. Raufaste-Cazavieille V, Santiago R, Droit A. Multi-omics analysis: Paving the path toward achieving precision medicine in cancer treatment and immuno-oncology. *Front Mol Biosci* (2022) 9:962743. doi: 10.3389/fmolb.2022.962743

frontiers in Oncology

REVIEW
published: 28 October 2021
doi: 10.3389/fonc.2021.777617

Recent Advances in the Mechanism Research and Clinical Treatment of Anti-Angiogenesis in Biliary Tract Cancer

*Yue Wang[1], Tianli Chen[1], Kangshuai Li[1], Wentao Mu[1], Zengli Liu[1], Anda Shi[1], Jialiang Liu[1], Wei Zhao[1], Shuo Lian[1], Shaohui Huang[1], Chang Pan[2] and Zongli Zhang[1]**

[1] Department of General Surgery, Qilu Hospital, Cheeloo College of Medicine, Shandong University, Jinan, China, [2] Department of Emergency, Qilu Hospital, Cheeloo College of Medicine, Shandong University, Jinan, China

Biliary tract cancers (BTCs), including cholangiocarcinoma (CCA) and gallbladder cancer (GC), are malignancies originating from the biliary tract with poor prognosis. In the early stage of BTCs, surgery is the only choice for cure. Unfortunately, most patients with BTC are diagnosed at an advanced stage and lose the opportunity for surgery. For many advanced solid tumors, antiangiogenic therapy has achieved encouraging results. While most clinical studies on antiangiogenic therapy in advanced BTCs have shown an excellent disease control rate (DCR), the improvement in overall survival (OS) is controversial. Understanding how the relevant signaling molecules influence the angiogenic response and the functional interaction is necessary for the formulation of new treatment regimens and the selection of enrolled patients. In this review, we aim to summarize and discuss the latest advances in antiangeogenesis for BTCs, mainly focusing on the molecular mechanism of angiogenesis in BTCs and the therapeutic effects from clinical trials. Furthermore, the horizon of antiangiogenesis for BTCs is highlighted.

Keywords: angiogenesis, gallbladder carcinoma, biliary tract cancers, cholangiocarcinoma, targeted therapy, mechanism, antiangiogenic therapy

OPEN ACCESS

Edited by:
Xuesong Gu,
Beth Israel Deaconess Medical Center and Harvard Medical School, United States

Reviewed by:
Zhaochen Liu,
Zhengzhou University, China
Zheng Liu,
National Cancer Center of China, China
Zhongqi Fan,
First Affiliated Hospital of Jilin University, China

***Correspondence:**
Zongli Zhang
zzlzzl1900@163.com

Specialty section:
This article was submitted to Cancer Immunity and Immunotherapy, a section of the journal Frontiers in Oncology

Received: *15 September 2021*
Accepted: *11 October 2021*
Published: *28 October 2021*

Citation:
Wang Y, Chen T, Li K, Mu W, Liu Z, Shi A, Liu J, Zhao W, Lian S, Huang S, Pan C and Zhang Z (2021) Recent Advances in the Mechanism Research and Clinical Treatment of Anti-Angiogenesis in Biliary Tract Cancer. Front. Oncol. 11:777617. doi: 10.3389/fonc.2021.777617

INTRODUCTION

Biliary tract cancers (BTCs) are a diverse group of malignancies originating in the biliary epithelium (1). According to their anatomical site of origin, BTCs are divided into cholangiocarcinoma (CCA) and gallbladder cancer (GC). CCAs are further classified as intrahepatic CCA (iCCA), perihilar CCA (pCCA), and distal CCA (dCCA) (2). PCCA and dCAA are also collectively called eCCA. BTCs account for only 3% of all gastrointestinal cancers, and the incidence of BTCs has increased over the past few decades (3). At present, surgical resection is still the only radical cure for BTCs (4).

However, because the symptoms of BTCs in the early stage are atypical, most cases are diagnosed at an advanced stage of disease and therefore lose the opportunity for radical surgical treatment. For patients with advanced unresectable or metastatic BTCs, systemic therapy might be the only beneficial treatment option (5). Unfortunately, due to the insensitivity to systemic therapies such as chemotherapy, the outcome of advanced and metastatic BTCs is unsatisfactory, with a 5-year survival rate of approximately 10%. Therefore, new therapies for BTC are urgently needed to improve the OS rate (6). In the era of precise treatment, antiangiogenic drugs are a main component of targeted therapy. However, the application of antiangiogenic therapy in BTC lacks consensus, and the criteria to select appropriate patients for antiangiogenic therapy have not been studied (7).

Metastasis is the main cause of individual death during tumor progression. There is sufficient evidence that tumor neovascularization is the pathological basis and necessary condition for the growth and metastasis of solid tumors (8). Tumor ischemia, on the one hand, affects the nutritional supply of the tumor, but on the other hand, it also impedes drug accessibility to the tumor and even promotes the selection of more aggressive tumor cells. Some scholars believe that promoting the normalization of tumor blood vessels will be an effective treatment (7).

Tumor-associated angiogenesis is active, and microvascular density is increased in BTCs, which contributes to the low cure and high recurrence rates after surgical resection. Microvessel density (MVD) is an indicator of tumor-driven neovascularization. MVD is significantly associated with survival and prognosis in GC, iCCA and extrahepatic cholangiocarcinoma (eCCA) (9–11). Studies confirmed that higher MVD was associated with advanced tumor stage and lower tumor resection rate and that MVD was an independent prognostic factor in a multivariate analysis. The 5-year survival rate of the high MVD group (2.2%) was significantly lower than that of the low MVD group (42.1%) (11), which suggested that the prognosis of BTCs is closely related to tumor angiogenesis. Although some antiangiogenic drugs have been approved for clinical trials in BTCs, the results are unsatisfactory. At present, the mechanism of tumor angiogenesis in BTCs is not clear, and the relevant targeted therapy needs to be further studied (12). This review summarizes the current consensus on tumor angiogenesis, with a focus on angiogenesis as the driving force in BTC development, and the status of the research and application of antiangiogenic therapy in BTCs.

Abbreviations: BTCs, Biliary tract cancers; CCA, Cholangiocarcinoma; iCCA, intrahepatic cholangiocarcinoma; pCCA, perihilar cholangiocarcinoma; dCCA, distal cholangiocarcinoma; eCCA, extrahepatic cholangiocarcinoma; GC, gallbladder cancer; DCR, disease control rate; OS, overall survival; PFS, progress free survival; mPFS, median progression-free survival; mTTP, median time to progression; mOS, median overall survival; ORR, objective response rate; MVD, microvessel density; ROS, reactive oxygen species; VEGF, Vascular Endothelial Growth Factor; VEGFR, Vascular Endothelial Growth Factor Receptor; RTK, tyrosine kinases; MMPs, matrix metalloproteinases; TGFβ1, Transforming Growth Factor Beta 1; TNF-α, Tumor necrosis factor-α; PDGF, The platelet-derived growth factor family; PDGFR-β, platelet-derived growth factor; Ang1, Angiogenin-1; Ang2, Angiogenin-2; bFGF, basic fibroblast growth factor; HPC, hepatic stem/progenitor cells; PBC, primary biliary cirrhosis; Tems, TIE-2-expend monocytes; VM, Vasculogenic mimicry; RTKs, receptor tyrosine kinase; aCECs, activated circulating vascular epithelial cells; RECIST, Response Evaluation Criteria in Solid Tumours; BF, bloodflow; BV, blood volume; GEM, Gemcitabine; GC, Gemcitabine + Cisplatin; GemCap, Gemcitabine + Capecitabine; GEMOX, Gemcitabine + Oxaliplatin; GEMOX-B, Gemcitabine + Oxaliplatin + Bevacizumab; L-OHPL, Oxaliplatin; Cape, Capecitabine.

TUMOR ANGIOGENESIS AND TUMOR VASCULAR NORMALIZATION

Tumor blood vessels are characterized by structural disorder, incomplete wall structure and high permeability, which can lead to local hypoperfusion of the tumor (13). Thus, it is difficult for either oxygen or drugs transported through blood vessels to enter the tumor parenchyma, which will greatly reduce the effectiveness of radiotherapy, chemotherapy and immunotherapy (14–16). The ionizing radiation of radiotherapy can locally produce reactive oxygen species (ROS) in the presence of oxygen. ROS can damage DNA and directly result in the death of tumor cells (17). However, the low-oxygen tumor microenvironment weakens the effect of this treatment. Systemic chemotherapy drugs need to attach to the local tumor area through the blood circulation system. A low perfusion state and increased interstitial pressure prevent drugs from attaching to the tumor area or reduce the amount of drugs entering the tumor parenchyma, thereby affecting the efficacy of chemotherapy. For the tumor itself, the lack of effective blood perfusion leads to a hypoxic tumor microenvironment (18). Hypoxia can activates the HIF (Hypoxia-inducible factor) signaling pathway, which promotes tumor cells to overexpress VEGF to induce tumor angiogenesis (19); In addition, tumor cells with more aggressive and metastatic ability will be screened out because of the harsh tumor microenvironment (20). The RhoA-ROCK1 signaling can be activated by HIF to enhance cell motility (21). Hypoxia increases hypermethylation of tumor suppressor gene, which makes epigenetic aberration and then promotes tumor growth and metastasis (22). Furthermore, hypoxia inhibits tumor immunity by inhibiting cytotoxic T cell activity, promoting local tumor recruitment of Treg cells, and inhibiting the synthesis of pro-inflammatory cytokines. These effects involve a series of factors including cAMP, HIF, COX2, SDF1, IL-10, etc. (23–26).

In the past, antiangiogenic therapy was thought to work by blocking the pathway of tumor angiogenesis and cutting off the nutrient supply to the tumor. However, with clinical research in recent years, it has been found that the effect of antiangiogenic therapy is limited, and some patients are more prone to tumor metastasis after antiangiogenic therapy (27). This is because antiangiogenic drugs severely degenerate tumor blood vessels, while blocking the nutritional supply of tumor, the supply of drugs and oxygen also been hindered. Such conditions can help tumor tissue resist the effects of radiotherapy and chemotherapy, and further deepen the hypoxia condition of tumor microenvironment (28). As mentioned above, hypoxia increases tumor malignant phenotype and inhibits tumor immunity, which is obviously not conducive to tumor therapy. Until the theory of tumor vascular normalization was proposed in 2005 (13), the purpose of antiangiogenic therapy has not changed from degrading tumor blood vessels to promoting the

maturation of tumor blood vessels, thereby improving local blood perfusion and material transportation in the tumor microenvironment. This notion partly addresses the limitations of antiangiogenic therapy and provides a theoretical basis for antiangiogenic therapy combined with chemotherapy or targeted therapy. After antiangiogenic treatment, there will be a specific time window. At this time, the tumor blood vessels will be temporarily and reversibly normalized, and drugs are easier to enter the tumor microenvironment (29).

Inhibition of tumor angiogenesis and induction of tumor vascular normalization are of great significance in the treatment of tumors (30). Unfortunately, the existing antiangiogenic therapies have not shown promising therapeutic effects, especially in the field of BTCs. Existing studies have shown that anti-VEGF therapy not only inhibits tumor angiogenesis, but also promotes normalization of tumor blood vessels (31). There are also reports showing that treatments targeting VEGF can increase the invasion and metastatic phenotype of tumors (32). These contradictory results are believed to be related to the complex regulatory network of tumor angiogenesis. Vascular endothelial protein tyrosine phosphatase (VE-PTP) inhibitors can mature tumor vessels by activating Tie-2 (33). Overexpression of proteins such as R-RAS and HRG which contribute to vascular maturation can normalize abnormal tumor vessels (34, 35). These findings provide new targets for tumor vascular normalization. In addition to the drug itself, the dose and duration of drugs are crucial for abnormal tumor vascular development to different outcomes, tumor vascular normalization and tumor vascular degeneration. While methods to assess the time window of tumor vessel normalization are still scarce, and the control of drug dose and time is not ideal (36). Furthermore, the mechanism of angiogenesis is ambiguous in tumors, and there are no therapeutic targets that can bypass normal blood vessels. Therefore, further research is needed to clarify the mechanism and explore more effective targets and treatment strategies (7).

FACTORS AND MECHANISMS THAT REGULATE ANGIOGENESIS IN BTCs

The growth of solid tumors is accompanied by tumor angiogenesis, and it is reasonable that anti-angiogenic therapy should be an important part of anti-tumor therapy. However, therapeutic regimens targeting VEGF/VEGFR have consistently failed to provide encouraging results (37). The main reasons is that there are many ways to promote angiogenesis (**Figure 1**). VEGF-dependent or VEGF-independent neovascularization and angiogenesis mimicry can all provide blood vessels for tumor tissues. Inhibition of one pathway leads to compensatory activation of other pathways. Besides, classical proangiogenic pathways, such as the VEGF/VEGFR pathway, also play a role in normal tissue. That makes treatment easier to be interrupted by on-target off-tumor toxicities (38). Therefore, it is critical to find tumor-specific antiangiogenic targets and the common pathways in different angiogenesis mechanisms. Understanding the pro- and anti-angiogenesis factors as well as their interaction and molecular mechanisms is essential for the development of durable and effective anti-angiogenesis drugs (39). In the following content, we will describe the role of pro-angiogenic and anti-angiogenic factors in BTCs, especially their regulatory mechanism.

VEGF/VEGFR SIGNALING PATHWAY

VEGF is a growth factor with the strongest angiogenic activity. The VEGF growth factor family includes VEGF-A, -B, -C, -D, -E, -F and placental growth factor (40). Among these types of VEGF, VEGF-A is generally believed to play the most obvious role in promoting angiogenesis. During mouse embryonic development, VEGF or VEGF receptor (VEGFR) gene deletion leads to embryonic death due to angiogenesis disorder. Additionally, VEGF plays an important role in tumor angiogenesis. VEGF is

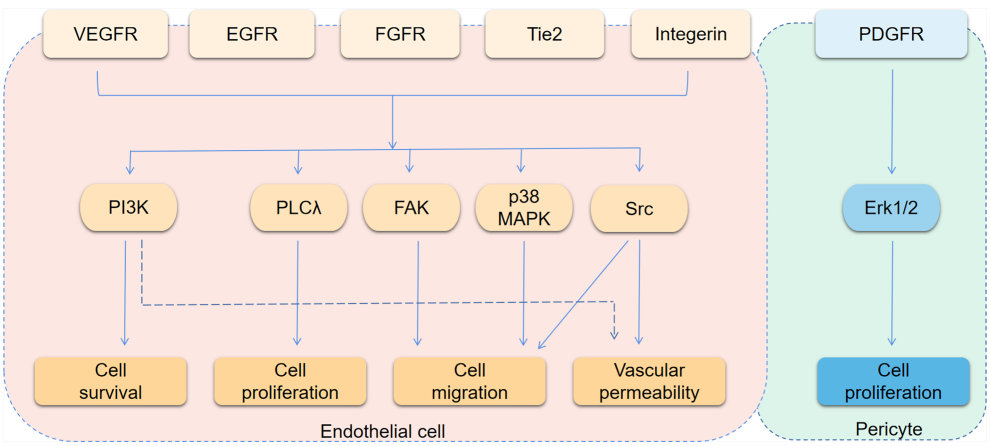

FIGURE 1 | Angiogenesis signaling pathways. The figure shows the main downstream pathways of receptors associated with angiogenesis. The main phenotypes affected by each pathway are indicated by arrows.

overexpressed in many epithelial tumor cells. A large number of studies have reported that the level of VEGF in peripheral blood is directly related to tumor prognosis (41).

VEGF mainly acts through the corresponding receptors Flt-1 and KDR, also known as VEGFR-1 and VEGFR-2 (42). Both Flt-1 and KDR are receptors for tyrosine kinase receptors (RTKs). The binding of VEGF and KDR activates the MAPK signaling pathway and promotes endothelial cell proliferation and angiogenesis. The function of Flt-1 is more complicated. In addition to promoting angiogenesis, the combination of VEGF can also activate matrix metalloproteinases (MMPs). The increased expression of VEGF in tumor tissues is related to hypoxia-inducible factors, which can promote the expression of VEGF. The traditional concept states that VEGFR is specifically expressed in endothelial cells. However, an increasing number of recent studies have shown that tumor cells can also express VEGFR. VEGF secreted by tumor cells can promote angiogenesis and tumor cell proliferation through paracrine (acting on endothelial cells VEGFR) and autocrine (acting on the VEGFR of tumor cells) pathways.

Some researchers examined VEGF expression in four CCA cell lines and their culture supernatants. The results show that CCA cells can express and secrete VEGF (43). VEGF can be detected in bile and can be used as a diagnostic and predictive biomarker for different biliary diseases (44). Studies have shown that the positive expression rates of VEGF in clinical samples of iCCA, eCCA and GC are 53.8%, 59.2% and 56.3% (45–47). The overexpression of VEGF is related to the intrahepatic metastasis of iCCA (P=0.0224), while there was no significant correlation between VEGF and the clinical features of eCCA in this study (46). Other studies have shown that the expression of VEGF-A tends to increase in hypervascularized eCCA, but it did not reach statistical significance (P=0.08) (48). Further studies on eCCA have shown that, compared with pCCA, the positive expression rate of VEGF-A in dCCA is higher (69% *vs.* 25%, P <0.0001), and it is related to an increase in microvessel density (49). When VEGF was neutralized by adding 10 mg/mL anti-VEGF antibody to the medium, vascular endothelial cells decreased to 63.8% of the control group (P <0.02) (43). Any factor that destroys the expression of VEGF or VEGFR may affect the angiogenesis of BTCs. The following factors, hormones or drugs that may affect the VEGF signaling pathway were identified in the study of BTCs (**Figure 2**). TGF-β1 is expressed in tumor cells or surrounding mesenchymal cells, and immunostaining shows that its receptors TβR-I and TβR-II are strongly positively expressed in tumor cells. Studies have shown that TGFβ1 can promote the expression of VEGF in tumor cells through autocrine or paracrine modes and then affect tumor angiogenesis (50). S100A8 is highly expressed in CCA cells and increases the secretion of VEGF by activating the Toll-like receptor 4 (TLR4)/NF-κB pathway, thereby inducing the migration of vascular endothelial cells (51). Studies also show that COX-2 is related to angiogenesis. COX-2 is highly expressed in CCA tissues, especially advanced CCA (52). COX-2 inhibitors have been approved for adjuvant treatment of CCA, but *in vitro* experiments show that they have no inhibitory effect on the growth of tumor cells. COX-2 inhibitors can inhibit the expression and secretion of VEGF-C, thereby affecting the invasion of cholangiocarcinoma (52). MiR-101 can also inhibit COX-2 or directly target the 3' untranslated region of VEGF mRNA to inhibit VEGF transcription (53). AKirin2 is overexpressed in CCA and promotes VEGF-A expression by activating the IL-6/STAT3 signaling pathway. This process can be inhibited by miR-490-3p (54). The highly conserved cell surface protein B7-H3 is reported to correlate with pathological rather than physiological angiogenesis and is regarded as an attractive target for the selective destruction of tumor vasculature (55). Estrogen can significantly increase the expression and secretion of VEGF-A in CCA cells. This effect is

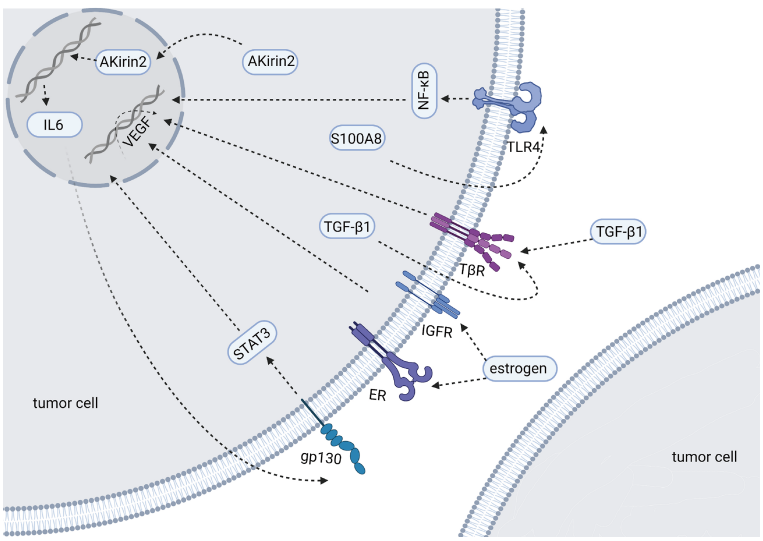

FIGURE 2 | Molecules and mechanisms regulating the expression of VEGF in BTCs (Created in BioRender.com). The figure mainly shows the factors have been reported to affect the expression of VEGF in BTCs. These factors are overexpressed in tumor cells and their downstream signaling pathways of affecting VEGF have been described by researchers.

partially inhibited by estrogen receptor antagonists and completely blocked when used in combination with IGF1-R blocking antibodies (56). Tumor necrosis factor-α (TNF-α) can promote or inhibit endothelial cell growth and angiogenesis, depending on the cell condition. Treatment with lupeol or stigmasterol significantly reduced the secretion of TNF-α in umbilical vein endothelial cells, and then, the transcription level of VEGFR-2 decreased, which interfered with tumor angiogenesis by inhibiting VEGF signaling (57). HMGB1 induces angiogenesis by promoting the expression of VEGFR-2 in vascular endothelial cells (58). Histamine can increase the expression of VEGF-A/-C. Histamine stimulation has an effect on the angiogenesis observed in the tumor microenvironment. This effect can be inhibited by the HDC inhibitor α-methyl-DL-histidine dihydrochloride or the H1HR antagonist terfenadine (59). In addition, a drug, phenformin, can increase the expression and secretion of VEGF (60).

VEGF also has a close relationship with precancerous lesions. There are stem cells called hepatic stem/progenitor cells (HPCs) around the biliary tree. In primary biliary cirrhosis (PBC), a precancerous lesion of CCA, HPC is activated, and VEGF-A and VEGF-C are highly expressed (61). Higher angiogenesis can be observed in PBC samples. These studies indicate that the VEGF/VEGFR signaling pathway and angiogenesis may play an important role in the occurrence and development of BTCs.

PDGF/PDGFR SIGNALING PATHWAY

The platelet-derived growth factor family (PDGF) regulates angiogenesis in tumors, and four family members have been identified, including PDGF-A, B, C, and D (62). PDGF can be synthesized and secreted by platelets, smooth muscle cells, vascular endothelial cells, pericytes and tumor cells. As a growth factor, PDGF combines with its receptor PDGFR to promote the growth of pericytes, vascular endothelial cells, fibroblasts, vascular smooth muscle cells and tumor cells by activating the Erk1/2 signalling pathway (63). PDGF promotes tumor cells migration by activating the p38/MAPK signalling pathway and overexpressing the MMPs. PDGF can also promote the directional migration and vascular envelopment of pericytes, thereby regulating the maturation and stability of tumor blood vessels. PDGF has been found to be highly expressed in a variety of solid tumors and as a predictor of poor prognosis. In biliary tumors, PDGF has been shown to be highly expressed and associated with poor prognosis (64, 65). Excessive activation of platelets has been found in CCA, which may be the source of PDGF in CCA (65). TCF-21 has been identified as a tumor suppressor gene in a variety of tumors, including CCA. When TCF-21 is overexpressed in CCA cells, it can inhibit the expression of PDGF (66).

ANG-TIE-2 SIGNALING PATHWAY

Another important group of angiogenesis regulators is the angiopoietin family, including Ang1 and Ang2, which act through their receptor Tie-2. In recent years, this family of proteins has received increasing attention (67). When VEGF-mediated angiogenesis is blocked, the upregulation of Ang expression has been shown to be part of the angiogenesis rescue response, leading to accelerated tumor metastasis. Ang1 and Ang2 have opposite effects. Ang1 is the agonist ligand TiE-2 (68), which activates downstream pathways after phosphorylation of the receptor, protects blood vessels, maintains endothelial cell survival, and inhibits inflammation and vascular leakage. Ang1 can be expressed in a variety of cells, such as pericytes, smooth muscle cells and fibroblasts. Ang2, which is mainly expressed in vascular endothelial cells, has the opposite effect as Ang1. Ang2 is an inhibitory ligand of TiE-2 that can block Ang1-induced TiE-2 activation. Ang2 can also destroy vascular stability and promote inflammation and leakage (69). Therefore, both Ang1 and Ang2 play important roles in vascular remodeling and angiogenesis (70).

Ang1 has been shown to be highly expressed in a variety of tumor cells. Tumor-associated endothelial cells express high levels of Ang2, and the Ang2 concentration in peripheral blood is thought to be related to the tumor progression of BTCs (71). The TIE-2 receptor has also been detected in the tumor vascular endothelium (68). Although reported to promote tumor growth, Ang1 usually exerts an antitumor effect. In a study of biliary tract tumors, a team found that the expression of Ang1 in pCCA was negatively correlated with the metastasis rate, and the presence of TIE-2-expanded monocytes (Tems) in tumor tissues was associated with a lower recurrence rate (70). Ang2 expression was correlated with higher MVD in CCA (P=0.015). When both Ang2 and VEGF are positive, the MVD of CCA tissue is significantly increased (45).

bFGF/FGFR SIGNALING PATHWAY

There are 22 members of the FGF family, from FGF-1 to FGF-23, except for FGF15 (human FGF19 and mouse FGF15 are homologous) (72). Among them, basic fibroblast growth factor (bFGF, also called FGF2) can affect vascular endothelial cells and stimulate angiogenesis. FGF receptor (FGFR) is expressed in endothelial cells. bFGF has been shown to be overexpressed in CCA (72, 73). Four CCA cell lines and their culture media were tested, and it was found that two of them can express and secrete bFGF, and all of them can express FGFR-1. The addition of anti-bFGF neutralizing antibody did not affect the proliferation of CCA cells but reduced the vascular endothelial cells to 58.9% of the control group (P<0.001). These results indicate that bFGF can affect the survival of the vascular endothelium in the form of paracrine signaling (43).

APELIN/APLNR SIGNALING PATHWAY

The apelin/APLNR axis plays important roles in regulating blood pressure and cardiovascular disease and in regulating angiogenesis and the endothelial cell response to hypoxia (74, 75). Studies have shown that high expression of apelin can

promote tumor angiogenesis in malignant tumors such as lung and liver cancers (76, 77). In CCA, researchers found that high expression levels of apelin and APLNR promote CCA cell proliferation and angiogenesis. Exogenous apelin stimulation can significantly increase the expression of angiogenesis factors (VEGF and Ang). Anti-APLNR reduces not only the expression of angiogenesis factors (VEGF and Ang) but also the expression of vimentin, MMP-9 and MMP-3 (78). These results suggest that the apelin/APLNR axis plays an important role in tumor angiogenesis. The mechanism regulating the expression of apelin/APLNR is not clear, but it has been extensively studied in different tumors. Apelin expression is related to oral squamous cell carcinoma hypoxia (79), and circulating apelin concentration is related to C-reactive protein in gastric and esophageal cancers (80). In prostate cancer, the level of apelin is regulated by microRNA-224 (81). Further research is needed in CCA.

OTHER FACTORS AND MECHANISM

MMP can degrade the extracellular matrix and promote tumor angiogenesis. The expression of MMP2/MMP9 is increased in CCA and associated with poor prognosis. The overexpression of PDGF can contribute to the overexpression of MMP2/MMP9 (65). The roles of TSP-1 in tumor angiogenesis and tumor progression are still controversial. The expression of TSP-1 is associated with a significant decrease in MVD levels in CCA (45), which suggests that TSP-1 may play a role in inhibiting angiogenesis in CCA. However, the incidence of intrahepatic metastasis is higher when TSP-1 is positive (45). In a study of iCCA, TSP-1 was also positively correlated with lymphatic invasion (82). LOXL1 is a classic member of the LOX family. It is overexpressed in iCCA and can be secreted outside the cell. LOXL1 protein can bind to the exposed RGD domain of FBLN5, then the complex can bind to Integrin alpha V beta 3 on the surface of vascular endothelial cells and promotes angiogenesis *via* the downstream FAK and MAPK signaling pathways (83). In addition, angiostatin and endostatin can also inhibit angiogenesis (84, 85). Recombinant human endostatin (ENDOSTAR) can act on a variety of cell signaling pathways. It reduces tumor angiogenesis-related proteins and inhibits tumor lymphangiogenesis to inhibit angiogenesis. Moreover, it has been shown to have a good therapeutic effect on nonsmall cell lung cancer (46). Recent studies have shown that recombinant human endostatin can bring clinical benefits to patients with advanced cervical cancer. However, the expression and role of angiostatin in CCA remain unclear. Integrins belong to the family of cell adhesion molecules and are involved in tumor angiogenesis. Multiple subtypes of integrin are highly expressed in BTCs (86, 87). Integrin as a receptor can promote endothelial cell migration by activating FAK and MAPK signaling pathways. Moreover, integrin on the surface of vascular endothelial cells can bind to a certain structure of the extracellular matrix to accelerate the migration of endothelial cells and the formation of tumor blood vessels (88). Cilengitide is an integrin antagonist that can recognize and interact with integrins. Their interaction induces tumor cell apoptosis and inhibits tumor angiogenesis (89). Thalidomide can also inhibit angiogenesis by blocking the secretion of VEGF and basic fibroblast growth factor (bFGF) (90).

Vasculogenic mimicry (VM) is a form of vessels that is different from vessels derived from classic tumor angiogenesis and is independent of the vascular endothelium (91). It is composed of a cord formed by aggressive and poorly differentiated tumor cells, through which blood can be seen (92). The pipeline is connected with the host's blood vessels so that the tumor cells can obtain blood supply to meet the needs of tumor growth, invasion and metastasis (93). VM has been found in liver cancer, lung cancer, prostate cancer and ovarian cancer, and it has been proven to correlate with tumor growth, differentiation and invasion. However, there is still a lack of research in BTCs.

CLINICAL PROGRESS OF ANTIANGIOGENIC THERAPY IN BTCs

Anti-angiogenic drugs (**Figure 3**) are currently divided into three categories: anti-VEGF monoclonal antibodies such as bevacizumab; signaling pathway inhibitors, represented by the small molecule tyrosine kinase inhibitors; and recombinant human vascular endostatin (94). Bevacizumab monotherapy has been shown to be less effective. Long-term clinical studies have shown that bevacizumab monotherapy can prolong progression-free survival (PFS) but not overall survival (OS), suggesting that inhibition of the classic VEGF pathway may activate compensatory pathways that promote tumor angiogenesis or metastasis, thereby leading to a rebound in tumor malignancy. Small molecule multitargeted receptor tyrosine kinase (RTK) inhibitors such as solafinib can simultaneously suppress multiple signaling pathways (95). This effect is expected to solve the problems of the abnormal activation of other signaling pathways in the case of a single inhibition of VEGF signaling pathways. Although TKI drugs, including sorafenib, axitinib, and sunitinib, are all multitarget inhibitors, their effects are mostly the same (96, 97). For example, the main targets of axitinib are VEGFR-1, VEGFR-2, VEGFR-3, the role of those are mainly angiogenesis (98). The inhibitory effect is not obvious on the target of whose roles are mainly promoting tumor cell survival and proliferation. Besides, these small molecule tyrosine kinase inhibitors have minimal effect on the tumor microenvironment. To improve the efficacy, on the one hand, a combination of drugs can be applied to interfere with angiogenesis and tumor proliferation simultaneously; on the other hand, a new generation of antiangiogenic drugs should cover more targets involved in the tumor growth. Anlotinib, as a new generation of antiangiogenic drugs, can inhibit tumor angiogenesis by targeting VEGFR, FGFR and PDGFR, meanwhile, it can also inhibits tumor growth by targeting c-kit (99). The significantly prolonged PFS and OS achieved in anlotinib treated drug-resistant NSCLC patients may be due to this dual effect (100). Currently, antiangiogenesis-based drug

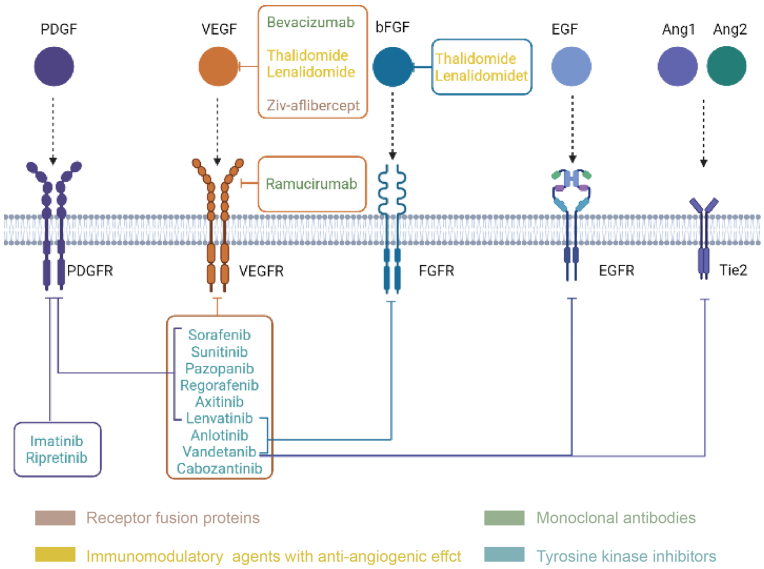

FIGURE 3 | Classification and targets of anti-angiogenic drugs (Created in BioRender.com). Every drug in the picture points to its own targets, and the four drug types are distinguished by four colors.

strategies for the treatment of malignant tumors include single-drug therapies with targeted drugs, combinations of chemotherapy and targeted drugs, combinations of immunotherapy and targeted drugs, and combined applications of targeted drugs. At present, antiangiogenic therapy has not been approved for the clinical treatment of biliary tract tumors, and most of the relevant studies are in the clinical trial stage. The following will summarize the research progress of antiangiogenic therapy for biliary tumors (**Table 1**).

MONOTHERAPY REGIMENS

The single-drug regimens of antiangiogenic therapy mostly use signaling pathway inhibitors, which can act on multiple targets simultaneously. Although more targets can increase the efficacy, the possibility of the corresponding side effects is also increased. Sunitinib, a multitarget tyrosine kinase inhibitor that targets PDGFR, VEGFR, KIT, FLT-3 and RET, can inhibit not only tumor proliferation but also angiogenesis at the same time. Sunitinib has been shown to be effective in the treatment of several solid tumors. In a study of advanced biliary tract tumors, Jun Ho Yi et al. believed that sunitinib monotherapy had a poor clinical effect. The PFS was only 1.7 months, and the incidence of grade 3–4 toxicities was high (46.4%) (101). Dreyer C et al. reported three cases of ICC patients with tumor progression after receiving first-line chemotherapy and treated them with sunitinib. Reductions in tumor size and density were observed in all three cases; one achieved partial remission, and two achieved stable disease (SD). They concluded that sunitinib was well tolerated and had manageable side effects. Based on these encouraging results, they initiated a phase II clinical study of sunitinib for second-line treatment in patients with advanced intrahepatic cholangiocarcinoma who had received chemotherapy (102). Fifty-three patients were included in this study, of whom 15% achieved partial remission, 71% achieved disease stability, the median PFS (mPFS) was 5.2 months and the median OS (mOS) was 9.6 months [95% CI: 5.8–13.1] (103). Thus, sunitinib monotherapy shows promising activity in advanced intrahepatic cholangiocarcinoma. Sorafenib, a hot multitarget tyrosine kinase inhibitor that targets VEGFR-2/-3, PDGFR-B, B-Raf, and C-Raf, achieved a 2% disease remission rate in the second-line treatment of 46 patients with advanced cholangiocarcinoma. The median progression-free survival was 2.3 months (range: 0–12 months), and the median overall survival was 4.4 months (range: 0–22 months) (104). Another study using sorafenib as a first-line regimen for advanced biliary tumors showed that the median PFS was 3 months (95% CI: 2–4 months) and the median OS was 9 months (95% CI: 4–12 months) (105). The results of these two clinical trials indicate that sorafenib did not achieve positive resultes in the treatment of advanced biliary tumors as a Monotherapy, and the combination therapy of sorafenib with other drugsit may be a promissing future direction. Lenvatinib is an inhibitor of VEGFR, FGFR and PDGFR. A phase II clinical trial was conducted with lenvatinib as a single agent for advanced biliary tract tumors. An interim evaluation of 17 patients showed a DCR of 82% (106). Finally, 26 patients were recruited into the study, and the results showed that the median PFS was 3.19 months (95% CI: 2.79–7.23) and the median OS was 7.35 months (95% CI: 4.50–11.27). Therefore, the study authors concluded that lenvatinib showed promising therapeutic effects in advanced biliary tract tumors with manageable side effects (107). Regorafenib is a multitarget inhibitor that targets VEGFR, PDGFR-β, KIT, RET and RAF-1. For patients with advanced biliary tract tumors who received failing first-line treatment, the average progression-free survival

TABLE 1 | Anti-angiogenic drugs of BTCs in phase II.

Therapy	Target	NCT	Line	Phase	n	Patients	mPFS/mTTP months (95% CI)	mOS months (95% CI)	ORR	DCR
monotherapies										
Sorafenib	VEGFR, PDGFR, Raf	NCT 00238212	first	II	31	advanced BTC	3.0 (2.0-4.0)	9.0 (4.0-12.0)	0.0%	39.0%
Sunitinib	VEGFR, PDGFR, c-Kit, IRE1α	NCT 01718327	second	II	53	advanced iCCA	5.2	9.6 (5.8-13.1)	15.0%	85.0%
Sunitinib	VEGFR, PDGFR, c-Kit, IRE1α	NCT 01082809	second	II	56	advanced BTC	1.7 (1.0-2.4)*	4.8 (3.8-4.8)	8.9%	50.0%
Lenvatinib	VEGFR, FGFR, PDGFR, Kit, RET	NCT 02579616	second	II	17	advanced BTC			6.0%	82.0%
Lenvatinib	VEGFR, FGFR, PDGFR, Kit, RET	NCT 02579616	second	II	26	advanced BTC	3.2 (2.79-7.23)	7.4 (4.5-11.3)	11.5%	85.0%
Regorafenib	VEGFR, PDGFR, Kit, RET, Raf	NCT 02053376	second	II	43	advanced BTC	3.9 (3.2-6.2)	8.0 (3.3-18.6)	11.0%	56.0%
Apatinib	VEGFR-2	NCT 03521219	second	II	24	advanced iCCA	3.2 (2.7-5.1)	8.3 (3.8-12.9)	20.8%	62.5%
Apatinib	VEGFR-2	NCT 03251443	second	II	26	advanced iCCA	2.0 (0.7-3.3)	9. 0 (4.6-13.4)	11.5%	50.3%
Vandetanib	VEGFR, EGFR, PDGFR, Tie-2, FGFR	NCT 00753675	first	II	56	advanced BTC	3.4 (2.3-5)	7.4 (6.1 -11.7)	3.6%	25.0%
Cytotoxic + targeted therapies										
GEM+ Vandetanib	VEGFR, EGFR, PDGFR, Tie-2, FGFR	NCT 00753675	first	II	57		3.7 (2.9-6.2)	9.2 (6.9-11.6)	19.3%	29.8%
GEM+ placebo					52	advanced BTC	4.8 (1.9-7.3)	9.9 (8.2-16.9)	13.5%	20.0%
GC+ Sorafenib	VEGFR, PDGFR, Raf	NCT 00919061	first	II	39	advanced BTC	6.5 (3.5-8.3)	14.4 (11.6-19.2)		
GemCap+ Bevacizumab	VEGF	NCT 01007552	first	II	50	advanced BTC	8.1 (5.3-9.9)	10.2 (7.5-13.7)	24.0%	72.0%
GEMOX+ Bevacizumab	VEGF	NCT 00361231	first + second	II	35	advanced BTC	7.0 (5.3-10.3)	12.7 (7.3-18.1)	40.0%	69.0%
GEM+L-OHPL+ Cape+Panitumumab	EGFR	NCT 01206049	first	II	45	advanced BTC	6.1 (5.8-8.1)	9.5 (8.3-13.3)	46.0%	
GEM+L-OHPL+ Cape+Bevacizumab	VEGF				43		8.2 (5.3-10.6)	12.3 (8.8-13.3)	18.0%	
GEM+placebo	VEGFR, PDGFR, RAF, KIT, FLT-3	NCT 00661830	first	II	36	advanced BTC	4.9 (3.5-7.7)	11.2	10.0%	90.0%
GEM+Sorafenib					41		3.0 (1.8-7.2)	8.4	14.0%	86.0%
GC+Cediranib	VEGFR, PDGFR, c-kit	NCT 00939848	first	II	62	advanced BTC	8.0 (6.5-9.3)	14.1 (10.2-16.4)	44.0%	78.0%
GC+placebo					62		7.4 (5.7-8.5)	11.9 (9.2-14.3)	19.0%	65.0%
Targeted + targeted therapies										
Lenvatinib+ Pembrolizumab	VEGFR, FGFR, PDGFR, Kit, RET, PD-1	NCT 03895970	second	II	32	advanced BTC	4.9 (4.7-5.2)	11.0 (9.6-12.3)	25.0%	78.1%
Sorafenib +Erlotinib	VEGFR, PDGFR, RAF, KIT, FLT-3, EGFR	NCT 01093222	first	II	34	advanced BTC	2.0 (2.0-3.0)	6.0 (3.0-8.0)	6.0%	35.0%
Bevacizumab +Erlotinib	VEGF +EGFR	NCT 00356889	first	II	49	advanced BTC	4.4 (3.0-7.8)*	9.9 (7.2-13.6)	12.0%	63.0%

**These data represent mTTP.*

GEM, Gemcitabine; GC, Gemcitabine + Cisplatin; GemCap, Gemcitabine + Capecitabine; GEMOX, Gemcitabine + Oxaliplatin; L-OHPL, Oxaliplatin; Cape, Capecitabine; NCT, National Clinical Trial; mPFS, median progression-free survival; mTTP, median time to progression; mOS, median overall survival; ORR, objective response rate; DCR, disease control rate.

of regorafenib treatment was 3.9 months (95% CI: 3.2–6.2), and the average overall survival time was 8 months (95% CI: 3.3–18.6). Regorafenib may exert its promising efficacy in advanced biliary tract tumors, which is worthy of further study (108).

COMBINATION THERAPY REGIMENS

Chemotherapy Combined With Targeted Therapy

A phase II study of bevacizumab combined with gemcitabine/capecitabine in the treatment of advanced BTCs showed that the mPFS was 8.1 months, and the mOS was 10.2 months. Compared with the results of the gemcitabine/cisplatin combination in the ABC-02 trial (8 months of PFS and 11.7 months of OS), it could not be concluded that bevacizumab combined with Gemcitabine plus Capecitabine (GemCap) would benefit patients. However, more clinical stage IV patients were enrolled in the former group than in the latter group, and the proportion of patients with stage III disease was relatively low (6% vs. 25%) (109). Gemcitabine plus Oxaliplatin (GEMOX) in BTCs achieved an ORR of 26%-50% and a median overall survival of 11–12 months. The ORR of Gemox-B (the addition of bevacizumab to GEMOX) in BTCS reached 40%, the median progression-free survival reached 7.0 months, and the median overall survival reached 12.7 months (110). A phase II clinical trial showed that after two treatment cycles of bevacizumab combined with gemcitabine and oxaliplatin, the maximum standardized uptake value on FDG-PET scans was significantly decreased, indicating disease control and longer PFS and OS (110). A phase II clinical trial of the multitarget tyrosine kinase inhibitor cediranib combined with first-line chemotherapy in the treatment of advanced biliary tract cancer was conducted. Patients were randomly divided into two groups: cediranib combined with chemotherapy or placebo combined with chemotherapy. However, only ORR but not mPFS or mOSz showed a statistically significant difference, with 44% in the cediranib group versus 19% in the placebo group (111). In addition, sorafenib has also been introduced into several clinical trials of combination therapy regimens. However, the strategy of sorafenib combined with gemcitabine and cisplatin failed to improve the efficacy (112). Another trial on sorafenib combined with gemcitabine versus gemcitabine combined with placebo showed that the addition of sorafenib did not improve the outcome of advanced biliary tumors (113). Vandetanib is also a kinase inhibitor that has been shown to inhibit angiogenesis *in vivo* and *in vitro*. The efficacy and side effects of vandetanib as a monotherapy, vandetanib combined with gemcitabine and gemcitabine combined with placebo were studied. There was no difference in side effects among the three groups, while the objective response rate (ORR) of the vandetanib combined with gemcitabine group was higher than those of the other two groups (114). The efficacy of chemotherapy combined with EGFR inhibitor and VEGF monoclonal antibody was also studied, and the results showed no significant difference in mOS and mPFs between the GEM + L-OHPL + CAPE + panitumumab group and the GEM + L-OHPL + CAPE + bevacizumab group, although the former group had a higher ORR (115). From the results above, a conclusion can be drawn that cytotoxic drugs combined with anti-angiogenic drugs may achieve a better ORR in patients with BTCs, although little improvements in mPFS and mOS was observed.

Combination Therapy With Multiple Targeted Drugs

A phase II multicenter clinical trial of bevacizumab and erlotinib (an EGFR tyrosine kinase inhibitor) showed that 12% of patients had a confirmed partial response, 51% achieved stable disease, the median TTP was 4.4 months (95% CI: 3.0–7.8), and the median overall survival was 9.9 months (95% CI: 7.2–13.6) (116). Another clinical trial recruited 32 patients who were pretreated with systemic antitumor treatments to receive treatment with pembrolizumab combined with lenvatinib. The ORR of all patients was 25%, the median OS was 11.0 months (95% CI: 9.6–12.3), and the median PFS was 4.9 months (95% CI: 4.7–5.2) (117). Furthermore, a phase II SWOG study with sorafenib and erlotinib for advanced cholangiocarcinoma yielded a median progression-free survival of 2 months (95% CI: 2–3 months) and a median overall survival of 6 months (95% CI: 3–8 months) (118). The combination of multiple targeted drugs as an alternative strategy for advanced BTCs has preclinical evidences. The activity of this combination has been verified in some clinical trails, Although, the improvement in OS or PFS should be investigated by further clinical trails.

DISCUSSION

Biliary tract tumors account for 3% of all digestive tract tumors. Their incidence has been increasing in recent years for various reasons (119). Therefore, it is urgent to increase the treatment selection of BTCs (120, 121). The development of individualized treatment plans is of great significance for cholangiocarcinoma with high heterogeneity (122, 123). The clinical trial results revealed that most antiangiogenic drugs alone or in combination did not significantly prolong OS and PFS in patients with biliary tract tumors. However, some of these clinical trials achieved considerable ORR, indicating significant tumor regression at the early stage of treatment. There are two possible reasons for the unsatisfactory results of antiangiogenic therapy. On the one hand, a compensatory feedback pathway may be activated when one angiogenesis pathway is inhibited. For example, inhibiting VEGF signaling pathways may activate Ang pathways. On the other hand, inhibition of angiogenesis leads to hypoxia in the local environment, which may promote the expression of tumor proliferation and migration genes. For example, HIF-1 and downstream gene expression levels were increased after VEGF inhibition. Therefore, combination therapy as the future direction of antiangiogenic therapy seems to be feasible. The combination of the antiangiogenic drug bevacizumab and the antiproliferative drug acetazolamide results in tumor inhibition in mice (124). Further clinical

studies should be performed in the future to test this hypothesis. Based on the theory that antiangiogenic agents help target drugs penetrate into the tumor microenvironment, the effect of pemigatinib, a novel drug, which is approved by the FDA for the treatment of cholangiocarcinoma, in combined with should also be investigated for the treatment of patients with FGFR mutations.

The selection of potential patients who will benefit from antiangiogenic drugs is also crucial for the design of clinical trials and may be a critical factor for reaching the main endpoint. Dreyer C et al. reported promising results in three iCCA patients who were selected with hypervascular features. Therefore, the selection of cases with active tumor angiogenesis through imaging or histological evaluation may be conducive to improving the ORR. Some researchers have confirmed that the DWI phase of MRI is effective in evaluating tumor angiogenesis (125). Wu Xin et al. analyzed 88 cases of eCCA and found that ADC values were negatively correlated with MVD and VEGF ($p < 0.05$), indicating that DWI could be performed for the selection of BTC patients who may benefit from antiangiogenic treatment. It is critical to find more useful methods and markers to help clinicians assess whether patients can benefit from antiangiogenic therapy before medication.

At present, in clinical studies, RECIST is mostly applied to evaluate the effect of antiangiogenic therapy. However, antiangiogenic treatment may not result in a significant change in tumor volume in BTCs. After vascular degeneration, the interior of the tumor is necrotic, and the volume may not change. Therefore, traditional RECIST is not appropriate to evaluate the efficacy. Some researchers have proposed new ways to assess efficacy. It has been suggested that activated circulating vascular epithelial cells (aCECs) have higher sensitivity and reliability in efficacy evaluation than upstream factors such as VEGF. Some scholars have proposed using intratumor blood perfusion indicators [such as blood flow (BF) and blood volume (BV)] to reflect changes in blood supply. In particular, in view of the theory of vascular normalization proposed in recent years, how to evaluate the time window of anti-vascular therapy has become an urgent problem to be solved.

There are many kinds of cells in the tumor microenvironment, and the cytokines secreted and the receptors expressed by them constitute multiple signaling pathways that interact with each other. These signaling pathways are involved in tumor angiogenesis (126). Inhibition of one target or one pathway may result in short-term tumor regression, but inhibition of one pathway may promote another pathway. Therefore, effective antiangiogenic therapy needs to focus on common targets or multiple targets of multiple pathways and solve drug delivery problems in the leaky and poorly perfused tumor microenvironment. The study of improving the mechanism of angiogenesis in cholangiocarcinoma is helpful to find new therapeutic targets. Strengthening the construction of methods to evaluate tumor vascular normalization is helpful for the clinical development of reasonable antivascular therapy.

In conclusion, as highly heterogeneous tumors, the treatment and management of BTCs needs comprehensive evaluation and individualized medication, for which antiangiogenic therapy is a promising treatment method.

AUTHOR CONTRIBUTIONS

YW collected and analyzed the previous research fruits, and wrote the manuscript. TC, KL, and WM modified this article. ZL, AS, JL, WZ, SL, SH and CP contributed to the search for literature. ZZ designed and supervised the review. All authors contributed to the article and approved the submitted version.

FUNDING

Our study was supported by Shandong University Multidisciplinary Research and Innovation Team of Young Scholars (Grant No. 2020QNQT002), National Natural Science Foundation of China (Grant No. 82072676, 82172791), China Postdoctoral Science Foundation(Grant No. 2020M682190, 2020M682195), Clinical Research Foundation of Shandong University(Grant No. 2020SDUCRCA018), Natural Science Foundation of Shandong Province(ZR2019MH008), Jinan City Science and Technology Development Program (Grant No. 201805017, 201805013), Clinical Research Innovation Fund Project (CXPJJH11800001-2018240), Hengrui Hepatobiliary and Pancreatic Foundation (Grant No.Y-2017-144), and Beijing Medical Award Foundation (YXJL-2020-0785-0967, YXJL-2020-0785-0968).

REFERENCES

1. Labib PL, Goodchild G, Pereira SP. Molecular Pathogenesis of Cholangiocarcinoma. *BMC Cancer* (2019) 19(1). doi: 10.1186/s12885-019-5391-0
2. Valle JW, Kelley RK, Nervi B, Oh DY, Zhu AX. Biliary Tract Cancer. *Lancet* (2021) 397(10272):428–44. doi: 10.1016/S0140-6736(21)00153-7
3. Banales JM, Cardinale V, Carpino G, Marzioni M, Andersen JB, Invernizzi P, et al. Expert Consensus Document: Cholangiocarcinoma: Current Knowledge and Future Perspectives Consensus Statement From the European Network for the Study of Cholangiocarcinoma (ENS-CCA). *Nat Rev Gastroenterol Hepatol* (2016) 13(5):261–80. doi: 10.1038/nrgastro.2016.51
4. Marin JJG, Prete MG, Lamarca A, Tavolari S, Landa-Magdalena A, Brandi G, et al. Current and Novel Therapeutic Opportunities for Systemic Therapy in Biliary Cancer. *Br J Cancer* (2020) 123(7):1047–59. doi: 10.1038/s41416-020-0987-3
5. Banales JM, Marin JJG, Lamarca A, Rodrigues PM, Khan SA, Roberts LR, et al. Cholangiocarcinoma 2020: The Next Horizon in Mechanisms and Management. *Nat Rev Gastroenterol Hepatol* (2020) 17(9):557–88. doi: 10.1038/s41575-020-0310-z
6. Chen T, Li K, Liu Z, Liu J, Wang Y, Sun R, et al. WDR5 Facilitates EMT and Metastasis of CCA by Increasing HIF-1α Accumulation in Myc-Dependent and Independent Pathways. *Mol Ther* (2021) 29(6):2134–50. doi: 10.1016/j.ymthe.2021.02.017
7. Viallard C, Larrivée B. Tumor Angiogenesis and Vascular Normalization: Alternative Therapeutic Targets. *Angiogenesis* (2017) 20(4):409–26. doi: 10.1007/s10456-017-9562-9
8. Folkman J. Tumor Angiogenesis: Therapeutic Implications. *N Engl J Med* (1971) 285(21):1182–6. doi: 10.1111/1523-1747.ep12625746

9. Chen Y, Yu Y, Ding G, Ding H. Lymphangiogenic and Angiogentic Microvessel Density in Gallbladder Carcinoma. *Hepatogastroenterology* (2011) 58(105):20–5. doi: 10.1136/gut.2008.170811corr1
10. Thelen A, Scholz A, Benckert C, Schröder M, Weichert W, Wiedenmann B, et al. Microvessel Density Correlates With Lymph Node Metastases and Prognosis in Hilar Cholangiocarcinoma. *J Gastroenterol* (2008) 43(12):959–66. doi: 10.1007/s00535-008-2255-9
11. Thelen A, Scholz A, Weichert W, Wiedenmann B, Neuhaus P, Gessner R, et al. Tumor-Associated Angiogenesis and Lymphangiogenesis Correlate With Progression of Intrahepatic Cholangiocarcinoma. *Am J Gastroenterol* (2010) 105(5):1123–32. doi: 10.1038/ajg.2009.674
12. Weinberg BA, Xiu J, Lindberg MR, Shields AF, Hwang JJ, Poorman K, et al. Molecular Profiling of Biliary Cancers Reveals Distinct Molecular Alterations and Potential Therapeutic Targets. *J Gastrointest Oncol* (2019) 10(4):652–62. doi: 10.21037/jgo.2018.08.18
13. Jain RK. Normalization of Tumor Vasculature: An Emerging Concept in Antiangiogenic Therapy. *Science* (2005) 307(5706):58–62. doi: 10.1126/science.1104819
14. Murata R, Nishimura Y, Hiraoka M. An Antiangiogenic Agent (TNP-470) Inhibited Reoxygenation During Fractionated Radiotherapy of Murine Mammary Carcinoma. *Int J Radiat Oncol Biol Phys* (1997) 37(5):1107–13. doi: 10.1016/S0360-3016(96)00628-1
15. Fenton BM, Paoni SF, Ding I. Effect of VEGF Receptor-2 Antibody on Vascular Function and Oxygenation in Spontaneous and Transplanted Tumors. *Radiother Oncol* (2004) 72(2):221–30. doi: 10.1016/j.radonc.2004.05.005
16. Ma J, Pulfer S, Li S, Chu J, Reed K, Gallo JM, et al. Pharmacodynamic-Mediated Reduction of Temozolomide Tumor Concentrations by the Angiogenesis Inhibitor TNP-470. *Cancer Res* (2001) 61(14):5491–8. doi: 10.1016/S0165-4608(01)00481-2
17. Lacerda Q, Tantawi M, Leeper DB, Wheatley MA, Eisenbrey JR. Emerging Applications of Ultrasound-Contrast Agents in Radiation Therapy. *Ultrasound Med Biol* (2021) 47(6):1465–74. doi: 10.1016/j.ultrasmedbio.2021.01.032
18. Padera TP, Stoll BR, Tooredman JB, Capen D, di Tomaso E, Jain RK. Pathology: Cancer Cells Compress Intratumour Vessels. *Nature* (2004) 427(6976):695. doi: 10.1038/427695a
19. Fong GH. Mechanisms of Adaptive Angiogenesis to Tissue Hypoxia. *Angiogenesis* (2008) 11(2):121–40. doi: 10.1007/s10456-008-9107-3
20. Bottaro DP, Liotta LA. Cancer: Out of Air Is Not Out of Action. *Nature* (2003) 423(6940):593–5. doi: 10.1038/423593a
21. Gilkes DM, Xiang L, Lee SJ, Chaturvedi P, Hubbi ME, Wirtz D, et al. Hypoxia-Inducible Factors Mediate Coordinated RhoA-ROCK1 Expression and Signaling in Breast Cancer Cells. *Proc Natl Acad Sci* (2014) 111(3):E384–93. doi: 10.1073/pnas.1321510111
22. Thienpont B, Steinbacher J, Zhao H, D'Anna F, Kuchnio A, Ploumakis A, et al. Tumour Hypoxia Causes DNA Hypermethylation by Reducing TET Activity. *Nature* (2016) 537(7618):63–8. doi: 10.1038/nature19081
23. Chen Y, Chang G, Chen X, Li Y, Li H, Cheng D, et al. IL-6-miR-210 Suppresses Regulatory T Cell Function and Promotes Atrial Fibrosis by Targeting Foxp3. *Mol Cells* (2020) 43(5):438–47. doi: 10.14348/molcells.2019.2275
24. Kerber EL, Padberg C, Koll N, Schuetzhold V, Fandrey J, Winningh S, et al. The Importance of Hypoxia-Inducible Factors (HIF-1 and HIF-2) for the Pathophysiology of Inflammatory Bowel Disease. *Int J Mol Sci* (2020) 21(22):8551. doi: 10.3390/ijms21228551
25. Kumar V, Gabrilovich DI. Hypoxia-Inducible Factors in Regulation of Immune Responses in Tumour Microenvironment. *Immunology* (2014) 143(4):512–9. doi: 10.1111/imm.12380
26. Lequeux A, Noman MZ, Xiao M, Van Moer K, Hasmim M, Benoit A, et al. Targeting HIF-1 Alpha Transcriptional Activity Drives Cytotoxic Immune Effector Cells Into Melanoma and Improves Combination Immunotherapy. *Oncogene* (2021) 40(28):4725–35. doi: 10.1038/s41388-021-01846-x
27. Vasudev NS, Reynolds AR. Anti-Angiogenic Therapy for Cancer: Current Progress, Unresolved Questions and Future Directions. *Angiogenesis* (2014) 17(3):471–94. doi: 10.1007/s10456-014-9420-y
28. Seton-Rogers S. When Good Drugs do Bad Things. *Nat Rev Cancer* (2009) 9(4):228–9. doi: 10.1038/nrc2632
29. Jain RK. Normalizing Tumor Vasculature With Anti-Angiogenic Therapy: A New Paradigm for Combination Therapy. *Nat Med* (2001) 7(9):987–9. doi: 10.1038/nm0901-987
30. Chen P, Bonaldo P. Role of Macrophage Polarization in Tumor Angiogenesis and Vessel Normalization: Implications for New Anticancer Therapies. *Int Rev Cell Mol Biol* (2013) 301:1–35. doi: 10.1016/B978-0-12-407704-1.00001-4
31. Carmeliet P, Jain RK. Principles and Mechanisms of Vessel Normalization for Cancer and Other Angiogenic Diseases. *Nat Rev Drug Discov* (2011) 10(6):417–27. doi: 10.1038/nrd3455
32. Ebos JM, Lee CR, Cruz-Munoz W, Bjarnason GA, Christensen JG, Kerbel RS. Accelerated Metastasis After Short-Term Treatment With a Potent Inhibitor of Tumor Angiogenesis. *Cancer Cell* (2009) 15(3):232–9. doi: 10.1016/j.ccr.2009.01.021
33. Kontos CD, Willett CG. Inhibiting the Inhibitor: Targeting Vascular Endothelial Protein Tyrosine Phosphatase to Promote Tumor Vascular Maturation. *J Natl Cancer Inst* (2013) 105(16):1163–5. doi: 10.1093/jnci/djt199
34. Rolny C, Mazzone M, Tugues S, Laoui D, Johansson I, Coulon C, et al. HRG Inhibits Tumor Growth and Metastasis by Inducing Macrophage Polarization and Vessel Normalization Through Downregulation of PlGF. *Cancer Cell* (2011) 19(1):31–44. doi: 10.1016/j.ccr.2010.11.009
35. Sawada J, Urakami T, Li F, Urakami A, Zhu W, Fukuda M, et al. Small GTPase R-Ras Regulates Integrity and Functionality of Tumor Blood Vessels. *Cancer Cell* (2012) 22(2):235–49. doi: 10.1016/j.ccr.2012.06.013
36. Li W, Quan YY, Li Y, Lu L, Cui M, et al. Monitoring of Tumor Vascular Normalization: The Key Points From Basic Research to Clinical Application. *Cancer Manag Res* (2018) 10:4163–72. doi: 10.2147/CMAR.S174712
37. Abdalla A, Xiao L, Ullah MW, Yu M, Ouyang C, Yang G. Current Challenges of Cancer Anti-Angiogenic Therapy and the Promise of Nanotherapeutics. *Theranostics* (2018) 8(2):533–48. doi: 10.7150/thno.21674
38. Mukherjee A, Madamsetty VS, Paul MK, Mukherjee S. Recent Advancements of Nanomedicine Towards Antiangiogenic Therapy in Cancer. *Int J Mol Sci* (2020) 21(2). doi: 10.3390/ijms21020455
39. Huang D, Lan H, Liu F, Wang S, Chen X, Jin K, et al. Anti-Angiogenesis or Pro-Angiogenesis for Cancer Treatment: Focus on Drug Distribution. *Int J Clin Exp Med* (2015) 8(6):8369–76.
40. Dai J, Rabie AB. VEGF: An Essential Mediator of Both Angiogenesis and Endochondral Ossification. *J Dent Res* (2007) 86(10):937–50. doi: 10.1177/154405910708601006
41. Lange C, Storkebaum E, de Almodóvar CR, Dewerchin M, Carmeliet P. Vascular Endothelial Growth Factor: A Neurovascular Target in Neurological Diseases. *Nat Rev Neurol* (2016) 12(8):439–54. doi: 10.1038/nrneurol.2016.88
42. Shibuya M. VEGF-VEGFR System as a Target for Suppressing Inflammation and Other Diseases. *Endocr Metab Immune Disord Drug Targets* (2015) 15(2):135–44. doi: 10.2174/1871530315666150316121956
43. Ogasawara S, Yano H, Higaki K, Takayama A, Akiba J, Shiota K, et al. Expression of Angiogenic Factors, Basic Fibroblast Growth Factor and Vascular Endothelial Growth Factor, in Human Biliary Tract Carcinoma Cell Lines. *Hepatol Res* (2001) 20(1):97–113. doi: 10.1016/S1386-6346(00)00117-0
44. Navaneethan U, Gutierrez NG, Jegadeesan R, Venkatesh PG, Poptic E, Liu X, et al. Vascular Endothelial Growth Factor Levels in Bile Distinguishes Pancreatic Cancer From Other Etiologies of Biliary Stricture: A Pilot Study. *Dig Dis Sci* (2013) 58(10):2986–92. doi: 10.1007/s10620-013-2764-0
45. Tang D, Nagano H, Yamamoto H, Wada H, Nakamura M, Kondo M, et al. Angiogenesis in Cholangiocellular Carcinoma: Expression of Vascular Endothelial Growth Factor, Angiopoietin-1/2, Thrombospondin-1 and Clinicopathological Significance. *Oncol Rep* (2006) 15(3):525–32. doi: 10.3892/or.15.3.525
46. Yoshikawal D, Ojima H, Iwasaki M, Hiraoka N, Kosuge TK. Clinicopathological and Prognostic Significance of EGFR, VEGF, and HER2 Expression in Cholangiocarcinoma. *Br J Cancer* (2008) 98(2):418–25. doi: 10.1038/sj.bjc.6604129
47. Sun XN, Cao WG, Wang X, Wang Q, Gu BX, Yang QC, et al. Prognostic Impact of Vascular Endothelial Growth Factor-A Expression in Resected

Gallbladder Carcinoma. *Tumour Biol* (2011) 32(6):1183–90. doi: 10.1007/s13277-011-0221-2
48. Mobius C, Demuth C, Aigner T, Wiedmann M, Wittekind C, Mössner J, et al. Evaluation of VEGF A Expression and Microvascular Density as Prognostic Factors in Extrahepatic Cholangiocarcinoma. *Eur J Surg Oncol* (2007) 33(8):1025–9. doi: 10.1016/j.ejso.2007.02.020
49. Guedj N, Zhan Q, Perigny M, Rautou PE, Degos F, et al. Comparative Protein Expression Profiles of Hilar and Peripheral Hepatic Cholangiocarcinomas. *J Hepatol* (2009) 51(1):93–101. doi: 10.1016/j.jhep.2009.03.017
50. Benckert C, Jonas S, Cramer T, Von Marschall Z, Schäfer G, Peters M, et al. Transforming Growth Factor Beta 1 Stimulates Vascular Endothelial Growth Factor Gene Transcription in Human Cholangiocellular Carcinoma Cells. *Cancer Res* (2003) 63(5):1083–92.
51. Pan S, Hu Y, Hu M, Xu Y, Chen M, Du C, et al. S100A8 Facilitates Cholangiocarcinoma Metastasis *via* Upregulation of VEGF Through TLR4/NF−κb Pathway Activation. *Int J Oncol* (2020) 56(1):101–12. doi: 10.3892/ijo.2020.4977
52. You Z, Bei L, Cheng LP, Cheng NS. Expression of COX-2 and VEGF-C in Cholangiocarcinomas at Different Clinical and Pathological Stages. *Genet Mol Res* (2015) 14(2):6239–46. doi: 10.4238/2015.June.9.9
53. Zhang J, Han C, Zhu H, Song K, Wu T. miR-101 Inhibits Cholangiocarcinoma Angiogenesis Through Targeting Vascular Endothelial Growth Factor (VEGF). *Am J Pathol* (2013) 182(5):1629–39. doi: 10.1016/j.ajpath.2013.01.045
54. Leng K, Xu Y, Kang P, Qin W, Cai H, Wang H, et al. Akirin2 Is Modulated by miR-490-3p and Facilitates Angiogenesis in Cholangiocarcinoma Through the IL-6/STAT3/VEGFA Signaling Pathway. *Cell Death Dis* (2019) 10(4):262. doi: 10.1038/s41419-019-1506-4
55. Cheng R, Chen Y, Zhou H, Wang B, Du Q, Chen Y. B7-H3 Expression and its Correlation With Clinicopathologic Features, Angiogenesis, and Prognosis in Intrahepatic Cholangiocarcinoma. *APMIS* (2018) 126(5):396–402. doi: 10.1111/apm.12837
56. Mancino A, Mancino MG, Glaser SS, Alpini G, Bolognese A, Izzo L, et al. Estrogens Stimulate the Proliferation of Human Cholangiocarcinoma by Inducing the Expression and Secretion of Vascular Endothelial Growth Factor. *Dig Liver Dis* (2009) 41(2):156–63. doi: 10.1016/j.dld.2008.02.015
57. Kangsamaksin T, Chaithongyot S, Wootthichairangsan C, Hanchaina R, Tangshewinsirikul C, Svasti J. Lupeol and Stigmasterol Suppress Tumor Angiogenesis and Inhibit Cholangiocarcinoma Growth in Mice *via* Downregulation of Tumor Necrosis Factor-α. *PloS One* (2017) 12(12):e0189628. doi: 10.1371/journal.pone.0189628
58. Xu YF, Liu ZL, Pan C, Yang XQ, Ning SL, Liu HD, et al. HMGB1 Correlates With Angiogenesis and Poor Prognosis of Perihilar Cholangiocarcinoma *via* Elevating VEGFR2 of Vessel Endothelium. *Oncogene* (2019) 38(6):868–80. doi: 10.1038/s41388-018-0485-8
59. Francis H, DeMorrow S, Venter J, Onori P, White M, Gaudio E, et al. Inhibition of Histidine Decarboxylase Ablates the Autocrine Tumorigenic Effects of Histamine in Human Cholangiocarcinoma. *Gut* (2012) 61(5):753–64. doi: 10.1136/gutjnl-2011-300007
60. Jaidee R, Kongpetch S, Senggunprai L, Prawan A, Kukongviriyapan U, Kukongviriyapan V, et al. Phenformin Inhibits Proliferation, Invasion, and Angiogenesis of Cholangiocarcinoma Cells *via* AMPK-mTOR and HIF-1A Pathways. *Naunyn Schmiedebergs Arch Pharmacol* (2020) 393(9):1681–90. doi: 10.1007/s00210-020-01885-3
61. Franchitto A, Onori P, Renzi A, Carpino G, Mancinelli R, Alvaro D, et al. Expression of Vascular Endothelial Growth Factors and Their Receptors by Hepatic Progenitor Cells in Human Liver Diseases. *Hepatobiliary Surg Nutr* (2013) 2(2):68–77. doi: 10.3978/j.issn.2304-3881.2012.10.11
62. Manzat Saplacan RM, Balacescu L, Gherman C, Chira RI, Craiu A, Mircea PA, et al. The Role of PDGFs and PDGFRs in Colorectal Cancer. *Mediators Inflamm* (2017) 2017:4708076. doi: 10.1155/2017/4708076
63. Heldin CH, Westermark B. Platelet-Derived Growth Factor: Three Isoforms and Two Receptor Types. *Trends Genet* (1989) 5(4):108–11. doi: 10.1016/0168-9525(89)90040-1
64. Boonjaraspinyo S, Boonmars T, Wu Z, Loilome W, Sithithaworn P, Nagano I, et al. Platelet-Derived Growth Factor May be a Potential Diagnostic and Prognostic Marker for Cholangiocarcinoma. *Tumor Biol* (2012) 33(5):1785–802. doi: 10.1007/s13277-012-0438-8
65. Pan S, Hu Y, Hu M, Jian H, Chen M, Gan L, et al. Platelet-Derived PDGF Promotes the Invasion and Metastasis of Cholangiocarcinoma by Upregulating MMP2/MMP9 Expression and Inducing EMT *via* the P38/MAPK Signalling Pathway. *Am J Transl Res* (2020) 12(7):3577–95.
66. Duan HX, Li BW, Zhuang X, Wang LT, Cao Q, Tan LH, et al. TCF21 Inhibits Tumor-Associated Angiogenesis and Suppresses the Growth of Cholangiocarcinoma by Targeting PI3K/Akt and ERK Signaling. *Am J Physiol Gastrointest Liver Physiol* (2019) 316(6):G763–73. doi: 10.1152/ajpgi.00264.2018
67. Augustin HG, Koh GY, Thurston G, Alitalo K. Control of Vascular Morphogenesis and Homeostasis Through the Angiopoietin–Tie System. *Nat Rev Mol Cell Biol* (2009) 10(3):165–77. doi: 10.1038/nrm2639
68. Suri C, Jones PF, Patan S, Bartunkova S, Maisonpierre PC, Davis S, et al. Requisite Role of Angiopoietin-1, a Ligand for the TIE2 Receptor, During Embryonic Angiogenesis. *Cell (Cambridge)* (1996) 87(7):1171–80. doi: 10.1016/S0092-8674(00)81813-9
69. Maisonpierre PC, Suri C, Jones PF, Bartunkova S, Wiegand SJ, Radziejewski C, et al. Angiopoietin-2, a Natural Antagonist for Tie2 That Disrupts *In Vivo* Angiogenesis. *Science* (1997) 277(5322):55–60. doi: 10.1126/science.277.5322.55
70. Atanasov G, Hau HM, Dietel C, Benzing C, Krenzien F, Brandl A, et al. Prognostic Significance of TIE2-Expressing Monocytes in Hilar Cholangiocarcinoma. *J Surg Oncol* (2016) 114(1):91–8. doi: 10.1002/jso.24249
71. Voigtländer T, David S, Thamm K, Schlué J, Metzger J, Manns MP, et al. Angiopoietin-2 and Biliary Diseases: Elevated Serum, But Not Bile Levels Are Associated With Cholangiocarcinoma. *PloS One* (2014) 9(5):e97046. doi: 10.1371/journal.pone.0097046
72. Xu YF, Yang XQ, Lu XF, Guo S, Liu Y, Iqbal M, et al. Fibroblast Growth Factor Receptor 4 Promotes Progression and Correlates to Poor Prognosis in Cholangiocarcinoma. *Biochem Biophys Res Commun* (2014) 446(1):54–60. doi: 10.1016/j.bbrc.2014.02.050
73. Su WC, Shiesh SC, Liu HS, Chen CY, Chow NH, Lin XZ, et al. Expression of Oncogene Products HER2/Neu and Ras and Fibrosis-Related Growth Factors bFGF, TGF-Beta, and PDGF in Bile From Biliary Malignancies and Inflammatory Disorders. *Dig Dis Sci* (2001) 46(7):1387–92. doi: 10.1023/A:1010619316436
74. Eyries M, Siegfried G, Ciumas M, Montagne K, Agrapart M, Lebrin F, et al. Hypoxia-Induced Apelin Expression Regulates Endothelial Cell Proliferation and Regenerative Angiogenesis. *Circ Res* (2008) 103(4):432–40. doi: 10.1161/CIRCRESAHA.108.179333
75. Kidoya H, Ueno M, Yamada Y, Mochizuki N, Nakata M, Yano T, et al. Spatial and Temporal Role of the Apelin/APJ System in the Caliber Size Regulation of Blood Vessels During Angiogenesis. *EMBO J* (2008) 27(3):522–34. doi: 10.1038/sj.emboj.7601982
76. Berta J, Kenessey I, Dobos J, Tovari J, Klepetko W, Jan Ankersmit H, et al. Apelin Expression in Human Non-Small Cell Lung Cancer: Role in Angiogenesis and Prognosis. *J Thorac Oncol* (2010) 5(8):1120–9. doi: 10.1097/JTO.0b013e3181e2c1ff
77. Muto J, Shirabe K, Yoshizumi T, Ikegami T, Aishima S, Ishigami K, et al. The Apelin-APJ System Induces Tumor Arteriogenesis in Hepatocellular Carcinoma. *Anticancer Res* (2014) 34(10):5313–20.
78. Hall C, Ehrlich L, Venter J, O'Brien A, White T, Zhou T, et al. Inhibition of the Apelin/Apelin Receptor Axis Decreases Cholangiocarcinoma Growth. *Cancer Lett* (2017) 386:179–88. doi: 10.1016/j.canlet.2016.11.025
79. Heo K, Kim YH, Sung HJ, Li HY, Yoo CW, Kim JY, et al. Hypoxia-Induced Up-Regulation of Apelin Is Associated With a Poor Prognosis in Oral Squamous Cell Carcinoma Patients. *Oral Oncol* (2012) 48(6):500–6. doi: 10.1016/j.oraloncology.2011.12.015
80. Diakowska D, Markocka-Mączka K, Szelachowski P, Grabowski K. Serum Levels of Resistin, Adiponectin, and Apelin in Gastroesophageal Cancer Patients. *Dis Markers* (2014) 2014:1–8. doi: 10.1155/2014/619649
81. Wan Y, Zeng ZC, Xi M, Wan S, Hua W, Liu YL, et al. Dysregulated microRNA-224/Apelin Axis Associated With Aggressive Progression and Poor Prognosis in Patients With Prostate Cancer. *Hum Pathol* (2015) 46(2):295–303. doi: 10.1016/j.humpath.2014.10.027
82. Aishima S, Taguchi K, Sugimachi K, Asayama Y, Nishi H, Shimada M, et al. The Role of Thymidine Phosphorylase and Thrombospondin-1 in

Angiogenesis and Progression of Intrahepatic Cholangiocarcinoma. *Int J Surg Pathol* (2002) 10(1):47–56. doi: 10.1177/106689690201000108
83. Yuan R, Li Y, Yang B, Jin Z, Xu J, Shao Z, et al. LOXL1 Exerts Oncogenesis and Stimulates Angiogenesis Through the LOXL1-FBLN5/alphavbeta3 Integrin/FAK-MAPK Axis in ICC. *Mol Ther Nucleic Acids* (2021) 23:797–810. doi: 10.1016/j.omtn.2021.01.001
84. Cao Y, Xue L. Angiostatin. *Semin Thromb Hemost* (2004) 30(1):83–93. doi: 10.1055/s-2004-822973
85. Walia A, Yang JF, Huang YH, Rosenblatt MI, Chang JH, Azar DT. Endostatin's Emerging Roles in Angiogenesis, Lymphangiogenesis, Disease, and Clinical Applications. *Biochim Biophys Acta* (2015) 1850 (12):2422–38. doi: 10.1016/j.bbagen.2015.09.007
86. Phanthaphol N, Somboonpatarakun C, Suwanchiwasiri K, Chieochansin T, Sujjitjoon J, Wongkham S, et al. Chimeric Antigen Receptor T Cells Targeting Integrin αvβ6 Expressed on Cholangiocarcinoma Cells. *Front Oncol* (2021) 11. doi: 10.3389/fonc.2021.657868
87. Huang Y, Kong Y, Zhang L, He T, Zhou X, Yan Y, et al. High Expression of ITGA3 Promotes Proliferation and Cell Cycle Progression and Indicates Poor Prognosis in Intrahepatic Cholangiocarcinoma. *BioMed Res Int* (2018) 2018:1–9. doi: 10.1155/2018/2352139
88. Duro-Castano A, Gallon E, Decker C, Vicent MJ. Modulating Angiogenesis With Integrin-Targeted Nanomedicines. *Adv Drug Deliv Rev* (2017) 119:101–19. doi: 10.1016/j.addr.2017.05.008
89. Desgrosellier JS, Cheresh DA. Integrins in Cancer: Biological Implications and Therapeutic Opportunities. *Nat Rev Cancer* (2010) 10(1):9–22. doi: 10.1038/nrc2748
90. D'Amato RJ, Loughnan MS, Flynn E, Folkman J. Thalidomide Is an Inhibitor of Angiogenesis. *Proc Natl Acad Sci USA* (1994) 91(9):4082–5. doi: 10.1073/pnas.91.9.4082
91. Zhang J, Qiao L, Liang N, Xie J, Luo H, Deng G, et al. Vasculogenic Mimicry and Tumor Metastasis. *J Buon* (2016) 21(3):533–41.
92. Fernández-Cortés M, Delgado-Bellido D, Oliver FJ. Vasculogenic Mimicry: Become an Endothelial Cell "But Not So Much". *Front Oncol* (2019) 9:803. doi: 10.3389/fonc.2019.00803
93. Wei X, Chen Y, Jiang X, Peng M, Liu Y, Mo Y, et al. Mechanisms of Vasculogenic Mimicry in Hypoxic Tumor Microenvironments. *Mol Cancer* (2021) 20(1):7. doi: 10.1186/s12943-020-01288-1
94. Mauriz JL, González-Gallego J. Antiangiogenic Drugs: Current Knowledge and New Approaches to Cancer Therapy. *J Pharm Sci* (2008) 97(10):4129–54. doi: 10.1002/jps.21286
95. Marisi G, Cucchetti A, Ulivi P, Canale M, Cabibbo G, Solaini L, et al. Ten Years of Sorafenib in Hepatocellular Carcinoma: Are There Any Predictive and/or Prognostic Markers? *World J Gastroenterol* (2018) 24(36):4152–63. doi: 10.3748/wjg.v24.i36.4152
96. Abdelgalil AA, Alkahtani HM, Al-Jenoobi FI. Sorafenib. *Profiles Drug Subst Excip Relat Methodol* (2019) 44:239–66. doi: 10.1016/bs.podrm.2018.11.003
97. Grimaldi AM, Guida T, D'Attino R, Perrotta E, Otero M, Masala A, et al. Sunitinib: Bridging Present and Future Cancer Treatment. *Ann Oncol* (2007) 18 Suppl 6:vi31–4. doi: 10.1093/annonc/mdm221
98. Kelly RJ, Rixe O. Axitinib (AG-013736). *Recent Results Cancer Res* (2010) 184:33–44. doi: 10.1007/978-3-642-01222-8_3
99. Shen G, Zheng F, Ren D, Du F, Dong Q, Wang Z, et al. Anlotinib: A Novel Multi-Targeting Tyrosine Kinase Inhibitor in Clinical Development. *J Hematol Oncol* (2018) 11(1):120. doi: 10.1186/s13045-018-0664-7
100. Han B, Li K, Wang Q, Zhang L, Shi J, Wang Z, et al. Effect of Anlotinib as a Third-Line or Further Treatment on Overall Survival of Patients With Advanced Non-Small Cell Lung Cancer: The ALTER 0303 Phase 3 Randomized Clinical Trial. *JAMA Oncol* (2018) 4(11):1569–75. doi: 10.1001/jamaoncol.2018.3039
101. Yi JH, Thongprasert S, Lee J, Doval DC, Park SH, Park JO, et al. A Phase II Study of Sunitinib as a Second-Line Treatment in Advanced Biliary Tract Carcinoma: A Multicentre, Multinational Study. *Eur J Cancer (1990)* (2011) 48(2):196–201. doi: 10.1200/jco.2011.29.15_suppl.e14653
102. Dreyer C. Disease Control With Sunitinib in Advanced Intrahepatic Cholangiocarcinoma Resistant to Gemcitabine-Oxaliplatin Chemotherapy. *World J Hepatol* (2015) 7(6):910. doi: 10.4254/wjh.v7.i6.910
103. Neuzillet CSJFL. Sunitinib as Second-Line Treatment in Patients With Advanced Intrahepatic Cholangiocarcinoma (SUN-CK Phase II Trial): Safety, Efficacy, and Updated Translational Results. *J Clin Oncol* (2015) 33 (3_suppl):343. doi: 10.1200/jco.2015.33.3_suppl.343
104. Bengala C, Bertolini F, Malavasi N, Boni C, Aitini E, Dealis C, et al. Sorafenib in Patients With Advanced Biliary Tract Carcinoma: A Phase II Trial. *Br J Cancer* (2010) 102(1):68–72. doi: 10.1038/sj.bjc.6605458
105. El-Khoueiry AB, Rankin CJ, Ben-Josef E, Lenz HJ, Gold PJ, Hamilton RD, et al. SWOG 0514: A Phase II Study of Sorafenib in Patients With Unresectable or Metastatic Gallbladder Carcinoma and Cholangiocarcinoma. *Invest New Drugs* (2012) 30(4):1646–51. doi: 10.1007/s10637-011-9719-0
106. Morizane C, Ueno M, Sasaki T, Nagashima F, Mizuno N, Shimizu S. Interim Analysis of a Phase 2 Study of Lenvatinib (LEN) Monotherapy as Second-Line Treatment in Unresectable Biliary Tract Cancer (BTC). *Ann Oncol* (2017) 35(4_suppl):310. doi: 10.1200/JCO.2017.35.4_suppl.310
107. Ueno M, Ikeda M, Sasaki T, Nagashima F, Mizuno N, Shimizu S, et al. Phase 2 Study of Lenvatinib Monotherapy as Second-Line Treatment in Unresectable Biliary Tract Cancer: Primary Analysis Results. *BMC Cancer* (2020) 20(1). doi: 10.1186/s12885-020-07365-4
108. Sun W, Patel A, Normolle D, Patel K, Ohr J, Lee JJ, et al. A Phase 2 Trial of Regorafenib as a Single Agent in Patients With Chemotherapy-Refractory, Advanced, and Metastatic Biliary Tract Adenocarcinoma. *Cancer* (2019) 125 (6):902–9. doi: 10.1002/cncr.31872
109. Iyer RV, Pokuri VK, Groman A, Ma WW, Malhotra U, Iancu DM, et al. A Multicenter Phase II Study of Gemcitabine, Capecitabine, and Bevacizumab for Locally Advanced or Metastatic Biliary Tract Cancer. *Am J Clin Oncol* (2018) 41(7):649–55. doi: 10.1097/COC.0000000000000347
110. Zhu AX, Meyerhardt JA, Blaszkowsky LS, Kambadakone AR, Muzikansky A, Zheng H, et al. Efficacy and Safety of Gemcitabine, Oxaliplatin, and Bevacizumab in Advanced Biliary-Tract Cancers and Correlation of Changes in 18-Fluorodeoxyglucose PET With Clinical Outcome: A Phase 2 Study. *Lancet Oncol* (2010) 11(1):48–54. doi: 10.1016/S1470-2045(09)70333-X
111. Valle JW, Wasan H, Lopes A, Backen AC, Palmer DH, Morris K, et al. Cediranib or Placebo in Combination With Cisplatin and Gemcitabine Chemotherapy for Patients With Advanced Biliary Tract Cancer (ABC-03): A Randomised Phase 2 Trial. *Lancet Oncol* (2015) 16(8):967–78. doi: 10.1016/S1470-2045(15)00139-4
112. Lee JK, Capanu M, O'Reilly EM, Ma J, Chou JF, Shia J, et al. A Phase II Study of Gemcitabine and Cisplatin Plus Sorafenib in Patients With Advanced Biliary Adenocarcinomas. *Br J Cancer* (2013) 109(4):915–9. doi: 10.1038/bjc.2013.432
113. Moehler M, Maderer A, Schimanski C, Kanzler S, Denzer U, Kolligs FT, et al. Gemcitabine Plus Sorafenib Versus Gemcitabine Alone in Advanced Biliary Tract Cancer: A Double-Blind Placebo-Controlled Multicentre Phase II AIO Study With Biomarker and Serum Programme. *Eur J Cancer* (2014) 50 (18):3125–35. doi: 10.1016/j.ejca.2014.09.013
114. Santoro A, Gebbia V, Pressiani T, Testa A, Personeni N, Arrivas Bajardi E, et al. A Randomized, Multicenter, Phase II Study of Vandetanib Monotherapy Versus Vandetanib in Combination With Gemcitabine Versus Gemcitabine Plus Placebo in Subjects With Advanced Biliary Tract Cancer: The VanGogh Study. *Ann Oncol* (2015) 26(3):542–7. doi: 10.1093/annonc/mdu576
115. Jensen LFEPJ. Randomized Phase II Crossover Trial Exploring the Clinical Benefit From Targeting EGFR or VEGF With Combination Chemotherapy in Patients With Non-Resectable Biliary Tract Cancer. *J Clin Oncol* (2015) 33 (15_suppl):4071. doi: 10.1200/jco.2015.33.15_suppl.4071
116. Lubner SJ, Mahoney MR, Kolesar JL, Loconte NK, Kim GP, Pitot HC, et al. Report of a Multicenter Phase II Trial Testing a Combination of Biweekly Bevacizumab and Daily Erlotinib in Patients With Unresectable Biliary Cancer: A Phase II Consortium Study. *J Clin Oncol* (2010) 28(21):3491–7. doi: 10.1200/JCO.2010.28.4075
117. Lin J, Yang X, Long J, Zhao S, Mao J, Wang D, et al. Pembrolizumab Combined With Lenvatinib as Non-First-Line Therapy in Patients With Refractory Biliary Tract Carcinoma. *Hepatobiliary Surg Nutr* (2020) 9 (4):414–24. doi: 10.21037/hbsn-20-338
118. El-Khoueiry AB, Rankin C, Siegel AB, Iqbal S, Gong IY, Micetich KC, et al. S0941: A Phase 2 SWOG Study of Sorafenib and Erlotinib in Patients With Advanced Gallbladder Carcinoma or Cholangiocarcinoma. *Br J Cancer* (2014) 110(4):882–7. doi: 10.1038/bjc.2013.801

119. Oneda E, Abu HM, Zaniboni A. Biliary Tract Cancer: Current Medical Treatment Strategies. *Cancers (Basel)* (2020) 12(5). doi: 10.3390/cancers12051237
120. Qiu B, Chen T, Sun R, Liu Z, Zhang X, Li Z, et al. Sprouty4 Correlates With Favorable Prognosis in Perihilar Cholangiocarcinoma by Blocking the FGFR-ERK Signaling Pathway and Arresting the Cell Cycle. *EBioMedicine* (2019) 50:166–77. doi: 10.1016/j.ebiom.2019.11.021
121. Li Z, Liu J, Chen T, Sun R, Liu Z, Qiu B, et al. HMGA1-TRIP13 Axis Promotes Stemness and Epithelial Mesenchymal Transition of Perihilar Cholangiocarcinoma in a Positive Feedback Loop Dependent on C-Myc. *J Exp Clin Cancer Res* (2021) 40(1):86. doi: 10.1186/s13046-021-01890-1
122. Liu Z, Sun R, Zhang X, Qiu B, Chen T, Li Z, et al. Transcription Factor 7 Promotes the Progression of Perihilar Cholangiocarcinoma by Inducing the Transcription of C-Myc and FOS-Like Antigen 1. *EBioMedicine* (2019) 45:181–91. doi: 10.1016/j.ebiom.2019.06.023
123. Sun R, Liu Z, Qiu B, Chen T, Li Z, Zhang X, et al. Annexin10 Promotes Extrahepatic Cholangiocarcinoma Metastasis by Facilitating EMT *via* PLA2G4A/PGE2/STAT3 Pathway. *EBioMedicine* (2019) 47:142–55. doi: 10.1016/j.ebiom.2019.08.062
124. Vaeteewoottacharn K, Kariya R, Dana P, Fujikawa S, Matsuda K, Ohkuma K, et al. Inhibition of Carbonic Anhydrase Potentiates Bevacizumab Treatment in Cholangiocarcinoma. *Tumor Biol* (2016) 37(7):9023–35. doi: 10.1007/s13277-016-4785-8
125. Meyer H, Wienke A, Surov A. Association Between VEGF Expression and Diffusion Weighted Imaging in Several Tumors—A Systematic Review and Meta-Analysis. *Diagnostics* (2019) 9(4):126. doi: 10.3390/diagnostics 9040126
126. Weis SM, Cheresh DA. Tumor Angiogenesis: Molecular Pathways and Therapeutic Targets. *Nat Med* (2011) 17(11):1359–70. doi: 10.1038/nm.2537

Conflict of Interest: The authors declare that the research was conducted in the absence of any commercial or financial relationships that could be construed as a potential conflict of interest.

The reviewer ZL declared a shared affiliation, with no collaboration, with TC to the handling editor at the time of review.

Publisher's Note: All claims expressed in this article are solely those of the authors and do not necessarily represent those of their affiliated organizations, or those of the publisher, the editors and the reviewers. Any product that may be evaluated in this article, or claim that may be made by its manufacturer, is not guaranteed or endorsed by the publisher.

frontiers in Immunology

ORIGINAL RESEARCH
published: 03 December 2021
doi: 10.3389/fimmu.2021.790661

Prognostic Stratification Based on HIF-1 Signaling for Evaluating Hypoxic Status and Immune Infiltration in Pancreatic Ductal Adenocarcinomas

Hongkai Zhuang[1,2†], Shujie Wang[1†], Bo Chen[3†], Zedan Zhang[4†], Zuyi Ma[1], Zhenchong Li[1], Chunsheng Liu[1], Zixuan Zhou[1], Yuanfeng Gong[1], Shanzhou Huang[1], Baohua Hou[1], Yajin Chen[2*] and Chuanzhao Zhang[1*]*

[1] Department of General Surgery, Guangdong Provincial People's Hospital, Guangdong Academy of Medical Sciences, Guangzhou, China, [2] Department of Hepatobiliary Surgery, Sun Yat-Sen Memorial Hospital, Sun Yat-Sen University, Guangzhou, China, [3] Department of Breast Cancer, Cancer Center, Guangdong Provincial People's Hospital, Guangdong Academy of Medical Sciences, Guangzhou, China, [4] Department of Urology, Peking University First Hospital, Beijing, China

OPEN ACCESS

Edited by:
Yunfei Xu,
Shandong University, China

Reviewed by:
Qianjin Liao,
Central South University, China
M. Celeste Simon,
University of Pennsylvania, United States

***Correspondence:**
Baohua Hou
15917919681@163.com
Yajin Chen
cyj0509@126.com
Chuanzhao Zhang
zhangchuanzhao@gdph.org.cn

†These authors have contributed equally to this work

Specialty section:
This article was submitted to Cancer Immunity and Immunotherapy, a section of the journal Frontiers in Immunology

Received: 07 October 2021
Accepted: 19 November 2021
Published: 03 December 2021

Citation:
Zhuang H, Wang S, Chen B, Zhang Z, Ma Z, Li Z, Liu C, Zhou Z, Gong Y, Huang S, Hou B, Chen Y and Zhang C (2021) Prognostic Stratification Based on HIF-1 Signaling for Evaluating Hypoxic Status and Immune Infiltration in Pancreatic Ductal Adenocarcinomas. Front. Immunol. 12:790661. doi: 10.3389/fimmu.2021.790661

Pancreatic ductal adenocarcinoma (PDAC) has a hypoxic and desmoplastic tumor microenvironment (TME), leading to treatment failure. We aimed to develop a prognostic classifier to evaluate hypoxia status and hypoxia-related molecular characteristics of PDAC. In this study, we classified PDAC into three clusters based on 16 known hypoxia-inducible factor 1 (HIF-1)-related genes. Nine differentially expressed genes were identified to construct an HIF-1 score system, whose predictive efficacy was evaluated. Furthermore, we investigated oncogenic pathways and immune-cell infiltration status of PDAC with different scores. The C-index of the HIF-1score system for OS prediction in the meta-PDAC cohort and the other two validation cohorts were 0.67, 0.63, and 0.65, respectively, indicating that it had a good predictive value for patient survival. Furthermore, the area under the curve (AUC) of the receiver operating characteristic (ROC) curve of the HIF-1α score system for predicting 1-, 3-, and 4-year OS indicated the HIF-1α score system had an optimal discrimination of prognostic prediction for PDAC. Importantly, our model showed superior predictive ability compared to previous hypoxia signatures. We also classified PDAC into HIF-1 scores of low, medium, and high groups. Then, we found high enrichment of glycolysis, mTORC1 signaling, and MYC signaling in the HIF-1 score high group, whereas the cGMP metabolic process was activated in the low score group. Of note, analysis of public datasets and our own dataset showed a high HIF-1 score was associated with high immunosuppressive TME, evidenced by fewer infiltrated $CD8^+$ T cells, B cells, and type 1 T-helper cells and reduced cytolytic activity of $CD8^+$ T cells. In summary, we established a specific HIF-1 score system to discriminate

PDAC with various hypoxia statuses and immune microenvironments. For highly hypoxic and immunosuppressive tumors, a combination treatment strategy should be considered in the future.

Keywords: PDAC, HIF-1, hypoxia, ICB, immunosuppression, immune infiltration

INTRODUCTION

Pancreatic ductal adenocarcinoma (PDAC) is one of the deadliest malignancies and accounts for nearly 4.5% of all cancer-related deaths worldwide, with a 5-year survival rate of less than 10% (1, 2). Despite major efforts to improve the diagnosis and treatment of PDAC, the survival rate of patients with PDAC has not significantly improved (3). In particular, novel treatments were found to have limited indications or low response rates (2–5). For example, olaparib, is only effective in patients with germline BRCA mutations (6–8). PD-1/PD-L1 inhibition-based immunotherapy is under investigation, and preliminary data showed limited efficacy for single drug treatment (9, 10). These are due to tumor heterogeneity and the specific tumor microenvironment (TME) in PDAC (11–13). In addition, the traditional prognostic clinicopathological characteristics, such as American Joint Committee on Cancer (AJCC) stage and histologic grade, have less accurate predictive value for the clinical outcome of patients with PDAC (14–16). Therefore, exploring the molecular classification and mechanisms leading to TME development and tumor progression will help in designing more effective precision treatments for PDAC.

Desmoplasia and hypoxia are the major characteristics of TME in PDAC, in which desmoplasia worsens tumor hypoxia, and hypoxic conditions promote the proliferation of stromal cells such as CAFs, leading to severe desmoplasia (17–19). Hypoxia-inducible factor-1 (HIF-1) is a master regulator of tumor hypoxia and plays a critical role in promoting the malignant phenotypes of PDAC (20, 21). For example, HIF-1 was reported to enhance the transcription of Snail by binding to its hypoxia response elements, inducing epithelial-mesenchymal transition and cancer metastasis in PDAC (22). In addition, the hypoxic TME of PDAC could upregulate the expression of multidrug resistance 1 (MDR1) through the HIF-1 signaling pathway, thereby mediating chemotherapy resistance (23). Importantly, HIF-1 regulates anti-tumor immunity by regulating the expression of PD-L1 or CD47, resulting in an immunosuppressive TME (24–27). Thus, hypoxia and HIF-1 may affect the expression of different genes and lead to corresponding cancer cell behaviors. Therefore, it is of great interest to establish a prognostic classifier to evaluate the different hypoxia status and characteristics of hypoxia-related subtypes of PDAC.

In the current study, using multiple bioinformatics analysis, we classified patients with PDAC into three clusters based on HIF-1 related genes. Nine differentially expressed genes among the three HIF-1 clusters were identified from the meta-PDAC cohort to construct an HIF-1 score system for prognostic stratification of patients with PDAC. The predictive efficacy of the HIF-1 score system was evaluated in meta-PDAC cohort and validation cohort. Of note, we also comprehensively assessed the oncologic biological pathways and immune-cell infiltration status for pancreatic cancers with different HIF-1 scores.

MATERIALS AND METHODS

PDAC Datasets and Preprocessing

Publicly available PDAC mRNA-sequencing data and corresponding clinical information of patients were obtained from the Gene Expression Omnibus (GEO, https://www.ncbi.nlm.nih.gov/geo/), the Cancer Genome Atlas (TCGA, https://cancergenome.nih.gov/), and the International Cancer Genome Consortium (ICGC, https://icgc.org/) databases. The PDAC dataset GSE62452 (Platform: GPL6244; 61 non-tumor samples and 69 tumor samples) from the GEO database and TCGA PDAC dataset (4 non-tumor samples and 146 tumor samples) were integrated into a meta-PDAC cohort (65 non-tumor samples and 215 tumor samples). The R package 'sva' was used to eliminate batch effects. Of the 215 PDAC cases in the meta-PDAC cohort, 205 were cases with OS > 1 month and were used as the training cohort for prognostic stratification based on HIF-1 signaling. Transcriptomic data from the ICGC PDAC cohort (N = 96; validation cohort 1) and GSE79668 cohorts (Platform: GPL11154; N = 51; validation cohort 2) were used for validation.

Identification of HIF-1 Related Genes in PDAC

A total of 16 HIF-1 related genes were identified, corroborating previous studies (28, 29). The differential expression of these genes between non-tumor and tumor samples was evaluated in the meta-PDAC cohort. The prognostic value of HIF-1-related genes in PDAC was evaluated in a meta-PDAC cohort using Kaplan–Meier (KM) survival analysis.

Consensus Clustering Analysis

Using the R package 'ConsensusClusterPlus', consensus clustering was conducted to categorize PDAC patients into subgroups based on the expression of HIF-1 related genes. Principal component analysis (PCA) was performed to evaluate the clustering efficacy. KM survival analysis was then performed to assess the OS difference between different subgroups. The differential expression of HIF-1 related genes between different subgroups was visualized using the R package 'pheatmap'. Then, the association between subgroups and clinicopathological characteristics, including AJCC stage and

histologic grade, was evaluated using the chi-square test or Fisher's exact test. Differentially expressed genes between different subgroups were identified using the R package 'limma' under the threshold of |log2 fold change (FC)| > 0.5. The overlapping differentially expressed genes (ODEGs) were selected for subsequent analysis.

Development and Validation of the HIF-1 Score System

Using the R package 'survival', we performed univariate Cox regression analysis to assess the association between the ODEGs and OS in batches in the meta-PDAC cohort. Then, using the R package 'glmnet', the critical prognosis-associated ODEGs were further determined through least absolute shrinkage and selection operator (LASSO) regression analysis. KM survival analysis was also conducted to evaluate the prognostic association of the critical prognosis-associated ODEGs according to the optimal cutoff point using the R package 'survminer'. Using the R package 'survival', an HIF-1 score system was developed based on a linear combination of the expression of the critical prognosis-associated ODEGs and the multivariable Cox regression coefficients as the weight. For external validation of the HIF-1 score system, the HIF-1 score was also calculated for patients with PDAC in the ICGC PDAC cohort and GSE79668 cohort with the same multivariable Cox regression coefficients in the meta-PDAC cohort.

Using the R package 'survminer', KM survival curves for OS were constructed according to the optimal cutoff points obtained from X-tile software version 3.6.1 (low HIF-1 score, medium HIF-1 score, and high HIF-1 score) (30). The predictive performance of the HIF-1 score system was evaluated using the C-index and AUC of the ROC curves. PCA was performed to evaluate prognostic stratification efficacy. In addition, the association between HIF-1 score and clinicopathological characteristics, including AJCC stage and histologic grade, was evaluated using the chi-square test.

Association Between HIF-1 Score and Somatic Mutation in PDAC

Using the R package 'maftools', we visualized the somatic mutation profile of PDAC in the TCGA PDAC cohort. We further investigated the association between HIF-1 score and somatic mutation using the chi-square test. We also assessed the association between tumor mutation burden (TMB) and HIF-1 score. In summary, we aimed at preliminarily determining whether somatic mutation status affected hypoxia status in PDAC.

Gene Set Variation Analysis (GSVA)

GSVA is an analytical method used to calculate the enrichment scores of specific gene sets for each sample based on RNA-seq (31). Using the R package 'gsva', we conducted GSVA to estimate the enrichment scores of 50 gene ontology gene sets (h.all.v7.0.symbols.gmt), and 231 metabolic process gene sets (c5.go.bp.v7.4.symbols.gmt) obtained from the Molecular Signature Database (MSigDB, http://software.broadinstitute.org/gsea/msigdb) in the meta-PDAC cohort. Furthermore, GSVA was also implanted to calculate the enrichment scores of 25 immune-related terms extracted from previous studies (32).

Association Between HIF-1 Score and Hypoxia Scores

A total of three hypoxia scores based on the TCGA PDAC dataset were obtained from the cBioportal database (http://www.cbioportal.org/), including Buffa hypoxia, Ragnum hypoxia score, and Winter hypoxia score (33–35). We then evaluated the differences in these three hypoxia scores between different HIF-1 score subgroups. Correlation analysis between the HIF-1 score and these three hypoxia scores was conducted using Pearson correlation coefficients. KM survival curves were obtained for HIF-1 and the three hypoxia scores in the sample TCGA PDAC cohort. Then, ROC curves for 1-, 2-, and 3-year OS were performed for HIF-1 score and these three hypoxia scores to compare their predictive reliability for OS.

Real-Time Polymerase Chain Reaction (RT-qPCR)

A total of 28 samples of PDAC patients were collected after surgical resection in Guangdong Provincial People's Hospital during 2015-2021. The total mRNA of PDAC tissues were isolated using TRIzol (Invitrogen, USA) following the manufacturer's instruction. The RT-qPCR was conducted in triplicate using Taqman™ Assay kit (Applied Biosystems, USA). The expressions were estimated by $2^{-\triangle\triangle Ct}$ method andβ-actin was used as an internal control. The sequences of primers for the nine genes of our model were shown in **Table S1**. Informed consent was obtained from all patients, and the study was approved by the Ethics Committee of Guangdong Provincial People's Hospital.

Immunohistochemistry

The formalin-fixed paraffin-embedded sections (4-μm thick) from the corresponding PDAC samples were deparaffinized and rehydrated, followed by antigen retrieval using citrate buffer (pH 8.0). Staining for CD8+ T cells were performed using a rabbit anti-CD8A monoclonal antibody (GB13429, Servicebio, China) and the LSAB+ System HRP kit (DAKO, Carpineteria, CA) according to the manufacturer's instructions. The levels of CD8A-positive cells was quantified by whole slide digital scanning using Aperio VERSA scanner (Leica Bioosystems, USA), and converted to number/mm^2.

Statistical Analysis

GraphPad Prism 8.0 software (GraphPad Software, Inc.) and the R software version 3.5.2 (http://r-project.org/) were used to conduct all statistical analyses. Group differences analysis were performed using Wilcoxon test or Kruskal–Wallis test, and expressed as means ± standard deviation (SD). Pearson correlation coefficient was used for correlation analysis. A two-sided P value < 0.05 was considered as statistically significant.

RESULTS

The mRNA Expression of HIF-1 Related Genes in PDAC

We analyzed 16 known HIF-1 related genes and found that 15 were significantly overexpressed in tumor samples in the meta-PDAC cohort, including *ALDOA*, *ALDOC*, *ENO1*, *GAPDH*, *HIF1A*, *HK1*, *HK2*, *LDHA*, *PDK1*, *PFKFB3*, *PFKL*, *PGK1*, *PKM*, *SLC2A1*, and *SLCS2A3*, whereas only one (*BNIP3*) was significantly downregulated (**Figure S1A**). KM survival analysis demonstrated that 13 HIF-1 related genes were significantly associated with shorter OS of PDAC patients, namely *ALDOA*, *ALDOC*, *ENO1*, *GAPDH*, *HIF1A*, *HK1*, *HK2*, *LDHA*, *PDK1*, *PGK1*, *PKM*, *SLC2A1*, and *SLCS2A3*. (**Figure S1B**).

Consensus Clustering Analysis Identified Three HIF-1 Clusters of PDAC With Different Clinical Outcomes

According to the mRNA expression similarity of HIF-1 related genes, k = 3 was the most appropriate choice for classifying patients with PDAC into three clusters, namely HIF-1 clusters A, B, and C (**Figures 1A, B**). PCA demonstrated that HIF-1 related genes worked well with significant clustering efficacy (**Figure 1C**). The KM survival curve for OS showed that HIF-1 cluster C had the best survival, and HIF-1 cluster B had shorter medium OS than HIF-1 cluster A, though survival differences between cluster A and cluster B was not statistically significant (**Figure 1D**). A heatmap was constructed to visualize the distribution of these 16 HIF-1 related genes, AJCC stage, and the histologic grade among the three HIF-1 clusters (**Figure 1E**). Furthermore, we found that the HIF-1 cluster was not significantly associated with AJCC stage but significantly associated with histologic grade (**Figures 1F, G**), in which HIF-1 cluster B was significantly correlated with advanced histologic grade and HIF-1 cluster C was correlated with low histologic grade. These results indicate that different HIF-1 clusters are associated with different clinical outcomes.

Development and Validation of the HIF-1 Score System

The DEGs between different HIF-1 clusters were visualized using volcano plots (**Figures S2A–C**). There were 249 ODEGs among the three HIF-1 clusters (**Figure S2D**). Univariable Cox regression analysis demonstrated that 130 ODEGs were significantly associated with OS of patients with PDAC ($P < 0.05$) (**Table S2**). Moreover, LASSO regression analysis identified nine critical prognosis-associated ODEGs, and the KM survival analysis is shown in the forest plots (**Figure 2**). Subsequently, based on these nine critical prognosis-associated ODEGs, we constructed an HIF-1 score system using multivariable Cox

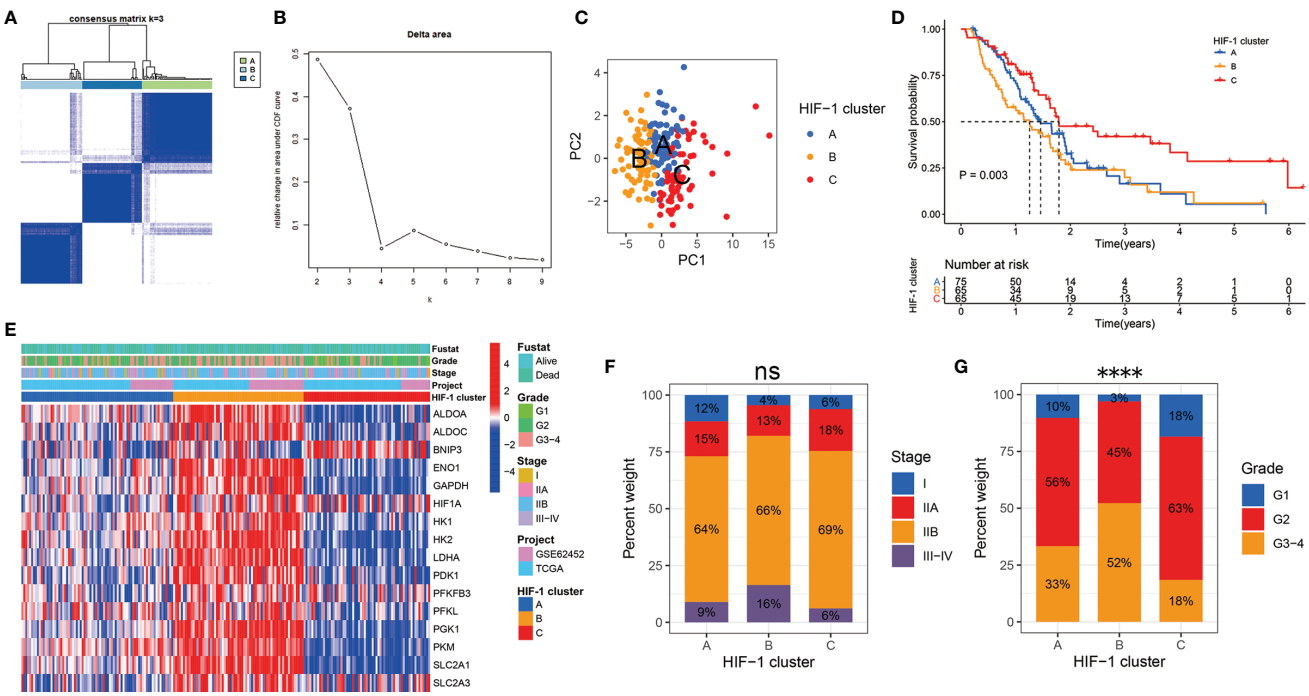

FIGURE 1 | Consensus clustering analysis identified three HIF-1 clusters of PDAC with different clinical outcomes. **(A)** The meta-PDAC cohort was divided into three distinct clusters when k = 3. **(B)** Relative change in area under consensus clustering cumulative distribution function curve for k = 2 to 9. **(C)** PCA demonstrated that HIF-1 related genes worked well with significant clustering efficacy. **(D)** The KM survival curve for OS showed a significant difference among these three HIF-1 clusters. **(E)** Heatmap to show the 16 HIF-1 related genes expression and corresponding clinicopathological information in the three HIF-1 clusters. **(F)** HIF-1 cluster was not significantly associated with AJCC stage. **(G)** HIF-1 cluster was significantly associated with histologic grade. PDAC, pancreatic ductal adenocarcinoma; PCA, principal component analysis; KM, Kaplan-Meier; OS, overall survival; AJCC, American Joint Committee on Cancer. ns > 0.05; ****P value < 0.0001.

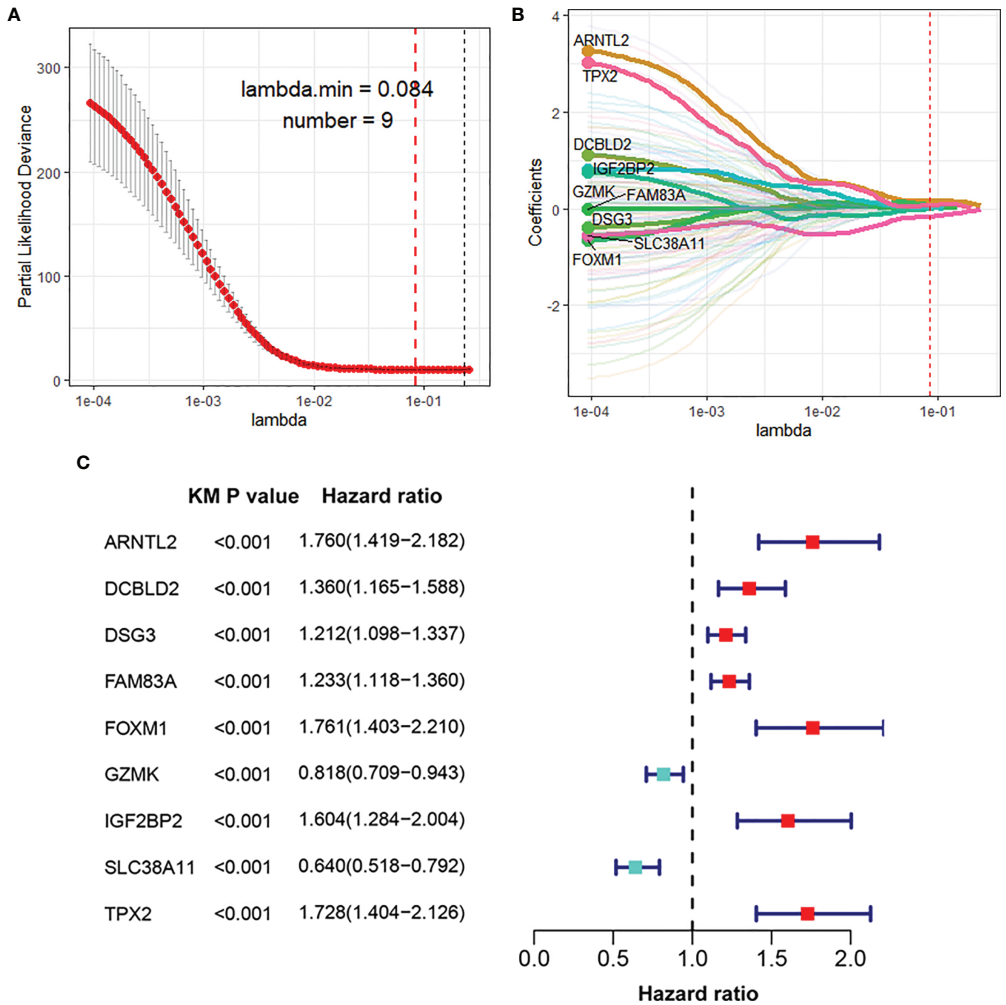

FIGURE 2 | Identification of nine critical prognosis-associated ODEGs for PDAC. **(A, B)** LASSO regression analysis identified nine critical prognosis-associated ODEGs for PDAC. **(C)** Forest plots to show the results of KM survival analysis of the nine critical prognosis ODEGs. ODEGs, overlapping differentially expressed genes; PDAC, pancreatic ductal adenocarcinoma; KM, Kaplan-Meier.

regression analysis in the meta-PDAC cohort (training cohort). The HIF-1 score was calculated by multiplying the expression of these nine critical prognosis-associated ODEGs by the corresponding multivariable Cox regression coefficients: HIF-1 score = (0.159789 × the expression value of ARNTL2) + (-0.005245 × the expression value of TPX2) + (0.105759 × the expression value of DCBLD2) + (0.045574 × the expression value of IGF2BP2) + (-0.088258 × the expression value of GZMK) + (-0.001925 × the expression value of FAM83A) + (-0.245471 × the expression value of SLC38A11) + (0.214995 × the expression value of FOXM1) + (0.103582 × the expression value of DSG3). Then, we classified patients in the meta-PDAC cohort into high-, medium-, and low-HIF-1 score groups according to the optimal cutoff point obtained from X-tile 3.6.1 software (low HIF-1 score, < 1.006; medium HIF-1 score, 1.006 ≥ & < 2.349; high HIF-1 score, ≥ 2.349). The KM survival curves for OS showed significant differences among these three HIF-1 score subgroups, in which the low-HIF-1 score group had the best survival and the high-HIF-1 score group had the worst survival (**Figure 3A**). For validation, HIF-1 scores were also calculated for 96 patients with PDAC in the ICGC PDAC cohort (validation cohort 1) and 51 patients with PDAC in the GSE79668 cohort (validation cohort 2). Similar results of KM survival analysis were also observed in the validation cohorts (**Figures 3B, C**).

The C-index of the HIF-1 score system for OS prediction in the meta-PDAC cohort were 0.67 (95%CI, 0.62–0.72). For validation cohorts, the HIF-1 score system also exhibited a high accuracy of OS prediction, with a C-index of 0.63 (95% CI, 0.56–0.70) in the ICGC PDAC cohort and a C-index of 0.65 (95%CI, 0.57–0.73) in the GSE79668 cohort. In addition, for the meta-PDAC cohort, the AUC values of the HIF-1 score system for predicting 1-, 2-, and 3-year OS were 0.716, 0.729, and 0.751, respectively (**Figure 3D**). Consistently, the AUC of the HIF-1 score for 1-, 2-, and 3-year OS were 0.720, 0.623, and 0.604 in the

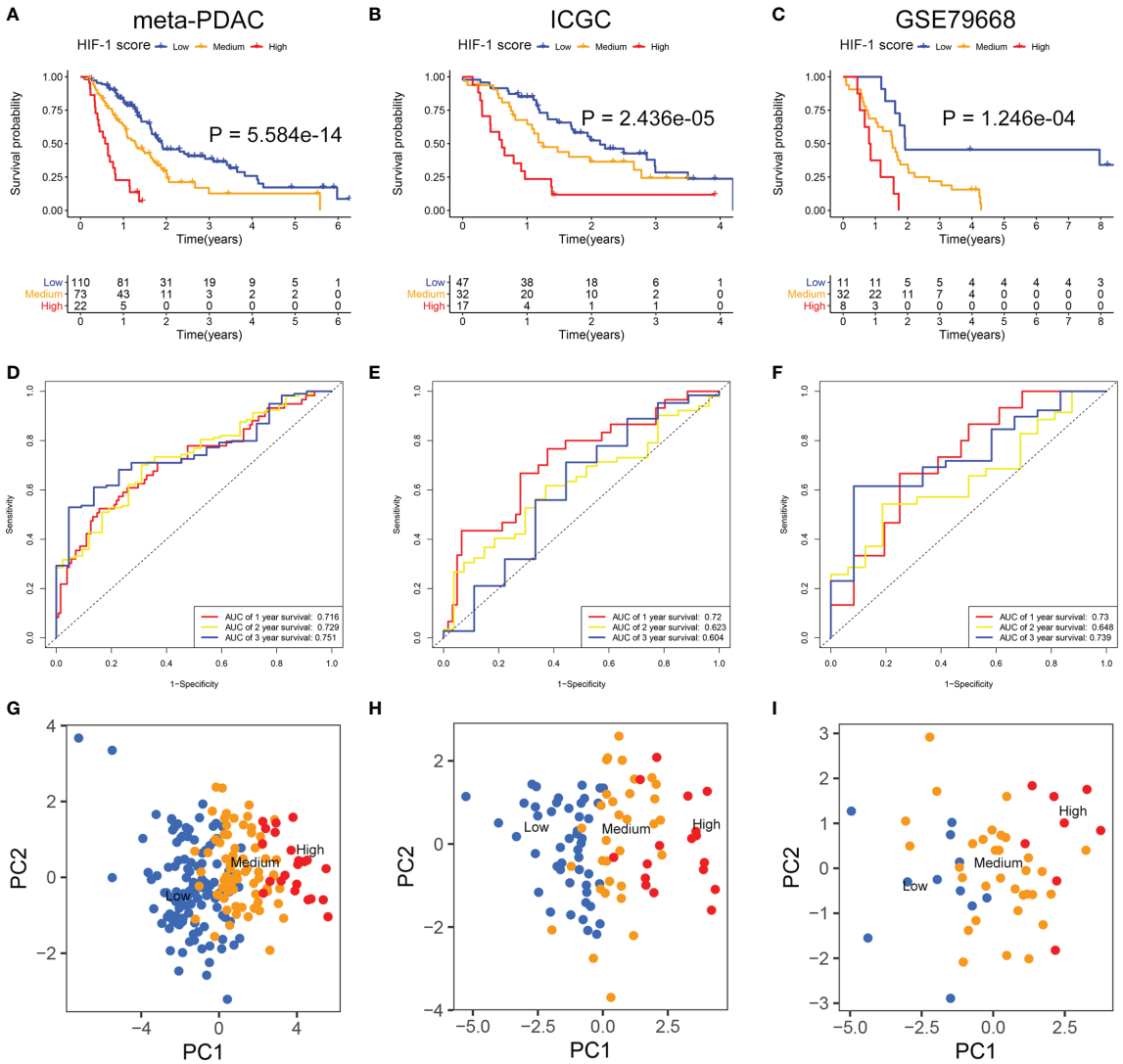

FIGURE 3 | Development and validation of the HIF-1 score system. **(A–C)** KM survival curves for OS of patients with PDAC according to the HIF-1 score groups in the meta-PDAC cohort, ICGC PDAC cohort, and GSE79668 cohort. **(D–F)** ROC curve analysis of the HIF-1 score system for 1-, 2-, and 3-year OS prediction in the meta-PDAC cohort, ICGC PDAC cohort, and GSE79668 cohort. **(G–I)** PCA to confirm the cluster efficacy of the HIF-1 score system in the meta-PDAC cohort, ICGC PDAC cohort, and GSE79668 cohort. KM, Kaplan-Meier; OS, overall survival; PDAC, pancreatic ductal adenocarcinoma; PCA, principal component analysis; ROC, the receiver operating characteristic curve.

ICGC PDAC cohort, and 0.730, 0.648, and 0.739 in the GSE79668 cohort, respectively (**Figures 3E, F**). PCA confirmed the cluster efficacy of the HIF-1 score system (**Figures 3G–I**). These results suggest an optimal discrimination of prognostic prediction using the HIF-1 score system for PDAC.

Association Between HIF-1 Score and Clinicopathological Characteristics in PDAC

Chi-square analysis indicated that the HIF-1 score system was not significantly correlated with AJCC stage in patients with PDAC, and no significant difference in HIF-1 score was found among different AJCC stages (**Figures 4A, B**). However, the HIF-1 score system was significantly associated with advanced histologic grade, and PDAC patients with higher histologic grade had higher HIF-1 scores than those with lower histologic grades (**Figures 4C, D**). In addition, univariate and multivariate Cox regression analyses demonstrated that the HIF-1 score system was an independent prognostic factor for OS in patients with PDAC (**Figures 4E, F**).

Association Between HIF-1 Score and Genomic Alteration

In line with published studies, we verified that mutations in *KRAS*, *TP53*, *CDKN2A*, and *SMAD4* are four of the most

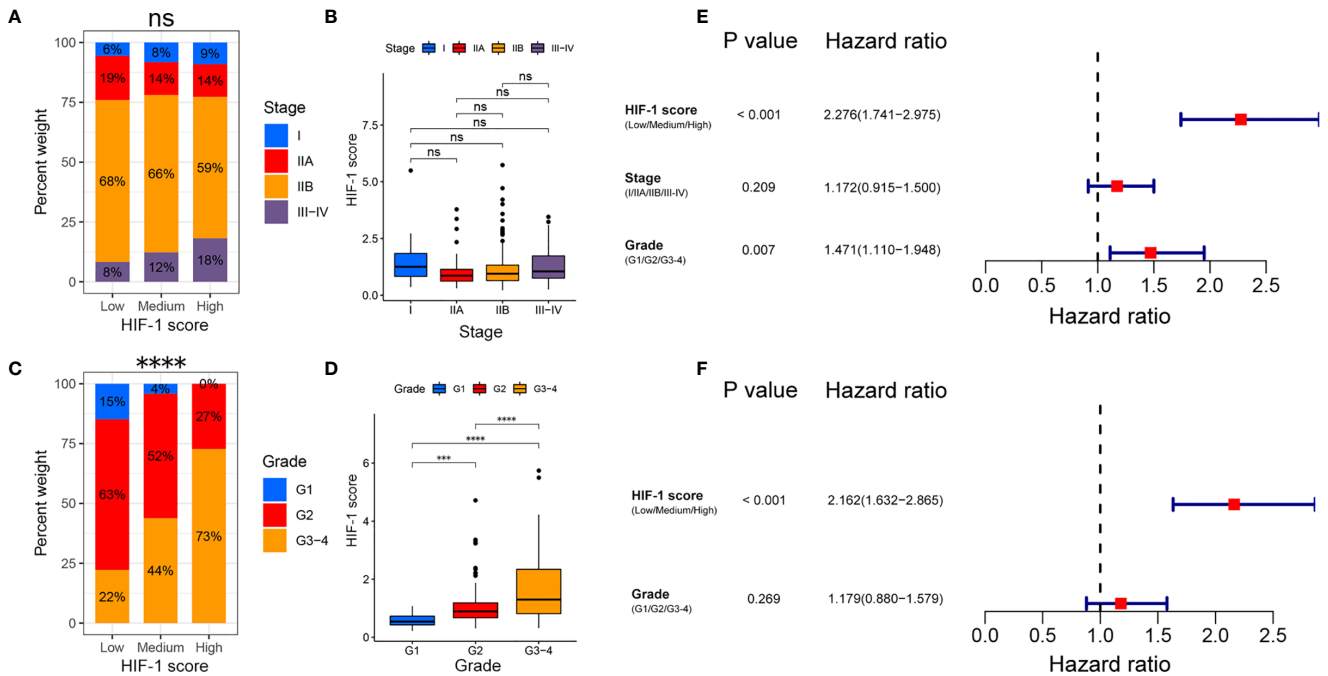

FIGURE 4 | Association between the HIF-1 score and clinicopathological characteristics in PDAC. **(A, B)** No significant association between HIF-1 score and AJCC stage were found in PDAC. **(C, D)** Significant positive correlation between HIF-1 score and histologic grade were observed in PDAC. **(E)** Univariate Cox regression analysis demonstrated that HIF-1 score system and histologic grade were prognostic factor for OS of patients with PDAC. **(F)** Multivariate Cox regression analysis demonstrated that the HIF-1 score system was an independent unfavorable prognostic factor for OS of patients with PDAC. PDAC, pancreatic ductal adenocarcinoma; OS, overall survival. ns > 0.05; ***P value < 0.001; ****P value < 0.0001.

frequent genetic alterations in PDAC (**Figure 5A**). The most common nucleotide change was the C > T transversion (**Figure 5A**). Furthermore, our study revealed that *KRAS* and *TP53* mutation status were significantly correlated with the HIF-1 score (**Figure 5A**). Patients with *KRAS* and *TP53* alterations had significantly higher HIF-1 scores than those with wild type *KRAS* and *TP53* (**Figures 5B, C**). In addition, patients with higher HIF-1 scores had a much higher TMB than those with lower HIF-1 scores (**Figures 5D, E**).

Analysis of Biological Pathways Among Different HIF-1 Score Groups

The top 20 differential oncologic biological pathways and metabolic processes between different HIF-1 score groups were presented using heatmaps (**Figure S3**). Ten critical oncologic biological pathways were found intersected among these three HIF-1 clutters (**Figure 6A**). The high HIF-1 score group had the highest enrichment scores for hypoxia, glycolysis, mTORC1 signaling, MYC signaling (MYC target V1 and MYC target V2), mitotic spindle, DNA repair, G2M targets, and E2F targets, while the low-HIF-1 score group showed the lowest enrichment. By analyzing the metabolic process, we found that the high HIF-1 score group had significant enrichment of nucleobase metabolic processes (**Figure S3E, F**). However, cGMP metabolic process, on the contrary, was significantly downregulated in the high HIF-1 score group but upregulated in the low-HIF-1 score group (**Figure S3E**).

Comparison With Our HIF-1 Score System With Other Hypoxia Score Systems

Previous studies have reported the hypoxia score system in other cancer types based on transcriptional data. In this study, we compared the predictive ability of our HIF-1 score system with these published hypoxia score systems in pancreatic cancer. First, we observed stepwise scores from HIF-1 low to high score groups calculated by the Buffa hypoxia, Ragnum hypoxia, and Winter hypoxia score systems (**Figures 6B–D**). These results validated our HIF-1 score system reflecting hypoxia status in pancreatic cancer. Furthermore, we found that HIF-1 score was significantly correlated with these three hypoxia score systems (Cor = 0.70, P < 0.0001 for Buffa hypoxia score; Cor = 0.76, P < 0.0001 for Ragnum hypoxia score; Cor = 0.67, P < 0.0001 for Winter hypoxia score) (**Figures 6E–G**). We then compared the prognostic stratification ability of the HIF-1 score system and these three hypoxia scores through KM survival analysis in TCGA PDAC cohort, which showed that the HIF-1 score system had the best performance in prognostic stratification (**Figures 6H–K**). We also compared the discriminatory ability of the HIF-1 score system and these three hypoxia scores in prognostic prediction through AUC of the ROC curves, which demonstrated that the HIF-1 score system had the best predictive efficacy for 1-, 2-, and 3-year OS of

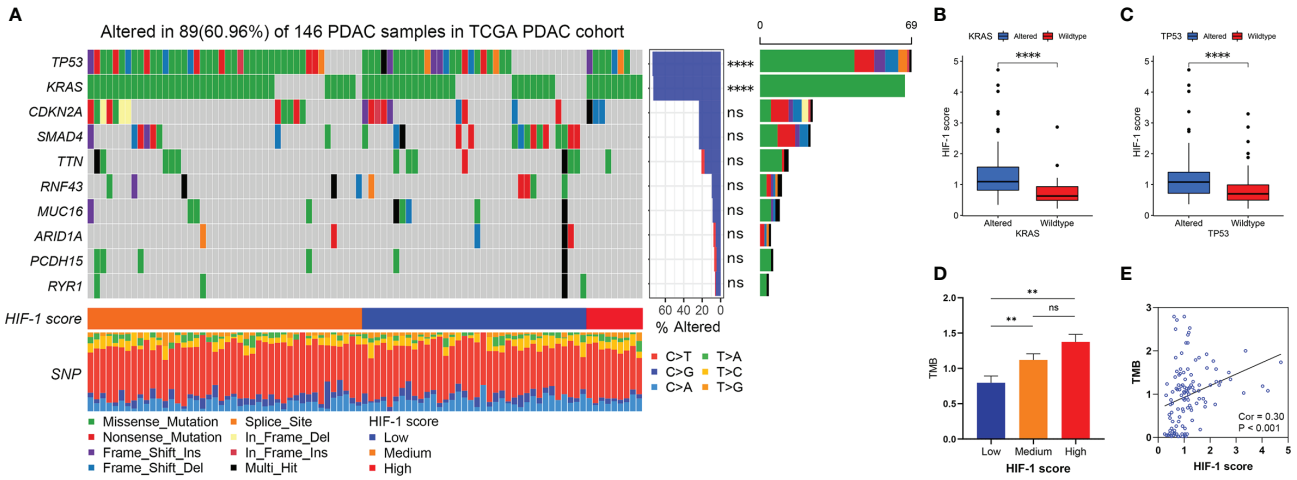

FIGURE 5 | Association between HIF-1 score and genomic alteration in PDAC. **(A)** The waterfall plot shows the top 10 most commonly mutated genes in patients with PDAC. HIF-1 score was significantly correlated with KRAS and TP53 mutation. **(B)** Higher HIF-1 score was found in KRAS altered PDAC. **(C)** Higher HIF-1 score was found in TP53 altered PDAC. **(D)** TMB in low HIF-1 score group PDAC was much lower than those in medium and high HIF-1 score group PDAC. **(E)** HIF-1 score was positively associated with TMB in PDAC. PDAC, pancreatic ductal adenocarcinoma; TMB, tumor mutation burden. ns > 0.05; **P value < 0.01; ****P value < 0.0001.

PDAC patients (**Figures 6L–N**). These results suggest that our score system had superior predictive ability for patient prognoses.

Tumors With High HIF-1 Score Were Associated With Immunosuppressive Phenotype

The 25 immune-related terms were visualized using a heatmap, including CD56dim natural killer cells, type-17 T-helper cells, plasmacytoid dendritic cells, gamma delta T cells, macrophages, T follicular helper cells, myeloid-derived suppressor cells, regulatory T cells, natural killer T cells, natural killer cells, activated dendritic cells, immature dendritic cells, monocytes, eosinophils, mast cells, activated $CD4^+$ T cells, cytolytic activity, activated $CD8^+$ T cells, tumor-infiltrating lymphocytes (TILs), type 1 T-helper cells, neutrophils, CD56bright natural killer cells, and type 2 T-helper cells (**Figure 7A**). Furthermore, significant differences in the infiltration and cytolytic activity of TILs were observed among different HIF-1 score groups, especially for activated $CD8^+$ T cells, B cells (activated and immature), and type 1 T-helper cells (**Figures 7B–G**). Of note, patients in the high HIF-1 score group exhibited the lowest infiltration and cytolytic activity of CD8+ T cells, while those in the low-HIF-1 score group exhibited the highest (**Figures 7C, D**). To further confirm these findings, we investigated the correlation between the HIF-1 score and the infiltration of $CD8^+$ T cell using our own dataset. Based on the results of RT-qPCR, we calculated the HIF-1 score for the 28 PDAC tissues, and divided them into low- and high-HIF-1 score according to the medium cutoff of HIF-1 scores. Representative image of CD8A immunostaining of low- and high-HIF-1 score PDAC samples were shown in **Figures 7H, I**. Negative association between the HIF-1 score and $CD8^+$ T cell infiltration was observed (**Figure 7J**). And tumors with high HIF-1 scores exhibited decreased infiltration of $CD8^+$ T cells compared with those with low HIF-1 score (**Figure 7K**).

We also found that higher HIF-1 scores were significantly correlated with higher PD-L1 and B7-H3 expression in PDAC, which are important molecules regulating the immunosuppressive phenotype (**Figures S4A, B**). In addition, we assessed the differences in HIF-1 scores between various subtypes defined by Bailey et al., which were squamous, immunogenic, pancreatic progenitor, and aberrantly differentiated endocrine exocrine (ADEX) (36). In their study, the squamous subtype showed significantly increased hypoxia response and limited immune infiltration and the worst survival. Consistently, we found that tumors of the squamous subtype had significantly higher HIF-1 scores than those in the immunogenic subtype ("hot tumor") (**Figure S4C**), suggesting that the squamous subtype had a highly hypoxic status. These results indicate that the HIF-1 score system might be an indicator of the immune-cell infiltration profile in PDAC. In particular, our results suggest an immunosuppressive status of tumors with high HIF-1 score ("cold tumor").

DISCUSSION

PDAC is one of the most lethal malignancies with a heterogeneous molecular profile and various hypoxic TMEs (13, 37–39). Over the past decade, molecular target therapy and immune checkpoint inhibitors have been breakthrough advancements in the treatment of various malignancies, such as non-small cell lung cancer, hepatocellular carcinoma, and melanoma (40–42). However, limited therapeutic efficacy has been observed in PDAC due to the limited infiltration of anti-tumor immune cells in the hypoxic TME (43–45). Indeed, the hypoxic TME of PDAC contributes

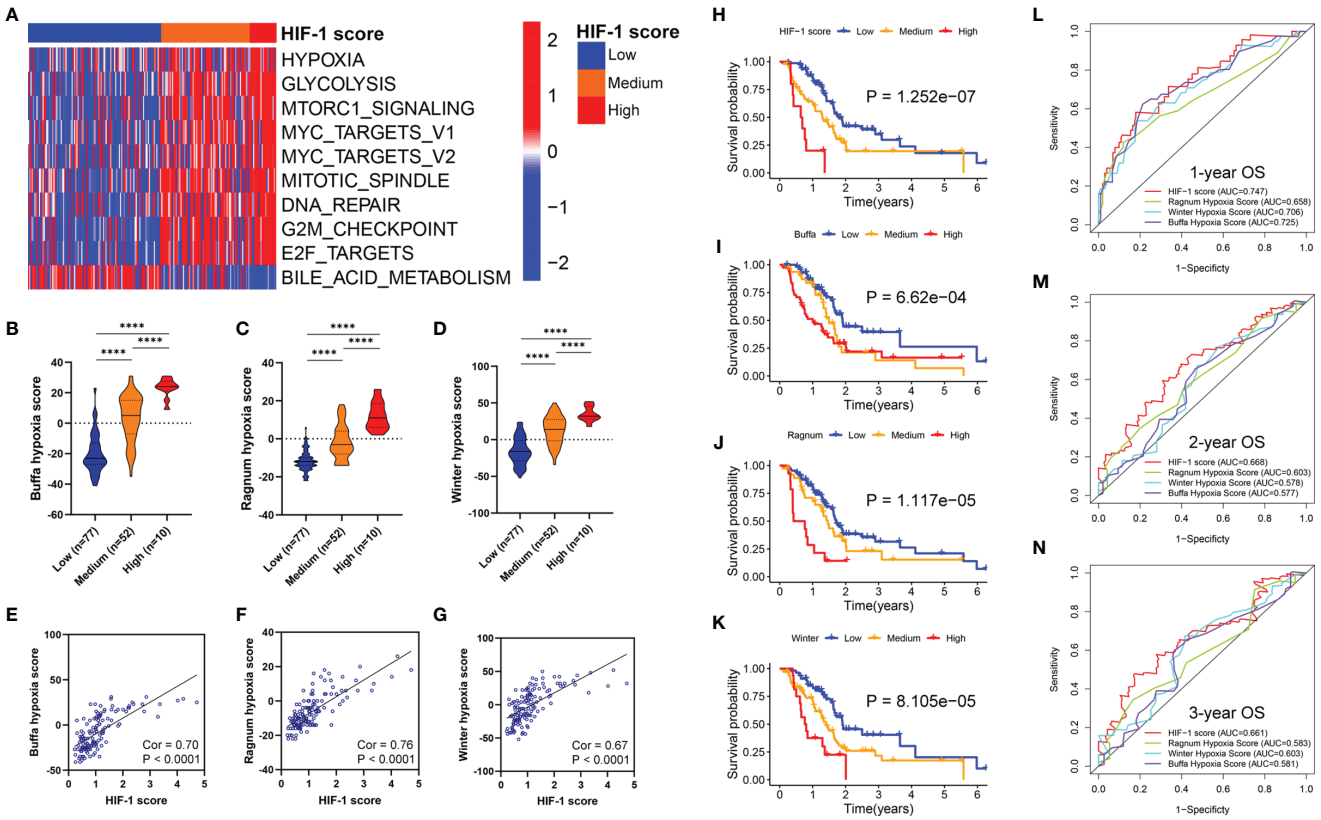

FIGURE 6 | Association between HIF-1 score and hypoxia status and oncologic biological processes in PDAC. **(A)** Heatmap to show the ten critical oncologic biological pathways intersected among the three HIF-1 clutters. **(B–D)** Stepwise scores from HIF-1 score low to high group based on the Buffa hypoxia, Ragnum hypoxia score, and Winter hypoxia score system. **(E–G)** HIF-1 score was significantly correlated with Buffa hypoxia, Ragnum hypoxia score, and Winter hypoxia score system. **(H–K)** KM survival curves for OS of patients with PDAC according to the HIF-1 score system, Buffa hypoxia, Ragnum hypoxia score, and Winter hypoxia score system in TCGA PDAC cohort. **(L–N)** ROC curve analysis for 1-, 2-, and 3-year OS prediction based on the HIF-1 score system, Buffa hypoxia, Ragnum hypoxia score, and Winter hypoxia score system in TCGA PDAC cohort. PDAC, pancreatic ductal adenocarcinoma; KM, Kaplan-Meier; OS, overall survival; TCGA, the Cancer Genome Atlas; ROC, the receiver operating characteristic curve. ****P value < 0.0001.

significantly to treatment failure of chemotherapy, target therapy, and immunotherapy (46–50). Targeting tumor hypoxia and HIF-1 signaling might be a promising approach to improve the therapeutic response of chemotherapies or immunotherapies for patients with PDAC. However, a previous study by J. Board et al. found no survival improvement with the combination treatment of a hypoxia inhibitor (TH-302) with gemcitabine in advanced PDAC (51). The disappointing results might be due to several reasons, including not recruiting appropriate patients because they did not check the hypoxic status of the PDAC before treatment. Therefore, to facilitate clinicians in individualized treatment decisions, it is of great value to develop a prognostic classifier to assess the hypoxic status and the corresponding molecular profile of PDAC.

In the present study, based on the known 16 HIF-1 related genes, we constructed a consensus clustering analysis to classify PDAC patients from the meta-PDAC cohort into three HIF-1 clusters. We then developed an HIF-1 score system integrated with nine prognosis-associated ODEGs among the three HIF-1 clusters, which showed reliable predictive efficacy for OS of PDAC patients through KM survival analysis, C-indexes, and AUC of the ROC curves in the training cohort and validation cohorts. In addition, by comparing our HIF-1 score system with other hypoxia score systems established based on other cancer types, we found that our model had the highest prognostic predictive value in PDAC. Taken together, we developed a specific HIF-1 score system for PDAC, which reflects the hypoxic status of tumors and has satisfactory predictive value for patient prognoses.

Some of the nine genes utilized in the HIF-1 score system play critical roles in pancreatic carcinogenesis. For example, Wand et al. indicated that *ARNTL2* is involved in pancreatic carcinogenesis by regulating the TGF-β signaling pathway (52). *IGF2BP2* overexpression promotes PDAC progression through the PI3K/Akt signaling pathway (53). *TPX2* is a critical target of the KRAS signaling pathway and a potential therapeutic target in PDAC (54, 55). Parameswaran et al. demonstrated that *FAM83A* overexpression promotes tumor progression through the MEK-ERK signaling pathway in PDAC (56). *DCBLD2* and *DSG* were identified as unfavorable prognostic biomarkers in PDAC (57, 58). Notably, it has been reported that *FOXM1* is overexpressed in hypoxic cancer cells, which is mediated by HIF-1 (59). Cui

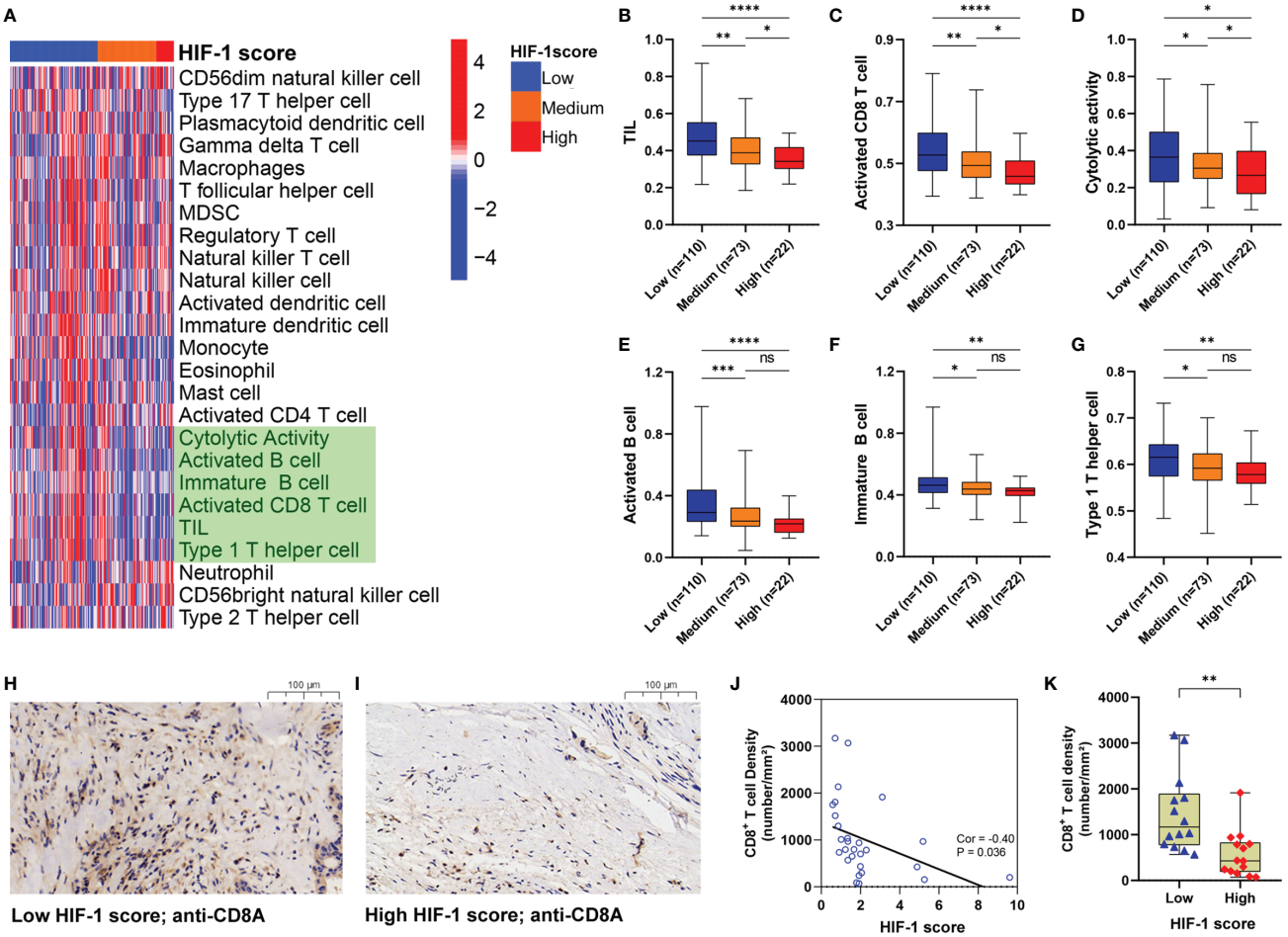

FIGURE 7 | Tumors with high HIF-1 score were associated with immunosuppressive phenotype. **(A)** Heatmap to show the 25 immune-related terms in the three HIF-1 score groups. **(B–G)** Differences of TIL, activated $CD8^+$ T cell, cytolytic activity, activated B cell, immature B cell, and Type 1 T helper cell among the three HIF-1 score groups. **(H)** Representative image of CD8A immunostaining in low-HIF-1 score tumor. **(I)** Representative image of CD8A immunostaining in high-HIF-1 score tumor. **(J)** Negative association between the HIF-1 score and $CD8^+$ T cell infiltration. **(K)** Tumors with high HIF-1 scores exhibited decreased $CD8^+$ T cell infiltration compared with those with low HIF-1 scores. TIL, tumor-infiltrating lymphocytes. ns > 0.05; *P value < 0.05; **P value < 0.01;***P value < 0.001; ****P value < 0.0001.

et al. also demonstrated that *FOXM1* impelled the Warburg effect and tumor progression in PDAC through transcriptional modulation of LDHA expression, indicating that *FOXM1* is a HIF-1 target affecting PDAC metabolism and progression (60). It should be pointed out, based on the method of data mining, that all the nine genes of our model should be HIF-1-related genes. However, many of them have not been reported to be directly regulated by HIF-1. Further studies are needed to investigate how HIF regulates or interacts with these genes.

In our study, we classified pancreatic cancer patients into three groups based on HIF-1 score system, which were HIF-1 low, medium, and high score groups. Compared to HIF-1 low and medium score groups, pancreatic cancers with HIF-1 high scores are considered more aggressive and refractory because they are associated with worse survival and more advanced grade. By exploring the molecular profile between tumors in HIF-1 low, medium, and high score groups, we found significant enrichment of the MYC and mTORC pathways in the HIF-1 high score group. MYC has been identified as one of the main drivers of PDAC initiation and metastasis (61). Pre-clinical studies have found that inhibition of c-MYC induces cell cycle arrest and chemosensitivity and impairs hypoxia signaling in PDAC (62–65). The mTORC1 pathway is also an oncogenic signaling pathway involved in the proliferation of tumor cells through the modulation of autophagy and angiogenesis (66). Of note, a previous studies revealed that mTORC1 upregulated the transcription and translation of HIF-1 (67–69). Everolimus, an inhibitor of mTORC1, has been shown to impair tumor progression in gemcitabine-resistant PDAC by diminishing the Warburg effect (70). However, Wolpin et al. demonstrated that daily everolimus administered as a single agent had little clinical efficacy in patients with gemcitabine-resistant PDAC (71). Similarly, the combination of everolimus with cytotoxic therapies (e.g., gemcitabine and cisplatin) also failed to achieve

meaningful therapeutic responses in patients with PDAC (72–74). These results suggest that single-target therapy may not be sufficient for the eradication of pancreatic cancer cells, especially for refractory and chemoresistant cancer cells. Therefore, combination target therapy may be a promising treatment. Our findings indicate that MYC and mTORC pathways are critical driver in HIF-1 high score tumors, which provides a preliminary rationale for combination treatment using HIF-1 inhibitor and MYC inhibitor, or using HIF-1 inhibitor and everolimus in these highly hypoxic and aggressive pancreatic cancers in future studies.

In addition to activation of MYC and mTORC signaling, we revealed that pancreatic cancers with HIF-1 high scores were more immunosuppressive by further investigation into the hypoxia-immune profiles. In particular, tumors with high HIF-1 scores were associated with low infiltration of TILs, including active $CD8^+$ T cells, active and immature B cells, and type 1 helper T cells. These tumors had high expression of PD-L1 and B7-H3, which are important immune checkpoint proteins. Tumor hypoxia and HIF-1 activation regulate many processes of anti-tumor immunity, leading to impaired immune responses and immune evasion (75–78). For example, HIF-1 decreases the production of IL2 and IFN-γ by CD8+ T cells, thereby diminishing the cytolytic activity (75). Hypoxia-mediated ROS also results in immunosuppressive and even lethal toxicity in $CD8^+$ T cells (76). Interestingly, using a genetic animal model, Lee et al. demonstrated accumulation of HIF-1α in early pancreatic neoplasia but HIF-1α deletion accelerates PDAC initiation by increasing B cell infiltration, suggesting the pro-neoplastic effect of B cells (79). However, the role of B cells in anti-tumor immunity is still controversial (80, 81). Therefore, further studies are needed to clarify the role of B cell immunity in human PDAC and its interaction with HIF-1. Notably, hypoxia-mediated HIF-1 increases the expression of PD-L1 in multiple solid tumors through PTEN/PI3K signaling, thereby inducing anergy or apoptosis of T cells (78, 82, 83). In addition, we found that a higher HIF-1 score was also observed in the squamous tumor subtype defined by Bailey et al., which was characterized by enrichment for hypoxia response, metabolic reprogramming, and MYC signaling and associated with poor prognosis and limited immune infiltration (36). Taken together, pancreatic cancers with higher HIF-1 scores have a more immunosuppressive TME. Tumors with low/medium HIF-1 scores tend to be good candidates for immunotherapy, especially single treatment with PD-1/PD-L1 inhibitor. For highly hypoxic and immunogenic cold tumors, strategies to break immune-cell infiltrating barriers by inhibiting HIF-1 or reducing desmoplasia may be beneficial for strengthening the efficacy of immunotherapy.

Several limitations of the current study should be noticed. First, a multi-cent and large cohort should be performed to validate the prognostic prediction ability of the HIF-1 score system. Second, further experiment studies should be conducted to investigate the underlying mechanisms by which the HIF-1 related genes regulate anti-tumor immunity in PDAC.

In summary, our study established a specific HIF-1 score system to discriminate pancreatic cancers with various degrees of hypoxia status and immunosuppressive TMEs, which provides accurate predictive value for patient prognoses. In addition, we present distinctive molecular profiles and critical oncogenic pathways for tumors with low/medium HIF-1 scores and high HIF-1 scores, which provide distinctive strategies for treating these pancreatic cancers individually.

DATA AVAILABILITY STATEMENT

The original contributions presented in the study are included in the article/**Supplementary Material**. Further inquiries can be directed to the corresponding authors.

ETHICS STATEMENT

The study was reviewed and approved by the Ethics Committee of Guangdong Provincial People's Hospital. The patients/participants provided their written informed consent to participate in this study.

AUTHOR CONTRIBUTIONS

Conceptualization: HZ, BH, YC, and CZ. Methodology: HZ, BC, and SW. Investigation: HZ, SW, ZDZ, and BC. Writing – original draft: HZ and CZ. Writing – review and editing: HZ, SW, ZDZ, ZM, ZL, CL, ZXZ, YG, and SH. Visualization: HZ. Supervision: HZ, SW, BC, SH, BH, and CZ. Funding acquisition: BC, BH, and CZ. All authors contributed to the article and approved the submitted version.

FUNDING

This study was supported by National Natural Science Foundation of China (NO.: 82072637, 82072635, 81672475 and 81702783), High-level Hospital Construction Project (DFJH201921), and Fundamental Research Funds for the Central Universities (y2syD2192230).

ACKNOWLEDGMENTS

The authors would like to give their sincere appreciation to the reviewers for their helpful comments on this article and research groups for the TCGA and CEO, which provided data for this collection.

SUPPLEMENTARY MATERIAL

The Supplementary Material for this article can be found online at: https://www.frontiersin.org/articles/10.3389/fimmu.2021.790661/full#supplementary-material

Supplementary Figure 1 | (A) Differential expression analysis of the 16 HIF-1 related genes between non-tumor and tumor samples. **(B)** Forest plots to show the results of KM survival analysis of the 16 HIF-1 related genes. KM, Kaplan-Meier. **P value < 0.01; ***P value < 0.001; ****P value < 0.0001.

Supplementary Figure 2 | (A) Differential expression analysis between HIF-1 cluster **(A, B)**. **(B)** Differential expression analysis between HIF-1 cluster **(A, C)**. **(C)** Differential expression analysis between HIF-1 cluster **(B, C)**. **(D)** Intersection of differential expressed genes among these three HIF-1 clusters.

Supplementary Figure 3 | Heatmaps to show the top 20 differential oncologic biological pathways and metabolic processes between different HIF-1 score groups were respectively presented using heatmaps.

Supplementary Figure 4 | (A) Association between HIF-1 score and PD-L1 expression in PDAC. **(B)** Association between HIF-1 score and B7-H3 expression in PDAC. **(C)** Patients in patients in squamous subtype had significant higher HIF-1 score than those in immunogenic subtype. PDAC, pancreatic ductal adenocarcinoma. ****P value < 0.0001.

REFERENCES

1. Mizrahi JD, Surana R, Valle JW, Shroff RT. Pancreatic Cancer. *Lancet* (2020) 395:2008–20. doi: 10.1016/S0140-6736(20)30974-0
2. McGuigan A, Kelly P, Turkington RC, Jones C, Coleman HG, McCain RS. Pancreatic Cancer: A Review of Clinical Diagnosis, Epidemiology, Treatment and Outcomes. *World J Gastroenterol* (2018) 24:4846–61. doi: 10.3748/wjg.v24.i43.4846
3. Neoptolemos JP, Kleeff J, Michl P, Costello E, Greenhalf W, Palmer DH. Therapeutic Developments in Pancreatic Cancer: Current and Future Perspectives. *Nat Rev Gastroenterol Hepatol* (2018) 15:333–48. doi: 10.1038/s41575-018-0005-x
4. Elaileh A, Saharia A, Potter L, Baio F, Ghafel A, Abdelrahim M, et al. Promising New Treatments for Pancreatic Cancer in the Era of Targeted and Immune Therapies. *Am J Cancer Res* (2019) 9:1871–88.
5. Kowalewski A, Szylberg L, Saganek M, Napiontek W, Antosik P, Grzanka D. Emerging Strategies in BRCA-Positive Pancreatic Cancer. *J Cancer Res Clin Oncol* (2018) 144:1503–7. doi: 10.1007/s00432-018-2666-9
6. Furuse J. A PARP Inhibitor in Pancreatic Cancer: Enhancement Anti-Tumour Activity of Chemoradiation Therapy Against Pancreatic Cancer? *EBioMedicine* (2019) 40:9–10. doi: 10.1016/j.ebiom.2019.01.039
7. Kaufman B, Shapira-Frommer R, Schmutzler RK, Audeh MW, Friedlander M, Balmana J, et al. Olaparib Monotherapy in Patients With Advanced Cancer and a Germline BRCA1/2 Mutation. *J Clin Oncol* (2015) 33:244–50. doi: 10.1200/JCO.2014.56.2728
8. Zhu H, Wei M, Xu J, Hua J, Liang C, Meng Q, et al. PARP Inhibitors in Pancreatic Cancer: Molecular Mechanisms and Clinical Applications. *Mol Cancer* (2020) 19:49. doi: 10.1186/s12943-020-01167-9
9. Wang BC, Li PC, Fan JQ, Lin GH, Liu Q. Durvalumab and Tremelimumab Combination Therapy Versus Durvalumab or Tremelimumab Monotherapy for Patients With Solid Tumors: A Systematic Review and Meta-Analysis. *Med (Baltimore)* (2020) 99:e21273. doi: 10.1097/MD.0000000000021273
10. O'Reilly EM, Oh DY, Dhani N, Renouf DJ, Lee MA, Sun W, et al. Durvalumab With or Without Tremelimumab for Patients With Metastatic Pancreatic Ductal Adenocarcinoma: A Phase 2 Randomized Clinical Trial. *JAMA Oncol* (2019) 5:1431–8. doi: 10.1001/jamaoncol.2019.1588
11. Ho WJ, Jaffee EM, Zheng L. The Tumour Microenvironment in Pancreatic Cancer - Clinical Challenges and Opportunities. *Nat Rev Clin Oncol* (2020) 17:527–40. doi: 10.1038/s41571-020-0363-5
12. Torphy RJ, Schulick RD, Zhu Y. Understanding the Immune Landscape and Tumor Microenvironment of Pancreatic Cancer to Improve Immunotherapy. *Mol Carcinog* (2020) 59:775–82. doi: 10.1002/mc.23179
13. Tao J, Yang G, Zhou W, Qiu J, Chen G, Luo W, et al. Targeting Hypoxic Tumor Microenvironment in Pancreatic Cancer. *J Hematol Oncol* (2021) 14:14. doi: 10.1186/s13045-020-01030-w
14. Liu L, Xu HX, He M, Wang W, Wang WQ, Wu CT, et al. A Novel Scoring System Predicts Postsurgical Survival and Adjuvant Chemotherapeutic Benefits in Patients With Pancreatic Adenocarcinoma: Implications for AJCC-TNM Staging. *Surg* (2018) 163:1280–94. doi: 10.1016/j.surg.2018.01.017
15. Yan X, Wan H, Hao X, Lan T, Li W, Xu L, et al. Importance of Gene Expression Signatures in Pancreatic Cancer Prognosis and the Establishment of a Prediction Model. *Cancer Manag Res* (2019) 11:273–83. doi: 10.2147/CMAR.S185205
16. Liu ZQ, Xiao ZW, Luo GP, Liu L, Liu C, Xu J, et al. Effect of the Number of Positive Lymph Nodes and Lymph Node Ratio on Prognosis of Patients After Resection of Pancreatic Adenocarcinoma. *Hepatobiliary Pancreat Dis Int* (2014) 13:634–41. doi: 10.1016/s1499-3872(14)60264-2
17. Sada M, Ohuchida K, Horioka K, Okumura T, Moriyama T, Miyasaka Y, et al. Hypoxic Stellate Cells of Pancreatic Cancer Stroma Regulate Extracellular Matrix Fiber Organization and Cancer Cell Motility. *Cancer Lett* (2016) 372:210–8. doi: 10.1016/j.canlet.2016.01.016
18. Mangge H, Niedrist T, Renner W, Lyer S, Alexiou C, Haybaeck J. New Diagnostic and Therapeutic Aspects of Pancreatic Ductal Adenocarcinoma. *Curr Med Chem* (2017) 24:3012–24. doi: 10.2174/0929867324666170510150124
19. Sharbeen G, McCarroll JA, Akerman A, Kopecky C, Youkhana J, Kokkinos J, et al. Cancer-Associated Fibroblasts in Pancreatic Ductal Adenocarcinoma Determine Response to SLC7A11 Inhibition. *Cancer Res* (2021) 18:3461. doi: 10.1158/0008-5472.CAN-20-2496
20. Duffy JP, Eibl G, Reber HA, Hines OJ. Influence of Hypoxia and Neoangiogenesis on the Growth of Pancreatic Cancer. *Mol Cancer* (2003) 2:12. doi: 10.1186/1476-4598-2-12
21. Shah VM, Sheppard BC, Sears RC, Alani AW. Hypoxia: Friend or Foe for Drug Delivery in Pancreatic Cancer. *Cancer Lett* (2020) 492:63–70. doi: 10.1016/j.canlet.2020.07.041
22. Zhu GH, Huang C, Feng ZZ, Lv XH, Qiu ZJ. Hypoxia-Induced Snail Expression Through Transcriptional Regulation by HIF-1alpha in Pancreatic Cancer Cells. *Dig Dis Sci* (2013) 58:3503–15. doi: 10.1007/s10620-013-2841-4
23. Yang SY, Song BQ, Dai SL, Yang KX, Jin Z, Shi KW. Effects of Hypoxia-Inducible Factor-1alpha Silencing on Drug Resistance of Human Pancreatic Cancer Cell Line Patu8988/5-Fu. *Hepatogastroenterol* (2014) 61:2395–401.
24. You L, Wu W, Wang X, Fang L, Adam V, Nepovimova E, et al. The Role of Hypoxia-Inducible Factor 1 in Tumor Immune Evasion. *Med Res Rev* (2021) 41:1622–43. doi: 10.1002/med.21771
25. Noman MZ, Desantis G, Janji B, Hasmim M, Karray S, Dessen P, et al. PD-L1 Is a Novel Direct Target of HIF-1alpha, and Its Blockade Under Hypoxia Enhanced MDSC-Mediated T Cell Activation. *J Exp Med* (2014) 211:781–90. doi: 10.1084/jem.20131916
26. Samanta D, Park Y, Ni X, Li H, Zahnow CA, Gabrielson E, et al. Chemotherapy Induces Enrichment of CD47(+)/CD73(+)/PDL1(+) Immune Evasive Triple-Negative Breast Cancer Cells. *Proc Natl Acad Sci USA* (2018) 115:E1239–48. doi: 10.1073/pnas.1718197115
27. Zhang H, Lu H, Xiang L, Bullen JW, Zhang C, Samanta D, et al. HIF-1 Regulates CD47 Expression in Breast Cancer Cells to Promote Evasion of Phagocytosis and Maintenance of Cancer Stem Cells. *Proc Natl Acad Sci USA* (2015) 112:E6215–23. doi: 10.1073/pnas.1520032112
28. Semenza GL. HIF-1: Upstream and Downstream of Cancer Metabolism. *Curr Opin Genet Dev* (2010) 20:51–6. doi: 10.1016/j.gde.2009.10.009
29. Deng F, Chen D, Wei X, Lu S, Luo X, He J, et al. Development and Validation of a Prognostic Classifier Based on HIF-1 Signaling for Hepatocellular Carcinoma. *Aging (Albany NY)* (2020) 12:3431–50. doi: 10.18632/aging.102820
30. Camp RL, Dolled-Filhart M. Rimm DL. X-Tile: A New Bio-Informatics Tool for Biomarker Assessment and Outcome-Based Cut-Point Optimization. *Clin Cancer Res* (2004) 10:7252–9. doi: 10.1158/1078-0432.CCR-04-0713
31. Hanzelmann S, Castelo R, Guinney J. GSVA: Gene Set Variation Analysis for Microarray and RNA-Seq Data. *BMC Bioinf* (2013) 14:7. doi: 10.1186/1471-2105-14-7
32. Bindea G, Mlecnik B, Tosolini M, Kirilovsky A, Waldner M, Obenauf AC, et al. Spatiotemporal Dynamics of Intratumoral Immune Cells Reveal the Immune Landscape in Human Cancer. *Immun* (2013) 39:782–95. doi: 10.1016/j.immuni.2013.10.003

33. Buffa FM, Harris AL, West CM, Miller CJ. Large Meta-Analysis of Multiple Cancers Reveals a Common, Compact and Highly Prognostic Hypoxia Metagene. *Br J Cancer* (2010) 102:428–35. doi: 10.1038/sj.bjc.6605450
34. Ragnum HB, Vlatkovic L, Lie AK, Axcrona K, Julin CH, Frikstad KM, et al. The Tumour Hypoxia Marker Pimonidazole Reflects a Transcriptional Programme Associated With Aggressive Prostate Cancer. *Br J Cancer* (2015) 112:382–90. doi: 10.1038/bjc.2014.604
35. Winter SC, Buffa FM, Silva P, Miller C, Valentine HR, Turley H, et al. Relation of a Hypoxia Metagene Derived From Head and Neck Cancer to Prognosis of Multiple Cancers. *Cancer Res* (2007) 67:3441–9. doi: 10.1158/0008-5472.CAN-06-3322
36. Bailey P, Chang DK, Nones K, Johns AL, Patch AM, Gingras MC, et al. Genomic Analyses Identify Molecular Subtypes of Pancreatic Cancer. *Nat* (2016) 531:47–52. doi: 10.1038/nature16965
37. Yamasaki A, Yanai K, Onishi H. Hypoxia and Pancreatic Ductal Adenocarcinoma. *Cancer Lett* (2020) 484:9–15. doi: 10.1016/j.canlet.2020.04.018
38. Biancur DE, Kimmelman AC. The Plasticity of Pancreatic Cancer Metabolism in Tumor Progression and Therapeutic Resistance. *Biochim Biophys Acta Rev Cancer* (2018) 1870:67–75. doi: 10.1016/j.bbcan.2018.04.011
39. Espiau-Romera P, Courtois S, Parejo-Alonso B, Sancho P. Molecular and Metabolic Subtypes Correspondence for Pancreatic Ductal Adenocarcinoma Classification. *J Clin Med* (2020) 9:4128. doi: 10.3390/jcm9124128
40. Fournel L, Wu Z, Stadler N, Damotte D, Lococo F, Boulle G, et al. Cisplatin Increases PD-L1 Expression and Optimizes Immune Check-Point Blockade in Non-Small Cell Lung Cancer. *Cancer Lett* (2019) 464:5–14. doi: 10.1016/j.canlet.2019.08.005
41. Fu Y, Liu S, Zeng S, Shen H. From Bench to Bed: The Tumor Immune Microenvironment and Current Immunotherapeutic Strategies for Hepatocellular Carcinoma. *J Exp Clin Cancer Res* (2019) 38:396. doi: 10.1186/s13046-019-1396-4
42. Ridolfi L, De Rosa F, Petracci E, Tanda ET, Marra E, Pigozzo J, et al. Anti-PD1 Antibodies in Patients Aged >/= 75 Years With Metastatic Melanoma: A Retrospective Multicentre Study. *J Geriatr Oncol* (2020) 11. doi: 10.1016/j.jgo.2019.12.012
43. Hou YC, Chao YJ, Hsieh MH, Tung HL, Wang HC, Shan YS. Low CD8(+) T Cell Infiltration and High PD-L1 Expression Are Associated With Level of CD44(+)/CD133(+) Cancer Stem Cells and Predict an Unfavorable Prognosis in Pancreatic Cancer. *Cancers (Basel)* (2019) 11:541. doi: 10.3390/cancers11040541
44. Li J, Yuan S, Norgard RJ, Yan F, Yamazoe T, Blanco A, et al. Tumor Cell-Intrinsic USP22 Suppresses Antitumor Immunity in Pancreatic Cancer. *Cancer Immunol Res* (2019) 8:282–91. doi: 10.1158/2326-6066.CIR-19-0661
45. Balachandran VP, Beatty GL, Dougan SK. Broadening the Impact of Immunotherapy to Pancreatic Cancer: Challenges and Opportunities. *Gastroenterol* (2019) 156:2056–72. doi: 10.1053/j.gastro.2018.12.038
46. Shukla SK, Purohit V, Mehla K, Gunda V, Chaika NV, Vernucci E, et al. MUC1 and HIF-1alpha Signaling Crosstalk Induces Anabolic Glucose Metabolism to Impart Gemcitabine Resistance to Pancreatic Cancer. *Cancer Cell* (2017) 32:71–87 e7. doi: 10.1016/j.ccell.2017.06.004
47. Ma J, Weng L, Jia Y, Liu B, Wu S, Xue L, et al. PTBP3 Promotes Malignancy and Hypoxia-Induced Chemoresistance in Pancreatic Cancer Cells by ATG12 Up-Regulation. *J Cell Mol Med* (2020) 24:2917–30. doi: 10.1111/jcmm.14896
48. Daniel SK, Sullivan KM, Labadie KP, Pillarisetty VG. Hypoxia as a Barrier to Immunotherapy in Pancreatic Adenocarcinoma. *Clin Transl Med* (2019) 8:10. doi: 10.1186/s40169-019-0226-9
49. Yang X, Lu Y, Hang J, Zhang J, Zhang T, Huo Y, et al. Lactate-Modulated Immunosuppression of Myeloid-Derived Suppressor Cells Contributes to the Radioresistance of Pancreatic Cancer. *Cancer Immunol Res* (2020) 8:1440–51. doi: 10.1158/2326-6066.CIR-20-0111
50. Luo W, Qiu J, Zheng L, Zhang T. Novel Therapies Targeting Hypoxia Mechanism to Treat Pancreatic Cancer. *Chin J Cancer Res* (2021) 33:216–31. doi: 10.21147/j.issn.1000-9604.2021.02.09
51. Borad MJ, Reddy SG, Bahary N, Uronis HE, Sigal D, Cohn AL, et al. Randomized Phase II Trial of Gemcitabine Plus TH-302 Versus Gemcitabine in Patients With Advanced Pancreatic Cancer. *J Clin Oncol* (2015) 33:1475–81. doi: 10.1200/JCO.2014.55.7504
52. Wang Z, Liu T, Xue W, Fang Y, Chen X, Xu L, et al. ARNTL2 Promotes Pancreatic Ductal Adenocarcinoma Progression Through TGF/BETA Pathway and Is Regulated by miR-26a-5p. *Cell Death Dis* (2020) 11:692. doi: 10.1038/s41419-020-02839-6
53. Xu X, Yu Y, Zong K, Lv P, Gu Y. Up-Regulation of IGF2BP2 by Multiple Mechanisms in Pancreatic Cancer Promotes Cancer Proliferation by Activating the PI3K/Akt Signaling Pathway. *J Exp Clin Cancer Res* (2019) 38:497. doi: 10.1186/s13046-019-1470-y
54. Warner SL, Stephens BJ, Nwokenkwo S, Hostetter G, Sugeng A, Hidalgo M, et al. Validation of TPX2 as a Potential Therapeutic Target in Pancreatic Cancer Cells. *Clin Cancer Res* (2009) 15:6519–28. doi: 10.1158/1078-0432.CCR-09-0077
55. Gomes-Filho SM, Dos Santos EO, Bertoldi ERM, Scalabrini LC, Heidrich V, Dazzani B, et al. Aurora A Kinase and Its Activator TPX2 Are Potential Therapeutic Targets in KRAS-Induced Pancreatic Cancer. *Cell Oncol (Dordr)* (2020) 43:445–60. doi: 10.1007/s13402-020-00498-5
56. Parameswaran N, Bartel CA, Hernandez-Sanchez W, Miskimen KL, Smigiel JM, Khalil AM, et al. A FAM83A Positive Feed-Back Loop Drives Survival and Tumorigenicity of Pancreatic Ductal Adenocarcinomas. *Sci Rep* (2019) 9:13396. doi: 10.1038/s41598-019-49475-5
57. Feng Z, Li K, Wu Y, Peng C. Transcriptomic Profiling Identifies DCBLD2 as a Diagnostic and Prognostic Biomarker in Pancreatic Ductal Adenocarcinoma. *Front Mol Biosci* (2021) 8:659168. doi: 10.3389/fmolb.2021.659168
58. Ormanns S, Altendorf-Hofmann A, Jackstadt R, Horst D, Assmann G, Zhao Y, et al. Desmogleins as Prognostic Biomarkers in Resected Pancreatic Ductal Adenocarcinoma. *Br J Cancer* (2015) 113:1460–6. doi: 10.1038/bjc.2015.362
59. Xia LM, Huang WJ, Wang B, Liu M, Zhang Q, Yan W, et al. Transcriptional Up-Regulation of FoxM1 in Response to Hypoxia Is Mediated by HIF-1. *J Cell Biochem* (2009) 106:247–56. doi: 10.1002/jcb.21996
60. Cui J, Shi M, Xie D, Wei D, Jia Z, Zheng S, et al. FOXM1 Promotes the Warburg Effect and Pancreatic Cancer Progression *via* Transactivation of LDHA Expression. *Clin Cancer Res* (2014) 20:2595–606. doi: 10.1158/1078-0432.CCR-13-2407
61. Ischenko I, Petrenko O, Hayman MJ. Analysis of the Tumor-Initiating and Metastatic Capacity of PDX1-Positive Cells From the Adult Pancreas. *Proc Natl Acad Sci USA* (2014) 111:3466–71. doi: 10.1073/pnas.1319911111
62. Liu X, Zhou Y, Peng J, Xie B, Shou Q, Wang J. Silencing C-Myc Enhances the Antitumor Activity of Bufalin by Suppressing the HIF-1alpha/SDF-1/CXCR4 Pathway in Pancreatic Cancer Cells. *Front Pharmacol* (2020) 11:495. doi: 10.3389/fphar.2020.00495
63. Liu X, Xiao XY, Shou QY, Yan JF, Chen L, Fu HY, et al. Bufalin Inhibits Pancreatic Cancer by Inducing Cell Cycle Arrest *via* the C-Myc/NF-kappaB Pathway. *J Ethnopharmacol* (2016) 193:538–45. doi: 10.1016/j.jep.2016.09.047
64. Chien W, Lee DH, Zheng Y, Wuensche P, Alvarez R, Wen DL, et al. Growth Inhibition of Pancreatic Cancer Cells by Histone Deacetylase Inhibitor Belinostat Through Suppression of Multiple Pathways Including HIF, NFkB, and mTOR Signaling *In Vitro* and *In Vivo*. *Mol Carcinog* (2014) 53:722–35. doi: 10.1002/mc.22024
65. Zhang M, Fan HY, Li SC. Inhibition of C-Myc by 10058-F4 Induces Growth Arrest and Chemosensitivity in Pancreatic Ductal Adenocarcinoma. *BioMed Pharmacother* (2015) 73:123–8. doi: 10.1016/j.biopha.2015.05.019
66. Babiker HM, Karass M, Recio-Boiles A, Chandana SR, McBride A, Mahadevan D. Everolimus for the Treatment of Advanced Pancreatic Ductal Adenocarcinoma (PDAC). *Expert Opin Investig Drugs* (2019) 28:583–92. doi: 10.1080/13543784.2019.1632289
67. Semenza GL. Targeting HIF-1 for Cancer Therapy. *Nat Rev Cancer* (2003) 3:721–32. doi: 10.1038/nrc1187
68. Wang Y, Zhao Q, Ma S, Yang F, Gong Y, Ke C. Sirolimus Inhibits Human Pancreatic Carcinoma Cell Proliferation by a Mechanism Linked to the Targeting of mTOR/HIF-1 Alpha/VEGF Signaling. *IUBMB Life* (2007) 59:717–21. doi: 10.1080/15216540701646484
69. Huang C, Li Y, Li Z, Xu Y, Li N, Ge Y, et al. LIMS1 Promotes Pancreatic Cancer Cell Survival Under Oxygen-Glucose Deprivation Conditions by Enhancing HIF1A Protein Translation. *Clin Cancer Res* (2019) 25:4091–103. doi: 10.1158/1078-0432.CCR-18-3533
70. Cui J, Guo Y, Wu H, Xiong J, Peng T. Everolimus Regulates the Activity of Gemcitabine-Resistant Pancreatic Cancer Cells by Targeting the Warburg Effect *via* PI3K/AKT/mTOR Signaling. *Mol Med* (2021) 27:38. doi: 10.1186/s10020-021-00300-8

71. Wolpin BM, Hezel AF, Abrams T, Blaszkowsky LS, Meyerhardt JA, Chan JA, et al. Oral mTOR Inhibitor Everolimus in Patients With Gemcitabine-Refractory Metastatic Pancreatic Cancer. *J Clin Oncol* (2009) 27:193–8. doi: 10.1200/JCO.2008.18.9514
72. Costello BA, Borad MJ, Qi Y, Kim GP, Northfelt DW, Erlichman C, et al. Phase I Trial of Everolimus, Gemcitabine and Cisplatin in Patients With Solid Tumors. *Invest New Drugs* (2014) 32:710–6. doi: 10.1007/s10637-014-0096-3
73. Joka M, Boeck S, Zech CJ, Seufferlein T, Wichert G, Licht T, et al. Combination of Antiangiogenic Therapy Using the mTOR-Inhibitor Everolimus and Low-Dose Chemotherapy for Locally Advanced and/or Metastatic Pancreatic Cancer: A Dose-Finding Study. *Anticancer Drugs* (2014) 25:1095–101. doi: 10.1097/CAD.0000000000000146
74. Weinberg BA, Wang H, Witkiewicz AK, Marshall JL, He AR, Vail P, et al. A Phase I Study of Ribociclib Plus Everolimus in Patients With Metastatic Pancreatic Adenocarcinoma Refractory to Chemotherapy. *J Pancreat Cancer* (2020) 6:45–54. doi: 10.1089/pancan.2020.0005
75. Caldwell CC, Kojima H, Lukashev D, Armstrong J, Farber M, Apasov SG, et al. Differential Effects of Physiologically Relevant Hypoxic Conditions on T Lymphocyte Development and Effector Functions. *J Immunol* (2001) 167:6140–9. doi: 10.4049/jimmunol.167.11.6140
76. Hildeman DA, Mitchell T, Teague TK, Henson P, Day BJ, Kappler J, et al. Reactive Oxygen Species Regulate Activation-Induced T Cell Apoptosis. *Immun* (1999) 10:735–44. doi: 10.1016/s1074-7613(00)80072-2
77. Chen J, Jiang CC, Jin L, Zhang XD. Regulation of PD-L1: A Novel Role of Pro-Survival Signalling in Cancer. *Ann Oncol* (2016) 27:409–16. doi: 10.1093/annonc/mdv615
78. Barsoum IB, Smallwood CA, Siemens DR. Graham CH. A Mechanism of Hypoxia-Mediated Escape From Adaptive Immunity in Cancer Cells. *Cancer Res* (2014) 74:665–74. doi: 10.1158/0008-5472.CAN-13-0992
79. Lee KE, Spata M, Bayne LJ, Buza EL, Durham AC, Allman D, et al. Hif1a Deletion Reveals Pro-Neoplastic Function of B Cells in Pancreatic Neoplasia. *Cancer Discov* (2016) 6:256–69. doi: 10.1158/2159-8290.CD-15-0822
80. Wouters MCA, Nelson BH. Prognostic Significance of Tumor-Infiltrating B Cells and Plasma Cells in Human Cancer. *Clin Cancer Res* (2018) 24:6125–35. doi: 10.1158/1078-0432.CCR-18-1481
81. Pineda S, Lopez de Maturana E, Yu K, Ravoor A, Wood I, Malats N, et al. Tumor-Infiltrating B- and T-Cell Repertoire in Pancreatic Cancer Associated With Host and Tumor Features. *Front Immunol* (2021) 12:730746. doi: 10.3389/fimmu.2021.730746
82. Parsa AT, Waldron JS, Panner A, Crane CA, Parney IF, Barry JJ, et al. Loss of Tumor Suppressor PTEN Function Increases B7-H1 Expression and Immunoresistance in Glioma. *Nat Med* (2007) 13:84–8. doi: 10.1038/nm1517
83. Dong H, Strome SE, Salomao DR, Tamura H, Hirano F, Flies DB, et al. Tumor-Associated B7-H1 Promotes T-Cell Apoptosis: A Potential Mechanism of Immune Evasion. *Nat Med* (2002) 8:793–800. doi: 10.1038/nm730

Conflict of Interest: The authors declare that the research was conducted in the absence of any commercial or financial relationships that could be construed as a potential conflict of interest.

Publisher's Note: All claims expressed in this article are solely those of the authors and do not necessarily represent those of their affiliated organizations, or those of the publisher, the editors and the reviewers. Any product that may be evaluated in this article, or claim that may be made by its manufacturer, is not guaranteed or endorsed by the publisher.

frontiers in Immunology

ORIGINAL RESEARCH
published: 08 December 2021
doi: 10.3389/fimmu.2021.800268

Prognostic Risk Model and Tumor Immune Environment Modulation of m5C-Related LncRNAs in Pancreatic Ductal Adenocarcinoma

Hao Yuan[1,2†], Jinhui Liu[3†], Li Zhao[1,2†], Pengfei Wu[1,2†], Guosheng Chen[1,2], Qun Chen[1,2], Peng Shen[1,2], Taoyue Yang[1,2], Shaoqing Fan[1,2], Bin Xiao[1,2] and Kuirong Jiang[1,2*]*

[1] Pancreas Center, Department of General Surgery, The First Affiliated Hospital of Nanjing Medical University, Nanjing, China, [2] Pancreas Institute, Nanjing Medical University, Nanjing, China, [3] Department of Gynecology, The First Affiliated Hospital of Nanjing Medical University, Nanjing, China

OPEN ACCESS

Edited by:
Yunfei Xu,
Shandong University, China

Reviewed by:
Ning Pu,
Fudan University, China
Yongsong Chen,
Shantou University, China

***Correspondence:**
Kuirong Jiang
jiangkuirong@njmu.edu.cn
Bin Xiao
xiaobin@jsph.org.cn

[†]These authors have contributed equally to this work

Specialty section:
This article was submitted to Cancer Immunity and Immunotherapy, a section of the journal Frontiers in Immunology

Received: *22 October 2021*
Accepted: *19 November 2021*
Published: *08 December 2021*

Citation:
Yuan H, Liu J, Zhao L, Wu P, Chen G, Chen Q, Shen P, Yang T, Fan S, Xiao B and Jiang K (2021) Prognostic Risk Model and Tumor Immune Environment Modulation of m5C-Related LncRNAs in Pancreatic Ductal Adenocarcinoma. Front. Immunol. 12:800268. doi: 10.3389/fimmu.2021.800268

RNA methylation modification is a key process in epigenetics that regulates posttranscriptional gene expression. With advances in next-generation sequencing technology, 5-methylcytosine (m5C) modification has also been found in multiple RNAs. Long non-coding RNAs (lncRNAs) were proved to have a key role in cancer progression and closely related to the tumor immune microenvironment. Thus, based on the PDAC patients' clinical information and genetic transcriptome data from the TCGA database, we performed a detailed bioinformatic analysis to establish a m5C-related lncRNA prognostic risk model for PDAC patients and discovered the relationship between the risk model and PDAC immune microenvironment. Pearson correlation coefficient analysis was applied to conduct a m5C regulatory gene and m5C-related lncRNA co-expression network. Expression of m5C-related lncRNAs screened by univariate regression analysis with prognostic value showed a significant difference between pancreatic cancer and normal tissues. The least absolute shrinkage and selection operator (LASSO) Cox regression method was applied to determine an 8-m5C-related lncRNA prognostic risk model. We used principal component analysis to indicate that the risk model could distinguish all the samples clearly. The clinical nomogram also accurately predicted 1-, 1.5-, 2-, and 3-year survival time among PDAC patients. Additionally, this risk model was validated in the entire group and sub-test groups using KM analysis and ROC analysis. Combined with the clinical characteristics, the risk score was found to be an independent factor for predicting the survival of PDAC patients. Furthermore, the association between the risk model and tumor immune microenvironment was evaluated *via* the ESTIMATE R package and CIBERSORT method. Consequently, the results indicated that immune cells were associated with m5C-related lncRNA risk model scores and had different distribution in the high- and low-risk groups. Based on all these analyses, the m5C-related lncRNA risk model could be a reliable prognostic tool and therapeutic target for PDAC patients.

Keywords: lncRNA, m5C methylation, tumor immune microenvironment, PDAC, prognostic model

INTRODUCTION

Pancreatic ductal adenocarcinoma (PDAC) is a common malignant tumor of the digestive system, which is characterized by high degree of malignancy, easy recurrence, and metastasis (1). Recently, the incidence rate of PDAC has increased year by year. Due to the lack of early diagnosis methods, most patients were diagnosed at an advanced stage and lost the chance of radical resection (2). Lately, personalized molecular therapies targeting specific tumor-associated genes and the application of immune checkpoint inhibitors have effectually meliorated the prognostic effect of patients with advanced cancer (3). However, pancreatic cancer is characterized by high rates of drug resistance and metastasis due to its specific tumor microenvironment, current therapies have not effectively contributed to the prognosis of patients with PDAC, and researchers still need more specific biomarkers for developing more effective diagnostic and treatment strategies (4). Hence, it is essential to find new molecular biomarkers for early diagnosis of PDAC.

Epigenetics study aims to research gene differential expression without changing nucleotide sequence (5), and epigenetic modification has been proven to play an important role in the progress of tumor biology (6), such as DNA and RNA methylation, genomic imprinting, gene silencing, and non-coding RNA modification. In recent years, N6-methyladenine (m6A) and 5-methylcytosine (m5C) RNA methylation have become a vital direction in detecting the regulation of RNA epigenetic modification upon the growth of various malignant tumors (7, 8). With the advance of high-throughput sequencing technology, the distribution and biological functions of RNA m5C modification at mRNA and non-coding RNA have been gradually discovered (9). RNA m5C methylation is catalyzed by a methyltransferase complex, which consists of three methylation-related enzymes, including methyltransferase ("Writer"), demethylase ("Erase"), and m5C binding protein ("Reader"). Similar to functions of m6A methylation, m5C methylation exerted biological effects mainly by regulating RNA stability, affecting transcription efficiency, and mediating RNA localization (10). In addition, abnormal expression of m5C methylation is associated with the occurrence and development of several malignant tumors (11, 12). Recent reports have also demonstrated that m5C-related gene expression is associated with prognosis in patients with lung and pancreatic cancers, which further indicated that m5C methylation may have an essential role in malignant tumor growth (13, 14).

Long non-coding RNAs are transcribed by corresponding genes and have a similar structure to mRNA including polyA tail and promoter structure (15). Due to different splicing methods, multiple lncRNAs were formed during the differentiation process. Several research unveiled that lncRNAs could modulate downstream genes in epigenetic, transcriptional, and post-transcriptional levels including gene silencing, histone processing, transcriptional regulation, transcriptional interference, and nuclear transport, which were closely related to the development of various human diseases (16). In malignant tumors, methylation-related genes could affect tumor progression by regulating the methylation level of lncRNA. For instance, LINC00942-specific sequence recruited methylated transferase METTL14 and stabilized the downstream targets of LNC942, which could promote tumorigenesis and development in breast cancer (17). Several reports have demonstrated that m5C modification existed widely in non-coding RNAs; nevertheless, the reports about m5C methylation regulation in lncRNAs were still few. Thus, it is essential to further research the relationship between m5C methylation and lncRNAs, especially in malignant tumor.

Tumor microenvironment (TME) is a mixture of fluid, immune cells, and blood vessels surrounding the tumor (18). The interaction between tumor cells and TME could determine the progression and fate of tumor. Therefore, understanding the composition and function of TME is crucial to research cancer progression (19). Studies have indicated that multiple genetic mutations could increase the incidence of cancer. However, the impact of TME on cancer development is still unclear. Accumulating evidence revealed that lncRNAs were important regulators in the immune system, which could control the distribution and activation of immune cells and mediate the tumor cells' immune evasion. For instance, LncRNA-MALAT1 could promote thyroid cancer progression *via* modulating tumor-associated macrophages secreting FGF2 protein (20). In colorectal cancer, lncRNA SATB2-AS1 could regulate tumor tissue immune cell density *via* combining with downstream proteins WDR5 and GADD45A and regulating TH1-type chemokines (21). Furthermore, the relationship between lncRNAs and tumor immune microenvironment has also been reported in pancreatic cancer (22). However, the relationship between m5C-related lncRNAs and tumor-infiltrating lymph cell distribution has never been reported in PDAC.

In our study, we summarized 177 PDAC patients' clinical information together with transcriptome expression data, and constructed an mRNA–lncRNA co-expression network between m5C-related mRNAs and lncRNAs. A total of 17 prognostic lncRNAs were screened *via* univariate Cox analysis. Consequently, we generated a PDAC prognostic risk model consisting of 8 m5C-related lncRNAs *via* LASSO regression analysis. We further verified the prognostic risk model in subgroups *via* Kaplan–Meier (KM) analysis and receiver operating characteristic curve (ROC) analysis. Additionally, the association between the risk model and tumor immune environment was measured *via* the ESTIMATE R package and CIBERSORT tool. Finally, 6 types of immune cells were identified in high- or low-risk groups. Moreover, m5C-related lncRNAs had statistically significant association with immune related genes and 5 types of tumor-infiltrating lymph cells were negatively correlated with the risk scores. In summary, our research indicated that the m5C-related lncRNA risk model might offer a promising prognostic tool and play an essential role in regulating PDAC immune cell distribution.

MATERIALS AND METHODS

Data Collection and Processing

We downloaded a total of 182 patient data from the TCGA data website including clinical and transcriptome expression raw data

(https://portal.gdc.cancer.gov/repository). Compared with the Ensemble Genes ID, 14,086 lncRNAs were identified in the TCGA dataset. Online bioinformatic tool GEPIA (http://gepia.cancer-pku.cn/index.html) was used to detect the expression of m5C-related genes in pancreatic normal and tumor tissues (|Log2FC| Cutoff = 1, *p*-value cutoff = 0.01; Match TCGA normal and GTEx data).

LASSO Analysis

The LASSO regression method was introduced to construct a m5C regulatory gene-related lncRNA predicted risk model *via* R package. It is a widely used high-dimensional index regression method that screened the m5C-related lnRNAs with prognostic value and constructed a predicted risk model by applying a penalty proportional to the contraction of the regression coefficient. We established a m5C-related lncRNA risk model consisting of 8 lncRNAs depending on this method.

GSEA

We divided all samples into two groups according to the median risk score of the m5C-related lncRNAs. GSEA software (GSEA_4.1.0) was performed to analyze the data. Enrichments of gene sets with a normalized *p*-value less than 0.05 were considered to be significant.

Cell Culture

HPNE cell lines (human pancreatic ductal epithelial cell line) and all the three human pancreatic cancer cell lines (Mia-PaCa-2, Panc-1, and CFPAC-1) were purchased from the Cell Bank of Type Culture Collection of the Chinese Academy of Sciences in Shanghai, China. The cells were cultured in RPMI 1640 medium (Gibco, United States) or Dulbecco's modified Eagle's medium (Gibco, United States) with 10% fetal bovine serum (Wisent, Montreal, QC, Canada), 100 U/ml penicillin, and 100 μg/ml streptomycin in the incubator at 37°C and 5% CO_2 concentration.

RNA Isolation and Quantitative Real-Time PCR

Total RNA was isolated from pancreatic cancer cells and HPNE cells by Trizol reagent (Life Technologies, Carlsbad, CA, USA) based on the manufacturer's instruction. After quality validation, iScript cDNA Synthesis Kit (Bio-Rad, Hercules, CA, USA) was used to perform reverse transcription. Total cDNA was further used for qRT-PCR with the TaqMan Gene Expression Assay (Thermo Fisher Scientific, Rockford, IL, USA). The expression of GAPDH was used as an internal control to calibrate the original mRNA expression level. The m5C-related lncRNA expression was calculated *via* the $2^{-\Delta\Delta CT}$ method. All primer sequences used in this research are listed in **Supplementary Table 1**.

Identification Tumor-Infiltrating Immune Cells

CIBERSORT is a typical tool to deconvolute the expression matrix of immune cells based on linear support vector regression, which quantified the infiltrating immune cells proportion *via* detecting marker gene expression. In our study, we combined the expression of marker genes from 22 types of immune cells and all the PDAC patients' transcriptome data to acquire the tumor-infiltrating lymph cell distribution scores *via* CIBERSORT. ESTIMATE R package could use gene expression profile to predict stromal cell and immune cell scores, and then calculate the amount of these two types of cells, which was performed to analyze the pancreatic cancer purity in this research.

Statistical Analysis

The data flow chart is shown in **Supplementary Table 2**. The m5C-related lncRNAs with correlation index > 0.3 and $p < 0.05$ were regarded as statistically significant. Univariate and multivariate Cox regression analyses were performed to identify the m5C-related lncRNA risk score as an independent prognostic factor for PDAC. The Kaplan–Meier method was performed to compare OS time of PDAC patients. ROC analysis was expended to measure the prognostic competence between the prognostic risk scores and other clinical parameters. The qRT-PCR experiments were analyzed by PRISM 7. The relationship between the m5C-related lncRNA risk score and tumor-infiltrating lymph cell distribution was analyzed by CIBERSORT and ESTIMATE R package.

RESULTS

Identification of m5C Regulator-Related LncRNAs in PDAC Patients

Initially, we screened the m5C methylation modification-related genes based on the published articles. A total of 13 m5C regulators were selected, namely, YBX1, ALYREF, DNMT1, NSUN4, TRDMT1, TET2, NSUN7, NSUN6, NSUN5, NSUN3, NSUN2, DNMT3a, and DNMT3b. We summarized the m5C regulator genes and then compared the expression of m5C regulator genes in 179 normal pancreas tissues and 171 pancreatic cancer tissues using online data base GEPIA (http://gepia.cancer-pku.cn/). We found that among the m5C regulators, the expression of YBX1, ALYREF, DNMT1, and NSUN4 was obviously higher in PDAC patient's tissues ($p < 0.05$), whereas no notable variances were detected in TRDMT1, TET2, NSUN7, NSUN6, NSUN5, NSUN3, NSUN2, DNMT3a, and DNMT3b (**Supplementary Figure 1**). Moreover, the m5C-related lncRNAs were recognized by correlation analysis depending on the expression of m5C regulators and lncRNAs in a total of 177 PDAC samples. Use correlation coefficient > 0.3 and *p*-value > 0.05 as filter criterion; finally, 242 m5C-related lncRNAs were screened. We also constructed a network between m5C-related genes and their co-expressing lncRNAs to show m5C-related lncRNA co-expressing relationship (**Figure 1A**). Based on the screened m5C-related lncRNAs, we use univariate Cox analysis ($p < 0.001$) to further filter the prognostic m5C-related lncRNA in PDAC patients combined with the patient survival data. The results indicated that a total of 17 PDAC prognostic lncRNAs were screened, and most of the m5C-related lncRNAs were protective factors (hazard ratio, HR < 1), only CASC8 was a risk factor (HR > 1) in PDAC. In addition, the Circos picture showed that the protective m5C-related

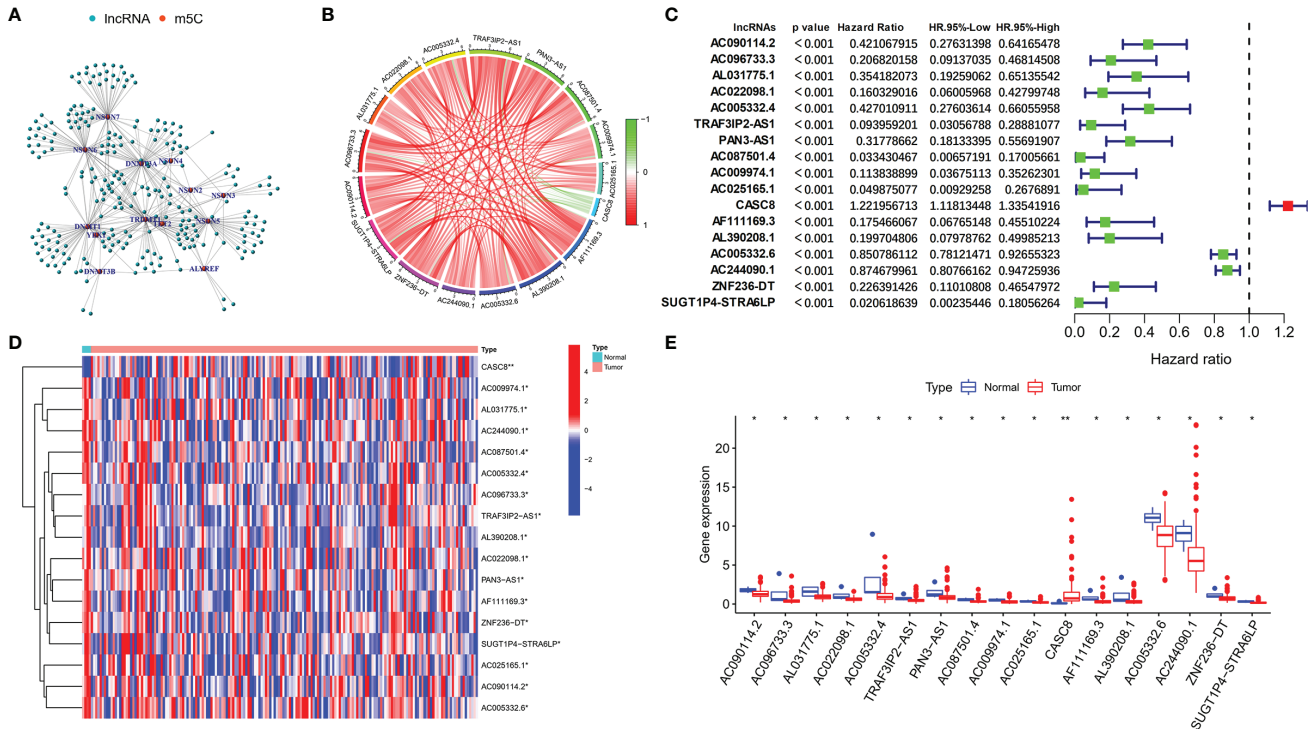

FIGURE 1 | Identification of m5C regulator-related lncRNAs with prognostic value in PDAC patients. **(A)** Co-expression relationship between m5C-related lncRNAs and m5C regulators. **(B)** Circos figure exhibited the expression correlation between the m5C-related lncRNAs with prognostic value (red line represents positive relationship and the green line represents negative relationship). **(C)** Forest plot showed the prognostic risk value of the 17 screened m5C-related lncRNAs *via* univariate Cox regression analysis. **(D, E)** Heatmap and scatter diagram indicated the different expression of m5C-related lncRNAs in normal and tumor tissues. $^{*}p < 0.05$, $^{**}p < 0.01$.

lncRNAs had positive expression correlation and risk factor CASC8 was negatively correlated with others (**Figures 1B, C**). Furthermore, we tried to clarify the expression of the screened prognostic m5C-related lncRNAs in PDAC patients depending on the TCGA database. The heatmap revealed that all the lncRNAs had statistical differences between the normal and tumor pancreatic tissues, which indicated that the m5C-related lncRNAs might play a key role in PDAC progression (**Figures 1D, E**).

Establishing an 8 m5C-Related LncRNA Risk Model for PDAC Patients

Depending on the primary screen of the m5C-related lncRNAs, the LASSO regression technique was further performed randomly to construct a prognostic risk model for PDAC, which showed that eight m5C-related lncRNAs were appropriate for building the prognostic risk model (**Figures 2A, B** and **Table 1**). The risk score was calculated as follows: risk score = (-0.780839063578865 * AC022098.1. expression) + (-0.220638925265728 * AL031775.1 expression) + (-0.0579614996945241 * AC005332.6 expression) + (-0.367271578600146 * AC096733.3 expression) + (-0.0490022123517058 * AC025165.1 expression) + (0.0600252490282948 * CASC8 expression) + (-0.528438814531151 * AC009974.1 expression) + (-0.113641932851614 * PAN3-AS1 expression). The Sankey diagram indicated the relationship between the 6 m5C regulators mRNAs and 8 screened lncRNAs, of which CASC8 belonged to risk factors and the others were protective factors (**Figure 2C**). Furthermore, all the PDAC patients were divided into low- or high-risk groups based on the median risk scores calculated by the above formula. The principal component analysis (PCA) and three-dimensional PCA showed that patients with different risks were well separated into two clusters (**Figures 2D, E**). Patients in the high-risk group had significantly shorter survival time than the patients in the low-risk group. A distinguished difference in OS time was detected between the low- and high-risk groups *via* Kaplan–Meier survival analysis (HR = 2.47, 95% CI: 1.64–3.73, $p < 0.001$, **Figure 2F**).

Relationships Between m5C-Related LncRNAs and Clinical Pathological Parameters

We further detected the impact of the selected eight lncRNAs on PDAC patients' overall survival time, respectively. The OS curve of the m5C-related lncRNAs showed that patients with risk lncRNA high expression (CASC8) had shorter survival time, whereas those with protective lncRNA high expression (AC022098.1, AL031775.1, AC005332.6, AC096733.3, AC025165.1, AC009974.1, and PAN3-AS1) had longer survival time (**Figure 3A**). According to the heatmap, the pancreatic

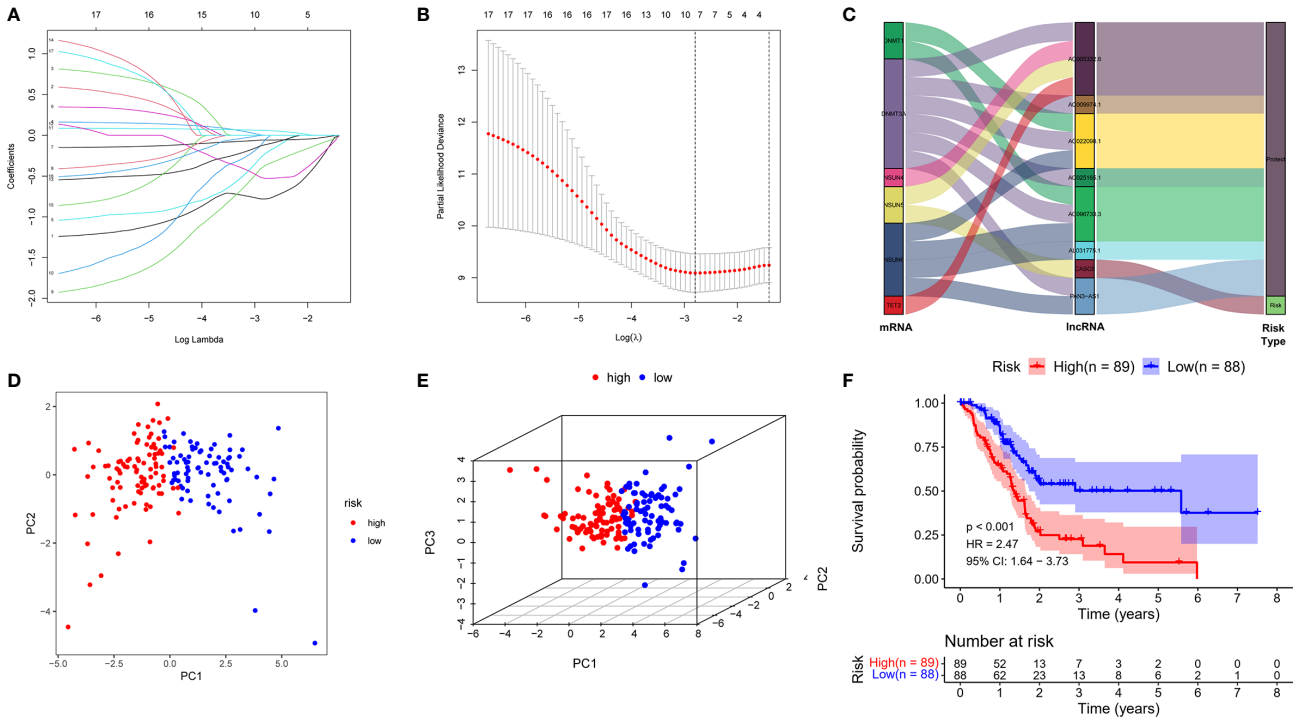

FIGURE 2 | Constructed a m5C-related lncRNA risk model in the PDAC cohort. **(A)** LASSO regression of the 17 m5C-related lncRNAs. **(B)** Cross-validation for optimizing the parameter in LASSO regression. **(C)** The Sankey diagram displayed the relationship between the 6 m5C regulators mRNA expression and the 8 m5C-related lncRNAs. **(D, E)** PCA and three-dimensional PCA analysis derived from the m5C-related lncRNAs indicated that the patients were divided into two significantly high- or low-risk distribution patterns. **(F)** KM curve shows that patients in the m5C-related lncRNA low-risk group survived dramatically longer than those in the high-risk group.

TABLE 1 | The 8 m5C-related lncRNA risk model parameters.

LncRNAs	AC022098.1	AL031775.1	AC005332.6	AC096733.3	AC025165.1	CASC8	AC009974.1	PAN3-AS1
Correlation coefficient	-0.780839064	-0.220638925	-0.0579615	-0.367271579	-0.049002212	-0.060025249	-0.528438815	-0.113641933

tumor size was significantly different between the high- and low-risk groups ($p < 0.05$). Nevertheless, the other clinical factors including patient age, gender, tumor stage, and grade had no statistical differences (**Figure 3B**). Moreover, we further subdivide these clinical indicators severally and analyzed the risk scores in the subgroups. The KM survival curve showed that the patients with high-risk scores had a shorter OS in male patients' group, younger patients (age less than 65 years), Stage I–II groups, Grade I–II or Grade III–IV groups, T I–II or T III–IV groups, N0 or N I–III groups, and patients without any metastasis group (**Figure 3C** and **Supplementary Figure 2**).

The m5C-Related LncRNA Risk Score Was an Independent Prognostic Factor for PDAC

We ordered the patients based on the risk scores. Heatmap revealed that the expression of 8 m5C-related lncRNAs were considerably different in the PDAC patients with different risk scores. Furthermore, the scatter dot plot also unveiled that the mortality of the PDAC patients increased with the risk scores, and patients with lower risk scores exhibited longer survival time (**Figure 4A**). Next, we performed univariate and multivariable Cox regression analyses to validate if the risk score calculated by the m5C-related lncRNA risk model could work as an independent prognostic factor for PDAC patients. As shown in **Figure 4B**, univariate Cox regression analysis demonstrated that only the m5C-related lncRNA risk scores were obviously positively related with OS (HR: 197.088, 95% CI: 10.283–3777.290, $p < 0.001$). Multivariate analysis also revealed that m5C-related lncRNAs prognostic risk score (HR: 116.786, 95% CI: 3.668–3718.415, $p = 0.007$) had a significant relationship with PDAC patients' OS and could act as an independent prognostic factor (**Figure 4C**). Our results suggested that the m5C-related lncRNA risk model was an independent prognostic factor for PDAC and took advantage of the traditional clinicopathological indicators including patient age, gender, and tumor stage. Moreover, the 1-year ROC curve proved that the AUC value for the m5C-related lncRNA risk model was 0.716, which was

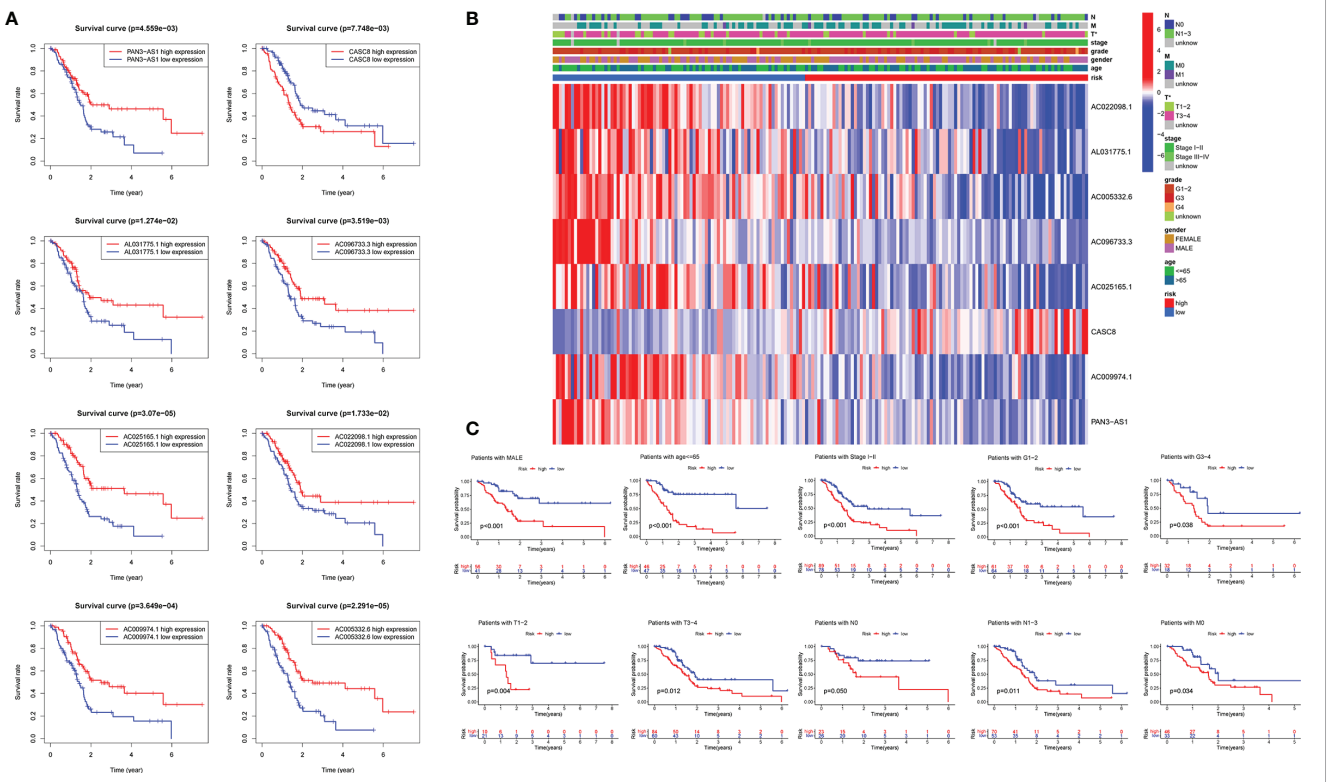

FIGURE 3 | Relationships between m5C-related lncRNAs and clinical pathological parameters. **(A)** Eight survival curves based on the m5C-related lncRNAs expression. **(B)** Heatmap displayed the clinical characteristics and differences in the high- and low-risk group calculated by m5C-related lncRNA risk scores. **(C)** Survival analysis in subgroups including gender, age and tumor stages.

better than the traditional clinical factors such as age (AUC = 0.554), gender (AUC = 0.588), grade (AUC = 0.614), AJCC stage (AUC = 0.447), T stage (AUC = 0.447), N stage (AUC = 0.512), and M stage (AUC = 0.467) (**Figure 4D**). In addition, the 3-year ROC curve analysis also suggested that the risk score AUC value (AUC = 0.639) was a superior prognostic factor for PDAC patients (**Figure 4E**).

Exanimating the Prediction Value of the m5C-Related LncRNA Risk Model

In order to predict the PDAC patient overall survival accurately, a nomogram was constructed to reveal the 1-, 3-, and 5-year survival rates based on the m5C-related lncRNAs expression risk scores together with clinicopathologic features (including age, gender, grade, T stage, M stage, and N stage) (**Figure 5A**). In addition, we used a calibration curve to compare the consistency of the actual and the predicted 1-, 1.5-, 2-, and 3-year patient survival. We found that the actual and the predicted line were almost in accordance within 3 years (**Figure 5B**). The above results proved that the nomogram we generated *via* m5C-related lncRNA prognostic risk scores was dependable. In addition, we randomly divided all the PDAC patients from TCGA into two subgroups (group A and B) in a 1:1 ratio and performed an internal validation for the m5C-related lncRNA risk model. The KM survival curve and 5-year ROC curve were examined in each subgroup. Our results showed that the patients with higher m5C-related lncRNA risk scores had shorter OS in group A (HR: 2.05, 95% CI: 1.13–3.71, p = 0.019) and the AUC value of the 5-year ROC curve was 0.814 (**Figures 5C, D**). The patients in group B had a similar OS trend (HR: 2.56, 95% CI: 1.44–4.56, p = 0.001) and the AUC value was 0.903 (**Figures 5E, F**). Moreover, the scatter dot plot also revealed an obvious difference expression of the screened lncRNAs in high- or low-risk groups, and the patient survival time was positively related with the risk scores in all the subgroups (**Supplementary Figure 3**). The above results demonstrated that the m5C-related lncRNA risk model was a reliable predictive factor for the PDAC patient.

Detecting LnRNA Expression *In Vitro* and Functional Enrichment Analysis

The m5C-related lncRNA expression profiles from the TCGA database indicated that AC022098.1, AL031775.1, AC005332.6, AC096733.3, AC025165.1, AC009974.1, and PAN3-AS1 were downregulated, and the CASC8 was overexpressed in PDAC. In order to examine the lncRNAs' expression level *in vitro*, three pancreatic cancer cell lines and a normal pancreatic duct cell line were used to perform the qRT-PCR experiments. The *in vitro* results were not completely consistent with the data from TCGA (**Figure 6A**). We found that CASC8 was upregulated in pancreatic

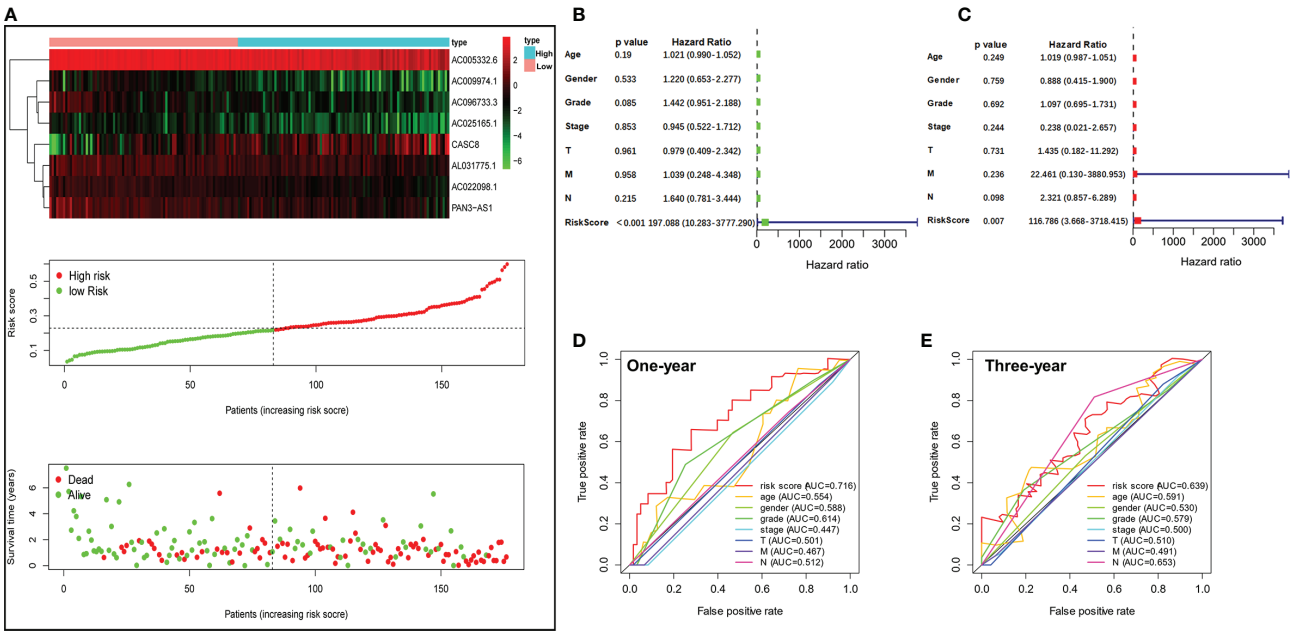

FIGURE 4 | Valuation of the m5C-related lncRNA risk model as an independent prognostic factor for PDAC. **(A)** Heatmap showed the differential expression of the 8 m5C-related lncRNAs in the high- or low-risk group. Scatter plot displayed risk score distribution of high-risk and low-risk PDAC patients based on the m5C-related lncRNA risk model and the relationship between survival time and PDAC patients risk score. **(B)** Univariate Cox regression analysis revealed the association between patients' survival and clinicopathological parameters along with m5C-related lncRNA risk score. **(C)** Multivariate Cox regression analysis uncovered that only the risk score (p = 0.009) was an independent prognostic factor for PDAC patients. **(D, E)** The 1-year **(D)** and 3-year **(E)** ROC analysis revealed the AUCs of m5C-related lncRNA risk score and other clinical characteristics.

cancer cells (Mia-PaCa-2, CFPAC-1, and Panc-1 cells) and AC096733.3 was in low expression compared with HPNE cells, which were with the same expression profile with TCGA data. AC096733.3, AC025165.1, PAN3-AS1, and AC009974.1 were downregulated in at least two cancer cell lines and may play as tumor suppressor genes in PDAC. The above results were partly consistent with the patients' OS analysis data from TCGA. However, AC022098.1 and AC005332.6 were suppressed in Mia-PaCa-2 and overexpressed in CFPAC-1, and their expression was inconsistent in different cells. In addition, AL031775.1 was only downregulated in Panc-1 cells. Hence, the underlying mechanisms that m5C-related lncRNAs regulating PDAC patient OS time still needs to be further explored. To seek the signal pathways that m5C-related lncRNAs might involve in the low- or high-risk groups, GSEA was performed. We found that the MTORC1 signaling pathway was activated in the high-risk group; nevertheless, MYOGENESIS and KRAS signaling pathways were activated in the low-risk group (**Figures 6B, C**). Furthermore, we summarized differential genes in the low- or high-risk groups to conduct GO and KEGG enrichment analysis. The top five GO enrichment biological processes were T-cell activation, Calcium ion homeostasis, Hormone transport, Modulation of chemical synaptic transmission, and Regulation of trans-synaptic signaling pathway (**Figures 6D–F**). Additionally, KEGG analysis revealed that several immune-related pathways were enriched such as Primary immunodeficiency, T-cell receptor signaling pathway, Leukocyte transendothelial migration, and Th1/Th2 cell differentiation (**Figures 6G, H**).

The Relationship Between m5C-Related LncRNAs and Tumor-Infiltrating Lymph Cells

We analyzed the differences of tumor microenvironment in the high- or low-risk groups. By using CIBERSORT tool with values of $p < 0.05$, a total of 22 tumor-infiltrating immune cells were screened (**Figure 7A**). The results demonstrated that naïve B cells, $CD8^{+}$T cells, regulatory T (Treg) cells, and resting NK cells exhibited a higher expression in the low-risk group ($p < 0.05$), whereas the M0 and M2 phenotype macrophages had a higher expression in the high-risk group. M2 phenotype macrophage has been proven as a co-carcinogenic factor in pancreatic cancer. Hence, m5C-related lncRNAs may promote M2 phenotype macrophage polarization or infiltration in PDAC. Additionally, we further detected the relationship between m5C-related lncRNAs and immune-related genes (LMTK3, LAG3, CD27, CD28, CD86, and BTLA), which indicated that most of the lncRNAs had statistical correlation with immune-related genes except AC025165.1 ($p < 0.05$) (**Figure 7B**). Gene expression analysis also showed that expression of the above immune-related genes are different in low- or high-risk groups (**Figure 7C**). Moreover, tumor microenvironment scores were performed to analyze the stromal and immune cell proportion in

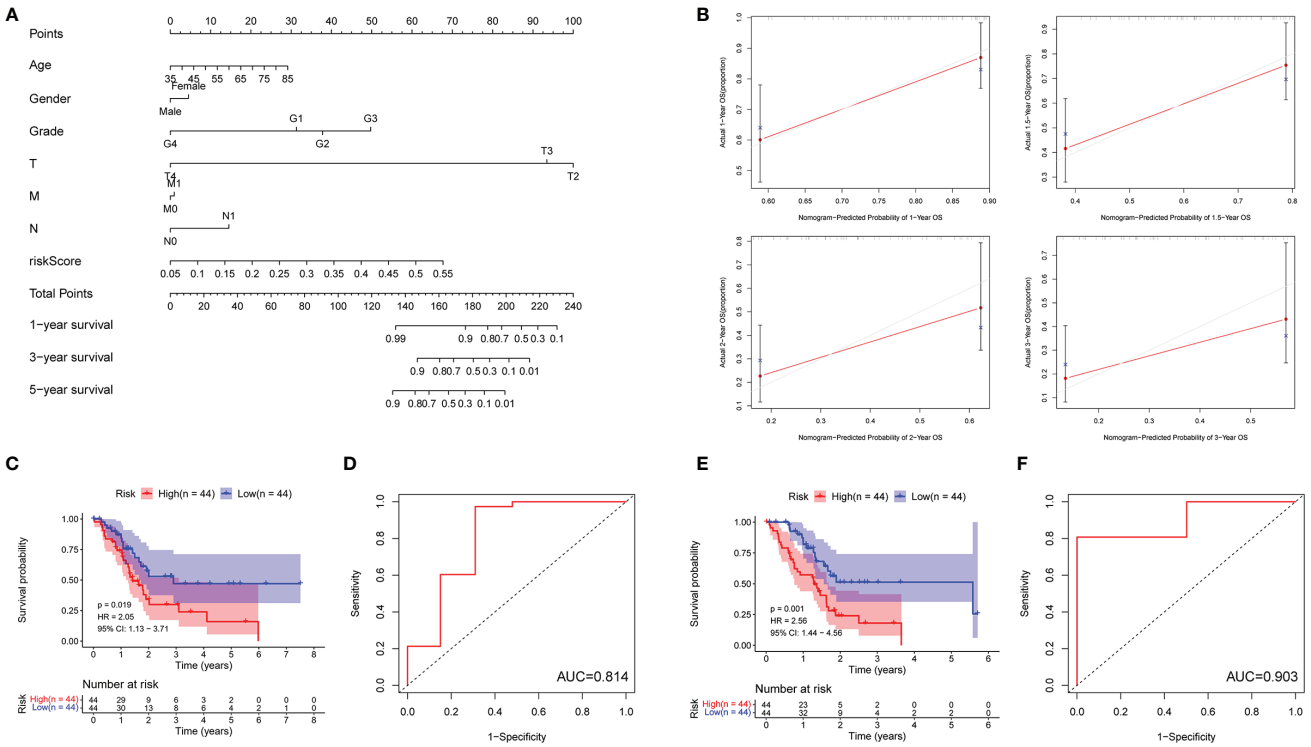

FIGURE 5 | Detecting the prediction value of the m5C-related lncRNA risk model. **(A)** The prediction of 1-, 3-, and 5-year survival for PDAC patients based on the prognostic nomogram derived from the m5C-related lncRNA risk score and other clinicopathologic feature. **(B)** Calibration curves illustrated the consistency between predicted and observed 1-, 1.5-, 2-, and 3-year survival rates in PDAC patients depending on the prognostic nomogram. **(C–F)** Overall survival and ROC analysis in subgroups (**C**, **D**: Group **A**; **E**, **F**: Group **B**).

the tumor environment *via* ESTIMATE R package. We obviously found that the PDAC tissues with low m5C-related lncRNA risk scores had higher immune scores, stromal scores, and overall ESTIMATE scores, which indicated that the PDAC in the low-risk group had lower pancreatic tumor proportion (**Figure 7D**). Lastly, we also investigated the association between the m5C-related lncRNA risk score and tumor lymph cells. Spearman's correlation analysis revealed that the risk score was positively related with 3 tumor-infiltrating lymph cells (NK cells, M0, and M2 phenotype macrophages), but was negatively correlated with regulatory T cells, $CD8^{+}$T cells, activated memory $CD4^{+}$T cells, naïve B cells, and plasma cells ($p < 0.05$) (**Figure 7E**). These outcomes revealed that the m5C-related risk scores could discriminate the different features of tumor-infiltrating lymph cells in PDAC.

DISCUSSION

Pancreatic cancer is an extremely malignant cancer, and its incidence is close to mortality rate. In recent years, although comprehensive treatments based on surgery have made some progress in the treatment of PDAC patients, the diagnosis and prognosis of PDAC are still unsatisfactory, and the survival rate is still less than 10%. Early diagnosis is the key to the treatment of pancreatic cancer (23). However, the etiology of pancreatic cancer is still unclear and there is a lack of effective biomarkers for early diagnosis. Therefore, it is urgent to explore the genetic or epigenetic factors of the occurrence and development of pancreatic cancer to identify new therapeutic targets or biomarkers.

RNA methylation is one of the most important epigenetic modification in RNA post-transcriptional regulation and has been a research frontier and hotspot recently. RNA methylation includes several types such as m6A, m1A, m5C, m7G, and Nm, among which RNA m5C methylation refers to the modification of the fifth cytosine of RNA by methylation (24–26). At present, relevant studies have shown that RNA m5C methylation widely existed in cells and played an important role in various physiological and pathological processes (27–29). In this study, we downloaded 177 PDAC patients' gene expression profiles from the TCGA database and constructed an 8-m5C-related lncRNA risk model. As far as we know, this is the first prognostic analysis of the m5C regulator-related lncRNAs in PDAC.

Long non-coding RNAs are more than 200 nucleotides, which were initially considered as "junk sequence" without specific biological functions. However, recent reports have proved that lncRNAs were widely expressed in human cells and closely related to the occurrence and development of tumors, which

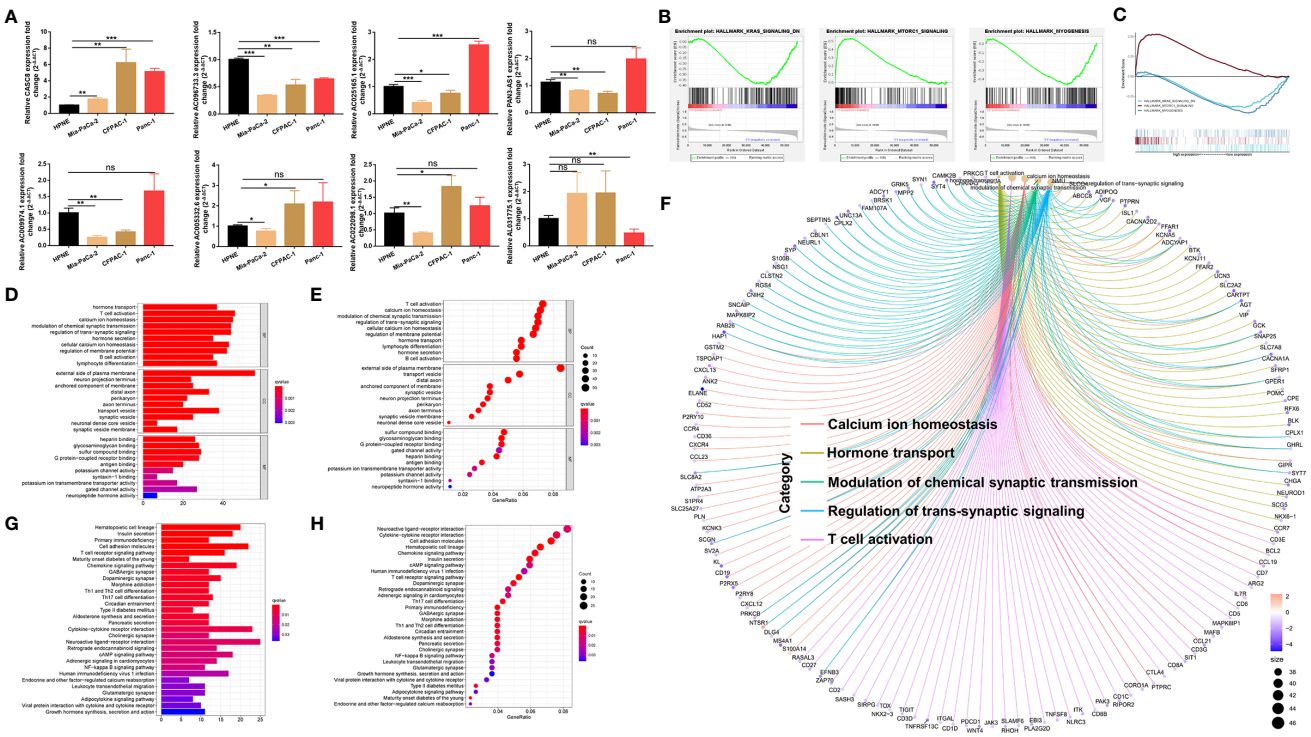

FIGURE 6 | Validating the expression level of the m5C related lncRNAs *in vitro* and functional enrichment analysis. **(A)** qRT-PCR experiments were performed to detect the expression of the 8 m5C related lncRNAs in HPNE cells and three pancreatic cancer cells respectively. **(B, C)** GSEA results showed significant enrichment signaling pathways in the high-and low-risk groups. **(D–F)** GO analysis was performed to detect biological processes that involved in the high-or low-risk groups. **(G, H)** KEGG pathway analysis results indicated the enriched signaling pathways associated with the m5C related lncRNAs risk scores. ns, not significant, *P < 0.05, **P < 0.01, ***P < 0.001.

suggested that lncRNAs may be potential prognostic markers and therapeutic targets for malignant tumors (30). In addition, lncRNAs could regulate tumor growth in several ways including *in situ* regulation and molecular sink, combining with protein and molecular scaffold. Among them, the most essential way was regulating related gene expression (31, 32). Hence, we focused on the lncRNAs that had co-expression relationship with m5C regulators in PDAC and used bioinformatic and statistical methods to generate a prognostic risk model for PDAC.

In our research, we compared the expression of 13 m5C regulator genes in pancreatic cancer and normal tissues *via* the GEPIA online tool and identified a total of 242 m5C-related lncRNAs depending on the co-expression relationship. Furthermore, we analyzed the PDAC patients' clinical information together with gene transcriptome data downloaded from TCGA. Finally, 17 prognostic m5C-related lncRNAs were detected and all the prognostic m5C-related lncRNA expression was significantly different between pancreas normal and tumor tissues. In addition, LASSO regression was performed, and we constructed an 8-m5C-related lncRNA risk model and separated all the 177 PDAC patients into high- and low-risk groups based on the risk scores. The PCA and patients' overall survival analysis confirmed that the 8-m5C-related lncRNA risk model could predict PDAC patient prognosis effectively. Typically, clinicians would make a rough judgment on PDAC patients' long-term survival based on clinical indicators such as general patient profile, pancreatic tumor size, invasion of peripheral blood vessels and nerves, presence of metastasis, and tumor pathological type. However, with advances in cancer gene research technology, scientists began to pay more attention to the changes in gene expression levels during tumor progression (33, 34). In our work, univariate and multivariate Cox regression analysis indicated that the risk scores depending on the m5C-related lncRNAs expression were the independent risk factor for PDAC and better than traditional indexes including age, tumor grade, and stage on predicting patient survival rate. The currently constructed PDAC prognostic risk model mainly focused on a single molecular biomarker. However, only one biomarker could not work as a precise tumor biomarker in clinical diagnosis such as the typical PDAC biomarker CA19-9 that was not aberrant in every PDAC patient. It has been reported that lncRNAs could be released in serum, saliva, and urine (35). Hence, it has the potential to be a stable biomarker in human blood or other body fluid. A lot of studies have demonstrated that lncRNAs could work as a new type of biomarker in several malignant tumors including hepatocellular carcinoma, breast cancer, lung cancer, and pancreatic cancer (36). Nevertheless, our research was the first

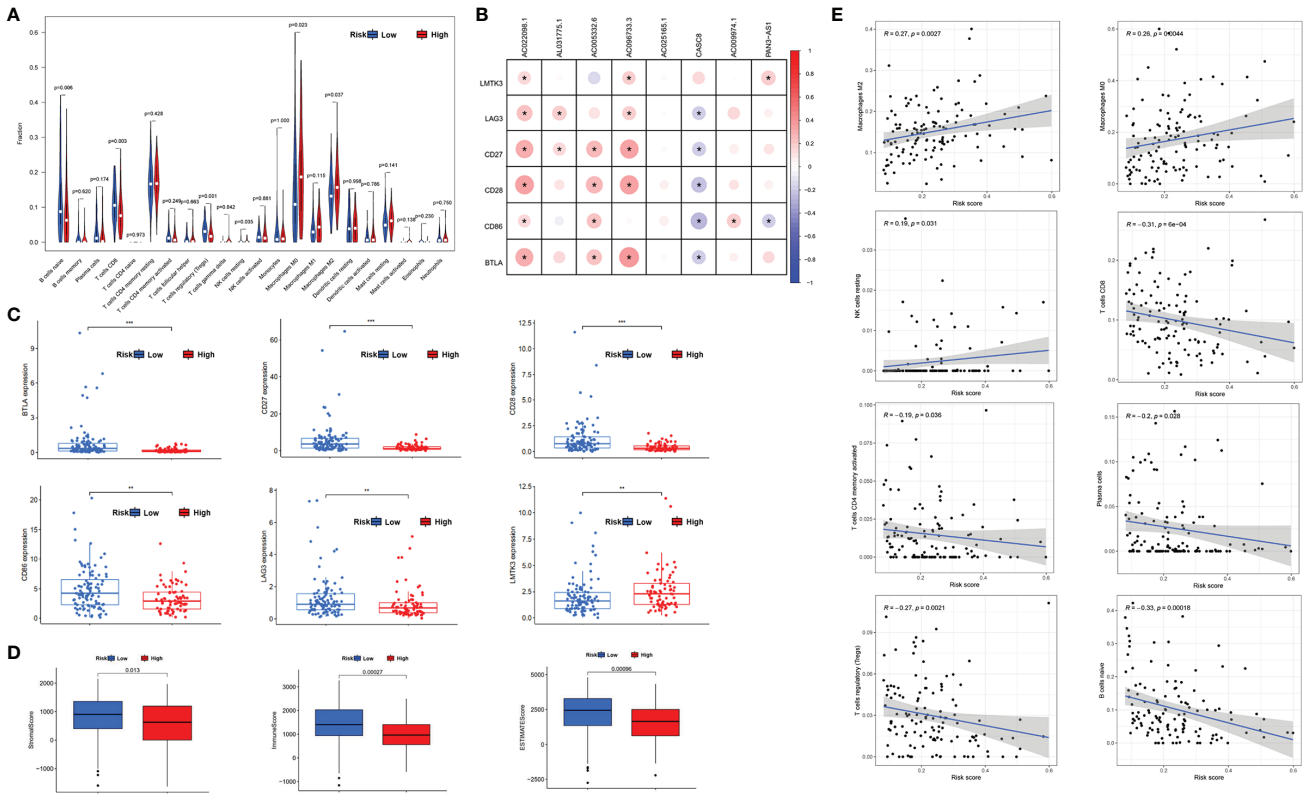

FIGURE 7 | The relationship between m5C-related lncRNAs and tumor-infiltrating lymph cells. **(A)** Violet plot showed the 22 tumor-infiltrating lymph cells distribution in PDAC patients with different m5C-related lncRNA risk scores. **(B)** The connection between the immune associated genes and the selected m5C-related lncRNAs. **(C)** Scatter diagram revealed the expression of immune-related genes in low- or high-risk groups, respectively. **(D)** Box plots indicated the proportion of stromal and immune cells in PDAC tissues *via* ESTIMATE R package method. **(E)** Correlation between the lymph cells and m5C-related lncRNA risk scores. $^{*}p < 0.05$, $^{**}p < 0.01$, $^{***}p < 0.001$.

study to report an 8-prognostic m5C-related lncRNA risk model and validated that the prognostic risk model could predict PDAC patients' OS accurately. In our research, 8 m5C-related lncRNAs were carefully chosen *via* a bioinformatic method, 7 of which have never been previously studied in PDAC (AC022098.1, AL031775.1, AC005332.6, AC096733.3, AC025165.1, AC009974.1, and PAN3-AS1). Only the CASC8 has been reported in the multiple malignant tumor such as colorectal cancer, lung cancer, and hepatocellular carcinoma (37–39). We checked the above lncRNA expression in the human pancreatic ductal cell line and three pancreatic cancer cell lines. The results showed that CASC8 was overexpressed in all pancreatic cancer lines, which indicated that CACS8 may also play a key role in promoting pancreatic cancer progression.

Recent research showed that m5C-related genes could regulate tumor immune microenvironment in breast cancer (40). LncRNAs are also known to be involved in regulating tumor-infiltrating lymph cells in malignant tumors (41).

In our study, we carefully evaluated the relationship between m5C-related lncRNAs and PDAC-infiltrating immune cells. Our results exhibited that the distribution of tumor-infiltrating immune cells in PDAC were different in high- or low-risk groups. The immune scores and stromal scores of the high-risk group were also lower than the low-risk group. We found that naïve B cells, CD8+T cells, Treg cells, and resting NK cells had a higher expression level in the low-risk group. CD8+T cells, Treg cells, and NK cells were considered as tumor suppressors in malignant tumors. In pancreatic cancer, the depletion of Treg cells made the abnormal distribution of fibroblast, which could recruit myeloid cells and restore the immune suppression environment *via* secreting multiple cell chemokine including CCL3, CCL6, and CCL8 (42). In addition, the M0 and M2 phenotype macrophages had a higher expression level in the high-risk group. Based on the previous study, M2 phenotype macrophage has been proven as a co-carcinogenic factor in pancreatic cancer (43). Therefore, m5C-related lncRNAs may regulate pancreatic cancer progression *via* promoting M2 phenotype macrophage polarization or infiltration in PDAC. As we know, there were no published reports about detecting the potential function of m5C-related lncRNAs in regulating the distribution of tumor-infiltrating lymph cells in PDAC at present.

However, there are still some limitations in our study. For example, all the PDAC patients' transcriptome expression data

and clinical information were downloaded and analyzed from the TCGA database or GEPIA online database. We only evaluated the m5C-related lncRNA risk model *via* internal validation, lacking external database validation. Nevertheless, we tried to download the PDAC patients' information from ICGC (International Cancer Genome Consortium) or GEO database, but the corresponding risk scores could not be calculated due to the lack of expression data of the selected m5C-related lncRNAs in these databases. In addition, we only detected the screened m5C-related lncRNA expression *in vitro*, and the *in vivo* experiments and PDAC patients' tumor tissue validation should still be performed in the future to make the prediction results more reliable. Moreover, the nomogram we constructed only calibrated within 3 years, because of the small number of PDAC patients and the lack of T1 stage patients, which suggested that our findings need further validation in larger PDAC patient follow-up cohorts. Additionally, there was a lack of molecular mechanism research in our study. Identifying which m5C-related lncRNAs could regulate pancreatic cancer survival is just the beginning. We will explore the specific mechanism of the screened lncRNAs that affected PDAC progression in our next work.

CONCLUSION

We constructed an 8-m5C-related lncRNA prognostic risk model for PDAC patients based on the transcriptome expression and clinical data from TCGA. The m5C-related lncRNA risk model was proved to have an independent prognostic value and provided an accurate survival prediction for PDAC patients. In addition, our research also offered us a better understanding of the regulation of tumor-infiltrating lymph cells in PDAC. In brief, the m5C-related lncRNA risk model may provide us the potential biomarkers or treatment targets for PDAC.

DATA AVAILABILITY STATEMENT

The datasets presented in this study can be found in online repositories. The names of the repository/repositories and accession number(s) can be found in the article/**Supplementary Material**.

ETHICS STATEMENT

All the patient's raw data in our study were downloaded from TCGA, so there are no ethical issues and other conflicts of interest. The patients/participants provided their written informed consent to participate in this study.

AUTHOR CONTRIBUTIONS

HY, JL, and LZ summarized and analyzed the TCGA patients' data. HY and PW drafted the manuscript. KJ and BX designed and monitored the research. All authors contributed to the article and approved the submitted version.

FUNDING

This research was funded by the National Natural Science Foundation of China (Nos. 82072706 and 81871980) and Jiangsu Key Medical Discipline (General Surgery, ZDXKA2016005).

ACKNOWLEDGMENTS

We acknowledge TCGA as a public database, which provided relevant data for free for research.

SUPPLEMENTARY MATERIAL

The Supplementary Material for this article can be found online at: https://www.frontiersin.org/articles/10.3389/fimmu.2021.800268/full#supplementary-material

Supplementary Figure 1 | Detecting the expression of m5C regulators *via* GEPIA online database. *P < 0.05.

Supplementary Figure 2 | The overall survival in other clinical factors subgroups.

Supplementary Figure 3 | Heatmaps showed the differential expression of the 8 m5C-related lncRNAs in subgroups. Scatter plot revealed the risk score location of high-risk and low-risk PDAC patients and the relationship between survival time and risk score in subgroups (**A**: Group **A**; **B**: Group **B**).

REFERENCES

1. Vincent A, Herman J, Schulick R, Hruban RH, Goggins M. Pancreatic Cancer. *CA Cancer J Clin* (2011) 378:607–20. doi: 10.1016/S0140-6736(10)62307-0
2. Siegel RL, Miller KD, Fuchs HE, Jemal A. Cancer Statistics, 2021. *CA Cancer J Clin* (2021) 71:7–33. doi: 10.3322/caac.21654
3. Schizas D, Charalampakis N, Kole C, Economopoulou P, Koustas E, Gkotsis E, et al. Immunotherapy for Pancreatic Cancer: A 2020 Update. *Cancer Treat Rev* (2020) 86:102016. doi: 10.1016/j.ctrv.2020.102016
4. Jain T, Dudeja V. The War Against Pancreatic Cancer in 2020 - Advances on All Fronts. *Nat Rev Gastroenterol Hepatol* (2021) 18:99–100. doi: 10.1038/s41575-020-00410-4
5. Kaliman P. Epigenetics and Meditation. *Curr Opin Psychol* (2019) 28:76–80. doi: 10.1016/j.copsyc.2018.11.010
6. Kanwal R, Gupta K, Gupta S. Cancer Epigenetics: An Introduction. *Methods Mol Biol (Clifton NJ)* (2015) 1238:3–25. doi: 10.1007/978-1-4939-1804-1_1
7. Ma S, Chen C, Ji X, Liu J, Zhou Q, Wang G, et al. The Interplay Between M6a RNA Methylation and Noncoding RNA in Cancer. *J Hematol Oncol* (2019) 12:121. doi: 10.1186/s13045-019-0805-7
8. He L, Li H, Wu A, Peng Y, Shu G, Yin G. Functions of N6-Methyladenosine and its Role in Cancer. *Mol Cancer* (2019) 18:176. doi: 10.1186/s12943-019-1109-9
9. Chellamuthu A, Gray SG. The RNA Methyltransferase NSUN2 and Its Potential Roles in Cancer. *Cells* (2020) 9. doi: 10.3390/cells9081758
10. Nombela P, Miguel-López B, Blanco S. The Role of M(6)A, M(5)C and Ψ RNA Modifications in Cancer: Novel Therapeutic Opportunities. *Mol Cancer* (2021) 20:18. doi: 10.1186/s12943-020-01263-w

11. Chen X, Li A, Sun BF, Yang Y, Han YN, Yuan X, et al. 5-Methylcytosine Promotes Pathogenesis of Bladder Cancer Through Stabilizing mRNAs. *Nat Cell Biol* (2019) 21:978–90. doi: 10.1038/s41556-019-0361-y
12. Yang R, Liang X, Wang H, Guo M, Shen H, Shi Y, et al. The RNA Methyltransferase NSUN6 Suppresses Pancreatic Cancer Development by Regulating Cell Proliferation. *EBioMedicine* (2021) 63:103195. doi: 10.1016/j.ebiom.2020.103195
13. Yu X, Zhang Q, Gao F, Zhang M, Zheng Q, He Y, et al. Predictive Value of M5c Regulatory Gene Expression in Pancreatic Adenocarcinoma. *Sci Rep* (2021) 11:17529. doi: 10.1038/s41598-021-96470-w
14. Pan J, Huang Z, Xu Y. M5c-Related lncRNAs Predict Overall Survival of Patients and Regulate the Tumor Immune Microenvironment in Lung Adenocarcinoma. *Front Cell Dev Biol* (2021) 9:671821. doi: 10.3389/fcell.2021.671821
15. Qian X, Zhao J, Yeung PY, Zhang QC, Kwok CK. Revealing lncRNA Structures and Interactions by Sequencing-Based Approaches. *Trends Biochem Sci* (2019) 44:33–52. doi: 10.1016/j.tibs.2018.09.012
16. Bridges MC, Daulagala AC, Kourtidis A. LNCcation: lncRNA Localization and Function. *J Cell Biol* (2021) 220. doi: 10.1083/jcb.202009045
17. Sun T, Wu Z, Wang X, Wang Y, Hu X, Qin W, et al. LNC942 Promoting METTL14-Mediated M(6)A Methylation in Breast Cancer Cell Proliferation and Progression. *Oncogene* (2020) 39:5358–72. doi: 10.1038/s41388-020-1338-9
18. Arneth B. Tumor Microenvironment. *Medicina (Kaunas Lithuania)* (2019) 56 (1):15. doi: 10.3390/medicina56010015
19. Hinshaw DC, Shevde LA. The Tumor Microenvironment Innately Modulates Cancer Progression. *Cancer Res* (2019) 79:4557–66. doi: 10.1158/0008-5472.CAN-18-3962
20. Huang JK, Ma L, Song WH, Lu BY, Huang YB, Dong HM, et al. LncRNA-MALAT1 Promotes Angiogenesis of Thyroid Cancer by Modulating Tumor-Associated Macrophage FGF2 Protein Secretion. *J Cell Biochem* (2017) 118:4821–30. doi: 10.1002/jcb.26153
21. Xu M, Xu X, Pan B, Chen X, Lin K, Zeng K, et al. LncRNA SATB2-AS1 Inhibits Tumor Metastasis and Affects the Tumor Immune Cell Microenvironment in Colorectal Cancer by Regulating SATB2. *Mol Cancer* (2019) 18:135. doi: 10.1186/s12943-019-1063-6
22. Wei C, Liang Q, Li X, Li H, Liu Y, Huang X, et al. Bioinformatics Profiling Utilized a Nine Immune-Related Long Noncoding RNA Signature as a Prognostic Target for Pancreatic Cancer. *J Cell Biochem* (2019) 120:14916–27. doi: 10.1002/jcb.28754
23. Lin QJ, Yang F, Jin C, Fu DL. Current Status and Progress of Pancreatic Cancer in China. *World J Gastroenterol* (2015) 21:7988–8003. doi: 10.3748/wjg.v21.i26.7988
24. Mongan NP, Emes RD, Archer N. Detection and Analysis of RNA Methylation. *F1000Research* (2019) 26:8. doi: 10.12688/f1000research.17956.1
25. Traube FR, Carell T. The Chemistries and Consequences of DNA and RNA Methylation and Demethylation. *RNA Biol* (2017) 14:1099–107. doi: 10.1080/15476286.2017.1318241
26. Xie S, Chen W, Chen K, Chang Y, Yang F, Lin A, et al. Emerging Roles of RNA Methylation in Gastrointestinal Cancers. *Cancer Cell Int* (2020) 20:585. doi: 10.1186/s12935-020-01679-w
27. Li Q, Li X, Tang H, Jiang B, Dou Y, Gorospe M, et al. NSUN2-Mediated M5c Methylation and METTL3/METTL14-Mediated M6a Methylation Cooperatively Enhance P21 Translation. *J Cell Biochem* (2017) 118:2587–98. doi: 10.1002/jcb.25957
28. Bohnsack KE, Höbartner C, Bohnsack MT. Eukaryotic 5-Methylcytosine (M^5C) RNA Methyltransferases: Mechanisms, Cellular Functions, and Links to Disease. *Genes* (2019) 10(2):102. doi: 10.3390/genes10020102
29. Zhao BS, Roundtree IA, He C. Post-Transcriptional Gene Regulation by mRNA Modifications. *Nat Rev Mol Cell Biol* (2017) 18:31–42. doi: 10.1038/nrm.2016.132
30. Nandwani A, Rathore S, Datta M. LncRNAs in Cancer: Regulatory and Therapeutic Implications. *Cancer Lett* (2021) 501:162–71. doi: 10.1016/j.canlet.2020.11.048
31. Gil N, Ulitsky I. Regulation of Gene Expression by Cis-Acting Long Non-Coding RNAs. *Nat Rev Genet* (2020) 21:102–17. doi: 10.1038/s41576-019-0184-5
32. Kopp F, Mendell JT. Functional Classification and Experimental Dissection of Long Noncoding RNAs. *Cell* (2018) 172:393–407. doi: 10.1016/j.cell.2018.01.011
33. Best MG, Wesseling P, Wurdinger T. Tumor-Educated Platelets as a Noninvasive Biomarker Source for Cancer Detection and Progression Monitoring. *Cancer Res* (2018) 78:3407–12. doi: 10.1158/0008-5472.CAN-18-0887
34. Soria F, Krabbe LM, Todenhöfer T, Dobruch J, Mitra AP, Inman BA, et al. Molecular Markers in Bladder Cancer. *World J Urol* (2019) 37:31–40. doi: 10.1007/s00345-018-2503-4
35. Chandra Gupta S, Nandan Tripathi Y. Potential of Long Non-Coding RNAs in Cancer Patients: From Biomarkers to Therapeutic Targets. *Int J Cancer* (2017) 140:1955–67. doi: 10.1002/ijc.30546
36. Li Y, Jiang T, Zhou W, Li J, Li X, Wang Q, et al. Pan-Cancer Characterization of Immune-Related lncRNAs Identifies Potential Oncogenic Biomarkers. *Nat Commun* (2020) 11:1000. doi: 10.1038/s41467-020-14802-2
37. Jiang X, Guan J, Xu Y, Ren H, Jiang J, Wudu M, et al. Silencing of CASC8 Inhibits Non-Small Cell Lung Cancer Cells Function and Promotes Sensitivity to Osimertinib *via* FOXM1. *J Cancer* (2021) 12:387–96. doi: 10.7150/jca.47863
38. Haerian MS, Haerian BS, Molanaei S, Kosari F, Sabeti S, Bidari-Zerehpoosh F, et al. Lack of Association of CASC8 Rs1447295 With Colorectal Cancer in Iranian Population: A Multicenter Case-Control Study. *Gene* (2017) 634:74–6. doi: 10.1016/j.gene.2017.08.042
39. Wu ER, Hsieh MJ, Chiang WL, Hsueh KC, Yang SF, Su SC. Association of lncRNA CCAT2 and CASC8 Gene Polymorphisms With Hepatocellular Carcinoma. *Int J Environ Res Public Health* (2019) 16(16):2833. doi: 10.3390/ijerph16162833
40. Huang Z, Pan J, Wang H, Du X, Xu Y, Wang Z, et al. Prognostic Significance and Tumor Immune Microenvironment Heterogenicity of M5c RNA Methylation Regulators in Triple-Negative Breast Cancer. *Front Cell Dev Biol* (2021) 9:657547. doi: 10.3389/fcell.2021.657547
41. Sun J, Zhang Z, Bao S, Yan C, Hou P, Wu N, et al. Identification of Tumor Immune Infiltration-Associated lncRNAs for Improving Prognosis and Immunotherapy Response of Patients With Non-Small Cell Lung Cancer. *J Immunother Cancer* (2020) 8(1):e000110. doi: 10.1136/jitc-2019-000110
42. Zhang Y, Lazarus J, Steele NG, Yan W, Lee HJ, Nwosu ZC, et al. Regulatory T-Cell Depletion Alters the Tumor Microenvironment and Accelerates Pancreatic Carcinogenesis. *Cancer Discov* (2020) 10:422–39. doi: 10.1158/2159-8290.CD-19-0958
43. Yang J, Li Y, Sun Z, Zhan H. Macrophages in Pancreatic Cancer: An Immunometabolic Perspective. *Cancer Lett* (2021) 498:188–200. doi: 10.1016/j.canlet.2020.10.029

Conflict of Interest: The authors declare that the research was conducted in the absence of any commercial or financial relationships that could be construed as a potential conflict of interest.

Publisher's Note: All claims expressed in this article are solely those of the authors and do not necessarily represent those of their affiliated organizations, or those of the publisher, the editors and the reviewers. Any product that may be evaluated in this article, or claim that may be made by its manufacturer, is not guaranteed or endorsed by the publisher.

frontiers in Immunology

REVIEW
published: 15 December 2021
doi: 10.3389/fimmu.2021.792781

Combination of Ablation and Immunotherapy for Hepatocellular Carcinoma: Where We Are and Where to Go

Kunpeng Wang[1], Cong Wang[2], Hao Jiang[1], Yaqiong Zhang[3], Weidong Lin[1], Jinggang Mo[1] and Chong Jin[1]**

[1] Department of General Surgery, Taizhou Central Hospital (Taizhou University Hospital), Taizhou, China, [2] Department of General Surgery, Second Xiangya Hospital, Central South University, Changsha, China, [3] Department of Clinical Laboratory, Taizhou Central Hospital (Taizhou University Hospital), Taizhou, China

OPEN ACCESS

Edited by:
Xuesong Gu,
Beth Israel Deaconess Medical Center and Harvard Medical School, United States

Reviewed by:
James Ahodantin,
University of Maryland, Baltimore, United States
Antonio Facciorusso,
University of Foggia, Italy

***Correspondence:**
Chong Jin
jinc@tzzxyy.com
Jinggang Mo
mojg@tzzxyy.com

Specialty section:
This article was submitted to Cancer Immunity and Immunotherapy, a section of the journal Frontiers in Immunology

Received: 11 October 2021
Accepted: 25 November 2021
Published: 15 December 2021

Citation:
Wang K, Wang C, Jiang H, Zhang Y, Lin W, Mo J and Jin C (2021) Combination of Ablation and Immunotherapy for Hepatocellular Carcinoma: Where We Are and Where to Go. Front. Immunol. 12:792781. doi: 10.3389/fimmu.2021.792781

Hepatocellular carcinoma (HCC) is the third leading cause of cancer-related deaths worldwide and is increasing in incidence. Local ablative therapy plays a leading role in HCC treatment. Radiofrequency (RFA) is one of the first-line therapies for early local ablation. Other local ablation techniques (e.g., microwave ablation, cryoablation, irreversible electroporation, phototherapy.) have been extensively explored in clinical trials or cell/animal studies but have not yet been established as a standard treatment or applied clinically. On the one hand, single treatment may not meet the needs. On the other hand, ablative therapy can stimulate local and systemic immune effects. The combination strategy of immunotherapy and ablation is reasonable. In this review, we briefly summarized the current status and progress of ablation and immunotherapy for HCC. The immune effects of local ablation and the strategies of combination therapy, especially synergistic strategies based on biomedical materials, were discussed. This review is hoped to provide references for future researches on ablative immunotherapy to arrive to a promising new era of HCC treatment.

Keywords: hepatocellular carcinoma, ablation, immunotherapy, synergistic therapy, multifunctional nanoplatform, nanomedicine

INTRODUCTION

Primary liver cancer is one of the most common malignant tumors in the digestive system and the third leading cause of cancer-related deaths (1). Hepatocellular carcinoma (HCC), which comprises ~90% of cases, is the most common type of primary liver cancer. The management of HCC lies on the Barcelona Clinic Liver Cancer (BCLC) staging system. Most clinical practices guidelines recommend resection, thermal ablation and transplantation for patients with early HCC (BCLC 0, A), whereas transarterial chemoembolization (TACE) and systemic therapies are preferred for patients with intermediate (BCLC B) and advanced (BCLC C) HCCs, respectively (2–5). Surgical resection and transplantation could offer the best chance for a cure in early HCC, but not all patients with early-stage HCC, especially those with cirrhosis, benefit from these treatments. Liver function

and portal hypertension are the fatal selection criteria of resection, because 80%-90% HCCs develop from cirrhosis (6). Moreover, the recurrence rate after HCC resection reaches as high as 68% (7). Scientists and surgeons have exerted much effort into the removal of tumors (8). However, this task is still an insurmountable mountain, because HCC cannot be considered a local disease even in the early stage. The outcomes of liver transplantation are superior to that of hepatic resection. However, organ shortage, long waiting time, and high cost are deterred, except for the strict transplantation indication. Locoregional ablative therapy including radiofrequency ablation (RFA) and microwave ablation (MWA), is a potentially curative strategy for early HCC, coming into sight. The advent of the genomic era, as well as the increase in the understanding of the role of immunity in HCC progression, support targeted therapy and immunotherapy. The combination of ablative therapy and immunotherapy has been a subject of recent clinical and basic researches. Herein, we summarized ablative therapy and immunotherapy for HCC, discussed their synergistic anti-tumor effects, and envisaged the current trends and future prospects of their combination.

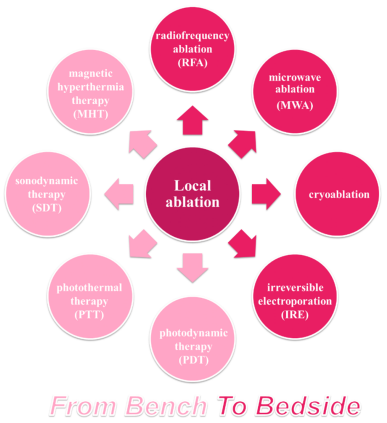

FIGURE 1 | Overview of ablative techniques for HCC. Ablative strategy has occupied an important position among HCC therapies, based on thermal or non-thermal tumor destruction. RFA, the most common ablation technique applied for patients with HCC, has been developed as a standard treatment, while other ablative techniques have been explored in clinical or preclinical researches.

ABLATION THERAPY

Thermal ablation, demonstrates similar outcomes as hepatic resection in early HCC (tumors size < 2–3 cm) (9, 10). Other ablation therapies, such as cryoablation, have not established a standard clinic procedure and are therefore less used. In recent years, photodynamic therapy (PDT), photothermal therapy (PTT), magnetic hyperthermia therapy (MHT), and irreversible electroporation (IRE) have shown potential applications in HCC with the prevalence of biomaterials in medicine. The major mechanism of ablative therapies is to induce irreversible thermal (i.e., RFA, MWA, and PTT) or non-thermal tumor destruction (i.e., IRE and PDT) *via* electromagnetic or light energy. This section gives a brief retrospect of traditional ablative therapies for HCC, as well as novel ablative techniques (**Figure 1**), and discusses their immunological effects.

Clinical Applications

RFA, a standard ablative and first-line therapy for small-sized HCC, is more cost-effective than hepatic resection (10). RFA can achieve tumor necrosis at 375–480 kHz and > 60°C (11). However, traditional monopolar RFA is limited in tumors less than 2–3 cm or near vessels due to heat sink effect, which is also related to recurrence (12). Novel techniques are developed to improve ablation efficacy. No-touch multibipolar RFA can be used to tumors up to 5 cm with similar disease-free survival (DFS) and overall survival (OS) rates compared with resection (13). However, insufficient RFA (iRFA) is one of the major reasons for recurrence after RFA. iRFA could lead to HCC with a more aggressive phenotype, drug resistance and worse prognosis (**Table 1**). The ablative margin assessed by computed tomography (CT) after RFA can be an important predictor of local tumor progression (LTP) and overall recurrence. A study indicated that insufficient ablative margin (<5 mm) was associated with higher rates of LTP and overall recurrence in HCC, but the sensitivity values were only 36.4% and 46.2%, respectively (26). iRFA could promote the proliferation, migration, invasion, epithelial-mesenchymal transition (EMT), and angiogenesis of residual tumors through the transcriptional and epigenetic regulation. Some signaling pathways associated with tumor growth and progression, such as the Akt signaling pathway involved in cellular proliferation, survival and angiogenesis are activated after iRFA (20, 22, 24, 25).

Several strategies have been used to counter iRFA. One of which is to improve the accuracy of imaging guidance for the specific identification of tumor boundaries, especially with the application of nanotechnology. Jiang and colleagues developed a nanobubble conjugated with colony-stimulating factor 1 receptor (CSF-1R), called NBCSF-1R, for HCC margin detection (27). NBCSF-1R provided a non-invasive effective ultrasound imaging capabilities for evaluating therapy response of RFA through the high specificity targeting of CSF-1R-overexpressing macrophages and HCC tumor margin. Another strategy is the combination therapy for salvage. For instance, sorafenib and IFN-α combined with herbal compound inhibited the EMT of HCC cells after iRFA (28, 29); bevacizumab inhibited the tumor growth and angiogenesis induced by iRFA (30); and CTLA-4 blockade suppressed the growth of residual tumors and improved survival in a subcutaneous murine HCC model (31). Other agents include metformin (32) and hydroxychloroquine (HCQ) (33). However, one study demonstrated that ATPase inhibitory factor 1 (IF1) increased HCC cells' resistance to sorafenib after iRFA (16). These results indicated that the application of systemic therapy or immunotherapy could cope with the adverse impacts of iRFA but the choice of agents could be limited by iRFA-induced resistance.

TABLE 1 | Mechanisms of phenotype changes after iRFA.

Objects	Phenotypes	Mechanisms	Years	Refs.
HepG2 and MHCC97 cell lines and HCC patient-derived xenograft mouse model	Promoted cell viability and metastasis	m^6 A-YTHDF1-EGFR axis	2021	(14)
Tumor-associated endothelial cell (TAEC), platelet, HepG2 and SMMC7721 cell lines, and orthotopic tumor mouse model	Enhanced TAEC permeability; activated platelets *in vitro*; and promoted tumor growth, metastasis and endothelial permeability *in vivo*	Upregulation of vascular endothelial-cadherin and ICAM-1	2021	(15)
Hep3B and Huh7 cell lines	Enhanced colony formation, migration, EMT, and angiogenesis; increased resistance to sorafenib	IF1 overexpression and NF-κB activation	2020	(16)
Huh7 cell line, xenograft nude mouse model, and liver metastasis model by tail vein injection	Facilitated cell growth and metastasis *in vitro* and *in vivo*	ceRNA mechanism: ASMTL-AS1/miR-342-3p/NLK/YAP axis	2020	(17)
Huh7 and MHCC97 cell lines	Promoted cell proliferation, migration, invasion, epithelial-mesenchymal transition, and stemness	ceRNA mechanism: GAS6-AS2/miR-3619-5p/ARL2 axis	2020	(18)
HepG2 cell line	Enhanced cell proliferation, colony formation, and migration	c-Met overexpression and MAPK signal pathway activation	2020	(19)
HCCLM3 cell line, xenograft nude mouse model	Induced tumor growth, EMT changes, and metastasis *in vitro* and *in vivo*	Flotillin-1/2 overexpression and Akt/Wnt/β-catenin signaling pathway activation	2019	(20)
HepG2 and SMMC7721 cell lines	Increased cell proliferation, migration, invasion and autophagy *in vitro*	HIF-1α/BNIP3 pathway	2019	(21)
HCCLM3 and HepG2 cell lines, orthotopic nude mouse model	Promoted lung and intrahepatic residual tumor cells *in vivo* and promoted cell migration and invasion *in vitro*	ITGB3 overexpression and FAK/PI3K/AKT signaling pathway activation	2017	(22)
HCCLM3 and HepG2 cell lines, orthotopic nude mouse model	Changed cellular morphology, motility, metastasis, and EMT *in vitro* and *in vivo*	β-catenin signaling activation	2014	(23)
SMMC7721 and Huh7 cell lines, ectopic nude mouse model, and metastasis model by tail vein injection	Enhanced cell proliferation, migration, invasion, and EMT *in vitro*; increased tumor size and lung metastasis *in vivo*	Akt and ERK signaling pathways	2013	(24)
TAEC, HepG2 and HCCLM3 cell lines	Inhibited TAECs proliferation, enhanced TAECs migration and tube formation (angiogenesis); and promoted HCC cell invasiveness	Activation of Akt, ERK1/2 and NF-κB signaling pathways and inhibition of STAT3 signaling pathways	2012	(25)

MWA could provide higher temperature with expanded ablation zone and shorter ablation time because of its higher frequency (900–2,450 MHz) (11). A recent study showed that MWA provided more excellent tumor control than RFA for patients with perivascular HCC (34, 35). In addition, a meta-analysis of randomized-controlled trials demonstrated that MWA seemed to benefit disease-free survivals at 5 years compared with RFA (36). New microwave thermosphere ablation (MTA) may provide a safer and more effective ablation with shorter time than RFA with the developments of novel MWA systems (37).

Cryoablation is also a thermal technique that could be more effective and safer for tumors not suitable for RFA or MWA, such as perivascular HCC. The goal of cryoablation is to destroy tumor tissue by alternating freezing and thawing on the basis of the Joule-Thomson effect, which benefits low risk vascular complications (38). Moreover, a multicenter randomized controlled trial demonstrated that cryoablation achieved lower local tumor progression than RFA with similar OS and DFS rates (39). IRE is a non-thermal ablative technique that mediates cell damage by changing cell permeability and cellular homeostasis, which lead to cell death (40). Although IRE is a relatively new technique and few clinical studies have been conducted, its safety and efficacy have been proven (41, 42). Similar to cryoablation, one of advantages of IRE is that this technique can be used for tumors not suitable for RFA or MWA, such as perivascular HCC (43).

In a word, ablation take an indispensable place in the clinical treatment of HCC. A series of new techniques have been developed to improve the ablation efficacy and zone to benefit more patients. However, these technologies are image-guided, and their efficacy is closely related to the skills of operators to some extent. This factor is a major barrier to application and an interfering factor that is difficult to eliminate in comparative studies.

Emerging Ablative Strategies

Phototherapy (e.g., PDT and PTT) is an emerging and prospective cancer therapeutic strategy. Phototherapy kills cancer cells through photochemical or photophysical effects to achieve therapeutic effects. Various photosensitizers (PSs), such as porphyrin-based PDT (44), 5-aminolaevulinic acid-PDT (45) and Radachlorin-PDT (46), could be applied for HCC. However, several factors need to be improved before these methods could be clinically used. First, light (laser) is one of the most indispensable elements in PDT and PTT, on which the therapeutic effect mostly depends. PSs and photothermal agents can be activated only when the light wavelength is in a specific range, known as therapeutic window. Moreover, light wavelength also determines the depth of tissue penetration, which limits percutaneous application of phototherapy to tumors in abdominal parenchymal organs, especially in deep parts. The rapid development of endoscopic techniques and biomedical materials gave rise to strategies to overcome the depth dependence. For example, Li et al. reported laparoscopic-assisted photothermal ablation method based on superparamagnetic iron oxide (SPIO) and new indocyanine green (ICG), called IR820@PEG-SPIO (47). More surprisingly, IR820@PEG-SPIO completely ablated orthotopic liver cancer in nude mice model, as well as detect early-stage HCC (diameter < 2 mm) *via* fluorescence,

photoacoustic and magnetic resonance (MR) imaging. Compared with visible light, near infrared (NIR) light and X-Ray can provide deeper penetration (48–51). Besides, MHT, an alternative strategy, has been proposed to further overcome the limitation of penetration depth. Qian and colleagues developed a ferrimagnetic silk fibroin hydrogel (FSH) and demonstrated that FSH-mediated MHT, without depth limitation, could be more suitable for treating liver tumors compared with traditional PTT (52).

Nanoplatforms have stood out because they have improved therapeutic effects and reduced adverse effects, provide precise operation with optimized imaging guidance, and combine therapeutic strategies for synergistic anti-tumor effects. Zhu et al. designed a nanoparticle (ZnPc/SFB@BSA) that combined PDT, PTT and sorafenib with increased efficacy and decreased side effects of sorafenib (53). Jin and colleagues reported another nanoparticle loaded with sorafenib/indocyanine for PDT/PTT/chemotherapy, which could provide synergistic effects against HCC (54). Liu's group has been devoted to designing different nanoplatforms for combined phototherapy/chemotherapy by aptamer (TLS11a) modification to enhance HCC-specific targeting (55–57). Nanoplatforms may provide more detailed and comprehensive information about tumor size, anatomical structure, and location and realize precise theranostic guidance by applying dual- or multimodal images that integrate optical and traditional medical images (e.g., CT and MR images). For instance, Qi et al. synthesized a NIR-II photoacoustic (PA) CT imaging-guided nanoagent for HCC theranostic strategy, called Pt@PDA-c (58). Pt@PDA-c had deep tissue penetration and high resolution, which provided accurate location of deep (~4 mm intraabdominal depth) and small (diameter < 5 mm) HCC lesions. Moreover, Pt@PDA-c-mediated PTT could eliminated HCC without recurrence under the guidance of real-time PACT.

Immunological Effects of Ablation

Ablation has long been considered a local treatment. However, growing evidence shows that ablation does more than physically eliminating tumors; it can also play a considerable role in distant lesions through immune effects, also known as abscopal effect. Changes in circulating immune cells/factors and tumor immune microenvironments have been explored by analyzing peripheral blood and tumor models. In 2005, Michael Geissler and colleagues found that local tumor ablation (percutaneous ethanol injection [PEI]/RFA) increased HCC immunogenicity in patients thus to promote endogenous adjuvants release and dendritic cell (DC) activation (59). Besides, RFA induced systemic immune variation in innate immune cells (including natural killer (NK) cells and plasmacytoid DCs) and adaptive immune cells (including tumor-specific T cells, antigen-presenting cells [APCs] and CD8 central memory T cells) (60–62). *De novo* or enhanced tumor-specific immune responses could be observed in patients with HCC after MWA (63). Wu and colleagues observed that neutrophil, monocyte and NK cell were increased to induce innate immune response and immunosuppressive lymphocyte was decreased in patients with HCC post-IRE (64). Moreover, their results indicated an ideal treatment window for immunotherapy (3–14 days post-IRE) to further control tumor recurrence and metastasis. Moreover, the expression of immune checkpoints (programmed cell death protein-1 [PD-1] and PD-1 cognate ligand [PD-L1]), which are associated with HCC tumor size, blood vessel invasion, and BCLC staging, can be downregulated by cryoablation but upregulated at recurrence (65).

The results observed in patients have also been further validated in various animal models. RFA increased CD8+ T cells, memory CD8+ T cells, and DCs and decreased regulatory T (Treg) cells in a unique murine model developed through a combination of intrasplenic inoculated oncogenic hepatocytes and carbon tetrachloride (66). Dai et al. reported that IRE could increase anti-tumor CD8+ T cells to prevent local tumor regrowth and distant metastasis and decrease immunosuppressive Treg and PD-1+ T cells in C57BL/6J mouse model bearing subcutaneous H22 hepatoma (67). Fong's group demonstrated that IRE induced tumor antigens and facilitated granulocyte macrophage colony-stimulating factor plasmid transfer to achieve local and systemic anti-tumor responses in Yorkshire pig models (68, 69). Similarly, in other solid tumors, RFA can not only reduce the proportions of immunosuppressive cells (including Treg cells, tumor-associated macrophages and neutrophils), but increase the T cell infiltration as well as expression of the immune checkpoints (PD-1/PD-L1 and lymphocyte-activation gene 3 [LAG3]) in RFA-treated tumors and distant non-RFA tumors (70, 71). Moreover, serum and intra-tumoral cytokines, such as IFN-γ, IL-1α/β, IL-2/6/8/10, and TNFα/β, were also increased or activated (64, 72–75).

Increasing evidence have proved that ablation therapy could activate systemic anti-tumor immunological effects and inhibit immunosuppressive effects (**Figure 2**). However, RFA could also increase PD-1/PD-L1 expression, which was repressed by

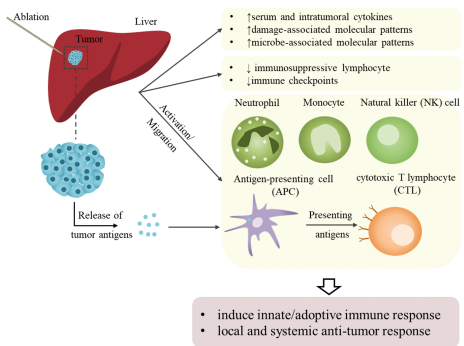

FIGURE 2 | Schematic representation of ablation-induced immunological effects on HCC. Ablation assists local and systemic antitumor responses by activating antitumor immunity and suppressing immunosuppressive effects. On the one hand, the activation of or increase in innate immune cells and cytokines that kill tumor cells achieves non-specific tumor killing. The activation of or increase in adoptive immune cells and the release of tumor-associated or tumor-specific antigens mediates specific anti-tumor immunity. However, these immune effects brought by local ablation are relatively weak and could not meet the requirement needed to sustain anti-tumor effects and prevent recurrence.

sunitinib with activation of immune response (66). This effect may facilitate checkpoint inhibitor therapy by constructing an immune-supportive microenvironment. Thus, combining ablation with immunotherapy is rational to achieve augmented and longer anti-tumor effects and prevent HCC progression with improved outcomes.

IMMUNOTHERAPY

The 5-year recurrence rates of early HCC with operation or ablation are as high as 70% (6). A retrospective study found that 64 of 103 patients with early/intermediate HCC who received RFA experienced recurrence (76). In addition to the pathophysiological characteristics of the HCC, incomplete treatment response results in the high post-operative recurrence rate, which negatively affects long-term survival. In a meta-analysis reviewing the recurrence rate of HCC after RFA over a ten-year period, the size, number, and location of tumors are partly responsible for incomplete treatment response, limiting the application of RFA in the early 2000s (77). With the introduction of multiple treatment modalities, such as RFA + PEI/TACE, these limitations have been broken and post-recurrence rates have been significantly reduced. However, to complicate matters further, recurrent tumors may be more aggressive (23, 78–80). Thus, adjuvant systemic therapy is taken in consideration. Sorafenib, a multi-tyrosine kinase inhibitor (TKI), has considerably improved the survival of patients with advanced HCC, whereas chemotherapy does not (81). Other emerging TKI drugs, including lenvatinib, regorafenib, cabozantinib and donafenib have been proved to improve the survival benefit of patients with advanced HCC (82–86). However, sorafenib, as an adjuvant therapy for HCC after resection or ablation, did not improved recurrence-free survival (RFS) (82). Furthermore, a phase III STORM trial established a predictive 146-gene signature, which comprised some genes involved in immune-related processes; however, the tested biomarkers and reported prognostic gene signatures lacked value in predicting adjuvant sorafenib on RFS (87). Surprisingly, iodine (131I)-labeled metuximab, an immunotherapeutic agent, proved to benefit RFS of post-operative or post-ablative patients with HCC, in particularly those with CD147+ (88, 89).

The immune system plays a critical role in HCC, particularly in the HCC development and progression, as well as the treatment response or tolerance (**Figure 3**). Bruno et al. elaborated the HCC immune microenvironment (e.g., antigens, molecular features, and immune cells), and reviewed HCC immunotherapies including immune checkpoint inhibitor (ICI)-based therapies, as well as others based on adoptive cells and vaccines (90). This section will not dwell on the above; instead, it will give a brief retrospect of the application of immune modulators and the advances in novel immunomodulatory strategies.

In short, the goal of immunomodulatory strategies is to activate anti-tumor immune response and/or suppress immune evasion. Immune checkpoints, the surface receptors expressed on immune system cells, include PD-1, PD-L1, cytotoxic T lymphocyte associated antigen 4 (CTLA4), LAG3, and T cell immunoglobulin and mucin domain containing-3 (TIM3) (91). Overexpressed PD-L1 in HCC cells can promote its binding with PD-1 on effector T cells, resulting in immune escape of tumor cells and apoptosis of T cells, which is conducive to the growth and progression of HCC (92). Overexpression of CTLA4 and TIM3 in Treg cells and overexpression of LAG3 and TIM3 in tumor infiltrating T lymphocytes can prevent the activation of effector T cells, also resulting in immune escape of tumor cells (90). The immune checkpoint is one of the immunosuppressive mechanisms that can help HCC immune escape by binding to corresponding ligands in HCC, which is also the rationale for the therapeutic application of ICIs. Recent clinical trials suggested that ICIs, whether alone or in combination with other agents, had a positive effect in HCC. Nivolumab (anti-PD-1), atezolizumab (anti-PD-L1), and tremelimumab (anti- CTLA4), have been proved to be safe and have effective anti-tumor responses for treating HCC (93–95). Notably, nivolumab and pembrolizumab well tolerated and effective in patients with advanced HCC after sorafenib failure with promising effects on long-term survival (96, 97). Atezolizumab, particularly in combination with bevacizumab (anti-VEGF), has superior performance compared with sorafenib in term of survival outcomes and the life quality of patients with unresectable HCC (98, 99).

Other immunotherapies, including adoptive immunotherapies (AITs) and immunotherapeutic vaccinations, activate anti-tumor immune response. AIT improves anti-tumor immunity by expanding or sensitizing lymphocytes *in vitro* and reinjecting them into patients, and cancer vaccines aim to enhance tumor-

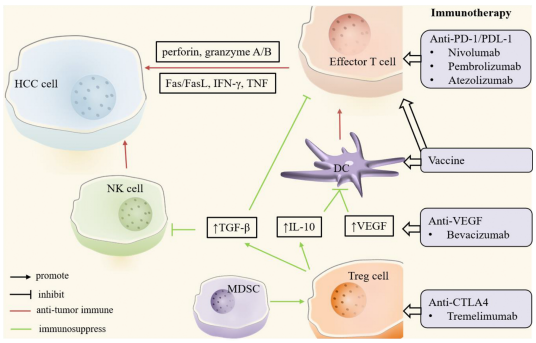

FIGURE 3 | Key players in HCC immune microenvironment. In the HCC microenvironment, natural killer (NK) cells, dendritic cells (DCs) and effector T cells mainly play an anti-tumor immune role (red). Regulatory T (Treg) cells and myeloid-derived suppressor cells (MDSCs) promote tumor immune escape or drug resistance through immunosuppressive effects (green). In addition, tumor growth factor-β (TGF-β), interleukin-10 (IL-10) and other cytokines play an important role in tumor immunity. Immunotherapy enhances anti-tumor immunity or suppresses immunosuppression by targeting these critical cells and molecules. CTLA4, cytotoxic T lymphocyte-associated antigen 4; DC, dendritic cell; FasL, Fas ligand; HCC, hepatocellular carcinoma; IFN-γ, interferon-γ; IL-10, interleukin-10; MDSC, myeloid-derived suppressor cell; NK, natural killer; PD-1, programmed cell death protein-1; PDL-1, programmed cell death protein ligand -1; TGF-β, tumor growth factor-β; Treg, regulatory T; VEGF, vascular endothelial growth factor.

specific immune responses that are primarily activated by antigen-presenting cells (e.g., DCs) and produce endogenous TAAs. Although these treatments have not been studied as extensively as ICIs, they are under clinical studies. Clinical trials demonstrated the safety and efficacy of T cell- (100), DC- (101), and activated cytokine-induced killer (CIK) cell- (102) based adoptive immunotherapies, as well as oncolytic virus (103, 104) and peptide (105–107) vaccines for HCC. Glypican-3 (GPC3), a carcinoembryonic antigen ideal for immunotherapy target, has been studied extensively as an anti-tumor vaccine of HCC. Phase I/II clinical trials suggested that GPC3 peptide vaccine is effective in inducing cytotoxic T lymphocyte (CTL) killing cancer cells, reducing RFS, and improving OS, particularly in patients with GPC3-overexpressing HCC (105, 108, 109). An animal experiment demonstrated that the synergistic anti-tumor effects depended on increased GPC3-induced CTL though the combination of PD-1/PD-L1 blockade and GPC3 peptide vaccine (110). Moreover, a series of novel GPC3-targeting vaccine (111, 112) and antibodies (113–115) and cellular immunotherapeutic strategies (116–118) against GPC3 rely on the role of GPC3 in HCC and immunotherapy.

Strategies for enhancing therapeutic effects and monitoring immunotherapies have been developed based on advanced technologies. For instance, Liao et al. successfully applied NIR-II fluorescent imaging to NK cell-based immunotherapy for the real-time quantitative tracking and visualization of the viability of adoptive NK cells *in vivo* (119). The potency of immunotherapies can be enhanced by modification with specific antigens (120–122), mRNA optimization (123) and combination with adjuvants (124, 125).

COMBINED ABLATIVE-IMMUNOTHERAPY

As mentioned in Section 2.3, ablation techniques could induce local and systemic antitumor immune responses, but these responses are relatively weak, and cannot completely control the tumor. This reason explains the high local recurrence rates after treatment. RFA activated tumor-specific T cells, but it could not identify a new grown tumor or a recurrent tumor, which resulted in the tumor immune escape and recurrence in a HCC patient (60). Moreover, only 30% of patients with HCC achieved long-term remission and better DFS, because of the tumor-specific immune responses induced by MWA (63). The facts that the application of a single locoregional therapy has a high recurrence rate and locoregional ablation can induce anti-tumor immune responses, have led to the development of combined ablative and systemic therapy studies for recurrence reduction or treatment, as well as improved survival outcomes. Indeed, the advent of TKIs and immunotherapy have improved the outcomes of patients with HCC. Sorafenib, the most promising candidate for adjuvant chemotherapy, failed in patients with HCC after resection or ablation. Results from STORM trial in 2005 showed that compared with placebo, adjuvant sorafenib did not significantly improve RFS in patients with HCC post resection or ablation (126), which is consistent with the findings of existing randomized trials that showed no survival benefit for HCC patients after ablation with adjuvant sorafenib (127, 128). In addition, a study has shown that vitamin K combined with angiotensin converting enzyme inhibitors can inhibit the cumulative recurrence of HCC after treatment (129). A retrospective study has shown that angiotensin II receptor 1 blockers (sartans) can significantly improve overall survival and recurrence time in HCC patients after RFA (130), while another study have shown that this combination can only improve recurrence time (131). These results suggest that more rigorous randomized clinical trials are needed to verify the efficacy of this combination for HCC. On the other hand, the unsatisfying combinations indicated the emergence of immunotherapy as an adjuvant candidate.

In the VX2 tumor model, the combination of RFA and CpG-oligodeoxynuleotides vaccine prevented tumor progression and improved survival outcomes by enhancing anti-tumor T cell response and cytotoxicity (132). Using the CT26 tumor model, Liu et al. studied the roles of palliative RFA (pRFA) in T-cell immune responses and tumor recurrence, which could be more significant in combination with antibodies (74). Likewise, MWA combined with anti-PD-1/anti-CTLA-4 protected mice from recurrence with improved survival (133).

Clinical Combination on the Way

Table 2 reviews the finished clinical trials of the combinations of ablation and immunotherapy. Nivolumab and pembrolizumab, which are PD-1 blockades, received quick approvals as second line therapy for patients with HCC after sorafenib failure on the basis of CheckMate-040 (93) and KEYNOTE-224 (97). A recent proof-of-concept clinical trial suggested that the application of RFA or MWA enhanced the anti-tumor effects and response rates (from 10% to 24%) of nivolumab and pembrolizumab (135). The explanation for synergistic effects may be found in Section 2.3 in this review. In brief, the critical roles of RFA in T cell infiltration/response and PD-1 expression may be one of rationales for combining RFA with PD-1 blockade. Besides, the combination of RFA with tremelimumab (CTLA-4 blockade) have been also explored (134, 135).

Various studies have demonstrated the safe and effective to applicate adjuvant adoptive cellular immunotherapies to patients with HCC post-ablation with improved RFS and OS (102, 139–141). For patients with metastatic HCC, the combination of cryoablation and DC-CIK cell immunotherapy also achieved a significantly higher OS (median: 32 months) than cryoablation (median: 17.5 months) and the untreated group (median: 3 months) (144). Moreover, the multiple treatment modality for cryo-immunotherapy could provide better prognosis than the single one.

Notably, Tetsuya Nakatsura's team found that RFA stood out among other locoregional therapies (including surgical resection and TACE) by referring to GPC3-specific T-cell-mediated immune response for HCC (145). Compared with resection, RFA significantly induced GPC3-specific CTLs, especially in patients with GPC3-overexpressing HCC. Consequently, the phase II study of GPC3 peptide vaccine for adjuvant immunotherapy was carried out, laying a foundation of

TABLE 2 | Clinical combinations of ablation and immunotherapy.

Ablation technique	Immunotherapy	Efficacies/Outcomes	Research type	Years	Ref.
RFA	CTLA-4 blockade (tremelimumab)	Accumulation of intratumoral $CD8^+$ T cells and reduction of HCV load	Phase II trial	2017	(134)
RFA	CTLA-4 blockade (tremelimumab)	Activation of tumor-specific T cell with decreased T-cell clonality	Correlative study	2019	(135)
RFA	PD-1 blockade (camrelizumab)	improved 1-year RFS and OS of patients with recurrent HCC	propensity score matching analysis	2021	(136)
RFA/MWA	PD-1 blockade (nivolumab/pembrolizumab)	Increased response rate with improved survival in patients with advanced HCC after sorafenib failure	Proof-of-concept clinical trial	2020	(137)
RFA	Adoptive immunotherapy (RAK cell)	Feasibility and safety with no severe adverse events, recurrences or deaths in a 7-month follow-up	–	2010	(138)
RFA	Adoptive immunotherapy (NK/γδT/CIK)	Efficiency and safety with improved progression-free survival (PFS) and survival prognosis, decreased HVC load	Open-label	2014	(139)
RFA	Adoptive immunotherapy (CIK)	Increased RFS and OS	Multicenter, randomized, open-label, phase III trial	2015	(102)
RFA	Adoptive immunotherapy (CIK)	Safety with prolonged RFS	Real-word study	2019	(140)
RFA	Adoptive immunotherapy (OK432-stimulated monocyte-derived DC)	Safety with longer RFS; associated with enhanced TAA-specific T-cell responses	Randomized phase I/II trial	2020	(141)
RFA	Vaccine (DC) + multiple antigen (AFP/GPC3/MAGE-1)	Safety and tolerance	Phase I/IIa trial	2015	(109)
RFA	Vaccine (GPC3 antigen)	Improved 1-year recurrence rates in patients with GPC3-positive HCC	Open-label, single-arm phase II trial	2016	(142)
MWA	Adoptive immunotherapy (DC/CIK/CTL)	Safety with ameliorated peripheral lymphocyte percentage	Phase I trial	2011	(143)
cryoablation	Adoptive immunotherapy (DC-CIK)	Increased OS	Retrospective study	2013	(144)

antitumor efficacy of GPC3 peptide vaccine and induced GPC3-specific CTL (105). Although the combination of resection or RFA with GPC3 peptide vaccine decreased the 1-year recurrence rate (142), whether different local strategies had an impact on the prognosis of the combination treatment remained unclear. However, another randomized phase II study showed that adjuvant immunotherapy with tumor associated antigen (TAA)-pulsed DC vaccine prolonged the RFS of patients with complete remission in non-RFA (including surgical resection, TACE, and PEI) groups compared with those in the RFA group (102). These results suggest that combination strategy benefits patients, but the choice of optimal combinations is thought provoking.

Springing Synergistic Strategies Based on Nanoplatforms

While the clinical trials are in full force, the combination of ablation and immunotherapy is also attracting the attention of scientists in basic medicine and biomedical materials. The development and application of multi-functional nanoplatforms have enabled synergistic ablative-immunotherapy strategy to flourish, instead of the sequential combination. On the one hand, a nanoplatform can deliver multiple drugs with optimized drug performance and therapeutic efficiency, as well as reduced drug toxicity. On the other hand, nanoplatforms can apply imaging technology to identify and locate tumors, guide ablation procedures, as well as monitor drug responses and therapy efficacy. Moreover, such a combination strategy may maximize the synergistic anti-tumor effects and thus achieve a greater therapeutic efficacy than the mere sum of the parts.

First, nanoplatforms can improve the targeting ability of agents through the innate enhanced permeability and retention effect and modifications with specific targets to enhance the anti-tumor effects (8). A mesoporous silica based nanosystem co-loading ICG and sorafenib, named (ICG+S)@mSiO2, was developed for synergetic PTT/immuno-enhanced therapy (146). (ICG+S)@mSiO2 improved endocytosis of HCC cells and photothermal efficiency. Active targeting deliveries were achieved in SP94-PB-SF-Cy5.5 nanoparticles (NPs) (147) and PCN-ACF-CpG@HA NPs (148) by conjugated with HCC specific targeting peptide (such as SP94) and HA (targeting CD44 receptor-overexpressed HCC cells), respectively. Moreover, SP94-PB-SF-Cy5.5 and PCN-ACF-CpG@HA, in combination with PD-L1 blockade and an immunologic adjuvant (CpG), enhanced the PTT- and PDT-induced weak immunogenic cell death of cancer cells. Similarly, these strategies for enhanced immune responses also applied sonodynamic immunotherapy as recently reported by Tan et al. (149) and Lin et al. (150). Moreover, anti-TGF-β antibody modification is an active targeting strategy that enhances cell endocytosis for improved PTT and an immunotherapeutic strategy for immune activation (151). Besides, ICG/ICG-SF-Gel-based photothermal-immunotherapy inhibited primary and distal tumor growth, with improved survival time with the help of Ganoderma lucidum polysaccharides (GLP) for enhancing the antitumor immunity (152).

These combined anti-tumor effects led to the application of TAAs in *in situ* vaccination to eliminate residual and distant lesions, as well as inhibit tumor recurrence and metastasis.

Biomimetic nanotechnology, which integrates advantages of nanoplatform delivery and cellular immunotherapy, provides novel strategies for synergistic ablative immunotherapy. On the one hand, biomimetic nanoplatforms are ideal for targeted drug delivery because of their superior biological characteristics. For instance, Wang et al. developed a photothermal immunotherapy nanoplatform based on synthetic high-density lipoprotein (sHDL) (153). The higher expression of sHDL in HCC cells than in other normal cells of liver facilitates the preferential delivery of agents into the cytosol of HCC cells. Ma and colleagues designed a CAR-T cell membrane-coated mesoporous silica NP, which specifically recognized GPC3+ HCC cells (154). On the other hand, a programmable therapeutic strategy based on engineered immune cells provide a possibility for the synergy of ablation and cellular immunotherapy. Zhang et al. constructed an artificial engineered NK cell decorated with TLS11a (a HCC-specific targeting aptamer) for photothermal immunotherapy (56).

DISCUSSION

The development of science and technology and the deepening of researches on HCC have promoted vigorous developments of treatment strategies for HCC, including the local treatment represented by the clinical standard treatment (RFA) and the emerging phototherapy, and the systematic treatment represented by sorafenib and immune blockers. However, monotherapies have shown some limitations. RFA is a first-line ablative therapy with established technical standard for patients with HCC. However, over 30% of patients suffer from recurrence or metastasis after iRFA (27). The solutions to the problems after iRFA include two aspects: improving the efficiency of RFA and applying combination therapy. The former can be solved well with the development of imaging technology based on nanomaterials, but the process from new drug development to clinical application is long and slow. The latter provides a salvage alternative for residual tumors, but the choice of drugs is thought provoking because of possible drug resistance after iRFA. Moreover, high-quality evidence-based medicine are lacking to support these solutions.

In comparison, increasing evidence support combination therapy. Thus, the combination of ablation and immunotherapy is rationale. On the one hand, ablation can promote anti-tumor immune responses. However, these responses are not strong enough to completely control tumors. On the other hand, the addition of immunotherapy may synergistically amplify the anti-tumor immune effect. The application of nanotechnology and nanomaterials in ablative immunotherapy strengthens the combination; enhances therapeutic effects by improving the physical, chemical, and physiological properties of agents; and achieves a synergistic effect through theranostic nanoplatforms.

Of course, many controversies and challenges need to be resolved. How to develop individualized treatment strategies to obtain the best treatment effect needs to be taken into consideration in clinical research. First, most clinical trials of ablative immunotherapy apply adjuvant immunotherapy after ablation. The frequency of ablation and the optimal time of immunotherapy application need to be specified. For example, a study showed that the ideal time window for immunotherapy after IRE is 3-14 days post-ablation (64). Another study suggested that the frequency of cryoablation is related to prognosis (144). Second, the expression difference of specific genes, such as GPC3 (105, 108, 109), in some patients with HCC leads to different immunotherapy responses and outcomes. Third, the combinations of ablative immunotherapy are diverse. Although some studies demonstrated that ablative immunotherapy provides better outcomes than single ablation or immunotherapy, whether different combinations have differences is unknown. In addition, more multicenter, randomized clinical trials with large samples are needed to confirm the benefits of the ablative immunotherapy. With regard to basic researches, the animal models used in ablative therapy, especially phototherapy, and subcutaneous tumor transplantation model are not suitable because the penetration depth of such techniques is limited. Moreover, tumors in solid organs such as liver, are difficult to reach by percutaneous or laparoscopic ablative techniques, unless the tumor is on the surface of the organ. The development of new drugs based on nanomaterials (such as NIR/X-Ray activated PSs and photothermal drugs) and novel technologies (such as SDT), has been devoted to address these problems. Of course, the success of these advances in cell and animal levels is still a long way from clinical applications. Nonetheless, ablative immunotherapy is expected to gain a place in HCC therapy and benefit patients in the near future.

AUTHOR CONTRIBUTIONS

KW and CJ contributed to conceive and design the study. CW, KW, and JM performed the article searching. HJ, WL, and YZ extracted the data. CW and KW wrote the manuscript. CJ and JM supervised the manuscript. All authors contributed to the article and approved the submitted version.

FUNDING

This project is supported by the grants from Zhejiang Province Public Welfare Technology Application Research Project (No. LGF21H160022), Natural Science Foundation of Zhejiang Province (No. LQ22H160055), Science and Technology Plan Project of Taizhou (No. 21ywb26 and 21ywb29), Medical Science and Technology Project of Zhejiang Province (No. 2017KY711), and Project of Taizhou University (No.2018PY057).

REFERENCES

1. Sung H, Ferlay J, Siegel RL, Laversanne M, Soerjomataram I, Jemal A, et al. Global Cancer Statistics 2020: GLOBOCAN Estimates of Incidence and Mortality Worldwide for 36 Cancers in 185 Countries. *CA: Cancer J Clin* (2021) 71(3):209–49. doi: 10.3322/caac.21660
2. Vogel A, Cervantes A, Chau I, Daniele B, Llovet JM, Meyer T, et al. Hepatocellular Carcinoma: ESMO Clinical Practice Guidelines for Diagnosis, Treatment and Follow-Up. *Ann Oncol* (2018) 29(Suppl 4): iv238–55. doi: 10.1093/annonc/mdy308
3. Chen LT, Martinelli E, Cheng AL, Pentheroudakis G, Qin S, Bhattacharyya GS, et al. Pan-Asian Adapted ESMO Clinical Practice Guidelines for the Management of Patients With Intermediate and Advanced/Relapsed Hepatocellular Carcinoma: A TOS-ESMO Initiative Endorsed by CSCO, ISMPO, JSMO, KSMO, MOS and SSO. *Ann Oncol* (2020) 31(3):334–51. doi: 10.1016/j.annonc.2019.12.001
4. Gordan JD, Kennedy EB, Abou-Alfa GK, Beg MS, Brower ST, Gade TP, et al. Systemic Therapy for Advanced Hepatocellular Carcinoma: ASCO Guideline. *J Clin Oncol* (2020) 38(36):4317–45. doi: 10.1200/JCO.20.02672
5. Benson AB, D'Angelica MI, Abbott DE, Abrams TA, Alberts SR, Anaya DA, et al. Guidelines Insights: Hepatobiliary Cancers, Version 2.2019. *J Natl Compr Cancer Netw: JNCCN* (2019) 17(4):302–10. doi: 10.6004/jnccn.2019.0019
6. Llovet JM, Kelley RK, Villanueva A, Singal AG, Pikarsky E, Roayaie S, et al. Hepatocellular Carcinoma. *Nat Rev Dis Primers* (2021) 7(1):6. doi: 10.1038/s41572-020-00240-3
7. Roayaie S, Obeidat K, Sposito C, Mariani L, Bhoori S, Pellegrinelli A, et al. Resection of Hepatocellular Cancer ≤2 Cm: Results From Two Western Centers. *Hepatol (Baltimore Md)* (2013) 57(4):1426–35. doi: 10.1002/hep.25832
8. Wang C, Fan W, Zhang Z, Wen Y, Xiong L, Chen X. Advanced Nanotechnology Leading the Way to Multimodal Imaging-Guided Precision Surgical Therapy. *Adv Mater* (2019) 31(49):1904329. doi: 10.1002/adma.201904329
9. Peng Z-W, Liu F-R, Ye S, Xu L, Zhang Y-J, Liang H-H, et al. Radiofrequency Ablation Versus Open Hepatic Resection for Elderly Patients (> 65 Years) With Very Early or Early Hepatocellular Carcinoma. *Cancer* (2013) 119 (21):3812–20. doi: 10.1002/cncr.28293
10. Cucchetti A, Piscaglia F, Cescon M, Colecchia A, Ercolani G, Bolondi L, et al. Cost-Effectiveness of Hepatic Resection Versus Percutaneous Radiofrequency Ablation for Early Hepatocellular Carcinoma. *J Hepatol* (2013) 59(2):300–7. doi: 10.1016/j.jhep.2013.04.009
11. Breen DJ, Lencioni R. Image-Guided Ablation of Primary Liver and Renal Tumours. *Nat Rev Clin Oncol* (2015) 12(3):175–86. doi: 10.1038/nrclinonc.2014.237
12. Lehmann KS, Poch FGM, Rieder C, Schenk A, Stroux A, Frericks BB, et al. Minimal Vascular Flows Cause Strong Heat Sink Effects in Hepatic Radiofrequency Ablation Ex Vivo. *J Hepatobiliary Pancreat Sci* (2016) 23 (8):508–16. doi: 10.1002/jhbp.370
13. Mohkam K, Dumont P-N, Manichon A-F, Jouvet J-C, Boussel L, Merle P, et al. No-Touch Multibipolar Radiofrequency Ablation vs. Surgical Resection for Solitary Hepatocellular Carcinoma Ranging From 2 to 5 Cm. *J Hepatol* (2018) 68(6):1172–80. doi: 10.1016/j.jhep.2018.01.014
14. Su T, Huang M, Liao J, Lin S, Yu P, Yang J, et al. Insufficient Radiofrequency Ablation Promotes Hepatocellular Carcinoma Metastasis Through M A mRNA Methylation Dependent Mechanism. *Hepatol (Baltimore Md)* (2021) 74(3):1339–56. doi: 10.1002/hep.31766
15. Kong J, Yao C, Dong S, Wu S, Xu Y, Li K, et al. ICAM-1 Activates Platelets and Promotes Endothelial Permeability Through VE-Cadherin After Insufficient Radiofrequency Ablation. *Adv Sci (Weinheim Baden-Wurttemberg Germany)* (2021) 8(4):2002228. doi: 10.1002/advs.202002228
16. Kong J, Yao C, Ding X, Dong S, Wu S, Sun W, et al. ATPase Inhibitory Factor 1 Promotes Hepatocellular Carcinoma Progression After Insufficient Radiofrequency Ablation, and Attenuates Cell Sensitivity to Sorafenib Therapy. *Front Oncol* (2020) 10:1080. doi: 10.3389/fonc.2020.01080
17. Ma D, Gao X, Liu Z, Lu X, Ju H, Zhang N. Exosome-Transferred Long non-Coding RNA ASMTL-AS1 Contributes to Malignant Phenotypes in Residual Hepatocellular Carcinoma After Insufficient Radiofrequency Ablation. *Cell Prolif* (2020) 53(9):e12795. doi: 10.1111/cpr.12795
18. Li Z, Jiang M, Zhang T, Liu S. Promotes Hepatocellular Carcinoma via Axis Under Insufficient Radiofrequency Ablation Condition. *Cancer Biother Radiopharm* (2020). doi: 10.1089/cbr.2019.3541
19. Jia G, Li F, Tong R, Liu Y, Zuo M, Ma L, et al. C-Met/MAPK Pathway Promotes the Malignant Progression of Residual Hepatocellular Carcinoma Cells After Insufficient Radiofrequency Ablation. *Med Oncol (Northwood Lond Engl)* (2020) 37(12):117. doi: 10.1007/s12032-020-01444-z
20. Zhang N, Li H, Qin C, Ma D, Zhao Y, Zhu W, et al. Insufficient Radiofrequency Ablation Promotes the Metastasis of Residual Hepatocellular Carcinoma Cells *via* Upregulating Flotillin Proteins. *J Cancer Res Clin Oncol* (2019) 145(4):895–907. doi: 10.1007/s00432-019-02852-z
21. Xu W-L, Wang S-H, Sun W-B, Gao J, Ding X-M, Kong J, et al. Insufficient Radiofrequency Ablation-Induced Autophagy Contributes to the Rapid Progression of Residual Hepatocellular Carcinoma Through the HIF-1α/BNIP3 Signaling Pathway. *BMB Rep* (2019) 52(4):277–82. doi: 10.5483/BMBRep.2019.52.4.263
22. Zhang N, Ma D, Wang L, Zhu X, Pan Q, Zhao Y, et al. Insufficient Radiofrequency Ablation Treated Hepatocellular Carcinoma Cells Promote Metastasis by Up-Regulation Itgb3. *J Cancer* (2017) 8(18):3742–54. doi: 10.7150/jca.20816
23. Zhang N, Wang L, Chai Z-T, Zhu Z-M, Zhu X-D, Ma D-N, et al. Incomplete Radiofrequency Ablation Enhances Invasiveness and Metastasis of Residual Cancer of Hepatocellular Carcinoma Cell HCCLM3 *via* Activating β-Catenin Signaling. *PLoS One* (2014) 9(12):e115949. doi: 10.1371/journal.pone.0115949
24. Dong S, Kong J, Kong F, Kong J, Gao J, Ke S, et al. Insufficient Radiofrequency Ablation Promotes Epithelial-Mesenchymal Transition of Hepatocellular Carcinoma Cells Through Akt and ERK Signaling Pathways. *J Transl Med* (2013) 11:273. doi: 10.1186/1479-5876-11-273
25. Kong J, Kong L, Kong J, Ke S, Gao J, Ding X, et al. After Insufficient Radiofrequency Ablation, Tumor-Associated Endothelial Cells Exhibit Enhanced Angiogenesis and Promote Invasiveness of Residual Hepatocellular Carcinoma. *J Transl Med* (2012) 10:230. doi: 10.1186/1479-5876-10-230
26. Teng W, Liu K-W, Lin C-C, Jeng W-J, Chen W-T, Sheen IS, et al. Insufficient Ablative Margin Determined by Early Computed Tomography may Predict the Recurrence of Hepatocellular Carcinoma After Radiofrequency Ablation. *Liver Cancer* (2015) 4(1):26–38. doi: 10.1159/000343877
27. Jiang Q, Zeng Y, Xu Y, Xiao X, Liu H, Zhou B, et al. Ultrasound Molecular Imaging as a Potential Non-Invasive Diagnosis to Detect the Margin of Hepatocarcinoma *via* CSF-1r Targeting. *Front Bioeng Biotechnol* (2020) 8:783. doi: 10.3389/fbioe.2020.00783
28. Dong S, Kong J, Kong F, Kong J, Gao J, Ji L, et al. Sorafenib Suppresses the Epithelial-Mesenchymal Transition of Hepatocellular Carcinoma Cells After Insufficient Radiofrequency Ablation. *BMC Cancer* (2015) 15:939. doi: 10.1186/s12885-015-1949-7
29. Zhang N, Wang L-R, Li D-D, Ma D-N, Wang C-H, He X-G, et al. Interferon-α Combined With Herbal Compound "Songyou Yin" Effectively Inhibits the Increased Invasiveness and Metastasis by Insufficient Radiofrequency Ablation of Hepatocellular Carcinoma in an Animal Model. *Integr Cancer Ther* (2018) 17(4):1260–9. doi: 10.1177/1534735418801525
30. Kong J, Kong J, Pan B, Ke S, Dong S, Li X, et al. Insufficient Radiofrequency Ablation Promotes Angiogenesis of Residual Hepatocellular Carcinoma *via* HIF-1α/VEGFA. *PLoS One* (2012) 7(5):e37266. doi: 10.1371/journal.pone.0037266
31. Zhang L, Wang J, Jiang J, Zhang M, Shen J. CTLA-4 Blockade Suppresses Progression of Residual Tumors and Improves Survival After Insufficient Radiofrequency Ablation in a Subcutaneous Murine Hepatoma Model. *Cardiovasc Intervent Radiol* (2020) 43(9):1353–61. doi: 10.1007/s00270-020-02505-6
32. Zhang Q, Kong J, Dong S, Xu W, Sun W. Metformin Exhibits the Anti-Proliferation and Anti-Invasion Effects in Hepatocellular Carcinoma Cells After Insufficient Radiofrequency Ablation. *Cancer Cell Int* (2017) 17:48. doi: 10.1186/s12935-017-0418-6
33. Zhao Z, Wu J, Liu X, Liang M, Zhou X, Ouyang S, et al. Insufficient Radiofrequency Ablation Promotes Proliferation of Residual Hepatocellular Carcinoma *via* Autophagy. *Cancer Lett* (2018) 421:73–81. doi: 10.1016/j.canlet.2018.02.024

34. An C, Li W-Z, Huang Z-M, Yu X-L, Han Y-Z, Liu F-Y, et al. Small Single Perivascular Hepatocellular Carcinoma: Comparisons of Radiofrequency Ablation and Microwave Ablation by Using Propensity Score Analysis. *Eur Radiol* (2021) 31(7):4764–73. doi: 10.1007/s00330-020-07571-5
35. Feng Y, Wang L, Lv H, Shi T, Xu C, Zheng H, et al. Microwave Ablation Versus Radiofrequency Ablation for Perivascular Hepatocellular Carcinoma: A Propensity Score Analysis. *HPB* (2021) 23(4):512–9. doi: 10.1016/j.hpb.2020.08.006
36. Facciorusso A, Abd El Aziz MA, Tartaglia N, Ramai D, Mohan BP, Cotsoglou C, et al. Microwave Ablation Versus Radiofrequency Ablation for Treatment of Hepatocellular Carcinoma: A Meta-Analysis of Randomized Controlled Trials. *Cancers (Basel)* (2020) 12(12):3796–806. doi: 10.3390/cancers12123796
37. Tamai H, Okamura J. New Next-Generation Microwave Thermosphere Ablation for Small Hepatocellular Carcinoma. *Clin Mol Hepatol* (2021) 27 (4):564–74. doi: 10.3350/cmh.2021.0136
38. Kim R, Kang TW, Cha DI, Song KD, Lee MW, Rhim H, et al. Percutaneous Cryoablation for Perivascular Hepatocellular Carcinoma: Therapeutic Efficacy and Vascular Complications. *Eur Radiol* (2019) 29(2):654–62. doi: 10.1007/s00330-018-5617-6
39. Wang C, Wang H, Yang W, Hu K, Xie H, Hu K-Q, et al. Multicenter Randomized Controlled Trial of Percutaneous Cryoablation Versus Radiofrequency Ablation in Hepatocellular Carcinoma. *Hepatol (Baltimore Md)* (2015) 61(5):1579–90. doi: 10.1002/hep.27548
40. Saini A, Breen I, Alzubaidi S, Pershad Y, Sheth R, Naidu S, et al. Irreversible Electroporation in Liver Cancers and Whole Organ Engineering. *J Clin Med* (2018) 8(1):22–32. doi: 10.3390/jcm8010022
41. Sutter O, Calvo J, N'Kontchou G, Nault J-C, Ourabia R, Nahon P, et al. Safety and Efficacy of Irreversible Electroporation for the Treatment of Hepatocellular Carcinoma Not Amenable to Thermal Ablation Techniques: A Retrospective Single-Center Case Series. *Radiology* (2017) 284(3):877–86. doi: 10.1148/radiol.2017161413
42. Frühling P, Nilsson A, Duraj F, Haglund U, Norén A. Single-Center Nonrandomized Clinical Trial to Assess the Safety and Efficacy of Irreversible Electroporation (IRE) Ablation of Liver Tumors in Humans: Short to Mid-Term Results. *Eur J Surg Oncol* (2017) 43(4):751–7. doi: 10.1016/j.ejso.2016.12.004
43. Niessen C, Igl J, Pregler B, Beyer L, Noeva E, Dollinger M, et al. Factors Associated With Short-Term Local Recurrence of Liver Cancer After Percutaneous Ablation Using Irreversible Electroporation: A Prospective Single-Center Study. *J Vasc Intervent Radiol JVIR* (2015) 26(5):694–702. doi: 10.1016/j.jvir.2015.02.001
44. Egger NG, Schoenecker JA, Gourley WK, Motamedi M, Anderson KE, Weinman SA. Photosensitization of Experimental Hepatocellular Carcinoma With Protoporphyrin Synthesized From Administered Delta-Aminolevulinic Acid: Studies With Cultured Cells and Implanted Tumors. *J Hepatol* (1997) 26(4):913–20. doi: 10.1016/S0168-8278(97)80260-7
45. Otake M, Nishiwaki M, Kobayashi Y, Baba S, Kohno E, Kawasaki T, et al. Selective Accumulation of ALA-Induced PpIX and Photodynamic Effect in Chemically Induced Hepatocellular Carcinoma. *Br J Cancer* (2003) 89 (4):730–6. doi: 10.1038/sj.bjc.6601135
46. Mirzaei H, Djavid GE, Hadizadeh M, Jahanshiri-Moghadam M, Hajian P. The Efficacy of Radachlorin-Mediated Photodynamic Therapy in Human Hepatocellular Carcinoma Cells. *J Photochem Photobiol B* (2015) 142:86–91. doi: 10.1016/j.jphotobiol.2014.11.007
47. Li Q, Chen K, Huang W, Ma H, Zhao X, Zhang J, et al. Minimally Invasive Photothermal Ablation Assisted by Laparoscopy as an Effective Preoperative Neoadjuvant Treatment for Orthotopic Hepatocellular Carcinoma. *Cancer Lett* (2021) 496:169–78. doi: 10.1016/j.canlet.2020.09.024
48. Fan W, Tang W, Lau J, Shen Z, Xie J, Shi J, et al. Breaking the Depth Dependence by Nanotechnology-Enhanced X-Ray-Excited Deep Cancer Theranostics. *Adv Mater (Deerfield Beach Fla)* (2019) 31(12):e1806381. doi: 10.1002/adma.201806381
49. Sun W, Zhou Z, Pratx G, Chen X, Chen H. Nanoscintillator-Mediated X-Ray Induced Photodynamic Therapy for Deep-Seated Tumors: From Concept to Biomedical Applications. *Theranostics* (2020) 10(3):1296–318. doi: 10.7150/thno.41578
50. Jin G, He R, Liu Q, Lin M, Dong Y, Li K, et al. Near-Infrared Light-Regulated Cancer Theranostic Nanoplatform Based on Aggregation-Induced Emission Luminogen Encapsulated Upconversion Nanoparticles. *Theranostics* (2019) 9(1):246–64. doi: 10.7150/thno.30174
51. Li S, Deng Q, Zhang Y, Li X, Wen G, Cui X, et al. Rational Design of Conjugated Small Molecules for Superior Photothermal Theranostics in the NIR-II Biowindow. *Adv Mater (Deerfield Beach Fla)* (2020) 32(33): e2001146. doi: 10.1002/adma.202001146
52. Qian K-Y, Song Y, Yan X, Dong L, Xue J, Xu Y, et al. Injectable Ferrimagnetic Silk Fibroin Hydrogel for Magnetic Hyperthermia Ablation of Deep Tumor. *Biomaterials* (2020) 259:120299. doi: 10.1016/j.biomaterials.2020.120299
53. Yu X-N, Deng Y, Zhang G-C, Liu J, Liu T-T, Dong L, et al. Sorafenib-Conjugated Zinc Phthalocyanine Based Nanocapsule for Trimodal Therapy in an Orthotopic Hepatocellular Carcinoma Xenograft Mouse Model. *ACS Appl Mater Interfaces* (2020) 12(15):17193–206. doi: 10.1021/acsami.0c00375
54. Wu H, Wang C, Sun J, Sun L, Wan J, Wang S, et al. Self-Assembled and Self-Monitored Sorafenib/Indocyanine Green Nanodrug With Synergistic Antitumor Activity Mediated by Hyperthermia and Reactive Oxygen Species-Induced Apoptosis. *ACS Appl Mater Interfaces* (2019) 11 (47):43996–4006. doi: 10.1021/acsami.9b18086
55. Zhang D, Zheng A, Li J, Wu M, Wu L, Wei Z, et al. Smart Cu(II)-Aptamer Complexes Based Gold Nanoplatform for Tumor Micro-Environment Triggered Programmable Intracellular Prodrug Release, Photodynamic Treatment and Aggregation Induced Photothermal Therapy of Hepatocellular Carcinoma. *Theranostics* (2017) 7(1):164–79. doi: 10.7150/thno.17099
56. Zhang D, Zheng Y, Lin Z, Lan S, Zhang X, Zheng A, et al. Artificial Engineered Natural Killer Cells Combined With Antiheat Endurance as a Powerful Strategy for Enhancing Photothermal-Immunotherapy Efficiency of Solid Tumors. *Small (Weinheim an der Bergstrasse Germany)* (2019) 15 (42):e1902636. doi: 10.1002/smll.201902636
57. Lan S, Lin Z, Zhang D, Zeng Y, Liu X. Photocatalysis Enhancement for Programmable Killing of Hepatocellular Carcinoma Through Self-Compensation Mechanisms Based on Black Phosphorus Quantum-Dot-Hybridized Nanocatalysts. *ACS Appl Mater Interfaces* (2019) 11(10):9804–13. doi: 10.1021/acsami.8b21820
58. Qi S, Zhang Y, Liu G, Chen J, Li X, Zhu Q, et al. Plasmonic-Doped Melanin-Mimic for CXCR4-Targeted NIR-II Photoacoustic Computed Tomography-Guided Photothermal Ablation of Orthotopic Hepatocellular Carcinoma. *Acta Biomater* (2021) 129:245–57. doi: 10.1016/j.actbio.2021.05.034
59. Ali MY, Grimm CF, Ritter M, Mohr L, Allgaier H-P, Weth R, et al. Activation of Dendritic Cells by Local Ablation of Hepatocellular Carcinoma. *J Hepatol* (2005) 43(5):817–22. doi: 10.1016/j.jhep.2005.04.016
60. Zerbini A, Pilli M, Penna A, Pelosi G, Schianchi C, Molinari A, et al. Radiofrequency Thermal Ablation of Hepatocellular Carcinoma Liver Nodules can Activate and Enhance Tumor-Specific T-Cell Responses. *Cancer Res* (2006) 66(2):1139–46. doi: 10.1158/0008-5472.CAN-05-2244
61. Zerbini A, Pilli M, Fagnoni F, Pelosi G, Pizzi MG, Schivazappa S, et al. Increased Immunostimulatory Activity Conferred to Antigen-Presenting Cells by Exposure to Antigen Extract From Hepatocellular Carcinoma After Radiofrequency Thermal Ablation. *J Immunother (Hagerstown Md 1997)* (2008) 31(3):271–82. doi: 10.1097/CJI.0b013e318160ff1c
62. Rochigneux P, Nault J-C, Mallet F, Chretien A-S, Barget N, Garcia AJ, et al. Dynamic of Systemic Immunity and its Impact on Tumor Recurrence After Radiofrequency Ablation of Hepatocellular Carcinoma. *Oncoimmunology* (2019) 8(8):1615818. doi: 10.1080/2162402X.2019.1615818
63. Leuchte K, Staib E, Thelen M, Gödel P, Lechner A, Zentis P, et al. Microwave Ablation Enhances Tumor-Specific Immune Response in Patients With Hepatocellular Carcinoma. *Cancer Immunol Immunother* (2021) 70 (4):893–907. doi: 10.1007/s00262-020-02734-1
64. Guo X, Du F, Liu Q, Guo Y, Wang Q, Huang W, et al. Immunological Effect of Irreversible Electroporation on Hepatocellular Carcinoma. *BMC Cancer* (2021) 21(1):443. doi: 10.1186/s12885-021-08176-x
65. Zeng Z, Shi F, Zhou L, Zhang M-N, Chen Y, Chang X-J, et al. Upregulation of Circulating PD-L1/PD-1 is Associated With Poor Post-Cryoablation Prognosis in Patients With HBV-Related Hepatocellular Carcinoma. *PLoS One* (2011) 6(9):e23621. doi: 10.1371/journal.pone.0023621
66. Qi X, Yang M, Ma L, Sauer M, Avella D, Kaifi JT, et al. Synergizing Sunitinib and Radiofrequency Ablation to Treat Hepatocellular Cancer by Triggering

the Antitumor Immune Response. *J Immunother Cancer* (2020) 8(2):1038–51. doi: 10.1136/jitc-2020-001038
67. Dai Z, Wang Z, Lei K, Liao J, Peng Z, Lin M, et al. Irreversible Electroporation Induces CD8 T Cell Immune Response Against Post-Ablation Hepatocellular Carcinoma Growth. *Cancer Lett* (2021) 503:1–10. doi: 10.1016/j.canlet.2021.01.001
68. Au JT, Wong J, Mittra A, Carpenter S, Haddad D, Carson J, et al. Irreversible Electroporation Is a Surgical Ablation Technique That Enhances Gene Transfer. *Surgery* (2011) 150(3):474–9. doi: 10.1016/j.surg.2011.07.007
69. Au JT, Mittra A, Song TJ, Cavnar M, Jun K, Carson J, et al. Irreversible Electroporation Facilitates Gene Transfer of a GM-CSF Plasmid With a Local and Systemic Response. *Surgery* (2013) 154(3):496–503. doi: 10.1016/j.surg.2013.06.005
70. Shi L, Chen L, Wu C, Zhu Y, Xu B, Zheng X, et al. PD-1 Blockade Boosts Radiofrequency Ablation-Elicited Adaptive Immune Responses Against Tumor. *Clin Cancer Res* (2016) 22(5):1173–84. doi: 10.1158/1078-0432.CCR-15-1352
71. Fei Q, Pan Y, Lin W, Zhou Y, Yu X, Hou Z, et al. High-Dimensional Single-Cell Analysis Delineates Radiofrequency Ablation Induced Immune Microenvironmental Remodeling in Pancreatic Cancer. *Cell Death Dis* (2020) 11(7):589. doi: 10.1038/s41419-020-02787-1
72. Chauhan A, Midha S, Kumar R, Meena R, Singh P, Jha SK, et al. Rapid Tumor Inhibition *via* Magnetic Hyperthermia Regulated by Caspase 3 With Time-Dependent Clearance of Iron Oxide Nanoparticles. *Biomater Sci* (2021) 9(8):2972–90. doi: 10.1039/d0bm01705a
73. Muñoz NM, Dupuis C, Williams M, Dixon K, McWatters A, Avritscher R, et al. Molecularly Targeted Photothermal Ablation Improves Tumor Specificity and Immune Modulation in a Rat Model of Hepatocellular Carcinoma. *Commun Biol* (2020) 3(1):783. doi: 10.1038/s42003-020-01522-y
74. Wu H, Li S-S, Zhou M, Jiang A-N, He Y, Wang S, et al. Palliative Radiofrequency Ablation Accelerates the Residual Tumor Progression Through Increasing Tumor-Infiltrating MDSCs and Reducing T-Cell-Mediated Anti-Tumor Immune Responses in Animal Model. *Front Oncol* (2020) 10:1308. doi: 10.3389/fonc.2020.01308
75. Zhao J, Li Q, Muktiali M, Ren B, Hu Y, Li D, et al. Effect of Microwave Ablation Treatment of Hepatic Malignancies on Serum Cytokine Levels. *BMC Cancer* (2020) 20(1):812. doi: 10.1186/s12885-020-07326-x
76. Facciorusso A, Del Prete V, Antonino M, Crucinio N, Neve V, Di Leo A, et al. Post-Recurrence Survival in Hepatocellular Carcinoma After Percutaneous Radiofrequency Ablation. *Dig Liver Dis* (2014) 46(11):1014–9. doi: 10.1016/j.dld.2014.07.012
77. Tiong L, Maddern GJ. Systematic Review and Meta-Analysis of Survival and Disease Recurrence After Radiofrequency Ablation for Hepatocellular Carcinoma. *Br J Surg* (2011) 98(9):1210–24. doi: 10.1002/bjs.7669
78. Yoshida S, Kornek M, Ikenaga N, Schmelzle M, Masuzaki R, Csizmadia E, et al. Sublethal Heat Treatment Promotes Epithelial-Mesenchymal Transition and Enhances the Malignant Potential of Hepatocellular Carcinoma. *Hepatol (Baltimore Md)* (2013) 58(5):1667–80. doi: 10.1002/hep.26526
79. Zhang R, Ma M, Lin X-H, Liu H-H, Chen J, Chen J, et al. Extracellular Matrix Collagen I Promotes the Tumor Progression of Residual Hepatocellular Carcinoma After Heat Treatment. *BMC Cancer* (2018) 18 (1):901. doi: 10.1186/s12885-018-4820-9
80. Su T, Liao J, Dai Z, Xu L, Chen S, Wang Y, et al. Stress-Induced Phosphoprotein 1 Mediates Hepatocellular Carcinoma Metastasis After Insufficient Radiofrequency Ablation. *Oncogene* (2018) 37(26):3514–27. doi: 10.1038/s41388-018-0169-4
81. Bruix J, Raoul J-L, Sherman M, Mazzaferro V, Bolondi L, Craxi A, et al. Efficacy and Safety of Sorafenib in Patients With Advanced Hepatocellular Carcinoma: Subanalyses of a Phase III Trial. *J Hepatol* (2012) 57(4):821–9. doi: 10.1016/j.jhep.2012.06.014
82. Kudo M, Finn RS, Qin S, Han K-H, Ikeda K, Piscaglia F, et al. Lenvatinib Versus Sorafenib in First-Line Treatment of Patients With Unresectable Hepatocellular Carcinoma: A Randomised Phase 3 Non-Inferiority Trial. *Lancet (Lond Engl)* (2018) 391(10126):1163–73. doi: 10.1016/S0140-6736(18)30207-1
83. Cheon J, Chon HJ, Bang Y, Park NH, Shin JW, Kim KM, et al. Real-World Efficacy and Safety of Lenvatinib in Korean Patients With Advanced Hepatocellular Carcinoma: A Multicenter Retrospective Analysis. *Liver Cancer* (2020) 9(5):613–24. doi: 10.1159/000508901
84. Qin S, Bi F, Gu S, Bai Y, Chen Z, Wang Z, et al. Donafenib Versus Sorafenib in First-Line Treatment of Unresectable or Metastatic Hepatocellular Carcinoma: A Randomized, Open-Label, Parallel-Controlled Phase II-III Trial. *J Clin Oncol* (2021) 39(27):3002–11. doi: 10.1200/JCO.21.00163
85. Bruix J, Qin S, Merle P, Granito A, Huang Y-H, Bodoky G, et al. Regorafenib for Patients With Hepatocellular Carcinoma Who Progressed on Sorafenib Treatment (RESORCE): A Randomised, Double-Blind, Placebo-Controlled, Phase 3 Trial. *Lancet (Lond Engl)* (2017) 389(10064):56–66. doi: 10.1016/S0140-6736(16)32453-9
86. Kelley RK, Ryoo B-Y, Merle P, Park J-W, Bolondi L, Chan SL, et al. Second-Line Cabozantinib After Sorafenib Treatment for Advanced Hepatocellular Carcinoma: A Subgroup Analysis of the Phase 3 CELESTIAL Trial. *ESMO Open* (2020) 5(4):714–22. doi: 10.1136/esmoopen-2020-000714
87. Pinyol R, Montal R, Bassaganyas L, Sia D, Takayama T, Chau G-Y, et al. Molecular Predictors of Prevention of Recurrence in HCC With Sorafenib as Adjuvant Treatment and Prognostic Factors in the Phase 3 STORM Trial. *Gut* (2019) 68(6):1065–75. doi: 10.1136/gutjnl-2018-316408
88. Bian H, Zheng J-S, Nan G, Li R, Chen C, Hu C-X, et al. Randomized Trial of [131I] Metuximab in Treatment of Hepatocellular Carcinoma After Percutaneous Radiofrequency Ablation. *J Natl Cancer Inst* (2014) 106 (9):239–43. doi: 10.1093/jnci/dju239
89. Li J, Xing J, Yang Y, Liu J, Wang W, Xia Y, et al. Adjuvant I-Metuximab for Hepatocellular Carcinoma After Liver Resection: A Randomised, Controlled, Multicentre, Open-Label, Phase 2 Trial. *Lancet Gastroenterol Hepatol* (2020) 5(6):548–60. doi: 10.1016/S2468-1253(19)30422-4
90. Sangro B, Sarobe P, Hervás-Stubbs S, Melero I. Advances in Immunotherapy for Hepatocellular Carcinoma. *Nat Rev Gastroenterol Hepatol* (2021) 18 (8):525–43. doi: 10.1038/s41575-021-00438-0
91. Pinter M, Jain RK, Duda DG. The Current Landscape of Immune Checkpoint Blockade in Hepatocellular Carcinoma: A Review. *JAMA Oncol* (2021) 7(1):113–23. doi: 10.1001/jamaoncol.2020.3381
92. Abd El Aziz MA, Facciorusso A, Nayfeh T, Saadi S, Elnaggar M, Cotsoglou C, et al. Immune Checkpoint Inhibitors for Unresectable Hepatocellular Carcinoma. *Vaccines (Basel)* (2020) 8(4):616–44. doi: 10.3390/vaccines8040616
93. El-Khoueiry AB, Sangro B, Yau T, Crocenzi TS, Kudo M, Hsu C, et al. Nivolumab in Patients With Advanced Hepatocellular Carcinoma (CheckMate 040): An Open-Label, Non-Comparative, Phase 1/2 Dose Escalation and Expansion Trial. *Lancet (Lond Engl)* (2017) 389 (10088):2492–502. doi: 10.1016/S0140-6736(17)31046-2
94. Lee MS, Ryoo B-Y, Hsu C-H, Numata K, Stein S, Verret W, et al. Atezolizumab With or Without Bevacizumab in Unresectable Hepatocellular Carcinoma (GO30140): An Open-Label, Multicentre, Phase 1b Study. *Lancet Oncol* (2020) 21(6):808–20. doi: 10.1016/S1470-2045(20)30156-X
95. Sangro B, Gomez-Martin C, de la Mata M, Iñarrairaegui M, Garralda E, Barrera P, et al. A Clinical Trial of CTLA-4 Blockade With Tremelimumab in Patients With Hepatocellular Carcinoma and Chronic Hepatitis C. *J Hepatol* (2013) 59(1):81–8. doi: 10.1016/j.jhep.2013.02.022
96. Yau T, Hsu C, Kim T-Y, Choo S-P, Kang Y-K, Hou M-M, et al. Nivolumab in Advanced Hepatocellular Carcinoma: Sorafenib-Experienced Asian Cohort Analysis. *J Hepatol* (2019) 71(3):543–52. doi: 10.1016/j.jhep.2019.05.014
97. Zhu AX, Finn RS, Edeline J, Cattan S, Ogasawara S, Palmer D, et al. Pembrolizumab in Patients With Advanced Hepatocellular Carcinoma Previously Treated With Sorafenib (KEYNOTE-224): A Non-Randomised, Open-Label Phase 2 Trial. *Lancet Oncol* (2018) 19(7):940–52. doi: 10.1016/S1470-2045(18)30351-6
98. Finn RS, Qin S, Ikeda M, Galle PR, Ducreux M, Kim T-Y, et al. Atezolizumab Plus Bevacizumab in Unresectable Hepatocellular Carcinoma. *N Engl J Med* (2020) 382(20):1894–905. doi: 10.1056/NEJMoa1915745
99. Galle PR, Finn RS, Qin S, Ikeda M, Zhu AX, Kim T-Y, et al. Patient-Reported Outcomes With Atezolizumab Plus Bevacizumab Versus Sorafenib in Patients With Unresectable Hepatocellular Carcinoma (IMbrave150): An Open-Label, Randomised, Phase 3 Trial. *Lancet Oncol* (2021) 22(7):991–1001. doi: 10.1016/S1470-2045(21)00151-0

100. Takayama T, Sekine T, Makuuchi M, Yamasaki S, Kosuge T, Yamamoto J, et al. Adoptive Immunotherapy to Lower Postsurgical Recurrence Rates of Hepatocellular Carcinoma: A Randomised Trial. *Lancet (London Engl)* (2000) 356(9232):802–7. doi: 10.1016/S0140-6736(00)02654-4
101. Palmer DH, Midgley RS, Mirza N, Torr EE, Ahmed F, Steele JC, et al. A Phase II Study of Adoptive Immunotherapy Using Dendritic Cells Pulsed With Tumor Lysate in Patients With Hepatocellular Carcinoma. *Hepatol (Baltimore Md)* (2009) 49(1):124–32. doi: 10.1002/hep.22626
102. Lee JH, Lee J-H, Lim Y-S, Yeon JE, Song T-J, Yu SJ, et al. Adjuvant Immunotherapy With Autologous Cytokine-Induced Killer Cells for Hepatocellular Carcinoma. *Gastroenterology* (2015) 148(7):1383–91. doi: 10.1053/j.gastro.2015.02.055
103. Heo J, Reid T, Ruo L, Breitbach CJ, Rose S, Bloomston M, et al. Randomized Dose-Finding Clinical Trial of Oncolytic Immunotherapeutic Vaccinia JX-594 in Liver Cancer. *Nat Med* (2013) 19(3):329–36. doi: 10.1038/nm.3089
104. Cripe TP, Ngo MC, Geller JI, Louis CU, Currier MA, Racadio JM, et al. Phase 1 Study of Intratumoral Pexa-Vec (JX-594), an Oncolytic and Immunotherapeutic Vaccinia Virus, in Pediatric Cancer Patients. *Mol Ther* (2015) 23(3):602–8. doi: 10.1038/mt.2014.243
105. Sawada Y, Yoshikawa T, Nobuoka D, Shirakawa H, Kuronuma T, Motomura Y, et al. Phase I Trial of a Glypican-3-Derived Peptide Vaccine for Advanced Hepatocellular Carcinoma: Immunologic Evidence and Potential for Improving Overall Survival. *Clin Cancer Res* (2012) 18(13):3686–96. doi: 10.1158/1078-0432.CCR-11-3044
106. Butterfield LH, Ribas A, Meng WS, Dissette VB, Amarnani S, Vu HT, et al. T-Cell Responses to HLA-A*0201 Immunodominant Peptides Derived From Alpha-Fetoprotein in Patients With Hepatocellular Cancer. *Clin Cancer Res* (2003) 9(16 Pt 1):5902–8.
107. Shang X-Y, Chen H-S, Zhang H-G, Pang X-W, Qiao H, Peng J-R, et al. The Spontaneous CD8+ T-Cell Response to HLA-A2-Restricted NY-ESO-1b Peptide in Hepatocellular Carcinoma Patients. *Clin Cancer Res* (2004) 10 (20):6946–55. doi: 10.1158/1078-0432.CCR-04-0502
108. Yoshikawa T, Nakatsugawa M, Suzuki S, Shirakawa H, Nobuoka D, Sakemura N, et al. HLA-A2-Restricted Glypican-3 Peptide-Specific CTL Clones Induced by Peptide Vaccine Show High Avidity and Antigen-Specific Killing Activity Against Tumor Cells. *Cancer Sci* (2011) 102(5):918–25. doi: 10.1111/j.1349-7006.2011.01896.x
109. Lee J-H, Lee Y, Lee M, Heo MK, Song J-S, Kim K-H, et al. A Phase I/IIa Study of Adjuvant Immunotherapy With Tumour Antigen-Pulsed Dendritic Cells in Patients With Hepatocellular Carcinoma. *Br J Cancer* (2015) 113 (12):1666–76. doi: 10.1038/bjc.2015.430
110. Sawada Y, Yoshikawa T, Shimomura M, Iwama T, Endo I, Nakatsura T. Programmed Death-1 Blockade Enhances the Antitumor Effects of Peptide Vaccine-Induced Peptide-Specific Cytotoxic T Lymphocytes. *Int J Oncol* (2015) 46(1):28–36. doi: 10.3892/ijo.2014.2737
111. Wu Q, Pi L, Le Trinh T, Zuo C, Xia M, Jiao Y, et al. A Novel Vaccine Targeting Glypican-3 as a Treatment for Hepatocellular Carcinoma. *Mol Ther* (2017) 25(10):2299–308. doi: 10.1016/j.ymthe.2017.08.005
112. Chen K, Wu Z, Zhao H, Wang Y, Ge Y, Wang D, et al. / Fusion Gene Immunization Generates Potent Antitumor Cellular Immunity and Enhances Anti-PD-1 Efficacy. *Cancer Immunol Res* (2020) 8(1):81–93. doi: 10.1158/2326-6066.CIR-19-0210
113. Yu L, Yang X, Huang N, Lang Q-L, He Q-L, Jian-Hua W, et al. A Novel Targeted GPC3/CD3 Bispecific Antibody for the Treatment Hepatocellular Carcinoma. *Cancer Biol Ther* (2020) 21(7):597–603. doi: 10.1080/15384047.2020.1743158
114. Liu X, Gao F, Jiang L, Jia M, Ao L, Lu M, et al. 32A9, a Novel Human Antibody for Designing an Immunotoxin and CAR-T Cells Against Glypican-3 in Hepatocellular Carcinoma. *J Transl Med* (2020) 18(1):295. doi: 10.1186/s12967-020-02462-1
115. Du K, Li Y, Liu J, Chen W, Wei Z, Luo Y, et al. A Bispecific Antibody Targeting GPC3 and CD47 Induced Enhanced Antitumor Efficacy Against Dual Antigen-Expressing HCC. *Mol Ther* (2021) 29(4):1572–84. doi: 10.1016/j.ymthe.2021.01.006
116. Li D, Li N, Zhang Y-F, Fu H, Feng M, Schneider D, et al. Persistent Polyfunctional Chimeric Antigen Receptor T Cells That Target Glypican 3 Eliminate Orthotopic Hepatocellular Carcinomas in Mice. *Gastroenterology* (2020) 158(8):2250–65. doi: 10.1053/j.gastro.2020.02.011
117. Sun L, Gao F, Gao Z, Ao L, Li N, Ma S, et al. Shed Antigen-Induced Blocking Effect on CAR-T Cells Targeting Glypican-3 in Hepatocellular Carcinoma. *J Immunother Cancer* (2021) 9(4):1875–88. doi: 10.1136/jitc-2020-001875
118. Yu M, Luo H, Fan M, Wu X, Shi B, Di S, et al. Development of GPC3-Specific Chimeric Antigen Receptor-Engineered Natural Killer Cells for the Treatment of Hepatocellular Carcinoma. *Mol Ther* (2018) 26(2):366–78. doi: 10.1016/j.ymthe.2017.12.012
119. Liao N, Su L, Zheng Y, Zhao B, Wu M, Zhang D, et al. *In Vivo* Tracking of Cell Viability for Adoptive Natural Killer Cell-Based Immunotherapy by Ratiometric NIR-II Fluorescence Imaging. *Angew Chem Int Ed Engl* (2021). doi: 10.1002/anie.202106730
120. Liu Q, Tian Y, Li Y, Zhang W, Cai W, Liu Y, et al. *In Vivo* Therapeutic Effects of Affinity-Improved-TCR Engineered T-Cells on HBV-Related Hepatocellular Carcinoma. *J Immunother Cancer* (2020) 8(2):1748–60. doi: 10.1136/jitc-2020-001748
121. Tseng H-C, Xiong W, Badeti S, Yang Y, Ma M, Liu T, et al. Efficacy of Anti-CD147 Chimeric Antigen Receptors Targeting Hepatocellular Carcinoma. *Nat Commun* (2020) 11(1):4810. doi: 10.1038/s41467-020-18444-2
122. Rettman P, Blunt MD, Fulton RJ, Vallejo AF, Bastidas-Legarda LY, España-Serrano L, et al. Peptide: MHC-Based DNA Vaccination Strategy to Activate Natural Killer Cells by Targeting Killer Cell Immunoglobulin-Like Receptors. *J Immunother Cancer* (2021) 9(5):1912–22. doi: 10.1136/jitc-2020-001912
123. Yang T, Li C, Wang X, Zhao D, Zhang M, Cao H, et al. Efficient Hepatic Delivery and Protein Expression Enabled by Optimized mRNA and Ionizable Lipid Nanoparticle. *Bioact Mater* (2020) 5(4):1053–61. doi: 10.1016/j.bioactmat.2020.07.003
124. Li G, Liu D, Kimchi ET, Kaifi JT, Qi X, Manjunath Y, et al. Nanoliposome C6-Ceramide Increases the Anti-Tumor Immune Response and Slows Growth of Liver Tumors in Mice. *Gastroenterology* (2018) 154(4):1024–36. doi: 10.1053/j.gastro.2017.10.050
125. Zuo B, Qi H, Lu Z, Chen L, Sun B, Yang R, et al. Alarmin-Painted Exosomes Elicit Persistent Antitumor Immunity in Large Established Tumors in Mice. *Nat Commun* (2020) 11(1):1790. doi: 10.1038/s41467-020-15569-2
126. Bruix J, Takayama T, Mazzaferro V, Chau G-Y, Yang J, Kudo M, et al. Adjuvant Sorafenib for Hepatocellular Carcinoma After Resection or Ablation (STORM): A Phase 3, Randomised, Double-Blind, Placebo-Controlled Trial. *Lancet Oncol* (2015) 16(13):1344–54. doi: 10.1016/S1470-2045(15)00198-9
127. Lencioni R, Llovet JM, Han G, Tak WY, Yang J, Guglielmi A, et al. Sorafenib or Placebo Plus TACE With Doxorubicin-Eluting Beads for Intermediate Stage HCC: The SPACE Trial. *J Hepatol* (2016) 64(5):1090–8. doi: 10.1016/j.jhep.2016.01.012
128. Meyer T, Fox R, Ma YT, Ross PJ, James MW, Sturgess R, et al. Sorafenib in Combination With Transarterial Chemoembolisation in Patients With Unresectable Hepatocellular Carcinoma (TACE 2): A Randomised Placebo-Controlled, Double-Blind, Phase 3 Trial. *Lancet Gastroenterol Hepatol* (2017) 2(8):565–75. doi: 10.1016/S2468-1253(17)30156-5
129. Yoshiji H, Noguchi R, Toyohara M, Ikenaka Y, Kitade M, Kaji K, et al. Combination of Vitamin K2 and Angiotensin-Converting Enzyme Inhibitor Ameliorates Cumulative Recurrence of Hepatocellular Carcinoma. *J Hepatol* (2009) 51(2):315–21. doi: 10.1016/j.jhep.2009.04.011
130. Facciorusso A, Del Prete V, Crucinio N, Muscatiello N, Carr BI, Di Leo A, et al. Angiotensin Receptor Blockers Improve Survival Outcomes After Radiofrequency Ablation in Hepatocarcinoma Patients. *J Gastroenterol Hepatol* (2015) 30(11):1643–50. doi: 10.1111/jgh.12988
131. Facciorusso A, Abd El Aziz MA, Cincione I, Cea UV, Germini A, Granieri S, et al. Angiotensin Receptor 1 Blockers Prolong Time to Recurrence After Radiofrequency Ablation in Hepatocellular Carcinoma Patients: A Retrospective Study. *Biomedicines* (2020) 8(10):399–410. doi: 10.3390/biomedicines8100399
132. Behm B, Di Fazio P, Michl P, Neureiter D, Kemmerling R, Hahn EG, et al. Additive Antitumour Response to the Rabbit VX2 Hepatoma by Combined Radio Frequency Ablation and Toll Like Receptor 9 Stimulation. *Gut* (2016) 65(1):134–43. doi: 10.1136/gutjnl-2014-308286
133. Duan X, Wang M, Han X, Ren J, Huang G, Ju S, et al. Combined Use of Microwave Ablation and Cell Immunotherapy Induces Nonspecific Immunity of Hepatocellular Carcinoma Model Mice. *Cell Cycle (Georgetown Tex)* (2020) 19 (24):3595–607. doi: 10.1080/15384101.2020.1853942

134. Duffy AG, Ulahannan SV, Makorova-Rusher O, Rahma O, Wedemeyer H, Pratt D, et al. Tremelimumab in Combination With Ablation in Patients With Advanced Hepatocellular Carcinoma. *J Hepatol* (2017) 66(3):545–51. doi: 10.1016/j.jhep.2016.10.029
135. Agdashian D, ElGindi M, Xie C, Sandhu M, Pratt D, Kleiner DE, et al. The Effect of Anti-CTLA4 Treatment on Peripheral and Intra-Tumoral T Cells in Patients With Hepatocellular Carcinoma. *Cancer Immunol Immunother* (2019) 68(4):599–608. doi: 10.1007/s00262-019-02299-8
136. Wang X, Liu G, Chen S, Bi H, Xia F, Feng K, et al. Combination Therapy With PD-1 Blockade and Radiofrequency Ablation for Recurrent Hepatocellular Carcinoma: A Propensity Score Matching Analysis. *Int J Hperthermia* (2021) 38(1):1519–28. doi: 10.1080/02656736.2021.1991011
137. Lyu N, Kong Y, Li X, Mu L, Deng H, Chen H, et al. Ablation Reboots the Response in Advanced Hepatocellular Carcinoma With Stable or Atypical Response During PD-1 Therapy: A Proof-Of-Concept Study. *Front Oncol* (2020) 10:580241. doi: 10.3389/fonc.2020.580241
138. Ma H, Zhang Y, Wang Q, Li Y, He J, Wang H, et al. Therapeutic Safety and Effects of Adjuvant Autologous RetroNectin Activated Killer Cell Immunotherapy for Patients With Primary Hepatocellular Carcinoma After Radiofrequency Ablation. *Cancer Biol Ther* (2010) 9(11):903–7. doi: 10.4161/cbt.9.11.11697
139. Cui J, Wang N, Zhao H, Jin H, Wang G, Niu C, et al. Combination of Radiofrequency Ablation and Sequential Cellular Immunotherapy Improves Progression-Free Survival for Patients With Hepatocellular Carcinoma. *Int J Cancer* (2014) 134(2):342–51. doi: 10.1002/ijc.28372
140. Yoon JS, Song BG, Lee J-H, Lee HY, Kim SW, Chang Y, et al. Adjuvant Cytokine-Induced Killer Cell Immunotherapy for Hepatocellular Carcinoma: A Propensity Score-Matched Analysis of Real-World Data. *BMC Cancer* (2019) 19(1):523. doi: 10.1186/s12885-019-5740-z
141. Kitahara M, Mizukoshi E, Terashima T, Nakagawa H, Horii R, Iida N, et al. Safety and Long-Term Outcome of Intratumoral Injection of OK432-Stimulated Dendritic Cells for Hepatocellular Carcinomas After Radiofrequency Ablation. *Transl Oncol* (2020) 13(7):100777. doi: 10.1016/j.tranon.2020.100777
142. Sawada Y, Yoshikawa T, Ofuji K, Yoshimura M, Tsuchiya N, Takahashi M, et al. Phase II Study of the GPC3-Derived Peptide Vaccine as an Adjuvant Therapy for Hepatocellular Carcinoma Patients. *Oncoimmunology* (2016) 5 (5):e1129483. doi: 10.1080/2162402X.2015.1129483
143. Zhou P, Liang P, Dong B, Yu X, Han Z, Xu Y. Phase I Clinical Study of Combination Therapy With Microwave Ablation and Cellular Immunotherapy in Hepatocellular Carcinoma. *Cancer Biol Ther* (2011) 11 (5):450–6. doi: 10.4161/cbt.11.5.14669
144. Niu L-Z, Li J-L, Zeng J-Y, Mu F, Liao M-T, Yao F, et al. Combination Treatment With Comprehensive Cryoablation and Immunotherapy in Metastatic Hepatocellular Cancer. *World J Gastroenterol* (2013) 19 (22):3473–80. doi: 10.3748/wjg.v19.i22.3473
145. Nobuoka D, Motomura Y, Shirakawa H, Yoshikawa T, Kuronuma T, Takahashi M, et al. Radiofrequency Ablation for Hepatocellular Carcinoma Induces Glypican-3 Peptide-Specific Cytotoxic T Lymphocytes. *Int J Oncol* (2012) 40(1):63–70. doi: 10.3892/ijo.2011.1202
146. Yang H, Liu H-S, Hou W, Gao J-X, Duan Y, Wei D, et al. An NIR-Responsive Mesoporous Silica Nanosystem for Synergetic Photothermal-Immunoenhancement Therapy of Hepatocellular Carcinoma. *J Mater Chem B* (2020) 8(2):251–9. doi: 10.1039/c9tb01891c
147. Zhou T, Liang X, Wang P, Hu Y, Qi Y, Jin Y, et al. A Hepatocellular Carcinoma Targeting Nanostrategy With Hypoxia-Ameliorating and Photothermal Abilities That, Combined With Immunotherapy, Inhibits Metastasis and Recurrence. *ACS Nano* (2020) 14(10):12679–96. doi: 10.1021/acsnano.0c01453
148. Cai Z, Xin F, Wei Z, Wu M, Lin X, Du X, et al. Photodynamic Therapy Combined With Antihypoxic Signaling and CpG Adjuvant as an *In Situ* Tumor Vaccine Based on Metal-Organic Framework Nanoparticles to Boost Cancer Immunotherapy. *Adv Healthc Mater* (2020) 9(1):e1900996. doi: 10.1002/adhm.201900996
149. Tan Y, Yang S, Ma Y, Li J, Xie Q, Liu C, et al. Nanobubbles Containing sPD-1 and Ce6 Mediate Combination Immunotherapy and Suppress Hepatocellular Carcinoma in Mice. *Int J Nanomed* (2021) 16:3241–54. doi: 10.2147/IJN.S305857
150. Lin X, Huang R, Huang Y, Wang K, Li H, Bao Y, et al. Nanosonosensitizer-Augmented Sonodynamic Therapy Combined With Checkpoint Blockade for Cancer Immunotherapy. *Int J Nanomed* (2021) 16:1889–99. doi: 10.2147/IJN.S290796
151. Cai H, Dai X, Guo X, Zhang L, Cao K, Yan F, et al. Ataxia Telangiectasia Mutated Inhibitor-Loaded Copper Sulfide Nanoparticles for Low-Temperature Photothermal Therapy of Hepatocellular Carcinoma. *Acta Biomater* (2021) 127:276–86. doi: 10.1016/j.actbio.2021.03.051
152. Xia Q-H, Lu C-T, Tong M-Q, Yue M, Chen R, Zhuge D-L, et al. Ganoderma Lucidum Polysaccharides Enhance the Abscopal Effect of Photothermal Therapy in Hepatoma-Bearing Mice Through Immunomodulatory, Anti-Proliferative, Pro-Apoptotic and Anti-Angiogenic. *Front Pharmacol* (2021) 12:648708. doi: 10.3389/fphar.2021.648708
153. Wang J, Meng J, Ran W, Lee RJ, Teng L, Zhang P, et al. Hepatocellular Carcinoma Growth Retardation and PD-1 Blockade Therapy Potentiation With Synthetic High-Density Lipoprotein. *Nano Lett* (2019) 19(8):5266–76. doi: 10.1021/acs.nanolett.9b01717
154. Ma W, Zhu D, Li J, Chen X, Xie W, Jiang X, et al. Coating Biomimetic Nanoparticles With Chimeric Antigen Receptor T Cell-Membrane Provides High Specificity for Hepatocellular Carcinoma Photothermal Therapy Treatment. *Theranostics* (2020) 10(3):1281–95. doi: 10.7150/thno.40291

Conflict of Interest: The authors declare that the research was conducted in the absence of any commercial or financial relationships that could be construed as a potential conflict of interest.

frontiers in Immunology

CASE REPORT
published: 23 December 2021
doi: 10.3389/fimmu.2021.788629

A Case Report of Non-Bacterial Cystitis Caused by Immune Checkpoint Inhibitors

Sihui Zhu[1,2†], *Lijuan Bian*[1,2†], *Jia Lv*[1,2†], *Baorui Liu*[1,2*] *and Jie Shen*[1,2*]

[1] Comprehensive Cancer Centre of Nanjing Drum Tower Hospital, Clinical College of Nanjing Medical University, Nanjing, China, [2] Comprehensive Cancer Centre of Drum Tower Hospital, Medical School of Nanjing University, Clinical Cancer Institute of Nanjing University, Nanjing, China

OPEN ACCESS

Edited by:
Xuesong Gu,
Beth Israel Deaconess Medical Center and Harvard Medical School, United States

Reviewed by:
Qiang Gao,
Fudan University, China
Feng Wang,
Jinling Hospital, China
Zhi Peng,
Peking University Cancer Hospital, China

***Correspondence:**
Jie Shen
shenjie2008nju@163.com
Baorui Liu
baoruiliu@nju.edu.cn

†These authors have contributed equally to this work

Specialty section:
This article was submitted to Cancer Immunity and Immunotherapy, a section of the journal Frontiers in Immunology

Received: 03 October 2021
Accepted: 06 December 2021
Published: 23 December 2021

Citation:
Zhu S, Bian L, Lv J, Liu B and Shen J (2021) A Case Report of Non-Bacterial Cystitis Caused by Immune Checkpoint Inhibitors. Front. Immunol. 12:788629. doi: 10.3389/fimmu.2021.788629

We report a case of non-bacterial cystitis after treatment with programmed death-1 (PD-1) and programmed cell death-ligand 1 (PD-L1) antibodies, which was considered an immune-related adverse event (irAE). A 48-year-old male patient with intrahepatic cholangiocarcinoma (ICC) was treated with nivolumab after postoperative multi-line treatment. This patient recurred worsening of psoriasis and repeated urinary tract discomfort. The drug was discontinued and surgery was performed due to the recurrence of the tumor suggested by imaging. After receiving three cycles of chemotherapy treatment combined with atezolizumab, urinary tract discomfort reappeared. No bacteria were found in multiple urine cultures, and non-bacterial bladder inflammation was considered after cystoscopy biopsy. This is a report of non-bacterial inflammation of the urinary tract caused by immunotherapy.

Keywords: programmed death-1 antibody, programmed cell death-ligand 1 antibody, intrahepatic cholangiocarcinoma, cystitis, immune-related adverse events

BACKGROUND

Immune checkpoint inhibitors (ICIs) induce antitumor immune responses by blocking immune checkpoints, such as cytotoxic T lymphocyte antigen-4 (CTLA-4) and programmed death-1 (PD-1) or its ligand, PD-L1. By increasing the activity of the immune system, these drugs produce excessive immunity to normal organs and cause toxicity different from standard chemotherapy or other biological agents (1). Among them, skin and gastrointestinal adverse reactions were the most commonly observed (2). Here, we reporte a case of cystitis after receiving nivolumab and atezolizumab (PD-1 and PD-L1 antibodies), which was considered a type of immune-related adverse event (irAE).

CASE REPORT

Our patient is a 48-year-old male with intrahepatic cholangiocarcinoma (ICC) with a history of psoriasis for more than 20 years. After receiving multi-line treatment, including surgery, chemotherapy, and radiotherapy, among others, the effect was not good and the patient's disease progressed. According to the results of clinical trials on biliary tumors (3), PD-1 antibody combined with lenvatinib was tried.

There was no obvious abnormality in urine routine during baseline examination; meanwhile, the patient's psoriasis was also in an inactive period, which has been stable for a long time and did not require drug control. However, after combination treatment with lenvatinib and nivolumab, psoriasis recurred, with scattered rashes all over the body, and skin toxicity symptoms aggravated with the increase of the cumulative dose of the PD-1 antibody. The patient developed urinary tract irritation after three cycles. Urine examination revealed 375/μl white blood cells (WBCs) in the urine (**Figure 1**). Although no bacteria were found in the urine culture, the possibility of bacterial cystitis was still considered after consultation with the urology department based on the patient's symptoms at that time. After antibiotic treatment, laboratory tests had indeed improved, but the patient's symptoms did not get better. Therefore, the treatment was discontinued. However, the patient's tumor indicators increased due to the discontinuation of lenvatinib and PD-1 antibody (**Figure 1**). Imaging examinations also revealed new lesions located on the right posterior lobe of the liver and above the duodenum on the right side of the pancreatic head in the abdominal cavity (**Figure 2**). In general surgery consultation, this patient was considered to have a chance of surgery, so an operation was performed. One month after the second operation, the patient's tumor indicators decreased and then increased again (**Figure 1**). Except for a slight thickening of the local omentum, no lesions were found on imaging. At the same time, the patient's urinary tract symptoms improved after the drug has been withdrawn for more than 3 months. Therefore, Gemox chemotherapy (gemcitabine +oxaliplatin) was considered after the operation. Meanwhile, the patient's immunohistochemistry was positive for PD-L1. Taking the improvement of curative effect into account, and with the patient's insistence on trying, the treatment plan was finally determined as Gemox combined with the PD-L1 antibody. The patient then did not develop skin toxicity. After three cycles, the tumor markers dropped significantly, but bladder irritation reoccurred, which was significantly worse than before. Urine examination revealed that WBCs were 2,818/μl (**Figure 1**) and bacteria were 512/μl. After consultation with the Department of Urology and Nephrology, bilateral ureteral stent implantation and cystoscopy and biopsy were decided. The result of the bladder biopsy indicated chronic inflammation of mucosal tissue, mucosal erosion in some areas, and proliferation of granulation tissues and fibroblasts (**Figure 3**). After the multidisciplinary consultation, immune-related cystitis was considered; treatment with steroid hormones was given, which started at 2 mg/kg, then slowly decreased. The urinary tract irritation symptoms were relieved, and the laboratory examination was also significantly improved. After 4 weeks, the urine routine was reviewed, and the WBC count was 66/μl. At present, during the hormone reduction period, urine routine and carbohydrate antigen 19-9 (CA19-9) are continued to be monitored, and imaging examinations are performed regularly (including MRI and PET-CT). In the follow-up treatment, it was considered that this patient cannot tolerate the side effects of immunotherapy. Whether hormones affect the efficacy of immunotherapy is currently controversial, so chemotherapy only was considered.

DISCUSSION

We report a case of non-bacterial cystitis that is related to PD-1 and PD-L1 antibodies after treatment. As far as we know, there are currently few reports of irAEs in the urinary system, and non-bacterial cystitis is even rarer. This adverse reaction usually causes bladder irritation symptoms, such as frequent urination and pain on urination. For example, a case of immune-related cystitis after the use of nivolumab has been reported by Ozaki et al. This patient developed frequent urination, painful urination, and gross hematuria (4). In addition, two cases reported by Shimatani et al. had symptoms such as frequent urination and diarrhea, and the final pathological examination results were clear as immune-related cystitis (5). According to the relevant literature and guidelines, once irAE is suspected, it is best to have a specialist consultation to rule out infection or other accidental conditions (4). Management after diagnosis generally relies on steroid hormones and other immunomodulatory agents (6).

The exact pathophysiological mechanism of irAE is still unclear, and the side effects and severity caused by different ICI drugs or even different doses also vary (1). In an analysis of advanced melanoma, 71% of patients treated with nivolumab had irAEs, the most common of which were fatigue, pruritus, diarrhea, and rash. Of the patients, 10% reached grade 3 or 4 (7). On the other hand, 84.6% of patients treated with ipilimumab

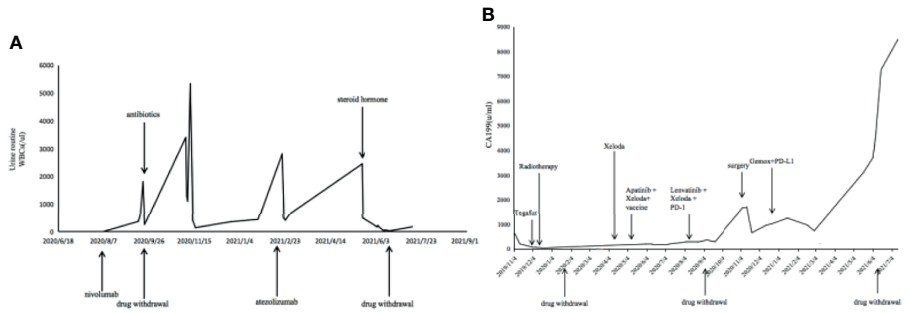

FIGURE 1 | **(A)** Clinical course. **(B)** Carbohydrate antigen 19-9 (CA19-9) change curve.

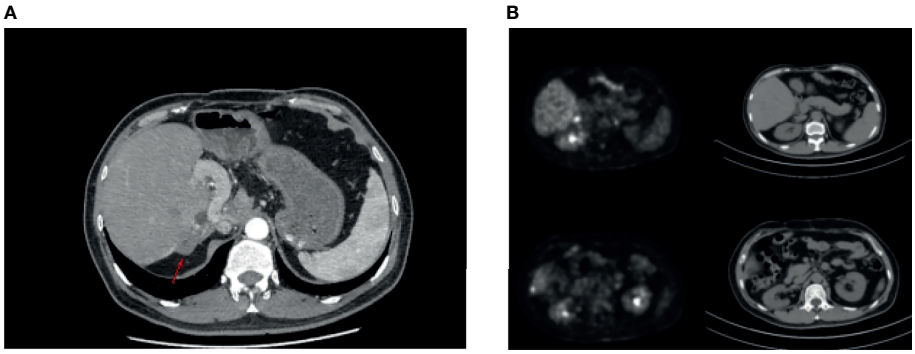

FIGURE 2 | **(A)** October 22, 2019: magnetic resonance cholangiopancreatography showed the density of the soft tissue under the capsule of the right lobe of the liver. The possibility of metastasis was considered. **(B)** November 4, 2020: discovery of new lesions; tumor metastasis was considered (PET/CT showed nodular thickening of the capsule of the right posterior lobe of the liver, soft tissue density nodules in the fat space above the duodenum on the right side of pancreatic head in the abdominal cavity, and abnormal increase of glucose metabolism). Compared with the previous film, it was a new lesion. A high possibility of tumor metastasis was considered.

had irAEs and 25.2% of patients reached grade 3 or 4, which mainly occurred in the gastrointestinal tract, liver, skin, and the endocrine system (7). As far as we know, the non-bacterial cystitis that we have reported in the urinary system is relatively rare, and there are very few reports. Multiple studies have shown that patients with a history of autoimmune diseases have an increased risk of irAEs (1, 8). But these adverse reactions can often be controlled by active treatment, so this is not an absolute contraindication for ICI use. Such patients can still obtain long-lasting antitumor effects from immunotherapy (9).

Steroid hormones can regulate immune activity by inducing the apoptosis of T lymphocytes (10), but its influence on ICI therapy is still controversial. Horvat et al. found that one-third of patients receiving ipilimumab required systemic corticosteroid therapy. But it did not affect the efficacy of immunotherapy. They found that receiving corticosteroid therapy had no significant relationship with the patients' overall survival (OS) (11). However, there are some studies suggesting that a high baseline prednisone dose is associated with poor survival (12). They speculated that the use of steroid hormones before ICI treatment may affect the activation of primitive T cells, thereby affecting the efficacy of immunotherapy, while the use of steroid hormones during treatment would only affect the activated T cells, and this effect cannot reduce the overall efficacy of immunotherapy (12). In this case, the patient had a history of psoriasis. After using PD-1, psoriasis worsened and the symptoms were relieved after symptomatic treatment, so his underlying disease did not affect the ICI treatment. After three cycles, the patient developed symptoms of bladder irritation, but because of the unsatisfactory treatment effect, the disease progression was found on imaging examination to be the reason for the patient's discontinuation of the PD-1 antibody. In the subsequent PD-L1 antibody treatment, the patient did not develop skin toxicity, but the bladder symptoms continued and were worse than before. It may be that the signal pathways of PD-1 and PD-L1 are not the same and that the mechanisms of adverse reactions are also different. After multidisciplinary consultation, the bladder biopsy was considered to be non-bacterial cystitis caused by immunotherapy. After hormone therapy, the patient's own symptoms and laboratory examinations were significantly improved. Since the patient complained that he cannot tolerate such symptoms, and whether hormone therapy would affect the

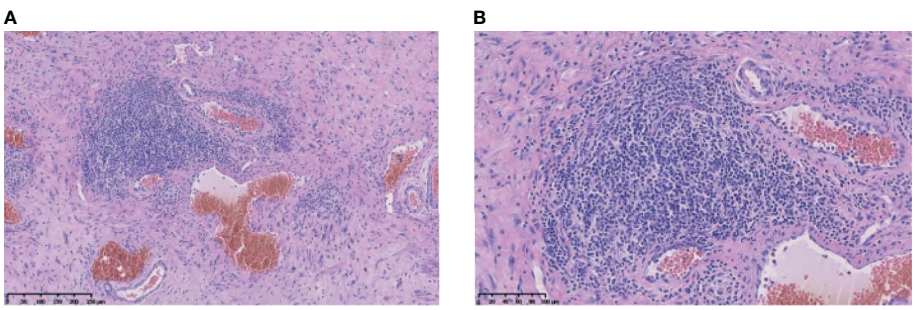

FIGURE 3 | Histopathological findings. **(A)** was taken at 10x, and **(B)** was taken at 20x.

efficacy of ICI is currently controversial, he did not continue using immunotherapy.

According to statistics, globally, the probability of death due to irAEs that received ICI treatment is about 0.6%. Of this, PD-1 antibody contributes 0.36% and PD-L1 0.38% (13). The cause of death is usually pneumonia, hepatitis, or neurotoxicity. CTLA-4 and combined immunotherapy have higher mortality rates, 1.08% and 1.23%, respectively (13). Studies have found that certain antibodies in the serum before treatment may be related to the risk of irAEs (9). An early increase in peripheral lymphocyte counts can also be used as a biomarker of irAE risk (14). B cells in the body and some cytokines such as interleukin 17 (IL-17) can also help identify the risk of irAE in patients (15, 16), but they appear to lack sensitivity. Further research is needed in the future (1, 9).

More and more studies have shown that the onset of irAE can be used as a potential biomarker to predict the efficacy of PD-1 and PD-L1 in various solid tumors (17). Patients with irAEs show better efficacy than those without irAE (14, 18, 19). The mechanism is unclear, but may be due to the bystander effect of ICI-activated T cells, which target not only tumor cells but also normal tissues to produce side effects (20). The specific antigens preexisting in normal organs may also be the predisposing factors of irAEs and produce autoimmune toxic reactions that are not antitumor related (21). Of course, this conclusion also needs the support of more clinical data.

DATA AVAILABILITY STATEMENT

The raw data supporting the conclusions of this article will be made available by the authors, without undue reservation.

ETHICS STATEMENT

The studies involving human participants were reviewed and approved by the Ethics Committee of the Comprehensive Cancer Center of Drum Tower Hospital of Nanjing University. The patients/participants provided written informed consent to participate in this study. Written informed consent was obtained from the individual(s) for the publication of any potentially identifiable images or data included in this article.

AUTHOR CONTRIBUTIONS

JS and BL designed the clinical trial. SZ, JS, and BL drafted the manuscript and provided figures. SZ, LB, JL, BL, and JS acquired, analyzed, and interpreted the data. JS, LB, and BL revised the manuscript critically for important intellectual content and agreed to be accountable for all aspects of the work in ensuring that questions related to the accuracy or integrity of any part of the work are appropriately investigated and resolved. All authors contributed to the article and approved the submitted version.

FUNDING

This study was supported by the National Natural Science Foundation of China (no. 81902914), Jiangsu Provincial Medical Youth Talent (no. QNRC2016043), and the Key Medical Science and Technology Development Project of Nanjing (no. ZKX16032).

REFERENCES

1. Postow M, Sidlow R, Hellmann M. Immune-Related Adverse Events Associated With Immune Checkpoint Blockade. *N Engl J Med* (2018) 378:158–68. doi: 10.1056/NEJMra1703481
2. Weber J, Hodi F, Wolchok J, Topalian S, Schadendorf D, Larkin J, et al. Safety Profile of Nivolumab Monotherapy: A Pooled Analysis of Patients With Advanced Melanoma. *J Clin Oncol* (2017) 35:785–92. doi: 10.1200/JCO.2015.66.1389
3. Lin J, Yang X, Long J, Zhao S, Mao J, Wang D, et al. Pembrolizumab Combined With Lenvatinib as Non-First-Line Therapy in Patients With Refractory Biliary Tract Carcinoma. *Hepatobiliary Surg Nutr* (2020) 9:414–24. doi: 10.21037/hbsn-20-338
4. Ozaki K, Takahashi H, Murakami Y, Kiyoku H, Kanayama H. A Case of Cystitis After Administration of Nivolumab. *Int Cancer Conf J* (2017) 6:164–6. doi: 10.1007/s13691-017-0298-6
5. Shimatani K, Yoshimoto T, Doi Y, Sonoda T, Yamamoto S, Kanematsu A. Two Cases of Nonbacterial Cystitis Associated With Nivolumab, the Anti-Programmed-Death-Receptor-1 Inhibitor. *Urol Case Rep* (2018) 17:97–9. doi: 10.1016/j.eucr.2017.12.006
6. Puzanov I, Diab A, Abdallah K, Bingham C, Brogdon C, Dadu R, et al. Managing Toxicities Associated With Immune Checkpoint Inhibitors: Consensus Recommendations From the Society for Immunotherapy of Cancer (SITC) Toxicity Management Working Group. *J Immunother Cancer* (2017) 5:95. doi: 10.1186/s40425-017-0300-z
7. Weber J, Kähler K, Hauschild A. Management of Immune-Related Adverse Events and Kinetics of Response With Ipilimumab. *J Clin Oncol* (2012) 30:2691–7. doi: 10.1200/JCO.2012.41.6750
8. Abdel-Wahab N, Shah M, Lopez-Olivo M, Suarez-Almazor M. Use of Immune Checkpoint Inhibitors in the Treatment of Patients With Cancer and Preexisting Autoimmune Disease: A Systematic Review. *Ann Internal Med* (2018) 168:121–30. doi: 10.7326/M17-2073
9. Yoest J. Clinical Features, Predictive Correlates, and Pathophysiology of Immune-Related Adverse Events in Immune Checkpoint Inhibitor Treatments in Cancer: A Short Review. *ImmunoTargets Ther* (2017) 6:73–82. doi: 10.2147/ITT.S126227
10. Herold M, McPherson K, Reichardt H. Glucocorticoids in T Cell Apoptosis and Function. *Cell Mol Life Sci CMLS* (2006) 63:60–72. doi: 10.1007/s00018-005-5390-y
11. Horvat T, Adel N, Dang T, Momtaz P, Postow M, Callahan M, et al. Immune-Related Adverse Events, Need for Systemic Immunosuppression, and Effects on Survival and Time to Treatment Failure in Patients With Melanoma Treated With Ipilimumab at Memorial Sloan Kettering Cancer Center. *J Clin Oncol* (2015) 33:3193–8. doi: 10.1200/JCO.2015.60.8448
12. Kartolo A, Deluce J, Holstead R, Hopman W, Lenehan J, Baetz T. Impact of Baseline Corticosteroids on Immunotherapy Efficacy in Patients With Advanced Melanoma. *J Immunother (Hagerstown Md 1997)* (2021) 44:167–74. doi: 10.1097/CJI.0000000000000360
13. Wang D, Salem J, Cohen J, Chandra S, Menzer C, Ye F, et al. Fatal Toxic Effects Associated With Immune Checkpoint Inhibitors: A Systematic Review and Meta-Analysis. *JAMA Oncol* (2018) 4:1721–8. doi: 10.1001/jamaoncol.2018.3923
14. Okada N, Kawazoe H, Takechi K, Matsudate Y, Utsunomiya R, Zamami Y, et al. Association Between Immune-Related Adverse Events and Clinical Efficacy in Patients With Melanoma Treated With Nivolumab: A

Multicenter Retrospective Study. *Clin Ther* (2019) 41:59–67. doi: 10.1016/j.clinthera.2018.11.004
15. Das R, Bar N, Ferreira M, Newman A, Zhang L, Bailur J, et al. Early B Cell Changes Predict Autoimmunity Following Combination Immune Checkpoint Blockade. *J Clin Invest* (2018) 128:715–20. doi: 10.1172/JCI96798
16. Young A, Quandt Z, Bluestone J. The Balancing Act Between Cancer Immunity and Autoimmunity in Response to Immunotherapy. *Cancer Immunol Res* (2018) 6:1445–52. doi: 10.1158/2326-6066.CIR-18-0487
17. Das S, Johnson D. Immune-Related Adverse Events and Anti-Tumor Efficacy of Immune Checkpoint Inhibitors. *J Immunother Cancer* (2019) 7:306. doi: 10.1186/s40425-019-0805-8
18. Rogado J, Sánchez-Torres J, Romero-Laorden N, Ballesteros A, Pacheco-Barcia V, Ramos-Leví A, et al. Immune-Related Adverse Events Predict the Therapeutic Efficacy of Anti-PD-1 Antibodies in Cancer Patients. *Eur J Cancer (Oxford Engl 1990)* (2019) 109:21–7. doi: 10.1016/j.ejca.2018.10.014
19. Ricciuti B, Genova C, De Giglio A, Bassanelli M, Dal Bello M, Metroí G, et al. Impact of Immune-Related Adverse Events on Survival in Patients With Advanced Non-Small Cell Lung Cancer Treated With Nivolumab: Long-Term Outcomes From a Multi-Institutional Analysis. *J Cancer Res Clin Oncol* (2019) 145:479–85. doi: 10.1007/s00432-018-2805-3
20. Passat T, Touchefeu Y, Gervois N, Jarry A, Bossard C, Bennouna J. [Physiopathological Mechanisms of Immune-Related Adverse Events Induced by Anti-CTLA-4, Anti-PD-1 and Anti-PD-L1 Antibodies in Cancer Treatment]. *Bull du Cancer* (2018) 105:1033–41. doi: 10.1016/j.bulcan.2018.07.005
21. Iwama S, De Remigis A, Callahan M, Slovin S, Wolchok J, Caturegli P. Pituitary Expression of CTLA-4 Mediates Hypophysitis Secondary to Administration of CTLA-4 Blocking Antibody. *Sci Trans Med* (2014) 6:230ra45. doi: 10.1126/scitranslmed.3008002

Conflict of Interest: The authors declare that the research was conducted in the absence of any commercial or financial relationships that could be construed as a potential conflict of interest.

frontiers in Immunology

ORIGINAL RESEARCH
published: 03 January 2022
doi: 10.3389/fimmu.2021.774435

Comprehensive Analysis of Expression, Prognostic Value, and Immune Infiltration for Ubiquitination-Related FBXOs in Pancreatic Ductal Adenocarcinoma

Yalu Zhang[†], *Qiaofei Liu*[†], *Ming Cui*, *Mengyi Wang*, *Surong Hua*, *Junyi Gao* and *Quan Liao*[*]

Department of General Surgery, State Key Laboratory of Complex Severe and Rare Diseases, Peking Union Medical College Hospital, Chinese Academy of Medical Science and Peking Union Medical College, Beijing, China

Pancreatic ductal adenocarcinoma (PDAC) is one of the most refractory human malignancies. F-box only proteins (FBXO) are the core components of SKP1-cullin 1-F-box E3 ubiquitin ligase, which have been reported to play crucial roles in tumor initiation and progression *via* ubiquitination-mediated proteasomal degradation. However, the clinical implications and biological functions of FBXOs in PDAC have not been fully clarified. Herein we perform a comprehensive analysis for the clinical values and functional roles of FBXOs in PDAC using different public databases. We found that FBXO1 (CCNF), FBXO20 (LMO7), FBXO22, FBXO28, FBXO32, and FBXO45 (designated six-FBXOs) were robustly upregulated in PDAC tissues, which predicted an adverse prognosis of PDAC patients. There was a significant correlation between the expression levels of six-FBXOs and the clinicopathological features in PDAC. The transcriptional levels of six-FBXOs were subjected to the influence of promoter methylation levels. There were more than 40% genetic alterations and mutations of six-FBXOs, which affected the clinical outcome of PDAC patients. Furthermore, the expression of six-FBXOs was associated with immune infiltrations and activated status, including B cells, $CD8^+$ T cells, $CD4^+$ T cells, NK cells, macrophages, and dendritic cells. The functional prediction revealed that the six-FBXOs were involved in ubiquitination-related pathways and other vital signaling pathways, such as p53, PI3K/Akt, and Hippo pathway. Therefore, six-FBXOs are the promising prognostic biomarkers or potential targets for PDAC diagnosis and treatment.

Keywords: FBXOs, pancreatic ductal adenocarcinoma, prognostic value, immune infiltration, bioinformatics analysis

OPEN ACCESS

Edited by:
Yunfei Xu,
Shandong University, China

Reviewed by:
Zheng Wang,
Xi'an Jiaotong University, China
Tong Wu,
Erasmus Medical Center, Netherlands
Yanyan Zhang,
University of Chinese Academy of Sciences, China

***Correspondence:**
Quan Liao
liaoq@pumch.cn

[†]*These authors have contributed equally to this work*

Specialty section:
This article was submitted to Cancer Immunity and Immunotherapy, a section of the journal Frontiers in Immunology

Received: *12 September 2021*
Accepted: *22 November 2021*
Published: *03 January 2022*

Citation:
Zhang Y, Liu Q, Cui M, Wang M, Hua S, Gao J and Liao Q (2022) Comprehensive Analysis of Expression, Prognostic Value, and Immune Infiltration for Ubiquitination-Related FBXOs in Pancreatic Ductal Adenocarcinoma. Front. Immunol. 12:774435. doi: 10.3389/fimmu.2021.774435

INTRODUCTION

According to the 2017 cancer statistics of the National Cancer Center of China, the incidence of pancreatic cancer ranked 11th among women and 7th among men, and the mortality rate ranked 6th among malignant tumors in China (1). Pancreatic ductal adenocarcinoma (PDAC) is the most common pathological type of pancreatic cancer, accounting for about 90% of pancreatic cancer (2). The clinical outcome of PDAC patients is often extremely poor, and the 5-year survival rate is only around 9% due to difficulties in early diagnosis, low success rate in surgical dissection, and chemotherapy resistance (3, 4). Therefore, it is necessary to find diagnostic or therapeutic targets of PDAC to improve the clinical outcomes of patients.

The occurrence and development of PDAC are responsible for multi-factor and multi-step processes, such as the activation/inactivation of oncogenes/tumor suppressor genes, tumor stem cell, gene mutation, epigenetic modification, and post-translational regulation as well as tumor immune microenvironment (5–8). Among them, ubiquitination-mediated degradation of target protein with high selectivity is a key pathway for post-translational modification, which plays a significant role in oncogenesis and pathological mechanism (9). E3 ubiquitin ligase is a vital component of the ubiquitination cascade that binds directly to substrates by controlling mutual specificity, which is regarded as a promising anticancer drug target (10). F-box only (FBXO) proteins are the substrate-recognizing subunits of SKP1-cullin 1-F-box (SCF) E3 ligase. An increasing number of studies have revealed that FBXO family members, as important molecular regulators, are implicated in cell apoptosis, angiogenesis, epithelial–mesenchymal transition (EMT), and multiple important signaling pathways, like p53, NF-κB, PI3K/AKT, and Hippo signaling pathway, in a variety of tumors (11); for example, FBXO1, also known as cyclin F (CCNF), participates in the formation of SCF ubiquitin ligase complex and is involved in tuning centrosome duplication, DNA repair, and genome stability (12). FBXO20, also known as LIM (Lin11, Isl-1, and Mec-3) domain 7 (LMO7), belongs to PDZ and the LIM domain-containing protein family. It has been reported that LMO7 played a role in the regulation of cell adhesion, mitosis, and cancer metastasis and progression, including breast cancer, lung adenocarcinoma, and pancreatic cancer (13–16). Clinically, some FBXO family members were closely linked to the overall survival (OS) and disease-free survival (DFS) of patients with breast cancer (17). However, the clinical significance and biological role of FBXOs in PDAC are still unclear as yet and remain to be elucidated.

Among FBXO1–50, FBXO12 is also called FBXO35, FBXO17 is also called FBXO26, FBXO14 is also called FBXO31, and FBXO19 is absent. In the present study, we mainly focused on six FBXO family members with limited studies in the field of PDAC research, including FBXO1, FBXO20, FBXO22, FBXO28, FBXO32, and FBXO45 (designated six-FBXOs in the following text). We compared the different expression levels of the six ubiquitination-related FBXOs between PDAC tissues and paracarcinoma tissues or normal pancreatic tissues. Furthermore, using diverse public databases, we comprehensively analyzed their correlation with clinicopathologic characteristics, promoter methylation in epigenetic regulation, fluorescence localization, gene mutation, immune infiltration, and prognostic values as well as the functional enrichment analysis and the prediction of Kyoto Encyclopedia of Genes and Genomes (KEGG) pathway. Finally, we validated the expression levels of six-FBXOs in five different PDAC cell lines compared with human normal pancreas cells.

Abbreviations: ANCT, adjacent non-cancerous tissues; BP, biological process; CC, cellular component; CCNF, cyclin F; CI, confidence interval; DFS, disease-free survival; EMT, epithelial–mesenchymal transition; GO, gene ontology; hn-PDEC, human normal pancreatic ductal epithelial cells; HPA, Human Protein Atlas; HR, hazard ratio; IHC, immunohistochemistry; IPMA, intraductal papillary-mucinous adenoma; IPMC, intraductal papillary-mucinous carcinoma; IPMN, intraductal papillary-mucinous neoplasm; KEGG, Kyoto Encyclopedia of Genes and Genomes; LMO7, LIM (Lin11, Isl-1, and Mec-3) domain 7; MF, molecular function; OS, overall survival; PAAD, pancreatic adenocarcinoma; PanIN, pancreatic duct intraepithelial neoplasia; PDAC, pancreatic ductal adenocarcinoma; RRM2, ribonucleotide reductase M2; SCF, SKP1-cullin 1-F-box.

MATERIALS AND METHODS

GEPIA

GEPIA is an interactive online web tool for investigators to explore diverse functional modules based on TCGA and GTEx databases (18). Using the GEPIA database, we analyzed the gene expression profile of FBXO family members across 33 tumor samples and paired normal tissues, including pancreatic adenocarcinoma (PAAD), and performed the pathological stage plot of the FBXOs as well as evaluated the prognostic values of FBXOs in PDAC patients. "Median" was selected as the "Group Cutoff".

Oncomine and UALCAN

Oncomine is a public database that contains substantial tumor microarray datasets (19). Log2-transformed form was utilized to represent the transcriptional levels of FBXOs. Fold change >2 and p-value <0.05 were selected as the inclusion criteria. UALCAN is a user-friendly database for the analysis of gene expression and clinical parameters from thirty-one different types of tumors, including PDAC (20). In this study, PDAC staging, grading, TP53 mutation, and methylation data were obtained from the UALCAN database.

GEO

GEO database includes a large number of high-throughput sequencing data, including PDAC datasets. We used five GEO datasets to compare the expression levels of FBXOs in PDAC tissues and normal pancreatic tissues (GSE16515 and GSE62165) or para-carcinoma tissues (GSE62452, GSE28735, and GSE15471). Besides these, five GEO datasets were used to analyze correlations between the expression levels of FBXOs and the clinicopathologic characteristics of PDAC. GSE21501 was used for the analysis of tumor size (T1–T2 *vs.* T3–T4) and

lymphatic metastasis (N0 *vs*. N1); GSE62165, GSE62452, GSE19650, and GSE51971 were used for the analysis of tumor location (head *vs*. body/tail), differentiation degree (G1–G2 *vs*. G3–G4), different pancreatic precancerous lesions, and cell stemness, respectively.

The Human Protein Atlas

The Human Protein Atlas (HPA) database is an integrated and accessible data mining platform containing a substantial distribution of information of human protein from more than twenty kinds of cancer in cellular and histopathological levels. The immunohistochemical (IHC) staining images of FBXO family members and the confocal images of their cellular localization were acquired from the HPA database.

Kaplan–Meier Plotter

The Kaplan–Meier plotter is an interactive and public online database for analyzing the survival of twenty-one tumor types based on substantial RNA-seq and next-generation sequencing (21). The prognostic values of FBXO family members and their prognostic subgroup analysis in gender, mutation burden, and immune infiltration were evaluated by the Kaplan–Meier plotter database. Hazard ratio (HR) and 95% confidence interval (CI) were calculated automatically according to "Auto select best cutoff".

SurvExpress and LinkedOmics

SurvExpress is a bioinformatics web server for gene expression and clinical data in tumors (22). The prognosis of FBXO family members and the transcriptional levels in low- and high-risk groups were assessed by using this database. "PAAD-TCGA-Pancreatic adenocarcinoma" (n = 176) was selected. The PDAC cohorts were divided into low- and high-risk groups based on the prognostic index to compare the expression levels of FBXOs. LinkedOmics is an available web portal for users to analyze multi-omics data within and across 32 cancer types (23). This database was used to evaluate the prognosis of promoter methylation of the FBXOs and top 200 co-expressed genes with individual FBXOs in PDAC patients.

Immune Infiltration Analysis of FBXOs

TIMER is a user-friendly web server for the systematic and comprehensive analysis of immune infiltration across various tumor types *via* inputting function-specific parameters (24). The immune infiltration of FBXOs in PDAC tissues was estimated using TIMER database (Spearman correlation). Furthermore, TISIDB is a public portal for tumor and immune system interaction as well as integration of numerous heterogeneous data types (25). We used this database to perform a further detailed analysis of immune infiltration of FBXOs in PDAC based on high-throughput data.

cBioPortal Database

The cBioPortal database is an accessible online resource to interactively explore and visualize multidimensional genomics data and clinical profiles in diverse cancer samples (26). Using cBioPortal database, we analyzed the genetic alteration, mutation, and related prognosis of FBXOs in PDAC and identified the top 200 co-expressed genes of FBXOs. The "Pancreatic adenocarcinoma (TCGA, PanCancer Atlas)" (184 samples) was selected. In terms of "Select Genomic Profiles", the "Mutation", "Structural Variant", "Putative copy-number alterations from GISTIC", "mRNA Expression", and "Protein expression z-scores (RPPA)" were selected. Besides these, "Complete sample (168)" was selected as the option of "Select Patient/Case Set".

DAVID

DAVID is a bioinformatic analytic tool for the functional enrichment of genes derived from high-throughput genomic experiments, such as functional classification and annotation, to acquire an in-depth understanding of the biological function of gene lists (27). Functional enrichment and prediction of FBXOs were performed using gene ontology (GO) and KEGG pathway analysis from DAVID. GO functional enrichment consists of biological process (BP), cellular component (CC), and molecular function (MF).

Cell Culture

Human immortal pancreatic epithelial cell line HPDE6 and PDAC cell lines (Panc-1, AsPC-1, SW1990, T3M4, and CAPAC-1) were purchased from the National Infrastructure of Cell Line Resource (Beijing, China). HPDE6, Panc-1, and T3M4 were cultured in DMEM medium (HyClone); AsPC-1, SW1990, and CFPAC-1 were cultured in RPMI-1640, Leibovitz's L-15, and IMDM medium (Coning), respectively. All media were supplemented with 10% fetal bovine serum (Gibco) and 1% penicillin–streptomycin (Sigma), and cells were incubated in a humidified atmosphere at 37°C and 5% CO_2.

RNA Extraction and Quantitative PCR

Total RNA was isolated from exponentially divided cell lines using Trizol Reagent (RNAiso Plus, #9109, Takara) and then concentrated with trichloromethane, isopropanol, and ethanol according to standard protocols. The RNA was reverse-transcribed with PrimeScript™ RT reagent Kit (#RR037A, Takara). Real-time qPCR was administrated in three duplicates for each sample with TB Green® Premix Ex Taq™ (#RR420A, Takara) on the QuantStudio3 apparatus (ThermoFisher, USA). GAPDH was used for standard normalization, and the data were analyzed using the $2^{-\Delta\Delta CT}$ method. The primer sequences were summarized in **Supplementary Table S1**.

Statistical Analysis

Statistical analysis and graphs were performed and plotted by GraphPad Prism 6.0 (Lajolla, CA, USA). Comparisons between the two groups were conducted using a two-tailed Student's t-test. For comparisons of three or more groups, one-way ANOVA with *post-hoc* Dunnett test or Tukey's test was utilized. Statistical significance was indicated as p-value <0.05.

RESULTS

Aberrant Transcriptional Levels of FBXOs in Patients With PDAC

To investigate the expression profiles of FBXO family members in PDAC, the GEPIA database, an online analysis tool based on

TCGA and GTEx datasets, was used to compare the difference between the mRNA expression levels of FBXOs in PDAC tissues (N = 179) and normal pancreatic tissues (N = 171). A total of twenty-one aberrantly expressed genes were identified within the human PDAC tissues. Of them, FBXO1, FBXO5, FBXO7, FBXO8, FBXO11, FBXO13, FBXO18, FBXO20, FBXO22, FBXO23, FBXO28, FBXO32, FBXO34, FBXO38, FBXO42, FBXO45, and FBXO46 were upregulated, while FBXO2, FBXO12, FBXO35, and FBXO50 were downregulated in PDAC tissues (**Figure 1**). No abnormal expression was found in other FBXO members (**Supplementary Figure S1**). By consulting the previously published literature, there are extremely limited reports related to FBXO1, FBXO20, FBXO22, FBXO28, FBXO32, and FBXO45 in PDAC, and we therefore further explored the six genes. Furthermore, the transcriptional levels of six-FBXOs were explored in 32 other types of tumor. We found that six-FBXOs were also abnormally expressed in the other multiple tumors (**Supplementary Figure S2**). Next, Oncomine databases were also used to investigate the expression of six-FBXOs in PDAC tissues *versus* normal pancreatic tissues. The results confirmed that the mRNA expression levels of FBXO20, FBXO32, and FBXO45 were strongly upregulated in patients with PDAC in different datasets (**Supplementary Figures S3A–D** and **Table 1**). In Buchholz's data, FBXO32 exhibited a higher expression in pancreatic duct intraepithelial neoplasia (PanIN) than in normal pancreatic tissues (**Supplementary Figure 3C**). Moreover, five GEO datasets were

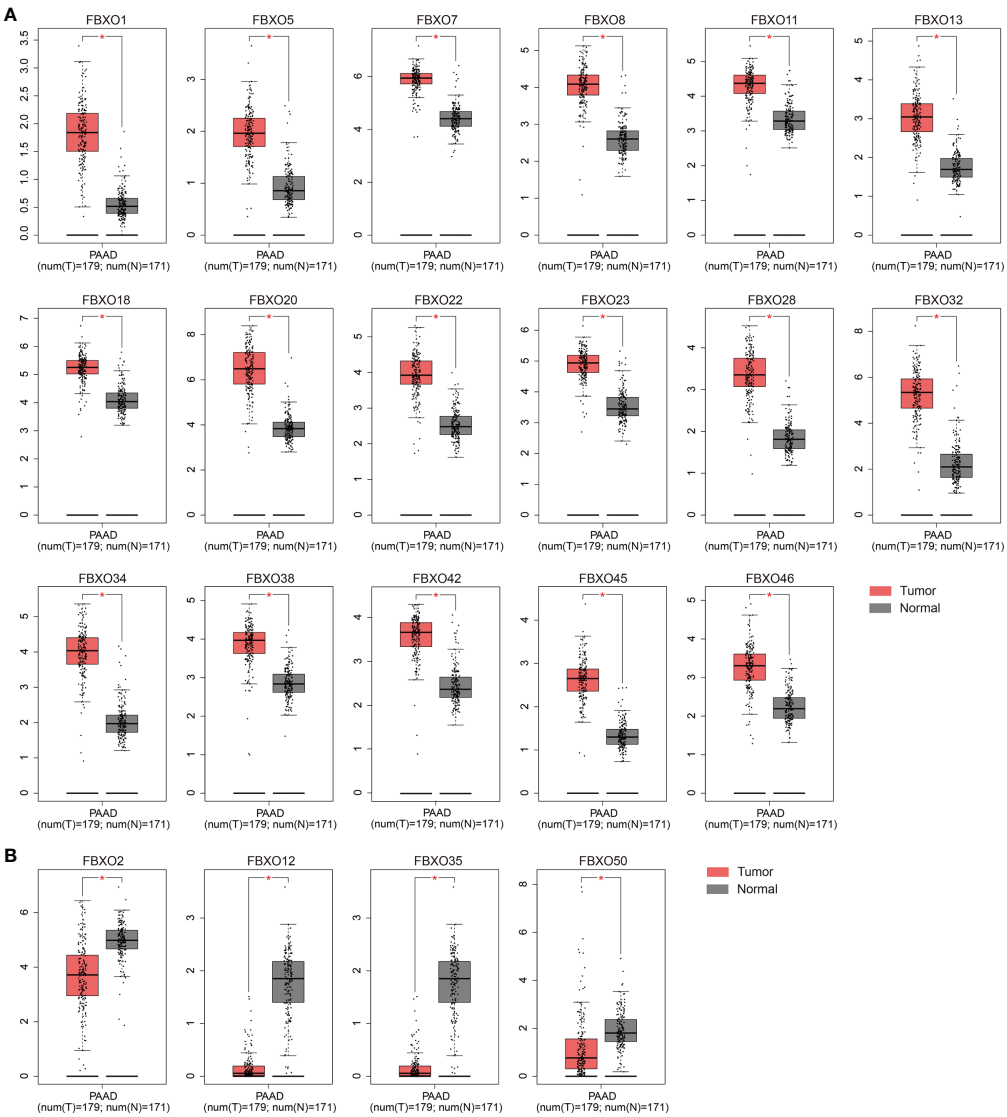

FIGURE 1 | Using GEPIA database, FBXO family members that are aberrantly expressed in pancreatic ductal adenocarcinoma (PDAC) tissues (n = 179) *versus* normal pancreatic tissues (n = 171). **(A)** FBXO family members that are highly expressed in PDAC tissues. **(B)** FBXO family members that are lowly expressed in PDAC tissues. *P < 0.05.

TABLE 1 | The significant changes of FBXO transcription levels between PDAC tissues and normal pancreatic tissues (Oncomine).

Genes	Source	Type of pancreatic cancer *versus* normal pancreatic tissue	Platform	*t*-test	Fold change	*p*-value
FBXO20 (LMO7)	Pei pancreas	Pancreatic carcinoma *vs*. normal	Human Genome U133 Plus 2.0 Array	7.962	3.535	1.56E-10
	Iacobuzio-Donahue pancreas 2	Pancreatic adenocarcinoma *vs*. normal	NA	6.309	4.305	1.04E-05
	Segara pancreas	Pancreatic carcinoma *vs*. normal	Human Genome U133A Array	3.061	1.481	0.005
FBXO32	Badea pancreas	Pancreatic ductal adenocarcinoma *vs*. normal	Human Genome U133 Plus 2.0 Array	10.146	3.427	6.17E-16
	Iacobuzio-Donahue pancreas 2	Pancreatic adenocarcinoma *vs*. normal	NA	4.855	2.640	1.10E-04
	Grutzmann pancreas	Pancreatic ductal adenocarcinoma epithelia *vs*. normal	Human Genome U133B Array	2.588	2.246	0.009
	Buchholz pancreas	Pancreatic intraepithelial neoplasia *vs*. normal	NA	3.191	1.339	0.004
	Buchholz pancreas	Pancreatic ductal adenocarcinoma *vs*. normal	NA	4.784	1.543	3.24E-04
	Pei pancreas	Pancreatic carcinoma *vs*. normal	Human Genome U133 Plus 2.0 Array	3.007	2.657	0.004
FBXO45	Grutzmann pancreas	Pancreatic ductal adenocarcinoma epithelia *vs*. normal	Human Genome U133B Array	2.530	2.173	0.010
	Badea pancreas	Pancreatic ductal adenocarcinoma *vs*. normal	Human Genome U133 Plus 2.0 Array	5.406	1.502	3.62E-07
	Iacobuzio-Donahue pancreas 2	Pancreatic adenocarcinoma *vs*. normal	NA	2.054	1.850	0.042
	Pei pancreas	Pancreatic carcinoma *vs*. normal	Human Genome U133 Plus 2.0 Array	3.020	1.348	0.003

NA, not available.

collected to verify the abnormality in the expression patterns of six-FBXOs found above *via* a comparison between PDAC and normal pancreatic tissues (GSE16515 and GSE62165) or adjacent non-cancerous tissues (ANCT) (GSE62452, GSE28735, and GSE15471). As shown in **Figure 2**, the overall results confirmed that the expression levels of six-FBXOs were robustly elevated, although FBXO1 and FBXO22 did not show statistical differences in two of the datasets (**Figures 2A–E**).

The Correlation Between Six-FBXO Expression and the Clinicopathological Features of PDAC Patients

Then, we evaluated the clinical significance of six-FBXOs in PDAC by using three GEO datasets (GSE62165, GSE21501, and GSE62452), GEPIA, and UALCAN databases. The data from GSE62165 showed that none of the six-FBXOs was associated with tumor location (N = 118) (**Supplementary Figure S4A**), while GSE21501 displayed that FBXO28 and FBXO32 were tightly linked to tumor size (N = 98); FBXO32 was also related to lymphatic metastasis (N = 101) (**Figures 3A, B**). GSE62452 demonstrated that the higher expression levels of FBXO1, FBXO20, FBXO32, and FBXO45 were correlated with poorer tumor differentiation (N = 68), apart from FBXO22 and FBXO38 (**Figure 3C**). Besides this, the GEPIA database manifested that, among six-FBXOs, FBXO32 was associated with tumor staging (N = 179); FBXO1, FBXO20, and FBXO45 had a related trend with tumor staging, whereas no correlation with tumor staging was observed for FBXO22 and FBXO28 (**Figure 3D**). It was worth mentioning that FBXO family members FBXO8, FBXO13, and FBXO34 were linked to tumor staging, and FBXO50 had an associated trend with tumor staging (**Supplementary Figure S4B**).

The results from the UALCAN database further confirmed the GSE21501 data that FBXO32 was closely relevant in the lymphatic metastasis of PDAC as well as showed that FBOX20 expression was relatively lower in PDAC patients with diabetes, compared with PDAC patients without diabetes (**Supplementary Figure S4C**). Furthermore, the UALCAN database displayed a more detailed analysis regarding tumor differentiation and staging based on TCGA samples. The data from the UALCAN database verified that the expression levels of six-FBXOs were strongly relevant in tumor differentiation, and patients who were in worse differentiation had the higher expression of six-FBXOs on the whole (**Supplementary Figure S5A**). Further validating the results of the GEPIA database, FBXO32 was related to the tumor stage of PDAC patients. It also indicated that the mRNA expression levels of FBXO20 and FBXO45 were closely related to the tumor stage of PDAC patients (**Supplementary Figure S5B**), which meant that patients who were in more advanced tumor staging tended to express higher transcripts of FBXO20, FBXO32, and FBXO45. TP53 mutation plays a crucial role in the initiation, formation, and maintenance of PDAC (28). Therefore, we also explored the effect of P53 mutation on the expression of six-FBXOs. The data showed that FBXO1, FBXO20, and FBXO45 exhibited higher expression levels in the TP53-mutant group than in the TP53-nonmutant group, while this kind of difference was not observed for FBXO22, FBXO28, and FBXO32 (**Supplementary Figure S5C**).

Pancreatic carcinogenesis is a gradual and multi-step process from precancerous lesions (8). We compared the expression of six-FBXOs in different precancerous lesions, including intraductal papillary-mucinous neoplasm (IPMN), intraductal papillary-mucinous carcinoma (IPMC), and intraductal papillary-mucinous adenoma (IPMA) by using the GSE19650 dataset. The results indicated that FBXO20 was highly expressed in these three kinds of precancerous lesions (IPMA, IPMC, and IPMN) in comparison to normal pancreatic tissues, and FBXO20 had the highest expression level among these three pathological types, while FBXO22 was downregulated in IPMA compared

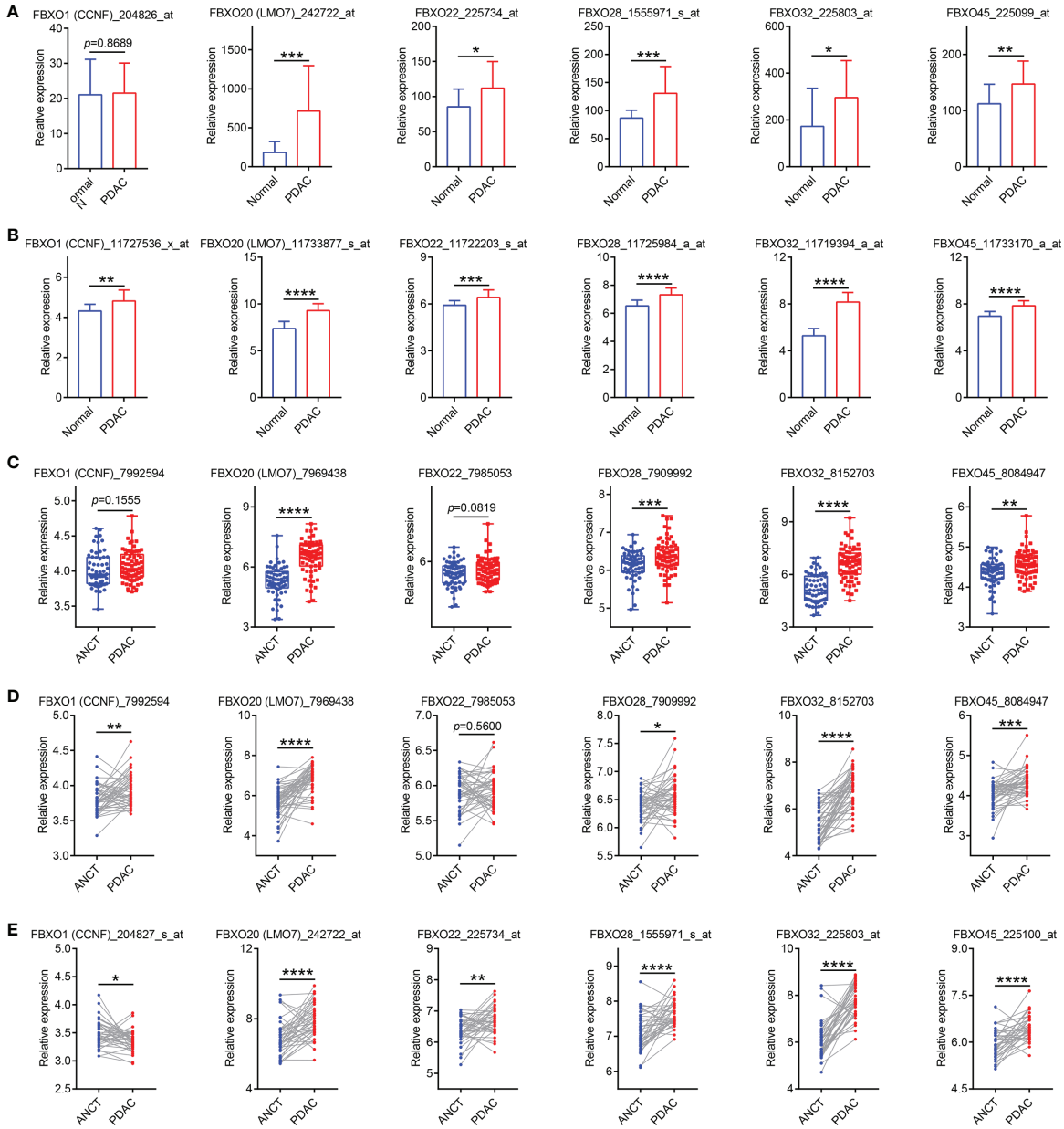

FIGURE 2 | Five GEO datasets were collected to validate the abnormality in the expression patterns of six-FBXOs in pancreatic ductal adenocarcinoma (PDAC). **(A)** The mRNA levels of six-FBXOs *via* the comparison between PDAC (n = 36) and normal pancreatic tissues (n = 16) in GSE16515 dataset. **(B)** The expression levels of six-FBXOs in PDAC tissues (n = 118) compared with normal tissues (n = 13) in GSE62165 dataset. **(C)** The expression levels of six-FBXOs in PDAC tissues (n = 69) *versus* adjacent non-cancerous tissues (ANCT) (n = 61) in GSE62452 dataset. **(D)** The transcriptional levels of six-FBXOs in PDAC tissues compared with ANCT (N = 45 pairs) in GSE28735 dataset. **(E)** The expression levels of six-FBXOs in PDAC tissues compared with ANCT (N = 39 pairs) in GSE15471 dataset. The code behind the gene is the probe name in different GEO datasets. *P < 0.05, **P < 0.01, ***P < 0.001, ****P < 0.0001.

with corresponding normal tissues (**Figure 3E**). FBXO32 and FBXO45 were significantly enhanced in IPMC, and FBXO32 exhibited the highest expression level among the other pathological types (**Figure 3E**). Taken together, these results demonstrated that FBXO20, FBXO22, FBXO32, and FBXO45 may act as markers of precancerous lesions and have the value of early diagnosis of pancreatic cancer.

The Correlation Between Promoter Methylation Levels of Six-FBXOs and Clinicopathological Characteristics

Promoter methylation is a critical epigenetic modification to regulate gene expression in human cancers (29). Therefore, we next investigated the promoter methylation levels of six-FBXOs. The results illustrated that FBXO1, FBXO20, and FBXO32 had

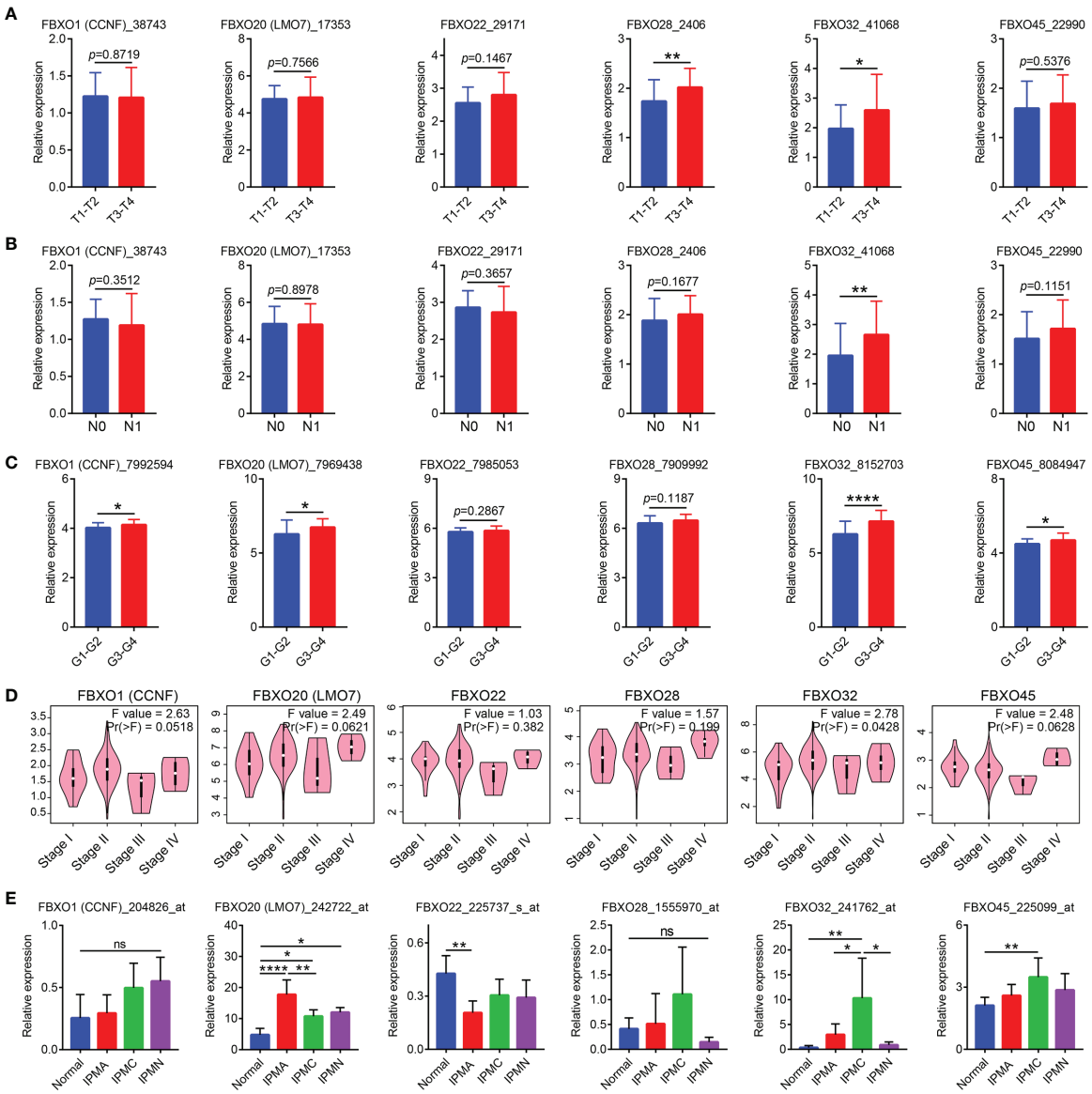

FIGURE 3 | Correlation between six-FBXO expression and the clinicopathological characteristics of pancreatic ductal adenocarcinoma (PDAC) patients in GEO datasets and GEPIA. **(A)** The expression levels of six-FBXOs *via* the comparison between T1–T2 (n = 18) and T3–T4 (n = 80) in GSE21501 dataset. **(B)** The expression levels of six-FBXOs in PDAC patients with/without lymphatic metastasis (N1/N0, 73 *vs*. 28) in GSE21501 dataset. **(C)** The mRNA levels of six-FBXOs in different differentiation degrees of PDAC (G1–G2 *vs*. G3–G4, 37 *vs*. 31) using GSE62452 dataset. **(D)** The expression levels of six-FBXOs in different pathological stages using GEPIA. **(E)** The transcriptional levels of six-FBXOs in different pancreatic precancerous lesions compared with normal pancreatic tissues using GSE19650 dataset. Normal (n = 7), IPMA (n = 6), IPMC (n = 6), and IPMN (n = 3). The code behind the gene is the probe name in different GEO datasets. *P < 0.05, **P < 0.01 ****P < 0.0001. n.s., not significant difference.

lower methylation levels in primary tumors than in normal pancreatic tissues, while FBXO45 had a higher methylation level in PDAC (**Supplementary Figure S6A**). In six-FBXOs, there were considerable differences in the promoter methylation level among divergent differentiated degrees or clinical stages. The methylation levels of FBXO1, FBXO20, FBXO32, and FBXO45 were associated with tumor differentiation (**Supplementary Figure S6B**). The methylation levels of FBXO1, FBXO20, FBXO22, FBXO32, and FBXO45 were correlated with clinical stages (**Supplementary Figure S7A**). In particular, FBXO1 exhibited a robust negative correlation between promoter methylation levels and differentiated degree or clinical stages. In addition, FBXO1, FBXO20, and FBXO45 had a lower methylation degree in the TP53-mutant group than in the TP53-nonmutant group, while FBXO22, FBXO28, and FBXO32 had no significant correlation between methylation level and TP53-mutant (**Supplementary Figure S7B**).

The Protein Expression, Cell Lines, Cellular Localization, and Cell Stemness of Six-FBXOs in PDAC

Next, we probed into the protein levels of six-FBXO expression between PDAC tissues and normal pancreatic tissues from the HPA database. The IHC staining of six-FBXOs revealed that the protein expression levels of FBXO1, FBXO20, and FBXO45 were markedly increased compared with the corresponding normal pancreatic tissues (**Figure 4A**), which corroborated the aforesaid result. The IHC data of FBXO22, FBXO28, and FBXO32 were pending cancer tissue analysis in the HPA database. Besides this, GSE45757 was used to evaluate the six-FBXO expression in human normal pancreatic ductal epithelial cells (hn-PDEC) and PDAC cell lines, including Panc-1, BxPC-3, Capan-2, Mia PaCa-2, SW1990, SU86.86, CFPAC-1, HPAF_II, and Hs766T. The data demonstrated that FBXO1, FBXO20, FBXO22, and FBXO28 were strongly upregulated in multiple PDAC cell lines relative to hn-PDEC (**Figures 4B–E**). The expression levels of FBXO32 and FBXO45 in cell lines were not available in the GSE45757 dataset. The cellular localization of gene expression often determines its corresponding significant function, so we explored the subcellular localization of six-FBXOs by using confocal images of the HPA database. The results warranted that FBXO1 was detected in the centrosome, FBXO20 was detected in actin filaments and cytosol, FBXO28 was detected in the nucleoplasm and focal adhesion sites, FBXO32 was detected in the nucleoplasm and cytosol, and FBXO45 was detected in the cytosol (**Figure 4F**). The confocal result of FBXO22 was absent in the HPA database. More importantly, we also explored the cell stemness of six-FBXOs in PDAC by using the GSE51971 dataset, whose data were classified into triple-positive group and triple-negative group according to whether these expressed the three important cancer stem cell markers, CD44, CD133, and EpCAM. The results showed that the expression levels of FBXO22, FBXO28, and FBXO32 were potently enhanced in the triple-negative group (**Figure 4G**). Overall, these results suggested that six-FBXOs are likely to play a vital role in PDAC initiation and progression.

The Prognostic Analysis of Six-FBXOs in PDAC Patients

In order to investigate the prognostic values, we explore the prognostic data of six-FBXOs from three primary public databases: GEPAI, Kaplan–Meier plotter, and SurvExpress. The data from GEPAI displayed that the high levels of six-FBXOs were tightly linked to a decreased probability of OS and DFS in PDAC (89 *vs.* 89) (**Supplementary Figure S8** and **Table 2**). The Kaplan–Meier plotter further substantiated the aforesaid prognostic results (**Figure 5** and **Table 2**). Specifically, FBXO20 had the highest HR in OS and DFS at 2.73 and 9.6, respectively, which meant that the FBXO20 high-expression group had 2.73 times and 9.6 times the risk of PDAC-related death and relapse, respectively, *versus* the FBXO20 low-expression group. The median OS time of the low- and high-expression groups was 18.93 and 10.27 months, respectively. More detailed prognostic information was shown in **Figure 5** and **Table 2**. Additionally, the SurvExpress online web tool also confirmed that six-FBXOs were the negative prognosis factors of PDAC patients (**Supplementary Figures S9**, **S10A**). The respective six-FBXO expression levels of PDAC patients in the SurvExpress datasets were divided into low- and high-risk groups (88 *vs.* 88) according to the prognostic index. The data from SurvExpress revealed that six-FBXOs had higher expression levels in the high-risk group than in the low-risk group (**Supplementary Figure S10B**). The LinkedOmics databases demonstrated that the hypermethylation group of FBXO1, FBXO20, and FBXO32 indicated a better OS than the hypomethylation group, while no significant correlation with OS was observed for FBXO22, FBXO28, and FBXO45 (**Supplementary Figure S11**). Collectively, these results in this section outlined the important prognostic values of six-FBXOs, which may act as effective prognostic markers for PDAC patients.

The Six-FBXO Expression and Immune Infiltration Level in PDAC

Then, we analyzed the relationship between the expression of six-FBXOs and the immune infiltration levels in PDAC using the TIMER online tool. The data revealed that the expression levels of FBXO1, FBXO22, FBXO28, and FBXO45 were associated with B cell infiltration; FBXO20, FBXO22, FBXO28, FBXO32, and FBXO45 were correlated with $CD8^+$ T cell infiltration; FBXO20 and FBXO45 were inversely related to $CD4^+$ T cell infiltration; FBXO22, FBXO28, FBXO32, and FBXO45 were linked to macrophage and neutrophil cell infiltration; FBXO1, FBXO22, FBXO28, FBXO32, and FBXO45 were relevant in dendritic cell infiltration (**Supplementary Figure S12**). However, it was contradictory that these negative prognostic genes were positively associated with immune infiltration, especially $CD8^+$ T cells, which often predicted a good clinical outcome. We speculated that this was related to whether immune cells were activated and contained different subgroups. Therefore, the TISIDB databases were utilized to perform a more detailed immune infiltration analysis of six-FBXOs in PDAC among subgroups with different functions. The results from TISIDB showed that, on the whole, six-FBXOs had a negative association with various immune infiltration, especially activated B cell, activated $CD8^+$ T cell, and macrophage infiltration (**Figures 6A, B**), indicating the expression of six-FBXOs might be associated with a suppressive tumor immune microenvironment in PDAC.

To determine whether these six-FBXOs affected the prognosis of immune subgroup in PDAC patients, the Kaplan–Meier plotter was used to evaluate it between the immune cell-enriched group and the immune cell-decreased group. The data from the Kaplan–Meier plotter illustrated that FBXO1, FBXO20, FBXO22, FBXO28, and FBXO32 were the negative prognosis factors in the B cell-decreased group and the macrophage-decreased group, while FBXO45 was the negative prognosis factor in the B cell-enriched group and the macrophage-enriched group. FBXO20 and FBXO45 were the negative prognosis factors in the $CD8^+$ T cell-decreased group, while FBXO1, FBXO22, FBXO28, and FBXO32 were the negative prognosis factors in the $CD8^+$ T cell-enriched group. All six-FBXOs were the negative prognosis factors in the regulatory T cell-enriched group (**Supplementary Figure S13**).

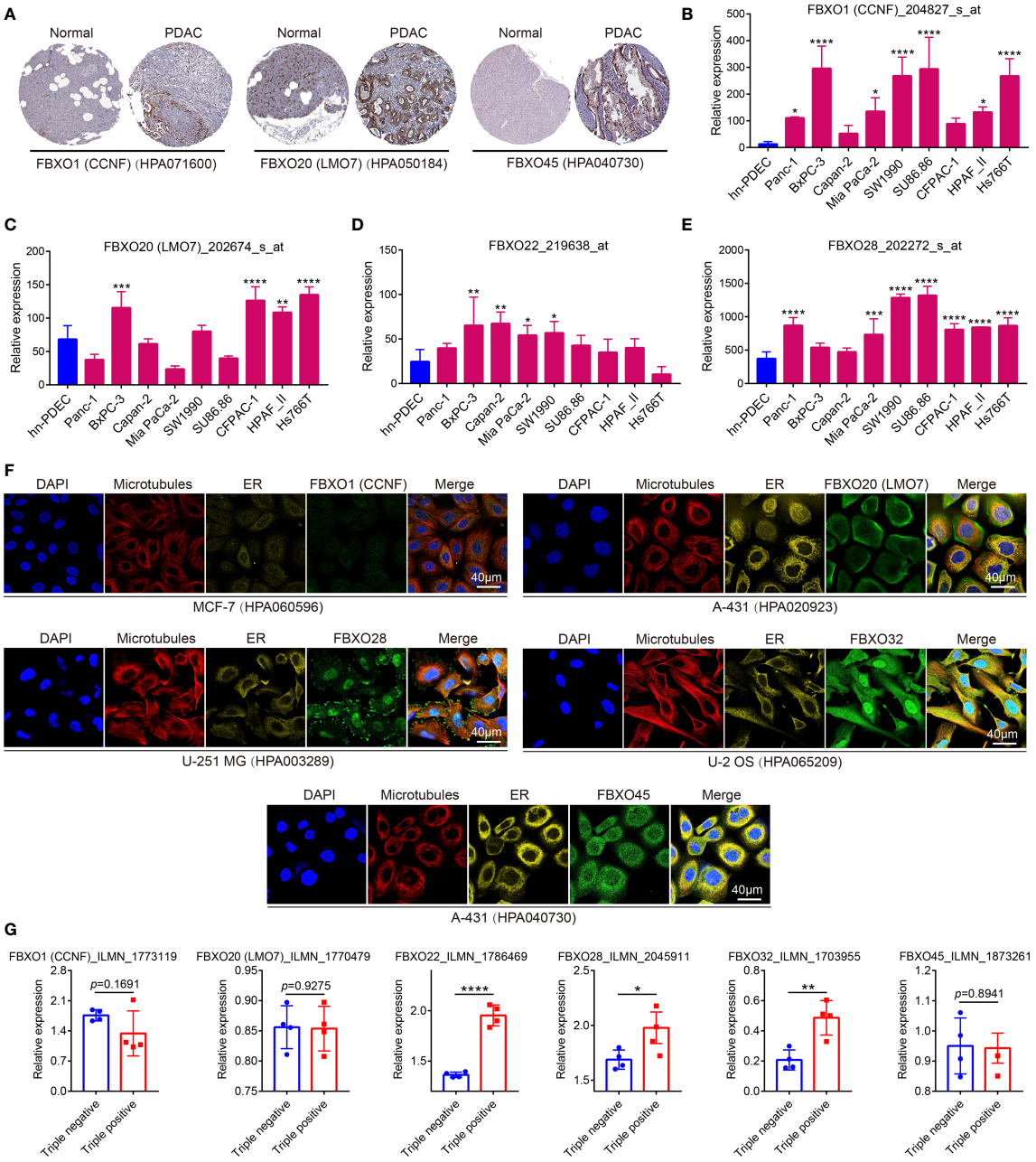

FIGURE 4 | The protein expression, cell lines, cellular localization, and cell stemness of six-FBXOs in pancreatic ductal adenocarcinoma (PDAC). **(A)** The protein expression of FBXO1, 20, and 45 in PDAC and normal tissues using immunohistochemistry (IHC) in Human Protein Atlas (HPA) database. The IHC images of FBXO22, 28, and 32 were absent. The code behind the gene is the related primary antibody in HPA. **(B–E)** The expression levels of FBXO1, 20, 22, and 28 in human normal pancreatic ductal epithelial cells (hn-PDEC) and multiple PDAC cell lines using GSE45757 dataset. The code behind the gene is the related probe name. FBXO32 and FBXO45 were not available. **(F)** The confocal images of cellular localization of six-FBXOs in different types of cells using HPA database. The code behind the cell line is the related primary antibody in HPA. ER, endoplasmic reticulum. **(G)** The expression levels of six-FBXOs in triple-positive group (n = 4) and triple-negative group (n = 4), which were classified by three key cancer stem cell markers, CD44, CD133, and EpCAM, using GSE51971 dataset. The code behind the gene is the related probe name. $^{*}P < 0.05$, $^{**}P < 0.01$, $^{***}P < 0.001$, $^{****}P < 0.0001$.

On the whole, the six-FBXOs tended to be the negative prognosis factors in the immunosuppressed state of PDAC. Furthermore, we also detected the prognostic analysis of subgroups in different gender or mutation burden. The results showed that FBXO1 and FBXO32 were the negative prognosis factors in the female group, whereas FBXO20, FBXO22, FBXO28, and FBXO45 were the negative prognosis factors in the male group. FBXO1, FBXO20, FBXO22, FBXO28, and FBXO32 were the negative prognosis

TABLE 2 | Prognostic analysis of the six-FBXOs in GEPIA and Kaplan–Meier plotter.

Genes	Expression	GEPIA				Kaplan–Meier plotter			
		OS		DFS		OS		RFS	
		HR (high)	*p*-value	HR (high)	*p*-value	HR (95% CI)	*p*-value	HR (95% CI)	*p*-value
FBXO1 (CCNF)	Upregulated	1.6	0.024	1.4	0.098	1.73 (1.13–2.63)	0.0102	3.31 (1.12–9.79)	0.0224
FBXO20 (LMO7)	Upregulated	1.7	0.012	1.6	0.033	2.73 (1.54–4.83)	0.0004	9.60 (2.24–41.23)	0.0002
FBXO22	Upregulated	2.0	0.0014	1.6	0.037	2.07 (1.23–3.47)	0.0048	2.77 (0.93–8.21)	0.0561
FBXO28	Upregulated	1.6	0.026	1.6	0.026	1.78 (1.17–2.72)	0.0068	NA	0.0035
FBXO32	Upregulated	1.5	0.048	1.6	0.051	1.71 (1.13–2.61)	0.0110	3.20 (1.38–7.42)	0.0045
FBXO45	Upregulated	1.7	0.013	1.7	0.015	1.99 (1.30–3.05)	0.0012	3.15 (1.36–7.30)	0.0050

OS, overall survival; DFS, disease-free survival; RFS, relapse-free survival; HR, hazard ratio; CI, confidence interval; NA, not available.

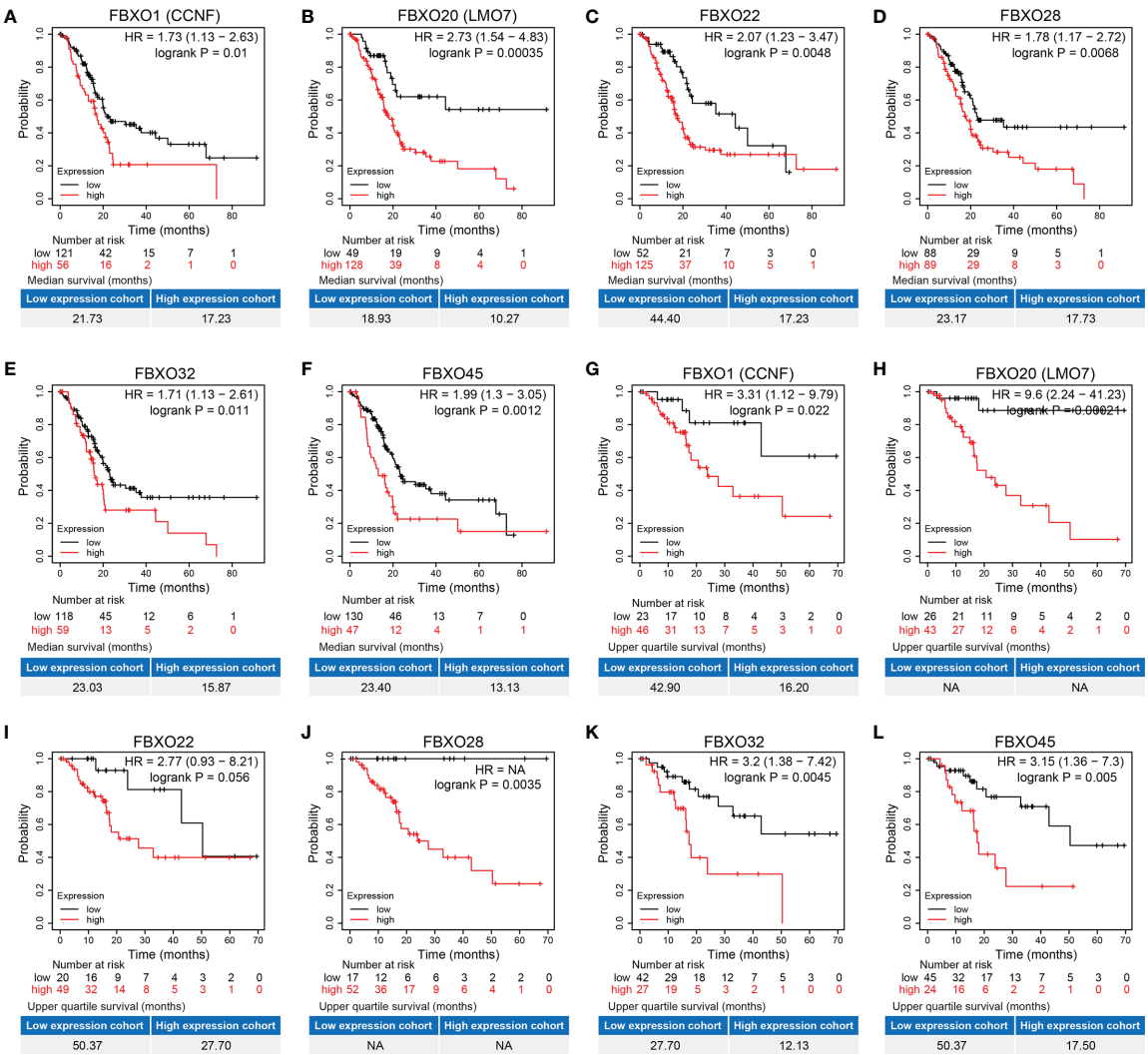

FIGURE 5 | The prognostic analysis of the six-FBXOs in pancreatic ductal adenocarcinoma (PDAC) using Kaplan–Meier plotter. **(A–F)** The overall survival of the six-FBXOs in PDAC patients (*N* = 177). **(G–L)** The disease-free survival of the six-FBXOs in PDAC patients (*N* = 69). "Auto-select best cutoff" was selected. NA, not available.

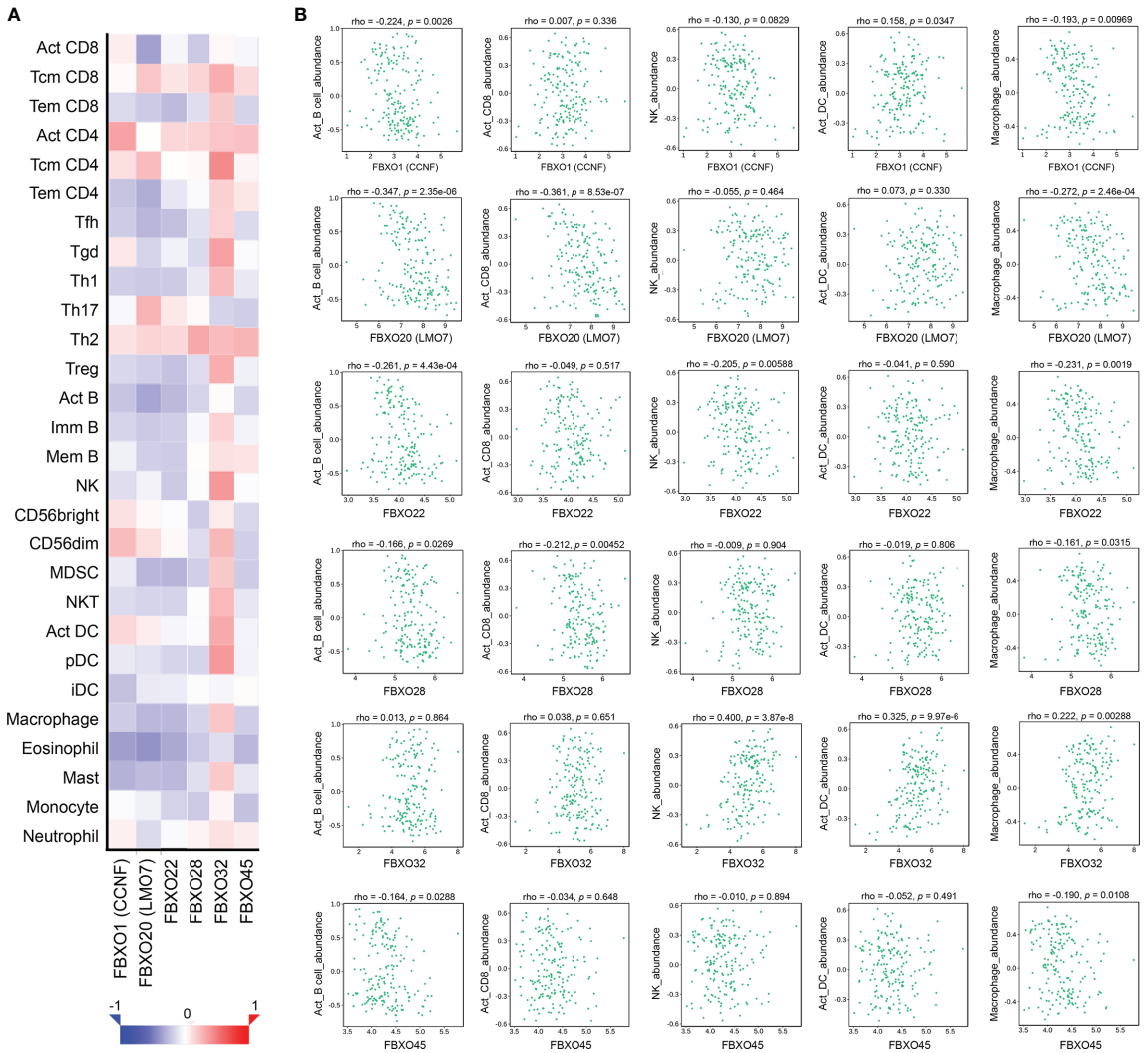

FIGURE 6 | Association of six-FBXO expression with immune infiltration level in pancreatic ductal adenocarcinoma (PDAC) (TISIDB). **(A)** Heat map of immune infiltrate correlation for six-FBXOs. **(B)** Scatter plot of the correlation between the expression level of six-FBXOs and immune cell infiltration, including Act_B cells, Act_CD8$^+$ T cells, NK cells, Act_DC, macrophages (Spearman correlation, N = 179). Act, activated; NK, natural killer cells; DC, dendritic cells.

factors in the low-mutation-burden group, and FBXO45 was the negative prognosis factor in the high-nutation-burden group (**Supplementary Figure S13**). For the subgroup analysis of DFS, the data are shown in **Supplementary Figure S14**. The HR, 95% CI, and p-value for the OS and DFS of six-FBXOs in different subgroups are summarized in **Supplementary Table S2**.

The Genetic Alteration and Mutation of Six-FBXOs in PDAC

We investigated the genetic alterations of the six-FBXO and the mutation in the cBioPortal database for pancreatic adenocarcinoma (TCGA and PanCancer Atlas). The results indicated that the genetic alteration of six-FBXOs in PDAC patients accounted for more than 40% (**Figure 7A**). Genetic alterations account for about 10% of each gene on average (**Figures 7B, C**), including mutation, amplification, mRNA high, mRNA low, and multiple alterations. For the progression of the genetic alterations of six-FBXOs, the data manifested that the altered group had a worse OS (p = 0.0331) and progression-free survival (p = 0.0428) than the unaltered group (**Figures 7D, E** and **Supplementary Table S3**). There is also such a trend for disease-specific survival in PDAC (p = 0.0592), but no statistical difference for DFS of two groups (p = 0.2020) (**Figures 7F, G** and **Supplementary Table S3**). Besides these, the altered group always had the higher typical PDAC gene mutations than the unaltered group, such as KRAS, TP53, CDKN2A, *etc.* (**Figure 7H**). Next, we analyzed the difference in sample-level enrichments between the altered group and the unaltered group. Using p <0.05 and log ratio >2 as the screening conditions, 1,194 genes were obtained in the altered group. The top 20 differently

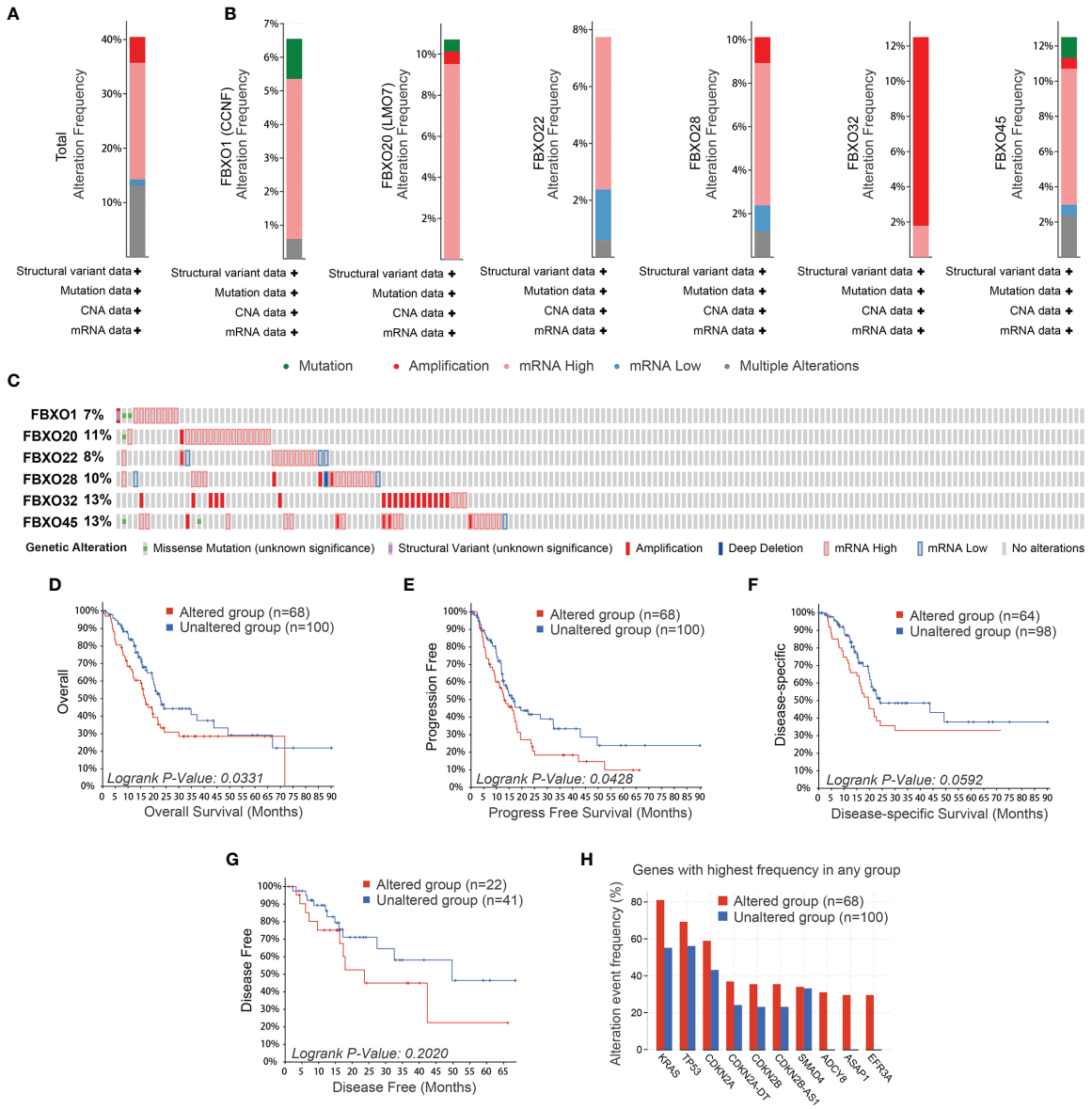

FIGURE 7 | The genetic alteration and mutation of six-FBXOs in PDAC using cBioPortal database. **(A)** Total alteration frequency of the six-FBXOs in PDAC. **(B, C)** Individual alteration frequency of six-FBXOs in PDAC. **(D–G)** The prognostic analysis of the genetic alteration of the six-FBXOs in PDAC, including overall (p = 0.0331), progression-free (p = 0.0428), disease-specific (p = 0.0592), and disease-free survival (p = 0.2020). **(H)** Alteration event frequency of common mutant genes between altered group (n = 68) and unaltered group (n = 100).

enriched genes are listed in **Supplementary Table S4**, such as ADCY8, ASAP1, EFR3A, KCNQ3, and PCAT1, which had been reported to play roles in tumor onset and progression (30–32).

Prediction of Functions and Pathways for Six-FBXOs in PDAC

We screened the top 200 positively co-expressed genes using the LinkedOmics database and the cBioPortal database, respectively, and obtained the intersected genes (**Figure 8A**). These shared gene sets were used to predict the functions and pathways of six-FBXOs by performing the GO and KEGG enrichment analysis. The GO enrichment analysis contains three points: BP, CC, and MF.

For FBXO1, BP terms indicated cell division, mitotic nuclear division, DNA replication, DNA repair, cell cycle, and cell proliferation. CC terms were implicated in nucleoplasm and condensed chromosome kinetochore, midbody. MF terms were involved in protein binding, ATP binding, and protein kinase binding. The KEGG pathways showed that FBXO1 was related to cell cycle, DNA replication, and p53 signaling pathway (**Figure 8B**). For FBXO20, BP terms were implicated in cell–cell adhesion, hemidesmosome assembly, actin cytoskeleton

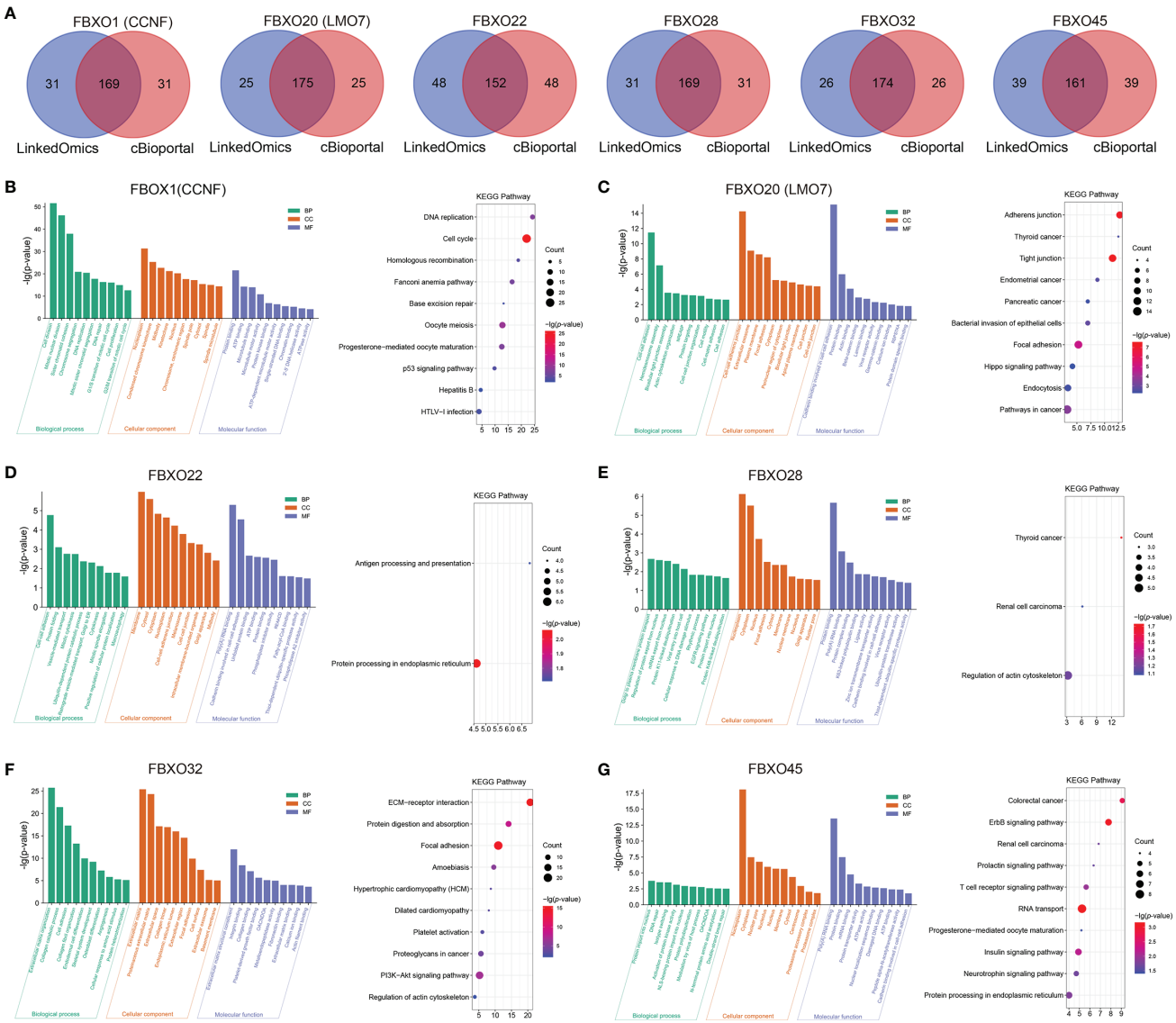

FIGURE 8 | Comprehensive bioinformatics analysis of six-FBXOs and individual co-expressed genes in pancreatic ductal adenocarcinoma. **(A)** Intersection of genes positively co-expressed in the top 200 of the LinkedOmics and the cBioPortal database (Spearman correlation). **(B–G)** The Gene Ontology enrichment analysis and Kyoto Encyclopedia of Genes and Genomes pathway prediction of six-FBXOs were performed. BP, biological processes; CC, cellular components; MF, molecular function.

organization, and negative regulation of extrinsic apoptotic signaling pathway. CC terms were involved in cell–cell adherens junction, extracellular exosome, plasma membrane, and focal adhesion. MF terms contained cadherin binding involved in cell–cell adhesion, protein binding, and actin binding. The KEGG pathways indicated that FBXO20 was related to tight junction, pathways in cancer, and Hippo signaling pathway (**Figure 8C**). For FBXO22, BP terms were implicated in protein folding, vesicle-mediated transport, and ubiquitin-dependent protein catabolic process. CC terms were involved in membrane, cytosol, and cytoplasm. MF terms contained poly(A) RNA binding, cadherin binding involved in cell–cell adhesion, and unfolded protein binding. The KEGG pathways indicated that FBXO22 was related to protein processing in the endoplasmic reticulum, antigen processing, and presentation (**Figure 8D**). For FBXO28, BP terms were implicated in Golgi to plasma membrane protein transport, regulation of protein export from nucleus, protein K11-linked deubiquitination, and EGFR signaling pathway. CC terms were involved in nucleoplasm, cytoplasm, and nucleus. MF terms contained protein complex binding, K63-linked polyubiquitin binding, and ubiquitin-protein transferase activity. The KEGG pathways indicated that FBXO28 was related to the regulation of actin cytoskeleton (**Figure 8E**). For FBXO32, BP terms were

implicated in extracellular matrix organization, collagen catabolic process, cell differentiation, and angiogenesis. CC terms were involved in extracellular matrix, proteinaceous extracellular matrix, and extracellular space. MF terms contained extracellular matrix structural constituent and integrin binding. The KEGG pathways indicated that FBXO32 was related to ECM–receptor interaction, PI3K-Akt signaling pathway, proteoglycans in cancer, and regulation of actin cytoskeleton (**Figure 8F**). For FBXO45, BP terms were implicated in protein import into the nucleus, DNA repair, and activation of protein kinase activity. CC terms were involved in nucleoplasm, cytoplasm, and nuclear pore. MF terms contained poly(A) RNA binding, protein binding, and mRNA binding. The KEGG pathways indicated that FBXO45 was related to RNA transport, ErbB signaling pathway, insulin signaling pathway, and T cell receptor signaling pathway (**Figure 8G**).

Validation of the Expression of Six-FBXOs in PDAC Cell Lines

To further validate the findings of the bioinformatics analysis, we used qPCR to confirm the transcriptional levels of six-FBXOs in five pancreatic cancer cell lines, respectively, that is, Panc-1, AsPC-1, SW1990, T3M4, and CFPAC-1, compared with human immortal pancreatic epithelial cell line HPDE6. The results revealed that, overall, the expression levels of six-FBXOs are markedly elevated in multiple PDAC cell lines (**Figure 9**), in concordance with the above-mentioned data, and it substantiated our bioinformatics analysis to some extent, although further *in vitro* and *in vivo* experiments were needed to support it.

DISCUSSION

Herein we comprehensively analyzed the clinical significance, function, and prognostic value of FBXO family genes, especially the six-FBXOs (FBXO1, FBXO20, FBXO22, FBXO28, FBXO32, and FBXO45). Firstly, we found the multiple FBXO family members to be aberrantly expressed in PDAC and identified six-FBXOs that were inversely associated with the OS and DFS of PDAC patients. Notably, although some differences of GEO data were not large, all of them were statistically significant and mutually verified using databases from different sources, which could confirm our findings on the six-FBXOs. Furthermore, their correlations between expression and clinicopathologic characteristics, as well as the promoter methylation levels, were further analyzed by using GEO, GEPIA, and UALCAN databases. Next, we investigated their protein expression, cell lines, cellular localization, and cell stemness. Using different databases, the related immune infiltration, genetic alteration, and mutation were evaluated in PDAC tissues. Finally, we predicted their functions and pathways through positively co-expressed genes using GO and KEGG enrichment analysis. Although some FBXO family members have been reported to be involved in oncogenesis and tumor advancement (11, 17, 33), comprehensive bioinformatics analyses of PDAC have yet to be investigated. The present study is the first time to analyze the transcription levels, clinicopathologic characteristics, promoter methylation, mutation, immune infiltration, and prognostic values of six FBXO family members (FBXO1, FBXO20, FBXO22, FBXO28, FBXO32, and FBXO45) in PDAC. We hope that these findings will help to replenish the available knowledge between the FBXO family and PDAC and contribute to improve the accuracy of prognostic prediction in PDAC patients as well as provide potential effective targets for the diagnosis and treatment of PDAC.

FBXO1

FBXO1 (CCNF) had been reported to be downregulated in hepatocellular carcinoma and was related to poor differentiation and adverse clinical outcome (34). In breast cancer, the overexpression of FBXO1 could suppress tumor progression, indicating that it has the role of a tumor suppressor (35). Intriguingly, FBXO1 mRNA was highly expressed in primary breast cancer tissues, but its protein level was strikingly reduced (35), hinting that FBXO1 was subjected to post-transcriptional modifications and protein degradation. Of note is the fact that FBXO1 was recently reported to be involved in the modification of the ubiquitination-proteasome system (36). FBXO1 was negatively regulated by the E3 ligase (FZR1) and the co-regulator of E3 ligase (FBXL8), which were known to play an oncogenic role in breast cancer, and FBXO1 could inhibit the expression of ribonucleotide reductase M2 (RRM2), a pro-tumorigenic protein (35). In contrast, FBXO1 was overexpressed in ovarian cancer tissues and facilitated the cell growth and invasion of ovarian cancer (37). Herein we found that FBXO1 was upregulated in PDAC tissues and the majority of PDAC cell lines as well as associated with the unfortunate prognosis of PDAC patients based on different public databases. These findings have been validated by a recently published study regarding the protein expression of FBXO1 in PDAC *via* IHC (38). Furthermore, our data showed that FBXO1 expression was linked to tumor differentiation, pathological grading, promoter methylation, P53 mutation, and immune infiltration in PDAC.

FBXO20

FBXO20 (LMO7) was downregulated in lung adenocarcinoma and relevant in tumor size, nodal involvement, and pathological stage as well as with a poor prognosis (15). The depletion of FBXO20 resulted in an increase of susceptibility for spontaneous lung cancer in the murine model (39). In contrast, FBXO20 could facilitate the migration ability of breast cancer cells in a cell-specific manner *via* modulating Rho-MRTF-SRF signaling (14). Liu et al. verified that the expression levels of FBXO20 mRNA and protein were increased in mouse and human pancreatic cancer tissues (16). The results of Liu were consistent with our findings in multiple public databases to some extent. FBXO20 acted an oncogenic role to promote metastasis and progression. In terms of proliferation, FBXO20 exhibited dual roles, that is, cell cycle acceleration and apoptosis inhibition (16). In addition, our data showed that a higher expression of FBXO20 tended to result in poorer pathological grading and worse tumor differentiation and predict an adverse prognosis in PDAC patients. FBXO20 was significantly elevated

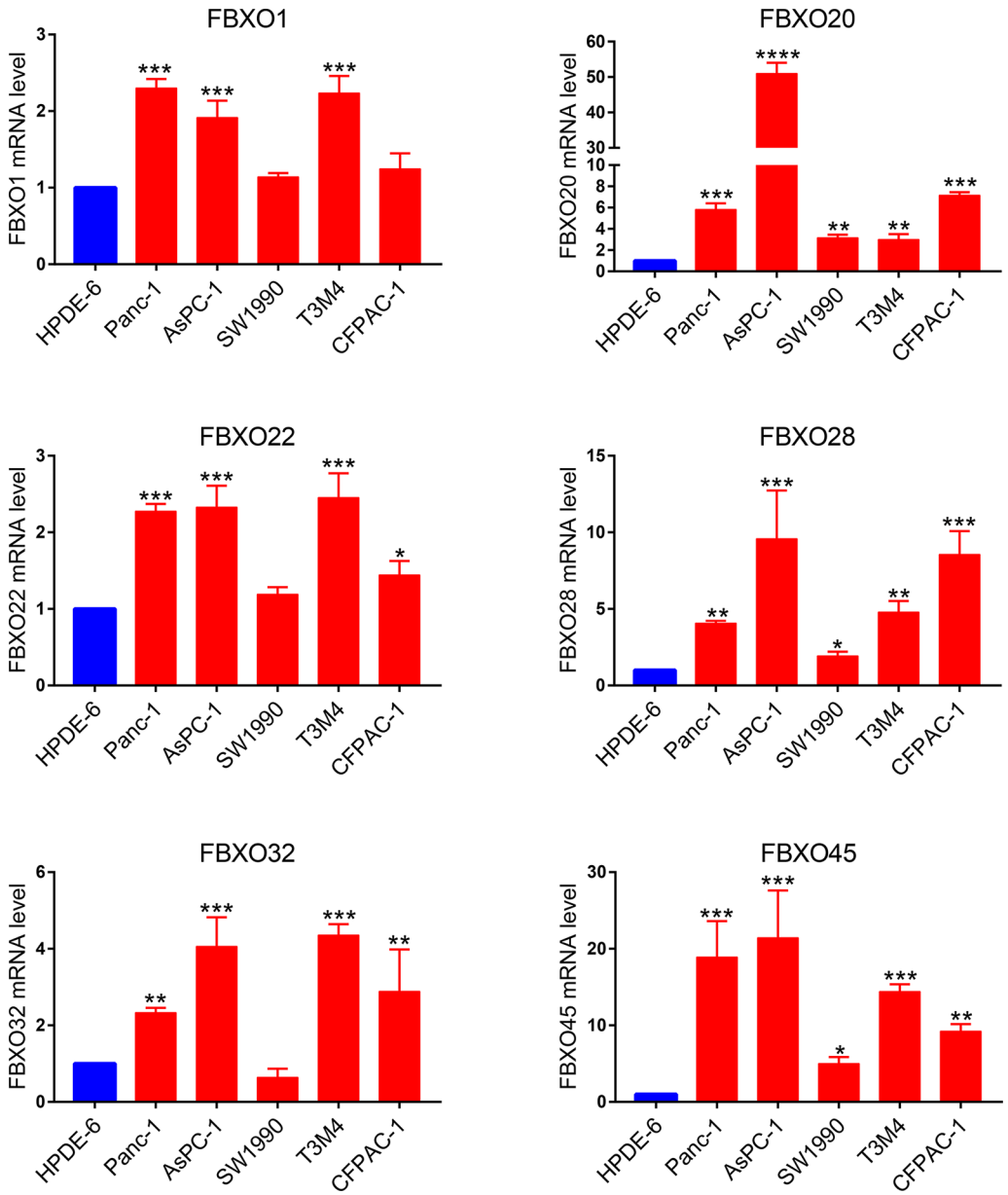

FIGURE 9 | The expression levels of six-FBXOs in human immortalized normal pancreatic epithelial cells HPDE6 and different pancreatic ductal adenocarcinoma cell lines were verified using real-time qPCR. *$P < 0.05$, **$P < 0.01$, ***$P < 0.001$, ****$P < 0.0001$.

in different pancreatic precancerous lesions, including IPMA, IPMC, and IPMN. Among them, IPMA had the highest expression levels of FBXO20. These data indicated that FBXO20 possessed the potential to be a sensitive indicator of precancerous lesions, which is important for the early diagnosis of PDAC. Besides this, FBXO20 was tightly correlated with diabetic status, promoter methylation, P53 mutation, and immune infiltration in PDAC. The functional analysis and KEGG pathways revealed that FBXO20 might be involved in apoptosis-related signaling pathway and Hippo signaling pathway, which deserve to be further investigated.

FBXO22

Accumulating evidence suggested that FBXO22 exerts its oncogenic functions through mediating the ubiquitination and degradation of substrates in many human malignancies (40). However, the roles it plays in different tumors is inconsistent in physiological and pathological processes. In renal cell carcinoma, FBXO22 restrained cancer metastasis and progression by suppressing VEGF-induced angiogenesis and MMP-9-induced invasion and migration (41). On the contrary, FBXO22 facilitated tumorigenesis and progression *via* regulating the ubiquitination and degradation of p21 in hepatocellular carcinoma (42), of LKB1 in lung cancer, and

of nuclear PTEN in colorectal cancer (43). Interestingly, FBXO22 exhibits a paradoxical dual role of pro-tumorigenic and anti-metastatic function in breast cancer progression (44). The functional role of FBXO22 in PDAC has not yet been reported. Herein we explored that FBXO22 was upregulated in PDAC and associated with cell stemness, poor pathological grading, and worse clinical outcomes. Notably, FBXO22 expression was closely correlated with the infiltration of a variety of immune cells, including B cells, $CD8^+$ T cells, $CD4^+$ T cells, NK cells, macrophages, neutrophils, and dendritic cells, implicating that it might be involved in the reprogramming of the tumor immune microenvironment in PDAC. Similarly, our functional analysis suggested that FBXO22 was related to the ubiquitin-dependent protein catabolic process, protein processing in the endoplasmic reticulum, antigen processing, and presentation, which allows our data and the published literatures to be mutually corroborated.

FBXO28

SCF (Skp1/Cul1/F-box) ubiquitin ligase serves as a key modulator of cell homeostasis *via* regulating downstream a variety of critical proteins for ubiquitylation (45). The IHC analysis displayed that FBXO28 and its phosphorylation are strong and predicted a poor prognosis in breast cancer (46). The CDK1/2-driven activation of the E3 ubiquitin ligase SCF^{FBXO28} accelerated MYC-dependent transcription by non-proteolytic ubiquitylation and promoted transformation and tumorigenesis (46). Fagerholm et al. showed that FBXO28 had a correlation with survival and treatment outcome using interaction analysis of cis-eQTL variants in breast cancer (47). Herein we found that FBXO28 had a high level in the majority of PDAC cell lines and tissues, which often predicted an adverse clinical survival for PDAC patients. Besides this, FBXO28 expression was related to cell stemness, tumor size, and pathological grading, but no significant correlation with promoter methylation. Notably, FBXO28 expression was strongly linked to the infiltration of multiple immune cells, such as B cells, $CD8^+$ T cells, macrophages, neutrophils, and dendritic cells. The functional analysis revealed that FBXO28 may be involved in protein transport, protein deubiquitination, EGFR signaling pathway, and regulation of actin cytoskeleton.

FBXO32

The promoter hypermethylation of FBXO32 was responsible for its downregulation in ovarian cancer cells. A profound methylation frequency of FBXO32 was detected in advanced-stage ovarian cancer, which predicted a shorter progression-free survival (48). The re-expression of FBXO32 dampened cell growth in platinum-resistant ovarian cancer as a result of being re-sensitized to cisplatin and increased apoptosis (48). A similar situation of aberrant methylation of FBXO32 could be found in esophageal squamous cell carcinoma (49). Furthermore, FBXO32 inhibited breast cancer oncogenesis and progression *via* interacting with KLF4 for its ubiquitination and degradation, a critical factor for cell fate decisions (50). Consistent with our findings, we also found aberrant promoter methylation of FBXO32, but the discordant result was that FBXO32 was hypomethylated and highly expressed in PanIN and PDAC, in comparison to normal tissues, as well as closely relevant in cell stemness, tumor size, lymphatic metastasis, tumor differentiation, tumor staging, and the prognosis of PDAC patients. Among pancreatic precancerous lesions, FBXO32 had the highest expression in IPMC. Furthermore, FBXO32 expression is also related to immune infiltration, *e.g.*, $CD8^+$ T cells, NK cells, macrophages, neutrophils, and dendritic cells. The functional analysis demonstrated that FBXO32 may be involved in cell differentiation, angiogenesis, regulation of actin cytoskeleton, and PI3K-Akt signaling pathway, which remains to be further explored.

FBXO45

FBXO45 propelled ubiquitin-mediated proteolysis of the tumor-suppressor PAR4 to control cancer cell survival (51). Specifically, E3 ubiquitin ligase FBXO45 could interact with PAR4, a PRKC apoptosis WT1 regulator, *via* a short consensus sequence motif in the cytoplasm to influence its ubiquitylation and proteasomal degradation, which, in turn, governs cell apoptosis (51). Furthermore, FBXO45 modulated the process of EMT *via* mediating the ubiquitination and degradation of substantial EMT-related transcription factors, such as Twist1, Snai1/2, and Zeb1/2, in tumor cells (52). In gastric cancer, the expression levels of FBXO45 in tumor tissues were increased compared with those in normal tissues. Unexpectedly, patients with high FBXO45 expression had longer survival than those with low expression (53). Herein we found that FBXO45 expression was markedly upregulated in PDAC tissues in both mRNA and protein levels and was inversely relevant in the OS and DFS of PDAC patients based on multiple online databases. FBXO45 expression was related to the degree of tumor differentiation, tumor staging, and P53 mutation in PDAC. The expression level of FBXO45 was higher in IPMC than in normal pancreatic tissues. Additionally, the expression levels of FBXO45 were related to immune infiltration, *i.e.*, B cells, $CD8^+$ T cells, $CD4^+$ T cells, NK cells, macrophages, neutrophils, and dendritic cells. The functional analysis showed that FBXO45 was involved in ErbB signaling pathway and T cell receptor signaling pathway.

Among six-FBXOs, FBXO32 had attracted our attention since it exhibited a strong correlation with all the clinicopathological parameters investigated as detailed above. In terms of prognosis, FBXO32 expression could well predict the clinical outcomes of PDAC patients in both OS and DFS. For diagnosis, FBXO32 was tightly associated with clinicopathologic characteristics, cell stemness, and immune infiltration. Besides this, we noticed that FBXO32 was not only significantly upregulated in PDAC tissues but also highly expressed in some precancerous tissues, such as IPMC and PanIN, which provided a strong support for the early diagnosis of PDAC. Regarding treatment, we speculated that FBXO32 was likely to play a role in PDAC initiation and progression as well as reprogramming of the tumor immune microenvironment through regulating cell differentiation, angiogenesis, actin cytoskeleton, and some important signaling pathways, such as PI3K/Akt signaling pathway. By developing therapeutic agents targeting FBXO32, it is possible to control and block the development and malignant transformation of PDAC.

Therefore, FBXO32 might be a promising prognostic/diagnostic/therapeutic target for PDAC.

CONCLUSION

In the present study, we identified that FBXO1, FBXO20, FBXO22, FBXO28, FBXO32, and FBXO45 are highly expressed in PDAC tissues, which are potential unfavorable prognostic factors for PDAC patients. The six FBXOs are strongly associated with clinicopathological features, promoter methylation, immune infiltration, and genetic mutation in PDAC based on different public databases. So far, there is a paucity in the literature studying the roles of six-FBXOs in PDAC. Therefore, the specific roles and underlying mechanisms of six-FBXOs in PDAC are worth further investigation through a large number of related experiments *in vitro* and *in vivo*. To sum up, our study indicates that six-FBXOs might act an oncogenic role to promote PDAC progression and serve as the potential targets for PDAC diagnosis and treatment.

DATA AVAILABILITY STATEMENT

The datasets presented in this study can be found in online repositories. The names of the repository/repositories and accession number(s) can be found in the article/**Supplementary Material**.

ETHICS STATEMENT

The study has been approved by the Ethics Committee of Peking Union Medical College Hospital. Since all the data were collected and downloaded from the public online databases, it was certain that all written informed consent had already been obtained.

AUTHOR CONTRIBUTIONS

YZ conceived this study, analyzed the data, and drafted the manuscript. QLiu reviewed and revised the manuscript. MC, MW, SH, and JG collected the data and reviewed the manuscript. QLiao was responsible for project administration and supervision. All authors contributed to the article and approved the submitted version.

FUNDING

This work was supported by the National Natural Science Foundation of China (82172765, 81872501, 81673023, 81272573, and 81502068), Beijing Natural Science Foundation (7172177), CAMS Innovation Fund for Medical Sciences (CIFMS, 2021-I2M-1-002) and Youth Foundation of Peking Union Medical College Hospital (pumch201911866).

ACKNOWLEDGMENTS

We would like to acknowledge Dr. Yunfeng Zhang and Yinuo Zhang for their spiritual support and encouragement.

SUPPLEMENTARY MATERIAL

The Supplementary Material for this article can be found online at: https://www.frontiersin.org/articles/10.3389/fimmu.2021.774435/full#supplementary-material

REFERENCES

1. Yang Y, Bai X, Bian D, Cai S, Chen R, Cao F, et al. Guidelines for the Diagnosis and Treatment of Pancreatic Cancer in China (2021). *J Pancreatol* (2021) 4(2):49–66. doi: 10.1097/jp9.0000000000000072
2. Kamisawa T, Wood LD, Itoi T, Takaori K. Pancreatic Cancer. *Lancet* (2016) 388(10039):73–85. doi: 10.1016/S0140-6736(16)00141-0
3. Leonhardt CS, Traub B, Hackert T, Klaiber U, Strobel O, Büchler MW, et al. Adjuvant and Neoadjuvant Chemotherapy in Pancreatic Ductal Adenocarcinoma. *J Pancreatol* (2020) 3(1):1–11. doi: 10.1097/jp9.0000000000000040
4. Hussain SP. Pancreatic Cancer: Current Progress and Future Challenges. *Int J Biol Sci* (2016) 12(3):270–2. doi: 10.7150/ijbs.14950
5. Neoptolemos JP, Kleeff J, Michl P, Costello E, Greenhalf W, Palmer DH. Therapeutic Developments in Pancreatic Cancer: Current and Future Perspectives. *Nat Rev Gastroenterol Hepatol* (2018) 15(6):333–48. doi: 10.1038/s41575-018-0005-x
6. Zhang Y, Liu Q, Liu J, Liao Q. Upregulated CD58 Is Associated With Clinicopathological Characteristics and Poor Prognosis of Patients With Pancreatic Ductal Adenocarcinoma. *Cancer Cell Int* (2021) 21(1):327. doi: 10.1186/s12935-021-02037-0
7. Zhang Y, Liu Q, Yang S, Liao Q. CD58 Immunobiology at a Glance. *Front Immunol* (2021) 12:705260. doi: 10.3389/fimmu.2021.705260
8. Zhang Y, Liu Q, Liao Q. Long Noncoding RNA: A Dazzling Dancer in Tumor Immune Microenvironment. *J Exp Clin Cancer Res* (2020) 39(1):231. doi: 10.1186/s13046-020-01727-3
9. Ciechanover A. Intracellular Protein Degradation: From a Vague Idea Thru the Lysosome and the Ubiquitin-Proteasome System and Onto Human Diseases and Drug Targeting. *Best Pract Res Clin Haematol* (2017) 30(4):341–55. doi: 10.1016/j.beha.2017.09.001
10. Skaar JR, Pagan JK, Pagano M. Mechanisms and Function of Substrate Recruitment by F-Box Proteins. *Nat Rev Mol Cell Biol* (2013) 14(6):369–81. doi: 10.1038/nrm3582
11. Tekcham DS, Chen D, Liu Y, Ling T, Zhang Y, Chen H, et al. F-Box Proteins and Cancer: An Update From Functional and Regulatory Mechanism to Therapeutic Clinical Prospects. *Theranostics* (2020) 10(9):4150–67. doi: 10.7150/thno.42735
12. D'Angiolella V, Donato V, Forrester FM, Jeong YT, Pellacani C, Kudo Y, et al. Cyclin F-Mediated Degradation of Ribonucleotide Reductase M2 Controls Genome Integrity and DNA Repair. *Cell* (2012) 149(5):1023–34. doi: 10.1016/j.cell.2012.03.043
13. Tzeng YW, Li DY, Chen Y, Yang CH, Chang CY, Juang YL. LMO7 Exerts an Effect on Mitosis Progression and the Spindle Assembly Checkpoint. *Int J Biochem Cell Biol* (2018) 94:22–30. doi: 10.1016/j.biocel.2017.11.006
14. Hu Q, Guo C, Li Y, Aronow BJ, Zhang J. LMO7 Mediates Cell-Specific Activation of the Rho-Myocardin-Related Transcription Factor-Serum Response Factor Pathway and Plays an Important Role in Breast Cancer Cell Migration. *Mol Cell Biol* (2011) 31(16):3223–40. doi: 10.1128/MCB.01365-10
15. Nakamura H, Hori K, Tanaka-Okamoto M, Higashiyama M, Itoh Y, Inoue M, et al. Decreased Expression of LMO7 and its Clinicopathological Significance

in Human Lung Adenocarcinoma. *Exp Ther Med* (2011) 2(6):1053–7. doi: 10.3892/etm.2011.329
16. Liu X, Yuan H, Zhou J, Wang Q, Qi X, Bernal C, et al. LMO7 as an Unrecognized Factor Promoting Pancreatic Cancer Progression and Metastasis. *Front Cell Dev Biol* (2021) 9:647387. doi: 10.3389/fcell.2021.647387
17. Liu Y, Pan B, Qu W, Cao Y, Li J, Zhao H. Systematic Analysis of the Expression and Prognosis Relevance of FBXO Family Reveals the Significance of FBXO1 in Human Breast Cancer. *Cancer Cell Int* (2021) 21(1):130. doi: 10.1186/s12935-021-01833-y
18. Tang Z, Li C, Kang B, Gao G, Li C, Zhang Z. GEPIA: A Web Server for Cancer and Normal Gene Expression Profiling and Interactive Analyses. *Nucleic Acids Res* (2017) 45(W1):W98–W102. doi: 10.1093/nar/gkx247
19. Rhodes DR, Yu J, Shanker K, Deshpande N, Varambally R, Ghosh D, et al. ONCOMINE: A Cancer Microarray Database and Integrated Data-Mining Platform. *Neoplasia* (2004) 6(1):1–6. doi: 10.1016/s1476-5586(04)80047-2
20. Chandrashekar DS, Bashel B, Balasubramanya SAH, Creighton CJ, Ponce-Rodriguez I, Chakravarthi B, et al. UALCAN: A Portal for Facilitating Tumor Subgroup Gene Expression and Survival Analyses. *Neoplasia* (2017) 19(8):649–58. doi: 10.1016/j.neo.2017.05.002
21. Nagy A, Munkacsy G, Gyorffy B. Pancancer Survival Analysis of Cancer Hallmark Genes. *Sci Rep* (2021) 11(1):6047. doi: 10.1038/s41598-021-84787-5
22. Aguirre-Gamboa R, Gomez-Rueda H, Martinez-Ledesma E, Martinez-Torteya A, Chacolla-Huaringa R, Rodriguez-Barrientos A, et al. SurvExpress: An Online Biomarker Validation Tool and Database for Cancer Gene Expression Data Using Survival Analysis. *PloS One* (2013) 8(9):e74250. doi: 10.1371/journal.pone.0074250
23. Vasaikar SV, Straub P, Wang J, Zhang B. LinkedOmics: Analyzing Multi-Omics Data Within and Across 32 Cancer Types. *Nucleic Acids Res* (2018) 46(D1):D956–63. doi: 10.1093/nar/gkx1090
24. Li T, Fan J, Wang B, Traugh N, Chen Q, Liu JS, et al. TIMER: A Web Server for Comprehensive Analysis of Tumor-Infiltrating Immune Cells. *Cancer Res* (2017) 77(21):e108–e10. doi: 10.1158/0008-5472.CAN-17-0307
25. Ru B, Wong CN, Tong Y, Zhong JY, Zhong SSW, Wu WC, et al. TISIDB: An Integrated Repository Portal for Tumor-Immune System Interactions. *Bioinformatics* (2019) 35(20):4200–2. doi: 10.1093/bioinformatics/btz210
26. Gao J, Aksoy BA, Dogrusoz U, Dresdner G, Gross B, Sumer SO, et al. Integrative Analysis of Complex Cancer Genomics and Clinical Profiles Using the Cbioportal. *Sci Signal* (2013) 6(269):pl1. doi: 10.1126/scisignal.2004088
27. Huang da W, Sherman BT, Lempicki RA. Systematic and Integrative Analysis of Large Gene Lists Using DAVID Bioinformatics Resources. *Nat Protoc* (2009) 4(1):44–57. doi: 10.1038/nprot.2008.211
28. Schofield HK, Zeller J, Espinoza C, Halbrook CJ, Del Vecchio A, Magnuson B, et al. Mutant P53r270h Drives Altered Metabolism and Increased Invasion in Pancreatic Ductal Adenocarcinoma. *JCI Insight* (2018) 3(2):e97422. doi: 10.1172/jci.insight.97422
29. Liu Y, Baggerly KA, Orouji E, Manyam G, Chen H, Lam M, et al. Methylation-eQTL Analysis in Cancer Research. *Bioinformatics* (2021) 37:4014–22. doi: 10.1093/bioinformatics/btab443
30. Zheng Q, Min S, Zhou Q. Identification of Potential Diagnostic and Prognostic Biomarkers for LUAD Based on TCGA and GEO Databases. *Biosci Rep* (2021) 41(6):SR20204370. doi: 10.1042/BSR20204370
31. Hashimoto A, Handa H, Hata S, Tsutaho A, Yoshida T, Hirano S, et al. Inhibition of Mutant KRAS-Driven Overexpression of ARF6 and MYC by an Eif4a Inhibitor Drug Improves the Effects of Anti-PD-1 Immunotherapy for Pancreatic Cancer. *Cell Commun Signal* (2021) 19(1):54. doi: 10.1186/s12964-021-00733-y
32. Wang J, Chen X, Hu H, Yao M, Song Y, Yang A, et al. PCAT-1 Facilitates Breast Cancer Progression *via* Binding to RACK1 and Enhancing Oxygen-Independent Stability of HIF-1alpha. *Mol Ther Nucleic Acids* (2021) 24:310–24. doi: 10.1016/j.omtn.2021.02.034
33. Lin M, Wang ZW, Zhu X. FBXO45 Is a Potential Therapeutic Target for Cancer Therapy. *Cell Death Discovery* (2020) 6:55. doi: 10.1038/s41420-020-0291-2
34. Fu J, Qiu H, Cai M, Pan Y, Cao Y, Liu L, et al. Low Cyclin F Expression in Hepatocellular Carcinoma Associates With Poor Differentiation and Unfavorable Prognosis. *Cancer Sci* (2013) 104(4):508–15. doi: 10.1111/cas.12100
35. Chang SC, Hung CS, Zhang BX, Hsieh TH, Hsu W. Ding JL. A Novel Signature of CCNF-Associated E3 Ligases Collaborate and Counter Each Other in Breast Cancer. *Cancers (Basel)* (2021) 13(12):2873. doi: 10.3390/cancers13122873
36. Lee A, Rayner SL, Gwee SSL, De Luca A, Shahheydari H, Sundaramoorthy V, et al. Pathogenic Mutation in the ALS/FTD Gene, CCNF, Causes Elevated Lys48-Linked Ubiquitylation and Defective Autophagy. *Cell Mol Life Sci* (2018) 75(2):335–54. doi: 10.1007/s00018-017-2632-8
37. Li Y, Guo H, Wang Z, Bu H, Wang S, Wang H, et al. Cyclin F and KIF20A, FOXM1 Target Genes, Increase Proliferation and Invasion of Ovarian Cancer Cells. *Exp Cell Res* (2020) 395(2):112212. doi: 10.1016/j.yexcr.2020.112212
38. Klimaszewska-Wisniewska A, Buchholz K, Neska-Dlugosz I, Durslewicz J, Grzanka D, Zabrzynski J, et al. Expression of Genomic Instability-Related Molecules: Cyclin F, RRM2 and SPDL1 and Their Prognostic Significance in Pancreatic Adenocarcinoma. *Cancers (Basel)* (2021) 13(4):859. doi: 10.3390/cancers13040859
39. Tanaka-Okamoto M, Hori K, Ishizaki H, Hosoi A, Itoh Y, Wei M, et al. Increased Susceptibility to Spontaneous Lung Cancer in Mice Lacking LIM-Domain Only 7. *Cancer Sci* (2009) 100(4):608–16. doi: 10.1111/j.1349-7006.2009.01091.x
40. Cheng J, Lin M, Chu M, Gong L, Bi Y, Zhao Y. Emerging Role of FBXO22 in Carcinogenesis. *Cell Death Discov* (2020) 6:66. doi: 10.1038/s41420-020-00303-0
41. Guo F, Liu J, Han X, Zhang X, Lin T, Wang Y, et al. FBXO22 Suppresses Metastasis in Human Renal Cell Carcinoma *via* Inhibiting MMP-9-Mediated Migration and Invasion and VEGF-Mediated Angiogenesis. *Int J Biol Sci* (2019) 15(3):647–56. doi: 10.7150/ijbs.31293
42. Zhang L, Chen J, Ning D, Liu Q, Wang C, Zhang Z, et al. FBXO22 Promotes the Development of Hepatocellular Carcinoma by Regulating the Ubiquitination and Degradation of P21. *J Exp Clin Cancer Res* (2019) 38(1):101. doi: 10.1186/s13046-019-1058-6
43. Ge MK, Zhang N, Xia L, Zhang C, Dong SS, Li ZM, et al. FBXO22 Degrades Nuclear PTEN to Promote Tumorigenesis. *Nat Commun* (2020) 11(1):1720. doi: 10.1038/s41467-020-15578-1
44. Sun R, Xie HY, Qian JX, Huang YN, Yang F, Zhang FL, et al. FBXO22 Possesses Both Protumorigenic and Antimetastatic Roles in Breast Cancer Progression. *Cancer Res* (2018) 78(18):5274–86. doi: 10.1158/0008-5472.CAN-17-3647
45. Weissman AM. Themes and Variations on Ubiquitylation. *Nat Rev Mol Cell Biol* (2001) 2(3):169–78. doi: 10.1038/35056563
46. Cepeda D, Ng HF, Sharifi HR, Mahmoudi S, Cerrato VS, Fredlund E, et al. CDK-Mediated Activation of the SCF(FBXO) (28) Ubiquitin Ligase Promotes MYC-Driven Transcription and Tumourigenesis and Predicts Poor Survival in Breast Cancer. *EMBO Mol Med* (2013) 5(7):1067–86. doi: 10.1002/emmm.201202341
47. Fagerholm R, Khan S, Schmidt MK, Garcia-Closas M, Heikkila P, Saarela J, et al. TP53-Based Interaction Analysis Identifies cis-eQTL Variants for TP53BP2, FBXO28, and FAM53A That Associate With Survival and Treatment Outcome in Breast Cancer. *Oncotarget* (2017) 8(11):18381–98. doi: 10.18632/oncotarget.15110
48. Chou JL, Su HY, Chen LY, Liao YP, Hartman-Frey C, Lai YH, et al. Promoter Hypermethylation of FBXO32, a Novel TGF-Beta/SMAD4 Target Gene and Tumor Suppressor, Is Associated With Poor Prognosis in Human Ovarian Cancer. *Lab Invest* (2010) 90(3):414–25. doi: 10.1038/labinvest.2009.138
49. Guo W, Zhang M, Shen S, Guo Y, Kuang G, Yang Z, et al. Aberrant Methylation and Decreased Expression of the TGF-Beta/Smad Target Gene FBXO32 in Esophageal Squamous Cell Carcinoma. *Cancer* (2014) 120(16):2412–23. doi: 10.1002/cncr.28764
50. Zhou H, Liu Y, Zhu R, Ding F, Wan Y, Li Y, et al. FBXO32 Suppresses Breast Cancer Tumorigenesis Through Targeting KLF4 to Proteasomal Degradation. *Oncogene* (2017) 36(23):3312–21. doi: 10.1038/onc.2016.479
51. Chen X, Sahasrabuddhe AA, Szankasi P, Chung F, Basrur V, Rangnekar VM, et al. Fbxo45-Mediated Degradation of the Tumor-Suppressor Par-4 Regulates Cancer Cell Survival. *Cell Death Differ* (2014) 21(10):1535–45. doi: 10.1038/cdd.2014.92
52. Xu M, Zhu C, Zhao X, Chen C, Zhang H, Yuan H, et al. Atypical Ubiquitin E3 Ligase Complex Skp1-Pam-Fbxo45 Controls the Core Epithelial-to-Mesenchymal Transition-Inducing Transcription Factors. *Oncotarget* (2015) 6(2):979–94. doi: 10.18632/oncotarget.2825

53. Kogure N, Yokobori T, Ogata K, Altan B, Mochiki E, Ohno T, et al. Low Expression of FBXO45 Is Associated With Gastric Cancer Progression and Poor Prognosis. *Anticancer Res* (2017) 37(1):191–6. doi: 10.21873/anticanres.11305

Conflict of Interest: The authors declare that the research was conducted in the absence of any commercial or financial relationships that could be construed as a potential conflict of interest.

Publisher's Note: All claims expressed in this article are solely those of the authors and do not necessarily represent those of their affiliated organizations, or those of the publisher, the editors and the reviewers. Any product that may be evaluated in this article, or claim that may be made by its manufacturer, is not guaranteed or endorsed by the publisher.

frontiers in Immunology

ORIGINAL RESEARCH
published: 05 January 2022
doi: 10.3389/fimmu.2021.781087

Comprehensive Pan-Cancer Genomic Analysis Reveals PHF19 as a Carcinogenic Indicator Related to Immune Infiltration and Prognosis of Hepatocellular Carcinoma

Zheng-yi Zhu[1†], *Ning Tang*[1,2†], *Ming-fu Wang*[1,3], *Jing-chao Zhou*[1,3], *Jing-lin Wang*[1,2,3*], *Hao-zhen Ren*[1,2,3*] *and Xiao-lei Shi*[1,2,3*]

[1] Department of Hepatobiliary Surgery, Affiliated Drum Tower Hospital of Nanjing University Medical School, Nanjing, China, [2] Nanjing Drum Tower Hospital Clinical College of Nanjing Medical University, Nanjing, China, [3] Nanjing Drum Tower Hospital Clinical College of Traditional Chinese and Western Medicine, Nanjing University of Chinese Medicine, Nanjing, China

Background: As a crucial constituent part of Polycomb repressive complex 2, PHD finger protein 19 (PHF19) plays a pivotal role in epigenetic regulation, and acts as a critical regulator of multiple pathophysiological processes. However, the exact roles of PHF19 in cancers remain enigmatic. The present research was primarily designed to provide the prognostic landscape visualizations of PHF19 in cancers, and study the correlations between PHF19 expression and immune infiltration characteristics in tumor microenvironment.

Methods: Raw data in regard to PHF19 expression were extracted from TCGA and GEO data portals. We examined the expression patterns, prognostic values, mutation landscapes, and protein-protein interaction network of PHF19 in pan-cancer utilizing multiple databases, and investigated the relationship of PHF19 expression with immune infiltrates across TCGA-sequenced cancers. The R language was used to conduct KEGG and GO enrichment analyses. Besides, we built a risk-score model of hepatocellular carcinoma (HCC) and validated its prognostic classification efficiency.

Results: On balance, PHF19 expression was significantly higher in cancers in comparison with that in noncancerous samples. Increased expression of PHF19 was detrimental to the clinical prognoses of cancer patients, especially HCC. There were significant correlations between PHF19 expression and TMB or MSI in several cancers. High PHF19 levels were critically associated with the infiltration of myeloid-derived suppressor cells (MDSCs) and Th2 subsets of CD4+ T cells in most cancers. Enrichment analyses revealed that PHF19 participated in regulating carcinogenic processes including cell cycle and DNA replication, and was correlated with the progression of HCC. Intriguingly, GSEA suggested that PHF19 was correlated with the

OPEN ACCESS

Edited by:
Yunfei Xu,
Shandong University, China

Reviewed by:
Geoffrey William Mccaughan,
The University of Sydney, Australia
Doriana Fruci,
Bambino Gesù Children's Hospital (IRCCS), Italy

***Correspondence:**
Jing-lin Wang
cw20120817@163.com
Hao-zhen Ren
renhaozhen1984@163.com
Xiao-lei Shi
sxl@nju.edu.cn

[†]*These authors have contributed equally to this work*

Specialty section:
This article was submitted to Cancer Immunity and Immunotherapy, a section of the journal Frontiers in Immunology

Received: *22 September 2021*
Accepted: *14 December 2021*
Published: *05 January 2022*

Citation:
Zhu Z-y, Tang N, Wang M-f, Zhou J-c, Wang J-l, Ren H-z and Shi X-l (2022) Comprehensive Pan-Cancer Genomic Analysis Reveals PHF19 as a Carcinogenic Indicator Related to Immune Infiltration and Prognosis of Hepatocellular Carcinoma. Front. Immunol. 12:781087. doi: 10.3389/fimmu.2021.781087

cellular components including immunoglobulin complex and T cell receptor complex in HCC. Based on PHF19-associated functional gene sets, an eleven-gene prognostic signature was constructed to predict HCC prognosis. Finally, we validated pan-cancer PHF19 expression, and its impacts on immune infiltrates in HCC.

Conclusion: The epigenetic related regulator PHF19 participates in the carcinogenic progression of multiple cancers, and may contribute to the immune infiltration in tumor microenvironment. Our study suggests that PHF19 can serve as a carcinogenic indicator related to prognosis in pan-cancer, especially HCC, and shed new light on therapeutics of cancers for clinicians.

Keywords: PHD finger protein 19 (PHF19), pan-cancer, immune infiltration, prognosis, The Cancer Genome Atlas (TCGA), hepatocellular carcinoma (HCC), predictive model, tumor microenvironment (TME)

INTRODUCTION

Cancer is a major concern regarding public health and the primary cause of death worldwide, and the incidence and mortality are rapidly increasing globally (1). Although cancer treatment has improved substantially over the last decades and currently allows cures for many previously fatal cases, large quantities of patients still experienced therapeutic failure and succumbed to cancer (2). Accordingly, there is a dire need to clarify the molecular mechanisms elucidating patterns of cancer pathogenesis and to identify reliable biomarkers for the early detection, diagnosis and treatment of cancers (3). Since the first human genome sequencing in 2001, comprehensive genomic characterization of tumors has become a major goal in the field of cancer research, and recent advances in sequencing technologies and computational analytical methods have revolutionized cancer research studies (4). Large-scale genomics projects like The Cancer Genome Atlas (TCGA) database, and the public repository named the NCBI Gene Expression Omnibus (GEO), provide matched molecular and clinical data of various cancers, which helps systematically analyze the survival impact of single gene expression. Currently, the application of cancer biomarkers has aroused great interest among scientists, which encourages researchers to explore novel prognostic biomarkers and therapeutic targets.

Polycomb group (PcG) proteins, as a class of widely-studied epigenetic modifiers, form large multiprotein complexes that serve as chromatin-modifying or -remodeling enzymes and participate in maintaining cell identity and cell differentiation, by keeping the transcriptional repression of functional genes which regulate developmental processes or cell-cycle progression (5, 6). Dysregulation of PcG proteins was reported to play pivotal roles in the anomalous activation of cellular differentiation, carcinogenesis, cancer development and progression (7). PcG proteins generally assemble in two functionally distinct Polycomb repressive complexes (PRCs) referred to as PRC1 (responsible for H2AK119 monoubiquitylation) and PRC2 (catalyzing H3K27 methylation) (8). The PRC2 core formed by enhancer of zeste homolog 1/2 (EZH1/2), suppressor of zeste 12 (SUZ12), the embryonic ectoderm development (EED) and retinoblastoma-binding protein 4/7 (RBBP4/7), can interact with several substoichiometrical accessory proteins that modulate its function, including Polycomb-like (PCL) proteins (9, 10). The *Pcl* gene was initially identified in *Drosophila melanogaster* (11), and three mammalian homologs of *Drosophila Pcl* have been characterized to date, termed PCL1 [also named PHD finger protein 1 (PHF1)], PCL2 [also named Metal response element binding transcription factor 2 (MTF2)], and PCL3 [also named PHD finger protein 19 (PHF19)], respectively (12). These PCL proteins are PRC2-relevant factors that form sub-complexes with PRC2 core components, and regulate the enzyme activity of PRC2 or its recruitment to the target loci (13).

PHD finger protein 19 (PHF19), namely PCL3, is an critical component of PRC2 that acts as a transcriptional repressor of several developmentally regulated genes and functions as a pivotal regulator of various biological processes (14). PHF19 protein contains a single Tudor domain followed by two plant homeodomain (PHD) fingers and an extended homologous (EH) domain, and binds trimethylated histone H3 Lys36 (H3K36me3) through its Tudor domain (15, 16). Direct recognition of H3K36me3 by PHF19 is a requisite for the complete enzyme activity of PRC2 complex and serves to recruit PRC2 and H3K36me3 demethylases NO66 or KDM2b to specific genomic loci to facilitate the removal of H3K36me3 active mark and deposition of histone H3 Lys27 trimethylation (H3K27me3) (16, 17). Previous researches have elucidated that PHF19 is overexpressed in multiple cancerous tissues compared with the normal tissue counterparts. For instance, PHF19 expression is present in all subgroups of multiple myeloma (MM) and is preferentially upregulated in high-risk MM (18). Aberrant overexpression of PHF19 has also implicated in gastric cancer, associated with cancer cell differentiation and poor prognosis for patients (19). Significantly elevated in the advanced stages of Glioblastoma (GBM), PHF19 was reported to block the degradation of β-catenin *via* transcriptional repression of SIAH1 and promote the progression of GBM (20). Tissue microarray analysis of surgically resected paired colorectal cancer (CRC) samples showed that PHF19 protein was overexpressed in CRC tissues compared with paired adjacent normal tissues (21). Nevertheless, despite the efforts to understand the roles of PHF19 in multiple cancers, a

comprehensive analysis that determines the genetic targets and mis-regulated pathways controlled by PHF19 has not been reported so far, and the molecular contributions of PHF19 remain elusive.

In the current research, we conducted a integrative pan-cancer analysis of tumor samples from public databases. We investigated the expression patterns of PHF19 in normal tissues, various cell lines and cancers, and estimated the prognostic values of PHF19 in pan-cancer based on multiple databases. Besides, we explored the links between PHF19 expression and tumor mutation burden (TMB), microsatellite instability (MSI), immune checkpoints and immune infiltration, and identified the specific genes and signaling pathways involved in the regulation of cancer development by PHF19. Finally, due to the fact that functional enrichment analysis of PHF19 was obviously correlated with hepatocellular carcinoma (HCC), we constructed a PHF19-related prognostic risk-score model for HCC patients and performed a validation of this model in an external dataset. These findings may have important implications in guiding basic research as well as clinical practice.

MATERIALS AND METHODS

Data Acquisition and Processing

As a landmark cancer genomics project, TCGA molecularly characterized more than 20,000 primary cancer and corresponding normal tissues across 33 cancer types (22). In our analysis, TCGA transcriptome RNA-seq data and clinical information were downloaded using the UCSC Xena platform (23). Transcripts per million (TPM) and fragments per kilobase million (FPKM) were used for quantification and comparison. Besides, two liver hepatocellular carcinoma (LIHC) cohorts and matched clinical data used in our study were respectively obtained from the Genomic Data Commons (GDC) Data Portal (https://portal.gdc.cancer.gov/) and the GSE14520 dataset from the GEO database (24).

Patients and Clinical Specimens

All the biospecimens are provided by Nanjing multicenter biobank, biobank of Nanjing Drum Tower Hospital, the Affiliated Hospital of Nanjing University Medical School. Written informed consents were obtained from all subjects, and normalized ethnic audit has been proceeded.

Reagents

Antibody recognizing PHF19 (Proteintech, 11895-1-AP) was purchased from Proteintech. For flow cytometry analysis, antibodies against CD14 (clone M5E2, 301808), CD11b (clone M1/70, 101205), CD33(clone WM53, 303404), CD4 (clone OKT4, 317416), IL-4 (clone MP4-25D2, 500806) were purchased from BioLegend. For RT-qPCR, the primers were as follows: PHF19 forward primer 5'-ACTCGGGACTCCTATGGTGC-3', reverse primer 5'-CCTCCGTCAGTTTGGACATCA-3'; and GAPDH forward primer 5'-GGAGCGAGATCCCTCCAAAAT-3', reverse primer 5'-GGCTGTTGTCATACTTCTCATGG-3'.

Analysis of PHF19 mRNA Expression Profiles

The mRNA expression profiles of PHF19 in major tissues and organs of human body were explored in the Human Protein Atlas (HPA), as well as the single cell transcriptomics analysis (25). Transcript levels of PHF19 in different cancers were analyzed using the ONCOMINE database (26), under the settings of P-value = 0.001 and fold change (FC) = 1.5, and in the "Gene_DE" module of TIMER2.0 database (27). Differential mRNA expression analysis of normal and tumor samples, and pathological stage analysis of PHF19, were performed in the "Single Gene Analysis" module of GEPIA (28). "Expression on Box Plots" module was used to depict box plots of expression differences between tumors and matched normal samples of the GTEx database, with the thresholds set as a P-value cutoff of 0.01 and $\log_2$FC cutoff of 1, and "Match TCGA normal and GTEx data" was set. The $\log_2$(TPM + 1) data was applied for log-scale.

Survival Analysis

Cox regression analysis for TCGA datasets was performed using RStudio software (version 1.2.5042) with the "survival" and "forestplot" package to investigate the correlation between PHF19 expression and cancer prognosis, including overall survival (OS) and disease-specific survival (DSS). We calculated the log-rank P-value and hazard ratio (HR) with 95% confidence intervals (95% CI) *via* the "survival" package and utilized the "forestplot" package to visualize the survival analysis. The Kaplan-Meier plotter, which is a web database aiming to evaluate the effect of 54,000 genes on survival in 21 tumor types (29), was used to determine PHF19 expression-associated OS outcomes of patients. Additionally, the GEPIA2 database was also utilized to determine the correlation between PHF19 mRNA expression and OS and disease-free survival (DFS) of cancers (30).

Genomic Alterations and Mutation Profiles

Based on the cBioPortal tool (http://www.cbioportal.org/), PHF19 mutation frequency and general mutation count in cancer patients were calculated to analyze the genomic alterations of PHF19 in various TCGA cancer types (31). The genome alterations of PHF19 included copy number amplification, deep or shallow deletion, missense mutation with uncertain significance and mRNA upregulation. Tumor mutation burden (TMB) is calculated as total somatic nonsynonymous mutation counts in coding regions and emerging as a biomarker for predicting immunotherapy effect. Microsatellite instability (MSI) refers to the nucleotide insertions or deletions in the microsatellite loci. The TMB and MSI scores were obtained from TCGA database and analyses regarding association between PHF19 expression and TMB or MSI were conducted by R language.

Immune Infiltration Analysis

The ESTIMATE algorithm (32), which is a method that infers the fraction of immune and stromal cells in tumor samples *via* analysis of gene expression signatures, was applied to evaluate

the immune cell infiltration levels (ImmuneScore) and the abundance of stromal components (StromalScore) for each TCGA sample in the RStudio software with the "estimate" package. The relationships of PHF19 expression with immune or stromal scores in several cancers were visualized as scatter plots. Higher ImmuneScore or StromalScore indicated larger proportion of immune or stromal components in tumor microenvironment (TME).

"Gene_Corr" module of TIMER2.0 database was utilized to explore the correlations between PHF19 expression and immune checkpoint-associated genes, including BTLA, CD27, CD274, CD276, CD28, CD40, CD70, CD80, CD86, CTLA4, HAVCR2, HHLA2, ICOS, ICOSLG, IDO1, IDO2, LAG3, PDCD1, TIGIT, TNFRSF9, and TNFSF9 across human cancers from the TCGA cohorts (33). The generated heatmap suggested statistical significance and provided the purity-adjusted partial Spearman's rho value, which avoided the effect of outliers. Besides, "Immune-Gene" tool of TIMER2.0 database was applied to explore the association between PHF19 level and immune cell infiltration in all TCGA cancers. Immune cells including myeloid-derived suppressor cells (MDSCs), Th1 and Th2 subsets of CD4+ T cells were selected. The TIDE and XCELL algorithms were applied to estimate the immune infiltration and the results were depicted as a heatmap and scatter plots.

Enrichment Analysis

The protein-protein interaction (PPI) network was established applying the Search Tool for the Retrieval of Interacting Genes (STRING) with the following input parameters: "evidence", "experiments", and 0.200 confidence level (34). The protein interaction file from STRING database was imported into the Cytoscape software (version 3.8.2) for PPI network construction, visualization and analysis (35). Besides, we adjusted the parameter "minimum required interaction score" to conformity = 0.150 and set the parameter "max number of interactors to show" as "no more than 50 interactors", in order to get access to experimentally determined PHF19-binding proteins.

"Similar Genes Detection" function of GEPIA2 database was utilized to acquire the first 100 PHF19-correlated genes based on the TCGA and GTEx datasets. "Correlation Analysis" module of GEPIA2 was applied to compute pair-wise gene expression correlations between PHF19 and selected genes, using the Pearson correlation method. We also used the "Gene_Corr" function of TIMER2.0 database to acquire the heatmap data of corresponding genes, containing the partial correlation coefficient (cor) and P-value calculated by the purity-adjusted Spearman's rank correlation test. Meanwhile, the Venn diagram was generated by a Venn diagram tool (http://bioinformatics.psb.ugent.be/webtools/Venn/) to perform the intersection analysis of the PHF19-binding and associated genes. These two sets of genes were combined to perform Kyoto Encyclopedia of Genes and Genomes (KEGG) pathway enrichment analysis by Metascape portal, which is designed to offer a comprehensive gene list annotation and analysis resource for experimental biologists (36). The resulting enriched pathways were visualized using the "ggplot2" R package. Besides, we conducted the Gene Ontology (GO) analysis to access the molecular functions (MF) *via* the "clusterProfiler" R package and the result was visualized using the cnetplot function.

CancerSEA is a dedicated database that portrays single-cell functional status maps that involve fourteen functional states of more than 40,000 single cells across 25 cancer types, aiming at comprehensively decoding distinct functional states of cancer cells at single-cell resolution (37). In the present research, the CancerSEA database was applied for the functional analysis of PHF19. Further gene set enrichment analysis (GSEA) was performed to identify the significant pathways between low expression and high expression group of PHF19, and the top four terms of GO analysis and transcription factor targets were exhibited, using the "clusterProfiler" R package.

Construction and Evaluation of Prognostic Risk Model

Forty genes were extracted from the PHF19 functionally associated gene set obtained by GO-MF analysis as described above, and the "limma" R package was used to determine differentially expressed genes (DEGs) between TCGA HCC samples and normal controls. We conducted univariate and multivariate Cox regression analyses by the "survival" package, and performed LASSO regression using the "glmnet" package to acquire the most useful predictive genes. The risk assessment model was constructed based on the corresponding coefficients and then applied to patients to generate the risk score of each patient. Patients in TCGA LIHC cohort and GSE14520 cohort were respectively separated into high- and low-risk groups in accordance with the median value of risk scores. We evaluated the predictive capability of the risk model by survival analysis and Receiver Operating Characteristic (ROC) curves. Univariate and multivariate Cox regression analyses were then conducted to confirm the prognostic efficiency of the risk-score model, as well as other clinicopathological features. Nomograms were formulated by using the "rms" R package in RStudio.

Statistical Analysis

For experimental studies, at least three biological replicates were repeated. Data were shown as average values ± SEM. The P value was calculated using GraphPad Software.

RESULTS

PHF19 Expression Profiles in Human Normal Tissues and Cancers

To determine the expression profiles of PHF19 in human normal tissues, we investigated the mRNA expression patterns of PHF19 in various non-tumor tissues and single cell types based on publicly available genome-wide expression data. As shown in **Figure 1A**, among all detected tissues and cell types, the highest PHF19 expression was observed in the monocytes, followed by the bone marrow and tonsil, based on the Consensus dataset created by integrating the data from three transcriptomics datasets (HPA, GTEx and FANTOM5). Low RNA tissue

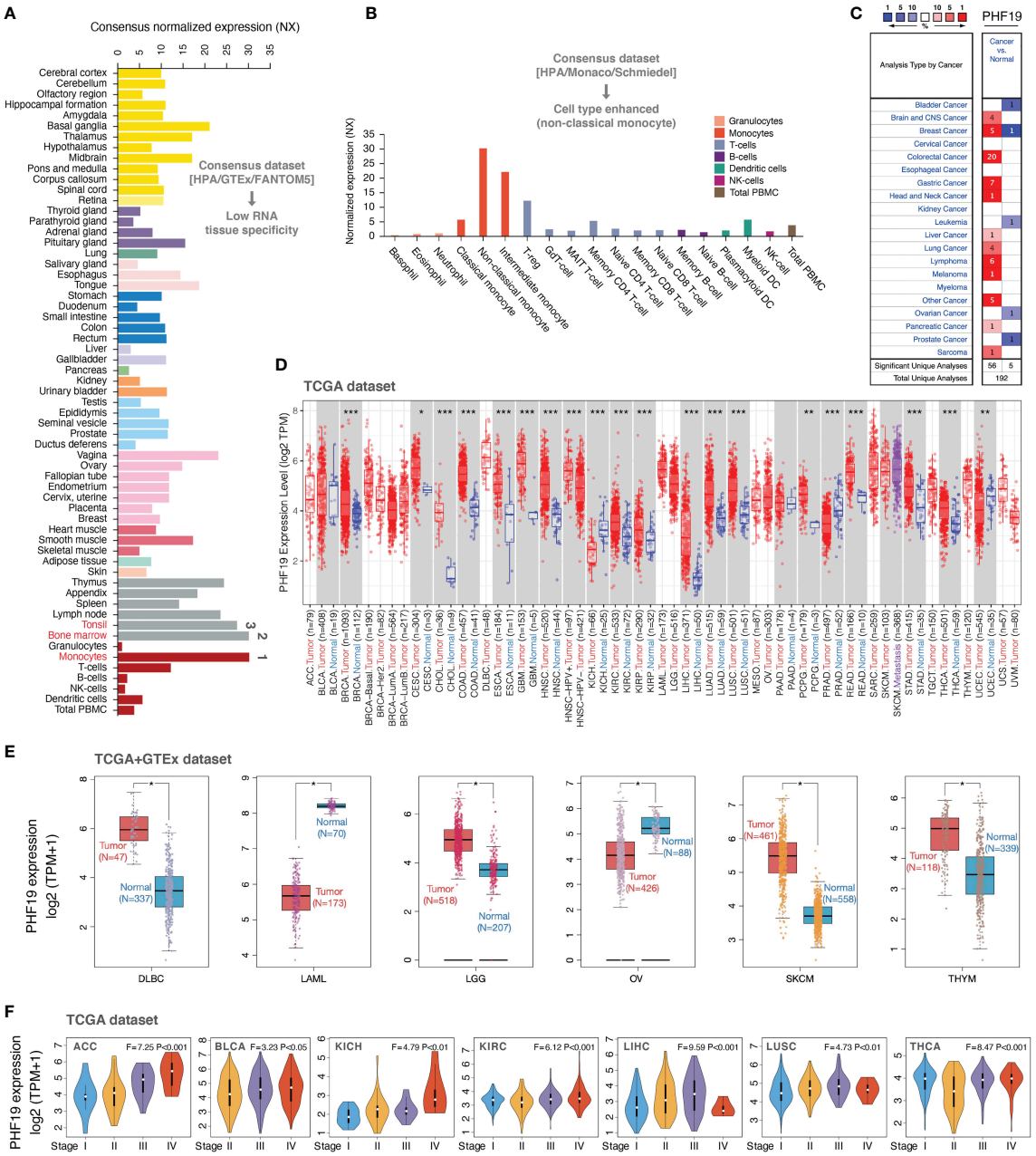

FIGURE 1 | PHF19 expression profiles in normal tissues and cancers. **(A)** PHF19 expression levels in normal tissues and cell types. **(B)** PHF19 expression levels in blood cell types. **(C)** Transcription levels of PHF19 in datasets of multiple cancers compared with noncancerous tissues. The figure was generated from the ONCOMINE database. **(D)** Expression levels of PHF19 in TCGA cancers were analyzed by TIMER2.0 database (*P < 0.05; **P < 0.01; ***P < 0.001). **(E)** Differences of PHF19 expression between cancers from the TCGA database and normal samples from the GTEx database (*P < 0.05). **(F)** PHF19 expression levels were assessed by the main pathological stages of ACC, BLCA, KICH, KIRC, LIHC, LUSC, and THCA. The $\log_2$(TPM + 1) for log-scale was used.

specificity was indicated since PHF19 was expressed in all tissues tested, with the consensus normalized expression (NX) in the vast majority of tissues > 1. With regard to RNA blood cell type specificity, interestingly, the PHF19 mRNA expression was obviously enriched in non-classical monocytes, when analyzing in the HPA/Monaco/Schmiedel datasets (**Figure 1B**). Non-classical monocytes express $CD14^{low}CD16^{+}$ antigen and constitute about 10%-15% of blood monocytes (38). Our result indicated that PHF19 might be implicated in specific functions of these monocytes.

We next retrieved PHF19 mRNA expression levels over a cancer-wide range *via* the ONCOMINE database. The results

determined that compared with that in the corresponding normal groups, PHF19 expression was higher in cancer tissues, such as brain and CNS cancer, breast cancer, colorectal cancer, gastric cancer, head and neck cancer, liver cancer, lung cancer, lymphoma, melanoma, pancreatic cancer, and sarcoma (**Figure 1C**). Yet in certain studies, PHF19 expression was lower in bladder cancer, breast cancer, leukemia, ovarian cancer, and prostate cancer. To further evaluate the expression status of PHF19 spanning various cancer types, we analyzed the TCGA RNA sequencing data by applying the TIMER2.0 approach. As presented in **Figure 1D**, PHF19 expression was significantly elevated in multiple cancer types, including BRCA (breast invasive carcinoma), CESC (cervical and endocervical cancer), CHOL (cholangiocarcinoma), COAD (colon adenocarcinoma), ESCA (esophageal carcinoma), GBM (glioblastoma multiforme), HNSC (head and neck cancer), KIRC (kidney renal clear cell carcinoma), KIRP (kidney renal papillary cell carcinoma), LIHC (liver hepatocellular carcinoma), LUAD (lung adenocarcinoma), LUSC (lung squamous cell carcinoma), PCPG (pheochromocytoma and paraganglioma), READ (rectum adenocarcinoma), STAD (stomach adenocarcinoma), and THCA (thyroid carcinoma), compared with their corresponding adjacent non-cancerous tissues. Meanwhile, PHF19 expression was markedly decreased in KICH (kidney chromophobe), PRAD (prostate adenocarcinoma), and UCEC (uterine corpus) than in their respective normal samples. By integrating data from the GTEx database as normal controls, we further performed differential-expression analysis of PHF19 between tumor and normal samples of DLBC (diffuse large B-cell lymphoma), LAML (acute myeloid leukemia), LGG (lower grade glioma), OV (ovarian serous), SKCM (skin cutaneous melanoma), and THYM (thymoma) (**Figure 1E**). Besides, we further evaluated the correlation of PHF19 expression with cancer pathological stages, including ACC (adrenocortical carcinoma), BLCA (bladder urothelial carcinoma), KICH, KIRC, LIHC, LUSC, and THCA (**Figure 1F**). The results determined a positive relationship between PHF19 level and advanced tumor stages.

Multifaceted Prognostic Analysis of PHF19 in Cancers

To investigate the clinical significance of PHF19 in cancer patients, we downloaded the TCGA mRNA sequencing and clinical information of 33 cancer types from the UCSC Xena platform and calculated the correlations of PHF19 expression with overall survival (OS) and disease-specific survival (DSS) of patients using the univariate Cox survival analysis. As shown in **Figure 2A**, the forest plots suggested that elevated PHF19 expression was significantly associated with worse OS in ACC (HR = 4.18, P < 0.001), KICH (HR = 5.06, P < 0.001), KIRC (HR = 2.64, P < 0.001), LGG (HR = 1.69, P = 0.002), LIHC (HR = 1.57, P < 0.001), MESO (mesothelioma) (HR = 2.16, P < 0.001), and PCPG (HR = 9.76, P < 0.001) patients, and also clearly correlated with worse DSS in ACC (HR = 4.27, P < 0.001), KICH (HR = 5.82, P < 0.001), KIRC (HR = 3.18, P < 0.001), LGG (HR = 1.83, P < 0.001), LIHC (HR = 1.48, P = 0.005), MESO (HR = 2.43, P = 0.006), and PCPG (HR = 12.65, P < 0.001) patients. These data showed that high expression of PHF19 was strongly associated with poor patient outcomes in multiple cancer types, which suggested that PHF19 may serve as a potential prognostic biomarker in pan-cancer. Of note, and in contrast, increased PHF19 expression was implicated in prolonged OS in THYM (HR = 0.32, P = 0.011).

Kaplan-Meier (KM) survival curves comparing PHF19 high and low expressing patients were also constructed to further evaluate the prognostic potential of PHF19 *via* the Kaplan-Meier plotter database. The results revealed that high PHF19 expression predicted worse OS in BC (bladder carcinoma), KIRC, KIRP, LIHC, LUAD, LUSC, and UCEC, nevertheless, patients with higher PHF19 expression showed remarkably improved OS in HNSC, SARC, THCA, and THYM (all log-rank P values < 0.05) (**Figure 2B**). We next compared the survival contribution of PHF19 in multiple cancer types, estimated using Mantel-Cox test through the GEPIA2 database, and the survival maps accompanied with OS curves and disease-free survival (DFS) curves are presented in **Figure 2C**. High transcriptional levels of PHF19 were linked to unfavorable prognosis in OS of ACC, LIHC, MESO, and SKCM, and DFS analysis data showed that elevated PHF19 level was related to unfavorable prognosis for ACC, LGG, LIHC, and UVM (uveal melanoma) (all log-rank P values < 0.05). Overall, the above data indicated that PHF19 expression was significantly correlated with patient prognosis in various cancers, especially in LIHC, and the relevance of PHF19 to clinical outcomes may shed new light on the underlying pathogenesis of different tumors.

Mutation Landscape of PHF19 in Cancers

We inspected the genomic alterations and mutation profiles of PHF19 in the TCGA cancer cohorts by employing the cBioPortal database. As presented in **Figure 3A**, the highest alteration frequency of PHF19 appeared in UCEC patients with "mutation" as the predominant type, while the "amplification" type of copy number alteration (CNA) and copy number "deep deletion" were respectively the primary type in KICH and THCA. Besides, we detected altogether 72 mutation sites including 65 missense, 4 truncating, 2 inframe, and 1 fusion mutation between amino acids 0 and 580, and the types, sites and case number of PHF19 genomic alterations were shown in **Figure 3B**. We also analyzed the general mutation count of PHF19 in 10953 patients/10967 samples from TCGA datasets (**Figure 3C**). In addition, we investigated the association between PHF19 alteration and the clinical outcomes of UCEC cases, and found that UCEC patients with altered PHF19 showed improved prognosis in terms of progression-free survival (PFS) (log-rank P = 0.035), but not OS (log-rank P = 0.077), DFS (log-rank P = 0.101), and DSS (log-rank P = 0.224), compared with those without PHF19 alteration (**Figure 3D**). Meanwhile, since TMB and MSI are regarded as critical factors impacting on oncogenesis and progression of tumors, and affecting response to immunotherapy in cancers, we next performed association analyses between PHF19 expression and TMB/MSI spanning all

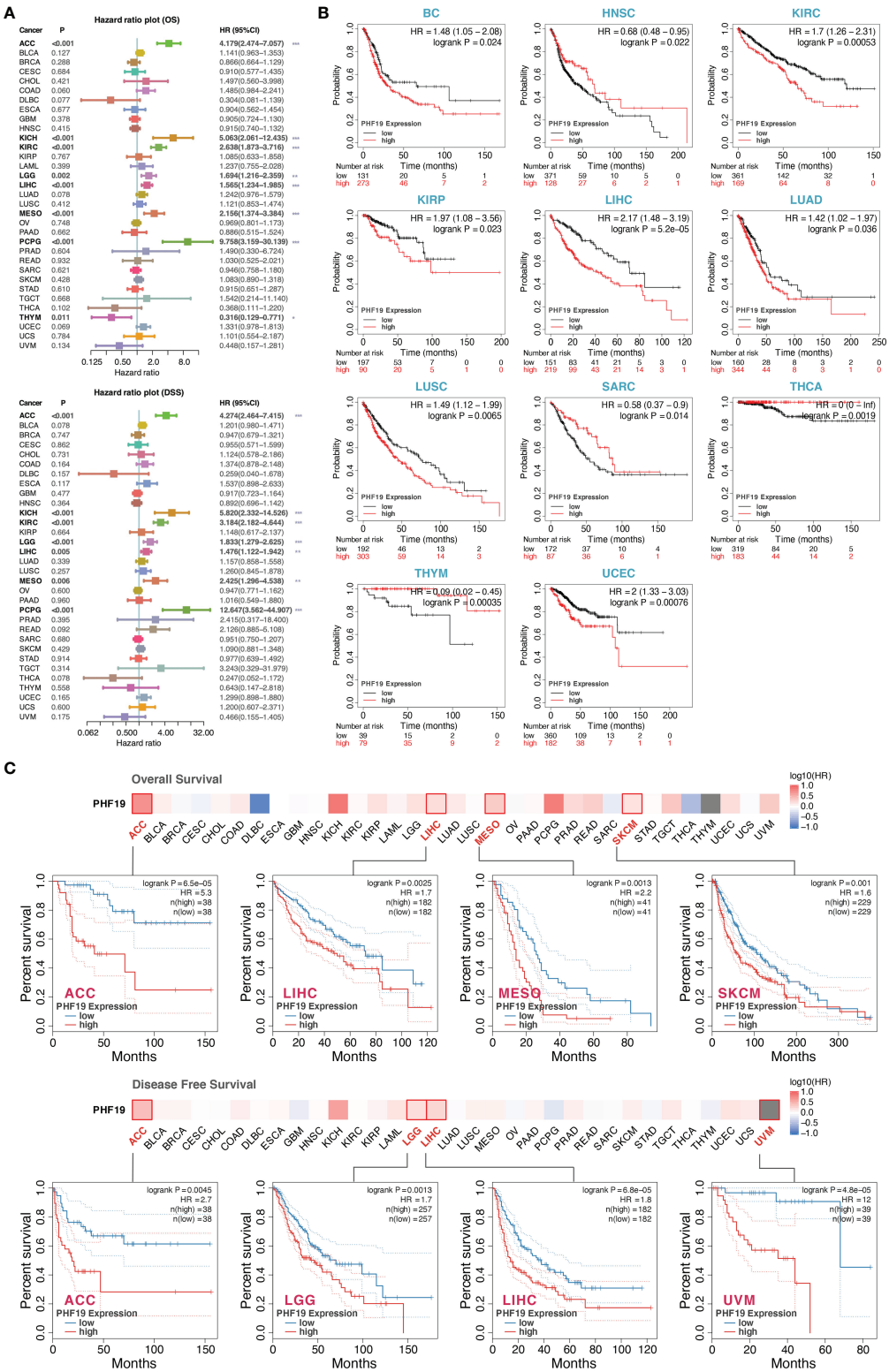

FIGURE 2 | Multifaceted prognostic analysis of PHF19 in cancers. **(A)** Correlations of PHF19 expression with OS and DSS of patients using the Cox regression survival analysis (*P < 0.05; **P < 0.01; ***P < 0.001). **(B)** KM survival curves showed that PHF19 expression was highly associated with clinical outcomes in different cancers. **(C)** The survival maps and survival curves were depicted to perform OS and DFS analyses in cancers.

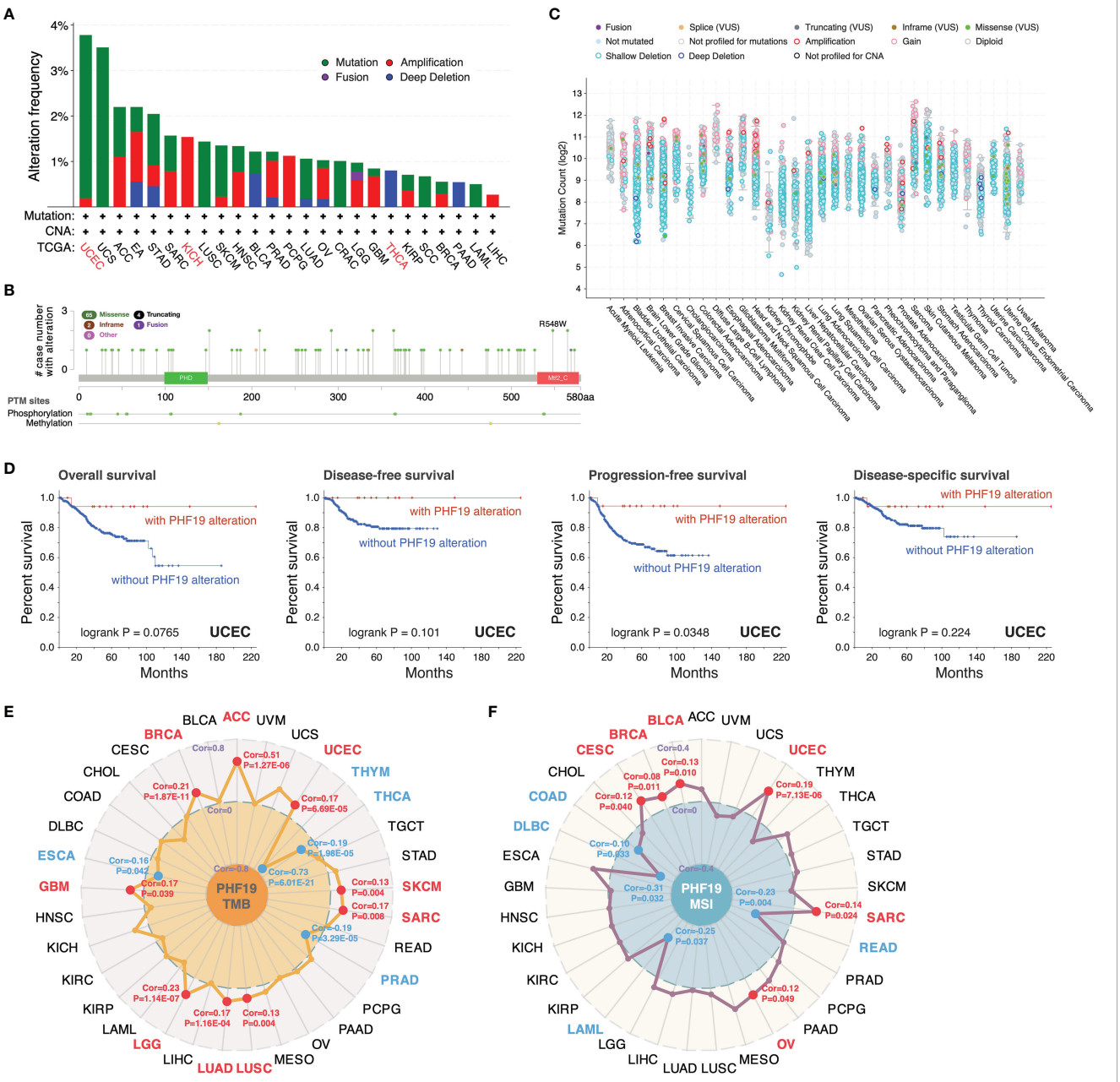

FIGURE 3 | Mutation landscape of PHF19 in cancers. PHF19 alteration frequencies in various cancers **(A)** and mutation sites **(B)** were visualized. **(C)** The general mutation counts of PHF19 in TCGA samples. **(D)** Correlations between PHF19 alteration status and OS, DFS, PFS, and DSS of UCEC. Radar maps of correlations between PHF19 expression and TMB **(E)** or MSI **(F)** were plotted.

TCGA tumor types. As shown in **Figure 3E**, PHF19 expression was positively correlated with TMB in ACC, BRCA, GBM, LGG, LUAD, LUSC, SARC, SKCM, and UCEC, while negatively correlated with TMB in ESCA, PRAD, THCA, and THYM cohorts (all P-values < 0.05). PHF19 expression was also positively correlated with MSI of BLCA, BRCA, CESC, OV, SARC, and UCEC, but negatively correlated with that of COAD, DLBC, LAML, and READ (all P-values < 0.05) (**Figure 3F**). These results may deserve further in-depth investigations.

PHF19 Expression Correlates With Tumor Immune Infiltration

Tumor-infiltrating immune cells, as principal compositions of the TME, are frequently involved in tumor behaviors including cancer initiation, progression or metastasis, and are deemed as independent predictors of sentinel lymph node status and cancer prognosis (39). Given that PHF19 expression correlates with TMB and MSI which affect response to cancer

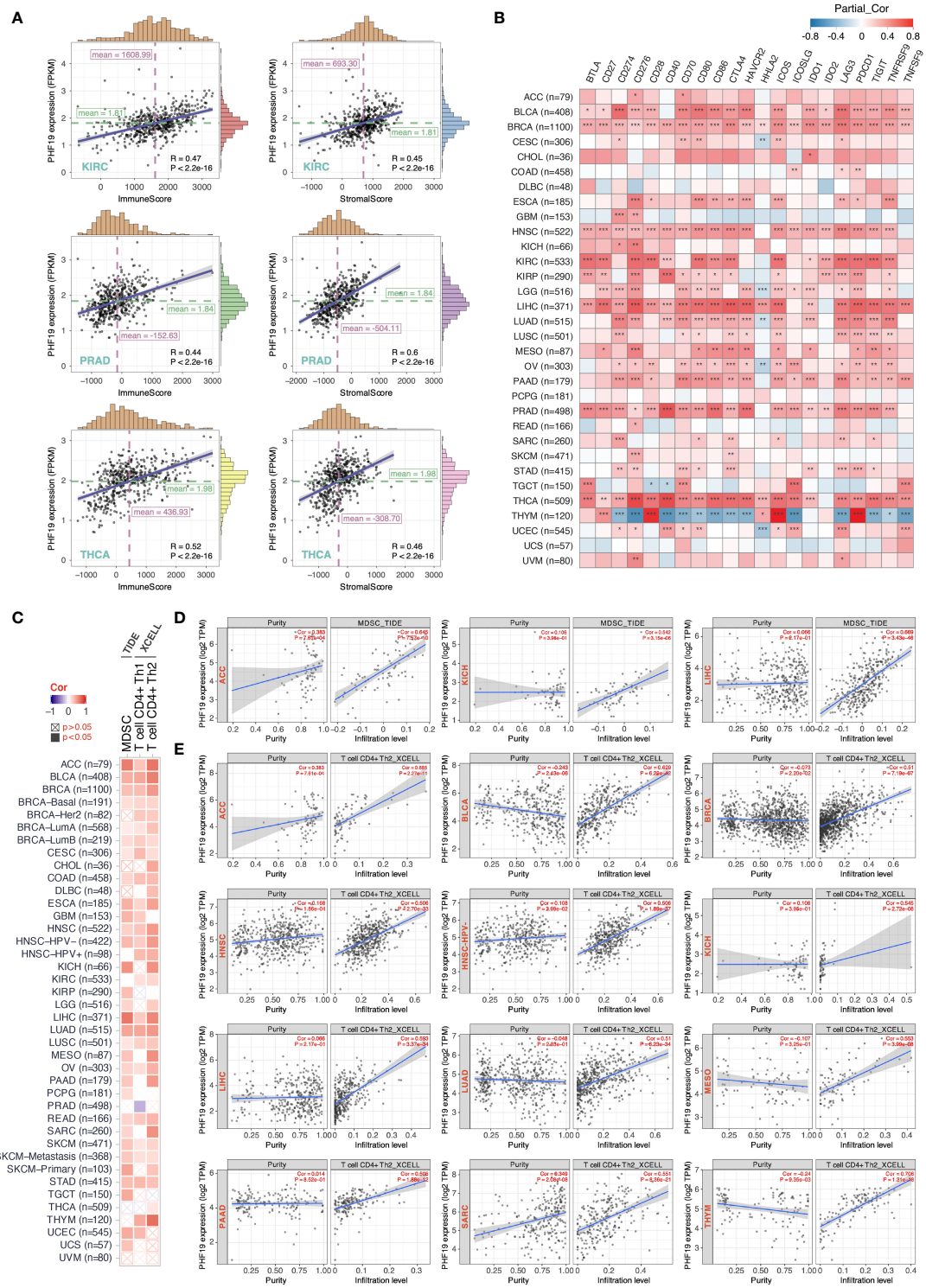

FIGURE 4 | PHF19 expression correlates with the immune infiltrates of tumors. **(A)** Top three scatter plots of correlation between PHF19 expression and immune and stromal scores in multiple cancers. **(B)** Correlations between PHF19 expression level and immune checkpoint-associated genes. **(C)** Correlations between PHF19 expression level and the infiltration level of MDSCs, Th1 and Th2 subsets of CD4+ T cells across TCGA cancers. Scatter plots of MDSC **(D)** and CD4+ Th2 cell **(E)** infiltration level related to PHF19 expression were presented.

immunotherapy, we next explored the correlations between PHF19 expression level and the abundance of immune cell infiltrates. By adopting the ESTIMATE method, we first computed the immune and stromal scores of cancer tissues. As **Figure 4A** indicated, PHF19 was correlated with the immune and stromal scores in KIRC, PRAD and THCA (all data P-values < 0.001). Since immune checkpoint-associated genes participate in the immunosuppressive mechanism that allows tumor cells to escape anti-tumor immunity (40), we next investigated the correlations between PHF19 expression and immune checkpoint-related genes, including BTLA, CD27, CD274, CD276, CD28, CD40, CD70, CD80, CD86, CTLA4, HAVCR2, HHLA2, ICOS, ICOSLG, IDO1, IDO2, LAG3, PDCD1, TIGIT, TNFRSF9, and TNFSF9 across human cancers from the TCGA cohorts, as shown in **Figure 4B**. Our results suggested that PHF19 expression was closely associated with almost all immune checkpoint-associated genes in BLCA, BRCA, HNSC, LIHC, PRAD and THCA, implying that PHF19 might conduce to immune escape in these tumors. Further, we calculated the correlation coefficients of PHF19 expression and immune infiltration levels by employing the TIDE and XCELL algorithms, and depicted the landscape of PHF19 correlating with immune cell infiltrates in various TCGA cohorts. The heatmap exhibited that PHF19 expression was positively and statistically significantly correlated with the immune infiltration of myeloid-derived suppressor cells (MDSCs) and Th2 subset of CD4+ T cells in the majority of cancers (**Figure 4C**). Intriguingly, PHF19 expression was also positively relevant to the infiltration abundance of CD4+ Th1 cells in 18 cancer types, with all correlation coefficients < 0.45, and negatively relevant to that in PRAD, with the correlation coefficient = -0.29. Representative scatter plots of MDSC infiltration level related to PHF19 expression were presented in **Figure 4D**, using the TIDE algorithm (with the correlation coefficient > 0.5). The results indicated that PHF19 expression was obviously positively correlated with the infiltration abundance of MDSCs in ACC (Cor = 0.645, P = 7.57e-10), KICH (Cor = 0.542, P = 3.15e-06) and LIHC (Cor = 0.669, P = 3.43e-46). As shown in **Figure 4E**, PHF19 expression was also significantly associated with the infiltration levels of CD4+ Th2 cells in ACC (Cor = 0.685, P = 2.27e-11), BLCA (Cor = 0.629, P = 6.29e-42), BRCA (Cor = 0.51, P = 7.19e-67), HNSC (Cor = 0.506, P = 2.70e-33), HNSC-HPV- (Cor = 0.506, P = 1.89e-27), KICH (Cor = 0.545, P = 2.72e-06), LIHC (Cor = 0.593, P = 3.37e-34), LUAD (Cor = 0.51, P = 6.23e-34), MESO (Cor = 0.553, P = 3.99e-08), PAAD (Cor = 0.505, P = 1.88e-12), SARC (Cor = 0.551, P = 8.36e-21), and THYM (Cor = 0.706, P = 1.31e-18). The profiles illustrated that PHF19, to a certain extent, was engaged in the immune infiltration-related pathways and served a critical role in the immuno-oncological interactions.

Enrichment Analysis of PHF19-Related Partners

To further decipher the underlying molecular mechanisms by which PHF19 contributes to carcinogenesis, we next investigated the available experimentally confirmed PHF19-binding proteins and PHF19 expression-associated genes for pathway enrichment analyses. In total, 50 PHF19-interacted proteins were retrieved from the STRING database by experimental evidence, and the PPI network of proteins with confidence level > 0.200 was presented as **Figure 5A**. We next acquired the top 100 genes that associated with PHF19 expression based on TCGA and GTEx datasets by utilizing the GEPIA2 database. As seen in **Figure 5B**, the PHF19 expression was significantly positively correlated with the expression of WDR76 (WD repeat domain 76) (R = 0.62), FEN1 (flap structure-specific endonuclease 1) (R = 0.60), PRC1 (protein regulator of cytokinesis 1) (R = 0.59), KIFC1 (kinesin family member C1) (R = 0.59), NCAPG (non-SMC condensin I complex subunit G) (R = 0.59), and EZH2 (enhancer of zeste 2 polycomb repressive complex 2 subunit) (R = 0.57) genes (all P-values < 0.001). The correlation heatmap showed that PHF19 was positively related to the above genes in the majority of TCGA cancers (**Figure 5C**). Besides, we performed the Venn intersection analysis between the two datasets described above and identified a common member, namely EZH2 (**Figure 5D**). Further, these two datasets were combined to perform KEGG pathway and GO molecular function (MF) enrichment analyses. As presented in **Figure 5E**, several pathways including "p53 signaling pathway", "microRNAs in cancer", "hepatocellular carcinoma", "apoptosis", "DNA replication" and "cell cycle" were revealed as the most significantly enriched KEGG pathways, indicating that PHF19 was crucially involved in the development and progression of cancers, especially HCC. Meanwhile, the GO-MF enrichment analysis confirmed that five terms were highly enriched, such as histone binding, catalytic activity acting on DNA, DNA-dependent ATPase activity, helicase activity and ATPase activity (**Figure 5F**). We also performed single-cell analysis by using CancerSEA database, and determined that PHF19 clearly stimulated a multitude of carcinogenic processes, including promotion of the cell cycle, DNA damage, epithelial to mesenchymal transition (EMT), invasion, and proliferation in different cancer cell types (**Figure 5G**).

To gain insight into the potential effect of PHF19 on HCC progression, we then downloaded the LIHC RNA-seq data from TCGA portal and performed GSEA analysis based on PHF19 expression level to identify the relevant pathways and underlying mechanisms. Enrichment score (ES) was calculated to compare the enrichment of genes in a ranked list. Our results indicated that PHF19 was significantly enriched in humoral immune response mediated by circulating immunoglobulin, immunoglobulin production, and pathways related to immunoglobulin complex and T cell receptor complex (**Figure 5H**). Moreover, we conducted the transcription factor target analysis, and found that DICER1 (dicer 1, ribonuclease III), GTF3A (general transcription factor IIIA), RUVBL2 (RuvB like AAA ATPase 2), and ZNF704 (zinc finger protein 704) were the main transcription factors participating in the PHF19-regulated pathways in HCC.

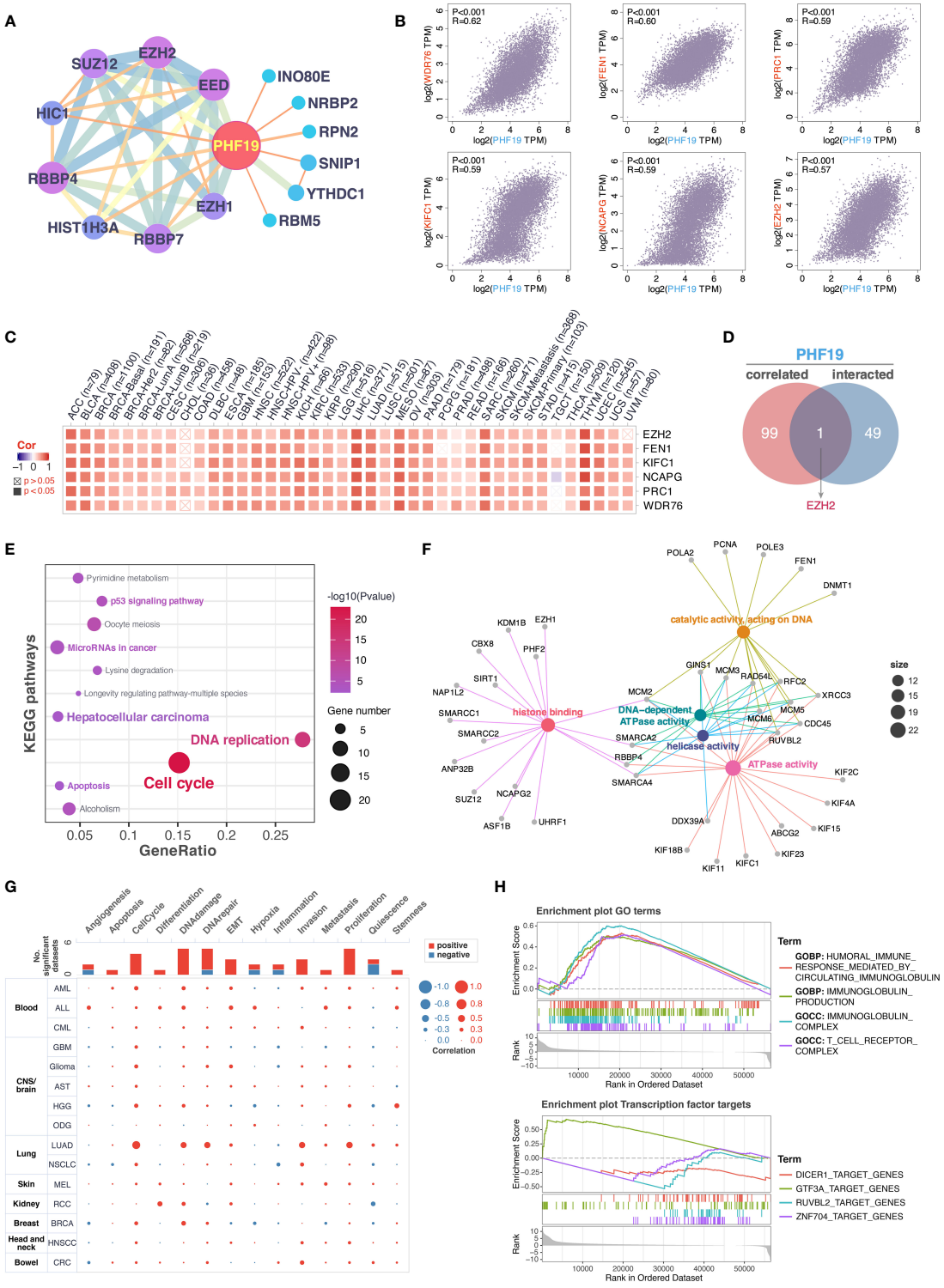

FIGURE 5 | Enrichment analysis of PHF19-related partners. **(A)** PPI network for PHF19 was constructed in Cytoscape. **(B)** The expression correlation between PHF19 and selected targeting genes, including WDR76, FEN1, PRC1, KIFC1, NCAPG, and EZH2. **(C)** The heatmap showed that PHF19 was positively related to the selected genes in TCGA cancers. **(D)** Venn diagram of PHF19-interacted and correlated genes. KEGG pathway **(E)** and GO molecular function **(F)** enrichment analyses were performed. **(G)** CancerSEA was utilized for single-cell analysis to determine the functions of PHF19. **(H)** GSEA analysis of PHF19-related signaling pathways in TCGA LIHC dataset.

Construction and Evaluation of Prognostic Risk-Score Model

For assessing the application of PHF19-associated functional gene sets in HCC prognosis, we entered the variables in **Figure 5F** into a univariable Cox proportional hazard regression to analyze the training set, namely the TCGA LIHC cohort. This strategy led to an optimal eleven-gene prognostic model in HCC, and the formula was applied to calculate the risk score of each patient, as follows: RiskScore = 0.081 ∗ KIF2C + 0.026 ∗ SMARCC1 − 0.005 ∗ ASF1B + 0.032 ∗ RBBP4 + 0.031 ∗ MCM6 − 0.012 ∗ KIF11 − 0.089 ∗ RAD54L + 0.069 ∗ GINS1 + 0.123 ∗ CBX8 + 0.001 ∗ ANP32B − 0.084 ∗ SUZ12. To better validate the robustness of the model, GSE14520 cohort was used as the independent external validation dataset.

We first calculated and plotted the prognostic Kaplan-Meier survival curves predicted by this model in both internal and external datasets (**Figures 6A, B**). The results showed that patients with high risk scores had obviously less survival probability than low-risk patients, which meant the higher the score, the worse the prognosis. The distribution of risk scores, survival statuses, and signature gene expression patterns for HCC patients in training and validation sets were visualized in **Figures 6C, D**, respectively. In TCGA LIHC cohort, both univariate (HR = 4.01, $p < 0.001$) and multivariate (HR = 3.71, $p < 0.001$) Cox regression analyses determined that the prognostic signature was strongly associated with prognosis (**Figure 6E**). Moreover, as shown in **Figure 6F**, the risk score was correlated with prognosis in univariate COX regression model (HR = 1.97, $p = 0.004$) in GSE14520 cohort, and the multivariate analysis suggested that the risk score was capable to independently predict the prognosis of HCC after adjusting for gender, age, AFP, ALT, tumor size, multinodular, BCLC staging, CLIP staging, and TNM staging (HR = 1.65, $p = 0.038$). These results suggested that the eleven-gene prognostic signature performed well in predicting the prognosis of HCC patients, and could function as a useful tool to supplement the gold standard for clinical diagnosis. Additionally, we further performed the time-dependent ROC curve analysis to validate the predictive classification efficiencies of risk-score model in HCC, and the area under the curve (AUC) values for 0.5-, 1-, 2-, 3-, and 5-years overall survival were presented in **Figure 6G**. Finally, as shown in **Figures 6H, I**, we formulated the prognostic nomograms to anticipate the individualized survival probability based on TCGA LIHC cohort and GSE14520 cohort, which might contribute to efficacy assessment and managing patients.

Validation of PHF19 Expression and Impacts of PHF19 on Immune Infiltrates in HCC

To ensure positive confirmation of pathophysiological roles of PHF19, we applied experimental validation to investigate its clinicopathological characteristics. We performed immunohistochemical (IHC) analyses in 78 cancer samples across BRCA, CESC, CHOL, COAD, ESCA, KIRC, KIRP, LIHC, LUAD, LUSC, PCPG, READ, and STAD, with three pairs of different surgical specimens analyzed per tumor type (**Figures 7A–M**). Adjacent or distant noncancerous tissues from the surgical margin were used as the control tissues. We found that the PHF19 protein expressions were significantly higher in tumor tissues in comparison with the control tissues, and the results were quantitated in **Figure 7N**, which indicated the extensive carcinogenic effects of PHF19.

In view of the prognostic value of PHF19 in HCC, we further studied the impacts of PHF19 expression on immune infiltration, by performing flow cytometry analysis on 15 clinical specimens diagnosed as HCC. MDSCs are a heterogeneous population of cells which expand during cancer, inflammation and infection, with a remarkable ability to suppress T-cell responses, and were defined as $CD11b^+$ $CD14^-$ $CD33^+$ in most tumors (41). We first determined the PHF19 mRNA levels in all samples, and patients were ranked according to PHF19 expression, and divided into low-, median- and high-PHF19 expression groups, respectively (**Figure 8A**). Significant differences were observed between these three groups. We found that the MDSC infiltration ratios were clearly higher in high-PHF19 expression group than in low-PHF19 group (**Figures 8B, C**), and PHF19 expression level was closely related to the degree of immune infiltration of MDSCs (**Figure 8D**). Similarly, we detected the infiltration of Th2 subsets of CD4+ T cells in specimens, which were defined as $CD4^+$ $IL4^+$. The results showed that hardly Th2 subsets can be detected in low-PHF19 expression group (**Figure 8E**). Collectively, these data indicated that PHF19 expression had noticeable effects on immune cell infiltration in HCC.

DISCUSSION

The physiological functions of PRC2 complex are subjected to intricate cellular regulation, which is correlated with the enormous complexity of PRC2 components (42). Previous studies have proved that H3K36me3-binding activity is harbored in the Tudor motif of PRC2-associated PCL protein named PHF19, and the Tudor function of PHF19 is also essential for H3K27me3 and repression of previously described 'poised' developmental genes (43). Although investigators have gained some understanding of the regulation of Polycomb activity by PHF19, little is known about whether and how it drives tumor initiation, progression, and metastasis (13). Collectively, as a critical epigenetic related gene, PHF19's potential roles in carcinogenesis and cancer development are worthwhile to be disclosed.

In the present study, we explored the pan-cancer expression profiles of PHF19, and the correlation between PHF19 aberrant expression and patient prognosis in different cancers. Compared with corresponding noncancerous tissues, PHF19 expression was significantly up-regulated across a range of cancers, which implied the extensively oncogenic characteristics of PHF19 in cancers and promising perspectives in the field of cancer research. This present result is consistent with findings of previous study in 2004 when PHF19 was first identified in human tissues and extends the work in important ways (44). COX regression analyses suggested that elevated PHF19

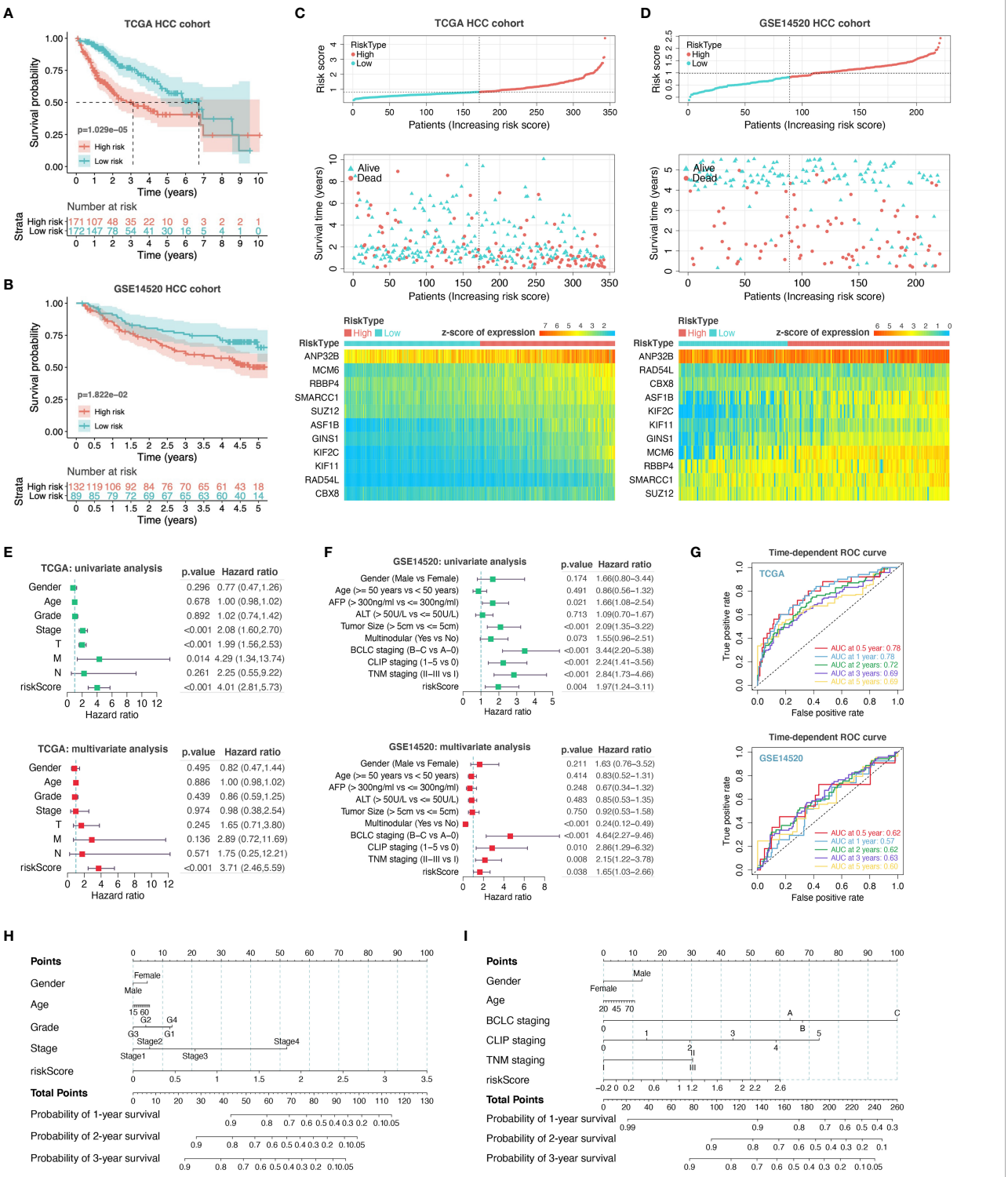

FIGURE 6 | Construction and evaluation of prognostic risk-score model. We performed survival analyses between the high- and low-risk score groups in TCGA HCC cohort **(A)** and GSE14520 HCC cohort **(B)**. The distribution of risk scores, survival statuses, and signature gene expression levels for HCC patients in training **(C)** and validation sets **(D)** were visualized. Univariate and multivariate Cox regression analyses were conducted for each clinical feature and risk-score model in TCGA dataset **(E)** and GSE14520 dataset **(F)**. T, T stage; M, M stage; N, N stage; riskScore, risk-score model. **(G)** Time-dependent ROC curve analysis to assess the predictive efficacy of the prognostic signature. **(H, I)** Nomograms for quantitatively predicting the probability of 1-, 2-, and 3-year OS for HCC patients.

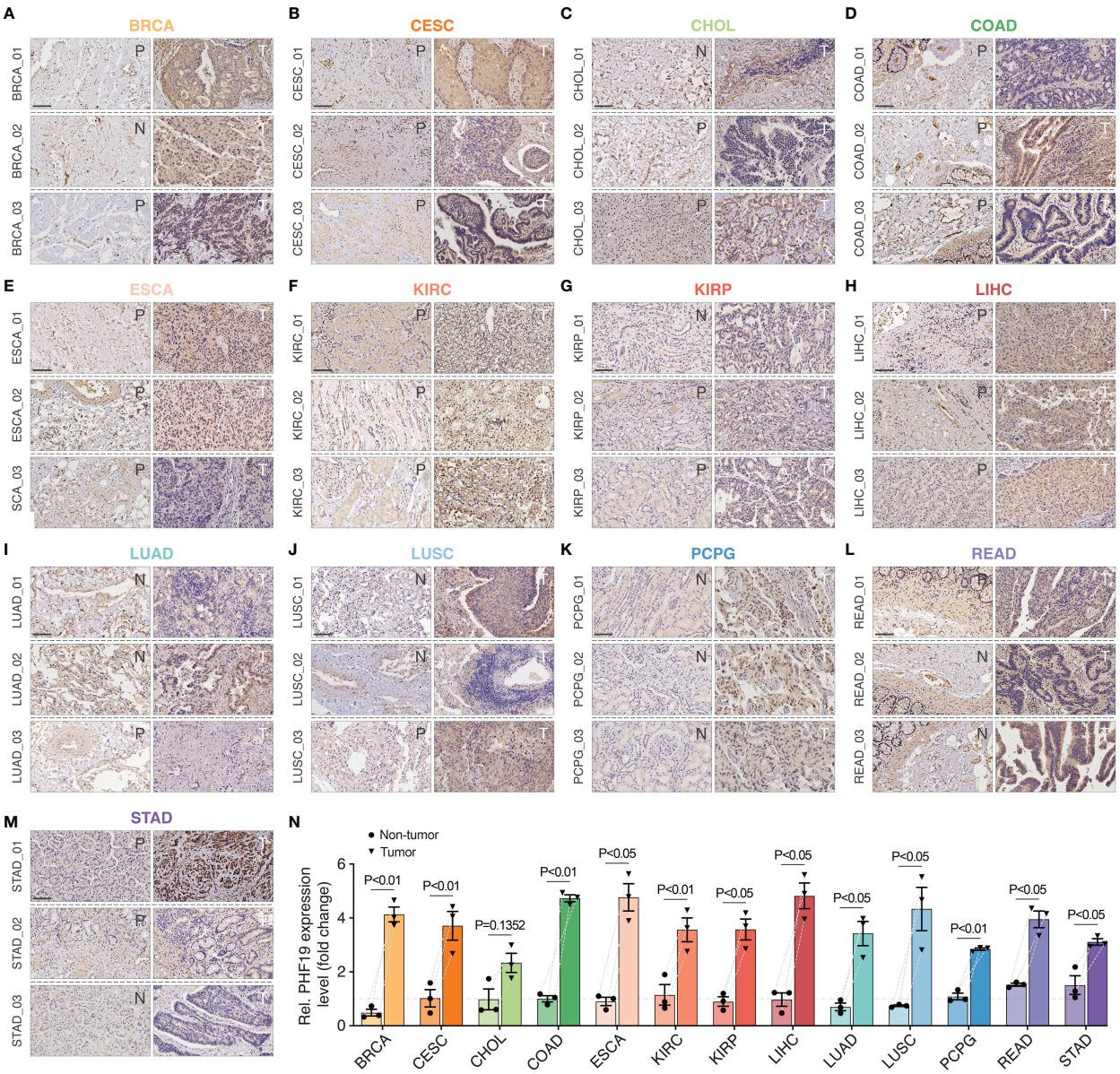

FIGURE 7 | Immunohistochemical stainings of PHF19 in cancers. We detected the PHF19 protein expressions in BRCA, CESC, CHOL, COAD, ESCA, KIRC, KIRP, LIHC, LUAD, LUSC, PCPG, READ, and STAD **(A–M)** (N, distant noncancerous tissues from the surgical margin; P, adjacent noncancerous tissues from the surgical margin; T, tumor tissues). **(N)** The results were then quantitated. Data represent mean ± SEM.

expression may lead to shorter OS and DSS in ACC, KICH, KIRC, LGG, LIHC, MESO, and PCPG, and Kaplan-Meier analyses revealed that high PHF19 expression predicted worse OS in BC, KIRC, KIRP, LIHC, LUAD, LUSC, and UCEC. Using Mantel-Cox test through the GEPIA2 database, we further validated that PHF19 overexpression was related to unfavorable DFS of ACC, LGG, LIHC, and UVM. Notably, these results particularly revealed PHF19 as a carcinogenic indicator of HCC prognosis, regardless of the prognostic algorithm. We further performed the enrichment analyses and identified that PHF19 was significantly enriched in cell cycle pathways, and related to the progression of HCC. Consistent with our results, past studies have shown that PHF19 knockdown resulted in the reduction of growth and cell cycle arrest in multiple myeloma (18), and reduced PHF19 levels in chronic myeloid leukemia cells arrested the cell cycle and promoted differentiation toward erythroid fate (45).

Cancer is a complicated disease involving complex reciprocal networks between tumor cells and the immune system. TME is composed of a variety of cell types, including mesenchymal cells and resident and infiltrating immune cells (46). Our initial exploration demonstrated that aberrant PHF19 expression was

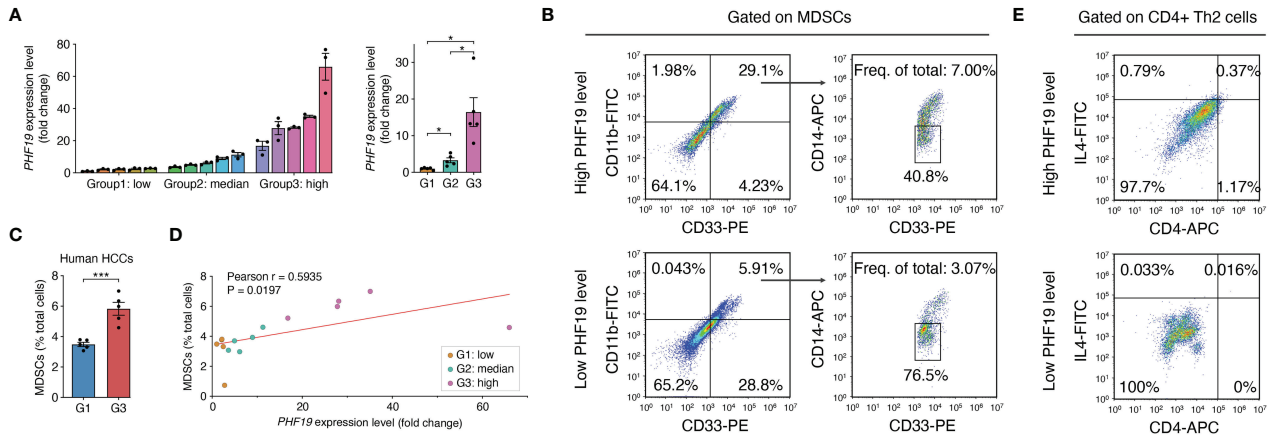

FIGURE 8 | PHF19 correlates with the immune infiltrates of MDSCs and Th2 subsets of CD4+ T cells in HCC. **(A)** PHF19 mRNA expression levels of HCC tissues from 15 patients, and patients were divided into low- (G1), median- (G2) and high-PHF19 expression (G3) groups. **(B)** Representative flow cytometric analysis of MDSCs proportion in specimens. **(C)** The degree of MDSC immune infiltration was higher in G3 group. **(D)** MDSCs proportions are proportional to the PHF19 levels. **(E)** Representative flow cytometric analysis of CD4+ Th2 cells proportion in specimens.

correlated with increased immune cell infiltration of MDSCs and Th2 subset of CD4+ T cells in the majority of cancers, which implied potential value of clinical application for PHF19 in cancer treatment. Ample evidence has supported that MDSCs are critical in regulating immune responses under pathological conditions, and play an prominent role in tumor angiogenesis, drug resistance, and promotion of cancer metastases (47). Past literature pointed that the discovery of CD4+ T cell subset-defining key transcription factors and framing of the Th1/Th2 paradigm ignited the CD4+ T cell field (48). CD4+ T cell subsets, such as Th1, Th2, Th17, and regulatory T (Treg) cells, serve pivotal functions in cancer immunity, among which the Th2 subset of CD4+ T cells secretes IL-4, IL-5, and IL-13, and activates B cells to become antibody-secreting plasma cells (49). It is worth noting that the balance between Th1 and Th2 differentiation is critical for immune homeostasis, and shift of Th1/Th2 balance towards Th2 cells is correlated with the immunosuppression and progression of cancer (50–52). Previously, researchers found that PHF19 restrained T cell senescence and sustained CD8+ T cell antitumor responses by orchestrating a transcriptional program extensively shared with miR-155 (53). Yet, more exact mechanisms underpinning the effects of PHF19 on tumor immunity remain to be elucidated. Cancer immunotherapies, especially immune checkpoint blockade therapy, have shifted the treatment of cancer by promoting complete and durable responses, and are now standard treatment for various malignant tumors (54). Unfortunately, only a small proportion of patients with certain cancer types respond to immunotherapy, probably due to inadequate immune activation to recognize tumor-specific antigens (55). Therefore, it is essential to identify additional potential therapeutic targets. Our current research showed that PHF19 levels demonstrated strong correlations with a variety of immune checkpoint molecules in BLCA, BRCA, HNSC, LIHC, PRAD and THCA. Moreover, in LIHC cohort, PHF19 was closely correlated with checkpoints including BTLA, CD27, CD274, CD276, CD28, CD40, CD70, CD80, CD86, CTLA4, HAVCR2, HHLA2, ICOS, IDO1, LAG3, PDCD1, TIGIT, TNFRSF9, and TNFSF9, indicating that PHF19 serves as a potential immune-related therapeutic target for HCC patients. In consequence, the present study points new directions for delineating the relationships between the epigenetic related PHF19 gene and immune cell infiltration within the TME, which may have important implications for exploring new strategies for cancer therapy.

As the fourth leading cause of cancer-related mortality globally, HCC imposes a huge health burden on society (56). To better explore new targets for early diagnosis and treatment, there is an urgent need to determine novel prognostic predictors and construct more reliable prognostic models of HCC. Our results provided evidence that elevated PHF19 expression indicated worse clinical outcomes in HCC patients. The GSEA results revealed that PHF19 was associated with the cellular components including immunoglobulin complex and T cell receptor complex in HCC, which provided new ideas for future research. Moreover, after the generation of eleven-gene prognostic signature, we performed a preliminary *in silico* validation using the external GEO dataset, which proved the effectiveness of the model. Taken together, the present study unveiled the complicated roles of PHF19 aberrant expression in the progression and prognoses of cancers, and summarized the pivotal signaling pathways associated with the pathophysiological functions of this epigenetic related gene. We also demonstrated that PHF19 played important roles in regulating tumor-infiltration of immune cells, and might exhibit beneficial therapeutic effects on cancer treatment. Enrichment Analysis highlighted the potential mechanistic basis of PHF19 in induction of HCC development, and the prognostic signatures derived from PHF19-related functional gene sets were validated to predict the overall survival of HCC independently. While these findings warrant further

investigation, our research provides novel insights into the promising application prospects of PHF19 in the field of cancer research.

DATA AVAILABILITY STATEMENT

Publicly available datasets were analyzed in this study. All relevant data can be found here: UCSC Xena (http://xena.ucsc.edu/), TCGA GDC Portal (https://portal.gdc.cancer.gov/), GSE14520 (https://www.ncbi.nlm.nih.gov/geo/query/acc.cgi?acc=GSE14520), Human Protein Atlas (https://www.proteinatlas.org), ONCOMINE (www.oncomine.org), TIMER2.0 (http://timer.cistrome.org/), GEPIA (http://gepia.cancer-pku.cn/index.html), GEPIA2 (http://gepia2.cancer-pku.cn), Kaplan-Meier plotter (https://kmplot.com/analysis/), cBioPortal (http://www.cbioportal.org/), STRING (https://www.string-db.org/), and CancerSEA (http://biocc.hrbmu.edu.cn/CancerSEA/).

ETHICS STATEMENT

The studies involving human participants were reviewed and approved by the human ethics committees of the Affiliated Drum Tower Hospital, Medical School of Nanjing University. The patients/participants provided their written informed consent to participate in this study.

AUTHOR CONTRIBUTIONS

Z-yZ and N-T conceived and designed the study, collected and assembled data, performed data analysis and interpretation, and wrote the manuscript. M-fW and J-cZ collected and assembled data, and performed data analysis and interpretation. J-lW, H-zR and X-lS conceived and designed the study, provided financial support and study material, performed data analysis and interpretation, wrote and gave final approval of the manuscript. All authors read and approved the manuscript.

FUNDING

This work was funded by the National Natural Science Foundation of China (81872359, to X-lS), Jiangsu Provincial Key Research and Development (BE2020752, to X-lS), Key Scientific Research Project of Jiangsu Provincial Health Commission (ZDA2020002, to X-lS), Jiangsu Province Natural Science Foundation (BK20190114, to J-lW), Jiangsu Province Postdoctoral Research Funding Program(2021K116B, to J-lW), the Nanjing Medical Science and Technique Development Foundation (QRX17129, to H-zR), the Nanjing health science and technology development project for Distinguished Young Scholars (JQX19002, to H-zR), the Fundamental Research Funds for the Central Universities (0214-14380510, to H-zR), the Nanjing health science and technology development project for Medical and health research (YKK19070, to J-lW), the Nanjing Science and technology project (201911039, to J-lW), Project of Modern Hospital Management and Development Institute, Nanjing University and Aid project of Nanjing Drum Tower Hospital Health, Education & Research Foundation (NDYG2020047, to J-lW), the Chen Xiao-ping Foundation for the Development of Science and Technology of Hubei Province, China (CXPJJH121001-2021073, to H-zR), the Innovation Capability Development Project of Jiangsu Province (No. BM2015004).

REFERENCES

1. Xu Z, Zeng S, Gong Z, Yan Y. Exosome-Based Immunotherapy: A Promising Approach for Cancer Treatment. *Mol Cancer* (2020) 19(1):160. doi: 10.1186/s12943-020-01278-3
2. Manzella G, Schreck LD, Breunis WB, Molenaar J, Merks H, Barr FG, et al. Phenotypic Profiling With a Living Biobank of Primary Rhabdomyosarcoma Unravels Disease Heterogeneity and AKT Sensitivity. *Nat Commun* (2020) 11 (1):4629. doi: 10.1038/s41467-020-18388-7
3. Yang Z, Wu L, Wang A, Tang W, Zhao Y, Zhao H, et al. dbDEMC 2.0: Updated Database of Differentially Expressed miRNAs in Human Cancers. *Nucleic Acids Res* (2017) 45(D1):D812–d8. doi: 10.1093/nar/gkw1079
4. Cieslik M, Chinnaiyan AM. Global Genomics Project Unravels Cancer's Complexity at Unprecedented Scale. *Nature* (2020) 578(7793):39–40. doi: 10.1038/d41586-020-00213-2
5. Abed JA, Jones RS. H3K36me3 Key to Polycomb-Mediated Gene Silencing in Lineage Specification. *Nat Struct Mol Biol* (2012) 19(12):1214–5. doi: 10.1038/nsmb.2458
6. Rose NR, King HW, Blackledge NP, Fursova NA, Ember KJ, Fischer R, et al. RYBP Stimulates PRC1 to Shape Chromatin-Based Communication Between Polycomb Repressive Complexes. *Elife* (2016) 5:e18591. doi: 10.7554/eLife.18591
7. Wang W, Qin JJ, Voruganti S, Nag S, Zhou J, Zhang R. Polycomb Group (PcG) Proteins and Human Cancers: Multifaceted Functions and Therapeutic Implications. *Med Res Rev* (2015) 35(6):1220–67. doi: 10.1002/med.21358
8. Di Croce L, Helin K. Transcriptional Regulation by Polycomb Group Proteins. *Nat Struct Mol Biol* (2013) 20(10):1147–55. doi: 10.1038/nsmb.2669
9. Sanna L, Marchesi I, Melone MAB, Bagella L. The Role of Enhancer of Zeste Homolog 2: From Viral Epigenetics to the Carcinogenesis of Hepatocellular Carcinoma. *J Cell Physiol* (2018) 233(9):6508–17. doi: 10.1002/jcp.26545
10. Laugesen A, Højfeldt JW, Helin K. Molecular Mechanisms Directing PRC2 Recruitment and H3K27 Methylation. *Mol Cell* (2019) 74(1):8–18. doi: 10.1016/j.molcel.2019.03.011
11. Duncan IM. Polycomblike: A Gene That Appears to be Required for the Normal Expression of the Bithorax and Antennapedia Gene Complexes of Drosophila Melanogaster. *Genetics* (1982) 102(1):49–70. doi: 10.1093/genetics/102.1.49
12. Hunkapiller J, Shen Y, Diaz A, Cagney G, McCleary D, Ramalho-Santos M, et al. Polycomb-Like 3 Promotes Polycomb Repressive Complex 2 Binding to CpG Islands and Embryonic Stem Cell Self-Renewal. *PloS Genet* (2012) 8(3): e1002576. doi: 10.1371/journal.pgen.1002576
13. Li H, Liefke R, Jiang J, Kurland JV, Tian W, Deng P, et al. Polycomb-Like Proteins Link the PRC2 Complex to CpG Islands. *Nature* (2017) 549 (7671):287–91. doi: 10.1038/nature23881
14. Ruan S, Zhang H, Tian X, Zhang Z, Huang H, Shi C, et al. PHD Finger Protein 19 Enhances the Resistance of Ovarian Cancer Cells to Compound Fuling Granule by Protecting Cell Growth, Invasion, Migration, and Stemness. *Front Pharmacol* (2020) 11:150. doi: 10.3389/fphar.2020.00150

15. Dong C, Nakagawa R, Oyama K, Yamamoto Y, Zhang W, Dong A, et al. Structural Basis for Histone Variant H3tK27me3 Recognition by PHF1 and PHF19. *Elife* (2020) 9:e58675. doi: 10.7554/eLife.58675
16. Brien GL, Gambero G, O'Connell DJ, Jerman E, Turner SA, Egan CM, et al. Polycomb PHF19 Binds H3K36me3 and Recruits PRC2 and Demethylase NO66 to Embryonic Stem Cell Genes During Differentiation. *Nat Struct Mol Biol* (2012) 19(12):1273–81. doi: 10.1038/nsmb.2449
17. Ballaré C, Lange M, Lapinaite A, Martin GM, Morey L, Pascual G, et al. Phf19 Links Methylated Lys36 of Histone H3 to Regulation of Polycomb Activity. *Nat Struct Mol Biol* (2012) 19(12):1257–65. doi: 10.1038/nsmb.2434
18. Mason MJ, Schinke C, Eng CLP, Towfic F, Gruber F, Dervan A, et al. Multiple Myeloma DREAM Challenge Reveals Epigenetic Regulator PHF19 as Marker of Aggressive Disease. *Leukemia* (2020) 34(7):1866–74. doi: 10.1038/s41375-020-0742-z
19. Wang H, Xu P, Sun G, Lv J, Cao J, Xu Z. Downregulation of PHF19 Inhibits Cell Growth and Migration in Gastric Cancer. *Scand J Gastroenterol* (2020) 55 (6):687–93. doi: 10.1080/00365521.2020.1766555
20. Deng Q, Hou J, Feng L, Lv A, Ke X, Liang H, et al. PHF19 Promotes the Proliferation, Migration, and Chemosensitivity of Glioblastoma to Doxorubicin Through Modulation of the SIAH1/β-Catenin Axis. *Cell Death Dis* (2018) 9(11):1049. doi: 10.1038/s41419-018-1082-z
21. Li P, Sun J, Ruan Y, Song L. High PHD Finger Protein 19 (PHF19) Expression Predicts Poor Prognosis in Colorectal Cancer: A Retrospective Study. *PeerJ* (2021) 9:e11551. doi: 10.7717/peerj.11551
22. Hutter C, Zenklusen JC. The Cancer Genome Atlas: Creating Lasting Value Beyond Its Data. *Cell* (2018) 173(2):283–5. doi: 10.1016/j.cell.2018.03.042
23. Goldman MJ, Craft B, Hastie M, Repečka K, McDade F, Kamath A, et al. Visualizing and Interpreting Cancer Genomics Data *via* the Xena platform. *Nat Biotechnol* (2020) 38(6):675–8. doi: 10.1038/s41587-020-0546-8
24. Roessler S, Jia HL, Budhu A, Forgues M, Ye QH, Lee JS, et al. A Unique Metastasis Gene Signature Enables Prediction of Tumor Relapse in Early-Stage Hepatocellular Carcinoma Patients. *Cancer Res* (2010) 70(24):10202–12. doi: 10.1158/0008-5472.Can-10-2607
25. Uhlén M, Fagerberg L, Hallström BM, Lindskog C, Oksvold P, Mardinoglu A, et al. Proteomics. Tissue-Based Map of the Human Proteome. *Science* (2015) 347(6220):1260419. doi: 10.1126/science.1260419
26. Rhodes DR, Yu J, Shanker K, Deshpande N, Varambally R, Ghosh D, et al. ONCOMINE: A Cancer Microarray Database and Integrated Data-Mining Platform. *Neoplasia* (2004) 6(1):1–6. doi: 10.1016/s1476-5586(04)80047-2
27. Li T, Fu J, Zeng Z, Cohen D, Li J, Chen Q, et al. TIMER2.0 for Analysis of Tumor-Infiltrating Immune Cells. *Nucleic Acids Res* (2020) 48(W1):W509–14. doi: 10.1093/nar/gkaa407
28. Tang Z, Li C, Kang B, Gao G, Li C, Zhang Z. GEPIA: A Web Server for Cancer and Normal Gene Expression Profiling and Interactive Analyses. *Nucleic Acids Res* (2017) 45(W1):W98–w102. doi: 10.1093/nar/gkx247
29. Nagy Á, Munkácsy G, Győrffy B. Pancancer Survival Analysis of Cancer Hallmark Genes. *Sci Rep* (2021) 11(1):6047. doi: 10.1038/s41598-021-84787-5
30. Tang Z, Kang B, Li C, Chen T, Zhang Z. GEPIA2: An Enhanced Web Server for Large-Scale Expression Profiling and Interactive Analysis. *Nucleic Acids Res* (2019) 47(W1):W556–60. doi: 10.1093/nar/gkz430
31. Gao J, Aksoy BA, Dogrusoz U, Dresdner G, Gross B, Sumer SO, et al. Integrative Analysis of Complex Cancer Genomics and Clinical Profiles Using the Cbioportal. *Sci Signal* (2013) 6(269):pl1. doi: 10.1126/scisignal.2004088
32. Yoshihara K, Shahmoradgoli M, Martínez E, Vegesna R, Kim H, Torres-Garcia W, et al. Inferring Tumour Purity and Stromal and Immune Cell Admixture From Expression Data. *Nat Commun* (2013) 4:2612. doi: 10.1038/ncomms3612
33. Zhao Y, Zhang M, Pu H, Guo S, Zhang S, Wang Y. Prognostic Implications of Pan-Cancer CMTM6 Expression and Its Relationship With the Immune Microenvironment. *Front Oncol* (2020) 10:585961. doi: 10.3389/fonc.2020.585961
34. Szklarczyk D, Gable AL, Lyon D, Junge A, Wyder S, Huerta-Cepas J, et al. STRING V11: Protein-Protein Association Networks With Increased Coverage, Supporting Functional Discovery in Genome-Wide Experimental Datasets. *Nucleic Acids Res* (2019) 47(D1):D607–13. doi: 10.1093/nar/gky1131
35. Otasek D, Morris JH, Bouças J, Pico AR, Demchak B. Cytoscape Automation: Empowering Workflow-Based Network Analysis. *Genome Biol* (2019) 20 (1):185. doi: 10.1186/s13059-019-1758-4
36. Zhou Y, Zhou B, Pache L, Chang M, Khodabakhshi AH, Tanaseichuk O, et al. Metascape Provides a Biologist-Oriented Resource for the Analysis of Systems-Level Datasets. *Nat Commun* (2019) 10(1):1523. doi: 10.1038/s41467-019-09234-6
37. Yuan H, Yan M, Zhang G, Liu W, Deng C, Liao G, et al. CancerSEA: A Cancer Single-Cell State Atlas. *Nucleic Acids Res* (2019) 47(D1):D900–8. doi: 10.1093/nar/gky939
38. Chang Y, Kang SY, Kim J, Kang HR, Kim HY. Functional Defects in Type 3 Innate Lymphoid Cells and Classical Monocytes in a Patient With Hyper-IgE Syndrome. *Immune Netw* (2017) 17(5):352–64. doi: 10.4110/in.2017.17.5.352
39. Shu L, Liu Y, Li J, Wu X, Li Y, Huang H. Landscape Profiling Analysis of DPP4 in Malignancies: Therapeutic Implication for Tumor Patients With Coronavirus Disease 2019. *Front Oncol* (2021) 11:624899. doi: 10.3389/fonc.2021.624899
40. Mo X, Huang X, Feng Y, Wei C, Liu H, Ru H, et al. Immune Infiltration and Immune Gene Signature Predict the Response to Fluoropyrimidine-Based Chemotherapy in Colorectal Cancer Patients. *Oncoimmunology* (2020) 9 (1):1832347. doi: 10.1080/2162402x.2020.1832347
41. Gabrilovich DI, Nagaraj S. Myeloid-Derived Suppressor Cells as Regulators of the Immune System. *Nat Rev Immunol* (2009) 9(3):162–74. doi: 10.1038/nri2506
42. Schuettengruber B, Bourbon HM, Di Croce L, Cavalli G. Genome Regulation by Polycomb and Trithorax: 70 Years and Counting. *Cell* (2017) 171(1):34–57. doi: 10.1016/j.cell.2017.08.002
43. Cai L, Rothbart SB, Lu R, Xu B, Chen WY, Tripathy A, et al. An H3K36 Methylation-Engaging Tudor Motif of Polycomb-Like Proteins Mediates PRC2 Complex Targeting. *Mol Cell* (2013) 49(3):571–82. doi: 10.1016/j.molcel.2012.11.026
44. Wang S, Robertson GP, Zhu J. A Novel Human Homologue of Drosophila Polycomblike Gene Is Up-Regulated in Multiple Cancers. *Gene* (2004) 343 (1):69–78. doi: 10.1016/j.gene.2004.09.006
45. García-Montolio M, Ballaré C, Blanco E, Gutiérrez A, Aranda S, Gómez A, et al. Polycomb Factor PHF19 Controls Cell Growth and Differentiation Toward Erythroid Pathway in Chronic Myeloid Leukemia Cells. *Front Cell Dev Biol* (2021) 9:655201. doi: 10.3389/fcell.2021.655201
46. Cioni B, Zaalberg A, van Beijnum JR, Melis MHM, van Burgsteden J, Muraro MJ, et al. Androgen Receptor Signalling in Macrophages Promotes TREM-1-Mediated Prostate Cancer Cell Line Migration and Invasion. *Nat Commun* (2020) 11(1):4498. doi: 10.1038/s41467-020-18313-y
47. Gabrilovich DI. Myeloid-Derived Suppressor Cells. *Cancer Immunol Res* (2017) 5(1):3–8. doi: 10.1158/2326-6066.Cir-16-0297
48. Ruterbusch M, Pruner KB, Shehata L, Pepper M. *In Vivo* CD4(+) T Cell Differentiation and Function: Revisiting the Th1/Th2 Paradigm. *Annu Rev Immunol* (2020) 38:705–25. doi: 10.1146/annurev-immunol-103019-085803
49. Li Q, Zou J, Wang M, Ding X, Chepelev I, Zhou X, et al. Critical Role of Histone Demethylase Jmjd3 in the Regulation of CD4+ T-Cell Differentiation. *Nat Commun* (2014) 5:5780. doi: 10.1038/ncomms6780
50. Ao L, Shi J, Bai Y, Zhang S, Gan J. Effects of Transcutaneous Electrical Acupoint Stimulation on Perioperative Immune Function and Postoperative Analgesia in Patients Undergoing Radical Mastectomy: A Randomized Controlled Trial. *Exp Ther Med* (2021) 21(3):184. doi: 10.3892/etm.2021.9615
51. Wang Z, Sokolovska A, Seymour R, Sundberg JP, Hogenesch H. SHARPIN Is Essential for Cytokine Production, NF-κb Signaling, and Induction of Th1 Differentiation by Dendritic Cells. *PloS One* (2012) 7(2):e31809. doi: 10.1371/journal.pone.0031809
52. Kantola T, Klintrup K, Väyrynen JP, Vornanen J, Bloigu R, Karhu T, et al. Stage-Dependent Alterations of the Serum Cytokine Pattern in Colorectal Carcinoma. *Br J Cancer* (2012) 107(10):1729–36. doi: 10.1038/bjc.2012.456
53. Ji Y, Fioravanti J, Zhu W, Wang H, Wu T, Hu J, et al. miR-155 Harnesses Phf19 to Potentiate Cancer Immunotherapy Through Epigenetic Reprogramming of CD8(+) T Cell Fate. *Nat Commun* (2019) 10(1):2157. doi: 10.1038/s41467-019-09882-8
54. Song W, Shen L, Wang Y, Liu Q, Goodwin TJ, Li J, et al. Synergistic and Low Adverse Effect Cancer Immunotherapy by Immunogenic Chemotherapy and Locally Expressed PD-L1 Trap. *Nat Commun* (2018) 9(1):2237. doi: 10.1038/s41467-018-04605-x

55. Lv M, Chen M, Zhang R, Zhang W, Wang C, Zhang Y, et al. Manganese Is Critical for Antitumor Immune Responses *via* cGAS-STING and Improves the Efficacy of Clinical Immunotherapy. *Cell Res* (2020) 30(11):966–79. doi: 10.1038/s41422-020-00395-4
56. Behary J, Amorim N, Jiang XT, Raposo A, Gong L, McGovern E, et al. Gut Microbiota Impact on the Peripheral Immune Response in Non-Alcoholic Fatty Liver Disease Related Hepatocellular Carcinoma. *Nat Commun* (2021) 12(1):187. doi: 10.1038/s41467-020-20422-7

Conflict of Interest: The authors declare that the research was conducted in the absence of any commercial or financial relationships that could be construed as a potential conflict of interest.

Publisher's Note: All claims expressed in this article are solely those of the authors and do not necessarily represent those of their affiliated organizations, or those of the publisher, the editors and the reviewers. Any product that may be evaluated in this article, or claim that may be made by its manufacturer, is not guaranteed or endorsed by the publisher.

frontiers in Immunology

ORIGINAL RESEARCH
published: 01 March 2022
doi: 10.3389/fimmu.2022.848387

Transarterial Chemoembolization Combined With Lenvatinib Plus PD-1 Inhibitor for Advanced Hepatocellular Carcinoma: A Retrospective Cohort Study

Mingyue Cai[1,2†], Wensou Huang[1,2†], Jingjun Huang[1,2†], Wenbo Shi[1,2], Yongjian Guo[1,2], Licong Liang[1,2], Jingwen Zhou[1,2], Liteng Lin[1,2], Bihui Cao[1,2], Ye Chen[1,2], Juan Zhou[3] and Kangshun Zhu[1,2]*

[1] Department of Minimally Invasive Interventional Radiology, The Second Affiliated Hospital of Guangzhou Medical University, Guangzhou, China, [2] Radiology Center, The Second Affiliated Hospital of Guangzhou Medical University, Guangzhou, China, [3] Department of Pharmacy, The Second Affiliated Hospital of Guangzhou Medical University, Guangzhou, China

Purpose: To investigate the efficacy and safety of transarterial chemoembolization (TACE) combined with lenvatinib plus PD-1 inhibitor (TACE-L-P) versus TACE combined with lenvatinib (TACE-L) for patients with advanced hepatocellular carcinoma (HCC).

Materials and Methods: Data of advanced HCC patients treated with TACE-L-P (TACE-L-P group) or TACE-L (TACE-L group) from January 2019 to December 2020 were prospectively collected and retrospectively analyzed. The differences in overall survival (OS), progression-free survival (PFS), tumor responses (based on modified Response Evaluation Criteria in Solid Tumors) and adverse events (AEs) were compared between the two groups. Potential factors affecting OS and PFS were determined.

Results: A total of 81 patients were included in this study. Among them, 41 received TACE-L-P and 40 received TACE-L. The patients in TACE-L-P group had prolonged OS (median, 16.9 *vs.* 12.1 months, *P*=0.009), longer PFS (median, 7.3 *vs.* 4.0 months, *P*=0.002) and higher objective response rate (56.1% *vs.* 32.5%, *P*=0.033) and disease control rate (85.4% *vs.* 62.5%, *P*=0.019) than those in TACE-L group. Multivariate analyses revealed that the treatment option of TACE-L, main portal vein invasion and extrahepatic metastasis were the independent risk factors for OS, while TACE-L and extrahepatic metastasis were the independent risk factors for PFS. In subgroup analyses, a superior survival benefit was achieved with TACE-L-P in patients with extrahepatic metastasis or tumor number >3 but not in those with main portal vein invasion.

OPEN ACCESS

Edited by:
Ignacio Melero, University of Navarra, Spain

Reviewed by:
Jianxun J. Song, Texas A&M Health Science Center, United States
Bin Xiong, Huazhong University of Science and Technology, China

***Correspondence:**
Kangshun Zhu
zhksh010@163.com

†These authors have contributed equally to this work and share first authorship

Specialty section:
This article was submitted to Cancer Immunity and Immunotherapy, a section of the journal Frontiers in Immunology

Received: *04 January 2022*
Accepted: *10 February 2022*
Published: *01 March 2022*

Citation:
Cai M, Huang W, Huang J, Shi W, Guo Y, Liang L, Zhou J, Lin L, Cao B, Chen Y, Zhou J and Zhu K (2022) Transarterial Chemoembolization Combined With Lenvatinib Plus PD-1 Inhibitor for Advanced Hepatocellular Carcinoma: A Retrospective Cohort Study. Front. Immunol. 13:848387. doi: 10.3389/fimmu.2022.848387

The incidence and severity of AEs in TACE-L-P group were comparable to those in TACE-L group (any grade, 92.7% *vs.* 95.0%, *P*=1.000; grade 3, 36.6% *vs.* 32.5%, *P*=0.699).

Conclusion: TACE-L-P significantly improved survival over TACE-L with an acceptable safety profile in advanced HCC patients, especially those with extrahepatic metastasis or tumor number >3 but without main portal vein invasion.

Keywords: hepatocellular carcinoma, transarterial chemoembolization, lenvatinib, immune checkpoint inhibitor, PD-1 inhibitor, combined therapy

INTRODUCTION

Hepatocellular carcinoma (HCC), representing 75%-85% of primary liver cancer, is one of the most prevalent and fatal malignancies worldwide (1). Although surgical resection, ablation and liver transplantation may provide curative potential for HCC, a majority of patients are diagnosed with advanced disease which is not amenable for these approaches and thus bear a poor prognosis with an expected median survival of 6-8 months (2–4).

The multikinase inhibitors sorafenib and lenvatinib are recommended as the first-line treatment of advanced HCC (2–4) on the basis of randomized trials demonstrating longer survival with sorafenib versus placebo (5, 6) and noninferiority of lenvatinib to sorafenib (7). However, the efficacy of monotherapy with these drugs is modest, and only a small survival benefit of about 3 months can be achieved with oral sorafenib (8). In this setting, transarterial chemoembolization (TACE) has been applied to providing local disease control in patients with acceptable liver function and tumor burden. It is supposed that the antiangiogenic agents in combination with TACE may effectively offset the post-TACE hypoxia-induced angiogenesis and, therefore, provide a superior antitumor effect for HCC (9, 10). In fact, many studies have suggested improved outcomes of this combination treatment compared with the use of a single drug or TACE alone for advanced HCC (11–14). But unfortunately, there still remained limited treatment responses with unsatisfied survival prolongation (11–13).

Recently, immune checkpoint inhibitors, including programmed death 1 (PD-1) and programmed death ligand 1 (PD-L1) inhibitors, have exhibited a promising clinical benefit to advanced HCC patients (15). Although phase III trials for anti-PD-1 monotherapy failed to meet their primary survival endpoints (16, 17), the studies testing combined treatments with PD-1/PD-L1 inhibitor and antiangiogenic agent showed exciting results (18–20). In a recent phase Ib study for evaluating the combination of lenvatinib and pembrolizumab (an anti-PD-1 antibody) in first-line treatment of unresectable HCC, an objective response rate (ORR) of 46.0% per modified Response Evaluation Criteria in Solid Tumors (mRECIST) and a median overall survival (OS) of 22.0 months were achieved (20). These impressive results suggested a promising therapeutic potential of the combination of lenvatinib plus PD-1 inhibitor in patients with HCC.

Since TACE possesses a local anticancer effect and may facilitate antitumor immunity but inevitably induces post-TACE angiogenesis (10, 21), and lenvatinib has an immunomodulatory effect on tumor microenvironment besides antiangiogenesis (22, 23), combining TACE and lenvatinib plus PD-1 inhibitor (TACE-L-P) may contribute to a synergistic anticancer activity for HCC. Accordingly, we hypothesized that the comprehensive therapy of TACE-L-P would be an effective treatment strategy for advanced HCC. Thus, we conducted this retrospective study to evaluate the efficacy and safety of TACE-L-P versus TACE combined with lenvatinib (TACE-L) in the patients with advanced HCC.

MATERIALS AND METHODS

Study Design and Patient Selection

This study was approved by our institutional review board, and written informed consent was obtained from every patient. Data of consecutive patients with advanced HCC who received TACE-L-P or TACE-L at our institution between January 2019 and December 2020 were prospectively collected and retrospectively analyzed.

The inclusion criteria for this study were as follows: 1) age between 18 and 75 years; 2) confirmed diagnosis with HCC (2, 4, 24) accompanied by macrovascular invasion and/or extrahepatic metastasis (BCLC stage C or CNLC Stage IIIa/IIIb); 3) tumor recurrence after curative resection or ablation was allowed; 4) Eastern Cooperative Oncology Group performance status (ECOG PS) of ≤1; and 5) Child-Pugh class A/B. Patients were excluded if they 1) had central nervous system metastasis; 2) had history of organ transplantation; 3) previously received TACE, hepatic arterial infusion chemotherapy (HAIC), radiotherapy or systemic therapy; 4) had other malignancies in addition to HCC; or 5) had severe medical comorbidities including severe cardiac, pulmonary, renal or coagulation dysfunction.

All laboratory test data were collected within 3 days before the initial treatment. Contrast-enhanced computed tomography (CT) or magnetic resonance imaging (MRI) was performed within 7 days before the initial treatment.

TACE Procedure

The patients received either conventional TACE (cTACE) or drug-eluting bead TACE (DEB-TACE) according to their own choice. For cTACE, an emulsion of 5-20 mL Lipiodol (Guerbet, Paris, France) mixed with 20-60 mg pirarubicin (Hisun Pfizer Pharmaceuticals, Fuyang, China) was administered into the tumor-feeding vessels, followed by embolization with polyvinyl alcohol particles (90-500 μm; Cook, Bloomington, Indiana, USA). For DEB-TACE, CalliSpheres (Hengrui Medical, Suzhou, China) or DC Bead (Biocompatibles, Farnham, Surrey, UK) with 100-300 μm in diameter was used as the drug carrier

and embolization agent. Typically, one vial of the beads was loaded with 60 mg pirarubicin. If blushed tumors were still visible after the embolization with one vial of beads, regular microspheres (8spheres, Hengrui Medical, Suzhou, China; Embosphere, Biosphere Medical, Roissy en France, France) with diameters of 100-700 μm were additionally injected (25).

During TACE, superselective catheterization was performed, and the embolization end point was blood stasis of the tumor-feeding arteries. In patients with huge or bilobar multiple lesions, in order to reduce the risk of complications, the embolization end point was not achieved in the initial TACE but in the second or third TACE session (26). In the case of arterioportal or arteriovenous fistula, the fistula would be embolized with 300-710 μm polyvinyl alcohol particles before administration of the drug-oil emulsion or drug-loaded beads.

TACE was repeated "on demand" upon the demonstration of viable tumor by follow-up CT or MRI in patients without deteriorated performance status or organ function.

Lenvatinib and PD-1 Inhibitor Administration

Lenvatinib (Eisai, Tokyo, Japan) and PD-1 inhibitor was initiated within 7 days after the first TACE. Lenvatinib at a dose of 12 mg (bodyweight ≥60 kg) or 8 mg (bodyweight <60 kg) was orally administered once a day. The PD-1 inhibitor sintilimab (Innovent Biologics, Suzhou, China), tislelizumab (BeiGene, Shanghai, China) or camrelizumab (Hengrui Pharma, Lianyungang, China) was injected intravenously at 200 mg once every 3 weeks. The interruption and discontinuation of drug administration depended on the presence and severity of toxicities according to the drug directions.

Follow-Up

Regular follow-up was conducted for all patients at a 3-6-week interval after the initial treatment. Each follow-up session included a detail history, physical examination, hematologic and biochemical tests, contrast-enhanced abdominal CT or MRI, chest CT, and other imaging examination if clinically indicated. The final follow-up ended on June 30, 2021.

During follow-up, the treatment of TACE-L-P or TACE-L was discontinued in cases of intolerable toxicity, progressive disease (PD) or change of treatment plan. And, the choice of the subsequent treatment, such as second-line targeted agent, PD-1 inhibitor (for the patients treated with TACE-L), radiotherapy (including iodine-125 seed brachytherapy), HAIC or best supportive care, was determined according to the results of discussion by our multidisciplinary team and the patients' request.

Assessments and Outcomes

OS and progression-free survival (PFS) were compared between TACE-L-P group and TACE-L group. OS was defined as the time from treatment initiation until death by any reason. PFS was

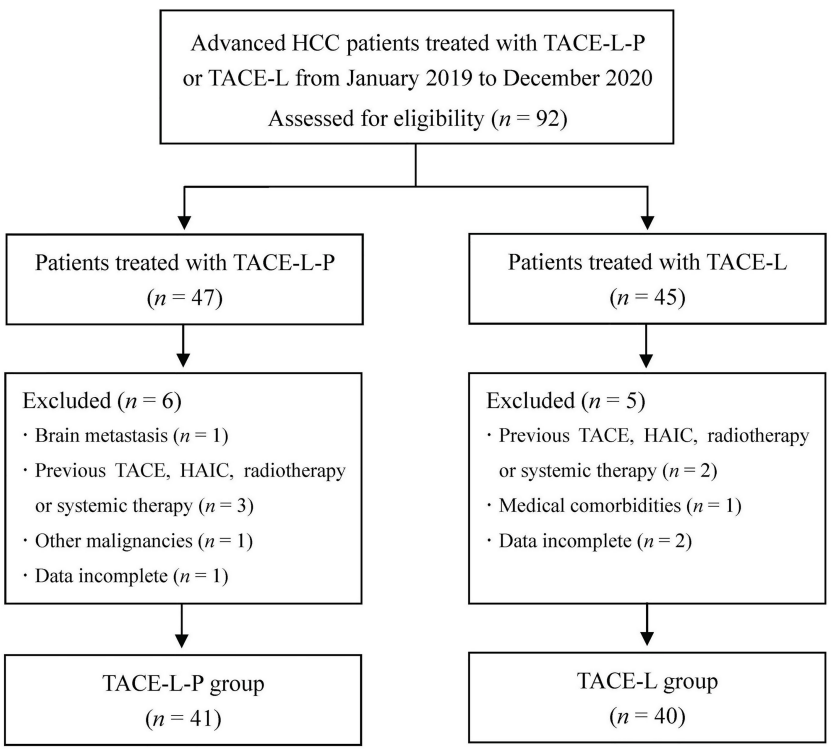

FIGURE 1 | Flow diagram of patient enrollment. HCC, hepatocellular carcinoma; TACE-L-P, transarterial chemoembolization combined with lenvatinib plus PD-1 inhibitor; TACE-L, transarterial chemoembolization combined with lenvatinib; TACE, transarterial chemoembolization; HAIC, hepatic arterial infusion chemotherapy.

defined as the time interval from treatment initiation to the first occurrence of PD or death, whichever occurred first.

Tumor responses were categorized as complete response (CR), partial response (PR), stable disease (SD) or PD according to mRECIST. Overall tumor response referred to the assessment of changes in tumor burden inside and outside the liver, while intrahepatic tumor response only included the assessment of changes in tumor burden inside the liver. ORR was defined as the percentage of patients who had a best tumor response rating of CR and PR. Disease control rate (DCR) was defined as the percentage of patients who had a best tumor response rating of CR, PR and SD.

Adverse events (AEs) related to treatments were recorded and assessed based on Common Terminology Criteria for Adverse Events (CTCAE) version 5.0. Postembolization syndrome (manifested by fever, abdominal pain, nausea, vomiting and increased white blood cell count) and transient abnormalities of liver enzyme after TACE (27, 28) were expected and would resolve within a short time, and therefore, they were not documented separately.

Statistical Analyses

Categorical data were expressed as number of patients (percentage). Quantitative data were expressed as mean ± standard deviation and median (range) for normally and non-normally distributed variables, respectively. Categorical data between the two groups were compared using χ^2 test or Fisher's exact test, as appropriate. Quantitative data were compared using Student's *t*-test or Mann-Whitney U test, as appropriate. Survival curves were analyzed by Kaplan-Meier method using

TABLE 1 | Baseline characteristics of the patients.

Characteristic	TACE-L-P group (*n*=41)	TACE-L group (*n*=40)	*P*
Sex			0.309
Female	4 (9.8)	7 (17.5)	
Male	37 (90.2)	33 (82.5)	
Age (years)	51.9 ± 10.3	54.6 ± 11.0	0.263
ECOG PS			0.274
1	8 (19.5)	12 (30.0)	
0	33 (80.5)	28 (70.0)	
HBsAg			0.779
Positive	35 (85.4)	35 (87.5)	
Negative	6 (14.6)	5 (12.5)	
Child-Pugh class			0.309
B	4 (9.8)	7 (17.5)	
A	37 (90.2)	33 (82.5)	
AFP level (μg/L)			0.733
≥400	21 (51.2)	22 (55.0)	
<400	20 (48.8)	18 (45.0)	
PIVKA-II (mAU/ml)			0.517
≥400	27 (65.9)	29 (72.5)	
<400	14 (34.1)	11 (27.5)	
Recurrent tumor			0.362
No	35 (85.4)	31 (77.5)	
Yes	6 (14.6)	9 (22.5)	
Number of tumors			0.439
>3	23 (56.1)	19 (47.5)	
≤3	18 (43.9)	21 (52.5)	
Tumor distribution			0.939
Bilobar	28 (68.3)	27 (67.5)	
Unilobar	13 (31.7)	13 (32.5)	
Largest tumor size (cm)	12.3 ± 4.8	13.6 ± 5.1	0.218
Main portal vein invasion			0.441
Yes	15 (36.6)	18 (45.0)	
No	26 (63.4)	22 (55.0)	
Hepatic vein invasion			0.581
Yes	12 (29.3)	14 (35.0)	
No	29 (70.7)	26 (65.0)	
Extrahepatic metastasis			0.585
Yes	17 (41.5)	19 (47.5)	
No	24 (58.5)	21 (52.5)	
TACE technique			0.223
cTACE	17 (41.5)	22 (55.0)	
DEB-TACE	24 (58.5)	18 (45.0)	

Data were presented as n (%) or mean ± standard deviation. TACE-L-P, transarterial chemoembolization combined with lenvatinib plus PD-1 inhibitor; TACE-L, transarterial chemoembolization combined with lenvatinib; ECOG PS, Eastern Cooperative Oncology Group Performance Status; HBsAg, hepatitis B surface antigen; AFP, α-fetoprotein; PIVKA-II, protein induced by vitamin K absence or antagonist-II; TACE, transarterial chemoembolization; cTACE, conventional transarterial chemoembolization; DEB-TACE, drug-eluting bead transarterial chemoembolization.

log-rank test. Variables with $P<0.10$ in univariate analysis were entered into a multivariate analysis using Cox regression model to identify the independent prognostic factors for OS and PFS. All statistical analyses were performed with SPSS Statistics version 22 (IBM, Armonk, New York, USA). All statistical tests were two-tailed, $P<0.05$ was considered statistically significant.

RESULTS

Study Population

During the study period, 92 patients with advanced HCC who received TACE-L-P or TACE-L were screened for eligibility. Of these patients, 11 were excluded because they met the excluded criteria (**Figure 1**). Finally, 81 patients were included in this study (41 in the TACE-L-P group and 40 in the TACE-L group). Detailed baseline characteristics of the patients were summarized in **Table 1**. In both groups, about half of the patients had more than 3 intrahepatic tumors at diagnosis. The mean largest tumor size of TACE-L-P group and TACE-L group was 12.3 ± 4.8 cm and 13.6 ± 5.1 cm, respectively. Two groups were comparable in the demographic, clinical and tumor characteristics.

The patients in TACE-L-P group underwent a total of 134 TACE procedures, with a median of 3 (range, 1-7). While the patients in TACE-L group underwent a total of 95 TACE procedures, with a median of 2 (range, 1-6). The mean duration of lenvatinib administration was 7.4 ± 3.8 (range, 1.2-15.6) months in TACE-L-P group and 4.3 ± 3.0 (range, 0.9-11.9) months in the TACE-L group ($P<0.001$). In the TACE-L-P group, the cycles of PD-1 inhibitor injection ranged from 2 to 22, with a mean of 9.9. The categories of PD-1 inhibitor the patients received were as follows: sintilimab for 30 (73.2%), tislelizumab for 6 (14.6%) and camrelizumab for 5 (12.2%).

Survival

The follow-up duration ranged from 4.6 to 29.8 months, with a median of 13.7 months. During follow-up, 27 patients (65.9%) in the TACE-L-P group and 30 patients (75.0%) in the TACE-L group died. Compared with the patients in TACE-L group, the patients in TACE-L-P group had significantly better survival outcomes (**Figure 2**). The median OS was 16.9 (95% confidence interval [CI] 14.9-18.8) months in TACE-L-P group and 12.1 (95% CI 10.7-13.5) months in TACE-L group ($P=0.009$). The median PFS was 7.3 (95% CI 6.0-8.7) months in TACE-L-P group and 4.0 (95% CI 2.7-5.3) months in TACE-L group ($P=0.002$). Additionally, the median OS and PFS of the patients treated with sintilimab were comparable to those of the patients treated with tislelizumab/camrelizumab (OS, 17.0 months [95% CI 14.4-19.6] *vs.* 16.9 months [95% CI 9.6-24.1], $P=0.210$; PFS, 7.5 months [95% CI 6.8-8.2] *vs.* 6.2 months [95% CI 4.6-7.7], $P=0.381$) in the TACE-L-P group (**Supplementary Figure 1**).

Prognostic Factors Analysis

Based on the results of the univariate and multivariate analyses (**Table 2**), treatment option (TACE-L *vs.* TACE-L-P; hazard ratio [HR]=2.065, 95% CI 1.208-3.533, $P=0.008$), extrahepatic metastasis (present *vs.* absent; HR=2.041, 95% CI 1.183-3.520, $P=0.010$) and main portal vein invasion (yes *vs.* no; HR=1.867, 95% CI 1.089-3.200, $P=0.023$) were identified as the independent prognostic factors for OS. In addition, treatment option (HR=2.243, 95% CI 1.344-3.743, $P=0.002$) and extrahepatic metastasis (HR=2.244, 95% CI 1.365-3.689, $P=0.001$) were also identified as the independent prognostic factors for PFS.

Subgroup analyses of factors for OS indicated that TACE-L-P treatment could provide a superior survival benefit in patients with no main portal vein invasion, tumor number >3 or extrahepatic metastasis, but failed to have a clinical benefit in

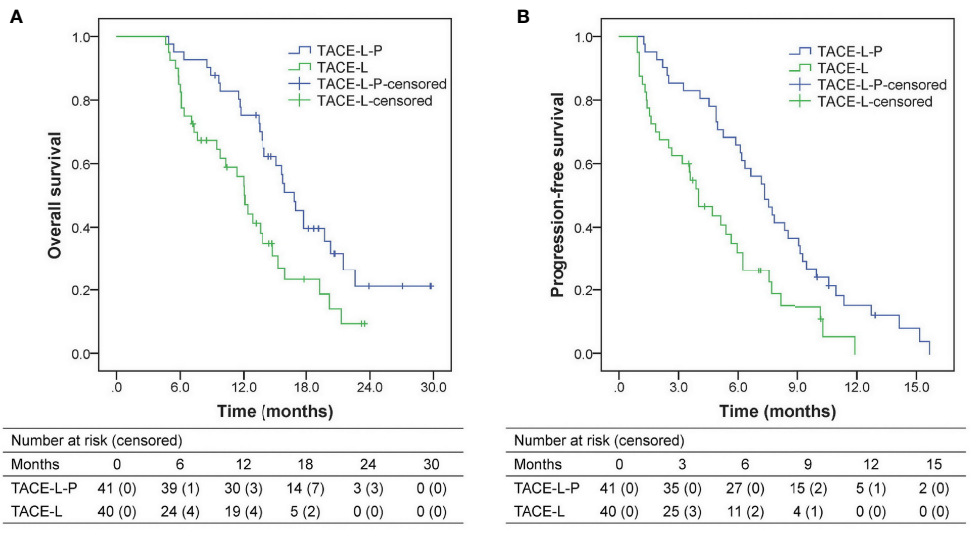

Number at risk (censored)						
Months	0	6	12	18	24	30
TACE-L-P	41 (0)	39 (1)	30 (3)	14 (7)	3 (3)	0 (0)
TACE-L	40 (0)	24 (4)	19 (4)	5 (2)	0 (0)	0 (0)

Number at risk (censored)						
Months	0	3	6	9	12	15
TACE-L-P	41 (0)	35 (0)	27 (0)	15 (2)	5 (1)	2 (0)
TACE-L	40 (0)	25 (3)	11 (2)	4 (1)	0 (0)	0 (0)

FIGURE 2 | Kaplan-Meier analyses of overall survival **(A)** and progression-free survival **(B)** according to treatment groups. TACE-L-P, transarterial chemoembolization combined with lenvatinib plus PD-1 inhibitor; TACE-L, transarterial chemoembolization combined with lenvatinib.

TABLE 2 | Analyses of prognostic factors for survival.

Factor	Overall survival				Progression-free survival			
	Univariate analysis		Multivariate analysis		Univariate analysis		Multivariate analysis	
	HR (95% CI)	*P*	HR (95% CI)	*P*	HR (95% CI)	*P*	HR (95% CI)	*P*
Sex								
Female/Male	1.459 (0.713-2.984)	0.301			0.951 (0.450-2.009)	0.895		
Age (years)								
<60/≥60	1.118 (0.631-1.981)	0.703			0.971 (0.581-1.626)	0.912		
ECOG PS								
1/0	1.587 (0.897-2.809)	0.113			1.271 (0.748-2.162)	0.376		
HBsAg								
Positive/Negative	1.632 (0.699-3.810)	0.257			1.045 (0.533-2.046)	0.899		
Child-Pugh class								
B/A	1.698 (0.800-3.606)	0.168			1.243 (0.631-2.448)	0.530		
AFP level (μg/L)								
≥400/<400	1.317 (0.779-2.225)	0.304			1.146 (0.718-1.828)	0.568		
PIVKA-II (mAU/mL)								
≥400/<400	1.275 (0.714-2.274)	0.411			1.387 (0.829-2.319)	0.212		
Recurrent tumor								
No/Yes	1.480 (0.723-3.030)	0.283			1.013 (0.561-1.829)	0.965		
Number of tumors								
>3/≤3	1.528 (0.893-2.615)	0.122			1.177 (0.733-1.888)	0.500		
Tumor distribution								
Bilobar/Unilobar	1.144 (0.647-2.022)	0.643			1.033 (0.623-1.711)	0.900		
Largest tumor size (cm)								
≥10/<10	1.531 (0.857-2.733)	0.150			1.388 (0.836-2.304)	0.205		
Main portal vein invasion								
Yes/No	1.638 (0.970-2.767)	0.065	1.867 (1.089-3.200)	0.023	1.025 (0.635-1.653)	0.920		
Hepatic vein invasion								
Yes/No	1.263 (0.721-2.211)	0.414			1.315 (0.783-2.206)	0.300		
Extrahepatic metastasis								
Yes/No	1.710 (1.013-2.888)	0.045	2.041 (1.183-3.520)	0.010	2.125 (1.313-3.438)	0.002	2.337 (1.430-3.820)	0.001
Treatment option								
TACE-L/TACE-L-P	1.987 (1.172-3.367)	0.011	2.065 (1.208-3.533)	0.008	2.100 (1.288-3.425)	0.003	2.312 (1.404-3.808)	0.001
TACE technique								
cTACE/DEB-TACE	1.188 (0.706-2.001)	0.517			1.311 (0.817-2.103)	0.262		

Analyses were performed using Cox proportional hazard regression model. HR, hazard ratio; CI, confidence interval; ECOG PS, Eastern Cooperative Oncology Group Performance Status; HBsAg, hepatitis B surface antigen; AFP, α-fetoprotein; PIVKA-II, protein induced by vitamin K absence or antagonist-II; TACE-L, transarterial chemoembolization combined with lenvatinib; TACE-L-P, transarterial chemoembolization combined with lenvatinib plus PD-1 inhibitor; TACE, transarterial chemoembolization; cTACE, conventional transarterial chemoembolization; DEB-TACE, drug-eluting bead transarterial chemoembolization.

patients with main portal vein invasion, tumor number ≤3 or no extrahepatic metastasis (**Figure 3**).

Tumor Responses

Tumor responses for patients in the two groups were shown in **Figure 4**. The ORR of both overall tumor (56.1% *vs.* 32.5%, *P*=0.033) and intrahepatic tumor (65.9% *vs.* 37.5%, *P*=0.011) was higher in the TACE-L-P group than in the TACE-L group. A higher DCR was also achieved in TACE-L-P group when compared with TACE-L group (overall tumor, 85.4% *vs.* 62.5%, *P*=0.019; intrahepatic tumor, 95.1% *vs.* 77.5%, *P*=0.021). In addition, the ORR (overall tumor, 56.7% *vs.* 54.5%, *P*=1.000; intrahepatic tumor, 66.7% *vs.* 63.6%, *P*=1.000) and DCR (overall tumor, 86.7% *vs.* 81.8%, *P*=1.000; intrahepatic tumor, 96.7% *vs.* 90.9%, *P*=0.470) of the patients treated with sintilimab were similar to those of the patients treated with tislelizumab/camrelizumab in the TACE-L-P group (**Supplementary Table 1**).

Safety

In total, treatment-related AEs were observed in 76 of the 81 patients (93.8%), and no grade 4/5 AEs occurred (**Table 3**). The frequency and severity of AEs was similar between the TACE-L-P group and the TACE-L group (any grade, 92.7% *vs.* 95.0%, *P*=1.000; grade 3, 36.6% *vs.* 32.5%, *P*=0.699). The AEs related to TACE, including ascites, pleural effusion, inguinal hematoma and intrahepatic biliary dilatation/biloma, were mild (≤ grade 2) and occurred in 6 (14.6%) and 7 (17.5%) patients in the TACE-L-P group and the TACE-L group (*P*=0.725), respectively. The AEs related to lenvatinib and/or PD-1 inhibitor occurred in 38 (92.7%) and 37 (90.0%) patients in the TACE-L-P group and the TACE-L group (*P*=1.000), respectively. In the TACE-L-P group, the incidences of overall and grade 3 AEs in the patients treated with sintilimab were similar to those in the patients treated with tislelizumab/camrelizumab (any grade, 93.3% *vs.* 90.9%, *P*=1.000; grade 3, 36.7% *vs.* 36.4%, *P*=1.000).

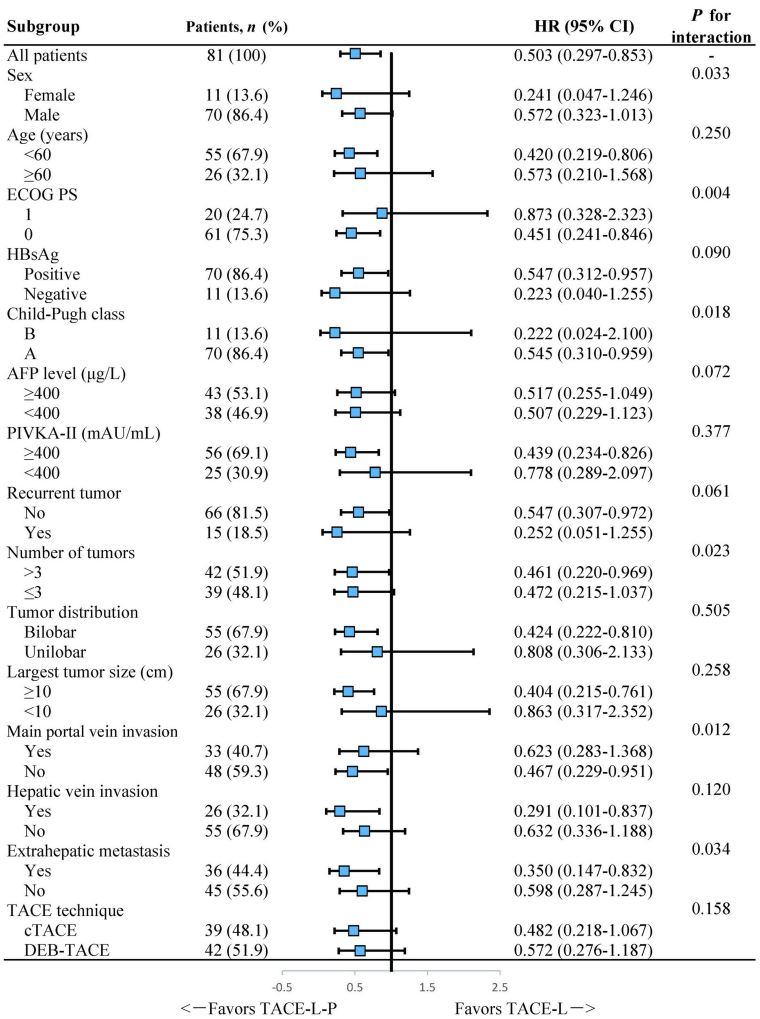

FIGURE 3 | Forest plot of the subgroup analyses for overall survival. HR, hazard ratio; CI, confidence interval; ECOG PS, Eastern Cooperative Oncology Group Performance Status; HBsAg, hepatitis B surface antigen; AFP, α-fetoprotein; PIVKA-II, protein induced by vitamin K absence or antagonist-II; TACE, transarterial chemoembolization; cTACE, conventional transarterial chemoembolization; DEB-TACE, drug-eluting bead transarterial chemoembolization; TACE-L-P, transarterial chemoembolization combined with lenvatinib plus PD-1 inhibitor; TACE-L, transarterial chemoembolization combined with lenvatinib.

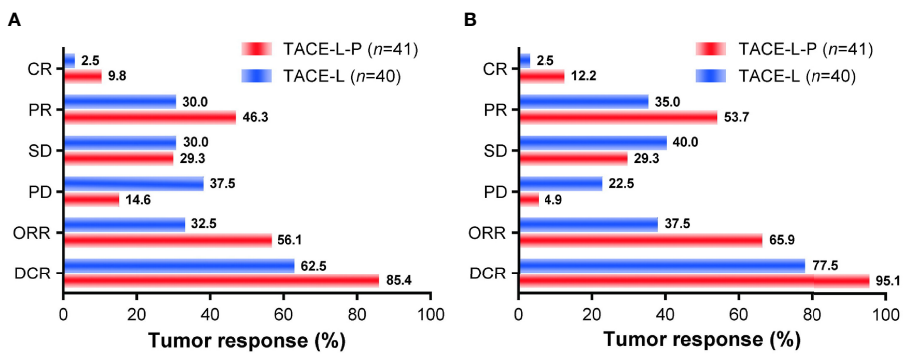

FIGURE 4 | Treatment responses of overall tumor **(A)** and intrahepatic tumor **(B)** for the two groups. TACE-L-P, transarterial chemoembolization combined with lenvatinib plus PD-1 inhibitor; TACE-L, transarterial chemoembolization combined with lenvatinib; CR, complete response; PR, partial response; SD, stable disease; PD, progressive disease; ORR, objective response rate; DCR, disease control rate.

TABLE 3 | Treatment-related adverse events in the two groups.

Adverse events	Any grade			Grade 3		
	TACE-L-P group (*n*=41)	TACE-L group (*n*=40)	*P*	TACE-L-P group (*n*=41)	TACE-L group (*n*=40)	*P*
Total	38 (92.7)	38 (95.0)	1.000	15 (36.6)	13 (32.5)	0.699
Related to TACE	6 (14.6)	7 (17.5)	0.725	0 (0.0)	0 (0.0)	–
New ascites	3 (7.3)	2 (5.0)	1.000	0 (0.0)	0 (0.0)	–
Pleural effusion	2 (4.9)	2 (5.0)	1.000	0 (0.0)	0 (0.0)	–
Inguinal hematoma	2 (4.9)	3 (7.5)	0.977	0 (0.0)	0 (0.0)	–
Biliary injury†	1 (2.4)	2 (5.0)	0.983	0 (0.0)	0 (0.0)	–
Related to drug*	38 (92.7)	37 (92.5)	1.000	15 (36.6)	13 (32.5)	0.699
Hypertension	16 (39.0)	14 (35.0)	0.708	9 (22.0)	8 (20.0)	0.829
Weight loss	14 (34.1)	11 (27.5)	0.517	1 (2.4)	0 (0.0)	1.000
Diarrhea	13 (31.7)	13 (32.5)	0.939	0 (0.0)	0 (0.0)	–
Hand-foot syndrome	11 (26.8)	13 (32.5)	0.576	0 (0.0)	0 (0.0)	–
Fatigue	11 (26.8)	9 (22.5)	0.651	1 (2.4)	0 (0.0)	1.000
Elevated AST	11 (26.8)	8 (20.0)	0.468	0 (0.0)	1 (2.5)	0.494
Decreased appetite	10 (24.4)	9 (22.5)	0.841	1 (2.4)	1 (2.5)	1.000
Hypothyroidism	10 (24.4)	8 (20.0)	0.635	0 (0.0)	0 (0.0)	–
Elevated ALP	9 (22.0)	11 (27.5)	0.563	0 (0.0)	0 (0.0)	–
Hypoalbuminemia	9 (22.0)	8 (20.0)	0.829	0 (0.0)	0 (0.0)	–
Abdominal pain	9 (22.0)	8 (20.0)	0.829	0 (0.0)	1 (2.5)	0.494
Pruritus	9 (22.0)	4 (10.0)	0.143	0 (0.0)	0 (0.0)	–
Elevated ALT	8 (19.5)	9 (22.5)	0.741	1 (2.4)	0 (0.0)	1.000
Thrombocytopenia	8 (19.5)	8 (20.0)	0.956	1 (2.4)	2 (5.0)	0.983
Neutropenia	8 (19.5)	6 (15.0)	0.591	2 (4.9)	2 (5.0)	1.000
Proteinuria	8 (19.5)	6 (15.0)	0.591	0 (0.0)	0 (0.0)	–
Rash	8 (19.5)	4 (10.0)	0.228	0 (0.0)	0 (0.0)	–
Anemia	7 (17.1)	5 (12.5)	0.562	0 (0.0)	1 (2.5)	0.494
Lymphopenia	7 (17.1)	4 (10.0)	0.353	1 (2.4)	0 (0.0)	1.000
Elevated TBi	6 (14.6)	7 (17.5)	0.725	1 (2.4)	1 (2.5)	1.000
Nausea	6 (14.6)	6 (15.0)	0.963	0 (0.0)	0 (0.0)	–
Elevated GGT	6 (14.6)	5 (12.5)	0.779	0 (0.0)	0 (0.0)	–
Ventosity	6 (14.6)	5 (12.5)	0.779	1 (2.4)	0 (0.0)	1.000
Arthralgia	6 (14.6)	5 (12.5)	0.779	0 (0.0)	0 (0.0)	–
Vomiting	5 (12.2)	6 (15.0)	0.713	0 (0.0)	0 (0.0)	–
Gingival bleeding	5 (12.2)	6 (15.0)	0.713	0 (0.0)	0 (0.0)	–
Dysphonia	4 (9.8)	6 (15.0)	0.704	0 (0.0)	0 (0.0)	–
Edema	3 (7.3)	4 (10.0)	0.973	0 (0.0)	0 (0.0)	–
Elevated uric acid	3 (7.3)	1 (2.5)	0.626	0 (0.0)	0 (0.0)	–
Insomnia	2 (4.9)	2 (5.0)	1.000	0 (0.0)	0 (0.0)	–
Infusion reaction	2 (4.9)	–	–	0 (0.0)	–	–
Hyperglycemia	1 (2.4)	0 (0.0)	1.000	0 (0.0)	0 (0.0)	–
Pneumonitis	1 (2.4)	0 (0.0)	1.000	1 (2.4)	0 (0.0)	1.000

*Data were presented as n (%). †Included intrahepatic biliary dilatation and biloma; *Referred to lenvatinib and/or PD-1 inhibitor. TACE-L-P, transarterial chemoembolization combined with lenvatinib plus PD-1 inhibitor; TACE-L, transarterial chemoembolization combined with lenvatinib; TACE, transarterial chemoembolization; AST, aspartate aminotransferase; ALT, alanine aminotransferase; ALP, alkaline phosphatase; TBi, total bilirubin; GGT, γ-glutamyl transpeptidase.*

Treatment-related AEs led to treatment interruption, dose reduction and treatment discontinuation of lenvatinib in 22 (53.7%), 21 (51.2%) and 3 (7.3%) patients, respectively, in the TACE-L-P group, and in 20 (50.0%), 20 (50.0%) and 3 (7.5%) patients, respectively, in the TACE-L group. Treatment-related AEs led to treatment interruption and discontinuation of PD-1 inhibitor in 10 (24.4%) and 6 (14.6%) patients in the TACE-L-P group, respectively. Discontinuation of both lenvatinib and PD-1 inhibitor because of AEs occurred in only 2 patients (4.9%).

DISCUSSION

Our study showed that TACE-L-P conferred a significant survival benefit when compared with TACE-L in patients with advanced HCC. This finding was associated with an increase in median OS from 12.1 months to 16.9 months, which might be attributed to the higher ORR and DCR and the longer PFS achieved in patients receiving TACE-L-P rather than TACE-L. Multivariate analyses also revealed that combining PD-1 inhibitor on the basis of TACE-L was an independent predictor for prolonged OS and PFS. These results indicated that the triple combination treatment of TACE-L-P might be a superior treatment option in advanced HCC patients. The reasons might be as follows: 1) TACE lead to an extensive local necrosis of the tumor and may subsequently elicit anticancer immune responses that may be further boosted with PD-1 inhibitors (10, 21). 2) Lenvatinib is a multikinase inhibitor with antiproliferative and antiangiogenitic activities (22), which may counteract the hypoxia-induced angiogenesis after TACE

(9, 10) and can regulate the tumor immune microenvironment and enhance immune response of PD-1 inhibitor in HCC (22, 23). Therefore, the combination of TACE, lenvatinib and PD-1 inhibitor may bring about a synergistic antitumor activity, contributing to improved clinical outcomes in advanced HCC patients.

Previous studies (29, 30) have assessed the combination of TACE, lenvatinib and PD-1 inhibitor for patients with unresectable HCC and reported a PFS of 11.4-13.3 months and an OS of 23.6-24.0 months, which seemed much longer than those for the patients treated with TACE-L-P in our study. However, it was worth noting that these studies enrolled a large proportion (25.0%-54.5%) of patients with HCC at BCLC stage B, who were expected to achieve better outcomes than those with BCLC stage C HCC in the present study. Additionally, the heavier tumor burden the patients borne in our study (largest tumor size of 12.3 ± 4.8 cm and a considerable proportion of patients with >3 intrahepatic tumors, bilobar tumor distribution, main portal vein invasion or extrahepatic metastasis) might also lead to a limited survival benefit of treatment. But then again, compared with TACE-L, TACE-L-P did provide a significant improvement in survival for the HCC patients with advanced disease.

In our study, the presence of main portal vein invasion or extrahepatic metastasis was identified as the independent risk factor for survival. These results were consistent with previous studies (31–34) and further confirmed that main portal vein invasion or extrahepatic spread had a profound adverse effect on prognosis in HCC patients. More notably, in subgroup analyses, a prolonged OS was observed with the treatment of TACE-L-P not in patients with main portal vein invasion but in those without main portal vein invasion, which implied that TACE-L-P might be better employed for HCC patients before the main portal trunk was involved so that an improved survival could be achieved. Furthermore, subgroup analyses also showed that TACE-L-P provided a better OS than TACE-L in the patients with extrahepatic metastasis or tumor number >3 but not in those with no extrahepatic metastasis or tumor number ≤3. The reasons might be that TACE exerted its antitumor property mainly by controlling intrahepatic lesions rather than extrahepatic metastases (9) and its effect on multiple tumors was also limited (35). Thus, a treatment strategy combining TACE with a more potent systemic therapy was urgently needed for patients with extrahepatic metastasis or multiple tumors. Our results revealed the necessity of the additional treatment with PD-1 inhibitor to TACE-L for such patients.

In our study, all the AEs with the combination of TACE and lenvatinib with/without PD-1 inhibitor were manageable and consistent with previously reported data on each individual treatment (7, 10, 12, 36). There were no new or unexpected AEs observed. Additionally, the incidence and severity of AEs in TACE-L-P group were comparable to those in TACE-L group. These results suggested that both the treatments of TACE-L-P and TACE-L were tolerable and combining PD-1 inhibitor with TACE-L did not significantly increase the risk of AEs compared with TACE-L, which revealed an acceptable safety profile of TACE-L-P.

In the present study, three different PD-1 inhibitors were used for the treatment of patients in TACE-L-P group. Although our results suggested that the tumor responses, survival and incidence of AEs in the patients treated with sintilimab were similar to those in the patients treated with tislelizumab/camrelizumab, the inconformity of treatment with these PD-1 inhibitors and its potential effects on treatment outcomes remained to be concerned. Additionally, our study had some other limitations. First, this study was a retrospective study, and the treatment option was individually determined based on the preference of the attending physician and the patient, which inevitably resulted in selection bias. Second, the sample size of this study was limited. The results of subgroup analyses should be cautiously interpreted. Consequently, validation of our findings by further randomized trials is necessary.

In conclusion, our study showed safety and promising outcomes with the treatment of TACE-L-P in patients with advanced HCC. These patients could benefit from TACE-L-P and had markedly better treatment responses and improved survival in comparison with TACE-L. These findings need to be confirmed in large sample, prospective randomized controlled trials.

DATA AVAILABILITY STATEMENT

The raw data supporting the conclusions of this article will be made available by the authors, without undue reservation.

ETHICS STATEMENT

The studies involving human participants were reviewed and approved by the Clinical Research and Application Ethics Committee of the Second Affiliated Hospital of Guangzhou Medical University. The patients/participants provided their written informed consent to participate in this study.

AUTHOR CONTRIBUTIONS

MC, WH, and JH conceived and designed the study with supervision from KZ. MC, WH, YG, JWZ, and KZ provided the provision of study materials or patients. WS, LCL, LTL, BC, YC, and JZ collected and assembled the data. MC, JH, and WS performed or supervised analyses. MC, WH, and KZ interpreted the results. MC, JH, and KZ wrote the manuscript. All authors reviewed the manuscript and approved the final version.

FUNDING

This work was supported by the National Natural Science Foundation of China (81873920, 82001930, 82001929), the Science and Technology Project of Guangzhou, China

(202002030135, 202102010082), the High-Level University Clinical Research Promotion Program of Guangzhou Medical University (B185004019), and the Doctoral Scientific Research Fund of the Second Affiliated Hospital of Guangzhou Medical University (010G271073).

SUPPLEMENTARY MATERIAL

The Supplementary Material for this article can be found online at: https://www.frontiersin.org/articles/10.3389/fimmu.2022.848387/full#supplementary-material

REFERENCES

1. Sung H, Ferlay J, Siegel RL, Laversanne M, Soerjomataram I, Jemal A, et al. Global Cancer Statistics 2020: GLOBOCAN Estimates of Incidence and Mortality Worldwide for 36 Cancers in 185 Countries. *CA Cancer J Clin* (2021) 71(3):209–49. doi: 10.3322/caac.21660
2. Zhou J, Sun H, Wang Z, Cong W, Wang J, Zeng M, et al. Guidelines for the Diagnosis and Treatment of Hepatocellular Carcinoma (2019 Edition). *Liver Cancer* (2020) 9(6):682–720. doi: 10.1159/000509424
3. Benson AB, D'Angelica MI, Abbott DE, Anaya DA, Anders R, Are C, et al. Hepatobiliary Cancers, Version 2.2021, NCCN Clinical Practice Guidelines in Oncology. *J Natl Compr Canc Netw* (2021) 19(5):541–65. doi: 10.6004/jnccn.2021.0022
4. European Association for the Study of the Liver. EASL. Clinical Practice Guidelines: Management of Hepatocellular Carcinoma. *J Hepatol* (2018) 69 (1):182–236. doi: 10.1016/j.jhep.2018.03.019
5. Llovet JM, Ricci S, Mazzaferro V, Hilgard P, Gane E, Blanc JF, et al. Sorafenib in Advanced Hepatocellular Carcinoma. *N Engl J Med* (2008) 359(4):378–90. doi: 10.1056/NEJMoa0708857
6. Cheng AL, Kang YK, Chen Z, Tsao CJ, Qin S, Kim JS, et al. Efficacy and Safety of Sorafenib in Patients in the Asia-Pacific Region With Advanced Hepatocellular Carcinoma: A Phase III Randomised, Double-Blind, Placebo-Controlled Trial. *Lancet Oncol* (2009) 10(1):25–34. doi: 10.1016/S1470-2045(08)70285-7
7. Kudo M, Finn RS, Qin S, Han KH, Ikeda K, Piscaglia F, et al. Lenvatinib Versus Sorafenib in First-Line Treatment of Patients With Unresectable Hepatocellular Carcinoma: A Randomised Phase 3 non-Inferiority Trial. *Lancet* (2018) 391(10126):1163–73. doi: 10.1016/S0140-6736(18)30207-1
8. Cai M, Li B, Lin L, Huang J, An Y, Huang W, et al. A Reduction and pH Dual-Sensitive Nanodrug for Targeted Theranostics in Hepatocellular Carcinoma. *Biomater Sci* (2020) 8(12):3485–99. doi: 10.1039/d0bm00295j
9. Kishore SA, Bajwa R, Madoff DC. Embolotherapeutic Strategies for Hepatocellular Carcinoma: 2020 Update. *Cancers (Basel)* (2020) 12(4):791. doi: 10.3390/cancers12040791
10. Chang Y, Jeong SW, Young JJ, Jae KY. Recent Updates of Transarterial Chemoembolilzation in Hepatocellular Carcinoma. *Int J Mol Sci* (2020) 21 (21):8165. doi: 10.3390/ijms21218165
11. Choi GH, Shim JH, Kim MJ, Ryu MH, Ryoo BY, Kang YK, et al. Sorafenib Alone Versus Sorafenib Combined With Transarterial Chemoembolization for Advanced-Stage Hepatocellular Carcinoma: Results of Propensity Score Analyses. *Radiology* (2013) 269(2):603–11. doi: 10.1148/radiol.13130150
12. Zhu K, Chen J, Lai L, Meng X, Zhou B, Huang W, et al. Hepatocellular Carcinoma With Portal Vein Tumor Thrombus: Treatment With Transarterial Chemoembolization Combined With Sorafenib–A Retrospective Controlled Study. *Radiology* (2014) 272(1):284–93. doi: 10.1148/radiol.14131946
13. Fu Z, Li X, Zhong J, Chen X, Cao K, Ding N, et al. Lenvatinib in Combination With Transarterial Chemoembolization for Treatment of Unresectable Hepatocellular Carcinoma (uHCC): A Retrospective Controlled Study. *Hepatol Int* (2021) 15(3):663–75. doi: 10.1007/s12072-021-10184-9
14. Geschwind JF, Kudo M, Marrero JA, Venook AP, Chen XP, Bronowicki JP, et al. TACE Treatment in Patients With Sorafenib-Treated Unresectable Hepatocellular Carcinoma in Clinical Practice: Final Analysis of GIDEON. *Radiology* (2016) 279(2):630–40. doi: 10.1148/radiol.2015150667
15. Cheng AL, Hsu C, Chan SL, Choo SP, Kudo M. Challenges of Combination Therapy With Immune Checkpoint Inhibitors for Hepatocellular Carcinoma. *J Hepatol* (2020) 72(2):307–19. doi: 10.1016/j.jhep.2019.09.025
16. Yau T, Park JW, Finn RS, Cheng A, Mathurin P, Edeline J, et al. CheckMate 459: A Randomized, Multi-Center Phase III Study of Nivolumab (NIVO) vs Sorafenib (SOR) as First-Line (1L) Treatment in Patients (Pts) With Advanced Hepatocellular Carcinoma (aHCC). *Ann Oncol* (2019) 30(suppl 5):v874–5. doi: 10.1093/annonc/mdz394.029
17. Finn RS, Ryoo BY, Merle P, Kudo M, Bouattour M, Lim HY, et al. Pembrolizumab As Second-Line Therapy in Patients With Advanced Hepatocellular Carcinoma in KEYNOTE-240: A Randomized, Double-Blind, Phase III Trial. *J Clin Oncol* (2020) 38(3):193–202. doi: 10.1200/JCO.19.01307
18. Finn RS, Qin S, Ikeda M, Galle PR, Ducreux M, Kim TY, et al. Atezolizumab Plus Bevacizumab in Unresectable Hepatocellular Carcinoma. *N Engl J Med* (2020) 382(20):1894–905. doi: 10.1056/NEJMoa1915745
19. Ren Z, Xu J, Bai Y, Xu A, Cang S, Du C, et al. Sintilimab Plus a Bevacizumab Biosimilar (IBI305) Versus Sorafenib in Unresectable Hepatocellular Carcinoma (ORIENT-32): A Randomised, Open-Label, Phase 2-3 Study. *Lancet Oncol* (2021) 22(7):977–90. doi: 10.1016/S1470-2045(21)00252-7
20. Finn RS, Ikeda M, Zhu AX, Sung MW, Baron AD, Kudo M, et al. Phase Ib Study of Lenvatinib Plus Pembrolizumab in Patients With Unresectable Hepatocellular Carcinoma. *J Clin Oncol* (2020) 38(26):2960–70. doi: 10.1200/JCO.20.00808
21. Cheu JW, Wong CC. Mechanistic Rationales Guiding Combination Hepatocellular Carcinoma Therapies Involving Immune Checkpoint Inhibitors. *Hepatology* (2021) 74(4):2264–76. doi: 10.1002/hep.31840
22. Kimura T, Kato Y, Ozawa Y, Kodama K, Ito J, Ichikawa K, et al. Immunomodulatory Activity of Lenvatinib Contributes to Antitumor Activity in the Hepa1-6 Hepatocellular Carcinoma Model. *Cancer Sci* (2018) 109(12):3993–4002. doi: 10.1111/cas.13806
23. Yi C, Chen L, Lin Z, Liu L, Shao W, Zhang R, et al. Lenvatinib Targets FGF Receptor 4 to Enhance Antitumor Immune Response of Anti–Programmed Cell Death-1 in HCC. *Hepatology* (2021) 74(5):2544–60. doi: 10.1002/hep.31921
24. Zhou J, Sun HC, Wang Z, Cong WM, Wang JH, Zeng MS, et al. Guidelines for Diagnosis and Treatment of Primary Liver Cancer in China (2017 Edition). *Liver Cancer* (2018) 7(3):235–60. doi: 10.1159/000488035
25. Liu Y, Huang W, He M, Lian H, Guo Y, Huang J, et al. Efficacy and Safety of CalliSpheres((R)) Drug-Eluting Beads Transarterial Chemoembolization in Barcelona Clinic Liver Cancer Stage C Patients. *Oncol Res* (2019) 27(5):565–73. doi: 10.3727/096504018X15313896322888
26. Lencioni R, de Baere T, Burrel M, Caridi JG, Lammer J, Malagari K, et al. Transcatheter Treatment of Hepatocellular Carcinoma With Doxorubicin-Loaded DC Bead (DEBDOX): Technical Recommendations. *Cardiovasc Intervent Radiol* (2012) 35(5):980–5. doi: 10.1007/s00270-011-0287-7
27. Lencioni R, de Baere T, Soulen MC, Rilling WS, Geschwind JF. Lipiodol Transarterial Chemoembolization for Hepatocellular Carcinoma: A Systematic Review of Efficacy and Safety Data. *Hepatology* (2016) 64 (1):106–16. doi: 10.1002/hep.28453
28. Gaba RC, Lewandowski RJ, Hickey R, Baerlocher MO, Cohen EI, Dariushnia SR, et al. Transcatheter Therapy for Hepatic Malignancy: Standardization of Terminology and Reporting Criteria. *J Vasc Interv Radiol* (2016) 27(4):457–73. doi: 10.1016/j.jvir.2015.12.752
29. Liu J, Li Z, Zhang W, Lu H, Sun Z, Wang G, et al. Comprehensive Treatment of Trans-Arterial Chemoembolization Plus Lenvatinib Followed by Camrelizumab for Advanced Hepatocellular Carcinoma Patients. *Front Pharmacol* (2021) 12:709060. doi: 10.3389/fphar.2021.709060
30. Cao F, Yang Y, Si T, Luo J, Zeng H, Zhang Z, et al. The Efficacy of TACE Combined With Lenvatinib Plus Sintilimab in Unresectable Hepatocellular Carcinoma: A Multicenter Retrospective Study. *Front Oncol* (2021) 11:783480. doi: 10.3389/fonc.2021.783480
31. Cheng S, Yang J, Shen F, Zhou W, Wang Y, Cong W, et al. Multidisciplinary Management of Hepatocellular Carcinoma With Portal Vein Tumor

Thrombus - Eastern Hepatobiliary Surgical Hospital Consensus Statement. *Oncotarget* (2016) 7(26):40816–29. doi: 10.18632/oncotarget.8386
32. Huang JJ, Cai MY, Huang WS, Guo YJ, Zhou JW, Liang LC, et al. Transarterial Chemoembolization Combined With Sorafenib and Iodine-125 Seed Brachytherapy for Hepatocellular Carcinoma With Portal Vein Tumor Thrombus: A Retrospective Controlled Study. *Chin Med J (Engl)* (2021) 135 (1):113–5. doi: 10.1097/CM9.0000000000001537
33. Natsuizaka M, Omura T, Akaike T, Kuwata Y, Yamazaki K, Sato T, et al. Clinical Features of Hepatocellular Carcinoma With Extrahepatic Metastases. *J Gastroenterol Hepatol* (2005) 20(11):1781–7. doi: 10.1111/j.1440-1746.2005.03919.x
34. Labeur TA, Berhane S, Edeline J, Blanc JF, Bettinger D, Meyer T, et al. Improved Survival Prediction and Comparison of Prognostic Models for Patients With Hepatocellular Carcinoma Treated With Sorafenib. *Liver Int* (2020) 40(1):215–28. doi: 10.1111/liv.14270
35. Miyayama S, Kikuchi Y, Yoshida M, Yamashiro M, Sugimori N, Ikeda R, et al. Outcomes of Conventional Transarterial Chemoembolization for Hepatocellular Carcinoma ≥10 Cm. *Hepatol Res* (2019) 49(7):787–98. doi: 10.1111/hepr.13335
36. Sangro B, Chan SL, Meyer T, Reig M, El-Khoueiry A, Galle PR. Diagnosis and Management of Toxicities of Immune Checkpoint Inhibitors in Hepatocellular Carcinoma. *J Hepatol* (2020) 72(2):320–41. doi: 10.1016/j.jhep.2019.10.021

Conflict of Interest: The authors declare that the research was conducted in the absence of any commercial or financial relationships that could be construed as a potential conflict of interest.

Publisher's Note: All claims expressed in this article are solely those of the authors and do not necessarily represent those of their affiliated organizations, or those of the publisher, the editors and the reviewers. Any product that may be evaluated in this article, or claim that may be made by its manufacturer, is not guaranteed or endorsed by the publisher.

frontiers in Immunology

SYSTEMATIC REVIEW
published: 02 March 2022
doi: 10.3389/fimmu.2022.801909

Efficacy and Safety of Anti-PD1/PDL1 in Advanced Biliary Tract Cancer: A Systematic Review and Meta-Analysis

Qi Jiang[1,2,3†], Jinsheng Huang[1,2,3†], Bei Zhang[1,2,3], Xujia Li[1,2,3], Xiuxing Chen[4], Bokang Cui[2,3,5], Shengping Li[2,3,5] and Guifang Guo[1,2,3*]*

[1] VIP Department, Sun Yat-sen University Cancer Center, Guangzhou, China, [2] State Key Laboratory of Oncology in South China, Sun Yat-sen University Cancer Center, Guangzhou, China, [3] Collaborative Innovation Center for Cancer Medicine, Sun Yat-sen University Cancer Center, Guangzhou, China, [4] Guangdong Provincial Key Laboratory of Malignant Tumor Epigenetics and Gene Regulation, Department of Medical Oncology, Sun Yat-sen Memorial Hospital, Sun Yat-sen University, Guangzhou, China, [5] Department of Pancreaticobiliary Surgery, Sun Yat-sen University Cancer Center, Guangzhou, China

OPEN ACCESS

Edited by:
Hongda Liu,
Nanjing Medical University, China

Reviewed by:
Alessandra Bettiol,
University of Florence, Italy
Alessandro Rizzo,
National Cancer Institute Foundation (IRCCS), Italy
Yasuo Hamamoto,
Keio University School of Medicine, Japan

***Correspondence:**
Guifang Guo
guogf@sysucc.org.cn
Shengping Li
lishp@sysucc.org.cn

[†]These authors have contributed equally to this work and share first authorship

Specialty section:
This article was submitted to Cancer Immunity and Immunotherapy, a section of the journal Frontiers in Immunology

Received: 26 October 2021
Accepted: 03 February 2022
Published: 02 March 2022

Citation:
Jiang Q, Huang J, Zhang B, Li X, Chen X, Cui B, Li S and Guo G (2022) Efficacy and Safety of Anti-PD1/PDL1 in Advanced Biliary Tract Cancer: A Systematic Review and Meta-Analysis. Front. Immunol. 13:801909. doi: 10.3389/fimmu.2022.801909

Background: Anti-programmed cell death protein 1 and its ligand (anti-PD1/PDL1) have been proposed as a promising therapeutic option for advanced biliary tract cancer (aBTC). Given the scarce quantitative analyses of anti-PD1/PDL1 in aBTC, we thus did a meta-analysis to assess the benefits and risks of this emerging treatment strategy in patients with aBTC.

Methods: PubMed, Embase, the Cochrane Library, Web of Science, and meeting resources were searched for relevant studies. The main endpoints were median progression-free survival (mPFS), median overall survival (mOS), objective response rate (ORR), disease control rate (DCR), any-grade adverse events (AEs), and grade 3–4 AEs.

Results: Twenty-eight studies with 1,338 participants were included. The best curative effect was found in the anti-PD1/PDL1 combined with anti-CTLA4 and chemotherapy group (mPFS: 12.4 months; mOS: 16.0 months; ORR: 45.1%; DCR: 95.0%), followed by the anti-PD1/PDL1 plus chemotherapy group (mPFS: 8.2 months; mOS: 14.8 months; ORR: 36.3%; DCR: 84.6%), the anti-PD1/PDL1 plus antiangiogenesis group (mPFS: 4.9 months; mOS: 10.2 months; ORR: 17.5%; DCR: 68.7%), the anti-PD1/PDL1 plus anti-cytotoxic T lymphocyte antigen 4 (anti-CTLA4) group (mPFS: 2.9 months; mOS: 8.3 months; ORR: 9.9%; DCR: 36.8%), and the anti-PD1/PDL1 monotherapy group (mPFS: 2.5 months; mOS: 7.6 months; ORR: 6.8%; DCR: 34.7%). Compared with anti-PD1-containing regimens, anti-PDL1-containing regimens achieved preferable mPFS (11.1 vs. 3.8 months), mOS (12.2 vs. 9.8 months), and ORR (23.7% vs. 17.4%), despite a similar DCR (61.1% vs. 61.3%). The mPFS, mOS, ORR, and DCR were 10.6 months, 15.8 months, 42.3%, and 88.6% of first-line anti-PD1/PDL1 and 3.0 months, 9.1 months, 11.6%, and 51.1% of second-line therapy or beyond, respectively. There were 80.6% and 34.0% of the patients suffering any-grade AEs and grade 3–4 AEs. Anti-PD1/PDL1 monotherapy might be considered as a safer alternative

than combination regimens. Meanwhile, obvious toxicities in the first-line setting could not be neglected.

Conclusions: Anti-PD1/PDL1 showed encouraging efficacy and acceptable safety profile in aBTC and, thus, could be an alternative treatment.

Keywords: biliary tract cancer (BTC), anti-PD1, anti-PDL1, anti-CTLA4, antiangiogenesis, chemotherapy, meta-analysis

INTRODUCTION

Biliary tract cancer (BTC), including intrahepatic cholangiocarcinoma (ICC), extrahepatic cholangiocarcinoma, and gallbladder cancer, is a heterogeneous group of malignant tumors that arises from the epithelium of the bile duct or gallbladder. The incidence of BTC, which accounts for roughly 10%–15% of hepatobiliary malignancies, is increasing progressively worldwide (1–3). Unfortunately, BTC carries a poor prognosis with a 5-year survival rate between 5% and 18%. Diagnosing BTC at an early stage remains elusive given its insidious onset and strong invasion, which poses a barrier to prompt surgical intervention, the only potentially curative treatment for BTC (4). Even for patients suitable for surgery, radical resection rate is still low and relapse rate cannot be ignored (5). Accordingly, palliative chemotherapy remains the mainstay of treatment for the majority of patients suffering BTC. The ABC-02 and ABC-06 studies demonstrated the antitumor effects of gemcitabine plus cisplatin (GemCis) and modified fluorouracil plus oxaliplatin (mFOLFOX), respectively, which established GemCis as first-line therapy and mFOLFOX as second-line therapy (6, 7). Notwithstanding the above, the exact benefits of the recognized chemotherapy regimens are still dismal. Furthermore, beyond the second line, no standard chemotherapy regimen has emerged.

Immune checkpoint inhibitor (ICI) has the power to restore T-cell-mediated tumor cell killing and deplete regulatory T cells (Treg) by blocking immune checkpoint molecules like programmed cell death protein 1 (PD1), programmed cell death ligand 1 (PDL1), and cytotoxic T lymphocyte antigen 4 (CTLA4) (8, 9). This ability has earned extensive interest from researchers. The past decade has yielded tremendous insights into the antitumor activity of PD1/PDL1 antibodies, which has scored marvelous achievements in a range of solid tumors such as melanoma, non-small cell lung cancer, renal cell carcinoma, bladder cancer, and Hodgkin's lymphoma (10–14). Upregulation of PD1 or PDL1 has been observed in BTC tumor tissues, justifying the use of anti-PD1/PDL1 in BTC (15–17). On the other hand, considerable attention has also been paid to the limited objective response rate (ORR) and acquired resistance of anti-PD1/PDL1 monotherapy (18, 19). That is why it is desirable to exploit efficient combination regimens with PD1/PDL1 inhibitors for BTC.

The addition of anti-CTLA4 to anti-PD1/PDL1 may have an enhanced efficacy on T-cell-mediated antitumor responses through non-redundant immune checkpoint blockade (20). The clinical benefits of this combination have been demonstrated in melanoma, renal cell carcinoma, and colorectal cancer (21–23). Meanwhile, the combination of anti-PD1/PDL1 and antiangiogenesis is another treatment regimen worth looking forward to. Apart from overexpression of vascular endothelial growth factor found in 53% ICC, antiangiogenic therapy also has synergistic effects with anti-PD1/PDL1 in the treatment of cancer through reducing Treg and immunosuppressive cytokines as well as converting the complex tumor microenvironment (24–27). Anti-PDL1 plus bevacizumab has shown amazing efficacy for hepatocellular carcinoma in the IMbrave150 study (28). What is more, conventional chemotherapy may enhance both innate and adaptive immunity and help recover immunosurveillance, supporting the rationale of using anti-PD1/PDL1 combined with chemotherapy (29, 30).

Herein, we did a meta-analysis for the following purposes: 1) to delineate the role of anti-PD1/PDL1 in advanced biliary tract cancer (aBTC), either as monotherapy or in combination with other therapies; 2) to make a comparison between anti-PD1 and anti-PDL1; and 3) to figure out the differences between first-line therapy and second-line therapy or beyond.

MATERIALS AND METHODS

This meta-analysis was performed in accordance with the Preferred Reporting Items for Systematic Reviews and Meta-Analyses (PRISMA) guidelines. This study was not registered.

Search Strategy

We systematically retrieved literature published from database inception up until May 7, 2021, by searching PubMed, Embase, the Cochrane Library, and Web of Science. There were no limitations on language, region, age, and duration of follow-up. We searched the following combined Medical Subject Headings (MeSH) terms and text word: "Biliary Tract Cancers," "Cholangiocarcinomas," "Gallbladder Cancers," "PD1," and "PDL1." The search strategy used for PubMed is available in **Supplementary File 1**. In addition, reference lists of reviews and meeting resources (including abstracts and posters) of the American Society of Clinical Oncology (ASCO) and European Society of Medicine Oncology (ESMO) until September 30, 2021, were also scanned through manual search.

Selection Criteria

The inclusion criteria were as follows: 1) prospective or retrospective clinical studies; 2) patients diagnosed with aBTC and treated with anti-PD1/PDL1, either as monotherapy or combined with antiangiogenensis, anti-CTLA4, or chemotherapy; and 3) studies reporting any of the following outcomes: progression-free survival

(PFS), overall survival (OS), ORR, disease control rate (DCR), any-grade adverse events (AEs), and grade 3–4 AEs.

The exclusion criteria were as follows: 1) editorials, letters, reviews, and case reports; 2) cell or animal experiments; 3) anti-PD1/PDL1 combined with drugs other than antiangiogenensis, anti-CTLA4, or chemotherapeutic agents; 4) no results provided or outcomes not relevant; and 5) duplicate studies.

Quality Assessment

Thirteen studies consisted of 11 prospective studies (31–41) and 2 retrospective studies (42, 43), which were assessed by the Risk Of Bias In Non-randomized Studies of Interventions (ROBINS-I) (44) and the JBI critical appraisal tool for case series (45), respectively. There were 14 studies [1 randomized study (46), 2 non-randomized comparative studies (47, 48), 10 single-arm studies (49–58), and 1 retrospective study (59)] with no full text available, which is why we gave up the corresponding quality assessments. What is more, we also did not assess the quality of one study reporting safety run-in results of a randomized, two-arm, non-comparative trial (60) due to the paucity of validated evaluation tools designed for this kind of trial.

Data Extraction

Data extraction was performed independently by two investigators (QJ and XL) whose disagreements would be settled by further discussion with a third investigator (GG). The following information from each study was recorded: first author, publication year, region, study type, median follow-up, disease status, drug, clinical setting, line of therapy, sample size, median age, gender, efficacy outcomes [including median progression-free survival (mPFS), 6-month PFS and 12-month PFS, median overall survival (mOS), 6-month OS, 12-month OS, ORR, DCR, complete response (CR), partial response (PR), stable disease (SD)], and safety outcomes (including any-grade AEs and grade 3–4 AEs). We used the package digitize of software R version 3.6.3 for obtaining survival data from the Kaplan–Meier curves (K-M curves). The number at risk, number censored, and number of events were estimated based on the method proposed by Tierney et al. (61).

Statistical Analysis

The pooled estimates of ORR, DCR, CR, PR, SD, any-grade AEs, and grade 3–4 AEs were calculated using STATA SE version 15. Besides subgroup analyses, we also provided pooled results after omitting studies that may be the source of heterogeneity. Heterogeneity across studies was evaluated by the Cochran Q chi-square test and I^2 statistic, with P <0.1 for the Q test deemed to have high heterogeneity and I^2 >50% regarded as an indicator of moderate-to-high heterogeneity. If separate verdicts from the Q test and I^2 statistic were at opposite poles, we would give priority to the conclusion from the I^2 statistic since the former is proverbially underpowered to detect heterogeneity (62). The robustness of the results was checked by sensitivity analyses. Funnel plots were drawn to evaluate publication bias. Moreover, Egger's test was used to assess funnel plot asymmetry and P <0.1 indicated significant publication bias. Of note, the sensitivity of Egger's test decreases when the number of included data was smaller than 20 (63), in which case we did not perform Egger's test. Differences between groups were tested by the chi-square test using IBM SPSS Statistics 22.0, with two-sided P-value <0.05 considered significant.

The pooled K-M curves were plotted and analyzed using the package MetaSurv of software R version 3.6.3 (64). Heterogeneity was assessed by H statistic, with H <1.2 considered as being indicative of insignificant heterogeneity (65).

The fixed-effects model was used for analysis on the premise of low heterogeneity between studies; otherwise, the random-effects model was applied to pooled results.

RESULTS

Study Selection and Characteristics

As shown in **Figure 1**, 887 studies were obtained through database searching and an additional five studies were found in other sources (reference lists of reviews, ASCO meetings, and ESMO meetings). Therefore, a total of 892 studies were identified. After removing duplicates, screening the title and abstract of the remaining studies, and assessing potentially relevant studies in detail, 28 studies were included in this meta-analysis.

Twenty-eight studies involved 1,338 participants and 34 sets of data (five studies had more than one subgroup of interest (39, 43, 47, 48, 60), and we distinguished different subgroups by numbers, such as Oh2020[1], Oh2020[2], and Oh2020[3]). **Tables 1**, **2** provide details of the baseline characteristics and main outcomes of the included studies, respectively.

Quality Assessment

Thirteen studies were performed with quality appraisal (**Supplementary Table 1**). Eleven prospective studies [including 1 non-randomized comparative study (39) and 10 single-arm studies (31–38, 40, 41)] evaluated by ROBINS-I were all at moderate risk of bias, thereby meeting the inclusion criteria. Two retrospective studies (42, 43) assessed by the JBI tool were also included in this meta-analysis.

Efficacy

Anti-PD1/PDL1 Monotherapy or in Combination With Other Therapies

The pooled K-M curves were built by data extracted from published K-M curves in 19 included studies (31–43, 47, 48, 50, 51, 54, 55). The pooled mPFS was 5.9 months (95% CI 5.2 to 6.6), and the estimated PFS rates were 49.5% at 6 months and 25.9% at 12 months (**Figure 2A**). The pooled mOS was 10.9 months (95% CI 10.1 to 11.7), and the 6- and 12-month OS rates were 70.4% and 45.2%, respectively (**Figure 3A**).

Among patients treated with anti-PD1/PDL1 monotherapy, the pooled mPFS was 2.5 months (95% CI 2.2 to 2.8), and the estimated PFS rates were 26.0% at 6 months and 14.4% at 12 months. The anti-PD1/PDL1 plus anti-CTLA4 group ended up with a similar mPFS of 2.9 months (95% CI 2.3 to 4.5), and the 6- and 12-month PFS rates were 27.5% and 8.1%, respectively. For patients receiving anti-PD1/PDL1 plus antiangiogenesis, the pooled mPFS was 4.9 months (95% CI 3.9 to 6.2), and the estimated PFS rates were 43.8% at 6 months and 17.0% at 12 months. For patients taking anti-PD1/PDL1 plus chemotherapy, the pooled mPFS was

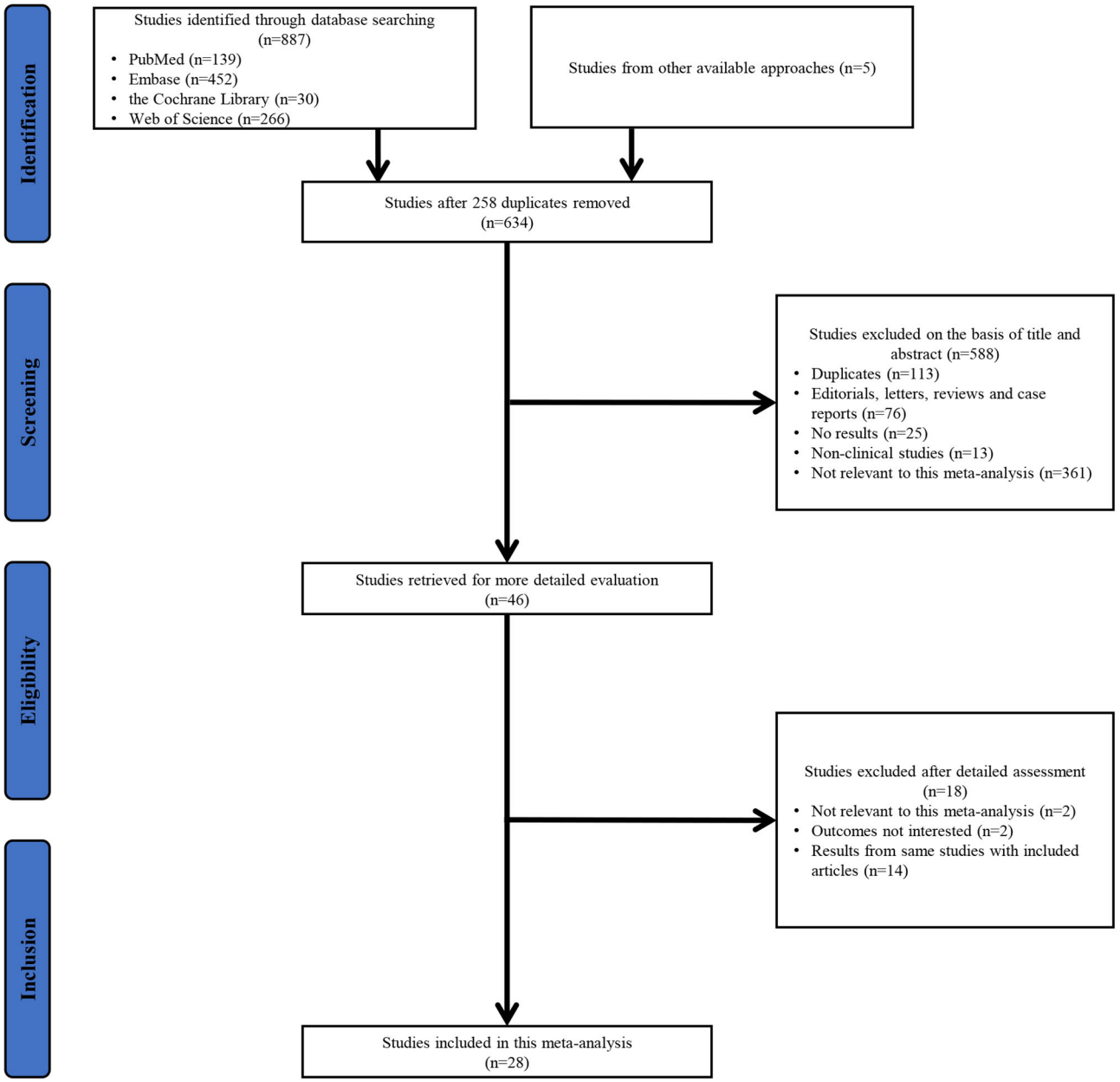

FIGURE 1 | PRISMA flowchart of the study selection process. PRISMA, Preferred Reporting Items for Systematic Reviews and Meta-Analyses.

8.2 months (95% CI 6.4 to 9.7), and the estimated PFS rates were 63.1% at 6 months and 26.9% at 12 months. Anti-PD1/PDL1 combined with anti-CTLA4 and chemotherapy elicited a longer mPFS of 12.4 months (95% CI 9.7 to 15.0), and the 6- and 12-month PFS rates were 83.8% and 51.9%, respectively (**Figure 2B**).

A similar trend was found in mOS. Anti-PD1/PDL1 monotherapy and anti-PD1/PDL1 plus anti-CTLA4 were very much similar [7.6 months (95% CI 6.4 to 9.2) vs. 8.3 months (95% CI 5.9 to 10.8)]. Anti-PD1/PDL1 plus antiangiogenesis reported a longer mOS of 10.2 months (95% CI 7.6 to 12.2), while the most impressive mOS was observed in anti-PD1/PDL1 plus chemotherapy with or without anti-CTLA4 [anti-PD1/PDL1 + chemotherapy + anti-CTLA4: 16.0 months (95% CI 11.9 to 19.1); anti-PD1/PDL1 + chemotherapy: 14.8 months (95% CI 12.3 to 17.5)]. The 6- and 12-month OS rates were 57.2% and 32.2% in anti-PD1/PDL1 monotherapy, 59.8% and 37.0% in anti-PD1/PDL1 plus anti-CTLA4, 68.7% and 43.2% in anti-PD1/PDL1 plus antiangiogenesis, 89.0% and 62.0% in anti-PD1/PDL1 plus chemotherapy, and 87.5% and 63.3% in anti-PD1/PDL1 combined with anti-CTLA4 and chemotherapy, respectively (**Figure 3B**).

In 28 studies reporting ORR (31–43, 46–60), the pooled ORR was 19.3%. The pooled ORRs of anti-PD1/PDL1 monotherapy,

TABLE 1 | Baseline characteristics of included studies with anti-PD1/PDL1 in aBTC.

Study	Region	Study type	Median follow-up, months	Disease status	Drug	Clinical setting	Line of therapy	Sample size	Median age (range), years	Male, %
Kim et al. (32)/ NCT02829918	USA	Open-label, multi-institutional, single-group, phase 2	12.4	Advanced refractory BTC	Nivolumab	240 mg, i.v., Q2W for 16 weeks, and then 480 mg, i.v., Q4W	2nd line and beyond	54	65 (28–86)	50
Ueno et al. (39)/ JapicCTI-153098	Japan	Open-label, multicenter, non-randomized, phase 1	5.1	Unresectable or recurrent BTC	1) Nivolumab	240 mg, i.v., Q2W	2nd line and beyond	30	68.0	60
			8.2	Unresectable or recurrent BTC	2) Nivolumab + GemCis	Nivolumab 240 mg, i.v., Q2W + cisplatin 25 mg/m^2, i.v. + gemcitabine 1,000 mg/m^2, i.v.	1st-line	30	67.5	47
Lee et al. (42)	Korea	Multicenter retrospective study	3.8	PDL1-positive GemCis-refractory BTC	Pembrolizumab	200 mg, i.v., Q3W	2nd line and beyond	51	66 (43–83)	56.9
Kang et al. (33)/ NCT03695952	Korea	Single-center, prospective cohort study	9.6	PDL1-positive advanced refractory BTC	Pembrolizumab	200 mg, i.v., Q3W	2nd line and beyond	40	61 (41–76)	57.5
KEYNOTE-028/ NCT02054806 (40, 41)	NR	Open-label, multicenter, non-randomized, phase 1b	5.7	aBTC	Pembrolizumab	10 mg/kg, Q2W for ≤2 years	2nd line and beyond	24	64 (43–70)	58.3
KEYNOTE-158/ NCT02628067 (40)	NR	Open-label, multicenter, non-randomized, phase 2	7.5	aBTC	Pembrolizumab	200 mg, Q3W	2nd line and beyond	104	63 (34–81)	49.0
Sun et al. (43)	China	Single-center, retrospective study	NR	aBTC	1) PD1 inhibitor monotherapy	NR	2nd line and beyond	20	NR	55
			NR	aBTC	2) PD1 inhibitor + chemotherapy	NR	2nd line and beyond	38	NR	63.2
Yarchoan et al. (46)/ NCT03201458	USA	Randomized, open-label, multicenter, phase 2	NR	aBTC	atezolizumab	840 mg, i.v., Q2W	2nd line and beyond	39	NR	NR
Ioka et al. (48)/ NCT01938612	Asia	Open-label, multicenter, phase 1	NR	aBTC	1) Durvalumab	10 mg/kg, Q2W	2nd line and beyond	42	64	NR
			NR	aBTC	2) Durvalumab + tremelimumab	durvalumab 20 mg/kg + tremelimumab 1.0 mg/kg, Q4W	2nd line and beyond	65	62	NR
Yoo et al. (31)/ NCT02699515	Japan, Korea, Taiwan	Open-label, phase 1	15.3	Metastatic or locally advanced BTC	Bintrafusp alpha	1,200 mg, i.v., Q2W	2nd line and beyond	30	67	63
Merck et al. (49)/ NCT03833661	NR	Open-label, multicenter, single-group, phase 2	NR	Locally advanced or metastatic BTC	Bintrafusp alpha	1,200 mg, i.v., Q2W	2nd line	159	NR	NR
Villanueva et al. (51)/ NCT03797326	NR	Open-label, non-randomized, phase 2	NR	aBTC	Pembrolizumab + lenvatinib	Pembrolizumab 200 mg, Q3W + lenvatinib 20 mg, q.d.	2nd line and beyond	31	NR	NR

(Continued)

TABLE 1 | Continued

Study	Region	Study type	Median follow-up, months	Disease status	Drug	Clinical setting	Line of therapy	Sample size	Median age (range), years	Male, %
Lin et al. (35)/ NCT03895970	NR	Single-arm	9.5	aBTC	Pembrolizumab + lenvatinib	Pembrolizumab 200 mg, Q3W (n = 11) or 3 mg/kg, Q3W (n = 21) + lenvatinib 12 mg (body weight ≥ 60 kg) or 8 mg (body weight < 60 kg), p.o., q.d.	2nd line and beyond	32	56.5	56
Arkenau et al. (36)/ NCT02443324	5 countries	Open-label, multicenter, non-randomized, phase 1	15.7	Previously treated advanced or metastatic BTC	Pembrolizumab + ramucirumab	Pembrolizumab 200 mg, i.v., d1, Q3W + ramucirumab 8 mg/kg, i.v., d1, d8	2nd line and beyond	26	63 (36–78)	30.8
Wang et al. (34)/ NCT04642664	China	Open-label, single-center, non-randomized, prospective	13.4	Previously treated aBTC	Camrelizumab + apatinib	Camrelizumab 200 mg, i.v., Q3W + apatinib 250 mg, p.o., q.d.	2nd line and beyond	22	60 (39–72)	52.4
Zong et al. (52)/ ChiCTR1900022003	China	Phase 2	8.76	Previously treated aBTC	Sintilimab + anlotinib	Sintilimab 200 mg, i.v., d1, Q3W + anlotinib 12 mg, p.o., d1~d14, Q3W	2nd line	17	59 (43–69)	52.9
Zhou et al. (50)/ NCT03996408	China	Open-label, dose-escalating, dose-expansion, phase 1b	NR	Advanced refractory BTC	TQB2450 + anlotinib	Anlotinib 10 mg and then 12 mg, p.o., d1~d14, Q3W + TQB2450 1,200 mg, i.v., d1, Q3W	2nd line and beyond	25	NR	NR
Sun et al. (53)/ NCT03825705	China	phase 1b	14.9	aBTC	TQB2450 + anlotinib	Anlotinib 10 mg (n = 22) or 12 mg (n = 12), d1~d14, Q3W + TQB2450 1,200 mg, Q3W	2nd line	34	57 (37–72)	44.1
Cousin et al. (54)/ NCT03475953	France	Open-label, multicenter, single-arm, phase 2	9.8	Advanced refractory BTC	Avelumab + regorafenib	Regorafenib 160 mg, q.d., d1~d21, Q4W + avelumab 10 mg/kg, Q2W	2nd line and beyond	34	63 (36–80)	NR
Oh et al. (47)/ NCT03046862	Korea	Phase 2	28.5	Chemo-naive aBTC	1) Durvalumab + tremelimumab + GemCis (biomarker cohort)	Gemcitabine 1,000 mg/m^2 + cisplatin 25 mg/m^2, d1, d8, followed by GemCis + durvalumab 1,120 mg + tremelimumab 75 mg, Q3W	1st line	30	NR	NR
			11.9	Chemo-naive aBTC	2) Durvalumab + tremelimumab + GemCis	NR	1st line	46	NR	NR
			11.3	Chemo-naive aBTC	3) Durvalumab + GemCis	NR	1st line	45	NR	NR
Boileve et al. (60)/ NCT03704480	France	Safety run-in results of the randomized IMMUNOBIL PRODIGE 57 phase 2 trial	NR	aBTC	1) Durvalumab + tremelimumab	Durvalumab 1,500 mg, i.v., d1 + tremelimumab 75 mg, i.v., d1, Q4W	2nd line	10	67 (60–75)	50
			9.8	aBTC	2) Durvalumab + tremelimumab + paclitaxel	Durvalumab 1,500 mg, i.v., d1 + tremelimumab 75 mg, i.v., d1, Q4W + paclitaxel 80 mg/m^2, i.v., d1, d8, d15	2nd line	10	70 (61–75)	70
Floudas et al. (55)/ NCT02821754	USA	Non-randomized, phase 2	NR	aBTC	Durvalumab + tremelimumab	Tremelimumab 75 mg, Q4W + durvalumab 1,500 mg for 4 doses, followed by durvalumab monotherapy 1,500 mg, Q4W	NR	12	NR	NR

(Continued)

TABLE 1 | Continued

Study	Region	Study type	Median follow-up, months	Disease status	Drug	Clinical setting	Line of therapy	Sample size	Median age (range), years	Male, %
Klein et al. (37)/ NCT02923934	Australia	Open-label, multicenter, non-randomized, phase 2	NR	aBTC	Nivolumab + ipilimumab	Nivolumab 3 mg/kg + ipilimumab 1 mg/kg, Q3W for 4 doses, followed by nivolumab monotherapy 3 mg/kg, Q2W	2nd line and beyond	39	65 (37–81)	51
Chiang et al. (58)/ NCT04172402	Taiwan	Single arm, phase 2	6.4	aBTC	Nivolumab + GS	Nivolumab 240 mg + gemcitabine 800 mg/m^2, d1 + S-1 80/100/120 mg, q.d., d1~d10, Q2W	1st line	48	66 (30–80)	46
Liu et al. (56)/ NCT03796429	China	Open-label, phase 2	10	aBTC	Toripalimab + GS	Toripalimab 240 mg, i.v., Q3W + gemcitabine 1,000 mg/m^2, i.v., d1, d8 + S-1 40–60 mg, b.i.d. * 14 days, Q3W	1st line	39	64	48.7
Chen et al. (38)/ NCT03486678	China	Open-label, single-arm, phase 2	11.8	aBTC	Camrelizumab + GEMOX	Camrelizumab 3 mg/kg, total dose ≤200 mg, i.v. drip, d1 + gemcitabine 800 mg/m^2, i.v. drip, d1 + oxaliplatin 85 mg/m^2, i.v. drip, d2, Q2W	1st line	37	64 (41–74)	70.3
Qin et al. (57)/ NCT0309289	China	Multicenter, single-arm, phase 2	NR	aBTC	Camrelizumab + FOLFOX4 or GEMOX	Camrelizumab 3 mg/kg, i.v., Q2W + typical FOLFOX4 or GEMOX	1st line	43	NR	NR
Gou et al. (59)	China	Retrospective study	NR	aBTC	PD1 inhibitors + nab-paclitaxel + S-1	NR	1st line	32	NR	NR

PD1, programmed cell death protein 1; PDL1, programmed cell death ligand 1; aBTC, advanced biliary tract cancer; BTC, biliary tract cancer; USA, United States; GemCis, gemcitabine + cisplatin; S-1, tegafur-gimeracil-oteracil; GS, gemcitabine + tegafur-gimeracil-oteracil; GEMOX, gemcitabine + oxaliplatin; FOLFOX4, fluorouracil + leucovorin + oxaliplatin; i.v., intravenously; i.v. drip, intravenous drips; p.o., orally; q.d., once daily; b.i.d., twice daily; Q2W, every 2 weeks; Q3W, every 3 weeks; Q4W, every 4 weeks; d1, day 1; d2, day 2; d8, day 8; d10, day 10; d14, day 14; d15, day 15; d21, day 21; 1st, first; 2nd, second; NR, not reported.

TABLE 2 | Main outcomes extracted from included studies with anti-PD1/PDL1 in aBTC.

Study	Sample size	mPFS (95% CI), months	6m-PFS, %	12m-PFS, %	mOS (95% CI), months	6m-OS, %	12m-OS, %	ORR, %	DCR, %	CR, %	PR, %	SD, %	Any-grade AEs, %	Grade 3–4 AEs, %
Kim et al. (32)/ NCT02829918	54	3.68 (2.3–5.69)	NR	NR	14.24 (5.98–NE)	NR	NR	11	50	0	11	39	NR	17
Ueno et al. (39)/	(1) 30	1.4 (1.4–1.4)	NR	NR	5.2 (4.5–8.7)	NR	NR	3	23	0	3	20	57	10
JapicCTI-153098	(2) 30	4.2 (2.8–5.6)	NR	NR	15.4 (11.8–NE)	NR	NR	37	63	0	37	27	100	90
Lee et al. (42)	51	2.1 (1.7–2.4)	NR	NR	6.9 (5.4–8.3)	NR	NR	9.8	35.3	0	9.8	25.5	58.8	7.8
Kang et al. (33)/ NCT03695952	40	1.5 (0.0–3.0)	13.1	NR	4.3 (3.5–5.1)	27.5	NR	10.0	47.5	0	10.0	37.5	20.5	0
KEYNOTE-028/ NCT02054806 (40, 41)	24	1.8 (1.4–3.1)	13.0	13.0	5.7 (3.1–9.8)	45.8	20.8	13.0	26.1	0	13.0	13.0	66.7	16.7
KEYNOTE-158/ NCT02628067 (40)	104	2.0 (1.9–2.1)	11.4	5.2	7.4 (5.5–9.6)	56.4	32.7	5.8	22.1	0	5.8	16.3	54.8	12.5
Sun et al. (43)	(1) 20	2.2 (1.10–3.30)	NR	NR	4.1 (2.79–5.42)	NR	NR	0	65	0	0	65	20.0	5.0
	(2) 38	5.1 (3.59–6.61)	NR	NR	14.9 (10.73–19.07)	NR	NR	34.2	89.5	7.9	26.3	55.3	76.3	34.2
Yarchoan et al. (46)/ NCT03201458	39	1.87	NR	NR	NR	NR	NR	2.9	32.4	0	2.9	29.4	NR	NR
Ioka et al. (48)/	(1) 42	NR	NR	NR	8.1 (5.6–10.1)	NR	NR	4.8	16.7	0	4.8	11.9	64	NR
NCT01938612	(2) 65	NR	NR	NR	10.1 (6.2–11.4)	NR	NR	10.8	32.2	0	10.8	21.5	82	NR
Yoo et al. (31)/ NCT02699515	30	2.5 (1.3–5.6)	32	24	12.7 (6.7–15.7)	73	52	20	40	7	13	20	63	37

(Continued)

TABLE 2 | Continued

Study	Sample size	mPFS (95% CI), months	6m-PFS, %	12m-PFS, %	mOS (95% CI), months	6m-OS, %	12m-OS, %	ORR, %	DCR, %	CR, %	PR, %	SD, %	Any-grade AEs, %	Grade 3–4 AEs, %
Merck et al. (49)/ NCT03833661	159	NR	NR	NR	NR	NR	NR	10.1	NR	NR	NR	NR	NR	NR
Villanueva et al. (51)/ NCT03797326	31	6.1 (2.1–6.4)	NR	NR	8.6 (5.6–NE)	NR	NR	10	68	0	10	58	97	48
Lin et al. (35)/ NCT03895970	32	4.9 (4.7–5.2)	33.7	6.25	11.0 (9.6–12.3)	71.9	39.4	25	78.1	0	25	53	100	62.5
Arkenau et al. (36)/ NCT02443324	26	1.64 (1.38–2.76)	18.0	NR	6.44 (4.17–13.27)	61.8	30.0	3.8	38.5	0	3.8	34.6	NR	38.5
Wang et al. (34)/ NCT04642664	22	4.4 (2.4–6.3)	NR	NR	13.1 (8.1–18.2)	NR	NR	19.0	71.4	0	19.0	52.3	100	63.6
Zong et al. (52)/ ChiCTR1900022003	17	6.5 (3.6–9.4)	NR	NR	Not reached	NR	NR	40.0	86.7	NR	NR	46.7	70.6	NR
Zhou et al. (50)/ NCT03996408	25	8	NR	NR	NR	NR	NR	41.67	75	12.5	29.2	33.3	83.3	16.7
Sun et al. (53)/ NCT03825705	34	5.95 (3.78–11.50)	NR	NR	NR	NR	64.71	11.8	76.5	0	11.8	64.7	NR	NR
Cousin et al. (54)/ NCT03475953	34	2.5 (1.9–5.5)	NR	NR	11.9 (6.2–NE)	NR	NR	13.8	51.7	0	13.8	37.9	NR	NR
Oh et al. (47)/	(1) 30	13.0	NR	NR	15.0	NR	NR	50.0	96.7	NR	NR	46.7	NR	NR
NCT03046862	(2) 46	11.9	NR	NR	20.7	NR	NR	73.3	97.8	NR	NR	23.9	NR	NR
	(3) 45	11.0	NR	NR	18.1	NR	NR	73.4	100	NR	NR	26.7	NR	NR
Boileve et al. (60)/	(1) 10	NR	NR	NR	NR	NR	NR	NR	NR	NR	NR	NR	NR	40
NCT03704480	(2) 10	NR	NR	NR	NR	NR	NR	10	60	10	0	50	NR	60
Floudas et al. (55)/ NCT02821754	12	3.1 (0.8–4.6)	NR	NR	5.45 (4.60–8.3)	NR	NR	0	41.7	0	0	41.7	NR	NR
Klein et al. (37)/ NCT02923934	39	2.9 (2.2–4.6)	NR	NR	5.7 (2.7–11.9)	NR	NR	23	44	0	23	21	NR	NR
Chiang et al. (58)/ NCT04172402	48	8.0 (5.8–not reached)	NR	NR	Not reached (10.7–not reached)	NR	NR	41.7	87.5	NR	NR	45.8	NR	NR
Liu et al. (56)/ NCT03796429	39	6.7	NR	NR	NR	NR	NR	20.6	85.3	0	20.6	64.7	NR	NR
Chen et al. (38)/ NCT03486678	37	6.1 (5.1–6.8)	50	NR	11.8 (8.3–15.4)	NR	NR	54	89	0	54	35	97	70
Qin et al. (57)/ NCT03092895	47	NR	NR	NR	NR	NR	NR	7.0	67.4	NR	NR	60.5	NR	NR
Gou et al. (59)	32	5.43	NR	NR	NR	NR	NR	25	84.3	NR	NR	59.4	NR	NR

All patients in most studies were evaluated except that the tumor responses were 46/54 in the Kim2020 study, 23/24 in the KEYNOTE-028 study, 34/39 in the Yarchoan2020 study, 21/22 in the Wang2021 study, 15/17 in the Zong2021 study, 24/25 in the Zhou2021 study, 29/34 in the Cousin2021 study, 34/39 in the Liu2020 study, and 43/47 in the Qin2019 study; PFS was 23/24 in the KEYNOTE-028 study and 21/22 in the Wang2021 study; OS was 21/22 in the Wang2021 study; and safety results were 39/40 in the Kang2020 study and 24/25 in the Zhou2021 study. Five studies had more than one subgroup of interest. Specifically, patients were allocated to the nivolumab group [Ueno20191)] or the nivolumab/GemCis group [Ueno2019(2)] in the Ueno2019 study; the PD1 inhibitor monotherapy group [Sun2019(1)] or the PD1 inhibitor plus chemotherapy group [Sun2019(2)] in the Sun2019 study; the durvalumab group [Ioka2019(1)] or the durvalumab/tremelimumab group [Ioka2019(2)] in the Ioka2019 study; the biomarker group [receiving durvalumab/tremelimumab with GemCis, [Oh2020(1)], the durvalumab/tremelimumab with GemCis group [Oh2020(2)] or the durvalumab with GemCis group [Oh2020(3)] in the Oh2020 study; the durvalumab/tremelimumab group [Boileve2021(1)] or the durvalumab/tremelimumab with paclitaxel group [Boileve2021(2)] in the Boileve2021 study.

PD1, programmed cell death protein 1; PDL1, programmed cell death ligand 1; aBTC, advanced biliary tract cancer; mPFS, medium progression-free survival; CI, confidence interval; 6m-PFS, 6-month progression-free survival; 12m-PFS, 12-month progression-free survival; mOS, medium overall survival; 6m-OS, 6-month overall survival; 12m-OS, 12-month overall survival; ORR, objective response rate; DCR, disease control rate; CR, complete response; PR, partial response; SD, stable disease; AEs, adverse events; NR, not reported; NE, not estimable; PFS, progression-free survival; OS, overall survival; GemCis, gemcitabine + cisplatin.

anti-PD1/PDL1 plus antiangiogenesis, anti-PD1/PDL1 plus anti-CTLA4, anti-PD1/PDL1 plus chemotherapy, and anti-PD1/PDL1 combined with anti-CTLA4 and chemotherapy were 6.8%, 17.5%, 9.9%, 36.3%, and 45.1% respectively, (**Figure 4A**).

There were 27 studies reporting DCR (31–43, 46–48, 50–60), resulting in a pooled DCR of 61.1%. The pooled DCRs of anti-PD1/PDL1 monotherapy, anti-PD1/PDL1 plus antiangiogenesis, anti-PD1/PDL1 plus anti-CTLA4, anti-PD1/PDL1 plus chemotherapy, and anti-PD1/PDL1 combined with anti-CTLA4 and chemotherapy were 34.7%, 68.7%, 36.8%, 84.6%, and 95.0%, respectively (**Figure 4B**).

CR and PR were reported in 22 studies (31–43, 46, 48, 50, 51, 53–56, 60), while SD was reported in 27 studies (31–43, 46–48, 50–60). The pooled CR, PR, and SD in total and by medication regimen subgroup are recorded in **Table 3**.

Anti-PD1-Containing Regimens and Anti-PDL1-Containing Regimens

Among patients taking anti-PD1-containing regimens, the pooled mPFS was 3.8 months (95% CI 3.0 to 4.3) and the 6- and 12-month PFS rates were 32.9% and 14.2%, respectively. The anti-PDL1-containing regimen group demonstrated a much longer mPFS of

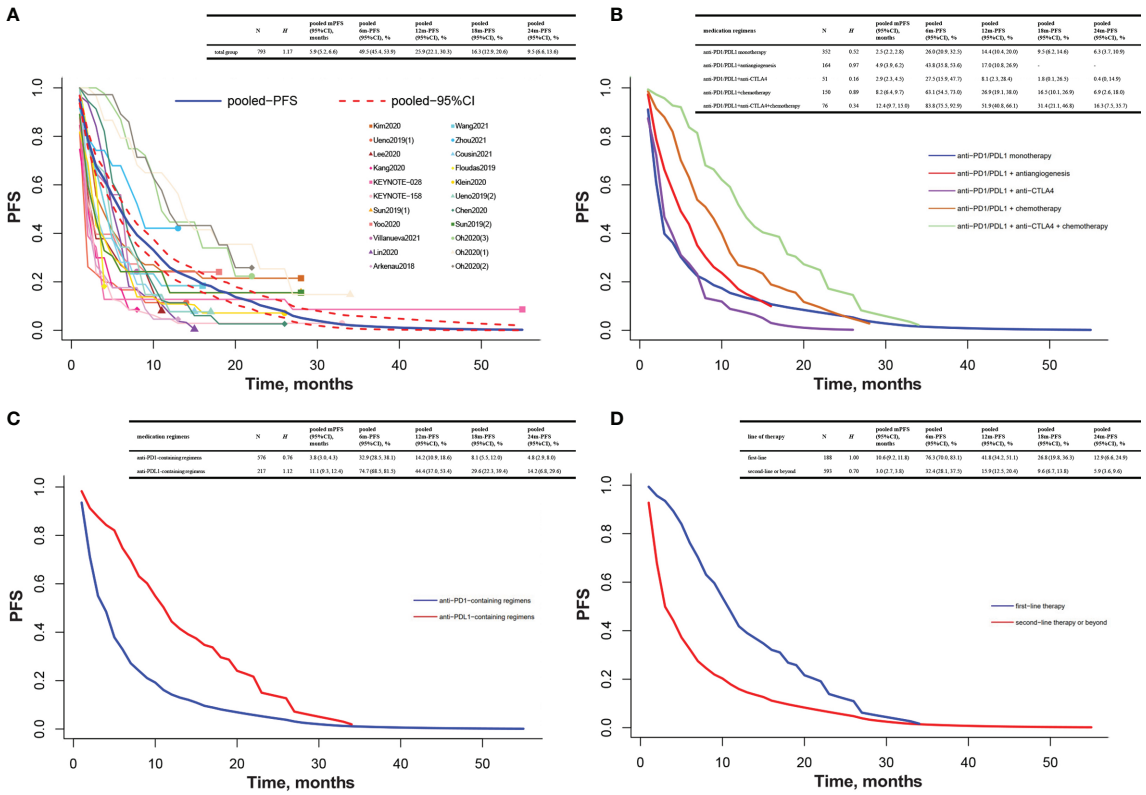

FIGURE 2 | Pooled Kaplan–Meier estimate of PFS. **(A)** Total group; **(B)** anti-PD1/PDL1 monotherapy, anti-PD1/PDL1 combined with antiangiogenesis or anti-CTLA4 or chemotherapy, or combination of anti-PD1/PDL1, anti-CTLA4, and chemotherapy; **(C)** anti-PD1-containing regimens and anti-PDL1-containing regimens; **(D)** first-line therapy and second-line therapy or beyond. Note: Heterogeneity was assessed by *H* statistic, with *H* <1.2 considered as being indicative of insignificant heterogeneity. Three studies had more than one subgroup of interest. Specifically, patients were allocated to the nivolumab group [Ueno2019(1)] or the nivolumab/GemCis group [Ueno2019(2)] in the Ueno2019 study; the PD1 inhibitor monotherapy group [Sun2019(1)] or the PD1 inhibitor plus chemotherapy group [Sun2019(2)] in the Sun2019 study; the biomarker group [receiving durvalumab/tremelimumab with GemCis, [Oh2020(1)], the durvalumab/tremelimumab with GemCis group [Oh2020(2)], or the durvalumab with GemCis group [Oh2020(3)] in the Oh2020 study. PFS, progression-free survival; mPFS, medium progression-free survival; CI, confidence interval; 6m-PFS, 6-month progression-free survival; 12m-PFS, 12-month progression-free survival; 18m-PFS, 18-month progression-free survival; 24m-PFS, 24-month progression-free survival; PD1, programmed cell death protein 1; PDL1, programmed cell death ligand 1; CTLA4, cytotoxic T lymphocyte antigen 4; GemCis, gemcitabine + cisplatin.

11.1 months (95% CI 9.3 to 12.4), and the 6- and 12-month PFS rates were 74.7% and 44.4%, respectively (**Figure 2C**). Furthermore, the gap in mOS between these two regimens was nearly 3 months [9.8 months (95% CI 8.5 to 10.9) vs. 12.2 months (95% CI 10.9 to 14.1)]. The 6- and 12-month OS rates were 65.0% and 41.4% in the anti-PD1-containing regimen group and 78.9% and 50.9% in the anti-PDL1-containing regimen group, respectively (**Figure 3C**).

Eighteen studies (32–43, 51, 52, 56–59) reported the tumor response of anti-PD1-containing regimens, and 10 studies (31, 46–50, 53–55, 60) described that of anti-PDL1-containing regimens. Anti-PDL1-containing regimens yielded a higher ORR than anti-PD1-containing regimens (23.7% vs. 17.4%, *P*-value = 0.005), albeit an unconspicuous disadvantage in DCR (61.1% vs. 61.3%, *P*-value = 0.933). When combined with antiangiogenesis, anti-PDL1 was also superior to anti-PD1 in ORR (20.3% vs. 16.3%, *P*-value = 0.381), but they were equally matched in DCR (68.4% vs. 68.9%, *P*-value = 0.980). On the contrary, despite a narrow victory in ORR (7.6% vs. 6.2%, *P*-value = 0.474), anti-PDL1 monotherapy was defeated by anti-PD1 monotherapy in DCR (28.4% vs. 37.4%, *P*-value = 0.094). The detailed discrepancies between anti-PD1-containing regimens and anti-PDL1-containing regimens are elaborated in **Table 4**.

First-Line Therapy and Second-Line Therapy or Beyond

The mPFS was 10.6 months (95% CI 9.2 to 11.8) for first-line therapy and 3.0 months (95% CI 2.7 to 3.8) for second-line therapy or beyond. The 6- and 12-month PFS rates were 76.3% and 41.8% for first line and 32.4% and 15.9% for second line or beyond (**Figure 2D**). Likewise, the mOS was also longer at first-line settings than at second-line settings or beyond [15.8 months (95% CI 12.7 to 18.2) vs. 9.1 months (95% CI 7.7 to 10.1)]. The 6- and 12-month OS rates were 90.4% and 62.4% for first line and 62.1% and 38.5% for second line or beyond (**Figure 3D**).

A comparison of the tumor response between first line and second line or beyond is shown in **Table 5**. At first-line setting, the ORR was obviously higher than that at second-line setting or beyond (42.3% vs. 11.6%, *P*-value < 0.001). The difference in

DCR was also significant, with a higher rate being observed in first-line therapy than in second-line therapy or beyond (88.6% vs. 51.1%, *P*-value < 0.001).

Safety

There were 14 studies (31, 33–35, 38–43, 48, 50–52) reporting any-grade AEs and 15 studies (31–36, 38–43, 50, 51, 60) reporting grade 3–4 AEs. The overall pooled any-grade AE rate and grade 3–4 AE rate were 80.6% and 34.0% (**Figures 4C, D**). The most frequent any-grade AE was reactive cutaneous capillary endothelial proliferation (RCCEP, 45.1%), followed by hypertension (39.9%), hypoalbuminemia (36.0%), leukopenia (34.0%), decreased appetite (26.2%), and asthenia (25.8%) (**Supplementary Table 2**). Of note, RCCEP and hypoalbuminemia were only reported in two studies using camrelizumab (34, 38). Grade 3–4 AEs that occurred in more than 3% of the patients were hypertension (15.4%), γ-glutamyltransferase increase (9.4%), gastrointestinal hemorrhage (9.3%), elevated bilirubin (8.9%), leukopenia (6.2%), and thrombocytopenia (3.5%) (**Supplementary Table 2**).

Any-grade AEs occurred in 50.5% of the patients in the anti-PD1/PDL1 alone group, 99.4% of the patients taking anti-PD1/PDL1 plus antiangiogenesis, and 94.6% of the patients receiving anti-PD1/PDL1 plus chemotherapy (**Figure 4C**). After omitting two studies using anlotinib (50, 52), the incidence of any-grade AEs in the anti-PD1/PDL1 plus antiangiogenesis group was 99.9% (95% CI 99.4% to 100.4%; I^2 = 0.0%; *P* = 0.605).

Grade 3–4 AEs occurred in 11.5% of the patients treated with anti-PD1/PDL1 monotherapy, 45.5% of the patients taking anti-PD1/PDL1 plus antiangiogenesis, and 65.1% of the patients receiving anti-PD1/PDL1 plus chemotherapy (**Figure 4D**). After omitting one study using anlotinib (50), the incidence of grade 3–4 AEs in the anti-PD1/PDL1 combined with antiangiogenesis group was 53.2% (95% CI 41.6% to 64.9%; I^2 = 38.6%; *P* = 0.180).

At the safety evaluation, there were some differences between anti-PD1-containing regimens and anti-PDL1-containing regimens regarding any-grade AE rate (82.5% vs. 74.2%, *P*-value = 0.017) and grade 3–4 AE rate (33.3% vs. 35.1%,

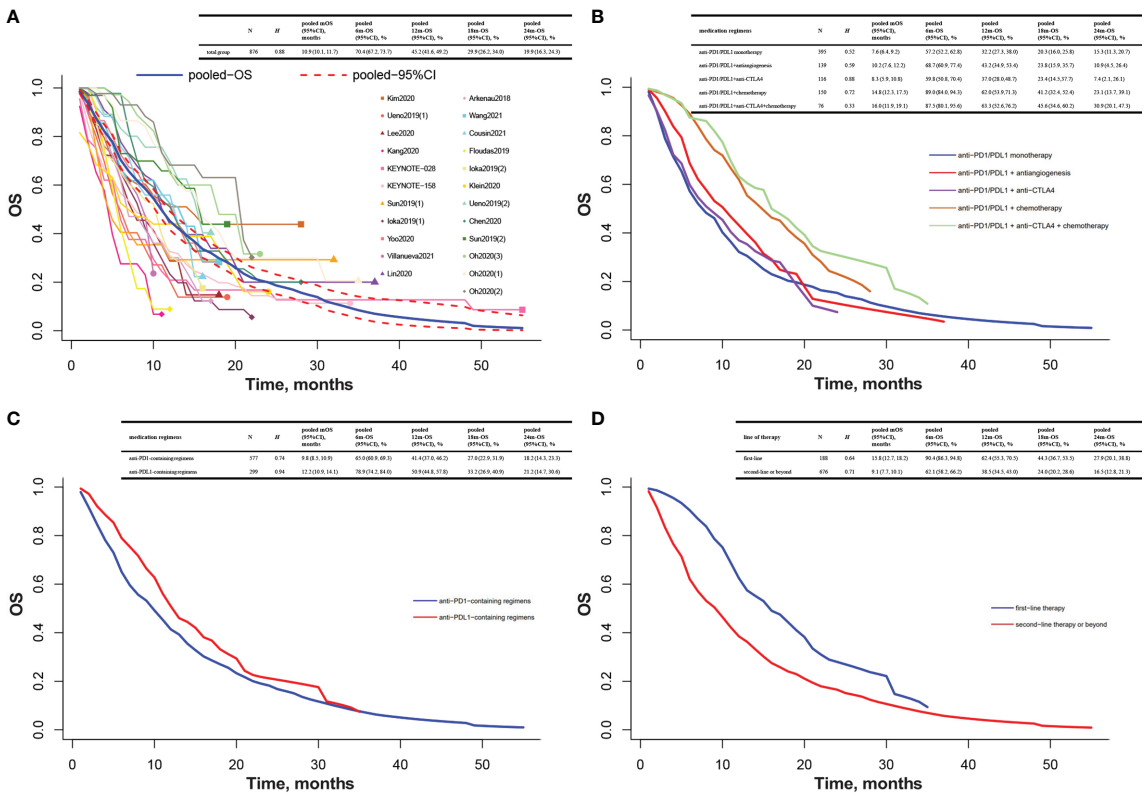

FIGURE 3 | Pooled Kaplan–Meier estimate of OS. **(A)** Total group; **(B)** anti-PD1/PDL1 monotherapy, anti-PD1/PDL1 combined with antiangiogenesis or anti-CTLA4 or chemotherapy, or combination of anti-PD1/PDL1, anti-CTLA4, and chemotherapy; **(C)** anti-PD1-containing regimens and anti-PDL1-containing regimens; **(D)** first-line therapy and second-line therapy or beyond. Heterogeneity was assessed by *H* statistic, with *H* <1.2 considered as being indicative of insignificant heterogeneity. Four studies had more than one subgroup of interest. Specifically, patients were allocated to the nivolumab group [Ueno2019(1)] or the nivolumab/GemCis group [Ueno2019(2)] in the Ueno2019 study; the PD1 inhibitor monotherapy group [Sun2019(1)] or the PD1 inhibitor plus chemotherapy group [Sun2019(2)] in the Sun2019 study; the durvalumab group [Ioka2019(1)] or the durvalumab/tremelimumab group [Ioka2019(2)] in the Ioka2019 study; the biomarker group [receiving durvalumab/tremelimumab with GemCis, Oh2020(1)], the durvalumab/tremelimumab with GemCis group [Oh2020(2)], or the durvalumab with GemCis group [Oh2020(3)] in the Oh2020 study. OS, overall survival; mOS, medium overall survival; CI, confidence interval; 6m-OS, 6-month overall survival; 12m-OS, 12-month overall survival; 18m-OS, 18-month overall survival; 24m-OS, 24-month overall survival; PD1, programmed cell death protein 1; PDL1, programmed cell death ligand 1; CTLA4, cytotoxic T lymphocyte antigen 4; GemCis, gemcitabine + cisplatin.

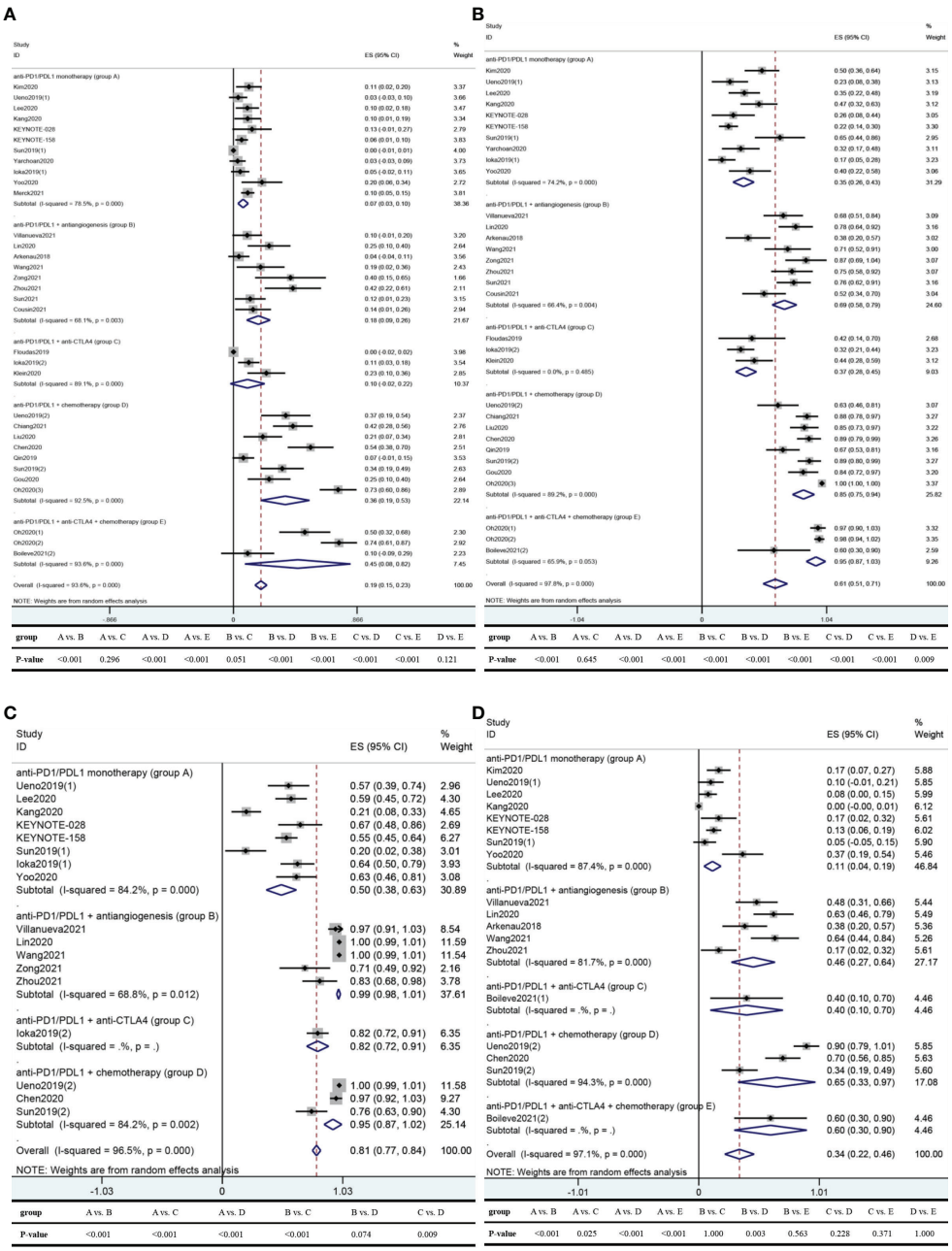

FIGURE 4 | Pooled results of ORR, DCR, any-grade AEs, and grade 3–4 AEs in total and by medication regimen subgroup. **(A)** ORR; **(B)** DCR; **(C)** any-grade AEs; **(D)** grade 3–4 AEs. Five studies had more than one subgroup of interest. Specifically, patients were allocated to the nivolumab group [Ueno2019(1)] or the nivolumab/GemCis group [Ueno2019(2)] in the Ueno2019 study; the PD1 inhibitor monotherapy group [Sun2019(1)] or the PD1 inhibitor plus chemotherapy group [Sun2019(2)] in the Sun2019 study; the durvalumab group [Ioka2019(1)] or the durvalumab/tremelimumab group [Ioka2019(2)] in the Ioka2019 study; the biomarker group [receiving durvalumab/tremelimumab with GemCis, Oh2020(1)], the durvalumab/tremelimumab with GemCis group [Oh2020(2)], or the durvalumab with GemCis group [Oh2020(3)] in the Oh2020 study; the durvalumab/tremelimumab group [Boileve2021(1)] or the durvalumab/tremelimumab with paclitaxel group [Boileve2021(2)] in the Boileve2021 study. Note: Heterogeneity across studies was evaluated by the Cochran *Q* chi-square test and I^2 statistic, with P <0.1 for the *Q* test deemed to have high heterogeneity and I^2 >50% regarded as an indicator of moderate-to-high heterogeneity. If separate verdicts from the *Q* test and I^2 statistic were at opposite poles, we would give priority to the conclusion from the I^2 statistic since the former is proverbially underpowered to detect heterogeneity. Differences between groups were tested by the chi-square test using IBM SPSS Statistics 22.0, with two-sided *P*-value <0.05 considered significant. ORR, objective response rate; DCR, disease control rate; AEs, adverse events; ES, effect size; CI, confidence interval; PD1, programmed cell death protein 1; PDL1, programmed cell death ligand 1; CTLA4, cytotoxic T lymphocyte antigen 4; GemCis, gemcitabine + cisplatin.

TABLE 3 | Pooled results of CR, PR, SD in total and by medication regimens subgroup with anti-PD1/PDL1 in aBTC.

Medication regimens	CR				PR				SD			
	N	ES (95% CI), %	I^2, %	*P*	*N*	ES (95% CI), %	I^2, %	*P*	*N*	ES (95% CI), %	I^2, %	*P*
Anti-PD1/PDL1 monotherapy	420	0.0 (–0.1, 0.2)	0.0	0.989	420	5.9 (2.5, 9.2)	69.8	<0.001	420	26.1 (18.1, 34.1)	74.6	<0.001
Anti-PD1/PDL1 + antiangiogenesis	197	0.0 (–0.2, 0.3)	0.0	0.756	197	13.8 (7.3, 20.3)	49.5	0.065	212	48.0 (39.5, 56.5)	39.5	0.116
Anti-PD1/PDL1 + anti-CTLA4	116	0.0 (–0.2, 0.3)	0.0	0.996	116	9.9 (–2.2, 21.9)	89.1	<0.001	116	22.7 (15.1, 30.2)	0.0	0.379
Anti-PD1/PDL1 + chemotherapy	139	0.0 (–0.3, 0.4)	7.1	0.358	139	33.9 (19.5, 48.3)	72.3	0.013	307	46.5 (35.6, 57.4)	75.8	<0.001
Anti-PD1/PDL1 + anti-CTLA4 + chemotherapy	10	10.0 (–8.6, 28.6)	–	–	10	0.1 (–1.9, 2.1)	–	–	86	37.5 (19.3, 55.7)	63.6	0.064
Overall	882	0.0 (–0.1, 0.1)	0.0	0.995	882	10.1 (7.3, 12.9)	85.1	<0.001	1,141	37.6 (31.6, 43.6)	80.9	<0.001

Heterogeneity across studies was evaluated by the Cochran Q chi-square test and I^2 statistic, with P <0.1 for the Q test deemed to have high heterogeneity and I^2 >50% regarded as an indicator of moderate-to-high heterogeneity. If separate verdicts from the Q test and I^2 statistic were at opposite poles, we would give priority to the conclusion from the I^2 statistic since the former is proverbially underpowered to detect heterogeneity.

CR, complete response; PR, partial response; SD, stable disease; PD1, programmed cell death protein 1; PDL1, programmed cell death ligand 1; aBTC, advanced biliary tract cancer; ES, effect size; CI, confidence interval; CTLA4, cytotoxic T lymphocyte antigen.

P-value = 0.750). Patients taking anti-PDL1 monotherapy were much more likely to have any-grade AEs than patients in the anti-PD1 monotherapy group (63.9% vs. 46.1%, *P*-value = 0.008) (**Table 4**). Heterogeneity for any-grade AEs of the anti-PD1 monotherapy group changed significantly after omitting two single-center studies (33, 43), which resulted in 57.5% (95% CI 50.9% to 64.2%; I^2 = 0.0%; *P* = 0.739). In addition, when Sun2019 (1) (43) was removed, there was no evidence of heterogeneity for grade 3–4 AEs of the anti-PD1 monotherapy group [11.8% (95% CI 7.9% to 15.7%; I^2 = 0.0%; *P* = 0.629)].

TABLE 4 | Pooled results of ORR, DCR, any-grade AEs, and grade 3–4 AEs of anti-PD1-containing regimens or anti-PDL1-containing regimens in aBTC.

Medication regimens	ORR					DCR				
	N	ES (95% CI), %	I^2, %	*P*	*P*-value	*N*	ES (95% CI), %	I^2, %	*P*	*P*-value
Overall					0.005					0.933
Anti-PD1	740	17.4 (11.9, 22.8)	89.8	<0.001		740	61.3 (49.4, 73.1)	93.6	<0.001	
Anti-PDL1	560	23.7 (13.8, 33.6)	96.1	<0.001		401	61.1 (46.6, 75.5)	97.9	<0.001	
Monotherapy					0.474					0.094
Anti-PD1	314	6.2 (1.8, 10.5)	74.9	0.001		314	37.4 (26.1, 48.7)	77.9	<0.001	
Anti-PDL1	265	7.6 (2.3, 12.8)	58.5	0.065		106	28.4 (14.1, 42.8)	65.0	0.058	
Combined with antiangiogenesis					0.381					0.980
Anti-PD1	125	16.3 (5.5, 27.0)	69.6	0.011		125	68.9 (53.7, 84.1)	74.8	0.003	
anti-PDL1	87	20.3 (5.2, 35.5)	72.1	0.028		87	68.4 (53.3, 83.4)	59.8	0.083	
Combined with anti-CTLA4					0.010					0.301
Anti-PD1	39	23.1 (9.9, 36.3)	–	–		39	43.6 (28.0, 59.2)	–	–	
Anti-PDL1	77	4.8 (-5.6, 15.2)	86.4	0.007		77	33.6 (23.1, 44.2)	0.0	0.543	
Combined with chemotherapy					<0.001					0.002
Anti-PD1	262	30.7 (17.2, 44.2)	86.0	<0.001		262	82.6 (75.9, 89.3)	56.2	0.033	
Anti-PDL1	45	73.3 (60.4, 86.3)	–	–		45	100.0 (99.5, 100.4)	–	–	
Combined with anti-CTLA4 + chemotherapy					–					–
Anti-PD1	–	–	–	–		–	–	–	–	
Anti-PDL1	86	45.1 (8.1, 82.1)	93.6	<0.001		86	95.0 (87.0, 103.0)	65.9	0.053	
Medication regimens	**Any-grade AEs**					**Grade 3–4 AEs**				
	N	ES (95% CI), %	I^2, %	*P*	*P*-value	*N*	ES (95% CI), %	I^2, %	*P*	*P*-value
Overall					0.017					0.750
Anti-PD1	475	82.5 (78.8, 86.3)	97.0	<0.001		538	33.3 (19.4, 47.2)	97.6	<0.001	
Anti-PDL1	161	74.2 (63.9, 84.5)	56.1	0.077		74	35.1 (17.6, 52.7)	61.5	0.050	
Monotherapy					0.008					<0.001
Anti-PD1	268	46.1 (30.3, 61.9)	86.4	<0.001		322	9.0 (2.6, 15.4)	84.4	<0.001	
Anti-PDL1	72	63.9 (52.8, 75.0)	0.0	0.934		30	36.7 (19.4, 53.9)	–	–	
Combined with antiangiogenesis					0.001					0.001
Anti-PD1	102	99.7 (98.4, 101.0)	62.8	0.045		111	53.2 (41.6, 64.9)	38.6	0.180	
Anti-PDL1	24	83.3 (68.4, 98.2)	–	–		24	16.7 (1.8, 31.6)	–	–	
Combined with anti-CTLA4					–					–
Anti-PD1	–	–	–	–		–	–	–	–	
Anti-PDL1	65	81.5 (72.1, 91.0)	–	–		10	40.0 (9.6, 70.4)	–	–	
Combined with chemotherapy					–					–
Anti-PD1	105	94.6 (87.0, 102.2)	84.2	0.002		105	65.1 (32.8, 97.5)	94.3	<0.001	
Anti-PDL1	–	–	–	–		–	–	–	–	
Combined with anti-CTLA4 + chemotherapy					–					–
Anti-PD1	–	–	–	–		–	–	–	–	
Anti-PDL1	–	–	–	–		10	60.0 (29.6, 90.4)	–	–	

Heterogeneity across studies was evaluated by the Cochran Q chi-square test and I^2 statistic, with P <0.1 for the Q test deemed to have high heterogeneity and I^2 >50% regarded as an indicator of moderate-to-high heterogeneity. If separate verdicts from the Q test and I^2 statistic were at opposite poles, we would give priority to the conclusion from the I^2 statistic since the former is proverbially underpowered to detect heterogeneity. Differences between groups were tested by the chi-square test using IBM SPSS Statistics 22.0, with two-sided P-value <0.05 considered significant.

ORR, objective response rate; DCR, disease control rate; AEs, adverse events; PD1, programmed cell death protein 1; PDL1, programmed cell death ligand 1; aBTC, advanced biliary tract cancer; ES, effect size; CI, confidence interval; CTLA4, cytotoxic T lymphocyte antigen 4.

We also saw a significant difference between first-line therapy and second-line therapy or beyond in the incidence of any-grade AEs (99.9% vs. 72.2%, *P*-value < 0.001). Additionally, first-line therapy revealed a higher grade 3–4 AE rate than second-line therapy or beyond (80.8% vs. 26.8%, *P*-value < 0.001) (**Table 5**).

Sensitivity Analyses

The sensitivity analyses of pooled estimates of tumor response and safety proved to be robust except any-grade AEs in the total group, in the anti-PD1/PDL1 plus antiangiogenesis group, in the anti-PD1 plus antiangiogenesis group, and in the second-line therapy or beyond. **Supplementary Table 3** offers the pooled results after omitting the study that influenced the robustness of pooled any-grade AEs discussed above.

Publication Bias

Funnel plots and Egger's tests were conducted in tumor response of the total group, ORR of anti-PD1-containing regimens, and ORR and DCR of second-line therapy or beyond (**Supplementary Figure 1**), all of which included no fewer than 20 sets of data. Except for DCR of second-line therapy or beyond ($P = 0.235$), the results of Egger's test represented a possibility of publication bias ($P < 0.001$).

DISCUSSION

To our knowledge, this meta-analysis was the first quantitative analysis to evaluate the efficacy and safety of anti-PD1/PDL1 in aBTC. With a majority of studies being non-comparative, we selectively extracted and analyzed data on survival, tumor response, and safety of the anti-PD1/PDL1 included arm.

On the whole, the pooled mPFS, mOS, ORR, DCR, any-grade AEs, and grade 3–4 AEs of aBTC patients receiving anti-PD1/PDL1 were 5.9 months, 10.9 months, 19.3%, 61.1%, 80.6%, and 34.0%, respectively. Nevertheless, heterogeneity caused by medication regimens and line of therapy came to light through subgroup analyses.

Our results showed that combination regimens with anti-PD1/PDL1 conferred an advantage in PFS, OS, ORR, DCR, PR, and SD over anti-PD1/PDL1 monotherapy. Furthermore, anti-PD1/PDL1 combined with chemotherapy with or without anti-CTLA4 was associated with impressively longer mPFS and mOS than other combination regimens. Likewise, tumor response was also better in this treatment plan. We noticed that the combinations of anti-PD1/PDL1 and chemotherapeutic drugs with or without anti-CTLA4 were mostly used as first-line therapy, while anti-PD1/PDL1 monotherapy or combined with antiangiogenesis or anti-CTLA4 was entirely applied in second-line setting or beyond. Hence, this obvious distinction in efficacy could be partly attributable to the difference in the line of therapy. The compelling safety benefits of anti-PD1/PDL1 monotherapy over combination therapy were observed (*P*-value < 0.05). Despite a slight decrease in the incidence of any-grade AEs compared with anti-PD1/PDL1 plus antiangiogenesis (94.6% vs. 99.4%, *P*-value = 0.074), anti-PD1/PDL1 plus chemotherapy was more likely to develop grade 3–4 AEs (65.1% vs. 45.5%, *P*-value = 0.003). The heterogeneity for any-grade AEs and grade 3–4 AEs of anti-PD1/PDL1 plus antiangiogenesis may result from the use of anlotinib in the Zhou2021 and Zong2021 studies (50, 52), probably because anlotinib is a multitarget tyrosine kinase inhibitor which is known for its more manageable toxicity (66). A phase 3 study of anlotinib plus TQB2450 versus chemotherapy as second-line treatment for aBTC is currently ongoing (NCT04809142).

Overall, anti-PDL1-containing regimens did better than anti-PD1-containing regimens in mPFS (11.1 vs. 3.8 months), mOS (12.2 vs. 9.8 months), ORR (23.7% vs. 17.4%, *P*-value = 0.005), and any-grade AEs (74.2% vs. 82.5%, *P*-value = 0.017), while no significant differences in DCR and grade 3–4 AEs were noted (*P*-value = 0.933 for DCR and *P*-value = 0.750 for grade 3–4 AEs). When used as monotherapy or combined with antiangiogenesis, the differences in ORR and DCR were also insignificant. Intriguingly, the comparison of any-grade AEs between single-agent anti-PD1 and anti-PDL1 was in stark contrast to the overall situation, with a trend favoring anti-PD1 monotherapy (46.1% vs. 63.9%, *P*-value = 0.008). We next sought to probe into the reasons for this phenomenon. Firstly, a much higher any-grade AE rate (>94%) exists in anti-PD1/PDL1 plus antiangiogenesis or chemotherapy (**Figure 4C**). Secondly, from the forest plot of any-grade AEs (**Supplementary Figure 2**), the weight of these two combinations in anti-PDL1-containing regimens was far smaller than that in anti-PD1-containing regimens (23.27% vs. 72.38%). Hence, we fostered

TABLE 5 | Pooled results of ORR, DCR, any-grade AEs, and grade 3–4 AEs by line of therapy subgroup in aBTC.

Line of therapy subgroup	ORR				DCR				Any-grade AEs				Grade 3–4 AEs			
	N	ES (95% CI), %	I^2, %	*P*	*N*	ES (95% CI), %	I^2, %	*P*	*N*	ES (95% CI), %	I^2, %	*P*	*N*	ES (95% CI), %	I^2, %	*P*
First-line therapy	345	42.3 (24.0, 60.6)	94.2	<0.001	345	88.6 (82.6, 94.5)	87.2	<0.001	67	99.9 (99.3, 100.6)	0.0	0.320	67	80.8 (61.5, 100.1)	77.8	0.034
Second-line therapy or beyond	943	11.6 (7.9, 15.2)	82.9	<0.001	784	51.1 (40.4, 61.8)	91.5	<0.001	569	72.2 (67.0, 77.3)	97.0	<0.001	545	26.8 (17.7, 35.9)	93.6	<0.001
P-value		<0.001				<0.001				<0.001				<0.001		

Heterogeneity across studies was evaluated by the Cochran Q chi-square test and I^2 statistic, with P <0.1 for the Q test deemed to have high heterogeneity and I^2 >50% regarded as an indicator of moderate-to-high heterogeneity. If separate verdicts from the Q test and I^2 statistic were at opposite poles, we would give priority to the conclusion from the I^2 statistic since the former is proverbially underpowered to detect heterogeneity. Differences between groups were tested by the chi-square test using IBM SPSS Statistics 22.0, with two-sided P-value <0.05 considered significant.

ORR, objective response rate; DCR, disease control rate; AEs, adverse events; aBTC, advanced biliary tract cancer; ES, effect size; CI, confidence interval.

the suspicion that the difference in weight gave anti-PDL1-containing regimens an advantage in any-grade AEs over anti-PD1-containing regimens. Regrettably, due to insufficiency of studies, it is utterly premature to jump to the conclusion that anti-PDL1 has an advantage over anti-PD1 in safety when combined with other therapies. For the same reason, the comparisons of tumor response between anti-PD1 and anti-PDL1, when combined with anti-CTLA4 or chemotherapy with or without anti-CTLA4, are getting nowhere. Six studies (33, 39–43) reporting any-grade AEs and seven studies (32, 33, 39–43) reporting grade 3–4 AEs of anti-PD1 monotherapy demonstrated significant heterogeneity, which may be due to the difference between the single-center design of Kang2020 and Sun2019(1) (33, 43) and the multicenter design of the remaining studies. There are several ongoing multicenter phase 3 trials regarding the combination of anti-PD1/PDL1 and chemotherapy in aBTC, such as pembrolizumab plus GemCis (NCT04924062; NCT04003636), durvalumab plus GemCis (NCT03875235), and KN035 plus gemcitabine/oxaliplatin (NCT03478488). We are looking forward to these results.

Regardless of medication regimens, the pooled mPFS, mOS, ORR, DCR, and grade 3–4 AE rate of first-line anti-PD1/PDL1 were 10.6 months, 15.8 months, 42.3%, 88.6%, and 80.8%, which seemed to exhibit superior tumor growth suppression but a greater risk compared with the GemCis group (mPFS: 8.0 months; mOS: 11.7 months; ORR: 26.1%; DCR: 81.4%; grade 3–4 AE rate: 70.7%) (6). The combined toxicity of anti-PD1/PDL1 and chemotherapy took the responsibility for the greater occurrence of AEs in the immunotherapy group. Compared with mFOLFOX (7), anti-PD1/PDL1 serving as second-line therapy or beyond offered potentially preferable efficacy and more satisfactory safety (mOS: 6.2 vs. 9.1 months; ORR: 5% vs. 11.6%; DCR: 33% vs. 51.1%; any-grade AE rate: 99% vs. 72.2%; grade 3–4 AE rate: 60% vs. 26.8%). The unnaturally greater risk of first-line anti-PD1/PDL1 than second-line therapy or beyond might be attributed to its zero weight of the monotherapy group which enjoyed lower incidence of AEs.

So far, there has been no large-scale, phase 3, randomized controlled trial verifying the benefits and risks of the abovementioned regimens in aBTC. Moreover, biomarkers capable of predicting the response to anti-PD1/PDL1 remain understudied, making the identification of reliable biomarkers a pressing task (17). The low incidence of BTC goes against the initiation of clinical trials of large scale, so we recommend multicenter collaborative efforts to bridge the major knowledge gaps. In this meta-analysis, we strictly followed the PRISMA guidelines, made the most efficient use of the available clinical studies, and conducted subgroup analyses as much as possible. We believe this article will generate more powerful evidence on when and how to prescribe anti-PD1/PDL1 for patients with aBTC.

Admittedly, our study still had some limitations. First of all was high heterogeneity which may be caused by methodological and clinical diversities between studies. On the one hand, the design of the included studies differed in several ways, such as the number of centers involved, clinical phase, duration of follow-up, and sample size. Additionally, with most of the studies being single arm, the comparison was based on data from the population with a different baseline, so comparability between studies was somewhat limited. On the other hand, baseline characteristics of participants differed greatly in that BTC is a heterogeneous group of malignancies. Considerable differences of epidemiology, biology, and management exist among the anatomical subtypes (4). Moreover, there were varied clinical interventions such as diverse medication regimens and different lines of therapy, which is why we performed subgroup analyses. The second one was publication bias primarily coming from the overwhelming preferences of sponsors, periodicals, and researchers for positive results. What is more, the significant between-study heterogeneity was another contributing factor to publication bias (63).

CONCLUSIONS

The head-to-head comparative trials concerning anti-PD1/PDL1 in BTC are consistently scarce in the context of increasing incidence of this tumor. Hence, it was timely and necessary to conduct this meta-analysis. Although further studies with control groups are warranted to confirm the efficacy and safety of anti-PD1/PDL1, our findings unequivocally lend support to the use of this treatment in patients with aBTC.

DATA AVAILABILITY STATEMENT

The original contributions presented in the study are included in the article/**Supplementary Material**. Further inquiries can be directed to the corresponding authors.

AUTHOR CONTRIBUTIONS

GG, QJ, and JH designed the study. QJ and XL screened the studies and extracted the data. Quality of evidence was judged by JH and BZ. XC and BC analyzed and interpreted the data. QJ and JH prepared the figures and drafted the manuscript. SL and GG contributed to the review and editing. All authors approved the final version of the article, including the authorship list.

FUNDING

This study was funded by the Guangdong Provincial Natural Science Foundation (grant no. 2021A1515012368).

SUPPLEMENTARY MATERIAL

The Supplementary Material for this article can be found online at: https://www.frontiersin.org/articles/10.3389/fimmu.2022.801909/full#supplementary-material

Supplementary Figure 1 | Funnel plots depicting the publication bias in included studies. **(A)** ORR of total group; **(B)** DCR of total group; **(C)** CR of total group; **(D)** PR of total group; **(E)** SD of total group; **(F)** ORR of anti-PD1-containing regimens; **(G)** ORR of second line therapy or beyond; **(H)** DCR of second line therapy or beyond. ORR, objective response rate; DCR, disease control rate; CR, complete response; PR, partial response; SD, stable disease; PD1, programmed cell death protein 1.

Supplementary Figure 2 | Forest plot of any-grade AEs in anti-PD1-containing regimens and anti-PDL1-containing regimens. **(A)** Anti-PD1-containing regimens; **(B)** anti-PDL1-containing regimens. Three studies had more than one subgroup of interest. Specifically, patients were allocated to nivolumab group [Ueno2019(1)] or nivolumab/GemCis group [Ueno2019(2)] in Ueno2019 study; PD1 inhibitor monotherapy group [Sun2019(1)] or PD1 inhibitor plus chemotherapy group [Sun2019(2)] in Sun2019 study; durvalumab group [Ioka2019(1)] or durvalumab/tremelimumab group [Ioka2019(2)] in Ioka2019 study. Heterogeneity across studies was evaluated by the Cochran *Q* chi-square test and I^2 statistic, with p<0.1 for the *Q* test deemed to have high heterogeneity and I^2 >50% regarded as an indicator of moderate-to-high heterogeneity. If separate verdicts from the *Q* test and I^2 statistic were at opposite poles, we would give priority to the conclusion from I^2 statistic since the former is proverbially underpowered to detect heterogeneity. AEs, adverse events; ES, effect size; CI, confidence interval; PD1, programmed cell death protein 1; PDL1, programmed cell death ligand 1; CTLA4, cytotoxic T lymphocyte antigen 4; GemCis, gemcitabine + cisplatin.

REFERENCES

1. Asrani SK, Devarbhavi H, Eaton J, Kamath PS. Burden of Liver Diseases in the World. *J Hepatol* (2019) 70(1):151–71. doi: 10.1016/j.jhep.2018.09.014
2. Banales JM, Marin JJG, Lamarca A, Rodrigues PM, Khan SA, Roberts LR, et al. Cholangiocarcinoma 2020: The Next Horizon in Mechanisms and Management. *Nat Rev Gastroenterol Hepatol* (2020) 17(9):557–88. doi: 10.1038/s41575-020-0310-z
3. Are C, Ahmad H, Ravipati A, Croo D, Clarey D, Smith L, et al. Global Epidemiological Trends and Variations in the Burden of Gallbladder Cancer. *J Surg Oncol* (2017) 115(5):580–90. doi: 10.1002/jso.24546
4. Rizvi S, Khan SA, Hallemeier CL, Kelley RK, Gores GJ. Cholangiocarcinoma - Evolving Concepts and Therapeutic Strategies. *Nat Rev Clin Oncol* (2018) 15 (2):95–111. doi: 10.1038/nrclinonc.2017.157
5. Rizzo A, Ricci AD, Brandi G. PD-L1, TMB, MSI, and Other Predictors of Response to Immune Checkpoint Inhibitors in Biliary Tract Cancer. *Cancers* (2021) 13(3):558. doi: 10.3390/cancers13030558
6. Valle J, Wasan H, Palmer DH, Cunningham D, Anthoney A, Maraveyas A, et al. Cisplatin Plus Gemcitabine Versus Gemcitabine for Biliary Tract Cancer. *New Engl J Med* (2010) 362(14):1273–81. doi: 10.1056/NEJMoa0908721
7. Lamarca A, Palmer DH, Wasan HS, Ross PJ, Ma YT, Arora A, et al. Second-Line FOLFOX Chemotherapy Versus Active Symptom Control for Advanced Biliary Tract Cancer (ABC-06): A Phase 3, Open-Label, Randomised, Controlled Trial. *Lancet Oncol* (2021) 22(5):690–701. doi: 10.1016/s1470-2045(21)00027-9
8. Abril-Rodriguez G, Ribas A. SnapShot: Immune Checkpoint Inhibitors. *Cancer Cell* (2017) 31(6):848–.e1. doi: 10.1016/j.ccell.2017.05.010
9. Wei SC, Duffy CR, Allison JP. Fundamental Mechanisms of Immune Checkpoint Blockade Therapy. *Cancer Discovery* (2018) 8(9):1069–86. doi: 10.1158/2159-8290.Cd-18-0367
10. Hamid O, Robert C, Daud A, Hodi FS, Hwu WJ, Kefford R, et al. Safety and Tumor Responses With Lambrolizumab (Anti-PD-1) in Melanoma. *New Engl J Med* (2013) 369(2):134–44. doi: 10.1056/NEJMoa1305133
11. Paz-Ares L, Luft A, Vicente D, Tafreshi A, Gümüş M, Mazières J, et al. Pembrolizumab Plus Chemotherapy for Squamous Non-Small-Cell Lung Cancer. *New Engl J Med* (2018) 379(21):2040–51. doi: 10.1056/NEJMoa1810865
12. Motzer RJ, Escudier B, McDermott DF, George S, Hammers HJ, Srinivas S, et al. Nivolumab Versus Everolimus in Advanced Renal-Cell Carcinoma. *New Engl J Med* (2015) 373(19):1803–13. doi: 10.1056/NEJMoa1510665
13. Powles T, Eder JP, Fine GD, Braiteh FS, Loriot Y, Cruz C, et al. MPDL3280A (Anti-PD-L1) Treatment Leads to Clinical Activity in Metastatic Bladder Cancer. *Nature* (2014) 515(7528):558–62. doi: 10.1038/nature13904
14. Ansell SM, Lesokhin AM, Borrello I, Halwani A, Scott EC, Gutierrez M, et al. PD-1 Blockade With Nivolumab in Relapsed or Refractory Hodgkin's Lymphoma. *New Engl J Med* (2015) 372(4):311–9. doi: 10.1056/NEJMoa1411087
15. Ye Y, Zhou L, Xie X, Jiang G, Xie H, Zheng S. Interaction of B7-H1 on Intrahepatic Cholangiocarcinoma Cells With PD-1 on Tumor-Infiltrating T Cells as a Mechanism of Immune Evasion. *J Surg Oncol* (2009) 100(6):500–4. doi: 10.1002/jso.21376
16. Weinberg BA, Xiu J, Lindberg MR, Shields AF, Hwang JJ, Poorman K, et al. Molecular Profiling of Biliary Cancers Reveals Distinct Molecular Alterations and Potential Therapeutic Targets. *J Gastrointest Oncol* (2019) 10(4):652–62. doi: 10.21037/jgo.2018.08.18
17. Rizzo A, Ricci AD, Brandi G. Recent Advances of Immunotherapy for Biliary Tract Cancer. *Expert Rev Gastroenterol Hepatol* (2021) 15(5):527–36. doi: 10.1080/17474124.2021.1853527
18. Wang D, Lin J, Yang X, Long J, Bai Y, Yang X, et al. Combination Regimens With PD-1/PD-L1 Immune Checkpoint Inhibitors for Gastrointestinal Malignancies. *J Hematol Oncol* (2019) 12(1):42. doi: 10.1186/s13045-019-0730-9
19. Ricci AD, Rizzo A, Brandi G. Immunotherapy in Biliary Tract Cancer: Worthy of a Second Look. *Cancer Control J Moffitt Cancer Center* (2020) 27 (3):1073274820948047. doi: 10.1177/1073274820948047
20. Rizvi NA, Cho BC, Reinmuth N, Lee KH, Luft A, Ahn MJ, et al. Durvalumab With or Without Tremelimumab vs Standard Chemotherapy in First-Line Treatment of Metastatic Non-Small Cell Lung Cancer: The MYSTIC Phase 3 Randomized Clinical Trial. *JAMA Oncol* (2020) 6(5):661–74. doi: 10.1001/jamaoncol.2020.0237
21. Larkin J, Chiarion-Sileni V, Gonzalez R, Grob JJ, Rutkowski P, Lao CD, et al. Five-Year Survival With Combined Nivolumab and Ipilimumab in Advanced Melanoma. *New Engl J Med* (2019) 381(16):1535–46. doi: 10.1056/NEJMoa1910836
22. Motzer RJ, Rini BI, McDermott DF, Arén Frontera O, Hammers HJ, Carducci MA, et al. Nivolumab Plus Ipilimumab Versus Sunitinib in First-Line Treatment for Advanced Renal Cell Carcinoma: Extended Follow-Up of Efficacy and Safety Results From a Randomised, Controlled, Phase 3 Trial. *Lancet Oncol* (2019) 20(10):1370–85. doi: 10.1016/s1470-2045(19)30413-9
23. Overman MJ, Lonardi S, Wong KYM, Lenz HJ, Gelsomino F, Aglietta M, et al. Durable Clinical Benefit With Nivolumab Plus Ipilimumab in DNA Mismatch Repair-Deficient/Microsatellite Instability-High Metastatic Colorectal Cancer. *J Clin Oncol Off J Am Soc Clin Oncol* (2018) 36(8):773–9. doi: 10.1200/jco.2017.76.9901
24. Sia D, Tovar V, Moeini A, Llovet JM. Intrahepatic Cholangiocarcinoma: Pathogenesis and Rationale for Molecular Therapies. *Oncogene* (2013) 32 (41):4861–70. doi: 10.1038/onc.2012.617
25. Terme M, Pernot S, Marcheteau E, Sandoval F, Benhamouda N, Colussi O, et al. VEGFA-VEGFR Pathway Blockade Inhibits Tumor-Induced Regulatory T-Cell Proliferation in Colorectal Cancer. *Cancer Res* (2013) 73(2):539–49. doi: 10.1158/0008-5472.Can-12-2325
26. Motz GT, Coukos G. The Parallel Lives of Angiogenesis and Immunosuppression: Cancer and Other Tales. *Nat Rev Immunol* (2011) 11 (10):702–11. doi: 10.1038/nri3064
27. Fabris L, Sato K, Alpini G, Strazzabosco M. The Tumor Microenvironment in Cholangiocarcinoma Progression. *Hepatol (Baltimore Md)* (2021) 73 Suppl 1 (Suppl 1):75–85. doi: 10.1002/hep.31410
28. Qin S, Ren Z, Feng YH, Yau T, Wang B, Zhao H, et al. Atezolizumab Plus Bevacizumab Versus Sorafenib in the Chinese Subpopulation With Unresectable Hepatocellular Carcinoma: Phase 3 Randomized, Open-Label IMbrave150 Study. *Liver Cancer* (2021) 10(4):296–308. doi: 10.1159/000513486
29. Bracci L, Schiavoni G, Sistigu A, Belardelli F. Immune-Based Mechanisms of Cytotoxic Chemotherapy: Implications for the Design of Novel and Rationale-Based Combined Treatments Against Cancer. *Cell Death Differ* (2014) 21 (1):15–25. doi: 10.1038/cdd.2013.67

30. Lesterhuis WJ, Punt CJ, Hato SV, Eleveld-Trancikova D, Jansen BJ, Nierkens S, et al. Platinum-Based Drugs Disrupt STAT6-Mediated Suppression of Immune Responses Against Cancer in Humans and Mice. *J Clin Invest* (2011) 121(8):3100–8. doi: 10.1172/jci43656
31. Yoo C, Oh Y, Choi HJ, Kudo M, Ueno M, Kondo S, et al. Phase I Study of Bintrafusp Alfa, a Bifunctional Fusion Protein Targeting TGF-Beta and PD-L1, in Patients With Pretreated Biliary Tract Cancer. *J Immunother Cancer* (2020) 8(1):e000564. doi: 10.1136/jitc-2020-000564
32. Kim RD, Chung V, Alese OB, El-Rayes BF, Li D, Al-Toubah TE, et al. A Phase 2 Multi-Institutional Study of Nivolumab for Patients With Advanced Refractory Biliary Tract Cancer. *JAMA Oncol* (2020) 6(6):888–94. doi: 10.1001/jamaoncol.2020.0930
33. Kang J, Jeong JH, Hwang H-S, Lee SS, Park DH, Oh DW, et al. Efficacy and Safety of Pembrolizumab in Patients With Refractory Advanced Biliary Tract Cancer: Tumor Proportion Score as a Potential Biomarker for Response. *Cancer Res Treat* (2020) 52(2):594–603. doi: 10.4143/crt.2019.493
34. Wang D, Yang X, Long J, Lin J, Mao J, Xie F, et al. The Efficacy and Safety of Apatinib Plus Camrelizumab in Patients With Previously Treated Advanced Biliary Tract Cancer: A Prospective Clinical Study. *Front Oncol* (2021) 11:646979. doi: 10.3389/fonc.2021.646979
35. Lin J, Yang X, Long J, Zhao S, Mao J, Wang D, et al. Pembrolizumab Combined With Lenvatinib as non-First-Line Therapy in Patients With Refractory Biliary Tract Carcinoma. *Hepatobil Surg Nutr* (2020) 9(4):414–24. doi: 10.21037/hbsn-20-338
36. Arkenau H-T, Martin-Liberal J, Calvo E, Penel N, Krebs MG, Herbst RS, et al. Ramucirumab Plus Pembrolizumab in Patients With Previously Treated Advanced or Metastatic Biliary Tract Cancer: Nonrandomized, Open-Label, Phase I Trial (JVDF). *Oncol* (2018) 23(12):1407–+. doi: 10.1634/theoncologist.2018-0044
37. Klein O, Kee D, Nagrial A, Markman B, Underhill C, Michael M, et al. Evaluation of Combination Nivolumab and Ipilimumab Immunotherapy in Patients With Advanced Biliary Tract Cancers: Subgroup Analysis of a Phase 2 Nonrandomized Clinical Trial. *JAMA Oncol* (2020) 6(9):1405–9. doi: 10.1001/jamaoncol.2020.2814
38. Chen X, Wu X, Wu H, Gu Y, Shao Y, Shao Q, et al. Camrelizumab Plus Gemcitabine and Oxaliplatin (GEMOX) in Patients With Advanced Biliary Tract Cancer: A Single-Arm, Open-Label, Phase II Trial. *J Immunother Cancer* (2020) 8(2):e001240. doi: 10.1136/jitc-2020-001240
39. Ueno M, Ikeda M, Morizane C, Kobayashi S, Ohno I, Kondo S, et al. Nivolumab Alone or in Combination With Cisplatin Plus Gemcitabine in Japanese Patients With Unresectable or Recurrent Biliary Tract Cancer: A non-Randomised, Multicentre, Open-Label, Phase 1 Study. *Lancet Gastroenterol Hepatol* (2019) 4(8):611–21. doi: 10.1016/s2468-1253(19)30086-x
40. Piha-Paul SA, Oh D-Y, Ueno M, Malka D, Chung HC, Nagrial A, et al. Efficacy and Safety of Pembrolizumab for the Treatment of Advanced Biliary Cancer: Results From the KEYNOTE-158 and KEYNOTE-028 Studies. *Int J Cancer* (2020) 147(8):2190–8. doi: 10.1002/ijc.33013
41. Ott PA, Bang YJ, Piha-Paul SA, Razak ARA, Bennouna J, Soria JC, et al. T-Cell-Inflamed Gene-Expression Profile, Programmed Death Ligand 1 Expression, and Tumor Mutational Burden Predict Efficacy in Patients Treated With Pembrolizumab Across 20 Cancers: KEYNOTE-028. *J Clin Oncol Off J Am Soc Clin Oncol* (2019) 37(4):318–27. doi: 10.1200/jco.2018.78.2276
42. Lee SH, Lee HS, Lee SH, Woo SM, Kim DU, Bang S. Efficacy and Safety of Pembrolizumab for Gemcitabine/Cisplatin-Refractory Biliary Tract Cancer: A Multicenter Retrospective Study. *J Clin Med* (2020) 9(6):1769. doi: 10.3390/jcm9061769
43. Sun D, Ma J, Wang J, Han C, Qian Y, Chen G, et al. Anti-PD-1 Therapy Combined With Chemotherapy in Patients With Advanced Biliary Tract Cancer. *Cancer Immunol Immunother CII* (2019) 68(9):1527–35. doi: 10.1007/s00262-019-02386-w
44. Sterne JA, Hernán MA, Reeves BC, Savović J, Berkman ND, Viswanathan M, et al. ROBINS-I: A Tool for Assessing Risk of Bias in non-Randomised Studies of Interventions. *BMJ (Clin Res ed)* (2016) 355:i4919. doi: 10.1136/bmj.i4919
45. Munn Z, Barker TH, Moola S, Tufanaru C, Stern C, McArthur A, et al. Methodological Quality of Case Series Studies: An Introduction to the JBI Critical Appraisal Tool. *JBI Evid Synthesis* (2020) 18(10):2127–33. doi: 10.11124/jbisrir-d-19-00099
46. Yarchoan M, Cope L, Anders RA, Noonan A, Goff LW, Goyal L, et al. A Multicenter Randomized Phase 2 Trial of Atezolizumab as Monotherapy or in Combination With Cobimetinib in Biliary Tract Cancers (BTCs): A NCIExperimental Therapeutics Clinical Trials Network(ETCTN) Study. *Cancer Res* (2020) 80(16 SUPPL):Abstract nr CT043.. doi: 10.1158/1538-7445.AM2020-CT043
47. Oh DY, Lee KH, Lee DW, Kim TY, Bang JH, Nam AR, et al. Phase II Study Assessing Tolerability, Efficacy, and Biomarkers for Durvalumab (D) ± Tremelimumab (T) and Gemcitabine/Cisplatin (GemCis) in Chemo-Naïve Advanced Biliary Tract Cancer (aBTC). *J Clin Oncol* (2020) 38(15):4520. doi: 10.1200/JCO.2020.38.15_suppl.4520
48. Ioka T, Ueno M, Oh DY, Fujiwara Y, Chen JS, Doki Y, et al. Evaluation of Safety and Tolerability of Durvalumab (D) With or Without Tremelimumab (T) in Patients (Pts) With Biliary Tract Cancer (BTC). *J Clin Oncol* (2019) 37:387. doi: 10.1200/JCO.2019.37.4_suppl.387
49. Merck. *Merck Reports Topline Data for Bintrafusp Alfa as Second-Line Monotherapy Treatment in Biliary Tract Cancer* (2021). Available at: https://www.merckgroup.com/en/news/bintrafusp-topline-data-biliary-tract-cancer-16-03-2021.html (Accessed March 16, 2021).
50. Zhou J, Gong J, Cao Y, Peng Z, Yuan J, Wang X, et al. Anlotinib Plus TQB2450 in Patients With Advanced Refractory Biliarytract Cancer (BTC): An Open-Label, Dose-Escalating, and Dose-Expansion Cohort of Phase Ib Trial. *J Clin Oncol* (2021) 39(3 SUPPL):292. doi: 10.1200/JCO.2021.39.3-suppl.292
51. Villanueva L, Lwin Z, Chung HC, Gomez-Roca C, Longo F, Yanez E, et al. Lenvatinib Plus Pembrolizumabfor Patients With Previouslytreated Biliary Tract Cancers in Themulticohort Phase II LEAP-005study. *J Clin Oncol* (2021) 39(3 SUPPL):321. doi: 10.1200/JCO.2021.39.3-suppl.321
52. Zong H, Zhong Q, Zhao R, Jin S, Zhou C, Zhang X, et al. Phase II Study of Anlotinib Plus Sintlimab as Second-Line Treatment for Patients With Advanced Biliary Tract Cancers. *J Clin Oncol Off J Am Soc Clin Oncol* (2021) 39(suppl 3):abstr 307. doi: 10.1200/JCO.2021.39.3_suppl.307
53. Sun Y, Zhou A, Zhang W, Jiang Z, Qu W. A Phase Ib Study of Anlotinib Plus TQB2450 as Second-Line Therapy for Advanced Biliary Tract Adenocarcinoma. *J Clin Oncol Off J Am Soc Clin Oncol* (2021) 39(suppl 15):abstr 4075. doi: 10.1200/JCO.2021.39.15_suppl.4075
54. Cousin S, Bellera CA, Guégan JP, Mazard T, Gomez-Roca CA, Metges JP, et al. Regomune: A Phase II Study of Regorafenib + Avelumab in Solid Tumors—Results of the Biliary Tract Cancer (BTC) Cohort. *J Clin Oncol Off J Am Soc Clin Oncol* (2021) 39(suppl 15):abstr 4096. doi: 10.1200/JCO.2021.39.15_suppl.4096
55. Floudas CS, Xie C, Brar G, Morelli MP, Fioravanti S, Walker M, et al. Combined Immune Checkpoint Inhibition (ICI) With Tremelimumab and Durvalumab in Patients With Advanced Hepatocellular Carcinoma (HCC) or Biliary Tract Carcinomas (BTC). *J Clin Oncol* (2019) 37:336. doi: 10.1200/JCO.2019.37.4_suppl.336
56. Liu T, Li W, Yu Y, Guo X, Xu X, Wang Y, et al. Toripalimab With Chemotherapy as First-Line Treatment for Advanced Biliary Tract Tumors: A Preliminary Analysis of Safety and Efficacy of an Open-Label Phase II Clinical Study. *Ann Oncol* (2020) 31:S261. doi: 10.1016/j.annonc.2020.08.031
57. Qin S, Chen Z, Liu Y, Xiong J, Ren Z, Meng Z, et al. A Phase II Study of Anti-PD1 Antibody Camrelizumab Plus FOLFOX4 or GEMOX Systemic Chemotherapy as First-Line Therapy for Advanced Hepatocellular Carcinoma or Biliary Tract Cancer. *J Clin Oncol* (2019) 37:4074. doi: 10.1200/JCO.2019.37.15-suppl.4074
58. Chiang N-J, Bai L-Y, Chen L-T, Huang C-J, Chen S-C, Shan Y-S, et al. A Phase II Trial of Nivolumab and Gemcitabine and S-1 as the First-Line Treatment in Patients With Advanced Biliary Tract Cancer. *Ann Oncol* (2021) 32(suppl_5):S376–S81. doi: 10.1016/annonc/annonc685
59. Gou M, Tie EL, Yan H, Si H, Wang Z, Qian N, et al. Pd-1 Inhibitors Plus Nab-Paclitaxel With S1 (AS) as First Line in Patients With Advanced Biliary Tract Cancer. *J Clin Oncol* (2020) 38(15):e15195. doi: 10.1200/JCO.2020.38.15_suppl.e15195
60. Boileve A, Hilmi M, Gougis P, Cohen R, Rousseau B, Blanc J-F, et al. Triplet Combination of Durvalumab, Tremelimumab, and Paclitaxel in Biliary Tract Carcinomas: Safety Run-in Results of the Randomized IMMUNOBIL PRODIGE 57 Phase II Trial. *Eur J Cancer* (2021) 143:55–63. doi: 10.1016/j.ejca.2020.10.027

61. Tierney JF, Stewart LA, Ghersi D, Burdett S, Sydes MR. Practical Methods for Incorporating Summary Time-to-Event Data Into Meta-Analysis. *Trials* (2007) 8:16. doi: 10.1186/1745-6215-8-16
62. Higgins JP, Thompson SG, Deeks JJ, Altman DG. Measuring Inconsistency in Meta-Analyses. *BMJ (Clin Res ed)* (2003) 327(7414):557–60. doi: 10.1136/bmj.327.7414.557
63. Sterne JA, Egger M, Smith GD. Systematic Reviews in Health Care: Investigating and Dealing With Publication and Other Biases in Meta-Analysis. *BMJ (Clin Res ed)* (2001) 323(7304):101–5. doi: 10.1136/bmj.323.7304.101
64. Combescure C, Foucher Y, Jackson D. Meta-Analysis of Single-Arm Survival Studies: A Distribution-Free Approach for Estimating Summary Survival Curves With Random Effects. *Stat Med* (2014) 33(15):2521–37. doi: 10.1002/sim.6111
65. Higgins JP, Thompson SG. Quantifying Heterogeneity in a Meta-Analysis. *Stat Med* (2002) 21(11):1539–58. doi: 10.1002/sim.1186
66. Shen G, Zheng F, Ren D, Du F, Dong Q, Wang Z, et al. Anlotinib: A Novel Multi-Targeting Tyrosine Kinase Inhibitor in Clinical Development. *J Hematol Oncol* (2018) 11(1):120. doi: 10.1186/s13045-018-0664-7

Conflict of Interest: The authors declare that the research was conducted in the absence of any commercial or financial relationships that could be construed as a potential conflict of interest.

frontiers in Oncology

CASE REPORT
published: 14 March 2022
doi: 10.3389/fonc.2022.818626

Camrelizumab Combined With Gemcitabine and Albumin-Bound Paclitaxel for Neoadjuvant Therapy in the Treatment of Progressive Gallbladder Cancer: A Case Report

Jing Wu[†], *Zheng Wang*[†], *Jing Li*, *Xue-Hui Peng*, *Yi-Chen Tang*, *Xiao-Bing Huang*[*] *and Yong-Gang He*[*]

Department of Hepatobiliary Surgery, The Second Affiliated Hospital of Army Medical University, Chongqing, China

OPEN ACCESS

Edited by:
Zheng Gong,
Jackson Laboratory, United States

Reviewed by:
Seyed Alireza Javadinia,
Sabzevar University of Medical Sciences, Iran
Faten Limaiem,
Hôpital Mongi Slim, Tunisia
Ruhi Dixit,
Banaras Hindu University, India

***Correspondence:**
Yong-Gang He
382948320@qq.com
Xiao-Bing Huang
1038915320@qq.com

[†]*These authors have contributed equally to this work*

Specialty section:
This article was submitted to Cancer Immunity and Immunotherapy, a section of the journal Frontiers in Oncology

Received: *19 November 2021*
Accepted: *24 January 2022*
Published: *14 March 2022*

Citation:
Wu J, Wang Z, Li J, Peng X-H, Tang Y-C, Huang X-B and He Y-G (2022) Camrelizumab Combined With Gemcitabine and Albumin-Bound Paclitaxel for Neoadjuvant Therapy in the Treatment of Progressive Gallbladder Cancer: A Case Report. Front. Oncol. 12:818626. doi: 10.3389/fonc.2022.818626

Background: The roles of immune checkpoint inhibitors in the treatment of gallbladder cancer are still unclear and challenged by controversial findings. Recent research has shown that immune checkpoint inhibitors in combination with chemotherapy may alleviate disease progression.

Case Summary: A 45-year-old female patient with gallbladder cancer accompanied by multiple abdominal lymph node metastasis was treated with camrelizumab combined with paclitaxel for injection (albumin-bound) and gemcitabine (AG) to downstage the tumor before a radical surgery could be performed. The postoperative quality of life was superior to the preoperative level.

Conclusion: Camrelizumab + AG offers a new therapeutic option for gallbladder cancer with multiple abdominal lymph node metastasis, which, however, warrants further validation in clinical trials.

Keywords: neoadjuvant therapy, immune checkpoint inhibitor, gallbladder cancer, chemotherapy, AG

INTRODUCTION

Gallbladder cancer is a common malignancy in the biliary system, and surgery offers the best chance for a cure (1). However, gallbladder cancer (GBC) is featured by difficulties in early diagnosis, rapid tumor progression, high degree of malignancy, easy recurrence/metastasis, and poor prognosis. Most patients would have already missed the opportunity for surgical resection at the time of diagnosis (1). Neoadjuvant therapy has provided a new treatment option for patients with unresectable advanced malignant tumors, which may downstage the tumor and prolong the survival time of patients. Neoadjuvant therapy may also increase the possibility of achieving a successful complete resection (2). At present, chemotherapy combined with gemcitabine + cisplatin (GC) is the standard treatment strategy for patients with advanced GBC (3). Research has shown that GC combined with paclitaxel for injection (albumin-bound) (PAB) prolonged the progression-free survival (PFS) and overall survival (OS) (4). PAB + gemcitabine (AG regimen) has been applied for the treatment of advanced biliary cancer (5). Notably, all mismatch repair protein (microsatellite instability, MSI)/deficient

mismatch repair protein (dMMR)-positive tumors can be treated with immune checkpoint inhibitors (6).

Preclinical studies have found that chemotherapeutic drugs could enhance the endogenous immune response through multiple mechanisms: firstly, chemotherapeutic drugs may activate the adaptive immune system by increasing the expression of human leukocyte antigen (HLA) and enhancing the stimulation of T cells; secondly, chemotherapeutic drugs may recover the immunological surveillance by disrupting STAT6-mediated immunosuppression (1). Based on these theories, a combination of immunotherapy and chemotherapy has been offered for patients with advanced biliary tract cancer (BTC) in the recent years and has shown promising efficacy (1, 7).

According to previous studies, neoadjuvant chemotherapy for degrading before surgical treatment will benefit advanced carcinoma patients. Here, we report on a case of GBC with multiple local lymph node metastasis who has been successfully treated with camrelizumab + AG.

CASE PRESENTATION

A 45-year-old woman was hospitalized because of right upper abdominal pain for 3 months. The patient had a cesarean delivery 20 years ago. The patient had no prior history of cancer and chronic viral hepatitis and no family history of BTC or other hereditary diseases related to the gallbladder or liver. Tenderness was examined in the right upper abdomen. The level of alpha-fetoprotein (AFP) was 334.66 ng/ml. The levels of carcinoembryonic antigen (CEA) and carbohydrate antigen 19-9 (CA 19-9) were within normal ranges (**Figure 1A**).

Abdominal contrast-enhanced computed tomography (CT) and magnetic resonance imaging (MRI) revealed GBC (3.2 cm × 2.7 cm in size) accompanied by localized multiple lymph node metastasis (the largest one was 2.5 cm × 3.6 cm) posterior to the pancreas, gallbladder enlargement, and gallbladder stones (**Figures 1B, C**). PET-CT indicated a cervical nodule shadow (approximately 3 cm in diameter) and increased FDG metabolism. All the aforementioned combined with the medical history indicated a primary tumor. In addition, a nodule shadow in the rear of the pancreatic head (approximately 2.5 × 3 cm in diameter), multiple primary lymph nodes in the para-abdominal aorta, and increased FDG metabolism indicated metastatic disease in these organs. PET/CT did not detect metastasis in other distant organs. Endoscopic ultrasound-guided fine-needle aspiration revealed positive lymph nodes posterior to the pancreas and a space-occupying lesion in the gallbladder. Ultrasonic endoscopy found one approximately 2.5 × 3-cm hypoechoic envelope block (without internal blood flow signal) and another approximately 3-cm moderate echo envelope block near the neck (without internal blood flow signal). The local gallbladder wall was not smooth, with a 2.3-cm stone at the bottom of the gallbladder. The puncture biopsy tissue was reddish brown. The presence of heterogeneous epithelioid cell groups combined with the immunohistochemistry (IHC) results supported the diagnosis of a poorly differentiated adenocarcinoma, although the possibility of neuroendocrine differentiation cannot be completely ruled out. The IHC results showed the following: CK+, Ki-67 (70%–80%)+, CK18+, Villin+, CgA a small amount+, SYN–, CD56–, TTF-1–, Hepatocyte–, AFP–, CDX-2–, CD34–, CA 19-9– (**Figures 2A–G**).

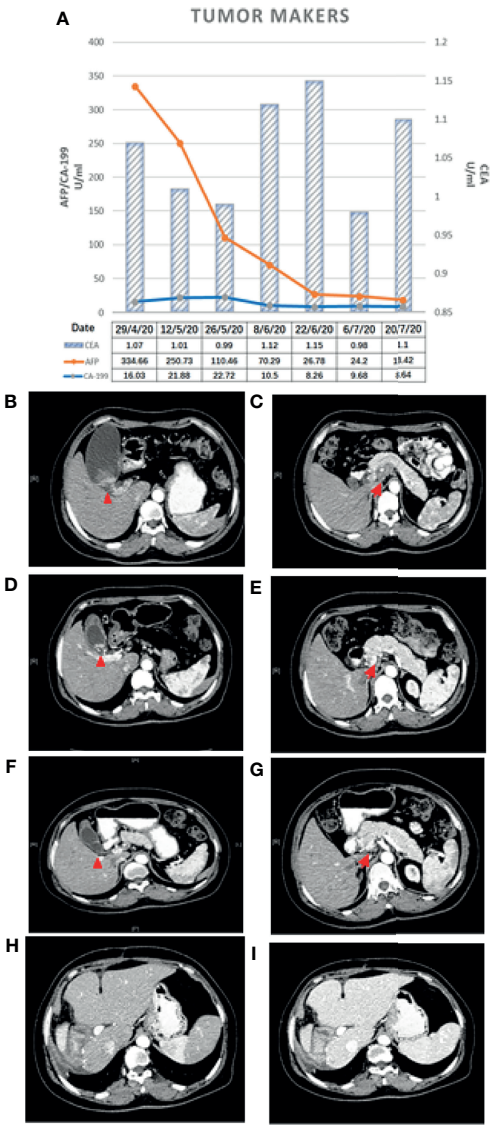

FIGURE 1 | **(A)** Changes in the tumor makers. **(B, C)** Baseline CT scan. **(D, E)** CT scan after the first treatment cycle. **(F, G)** CT scan after the second treatment cycle. Changes in CT findings: the primary gallbladder cancer and metastatic lymph nodes shrank after treatment with gemcitabine + albumin-bound paclitaxel combined with camrelizumab for two cycles. **(H, I)** CT examination after surgery. No recurrence or metastasis was found on abdominal CT at 14 months. The *red triangle* denotes the primary lesion and the *red arrow* indicates the metastatic lymph nodes posterior to the pancreas.

Final Diagnosis

No other obvious signs were shown. The examinations and imaging findings all indicated signs of GBC. According to the American Joint Committee on Cancer (AJCC) guidelines (8th

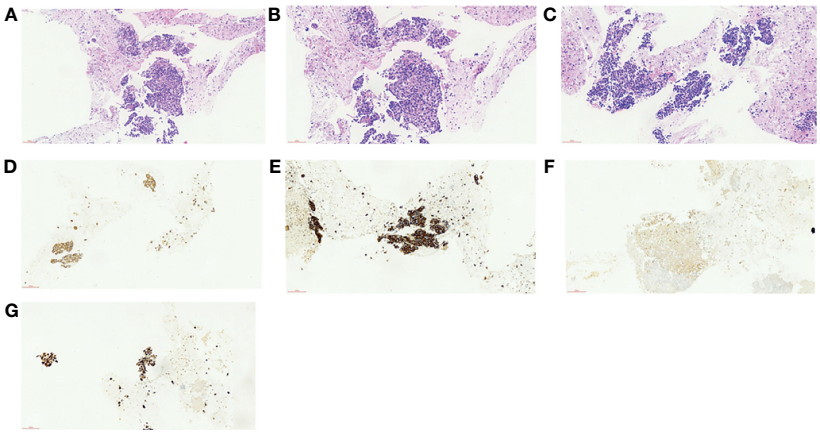

FIGURE 2 | **(A–F)** Results of histopathology before neoadjuvant therapy. **(A)** Hematoxylin–eosin (HE), ×40. **(B)** HE, ×200. **(C)** HE, ×200. **(D)** Cytokeratin 18 (CK18), ×200. **(E)** Pan cytokeratin (CK-pan), ×200. **(F, G)** Fibroblast activation protein (FAP), ×200.

edition), it was evaluated as T3N2M0 (IIIA) stage, for which surgical resection was not recommended.

Treatment

A multidisciplinary team (MDT) recommended the application of multidisciplinary treatment, for which genetic tests would be helpful. However, the patient refused to undergo genetic testing due to financial difficulties and requested to be treated directly with chemotherapy plus immunotherapy as soon as possible.

According to the guideline of the Chinese Society of Clinical Oncology (CSCO), the results of a randomized controlled phase III clinical trial did not support the benefit of neoadjuvant chemotherapy for biliary tract malignant tumor. Patients were recommended to attend the clinical trial. Referring to the literature reports and the CSCO guideline (5), the following treatment protocol was then chosen: 1,000 mg/m^2 gemcitabine (Stockhausen Pharmaceutical Co., Ltd., Jiangsu, China) plus 125 mg/m^2 PAB (Shiyao Group Ouyi Pharmaceutical Co., Ltd., Hebei, China) combined with 200 mg camrelizumab (an immune checkpoint inhibitor) (Hengrui Medicine Co., Ltd., Jiangsu, China). The patient was treated with 1,000 mg gemcitabine and 170 mg PAB on days 1, 8, and 15 and with 200 mg camrelizumab on day 1 every 3 weeks. The next cycle of treatment was repeated after a 2-week interval. Abdominal CT and measurements of the tumor markers were performed after each treatment cycle to assess the efficacy (**Figures 1D–G**) using the Response Evaluation Criteria in Solid Tumors (RECIST), version 1.1. After two cycles of treatment, the gallbladder tumor and metastatic lymph nodes shrank more than 30% (partial response, PR), and the AFP level decreased from 334.66 to 24.2 ng/ml. The tumor was then evaluated as resectable. During the therapy, the patient had good appetite without nausea and vomiting and scored 0 in the Eastern Cooperative Oncology Group (ECOG). Drug-induced myelosuppression was noted, as the white blood cell (WBC) count decreased to 2.14 × 10^9/L. The patient also experienced other hematologic toxicities during the treatment (**Table 1**). These adverse effects improved after subcutaneous injection of recombinant human granulocyte–macrophage colony-stimulating factors. In addition, the patient suffered from generalized pruritus and hemangioma-like changes at the forearms, back, and knee joints after the first dose in the second cycle (**Figure 3**), which were not alleviated after administration of loratadine (i.e., an anti-allergic drug). However, these symptoms were improved after intravenous infusion of 5 mg dexamethasone. The therapeutic tolerance decreased after the second cycle. After consultations with the MDT, the patient was encouraged to continue the current treatment protocol. However, considering the decreased tolerance to chemotherapy and the option of surgical resection, the patient refused further chemotherapy plus immunotherapy and requested a radical surgery. After preoperative examinations and informed consent of the patient, radical surgery was performed to remove the primary tumor, along with regional lymph node dissection under general anesthesia. The patient was also informed that hemihepatectomy + biliary–intestinal anastomosis or even pancreaticoduodenectomy might be performed during the surgery, depending on specific pathological findings. After informed consent was obtained from the patient's family, the surgery was performed under general anesthesia on August 10, 2020. During the surgery, the gallbladder was removed, and a cystic duct margin was found positive after a frozen section

TABLE 1 | Hematological and non-hematological toxicities during neoadjuvant therapy (grading according to CTCAE 3.0).

Hematological toxicities	Baseline	Grade	Non-hematological toxicities	Baseline	Grade
White blood cells	0	II	Nausea	0	I
Neutrophils (%)	0	I	Vomiting	0	I
Hemoglobin	0	I	Fatigue	0	I
Platelets	0	I	Pruritus	0	II

FIGURE 3 | Reactive cutaneous capillary endothelial proliferation (RCCEP) (*yellow arrows*) following immunotherapy.

pathological examination. Therefore, a partial bile duct resection was performed. Intraoperative pathological examination showed that the first resection margin of the common bile duct was positive and the second lower resection margin of the common bile duct was negative. In addition, the resection margin was positive for the right hepatic duct and negative for the left hepatic duct. According to the intraoperative pathological examination results, the surgical procedures were changed to right hemihepatectomy, radical cholecystectomy, and regional lymph node dissection, with informed consent of the family because the patient was unconscious.

After the surgery, the patient developed pulmonary infection and pleural effusion due to prolonged immobility, which were alleviated after antimicrobial therapy and ultrasound-guided thoracentesis and drainage. The patient was discharged on September 11, 2020. Postoperative pathology revealed that the lesion was a moderately differentiated adenocarcinoma of the gallbladder (**Figures 2D, E**) affecting the entire wall of the gallbladder, along with visible choroidal carcinoma thrombosis and nerve invasion. Metastases were found in lymph node stations 8 and 9, but not in stations 12, 14, and 16 (7). As it had been reported that postoperative adjuvant therapy could improve OS, the CSCO guideline recommended the use of capecitabine or participation in other clinical trials. Since the neoadjuvant chemotherapy plan of the patient was effective before surgery, we continued to treat this patient with chemotherapy plus immunotherapy after surgery. So far, the PFS of this patient has reached 14 months. The patient has maintained good quality of life in the past 9 months without disease progression (**Figures 1H, I**).

DISCUSSION

Most GBC patients are diagnosed at an advanced stage. The benefit of radiotherapy in the clinical treatment of GBC still needs further confirmation. As a result, the value of chemotherapy as a treatment option second only to surgery for GBC has been increasingly recognized (8). Gemcitabine + cisplatin has been reported as the first-line chemotherapy for GBC, but has a response rate of only about 20% (8). Most patients will suffer from disease progression soon after chemotherapy. Gallbladder cancer patients typically cannot tolerate high-intensity, long-duration chemotherapy due to various factors such as age, physical status, disease severity, and tumor burden. Therefore, for patients with inoperable GBC, a high-efficacy and low-toxicity chemotherapy regimen is particularly important.

For patients with advanced BTC, adding PAB to GC could achieve longer median progression-free survival (mPFS; 11.8 months) and median overall survival (mOS; 19.2 months) than the conventional GC regimen alone, with the mPFS and mOS in the GBC subgroup being 4.1 and 15.7 months, respectively (4). Treatment with PAB in combination with GC prolonged the mPFS and mOS compared with controls treated with GC alone (4).

For unresectable or metastatic extrahepatic cholangiocarcinoma, gemcitabine combined with PAB is feasible. In a phase II trial, Sahai et al. (4) found that PAB + gemcitabine was well tolerated when used as the first-line treatment for advanced or metastatic cholangiocarcinoma and concluded that this regimen might be an alternative option to the current therapeutic approaches for advanced cholangiocarcinoma.

The immunotherapy for cholangiocarcinoma included cancer vaccines, adoptive cellular immunotherapy, and immune checkpoint inhibitors (9). Some studies suggested that tumor vaccines combined with chemotherapy may increase the response rates of patients with BTC, including GBC, but validation in large-scale studies is lacking (1). Immune checkpoint inhibitors have become a new hotspot in current cancer research. By blocking specific pathways, these agents can release tumor-induced immunosuppression and activate the specific immune response to cancer cells, thus achieving immune-mediated clearance of cancer cells. Such efficacies are based on the effects on immunosuppression and tumor immune escape mediated by the interaction of programmed cell death 1 (PD-1), cytotoxic T-lymphocyte antigen 4 (CTLA-4), and their ligands. Camrelizumab (AiRuiKa^{TM}) is an immune checkpoint

inhibitor. It binds to the PD-1 receptor, blocks the binding between PD-1 and programmed death-ligand 1 (PD-L1) to wash and activate T cells, and produces sustained antitumor effects to inhibit tumor growth (10–12). Currently, camrelizumab has been used for the treatment of a variety of malignancies (13).

Wang et al. (14) reported that PD-1/PD-L1 blocking therapy may cause immune-related adverse reactions (immune-related adverse events, irAEs) and, hence, proposed combining immunotherapy with antitumor drugs to improve the therapeutic effect. However, there have been concerns that the combination therapy may also increase the incidence of more complex treatment-related adverse events. Chen et al. used camrelizumab + gemcitabine and oxaliplatin (GEMOX) to treat patients with advanced BTC and achieved promising outcomes with tolerable toxicities (8). Patients with GBC seemed to benefit more from this treatment. Gou et al. (15) reported that patients with advanced BTC who received a PD-1 inhibitor combined with a chemotherapy regimen had longer PFS (5.8 months) than those who received chemotherapy alone (3.2 months), providing supportive evidence for the efficacy of a combination treatment regimen for advanced BTC. Sun et al. (1) reported that the median OS of the PD-1 inhibitor combined with chemotherapy (14.9 months) was significantly longer than that of the PD-1 inhibitor monotherapy (4.1 months) and of the chemotherapy monotherapy (6.0 months). The combination of PD-1 inhibitor and chemotherapy also showed significantly longer median PFS (5.1 months) than that of PD-1 inhibitor monotherapy (2.2 months) and chemotherapy monotherapy (2.4 months). However, a considerable number of patients did not benefit from this therapy, which may also be associated with serious adverse events. Therefore, evaluation of predictive biomarkers of individual tumor tissues before therapy initiation is critical. Tumor mutation burden, mismatch repair genes, and MSI may be predictors of immunotherapy (16). Recent studies have found that the peripheral blood levels of circulating hematologic and serum cytokines and MAGE1 might serve as potential cancer biomarkers (17–19). Albrecht et al. (20) reported that there is limited evidence on the efficacy of PD-1 inhibitors combined with other chemotherapeutic agents for GBC. The authors also reported that PD-L1 is upregulated in tumors and immune cells in a subpopulation of advanced Western GBC, providing evidence that the TIGIT/CD155 axis is a novel immune checkpoint for complement therapy for GBC. This further confirms the need for a prospective study of PD-L1 in the treatment of advanced GBC.

Tumor mutation burden, mismatch repair genes, and high MSI may be predictive factors for immunotherapy. In this article, we reported our experience in treating a case of GBC with lymph node metastasis with camrelizumab + AG. Chemotherapy plus immunotherapy may have different tolerability profiles, such as bone marrow suppression and loss of appetite after chemotherapy. In addition to the many irAEs, camrelizumab also has a unique adverse event: reactive cutaneous capillary endothelial proliferation (RCCEP) (12). Our patient suffered from myelosuppression and the WBC count declined after the chemotherapy, which was alleviated after administration of recombinant human granulocyte colony-stimulating factor. In addition, RCCEP occurred in the trunk and extremities (**Figure 3**). After hormone therapy, RCCEP in the limb was slightly relieved. After discontinuation of camrelizumab, RCCEP was resolved and the patient's quality of life improved. The patient has been followed up for 14 months; currently, there is no tumor recurrence, the levels of CEA, CA19-9, and AFP are normal, and the quality of life is good.

Chemotherapy plus immunotherapy achieved definite efficacy in this patient, but the patient showed poor tolerance. The patient's physical tolerance decreased significantly after completing the second treatment cycle and requested direct surgery. Before the initiation of neoadjuvant therapy, the pathological diagnosis of the lesion was a poorly differentiated adenocarcinoma. After six sessions of neoadjuvant therapy, the gallbladder tumor and metastatic lymph nodes were reduced in size, and radical surgery was performed. Postoperative pathology revealed that the lesion was a moderately differentiated adenocarcinoma of the gallbladder, suggesting that the tumor had been downstaged after neoadjuvant therapy.

In this case, the patient was initially diagnosed with GBC with localized multiple lymph node metastasis, which made surgery infeasible. However, successful surgical resection was performed after treatment with camrelizumab + AG, and the patient has remained recurrence-free 14 months after surgery.

CONCLUSION

Locally advanced GBC could be downgraded after neoadjuvant therapy, which may improve the feasibility of performing a surgery. This strategy provides a new treatment option for GBC patients to prolong survival time and improve their quality of life. However, more accumulation of cases is necessary, and our finding needs to be further validated in large multicenter studies.

DATA AVAILABILITY STATEMENT

The original contributions presented in the study are included in the article/supplementary material. Further inquiries can be directed to the corresponding authors.

ETHICS STATEMENT

Informed written consent was obtained from the patient for the publication of this report and any accompanying images.

AUTHOR CONTRIBUTIONS

JW, ZW, X-BH, Y-GH, and JL contributed to the conception and design of the study and drafted the manuscript. X-HP, JW, and Y-CT contributed to the analysis and interpretation of data and revised the manuscript. X-BH participated in clinical treatment

and literature search. ZW contributed to participated in paper design, paper modification and use of pathological images. All authors read and approved the final manuscript.

FUNDING

This study was supported by grants from the National Natural Science Foundation of China (81672902) And the Hospital Research Fund (General Project) from The Second Affiliated Hospital of Army Medical University (no. 2016YLC18 and no. 2019XLC2006).

ACKNOWLEDGMENTS

We sincerely thank XinWei Diao for his assistance and contribution in completing this work.

REFERENCES

1. Sun D, Ma J, Wang J, Han C, Qian Y, Chen G, et al. Anti-PD-1 Therapy Combined With Chemotherapy in Patients With Advanced Biliary Tract Cancer. *Cancer Immunol Immunother* (2019) 68:1527–35. doi: 10.1007/s00262-019-02386-w
2. Gold DG, Miller RC, Haddock MG, Gunderson LL, Quevedo F, Donohue JH, et al. Adjuvant Therapy for Gallbladder Carcinoma: The Mayo Clinic Experience. *Int J Radiat Oncol Biol Phys* (2009) 75:150–5. doi: 10.1016/j.ijrobp.2008.10.052
3. Lee J, Park SH, Chang HM, Kim JS, Choi HJ, Lee MA, et al. Gemcitabine and Oxaliplatin With or Without Erlotinib in Advanced Biliary-Tract Cancer: A Multicentre, Open-Label, Randomised, Phase 3 Study. *Lancet Oncol* (2012) 13:181–8. doi: 10.1016/S1470-2045(11)70301-1
4. Shroff RT, Javle MM, Xiao L, Kaseb AO, Varadhachary GR, Wolff RA, et al. Gemcitabine, Cisplatin, and Nab-Paclitaxel for the Treatment of Advanced Biliary Tract Cancers: A Phase 2 Clinical Trial. *JAMA Oncol* (2019) 5:824–30. doi: 10.1001/jamaoncol.2019.0270
5. Sahai V, Catalano PJ, Zalupski MM, Lubner SJ, Menge MR, Nimeiri HS, et al. Nab-Paclitaxel and Gemcitabine as First-Line Treatment of Advanced or Metastatic Cholangiocarcinoma: A Phase 2 Clinical Trial. *JAMA Oncol* (2018) 4:1707–12. doi: 10.1001/jamaoncol.2018.3277
6. Lemery S, Keegan P, Pazdur R. First FDA Approval Agnostic of Cancer Site - When a Biomarker Defines the Indication. *N Engl J Med* (2017) 377:1409–12. doi: 10.1056/NEJMp1709968
7. Primrose JN, Fox RP, Palmer DH, Malik HZ, Prasad R, Mirza D, et al. Capecitabine Compared With Observation in Resected Biliary Tract Cancer (BILCAP): A Randomised, Controlled, Multicentre, Phase 3 Study. *Lancet Oncol* (2019) 20:663–73. doi: 10.1016/S1470-2045(18)30915-X
8. Chen X, Wu X, Wu H, Gu Y, Shao Y, Shao Q, et al. Camrelizumab Plus Gemcitabine and Oxaliplatin (GEMOX) in Patients With Advanced Biliary Tract Cancer: A Single-Arm, Open-Label, Phase II Trial. *J Immunother Cancer* (2020) 8. doi: 10.1136/jitc-2020-001240
9. Christofi T, Baritaki S, Falzone L, Libra M, Zaravinos A. Current Perspectives in Cancer Immunotherapy. *Cancers (Basel)* (2019) 11. doi: 10.3390/cancers11101472
10. Guo Y, Feng K, Liu Y, Wu Z, Dai H, Yang Q, et al. Phase I Study of Chimeric Antigen Receptor-Modified T Cells in Patients With EGFR-Positive Advanced Biliary Tract Cancers. *Clin Cancer Res* (2018) 24:1277–86. doi: 10.1158/1078-0432.CCR-17-0432
11. Hoos A. Development of Immuno-Oncology Drugs - From CTLA4 to PD1 to the Next Generations. *Nat Rev Drug Discov* (2016) 15:235–47. doi: 10.1038/nrd.2015.35
12. Francisco LM, Salinas VH, Brown KE, Vanguri VK, Freeman GJ, Kuchroo VK, et al. PD-L1 Regulates the Development, Maintenance, and Function of Induced Regulatory T Cells. *J Exp Med* (2009) 206:3015–29. doi: 10.1084/jem.20090847
13. Markham A, Keam SJ. Camrelizumab: First Global Approval. *Drugs* (2019) 79:1355–61. doi: 10.1007/s40265-019-01167-0
14. Wang D, Lin J, Yang X, Long J, Bai Y, Yang X, et al. Combination Regimens With PD-1/PD-L1 Immune Checkpoint Inhibitors for Gastrointestinal Malignancies. *J Hematol Oncol* (2019) 12:42. doi: 10.1186/s13045-019-0730-9
15. Gou M, Zhang Y, Liu T, Si H, Wang Z, Yan H, et al. PD-1 Inhibitors Could Improve the Efficacy of Chemotherapy as First-Line Treatment in Biliary Tract Cancers: A Propensity Score Matching Based Analysis. *Front Oncol* (2021) 11:648068. doi: 10.3389/fonc.2021.648068
16. Le DT, Durham JN, Smith KN, Wang H, Bartlett BR, Aulakh LK, et al. Mismatch Repair Deficiency Predicts Response of Solid Tumors to PD-1 Blockade. *Science* (2017) 357:409–13. doi: 10.1126/science.aan6733
17. Du F, Qiu Z, Ai W, Huang C, Ji J, Xiao X, et al. Blood Tests Predict the Therapeutic Prognosis of Anti-PD-1 in Advanced Biliary Tract Cancer. *J Leukoc Biol* (2021) 110:327–34. doi: 10.1002/JLB.5MA1220-631R
18. Anvari K, Pakdel AF, Memar B, Parsamanesh R, Ejlalzadeh SM, Javadinia SA. The Prevalence and Expression Pattern of Melanoma-Associated Antigen 1 in Esophageal Squamous Cell Carcinoma: A Historical Cohort Study. *Electron Physician* (2017) 9:3756–63. doi: 10.19082/3756
19. Fanipakdel A, Seilanian Toussi M, Rezazadeh F, Mohamadian Roshan N, Javadinia SA. Overexpression of Cancer-Testis Antigen Melanoma-Associated Antigen A1 in Lung Cancer: A Novel Biomarker for Prognosis, and a Possible Target for Immunotherapy. *J Cell Physiol* (2019) 234:12080–86. doi: 10.1002/jcp.27884
20. Albrecht T, Brinkmann F, Albrecht M, Lonsdorf AS, Mehrabi A, Hoffmann K, et al. Programmed Death Ligand-1 (PD-L1) Is an Independent Negative Prognosticator in Western-World Gallbladder Cancer. *Cancers (Basel)* (2021) 13. doi: 10.3390/cancers13071682

Conflict of Interest: The authors declare that the research was conducted in the absence of any commercial or financial relationships that could be construed as a potential conflict of interest.

frontiers in Oncology

REVIEW
published: 21 March 2022
doi: 10.3389/fonc.2022.870983

Biological Functions and Molecular Mechanisms of MiR-608 in Cancer

Juan Lu[†], *Danhua Zhu*[†] *and Lanjuan Li*[*]

State Key Laboratory for Diagnosis and Treatment of Infectious Diseases, National Clinical Research Center for Infectious Diseases, Collaborative Innovation Center for Diagnosis and Treatment of Infectious Diseases, The First Affiliated Hospital, College of Medicine, Zhejiang University, Hangzhou, China

In recent years, microRNAs (miRNAs) have attracted much attention because of their prominent role in cancer. An increasing number of studies have shown that miRNAs play an important role in a variety of tumors. miR-608 has been reported to be decreased in cancers, especially in solid tumors. miR-608 is regarded as a tumor suppressor, which has been verified through a large number of experiments both *in vivo* and *in vitro*. miR-608 participates in many biological processes, including cell proliferation, invasion, migration, and apoptosis, by inhibiting transmembrane proteins and many signaling pathways. Here, we summarize the expression profile and biological functions and mechanism of miR-608, suggesting that miR-608 is an ideal diagnostic and prognostic biomarker and a treatment target for cancer.

Keywords: miR-608, cancer, biomarker, molecular mechanism, tumor suppressor

OPEN ACCESS

Edited by:
Hongda Liu,
Nanjing Medical University, China

Reviewed by:
Zhendong Jin,
Second Military Medical University, China
Shuai Wang,
University of Pittsburgh Medical Center, United States

***Correspondence:**
Lanjuan Li
ljli@zju.edu.cn

[†]*These authors have contributed equally to this work*

Specialty section:
This article was submitted to Cancer Immunity and Immunotherapy, a section of the journal Frontiers in Oncology

Received: *07 February 2022*
Accepted: *28 February 2022*
Published: *21 March 2022*

Citation:
Lu J, Zhu D and Li L (2022) Biological Functions and Molecular Mechanisms of MiR-608 in Cancer. Front. Oncol. 12:870983. doi: 10.3389/fonc.2022.870983

BACKGROUND

MicroRNAs (miRNAs) are a class of nonprotein-coding single-stranded RNA with a length of approximately 18-25 nucleotides, and they are encoded by endogenous genes (1–4). miRNAs are highly conserved and tissue-specific (5). miRNAs were first found in Caenorhabditis elegans, and Lee et al. (6) also found that miRNAs participate in *lin-14* gene expression regulation through antisense RNA-RNA interactions. In the past 20 years, the number of miRNA studies has increased substantially. Researchers have shown that miRNAs are involved in the negative posttranscriptional regulation of gene expression and maintain cell homeostasis (7) in the human body by binding with the 3' untranslated region (3'-UTR) of mRNAs of target genes and degrading the target mRNAs. Generally, a single miRNA has a single mRNA target. However, a miRNAs can possess multiple targets, and a single miRNA target can also be shared by several miRNAs. Proper control of miRNA expression is required for a balanced physiological environment, as these small molecules influence almost every cellular process from the cell cycle and cell proliferation to apoptosis, with a wide range of target genes (8).

In recent research, numerous aberrantly expressed miRNAs were found to be related to the development and prognosis of cancers (9, 10). Among them, miR-608 (GeneID: 693 193), mapped to chromosome 10q24.31, has attracted extensive interest because its dysregulated expression plays a key role in the occurrence and development of various malignant tumors by affecting the posttranscriptional regulation of target genes (11). Further studies have demonstrated that miR-608 expression may affect the treatment efficacy in colorectal cancer (CRC) patients treated with chemotherapy alone or chemoradiotherapy alone (12). Choi et al. (13) demonstrated that miR-608

had the strongest inhibitory effect on the growth of A549 tumor cells by screening a miRNA library. Moreover, the expression level of miR-608 is decreased in many kinds of tumors, including acute myeloid leukaemia (14, 15), bladder cancer (BCa) (11), breast cancer (16), chordoma (17), clear cell renal cell carcinoma (18), gastric cancer (19), glioma (20, 21), melanoma (22), head and neck squamous cell carcinoma (23), hepatocellular carcinoma (HCC) (24, 25), lung cancer (LC) (26–28), osteosarcoma (29), ovarian cancer (30, 31), pancreatic cancer (32), and prostate cancer (33).

In this review, we summarize the latest progress of miR-608 research in the past decade and detail the expression, biogenesis, biological functions, and functional mechanisms of miR-608 in different cancers.

REGULATION OF MIR-608 EXPRESSION

The 3'-UTR is the crucial area by which miRNAs exert posttranscriptional regulatory functions. Upstream molecules can also bind to the 3'-UTR of miRNAs, downregulate miRNA levels and suppress the biological functions of miRNAs. Generally, upstream molecules mainly include lncRNAs, proteins, circular RNAs (circRNAs), chemical substances and drugs. Among these, 3'-UTR regions of CD44, which is a transmembrane glycoprotein, was firstly identified to bind to miR-608. The CD44 3'-UTR competitively binds with the 3'-UTR of miR-608, thus inhibiting miR-608 functions and releasing the inhibition of downstream mRNAs (34). As additional upstream molecules of miR-608, tumor suppressor candidate-2 pseudogene (TUSC2P) and tumor suppressor candidate 2 (TUSC2) arrest the functions of miR-608 *via* their 3'-UTRs, which subsequently increases translation of TUSC2. TUSC2 is a tumor suppressor, and TUSC2P represses cell invasion, migration, and colony formation *via* the TUSC2P/miR-608/TUSC2 axis (35). Moreover, the TUSC2P/miR-608/TUSC2 axis has been verified to be related to esophageal squamous cell carcinoma (ESCC) (36). In addition, in human lung adenocarcinoma (LUSC), B-cell lymphocyte xL (Bcl-xL), as an anti-apoptotic protein, can interact with hsa-miR-608 and further play a carcinogenic role through the PI3K/AKT, WNT, TGF-b, and ERK signaling pathways (37). Xu et al. (38) revealed that in neuroblastoma, 2,3,7,8-tetrachlorodibenzo-p-dioxin (TCDD) could bind to the aryl hydrocarbon receptor (AhR), induce upregulation of miR-608 and regulate the expression level of cell division cycle 42 (CDC42). An antagonist of AhR, CH223191, can reverse the effect of TCDD, further enhancing the reliability of the above results (38). Kang et al. (39) successfully demonstrated that during Kaposi's sarcoma-associated herpesvirus (KSHV) lytic infection, open reading frame 57 (ORF57) combined with miRNA and induces the expression of human interleukin 6 (hIL-6), accelerating cell proliferation and tumorigenesis. Thus, the virus can promote the occurrence and development of tumors by interfering with the function of miRNAs (39, 40). Equally notable is that natural products can influence the expression level of miR-608. For example, toosendanin (TSN) upregulates miR-608 and inhibits downstream targets, including Notch1 and Notch2 (41). In addition, circRNAs can also interact with miR-608, and Liu et al. (42) revealed that a circ_0089153/miR-608/EGFR/p53 interaction pathway exists in ameloblastoma (AB). The biological function of circ_0089153 relies on the MAPK signaling pathway (42).

Among the confirmed upstream targets of miR-608, long noncoding RNAs (lncRNAs) account for the highest proportion, which will be described in detail below. LINC00963 sponges miR-608 and upregulates the miR-608 target matrix metallopeptidase 15 (MMP-15) (14) in acute myeloid leukaemia (AML). Interestingly, in melanoma, LINC00963 can also interact with miR-608 and further elevate nucleus accumbens associated 1 (NACC1) expression, facilitating cell proliferation, migration and invasion (22), similar to what is seen in AML. Moreover, the lncRNA HOXD-AS1 was also found to bind with miR-608 and promote cell proliferation, migration, invasion, metastasis, and chemoresistance (43). Wang et al. (30) indicated that HOXD-AS1 combines with miR-608 and increases frizzled class receptor 4 (FZD4), participating in the development of ovarian cancer. The lncRNA NORAD has also been found to bind to miR-608 in cancer and upregulate forkhead box O6 (FOXO6) in gastric cancer, accelerating cell growth (19, 44). A similar axis also exists in ovarian cancer, but surprisingly, NORAD induces overexpression of signal transducer and activator of transcription 3 (STAT3) by interacting with miR-608 and functions as a tumor suppressor (31). Remarkably, Zhang et al. (20) also confirmed that lncHAS2-AS1 is another upstream target of miR-608, and STAT1 was found to be an upstream factor of lncHAS2-AS1. Both STAT1 and STAT3 belong to the STAT family. Thus, lncRNAs, miRNAs, mRNAs, and proteins can together form networks of mutual influence and interaction. With the increasing number of relevant studies, a more comprehensive and detailed understanding of these networks will be achieved. In addition, LINC02747, LINC00052, the lncRNA MALAT1, and the lncRNA BLACAT1 can also act as upstream molecules of miR-608 (**Table 1**) (**Figure 1**) (18, 23, 29, 45).

DYSREGULATION OF MIR-608 IN MALIGNANT DISEASES

MiR-608 in Acute Myeloid Leukaemia (AML)

For adults, AML is the most common leukaemia and is characterized by a reduction in normal haematopoietic cells and their replacement by primitive cells. At present, diagnosis is generally achieved by identifying cell immunophenotypes (46–48). Abnormal genetic examination results are recognized as an important prognostic factor. However, accumulating evidence has revealed that some people with normal genetic test results may also have AML (49). Therefore, it is necessary to find new diagnostic markers to screen these patients. Zuo et al. (14) demonstrated that both LINC00963 and MMP15 are

TABLE 1 | The upstream and target genes of miR-608 in multiple cancers.

Cancer type	Upstream factor	Target gene	Refs.
Acute myeloid leukaemia	LINC00963	MMP-15	(14)
Acute myeloid leukaemia	LncRNA HOTTIP	DDA1	(15)
Ameloblastoma	circ_0089153	EGFR, p53	(42)
Cancer	TUSC2P and TUSC2	TUSC2	(35)
Cancer	CD44	CDC42	(34)
Cancer	LncRNA HOXD-AS1		(43)
Cancer	LncRNA NORAD		(44)
Clear cell renal cell carcinoma	LINC02747	TFE3	(18)
Esophageal squamous cell carcinoma	TUSC2P	TUSC2	(36)
Gastric cancer	LncRNA NORAD	FOXO6	(19)
Glioblastoma	STAT1/lncHAS2-AS1	PRPS1	(20)
Glioma	toosendanin	Notch1 (Notch2)	(41)
Head and neck squamous cell carcinoma	LncRNA TMEM83	EGFR	(23)
Kaposi's sarcoma associated with herpesvirus	ORF57	vIL-6, hIL-6	(39)
Kaposi's sarcoma associated with herpesvirus	ORF57	vIL-6, hIL-6	(40)
Lung adenocarcinoma	Bcl-xL Silencing		
Melanoma	LINC00963	NACC1	(22)
Melanoma	LncRNA MALAT1/LINC00047		(45)
Neuroblastoma	TCDD/AhR	CDC42	(38)
Osteosarcoma	LncRNA BLACAT1	SOX12	(29)
Ovarian cancer	LncRNA HOXD-AS1	FZD4	(30)
Ovarian cancer	LncRNA NORAD	STAT3	(31)

upregulated in AML, while miR-608 is reduced. LINC00963 inhibits miR-608 and increases MMP15, which can repress AML cell growth and epithelial to mesenchymal transition (EMT) (14). Interestingly, Zhuang et al. (15) proposed that the lncRNA HOTTIP can upregulate DET1 and DDB1-associated 1 (DDA1) by sponging miR-608. However, the overexpression of DDA1 promotes AML cell proliferation and cell cycle progression (15), which contradicts the research results above. This is because the effector molecules MMP15 and DDA1 have different biological functions. These results remind us that if we want to utilize miRNA as a therapeutic target or diagnostic marker, there may be problems with low specificity.

MiR-608 in Bladder Cancer (BCa)

BCa is one of the most common cancers of the urinary system. The incidence rate of males is higher than that of females (50). BCa causes approximately 150000 deaths worldwide annually (51). Patients with BCa are often admitted to the hospital as an emergency, and the proportion of patients who are actively found through physical examination is not high. In addition, emergency admission often means poor prognosis (52, 53). Therefore, we urgently need to find new diagnostic biomarkers for the early detection of BCa. Liang et al. (11) found that miR-608 is always downregulated in BCa, which accelerates cell proliferation and cell cycle progression. When miR-608 is upregulated, it inhibits the expression of FLOT1 and induces G1 phase arrest *via* the AKT/FOXO3a signaling pathway. In a xenograft model *in vitro*, upregulated miR-608 was shown to repress BCa cell proliferation (11). In addition, another team also obtained the same results: overexpression of miR-608 can suppress cell survival and invasion and promote cell apoptosis (54). Therefore, miR-608 seems to have the potential to become a diagnostic marker or therapeutic target.

MiR-608 in Colorectal Cancer (CRC)

CRC currently has the fourth highest incidence rate in the world. In recent decades, with the continuous development of screening technology, the incidence rate of CRC has peaked. Early screening is one of the most effective measures to improve the prognosis of CRC patients, so finding new diagnostic markers remains important (55–57). In the past decade, there have been many meta-analyses and studies of the correlation of miR-608 rs4919510 and CRC, but the conclusions have not been consistent. Kupcinskas et al. (58) revealed that in Europe, miR-608 rs4919510 has no association with CRC. Interestingly, another team proposed that miR-608 rs4919510 is related to the risk of CRC in both African Americans and Caucasians (59). Both Dai et al. (60) and Ying et al. (61) further found that miR-608 rs4919510 is associated with decreased risk of CRC, although Gong's team disagrees (60–62). In addition, Pardini et al. (63) and Xing et al. (64) discovered that miR-608 rs4919510 is related to the prognosis of CRC, specifically, CRC recurrence-free survival (RFS). The rs4919510 variant G allele of miR-608 may upregulate MRPL43 by causing loss of its function, thus promoting CRC cell proliferation, invasion, and migration, inhibiting cell apoptosis, and ultimately increasing the risk of CRC (65). However, in 2018, another study reported that for the Iranian population, miR-608 rs4919510 was not associated with the incidence rate of CRC but was associated with metastatic risk (66). Therefore, we believe that miR-608 is a potential predictive biomarker of CRC.

MiR-608 in Hepatocellular Carcinoma (HCC)

HCC is the third leading cancer worldwide. The incidence rate of HCC has been high due to the pervasiveness of hepatitis B virus (HBV) and hepatitis C virus (HCV) infection. Therefore, HCC

has caused massive economic costs to human society. It is necessary to find new biomarkers to improve the prognosis of HCC (67–69). Wang et al. (25) found that miR-608 was downregulated in the HCC cell lines HepG2 and SK-Hep-1. Correlation analysis was performed with baseline clinical information. An elevated level of miR-608 was associated with a good prognosis of HCC and was specifically related to tumor size, differentiation, clinical stage, overall survival (OS) and disease-free survival (DFS). Moreover, the researchers also found that miR-608 inhibits its target macrophage migration inhibitory factor (MIF) and promotes cell proliferation (25). Surprisingly, He et al. (24) discovered almost the same pathway, except that the final effector molecule was not MIF but bromodomain-containing 4 (BRD4). This result further confirms that miRNAs can often play a role by targeting multiple targets. If there is synergy between these targets, the specific miRNAs can be considered potential biomarkers. Interestingly, another study revealed that miR-608 rs4919510 is significantly related to good prognosis (long OS) (70). Wang et al. (71) confirmed this conclusion by collecting clinical information from 993 HCC patients and 992 healthy individuals. Therefore, miR-608 has prognostic value and is expected to become a potential therapeutic target for HCC.

MiR-608 in Lung Cancer (LC)

Among cancers, the incidence rate of LC is the highest in the world, and the incidence rate of LC in women with a history of smoking is the third highest. LC also has the highest mortality among cancers, and the mortality rates in men and women are both the second highest (72–75). Therefore, it is of great significance to reveal the mechanisms underlying the occurrence and development of LC. In 2016, Li et al. (27) discovered that miR-608 rs4919510 was likely associated with both LC risk and susceptibility to LC. In 2019, Xu et al. (26) revealed that compared with that in normal lung tissue, miR-608 expression was downregulated in LC tissue. A dual-luciferase reporter experiment showed that BRD4 was a direct target of miR-608, and the expression level of BRD4 was upregulated in LC tissues. Reduced miR-608 can also promote LC cell proliferation, migration, and invasion through the JAK2/STAT3 signaling pathway (26). These results confirm the results of a study three years ago. Moreover, miR-608 was also found to be downregulated in non−small-cell lung cancer (NSCLC) by of sequencing samples from 106 NSCLC patients and 124 healthy people. Although miR-608 does not affect the incidence of NSCLC, miR-608 can target transcription factor AP-4 (TFAP4) *via* the Hippo-YAP signaling pathway, thereby promoting NSCLC cell apoptosis and inhibiting cell proliferation (28, 76). Through the Hippo-YAP signaling pathway, miR-608 can also target TEA domain transcription factor 2 (TEAD2) and increase cisplatin sensitivity in NSCLC (77). Moreover, miR-608 can exert a tumor-protecting function in small-cell lung cancer (78). What is more surprising is that in LUSC, miR-608 promotes LUAD cell death and increases the antiproliferative effect of gefitinib *via* the PI3K/AKT, WNT, TGF-β, and ERK signaling pathways (37, 79). Therefore, there is sufficient evidence to indicate that miR-608 is a potential therapeutic target and prognostic biomarker.

MiR-608 in Pancreatic Cancer

Pancreatic cancer has the worst prognosis of solid tumors (80, 81). Pancreatic cancer mortality ranks fourth among cancers worldwide and has risen considerably in the past few years (82, 83). The incidence of pancreatic cancer continues to slowly increase. This trend is because most pancreatic cancers are exocrine cell tumors, and the prognosis for exocrine cell tumors is worse than that of endocrine cell pancreatic cancers. Of exocrine cell tumors, pancreatic ductal adenocarcinomas (PDACs) are the most common subtype (84). Unfortunately, it is very difficult to detect pancreatic cancer early because of the lack of obvious symptoms. Thus, further discovery of new predictive biomarkers is urgently needed. In 2020, Nishiwada et al. (85) successfully constructed a diagnostic model that consisted of 6 miRNAs and had excellent performance in identifying lymph node metastasis in PDAC patients. The success of this model implies that miRNAs can be very valuable in the early diagnosis of pancreatic cancer. Interestingly, in pancreatic cancer, miR-608 is downregulated, and miR-608 can target ribonucleotide reductase M1 (RRM1) and cytidine deaminase (CDA) and control gemcitabine resistance (32). miR-608 also promotes PDAC cell apoptosis and prolongs PDAC patient OS by binding BRD4 (86, 87) and AKT serine/threonine kinase 2 (AKT2). Therefore, miR-608 has the potential to act as a new diagnostic and prognostic marker and even a treatment target for pancreatic cancer.

MiR-608 in Esophageal Squamous Cell Carcinoma (ESCC)

The incidence rate and mortality rate of esophageal cancer are among the top ten rates of all cancers (88–90). Esophageal adenocarcinoma (EAC) and ESCC are the two major subtypes of esophageal cancer (88). New biomarkers for ESCC are currently a hot topic of research, and miRNAs have already shown some advantages. Liu et al. (36) revealed that in ESCC EC109 and TE-1 cells, miR-608 targets TUSC2, inhibits cell proliferation and invasion, and promotes cell apoptosis. In addition, miR-608 rs4919510 can also act as a predictive factor for ESCC, as proven by bioinformatics methods (91).

MiR-608 in Other Cancers

In addition to the cancers mentioned above, miR-608 is also reduced in many other cancers. In chordoma, miR-608 is significantly downregulated and interacts with EGFR and Bcl-xL. The downregulation of miR-608 can accelerate chordoma cell proliferation and migration and repress cell apoptosis (17). In addition, miR-608 sponges RAC2/BCL2L1 and promotes prostate cancer cell proliferation, G2/M transition, and migration (33). In addition, miR-608 also exerts a tumor-inhibiting effect in breast cancer (92), clear cell renal cell carcinoma, gastric cancer, glioblastoma (GBM), glioma, head and neck squamous cell carcinoma, rectal cancer, Kaposi's sarcoma associated with herpesvirus infection, melanoma, nasopharyngeal

TABLE 2 | The expression profile and biological functions and mechanisms of miR-608.

Cancer type	Expression	Clinical features	Target gene	Function	Refs.
Acute myeloid leukaemia	downregulated		MMP-15	cell growth↓ and epithelial to mesenchymal transition (EMT)↓	(14)
Acute myeloid leukaemia	downregulated		DDA1	proliferation↑, cell cycle progression↑	(15)
Bladder cancer	downregulated		FLOT1	proliferation↑	(11)
Bladder cancer	upregulated			proliferation↓, invasion↓, apoptosis↑	(54)
Chordoma	downregulated		EGFR, Bcl-xL	proliferation↑, migration↑, apoptosis↓	(17)
Clear cell renal cell carcinoma	downregulated	high TNM stage and histological grade and poor prognosis	TFE3	proliferation↑	(18)
Colon cancer			NAA10	proliferation↓, migration↓, and cell cycle progression↓, apoptosis↑	(93)
Colorectal cancer			MRPL43	apoptosis↓, proliferation↑, invasion↑, migration↑, cell cycle progression↑	(65)
Colorectal cancer				metastasis↓	(66)
Colorectal cancer					(61)
Colorectal cancer					(58)
Colorectal cancer					(59)
Colorectal cancer					(62)
Colorectal cancer					(63)
Colorectal cancer		recurrence-free survival			(64)
Colorectal cancer					(60)
Metastatic colorectal cancer		tumor recurrence			(94)
Esophageal squamous cell carcinoma					(91)
Esophageal squamous cell carcinoma			TUSC2	proliferation↓, invasion↓, apoptosis↑	(36)
Gastric cancer	downregulated	poor prognosis	FOXO6	cell growth↑	(19)
Gastric cancer					(95)
Glioblastoma	downregulated	poor prognosis	PRPS1	migration↑, invasion↑	(20)
Glioma			Notch1 (Notch2)	apoptosis↑	(41)
Glioma stem cells	downregulated		MIF	proliferation↑, migration↑, invasion↑, apoptosis↓	(21)
Head and neck squamous cell carcinoma	downregulated		EGFR	progression↑	(23)
Head and neck squamous cell carcinoma				tumor growth↓	(96)
Hepatocellular carcinoma		good prognosis, long OS			(70)
Hepatocellular carcinoma					(71)
Hepatocellular carcinoma	downregulated		BRD4	proliferation↑	(24)
Hepatocellular carcinoma	downregulated	tumor size, differentiation, clinical stage, overall survival, disease-free survival	MIF	proliferation↑	(25)
Rectal cancer		better prognosis			(12)
Kaposi's sarcoma associated with herpesvirus (KSHV)			vIL-6, hIL-6	cell proliferation↑, tumorigenesis↑	(39)
Kaposi's sarcoma associated with herpesvirus (KSHV)			vIL-6, hIL-6		(40)
Lung adenocarcinoma/ non-small-cell lung cancer			AKT2	apoptosis↑	(87)
Lung adenocarcinoma		progression-free survival		anti-proliferation effect of gefitinib↑	(79)
Lung adenocarcinoma				cell death↑	(37)
Lung cancer	downregulated		BRD4	proliferation↑, migration↑, invasion↑	(26)
Lung cancer	downregulated			lung cancer risk↑, susceptibility to lung cancer↑	(27)
Non-small-cell lung cancer	downregulated	does not influence the incidence of NSCLC patients	TFAP4	apoptosis↓, migration↑	(76)
Non-small-cell lung cancer	downregulated		TEAD2	cisplatin sensitivity↓	(77)
Non-small-cell lung cancer	downregulated		TFAP4	apoptosis↓	(28)
Small-cell lung cancer					(78)
Melanoma	downregulated	poor prognosis	NACC1	proliferation↑, migration↑, invasion↑	(22)
Melanoma	downregulated			proliferation↑, migration↑, invasion↑	(45)
Nasopharyngeal carcinoma					(97)
Nasopharyngeal carcinoma					(98)

(Continued)

TABLE 2 | Continued

Cancer type	Expression	Clinical features	Target gene	Function	Refs.
Neuroblastoma			CDC42		(38)
Osteosarcoma	downregulated		SOX12	proliferation↑, migration↑, invasion↑	(29)
Ovarian cancer	downregulated	poor prognosis	FZD4	proliferation↑, colony formation↑, migration↑, invasion↑	(30)
Ovarian cancer	downregulated		STAT3	cancer growth-inhibiting effects of physcion 8-O-β-glucopyranoside↓, invasion↓, migration↓, apoptosis↑	(31)
Pancreatic cancer	downregulated		RRM1 and CDA	gemcitabine resistance↑	(32)
Pancreatic ductal adenocarcinoma		OS	BRD4	apoptosis↑	(86)
Prostate cancer	downregulated		RAC2/BCL2L1	proliferation↑, G2/M transition↑, migration↑	(33)

↑ *means promote and* ↓ *means inhibit.*

carcinoma (NPC), neuroblastoma, osteosarcoma, and ovarian cancer (**Table 2**).

Mechanism by Which MiR-608 Inhibits Tumor Growth

Clinically, in almost all cancers, tumor size is closely related to the prognosis of patients and influences the choice of treatment. Thus, the mechanisms of tumor growth and progression deserve attention. Tumor growth is closely related to the degrees of tumor cell proliferation and apoptosis. Whether a tumor grows often depends on which of these processes is stronger. Increasing evidence shows that miR-608 can significantly inhibit the proliferation of a variety of solid tumors, suggesting that miR-608 is closely related to cell proliferation and apoptosis. Next, we will elaborate the molecular mechanism by which miR-608 is involved in tumor growth from two perspectives.

MiR-608 and Transmembrane Proteins

Membrane proteins are the main executors of biofilm function. They can effectively participate in cell energy exchange, information recognition and transmission and material transport. According to the different positions of membrane proteins in the cell membrane, these proteins can be divided into peripheral membrane proteins and internal membrane proteins, which are also called transmembrane proteins (99). miR-608 can bind to the 3'-UTR of many transmembrane proteins to inhibit cancer cell proliferation and accelerate cell apoptosis. Among these transmembrane proteins, EGFR is especially important because EGFR can interact with epidermal growth factor (EGF) and induce receptor dimerization and tyrosine autophosphorylation, resulting in cell proliferation. Both Liu et al. (42) and Zhang et al. (17) reported that EGFR is a target of miR-608 and that miR-608 can indirectly attenuate cell proliferation by inhibiting EGFR. Moreover, MMP-15, another transmembrane protein, binds to miR-608 and participates in the progression of AML. Furthermore, rescue experiments indicate that overexpression of LINC00963 promotes cell proliferation and EMT by modulating MMP-15 (14). Interestingly, FZD4 is reported to be upregulated in ovarian cancer, and FZD4 is a transmembrane protein that belongs to the β-catenin signaling pathway. Generally, HOXD4-AS1 exerts tumor-promoting functions through the miR-608/FZD4 axis in ovarian cancer (30). These four studies all clearly indicate that the inhibition of transmembrane proteins by miR-608 leads to suppression of cell growth.

MiR-608 and Signaling Pathways

miR-608 modulates tumor growth not only by affecting transmembrane proteins but also by affecting multiple signaling pathways. The MAPK pathway has three levels of signal transmission: MAPK, MAPK kinase (MEK or MKK) and kinase of MAPK kinase (MEKK or MKKK). These three kinase levels can be activated in sequence and together regulate a variety of important physiological/pathological effects, such as cell growth and differentiation (100). Importantly, MAPK is also involved in the apoptosis induced by ultraviolet radiation (101). miR-608 targets EGFR and p53 and affects cell cycle processes *via* the MAPK pathway (42). Interestingly, p53 can further activate the PI3K/AKT pathway and influence the cell cycle and mitosis (102). In addition, miR-608 also affects the AKT/FOXO3a signaling pathway to control cell proliferation. miR-608 inhibits both the AKT and FOXO3a kinases and blocks the signaling pathway to attenuate cell proliferation (11) and accelerate cell apoptosis. Moreover, when miR-608 is overexpressed, the expression levels of BRD4, p-JAK2, p-STATA3, CD44, and MMP9 are significantly decreased, indicating that the JAK2/STAT3 signaling pathway is inhibited by miR-608 (26). The inhibition of miR-608 is essential for tumor suppression.

MiR-608 as a Biomarker

MiR-608 as a Diagnostic Biomarker

Early detection and diagnosis are key to improving the prognosis of cancers. An increasing number of studies have shown that the expression of miRNAs is significantly different between cancer tissues and normal tissues (12, 18, 33, 94). This difference can even be detected directly in body fluids (103), which has laid a foundation for the noninvasive detection of miRNA. single-nucleotide polymorphisms of genes encoding miRNAs significantly influence tumor susceptibility and can also act as diagnostic biomarkers for cancers. Ju et al. (18) demonstrated that in clear cell renal cell carcinoma, LINC02747 can sponge miR-608 and further upregulate the mRNA of the target TFE3. The authors suggest that LINC02747 has diagnostic potential for renal cell carcinoma (18). We also believe that miR-608 can be regarded as a diagnostic marker of renal cell tumors because

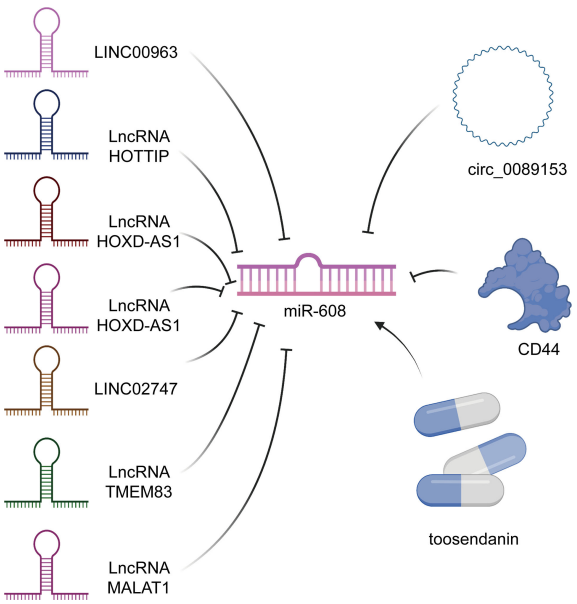

FIGURE 1 | Upstream targets of miR-608. Not only many lncRNAs can regulate the level of miR-608, but also some circRNAs and drugs, such as toosendanin, can also play the role of regulator of miR-608.

miR-608 is inhibited by upstream LINC02747. In addition, Tokarz et al. (94) found that single-nucleotide polymorphisms of the gene encoding miR-608 can also be used to accurately diagnose metastatic CRC. Moreover, after determining the genotypes of 1358 CRC patients and 1079 healthy controls through sequencing, another team found that miR-608 rs4919510 is obviously related to CRC susceptibility (61). Interestingly, researchers in LC also proposed that miR-608 rs4919510 can significantly affect tumor susceptibility (27).

MiR-608 as Prognostic Biomarker

In addition to its diagnostic biomarker potential, miR-608 also has the potential to become a prognostic marker for cancers. Expression of miR-608 is correlated with TNM stage, histological grade, and prognosis; and miR-608 has a close relationship with the prognosis of clear cell renal cell carcinoma (18). In addition, several studies have revealed that miR-608 can function as a prognostic marker (63, 65) and predict CRC recurrence (94). miR-608 rs4919510 was also found to be related to the RFS of CRC (64). Moreover, after collecting basic HCC clinicopathological information, Wang et al. (25) proved that miR-608 is highly correlated with HCC tumor size, differentiation, clinical stage, OS, and DFS. The researchers verified that a decrease in miR-608 facilitated the proliferation of the HCC cell lines HepG2 and SK-Hep-1 (25). Interestingly, Ma et al. (70) confirmed that miR-608 rs4919510 is associated with good prognosis and long OS. To our surprise, miR-608 was reported to be related to the PFS of LUSC patients, and miR-608 expression can indicate poor prognosis of ovarian cancer patients (30, 79). In summary, we found that miR-608 has unprecedented potential for predicting prognosis in solid tumors. However, there are few studies on the prognostic role of miR-608 in haematopoietic system tumors. miR-608 will likely

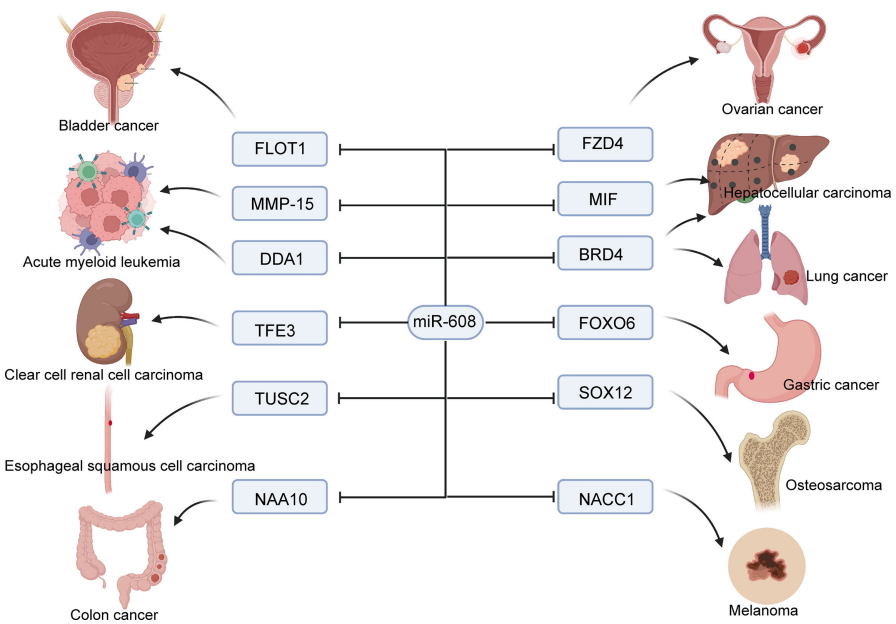

FIGURE 2 | Molecular mechanism of miR-608 affecting tumor cell proliferation. miR-608 targets a large number of genes to inhibit cancer cell growth, including bladder cancer, ovarian cancer, lung cancer, liver cancer, and renal cancer, etc.

be a promising prognostic marker for multiple tumors, including both solid tumors and non-solid tumors.

MiR-608 as Therapeutic Target

Intriguingly, miR-608 has already shown obvious therapeutic effects in tumors according to dozens of studies. TSN can elevate the expression level of miR-608, enhancing glioma cell apoptosis *via* the Notch signaling pathway. *In vivo* experiments also showed that TSN clearly inhibits tumor growth (41). Wang et al. (21) indicated that overexpression of miR-608 attenuates glioma stem cell proliferation, invasion, and migration and induces cell apoptosis, clearly explaining the therapeutic effect of miR-608 in tumors. Moreover, miR-608 can be sponged by LINC00052, regulate the expression of EGFR, and further promote the progression of head and neck squamous cell carcinoma *in vivo* and *in vitro* (23). Overexpression of miR-608 promoted doxorubicin-induced NSCLC cell apoptosis by repressing the expression of TFAP4, and TFAP4 was overexpressed in NSCLC tissues (28). Jiao et al. (22) illustrated that the LINC00963-miR-608-NACC1 pathway might be a potential treatment target for melanoma. Moreover, the roles of the BLACAT1/miR-608/SOX12 axis in osteosarcoma (29), HOXD4-AS1/miR-608/FZD4 axis (30) in ovarian cancer, and lncRNA NORAD/miR-608/STAT3 (31) axis in melanoma indicate that miR-608 could be an ideal therapeutic target. Li et al. (86) revealed that miR-608 can decrease the level of BRD4 and facilitate cell apoptosis. However, in PDAC, miR-608 is usually significantly reduced. A strategy to overexpress miR-608 utilizing gene editing technology or targeted therapy could significantly improve the prognosis for PDAC (86). Zhang et al. (33) also elucidated that miR-608 can obviously alleviate the progression of prostate cancer. Taken together, our findings provide valuable insights for the chemotherapy of multiple tumors, especially solid tumors.

CONCLUSIONS

In this review, we comprehensively summarized the latest and most valuable research on miR-608. Many researchers in the field of cancer are constantly looking for more potential tumor biomarkers to achieve tumor prevention and treatment. In recent decades, researchers have gradually found that miRNAs play an important role in the occurrence and development of tumors, and an increasing number of people have devoted themselves to studying this field. In addition, miR-608 is a novel miRNA with much potential. miR-608 is decreased in almost all solid tumors except bladder cancer (54). Interestingly, although the results of individual studies are different, miR-608 has been found to consistently play a role in inhibiting cancer in all tumors (**Figure 2**) . This result is surprising and provides new hope for tumor treatment.

Unfortunately, there are no clinical trials related to miR-608 yet, which may be a result of the failure of other drugs with similar targets, such as MRX34, which is miR-34a mimic (104). According to the results of previous clinical trials, the problems with such drugs are probably related to the multiple serious adverse reactions. We speculate that such reactions are caused by the low specificity of miRNA drugs. Thus, in future drug design, organ-specific drug dosages should be designed according to the characteristics of different organs to increase the accuracy of pharmacological effects and reduce complications. In addition, due to the wide distribution of RNases *in vivo*, miRNA drugs also face the challenge of RNA degradation. At present, most strategies use nanocarriers to reduce RNA degradation, but the toxicity of such drugs remains to be studied. In summary, miR-608 has obvious potential for the diagnosis, prognostication and treatment of cancer. To benefit patients in the future, new drugs need to be designed through potential technical routes, and clinical trials need to be carried out as soon as possible.

AUTHOR CONTRIBUTIONS

LL designed and guided the study. JL and DZ wrote and edited the manuscript. All authors contributed to the article and approved the submitted version.

FUNDING

This work was supported by the National Key Research and Development Program of China (2019YFC0840600 and 2019YFC0840609), and the Independent Project Fund of the State Key Laboratory for Diagnosis and Treatment of Infectious Diseases, the National Key Research and Development Program of China (2016YFC1101404/3).

REFERENCES

1. Rupaimoole R, Slack FJ. MicroRNA Therapeutics: Towards a New Era for the Management of Cancer and Other Diseases. *Nat Rev Drug Discov* (2017) 16:203–22. doi: 10.1038/nrd.2016.246
2. Simonson B, Das S. MicroRNA Therapeutics: The Next Magic Bullet? *Mini Rev Med Chem* (2015) 15:467–74. doi: 10.2174/1389557515666150324123208
3. Lu TX, Rothenberg ME. MicroRNA. *J Allergy Clin Immunol* (2018) 141:1202–7. doi: 10.1016/j.jaci.2017.08.034
4. Thorpe TE. Priestley in America, 1794–1804. *Nature* (1921) 108:394–7. doi: 10.1038/108394a0
5. Su JL, Chen PS, Johansson G, Kuo ML. Function and Regulation of Let-7 Family microRNAs. *Microrna* (2012) 1:34–9. doi: 10.2174/2211536611201010034
6. Lee RC, Feinbaum RL, Ambros V. The C. Elegans Heterochronic Gene Lin-4 Encodes Small RNAs With Antisense Complementarity to Lin-14. *Cell* (1993) 75:843–54. doi: 10.1016/0092-8674(93)90529-Y
7. Lee YS, Dutta A. MicroRNAs in Cancer. *Annu Rev Pathol* (2009) 4:199–227. doi: 10.1146/annurev.pathol.4.110807.092222
8. Mishra S, Yadav T, Rani V. Exploring miRNA Based Approaches in Cancer Diagnostics and Therapeutics. *Crit Rev Oncol Hematol* (2016) 98:12–23. doi: 10.1016/j.critrevonc.2015.10.003

9. Zhang L, Liao Y, Tang L. MicroRNA-34 Family: A Potential Tumor Suppressor and Therapeutic Candidate in Cancer. *J Exp Clin Cancer Res* (2019) 38:53. doi: 10.1186/s13046-019-1059-5
10. Okugawa Y, Grady WM, Goel A. Epigenetic Alterations in Colorectal Cancer: Emerging Biomarkers. *Gastroenterology* (2015) 149:1204–25.e12. doi: 10.1053/j.gastro.2015.07.011
11. Liang Z, Wang X, Xu X, Xie B, Ji A, Meng S, et al. MicroRNA-608 Inhibits Proliferation of Bladder Cancer *via* AKT/FOXO3a Signaling Pathway. *Mol Cancer* (2017) 16:96. doi: 10.1186/s12943-017-0664-1
12. Sclafani F, Chau I, Cunningham D, Lampis A, Hahne JC, Ghidini M, et al. Sequence Variation in Mature microRNA-608 and Benefit From Neo-Adjuvant Treatment in Locally Advanced Rectal Cancer Patients. *Carcinogenesis* (2016) 37:852–7. doi: 10.1093/carcin/bgw073
13. Choi YC, Yoon S, Byun Y, Lee G, Kee H, Jeong Y, et al. MicroRNA Library Screening Identifies Growth-Suppressive microRNAs That Regulate Genes Involved in Cell Cycle Progression and Apoptosis. *Exp Cell Res* (2015) 339:320–32. doi: 10.1016/j.yexcr.2015.10.012
14. Zuo W, Zhou K, Deng M, Lin Q, Yin Q, Zhang C, et al. LINC00963 Facilitates Acute Myeloid Leukemia Development by Modulating miR-608/MMP-15. *Aging (Albany NY)* (2020) 12:18970–81. doi: 10.18632/aging.103252
15. Zhuang MF, Li LJ, Ma JB. LncRNA HOTTIP Promotes Proliferation and Cell Cycle Progression of Acute Myeloid Leukemia Cells. *Eur Rev Med Pharmacol Sci* (2019) 23:2908–15. doi: 10.26355/eurrev_201904_17569
16. Hashemi M, Sanaei S, Rezaei M, Bahari G, Hashemi SM, Mashhadi MA, et al. miR-608 Rs4919510 C>G Polymorphism Decreased the Risk of Breast Cancer in an Iranian Subpopulation. *Exp Oncol* (2016) 38:57–9. doi: 10.31768/2312-8852.2016.38(1):57-59
17. Zhang Y, Schiff D, Park D, Abounader R. MicroRNA-608 and microRNA-34a Regulate Chordoma Malignancy by Targeting EGFR, Bcl-xL and MET. *PLoS One* (2014) 9:e91546. doi: 10.1371/journal.pone.0091546
18. Ju X, Sun Y, Zhang F, Wei X, Wang Z, He X. Long non-Coding RNA LINC02747 Promotes the Proliferation of Clear Cell Renal Cell Carcinoma by Inhibiting miR-608 and Activating TFE3. *Front Oncol* (2020) 10:573789. doi: 10.3389/fonc.2020.573789
19. Miao Z, Guo X, Tian L. The Long Noncoding RNA NORAD Promotes the Growth of Gastric Cancer Cells by Sponging miR-608. *Gene* (2019) 687:116–24. doi: 10.1016/j.gene.2018.11.052
20. Zhang L, Wang H, Xu M, Chen F, Li W, Hu H, et al. Long Noncoding RNA HAS2-AS1 Promotes Tumor Progression in Glioblastoma *via* Functioning as a Competing Endogenous RNA. *J Cell Biochem* (2020) 121:661–71. doi: 10.1002/jcb.29313
21. Wang Z, Xue Y, Wang P, Zhu J, Ma J. MiR-608 Inhibits the Migration and Invasion of Glioma Stem Cells by Targeting Macrophage Migration Inhibitory Factor. *Oncol Rep* (2016) 35:2733–42. doi: 10.3892/or.2016.4652
22. Jiao H, Jiang S, Wang H, Li Y, Zhang W. Upregulation of LINC00963 Facilitates Melanoma Progression Through miR-608/NACC1 Pathway and Predicts Poor Prognosis. *Biochem Biophys Res Commun* (2018) 504:34–9. doi: 10.1016/j.bbrc.2018.08.115
23. Ouyang T, Zhang Y, Tang S, Wang Y. Long non-Coding RNA LINC00052 Regulates miR-608/EGFR Axis to Promote Progression of Head and Neck Squamous Cell Carcinoma. *Exp Mol Pathol* (2019) 111:104321. doi: 10.1016/j.yexmp.2019.104321
24. He L, Meng D, Zhang SH, Zhang Y, Deng Z, Kong LB. microRNA-608 Inhibits Human Hepatocellular Carcinoma Cell Proliferation *via* Targeting the BET Family Protein BRD4. *Biochem Biophys Res Commun* (2018) 501:1060–7. doi: 10.1016/j.bbrc.2018.05.108
25. Wang K, Liang Q, Wei L, Zhang W, Zhu P. MicroRNA-608 Acts as a Prognostic Marker and Inhibits the Cell Proliferation in Hepatocellular Carcinoma by Macrophage Migration Inhibitory Factor. *Tumor Biol* (2016) 37:3823–30. doi: 10.1007/s13277-015-4213-5
26. Xu W, Sun D, Wang Y, Zheng X, Li Y, Xia Y, et al. Inhibitory Effect of microRNA-608 on Lung Cancer Cell Proliferation, Migration, and Invasion by Targeting BRD4 Through the JAK2/STAT3 Pathway. *Bosn J Basic Med Sci* (2020) 20:347–56. doi: 10.17305/bjbms.2019.4216
27. Li D, Zhu G, Di H, Li H, Liu X, Zhao M, et al. Associations Between Genetic Variants Located in Mature microRNAs and Risk of Lung Cancer. *Oncotarget* (2016) 7:41715–24. doi: 10.18632/oncotarget.9566
28. Wang YF, Ao X, Liu Y, Ding D, Jiao WJ, Yu Z, et al. MicroRNA-608 Promotes Apoptosis in non-Small Cell Lung Cancer Cells Treated With Doxorubicin Through the Inhibition of TFAP4. *Front Genet* (2019) 10:809. doi: 10.3389/fgene.2019.00809
29. Chen X, Cui Y, Ma Y. Long non-Coding RNA BLACAT1 Expedites Osteosarcoma Cell Proliferation, Migration and Invasion *via* Up-Regulating SOX12 Through miR-608. *J Bone Oncol* (2020) 25:100314. doi: 10.1016/j.jbo.2020.100314
30. Wang Y, Zhang W, Wang Y, Wang S. HOXD-AS1 Promotes Cell Proliferation, Migration and Invasion Through miR-608/FZD4 Axis in Ovarian Cancer. *Am J Cancer Res* (2018) 8:170–82.
31. Yang X, Yan Y, Chen Y, Li J, Yang J. Involvement of NORAD/miR-608/STAT3 Axis in Carcinostasis Effects of Physcion 8-O-β-Glucopyranoside on Ovarian Cancer Cells. *Artif Cells Nanomed Biotechnol* (2019) 47:2855–65. doi: 10.1080/21691401.2019.1637884
32. Rajabpour A, Afgar A, Mahmoodzadeh H, Radfar JE, Rajaei F, Teimoori-Toolabi L. MiR-608 Regulating the Expression of Ribonucleotide Reductase M1 and Cytidine Deaminase is Repressed Through Induced Gemcitabine Chemoresistance in Pancreatic Cancer Cells. *Cancer Chemother Pharmacol* (2017) 80:765–75. doi: 10.1007/s00280-017-3418-2
33. Zhang X, Fang J, Chen S, Wang W, Meng S, Liu B. Nonconserved miR-608 Suppresses Prostate Cancer Progression Through RAC2/PAK4/LIMK1 and BCL2L1/caspase-3 Pathways by Targeting the 3'-UTRs of RAC2/BCL2L1 and the Coding Region of PAK4. *Cancer Med* (2019) 8:5716–34. doi: 10.1002/cam4.2455
34. Jeyapalan Z, Deng Z, Shatseva T, Fang L, He C, Yang BB. Expression of CD44 3'-Untranslated Region Regulates Endogenous microRNA Functions in Tumorigenesis and Angiogenesis. *Nucleic Acids Res* (2011) 39:3026–41. doi: 10.1093/nar/gkq1003
35. Rutnam ZJ, Du WW, Yang W, Yang X, Yang BB. The Pseudogene TUSC2P Promotes TUSC2 Function by Binding Multiple microRNAs. *Nat Commun* (2014) 5:2914. doi: 10.1038/ncomms3914
36. Liu F, Gong R, He B, Chen F, Hu Z. TUSC2P Suppresses the Tumor Function of Esophageal Squamous Cell Carcinoma by Regulating TUSC2 Expression and Correlates With Disease Prognosis. *BMC Cancer* (2018) 18:894. doi: 10.1186/s12885-018-4804-9
37. Othman N, In LL, Harikrishna JA, Hasima N. Bcl-xL Silencing Induces Alterations in hsa-miR-608 Expression and Subsequent Cell Death in A549 and SK-LU1 Human Lung Adenocarcinoma Cells. *PLoS One* (2013) 8:e81735. doi: 10.1371/journal.pone.0081735
38. Xu T, Xie HQ, Li Y, Xia Y, Chen Y, Xu L, et al. CDC42 Expression is Altered by Dioxin Exposure and Mediated by Multilevel Regulations *via* AhR in Human Neuroblastoma Cells. *Sci Rep* (2017) 7:10103. doi: 10.1038/s41598-017-10311-3
39. Kang JG, Pripuzova N, Majerciak V, Kruhlak M, Le SY, Zheng ZM. Kaposi's Sarcoma-Associated Herpesvirus ORF57 Promotes Escape of Viral and Human Interleukin-6 From microRNA-Mediated Suppression. *J Virol* (2011) 85:2620–30. doi: 10.1128/JVI.02144-10
40. Kang JG, Majerciak V, Uldrick TS, Wang X, Kruhlak M, Yarchoan R, et al. Kaposi's Sarcoma-Associated Herpesviral IL-6 and Human IL-6 Open Reading Frames Contain miRNA Binding Sites and are Subject to Cellular miRNA Regulation. *J Pathol* (2011) 225:378–89. doi: 10.1002/path.2962
41. Wang Q, Wang Z, Hou G, Huang P. Toosendanin Suppresses Glioma Progression Property and Induces Apoptosis by Regulating miR-608/Notch Axis. *Cancer Manag Res* (2020) 12:3419–31. doi: 10.2147/CMAR.S240268
42. Liu J, Qiao X, Liu J, Zhong M. Identification of Circ_0089153/miR-608/EGFR P53 Axis in Ameloblastoma *via* MAPK Signaling Pathway. *Oral Dis* (2021) 28(3):756–70. doi: 10.1111/odi.13788
43. Xie SC, Yang YJ, Zhang JQ, Zhou S, Xie SW, Hua YY. HOXD-AS1: A Novel Oncogenic Long Intergenic non-Coding RNA in Humans. *Eur Rev Med Pharmacol Sci* (2019) 23:2898–907. doi: 10.26355/eurrev_201904_17568
44. Ghafouri-Fard S, Azimi T, Hussen BM, Abak A, Taheri M, Dilmaghani NA. Non-Coding RNA Activated by DNA Damage: Review of its Roles in the Carcinogenesis. *Front Cell Dev Biol* (2021) 9:714787. doi: 10.3389/fcell.2021.714787
45. Wu S, Chen H, Zuo L, Jiang H, Yan H. Suppression of Long Noncoding RNA MALAT1 Inhibits the Development of Uveal Melanoma *via*

microRNA-608-Mediated Inhibition of HOXC4. *Am J Physiol Cell Physiol* (2020) 318:C903–12. doi: 10.1152/ajpcell.00262.2019
46. Prada-Arismendy J, Arroyave JC, Röthlisberger S. Molecular Biomarkers in Acute Myeloid Leukemia. *Blood Rev* (2017) 31:63–76. doi: 10.1016/j.blre.2016.08.005
47. De Kouchkovsky I, Abdul-Hay M. 'Acute Myeloid Leukemia: A Comprehensive Review and 2016 Update'. *Blood Cancer J* (2016) 6:e441. doi: 10.1038/bcj.2016.50
48. Kayser S, Levis MJ. Clinical Implications of Molecular Markers in Acute Myeloid Leukemia. *Eur J Haematol* (2019) 102:20–35. doi: 10.1111/ejh.13172
49. Riva L, Luzi L, Pelicci PG. Genomics of Acute Myeloid Leukemia: The Next Generation. *Front Oncol* (2012) 2:40. doi: 10.3389/fonc.2012.00040
50. Dobruch J, Daneshmand S, Fisch M, Lotan Y, Noon AP, Resnick MJ, et al. Gender and Bladder Cancer: A Collaborative Review of Etiology, Biology, and Outcomes. *Eur Urol* (2016) 69:300–10. doi: 10.1016/j.eururo.2015.08.037
51. Aghaalikhani N, Rashtchizadeh N, Shadpour P, Allameh A, Mahmoodi M. Cancer Stem Cells as a Therapeutic Target in Bladder Cancer. *J Cell Physiol* (2019) 234:3197–206. doi: 10.1002/jcp.26916
52. Bladder Cancer: Diagnosis and Management of Bladder Cancer: © NICE (2015) Bladder Cancer: Diagnosis and Management of Bladder Cancer. *BJU Int* (2017) 120:755–65. doi: 10.1111/bju.14045
53. Seidl C. Targets for Therapy of Bladder Cancer. *Semin Nucl Med* (2020) 50:162–70. doi: 10.1053/j.semnuclmed.2020.02.006
54. Xiang M, Yuan W, Zhang W, Huang J. Expression of miR-490-5p, miR-148a-3p and miR-608 in Bladder Cancer and Their Effects on the Biological Characteristics of Bladder Cancer Cells. *Oncol Lett* (2019) 17:4437–42. doi: 10.3892/ol.2019.10143
55. Dekker E, Tanis PJ, Vleugels JLA, Kasi PM, Wallace MB. Colorectal Cancer. *Lancet* (2019) 394:1467–80. doi: 10.1016/S0140-6736(19)32319-0
56. Simon K. Colorectal Cancer Development and Advances in Screening. *Clin Interv Aging* (2016) 11:967–76. doi: 10.2147/CIA.S109285
57. Aran V, Victorino AP, Thuler LC, Ferreira CG. Colorectal Cancer: Epidemiology, Disease Mechanisms and Interventions to Reduce Onset and Mortality. *Clin Colorectal Cancer* (2016) 15:195–203. doi: 10.1016/j.clcc.2016.02.008
58. Kupcinskas J, Bruzaite I, Juzenas S, Gyvyte U, Jonaitis L, Kiudelis G, et al. Lack of Association Between miR-27a, miR-146a, miR-196a-2, miR-492 and miR-608 Gene Polymorphisms and Colorectal Cancer. *Sci Rep* (2014) 4:5993. doi: 10.1038/srep05993
59. Ryan BM, McClary AC, Valeri N, Robinson D, Paone A, Bowman ED, et al. Rs4919510 in Hsa-Mir-608 is Associated With Outcome But Not Risk of Colorectal Cancer. *PLoS One* (2012) 7:e36306. doi: 10.1371/journal.pone.0036306
60. Dai ZM, Lv JR, Liu K, Lei XM, Li W, Wu G, et al. The Role of microRNA-608 Polymorphism on the Susceptibility and Survival of Cancer: A Meta-Analysis. *Aging (Albany NY)* (2018) 10:1402–14. doi: 10.18632/aging.101476
61. Ying HQ, Peng HX, He BS, Pan YQ, Wang F, Sun HL, et al. MiR-608, pre-miR-124-1 and Pre-Mir26a-1 Polymorphisms Modify Susceptibility and Recurrence-Free Survival in Surgically Resected CRC Individuals. *Oncotarget* (2016) 7:75865–73. doi: 10.18632/oncotarget.12422
62. Rong GQ, Zhang XM, Chen B, Yang XD, Wu HR, Gong W. MicroRNA Gene Polymorphisms and the Risk of Colorectal Cancer. *Oncol Lett* (2017) 13:3617–23. doi: 10.3892/ol.2017.5885
63. Pardini B, Rosa F, Naccarati A, Vymetalkova V, Ye Y, Wu X, et al. Polymorphisms in microRNA Genes as Predictors of Clinical Outcomes in Colorectal Cancer Patients. *Carcinogenesis* (2015) 36:82–6. doi: 10.1093/carcin/bgu224
64. Xing J, Wan S, Zhou F, Qu F, Li B, Myers RE, et al. Genetic Polymorphisms in pre-microRNA Genes as Prognostic Markers of Colorectal Cancer. *Cancer Epidemiol Biomarkers Prev* (2012) 21:217–27. doi: 10.1158/1055-9965.EPI-11-0624
65. Zhu X, Liu Y, Xu J, Cheng Z, Yu Y, Chu M, et al. miR-608 Rs4919510 Polymorphism may Affect Susceptibility to Colorectal Cancer by Upregulating MRPL43 Expression. *DNA Cell Biol* (2020) 39:2017–27. doi: 10.1089/dna.2020.5689
66. Ranjbar R, Chaleshi V, Aghdaei HA, Morovvati S. Investigating the Association Between miR-608 Rs4919510 and miR-149 Rs2292832 With Colorectal Cancer in Iranian Population. *MicroRNA* (2018) 7:100–6. doi: 10.2174/2211536607666180206145540
67. Sherman M. Epidemiology of Hepatocellular Carcinoma. *Oncology* (2010) 78 Suppl 1:7–10. doi: 10.1159/000315223
68. Ferlay J, Shin HR, Bray F, Forman D, Mathers C, Parkin DM. Estimates of Worldwide Burden of Cancer in 2008: GLOBOCAN 2008. *Int J Cancer* (2010) 127:2893–917. doi: 10.1002/ijc.25516
69. Altekruse SF, Henley SJ, Cucinelli JE, McGlynn KA. Changing Hepatocellular Carcinoma Incidence and Liver Cancer Mortality Rates in the United States. *Am J Gastroenterol* (2014) 109:542–53. doi: 10.1038/ajg.2014.11
70. Ma XP, Yu G, Chen X, Xiao Q, Shi Z, Zhang LY, et al. MiR-608 Rs4919510 is Associated With Prognosis of Hepatocellular Carcinoma. *Tumor Biol* (2016) 37:9931–42. doi: 10.1007/s13277-016-4897-1
71. Wang R, Zhang J, Ma Y, Chen L, Guo S, Zhang X, et al. Association Study of Mir−149 Rs2292832 and Mir−608 Rs4919510 and the Risk of Hepatocellular Carcinoma in a Large−Scale Population. *Mol Med Rep* (2014) 10:2736–44. doi: 10.3892/mmr.2014.2536
72. Schwartz AG, Cote ML. Epidemiology of Lung Cancer. *Adv Exp Med Biol* (2016) 893:21–41. doi: 10.1007/978-3-319-24223-1_2
73. Nasim F, Sabath BF, Eapen GA. Lung Cancer. *Med Clin North Am* (2019) 103:463–73. doi: 10.1016/j.mcna.2018.12.006
74. Bade BC, Dela Cruz CS. Lung Cancer 2020: Epidemiology, Etiology, and Prevention. *Clin Chest Med* (2020) 41:1–24. doi: 10.1016/j.ccm.2019.10.001
75. Nanavaty P, Alvarez MS, Alberts WM. Lung Cancer Screening: Advantages, Controversies, and Applications. *Cancer Control* (2014) 21:9–14. doi: 10.1177/107327481402100102
76. Huang C, Yue W, Li L, Li S, Gao C, Si L, et al. Expression of MiR-608 in Nonsmall Cell Lung Cancer and Molecular Mechanism of Apoptosis and Migration of A549 Cells. *BioMed Res Int* (2020) 2020:8824519. doi: 10.1155/2020/8824519
77. Wang Y, Li F, Ma D, Gao Y, Li R, Gao Y. MicroRNA−608 Sensitizes non −Small Cell Lung Cancer Cells to Cisplatin by Targeting TEAD2. *Mol Med Rep* (2019) 20:3519–26. doi: 10.3892/mmr.2019.10616
78. Yan H, Xin S, Ma J, Wang H, Zhang H, Liu J. A Three microRNA-Based Prognostic Signature for Small Cell Lung Cancer Overall Survival. *J Cell Biochem* (2018) 1–8. doi: 10.1002/jcb.28159
79. Zhang N, Li Y, Zheng Y, Zhang L, Pan Y, Yu J, et al. miR-608 and miR-4513 Significantly Contribute to the Prognosis of Lung Adenocarcinoma Treated With EGFR-TKIs. *Lab Invest* (2019) 99:568–76. doi: 10.1038/s41374-018-0164-y
80. Goral V. Pancreatic Cancer: Pathogenesis and Diagnosis. *Asian Pac J Cancer Prev* (2015) 16:5619–24. doi: 10.7314/APJCP.2015.16.14.5619
81. Simoes PK, Olson SH, Saldia A, Kurtz RC. Epidemiology of Pancreatic Adenocarcinoma. *Chin Clin Oncol* (2017) 6:24. doi: 10.21037/cco.2017.06.32
82. Ilic M, Ilic I. Epidemiology of Pancreatic Cancer. *World J Gastroenterol* (2016) 22:9694–705. doi: 10.3748/wjg.v22.i44.9694
83. De La Cruz MS, Young AP, Ruffin MT. Diagnosis and Management of Pancreatic Cancer. *Am Fam Physician* (2014) 89:626–32.
84. Grossberg AJ, Chu LC, Deig CR, Fishman EK, Hwang WL, Maitra A, et al. Multidisciplinary Standards of Care and Recent Progress in Pancreatic Ductal Adenocarcinoma. *CA Cancer J Clin* (2020) 70:375–403. doi: 10.3322/caac.21626
85. Nishiwada S, Sho M, Banwait JK, Yamamura K, Akahori T, Nakamura K, et al. A MicroRNA Signature Identifies Pancreatic Ductal Adenocarcinoma Patients at Risk for Lymph Node Metastases. *Gastroenterology* (2020) 159:562–74. doi: 10.1053/j.gastro.2020.04.057
86. Li M, Li T, Ma W, Wang X, Zhao G. MicroRNA-608 Promotes Apoptosis *via* BRD4 Downregulation in Pancreatic Ductal Adenocarcinoma. *Oncol Lett* (2020) 19:1418–26. doi: 10.3892/ol.2019.11246
87. Othman N, Nagoor NH. miR-608 Regulates Apoptosis in Human Lung Adenocarcinoma *via* Regulation of AKT2. *Int J Oncol* (2017) 51:1757–64. doi: 10.3892/ijo.2017.4174
88. Reichenbach ZW, Murray MG, Saxena R, Farkas D, Karassik EG, Klochkova A, et al. Clinical and Translational Advances in Esophageal Squamous Cell Carcinoma. *Adv Cancer Res* (2019) 144:95–135. doi: 10.1016/bs.acr.2019.05.004

89. Uhlenhopp DJ, Then EO, Sunkara T, Gaduputi V. Epidemiology of Esophageal Cancer: Update in Global Trends, Etiology and Risk Factors. *Clin J Gastroenterol* (2020) 13:1010–21. doi: 10.1007/s12328-020-01237-x
90. Lam AK. Introduction: Esophageal Squamous Cell Carcinoma-Current Status and Future Advances. *Methods Mol Biol* (2020) 2129:1–6. doi: 10.1007/978-1-0716-0377-2_1
91. Yang PW, Huang YC, Hsieh CY, Hua KT, Huang YT, Chiang TH, et al. Association of miRNA-Related Genetic Polymorphisms and Prognosis in Patients With Esophageal Squamous Cell Carcinoma. *Ann Surg Oncol* (2014) 21 Suppl 4:S601–9. doi: 10.1245/s10434-014-3709-3
92. Huang AJ, Yu KD, Li J, Fan L, Shao ZM. Polymorphism Rs4919510:C>G in Mature Sequence of Human microRNA-608 Contributes to the Risk of HER2-Positive Breast Cancer But Not Other Subtypes. *PLoS One* (2012) 7: e35252. doi: 10.1371/journal.pone.0035252
93. Yang H, Li Q, Niu J, Li B, Jiang D, Wan Z, et al. microRNA-342-5p and miR-608 Inhibit Colon Cancer Tumorigenesis by Targeting NAA10. *Oncotarget* (2016) 7:2709–20. doi: 10.18632/oncotarget.6458
94. Tokarz P, Blasiak J. The Role of microRNA in Metastatic Colorectal Cancer and its Significance in Cancer Prognosis and Treatment. *Acta Biochim Pol* (2012) 59:467–74. doi: 10.18388/abp.2012_2079
95. Jiang J, Jia ZF, Cao DH, Wu YH, Sun ZW, Cao XY. Association of the miR-146a Rs2910164 Polymorphism With Gastric Cancer Susceptibility and Prognosis. *Future Oncol* (2016) 12:2215–26. doi: 10.2217/fon-2016-0224
96. Pan W, Wu C, Su Z, Duan Z, Li L, Mi F, et al. Genetic Polymorphisms of non-Coding RNAs Associated With Increased Head and Neck Cancer Susceptibility: A Systematic Review and Meta-Analysis. *Oncotarget* (2017) 8:62508–23. doi: 10.18632/oncotarget.20096
97. Zheng J, Deng J, Xiao M, Yang L, Zhang L, You Y, et al. A Sequence Polymorphism in miR-608 Predicts Recurrence After Radiotherapy for Nasopharyngeal Carcinoma. *Cancer Res* (2013) 73:5151–62. doi: 10.1158/0008-5472.CAN-13-0395
98. Qiu F, Yang L, Zhang L, Yang X, Yang R, Fang W, et al. Polymorphism in Mature microRNA-608 Sequence is Associated With an Increased Risk of Nasopharyngeal Carcinoma. *Gene* (2015) 565:180–6. doi: 10.1016/j.gene.2015.04.008
99. Haffke M, Duckely M, Bergsdorf C, Jaakola VP, Shrestha B. Development of a Biochemical and Biophysical Suite for Integral Membrane Protein Targets: A Review. *Protein Expr Purif* (2020) 167:105545. doi: 10.1016/j.pep.2019.105545
100. Guo YJ, Pan WW, Liu SB, Shen ZF, Xu Y, Hu LL. ERK/MAPK Signaling Pathway and Tumorigenesis. *Exp Ther Med* (2020) 19:1997–2007. doi: 10.3892/etm.2020.8454
101. Zhen AX, Piao MJ, Hyun YJ, Kang KA, Ryu YS, Cho SJ, et al. Purpurogallin Protects Keratinocytes From Damage and Apoptosis Induced by Ultraviolet B Radiation and Particulate Matter 2.5. *Biomol Ther (Seoul)* (2019) 27:395–403. doi: 10.4062/biomolther.2018.151
102. Schaefer T, Steiner R, Lengerke C. SOX2 and P53 Expression Control Converges in PI3K/AKT Signaling With Versatile Implications for Stemness and Cancer. *Int J Mol Sci* (2020) 21:4902. doi: 10.3390/ijms21144902
103. Cortez MA, Bueso-Ramos C, Ferdin J, Lopez-Berestein G, Sood AK, Calin GA. MicroRNAs in Body Fluids–the Mix of Hormones and Biomarkers. *Nat Rev Clin Oncol* (2011) 8:467–77. doi: 10.1038/nrclinonc.2011.76
104. Beg MS, Brenner AJ, Sachdev J, Borad M, Kang YK, Stoudemire J, et al. Phase I Study of MRX34, a Liposomal miR-34a Mimic, Administered Twice Weekly in Patients With Advanced Solid Tumors. *Invest New Drugs* (2017) 35:180–8. doi: 10.1007/s10637-016-0407-y

Conflict of Interest: The authors declare that the research was conducted in the absence of any commercial or financial relationships that could be construed as a potential conflict of interest.

Publisher's Note: All claims expressed in this article are solely those of the authors and do not necessarily represent those of their affiliated organizations, or those of the publisher, the editors and the reviewers. Any product that may be evaluated in this article, or claim that may be made by its manufacturer, is not guaranteed or endorsed by the publisher.

frontiers | Frontiers in Immunology

REVIEW
published: 13 April 2022
doi: 10.3389/fimmu.2022.810539

Research Progress of Biomarkers for Immune Checkpoint Inhibitors on Digestive System Cancers

Jingting Wang[1], *Xiao Ma*[1], *Zhongjun Ma*[1], *Yan Ma*[2], *Jing Wang*[1]* *and Bangwei Cao*[1]*

[1] Department of Oncology, Beijing Friendship Hospital, Capital Medical University, Beijing, China, [2] Department of Comprehensive Medicine, Beijing Shijingshan Hospital, Beijing, China

Immunotherapy represented by immune checkpoint inhibitors has gradually entered a new era of precision medicine. In view of the limited clinical benefits of immunotherapy in patients with digestive system cancers, as well as the side-effects and high treatment costs, development of biomarkers to predict the efficacy of immune therapy is a key imperative. In this article, we review the available evidence of the value of microsatellite mismatch repair, tumor mutation burden, specific mutated genes or pathways, PD-L1 expression, immune-related adverse reactions, blood biomarkers, and patient-related biomarkers in predicting the efficacy of immunotherapy against digestive system cancers. Establishment of dynamic personalized prediction models based on multiple biomarkers is a promising area for future research.

Keywords: immune check inhibitor (ICI), digestive system cancers, immunotherapy, predict therapeutic effectiveness, biomarker

OPEN ACCESS

Edited by:
Yunfei Xu,
Shandong University, China

Reviewed by:
C. Andrew Stewart,
National Cancer Institute (NIH), United States
Albino Eccher,
Integrated University Hospital Verona, Italy

***Correspondence:**
Jing Wang
wangjing1981@ccmu.edu.cn
Bangwei Cao
oncology@ccmu.edu.cn

Specialty section:
This article was submitted to Cancer Immunity and Immunotherapy, a section of the journal Frontiers in Immunology

Received: *07 November 2021*
Accepted: *21 March 2022*
Published: *13 April 2022*

Citation:
Wang J, Ma X, Ma Z, Ma Y, Wang J and Cao B (2022) Research Progress of Biomarkers for Immune Checkpoint Inhibitors on Digestive System Cancers. Front. Immunol. 13:810539. doi: 10.3389/fimmu.2022.810539

1 INTRODUCTION

Immune checkpoint inhibitor (ICI) therapy has transformed the treatment landscape for advanced-stage forms of many cancers, especially non-small cell lung cancer (NSCLC), melanoma, head and neck squamous cell carcinoma, kidney cancer and digestive system cancers. Despite several studies showing good long-term outcomes of these therapies, in clinical practice, the overall response rate (RR) in patients undergoing ICI treatment is unsatisfactory due to the heterogeneity of tumors, with only 20%–40% of patients benefiting from it in most scenarios. Therefore, identification of predictive biomarkers that can help screen patients who are most likely to respond to immunotherapy will help reduce unnecessary treatment costs and avoid immune-related adverse events (irAEs). In the era of personalized medicine, a variety of immunohistochemical techniques and high-throughput sequencing of the human genome are poised to play an increasingly important role by identifying clinically-relevant biomarkers using specimens such as blood samples and tissue specimens. In the context of cancer treatment, assessment of these biomarkers at baseline and at different time-points during treatment can provide valuable information to guide therapeutic decision-making. Moreover, use of a combination of clinical and molecular biomarkers is likely to play an important role in clinical decision-making. Extensive research has been conducted on biomarkers of immunotherapy efficacy in the context of NSCLC and melanoma, but there is a paucity of related studies on digestive system cancers. In this review, we discuss the currently

available biomarkers that can help predict the efficacy of ICI therapy in patients with digestive system cancers (**Figure 1**).

2 BIOMARKERS OF ICI THERAPEUTIC EFFICACY AGAINST DIGESTIVE SYSTEM CANCERS

2.1 Tumor Genome Biomarkers

2.1.1 Mismatch Repair Deficiency and Microsatellite Instability

Microsatellites are short tandem repeats throughout the human genome characterized by single nucleotide, dinucleotide or high nucleotide repetitions, and the number of repetitions is 10–50 times. Compared with normal cells, tumor cells exhibit altered length of microsatellites due to the insertion or deletion of repeat units, a phenomenon referred to as microsatellite instability (MSI). Mismatch repair (MMR) expression loss can cause accumulation of mismatches during DNA replication, leading to the occurrence of MSI. In 2017, the United States Food and Drug Administration (FDA) approved PD-1 antibody drugs for the treatment of "mismatch-repair-deficient (dMMR)/ microsatellite instability-high (MSI-H)" type solid tumors. This is the first anti-tumor therapy that is not based on the source of the tumor, but on molecular biomarkers in a wide range of tumors, laying the foundation for tumor ICI treatment markers. The reported incidence of MSI-H in gastric cancer (GC) and colorectal cancer (CRC) is 9% and 15%–20%, respectively, while the incidence is as high as 69.5% in Lynch syndrome adenocarcinoma (1–3). Clinically, MSI has been used as an important prognostic molecular biomarker in patients with CRC and other solid tumors, and has been used to inform formulation of adjuvant treatment plans; it has also been used to assist in the screening of Lynch syndrome.

In the landmark CHECKMATE 142 trial, MSI-H/dMMR patients with metastatic CRC showed a high degree of benefit from nivolumab treatment with an objective response rate (ORR) of 31%, of which 51 patients (69%) had disease control for ≥12 weeks, and all patients survived during the 12-month follow-up period (10). These patients showed a more sustained clinical benefit from nivolumab and ipilimumab dual immunotherapy, with ORR as high as 55% (11). In the study by Le et al. (9), ORR (40% vs 0%) and 20-week progression-free survival (PFS) rate (78% vs 11%) of metastatic CRC patients treated with pembrolizumab were significantly greater than those of proficient mismatch repair (pMMR) patients. The median progression-free survival (mPFS) and median overall survival (mOS) were not reached in the cohort with dMMR CRC, but were 2.2 and 5.0 months, respectively, in the cohort with pMMR CRC at a median follow-up period of 36 weeks (9). Subsequently, Le have expanded this study to evaluate efficacy of PD-1 blockade in patients with advanced dMMR cancers across 12 different tumor types. Objective radiographic response was observed in 53% and complete response (CR) was achieved in 21% of patients. Neither mPFS nor mOS has been reached yet over a

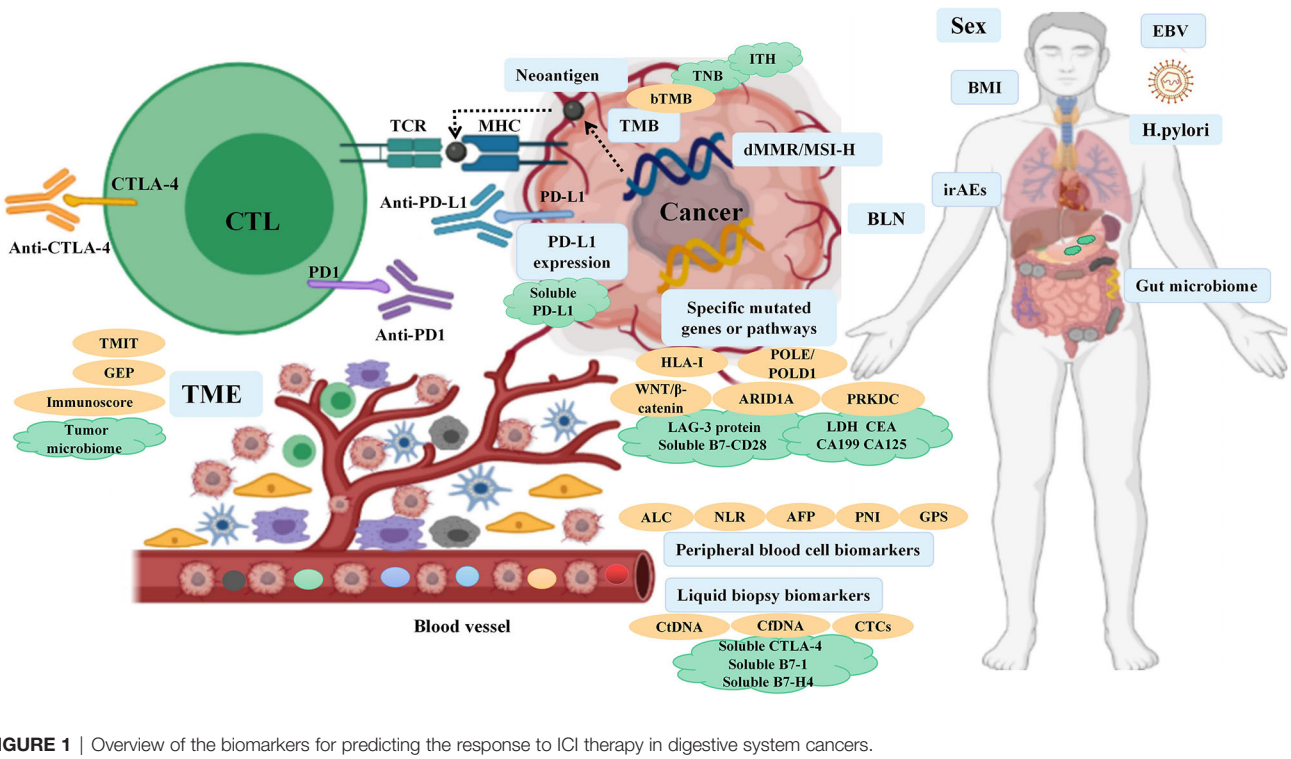

FIGURE 1 | Overview of the biomarkers for predicting the response to ICI therapy in digestive system cancers.

median follow-up time of 12.5 months (2). The results of KEYNOTE-164 and KEYNOTE-158 also further demonstrated the sustained clinical benefit of pembrolizumab in patients with MSI-H/dMMR metastatic CRC (13, 14). In the study by Noor et al., although the MSI-H/dMMR phenotype accounted for only 0.8% of pancreatic cancer patients, in the 7 patients treated with ICI, the mPFS was 8.2 months, and the mOS was not reached during the follow-up period of 6.8 months, resulting in better clinical benefit (12).

dMMR tumors often have a higher density of tumor infiltrating lymphocytes (TIL), and the "high immunogenicity" established by the large number of mutant neoantigens in dMMR tumors may be closely related to the efficacy of PD-1 inhibitors (9). The current National Comprehensive Cancer Network (NCCN) guidelines recommend the use of immunohistochemical staining methods to detect MSI from the protein level, and molecular-level polymerase chain reaction methods to detect specific microsatellite repeat sequence amplification to determine MSI status; however, there are still problems in the detection or interpretation process. With the widespread application of high-throughput sequencing platforms, next-generation gene sequencing (NGS) is being gradually applied for detection of microsatellite status, and can greatly increase the sensitivity of detection (18).

2.1.2 Tumor Mutation Burden

Tumor mutation burden (TMB) is an exploration of tumors at the level of human genome. TMB is defined as the number of somatic mutations in the whole genome after including the germ line DNA variants. The enhanced tumor immunogenicity and low immunosuppressive tumor micro-environment (TME) of high tumor mutation burden (TMB-H) can affect the sensitivity and clinical efficacy of ICI therapy based on the underlying assumption that TMB-H can create antigenic peptides (15, 19). In 2020, based on the findings from the phase 2 KEYNOTE-158, TMB was approved by FDA for the treatment of patients with any unresectable or metastatic non-dMMR/MSI TMB-H (TMB≥10 mut/MB) solid cancer that has progressed on prior therapy and for which no alternative treatment options are available. The KEYNOTE-158 study included patients with advanced malignancies involving the anal canal and biliary system; after a median follow-up of 37.1 months, objective response (OR) were observed in 30 (29%) of 102 patients in the tissue TMB-H (tTMB-H) group (≥10 mut/MB) and 43 (6%) of 688 patients in the non tTMB-H group. These findings indicated that the tTMB-H subgroup of patients may show a robust tumor response to pembrolizumab monotherapy (7). In a retrospective study of 1638 tumor patients, including CRC and hepatocellular carcinoma (HCC), who received immunotherapy and underwent full genetic testing and TMB assessment, TMB-H was independently related to efficacy of immunotherapy. TMB-H patients (TMB≥20 mut/MB) had significantly higher RR (58% vs 20%) and mPFS (12.8 vs 3.3 months) than those with low tumor mutation burden (TMB-L), and there was a positive linear correlation between TMB-H and the efficacy of anti-PD-1/PD-L1 monotherapy (4). In a study of 58 patients with advanced GC treated with toripalimab, TMB-H patients (TMB≥12 mut/MB) had significantly longer OS than patients with TMB-L (14.6 vs 4 months) (5). Furthermore, in the study by Schrock et al., the mPFS for TMB-H patients with metastatic CRC has not been reached (median follow-up >18 months) while the mPFS of TMB-L patients was 2 months (6). According to a recent research, TMB-H CRC in the Cancer Genome Atlas showed a trend towards increased RR and significantly improved prognosis (15). The above research results suggest that TMB is a novel and useful biomarker in patients with MSI-H mCRC, GC, and HCC, which can help stratify patients based on the likelihood of clinical benefit of ICI therapy.

However, the FDA approval for use of TMB has been met with mixed reviews. McGrail's analysis determined the correlation between TMB and survival benefit by analyzing genetic data of more than 10,000 cancer patients. The results failed to support the use of TMB-H as a biomarker for ICI treatment in all solid cancer types. TMB-H was found to predict the efficacy of immunotherapy for category I cancers types (such as CRC) where neoantigen load is related to CD8 T cell levels, while TMB-H was not found to predict response in category II cancer types where neoantigen load is not positively correlated with CD8 T-cell levels. Therefore, as the predictive value of TMB differs in different tumor types, further tumor type-specific research is necessary (15).

There is no clear consensus about several aspects of the use of TMB in predicting the efficacy of ICI therapy, such as the definition of the TMB-H threshold. In addition, whether TMB is a predictive or prognostic marker, or both, is not clear. Wu found that TMB has different effects on survival outcomes in different cancer types and can be incorporated in prognostic and risk stratification (20). Another important shortcoming is that TMB cannot more specifically reflect the immunogenicity of neoantigens. As an emerging auxiliary indicator of the TMB, the tumor neoantigen burden (TNB) is an indicator that reflects the total number of neoantigens in tumor cells. Tumor neoantigens can be presented by human MHC molecules and activate immune cells, and patients with more neoantigens are more likely to continue to benefit from immunotherapy. There is a highly significant correlation between TNB and anti-PD-1 treatment response, and TNB can directly and more accurately predict the response of anti-PD-1 treatment than TMB (21). TNB predicts the benefit of immunotherapy for digestive system cancers. Further research is required to explore whether TNB can replace TMB as a valuable immune predictor. In summary, the somatic mutation rate of tumors and the potential to form neoantigens are related to their sensitivity to ICI therapy. NGS technology used in combination with MSI and TMB analysis may be a more accurate tool for selecting cancer patients for immunotherapy (22).

In clinical settings, tissue biopsy is the standard for cancer diagnosis and treatment, and tTMB test is the primary choice when tumor tissue can be obtained or is adequate for use. However, TMB measurement in tumor tissue biopsy specimen is typically limited to a specific region of the tumor and may not accurately reflect the mutation panorama of the entire tumor; in particular, it may not capture the spatial and temporal heterogeneity found in patients with metastasis, and

the main reason for the failure of detection lies in insufficient tumor tissue and/or tumor cells. Recent studies have emphasized that detecting blood TMB (bTMB) offers practical advantages over use of tissue to detect tTMB. It is a simple and non-invasive alternative to tissue biopsy. It has advantages of fast turnaround time, high patient compliance, good specificity, low heterogeneity, and repeated sampling. Yang evaluated the bTMB of peripheral blood circulating tumor DNA (ctDNA) in patients with esophageal cancer, and found that the RR in the high bTMB group (bTMB >8) was significantly greater than that in the low bTMB group (bTMB ≤8) (61.5% vs 47.1%), confirming the feasibility of bTMB as an immunotherapy biomarker for esophageal cancer (8). In the MYSTIC study, bTMB was found to have a higher detection success rate than tissue samples (81% vs 63%) (23). However, the limitations of bTMB are that detection of mutations in plasma samples is influenced by the amount of tumor shedding, the depth of coverage, and clonal hematopoietic mutations. In addition, ctDNA content may also affect bTMB prediction efficiency. In order to overcome this limitation, in a study of lung cancer, ctDNA content of patients was incorporated into the algorithm model of bTMB, and the concept of low allele frequency bTMB was proposed, suggesting a significant correlation between ctDNA content and survival (24). It was more accurate than traditional bTMB in predicting the benefits of immunotherapy in this population. This study indicates the need to explore the potential biological mechanism of the predictive value of bTMB and to further optimize the predictive value of bTMB in digestive system tumors.

Intratumoral heterogeneity (ITH) refers to spatial or temporal heterogeneity with respect to the distribution of genomic diversity in a single tumor, resulting from cumulative gene mutations. Patients with low ITH were found to perform better in presentation and recognition of neoantigens during immunotherapy, predicting the prognosis in NSCLC (25). The research indicated that the response to immunotherapy can be optimally predicted by using the combination of ITH and TMB, and subsequently verified a consistent role of ITH in esophageal and GC. Further studies are required to expand the use of ITH in predicting the response of digestive system cancers to immunotherapy.

The level of correlation between subsets of biomarkers should also be noted, in particular, mutation metrics, such as subclonal TMB and cloned TMB. Kevin collated whole-exome and transcriptomic data from >1000 patients with 8 cancer types (including CRC) who were treated with ICI, to validate the multivariate predictors of immunotherapy (26). They found that clonal TMB was the strongest predictor of ICI response, followed by TMB and CXCL9 expression, while subclonal TMB and somatic copy alteration burden showed no significant predictive ability. They also observed a negative association between the burden of subclonal mutations and all indicators of immune infiltration, such as characteristics of CD8 effects, which is consistent with the recent emphasis on immunosuppressive effects of high burden of subclonal mutations. Tumors with high levels of neoantigens have a lower antigen dose than homogenous tumors with a high clonal neoantigen load, thus reducing the chances of recognizing T cells that respond to subclonal neoantigens (27). When T cells respond to subclonal neoantigens, these cells will not be able to target all tumor cells, thus limiting the attack on the tumor as a whole (28). These studies highlighted that neoantigen heterogeneity may influence immune surveillance and support the use of clonal neoantigens as biomarkers for predicting the efficacy of immunotherapy.

2.1.3 Specific Mutated Genes or Pathways

The NGS technology provides reliable targets and biomarkers of response to ICI treatment of digestive system cancers. The available data provides novel insights for defining biomarker-driven immunotherapy responses in specific genes mutations.

In the study by Harding, activation of altered Wnt/β-catenin signaling in HCC patients was found to be associated with lower disease control rate (DCR) (53% vs 0), shorter mPFS (7.4 vs 2.0 months) and mOS (15.2 vs 9.1 months) (16). In HCC, Wnt/CTNNB1 mutations characterize the immune excluded class and WNT activation leads to T-lymphocyte exclusion, making it a predictive biomarker of intrinsic innate resistance to ICI therapy in HCC (29). Therefore, HCC patients with alterations of non-WNT pathway notably respond or derive clinical benefit from immunotherapy. However, due to the small sample size and confounding factors in this study, further large-scale studies are required to confirm the clinical significance of Wnt/CTNNB1 mutations. In addition, *POLE* and *POLD1* are genes encoding DNA polymerase subunits that play a key role in the proofreading fidelity of DNA replication. *POLE* mutations are more common in patients with right colon cancer, stable microsatellites, and young men. In a study of 47,721 patients with various cancers including CRC, esophagogastric cancer, cholangiocarcinoma, HCC, and pancreatic ductal adenocarcinoma (PDAC), patients with *POLE* or *POLD1* mutations were found to have significantly higher TMB than those without these mutations, and their OS was significantly longer than that of wild-type populations (34 vs 18 months), which has been verified as an independent predictor of ICI treatment (17). Furthermore, Hu collectively reviewed the association between *ARID1A* inactivation and MMR, TMB, PD-L1, and TME. They found that *ARID1A* mutation may potentially serve as a predictive biomarker for ICI therapy in GC (30). The potential basis for *ARID1A* deficiency and immunotherapeutic sensitivity may be related to its disruption of mismatch repair, promotion of tumor mutation, increase of PD-L1 expression, and regulation of TME. In addition, the TMB of *PRKDC* mutation samples was significantly higher than that of *PRKDC* wild-type samples, especially in GC and CRC. Based on the TCGA tumor database, the expressions of CD8+T cells, NK cells, immune checkpoints, and chemokines were significantly increased in *PRKDC* mutation samples. *PRKDC* mutations predict favorable response to ICI therapy in lung cancer and melanoma, and can be further promoted in gastrointestinal (GI) cancers in the future (31). Moreover, human leukocyte antigen (*HLA*) gene is a polymorphic region in human genome. Increase in somatic mutation rate of *HLA* gene is significantly correlated with *HLA* dysfunction, which is a potential mechanism of immune escape, involved in carcinogenesis and tumor progression, and affects the efficacy of immunotherapy. *HLA* class I genotype polymorphism

was shown to be associated with better prognosis in patients with NSCLC and advanced melanoma (32). In patients with advanced esophageal cancer, the immunotherapy RR (85.71% vs 27.27%) and mPFS (7.683 vs 1.867 months) of patients with *HLA* heterozygous type were significantly higher and longer than those of homozygous type, respectively, suggesting that *HLA* typing may be a potential biomarker for predicting immunotherapy efficacy (see **Table 1**) (8).

Confirmation of the above preliminary data on the predictive effect of gene mutations in current and future clinical trials will widen the prospects of their use to inform treatment decision-making with respect to immunotherapy for digestive system cancers.

2.2 PD-L1 Expression

PD-L1, expressed on immune and tumor cells, interacts with PD-1 on immune checkpoint proteins that negatively regulate anti-tumor immune response, which enables tumor cells to evade immune surveillance. PD-L1 expression is closely related to a wide pattern of coregulated gene expression including T cell activation markers, T cell cytokine recruitment, and antigen presentation across multiple cell types (33). The expression

TABLE 1 | Predictive ability of tumor genome-related biomarkers for response to ICI therapy for digestive system cancers.

Type of predictors		Cancer type	ICI therapy	Number	Outcome	TMB-H	TMB-L	Reference
TMB	tTMB	Cancer (including CRC, HCC)	anti-PD-1/PD-L1	151	RR PFS OS	58% 12.8 months Not reached	20% 3.3 months 16.3 months	Goodman 2017 (4)
		Chemo-refractory AGC	anti-PD-1 (Toripalimab)	58	OS	14.6 months	4 months	Wang 2019 (5)
		MSI-H mCRC	anti-PD-1/PD-L1	22	mPFS	Not reached	2 months	Schrock 2019 (6)
		Advanced solid tumors (including anal and biliary)	anti-PD-1 (Pembrolizumab)	790	ORR	29%	6%	Marabelle 2020 (7)
	bTMB	Advanced esophageal cancer	anti-PD-1	30	RR	61.5%	47.1%	Yang 2019 (8)
MMR/MSI status						**dMMR**	**pMMR**	
		mCRC	anti-PD-1 (Pembrolizumab)	41	ORR 20-week PFS rate ORR DCR mPFS mOS	40% 78% 40% 90% Not reached Not reached	0% 11% 0% 11% 2.2 months 5.0 months	Le 2015 (9)
		MSI-H mCRC	anti-PD-1 (Nivolumab)	74	ORR	31%	–	Overman 2017 (10)
		MSI-H mCRC	Dual immunotherapy (Nivolumab plus Ipilimumab)	119	ORR	55%	–	Overman 2018 (11)
		PDAC	ICI therapy	7	mPFS mDOR	8.2 Not reached	– –	Noor 2021 (12)
		12 different cancers (including CRC/GEA/pancreas/small intestine/cholangiocarcinoma)	anti-PD-1 (Pembrolizumab)	86	CR	21%	–	Le 2017 (2)
		Treatment-refractory, MSI-H/dMMR mCRC	anti-PD-1 (Pembrolizumab)	128	ORR mDOR	33% Not reached	– –	Le 2019 (13)
		MSI-H/ dMMR cancers (including GC, cholangiocarcinoma, and pancreatic cancers)	anti-PD-1 (Pembrolizumab)	233	ORR mPFS mOS	34.3% 4.1 months 23.5 months	– – –	Marabelle 2019 (14)
		category I cancer types (including CRC)	anti-PD-1/PD-L1/CTLA-4	>10,000	ORR	39.8%	4.1%	McGrail 2021 (15)
						Gene mutation	**Gene wild**	
Gene mutation predictors	WNT/β-catenin pathway	HCC	anti-PD-1/PD-L1/CTLA-4	31	DCR PFS OS	0% 2.0 months 9.1 months	53% 7.4 months 15.2 months	Harding 2019 (16)
	POLE/POLD1 mutations	Multiple cancer (including CRC, esophagogastric cancer)	anti-PD-1/PD-L1/CTLA-4	47,721	OS	34 months	18 months	Wang F 2019 (17)
	HLA class I genotype (heterozygote/homozygous type)	Advanced esophageal cancer	anti-PD-1	25	RR mPFS	85.71% 7.683 months	27.27% 1.867 months	Yang 2019 (8)

AGC, advanced gastric cancer; CRC, colorectal cancer; HCC, hepatocellular carcinoma; TMB, tumor mutation burden; MMR, mismatch-repair; MSI, microsatellite instability; mCRC, metastatic colorectal cancer; DCR, disease control rate; PFS, progression-free survival; mOS, median overall survival; OS, overall survival; mPFS, median progression-free survival; mDOR, median disease control rate; ORR, objective response rate; RR, response rate; PDAC, pancreatic ductal carcinoma; RR, response rate.

level of PD-L1 seems to reflect the balance between host immune response and cancer immune escape, and it is higher in malignant tumor tissues than in precancerous lesions and normal tissues (34, 35). The combined positive score (CPS), tumor proportion score (TPS), and immune cell proportion score (IPS) are commonly used clinical evaluation criteria for PD-L1 expression, as a direct predictor of anti-PD-L1/PD-1 immunotherapy efficacy.

Several large randomized controlled trials have demonstrated the potential use of PD-L1 expression as a predictive biomarker (36, 38). In the KEYNOTE-059 study, 259 patients with previously treated advanced-stage GC or gastro-esophageal junction adenocarcinomas received pembrolizumab; the ORR was 15.5% in patients with a CPS of ≥1 versus 6.4% in those with a CPS of <1 (36). In the KEYNOTE-062 trial, among patients with advanced GC who received pembrolizumab as first-line treatment, those with CPS ≥ 10 showed longer OS (17.4 vs 10.6 months) than those with CPS ≥ 1 (38). Moreover, in heavily pretreated patients with advanced, metastatic adenocarcinoma (AC) or squamous cell carcinoma (SCC) of the esophagus, those with PD- L1 CPS ≥10 showed significantly greater ORR compared to those with CPS <10 (13.8% vs 6.3%) (41). For second-line treatment of AC or SCC, in the Chinese subgroup of the KEYNOTE-181 study, the mOS of those with PD-L1 CPS ≥ 10 was nearly two-fold greater than those with PD-L1 CPS <10 (12.0 vs 6.4 months) (37).

However, there is no clear consensus on the predictive ability of PD-L1 expression as a marker of response to ICI therapy. In the cohort of toripalimab monotherapy for advanced refractory GC, mPFS (5.5 vs 1.9 months, $P = 0.092$) and mOS (12.1 vs 5.3 months, $P = 0.45$) were highly increased in PD-L1 positive patients, but the differences in survival outcomes were not statistically significant (5). Furthermore, exploratory biomarker analysis of PD-L1 expression (≥1% or <1%) showed no significant difference in ORR (28.6% vs 27.7%) and DCR ≥12 weeks (52.4% vs 74.5%) in the nivolumab arm for CRC patients, suggesting that PD-L1 is not a predictive biomarker in these patients (10). Patients with dMMR/MSI-H mCRC showed response to nivolumab plus ipilimumab dual immunotherapy, irrespective of tumor PD-L1 expression (11). A meta-analysis of 9 studies found that high PD-L1 expression rate is associated with poor prognosis of ICI therapy for PDAC (43). In the CHECKMATE 040 study, baseline PD-L1 status in tumor cells showed no apparent effect on ORR in patients with advanced HCC treated with nivolumab (TPS≥1% 26% vs TPS<1% 19%) (40). Use of PD-L1 expression in combination with other biomarkers seems to reduce the offset of a single marker and predict ICI therapy efficacy more accurately. Chemo-refractory GC patients who were TMB-H and PD-L1 positive showed long-term benefits of toripalimab with respect to ORR (33.3% vs 3.0%), PFS (2.7 vs 1.9 months), and OS (12.1 vs 4 months) compared with those with TMB-L and PD-L1 negative status (5).

However, for PD-L1 expression assessment assays, CPS and TPS may have different values for predicting survival benefits. Compared with TPS, CPS is not limited to PD-L1 expression in tumor cells, but includes the sum of all PD- L1 positive cells (tumor cells, lymphocytes, and macrophages). In the KEYNOTE 224 trial, PD-L1 expression assessed by CPS score showed a correlation with the ORR benefit of pembrolizumab treatment in HCC patients (CPS≥1 32% vs CPS<1 20%); however, there was no significant correlation between TPS and therapeutic efficacy, suggesting that the combination of CPS score and TPS score may improve the predictive value of PD-L1 immunohistochemical assay (**Table 2**) (39). Moreover, the use of CPS to determine PD-L1 expression appears to be a more sensitive prognostic biomarker than TPS in GC, but this conclusion has not been generalized to all digestive system cancers (44).

Subclonal genotypes, transcriptome, and epigenetic changes may influence immune escape and explain intratumoral PD-L1 diversity. In MSS mCRC patients, PD-L1 mutations were shown to mediate immune escape of a subset of tumor subclones against avelumab, thereby affecting the efficacy of immunotherapy in a subset of patients expressing high-affinity FcγR3a (45). Patients with PD-L1 mutated subclones showed a higher-than average therapeutic benefit, showing slow dynamics reversing on avelumab withdrawal, which suggest that PD-L1 mutations may mediate the development of resistance to the direct antitumor effects of avelumab. Further trials are required to evaluate the specific clinical benefits of immunotherapy in this subset of MSS mCRC patients.

PD-L1 is a strong predictor of the efficacy of cancer immunotherapy, although it is not completely perfect. There is considerable heterogeneity in the expression of PD-L1 between tumors and within tumors, and its expression is not homogenous even in a pair of independent tumor lesions (46). Paolino found that PD-L1 expression was underestimated in biopsy compared with resected specimens, while the positive expression of PD-L1 was higher in metastatic lymph nodes than in primary tumors (47). In addition, the expression of PD-L1 is inducible and dynamic, and may be affected by interferons and toll-like receptor ligands, radiotherapy, targeted therapy, and chemotherapy (48, 49). Currently, PD-L1 expression is mainly detected using immunohistochemical methods, and there is considerable variability with respect to the positive thresholds set by different studies, the antibody detection platforms and the detection techniques used. Recent studies have analyzed assays for evaluating PD-L1 expression, and the results demonstrated that SP263 assay tended to increase the degree of positive expression while SP142 assay tended to stain better immune cells (50). Cerbelli explored the inter-observer reliability and correlation between PD-L1 expression assays, which revealed high agreement between the 22C3 PharmDx assay and the SP263 assay, suggesting that the two antibodies are interchangeability in immunotherapy (51). Furthermore, the lack of predictive utilization of PD-L1 expression is also attributable to dynamic changes in the TME and the fact that baseline tests may not reflect rapid variation of PD-L1 expression due to adaptive responses to treatment (52). These limitations further heighten concerns about the accuracy of PD-L1 expression. Therefore, formulation of a standardized PD-1/PD-L1 detection method is a key imperative. The expression of PD-L1 alone is not enough to screen people who can fully benefit from ICI treatment.

TABLE 2 | Predictive ability of PD-L1 expression for response to ICI therapy for digestive system cancers.

Cancer type	ICI therapy	Number	Assessment assay	Outcome	PD-L1 positive	PD-L1 negative	Reference
GC, AEG	anti-PD-1 (Pembrolizumab)	259	CPS	ORR CRR	15.5% 2.0%	6.4% 2.8%	Fuchs 2018 (36)
EAC, ESCC	anti-PD-1 (Pembrolizumab)	123	CPS	OS	12 months	6.4 months	Chen 2019 (37)
Advanced GC	anti-PD-1 (Pembrolizumab)	763	CPS	OS	17.4 months	10.6 months	Shitara 2020 (38)
Chemotherapy refractory GC	anti-PD-1 (Toripalimab)	55	TPS	ORR PFS OS	37.5% 5.5 months 12.1 months	8.5% 1.9 months 5.3 months	Wang 2019 (5)
MSI-H mCRC	anti-PD-1 (Nivolumab)	68	TPS	ORR DCR for ≥12 weeks	28.6% 52.4%	27.7% 74.5%	Overman 2017 (10)
MSI-H mCRC	Dual immunotherapy (Nivolumab plus Ipilimumab)	119	TPS	ORR DCR	54% 77%	52% 78%	Overman 2018 (11)
Advanced HCC previously treated with Sorafenib	anti-PD-1 (Pembrolizumab)	104	CPS TPS	ORR	32% 43%	20% 22%	Zhu 2018 (39)
Advanced HCC	anti-PD-1 (Pembrolizumab)	174	TPS	ORR	26%	19%	El-Khoueiry 2017 (40)
Pretreated advanced, metastatic adenocarcinoma or ESCC	anti-PD-1 (Pembrolizumab)	121	CPS	ORR	13.8%	6.3%	Shah 2018 (41)
					PD-L1 mRNA^{High}	PD-L1 mRNA ^{Low}	
MSS CRC	anti-PD-1	210	PD-L1 mRNA expression	mOS	Not reached	60 months	Liu 2021 (42)
Combined predictor							
					PD-L1 positive +TMB-H	**PD-L1 negative +TMB-L**	
Chemotherapy refractory GC	anti-PD-1 (Toripalimab)	55	TPS/TMB	ORR PFS OS	33.3% 2.7 months 12.1 months	3.0% 1.9 months 4 months	Wang 2019 (5)

GC, gastric cancer; CPS, combined positive score; TPS, tumor proportion score; AGC, advanced gastric cancer; MSI, microsatellite instability; mCRC, metastatic colorectal cancer; ORR, objective response rate; CRR, complete response rate; DCR, disease control rate; PFS, progression-free survival; OS, overall survival; PFS, progression-free survival; HCC, hepatocellular carcinoma; TMB, tumor mutation burden.

Moreover, amplification or higher expression of PD-L1 showed an independent association with dismal survival in HCC patients, authenticating the PD-1/PD-L1 axis as rational immunotherapeutic targets for HCC. Since the dynamics and turnover of translation and transcription levels may be different, clinical biomarker assessments usually adopt the PD-L1 protein level rather than the mRNA level for HCC (53). However, PD-L1 expression failed to predict the efficacy of ICI therapy in MSS CRC (10, 11). In a recent study, PD-L1 mRNA levels, but not the protein level, was associated with CD8+ T cell infiltration and better prognosis of immunotherapy for MSS CRC. The inconsistency between PD-L1 protein and mRNA expressions may indicate that PD-L1 regulation occurs post transcriptionally (42). Furthermore, some studies have shown a strong correlation of PD-L1 mRNA expression with prognosis in the context of NSCLC and malignant melanoma (54). The predictive value of PD-L1 or PD-L1 mRNA for immunotherapy is likely to vary due to cancer heterogeneity. Larger prospective clinical trials are required to verify whether PD-L1 mRNA can be a potential predictor of response to immunotherapy in patients with digestive system cancers. Moreover, there is a need to explore models that combine multiple biomarkers and/or assay methods to improve the predictive ability for immunotherapy efficacy.

2.3 Blood Biomarkers

2.3.1 Peripheral Blood Biomarkers

Peripheral blood biomarkers in routine clinical practice can help predict the treatment outcomes of digestive system cancers, and thereby facilitate risk-stratification and therapeutic decision-making for this patient population. Among the common laboratory tests, neutrophil-to-lymphocyte ratio (NLR) and absolute lymphocyte count (ALC) may be effective surrogate markers for predicting the outcome of immunotherapy for digestive system cancers. Namikawa found that the NLR after 4 weeks of nivolumab therapy in the CR or partial response (PR) group was significantly lower than that in the stable disease (SD) or progression disease (PD) group (2.2 vs 2.9, P=0.044) (55). Besides, another study of 26 advanced GC patients treated with nivolumab also investigated on the role of NLR before the first cycle (NLR_{pre}) and NLR at two weeks after the first administration (NLR_{post}) in predicting the efficacy of immune therapy (56). After stratifying patients into high NLR (≥5) and

low NLR (<5) groups, the mPFS was shorter in the high NLRpre arm (45 vs 87 days) and high NLRpost arm (28 vs 94 days). Consistently, high NLR_{pre} arm (175 vs 290 days) and high NLR_{post} arm (69 vs 290 days) showed significantly shorter OS. In the study by Ohta et al., the 6-month OS rate of patients with ALC>1,600/mL (100%) and NLR<4 (63%) was greater than that of patients with ALC<1600 mL (35%) and patients with NLR>4 (33%), respectively (57). The potential reason of dynamic changes in NLR as a predictive indicator may be related to changes in the relative proportion of circulating lymphocytes during nivolumab therapy. As a specific biomarker of HCC, alpha-foetoprotein (AFP) may also help predict the efficacy of immunotherapy. Patients with early response (decrease in AFP level by at least 20% from pre-treatment level within the initial 4 weeks of treatment) exhibited longer OS (28.0 vs 11.2 months) and PFS (15.2 vs 2.7 months), becoming an independent predictor of longer OS (58).

Some compound blood biomarkers also have ability to predict clinical efficacy. The association of such a cost-effective and widely accessible biomarker like NLR to TMB seems an implementable strategy worth exploring. Valero performed a retrospective cohort study of 1714 patients with various cancer types (including GC, CRC, HCC, PDAC, and ESCA) who were treated with ICI therapy; the probability of benefit from ICI was found to be significantly higher in the NLR low/TMB-H group compared to the NLR high/TMB-L group (62). Composite markers, such as prognostic nutrition index (PNI) and Glasgow prognostic score (GPS), which are based on a combination of routine blood parameters (serum albumin, lymphocyte count, C-reactive protein, and hypoalbuminemia), have been used to evaluate inflammatory status in GC patients. In a study, pre-treatment PNI in the CR or PR group was significantly better than that in the SD or PD group (37.1 vs 32.1, respectively; P=0.011). PNI at 8 weeks post-treatment and pre-treatment GPS showed significant association with poor efficacy of nivolumab therapy (55).

However, the methodology used to determine the cutoff levels of these peripheral blood biomarkers is unclear in many studies. Owing to different cutoff levels used in previous studies, further studies are required to determine the optimal cut-off levels of hematological markers for different cancers. In other cancers such as NSCLC or melanoma, the levels of lactate dehydrogenase, carcinoembryonic antigen, carbohydrate antigen199, and carbohydrate antigen125 have also been shown to be related to efficacy of immune therapy (63). Recent studies suggest that peripheral blood LAG-3 protein may be an important biomarker for predicting ICI efficacy in patients with melanoma (64). However, further research is required to explore accurate hematological markers in the context of digestive system cancers.

2.3.2 Liquid Biopsy Biomarkers

Long-term monitoring of the occurrence and development of cancers is an important aspect of precision medicine. However, tissue biopsy is not convenient enough for this purpose. Therefore, use of liquid biopsy in the context of cancer treatment is a useful evolving trend. Circulating tumor cells (CTCs), circulating tumor DNA (ctDNA), and exosomes together constitute the three major goals of liquid biopsy.

ctDNA mutation load can not only predict the response before treatment, but the change of ctDNA immediately after treatment can also strongly predict the response to immunotherapy. The ORR of patients with higher ctDNA mutation load was significantly greater than that of lower ctDNA (83% vs 7.7%, P=0.0014), and was shown to improve mPFS (87 days vs not reached). Besides, all patients who showed increasing ctDNA after treatment experienced PD within 100 days, and demonstrated significant decrease in DCR (92% vs 25%) and ORR (58% vs 0%), resulting in a shortened mPFS (123 days vs 66 days) (59). Moreover, Bratman found that the decline in ctDNA levels after pembrolizumab therapy was an independent predictor in patients with solid tumors. They also found that assessment of the changes in ctDNA levels in combination with the evaluation criteria for solid tumors in the third cycle of treatment could help identify patients who are unlikely to benefit from ICI treatment at an early stage. All 12 patients with ctDNA clearance during ICI therapy survived with median follow-up of 25 months (65). Furthermore, the proportion of CTCs with high PD-L1 expression at baseline and monitoring the early dynamic changes in CTC were found to predict the clinical efficacy of Sintilimab (61). At baseline, patients above the cutoff value of PD-$L1^{high}$ CTCs had significantly longer mPFS compared with those below the value (4.27 vs 2.07 months, P=0.002). At 9 weeks after the initiation of therapy, patients with PD-$L1^{high}$ CTCs <2 showed significantly better mPFS than patients with PD-$L1^{high}$ CTCs ≥2 (3.4 vs 2.1 months, P=0.031). The ratio of PD-$L1^{high}$ is of great value in predicting the efficacy of ICI therapy, and the results of a prospective study of this predictive marker have shown promising results. It is crucial to obtain enough high-purity CTC cells to determine the expression of PD-L1 protein.

Plasma cell free DNA (cfDNA) is a degraded DNA fragment released into plasma. Yang et al. constructed a copy number variations (CNV) risk score model based on peripheral blood cfDNA to predict the efficacy of ICI-based therapy in patients with hepatobiliary cancers. In cohorts receiving combination of ICI-based therapies, patients with lower CNV risk scores had longer OS [not reported (NR) vs 6.5 months] and PFS (6.17 vs 2.6 months) than those with high CNV risk scores (see **Table 3**) (60).

The above studies demonstrate the potential clinical utility of blood-based surveillance in patients receiving ICI therapy. Blood is a specimen that can be provided at the time of diagnosis. Compared with a single-point biopsy, blood tests are not easily interfered by sampling bias, which reduces the heterogeneity associated with sampling of tumor tissue. In addition, blood tests are minimally invasive, allow repeated sampling, and are associated with better patient compliance. Therefore, future basic and clinical research is required to further clarify the predictive value of soluble PD-L1 and bTMB in digestive system cancers (66). Furthermore, soluble B7-CD28 family inhibitory immune checkpoint proteins (including soluble CTLA-4, soluble B7-1 and soluble B7-H4) play a wide role in anti-cancer immunomodulatory regulation. Therefore, these

TABLE 3 | Predictive ability of hematological biomarkers for response to ICI therapy for digestive system cancers.

Type of predictors	Cancer type	ICI therapy	Number	Outcome	Beneficial outcome	Adverse outcome	Reference
ALC NLR	Advanced GC	anti-PD-1 (Nivolumab)	15	6-month OS rate	ALC>1,600/mL: 100% NLR<4: 63%	ALC<1600 mL: 35% NLR>4: 33%	Ohta 2020 (57)
NLR	Advanced GC	anti-PD-1 (Nivolumab)	26	mPFS mOS	Low NLR_{pre} (≥5): 87 days Low NLR_{post} (≥5): 94 days high NLR_{pre} (≥5): 290 days high NLR_{post} (≥5): 290 days	High NLR_{pre} (<5): 45 days High NLR_{post} (<5): 28 days low NLR_{pre} (<5): 175 days low NLR_{post} (<5): 69 days	Ogata T 2018 (56)
AFP	Advanced HCC	anti-PD-1/PD-L/ CTLA-4	60	OS PFS	Early AFP response: 28 Early AFP response: 15.2	early AFP nonresponders: 11.2 early AFP nonresponders: 2.7	Shao 2019 (58)
ctDNA	Metastatic GC	anti-PD-1 (Pembrolizumab)	61	ORR mPFS DCR	the upper tertile of ctDNA mutational load: 83% decreasing ctDNA: 58% the lower two tertiles of ctDNA mutational load: not reached decreasing ctDNA: 123 days decreasing ctDNA: 92%	the lower two tertiles of ctDNA mutational load: 7.7% increasing ctDNA: 0% the upper tertile of ctDNA mutational load: 87 days increasing ctDNA: 66 days increasing ctDNA: 25%	Kim 2018 (59)
cfDNA	Hepatobiliary cancers	anti-PD-1	108	mOS mPFS	lower CNV risk scores: not reached lower CNV risk scores: 6.17 months	Higher CNV risk scores:6.5 months Higher CNV risk scores:2.6months	Yang 2021 (60)
CTCs	Advanced solid tumor	anti-PD-1 (Sintilimab)	34	mPFS	High levels of PD-$L1^{high}$CTCs before therapy: 4.27 months PD-$L1^{high}$CTCs post therapy<2: 3.4 months	Low levels of PD-$L1^{high}$CTCs before therapy: 2.07 months PD-$L1^{high}$CTCs post therapy≥2: 2.1 months	Yue 2018 (61)

ALC, absolute lymphocyte count; NLR, neutrophil-to-lymphocyte ratio; AFP, alpha-foetoprotein; ctDNA, circulating tumor DNA; CTCs, circulating tumor cells; cfDNA, cell free DNA; GC, gastric cancer; HCC, hepatocellular carcinoma; PFS, progression-free survival; mOS, median overall survival; OS, overall survival; mPFS, median progression-free survival; DCR, disease control rate.

may serve as valuable prognostic biomarkers that can predict the therapeutic response, while also opening up new opportunities for anticancer immunotherapy (67).

2.4 Tumor Microenvironment (TME)

The TME is a complex tumor ecosystem that supports tumor growth and metastatic dissemination (68), and can reflect the response of the tumor to immunotherapy. TILs status is an important component of the heterogeneity of TME and mediates adaptive immunity.

A comprehensive immuno-genomic analysis of tumor microenvironment immunetypes (TMITs) classified it into four subgroups based on the expressions of PD-1 and CD8 in TILs. In the category of digestive system cancers, TIMT I subgroup (PD-L1 immunoreactivity of tumor cells and CD8 high expression of TILs) showed a significantly higher number of mutations or neoantigens in CRC and GC patients receiving anti- PD-1/PD-L1 therapy (69). On survival analysis according to TMIT, TMIT I showed the most prominent favorable prognostic effect. Furthermore, Noh performed another TMIT study in patients with small intestinal adenocarcinoma. TMIT I subgroup (PD-L1-positive tumor cells and CD8-high TILs) and TMIT III subgroup (PD-L1-positive tumor cells and CD8-low TILs) showed the best and worst outcomes of immunotherapy, respectively (73). However, the classification standards for immune type are not completely standardized, and further characterization of the immune type of patients with digestive system cancers may provide a breakthrough for ICI therapy in these patients.

Some studies indicated that tumors with high expression of T cell-"inflamed" phenotype show favorable response to immunotherapy. T-cell inflammatory gene expression profile (GEP) can be used as an inflammatory marker of T-cell inflamed TME, which was associated with longer PFS and higher ORR in patients treated with pembrolizumab (33). Tumors with "inflammatory" T cell infiltration are characterized by activation of type I IFN, immune potentiating chemokines that attract T cells, antigen presentation, and $CD8^+$ T cells, while tumor tissues with "non-inflammatory" T cell infiltration lack such expression and activation. The researchers hypothesized that a treatment regimen that converts non-inflammatory T-cell subtypes to inflammatory T-cell subtypes may enhance the sensitivity of the tumor to treatment regimens that depend on T-cell activity, thereby enhancing the therapeutic efficacy of immunotherapy (74). Additional analysis showed that combined use of TMB and GEP stratified Pan-tumor into groups that showed different clinical responses to pembrolizumab monotherapy, with both response rate and PFS strongest in groups with GEP high and TMB high (75). TMB and GEP independently predict the therapeutic response owing to their unique characteristics of capturing neoantigenicity and T cell activation to provide new patterns for predicting response to immunotherapy.

The tumor microbiome is composed of tumor type-specific intracellular bacteria, which is an important part of the TME. Different types of tumors have their own unique microbiota. Proteobacteria dominate the microbiota of pancreatic cancer. Bacteria can be found in CD45+ immune cells, which indicates that they may affect or reflect the immune status of the TME. Researchers have found differences in the differential abundance of microbes in immunotherapy responders and non-responders. Some microorganisms are related to the effectiveness of ICI therapy, which may be related to the metabolic ability of bacteria in the TME (76).

Immune score has attracted increasing clinical attention, which is determined using standardized operating procedures and specialized image-analysis software to quantify the density of CD3+ and CD8+ T cells in the tumor and its invasive edge. The 5-year recurrence risk of CRC patients with high immune scores (8%) was significantly lower than that of patients with lower than medium (19%) and low immune score (32%) (see **Table 4**) (70).

The TILs status and neoantigen changes after chemoradiotherapy can partly reflect the dynamic changes in the TME, which may induce immunotherapy response in patients who were hitherto non-responsive. How to screen such patients, or how to change the TME to improve response to immunotherapy, is an important direction for immunotherapy research to expand the application of immunotherapy and improve the effectiveness of immunotherapy.

2.5 Immune-Related Adverse Events

ICI treatment interferes with normal immune tolerance and triggers immune activation in normal tissues, leading to various irAEs. Of note, irAEs often indicate a good response to ICI treatment. In a multi-center retrospective study of patients with metastatic or unresectable GI cancer, patients with irAEs had longer mPFS (not reached vs 3.9 months) and mOS (not reached vs 7.4 months) than patients without irAEs (77). The above research highlighted the predictive potential of irAEs as a clinical biomarker in this population. In the studies of nivolumab for GC, a study of 65 GC patients showed significant improvement in mPFS (7.5 vs 1.4 months) and mOS (16.8 vs 3.2 months) in patients with irAEs compared with those without irAEs (78). Further study of 29 GC patients also confirmed the predictive effect of irAEs on PFS, with a significant increase in the median PFS in the irAEs group (5.8 vs 1.2 months) (55). Reactive causal capillary endothelial proliferation (RCCEP) is an extremely common skin irAE caused by camrelizumab. In a study, the mPFS (3.2 vs 1.9 months) and mOS (17.0 vs 5.8 months) of HCC patients with RCCEP was significantly greater than those of patients without RCCEP (79). In addition to HCC, camrelizumab therapy also increased the mOS of patients with RCCEP in a study of 228 patients with ESCC (10.1 vs 2.5 months) (see **Table 5**) (80).

The relationship between irAEs and ICI efficacy is potentially attributable to presence of similar antigens in tumor cells and other normal tissues (81). When the immune system is activated, it targets not only tumor cells but also non-tumor sites. Furthermore, infiltration of CD4+ and CD8+T cells in the damaged sites leads to auto-immune dysfunction, resulting in a series of clinical adverse reactions. However, not all irAEs indicate better efficacy of immunotherapy, because severe irAEs, such as immune-associated pneumonia and myocarditis, can be fatal. Therefore, dynamic management of irAEs should still be strictly cautious, following the five principles of prevent, anticipate, detect, treat and monitor.

2.6 Patient-Related Biomarkers

2.6.1 Sex

In a meta-analysis of 20 randomized trials of immunotherapy for multiple tumors, including GC, survival benefits of ICI therapy differed significantly between men and women [pooled OS hazard ratio (HR): 0.86 vs 0.72, P=0.0019]. Although the differences were statistically significant, due caution should be exercised before drawing any definitive conclusions. Future research should focus on improving treatment outcomes in women and exploring different immunotherapy regimens for men and women. New immunotherapy studies should be designed to ensure that more women are enrolled in trials to obtain a more comprehensive evaluation (82).

2.6.2 Gut Microbiome Biomarkers

The dynamic balance of gut microbiome plays a positive role in maintaining the homeostasis of the immune system. However, disruption of this balance may participate in the occurrence and development of malignant tumors by regulating host immune

TABLE 4 | Predictive ability of EBV, TME, BMI, and BLN for response to ICI therapy for digestive system cancers.

Type of predictors		Cancer type	ICI therapy	Number	Outcome	Beneficial outcome	Adverse outcome	Reference
EBV		Metastatic GC	anti-PD-1 (Pembrolizumab)	6	PR	EBV positive: 100%	–	Kim 2018 (62)
					mDOR	EBV positive: 8.5	–	
TME	TMIT	Small intestinal adenocarcinoma	anti-PD-1/PD-L1	195	mOS	TMIT Type I: 146.6 months	TMIT Type III: 12.1 months	NOH 2018 (69)
	Immunoscore	CRC	anti-PD-1/PD-L1/ CTLA-4	2,681	Risk of recurrence at 5 years	High immunoscore: 8%	Low immunoscore:32%	Pagès 2018 (74)
BMI		Advanced multiple cancers	anti-PD-1/PD-L1	976		**BMI≥25**	**BMI<25**	Cortellini 2019 (93)
					OS	26.6 months	6.6 months	
					PFS	11.7 months	3.7 months	
					TTF	9.3 months	3.6 months	
BLN		Refractory AGC	anti-PD-1	58		**BLN^{low} TMB-H**	**BLN^{high} TMB-L**	Wei 2021 (99)
					mPFS	Not reached	1.7 months	
					mOS	Not reached	2.7 months	
					ORR	37.5%	0%	
					DCR	62.5%	13.3%	

EBV, Epstein-barr virus; GC, gastric cancer; PR, partial response; PFS, progression-free survival; mOS, median overall survival; OS, overall survival; mPFS, median progression-free survival; TME, tumor micro-environment; TMIT, tumor microenvironment immunetypes; ICI, immune checkpoint inhibitors; CRC, colorectal cancer; BMI, body mass index; TTF, time to progression; ORR, objective response rate; DCR, disease control rate; TMB, tumor mutation burden; BLN, baseline lesion number; AGC, advanced gastric cancer; mDOR, median duration of response.

TABLE 5 | Predictive performance of irAES for response to ICI therapy for digestive system cancers.

Cancer type	ICI therapy	Number	Outcome	irAES	None-irAES	Reference
GI cancer	anti-PD-1	76	mPFS	Not reached	3.9 months	Das 2020 (77)
			mOS	Not reached	7.4 months	
Advanced GC	anti-PD-1 (Nivolumab)	65	mPFS	7.5 months	1.4 months	Masuda 2019 (78)
			mOS	16.8 months	3.2 months	
Advanced GC	anti-PD-1 (Nivolumab)	29	mOS	5.8 months	1.2 months	Namikawa 2020 (55)
HCC	anti-PD-1 (Camrelizumab)	217	mPFS	3.2 months	1.9 months	Wang 2020 (79)
			mOS	17.0 months	5.8 months	
ESCC	anti-PD-1 (Camrelizumab)	228	mOS	10.1 months	2.5 months	Huang 2020 (80)

GI, gastrointestinal; GC, gastric cancer; HCC, hepatocellular carcinoma; mPFS, median progression-free survival; mOS, median overall survival; ESCC, esophageal squamous cell carcinoma; irAES, immune-related adverse events.

regulation, apoptosis, autophagy, and other pathways. A recent study showed that gut microbiome can influence cancer immune reference point and it is thought to induce specific memory T cells by interferon-γ secreting CD4+and CD8+ T cells, which are associated with favorable results of anti-tumor immunotherapy (83).

Fluckiger identified major histocompatibility complex (MHC) class I-binding epitopes in the tail length tape measure protein (TMP) of a prophage found in the bacteriophage Enterococcus hirae. Mice carrying Enterococcus hirae containing this prophage mounted CD8+ T cell response upon anti-PD-1 immunotherapy, and improved the therapeutic effect of ICI therapy (83). In clinical studies, the response of patients to immunotherapy was shown to be related to the abundance of gut microbiome. Fecal samples from HCC patients responding to ICI therapy showed higher taxa richness than those of non-responders. At the 6th week of treatment, there was a significant difference in the beta diversity of the gut microbiome. In non-responders, Proteobacteria became predominant at week 12, while Akkermansia muciniphila and Ruminococcaceae, were significantly increased in ICI responders (84). Mager found that Bifidobacterium pseudolongum (B.pseudolongum), Lactobacillus johnsonii, and Olsenella species can enhance the efficacy of ICI therapy in CRC mouse models, and B. pseudolongum was found to enhance the response to immunotherapy through increased systemic translocation of inosine and activated anti-tumor T cells (85). Moreover, Drewes's study indicated that the efficacy of the anti-PD-L1 and anti-CTLA-4 in CRC patients is reliant on commensal bacteria, such as bifidobacteria and bacteroides (86). During the development of pancreatic cancer, tumor local immunity and gut microbiome interact with tumor and change synergistically with histopathological progression. Combined targeting of gut microbiome composition and metabolic pathways may effectively improve the efficacy of immunotherapy in PDAC (87).

These studies provide fascinating insights into the relationship between gut microbiome and antitumor efficacy of ICI therapy, suggesting that the gut microbiome can be used as a predictor of immunotherapy efficacy, and even become a potential treatment modifier. In the studies confirming the efficacy of intestinal microflora in regulating immunotherapy, different microflora were found to play a major role, which may be related to the tumor species and the patient population. Further studies should be conducted to explore the mechanism by which gut microbiome activates the TME (88). Given the biological and clinicopathologic heterogeneity among different tumors and individuals, the prospective value of gut microbiome biomarkers needs to be further explored in a larger cohort with a unitary tumor type.

2.6.3 Epstein-Barr Virus Biomarkers

Epstein-Barr virus associated gastric carcinoma (EBVaGC) has unique molecular biology characteristics, and is, therefore, considered as an independent gastric cancer subtype in studies. An estimated 8%–10% of GCs are associated with EBV infection, and patients with EBVaGC were found to have a better prognosis compared with other genotypes (89). With the ongoing advances in the field of precision medicine, especially in the field of immunotherapy, EBVaGC diagnosis and ICI therapy have become contemporary research hotspots. Follow-up studies have shown that EBVaGC shows greater sensitivity to ICI therapy. In a study by Panda et al., compared with MSI tumors, EBVaGC subtypes had a lower mutation burden, but showed stronger evidence of immune infiltration; in addition, RNA-SEQ data showed high expressions of immune checkpoint pathway (PD-1, CTLA-4 pathway) genes, which seemed to confer greater benefit of avelumab treatment against EBVaGC subtypes (90). Furthermore, in another study, the efficacy of pembrolizumab in GC patients was associated with positive EBV. All EBVaGC patients achieved PR with a median duration of response of 8.5 months and the ORR was 100% (59).

The above studies indicated that EBV may serve as a predictor of the efficacy of immunotherapy for GC, while the following studies provide a strong rationale for testing of PD-1 blockade in EBV-positive GC. EBVaGC is characterized by marked intratumoral or peritumoral infiltration of immune cells. The infiltrating lymphocytes are mainly CD8+ T cells, and large infiltration of CD8+T cells in GC tissues is often accompanied by high expression of PD-L1 (91). In addition, the IL-12 mediated signal intensity in EBV-positive tumors suggests the presence of a robust immune cell response, which provides a basis for the detection of ICI in EBVaGC (92). Besides, Derks reported enrichment of interferon-γ driven gene signature in EBVaGC and the amplification of PD-L1 in EBVaGC cells was significantly greater than that in other GC subtypes, which also implies that EBVaGC may show greater sensitivity to PD-1/PD-L1 immunotherapy (93). The 2020 NCCN guidelines for GC suggested that tumor EBV status may be a biomarker for

precision therapy of GC. Accurate detection is the premise of precise treatment, and EBV examination is crucial for ICI therapy and prognosis of EBVaGC patients.

2.6.4 Body Mass Index

Obesity is a global social and public health problem. Increased body mass index (BMI) is a known health hazard and is associated with an increased risk of cancer (94). A 5 kg/m^2 increase in BMI showed a strong association with oesophageal, colon, and gallbladder adenocarcinoma. However, recent studies have highlighted the potential role of obesity as a biomarker of the efficacy of cancer immunotherapy. Cortellini conducted a retrospective study of advanced cancer patients consecutively treated with anti-PD-1/PD-L1 inhibitors. They found that mPFS, mOS, and time to treatment failure were significantly longer for patients with BMI≥25 kg/m^2 (71).

The potential underlying mechanism by which obesity modulates the response to ICI therapy may involve obesity-induced immune aging and PD-1-mediated T cell dysfunction by leptin. PD-1-mediated T cell dysfunction was shown to enhance the efficacy of immune checkpoint blockade and confer long-term survival benefits (95). The relationship between BMI and OS should be interpreted with caution, as it may potentially be confounded by methodological limitations and heterogeneity with respect to study design. Therefore, it is vital to consider that patients with the same BMI may have significantly different body compositions and different prognosis, which reflect that BMI is not an adequate indicator of regional obesity. In addition to BMI, other indices such as waist circumference, visceral fat mass, subcutaneous fat mass, total body fat percentage, and trunk fat percentage should be integrated into comprehensive indicators to explore their relationship with benefits of ICI therapy (96). At present, the mechanism of "obesity paradox" needs to be further explored.

2.6.5 Nonalcoholic Steatohepatitis (NASH)

There are several etiological factors for HCC, among which NASH is an important driver of HCC. A recent study found that NASH limits the immunotherapy response of HCC to anti-tumor surveillance, and is a predictor of unfavorable outcomes of ICI therapy. After anti-PD1 treatment in NASH-related HCC mice, pre-existing HCC tissue showed no regression and there was an increase in CD8+/PD1+T cells in HCC tissue, suggesting that the activated immune cells may not play an immune surveillance role, but show the potential of tissue destruction (97). To further determine the clinical significance of disrupted immune surveillance in NASH after ICI treatment, Pfister conducted a meta-analysis of the three large randomized controlled trials (CHECKMATE-459, IMbrave150, and KEYNOTE-240) of patients with advanced HCC and found that non- alcoholic fatty liver disease (NAFLD) was associated with shorter mOS (5.4 vs 11.0 months) and mPFS (8.8 vs 17.7 months). After adjusting for potential confounders, NAFLD still showed an independent association with shorter survival in HCC patients treated with ICI. Due to the limited size of the study cohort, future prospective clinical studies are required to provide more robust evidence.

2.6.6 *Helicobacter pylori*

Helicobacter pylori (H. pylori) colonizes the gastric mucosa of 50% of the world's population and is related to geographical factors such as diet and lifestyle. H. pylori actively manipulates host tissue, establishes an immunosuppressive environment, and mediates immune regulation, which negatively affects a large number of immune cell types associated with antitumor immunity. Therefore, H. pylori infection is considered to attenuate the response to cancer immunotherapy (98). Oster's team used an MC38 colorectal adenoma tumor model to evaluate whether H. pylori reduces the efficacy of anti-CTLA-4 therapy. In this study, the tumor size of mice that were not infected with H. pylori was significantly smaller than that of the infected mice. Furthermore, they evaluated the effect of H. pylori infection on the immunotherapy efficacy in tumors developing *in situ* using a model of azoxymethane/dextran sodium sulfate colon cancer. Notably, the number of colon tumors in uninfected mice treated with anti-CTLA-4 was significantly lower than that in H. pylori infected mice. This study provided evidence that the presence of H. pylori in the gastric microbiota may jeopardize the efficacy of immunotherapies (99).

2.6.7 Other Predictive Markers

Patients with high initial tumor burden often have poor immune status and show poor response to immunotherapy. Recent research suggested that baseline lesion number (BLN) is a potential indicator of tumor burden, which takes priority over tumor size and can reflect the effect of tumor biology on immunotherapy sensitivity; in addition, BLN can be used in combination with TMB for better stratification of patients with respect to the risk of immunotherapy. The BLN-Low group showed better ORR and DCR compared with BLN-High group (15.4% vs 5.3% and 86.96% vs 54.29%, respectively). However, combined use of BLN and TMB showed better efficacy in predicting the benefits of immunotherapy. This study suggested that use of a combination of clinical and molecular biomarkers may have greater clinical relevance. The BLN-Low (≤ 5) and TMB-H (≥12 mutations/Mb) groups showed higher ORR (37.5% vs 0%) and DCR (62.5% vs 13.3%) , as well as longer PFS (not reached vs 1.7 months) and OS (not reached vs 2.7 months), compared with the BLN-High and TMB-L groups (see **Table 4**) (72).

3 CONCLUSION

In an era of immunotherapy, several biomarkers have been identified to predict the response to immunotherapy. However, the vast majority of biomarkers have shown limited predictive value in the context of digestive system cancers. This may be attributable to the fact that digestive system cancers is a large class of tumors with considerable heterogeneity, and which is possibly itself involved in regulation of gut microbiome and the TME. This may also be related to the lower response rate of digestive system tumors to immunotherapy compared with NSCLC and melanoma. At present, MSI is mainly used to predict the effectiveness of immunotherapy for digestive system

cancers; however, owing to the low overall incidence of MSI-H in the digestive system, it has limited clinical application. There is a need to explore novel biomarkers in the context of digestive system cancers.

The conflicting conclusions pertaining to the predictive efficacy of biomarkers in previous studies may be due to the differences with respect to tumor types, treatment methods, and detection standards used. A single biomarker is unlikely to accurately predict the effect of ICI treatment, and is liable to be affected by dynamic changes in the immunogenicity of the tumor and TME. Therefore, in the future, artificial intelligence and big data research can be used to build multidimensional and multivariable predictive models. Through large-sample analysis, multi-platform dynamic detection before and after treatment can be conducted, so as to obtain comprehensive predictive markers with the best predictive performance to guide clinical treatment. Timothy Chan team performed a comprehensive analysis of multiple biological factors (TMB, copy number change score, HLA-1 evolutionary difference, HLA-1 loss of heterozygosity, MSI, BMI, gender, NLR, tumor stage, immunotherapy drugs, age, tumor type, chemotherapy before immunotherapy, and blood indicators such as albumin, platelets and hemoglobin) (100) . The machine learning model (named RF16) was shown to predict the efficacy of ICI therapy with a high sensitivity and specificity, spanning 1479 patients with 16 cancer types (including CRC). The analysis demonstrated that TMB has the greatest influence on the immunotherapy efficacy, followed by the history of chemotherapy. However, the impact of MSI does not seem to be large, and researchers believe that this is most likely due to the very strong correlation between MSI and TMB. The prediction consistency index of RF16 was higher than that of TMB, and the response to immunotherapy predicted by RF16 was also significantly associated with longer OS.

Previous research has focused on sensitive markers to identify subsets of patients who are more likely to benefit from immunotherapy. In recent years, increasing attention has been paid to immunotherapy resistance genes and super-progressive genes. Exploration of new biomarkers should take into account both the sensitive and super-progressive directions. Further in-depth research on predictive biomarkers of immunotherapy will help leverage the full potential of ICI therapy in the realm of personalized medicine for cancer. Targeting different individuals, cancer types, and immune status, as well as TME-related data, such as molecular characteristics, microbial composition, T cell receptor library diversity, tumor-related gene mutations or drug resistance mutations, may help improve the model's predictive ability. Immunotherapy prediction models, especially for digestive system cancers, should be validated and improved using a larger and more representative patient population in the future. Improvement in the predictive models will help inform treatment strategies for digestive system cancers and open new vistas for individualized immunotherapy.

AUTHOR CONTRIBUTIONS

Data acquisition and data analysis were performed by JTW, JW, ZM, and XM. YM, and BC prepared the figure and tables. The first draft of the manuscript was written by JTW and JW, and the manuscript was further commented and approved by all authors. All authors contributed to the article and approved the submitted version.

FUNDING

This study was supported by the National Natural Science Foundation of People's Republic of China [grant number 82173056]; the Digestive Medical Coordinated Development Center of Beijing Hospitals Authority. No: XXT01; Beijing key clinical specialty (2018-2020); The pilot project of clinical collaboration with traditional Chinese medicine and western medicine in major refractory disease-Esophageal cancer (2019-ZX-005).

REFERENCES

1. Lee V, Le DT. Efficacy of PD-1 Blockade in Tumors With MMR Deficiency. *Immunother* (2016) 8(1):1–3. doi: 10.2217/imt.15.97
2. Le DT, Durham JN, Smith KN, Wang H, Bartlett BR, Aulakh LK, et al. Mismatch Repair Deficiency Predicts Response of Solid Tumors to PD-1 Blockade. *Science* (2017) 357(6349):409–13. doi: 10.1126/science.aan6733
3. Hause RJ, Pritchard CC, Shendure J, Salipante SJ. Classification and Characterization of Microsatellite Instability Across 18 Cancer Types. *Nat Med* (2016) 22(11):1342–50. doi: 10.1038/nm.4191
4. Goodman AM, Kato S, Bazhenova L, Patel SP, Frampton GM, Miller V, et al. Tumor Mutational Burden as an Independent Predictor of Response to Immunotherapy in Diverse Cancers. *Mol Cancer Ther* (2017) 16(11):2598–608. doi: 10.1158/1535-7163.MCT-17-0386
5. Wang F, Wei XL, Wang FH, Xu N, Shen L, Dai GH, et al. Safety, Efficacy and Tumor Mutational Burden as a Biomarker of Overall Survival Benefit in Chemo-Refractory Gastric Cancer Treated With Toripalimab, a PD1 Antibody in Phase Ib/II Clinical Trial NCT02915432. *Ann Oncol Off J Eur Soc Med Oncol* (2019) 30(9):1479–86. doi: 10.1093/annonc/mdz197
6. Schrock AB, Ouyang C, Sandhu J, Sokol E, Jin D, Ross JS, et al. Tumor Mutational Burden Is Predictive of Response to Immune Checkpoint Inhibitors in MSI-High Metastatic Colorectal Cancer. *Ann Oncol* (2019) 30(7):1096–103. doi: 10.1093/annonc/mdz134
7. Marabelle A, Fakih M, Lopez J, Shah M, Shapira-Frommer R, Nakagawa K, et al. Association of Tumour Mutational Burden With Outcomes in Patients With Advanced Solid Tumours Treated With Pembrolizumab: Prospective Biomarker Analysis of the Multicohort, Open-Label, Phase 2 KEYNOTE-158 Study. *Lancet Oncol* (2020) 21(10):1353–65. doi: 10.1016/S1470-2045(20)30445-9
8. Yang BB. Analysis of Immunotherapy Response and Potential Biomarkers of Advanced Esophageal Cancer by Liquid Biopsy. *Peking Union Med College* (2019) 2. doi: 10.27648/d.cnki.gzxhu.2019.000238.
9. Le DT, Uram JN, Wang H, Bartlett BR, Kemberling H, Eyring AD, et al. PD-1 Blockade in Tumors With Mismatch-Repair Deficiency. *N Engl J Med* (2015) 372(26):2509–20. doi: 10.1056/NEJMoa1500596
10. Overman MJ, McDermott R, Leach JL, Lonardi S, Lenz HJ, Morse MA, et al. Nivolumab in Patients With Metastatic DNA Mismatch Repair-Deficient or Microsatellite Instability-High Colorectal Cancer (CheckMate 142): An Open-Label, Multicentre, Phase 2 Study. *Lancet Oncol* (2017) 18(9):1182–91. doi: 10.1016/S1470-2045(17)30422-9
11. Overman MJ, Lonardi S, Wong KYM, Lenz HJ, Gelsomino F, Aglietta M, et al. Durable Clinical Benefit With Nivolumab Plus Ipilimumab in DNA Mismatch

Repair-Deficient/Microsatellite Instability-High Metastatic Colorectal Cancer. *J Clin Oncol* (2018) 36(8):773–9. doi: 10.1200/JCO.2017.76.9901
12. Noor A, Aguirre LE, Blue K, Avriett T, Kim DW. Abstract 415: Investigate the Efficacy of Immunotherapy for Treatment of Pancreatic Adenocarcinoma (PDAC) With Mismatch Repair Deficiency (dMMR). *J Clin Oncol* (2021) 39 (3_suppl):415. doi: 10.1200/JCO.2021.39.3_suppl.415
13. Le DT, Kim TW, Van Cutsem E, Geva R, Jäger D, Hara H, et al. Phase II Open-Label Study of Pembrolizumab in Treatment-Refractory, Microsatellite Instability–High/Mismatch Repair–Deficient Metastatic Colorectal Cancer: KEYNOTE-164. *J Clin Oncol* (2019) 38(1):JCO.19.02107. doi: 10.1200/JCO.19.02107
14. Marabelle A, Le DT, Ascierto PA, Di Giacomo AM, De Jesus-Acosta A, Delord JP, et al. Efficacy of Pembrolizumab in Patients With Noncolorectal High Microsatellite Instability/Mismatch Repair–Deficient Cancer: Results From the Phase II KEYNOTE-158 Study. *J Clin Oncol* (2019) 38(1): JCO.19.02105. doi: 10.1200/JCO.19.02105
15. McGrail DJ, Pilié PG, Rashid NU, Voorwerk L, Slagter M, Kok M, et al. High Tumor Mutation Burden Fails to Predict Immune Checkpoint Blockade Response Across All Cancer Types. *Ann Oncol* (2021) 32(5):661–72. doi: 10.1016/j.annonc.2021.02.006
16. Harding JJ, Nandakumar S, Armenia J, Khalil DN, Albano M, Ly M, et al. Prospective Genotyping of Hepatocellular Carcinoma: Clinical Implications of Next-Generation Sequencing for Matching Patients to Targeted and Immune Therapies. *Clin Cancer Res* (2019) 25(7):2116–26. doi: 10.1158/1078-0432.CCR-18-2293
17. Wang F, Zhao Q, Wang YN, Jin Y, He MM, Liu ZX, et al. Evaluation of POLE and POLD1 Mutations as Biomarkers for Immunotherapy Outcomes Across Multiple Cancer Types. *JAMA Oncol* (2019) 5(10):1504–6. doi: 10.1001/jamaoncol.2019.2963
18. Nowak JA, Yurgelun MB, Bruce JL, Rojas-Rudilla V, Hall DL, Shivdasani P, et al. Detection of Mismatch Repair Deficiency and Microsatellite Instability in Colorectal Adenocarcinoma by Targeted Next-Generation Sequencing. *J Mol Diagn* (2017) 19(1):84–91. doi: 10.1016/j.jmoldx.2016.07.010
19. Rizvi NA, Hellmann MD, Snyder A, Kvistborg P, Makarov V, Havel JJ, et al. Cancer Immunology. Mutational Landscape Determines Sensitivity to PD-1 Blockade in Non-Small Cell Lung Cancer. *Science* (2015) 348(6230):124–8. doi: 10.1126/science.aaa1348
20. Wu HX, Wang ZX, Zhao Q, Chen DL, He MM, Yang LP, et al. Tumor Mutational and Indel Burden: A Systematic Pan-Cancer Evaluation as Prognostic Biomarkers. *Ann Transl Med* (2019) 7(22):640. doi: 10.21037/atm.2019.10.116
21. Wang J, Boyle S, Lee C, Levy E, Chen R. Abstract 5710: Molecular Profiling of Anti-PD-1 Treated Melanoma Patients Reveals Importance of Assessing Neoantigen Burden and Tumor Escape Mechanisms for Clinical Treatment. *Cancer Res* (2018) 78:5710–0. doi: 10.1158/1538-7445.AM2018-5710
22. Luchini C, Bibeau F, Ligtenberg MJL, Singh N, Nottegar A, Bosse T, et al. ESMO Recommendations on Microsatellite Instability Testing for Immunotherapy in Cancer, and Its Relationship With PD-1/PD-L1 Expression and Tumour Mutational Burden: A Systematic Review-Based Approach. *Ann Oncol* (2019) 30(8):1232–43. doi: 10.1093/annonc/mdz116
23. Si H, Kuziora M, Quinn KJ, Helman E, Ye J, Liu F, et al. A Blood-Based Assay for Assessment of Tumor Mutational Burden in First-Line Metastatic NSCLC Treatment: Results From the MYSTIC Study. *Clin Cancer Res* (2020) 27 (6):1631–40. doi: 10.1016/j.ejca.2019.01.026
24. Wang Z, Duan J, Wang G, Zhao J, Xu J, Han J, et al. Allele Frequency-Adjusted Blood-Based Tumor Mutational Burden as a Predictor of Overall Survival for Non-Small Cell Lung Cancer Patients Treated With PD-1/PD-L1 Inhibitors. *J Thorac Oncol: Off Publ Int Assoc Study Lung Cancer* (2019) 15 (4):556–67. doi: 10.1016/j.jtho.2019.12.001.
25. Fang W, Jin H, Zhou H, Hong S, Zhang L. Intratumoral Heterogeneity as a Predictive Biomarker in Anti-PD-(L)1 Therapies for Non-Small Cell Lung Cancer. *Mol Cancer* (2021) 20(1):37. doi: 10.1186/s12943-021-01331-9
26. Litchfield K, Reading JL, Puttick C, Thakkar K, Swanton C. Meta-Analysis of Tumor and T Cell-Intrinsic Mechanisms of Sensitization to Checkpoint Inhibition. *Cell* (2021) 184(3):596–614.e14. doi: 10.1016/j.cell.2021.01.002
27. Wolf Y, Bartok O, Patkar S, Eli GB, Cohen S, Litchfield K. UVB-Induced Tumor Heterogeneity Diminishes Immune Response in Melanoma. *Cell* (2019) 179(1):219–35.e21. doi: 10.1016/j.cell.2019.08.032
28. McGranahan N, Furness AJ, Rosenthal R, Ramskov S, Lyngaa R, Saini SK, et al. Clonal Neoantigens Elicit T Cell Immunoreactivity and Sensitivity to Immune Checkpoint Blockade. *Science* (2016) 351(6280):1463–9. doi: 10.1126/science.aaf1490
29. Pinyol R, Sia D, Llovet JM. Immune Exclusion-Wnt/CTNNB1 Class Predicts Resistance to Immunotherapies in HCC. *Clin Cancer Res* (2019) 25(7):2021–3. doi: 10.1158/1078-0432.CCR-18-3778
30. Hu G, Tu W, Yang L, Peng G, Yang L. ARID1A Deficiency and Immune Checkpoint Blockade Therapy: From Mechanisms to Clinical Application. *Cancer Lett* (2020) 473:148–55. doi: 10.1016/j.canlet.2020.01.001
31. Chen Y, Li Y, Guan Y, Huang Y, Lin J, Chen L, et al. Prevalence of PRKDC Mutations and Association With Response to Immune Checkpoint Inhibitors in Solid Tumors. *Mol Oncol* (2020) 14(9):2096–110. doi: 10.1002/1878-0261.12739
32. Chowell D, Morris LGT, Grigg CM, Weber JK, Samstein RM, Makarov V, et al. Patient HLA Class I Genotype Influences Cancer Response to Checkpoint Blockade Immunotherapy. *Science* (2018) 359(6375):582–7. doi: 10.1126/science.aao4572
33. Ott PA, Bang YJ, Piha-Paul SA, Razak ARA, Bennouna J, Soria JC, et al. T-Cell-Inflamed Gene-Expression Profile, Programmed Death Ligand 1 Expression, and Tumor Mutational Burden Predict Efficacy in Patients Treated With Pembrolizumab Across 20 Cancers: KEYNOTE-028. *J Clin Oncol* (2019) 37(4):318–27. doi: 10.1200/JCO.2018.78.2276
34. Girolami I, Pantanowitz L, Munari E, Martini M, Nocini R, Bisi N, et al. Prevalence of PD-L1 Expression in Head and Neck Squamous Precancerous Lesions: A Systematic Review and Meta-Analysis. *Head Neck* (2020) 42 (10):3018–30. doi: 10.1002/hed.26339
35. Burtness B, Harrington KJ, Greil R, Soulières D, Tahara M, de Castro GJr, et al. Pembrolizumab Alone or With Chemotherapy Versus Cetuximab With Chemotherapy for Recurrent or Metastatic Squamous Cell Carcinoma of the Head and Neck (KEYNOTE-048): A Randomised, Open-Label, Phase 3 Study. *Lancet* (2019) 394(10212):1915–28. doi: 10.1016/S0140-6736(19)32591-7
36. Fuchs CS, Doi T, Jang RW, Muro K, Satoh T, Machado M, et al. Safety and Efficacy of Pembrolizumab Monotherapy in Patients With Previously Treated Advanced Gastric and Gastroesophageal Junction Cancer: Phase 2 Clinical KEYNOTE-059 Trial. *JAMA Oncol* (2018) 4(5):e180013. doi: 10.1001/jamaoncol.2018.0013
37. Chen J, Luo S, Qin S, Cheng Y, Li Z, Fan Y, et al. 760P Pembrolizumab vs Chemotherapy in Patients With Advanced/Metastatic Adenocarcinoma (AC) or Squamous Cell Carcinoma (SCC) of the Esophagus as Second-Line Therapy: Analysis of the Chinese Subgroup in KEYNOTE-181. *Ann Oncol* (2019) 30:mdz247–086. doi: 10.1093/annonc/mdz247.086
38. Shitara K, Van Cutsem E, Bang YJ, Fuchs C, Wyrwicz L, Lee KW, et al. Efficacy and Safety of Pembrolizumab or Pembrolizumab Plus Chemotherapy vs Chemotherapy Alone for Patients With First-Line, Advanced Gastric Cancer: The KEYNOTE-062 Phase 3 Randomized Clinical Trial. *JAMA Oncol* (2020) 6(10):1571–80. doi: 10.1001/jamaoncol.2020.3370
39. Zhu AX, Finn RS, Edeline J, Cattan S, Ogasawara S, Palmer D, et al. Pembrolizumab in Patients With Advanced Hepatocellular Carcinoma Previously Treated With Sorafenib (KEYNOTE-224): A Non-Randomised, Open-Label Phase 2 Trial. *Lancet Oncol* (2018) 19(7):940–52. doi: 10.1016/S1470-2045(18)30351-6
40. El-Khoueiry AB, Sangro B, Yau T, Crocenzi TS, Kudo M, Hsu C, et al. Nivolumab in Patients With Advanced Hepatocellular Carcinoma (CheckMate 040): An Open-Label, Non-Comparative, Phase 1/2 Dose Escalation and Expansion Trial. *Lancet* (2017) 389(10088):2492–502. doi: 10.1016/S0140-6736(17)31046-2
41. Shah MA, Kojima T, Hochhauser D, Enzinger P, Raimbourg J, Hollebecque A, et al. Efficacy and Safety of Pembrolizumab for Heavily Pretreated Patients With Advanced, Metastatic Adenocarcinoma or Squamous Cell Carcinoma of the Esophagus: The Phase 2 KEYNOTE-180 Study. *JAMA Oncol* (2019) 5 (4):546–50. doi: 10.1001/jamaoncol.2018.5441
42. Liu C, Liu R, Wang B, Lian J, Yao Y, Sun H, et al. Blocking IL-17A Enhances Tumor Response to Anti-PD-1 Immunotherapy in Microsatellite Stable Colorectal Cancer [Published Correction Appears in J Immunother Cancer. *J Immunother Cancer* (2021) 9(1):e001895. doi: 10.1136/jitc-2020-001895
43. Gao HL, Liu L, Qi ZH, Gao HL, Liu L, Qi ZH, et al. The Clinicopathological and Prognostic Significance of PD-L1 Expression in Pancreatic Cancer: A

Meta-Analysis. *Hepatobiliary Pancreat Dis Int* (2018) 17(2):95–100. doi: 10.1016/j.hbpd.2018.03.007
44. Yamashita K, Iwatsuki M, Harada K, Eto K, Hiyoshi Y, Ishimoto T, et al. Prognostic Impacts of the Combined Positive Score and the Tumor Proportion Score for Programmed Death Ligand-1 Expression by Double Immunohistochemical Staining in Patients With Advanced Gastric Cancer. *Gastric Cancer* (2020) 23(1):95–104. doi: 10.1007/s10120-019-00999-9
45. Stein A, Simnica D, Schultheiß C, Scholz R, Tintelnot J, Gökkurt E, et al. PD-L1 Targeting and Subclonal Immune Escape Mediated by PD-L1 Mutations in Metastatic Colorectal Cancer. *J Immunother Cancer* (2021) 9(7):e002844. doi: 10.1136/jitc-2021-002844
46. Mansfield AS, Murphy SJ, Peikert T, Yi ES, Vasmatzis G, Wigle DA, et al. Heterogeneity of Programmed Cell Death Ligand 1 Expression in Multifocal Lung Cancer. *Clin Cancer Res* (2016) 22(9):2177–82. doi: 10.1158/1078-0432.CCR-15-2246
47. Paolino G, Pantanowitz L, Barresi V, Pagni F, Munari E, Moretta L, et al. PD-L1 Evaluation in Head and Neck Squamous Cell Carcinoma: Insights Regarding Specimens, Heterogeneity and Therapy. *Pathol Res Pract* (2021) 226:153605. doi: 10.1016/j.prp.2021.153605
48. Chen J, Jiang CC, Jin L, Zhang XD. Regulation of PD-L1: A Novel Role of Pro-Survival Signalling in Cancer. *Ann Oncol* (2016) 27(3):409–16. doi: 10.1093/annonc/mdv615
49. Chen SF, Hou JY, Wu SY. Expression of Human GC Cell Line PD-L1 Is Up-Regulated by IFN-γ. *Chin J Pathophysiol* (2013) 29(11):1952–6. doi: 10.3969/j.issn.1000-4718.2013.11.006
50. Girolami I, Pantanowitz L, Barberis M, Paolino G, Brunelli M, Vigliar E, et al. Challenges Facing Pathologists Evaluating PD-L1 in Head & Neck Squamous Cell Carcinoma. *J Oral Pathol Med* (2021) 50(9):864–73. doi: 10.1111/jop.13220
51. Cerbelli B, Girolami I, Eccher A, Costarelli L, Taccogna S, Scialpi R, et al. Evaluating Programmed Death-Ligand 1 (PD-L1) in Head and Neck Squamous Cell Carcinoma: Concordance Between the 22C3 PharmDx Assay and the SP263 Assay on Whole Sections From a Multicentre Study. *Histopathol* (2022) 80(2):397–406. doi: 10.1111/his.14562
52. Doroshow DB, Bhalla S, Beasley MB, Sholl LM, Kerr KM, Gnjatic S, et al. PD-L1 as a Biomarker of Response to Immune-Checkpoint Inhibitors. *Nat Rev Clin Oncol* (2021) 18(6):345–62. doi: 10.1038/s41571-021-00473-5
53. Ma LJ, Feng FL, Dong LQ, Zhang Z, Duan M, Liu LZ, et al. Clinical Significance of PD-1/PD-Ls Gene Amplification and Overexpression in Patients With Hepatocellular Carcinoma. *Theranostics* (2018) 8(20):5690–702. doi: 10.7150/thno.28742
54. Duncan DJ, Scott M, Scorer P, Barker C. Assessment of PD-L1 mRNA and Protein Expression in Non-Small Cell Lung Cancer, Head and Neck Squamous Cell Carcinoma and Urothelial Carcinoma Tissue Specimens Using RNAScope and Immunohistochemistry. *PloS One* (2019) 14(4):e0215393. doi: 10.1371/journal.pone.0215393
55. Namikawa T, Yokota K, Tanioka N, Fukudome I, Iwabu J, Munekage M, et al. Systemic Inflammatory Response and Nutritional Biomarkers as Predictors of Nivolumab Efficacy for Gastric Cancer. *Surg Today* (2020) 50(11):1486–95. doi: 10.1007/s00595-020-02048-w
56. Ogata T, Satake H, Ogata M, Hatachi Y, Inoue K, Hamada M, et al. Neutrophil-To-Lymphocyte Ratio as a Predictive or Prognostic Factor for Gastric Cancer Treated With Nivolumab: A Multicenter Retrospective Study. *Oncotarget* (2018) 9(77):34520–7. doi: 10.18632/oncotarget.26145
57. Ohta A, Komatsu S, Tsuji R, Tanaka S, Kumano T, Imura K, et al. Clinical Evaluation of the Efficacy and Adverse Effects of Nivolumab Treatment for Patients With Advanced Gastric Cancer. *Gan To Kagaku Ryoho* (2020) 47(4):725–7.
58. Shao YY, Liu TH, Hsu C, Lu LC, Shen YC, Lin ZZ, et al. Early Alpha-Foetoprotein Response Associated With Treatment Efficacy of Immune Checkpoint Inhibitors for Advanced Hepatocellular Carcinoma. *Liver Int* (2019) 39(11):2184–9. doi: 10.1111/liv.14210
59. Kim ST, Cristescu R, Bass AJ, Kim KM, Odegaard JI, Kim K, et al. Comprehensive Molecular Characterization of Clinical Responses to PD-1 Inhibition in Metastatic Gastric Cancer. *Nat Med* (2018) 24(9):1449–58. doi: 10.1038/s41591-018-0101-z
60. Yang X, Hu Y, Yang K, Wang D, Lin J, Long J, et al. Cell-Free DNA Copy Number Variations Predict Efficacy of Immune Checkpoint Inhibitor-Based Therapy in Hepatobiliary Cancers. *J Immunother Cancer* (2021) 9(5):e001942. doi: 10.1136/jitc-2020-001942
61. Yue C, Jiang Y, Li P, Wang Y, Xue J, Li N, et al. Dynamic Change of PD-L1 Expression on Circulating Tumor Cells in Advanced Solid Tumor Patients Undergoing PD-1 Blockade Therapy. *Oncoimmunol* (2018) 7(7):e1438111. doi: 10.1080/2162402X.2018.1438111
62. Valero C, Lee M, Hoen D, Weiss K, Kelly DW, Adusumilli PS, et al. Pretreatment Neutrophil-to-Lymphocyte Ratio and Mutational Burden as Biomarkers of Tumor Response to Immune Checkpoint Inhibitors. *Nat Commun* (2021) 12(1):729. doi: 10.1038/s41467-021-20935-9
63. Van Wilpe S, Koornstra R, Den Brok M, De Groot JW, Blank C, De Vries J, et al. Lactate Dehydrogenase: A Marker of Diminished Antitumor Immunity. *Oncoimmunol* (2020) 9(1):1731942. doi: 10.1080/2162402X.2020.1731942
64. Shen R, Postow MA, Adamow M, Arora A, Hannum M, Maher C, et al. LAG-3 Expression on Peripheral Blood Cells Identifies Patients With Poorer Outcomes After Immune Checkpoint Blockade. *Sci Transl Med* (2021) 13(608):eabf5107. doi: 10.1126/scitranslmed.abf5107
65. Bratman SV, Yang SYC, Iafolla MAJ, Liu Z, Hansen AR, Bedard PL, et al. Personalized Circulating Tumor DNA Analysis as a Predictive Biomarker in Solid Tumor Patients Treated With Pembrolizumab. *Nat Cancer* (2020) 1(9):873–81. doi: 10.1038/s43018-020-0096-5
66. Zhou J, Mahoney KM, Giobbie-Hurder A, Zhao F, Lee S, Liao X, et al. Soluble PD-L1 as a Biomarker in Malignant Melanoma Treated With Checkpoint Blockade. *Cancer Immunol Res* (2017) 5(6):480–92. doi: 10.1158/2326-6066.CIR-16-0329
67. Khan M, Arooj S, Wang H. Soluble B7-CD28 Family Inhibitory Immune Checkpoint Proteins and Anti-Cancer Immunotherapy. *Front Immunol* (2021) 12:651634. doi: 10.3389/fimmu.2021.651634
68. Chen YP, Zhang Y, Lv JW, Li YQ, Wang YQ, He QM, et al. Genomic Analysis of Tumor Microenvironment Immune Types Across 14 Solid Cancer Types: Immunotherapeutic Implications. *Theranostics* (2017) 7(14):3585–94. doi: 10.7150/thno.21471
69. Noh BJ, Kim JH, Eom DW. Prognostic Significance of Categorizing Gastric Carcinoma by PD-L1 Expression and Tumor Infiltrating Lymphocytes. *Ann Clin Lab Sci* (2018) 48(6):695–706.
70. Pagès F, Mlecnik B, Marliot F, Bindea G, Ou FS, Bifulco C, et al. International Validation of the Consensus Immunoscore for the Classification of Colon Cancer: A Prognostic and Accuracy Study. *Lancet* (2018) 391(10135):2128–39. doi: 10.1016/S0140-6736(18)30789-X
71. Cortellini A, Bersanelli M, Buti S, Cannita K, Santini D, Perrone F, et al. A Multicenter Study of Body Mass Index in Cancer Patients Treated With Anti-PD-1/PD-L1 Immune Checkpoint Inhibitors: When Overweight Becomes Favorable. *J Immunother Cancer* (2019) 7(1):57. doi: 10.1186/s40425-019-0527-y
72. Wei XL, Xu JY, Wang DS, Chen DL, Ren C, Li JN, et al. Baseline Lesion Number as an Efficacy Predictive and Independent Prognostic Factor and Its Joint Utility With TMB for PD-1 Inhibitor Treatment in Advanced Gastric Cancer. *Ther Adv Med Oncol* (2021) 13:1758835921988996. doi: 10.1177/1758835921988996
73. Noh BJ, Hong SM, Jun SY, Eom DW. Prognostic Implications of Immune Classification in a Multicentre Cohort of Patients With Small Intestinal Adenocarcinoma. *Pathol* (2020) 52(2):228–35. doi: 10.1016/j.pathol.2019.09.004
74. Trujillo JA, Sweis RF, Bao R, Luke JJ. T Cell-Inflamed Versus Non-T Cell-Inflamed Tumors: A Conceptual Framework for Cancer Immunotherapy Drug Development and Combination Therapy Selection. *Cancer Immunol Res* (2018) 6(9):990–1000. doi: 10.1158/2326-6066.CIR-18-0277
75. Cristescu R, Mogg R, Ayers M, Albright A, Murphy E, Yearley J, et al. Pan-Tumor Genomic Biomarkers for PD-1 Checkpoint Blockade-Based Immunotherapy. *Science* (2018) 362(6411):eaar3593. doi: 10.1126/science.aar3593
76. Nejman D, Livyatan I, Fuks G, Gavert N, Zwang Y, Geller LT, et al. The Human Tumor Microbiome Is Composed of Tumor Type-Specific Intracellular Bacteria. *Science* (2020) 368(6494):973–80. doi: 10.1126/science.aay9189
77. Das S, Ciombor KK, Haraldsdottir S, Pumpalova Y, Sahin IH, Pineda G, et al. Immune-Related Adverse Events and Immune Checkpoint Inhibitor Efficacy in Patients With Gastrointestinal Cancer With Food and Drug Administration-Approved Indications for Immunotherapy. *Oncol* (2020) 25(8):669–79. doi: 10.1634/theoncologist.2019-0637

78. Masuda K, Shoji H, Nagashima K, Yamamoto S, Ishikawa M, Imazeki H, et al. Correlation Between Immune-Related Adverse Events and Prognosis in Patients With Gastric Cancer Treated With Nivolumab. *BMC Cancer* (2019) 19(1):974. doi: 10.1186/s12885-019-6150-y
79. Wang F, Qin S, Sun X, Ren Z, Meng Z, Chen Z, et al. Reactive Cutaneous Capillary Endothelial Proliferation in Advanced Hepatocellular Carcinoma Patients Treated With Camrelizumab: Data Derived From a Multicenter Phase 2 Trial. *J Hematol Oncol* (2020) 13(1):47. doi: 10.1186/s13045-020-00886-2
80. Huang J, Xu J, Chen Y, Zhuang W, Zhang Y, Chen Z, et al. Camrelizumab versus investigator's choice of chemotherapy as second-line therapy for advanced or metastatic oesophageal squamous cell carcinoma (ESCORT): A multicentre, randomised, open-label, phase 3 study. *Lancet Oncol* (2020) 21 (6):832–42. doi: 10.1016/S1470-2045(20)30110-8
81. Berner F, Bomze D, Diem S, Ali OH, Fässler M, Ring S, et al. Association of Checkpoint Inhibitor-Induced Toxic Effects With Shared Cancer and Tissue Antigens in Non-Small Cell Lung Cancer. *JAMA Oncol* (2019) 5(7):1043–7. doi: 10.1001/jamaoncol.2019.0402
82. Conforti F, Pala L, Bagnardi V, De Pas T, Martinetti M, Viale G, et al. Cancer Immunotherapy Efficacy and Patients' Sex: A Systematic Review and Meta-Analysis. *Lancet Oncol* (2018) 19(6):737–46. doi: 10.1016/S1470-2045(18) 30261-4
83. Fluckiger A, Daillère R, Sassi M, Sixt BS, Liu P, Loos F, et al. Cross-Reactivity Between Tumor MHC Class I-Restricted Antigens and an Enterococcal Bacteriophage. *Science* (2020) 369(6506):936–42. doi: 10.1126/science.aax0701
84. Zheng Y, Wang T, Tu X, Huang Y, Zhang H, Tan D, et al. Gut Microbiome Affects the Response to Anti-PD-1 Immunotherapy in Patients With Hepatocellular Carcinoma. *J Immunother Cancer* (2019) 7(1):193. doi: 10.1186/s40425-019-0650-9
85. Mager LF, Burkhard R, Pett N, Cooke NCA, Brown K, Ramay H, et al. Microbiome-Derived Inosine Modulates Response to Checkpoint Inhibitor Immunotherapy. *Science* (2020) 369(6510):1481–9. doi: 10.1126/science.abc3421
86. Drewes JL, Housseau F, Sears CL. Sporadic Colorectal Cancer: Microbial Contributors to Disease Prevention, Development and Therapy. *Br J Cancer* (2016) 115(3):273–80. doi: 10.1038/bjc.2016.189
87. Yang J. *Tracking the Dynamic Evolution of Tumor Local Immunity and Intestinal Flora to Explore the Optimization Strategy of Pancreatic Cancer Immunotherapy*. Zhejiang University (2020) 1. doi: 10.27461/d.cnki.gzjdx.2020.002120.
88. Jobin C. Precision Medicine Using Microbiota. *Science* (2018) 359(6371):32–4. doi: 10.1126/science.aar2946
89. Okabe A, Huang KK, Matsusaka K, Fukuyo M, Xing M, Ong X, et al. Cross-Species Chromatin Interactions Drive Transcriptional Rewiring in Epstein-Barr Virus-Positive Gastric Adenocarcinoma. *Nat Genet* (2020) 52(9):919–30. doi: 10.1038/s41588-020-0665-7
90. Panda A, Mehnert JM, Hirshfield KM, Riedlinger G, Damare S, Saunders T, et al. Immune Activation and Benefit From Avelumab in EBV-Positive Gastric Cancer. *J Natl Cancer Inst* (2018) 110(3):316–20. doi: 10.1093/jnci/djx213
91. Thompson ED, Zahurak M, Murphy A, Cornish T, Cuka N, Abdelfatah E, et al. Patterns of PD-L1 Expression and CD8 T Cell Infiltration in Gastric Adenocarcinomas and Associated Immune Stroma. *Gut* (2017) 66(5):794–801. doi: 10.1136/gutjnl-2015-310839
92. Bass, Thorsson, Shmulevich. Comprehensive Molecular Characterization of Gastric Adenocarcinoma. *Nature* (2014) 513(7517):202–9. doi: 10.1038/nature13480
93. Derks S, Liao X, Chiaravalli AM, Xu X, Camargo MC, Solcia E, et al. Abundant PD-L1 Expression in Epstein-Barr Virus-Infected Gastric Cancers. *Oncotarget* (2016) 7(22):32925–32. doi: 10.18632/oncotarget.9076
94. Renehan AG, Tyson M, Egger M, Heller RF, Zwahlen M. Body-Mass Index and Incidence of Cancer: A Systematic Review and Meta-Analysis of Prospective Observational Studies. *Lancet* (2008) 371(9612):569–78. doi: 10.1016/S0140-6736(08)60269-X
95. Wang Z, Aguilar EG, Luna JI, Dunai C, Khuat LT, Le CT, et al. Paradoxical Effects of Obesity on T Cell Function During Tumor Progression and PD-1 Checkpoint Blockade. *Nat Med* (2019) 25(1):141–51. doi: 10.1038/s41591-018-0221-5
96. Strulov Shachar S, Williams GR. The Obesity Paradox in Cancer-Moving Beyond BMI. *Cancer Epidemiol Biomarkers Prev* (2017) 26(1):13–6. doi: 10.1158/1055-9965.EPI-16-0439
97. Pfister D, Núñez NG, Pinyol R, Govaere O, Pinter M, Szydlowska M, et al. NASH Limits Anti-Tumour Surveillance in Immunotherapy-Treated HCC. *Nature* (2021) 592(7854):450–6. doi: 10.1038/s41586-021-03362-0
98. Moyat M, Velin D. Immune Responses to Helicobacter Pylori Infection. *World J Gastroenterol* (2014) 20(19):5583–93. doi: 10.3748/wjg.v20.i19.5583
99. Oster P, Vaillant L, Riva E, McMillan B, Begka C, Truntzer C, et al. Helicobacter Pylori Infection has a Detrimental Impact on the Efficacy of Cancer Immunotherapies. *Gut* (2021) 12:gutjnl-2020-323392. doi: 10.1136/gutjnl-2020-323392
100. Chowell D, Yoo SK, Valero C, Pastore A, Krishna C, Lee M, et al. Improved Prediction of Immune Checkpoint Blockade Efficacy Across Multiple Cancer Types. *Nat Biotechnol* (2021). doi: 10.1038/s41587-021-01070-8

Conflict of Interest: The authors declare that the research was conducted in the absence of any commercial or financial relationships that could be construed as a potential conflict of interest.

Publisher's Note: All claims expressed in this article are solely those of the authors and do not necessarily represent those of their affiliated organizations, or those of the publisher, the editors and the reviewers. Any product that may be evaluated in this article, or claim that may be made by its manufacturer, is not guaranteed or endorsed by the publisher.

frontiers | Frontiers in Immunology

ORIGINAL RESEARCH
published: 14 April 2022
doi: 10.3389/fimmu.2022.853213

Joint Analysis of Microbial and Immune Cell Abundance in Liver Cancer Tissue Using a Gene Expression Profile Deconvolution Algorithm Combined With Foreign Read Remapping

Dongmei Ai[1], Yonglian Xing[2], Qingchuan Zhang[3], Yishu Wang[2], Xiuqin Liu[2], Gang Liu[2] and Li C. Xia[4]**

[1] Basic Experimental Center of Natural Science, University of Science and Technology Beijing, Beijing, China, [2] School of Mathematics and Physics, University of Science and Technology Beijing, Beijing, China, [3] National Engineering Laboratory for Agri-Product Quality Traceability, Beijing Technology and Business University, Beijing, China, [4] School of Mathematics, South China University of Technology, Guangzhou, China

OPEN ACCESS

Edited by:
Hongda Liu,
Nanjing Medical University, China

Reviewed by:
Mahdi Hasanipanah,
Duy Tan University, Vietnam
Mingcong Deng,
Tokyo University of Agriculture and Technology, Japan

***Correspondence:**
Dongmei Ai
aidongmei@ustb.edu.cn
Li C. Xia
lcxia@scut.edu.cn

Specialty section:
This article was submitted to Cancer Immunity and Immunotherapy, a section of the journal Frontiers in Immunology

Received: 12 January 2022
Accepted: 07 March 2022
Published: 14 April 2022

Citation:
Ai D, Xing Y, Zhang Q, Wang Y, Liu X, Liu G and Xia LC (2022) Joint Analysis of Microbial and Immune Cell Abundance in Liver Cancer Tissue Using a Gene Expression Profile Deconvolution Algorithm Combined With Foreign Read Remapping. Front. Immunol. 13:853213. doi: 10.3389/fimmu.2022.853213

Recent transcriptomics and metagenomics studies showed that tissue-infiltrating immune cells and bacteria interact with cancer cells to shape oncogenesis. This interaction and its effects remain to be elucidated. However, it is technically difficult to co-quantify immune cells and bacteria in their respective microenvironments. To address this challenge, we herein report the development of a complete a bioinformatics pipeline, which accurately estimates the number of infiltrating immune cells using a novel Particle Swarming Optimized Support Vector Regression (PSO-SVR) algorithm, and the number of infiltrating bacterial using foreign read remapping and the GRAMMy algorithm. It also performs systematic differential abundance analyses between tumor-normal pairs. We applied the pipeline to a collection of paired liver cancer tumor and normal samples, and we identified bacteria and immune cell species that were significantly different between tissues in terms of health status. Our analysis showed that this dual model of microbial and immune cell abundance had a better differentiation (84%) between healthy and diseased tissue. *Caldatribacterium* sp., *Acidaminococcaceae* sp., *Planctopirus* sp., *Desulfobulbaceae* sp.,*Nocardia farcinica* as well as regulatory T cells (Tregs), resting mast cells, monocytes, M2 macrophases, neutrophils were identified as significantly different (Mann Whitney Test, FDR< 0.05). Our open-source software is freely available from GitHub at https://github.com/gutmicrobes/PSO-SVR.git.

Keywords: tumor microenvironment, RNA-seq, gene expression profiling, support vector regression, particle swarm algorithm

INTRODUCTION

Contrary to the intuition of most people, bacteria are present in almost every part of the human body, with over 1,000 species in the gut alone. Our commensal bacteria maintain a dynamic balance with each other, and their imbalance can lead to a variety of diseases in the human body, including many cancers (1). Indeed, approximately 20% of all lethal cancers in humans are induced by or associated with microorganisms (2). As a component of the tumor microenvironment (TME), bacteria can actively promote tumor development, as well as autoimmunity, contributing to mortality (3, 4).

Liver cancer is a malignant tumor and approximately 780,000 people were diagnosed with liver cancer worldwide yearly (5). Previous studies analyzed microbes inferred from the whole-genome sequencing data of liver cancer biopsies. They revealed a strong association between the occurrence of liver cancer and certain bacterial flora. For examples: Moffatt et al. found that the bacterium *Porphyromonas gingivalis* promotes hepatocellular carcinoma by affecting host cell signaling and thus cytokine response, cell cycle, and apoptosis (6); Garner et al. found that methoxysterigmatocystin, O-methylsterigmatocystin, and other metabolites induced DNA repair-deficient bacterial lesions and thus initiates hepatocellular carcinogenesis (7); Mangul et al. found that *Escherichia coli*, *Streptococcus faecalis*, and *Clostridium parvum* could act together to significantly promote liver tumorigenesis. However, such activity could be inhibited by the addition of intestinal bacteria (e.g., *Bifidobacterium longum* and *Lactobacillus acidophilus*) and rectal fungi (8).

However, these studies were mostly focused on the effects of intestinal bacteria upon hepatocellular carcinoma (HCC) while few have examined the bacteria present within hepatocellular carcinoma tissues. Tumor-infiltrating bacteria could be analyzed using sequencing reads of non-human source, however, these unmapped foreign reads are often overlooked. In fact, it is possible to accurately estimate microbial abundance in tissue biopsies using foreign reads remapping (9). In this study, we applied our previously developed GRAMMy (10) tool to identify the bacteria that are associated with liver cancer by adding a series of analyses on unmapped foreign reads filtered from RNA-seq data so as to estimate the relative abundance of infiltrating bacteria present within the tissue.

Studies have also shown that the infiltration of various immune cell populations, including monocytes/macrophages, natural killer cells (NK), NKT cells and T cells, is the main pathogenic feature for oncogenesis or other lesions in liver (11). Rohr-Udilova et al. observed considerable differences in the composition of immune cells between HCC and healthy liver. Pushpa Hegde et al. found a decrease in circulating mucosal-associated invariant T cells in patients with alcoholic or nonalcoholic fatty liver disease-related cirrhosis (12). Functional immune level changes were detected in a group of healthy people and liver transplant recipients (13). Microbial infection is very likely to occur in the clinical treatment of liver diseases, especially in the treatment of liver transplantation; bacterial infection being the most common (incidence of 31.45%) (14). Monitoring the immune status of transplant recipients is essential to predict the risk of infection.

Thus, researchers have just begun to understand the regulatory role of bacteria in the development of cancer, as well as oncogenesis at the interface of bacteria/immune cell interaction. Immune cells alone are a key component of the TME and play a critical role in cancer development and immunization. Therefore, in order to understand the dynamics of the TME, it is equally important to understand the presumed synergistic dynamics between bacteria and tissue-infiltrating immune cells. Computational deconvolution methods have become a convenient choice to assess tissue-infiltrating immune cells by formulating the problem as a system of equations used to describe the gene expression of a sample as a weighted sum of the expression profiles of mixed cell types. That is, once given the immune cell-type characteristic matrix and overall gene expression, by solving the deconvolution problem, immune cell types and levels can be reasonably co-quantified with bacteria using mRNA-seq data without resorting to additional experiments.

The deconvolution problem could be solved in several ways, such as by Support Vector Regression (SVR) (e.g., CIBERSORT) (15), linear least squares regression (e.g., TIMER) (16) and constrained least squares regression (e.g., EPIC and MCP-counter) (17, 18). CIBERSORT uses v-SVR linear regression to solve the linear equation model based on microarray data (RNA-seq data can also be used). The coefficient of the regression model represents the relative proportion of 22 immune cell types. TIMER calculates the abundance of six immune cells including CD4 T cells, CD8 T cells and B cells based on the constrained least square method, which better solved the multicollinearity problem caused by high-dimensional features. EPIC uses least square regression to infer the mRNA number of six immune cells and other cell types, and then converts the mRNA number into the relative proportion of related immune cells. Finally, through the verification of tumor active genes and clinical data of many patients, it is found that epic results are clinically applicable. Finally, the murine Microenvironment Cell Population counter (MCP-counter) was based on highly specific transcriptomic markers, allows a robust quantification of the count number of eight immune cell types and two stromal cell populations in heterogeneous tissues based on transcriptomic data, which represent the cell content.

At present, the main method of optimizing the SVR deconvolution problem uses an heuristic algorithm. Particle swarm optimization (PSO) is simple and easy to operate algorithm, and the optimization search process of PSO take into account the local search ability and global search ability, which can greatly improve the accuracy of SVR solution. At present, PSO- SVR algorithm has been applied in many fields. For example, Mingcong Deng et al. applied PSO- SVR algorithm to robotics in 2014 to predict the ball receiving time of a robot player (19). In 2017, the same team used PSO to optimize the parameters of the generalized Gaussian kernel model and confirmed that the algorithm also shows good performance in a pneumatic bending rubber actuator control system (20).

However, few teams have applied PSO- SVR to the field of tumor immune cell infiltration. This study aims to further study the universality of this algorithm and its advantages or limitations compared with other algorithms in this field through the results of liver cancer samples under this algorithm.

Mohammadi et al. evaluated several methods for solving the deconvolution problem and found that combining the loss function with regularization can improve the solution performance in the presence of highly correlated cell types in the mixture (21). However, the effect of the size of the regularization parameters on the effect of immune cell counting is unknown and the SVR model accuracy is affected by the initial parameters, such as the kernel function coefficients and penalty factors. To increase the robustness of the algorithm and reduce the influence of the initial self-defined parameters on the proportional counting results of immune cells, we introduced the particle swarm optimized support vector regression (PSO-SVR) algorithm, which uses PSO -a powerful parameter iterative optimization solution algorithm to improve the accuracy of the SVR solution. The algorithm was also used to compare with CIBERSORTX (22), EPIC, and MCP-counter on three real data sets, which confirmed its better accuracy.

Finally, we used the PSO-SVR algorithm and foreign read remapping to analyze a collection of paired liver cancer tumor and normal samples, identified bacteria and immune cell species that are significantly different between samples, and evaluated their joint effects by predicting the tumoral or normal pathological status of their originating tissue. The joint model identified B cells, T cells and *Caldatribacterium* sp., *Magnetobacteriaceae* sp. as pathological markers and together they were powerfully predictive for the pathologic status. Based on results from the three cases, classification accuracy when using only a single input feature is lower - only bacteria: 0.70, only immune cell feature: 0.74, and both features: 0.84. Such preliminary results are useful in resolving standing low response issue of immune checkpoint inhibitor-based immunotherapy (23, 24), in that microbial markers are potentially actionable targets (25, 26). As the joint immunomodulatory effects of the microbiome and immune cells are further elucidated for other cancer types, we could expect to find more novel biomarkers that could be intervened upon to improve normal tissue's immune response against tumor.

MATERIALS AND METHODS

The Liver Cancer mRNA Sequence Data Set

The mRNA-seq raw sequence data in BAM format of liver cancer patients' normal and tumor tissue biopsies for this study were downloaded from the Seven Bridges Cancer Genomics Cloud (CGC https://www.cancergenomicscloud.org/). The data set included 98 samples (49 pairs of RNA-Seq sequencing samples of primary liver cancer tumor tissue and adjacent normal tissue). The read sequences that did not map to the reference genome GRCH38 were extracted from the BAM files. These foreign reads were then mapped to the RefSeq (NCBI Reference Sequence Database) (https://www.ncbi.nlm.nih.gov/refseq/) - a large collection of bacterial genomes. The mapping results were then input to the GRAMMy pipeline for the relative abundance estimation of infiltrating bacteria. The obtained expression and microbial profiles were used for downstream analysis. The data processing flow is shown in **Figure 1**.

We first filtered the reads that were not matched to the human genome reference GRCH38 from the RNA-Seq samples in BAM format with SAMtools, which included reads that were not mapped at both ends and reads that were not mapped at one end (mapped at one end but not at the other). Apply Fastp to remove low-quality reads and partial reads, and excise poor quality bases. Use the BWA tool to remap the unmapped reads to a comprehensive microbial reference library RefSeq, containing the full genome sequence of 23,790 bacteria and archaea. We then applied GRAMMy algorithm to estimate the bacteria relative abundance.

The mRNA analysis pipeline begins with the Alignment Workflow, which is performed using a two-pass method with STAR. STAR aligns each read group separately and then merges the resulting alignments into one. Following alignment, BAM files are processed through the RNA Expression Workflow to determine RNA expression levels. The reads mapped to each gene are enumerated using HT-Seq-Count. Expression values are provided in a tab-delimited format.

Validation Data Sets for Immune Cell Infiltration

Three real data sets were used to validate the PSO-SVR algorithm as compared to the CIBERSORTX, EPIC, and MCP-counter algorithms. The first validation data set from the CIBERSORT article consists of the gene expression profiles of 20 peripheral blood mono nuclear cells (PBMC) samples and the ratio of immune cells determined through flow cytometry for the same samples. The second data set comes from the National Center for Biotechnology Information Search database (NCBI database) under the GEO Datasets GSE64385. It consists of the gene expression profile of 10 colorectal cancer (CRC) samples and the composition of immune cells as determined by immunohistochemistry of the same samples. The third data set from CIBERSORTX consists of the gene expression profiles of 19 melanoma samples and the composition of immune cells obtained through single-cell sequencing technique of the same samples. The full description of these data sets is shown in **Supplementary Table 1**.

Extracting Unmapped Reads

We first filtered the reads that did not matched to the human genome reference GRCH38 from the RNA-Seq samples in BAM format using SAMtools (27). The filtered reads included those that were not mapped at both ends and those that were not mapped at one end (mapped at one end but not the other). The process was as follows:

Extracting unmapped single reads: we used the command "samtools view -u -f 4 -F 264" to extract single-end unmapped reads in the format of FASTQ (28).

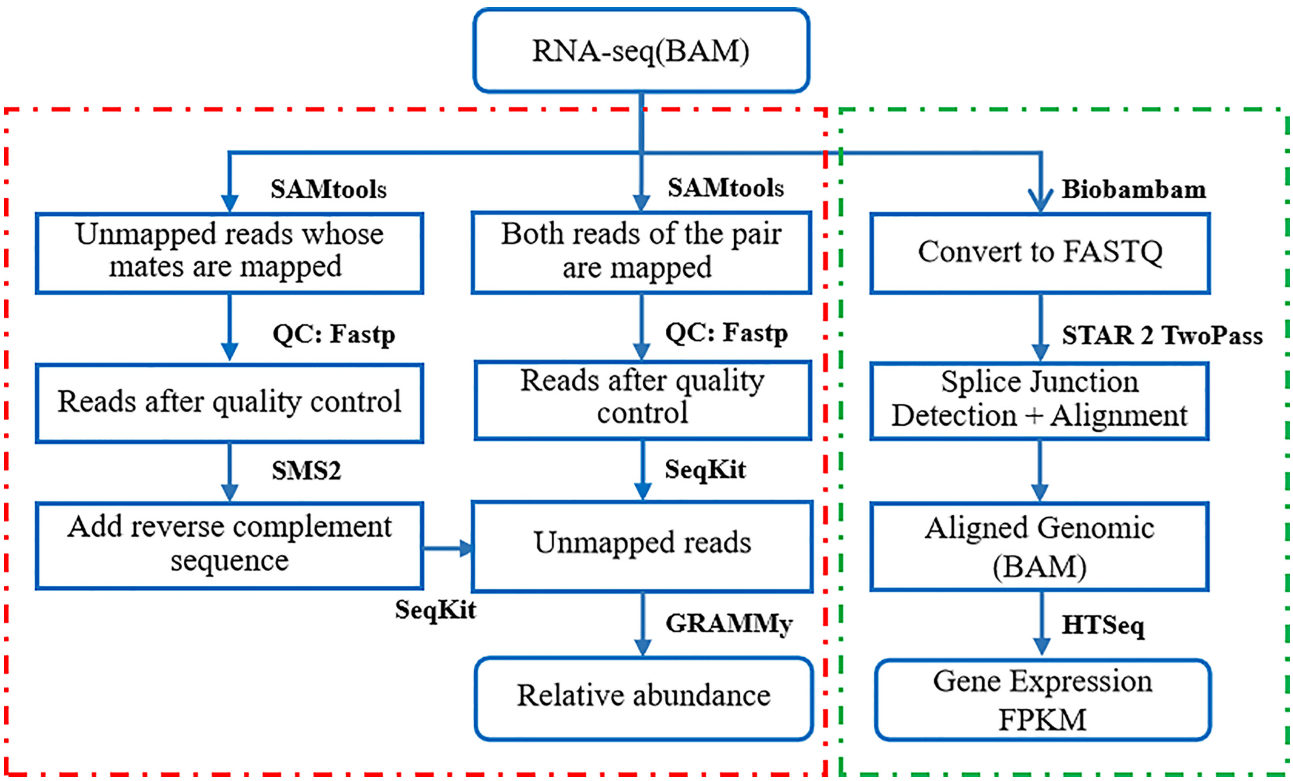

FIGURE 1 | Flow chart of RNA-Seq sequencing data processing.

Extracting unmapped paired-end reads: we used the command "samtools view -u -f 12 -F 256" to extract paired-end unmapped reads with the format FASTQ.

Sequencing Quality Control

Sequencing quality issues like low-confidence bases and sequence-specific bias complicate mRNA-seq analyses (29). We applied comprehensive quality control (QC) before analyses (30). We applied Fastp (31) to remove low-quality reads and partial reads, and to excise poor quality bases.

For the extracted unmapped paired-end reads, we used the command "fastp -q 0 -u 100 -n 10 -l 36 -A -G -M 0 -i" to delete sequences with base quality lower than 40% of Q15, sequences with N greater than 5, sequences with length less than 36, and broke up sequences, respectively. For the extracted unmapped single reads, we used the command "fastp -q 0 -u 100 -n 10 -l 36 -A -G -M 0 -i" to perform the same QC process on single-ended sequenced sequences. To merge the extracted single-end and paired-end unmapped reads, we used the SMS2 (32) software to add a reverse complementary sequence to the unmapped single reads. We then converted the resulting FASTQ formatted reads into the FASTA (33) format through SeqKit (34).

We then used the BWA tool (35) to remap the unmapped reads to a comprehensive microbial reference library RefSeq, containing the full genome sequence of 23,790 bacteria and archaea. We then applied the GRAMMy algorithm to estimate the relative abundance of bacteria to mitigate the problem of ambiguous mapping of short reads to relative reference sequences.

Statistical Analysis

The Mann Whitney U test, also known as "Mann Whitney rank sum test", was proposed by H.B.mann and D.Rwhitney in 1947. It assumes that any two samples are from two populations that are exactly the same except the population mean, in order to test for significant difference between the mean of the two populations.

Assuming that the mean values of two populations exist, they are recorded as μ_1,μ_2 respectively. With only one translation difference between f_1 and f_2 at most, we get: $\mu_1 = \mu_2 - \alpha$. The assumptions to be tested are as follows:

$$\begin{cases} H_0 : \mu_1 = \mu_2, H_1 : \mu_1 < \mu_2 \\ H_0 : \mu_1 = \mu_2, H_1 : \mu_1 > \mu_2 \end{cases}$$

The steps of Mann Whitney U test are:

1. Randomly select two independent random samples with capacity of N_A and N_B from two populations A and B, arrange (N_A + N_B) observations in order of size. If the same observations exist, the average of their bit order is used.

2. Calculate the grade and T_A and T_B of two samples.
3. The formula of Mann Whitney U test can be given according to T_A and T_B. The two calculated U values are not equal, but their sum is always equal to $N_A N_B$, that is, $U_A + U_B = N_A N_B$. If $N_A < 20$ and $N_B < 20$, the test statistics are:

$$U_A = N_A N_B + N_A(N_A + 1)/2 - T_A$$

$$U_B = N_A N_B + N_B(N_B + 1)/2 - T_B$$

In the test, because the critical value table of Mann Whitney U test only gives a smaller critical value, the smaller U value in U_A and U_B is used as the test statistic.

4. Select the smaller U value to compare with the critical value of U. if $U > U_\alpha(\alpha = 0.05$, accept the original assumption H_0. If $U < U_\alpha(\alpha = 0.05$, Then reject H_0 and accept H_1. The acceptance domain is the same as Wilcoxon test. U test can also be divided into small samples and large samples. In case of small samples, the critical values of U have been compiled into a table. In large samples, the distribution of U tends to be normal, so it can be treated by normal approximation.

The loss function is an index to measure the performance of the prediction model in predicting the expected results. The commonly used loss functions are mean squared error (MSE) and root mean squared error (RMSE). Since MSE squares the error (y – y^predicted = e), if e > 1, the value of the error will increase a lot. If there is an outlier in our data, the value of e will be very high and will be much greater than $|e|$. This will make the model with MSE loss give a higher weight to outliers. In order to minimize this outlier data point, we use the RMSE value, namely root mean square error, but at the expense of the prediction effect of other normal data points, which will eventually reduce the overall performance of the model.

$$RMSE = \left(\sum_{i=1}^{n} \frac{(\hat{y} - y_i)^2}{n}\right)^{\frac{1}{2}}$$

Correlation analysis refers to the analysis of two or more variable elements with correlation, so as to measure the correlation degree of two variable factors Correlation analysis can be carried out only when there is a certain connection or probability between the elements of correlation.

(1) Pearson correlation coefficient

Given two continuous variables x and y, the Pearson correlation coefficient is defined as:

$$\rho = \frac{\Sigma_{i=1}^{N}(x_i - \bar{x})(y_i - \bar{y})}{[\Sigma_{i=1}^{N}(x_i - \bar{x})^2 \Sigma_{I=1}^{N}(y_i - \bar{y})^2]^{\frac{1}{2}}}$$

Where $\bar{x}$ and $\bar{y}$ are the mean values of the variables x and y respectively.

ρ close to 0 indicates that there is no correlation between the two variables; whereas close 1 or - 1 indicates that the two variables are strongly correlated.

(2) Spearman correlation coefficient

Spearman correlation coefficient is defined as Pearson correlation coefficient ρ between hierarchical variables. For samples with a sample size of N, N original data are converted into hierarchical data. Compared with Pearson correlation coefficient, Spearman correlation coefficient is insensitive to data errors and extreme values, which is defined as.

$$\rho_s = \frac{\Sigma_{i=1}^{N}(R_i - \bar{R})(S_i - \bar{S})}{[\Sigma_{i=1}^{N}(R_i - \bar{R})^2 \Sigma_{I=1}^{N}(S_i - \bar{S})^2]^{\frac{1}{2}}}$$

Where R and S are the grades of observed values i respectively, $\bar{R}$ and $\bar{S}$ are the average grades of variables x and y respectively, and N is the total number of observed values.

Logistic regression, also known as log probability regression, is a machine learning method used to solve the binary classification problem, which is used to estimate the possibility of something. It does not need to scale the input features, and the interpretability of the model is very good. The influence of different features on the final result can be seen from the weight of features. We fit the following regularization model to binary features as:

$$\min_{\beta_0,\beta} -\left[\frac{1}{n}\sum_{i=1}^{n} y_i(\beta_0 + x_j^T\beta) - \log\left(1 + e^{\beta_0 + x_j^T\beta}\right)\right] + \mu\left[\frac{(1-\alpha)||\beta||_2^2}{2} + \alpha||\beta||_1\right]$$

Where β is the regression coefficient. Parameter α is the balanced lasso (L1) and ridge (L2) regularization, and λ determines their weights.

Therefore, we use the logistic regression classifier to classify 98 samples. Their corresponding bacterial relative abundance data and immune cell proportion data were used as input characteristics, and the sample status (normal/tumor) was used as the prediction variable 0 or 1. 75% of the data were used for training and 25% for testing. The association between hepatocarcinogenesis and tumor bacteria and invasive immune cells was analyzed through the classification results under different input characteristics.

RESULTS AND DISCUSSION

The Particle Swarm Optimized - Support Vector Regression Algorithm

Support Vector Regression (SVR) is a commonly used technique for non-linear unsupervised learning. The generalization ability and prediction accuracy of SVR depend on the choice of kernel function coefficients and penalty factors. Due to the large feature size, small sample size and unknown sample distribution, in order to avoid over fitting as much as possible, we used a simple and effective linear kernel function in order to avoid overfitting as much as possible. We introduced the particle swarm optimization (PSO) technique, which uses a powerful algorithm to invoke an iterative approach to solve parameter optimization. It can improve the accuracy of SVR results, and increase the robustness of the results through multiple iterations. The overall flowchart is shown in **Figure 2**.

We briefly introduce the SVR model for immune cell infiltration estimation. Based on a large amount of tissue gene

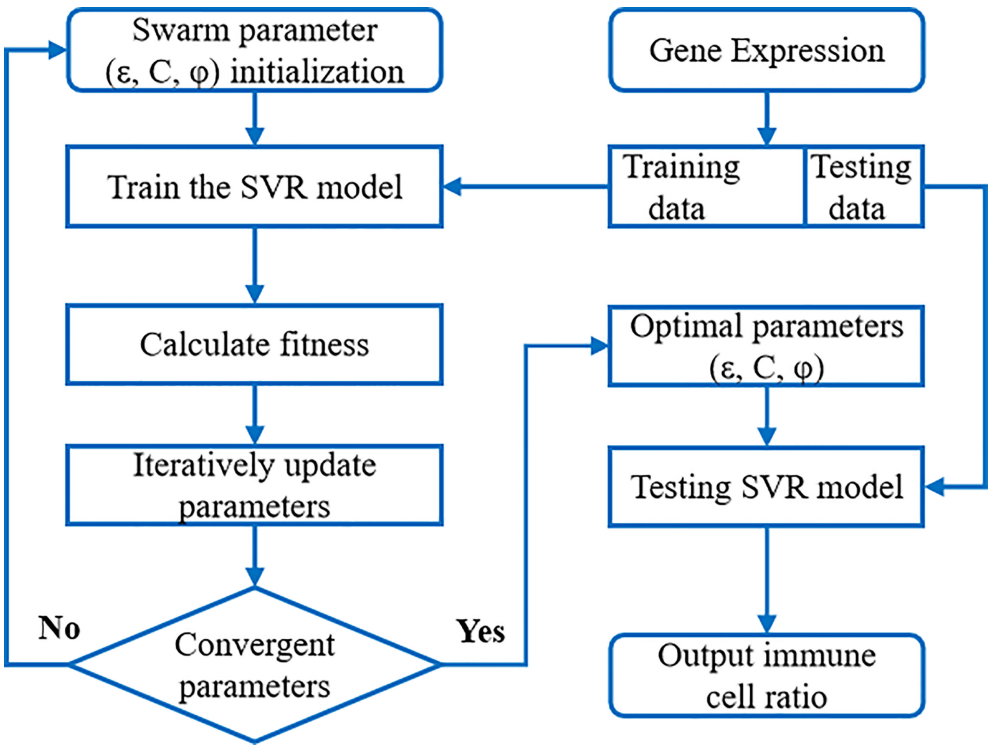

FIGURE 2 | The flow chart of PSO-SVR algorithm. SVR model was embedded into the PSO algorithm to calculate the optimal parameters; then SVR model with optimized parameters was applied to the immune cell ratios.

expression profile data combined with *a priori* knowledge of purified leukocyte subpopulation expression profile data (i.e., a "signature matrix" representing the expression profile data of each gene in different immune cells), the proportion of immune cells in tumor biopsies can be accurately estimated. The idea was first used in CIBERSORT. The gene expression profile data were first transformed into a linear combination of marker genes for immune cells to solve for f (representing the proportion of immune cells) in a linear combination equation. The linear combination equation was expressed as:

$$X_{n\times L} = S_{n\times m} \times f_{m\times L}$$

Where $X_{n\times L}$ denotes the expression profile data of n genes from L samples for deconvolution. $f_{m\times L}$ is the proportion of immune cells to be sought, specifically indicating the proportion of each immune cell in L samples among the m immune cell types. $S_{n\times m}$ is the signature matrix, indicating the expression profile data of n genes in each immune cell for m immune cells. The SVR algorithm solves the linear combinatorial equation using a deconvolution scheme.

The accuracy of the immune cell ratio calculated through the above SVR model is influenced by the model parameters such as the penalty factor C, sensitivity ϵ, and kernel function coefficient ϕ. These parameters are crucial to an SVR model's accuracy and generalizability. However, in practice, these parameters are largely manually chosen without justification. Here we propose to optimize (ϵ, C, ϕ) parameters through iterations using the particle swarm algorithm. In each iteration, the swarming particles update their velocity and position vectors by tracking two "optimal values" (p_{ibest}, g_{best}), where p_{ibest} denotes the individual optimal value of the particle and g_{best} is the global optimal value. In the computation, the expression data of each gene (i.e., each row vector in the $X_{n\times L}$ matrix) was treated as a particle in the swarming iteration.

$$v_{i+1} = qv_i + c_1r_1(p_{ibest} - x_i) + c_2r_2(g_{best} - x_i)$$

$$x_{i+1} = x_i + v_{i+1}$$

Where v_i and x_i represent the velocity vector and position vector of the i^{th} particle respectively, each gene is regarded as a particle respectively, and n represents the size of the population, specifically the number of genes; q is a non-negative inertia factor. The larger the value of q is, the stronger the global optimization ability is and the weaker the local optimization ability is; c_1 and c_2 are learning factors, general $c_1 = c_1 = 2$; r_1 and r_1 both represent random coefficients belonging to [0,1]; p_{ibest} represents the individual optimal value of the ith particle, and g_{best} is the global optimal value. We provide more detailed parameter explanation and algorithm flow in the **Supplementary Materials**. **Table 1** provides an explanation of key parameters.

We apply this iterative optimization process of particle swarm to solve the SVR model, so that its optimal input parameters are

TABLE 1 | PSO-SVR model parameter.

Parameter	Meaning	Reference range	Value
k(x,y)	kernel function	linear	k (x,y)=x·y
C	Penalty factor	[1,108]	3
ϵ	sensitivity	[0,0.2]	1.203564×10^{-5}
Φ	Kernel function coefficient	[0.01,2.0]	0.04545455

optimized according to the swarm fitness metric. Upon initialization, we specify the approximate ranges of the parameters ϵ, C, and ϕ as: ϵ = (0, 0.2), C = (1, 100), ϕ = (0.01, 2.0), and q_{max} and q_{min} values are 0.9 and 0.4 for the model. Upon convergence, we find the optimal parameter solution (ϵ, C, ϕ). SVR models using optimal parameters are validated using benchmark data sets. We apply model with these parameters to the expression data of liver cancer patients' tissues to solve for immune cell infiltration ratios.

The major innovation of PSO-SVR over previous SVR deconvolution methods is that it applies the machine learning technique – particle swarm algorithm, to do SVR iterative optimization. In the process, the swarming algorithm searches for SVR hyperplane formed by support vectors that capture as many data points as possible while satisfying the given constraints and avoiding overfitting, using a linear "ω-insensitive" loss function. The function penalizes only those data points outside a specific error radius. The support vectors were selected from the signature matrix of genes, and the standard reference expression profile (signature matrix) was selected from a composition of 22 immune cells including CD4 T, and CD8 T immune cells in CIBERSORTX, but other signature gene sets can be applied as well.

Benchmark of the PSO-SVR Algorithm

We gathered three data sets (see **Supplementary Table 1**), in which the immune cell proportions were determined through orthogonal flow cytometry (PBMC-FC), immunohistochemistry (CRC-IC), and single-cell RNA sequencing technologies (Melanoma-scRNA). Flow cytometry was an established technology to identify and determine different cell types in heterogeneous cell populations (36). immunohistochemistry is also well-established, using chemical reaction to label antibodies and to identify and quantify antigens within tissue cells. The genetic heterogeneity of cells of the same tissue can be also analyzed by scRNA-Seq at the level of individual cells to cluster and compute the composition immune cells (37). In order to verify the accuracy of PSO-SVR algorithm, we used data sets based on these technologies as the orthogonal control, and studied the deviation between PSO-SVR results and the control.

As shown in **Figure 3A**, for the PBMC-FC data, that the PSO-SVR estimated B cell, CD4 T cells, CD8 T cells and Monocytes levels were very close to the flow cytometry results. Overall, the four types of immune cells present a good correlation. The CD8 T cells showed relatively less consistency as compared to the other two types, maybe because CD8 T cells accounted for a relatively small number of T lymphocytes in PBMC (5%–20%) thus is subject to less accurate estimation. As shown in **Figure 3B**, the PSO-SVR estimates of B cells, monocytes, NK cells, and T cells were also in good concordance with the immunohistochemistry results. As shown in **Figure 3C**, PSO-SVR estimated immune cell fractions, such as CD4 T and CD8 T cells, also showed a good correlation with the scRNA-seq levels.

To further evaluate the PSO-SVR estimates using the PBMC-FC, CRC-IC and Melanoma-scRNA data sets, we used three metrics, namely root mean square error (RMSE), Pearson correlation coefficient, and Spearman's correlation coefficient. The individual indicators are shown in **Table 2**.

We observe in **Table 2** that the error was generally larger for B cells and that both Pearson and Spearman's correlation coefficients were relatively low. For CD4 T and CD8 T cells, the difference between the results presented in the PBMC-FC and Melanoma-scRNA is very small, and the RMSE and correlation coefficients for both are close, proving the reliability of the algorithm in this study.

Finally, the results calculated through PSO-SVR were compared with other algorithms such as CIBERSORTX, EPIC, MCP-counter, for calculating the proportion of immune cells in infiltrating tumors. From the results of PBMC-FC and Melanoma-scRNA (refer to **Supplementary Tables 2** and **5**), it can be observed that PSO-SVR outperforms CIBERSORTX, EPIC, MCP-counter, in terms of the three indicators, RMSE, Pearson, and Spearman correlation coefficients. However, the results of CRC-IC (refer to **Supplementary Table 3**) are not as good as the other three methods, which could be attributed to the small amount of CRC-IC data. Overall, our algorithm was highly accurate.

Joint Microbial- and Immune-Effect Analysis of Hepatocellular Carcinoma Samples

Differential Presence of Infiltrating Immune Cells Between Tumor and Normal Tissues

We analyzed the differences in the relative proportions of immune cells in tumor samples and normal solid tissue samples. The non-parametric Mann-Whitney-Wilcoxon test was conducted in R software and then corrected for p-values with the Benjamini-Hochberg correction (FDR). Immune cells with significant differences were identified as shown in **Supplementary Table 5** (FDR < 0.05).

As it can be seen in **Figure 4** and **Supplementary Table 6**, the relative proportions of regulatory T cells [confidence level=95%, FDR= 1.58E-07] and 59.87% significantly higher in tumor tissues, and the relative proportions of Monocytes and Neutrophils are 150.07% and 363.69% significantly lower [FDR= 6.77E-07, 1.37E-05], as compared to normal solid tissue samples. These results suggested that regulatory T cells, Monocytes

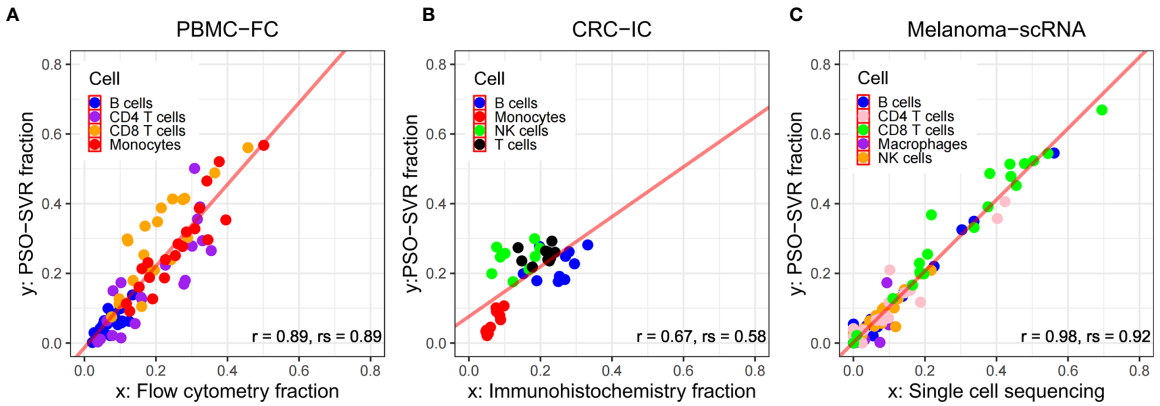

FIGURE 3 | Comparison between PSO-SVR and orthogonal technologies. Scatter plots of immune cell fractions with regression of **(A)** PBMC-FC; **(B)** CRC-IC; and **(C)** Melanoma-scRNA data; r for Pearson's correlation, rs for Spearman's correlation.

and Neutrophils were attracted toward tumor tissues who may act as host defense against invasive tumor growth. These findings were consistent with external knowledge and evidence.

As known, neutrophils provide the first line of defense for the innate immune system by phagocytosing, killing, and digesting bacteria and fungi (38). CD8 T cells are an important component of the immune system, and inducing an effective memory T cell response is a major target for vaccines against chronic infections and tumors (39). Studies have shown that the presence of Tregs in tumors of patients with hepatocellular carcinoma are suppressor cells and their increased levels are associated with immunosuppression and evasion in patients with cancer, where the inappropriate immune responses can be prevented by suppressing immune effector cells. In addition, the frequency of Tregs in lymphoid tissue, peripheral blood, and in the TME is greater than that in normal tissue (40).

Differential Presence of Infiltrating Bacteria Between Tumor and Normal Tissues

In **Table 3** and **Figure 5A**, we showed the most significant differentially present bacteria between tumor and normal tissues. These include *Caldatribacterium* sp. [↑74.94%, FDR=3.15×10^{-11}], *Acidaminococcaceae* sp. [↑73.58%, FDR=1.79×10^{-9}], among others. We used the nonparametric Mann-Whitney U test. The p-values were corrected for multiple testing through FDR.

Noticeably, *Caldatribacterium* sp., *Acidaminococcaceae* sp. (amino acid cocci), and *Planctopirus* sp. are significantly more abundant in infiltrating tumor tissues as compared to normal tissues and are likely associated with the pathological development of hepatocellular carcinoma.

These results were substantiated by external molecular biology and clinical evidence from previous studies. For examples it was found that the increase in *Caldatribacterium* sp. leads to DNA damage in hepatic stellate cells, which then promotes the development of hepatocellular carcinoma through metabolites or toxins from intestinal bacteria (41). Studies also showed the presence of *Planctopirus* sp. bacterial infection in serum and tissues derived from patients with chronic liver disease – a common presage of hepatocellular carcinoma; the enrichment of *Planctopirus* sp. bacteria in the serum of patients with chronic liver disease is significantly higher than that of healthy individuals, suggesting that it may be associated with the

TABLE 2 | Immune cell error table of three data sets.

	Cell type	Root mean square error (RMSE)	Pearson (r)	Spearman (rs)
PBMC-FC	B cells	0.028763	0.69534	0.67669
	Monocytes	0.056215	0.92192	0.93684
	CD4 T cells	0.073478	0.84827	0.88270
	CD8T cells	0.110915	0.84207	0.82105
CRC-IC	B cells	0.057609	0.39181	0.51515
	Monocytes	0.018876	0.87587	0.78181
	NK cells	0.116719	0.23098	0.30909
	T cells	0.060646	0.18626	0.16363
Melanoma-scRNA	B cells	0.019590	0.99128	0.85381
	Macrophages	0.028086	0.70316	0.67192
	NK cells	0.021296	0.92560	0.86315
	CD4 T cells	0.034945	0.95508	0.92847
	CD8 T cells	0.050518	0.97476	0.97543

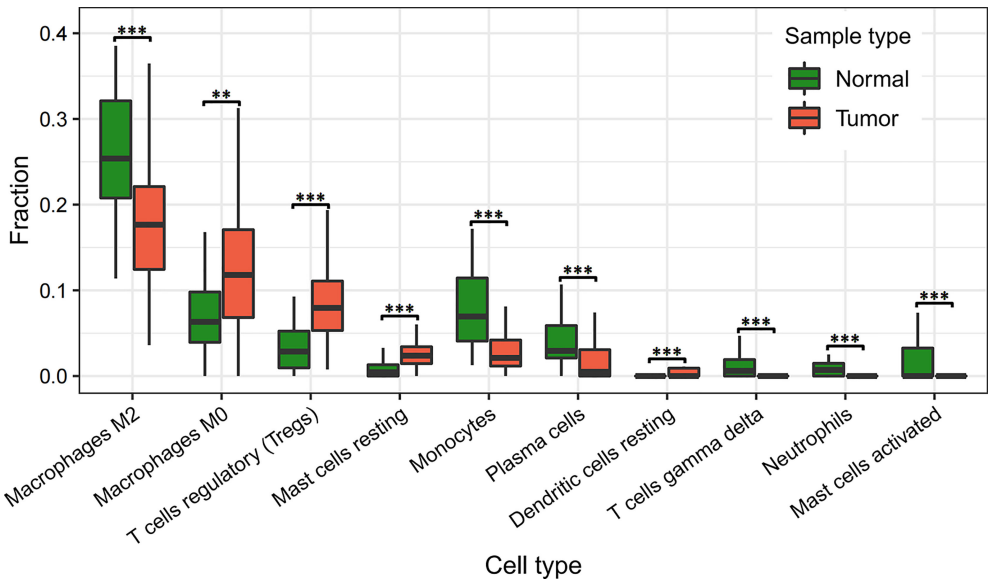

FIGURE 4 | Differetial analysis of immune cell infiltration in normal and tumor tissues. "***" indicates FDR < 0.01; "****" indicates FDR < 0.001.

development of chronic hepatitis B and primary liver cancer (42). The other bacteria identified in our study were also supported in the literature, where multiple species including *Gemmiger formicilis*, *Marithrix* sp., and *Haemophilus* sp. were found to be over-represented in in gut microbiome in patients with HCC (43).

We also found that the microbial diversity (Shannon Index) in the primary tumor tissue is significantly higher than that in normal tissue samples (see **Figure 5B**). This is somewhat contrary to the discoveries of higher gut microbiome diversity associated with healthy controls as known in many other related cancers (44).

Joint Effects of Infiltrating Immune Cells and Bacteria On Hepatocellular Carcinoma

In order to further analyze the impact of tumor infiltrating immune cells and bacteria on the occurrence and development of liver cancer, we used the downloaded gene expression data and transcriptome data of 98 liver cancer samples, and calculated the corresponding bacterial abundance data by using the estimation method of microbial relative abundance in this paper. The PSO-SVR algorithm described in Section 3.1 was used to calculate the relative proportion of immune cells in liver cancer samples.

Then the logistic regression classification method was applied to three cases: case 1, only bacterial abundance data were used as the input feature; In case 2, only the immune cell proportion data were used as the input feature; and in case 3, both bacterial abundance and immune cell ratio were used as input characteristics. From the classification results of the three cases (see **Table 4**), the classification accuracy of using only a single input feature is lower - only bacteria: 0.70, only immune cell feature: 0.74, and both features: 0.84. No matter which data feature is added, the classification accuracy can be improved. After adding the immune cell proportion data, the classification accuracy is improved by 20% compared with case 1; After adding bacterial abundance data, the accuracy of classifier is improved by 13.51% compared with case 2. This shows that the bacteria and infiltrating immune cells in liver cancer tissue contain key characteristics for cancer diagnosis, which can be used as a reference index for clinical cancer diagnosis.

TABLE 3 | Bacteria with significant variability between normal and primary tumor tissues.

Species	FDR	Difference %	State (↑↓)
Caldatribacterium sp.	3.15×10^{-11}	74.94%	↑
Acidaminococcaceae sp.	1.79×10^{-9}	73.58%	↑
Planctopirus sp.	2.50×10^{-9}	73.66%	↑
Desulfobulbaceae sp.	2.50×10^{-9}	71.10%	↑
Nocardia farcinica	8.02×10^{-9}	71.20%	↑

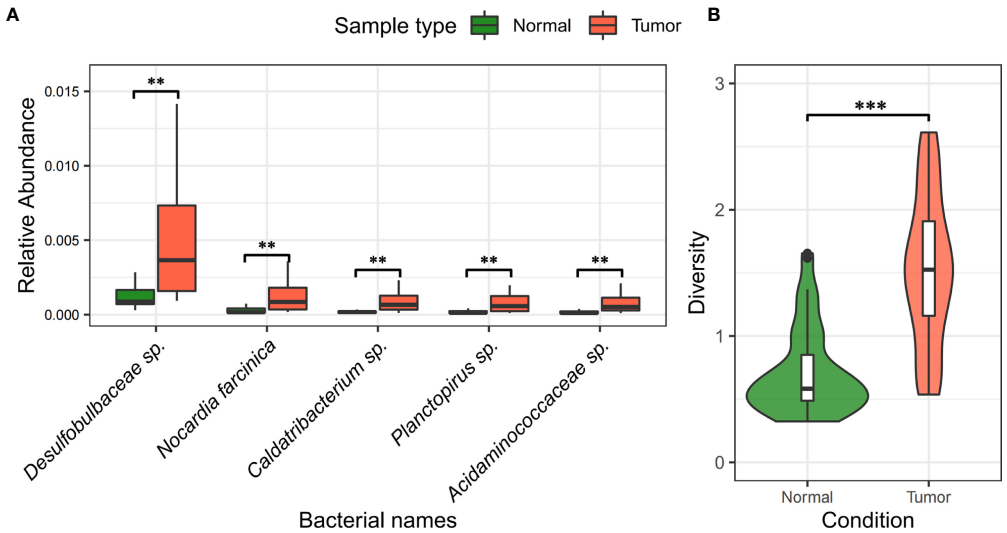

FIGURE 5 | Difference and diversity of bacteria in liver cancer samples. **(A)** Differentiation of bacteria between liver tumor tissue and normal tissue. "**" indicates FDR < 0.05; "****" indicates FDR < 0.001. **(B)** Analysis of alpha diversity of bacteria in tumor and normal tissues. The green color on the left indicates normal samples, the red part on the right indicates tumor samples, and the middle BASE part indicates the interquartile range.

CONCLUSIONS

We performed a joint analysis of microbial and immune cell abundance in liver cancer tissue using a gene expression profile deconvolution algorithm combined with foreign read remapping. First, we filtered out reads from the RNA-Seq data that did not map to the human reference genome. Second, we assembled the single-ended unmapped reads with a reverse complementary sequence to the double-ended unmapped reads, and the processed reads were then mapped to the microbial reference library. Finally, the GRAMMy algorithm was introduced to calculate the relative abundance of microorganisms. This algorithm overcomes the problem of mapping one read to different microbial reference sequences owing to small reads and enables a more accurate calculation of relative abundance.

This complete procedure was then applied to RNA-seq samples of 98 patients with hepatocellular carcinoma, and we found that microorganisms including *Caldatribacterium* sp. and *Planctopirus* sp. differed significantly between normal and tumor tissues, which was also reported in the literature.

To study the degree of immune cell response to microorganisms and the effect on liver cancer in the human microenvironment, we introduced SVR and particle swarm algorithm to estimate the relative proportion of infiltrating immune cells based on the deconvolution model. The results of our study were validated by actual data and then compared with some immune cell counting algorithms, such as CIBESORTX, EPIC, and MCP-counter, and were found to be relatively more reliable.

The PSO-SVR algorithm was applied to the gene expression profile data of liver cancer samples. The differential analysis revealed significant differences in regulatory T cells, monocytes, and neutrophils between normal and tumor tissues. Finally, using the classification regression algorithm within machine learning, we found that adding microbial characteristics can improve the accuracy of liver cancer prediction.

This study has some limitations that result from the limited sample size. For example, a small number of samples affects statistical power, which we anticipate correcting in further studies. Also, liver cancer has different cancer subtypes, which are not subdivided in this study; The model does not take gene variation into account; otherwise, there can be new information to improve the accuracy.

TABLE 4 | Classification effect of liver cancer samples under different input features.

	Case1: Bacteria	Case2: Immune cell	Case3: Bacteria-Cell
CIBERSORT	0.68	0.64	0.80
	0.75	0.71	0.88
	0.67	0.67	0.88
Average accuracy	0.70	0.67	0.85
PSO-SVR	0.68	0.76	0.80
	0.75	0.79	0.75
	0.67	0.67	0.96
Average accuracy	0.70	0.74	0.84

DATA AVAILABILITY STATEMENT

Publicly available datasets were analyzed in this study. This data can be found here: https://portal.gdc.cancer.gov/repository and http://www.cancergenomicscloud.org/.

AUTHOR CONTRIBUTIONS

DA, LCX and YX conceived and designed the study. YX and GL performed the analyses and summarized the data. LCX and DA supervised the study. DA, YX and LCX wrote the manuscript with inputs from GL, XL, and YW. All authors have read and agreed to the published version of the manuscript.

FUNDING

This work was supported by grants from the National Natural Science Foundation of China (61873027), open project of the National Engineering Laboratory for Agri-product Quality Traceability (No.AQT-2020-YB6), and GuangDong Basic and Applied Basic Research Foundation (2022A1515-011426).

SUPPLEMENTARY MATERIAL

The Supplementary Material for this article can be found online at: https://www.frontiersin.org/articles/10.3389/fimmu.2022.853213/full#supplementary-material.

REFERENCES

1. O'Hara AM, Shanahan F. The Gut Flora as a Forgotten Organ. *EMBO Rep* (2006) 7(7):688–93. doi: 10.1038/sj.embor.7400731
2. Elinav E, Nowarski R, Thaiss CA, Hu B, Jin C, Flavell RA. Inflammation-Induced Cancer: Crosstalk Between Tumours, Immune Cells and Microorganisms. *Nat Rev Cancer* (2013) 13(11):759–71. doi: 10.1038/nrc3611
3. Arleevskaya MI, Aminov R, Brooks WH, Manukyan G, Renaudineau Y. Editorial: Shaping of Human Immune System and Metabolic Processes by Viruses and Microorganisms. *Front Microbiol* (2019) 10:816. doi: 10.3389/fmicb.2019.00816
4. An Y, Zhang W, Liu T, Wang B, Cao H. The Intratumoural Microbiota in Cancer: New Insights From Inside. *Biochim Biophys Acta Rev Cancer* (2021) 1876(2):188626. doi: 10.1016/j.bbcan.2021.188626
5. Mizutani T, Mitsuoka T. Inhibitory Effect of Some Intestinal Bacteria on Liver Tumorigenesis in Gnotobiotic C3H/He Male Mice. *Cancer Lett* (1980) 11 (2):89–95. doi: 10.1016/0304-3835(80)90098-1
6. Moffatt CE, Lamont RJ. Porphyromonas Gingivalis Induction of MicroRNA-203 Expression Controls Suppressor of Cytokine Signaling 3 in Gingival Epithelial Cells. *Infect Immun* (2011) 79(7):2632–7. doi: 10.1128/Iai.00082-11
7. Garner RC, Wright CM. Induction of Mutations in DNA-Repair Deficient Bacteria by a Liver Microsomal Metabolite of Aflatoxin B1. *Br J Cancer* (1973) 28(6):544–51. doi: 10.1038/bjc.1973.184
8. Mangul S, Yang HT, Strauli N, Gruhl F, Porath HT, Hsieh K, et al. ROP: Dumpster Diving in RNA-Sequencing to Find the Source of 1 Trillion Reads Across Diverse Adult Human Tissues. *Genome Biol* (2018) 19(1):36. doi: 10.1186/s13059-018-1403-7
9. Zheng-Bradley X, Streeter I, Fairley S, Richardson D, Clarke L, Flicek P, et al. Alignment of 1000 Genomes Project Reads to Reference Assembly Grch38. *Gigascience* (2017) 6(7):1–8. doi: 10.1093/gigascience/gix038
10. Xia LC, Cram JA, Chen T, Fuhrman JA, Sun FZ. Accurate Genome Relative Abundance Estimation Based on Shotgun Metagenomic Reads. *PloS One* (2011) 6(12):e27992. doi: 10.1371/journal.pone.0027992
11. Karlmark KR, Wasmuth HE, Trautwein C, Tacke F. Chemokine-Directed Immune Cell Infiltration in Acute and Chronic Liver Disease. *Expert Rev Gastroenterol Hepatol* (2008) 2(2):233–42. doi: 10.1586/17474124.2.2.233
12. Hegde P, Weiss E, Paradis V, Wan J, Mabire M, Sukriti S, et al. Mucosal-Associated Invariant T Cells are a Profibrogenic Immune Cell Population in the Liver. *Nat Commun* (2018) 9(1):2146. doi: 10.1038/s41467-018-04450-y
13. Xue F, Zhang J, Han L, Li Q, Xu N, Zhou T, et al. Immune Cell Functional Assay in Monitoring of Adult Liver Transplantation Recipients With Infection. *Transplantation* (2010) 89(5):620–6. doi: 10.1097/tp.0b013e3181c690fa
14. Zhou T, Xue F, Han LZ, Xi ZF, Li QG, Xu N, et al. Invasive Fungal Infection After Liver Transplantation: Risk Factors and Significance of Immune Cell Function Monitoring. *J Dig Dis* (2011) 12(6):467–75. doi: 10.1111/j.1751-2980.2011.00542.x
15. Newman AM, Liu CL, Green MR, Gentles AJ, Feng WG, Xu Y, et al. Robust Enumeration of Cell Subsets From Tissue Expression Profiles. *Nat Methods* (2015) 12(5):453–7. doi: 10.1038/Nmeth.3337
16. Li B, Severson E, Pignon JC, Zhao HQ, Li TW, Novak J, et al. Comprehensive Analyses of Tumor Immunity: Implications for Cancer Immunotherapy. *Genome Biol* (2016) 17(1):174. doi: 10.1186/s13059-016-1028-7
17. Becht E, Giraldo NA, Lacroix L, Buttard B, Elarouci N, Petitprez F, et al. Estimating the Population Abundance of Tissue-Infiltrating Immune and Stromal Cell Populations Using Gene Expression. *Genome Biol* (2016) 17 (1):218. doi: 10.1186/s13059-016-1070-5
18. Racle J, de Jonge K, Baumgaertner P, Speiser DE, Gfeller D. Simultaneous Enumeration of Cancer and Immune Cell Types From Bulk Tumor Gene Expression Data. *Elife* (2017) 6:e26476. doi: 10.7554/eLife.26476
19. Deng M, Matsumoto N, Kitayama M, Inoue A. Online Estimation of Arriving Time for Robot to Soccer Ball in RoboCup Soccer Using PSO-SVR. In: Proceedings of the 2014 International Conference on Advanced Mechatronic Systems. (Institute of Electrical & Electronics Engineers) (2014). p. 543–6. doi: 10.1109/ICAMechS.2014.6911605
20. Fujita K, Deng M, Wakimoto S. A Miniature Pneumatic Bending Rubber Actuator Controlled by Using the PSO-SVR-Based Motion Estimation Method With the Generalized Gaussian Kernel. *Actuators* (2017) 6:6. doi: 10.3390/act6010006
21. Mohammadi S, Zuckerman N, Goldsmith A, Grama A. A Critical Survey of Deconvolution Methods for Separating Cell Types in Complex Tissues. *Proc IEEE* (2017) 105(2):340–66. doi: 10.1109/Jproc.2016.2607121
22. Newman AM, Steen CB, Liu CL, Gentles AJ, Chaudhuri AA, Scherer F, et al. Determining Cell Type Abundance and Expression From Bulk Tissues With Digital Cytometry. *Nat Biotechnol* (2019) 37(7):773–82. doi: 10.1038/s41587-019-0114-2
23. Gibney GT, Weiner LM, Atkins MB. Predictive Biomarkers for Checkpoint Inhibitor-Based Immunotherapy. *Lancet Oncol* (2016) 17(12):E542–51. doi: 10.1016/S1470-2045(16)30406-5
24. Hogan SA, Levesque MP, Cheng PF. Melanoma Immunotherapy: Next-Generation Biomarkers. *Front Oncol* (2018) 8:178. doi: 10.3389/fonc.2018.00178
25. Gopalakrishnan V, Spencer CN, Nezi L, Reuben A, Andrews MC, Karpinets TV, et al. Gut Microbiome Modulates Response to Anti-PD-1 Immunotherapy in Melanoma Patients. *Science* (2018) 359(6371):97–103. doi: 10.1126/science.aan4236
26. Matson V, Fessler J, Bao R, Chongsuwat T, Zha Y, Alegre ML, et al. The Commensal Microbiome Is Associated With Anti-PD-1 Efficacy in Metastatic Melanoma Patients. *Science* (2018) 359(6371):104–8. doi: 10.1126/science.aao3290
27. Li H, Handsaker B, Wysoker A, Fennell T, Ruan J, Homer N, et al. The Sequence Alignment/Map Format and SAMtools. *Bioinformatics* (2009) 25 (16):2078–9. doi: 10.1093/bioinformatics/btp352
28. Peter JA, Cock CJF, Naohisa G, Heuer ML, Rice PM. The Sanger FASTQ File Format for Sequences With Quality Scores, and the Solexa/Illumina FASTQ Variants. *Nucleic Acids Res* (2010) 38(6):1767–71. doi: 10.1093/nar/gkp1137
29. Yingjun YDG. Next Generation Sequencing in Quality Control and Analysis of Data. *Lab Med* (2017) 32(4):255–61. doi: 10.3969/j.issn.1673-8640.2017.04.003
30. Zhang C, Cleveland K, Schnoll-Sussman F, McClure B, Bigg M, Thakkar P, et al. Identification of Low Abundance Microbiome in Clinical Samples Using

Whole Genome Sequencing. *Genome Biol* (2015) 16:265. doi: 10.1186/s13059-015-0821-z
31. Chen SF, Zhou YQ, Chen YR, Gu J. Fastp: An Ultra-Fast All-in-One FASTQ Preprocessor. *Bioinformatics* (2018) 34(17):884–90. doi: 10.1093/bioinformatics/bty560
32. Tafesse FG, Huitema K, Hermansson M, van der Poel S, van den Dikkenberg J, Uphoff A, et al. Both Sphingomyelin Synthases SMS1 and SMS2 are Required for Sphingomyelin Homeostasis and Growth in Human HeLa Cells. *J Biol Chem* (2007) 282(24):17537–47. doi: 10.1074/jbc.M702423200
33. Pearson WR. Rapid and Sensitive Sequence Comparison With FASTP and FASTA. *Methods Enzymol* (1990) 183:63–98. doi: 10.1016/0076-6879(90)83007-v
34. Shen W, Le S, Li Y, Hu FQ. SeqKit: A Cross-Platform and Ultrafast Toolkit for FASTA/Q File Manipulation. *PloS One* (2016) 11(10):e0163962. doi: 10.1371/journal.pone.0163962
35. Li H, Durbin R. Fast and Accurate Short Read Alignment With Burrows-Wheeler Transform. *Bioinformatics* (2009) 25(14):1754–60. doi: 10.1093/bioinformatics/btp324
36. Al-Rubeai M, Emery AN. Flow Cytometry in Animal Cell Culture. *Bio/technology* (1993) 11(5):572–9. doi: 10.1038/nbt0593-572
37. Navin N, Kendall J, Troge J, Andrews P, Rodgers L, McIndoo J, et al. Tumour Evolution Inferred by Single-Cell Sequencing. *Nature* (2011) 472(7341):90–U119. doi: 10.1038/nature09807
38. Segal AW. How Neutrophils Kill Microbes. *Annu Rev Immunol* (2005) 23:197–223. doi: 10.1146/annurev.immunol.23.021704.115653
39. Araki K, Turner AP, Shaffer VO, Gangappa S, Keller SA, Bachmann MF, et al. mTOR Regulates Memory CD8 T-Cell Differentiation. *Nature* (2009) 460(7251):108–U124. doi: 10.1038/nature08155
40. Johdi NA, Ait-Tahar K, Sagap I, Jamal R. Molecular Signatures of Human Regulatory T Cells in Colorectal Cancer and Polyps. *Front Immunol* (2017) 8:620. doi: 10.3389/fimmu.2017.00620
41. Dodsworth JA, Blainey PC, Murugapiran SK, Swingley WD, Ross CA, Tringe SG, et al. Single-Cell and Metagenomic Analyses Indicate a Fermentative and Saccharolytic Lifestyle for Members of the OP9 Lineage. *Nat Commun* (2013) 4:1854. doi: 10.1038/ncomms2884
42. Kohn T, Wiegand S, Boedeker C, Rast P, Heuer A, Jetten MSM, et al. Planctopirus Ephydatiae, a Novel Planctomycete Isolated From a Freshwater Sponge. *Syst Appl Microbiol* (2020) 43(1):126022. doi: 10.1016/j.syapm.2019.126022
43. Ren ZG, Li A, Jiang JW, Zhou L, Yu ZJ, Lu HF, et al. Gut Microbiome Analysis as a Tool Towards Targeted Non-Invasive Biomarkers for Early Hepatocellular Carcinoma. *Gut* (2019) 68(6):1014–23. doi: 10.1136/gutjnl-2017-315084
44. Yelena L, Amnon A, Rita N, Atara U-Y, Ella V, Oranit C-E, et al. Alterations in the Gut Microbiome in the Progression of Cirrhosis to Hepatocellular Carcinoma. *mSystems* (2020) 5(3):e00153–20. doi: 10.1128/mSystems.00153-20

Conflict of Interest: The authors declare that the research was conducted in the absence of any commercial or financial relationships that could be construed as a potential conflict of interest.

frontiers | Frontiers in Immunology

ORIGINAL RESEARCH
published: 09 June 2022
doi: 10.3389/fimmu.2022.868809

Hepatic Tumor Stiffness Measured by Shear Wave Elastography Is Prognostic for HCC Progression Following Treatment With Anti-PD-1 Antibodies Plus Lenvatinib: A Retrospective Analysis of Two Independent Cohorts

Guosheng Yuan[1†], Fuli Xie[2†], Yangda Song[1†], Qi Li[1†], Rong Li[1], Xiaoyun Hu[1], Mengya Zang[1], Xiao Cheng[3], Guanting Lu[3], Jing Huang[3], Wenzhe Fan[4], Xiaoxiang Rong[2*], Jian Sun[1*] and Jinzhang Chen[1*]*

[1] Department of Infectious Diseases and Hepatology, Nanfang Hospital, Southern Medical University, Guangzhou, China, [2] Department of Oncology, Nanfang Hospital, Southern Medical University, Guangzhou, China, [3] Department of Hepatology, Zengcheng Branch, Nanfang Hospital, Southern Medical University, Guangzhou, China, [4] Department of Interventional Oncology, The First Affiliated Hospital of Sun Yat-Sen University, Guangzhou, China

Background: The clinical significance of liver stiffness (LS) measured by shear wave elastography (SWE) in programmed cell death protein-1 (PD-1) inhibitors treated advanced hepatocellular carcinoma (HCC) patients remains unknown. This study aimed to explore the prognostic value of baseline LS by SWE prior to PD-1 inhibitor treatment in combination with lenvatinib.

Methods: We retrospectively evaluated patients (n=133) with HCC who received anti-PD-1 antibodies plus lenvatinib at two high-volume medical centres, between January 2020 and June 2021. Univariate and multivariate logistic regression analysis were used to develop a novel nomogram. RNA sequencing and immunohistochemical staining were used to assess the heterogeneity of biological and immune characteristics associated with tumor stiffness.

Results: The objective response rate (ORR) and disease control rate (DCR) of the whole population were 23.4% and 72.2%, respectively. A LS value of the baseline tumorous foci of 19.53 kPa had the maximum sum of sensitivity and specificity, making it the optimal cut-off value for predicting PD-1 inhibitor efficacy. The nomogram comprised baseline tumor LS and albumin-bilirubin grade (ALBI), which provided favorable calibration and discrimination in the training dataset with an AUC of 0.840 (95%CI: 0.750-0.931) and a C-index of 0.828. Further, it showed acceptable discrimination in the validation cohort, with an AUC of 0.827 (95%CI: 0.673-0.980) and C-index of 0.803. The differentially expressed genes enriched in high stiffness tumors were predominantly associated with

OPEN ACCESS

Edited by:
Xuesong Gu,
Beth Israel Deaconess Medical Center and Harvard Medical School, United States

Reviewed by:
Shao-wei Li,
Taizhou Hospital of Zhejiang Province Affiliated to Wenzhou Medical University, China
Jian Ruan,
Zhejiang University, China
Tian Yang,
Eastern Hepatobiliary Surgery Hospital, China
Guoying Wang,
Third Affiliated Hospital of Sun Yat-sen University, China

***Correspondence:**
Wenzhe Fan
fanwz2007@126.com
Xiaoxiang Rong
rxiaoxiang@126.com
Jian Sun
doctorsunjian@qq.com
Jinzhang Chen
chenjinzhang@smu.edu.cn

[†]These authors have contributed equally to this work

Specialty section:
This article was submitted to Cancer Immunity and Immunotherapy, a section of the journal Frontiers in Immunology

Received: *03 February 2022*
Accepted: *03 May 2022*
Published: *09 June 2022*

metabolic pathways, while those enriched in low stiffness tumors were related to DNA damage repair. Furthermore, patients with high stiffness tumors had a relatively lower infiltration of immune cells and histone deacetylase pathway inhibitors were identified as candidate drugs to promote the efficacy of immunotherapy.

Conclusions: Baseline LS value of tumorous foci by SWE—that is, before administration of a PD-1 inhibitor in combination with lenvatinib—is a convenient predictor of PD-1 inhibitor efficacy in patients with advanced HCC, which has potential to be used for pretreatment stratification to optimize treatment of advanced HCC.

Keywords: hepatocellular carcinoma, pd-1, lenvatinib, shear wave elastography, stiffness

HIGHLIGHTS

- Question: Is hepatic tumor stiffness measured by shear wave elastography (SWE) useful in predicting HCC progression following treatment with Anti-PD-1 antibodies plus Lenvatinib?
- Pertinent Findings: Baseline tumor LS by SWE, before anti-PD-1 in combination with lenvatinib, is a convenient predictor of tumor progression in patients with advanced HCC through a retrospective analysis of two independent cohorts.
- Implications for Patient Care: Our data shed light on the application of tumor LS in predicting HCC progression, which might guide the development of rational strategies for use of anti-PD-1 in combination antiangiogenic agents, ultimately benefiting a broader range of patients.

INTRODUCTION

Despite the introduction of new targeted therapies for advanced hepatocellular carcinoma (HCC) over the last few decades, the prognosis of patients with advanced HCC remains poor as these treatment strategies are not wholly effective (1–3). In recent years, inhibitors of the programmed cell death-1 (PD-1)/programmed cell death ligand-1 (PD-L1) pathway have received much attention as HCC immunotherapies (4–6). However, previous studies showed that fewer than 20% of advanced HCC patients achieved an objective tumor response in anti-PD-1 monotherapy, indicating that combination regimens—e.g., anti-PD-1 with an antiangiogenic therapy—might be better options for systemic treatment (7–9). Indeed, the Imbrave150 study has demonstrated a new combination regimen (atezolizumab plus bevacizumab, also known as "T+A" strategy) to be superior to sorafenib (a kinase inhibitor), showing a 42% reduction in risk of death, resulting in the "T+A" strategy to be the recommended first-line treatment for patients with advanced HCC globally (10). In addition, the RESCUE trial showed that combined camrelizumab with apatinib was also promising, with an objective response rate (ORR) of 34.3% and a disease control rate (DCR) of 77.1% in advanced HCC patients when used as a first-line treatment (11). Nevertheless, in the above studies, only a fraction of patients benefited from anti-PD-1/PD-L1 antibodies in combination with an antiangiogenic therapy. Therefore, it's urgently needed to identify factors that can predict a curative effect to define which patients with advanced HCC are most likely to benefit from therapy with anti-PD-1 antibodies in combination with antiangiogenic therapy.

More than 80% of HCC cases arise in the cirrhotic liver (12) and the degree of liver fibrosis has been reported to be a negative prognostic factor for sorafenib therapy (13). With recent advances in ultrasound technology, various elastography techniques have been found to be effective in staging liver fibrosis, among which shear wave elastography (SWE)—which uses the supersonic shear imaging technique—is capable of predicting overall survival in patients after radiofrequency ablation for HCC (14). In addition, previous studies reported that liver stiffness (LS) values measured by SWE achieved better sensitivity and specificity than those measured by transient elastography (TE), the aspartate aminotransferase (AST) to Platelet Ratio Index, or the Fibrosis 4 score in patients with chronic hepatitis B (15–17). However, the clinical implications of baseline LS values by SWE in patients with advanced HCC who are treated with anti-PD-1/PD-L1 or in those treated with anti-PD-1/PD-L1 in combination with an antiangiogenic regimen have not been explored.

Herein, we aimed to investigate the clinical significance of tumor-LS by SWE in anti-PD-1 antibodies in combination with lenvatinib treated HCC patients. We demonstrated that the tumor LS value, as measured by SWE before combination treatment with anti-PD-1 antibodies plus lenvatinib, was a convenient predictor of tumor progression in patients with advanced HCC. We further explored the heterogeneity of biological and immune characteristics associated with tumor stiffness in 9 HCC tissue samples across two groups having different tumor LS values (a high LS group and a low LS group), using RNA sequencing and immunohistochemical (IHC) staining. Our data shed light on the application of tumor LS for predicting HCC progression, which might guide the development of rational regimens using anti-PD-1 antibodies in combination with an antiangiogenic therapy, to ultimately benefit a greater range of patients.

MATERIALS AND METHODS

Patients

This retrospective study included patients with HCC who underwent SWE before anti-PD-1 antibodies in combination with lenvatinib therapy, starting from June 1, 2020 to May 31, 2021 at Nanfang Hospital, Southern Medical University, and from January 1, 2020 to June 30, 2021 at the First Affiliated Hospital of Sun Yat-Sen University. All patients were aged ≥18 years with HCC diagnosed either by two imaging modalities or by biopsy according to the diagnostic criteria (18). This study was designed and performed according to the Declaration of Helsinki and was approved by the Medical Ethics Committee of Nanfang hospital and the First Affiliated Hospital of Sun Yat-Sen University. Written informed consent was obtained from each patient to retrospectively review and report on their medical records.

Patients with the following characteristics were excluded: (1) those who accepted locoregional therapy before treatment or during follow-up; (2) those with Child-Pugh C liver function; (3) those who were coinfected with hepatitis A, C, or D virus or HIV; (4) women who were pregnant or breastfeeding; (5) those whose Eastern Cooperative Oncology Group performance status was over 3; and (6) those who were lost to follow-up other than death within 3 months after treatment.

Ultimately, 93 patients with complete data were included in the training set. Furthermore, the validation cohort of 40 patients (7:3), who satisfied the inclusion and exclusion criteria, was selected by a random extraction of HCC patients treated at the First Affiliated Hospital of Sun Yat-Sen University. A flowchart showing patient selection is depicted in **Figure 1**.

LS Measurements Using SWE

LS values were measured in both tumorous foci and adjacent normal liver regions before the first dose of a PD-1 inhibitor using the ARFI imaging technology implemented on a Siemens Acuson S2000 ultrasound system (Siemens AG, Erlangen, Germany) at Nanfang hospital and on Aixplorer (SuperSonic Imagine, France) at the First Affiliated Hospital of Sun Yat-Sen University. Tumorous foci in the participants were previously identified as HCC by two imaging modalities or by biopsy, while the adjacent normal liver tissues were selected by the operator's preference. The physician who performed SWE had 17 years of experience. The SWE protocol was performed according to the European Federation of Societies for Ultrasound in Medicine and Biology and World Congress for Ultrasound in Medicine and Biology guidelines (19, 20). Results expressed in m/s from the virtual tissue quantification were converted to the Young's modulus and expressed in kiloPascals (kPa). LS measurements were considered reliable if they achieved an interquartile range interval/median ratio (IQR/M) of ≤0.3.

Treatment and Assessment

The dosage of anti-PD-1 therapy has been described in our previous studies (7, 21, 22); briefly, one of the following regimens was selected for each patient: toripalimab, 3 mg/kg body weight or 240 mg, once every 2 weeks by IV; camrelizumab, 200 mg, q2/3w, IV; or sintilimab, 200 mg, q3w, IV. The dosage of the antiangiogenic therapy lenvatinib was 8 mg once per day orally.

Demographic, clinical, and laboratory data were collected from all patients prior to initiating PD-1 inhibitor therapy. Data included the patient's age, gender, α-fetoprotein, alanine aminotransferase, aspartate transaminase, prothrombin time,

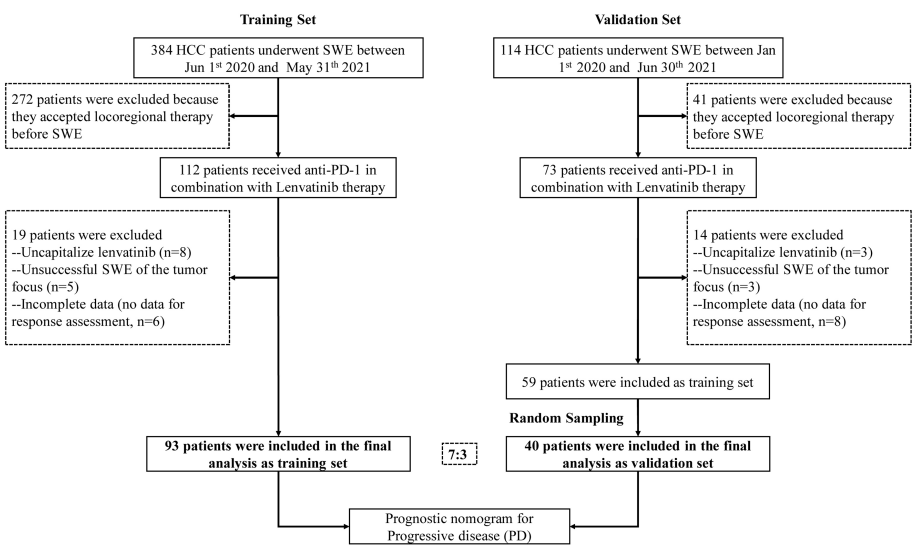

FIGURE 1 | Patient recruitment flowchart.

albumin level, platelet count, total bilirubin, Barcelona Clinic Liver Cancer (BCLC) stage, Eastern Cooperative Oncology Group (ECOG) performance, Child-Pugh score, tumor size, number, vascular invasion, and extrahepatic metastasis. The albumin-bilirubin (ALBI) score was calculated for each patient by the following formula: ALBI score = ($\log_{10}$ bilirubin × 0.66) + (albumin × −0.085), where bilirubin is in μmol/L and albumin in g/L.

Patients underwent computed tomography or magnetic resonance imaging at baseline, at 6-12 weeks after treatment initiation, and about every 3 months thereafter. Treatment-related Aes were recorded at every visit according to the US National Cancer Institute Common Terminology Criteria for Adverse Events (CTCAE v5.0). The modified response evaluation criteria in solid tumors (mRECIST) were used for tumor response evaluation (23) as follows: (1) complete response (CR), where the target lesions disappeared according to enhanced imaging in the arterial phase; (2) partial response (PR), where the diameter of the target lesions was reduced by ≥30% according to enhanced imaging in the arterial phase; (3) stable disease (SD), where the diameter of the target lesions was not reduced to threshold of PR, but it also did not increase past that in progressive disease (PD); (4) PD, which was marked by a total increase of ≥20% in the diameter of the target lesions according to enhanced imaging in the arterial phase compared with the baseline value, or if new lesions appeared.

Development and Validation of Combination Nomogram

Clinical characteristics were selected through univariate and multivariate logistic regression analysis and a nomogram was built based on the independent risk factors in the multivariate analysis. Details were also described in our previously report (22).

RNA Sequencing of Samples From Patients With HCC who Were Diagnosed in Nanfang Hospital

A total of 9 patients with HCC were recruited for RNA sequencing, of whom 5 had a high stiffness tumor (LS >19.53 kPa) and 4 had a low stiffness tumor (LS ≤19.53 kPa). All patients received a fine needle aspiration biopsy. The biopsy specimens were divided for both paraffin embedding and storing in RNA*later*® (Qiagen). MGISEQ-2000 was used to generate transcriptome data.

Immunohistochemistry

IHC was performed in accordance with previous reports (24, 25). Briefly, the 5-μm HCC sections embedded in paraffin were deparaffinized and treated with hydrogen peroxide to quench endogenous peroxidase activity. The following primary antibodies were used: Rabbit monoclonal [SP7] anti-CD3 antibody (100 μl; Abcam), and Rabbit monoclonal [CAL66] anti-CD8 antibody (100 μl; Abcam). All histopathological analyses were performed by an experienced histopathologist (with 21 years of experience), who was blinded to all clinical data. The CD3 and CD8 cell infiltrations were accessed by calculating the proportion of positive stained cells as follow: no staining, 1+; weak staining, 2+; moderate staining, 3+; strong staining, 4+; and intense staining, 5+. Accordingly, the score of 1+ and 2+ was defined as low expression while the other scores were defined as high expression.

Public Transcriptome Data Collection and Preprocessing

We accessed public transcriptome data of HCC patients from the Gene Expression Omnibus and TCGA databases. For samples from the TCGA database, we downloaded level three "HTSeq-Counts" data from the UCSC Xena website (https://xenabrowser.net/). The "voom" algorithm was used to transform RNA sequencing data, as previously described (26). For the GSE109211 dataset, we downloaded the "Series Matrix File(s)," containing normalized transcriptome data.

Development of a tumor Stiffness–Related Gene Expression Signature

To establish a tumor stiffness–related gene expression signature, we firstly performed differential expression gene (DEG) analysis between high and low stiffness HCC samples using the "DESeq2" package. The significance criterion for DEGs was set as an absolute log2FC value >1.0 and an adjusted P value <0.05. The top 100 genes with the largest absolute log2FC values in the log2FC value >1 group and the top 50 genes with the largest absolute log2FC values in the log2FC value <−1 group were separately selected to develop a tumor stiffness–related gene expression signature. The tumor stiffness of each sample was predicted using the nearest template prediction (NTP, Gene Pattern) algorithm based on our developed tumor stiffness–related gene expression signature.

Biological Processes and Tumor Microenvironment Characteristics Analysis

A biological process analysis was performed using gene set variation analysis (GSVA) based on the gene set files of "c2.cp.kegg. v6.2. symbols." The immune infiltration estimation was conducted using the "Microenvironment Cell Populations-counter (MCP-counter)" method by applying the "IOBR" R packages.

Connectivity Map Analysis

Cmap analysis was performed to identify effective candidate compounds following the instructions provided by the Cmap website (https://clue.io/).

Statistical Analysis

Statistical analyses were performed using SPSS 22.0 software (SPSS Inc., Chicago, IL) and R software (version 3.6.2, http://www.Rproject.org). Data were expressed as counts and percentages for categorical variables, such as those in baseline

characteristics, radiological tumor response, and adverse events (AEs). Qualitative differences between subgroups were analyzed using χ^2 tests or Fisher's exact test for categorical parameters. For analyzing the performance ability of quantitative LS to predict treatment outcome, the area under the receiver operator characteristic curve (AUROC) was calculated. AUROCs were compared by the Delong test by using the "pROC" package and the DCA curves were plotted by using the "RMDA" package. Sensitivity, specificity, positive likelihood ratio, and negative likelihood ratio of several cut-off values of LS levels were calculated to explore the best cut-off value in predicting treatment efficacy. Univariate and multivariate logistic regression analyses were performed to assess factors related to treatment outcomes. All statistical analyses were based on 2-tailed hypothesis tests with a significance level of $P<0.05$.

RESULTS

Patient Characteristics

For the analysis, a total of 93 and 40 patients (7:3) were included in the training and validation sets, respectively. **Table 1** shows the clinical characteristics of these patients at baseline. The proportion of patients with BCLC stage C disease was 77.4% (72/93) and 72.5% (29/40), and the proportion of patients with ALBI grade 1 were 55.9% (52/93) and 60.0% (24/40) in the training and validation sets, respectively. The LS values, as determined by SWE, of the tumorous foci and adjacent normal liver tissue in the training set were 17.70 ± 7.78 kPa and 13.96 ± 8.26 kPa, respectively, and the corresponding values in the validation set were 16.87 ± 6.68 kPa and 15.16 ± 8.44 kPa. Among the 133 patients, 96 (72.2%) achieved tumor control (CR + PR + SD), while 37 patients (27.8%) exhibited progressive disease (PD) (**Table 2**). The ORR was 23.4% and the DCR was 72.2% (**Table 2**).

Safety Analysis

All recorded treatment-related AEs are shown in **Table 3**. Forty-nine patients (49/133, 36.8%) experienced at least 1 AE during treatment with a PD-1 inhibitor in combination with lenvatinib. The 5 most frequent types of AEs were hepatitis (42/133, 31.6%), abdominal pain (36/133, 27.1%), thrombocytopenia (36/133, 27.1%), diarrhea (32/133, 24.1%), and hypothyroidism (31/133, 23.3%). A dose delay due to AEs was required in 10 patients. Steroids or immunosuppressive drugs were used to treat AEs in 14 patients, and no patients stop treatment due to AEs.

Correlation Between Baseline Variables and PD

To further evaluate baseline variables that might predict PD, a logistic regression analysis was conducted in the training set. A univariate regression analysis identified the following 2 factors as associated with PD: ALBI grade 1 (odds ratio [OR] 0.124, 95% CI 0.044-0.354, $P<0.001$) and LS value of tumorous foci by SWE (kPa) (OR 1.139, 95% CI 1.063-1.222, $P<0.001$). We then entered these significant factors into a multivariate analysis and found that along with an ALBI grade of 1 (OR 0.107, 95% CI 0.032-0.359, $P<0.001$), the baseline LS value of the tumor (OR 1.148, 95% CI 1.064-1.239, $P<0.001$) was an independent predictive factor for PD (**Table 4**).

Performance Ability of The Baseline LS Value in Predicting PD

To evaluate the correlation between PD and the baseline LS value, as determined by SWE prior to initiation of PD-1 inhibitor–based therapy, AUROCs were calculated (**Figure 2**). AUROCs of the LS values of the tumorous foci were higher than those of the adjacent normal liver tissue in both the training and validation sets (0.768 and 0.753, respectively). **Table 5** shows the sensitivity and specificity for predicting PD from the LS value of the tumorous foci in the training set. The sum of sensitivity and specificity was highest when the cut-off value was 19.53 kPa. Therefore, 19.53 kPa was adopted as the optimal cut-off value for LS of the tumorous foci in the following analyses.

Development and Validation of the Nomogram

A nomogram was established based on the results of multivariate logistic regression (**Figure 3A**). Variables of the nomogram included ALBI grade (grade 2) and baseline LS value of tumorous foci (>19.53kPa). Harrell's C-index was 0.828 and 0.803 respectively ($P>0.05$) in the training and validation set. In the training set, the nomogram yielded an AUC of 0.840 (95%CI 0.750-0.931) with a sensitivity of 55.6% and a specificity of 93.9%. In the validation set, the nomogram exhibited an AUC of 0.827 (95%CI 0.673-0.980) with a sensitivity of 40.0% and a specificity of 96.7% (**Figure 3B**). Calibration curves (**Figure 4**) and Hosmer-Lemeshow test indicated good consistency between the nomogram-predicted probability of PD and the actual PD rate in both sets ($P=0.548$ and $P=0.657$). DCA demonstrated a higher net benefit of the nomogram than treated-all and treat-non strategy, indicating that treatment strategies based on our nomogram prediction have favorable clinical utility (**Figure 5**).

Tumor Stiffness–Related Biological and Immune Characteristics in Patients With HCC of Nanfang Hospital Cohort

To explore the heterogeneity of biological and immune characteristics associated with tumor stiffness in HCC, we identified DEGs between tumors that were high stiffness (HS) versus low stiffness (LowS). A total of 483 tumor stiffness–related genes were found, 406 of which were upregulated in HS tumors, and the other 77 genes were more abundant in LowS tumors (**Figures 6A, B**). Kyoto Encyclopedia of Genes and Genomes (KEGG) analysis showed that the DEGs were enriched for multiple metabolism events (**Table S1**), indicating that

TABLE 1 | Baseline patient characteristics in the training and validation sets.

Characteristics	All patients (n = 133)	Training set (n = 93)	Validation set (n = 40)	*P* value[#]
Age (years)	53 ± 12	54 ± 12	51 ± 11	0.243
Gender				0.232
Men, n (%)	116 (87.2)	79 (84.9)	37 (92.5)	
Women, n (%)	17 (12.8)	14 (15.1)	3 (7.5)	
AFP (ng/ml)				0.807
<20	57 (42.9)	39 (41.9)	18 (45.0)	
20-400	24 (18.0)	16 (17.2)	8 (20.0)	
>400	52 (39.1)	38 (40.9)	14 (35.0)	
ALT (U/L)	29.0 (5.00, 1048.00)	26.00 (5.00, 1048.00)	35.00 (11.00, 125.00)	0.802
AST (U/L)	40.50 (9.00, 723.00)	38.00 (9.00, 723.00)	52.00(18.00, 324.00)	0.249
PT (s)	11.83 ± 1.62	11.88 ± 1.80	11.69 ± 1.09	0.538
ALB (g/L)	36.32 ± 5.59	36.00 ± 5.66	37.06 ± 5.36	0.287
PLT (10^9/L)	160.9 ± 84.8	159.92 ± 88.90	163.15 ± 75.58	0.970
TBIL (μmol/L)	17.80 ± 10.60	16.91 ± 9.59	19.59 ± 12.63	0.183
BCLC				0.543
B, n (%)	32 (24.1)	21 (22.6)	11 (27.5)	
C, n (%)	101 (75.9)	72 (77.4)	29 (72.5)	
ECOG performance*				0.973
0, n (%)	93 (69.9)	65 (69.9)	28 (70.0)	
1, n (%)	36 (27.1)	25 (26.9)	11 (27.5)	
2, n (%)	4 (3.0)	3 (3.2)	1 (2.5)	
3, n (%)	0	0	0	
Child-Pugh grade				0.877
A	114 (85.7)	80 (86.0)	34 (85.0)	
B	19 (14.3)	13 (14.0)	6 (15.0)	
ALBI	-2.29 ± 0.53	-2.29 ± 0.53	–2.29 ± 0.51	0.984
ALBI grade				0.662
1, n (%)	76 (57.1)	52 (55.9)	24 (60.0)	
2, n (%)	57 (42.9)	41 (44.1)	16 (40.0)	
Tumor number				0.773
<3 nodules, n (%)	84 (63.2)	58 (62.4)	26 (65.0)	
≥3 nodules, n (%)	49 (36.8)	35 (37.6)	14 (35.0)	
Tumor size (cm)	7.41 ± 4.30	7.43 ± 4.38	7.35 ± 4.16	0.922
Embolus				0.215
Absent, n (%)	74 (55.6)	55 (59.1)	19 (47.5)	
Present, n (%)	59 (44.4)	38 (40.9)	21 (52.5)	
Extrahepatic metastasis				0.845
Absent, n (%)	105 (78.9)	73 (78.5)	32 (80.0)	
Present, n (%)	28 (21.1)	20 (21.5)	8 (20.0)	
LS value of tumorous foci by SWE (kPa)	17.49 ± 7.47	17.70 ± 7.78	16.87 ± 6.68	0.557
LS value of adjacent normal liver tissue by SWE (kPa)	14.32 ± 8.30	13.96 ± 8.26	15.16 ± 8.44	0.409

*AFP, α-fetoprotein; ALB, albumin; ALBI, albumin-bilirubin; ALT, alanine aminotransferase; AST, aspartate aminotransferase; BCLC, Barcelona Clinic Liver Cancer; ECOG, Eastern Cooperative Oncology Group; LS, liver stiffness; PD-1, programmed cell death protein 1; PLT, platelet count; SWE, shear-wave elastography; PT, prothrombin time; TBIL, total bilirubin. ALBI score = (log_{10} bilirubin × 0.66) + (albumin × –0.085). *Fisher's exact test, others used χ^2 tests. [#]Comparison between the validation and training sets.*

metabolic differences might be the fundamental mechanisms underlying matrix stiffness effects on the tumor's biological behavior. To visually show the differences in pathway activation between the two groups, we performed GSVA enrichment against the KEGG gene set. As shown on the heatmap and volcano plot (**Figures 6C, D**), the HS tumor group presented enrichment pathways predominantly associated with metabolism pathways, including

TABLE 2 | Tumor responses.

Tumor response, n (%)	All patients (n = 133)	Training set (n = 93)	Validation set (n = 40)
Complete response (CR)	1 (0.8)	1 (1.1)	0
Partial response (PR)	30 (22.6)	19 (20.4)	11 (27.5)
Stable disease (SD)	65 (48.9)	46 (49.5)	19 (47.5)
Progressive disease (PD)	37 (27.8)	27 (29.0)	10 (25.0)
ORR (CR + PR)*	31 (23.4)	20 (21.5)	11 (27.5)
DCR (CR + PR + SD)[#]	96 (72.2)	66 (71.0)	30 (75.0)

DCR, disease control rate; ORR, objective response rate.
**Pearson χ^2 = 0.562, P = 0.453 (ORR comparison between the validation and training sets).*
[#]Pearson χ^2 = 0.226, P = 0.634 (DCR comparison between the validation and training sets).

TABLE 3 | Treatment-related adverse events in the training and validation sets.

Adverse Event	All patients (n = 133)		Training set (n = 93)		Validation set (n = 40)	
	All Grades, n (%)	Grades 3/4, n (%)	All Grades, n (%)	Grades 3/4, n (%)	All Grades, n (%)	Grades 3/4, n (%)
Hepatitis*	42 (31.6)	4 (3.0)	33 (35.5)	2 (2.2)	9 (22.5)	2 (5.0)
Abdominal pain	36 (27.1)	3 (2.3)	29 (31.2)	3 (3.2)	7 (17.5)	0
Thrombocytopenia	36 (27.1)	1 (0.8)	25 (26.9)	0	11 (27.5)	1 (2.5)
Diarrhea	32 (24.1)	4 (3.0)	23 (24.7)	3 (3.2)	9 (22.5)	1 (2.5)
Hypothyroidism	31 (23.3)	4 (3.0)	25 (26.9)	2 (2.2)	6 (15.0)	2 (5.0)
Hypertension	30 (22.6)	3 (2.3)	22 (23.7)	0	8 (20.0)	3 (7.5)
Headache	29 (21.8)	2 (1.5)	19 (20.4)	2 (2.2)	10 (25.0)	0
Fatigue	25 (18.8)	0	18 (19.4)	0	7 (17.5)	0
Proteinuria	24 (18.0)	3 (2.3)	18 (19.4)	1 (1.1)	6 (15.0)	2 (5.0)
Rash	22 (16.5)	4 (3.0)	19 (20.4)	3 (3.2)	3 (7.5)	1 (2.5)
Leukopenia	14 (10.5)	0	11 (11.8)	0	3 (7.5)	0
Vomiting	11 (8.3)	1 (0.8)	9 (9.7)	1 (1.1)	2 (5.0)	0
Hoarseness	6 (4.5)	0	4 (4.3)	0	2 (5.0)	0
Dental ulcer	3 (2.3)	0	3 (3.2)	0	0	0

There was no grade 5 adverse event (death) in any patient.

** Hepatitis was detected by Alanine aminotransferase (ALT) or aspartate aminotransferase (AST) increase.*

KEGG_SELENOAMINO_ACID_METABOLISM, and KEGG_TAURINE_AND_HYPOTAURINE_METABOLISM, while the LowS tumor group was significantly enriched in pathways related to DNA damage repair (abbreviations of the pathways on the heatmaps are shown in **Table S2**). As for the immune landscape, the results of MCP-counter analysis showed that the LowS group had a relatively higher amount of immune cell infiltration, especially of dendritic cells, total T cells, and CD8+ T cells, suggesting that LowS tumors present with a hot microenvironment (an immune cell-dense microenvironment) phenotype (**Figure 6E**). We further characterized immune cell infiltration with IHC and found results consistent with the

TABLE 4 | Univariate and multivariate logistic regression analyses of baseline variables predicting PD in training set (n = 93).

Factors	Univariate			Multivariate		
	OR	95% CI	*P* Value	OR	95% CI	*P* Value
Age	0.981	0.945-1.018	0.308			
Gender: Male/Female	1.439	0.434-4.773	0.552			
AFP (ng/mL):			0.514			
<20*						
20-400	2.000	0.569-7.028	0.280			
>400	1.538	0.560-4.230	0.404			
ALT (U/L)	0.998	0.992-1.005	0.629			
AST (U/L)	0.999	0.993-1.005	0.773			
PT (s)	1.053	0.814-1.362	0.694			
ALB (g/L)	1.009	0.932-1.093	0.829			
PLT (10^9/L)	1.001	0.997-1.006	0.592			
TBIL (μmol/L)	1.002	0.957-1.050	0.923			
BCLC stage: B/C	0.769	0.271-2.184	0.622			
ECOG performance:			0.909			
0*						
1	1.229	0.452-3.342	0.687			
2	1.306	0.111-15.299	0.832			
Child-Pugh: B/A	1.101	0.308-3.936	0.882			
ALBI grade:1/2	0.124	0.044-0.354	**<0.001**	0.107	0.032-0.359	**<0.001**
Tumor number: ≥3/<3	1.857	0.746-4.623	0.183			
Tumor size (cm)	0.938	0.841-1.046	0.252			
Embolus: Present/Absent	1.568	0.615-3.998	0.347			
Extrahepatic metastasis: Present/Absent	1.061	0.360-3.132	0.914			
LS value of tumor by SWE (kPa)	1.139	1.063-1.222	**<0.001**	1.148	1.064-1.239	**<0.001**
LS value of adjacent normal liver tissue by SWE (kPa)	0.999	0.946-1.055	0.962			

AFP, α-fetoprotein; ALB, albumin; ALBI, albumin-bilirubin; ALT, alanine aminotransferase; AST, aspartate aminotransferase; ECOG, Eastern Cooperative Oncology Group; LS, liver stiffness; PD, Progressive disease; PLT, platelet count; PT, prothrombin time; TBIL, total bilirubin; SWE, shear-wave elastography.

**Used as the reference category.*

Bold values are values with statistical differences (P value<0.05).

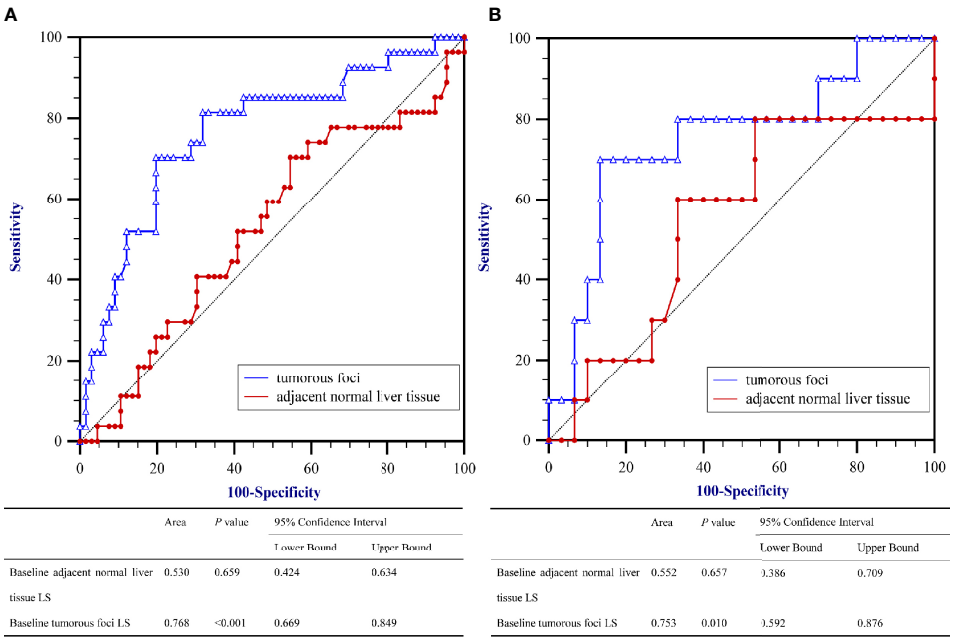

	Area	*P* value	95% Confidence Interval	
			Lower Bound	Upper Bound
Baseline adjacent normal liver tissue LS	0.530	0.659	0.424	0.634
Baseline tumorous foci LS	0.768	<0.001	0.669	0.849

	Area	*P* value	95% Confidence Interval	
			Lower Bound	Upper Bound
Baseline adjacent normal liver tissue LS	0.552	0.657	0.386	0.709
Baseline tumorous foci LS	0.753	0.010	0.592	0.876

FIGURE 2 | Area under the receiver operating characteristics curves (AUROC) for predicting Progressive Diseases (PD) after therapy with anti–programmed cell death protein 1 (PD-1) plus lenvatinib using baseline liver stiffness (LS) values of tumorous foci. **(A)** The training set (n = 93) and **(B)** the validation set (n = 40).

MCP-counter analysis (**Figure 6F**). Finally, we employed the Cmap tool to identify candidate drugs that might improve the efficacy of immunotherapy in patients with HS tumors. As shown in **Figures 7G, H**, 15 candidate drugs with absolute connectivity scores of <−90 were identified. Among them, 5 were histone deacetylase (HDAC) inhibitors, indicating that strategies to deactivate the HDAC pathway might be useful to promote infiltration of cytotoxic T cells into the microenvironment of HS tumors.

Validation of the Distinct Biological and Immune Characteristics Associated With Tumor Stiffness in The Cancer Genome Atlas Liver Hepatocellular Carcinoma and GSE109211 Cohorts

To further confirm the molecular changes underlying HCC tumors with different stiffness levels in patients from Nanfang hospital, we used the NTP algorithm to distinguish tumor tissues in the TCGA-LIHC cohort and the GSE109211 cohort according to the DEGs found between the HS and LowS groups. In the TCGA-LIHC cohort, 204 (54.5%) patients were assigned into the HS group. Similarly, in the GSE109211 cohort, 80 (57.6%) patients belonged to the HS group. Like the results from the Nanfang hospital analysis, the GSVA and immune analyses of the TCGA-LIHC and GSE109211 cohorts demonstrated that the tumors of the HS group also represented a metabolic activation phenotype and showed an absence of immune cell infiltration (**Figures 7A–C, J–L**). Moreover, we obtained data for intratumoral heterogeneity (ITH), tumor purity, tumor mutation burden (TMB), and number of neoantigens from the study of Thorsson et al. (27) and compared these values between HS and LowS groups. Patients in the HS group exhibited less ITH and a higher tumor purity (**Figures 7D, E**). However, there were no significant differences in TMB or in the number of neoantigens between HS and LowS groups (**Figures 7F, G**). Intriguingly, survival analysis of patients in the TCGA-LIHC cohort showed significant prognostic differences among the two different tumor stiffness groups, with the HS signature being associated with a better prognosis (**Figure 7H**). Finally, we analyzed the relationship between the tumor stiffness associated gene and pathway signature we developed and the efficacy of anti-vascular therapy. In the TCGA-LIHC cohort, we used the "pRRophetic" package to predict treatment response to both sorafenib and sunitinib. As shown in **Figure 7I**, the LowS group was more sensitive to sorafenib and sunitinib, although the estimated IC50 was significantly different between the HS and LowS groups only for sunitinib. In addition, by analyzing the GSE109211 cohort, we found that sorafenib-sensitive patients were mainly concentrated in the LowS group, and the tumor stiffness signature had the ability to predict response to sorafenib with an AUROC value of 0.801 (**Figures 7M, N**).

DISCUSSION

In recent decades, immune checkpoint inhibitors—particularly antibodies targeting the PD-1/PD-L1 pathway—have gained

TABLE 5 | Performance of baseline LS value in predicting PD in training set (n = 93).

Cut-off values	Sensitivity (%)	95% CI	Specificity (%)	95% CI	+LR	-LR
>=3.97	100	87.2 - 100.0	0	0.0 - 5.4	1	
>3.97	100	87.2 - 100.0	1.52	0.04 - 8.2	1.02	0
>5.07	100	87.2 - 100.0	3.03	0.4 - 10.5	1.03	0
>5.15	100	87.2 - 100.0	4.55	0.9 - 12.7	1.05	0
>5.39	100	87.2 - 100.0	6.06	1.7 - 14.8	1.06	0
>7.21	100	87.2 - 100.0	7.58	2.5 - 16.8	1.08	0
>7.66	96.3	81.0 - 99.9	7.58	2.5 - 16.8	1.04	0.49
>8.17	96.3	81.0 - 99.9	9.09	3.4 - 18.7	1.06	0.41
>8.27	96.3	81.0 - 99.9	10.61	4.4 - 20.6	1.08	0.35
>9.08	96.3	81.0 - 99.9	12.12	5.4 - 22.5	1.1	0.31
>9.19	96.3	81.0 - 99.9	13.64	6.4 - 24.3	1.12	0.27
>9.51	96.3	81.0 - 99.9	15.15	7.5 - 26.1	1.13	0.24
>9.61	96.3	81.0 - 99.9	16.67	8.6 - 27.9	1.16	0.22
>9.72	96.3	81.0 - 99.9	18.18	9.8 - 29.6	1.18	0.2
>10.16	96.3	81.0 - 99.9	19.7	10.9 - 31.3	1.2	0.19
>10.83	92.59	75.7 - 99.1	19.7	10.9 - 31.3	1.15	0.38
>10.94	92.59	75.7 - 99.1	24.24	14.5 - 36.4	1.22	0.31
>11.11	92.59	75.7 - 99.1	25.76	15.8 - 38.0	1.25	0.29
>11.17	92.59	75.7 - 99.1	27.27	17.0 - 39.6	1.27	0.27
>11.29	92.59	75.7 - 99.1	28.79	18.3 - 41.3	1.3	0.26
>11.52	92.59	75.7 - 99.1	30.3	19.6 - 42.9	1.33	0.24
>11.88	88.89	70.8 - 97.6	31.82	20.9 - 44.4	1.3	0.35
>12.2	85.19	66.3 - 95.8	31.82	20.9 - 44.4	1.25	0.47
>12.54	85.19	66.3 - 95.8	33.33	22.2 - 46.0	1.28	0.44
>12.6	85.19	66.3 - 95.8	34.85	23.5 - 47.6	1.31	0.43
>12.76	85.19	66.3 - 95.8	36.36	24.9 - 49.1	1.34	0.41
>13.02	85.19	66.3 - 95.8	37.88	26.2 - 50.7	1.37	0.39
>13.1	85.19	66.3 - 95.8	39.39	27.6 - 52.2	1.41	0.38
>13.23	85.19	66.3 - 95.8	40.91	29.0 - 53.7	1.44	0.36
>13.29	85.19	66.3 - 95.8	42.42	30.3 - 55.2	1.48	0.35
>13.36	85.19	66.3 - 95.8	43.94	31.7 - 56.7	1.52	0.34
>13.74	85.19	66.3 - 95.8	45.45	33.1 - 58.2	1.56	0.33
>14.39	85.19	66.3 - 95.8	46.97	34.6 - 59.7	1.61	0.32
>14.92	85.19	66.3 - 95.8	48.48	36.0 - 61.1	1.65	0.31
>15.05	85.19	66.3 - 95.8	50	37.4 - 62.6	1.7	0.3
>15.23	85.19	66.3 - 95.8	51.52	38.9 - 64.0	1.76	0.29
>15.32	85.19	66.3 - 95.8	53.03	40.3 - 65.4	1.81	0.28
>15.34	85.19	66.3 - 95.8	54.55	41.8 - 66.9	1.87	0.27
>15.35	85.19	66.3 - 95.8	56.06	43.3 - 68.3	1.94	0.26
>15.46	85.19	66.3 - 95.8	57.58	44.8 - 69.7	2.01	0.26
>15.5	81.48	61.9 - 93.7	57.58	44.8 - 69.7	1.92	0.32
>15.87	81.48	61.9 - 93.7	59.09	46.3 - 71.0	1.99	0.31
>16.22	81.48	61.9 - 93.7	60.61	47.8 - 72.4	2.07	0.31
>16.29	81.48	61.9 - 93.7	62.12	49.3 - 73.8	2.15	0.3
>16.64	81.48	61.9 - 93.7	63.64	50.9 - 75.1	2.24	0.29
>16.85	81.48	61.9 - 93.7	66.67	54.0 - 77.8	2.44	0.28
>17.13	81.48	61.9 - 93.7	68.18	55.6 - 79.1	2.56	0.27
>17.14	74.07	53.7 - 88.9	68.18	55.6 - 79.1	2.33	0.38
>18.09	74.07	53.7 - 88.9	69.7	57.1 - 80.4	2.44	0.37
>18.57	74.07	53.7 - 88.9	71.21	58.7 - 81.7	2.57	0.36
>18.6	70.37	49.8 - 86.2	71.21	58.7 - 81.7	2.44	0.42
>19.02	70.37	49.8 - 86.2	72.73	60.4 - 83.0	2.58	0.41
>19.2	70.37	49.8 - 86.2	75.76	63.6 - 85.5	2.9	0.39
>19.35	70.37	49.8 - 86.2	77.27	65.3 - 86.7	3.1	0.38
>19.51	70.37	49.8 - 86.2	78.79	67.0 - 87.9	3.32	0.38
>19.53 *	**70.37**	**49.8 - 86.2**	**80.3**	**68.7 - 89.1**	**3.57**	**0.37**
>19.81	66.67	46.0 - 83.5	80.3	68.7 - 89.1	3.38	0.42
>19.88	62.96	42.4 - 80.6	80.3	68.7 - 89.1	3.2	0.46
>19.94	59.26	38.8 - 77.6	80.3	68.7 - 89.1	3.01	0.51
>20.44	51.85	31.9 - 71.3	80.3	68.7 - 89.1	2.63	0.6
>20.75	51.85	31.9 - 71.3	84.85	73.9 - 92.5	3.42	0.57
>21.07	51.85	31.9 - 71.3	87.88	77.5 - 94.6	4.28	0.55
>22.03	48.15	28.7 - 68.1	87.88	77.5 - 94.6	3.97	0.59

(Continued)

TABLE 5 | Continued

Cut-off values	Sensitivity (%)	95% CI	Specificity (%)	95% CI	+LR	-LR
>22.87	44.44	25.5 - 64.7	87.88	77.5 - 94.6	3.67	0.63
>23.02	40.74	22.4 - 61.2	89.39	79.4 - 95.6	3.84	0.66
>23.09	40.74	22.4 - 61.2	90.91	81.3 - 96.6	4.48	0.65
>23.52	37.04	19.4 - 57.6	90.91	81.3 - 96.6	4.07	0.69
>23.86	33.33	16.5 - 54.0	90.91	81.3 - 96.6	3.67	0.73
>25.4	33.33	16.5 - 54.0	92.42	83.2 - 97.5	4.4	0.72
>26.46	29.63	13.8 - 50.2	92.42	83.2 - 97.5	3.91	0.76
>26.64	29.63	13.8 - 50.2	93.94	85.2 - 98.3	4.89	0.75
>26.96	25.93	11.1 - 46.3	93.94	85.2 - 98.3	4.28	0.79
>28.27	22.22	8.6 - 42.3	93.94	85.2 - 98.3	3.67	0.83
>29.14	22.22	8.6 - 42.3	95.45	87.3 - 99.1	4.89	0.81
>29.31	22.22	8.6 - 42.3	96.97	89.5 - 99.6	7.33	0.8
>30.91	18.52	6.3 - 38.1	96.97	89.5 - 99.6	6.11	0.84
>32.08	14.81	4.2 - 33.7	96.97	89.5 - 99.6	4.89	0.88
>33.07	14.81	4.2 - 33.7	98.48	91.8 - 100.0	9.78	0.86
>34.07	11.11	2.4 - 29.2	98.48	91.8 - 100.0	7.33	0.9
>35.29	7.41	0.9 - 24.3	98.48	91.8 - 100.0	4.89	0.94
>36.54	3.7	0.09 - 19.0	98.48	91.8 - 100.0	2.44	0.98
>38.02	3.7	0.09 - 19.0	100	94.6 - 100.0		0.96
>39.43	0	0.0 - 12.8	100	94.6 - 100.0		1

*LS, Liver stiffness; PD, Progressive disease; CI, confidence Interval; +LR, positive likelihood ratio; -LR, negative likelihood ratio; *: the cut-off value has the highest sum of sensitivity and specificity.*

Bold values are values with statistical differences (P value<0.05).

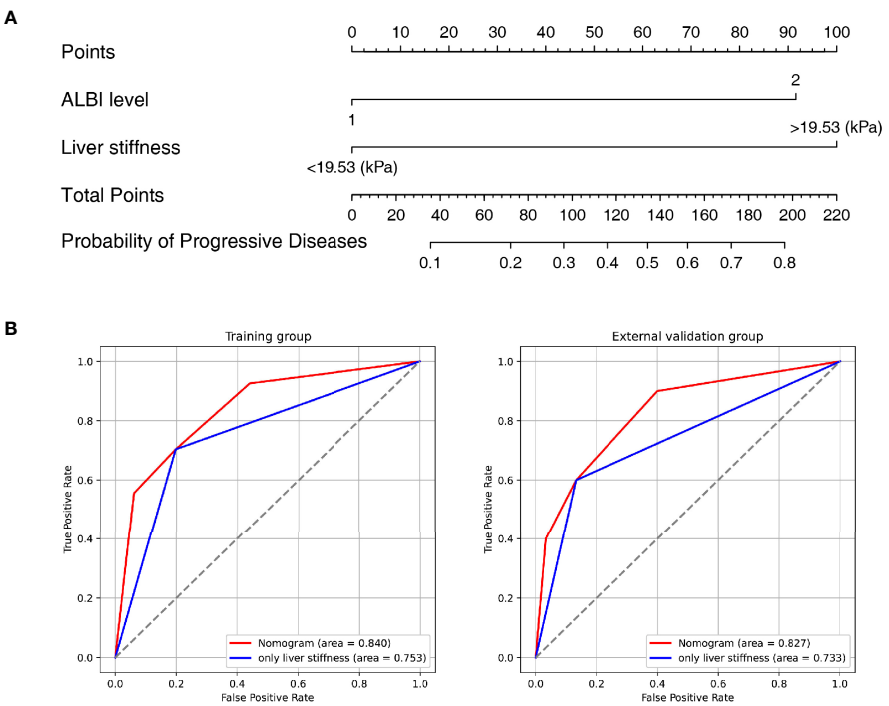

FIGURE 3 | Nomogram and Receiver operating characteristic (ROC) curves analysis. **(A)** Nomogram for predicting probability of Progressive Diseases (PD) after therapy with anti–programmed cell death protein 1 (PD-1) plus lenvatinib. **(B)** ROC curves for 2 models in the training (left) and validation (right) set. Model based on baseline liver stiffness (LS) values of tumorous foci >19.53 kPa were shown in blue. Nomogram contains both baseline LS of tumorous foci and ALBI grade were shown in red.

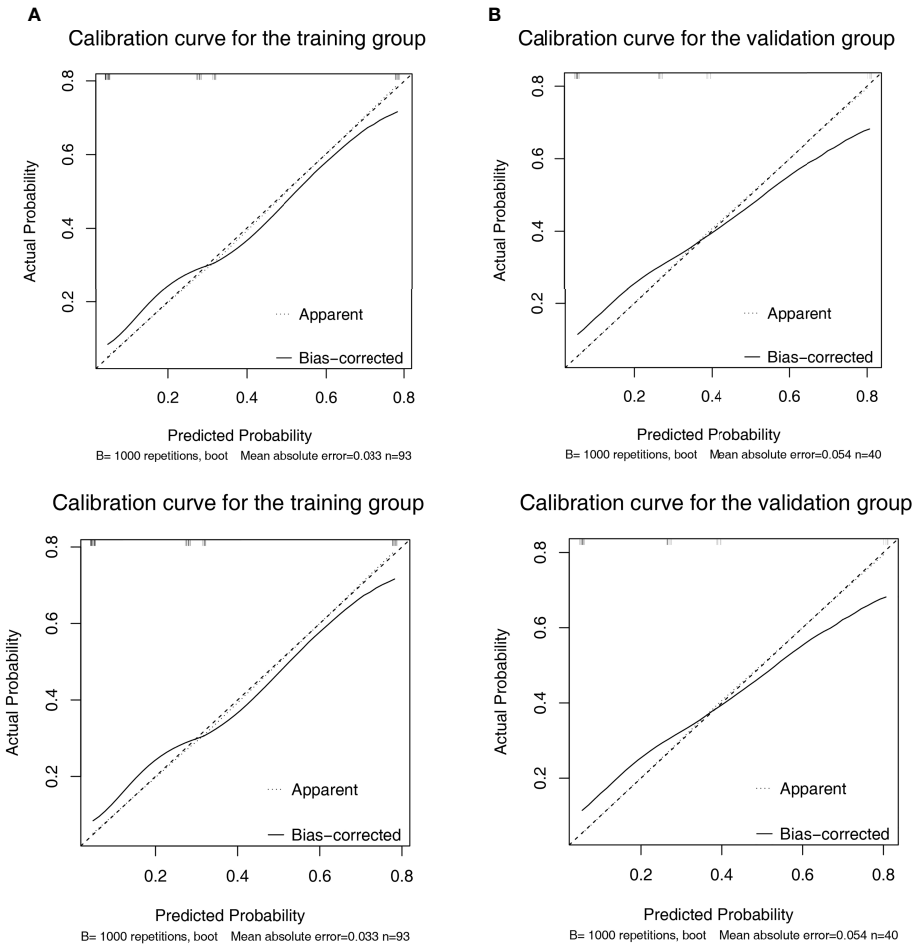

FIGURE 4 | Calibration curve of the nomogram in the training **(A)** and validation **(B)** set. X-axis represents the nomogram predicted probability of Progressive Diseases (PD). Y-axis represents the actual probability of PD, and the diagonal dashed line (represent ideal) indicates the ideal prediction by a perfect model. Results were plotted *via* bootstrapping with 1000 resamples. The closer the bias-corrected calibration curve (solid line) is to the diagonal line, the higher the prediction accuracy of the model.

popularity, becoming more commonly used in the clinic. However, with their widespread use came a gradual realization that they were effective in only a fraction of patients (10-30%), indicating it is urgently needed to develop robust predictors as useful tools for precise immunotherapy of advanced HCC (28, 29). In a previous study, we developed and validated a radiomics nomogram by incorporating pretreatment contrast-enhanced computed tomography images and clinical factors to estimate the efficacy of anti-PD-1 antibodies treatment in patients with advanced HCC (22). However, the development of a radiomics nomogram needs precise feature extraction of tumorous foci and professionals to carry out tedious machine learning, which greatly limits its application in our daily clinical practice. Therefore, more effective and convenient predictive tools are needed.

Previous studies have identified important HCC etiologies, like viral hepatitis, fatty liver disease, and alcoholic cirrhosis—each of which can induce fibrosis and lead to the development of HCC (30–32). Indeed, fibrosis is a verified factor that leads to HCC, and over 80% of patients with HCC have liver fibrosis (14, 33, 34). Accordingly, liver stiffness has been gradually accepted as an indicator of prognosis in patients with HCC. For example, Lee et al. found that LS values measured by 2D-SWE significantly predicted overall survival after radiofrequency ablation for HCC (14), while magnetic resonance elastography (MRE)-assessed LS has been highlighted as a potential radio-omics biomarker for predicting the prognosis of patients with chronic liver disease and HCC (13). However, no study has yet examined LS values as predictors for anti-PD-1 antibodies treatment efficacy. In the present report, we assessed the performance of LS values, as measured by SWE, for predicting response to therapy with anti-PD-1 antibodies in combination with lenvatinib in patients with advanced HCC. We demonstrated

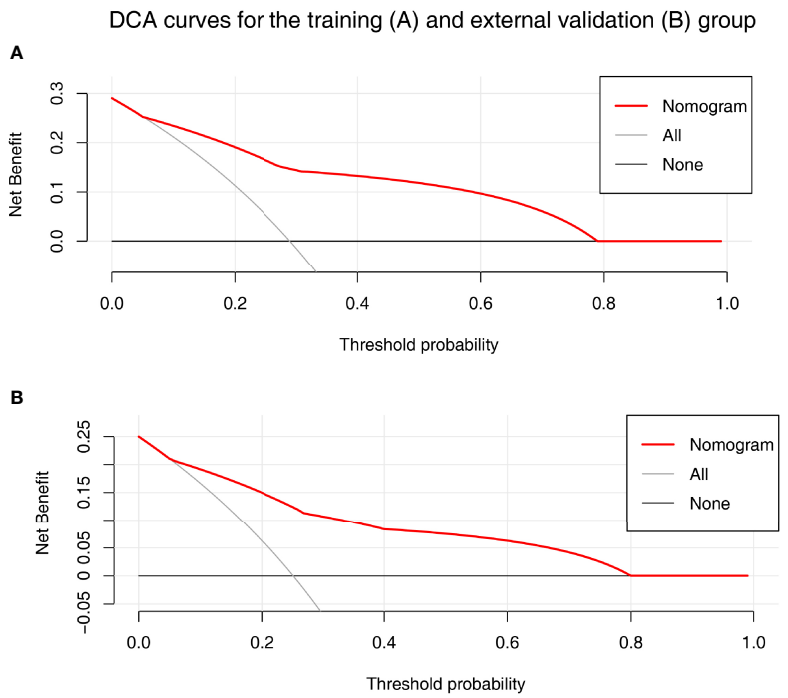

FIGURE 5 | The decision curve analysis (DCA) for the nomogram in training **(A)** and validation **(B)** set. Nomogram contains both baseline LS of tumorous foci and ALBI grade were shown in red. Result showed that using the nomogram for PD prediction has more benefit than the treat-all-patients scheme (gray curve). A larger area under the decision curve suggested a better clinical utility.

that a baseline tumor LS of >19.53 kPa was associated with higher rates of PD. We chose to test tumor LS values measured by SWE as a potential tool for predicting treatment efficacy of PD-1 inhibitor-based therapy for the following reasons: 1) with recent advances in ultrasound technology, various elastography techniques, including TE and SWE, have been confirmed to be effective tools for staging the degree of fibrosis (15–17); 2) in contrast to TE, SWE provides additional real-time information on tumorous foci, enabling a more detailed characterization that can help to predict the nature and behavior of the tumor (35); and 3) compared to TE, SWE shows a higher rate of reliable measurements and a similar predictive value for fibrosis, as determined in a meta-analysis of 13 studies (36).

To validate the predictive value of the data obtained from SWE, AUROCs were calculated for baseline tumor LS values in predicting PD after treatment with anti-PD-1 antibodies plus lenvatinib; we found that the AUROC was increased in both the training and validation sets compared with the normal liver tissue. Recently, Kim et al. reported that higher LS values, as assessed by MRE, are a potential biomarker for predicting poor overall survival and significant liver injury in patients with advanced HCC who were treated with sorafenib (13). This is in concordance with our current data, where tumor LS was identified as a strong predictor of treatment efficacy after anti-PD-1 antibodies in combination with lenvatinib. Furthermore, we have verified the predictive value of hepatic tumor stiffness by developing a nomogram, which showed favourable discrimination and calibration values.

The mechanism underlying the differential anti-PD-1 antibodies in combination with lenvatinib response associated with tumor stiffness in HCC remains unknown. This may be partly due to the dense extracellular matrix (ECM) that forms a barrier for T cells since the fibrotic state of desmoplastic tumors can cause immunosuppression through multiple mechanisms. First, it has been proposed that ECM may act as a physical barrier to $CD8^+$ T cells infiltration into tumors. In addition to physical exclusion, matrix density and architecture could induce the localization and migration of T cells into the tumor stroma rather than into tumor cell nests (37). Furthermore, cellular components of tumor-associated fibrosis, particularly the cancer-associated fibroblasts (CAF), can have both direct and indirect effects on T cell infiltration and function (38). To explore the heterogeneity of biological and immune characteristics associated with tumor stiffness in HCC—and thus, potential explanations of the differential response—we identified DEGs between high- and low-stiffness tumor groups using scRNA-seq and IHC staining. We found that the DEGs that were enriched in high stiffness tumors were predominantly associated with metabolic pathways, while those enriched in low stiffness tumors were related to DNA damage repair, indicating that metabolic differences might drive the matrix stiffness–induced effects on the tumor's biological behavior.

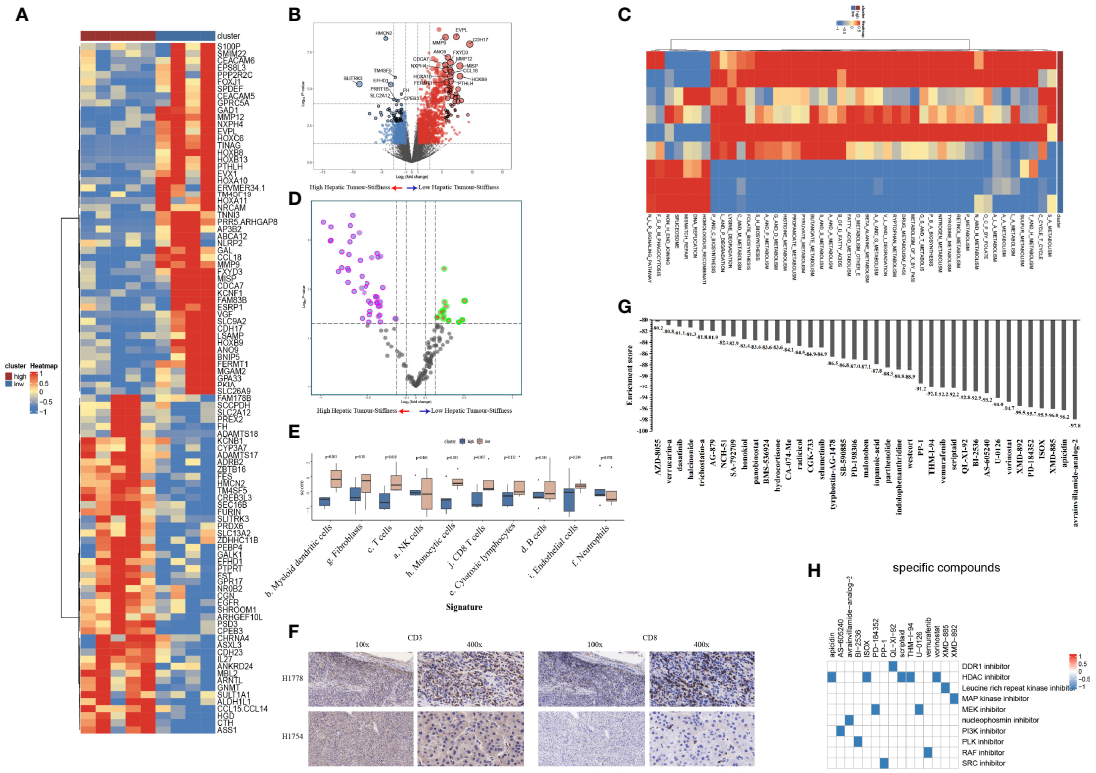

FIGURE 6 | Biological functions and immune characteristics of tumors with high (n = 5) or low (n = 4) stiffness. **(A, B)** Heatmap **(A)** and volcano plot **(B)** comparing differences in gene expression between tumors with high and low stiffness. **(C, D)** Heatmap **(C)** and volcano plot **(D)** comparing differences in Kyoto Encyclopedia of Genes and Genomes (KEGG) pathways between tumors with high and low stiffness. **(E)** Boxplots of cell infiltration levels calculated by the Microenvironment Cell Populations-counter among tumors with high and low stiffness. **(F)** Representative micrographs of CD3 and CD8 protein expression in tumor samples with high and low stiffness, as detected by immunohistochemistry (H1778 was a patient with low stiffness liver tumor, and H1754 was a patient with high stiffness liver tumor). **(G)** Bar plot showing the enrichment score of each candidate compound in the connectivity map analysis. Compounds are sorted from right to left as the highest to lowest enriched, as assessed using an enrichment analysis. **(H)** Heatmap showing the mechanisms of the action (rows) of each compound (columns) from the connectivity map analysis. A total of 15 candidate drugs with absolute connectivity scores of <–90 were identified. Among them, 5 were histone deacetylase (HDAC) inhibitors.

Further analyses using the MCP-counter and IHC were performed to explore the immune landscape based on matrix stiffness. Our data showed that patients with low tumor stiffness had relatively higher immune cell infiltration, suggesting low LS is associated with a hot immune microenvironment phenotype, which might explain the differential responses to anti-PD-1–based therapy. In addition, the above molecular changes associated with tumors of different stiffnesses were further validated in the TCGA-LIHC and GSE109211 cohorts. Finally, we identified candidate drugs targeting the HDAC pathway as potentially useful strategies for promoting the infiltration of cytotoxic T cells into the microenvironment of high LS tumors, with the idea that this would enhance the efficacy of immunotherapies. Further experimental research focusing on the efficacy and safety of HDAC inhibitors in HCC patients with high stiffness liver tumors is needed to verify our conjecture.

Several limitations should be considered while interpreting our results. First, this is a retrospective study, which may have selection bias. The conclusions drawn from this study should be verified in larger prospective studies. Second, only 9 HCC samples were collected for RNA sequencing and IHC analysis, and thus, selection bias and confounding factors could not be eliminated. Third, several factors affecting the stiffness of liver tumors—e.g., MAFLD (metabolic associated fatty liver disease), ascites and jaundice, have not been analyzed in our current study. Therefore, additional multicenter, randomized controlled prospective studies are needed, specifically in patients with advanced HCC who receive a PD-1 inhibitor in combination with lenvatinib as the first-line regimen, to evaluate the predictive ability of tumor LS and the underlying mechanisms of LS-associated disease progression.

In conclusion, baseline LS values of tumorous foci by SWE prior to initiation of treatment with a PD-1 inhibitor plus lenvatinib were found to conveniently predict PD-1 inhibitor efficacy in patients with advanced HCC. It may be possible to apply these findings in the future for pretreatment stratification aimed at optimizing treatment outcomes in patients with advanced HCC. Metabolic differences and immune cell infiltration abundance may be the underlying mechanisms driving matrix stiffness effects on the tumor's biological behavior.

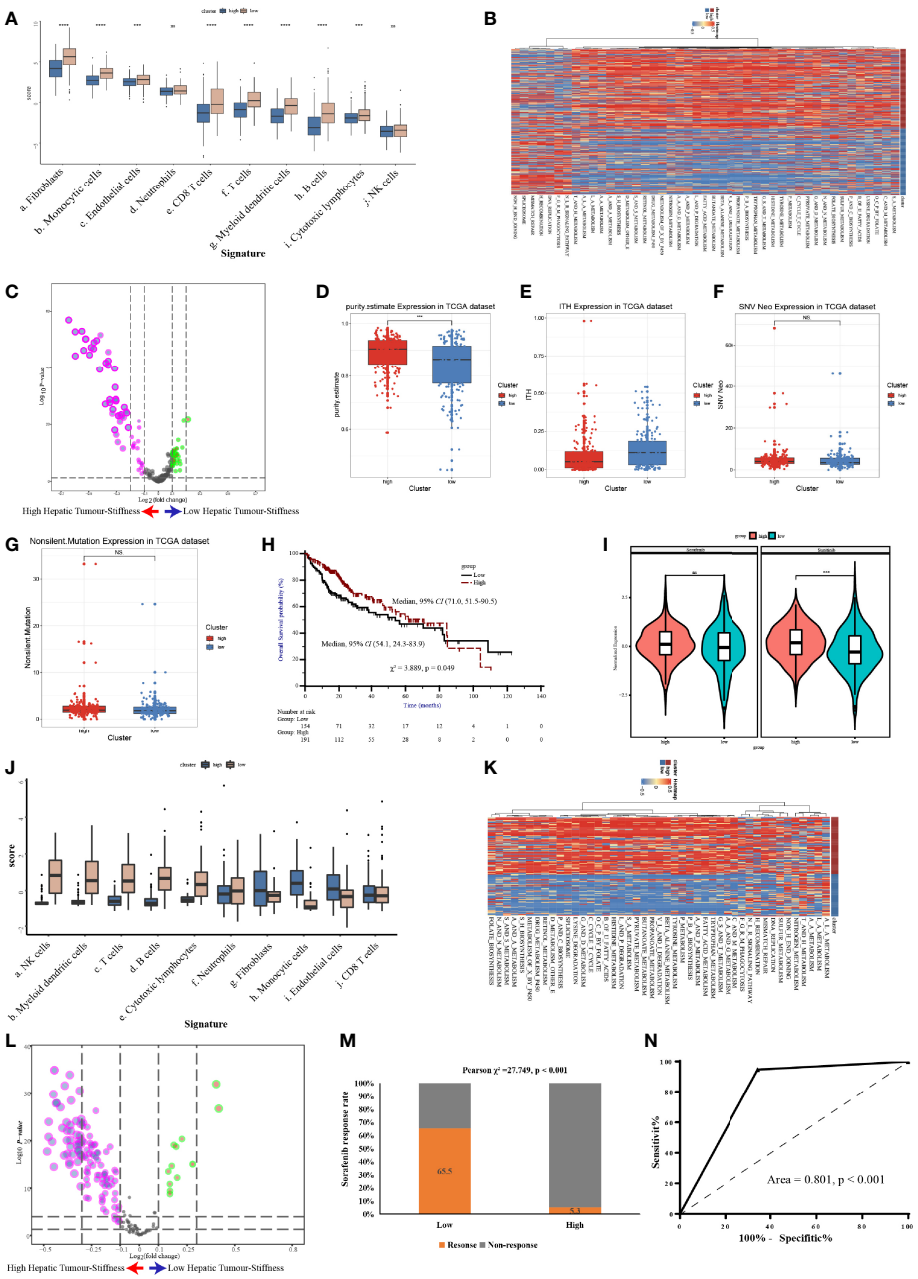

FIGURE 7 | Validation of the high stiffness signature in TCGA-LIHC and GSE109211 datasets. **(A)** Boxplots of cell infiltration, as calculated by the Microenvironment Cell Populations-counter (MCP-counter), among tumors with high and low stiffness from The Cancer Genome Atlas Liver Hepatocellular Carcinoma (TCGA-LIHC) cohort. **(B, C)** Heatmap **(B)** and volcano plot **(C)** comparing differences in the Kyoto Encyclopedia of Genes and Genomes (KEGG) pathways between tumors with high and low stiffness in the TCGA-LIHC cohort. **(D–G)** Boxplots of tumor purity **(D)**, intratumoral heterogeneity (ITH) **(E)**, neoantigen **(F)**, and tumor mutation burden **(G)** in the 4 studied histone modification patterns of the TCGA-LIHC cohort. **(H)** Kaplan-Meier curves of overall survival in the TCGA-LIHC cohort according to tumor stiffness. **(I)** Violin plot of the estimated IC50 value of sorafenib and sunitinib calculated based on the Genomics of Drug Sensitivity in Cancer database among tumors with high or low stiffness in the TCGA-LIHC cohort. **(J)** Boxplots of cell infiltration levels calculated by the MCP-counter among tumors with high and low stiffness in the GSE109211 cohort. **(K, L)** Heatmap **(K)** and volcano plot **(L)** comparing differences in KEGG pathways between tumors with high and low stiffness in the GSE109211 cohort. **(M)** Bar charts summarizing the proportions of patients with different sorafenib responses across different tumor stiffness groups in the GSE109211 cohort. **(N)** Receiver operating characteristic curves of treatment response predictions of sorafenib according to the tumor stiffness signature in the GSE109211 cohort. NS means not-siginificant (without statistical difference); *** means p value < 0.001; **** means p value < 0.0001.

DATA AVAILABILITY STATEMENT

The original contributions presented in the study are publicly available. This data can be found here: https://www.ncbi.nlm.nih.gov/, PRJNA816189

ETHICS STATEMENT

The studies involving human participants were reviewed and approved by the Medical Ethics Committee of Nanfang hospital and the First Affiliated Hospital of Sun Yat-Sen University. The patients/participants provided their written informed consent to participate in this study.

AUTHOR CONTRIBUTIONS

(I) Conception and design: GY, FX, YS, JS, JC. (II) Administrative support: JC. (III) Provision of study materials or patients: XH, QL, RL, MZ, XC, GL, JC, JH. (IV) Collection and assembly of data: GY, QL, RL, XH, MZ, XC, GL, JC. (V) Data analysis and interpretation: GY, FX, YS, XH, JC. (VI) Manuscript writing: All authors. (VII) Manuscript revised: GY, FX, YS, QL, WF, XR, JSu, JC. (VIII) Final approval of manuscript: All authors.

FUNDING

This study was supported by grants from the National Natural Science Foundation of China (82102879), the Natural Science Foundation of Guangdong Province (2021A1515012518), and the Postdoctoral Research Foundation of China (No. 2021M691468). The funding agencies had no role in the study design, data collection and analysis, decision to publish, or preparation of the manuscript.

SUPPLEMENTARY MATERIAL

The Supplementary Material for this article can be found online at: https://www.frontiersin.org/articles/10.3389/fimmu.2022.868809/full#supplementary-material

REFERENCES

1. Llovet JM, Kelley RK, Villanueva A, Singal AG, Pikarsky E, Roayaie S, et al. Hepatocellular Carcinoma. *Nat Rev Dis Primers* (2021) 7(1):6. doi: 10.1038/s41572-020-00240-3
2. Yang JD, Hainaut P, Gores GJ, Amadou A, Plymoth A, Roberts LR. A Global View of Hepatocellular Carcinoma: Trends, Risk, Prevention and Management. *Nat Rev Gastroenterol Hepatol* (2019) 16(10):589–604. doi: 10.1038/s41575-019-0186-y
3. Rimassa L, Pressiani T, Merle P. Systemic Treatment Options in Hepatocellular Carcinoma. *Liver Cancer* (2019) 8(6):427–46. doi: 10.1159/000499765
4. Kalasekar SM, Garrido Laguna I, Evason KJ. Immune Checkpoint Inhibitors in Novel Combinations for Hepatocellular Carcinoma. *Hepatology* (2021) 73(6):2591–2593. doi: 10.1002/hep.31706
5. Killock D. PD-1 Inhibition Enters the Frontline. *Nat Rev Clin Oncol* (2020) 17(2):69. doi: 10.1038/s41571-019-0303-4
6. Finn RS, Zhu AX. Evolution of Systemic Therapy for Hepatocellular Carcinoma. *Hepatology* (2020) 73(Suppl 1):150–157. doi: 10.1002/hep.31306
7. Chen J, Hu X, Li Q, Dai W, Cheng X, Huang W, et al. Effectiveness and Safety of Toripalimab, Camrelizumab, and Sintilimab in a Real-World Cohort of Hepatitis B Virus Associated Hepatocellular Carcinoma Patients. *Ann Transl Med* (2020) 8(18):1187. doi: 10.21037/atm-20-6063
8. Zhu AX, Finn RS, Edeline J, Cattan S, Ogasawara S, Palmer D, et al. Pembrolizumab in Patients With Advanced Hepatocellular Carcinoma Previously Treated With Sorafenib (KEYNOTE-224): A non-Randomised, Open-Label Phase 2 Trial. *Lancet Oncol* (2018) 19(7):940–52. doi: 10.1016/S1470-2045(18)30351-6
9. El-Khoueiry AB, Sangro B, Yau T, Crocenzi TS, Kudo M, Hsu C, et al. Nivolumab in Patients With Advanced Hepatocellular Carcinoma (CheckMate 040): An Open-Label, non-Comparative, Phase 1/2 Dose Escalation and Expansion Trial. *Lancet* (2017) 389(10088):2492–502. doi: 10.1016/S0140-6736(17)31046-2
10. Finn RS, Qin S, Ikeda M, Galle PR, Ducreux M, Kim TY, et al. Atezolizumab Plus Bevacizumab in Unresectable Hepatocellular Carcinoma. *N Engl J Med* (2020) 382(20):1894–905. doi: 10.1056/NEJMoa1915745
11. Xu J, Shen J, Gu S, Zhang Y, Wu L, Wu J, et al. Camrelizumab in Combination With Apatinib in Patients With Advanced Hepatocellular Carcinoma (RESCUE): A Nonrandomized, Open-Label, Phase II Trial. *Clin Cancer Res* (2021) 27(4):1003–11. doi: 10.1158/1078-0432.CCR-20-2571
12. Bray F, Ferlay J, Soerjomataram I, Siegel RL, Torre LA, Jemal A. Global Cancer Statistics 2018: GLOBOCAN Estimates of Incidence and Mortality Worldwide for 36 Cancers in 185 Countries. *CA: A Cancer J Clin* (2018) 68(6):394–424. doi: 10.3322/caac.21492
13. Kim B, Kim SS, Cho SW, Cheong JY, Huh J, Kim JK, et al. Liver Stiffness in Magnetic Resonance Elastography is Prognostic for Sorafenib-Treated Advanced Hepatocellular Carcinoma. *Eur Radiol* (2020) 31(4):2507–17. doi: 10.1007/s00330-020-07357-9
14. Lee DH, Lee JM, Yoon J, Kim YJ, Lee J, Yu SJ, et al. Liver Stiffness Measured by Two-Dimensional Shear-Wave Elastography: Prognostic Value After Radiofrequency Ablation for Hepatocellular Carcinoma. *Liver Cancer* (2018) 7(1):65–75. doi: 10.1159/000484445
15. Zhuang Y, Ding H, Zhang Y, Sun H, Xu C, Wang W. Two-Dimensional Shear-Wave Elastography Performance in the Noninvasive Evaluation of Liver Fibrosis in Patients With Chronic Hepatitis B: Comparison With Serum Fibrosis Indexes. *Radiology* (2017) 283(3):873–82. doi: 10.1148/radiol.2016160131
16. Zeng J, Zheng J, Jin J, Mao Y, Guo H, Lu M, et al. Shear Wave Elastography for Liver Fibrosis in Chronic Hepatitis B: Adapting the Cut-Offs to Alanine Aminotransferase Levels Improves Accuracy. *Eur Radiol* (2019) 29(2):857–65. doi: 10.1007/s00330-018-5621-x
17. Guo H, Liao M, Jin J, Zeng J, Li S, Schroeder DR, et al. How Intrahepatic Cholestasis Affects Liver Stiffness in Patients With Chronic Hepatitis B: A Study of 1197 Patients With Liver Biopsy. *Eur Radiol* (2020) 30(2):1096–104. doi: 10.1007/s00330-019-06451-x
18. Chen LT, Martinelli E, Cheng AL, Pentheroudakis G, Qin S, Bhattacharyya GS, et al. Pan-Asian Adapted ESMO Clinical Practice Guidelines for the Management of Patients With Intermediate and Advanced/Relapsed Hepatocellular Carcinoma: A TOS–ESMO Initiative Endorsed by CSCO, ISMPO, JSMO, KSMO, MOS and SSO. *Ann Oncol* (2020) 31(3):334–51. doi: 10.1016/j.annonc.2019.12.001
19. Barr RG. Foreword to the Second Set of WFUMB Guidelines and Recommendations on the Clinical Use of Ultrasound Elastography. *Ultrasound Med Biol* (2017) 43(1):1–3. doi: 10.1016/j.ultrasmedbio.2016.08.027
20. Dietrich CF. EFSUMB Guidelines 2015 on Interventional Ultrasound. *Med Ultrason* (2015) 17(4):521–7. doi: 10.11152/mu.2013.2066.174.efb

21. Yuan G, Cheng X, Li Q, Zang M, Huang W, Fan W, et al. Safety and Efficacy of Camrelizumab Combined With Apatinib for Advanced Hepatocellular Carcinoma With Portal Vein Tumor Thrombus: A Multicenter Retrospective Study. *Onco Targets Ther* (2020) 13:12683–93. doi: 10.2147/OTT.S286169
22. Yuan G, Song Y, Li Q, Hu X, Zang M, Dai W, et al. Development and Validation of a Contrast-Enhanced CT-Based Radiomics Nomogram for Prediction of Therapeutic Efficacy of Anti-PD-1 Antibodies in Advanced HCC Patients. *Front Immunol* (2021) 11:613946. doi: 10.3389/fimmu.2020.613946
23. Lencioni R, Llovet JM. Modified RECIST (mRECIST) Assessment for Hepatocellular Carcinoma. *Semin Liver Dis* (2010) 30(1):52–60. doi: 10.1055/s-0030-1247132
24. Kim HD, Song GW, Park S, Jung MK, Kim MH, Kang HJ, et al. Association Between Expression Level of PD1 by Tumor-Infiltrating CD8(+) T Cells and Features of Hepatocellular Carcinoma. *Gastroenterology* (2018) 155(6):1936–50.e17. doi: 10.1053/j.gastro.2018.08.030
25. Garnelo M, Tan A, Her Z, Yeong J, Lim CJ, Chen J, et al. Interaction Between Tumour-Infiltrating B Cells and T Cells Controls the Progression of Hepatocellular Carcinoma. *Gut* (2017) 66(2):342–51. doi: 10.1136/gutjnl-2015-310814
26. Zhou R, Zeng D, Zhang J, Sun H, Wu J, Li N, et al. A Robust Panel Based on Tumour Microenvironment Genes for Prognostic Prediction and Tailoring Therapies in Stage I-III Colon Cancer. *Ebiomedicine* (2019) 42:420–30. doi: 10.1016/j.ebiom.2019.03.043
27. Thorsson V, Gibbs DL, Brown SD, Wolf D, Bortone DS, Ou YT, et al. The Immune Landscape of Cancer. *Immunity* (2018) 48(4):812–830.e14. doi: 10.1016/j.immuni.2018.03.023
28. Qin S, Ren Z, Meng Z, Chen Z, Chai X, Xiong J, et al. Camrelizumab in Patients With Previously Treated Advanced Hepatocellular Carcinoma: A Multicentre, Open-Label, Parallel-Group, Randomised, Phase 2 Trial. *Lancet Oncol* (2020) 21(4):571–80. doi: 10.1016/S1470-2045(20)30011-5
29. Yau T, Hsu C, Kim T, Choo S, Kang Y, Hou M, et al. Nivolumab in Advanced Hepatocellular Carcinoma: Sorafenib-Experienced Asian Cohort Analysis. *J Hepatol* (2019) 71(3):543–52. doi: 10.1016/j.jhep.2019.05.014
30. Nguyen MH, Wong G, Gane E, Kao JH, Dusheiko G. Hepatitis B Virus: Advances in Prevention, Diagnosis, and Therapy. *Clin Microbiol Rev* (2020) 33(2):e00046–19. doi: 10.1128/CMR.00046-19
31. Yuen MF, Hou JL, Chutaputti A. Hepatocellular Carcinoma in the Asia Pacific Region. *J Gastroenterol Hepatol* (2009) 24(3):346–53. doi: 10.1111/j.1440-1746.2009.05784.x
32. Powell EE, Wong VW, Rinella M. Non-Alcoholic Fatty Liver Disease. *Lancet* (2021) 397(10290):2212–24. doi: 10.1016/S0140-6736(20)32511-3
33. EASL Clinical Practice Guidelines. Management of Hepatocellular Carcinoma. *J Hepatol* (2018) 69(1):182–236. doi: 10.1016/j.jhep.2018.03.019
34. Heimbach JK, Kulik LM, Finn RS, Sirlin CB, Abecassis MM, Roberts LR, et al. AASLD Guidelines for the Treatment of Hepatocellular Carcinoma. *Hepatology* (2018) 67(1):358–80. doi: 10.1002/hep.29086
35. Summers JA, Summers JA, Radhakrishnan M, Radhakrishnan M, Morris E, Morris E, et al. Virtual Touch™ Quantification to Diagnose and Monitor Liver Fibrosis in Hepatitis B and Hepatitis C: A NICE Medical Technology Guidance. *Appl Health Econ Hea* (2017) 15(2):139–54. doi: 10.1007/s40258-016-0277-7
36. Kim DW, Park C, Yoon HM, Jung AY, Lee JS, Jung SC, et al. Technical Performance of Shear Wave Elastography for Measuring Liver Stiffness in Pediatric and Adolescent Patients: A Systematic Review and Meta-Analysis. *Eur Radiol* (2019) 29(5):2560–72. doi: 10.1007/s00330-018-5900-6
37. Jiang H, Hegde S, Denardo DG. Tumor-Associated Fibrosis as a Regulator of Tumor Immunity and Response to Immunotherapy. *Cancer Immunol Immunother* (2017) 66(8):1037–48. doi: 10.1007/s00262-017-2003-1
38. Nicolas-Boluda A, Vaquero J, Vimeux L, Guilbert T, Barrin S, Kantari-Mimoun C, et al. Tumor Stiffening Reversion Through Collagen Crosslinking Inhibition Improves T Cell Migration and Anti-PD-1 Treatment. *Elife* (2021) 10:e58688. doi: 10.7554/eLife.58688

Conflict of Interest: The authors declare that the research was conducted in the absence of any commercial or financial relationships that could be construed as a potential conflict of interest.

The reviewer GW declared a shared parent affiliation with the author WF to the handling editor at the time of the review

Citation: *Yuan G, Xie F, Song Y, Li Q, Li R, Hu X, Zang M, Cheng X, Lu G, Huang J, Fan W, Rong X, Sun J and Chen J (2022) Hepatic Tumor Stiffness Measured by Shear Wave Elastography is Prognostic for HCC Progression Following Treatment With Anti-PD-1 Antibodies Plus Lenvatinib: A Retrospective Analysis of Two Independent Cohorts.*
Front. Immunol. 13:868809. doi: 10.3389/fimmu.2022.868809

frontiers | Frontiers in Immunology

ORIGINAL RESEARCH
published: 22 June 2022
doi: 10.3389/fimmu.2022.892750

Identification of CFHR4 as a Potential Prognosis Biomarker Associated With Immune Infiltrates in Hepatocellular Carcinoma

Hongjun Yu[1,2†], Chaoqun Wang[1,2†], Shanjia Ke[1,2†], Miaoyu Bai[1,2†], Yanan Xu[1,2], Shounan Lu[1,2], Zhigang Feng[1,2,3], Baolin Qian[1,2], Yue Xu[4], Menghua Zhou[1,2], Zihao Li[1,2], Bing Yin[1,2], Xinglong Li[1,2], Yongliang Hua[2,5], Yongzhi Zhou[1], Shangha Pan[2], Yao Fu[6] and Yong Ma[1,2*]*

[1] Department of Minimal Invasive Hepatic Surgery, The First Affiliated Hospital of Harbin Medical University, Harbin, China, [2] Key Laboratory of Hepatosplenic Surgery, Ministry of Education, The First Affiliated Hospital of Harbin Medical University, Harbin, China, [3] The First Department of General Surgery, Affiliated Hospital of Inner Mongolia Minzu University, Tongliao, China, [4] Department of Pediatrics, Hainan Hospital of PLA General Hospital, Sanya, China, [5] Department of Pediatric Surgery, The First Affiliated Hospital of Harbin Medical University, Harbin, China, [6] Department of Ultrasound, The First Affiliated Hospital of Harbin Medical University, Harbin, China

OPEN ACCESS

Edited by:
Xuesong Gu,
Beth Israel Deaconess Medical Center and Harvard Medical School, United States

Reviewed by:
Simon John Clark,
University of Tübingen, Germany
Manish Muhuri,
Biogen Idec, United States

***Correspondence:**
Yao Fu
drfuyao@163.com
Yong Ma
mayong@ems.hrbmu.edu.cn

[†]These authors have contributed equally to this work

Specialty section:
This article was submitted to Cancer Immunity and Immunotherapy, a section of the journal Frontiers in Immunology

Received: 09 March 2022
Accepted: 16 May 2022
Published: 22 June 2022

Citation:
Yu H, Wang C, Ke S, Bai M, Xu Y, Lu S, Feng Z, Qian B, Xu Y, Zhou M, Li Z, Yin B, Li X, Hua Y, Zhou Y, Pan S, Fu Y and Ma Y (2022) Identification of CFHR4 as a Potential Prognosis Biomarker Associated With Immune Infiltrates in Hepatocellular Carcinoma. Front. Immunol. 13:892750. doi: 10.3389/fimmu.2022.892750

Background: Complement factor H-related 4 (CFHR4) is a protein-coding gene that plays an essential role in multiple diseases. However, the prognostic value of CFHR4 in hepatocellular carcinoma (HCC) is unknown.

Methods: Using multiple databases, we investigated CFHR4 expression levels in HCC and multiple cancers. The relationship between CFHR4 expression levels and clinicopathological variables was further analyzed. Various potential biological functions and regulatory pathways of CFHR4 in HCC were identified by performing a Gene Ontology (GO) analysis, Kyoto Encyclopedia of Genes and Genomes (KEGG) analysis and Gene Set Enrichment Analysis (GSEA). Single-sample gene set enrichment analysis (ssGSEA) was performed to confirm the correlation between CFHR4 expression and immune cell infiltration. The correlations between CFHR4 expression levels in HCC and N6-methyladenosine (m6A) modifications and the competing endogenous RNA (ceRNA) regulatory networks were confirmed in TCGA cohort.

Results: CFHR4 expression levels were significantly decreased in HCC tissues. Low CFHR4 expression in HCC tissues was significantly correlated with the patients' sex, race, age, TNM stage, pathological stage, tumor status, residual tumor, histologic grade and alpha fetal protein (AFP) level. GO and KEGG analyses revealed that differentially expressed genes related to CFHR4 may be involved in the synaptic membrane, transmembrane transporter complex, gated channel activity, chemical carcinogenesis, retinol metabolism, calcium signaling pathway, PPAR signaling pathway, insulin and gastric acid secretion. GSEA revealed that the FCGR-activated reaction, PLK1 pathway, ATR pathway, MCM pathway, cascade reactions of PI3K and FGFR1, reactant-mediated MAPK activation and FOXM1 pathway were significantly enriched in

HCC with low CFHR4 expression. Moreover, CFHR4 expression was inversely correlated the levels of infiltrating Th2 cells, NK CD56bright cells and Tfh cells. In contrast, we observed positive correlations with the levels of infiltrating DCs, neutrophils, Th17 cells and mast cells. CFHR4 expression showed a strong correlation with various immunomarker groups in HCC. In addition, high CFHR4 expression significantly prolonged the overall survival (OS), disease-specific survival (DSS) and progression-free interval (PFI). We observed a substantial correlation between the expression of CFHR4 and multiple N6-methyladenosine genes in HCC and constructed potential CFHR4-related ceRNA regulatory networks.

Conclusions: CFHR4 might be a potential therapeutic target for improving the HCC prognosis and is closely related to immune cell infiltration.

Keywords: CFHR4, prognosis, biomarker, immune Infiltrate, hepatocellular carcinoma

INTRODUCTION

HCC is the sixth most common cancer worldwide. Over 900,000 new cases of HCC are confirmed each year, and approximately 800,000 people die of HCC annually, making it the third most common cause of cancer-related death. The morbidity and mortality rates of HCC are 2 to 3 times higher in men than in women in most areas (1). In China, the death rate of HCC is the highest among men over 60 years of age. The number of new cases of liver cancer diagnosed each year accounts for approximately 50% of all cases worldwide. The key determinants of liver cancer are chronic HBV infection, aflatoxin exposure or both (1, 2). The development of surgical procedures has improved the survival rate of patients with early-phase HCC, but many patients already have advanced HCC at the diagnosis, resulting in a poor overall survival rate. Therefore, the identification of new, relevant biomarkers is urgently needed to improve the early diagnosis, prognostic assessment and treatment of HCC (3–5).

Research shows that the complement system is a vitally important component of innate immunity and is extensively involved in innate immune recognition, adaptive cell stimulation and proinflammatory effector responses. The complement system exerts a regulatory effect on the tumor microenvironment, influencing the outcome of the immune response (6, 7). The factor H/CFHR family includes five complement F factor H-related proteins (CFHR1/2/3/4/5), factor H and complement factor H-like protein (CFHL1) (8, 9). CFHRs are secreted plasma proteins synthesized mainly by hepatocytes. CFHR4 is a key component of the innate immune system, and its expression is restricted to the liver (10). To date, numerous studies have suggested a role for CFHR4 in immune system disorders, such as age-related macular degeneration (AMD) (10, 11), systemic lupus erythematosus (12) and atypical hemolytic uremic syndrome (AHUS) (13, 14). However, the association of CFHR4 with HCC has not yet been characterized.

The N6-methyladenosine (m6A) RNA and competing endogenous RNA (ceRNA) regulatory network is currently a new direction in cancer therapy, and the mechanisms have been extensively studied in HCC (15). Current studies mainly focus on methyltransferases, demethylases and binding proteins (16, 17). Although the mechanism of the m6A regulatory factor requires further study, the roles of the m6A regulatory factor in tumor proliferation, invasion and metastasis have been confirmed (18). In addition, ceRNA regulatory networks are also crucial for the emergence and development of multiple cancers, including ovarian cancer (19), esophageal cancer (20) and gastric cancer (21). However, no studies have examined the ceRNA regulatory network of CFHR4 in HCC or reported on its association with m6A regulators.

In the present study, we analyzed CFHR4 expression levels in HCC tumors and normal liver tissue from multiple datasets. An analysis of RNA sequencing (RNA-seq) data from TCGA revealed the clinical relevance and potential diagnostic and prognostic roles of CFHR4 in HCC. In addition, we further explored the biological significance of CFHR4 by performing enrichment analyses and a protein–protein interaction (PPI) network analysis and determining the correlation with immune cell infiltration. After analyzing the correlation of CFHR4 and m6A, we constructed ceRNA regulatory networks involving CFHR4 in HCC.

MATERIALS AND METHODS

RNA-Seq Data Source

We first collected gene expression data and clinical data from 424 patients with HCC in TCGA (https://portal.gdc.cancer.gov). In addition, the RNA sequencing data (GSE14520) were downloaded from the Gene Expression Omnibus (GEO) database. HTSeq-FPKM of level 3 format was converted into transcripts per million (TPM). Screening was performed to exclude patients with incomplete information, and the TPM data from 374 patients were used in subsequent analyses (**Supplementary Table 1**). The evolution process used the "ggplot2" R package.

Cell Lines and Cell Culture

Normal human liver cells (WRL68) were purchased from AcceGen (Fairfield, USA), and HCC cell lines (BEL7402, SK-

hep1, HCCLM3, HepG2 and Huh7) were purchased from the Chinese Academy of Science (Shanghai, China). WRL68 cells were cultured in RPMI-1640 medium, and other cell lines were cultured in DMEM supplemented with 10% FBS and 1% penicillin-streptomycin. All cells were incubated in a 37°C incubator with 5% CO_2.

HCC Tissue Collection

We collected 30 pairs of HCC tissues and adjacent liver tissues at the First Affiliated Hospital of Harbin Medical University from 2006 to 2013 after obtaining informed consent from patients. The research project was conducted under the supervision of the Ethics Committee of the First Affiliated Hospital of Harbin Medical University.

Quantitative Real-Time PCR

Quantitative real-time PCR was performed on the samples as described previously (5). The following primers were used: CFHR4-F, 5'-TGCGGTTTAAGCTCCATGACA -3'; CFHR4-R, 5'-CCCATCTTCACCACACACTATG-3'; GAPDH-F, 5' -TGA CTTCAACAGCGACACCCA-3' and GAPDH-R, 5'-CACCCT GTTGCTGTAGCCAAA-3'. GAPDH was used as a control to determine changes in mRNA levels using the $2^{-\Delta\Delta CT}$ method.

Identification of Differentially Expressed Genes

The differentially expressed genes (DEGs) between high CFHR4 expression and low CFHR4 expression samples from TCGA database were analyzed using the DEseq2 (1.26.0) R package (22) with Student's t test. Differences were considered statistically significant for an adjusted p value < 0.05 and absolute log2-fold change > 1.5. Moreover, volcano plots and heatmaps were constructed to visualize the DEGs.

Gene Set Enrichment Analysis (GSEA)

Pathway enrichment analyses were performed with the "clusterProfiler" R package (23, 24). The c2.cp.v7.2.symbols.gmt curated gene sets were retrieved from the Molecular Signatures Database (MSigDB). Each analytical technique was conducted repeatedly a thousand times. An FDR-corrected q value < 0.25 and adjusted p value< 0.05 were considered statistically significant.

ssGSEA of Immune Cell Infiltration

We analyzed the levels of infiltration of 24 types of immune cells in HCC using the ssGSEA method with the GSVA package in R. We then quantified the enrichment score for each immune cell by performing gene expression profiling of each HCC sample based on the signature of immune cells (25, 26).

Construction and Evaluation of the Nomogram

The univariate Cox regression analysis of the correlation between CFHR4 expression and the values multiple clinical prognostic parameters in patients with HCC was performed using R software with the "survival" package. Using the RMS package (version 6.2-0) and survival package (version 3.2-10), nomograms including important clinical features and calibration plots were constructed. The 45° line represents the best-predicted value, and calibration curves were graphically evaluated by mapping the nomogram-predicted probability against observed occurrences. The consistency index (C-index) was used to measure the discriminative capability of the nomogram and to compare the predictive accuracy of nomograms and individual prognostic indicators. This process was calculated using the bootstrap method and repeated 1000 times. In the present study, one-way analysis of variance (ANOVA) and two-tailed Student's t test were used to analyze the data. A P value < 0.05 was considered statistically significant.

Prediction and Construction of ceRNA Networks

The TargetScan (http://www.targetscan.org), DIANA-microT (http://diana.imis.athena-innovation.gr/DianaTools/index) and RNAinter (http://www.rnainter.org) online sites were used together to predict and analyze the target miRNAs of CFHR4, compare the correlations between the expression of CFHR4 and target miRNAs and screen miRNAs that were more compatible with ceRNA networks. The target lncRNAs of the screened miRNAs were predicted and analyzed using miRNet2.0 (www.mirnet.ca/miRNet/home.xhtml) and starBase3.0 (www.starbase.sysu.edu.cn), and the correlation between the two was further analyzed to screen for additional eligible ceRNAs. A comprehensive analysis of negatively correlated miRNA–mRNA and miRNA-lncRNA expression levels was performed to establish an HCC-related lncRNA-miRNA–mRNA (CFHR4) ceRNA network.

Statistical Analysis

The R package (version 3.6.3) was used for statistical analyses and plotting. CFHR4 expression in unpaired and paired samples was analyzed using the Wilcoxon rank sum test and Wilcoxon signed rank test, respectively, with the pROC (1.17.0.1) package for ROC analysis. In addition, the Kruskal–Wallis test and univariate Cox analysis were applied to investigate whether CFHR4 expression was associated with clinicopathological factors. Using the KM method and log-rank test, we compared the differences in 10-year OS, DSS and PFI between patients with high CFHR4 expression and those with low CFHR4 expression in TCGA. In all studies, a P value < 0.05 was defined as statistically significant.

RESULTS

CFHR4 Expression Is Downregulated in HCC

By analyzing GTEx and TCGA datasets, we investigated the CFHR4 mRNA levels across cancer types using the Wilcoxon rank sum test, including adrenocortical carcinoma (ACC), bladder urothelial carcinoma (BLCA), breast invasive carcinoma (BRCA), cervical squamous cell carcinoma and endocervical adenocarcinoma (CESC), cholangiocarcinoma (CHOL), colon adenocarcinoma (COAD), esophageal carcinoma (ESCA), glioblastoma multiforme (GBM), head and neck squamous cell carcinoma (HNSC), kidney

chromophobe (KICH), kidney renal clear cell carcinoma (KIRC), kidney renal papillary cell carcinoma (KIRP), acute myeloid leukemia (LAML), brain lower grade glioma (LGG), liver hepatocellular carcinoma (LIHC), lung adenocarcinoma (LUAD), lung squamous cell carcinoma (LUSC), mesothelioma (MESO), ovarian serous cystadenocarcinoma (OV), pancreatic adenocarcinoma (PAAD), pheochromocytoma and paraganglioma (PCPG), prostate adenocarcinoma (PRAD), rectum adenocarcinoma (READ), stomach adenocarcinoma (STAD), skin cutaneous melanoma (SKCM), testicular germ cell tumors (TGCT), thyroid carcinoma (THCA), uterine corpus endometrial carcinoma (UCEC) and uterine carcinosarcoma (UCS). We found that CFHR4 expression was significantly decreased in LIHC and CHOL compared with normal tissues (**Figure 1A**). We obtained similar results from the Timer and GEPIA databases (**Supplementary Figures 1A, B**). According to the expression of CFHR4 in 374 HCC tissues and 50 normal liver tissues, we confirmed that the CFHR4 expression level was also noticeably decreased in HCC tissues ($P<0.001$) (**Figure 1B**). Furthermore, CFHR4 was underexpressed in the GSE14520 HCC cohort ($P<0.001$) (**Figure 1C**). Similar results were obtained for adjacent HCC tissues among the 50 matched HCC tissues and adjacent HCC tissues ($P<0.05$) (**Figure 1D**). We extracted protein from human normal hepatic cells (WRL68) and HCC cells (BEL7402, SK-hep1, HCCLM3, HepG2 and Huh7) and confirmed the low expression of CFHR4 in HCC cells using Western blot (**Figure 1E**). Subsequently, 30 pairs of HCC samples were validated, and similar conclusions were reached (**Figure 1F**). CFHR4 mRNA expression levels were further validated using quantitative real-time PCR analyses ($P<0.001$) (**Figures 1G, H**). In addition, we constructed the receiver operating characteristic (ROC) curve. The area under the curve (AUC) for CFHR4 was 0.698, and it has a significant diagnostic value for HCC (**Figure 1I**).

Identification of DEGs in HCC

According to the CFHR4 expression level, we divided the data from patients with HCC into high and low CFHR4 expression groups for comparison. The DESeq2 package was used to infer CFHR4-associated genes and analyze the DEGs between the high and low expression groups. An adjusted p value < 0.05 and absolute log2-fold change > 1.5 were considered statistically significant. A total of 721 significant DEGs were identified. 113 DEGs were associated with the high CFHR4 expression group, and 608 DEGs were associated with the low CFHR4 expression group (**Figure 1J** and **Supplementary Table 2**). The top 10 DEGs were identified, further analyzed using HTSeq-Counts and sorted by relative expression (**Figure 1K**).

GO and KEGG Enrichment Analyses

GO and KEGG enrichment analyses were performed using the "clusterProfiler" R package to further analyze the potential biological functions of CFHR4-related DEGs. The GO analysis indicated that CFHR4-related DEGs may be involved in gated channel activity, regulation of signal release, regulation of ion transmembrane transport, metal ion transmembrane transporter activity, synaptic membrane, transmembrane transporter complex and passive transmembrane transporter activity (**Figures 2A, B**; **Supplementary Table 3**). In the KEGG enrichment analysis, CFHR4-related DEGs were mainly involved in chemical carcinogenesis, retinol metabolism, the calcium signaling pathway, the PPAR signaling pathway, bile secretion, insulin secretion and gastric acid secretion (**Figures 2C, D**).

CFHR4-Related Signaling Pathways Based on GSEA

GSEA was conducted between the high and low CFHR4 expression groups to further reveal CFHR4-related signaling pathways in HCC. The following pathways were significantly enriched in patients with low CFHR4 expression: FCGR-activated reaction, PLK1 pathway, reactant FCERI-mediated MAPK activation, ATR pathway, MCM pathway, cascade reaction of PI3K and FGFR1, reactant-mediated MAPK activation and FOXM1 pathway (**Figures 2E–J**; **Supplementary Table 4**).

PPI Network Analysis

We explored the association between 721 DEGs in the HCC group using the STRING database by setting the interaction threshold to 0.70 and constructed a PPI network to further investigate the underlying mechanisms (**Figure 3A**; **Supplementary Table 5**). Subsequently, 301 proteins and 420 edges were screened, and five central gene clusters were identified using a total score ≥5000 (**Figures 3B–F**). In addition, the top 7 central genes were screened, including CENPA, CDC20, UBE2C, CEP55, BIRC5, FAM64A and TRIP13 (**Figure 3G**). By analyzing the GeneMANIA and STRING online datasets, potential CFHR4-interacting target genes were identified (**Supplementary Figures 2A, B**). CFHR4-related genes were selected by performing a crossover analysis, including C3, CRP, CFHR1, CFHR3 and CFHR5 (**Supplementary Figure 2C**). We subsequently analyzed the association between CFHR4 and the 5 intersecting genes (**Supplementary Figures 2D–H**).

Correlation Between CFHR4 Expression and Immune Cell Infiltration

Based on the ssGSEA algorithm, we confirmed and quantified the correlations between CFHR4 expression and the immune cell infiltration levels (**Figure 4A**). The expression of CFHR4 was negatively correlated with aDCs, TFH cells, NK CD56bright cells and Th2 cells, and it has positive correlations with Th17 cells, DCs, neutrophils, mast cells, Tgd cells, Tcm cells, cytotoxic cells, Tregs, NK cells, pDCs, eosinophils, iDCs, B cells, T cells, CD8 T cells, Tems, NK CD56dim cells, T helper cells, macrophages and Th1 cells (**Figures 4B–H**). We further confirmed the correlation between CFHR4 expression with immunomarker of various immune cells in HCC. The results showed that CFHR4 expression was significantly correlated with the immunomarkers IRF5 and INOS of M1 macrophages in HCC (**Table 1**). It indicated that CFHR4 may induce macrophages to M1 polarization in HCC. This analysis of immune markers of different functions T cells showed that CFHR4 expression was highly correlated with the most immunomarkers (CD8B, CD3D, STAT1, IFN-γ, STAT5A, IL21, TGFβ, PD-1, CTLA4, LAG3 and TIM-3) of T cells in HCC (**Table 1**). It turns out that CFHR4 may perform an indispensable role in the T cells' immune response to HCC. Especially for T cells

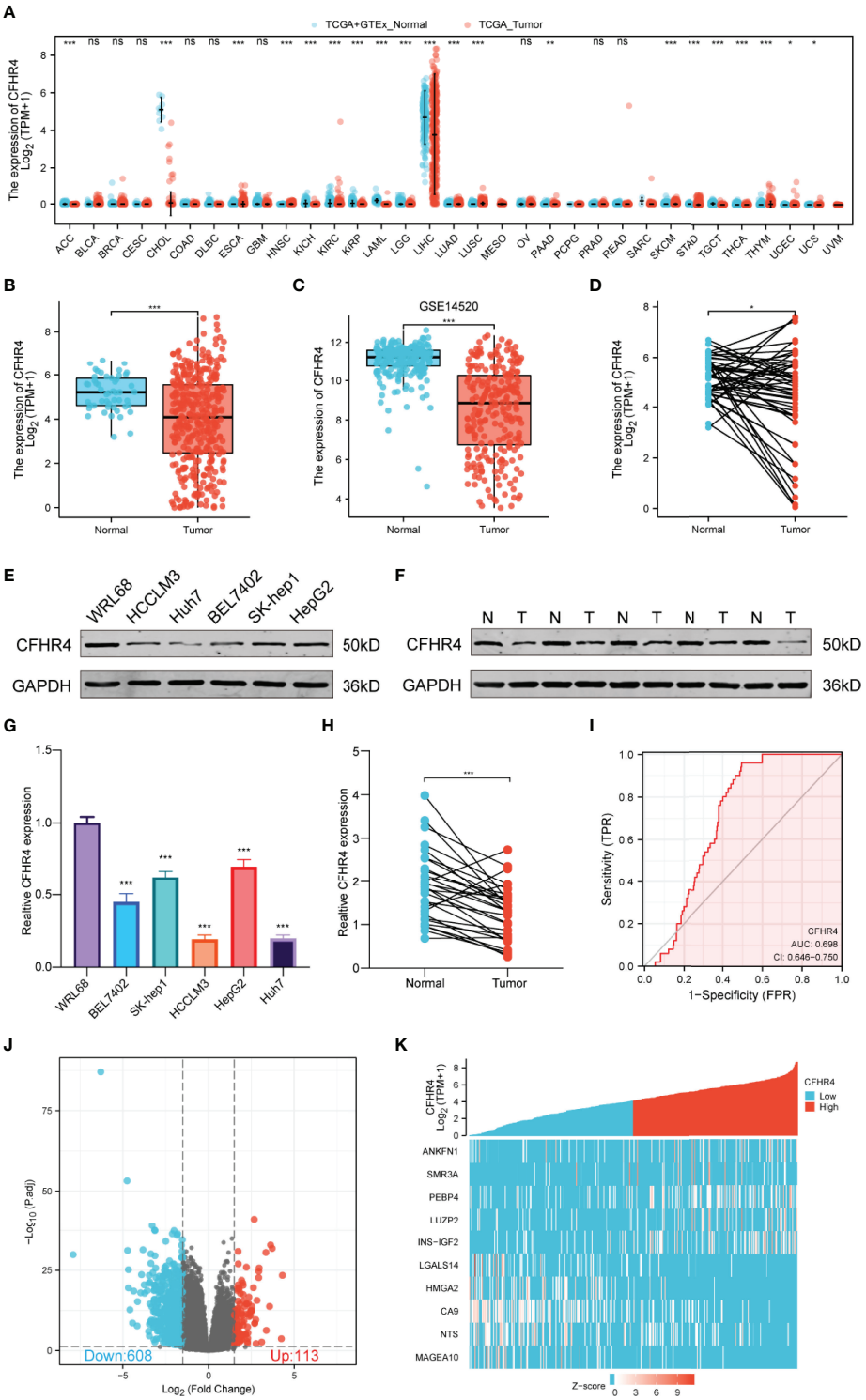

FIGURE 1 | Differences in the expression of CFHR4 and CFHR4-associated DEGs. **(A)** CFHR4 expression levels in different cancer tissues compared to normal tissues (TCGA). **(B–D)** CFHR4 expression in HCC samples. **(E)** CFHR4 expression was detected in WRL68, BEL7402, SK-Hep1, HCCLM3, HepG2, and Huh7 cell lines using Western blotting. **(F)** CFHR4 protein expression in 30 paired adjacent noncancerous tissues and HCC tissues. **(G)** CFHR4 expression was detected in WRL68, BEL7402, SK-Hep1, HCCLM3, HepG2, and Huh7 cell lines using PCR. **(H)** CFHR4 mRNA expression in 30 paired adjacent noncancerous tissues and HCC tissues. **(I)** ROC curves were created to investigate the value of CFHR4 in identifying HCC tissues. **(J, K)** Volcano plots of the DEGs and heatmap showing the top 10 DEGs. *$p < 0.05$, **$p < 0.01$, ***$p < 0.001$, NS, no significance.

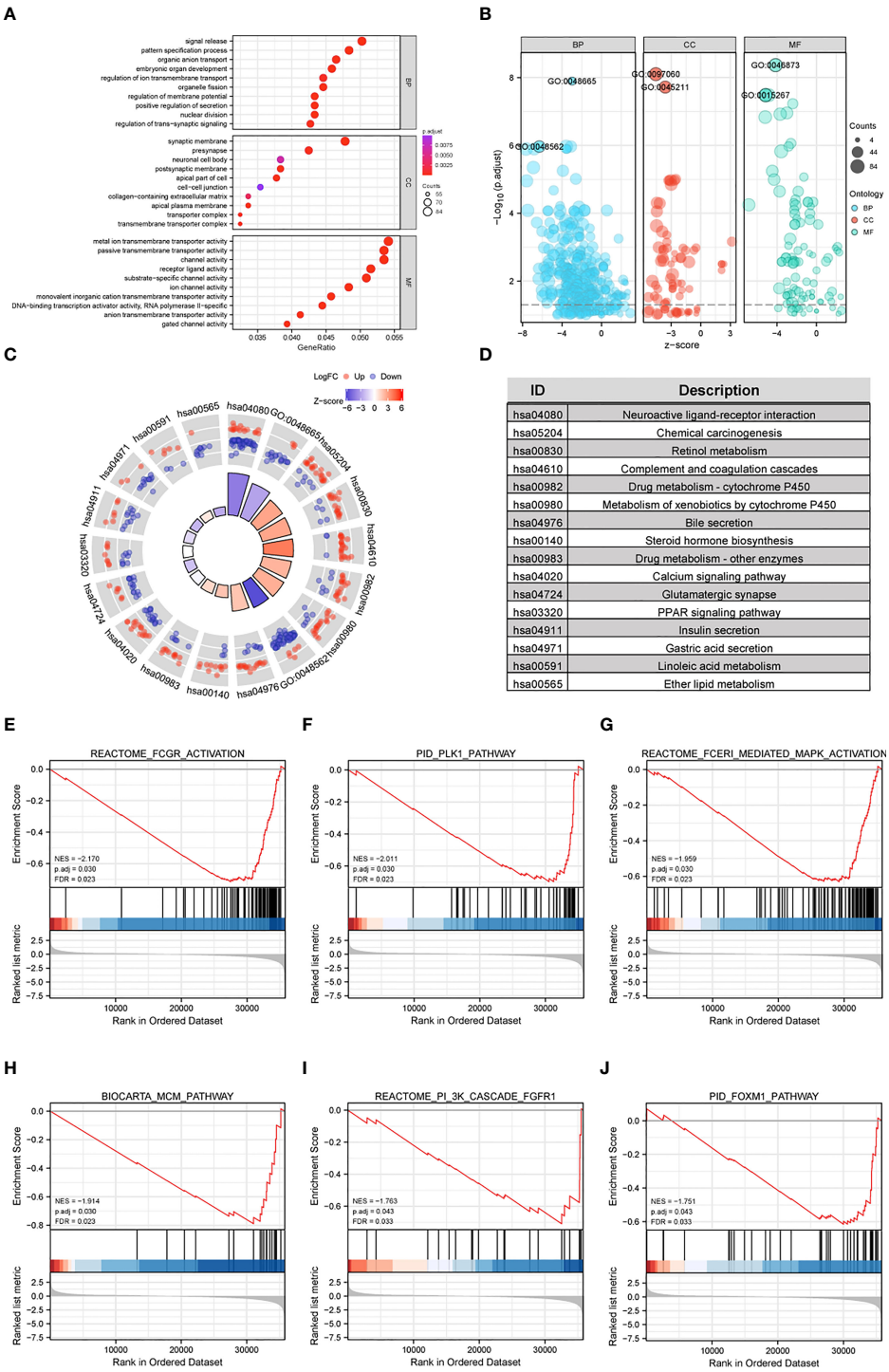

ID	Description
hsa04080	Neuroactive ligand-receptor interaction
hsa05204	Chemical carcinogenesis
hsa00830	Retinol metabolism
hsa04610	Complement and coagulation cascades
hsa00982	Drug metabolism - cytochrome P450
hsa00980	Metabolism of xenobiotics by cytochrome P450
hsa04976	Bile secretion
hsa00140	Steroid hormone biosynthesis
hsa00983	Drug metabolism - other enzymes
hsa04020	Calcium signaling pathway
hsa04724	Glutamatergic synapse
hsa03320	PPAR signaling pathway
hsa04911	Insulin secretion
hsa04971	Gastric acid secretion
hsa00591	Linoleic acid metabolism
hsa00565	Ether lipid metabolism

FIGURE 2 | Functional enrichment analyses of CFHR4-related genes in HCC. **(A, B)** The enriched terms in GO categories in HCC. **(C, D)** KEGG pathway analysis based on CFHR4-associated DEGs. **(E–J)** GSEA enrichment plots, including FCGR, activated reaction, PLK1 pathway, reactant FCERI-mediated MAPK activation, ATR pathway, MCM pathway, cascade reactions of PI3K and FGFR1, reactant-mediated MAPK activation and FOXM1 pathway.

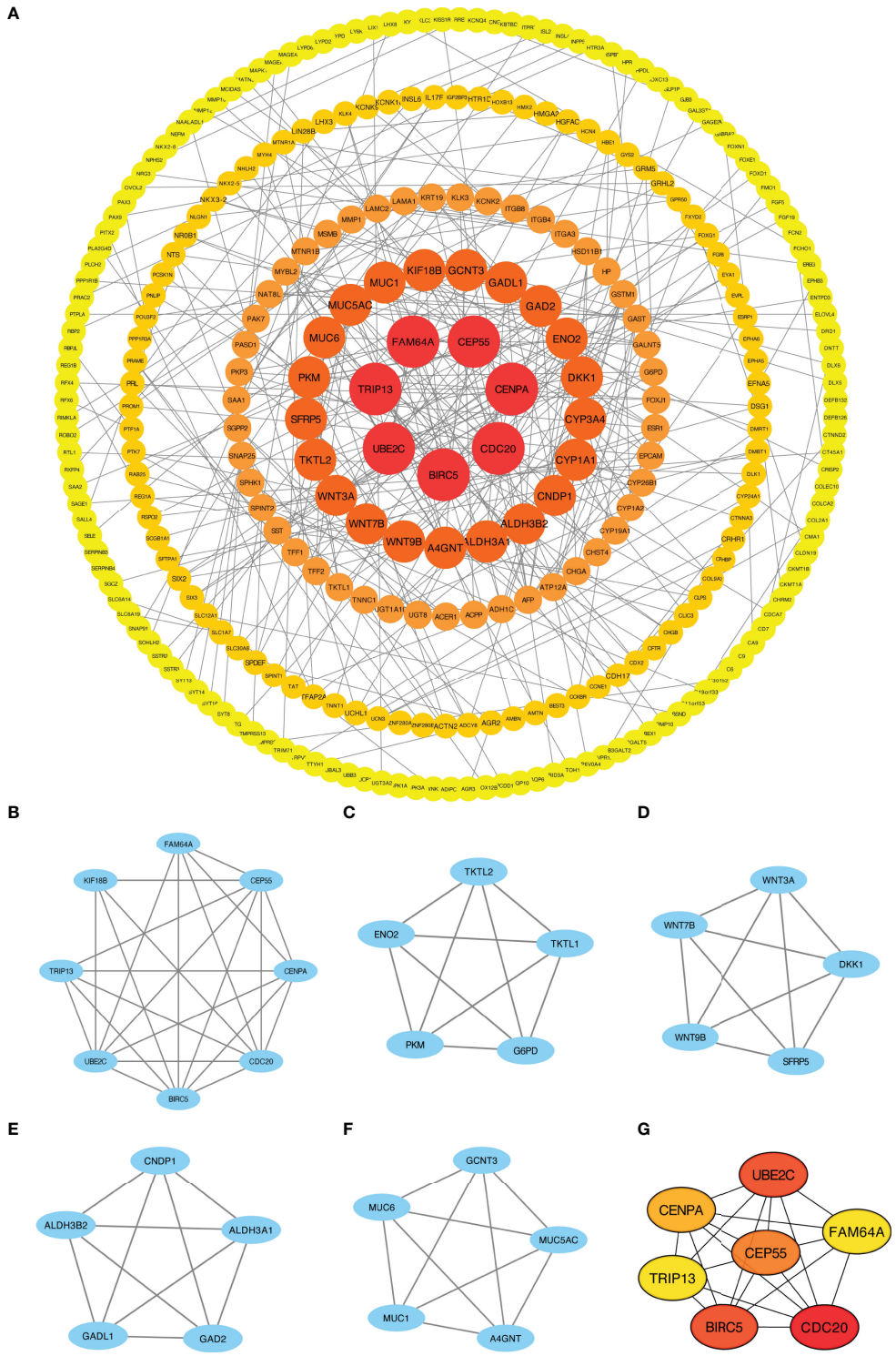

FIGURE 3 | PPI network enrichment analysis. **(A)** The PPI network was built based on PPI pairs identified by the STRING dataset. **(B–F)** Hub gene clusters were selected from the PPI network (criteria of total scores ≥ 5,000). **(G)** Top 7 hub genes in the PPI network.

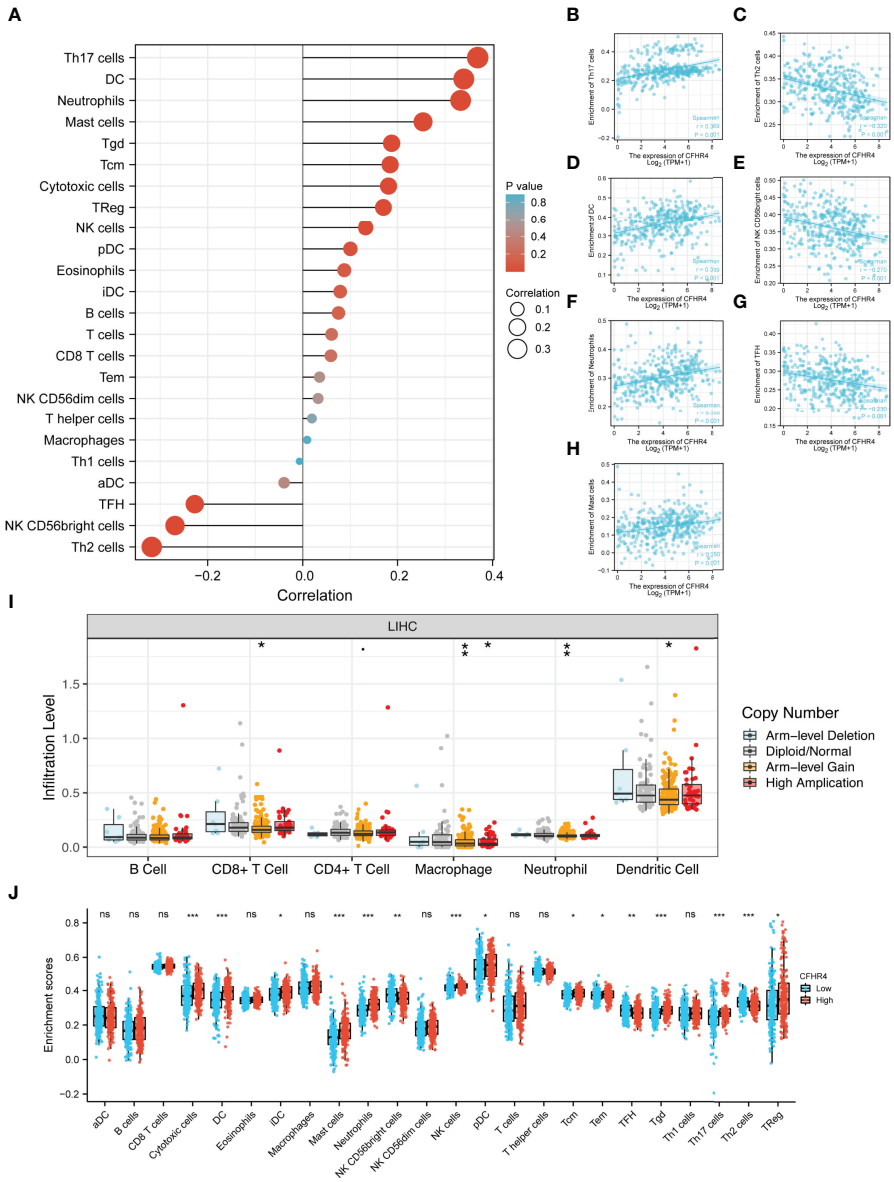

FIGURE 4 | Integrative analysis of CFHR4 expression in the infiltrating immune microenvironment. **(A)** The forest plot depicts the relationship between the level of CFHR4 expression and the relative abundances of 24 immune cells. **(B–H)** Scatter plots showing the differentiation of Th17 cells, Th2 cells, DCs, NK CD56bright cells, neutrophils, TFH cells and mast cells infiltration levels between high and low groups of CFHR4 expression. **(I)** The SCNA showed that CFHR4 expression correlated with the level of immune cell infiltration. **(J)** Scatter plots showing the correlations between 24 immune cells and CFHR4 expression levels. *p < 0.05, **p < 0.01, ***p < 0.001, NS, no significance.

exhaustion, consistent results with the GISTIC analysis were obtained. The somatic copy number alteration (SCNA) module demonstrated that the arm-level deletion of CFHR4 was markedly associated with immune cell infiltration levels in HCC (**Figure 4I**). In addition, the results also showed a correlation between CFHR4 expression and the immunomarkers of TAMs, neutrophils and dendritic cells (**Table 1**). Subsequently, according to the expression level of CFHR4, HCC samples were dichotomized into CFHR4-high and low expression groups, we aimed to reveal whether different expression groups of CFHR4 differ in the tumor immune microenvironment of HCC (**Figure 4J**). We found that cytotoxic cells, DCs, iDCs, mast cells, neutrophils, NK cells, pDCs, Tcm cells, Tem cells, Tgd cells, Th17 cells and Tregs were increased in the CFHR4 high expression group ($P < 0.05$), while the NK CD56bright cells, TFH cells and Th2 cells decreased ($P < 0.05$). These findings confirmed that reduced expression of CFHR4 in HCC was closely associated with immune cell infiltration.

TABLE 1 | Correlation analysis between CFHR4 expression and biomarkers of immune cells.

Description	Gene markers	LIHC	
		Cor	P value
CD8+ T cell	CD8A	−0.074	0.152
	CD8B	−0.120	**0.017**
T cell (general)	**CD3D**	−0.200	**< 0.001**
	CD3E	−0.054	0.301
	CD2	−0.089	0.087
B cell	**CD19**	−0.140	**0.006**
	CD79A	−0.072	0.165
Monocyte	**CD86**	−0.170	**0.001**
	CD115 (CSF1R)	−0.072	0.165
TAM	CCL2	−0.005	0.922
	CD68	−0.210	**< 0.001**
	IL10	−0.110	**0.04**
M1 Macrophage	**INOS (NOS2)**	0.22	**< 0.001**
	IRF5	−0.230	**< 0.001**
	COX2 (PTGS2)	0.006	0.9
M2 Macrophage	CD163	0.079	0.129
	VSIG4	0.03	0.564
	MS4A4A	0.063	0.223
Neutrophils	**CD66b (CEACAM8)**	−0.120	**0.021**
	CD11b (ITGAM)	−0.130	**0.009**
	CCR7	0.12	**0.023**
Natural killer cell	KIR2DL1	0.064	0.215
	KIR2DL3	−0.047	0.367
	KIR2DL4	−0.069	0.183
	KIR3DL1	−0.009	0.866
	KIR3DL2	0.026	0.612
	KIR3DL3	−0.065	0.209
	KIR2DS4	0.005	0.929
	HLA-DPB1	−0.110	**0.038**
	HLA-DQB1	−0.043	0.411
	HLA-DRA	−0.003	0.956
	HLA-DPA1	0.051	0.327
	BDCA-1 (CD1C)	0.005	0.926
Dendritic cell	**BDCA-4 (NRP1)**	−0.110	**0.028**
	CD11c (ITGAX)	−0.160	**0.002**
Th1	T-bet (TBX21)	0.061	0.239
	STAT4	−0.091	0.078
	STAT1	−0.120	**0.016**
	IFN-γ (IFNG)	−0.110	**0.03**
	TNF-α (TNF)	−0.069	0.182
Th2	GATA3	−0.094	0.069
	STAT6	0.03	0.568
	STAT5A	−0.190	**< 0.001**
	IL13	−0.013	0.802
Tfh	BCL6	−0.022	0.669
	IL21	−0.110	**0.041**
	STAT3	0.082	0.113
	IL17A	0.035	0.496
Th17	FOXP3	0.08	0.123
	CCR8	−0.081	0.116
	STAT5B	−0.016	0.763
	TGFβ (TGFB1)	−0.260	**< 0.001**
T cell exhaustion	**PD-1 (PDCD1)**	−0.220	**< 0.001**
	CTLA4	−0.200	**< 0.001**
	LAG3	−0.240	**< 0.001**
	TIM-3 (HAVCR2)	−0.190	**< 0.001**
	GZMB	−0.086	0.098
Treg	FOXP3	0.08	0.123

The bold values indicates that the correlation analysis between CFHR4 and biomarker of immune cell is statistically significant.

Correlation Between the CFHR4 Expression Level and Clinical Characteristics

The clinical data from patients with HCC in TCGA database were obtained to investigate the clinical characteristics of patients with different CFHR4 expression levels. After removing patients with incomplete clinical data, 374 patients remained for further analysis; the average age was 61.5 years (49.25 to 70.00 years), and 67% were male. **Table 2** provides a detailed description of the clinical data. We evaluated the differences in clinicopathological variables after stratifying patients based on CFHR4 expression using the Kruskal–Wallis test, and the level of CFHR4 was strongly correlated with age, sex, race, TNM stage, histologic grade, pathological stage, tumor status, residual tumor,

TABLE 2 | The correlations between clinicopathological variables and CFHR4 expression.

Characteristic	Low expression of CFHR4	High expression of CFHR4	p
n	187	187	
Gender, n (%)			0.122
Female	68 (18.2%)	53 (14.2%)	
Male	119 (31.8%)	134 (35.8%)	
Race, n (%)			< 0.001
Asian	100 (27.6%)	60 (16.6%)	
Black or African American	6 (1.7%)	11 (3%)	
White	78 (21.5%)	107 (29.6%)	
Age, n (%)			0.011
<=60	101 (27.1%)	76 (20.4%)	
>60	85 (22.8%)	111 (29.8%)	
T stage, n (%)			0.017
T1	78 (21%)	105 (28.3%)	
T2	51 (13.7%)	44 (11.9%)	
T3	50 (13.5%)	30 (8.1%)	
T4	8 (2.2%)	5 (1.3%)	
N stage, n (%)			0.128
N0	136 (52.7%)	118 (45.7%)	
N1	4 (1.6%)	0 (0%)	
M stage, n (%)			0.628
M0	145 (53.3%)	123 (45.2%)	
M1	3 (1.1%)	1 (0.4%)	
Pathologic stage, n (%)			0.004
Stage I	74 (21.1%)	99 (28.3%)	
Stage II	45 (12.9%)	42 (12%)	
Stage III	55 (15.7%)	30 (8.6%)	
Stage IV	4 (1.1%)	1 (0.3%)	
Tumor status, n (%)			0.001
Tumor free	85 (23.9%)	117 (33%)	
With tumor	92 (25.9%)	61 (17.2%)	
Residual tumor, n (%)			0.321
R0	164 (47.5%)	163 (47.2%)	
R1	11 (3.2%)	6 (1.7%)	
R2	0 (0%)	1 (0.3%)	
Histologic grade, n (%)			< 0.001
G1	17 (4.6%)	38 (10.3%)	
G2	77 (20.9%)	101 (27.4%)	
G3	80 (21.7%)	44 (11.9%)	
G4	11 (3%)	1 (0.3%)	
AFP (ng/ml), n (%)			< 0.001
<=400	87 (31.1%)	128 (45.7%)	
>400	46 (16.4%)	19 (6.8%)	

vascular invasion and AFP level (**Figures 5A–L**). Notably, CFHR4 was expressed at higher levels in the older age group (age>60 years) than in the younger age group (age ≤ 60 years) (P<0.05). Significant differences in CFHR4 expression levels were also noted in different races (P<0.001). Moreover, a higher histological grade, TNM grade, pathological stage and tumor status were also significantly associated with low CFHR4 expression. Subsequently, we further confirmed the lower CFHR4 expression level in the group with a high AFP level (>400 ng/mL) (P<0.001). Based on these results, patients with HCC presenting lower CFHR4 expression seemed to have a more advanced tumor stage.

Prognostic Potential of CFHR4 in HCC

Afterward, we performed a series of studies to determine the association of CFHR4 expression levels with the prognosis of patients with HCC. The Kaplan–Meier Plotter analysis revealed an association between low CFHR4 expression and a poor prognosis (**Figures 6A–C**). Moreover, we performed subgroup analyses of OS, DSS and PFI. Patients with high CFHR4 expression had a correspondingly better prognosis for OS, DSS and PFI in the Asian group (**Figures 6D–F**). However, OS, DSS and PFI in the white and black or African–American subgroups were not significantly different (**Supplementary Figures 3A–C**). In addition, patients with HCC presenting high CFHR4 expression who were aged ≤ 60 years experienced longer OS and DSS but had a worse prognosis in terms of PFI (**Figure 6G–I**). However, no significant differences were observed in the younger age subgroups for OS, DSS and PFI (age ≤ 60 years) (**Supplementary Figures 3D–F**). We further confirmed that the T3 and T4 subgroups and the stage III and stage IV subgroups experienced poorer OS (**Supplementary Figures 3G, H**).

A univariate Cox regression analysis was performed with TNM stage, pathological grade, tumor status and CFHR4 expression levels to further identify factors associated with different prognoses (**Supplementary Table 6**). The forest plot illustrated that low expression of CFHR4 was a risk factor for the

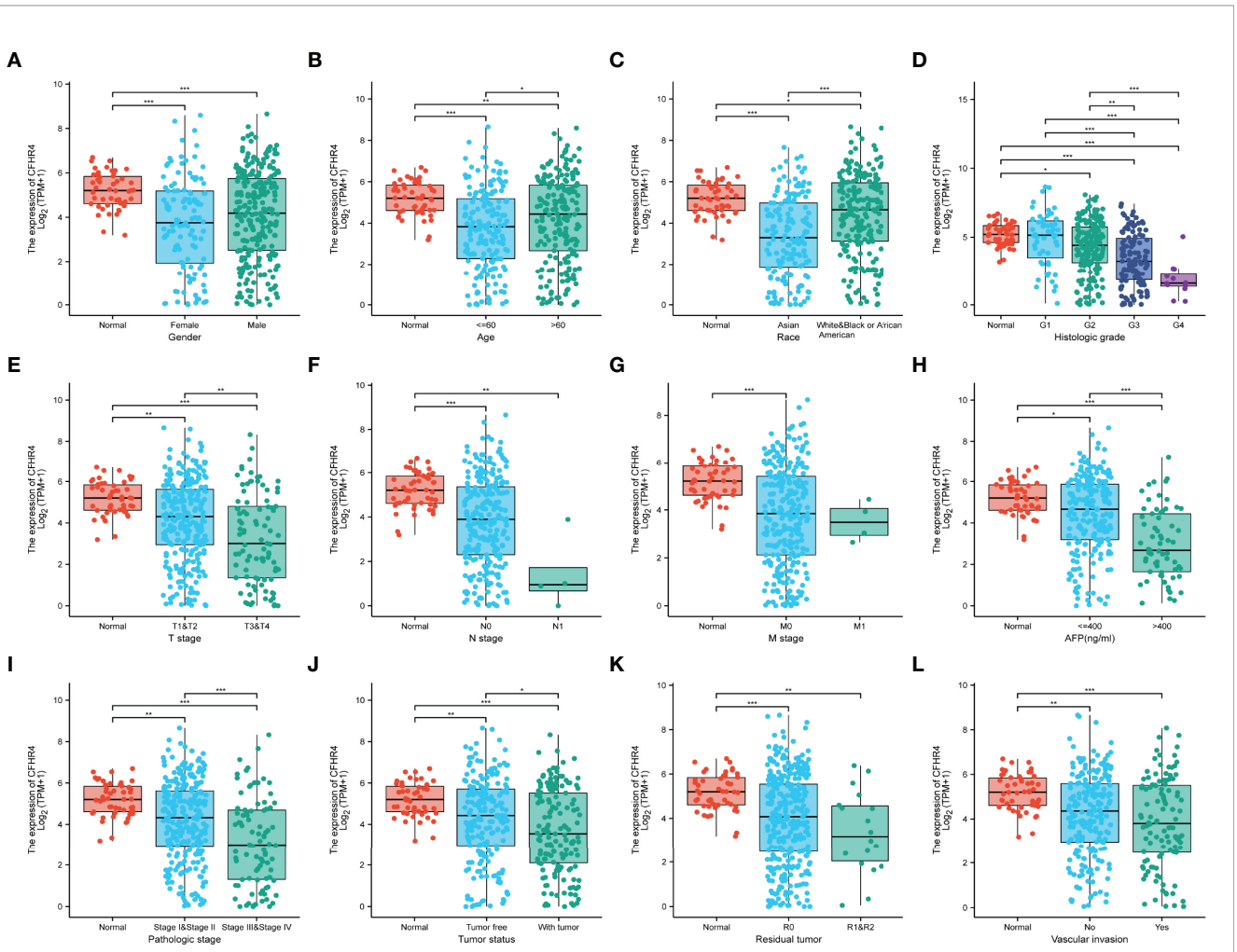

FIGURE 5 | Correlation of CFHR4 expression with clinicopathological characteristics. **(A)** Sex. **(B)** Age. **(C)** Race. **(D)** Histologic grade. **(E)** T stage. **(F)** N stage. **(G)** M stage. **(H)** AFP level. **(I)** Pathological stage. **(J)** Tumor status. **(K)** Residual tumor. **(L)** Vascular invasion. *p < 0.05, **p < 0.01, ***p < 0.001.

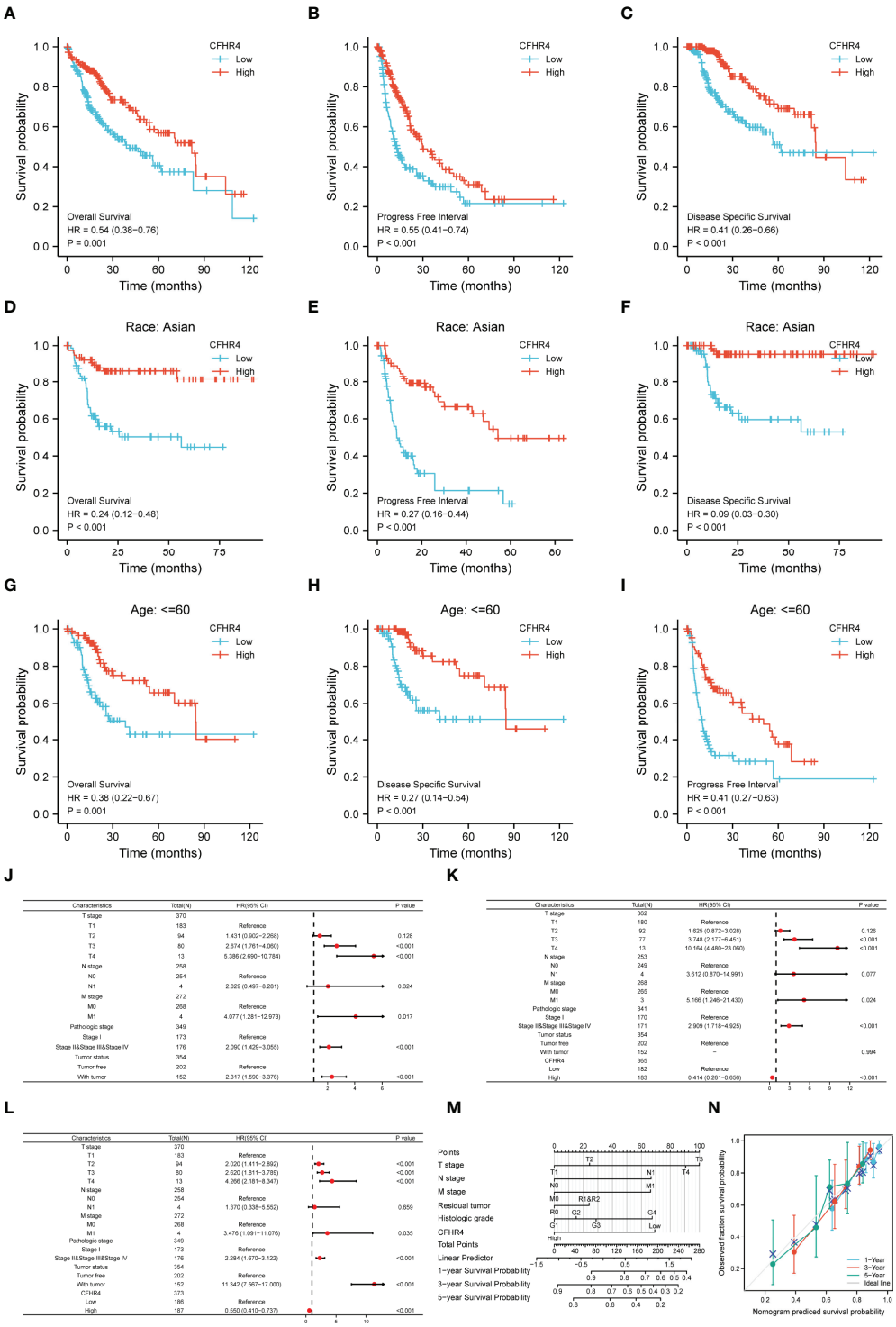

FIGURE 6 | The prognostic value of CFHR4 in HCC. **(A–C)** Survival curves showing a comparison of OS, DSS and PFI between patients with HCC presenting high and low CFHR4 expression. **(D–F)** OS, DSS and PFI survival curves for Asian patients with HCC presenting high and low CFHR4 expression. **(G–I)** OS, DSS and PFI survival curves for patients with HCC aged ≤60 years presenting with high and low CFHR4 expression. **(J–L)** Univariate survival analysis of OS, PFI, and DSS in patients from different subgroups stratified according to TNM stage, pathological grade, tumor status, and CFHR4 expression levels. **(M)** For patients with HCC, a nomogram was constructed to estimate the probability of 1-, 3-, and 5-year OS. **(N)** Nomogram calibration plots for determining the probability of OS at 1, 3, and 5 years.

OS (**Figure 6J**; **Supplementary Table 7**), DSS (**Figure 6K**; **Supplementary Table 6**) and PFI (**Figure 6L**; **Supplementary Table 8**) of patients with HCC. According to the results of the univariate Cox regression analysis, CFHR4 expression and other independent clinicopathological factors were used to construct the point scale of the nomogram. Each variable was scored with reference to the scale of the nomogram, and the total scores were dispatched to the outcome line and predicted the prognosis of patients with at 1, 3 and 5 years. The C-index of the nomogram was 0.706 (95% confidence interval: 0.671-0.741). This result suggested that the prognostic nomogram of CFHR4 had good discriminatory power (**Figure 6M**). The deviation correction line in the calibration analysis approached the ideal curve, indicating that the predicted values were consistent with the observed values (**Figure 6N**). Consistent results were obtained with the univariate Cox regression analysis.

CFHR4 Expression Is in Associated With m6A RNA Methylation Regulators in HCC

As reported in previous studies, m6A RNA methylation exerts an important effect on the development of HCC (27–29). The correlations between CFHR4 expression and the expression of 23 m6A-related genes were analyzed in TCGA (**Figure 7A**). The correlation analysis showed significant negative correlations between the expression of CFHR4 ($P < 0.05$) and 15 m6A-related genes in HCC (**Figures 7B–P**). Furthermore, groups were established based on the median CFHR4 expression, and 211 patients were assigned to the high expression group and 210 patients were assigned to in the low expression group. We determined the relationship between the CFHR4 expression level and m6A modification level in HCC by analyzing the differential expression of 23 m6A-related genes in different expression groups (**Figure 7Q**). The expression of YTHDC1, IGF2BP1, IGF2BP2, IGF2BP3, YTHDF1, YTHDF2, HNRNPA2B1, LRPPRC, HNRNPC, RBMX, METTL16, METTL3, RBM15, RBM15B, VIRMA, WTAP and ALKBH5 was reduced in the high CFHR4 expression group ($P < 0.05$). In summary, a strong correlation was observed between m6A RNA methylation in HCC and the CFHR4 expression level.

Construction of a CFHR4-Related ceRNA Triple Regulatory Network

Accumulating evidence highlights the regulatory role of lncRNA–miRNA–mRNA ceRNA networks in cancers. Therefore, we analyzed and constructed a ceRNA regulatory network for CFHR4 in HCC. Through TargetScan, DIANA-microT and RNAinter database predictions, the following 11 miRNAs were jointly predicted: hsa-miR-32-3p, hsa-miR-142-5p, hsa-miR-146a-5p, hsa-miR-302c-5p, hsa-miR-361-5p, hsa-miR-4775, hsa-miR-4786-5p, hsa-miR-4795-3p, hsa-miR-5590-3p, hsa-miR-580-3p and hsa-miR-590-3p (**Figure 8A**). Based on the regulatory relationship in the ceRNA network, a negative correlation was observed between mRNAs and miRNAs. Four miRNAs negatively correlated with CFHR4 expression were identified and screened by performing a correlation analysis. The scatter plots showed the correlation between CFHR4 expression and the target miRNAs, and the TargetScan database was used to predict the potential binding sites in CFHR4 for target miRNAs (**Figures 8B–E**). Subsequently, the lncRNAs that may interact with the target miRNAs (hsa-miR-146a-5p, hsa-miR-361-5p and hsa-miR-580-3p) were further predicted using the miRNet and starBase databases (**Figures 8F–H**). This interaction is due to the negative correlation between the expression of lncRNAs and miRNAs. Consequently, using the starBase database, we further screened and confirmed the lncRNAs in HCC that were negatively correlated with the three target miRNAs. Based on these results, the following 10 ceRNA regulatory networks that play a role in HCC were constructed: TMEM161B-AS1-hsa-miR-146a-5p-CFHR4, CCDC183-AS1-hsa-miR-146a-5p-CFHR4, NEAT1-hsa-miR-146a-5p-CFHR4, MALAT1-hsa-miR-146a-5p-CFHR4, XIST-hsa-miR-146a-5p-CFHR4, DNAAF4-CCPG1-hsa-miR-361-5p-CFHR4, NEAT1-hsa-miR-580-3p-CFHR4, LINC00641-hsa-miR-580-3p-CFHR4, DNAAF4-CCPG1-hsa-miR-580-3p-CFHR4 and DSCAM-AS1-hsa-miR-580-3p-CFHR4 (**Figure 8I**).

DISCUSSION

The CFHR family consists of five highly related proteins. Each CFHR gene has a completely duplicated structural domain in the plasma proteins, and they share high sequence identity (8, 9). Members of the CFHR family of proteins play key roles in the progression of multiple diseases through multiple mechanisms. For example, CFHR1 exacerbates atherosclerotic cardiovascular disease by altering the expression levels of C-reactive protein apolipoprotein and serum amyloid protein A (30). All CFHR genes are genetic risk factors for AMD (31). The CFHR family of genes is also important in AHUS and C3 glomerulopathy (11, 13, 32). In addition, some members of the CFHR family of proteins have been proven to exert a marked effect on the progression of a variety of cancers (33–35). However, few studies on CFHR4 have been conducted, and no studies have determined its role in cancer.

In the present study, we measured the expression level and prognostic value of CFHR4. We confirmed that CFHR4 mRNA expression was markedly downregulated in HCC and CHOL tissues, and these results were validated in multiple databases. The ROC curve analysis suggested that CFHR4 may be a promising diagnostic biomarker for differentiating HCC from normal tissue.

We confirmed the reduced expression of CFHR4 in HCC cell lines and HCC samples by performing *in vitro* experiments. We analyzed the DEGs related to CFHR4 to further assess the role of CFHR4 in HCC. By conducting GO and KEGG analyses, we found that differences in CFHR4 expression were significantly correlated with regulating signal release, regulation of ion transmembrane transport, gated channel activity, metal ion transmembrane transporter activity, calcium signaling pathway and the PPAR signaling pathway. Using GSEA, we also revealed that low CFHR4 expression was significantly associated with FCGR-activated reactions, the PLK1 pathway, reactant FCERI-

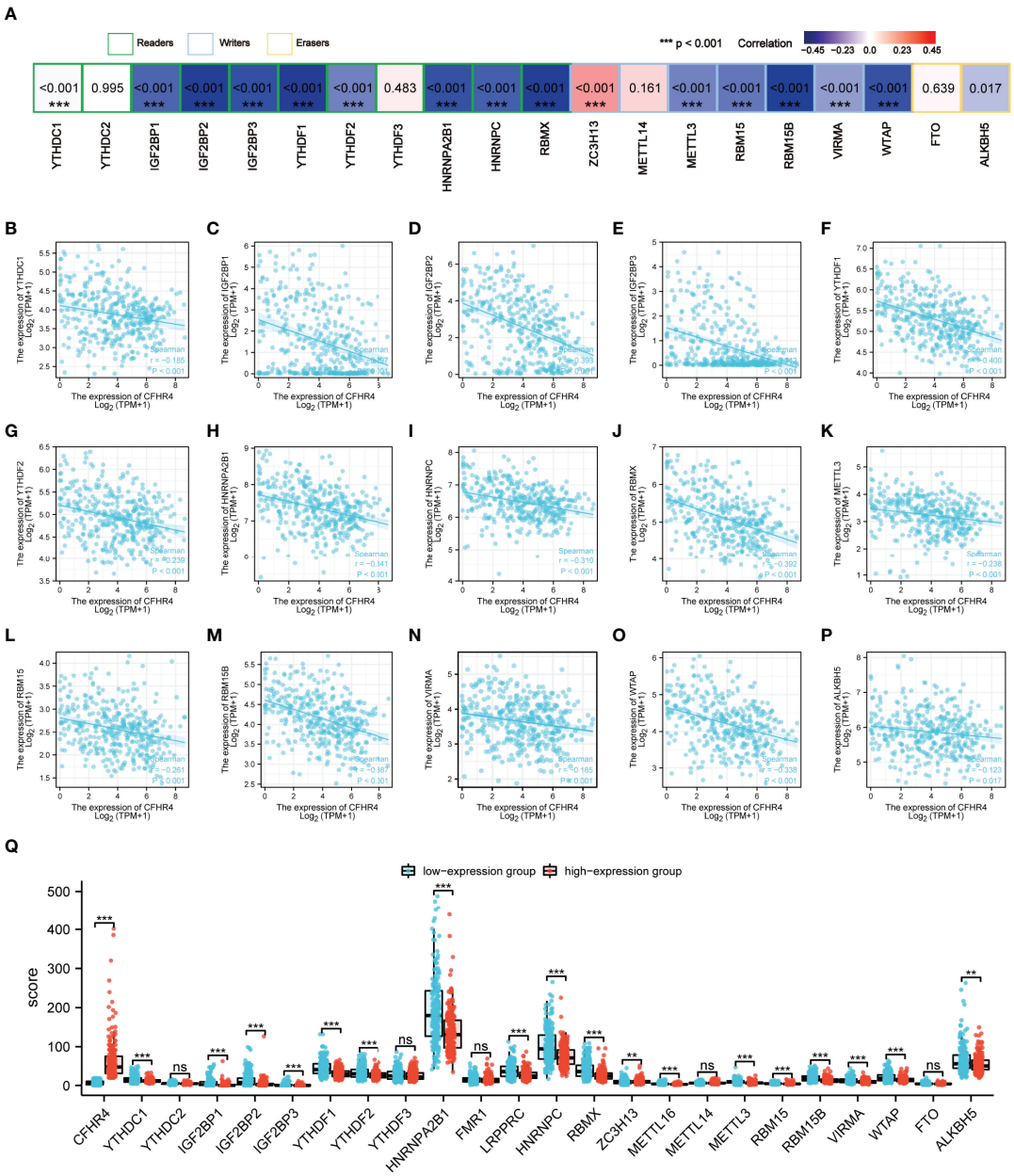

FIGURE 7 | Analysis of the association between the CFHR4 expression level and the expression of m6A-related genes in HCC. **(A)** Correlation of CFHR4 expression levels with m6A gene expression in HCC. **(B–P)** Scatter plot showing the relationship between CFHR4 and m6A genes. **(Q)** Correlation of m6A genes in the CFHR4 high and low expression groups of HCC tumor samples. **p < 0.01, ***p < 0.001, NS, no significance.

mediated MAPK activation, the ATR pathway, the MCM pathway, the cascade reactions of PI3K and FGFR1, reactant-mediated MAPK activation and the FOXM1 pathway in patients. PLK1 (36), MAPK (37), ATR (38), MCM (39), PI3K and FGFR1 (40) have been shown to play increasingly crucial regulatory roles in HCC, and these studies and our results indicated that CFHR4 may inhibit the development and progression of HCC by regulating these signaling pathways. However, the association of CFHR4 with these signaling pathways was first discovered here, and the regulatory mechanisms require further exploration. Furthermore, based on the DEGs, we constructed the PPI networks using the Cytoscape tool. Five central gene clusters (a total score ≥ 5000) and the top 7 central genes were screened, including CENPA, CDC20, UBE2C, CEP55, BIRC5, FAM64A and TRIP13. The CFHR4-interacting genes were generated using STRING and GeneMANIA online databases, and we observed five intersecting genes, including C3, CRP, CFHR1, CFHR3 and CFHR5. Existing studies have confirmed that CFHR4 regulates

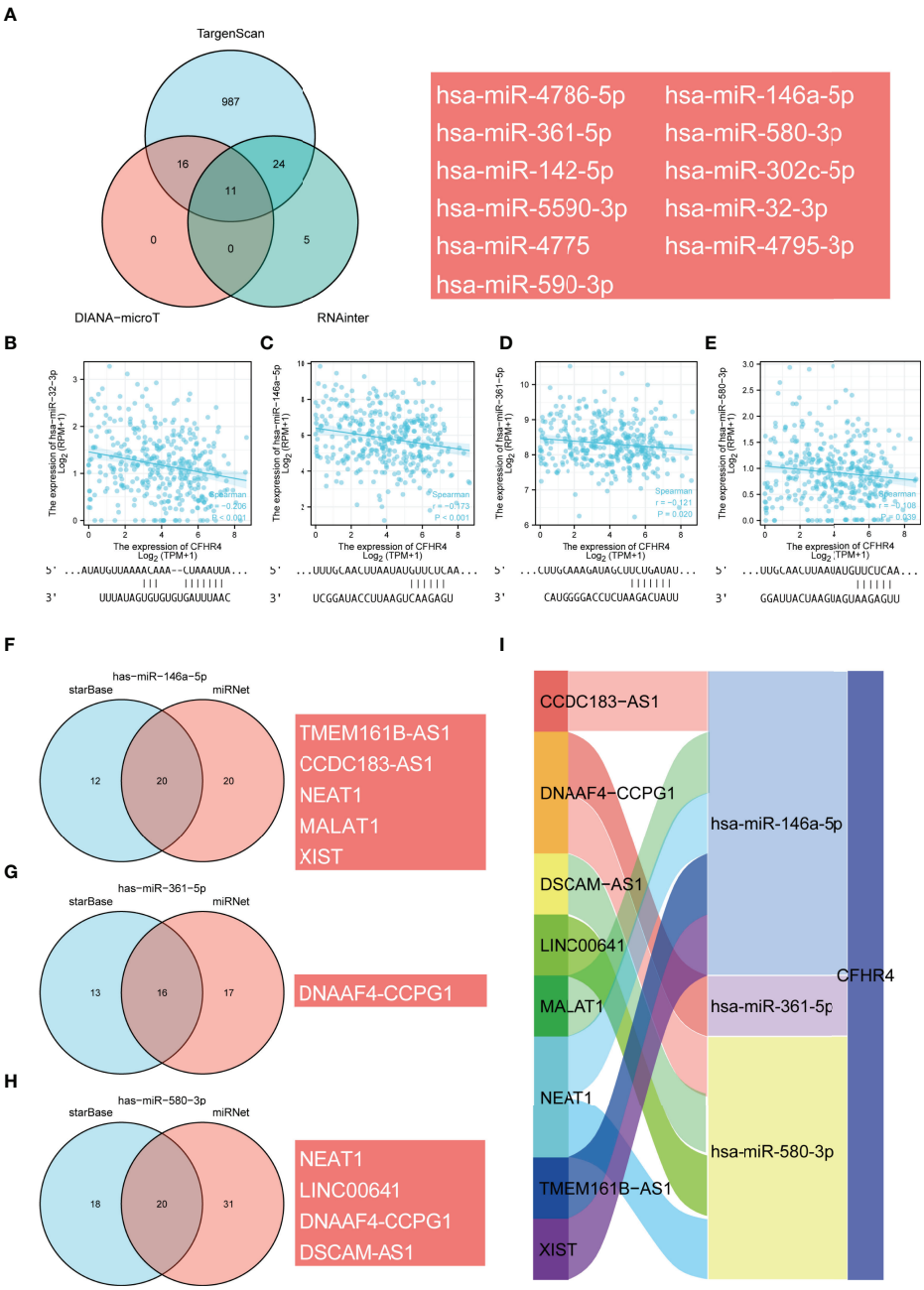

FIGURE 8 | Prediction of the ceRNA network in HCC. **(A)** Venn diagram showing the results for CFHR4 targets predicted using the TargetScan, DIANA-microT and RNAinter databases. **(B–E)** Scatter plots were generated to show miRNAs-mRNAs with significant correlations. TargetScan prediction of the potential binding sites in CFHR4 for the target miRNAs. **(F–H)** The lncRNAs that bind to target miRNAs were predicted using the miRNet and starBase online databases and displayed in a Venn diagram, including hsa–miR–146–5p, hsa–miR–361–5p and hsa–miR–580–3p. **(I)** Sankey diagram showing the CFHR4-related ceRNA regulatory network.

complement activation and opsonization on biological surfaces by interacting with native CRP (Hebecker et al., 2010). CFHR4 interacts with C3b (C3 activation fragment) (Hellwage et al., 1999, Hebecker and Jozsi, 2012). These conclusions promote the credibility of the predictions from the STRING database and will provide critical insights into the design of follow-up studies and experimental validation.

Among the results, tumor infiltrating immune cells (TIICs) were recently shown to play a pivotal regulatory role in tumor progression (41). The substantial accumulation of TIICs in HCC affects the prognosis of HCC (42). By revealing the relationship between CFHR4 expression and the level of immune cell infiltration in HCC, CFHR4 expression was clearly associated with the infiltration of Th17 cells, DCs, neutrophils and Th2

cells. Th17 cells are a major effector subset of CD4+ T cells that play a vital role in host protection and autoinflammatory disorders (43, 44). The differentiation of Th17 cells into Th1 and Th2 cell subsets participates in regulating the response to intracellular pathogens and extracellular organisms (45). Th1/17 cells produce IFN-γ to drive antitumor immune responses (46). Multiple studies reported that increased infiltration of Th17 cells inhibits the progression of breast cancer (47). Moreover, DCs are specialized antigen-presenting cells that play important roles in the initiation and regulation of innate and adaptive immune responses (48). The antitumor effect of DCs has been confirmed (49). Neutrophils have also been proven to exert bidirectional regulatory effects on the tumor immune microenvironment (50). Our studies indicated that high CFHR4 expression activated Th17 cells, DCs and neutrophils to promote antitumor immune responses. In addition, antigen-presenting cells might promote the polarization of CD4+ T cells toward Th1 and Th2 cell subsets. Th1 cells are mainly involved in cellular immunity and tumor clearance, and Th2 cells are involved in the stimulation of antibody production (51). Th2 cells have also been confirmed as an independent risk factor for cancer growth and progression (52, 53). The number of NK CD56bright cells is significantly increased in various cancers (54–56). Multiple studies reported that Tfh cells are a specialized subset of CD4+ T cells that support the germinal centers, which secrete high-affinity antibodies and provide help for memory B cells (57, 58). Additionally, Tfh cells were confirmed to be involved in human autoimmune responses and cancers (59, 60). Based on this information, CFHR4 modulates immune responses mediated by Th2 cells, NK CD56bright cells and Tfh cells in HCC. We also found that the CFHR4 CNV was significantly correlated with the levels of infiltrating CD8+ T cells, macrophages, neutrophils, and dendritic cells. In addition, CFHR4 expression is strongly correlated with various immunomarker groups in HCC. We confirmed significant correlations between CFHR4 expression and CD8+ T cells (CD8B), monocytes (CD86), TAMs (CD68 and IL10), M1 macrophages (NOS2 and IRF5), neutrophils (CD66b, CD11b, and CCR7), natural killer cells (HLA-DPB1), dendritic cells (NRP1 and ITGAX), Th1 cells (STAT1 and IFN-γ), Th2 cells (STAT5A), Tfh cells (IL21), Th17 cells (TGFβ) and exhausted T cells (PD-1, CTLA4, LAG3, and TIM-3). Our identified a potentially indispensable role for CFHR4 in regulating immune cell infiltration in HCC. We explored the relationship between CFHR4 expression with OS, PFI, DSS and clinical characteristics (TNM stage, residual tumor, and histological grade) by performing univariate Cox regression analysis. Calibration plots showed good agreement between predicted values of CFHR4-related column line plots and forecasted and observed values for 1-, 3- and 5-year OS probabilities. These results were consistent with those of the univariate Cox regression analysis.

The m6A methylation exerts a substantial effect on tumor cell proliferation, invasion and migration (61). Currently, m6A RNA and ceRNA regulatory networks are widely studied to determine HCC mechanisms (15). We further analyzed the relationship between CFHR4 expression and m6A modifications and determined that CFHR4 expression had inseparable relationships with IGF2BP2, IGF2BP3, YTHDF1, HNRNPA2B1, LRPPRC, HNRNPC, RBMX, RBM15B and WTAP expression. We also observed significant correlations between high CFHR4 expression and YTHDC1, IGF2BP1, IGF2BP2, IGF2BP3, YTHDF1, YTHDF2, HNRNPA2B1, LRPPRC, HNRNPC, RBMX, METTL16, METTL3, RBM15, RBM15B, VIRMA, WTAP and ALKBH5 expression. Multiple studies have now reported that IGF2BP1 (62), IGF2BP2 (28), IGF2BP3 (63), YTHDF1 (64), YTHDF2 (29), BRMX (65), RBM15 (66), METTL3 (67) and WTAP (27) are significantly upregulated in HCC, and their overexpression promotes HCC progression and is associated with a poor prognosis for patients with HCC. These discussions further supported our results. Thus, these findings suggested that the CFHR4 gene may be modified by m6A to increase the stability of its mRNA, which further inhibits the proliferation, invasion and migration of HCC. Subsequently, we constructed ceRNA regulatory networks based on the prediction. Because the ceRNA regulatory networks of CFHR4 were derived from a bioinformatics analysis, more experiments are needed to validate this network in future studies.

Although we increased our awareness of the regulatory mechanism of CFHR4 in HCC, the study had several limitations. Initially, the expression levels of CFHR4 and the important regulatory mechanisms and pathways related to CFHR4 in HCC should be further validated and evaluated by analyzing clinical samples from more centers. Secondly, However, the potential diagnostic value of the circulating CFHR4 content in HCC patients is not clear, and the clinical significance of circulating tumor markers remains to be further explored. In addition, the relationship between CFHR4 and interacting genes and m6A genes in HCC should be further explored and validated. In future studies, we will further elucidate the potential regulatory mechanisms of CFHR4 in HCC by performing more experiments.

CONCLUSIONS

In summary, this study represents the first in-depth analysis of CFHR4 in HCC. Our study suggested that CFHR4 was abnormally downregulated in HCC and that its reduced expression was correlated with a poorer prognosis. We confirmed the correlation between CFHR4 expression and the m6A modification, indicating that CFHR4 may be modified by m6A to improve mRNA stability. The construction of ceRNA networks suggested that CFHR4 may be involved in multiple molecular regulatory mechanisms of HCC. More importantly, CFHR4 expression was associated with multiple immune cells and may affect HCC tumor immunity by inducing M1 macrophage polarization and altering the infiltration of exhausted T cells. These findings provide additional insights into the mechanism by which CFHR4 may represent an important independent prognostic marker for HCC. The potential molecular mechanisms and regulatory networks of CFRH4 provide a basis for follow-up studies. The study also

provides important insights into the treatment of HCC based on genomics.

DATA AVAILABILITY STATEMENT

The article/**Supplementary Material** contains the original contributions presented in the study. Any additional questions can be forwarded to the corresponding authors.

ETHICS STATEMENT

The Ethics Committee of the First Affiliated Hospital of Harbin Medical University provided ethical review and approval. The patients provided their written informed consent to participate in this study.

AUTHOR CONTRIBUTIONS

HY, CW, SK, and MB made equal contributions to this article. HY, CW, and SK planned the research trials and engaged in article writing. YNX, SL, ZF, BQ, YX, and YF attended in information generation and analysis. MZ, ZL, BY, XL, YH, YZ, and SP also provided assistance with analysis. All authors made great efforts to the article and agreed to the version submitted.

FUNDING

This work was supported by the Research Fund of the National Natural Scientific Foundation of China (81100305, 81470876 and 81270527), Natural Science Foundation of Heilongjiang Province of China (QC2013C094, LC2018037), Chen Xiaoping Foundation for the Development of Science and Technology of Hubei Province (CXPJJH11900001-2019349), Outstanding Youth Training Fund from Academician Yu Weihan of Harbin Medical University (2014), and the First Affiliated Hospital of Harbin Medical University (2019L01, HYD2020JQ0007).

SUPPLEMENTARY MATERIAL

The Supplementary Material for this article can be found online at: https://www.frontiersin.org/articles/10.3389/fimmu.2022.892750/full#supplementary-material

Supplementary Figure 1 | CFHR4 expression levels in different cancer tissues compared to normal tissues. **(A)** CFHR4 expression levels in different cancer tissues compared to normal tissues in the Timer database. **(B)** CFHR4 expression levels in different cancer tissues compared to normal tissues in the GEPIA database. *p < 0.05, **p < 0.01, ***p < 0.001, NS, no significance.

Supplementary Figure 2 | PPI network and potential CFHR4-interacting target genes. **(A)** PPI networks were built using the STRING database. **(B)** PPI networks were built using the GeneMANIA database. **(C)** The intersecting genes identified by the STRING and GeneMANIA online databases are displayed in a Venn diagram. **(D)** Scatter plot showing the correlation between CFHR1 and CFHR4 expression. **(E)** Scatter plot showing the correlation between CFHR3 and CFHR4 expression. **(F)** Scatter plot showing the correlation between CFHR5 and CFHR4 expression. **(G)** Scatter plot showing the correlation between C3 and CFHR4 expression. **(H)** Scatter plot showing the correlation between CRP and CFHR4 expression.

Supplementary Figure 3 | The prognostic value of CFHR4 in HCC. **(A–C)** OS, DSS and PFI survival curves for white, black or African–American patients with HCC presenting high and low CFHR4 expression. **(D-F)** OS, DSS and PFI survival curves for patients with HCC aged > 60 years presenting with high and low CFHR4 expression. **(G)** OS curves for patients with stage T3 and T4 HCC presenting with high and low CFHR4 expression. **(H)** OS curves for patients with pathological stage III and IV HCC presenting with high and low CFHR4 expression.

Supplementary Table 1 | Characteristics of patients with HCC in TCGA.

Supplementary Table 2 | CFHR4-related DEGs.

Supplementary Table 3 | GO enrichment analysis of CFHR4.

Supplementary Table 4 | GSEA enrichment analysis of CFHR4.

Supplementary Table 5 | PPI network of CFHR4.

Supplementary Table 6 | OS of patients with HCC based on prognostic covariates.

Supplementary Table 7 | DSS patients with HCC based on prognostic covariates.

Supplementary Table 8 | PFI of patients with HCC based on prognostic covariates.

REFERENCES

1. Sung H, Ferlay J, Siegel RL, Laversanne M, Soerjomataram I, Jemal A, et al. Global Cancer Statistics 2020: GLOBOCAN Estimates of Incidence and Mortality Worldwide for 36 Cancers in 185 Countries. *CA Cancer J Clin* (2021) 71(3):209–49. doi: 10.3322/caac.21660
2. Chen W, Zheng R, Baade PD, Zhang S, Zeng H, Bray F, et al. Cancer Statistics in China, 2015. *CA Cancer J Clin* (2016) 66(2):115–32. doi: 10.3322/caac.21338
3. Forner A, Reig M, Bruix J. Hepatocellular Carcinoma. *Lancet* (2018) 391 (10127):1301–14. doi: 10.1016/S0140-6736(18)30010-2
4. Singal AG, Lampertico P, Nahon P. Epidemiology and Surveillance for Hepatocellular Carcinoma: New Trends. *J Hepatol* (2020) 72(2):250–61. doi: 10.1016/j.jhep.2019.08.025
5. Wang C, Dong L, Li X, Li Y, Zhang B, Wu H, et al. The PGC1alpha/NRF1-MPC1 Axis Suppresses Tumor Progression and Enhances the Sensitivity to Sorafenib/Doxorubicin Treatment in Hepatocellular Carcinoma. *Free Radic Biol Med* (2021) 163:141–52. doi: 10.1016/j.freeradbiomed.2020.11.035
6. Reis ES, Mastellos DC, Ricklin D, Mantovani A, Lambris JD. Complement in Cancer: Untangling an Intricate Relationship. *Nat Rev Immunol* (2018) 18 (1):5–18. doi: 10.1038/nri.2017.97
7. Yarmoska SK, Alawieh AM, Tomlinson S, Hoang KB. Modulation of the Complement System by Neoplastic Disease of the Central Nervous System. *Front Immunol* (2021) 12:689435. doi: 10.3389/fimmu.2021.689435
8. Poppelaars F, Goicoechea de Jorge E, Jongerius I, Baeumner AJ, Steiner MS, Jozsi M, et al. A Family Affair: Addressing the Challenges of Factor H and the Related Proteins. *Front Immunol* (2021) 12:660194. doi: 10.3389/fimmu.2021.660194
9. Skerka C, Chen Q, Fremeaux-Bacchi V, Roumenina LT. Complement Factor H Related Proteins (CFHRs). *Mol Immunol* (2013) 56(3):170–80. doi: 10.1016/j.molimm.2013.06.001
10. Lores-Motta L, Paun CC, Corominas J, Pauper M, Geerlings MJ, Altay L, et al. Genome-Wide Association Study Reveals Variants in CFH and CFHR4

Associated With Systemic Complement Activation: Implications in Age-Related Macular Degeneration. *Ophthalmology* (2018) 125(7):1064–74. doi: 10.1016/j.ophtha.2017.12.023
11. Cipriani V, Lores-Motta L, He F, Fathalla D, Tilakaratna V, McHarg S, et al. Increased Circulating Levels of Factor H-Related Protein 4 Are Strongly Associated With Age-Related Macular Degeneration. *Nat Commun* (2020) 11 (1):778. doi: 10.1038/s41467-020-14499-3
12. Zhao J, Wu H, Khosravi M, Cui H, Qian X, Kelly JA, et al. Association of Genetic Variants in Complement Factor H and Factor H-Related Genes With Systemic Lupus Erythematosus Susceptibility. *PLoS Genet* (2011) 7(5): e1002079. doi: 10.1371/journal.pgen.1002079
13. Zipfel PF, Wiech T, Stea ED, Skerka C. CFHR Gene Variations Provide Insights in the Pathogenesis of the Kidney Diseases Atypical Hemolytic Uremic Syndrome and C3 Glomerulopathy. *J Am Soc Nephrol* (2020) 31 (2):241–56. doi: 10.1681/ASN.2019050515
14. Moore I, Strain L, Pappworth I, Kavanagh D, Barlow PN, Herbert AP, et al. Association of Factor H Autoantibodies With Deletions of CFHR1, CFHR3, CFHR4, and With Mutations in CFH, CFI, CD46, and C3 in Patients With Atypical Hemolytic Uremic Syndrome. *Blood* (2010) 115(2):379–87. doi: 10.1182/blood-2009-05-221549
15. Wang P, Wang X, Zheng L, Zhuang C. Gene Signatures and Prognostic Values of M6a Regulators in Hepatocellular Carcinoma. *Front Genet* (2020) 11:540186. doi: 10.3389/fgene.2020.540186
16. Yang Y, Hsu PJ, Chen YS, Yang YG. Dynamic Transcriptomic M(6)A Decoration: Writers, Erasers, Readers and Functions in RNA Metabolism. *Cell Res* (2018) 28(6):616–24. doi: 10.1038/s41422-018-0040-8
17. Zaccara S, Ries RJ, Jaffrey SR. Reading, Writing and Erasing mRNA Methylation. *Nat Rev Mol Cell Biol* (2019) 20(10):608–24. doi: 10.1038/s41580-019-0168-5
18. Pan Y, Xiao K, Li Y, Li Y, Liu Q. RNA N6-Methyladenosine Regulator-Mediated Methylation Modifications Pattern and Immune Infiltration Features in Glioblastoma. *Front Oncol* (2021) 11:632934. doi: 10.3389/fonc.2021.632934
19. Zhang F, Luo BH, Wu QH, Li QL, Yang KD. LncRNA HCG18 Upregulates TRAF4/TRAF5 to Facilitate Proliferation, Migration and EMT of Epithelial Ovarian Cancer by Targeting miR-29a/B. *Mol Med* (2022) 28(1):2. doi: 10.1186/s10020-021-00415-y
20. Xue ST, Zheng B, Cao SQ, Ding JC, Hu GS, Liu W, et al. Long non-Coding RNA LINC00680 Functions as a ceRNA to Promote Esophageal Squamous Cell Carcinoma Progression Through the miR-423-5p/PAK6 Axis. *Mol Cancer* (2022) 21(1):69. doi: 10.1186/s12943-022-01539-3
21. Li D, Xu M, Wang Z, Huang P, Huang C, Chen Z, et al. The EMT-Induced lncRNA NR2F1-AS1 Positively Modulates NR2F1 Expression and Drives Gastric Cancer *via* miR-29a-3p/VAMP7 Axis. *Cell Death Dis* (2022) 13(1):84. doi: 10.1038/s41419-022-04540-2
22. Love MI, Huber W, Anders S. Moderated Estimation of Fold Change and Dispersion for RNA-Seq Data With Deseq2. *Genome Biol* (2014) 15(12):550. doi: 10.1186/s13059-014-0550-8
23. Subramanian A, Tamayo P, Mootha VK, Mukherjee S, Ebert BL, Gillette MA, et al. Gene Set Enrichment Analysis: A Knowledge-Based Approach for Interpreting Genome-Wide Expression Profiles. *Proc Natl Acad Sci USA* (2005) 102(43):15545–50. doi: 10.1073/pnas.0506580102
24. Yu G, Wang LG, Han Y, He QY. Clusterprofiler: An R Package for Comparing Biological Themes Among Gene Clusters. *OMICS* (2012) 16(5):284–7. doi: 10.1089/omi.2011.0118
25. Hanzelmann S, Castelo R, Guinney J. GSVA: Gene Set Variation Analysis for Microarray and RNA-Seq Data. *BMC Bioinf* (2013) 14:7. doi: 10.1186/1471-2105-14-7
26. Bindea G, Mlecnik B, Tosolini M, Kirilovsky A, Waldner M, Obenauf AC, et al. Spatiotemporal Dynamics of Intratumoral Immune Cells Reveal the Immune Landscape in Human Cancer. *Immunity* (2013) 39(4):782–95. doi: 10.1016/j.immuni.2013.10.003
27. Chen Y, Peng C, Chen J, Chen D, Yang B, He B, et al. WTAP Facilitates Progression of Hepatocellular Carcinoma *via* M6a-HuR-Dependent Epigenetic Silencing of ETS1. *Mol Cancer* (2019) 18(1):127. doi: 10.1186/s12943-019-1053-8
28. Pu J, Wang J, Qin Z, Wang A, Zhang Y, Wu X, et al. IGF2BP2 Promotes Liver Cancer Growth Through an M6a-FEN1-Dependent Mechanism. *Front Oncol* (2020) 10:578816. doi: 10.3389/fonc.2020.578816
29. Zhang C, Huang S, Zhuang H, Ruan S, Zhou Z, Huang K, et al. YTHDF2 Promotes the Liver Cancer Stem Cell Phenotype and Cancer Metastasis by Regulating OCT4 Expression *via* M6a RNA Methylation. *Oncogene* (2020) 39 (23):4507–18. doi: 10.1038/s41388-020-1303-7
30. Irmscher S, Zipfel SLH, Halder LD, Ivanov L, Gonzalez-Delgado A, Waldeyer C, et al. Factor H-Related Protein 1 (FHR-1) Is Associated With Atherosclerotic Cardiovascular Disease. *Sci Rep* (2021) 11(1):22511. doi: 10.1038/s41598-021-02011-w
31. Cipriani V, Tierney A, Griffiths JR, Zuber V, Sergouniotis PI, Yates JRW, et al. Beyond Factor H: The Impact of Genetic-Risk Variants for Age-Related Macular Degeneration on Circulating Factor-H-Like 1 and Factor-H-Related Protein Concentrations. *Am J Hum Genet* (2021) 108(8):1385–400. doi: 10.1016/j.ajhg.2021.05.015
32. Zuber J, Frimat M, Caillard S, Kamar N, Gatault P, Petitprez F, et al. Use of Highly Individualized Complement Blockade Has Revolutionized Clinical Outcomes After Kidney Transplantation and Renal Epidemiology of Atypical Hemolytic Uremic Syndrome. *J Am Soc Nephrol* (2019) 30(12):2449–63. doi: 10.1681/ASN.2019040331
33. Riihila PM, Nissinen LM, Ala-Aho R, Kallajoki M, Grenman R, Meri S, et al. Complement Factor H: A Biomarker for Progression of Cutaneous Squamous Cell Carcinoma. *J Invest Dermatol* (2014) 134(2):498–506. doi: 10.1038/jid.2013.346
34. Fan WL, Yang LY, Hsieh JC, Lin TC, Lu MJ, Liao CT. Prognostic Genetic Biomarkers Based on Oncogenic Signaling Pathways for Outcome Prediction in Patients With Oral Cavity Squamous Cell Carcinoma. *Cancers (Basel)* (2021) 13(11):2709. doi: 10.3390/cancers13112709
35. Zhu H, Li Q, Zhao Y, Peng H, Guo L, Zhu J, et al. Vaccinia-Related Kinase 2 Drives Pancreatic Cancer Progression by Protecting Plk1 From Chfr-Mediated Degradation. *Oncogene* (2021) 40(28):4663–74. doi: 10.1038/s41388-021-01893-4
36. Mok WC, Wasser S, Tan T, Lim SG. Polo-Like Kinase 1, a New Therapeutic Target in Hepatocellular Carcinoma. *World J Gastroenterol* (2012) 18 (27):3527–36. doi: 10.3748/wjg.v18.i27.3527
37. Dimri M, Satyanarayana A. Molecular Signaling Pathways and Therapeutic Targets in Hepatocellular Carcinoma. *Cancers (Basel)* (2020) 12(2):491. doi: 10.3390/cancers12020491
38. Sheng H, Huang Y, Xiao Y, Zhu Z, Shen M, Zhou P, et al. ATR Inhibitor AZD6738 Enhances the Antitumor Activity of Radiotherapy and Immune Checkpoint Inhibitors by Potentiating the Tumor Immune Microenvironment in Hepatocellular Carcinoma. *J Immunother Cancer* (2020) 8(1):e000340. doi: 10.1136/jitc-2019-000340
39. Lei Y, Wang S, Liu J, Yan W, Han P, Tian D. Identification of MCM Family as Potential Therapeutic and Prognostic Targets for Hepatocellular Carcinoma Based on Bioinformatics and Experiments. *Life Sci* (2021) 272:119227. doi: 10.1016/j.lfs.2021.119227
40. Liu Z, Mo H, Liu R, Niu Y, Chen T, Xu Q, et al. Matrix Stiffness Modulates Hepatic Stellate Cell Activation Into Tumor-Promoting Myofibroblasts *via* E2F3-Dependent Signaling and Regulates Malignant Progression. *Cell Death Dis* (2021) 12(12):1134. doi: 10.1038/s41419-021-04418-9
41. Domingues P, Gonzalez-Tablas M, Otero A, Pascual D, Miranda D, Ruiz L, et al. Tumor Infiltrating Immune Cells in Gliomas and Meningiomas. *Brain Behav Immun* (2016) 53:1–15. doi: 10.1016/j.bbi.2015.07.019
42. Sun H, Liu L, Huang Q, Liu H, Huang M, Wang J, et al. Accumulation of Tumor-Infiltrating CD49a(+) NK Cells Correlates With Poor Prognosis for Human Hepatocellular Carcinoma. *Cancer Immunol Res* (2019) 7(9):1535–46. doi: 10.1158/2326-6066.CIR-18-0757
43. Stockinger B, Veldhoen M. Differentiation and Function of Th17 T Cells. *Curr Opin Immunol* (2007) 19(3):281–6. doi: 10.1016/j.coi.2007.04.005
44. Lee YK, Turner H, Maynard CL, Oliver JR, Chen D, Elson CO, et al. Late Developmental Plasticity in the T Helper 17 Lineage. *Immunity* (2009) 30 (1):92–107. doi: 10.1016/j.immuni.2008.11.005
45. Bettelli E, Carrier Y, Gao W, Korn T, Strom TB, Oukka M, et al. Reciprocal Developmental Pathways for the Generation of Pathogenic Effector TH17 and Regulatory T Cells. *Nature* (2006) 441(7090):235–8. doi: 10.1038/nature04753
46. Chatterjee S, Daenthanasanmak A, Chakraborty P, Wyatt MW, Dhar P, Selvam SP, et al. CD38-NAD(+)Axis Regulates Immunotherapeutic Anti-Tumor T Cell Response. *Cell Metab* (2018) 27(1):85–100.e8. doi: 10.1016/j.cmet.2017.10.006

47. Karpisheh V, Ahmadi M, Abbaszadeh-Goudarzi K, Mohammadpour Saray M, Barshidi A, Mohammadi H, et al. The Role of Th17 Cells in the Pathogenesis and Treatment of Breast Cancer. *Cancer Cell Int* (2022) 22 (1):108. doi: 10.1186/s12935-022-02528-8
48. Wculek SK, Cueto FJ, Mujal AM, Melero I, Krummel MF, Sancho D. Dendritic Cells in Cancer Immunology and Immunotherapy. *Nat Rev Immunol* (2020) 20(1):7–24. doi: 10.1038/s41577-019-0210-z
49. Martinek J, Wu TC, Cadena D, Banchereau J, Palucka K. Interplay Between Dendritic Cells and Cancer Cells. *Int Rev Cell Mol Biol* (2019) 348:179–215. doi: 10.1016/bs.ircmb.2019.07.008
50. Shaul ME, Fridlender ZG. Neutrophils as Active Regulators of the Immune System in the Tumor Microenvironment. *J Leukoc Biol* (2017) 102(2):343–9. doi: 10.1189/jlb.5MR1216-508R
51. Roybal KT, Williams JZ, Morsut L, Rupp LJ, Kolinko I, Choe JH, et al. Engineering T Cells With Customized Therapeutic Response Programs Using Synthetic Notch Receptors. *Cell* (2016) 167(2):419–32.e16. doi: 10.1016/j.cell.2016.09.011
52. Orecchioni M, Bedognetti D, Newman L, Fuoco C, Spada F, Hendrickx W, et al. Single-Cell Mass Cytometry and Transcriptome Profiling Reveal the Impact of Graphene on Human Immune Cells. *Nat Commun* (2017) 8 (1):1109. doi: 10.1038/s41467-017-01015-3
53. Mantovani A, Romero P, Palucka AK, Marincola FM. Tumour Immunity: Effector Response to Tumour and Role of the Microenvironment. *Lancet* (2008) 371(9614):771–83. doi: 10.1016/S0140-6736(08)60241-X
54. Tonetti CR, de Souza-Araujo CN, Yoshida A, da Silva RF, Alves PCM, Mazzola TN, et al. Ovarian Cancer-Associated Ascites Have High Proportions of Cytokine-Responsive CD56bright NK Cells. *Cells* (2021) 10 (7):1702. doi: 10.3390/cells10071702
55. Nie Y, Liu D, Yang W, Li Y, Zhang L, Cheng X, et al. Increased Expression of TIGIT and KLRG1 Correlates With Impaired CD56(bright) NK Cell Immunity in HPV16-Related Cervical Intraepithelial Neoplasia. *Virol J* (2022) 19(1):68. doi: 10.1186/s12985-022-01776-4
56. Duan J, Lv G, Zhu N, Chen X, Shao Y, Liu Y, et al. Multidimensional Profiling Depicts Infiltrating Immune Cell Heterogeneity in the Tumor Microenvironment of Stage IA Non-Small Cell Lung Cancer. *Thorac Cancer* (2022) 13(7):947–55. doi: 10.1111/1759-7714.14329
57. Chen Z, Wang N, Yao Y, Yu D. Context-Dependent Regulation of Follicular Helper T Cell Survival. *Trends Immunol* (2022) 43(4):309–21. doi: 10.1016/j.it.2022.02.002
58. Walker LSK. The Link Between Circulating Follicular Helper T Cells and Autoimmunity. *Nat Rev Immunol* (2022) 11:1–9. doi: 10.1038/s41577-022-00693-5
59. Galdiero MR, Varricchi G, Marone G. The Immune Network in Thyroid Cancer. *Oncoimmunology* (2016) 5(6):e1168556. doi: 10.1080/2162402X.2016.1168556
60. Bian J, Lin J, Long J, Yang X, Yang X, Lu X, et al. T Lymphocytes in Hepatocellular Carcinoma Immune Microenvironment: Insights Into Human Immunology and Immunotherapy. *Am J Cancer Res* (2020) 10(12):4585–606.
61. Chen H, Gao S, Liu W, Wong CC, Wu J, Wu J, et al. RNA N(6)-Methyladenosine Methyltransferase METTL3 Facilitates Colorectal Cancer by Activating the M(6)A-GLUT1-Mtorc1 Axis and Is a Therapeutic Target. *Gastroenterology* (2021) 160(4):1284–300.e16. doi: 10.1053/j.gastro.2020.11.013
62. Zhang J, Hu K, Yang YQ, Wang Y, Zheng YF, Jin Y, et al. LIN28B-AS1-IGF2BP1 Binding Promotes Hepatocellular Carcinoma Cell Progression. *Cell Death Dis* (2020) 11(9):741. doi: 10.1038/s41419-020-02967-z
63. Jiang W, Cheng X, Wang T, Song X, Zheng Y, Wang L. LINC00467 Promotes Cell Proliferation and Metastasis by Binding With IGF2BP3 to Enhance the mRNA Stability of TRAF5 in Hepatocellular Carcinoma. *J Gene Med* (2020) 22(3):e3134. doi: 10.1002/jgm.3134
64. Su T, Huang M, Liao J, Lin S, Yu P, Yang J, et al. Insufficient Radiofrequency Ablation Promotes Hepatocellular Carcinoma Metastasis Through N6-Methyladenosine mRNA Methylation-Dependent Mechanism. *Hepatology* (2021) 74(3):1339–56. doi: 10.1002/hep.31766
65. Song Y, He S, Ma X, Zhang M, Zhuang J, Wang G, et al. RBMX Contributes to Hepatocellular Carcinoma Progression and Sorafenib Resistance by Specifically Binding and Stabilizing BLACAT1. *Am J Cancer Res* (2020) 10 (11):3644–65.
66. Cai X, Chen Y, Man D, Yang B, Feng X, Zhang D, et al. RBM15 Promotes Hepatocellular Carcinoma Progression by Regulating N6-Methyladenosine Modification of YES1 mRNA in an IGF2BP1-Dependent Manner. *Cell Death Discov* (2021) 7(1):315. doi: 10.1038/s41420-021-00703-w
67. Chen M, Wei L, Law CT, Tsang FH, Shen J, Cheng CL, et al. RNA N6-Methyladenosine Methyltransferase-Like 3 Promotes Liver Cancer Progression Through YTHDF2-Dependent Posttranscriptional Silencing of SOCS2. *Hepatology* (2018) 67(6):2254–70. doi: 10.1002/hep.29683

Conflict of Interest: The authors declare that the research was conducted in the absence of any commercial or financial relationships that could be construed as a potential conflict of interest.

Publisher's Note: All claims expressed in this article are solely those of the authors and do not necessarily represent those of their affiliated organizations, or those of the publisher, the editors and the reviewers. Any product that may be evaluated in this article, or claim that may be made by its manufacturer, is not guaranteed or endorsed by the publisher.

frontiers | Frontiers in Immunology

ORIGINAL RESEARCH
published: 07 July 2022
doi: 10.3389/fimmu.2022.930096

The Potential Predictive Biomarkers for Advanced Hepatocellular Carcinoma Treated With Anti-Angiogenic Drugs in Combination With PD-1 Antibody

Chenxi Liu[1†], *Sihui Zhu*[1,2†], *Yanbing Dong*[1], *Jie Shao*[1,2], *Baorui Liu*[1,2*] *and Jie Shen*[1,2*]

[1] *Comprehensive Cancer Centre of Drum Tower Hospital, Medical School of Nanjing University, Clinical Cancer Institute of Nanjing University, Nanjing, China,* [2] *Comprehensive Cancer Centre of Nanjing Drum Tower Hospital, Clinical College of Nanjing Medical University, Nanjing, China*

OPEN ACCESS

Edited by:
Zheng Gong,
Jackson Laboratory, United States

Reviewed by:
Shouju Wang,
Nanjing Medical University, China
Yixing Chen,
Fudan University, China

***Correspondence:**
Jie Shen
shenjie2008nju@163.com
Baorui Liu
baoruiliu@nju.edu.cn

†These authors have contributed equally to this work

Specialty section:
This article was submitted to Cancer Immunity and Immunotherapy, a section of the journal Frontiers in Immunology

Received: *27 April 2022*
Accepted: *14 June 2022*
Published: *07 July 2022*

Citation:
Liu C, Zhu S, Dong Y, Shao J, Liu B and Shen J (2022) The Potential Predictive Biomarkers for Advanced Hepatocellular Carcinoma Treated With Anti-Angiogenic Drugs in Combination With PD-1 Antibody. Front. Immunol. 13:930096. doi: 10.3389/fimmu.2022.930096

Background: Based on molecular biomarkers, anti-angiogenic drugs in combination with programmed cell death protein 1 (PD-1) antibodies can screen the potentially beneficial populations with hepatocellular carcinoma (HCC) and predict the efficacy after treatment. Therefore, we aimed to study predictive molecular biomarkers to improve the effectiveness of immuno-targeted combination therapy for HCC.

Patients and Methods: Baseline clinical data, blood samples, and imaging data of the first evaluation after two cycles of treatment were collected for 40 patients with advanced HCC who underwent combination therapy, and then these data were compared according to the efficacy. Since 15 patients had complete hematology samples, we additionally tested the T lymphocyte subpopulations of these 15 patients and also compared them according to the efficacy. In addition, we also selected five patients who benefited the most from the combination therapy and five patients with the worst curative effect for gene detection based on survival time and efficacy evaluation. Finally, the relationship between certain clinical characteristics, laboratory indicators, specific T lymphocyte subpopulations, gene mutations and the response of immuno-targeted combination therapy for HCC was evaluated.

Results: The high levels of $CD3^+CD4^+CD279^+$, $CD3^+CD8^+CD45RO^+CD62L^+$T lymphocytes and tumor mutational burden (TMB) were associated with good efficacy of the combination therapy (P=0.03, P<0.01 and P=0.03). The high levels of $CD3^+CD4^+CD28^+$ T lymphocytes were associated with poor efficacy of the combination therapy (P=0.02). The high mutation frequency of TP53 and ARID1A appeared in the non-response cohort. In addition, amplification mutation of 11q13-CCND1, FGF3, FGF4, and FGF19 was found in a patient with hyperprogression (HP).

Conclusions: The certain clinical characteristics, laboratory indicators, specific T lymphocyte subpopulations, and gene mutations established in this paper were potential predictive biomarkers for HCC patients treated with combination therapy.

Keywords: hepatocellular carcinoma, neoantigen reactive T cells, immunotherapy, PD-1 antibody, biomarker

BACKGROUND

In China, hepatocellular carcinoma (HCC) ranks the top five most frequently diagnosed cancer types that have high morbidity and mortality (1). So far, immune checkpoint inhibitors (ICIs) against programmed cell death protein 1 (PD-1), cytotoxic T lymphocyte antigen-4 (CTLA-4), and so on have brought new hope for the treatment of advanced HCC, especially in combination with targeted drugs, which can significantly improve the long-term prognosis of potentially beneficial populations. The GO30140 research has shown that patients with advanced HCC can obtain a progression-free survival (PFS) of 7.3 months and overall survival (OS) of 17.1 months when using the first-line combination of atezolizumab and bevacizumab (2). Imbrave150 research has shown that the global objective response rate (ORR) of atezolizumab in combination with bevacizumab can reach 27.3% in the treatment of unresectable HCC (3). The median overall survival (mOS) reaches 19.2 months (17.0-23.7 months) (HR=0.66; 95% CI: 0.52-0.85) (4), and the mOS of the Chinese subgroup is 24 months (17.1-NE) (HR=0.53; 95% CI: 0.35-0.80) (5).

Although combination therapies have achieved significant effects on the treatment of HCC, the less than 27.3%-46% response rate of drugs and high treatment costs have greatly restricted the application of immuno-targeted combination therapy (3, 6). Therefore, it is urgently necessary to improve the efficiency of combination therapy and identify potentially beneficial populations through laboratory characteristics, hallmark T lymphocyte subsets and other features.

The Tasuku Honjo team, who won the 2018 Nobel Prize in Physiology or Medicine, has discovered PD-1 and programmed cell death ligand 1 (PD-L1) (7). The binding of PD-1 and PD-L1 plays an important role in the mechanism underlying the tumor immune escape (8, 9), suggesting that inhibiting the interaction can mediate the body's anti-tumor activity. Since then, immunotherapy has been widely used in the field of tumor treatment.

The multi-kinase inhibitor sorafenib has become the standard treatment for HCC patients without indications for surgery since 2007 (10). However, its clinical efficacy is not satisfactory. The current emergence of anti-angiogenic drugs has broken this deadlock. A REFLECT study has reported the lenvatinib monotherapy for HCC patients, with a PFS of 7.4 months and an ORR of 24.1% (11), which is significantly higher compared with the sorafenib monotherapy (PFS of 3.7 months, ORR of 9.2%) (11).

As far as immunotherapy is concerned, the GO30140 study has shown that the ORR of atezolizumab as a single agent in advanced HCC is 17%, and the PFS is 3.4 months (1.9-5.2 months)(HR=0.55, 80% CI: 0.40-0.74 P=0.0108) (2). The Checkmate459 study has shown that when nivolumab monotherapy is used for unresectable HCC, the OS is 16.4 months (P= 0.075), PFS is 3.7 months (95%CI: 3.1-3.9), and ORR is 15% (12). The above-mentioned data all indicate that no more than 20% patients can benefit more from single PD-1 antibody treatment. A large number of research data in the past 5 years have shown that anti-angiogenic drugs in combination with PD-1 antibody therapy can further improve patient's survival, such as Imbrave150 (3), Rescue (13), Orient-32 (14), Keynote-524 (6) and so on.

At present, clinical trials of different types of anti-angiogenic drugs and PD-1 antibodies in the treatment of HCC are actively carried out in various tumor centers. However, the relevant indicators that can predict the potentially beneficial populations of combination therapy are only reported in malignant melanoma, non-small cell lung cancer (NSCLC), and other tumor types. There is no definite evidence in the field of HCC treatment.

In the present study, we performed statistics on the clinical characteristics, laboratory indicators, multiple T lymphocyte subtypes, and gene mutations of patients with advanced HCC in clinical trials who underwent immuno-targeted combination therapy. Moreover, we aim to explore sensitive response predictors of HCC combination therapy, and analyze the relationship between predictors and the sensitivity of combination therapy.

PATIENTS AND METHODS

Study Design and Participants

All specimens and relevant clinical data were obtained from the department of oncology, Drum Tower Hospital Affiliated to Medical School of Nanjing University. Baseline clinical data, blood samples, and imaging data of the first evaluation after two cycles of treatment were collected for 40 patients with advanced HCC treated with anti-angiogenic drugs in combination with PD-1 antibody. Patients started the combined treatment from May 2018. Since 15 patients had complete hematology samples, we additionally tested the T lymphocyte subpopulations. Based on the evaluation of response, the results of gene mutations of five patients each with the greatest and the worst clinical benefit were obtained. All HCC patients were confirmed by histopathology. Clinical data including the patient's age, gender, histopathological diagnosis, tumor location and stage, lymph node metastasis, and evaluation data after combination treatment. Clinical characteristics of the patients were summarized in **Table 1**. Informed consent was obtained from all patients. The protocols for our study were approved by the Human Research Protective Committee of Drum Tower Hospital.

Assessments

The blood sample was collected before the patients' first treatment, focusing on the patients' lymphocyte and neutrophil counts, and calculating the neutrophil to lymphocyte ratio (NLR). The first imaging evaluation was carried out within 28 days before the patients' initial treatment and was repeated every two cycles after medication. The Independent Radiological Review Committee (IRRC) evaluated the response according to RECIST V1.1. Since 15 patients had complete hematological samples, their T lymphocyte subpopulations were additionally tested. The peripheral venous blood of 15 patients were collected before treatment. CD3-FITC, CD19-PE, CD16-PE CD279-PE,

TABLE 1 | Baseline Demographic and Clinical Characteristics of Patients Receiving Combination Therapeutics (N =40).

Characteristic	No. (%)
Sex	
Male	36 (90)
Female	9 (10)
Age, years	
Median	57.1
Range	40-73
Age group, years	
<65	31 (77.5)
≥65	9 (22.5)
No.of involved disease site per patient	
1-2	7 (17.5)
3-4	28 (70.0)
≥5	5 (12.5)
No.of target lesions/total lesions	
Median	0.58
Range	0.33-1
Total diameter of target lesion,mm	
Median	51.88
Range	11.04-150.29
Involved disease sites	
Liver	29 (72.5)
Lung	13 (32.5)
Lymph nodes	11 (27.5)
Bone	13 (32.5)

CD223-PE, CD366-PE, CD137-PE, CD62L-PE, CD27-PE, CD4-PerCP, CD8-PerCP, CD8-APC, CD56-APC, CD45RO-APC, CD28-APC, IgG1 k, IgG2ak were used for direct labeling and staining with multiple combinations. The T lymphocyte subpopulations were detected by flow cytometry (The data of fluorescence-activated cell sorting were list in the **Supplementary Materials**). The five patients who benefited the most from the combination therapy and the five patients with the worst curative effect were selected for gene detection. The samples of gene detection came from tumor tissue and hematological samples. Comprehensive genomic alteration analysis of the tumor and matched blood samples were performed with an assay panel that captured 450 cancer-related genes and selected introns of 38 genes frequently rearranged in cancer (YuansuTM, OrigiMed). The genomic profile was produced using the NGS-based YuanSuTM 450 gene panel. The genes were captured and sequenced with a mean coverage of 900× by using Illumina NextSeq 500.

Statistical Analysis

As demonstrated by the overall workflow (**Figure 1**), pre-treatment clinical data, blood samples and imaging data were collected for 40 patients, and then these data were compared according to the efficacy. Among them, there were 9 partial remission (PR) patients named as Group PR, 30 stable disease (SD) patients and 1 progressive disease (PD) patient named as Group SD/PD at the first evaluation. T lymphocyte subtypes were measured in 15 patients, and the effect evaluation were also compared. Among them, there were 3 patients with PR and 12 patients with SD. Finally, we conducted gene detection on 10 patients based on the response evaluation. All statistical analyses were performed using SPSS 20.0. Chi-square test was used for qualitative data and t-test was used for quantitative data. $P<0.05$ was considered to be statistically significant. The Kaplan-Meier method was used to estimate PFS and OS.

RESULTS

Among 40 patients who received clinical data collection, hematological sample analysis, and imaging evaluation, 9 patients achieved PR, and 31 patients achieved SD/PD. The differences between the two cohorts were listed in **Table 2A**.

NLR Although there was no significant statistical difference in NLR (2.48 ± 2.07 and 3.53 ± 2.70) (P=0.291), there was still a trend that the PR group was lower than the SD/PD group.

Metastasis Among lung metastases, the PR group accounted for 44.44%, and the SD/PD group accounted for 29.03%. Although there was no significant statistical difference, it seemed that patients with lung metastasis had a higher rate of PR.

Lymphocyte Subpopulations Among 15 patients who received flow cytometry for the detection of lymphocyte

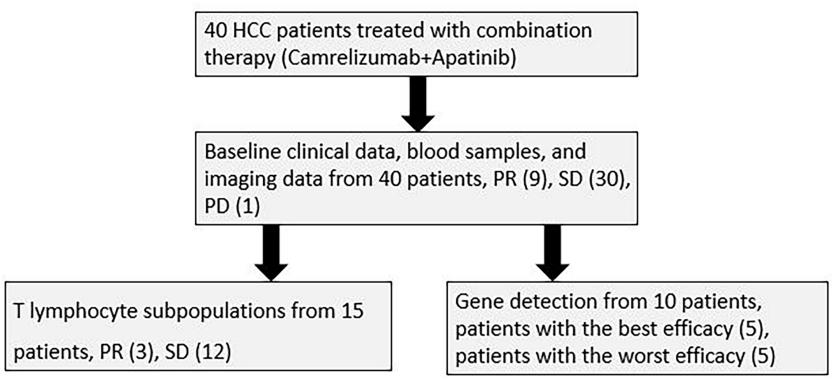

FIGURE 1 | The overall work flow of the whole study.

TABLE 2A | Differences in clinical data, hematology samples and imaging evaluations between the PR and SD/PD (n=40): PR (n=9), SD/PD (n=31).

	PR	SD/PD	t	P
gender	59.88 ± 10.43	56.29 ± 8.64	1.05	0.300
ANC	2.80 ± 1.03	3.95 ± 1.88	-1.76	0.087
LC	1.41 ± 0.59	1.53 ± 0.94	-0.36	0.724
NLR	2.48 ± 2.07	3.53 ± 2.70	-1.07	0.291
Target lesion/total lesion	13.26 ± 7.58	14.99 ± 8.28	-0.56	0.577
Liver metastasis	6 (66.67)	23 (74.19)	0.0004	0.983
Bone metastasis	0	1 (3.23)	/	1.00
Lung metastasis	4 (44.44)	9 (29.03)	0.216	0.642
Lymph node metastasis	3 (33.33)	8 (25.81)	0.0004	0.983

ANC, Absolute Neutrophil Count; LC, lymphocyte count.

subpopulations, 3 patients achieved PR, and 12 patients achieved SD. The differences between the two cohorts were listed in **Table 2B**. Among them, T lymphocytes with surface molecules expressing $CD3^+CD4^+CD279^+$,$CD3^+CD4^+CD28^+$, $CD3^+CD8^+CD45RO^+CD62L^+$ showed significant statistical differences (**Figure 2**; P=0.030, P=0.022, P=0.004). The high expression of $CD3^+CD4^+CD279^+$ and $CD3^+CD8^+CD45RO^+CD62L^+$ T lymphocytes indicated a good prognosis for the patient. The high expression of $CD3^+CD4^+CD28^+$ T lymphocytes suggested that immuno-targeted combination therapy was not effective.

Gene Mutations The OS (**Figure 3A**, 95% CI 0.08-0.55; p=0.025) and PFS (**Figure 3B**, 95% CI 0.08-0.48; p=0.014) of the patients evaluated as PR (n=9) for the first imaging assessment based on RECIST V1.1 were significantly longer than those of SD/PD patients (n=31). This suggested that the first evaluation of the efficacy could predict the long-term prognosis. So we selected the most and the least clinical benefit five patients each for gene detection and compared them based on the efficacy. The difference in gene mutation frequency between the two cohorts was shown in **Figure 4A**, and the difference in signal pathways was shown in **Figure 4B**. Among them, ARID1A and TP53 had a higher proportion in the SD/PD cohort(60% vs 0%;100% vs 40%), PI3K was enriched in the SD/PD cohort.

The TMB of patients was detected, and there was a significant statistical difference between the two cohorts. TMB of the PR was significantly higher than that of the SD/PD (P=0.025) (**Figure 5**). In addition, in a patient with hyperprogression within two months of the combination treatment, multiple gene amplification on the chromosomes of 11q13-CCND1, FGF3, FGF4, and FGF19 were found in gene sequencing.

DISCUSSION

In terms of the current research, although immuno-targeted combination therapy has brought new hope to patients with

TABLE 2B | Differences in lymphocyte subpopulation between the PR and SD (n=15): PR (n=3), SD (n=12).

	PR	SD	t	P
$CD3^+$	71.06 ± 12.74	59.39 ± 12.96	-1.40	0.185
$CD3^+CD8^+$	42.37 ± 6.11	55.18 ± 11.00	1.91	0.079
$CD3^+CD4^+$	35.13 ± 15.89	33.01 ± 11.16	-0.27	0.788
$CD8^+/CD4^+$	150.0 ± 98.04	193.9 ± 95.61	0.71	0.491
$CD56^+CD16^+$	11.67 ± 3.48	20.09 ± 10.14	1.38	0.189
$CD3^+CD19^+$	6.63 ± 4.37	8.83 ± 7.69	0.47	0.648
$CD3^+CD8^+CD279^+$	15.83 ± 14.52	13.79 ± 8.46	-0.33	0.748
$CD3^+CD8^+CD223^+$	2.33 ± 3.78	0.717 ± 0.529	-1.60	0.133
$CD3^+CD8^+CD366^+$	8.20 ± 9.68	5.51 ± 4.46	-0.74	0.470
$CD3^+CD8^+CD137^+$	0.53 ± 0.75	0.67 ± 0.60	0.33	0.747
$CD3^+CD4^+CD279^+$	**27.06 ± 20.07**	**11.18 ± 6.92**	**-2.43**	**0.030**
$CD3^+CD4^+CD223^+$	0.63 ± 0.92	0.60 ± 0.39	-0.10	0.921
$CD3^+CD4^+CD366^+$	2.70 ± 4.25	1.07 ± 0.81	-1.38	0.191
$CD3^+CD4^+CD137^+$	0.73 ± 0.58	0.52 ± 0.52	-0.61	0.554
$CD3^+CD8^+CD27^+$	72.76 ± 14.55	73.51 ± 14.04	0.08	0.935
$CD3^+CD8^+CD28^+$	70.90 ± 21.23	72.67 ± 15.68	0.17	0.871
$CD3^+CD4^+CD27^+$	60.83 ± 26.73	82.43 ± 12.73	2.13	0.053
$CD3^+CD4^+CD28^+$	**68.20 ± 25.07**	**90.54 ± 9.66**	**2.61**	**0.022**
$CD3^+CD8^+CD45RO^+CD62L^+$	**49.56 ± 8.68**	**29.65 ± 8.79**	**-3.52**	**0.004**
$CD3^+CD4^+CD45RO^+CD62L^+$	44.46 ± 16.18	57.08 ± 10.17	1.73	0.107
$CD3^+CD8^+CD45RO^+CD62L-$	34.06 ± 10.72	48.52 ± 11.51	1.96	0.071
$CD3^+CD4^+CD45RO^+CD62L-$	24.00 ± 12.35	26.25 ± 6.67	0.45	0.663

Bold values means that there are statistical differences in these T lymphocyte subpopulations.

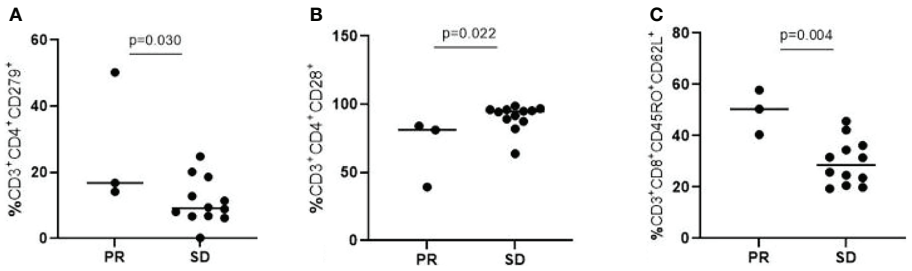

FIGURE 2 | T lymphocytes with surface molecules expressing CD3+CD4+CD279+ **(A)**, CD3+CD4+CD28+ **(B)**, CD3+CD8+CD45RO+CD62L+ **(C)** showed significant statistical differences (P=0.030, P=0.022, P=0.004).

advanced HCC, molecular biomarkers that can be applied to predict the efficacy of combination therapy are rarely systematically described due to the heterogeneity of HCC.

In this study, we preliminarily proved NLR through hematological sample analysis, $CD3^+CD4^+CD279^+$ T lymphocytes, $CD3^+CD4^+CD28^+$ T lymphocytes, and $CD3^+CD8^+CD45RO^+CD62L^+$T lymphocytes through lymphocyte subtype determination, and TP53, ARID1A, TMB, and 11q13 through genetic testing. These may be the predictive molecular biomarkers for screening effective populations for immuno-targeted combination therapy of HCC.

NLR is an inflammatory marker, which has been studied as a predictor of the efficacy of combination therapy for HCC. The median cut-off value of NLR is 4 (15). It has been confirmed that the increase in NLR has the same effect on OS in different tumor types, different sites, and different disease stages (HR=1.81, 95% CI=1.67-1.97; P <0.001), all suggesting a poor prognosis (15). Although there is no significant statistical difference in NLR in this research, there is still a trend that NLR in PR is lower compared with SD/PD. The sample size of this research is small, and the correlation between the NLR and HCC immuno-targeted combination therapy predictors still needs to be confirmed by a larger sample.

At present, only some studies believe that the detection of $CD279^+$ (PD-1) T lymphocytes can better predict the clinical outcome of patients (16). Studies have also found that after treatment with PD-1 antibody for NSCLC, low PD-1 T lymphocytes indicate a poor prognosis (17). In addition, T cells with memory phenotypes ($CD45RO^+$ and $CD62L^+$) show better anti-tumor ability and better endurance both *in vivo* and *in vitro* (18), and related adoptive cell-transfer (ACT) therapy is also in the fiery research stage. In this study, the high expression of $CD3^+CD4^+CD279^+$ and $CD3^+CD8^+CD45RO^+CD62L^+$ T lymphocytes reflects a correlation with a good prognosis. Nevertheless, whether $CD279^+$, $CD45RO^+$, and $CD62L^+$ can be used as predictors of HCC combination therapy still needs further retrospective research.

CD28 is a co-stimulatory molecule expressed on the surface of activated T cells. It can promote the proliferation and differentiation T cells by binding to B7 molecules on antigen-presenting cells (APCs). Recent studies have pointed out that the efficacy of PD-1 antibody treatment is related to the proliferation of cytotoxic T lymphocytes (CTLs), and the proliferation of CTLs depends on CD28 co-stimulation (19). This finding indicates that the CD28 pathway may reverse the immuno-suppressive state. Furthermore, in lung adenocarcinoma, patients with high CD28 expression have lower disease-free survival (DFS) (20). The high expression of CD28 in the SD in our study was consistent with the above-mentioned conclusion, indicating that the high baseline status of CD28 might exhaust the ability of the co-stimulatory pathway to reverse immunosuppression, which led to the occurrence and development of tumors.

TP53 mutation is not only related to HCC staging, but also related to lower OS and recurrence-free survival (RFS) of patients (21). At present, studies have confirmed that lung cancer patients carrying TP53 or KRAS mutations have significant clinical efficacy on PD-1 antibody therapy, which can be used as a potential predictor of immunotherapy (22). In addition,

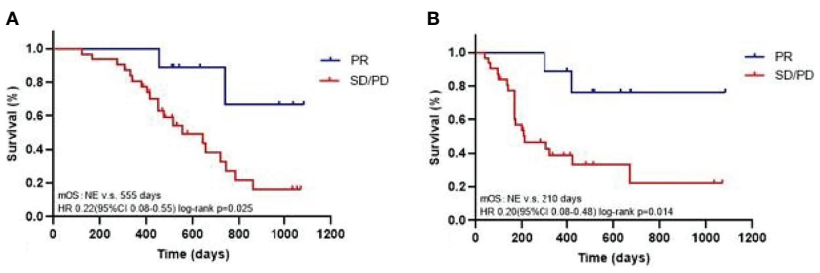

FIGURE 3 | Kaplan-Meier analysis of OS **(A)** and PFS (mRECIST; **B**).

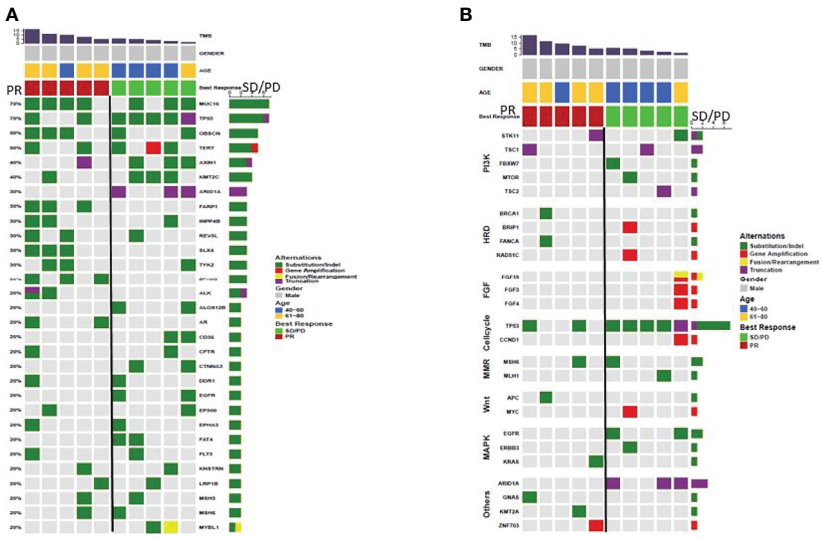

FIGURE 4 | **(A)** difference in gene mutation rate between PR (n=5) and SD/PD (n=5), **(B)** difference in signaling pathway between PR (n=5) and SD/PD (n=5).

ARID1A can exert a tumor suppressor effect by regulating the function of switching defective/sucrose non-fermenting (SWI/SNF) complex (23). At present, it is generally believed that the low expression of ARID1A is related to the poor prognosis of HCC (24), and patients with ARID1A mutations often get longer OS after immunotherapy (25). In this study, TP53 and ARID1A were enriched in the SD/PD cohort, and the contradictory conclusion might be attributed to the small test sample.

At present, many studies have confirmed that high TMB is related to the increased survival rate after immunotherapy for multiple tumor types. However, there is no uniform statement about the specific quantification of high TMB for different tumor types (26). The high TMB that appeared in the PR in this study was consistent with the above-mentioned statement, suggesting that it was a predictive factor for the efficacy of combination therapy for HCC.

Hyperprogression (HP) is closely related to the shortening of OS and PFS. At present, studies have found that the MDM2/MDM4 and copy number changes of several genes located on 11q13 are related to the HP of patients after treatment with ICIs (27). The 11q13 amplification mutation in hyperprogressive patients in this study was consistent with the above-mentioned conclusion, which preliminarily indicated that the immunotherapy was not effective for patients with 11q13 amplification mutation.

The above-mentioned laboratory indicators, lymphocyte subtypes, and gene mutations models might provide evidence for screening potentially beneficial populations for advanced HCC,

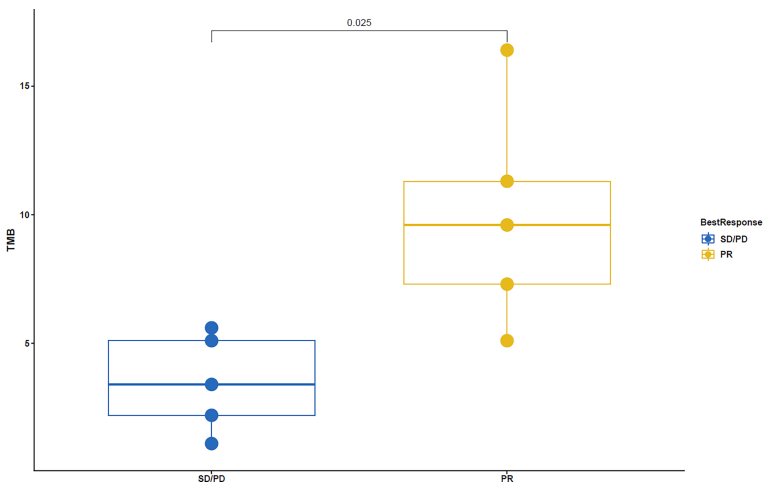

FIGURE 5 | TMB showed significant statistical difference between PR and SD/PD (P=0.025).

although the number of patients in our study was not large enough. From our primary study, it was indicated that NLR, $CD3^+CD4^+CD279^+$, $CD3^+CD4^+CD28^+$, and $CD3^+CD8^+CD45RO^+CD62L^+$ T lymphocytes in peripheral blood, and the mutations of TP53, ARID1A, TMB, and 11q13 could predict the efficacy of immuno-targeted combination therapy for patients with advanced HCC. We will expand the number of samples and conduct a more in-depth exploration in future studies.

DATA AVAILABILITY STATEMENT

The original contributions presented in the study are included in the article/**Supplementary Material**. Further inquiries can be directed to the corresponding authors.

ETHICS STATEMENT

The studies involving human participants were reviewed and approved by ethics committee of Comprehensive Cancer Center of Drum Tower Hospital of Nanjing University. The patients/participants provided their written informed consent to participate in this study.

AUTHOR CONTRIBUTIONS

JSo and BL conceived and designed the experiments. CL, SZ, YD, and JSn performed the experiments and analyzed the samples. CL, SZ, and YD analyzed the data. CL, SZ and YD composed the manuscript and provided figures. All authors interpreted the data, critically revised the manuscript for important intellectual contents and approved the final version.

FUNDING

This study was supported by National Natural Science Foundation of China (No. 81902914); Jiangsu Provincial Medical Youth Talent (No. QNRC2016043); and the Key Medical Science and Technology Development Project of Nanjing (No. ZKX16032).

SUPPLEMENTARY MATERIAL

The Supplementary Material for this article can be found online at: https://www.frontiersin.org/articles/10.3389/fimmu.2022.930096/full#supplementary-material

REFERENCES

1. Siegel RL, Miller KD, Jemal A. Cancer Statistics, 2018. *CA Cancer J Clin* (2018) 68(1):7–30. doi: 10.3322/caac.21442
2. Lee MS, Ryoo BY, Hsu CH, Numata K, Stein S, Verret W, et al. Atezolizumab With or Without Bevacizumab in Unresectable Hepatocellular Carcinoma (GO30140): An Open-Label, Multicentre, Phase 1b Study. *Lancet Oncol* (2020) 21(6):808–20. doi: 10.1016/S1470-2045(20)30156-X
3. Finn RS, Qin S, Ikeda M, Galle PR, Ducreux M, Kim TY, et al. Atezolizumab Plus Bevacizumab in Unresectable Hepatocellular Carcinoma. *N Engl J Med* (2020) 382(20):1894–905. doi: 10.1056/NEJMoa1915745
4. Cheng A, Qin S, Ikeda M, Galle PR, Ducreux M, Kim T, et al. Updated Efficacy and Safety Data From IMbrave150: Atezolizumab Plus Bevacizumab vs. Sorafenib for Unresectable Hepatocellular Carcinoma. *J Hepatol* (2022) 76:862–73. doi: 10.1016/j.jhep.2021.11.030
5. Finn RS, Qin SK, Ikeda M, Galle PR, Ducreux M, Kim TY, et al. IMbrave150: Updated Overall Survival (OS) Data From a Global, Randomized, Open-Label Phase III Study of Atezolizumab (Atezo) Plus Bevacizumab (Bev) Versus Sorafenib (Sor) in Patients (Pts) With Unresectable Hepatocellular Carcinoma (HCC). *J Clin Oncol* (2021) 39(3). doi: 10.1200/JCO.2021.39.3_suppl.267
6. Finn RS, Ikeda M, Zhu AX, Sung MW, Baron AD, Kudo M, et al. Phase Ib Study of Lenvatinib Plus Pembrolizumab in Patients With Unresectable Hepatocellular Carcinoma. *J Clin Oncol* (2020) 38(26):2960–70. doi: 10.1200/JCO.20.00808
7. Latchman Y, Wood CR, Chernova T, Chaudhary D, Borde M, Chernova I, et al. PD-L2 is a Second Ligand for PD-1 and Inhibits T Cell Activation. *Nat Immunol* (2001) 2(3):261–8. doi: 10.1038/85330
8. Freeman GJ, Long AJ, Iwai Y, Bourque K, Chernova T, Nishimura H, et al. Engagement of the PD-1 Immunoinhibitory Receptor by a Novel B7 Family Member Leads to Negative Regulation of Lymphocyte Activation. *J Exp Med* (2000) 192(7):1027–34. doi: 10.1084/jem.192.7.1027
9. Okazaki T, Honjo T. PD-1 and PD-1 Ligands: From Discovery to Clinical Application. *Int Immunol* (2007) 19:813–24. doi: 10.1093/intimm/dxm057
10. Llovet JM, Ricci S, Mazzaferro V, Hilgard P, Gane E, Blanc JF, et al. Sorafenib in Advanced Hepatocellular Carcinoma. *N Engl J Med* (2008) 359(4):378–90. doi: 10.1056/NEJMoa0708857
11. Kudo M, Finn RS, Qin S, Han KH, Ikeda K, Piscaglia F, et al. Lenvatinib Versus Sorafenib in First-Line Treatment of Patients With Unresectable Hepatocellular Carcinoma: A Randomised Phase 3 non-Inferiority Trial. *LANCET* (2018) 391(10126):1163–73. doi: 10.1016/S0140-6736(18)30207-1
12. Yau T, Park JW, Finn RS, Cheng AL, Mathurin P, Edeline J, et al. Nivolumab Versus Sorafenib in Advanced Hepatocellular Carcinoma (CheckMate 459): A Randomised, Multicentre, Open-Label, Phase 3 Trial. *Lancet Oncol* (2022) 23:77–90. doi: 10.1016/S1470-2045(21)00604-5
13. Xu J, Shen J, Gu S, Zhang Y, Wu L, Wu J, et al. Camrelizumab in Combination With Apatinib in Patients With Advanced Hepatocellular Carcinoma (RESCUE): A Nonrandomized, Open-Label, Phase II Trial. *Clin Cancer Res* (2021) 27(4):1003–11. doi: 10.1158/1078-0432.CCR-20-2571
14. Ren ZG, Xu JM, Bai YX, Xu AB, Cang SD, Du CY, et al. Sintilimab Plus a Bevacizumab Biosimilar (IBI305) Versus Sorafenib in Unresectable Hepatocellular Carcinoma (ORIENT-32): A Randomised, Open-Label, Phase 2-3 Study. *Lancet Oncol* (2021) 22(7):977–90. doi: 10.1016/S1470-2045(21)00252-7
15. Templeton AJ, McNamara MG, Seruga B, Vera-Badillo FE, Aneja P, Ocana A, et al. Prognostic Role Of neutrophil-to-Lymphocyte Ratio in Solid Tumors: A Systematic Review and Meta-Analysis. *J Natl Cancer Inst* (2014) 106(6):u124. doi: 10.1093/jnci/dju124
16. Kansy BA, Concha-Benavente F, Srivastava RM, Jie H, Shayan G, Lei Y, et al. PD-1 Status in CD8+T Cells Associates With Survival and Anti-PD-1 Therapeutic Outcomes in Head and Neck Cancer. *Cancer Res* (2017) 77(22):6353–64. doi: 10.1158/0008-5472.CAN-16-3167
17. Kamphorst AO, Pillai RN, Yang S, Nasti TH, Akondy RS, Wieland A, et al. Proliferation of PD-1+ CD8 T Cells in Peripheral Blood After PD-1–Targeted Therapy in Lung Cancer Patients. *Proceedings of the National Academy of Sciences* (2017) 114(19):4993–8. doi: 10.1073/pnas.1705327114
18. Liu Q, Sun Z, Chen L. Memory T Cells: Strategies for Optimizing Tumor Immunotherapy. *Protein Cell* (2020) 11(8):549–64. doi: 10.1007/s13238-020-00707-9
19. Kamphorst AO, Wieland A, Nasti T, Yang S, Zhang R, Barber DL, et al. Rescue of Exhausted CD8 T Cells by PD-1–Targeted Therapies Is CD28-Dependent.. *Science* (2017) 355(6332):1423–7. doi: 10.1126/science.aaf0683

20. Sun D, Tian L, Bian T, Zhao H, Tao J, Feng L, et al. CD28 in the Prognosis of Young Lung adenocarcinoma Patients. *Bmc Cancer* (2020) 20(1):910. doi: 10.1186/s12885-020-07412-0
21. Liu J, Ma Q, Zhang M, Wang X, Zhang D, Li W, et al. Alterations of TP53 Are Associated With a Poor Outcome for Patients With Hepatocellular Carcinoma: Evidence From a Systematic Review and Meta-Analysis. *Eur J Cancer* (2012) 48(15):2328–38. doi: 10.1016/j.ejca.2012.03.001
22. Dong ZY, Zhong WZ, Zhang XC, Su J, Xie Z, Liu SY, et al. Potential Predictive Value of TP53 and KRAS Mutation Status for Response to PD-1 Blockade Immunotherapy in Lung Adenocarcinoma. *Clin Cancer Res* (2017) 23 (12):3012–24. doi: 10.1158/1078-0432.CCR-16-2554
23. Kadoch C, Hargreaves DC, Hodges C, Elias L, Ho L, Ranish J, et al. Proteomic and Bioinformatic Analysis of Mammalian SWI/SNF Complexes Identifies Extensive Roles in Human Malignancy. *Nat Genet* (2013) 45(6):592–601. doi: 10.1038/ng.2628
24. Yim S, Kang S, Shin J, Jeong Y, Sohn B, Um S, et al. Low ARID1A Expression is Associated With Poor Prognosis in Hepatocellular Carcinoma. *CELLS-BASEL* (2020) 9(9):2002. doi: 10.3390/cells9092002
25. Jiang T, Chen X, Su C, Ren S, Zhou C. Pan-Cancer Analysis Ofarid1a Alterations as Biomarkers for Immunotherapy Outcomes. *J Cancer* (2020) 11(4):776–80. doi: 10.7150/jca.41296
26. Samstein RM, Lee C, Shoushtari AN, Hellmann MD, Shen R, Janjigian YY, et al. Tumor Mutational Load Predicts Survival After Immunotherapy Across Multiple Cancer Types. *Nat Genet* (2019) 51(2):202–6. doi: 10.1038/s41588-018-0312-8
27. Singavi AK, Menon S, Kilari D, Alqwasmi A, Ritch PS, Thomas JP, et al. 1140pdpredictive Biomarkers for Hyper-Progression (HP) in Response to Immune Checkpoint Inhibitors (ICI) – Analysis of Somatic Alterations (SAs). *Ann Oncol* (2017) 28. doi: 10.1093/annonc/mdx376.006

Conflict of Interest: The authors declare that the research was conducted in the absence of any commercial or financial relationships that could be construed as a potential conflict of interest.

The reviewer SW declared a shared parent affiliation with the authors to the handling editor at the time of the review.

Publisher's Note: All claims expressed in this article are solely those of the authors and do not necessarily represent those of their affiliated organizations, or those of the publisher, the editors and the reviewers. Any product that may be evaluated in this article, or claim that may be made by its manufacturer, is not guaranteed or endorsed by the publisher.

frontiers | Frontiers in Immunology

ORIGINAL RESEARCH
published: 08 July 2022
doi: 10.3389/fimmu.2022.940009

Efficacy and Safety of Drug-Eluting Beads Transarterial Chemoembolization Combining Immune Checkpoint Inhibitors in Unresectable Intrahepatic Cholangiocarcinoma: A Propensity Score Matching Analysis

Xue-Gang Yang[1,2], *Yan-Yuan Sun*[2], *De-Shan Li*[2], *Guo-Hui Xu*[2] *and Xiao-Qi Huang*[1*]

[1] Huaxi MR Research Center (HMRRC), Functional and Molecular Imaging Key Laboratory of Sichuan Province, Department of Radiology, West China Hospital, Sichuan University, Chengdu, China, [2] Department of Interventional Radiology, Sichuan Cancer Hospital and Institute, Chengdu, China

Purpose: To assess the effectiveness and safety of drug-eluting beads transarterial chemoembolization plus immune checkpoint inhibitors (DEB-TACE+ICIs) versus chemotherapy (gemcitabine+cisplatin) for patients with unresectable intrahepatic cholangiocarcinoma (iCCA).

Materials and Methods: This retrospective study included unresectable iCCA patients treated with DEB-TACE+ICIs or chemotherapy between May, 2019 and August, 2021. The differences in tumor responses, progression-free survival (PFS), overall survival (OS), and treatment-related adverse events (TRAEs) were compared between the 2 groups. Patient baseline characteristics, PFS, and OS were compared among 2 groups before and after propensity score-matching (PSM). Factors affecting PFS and OS were analyzed by Cox's proportional hazards regression model.

Results: The study included 49 patients with unresectable iCCA patients, 20 in the DEB-TACE+ICIs group and 29 in the chemotherapy group. PSM analysis created 20 pairs of patients in 2 groups. The patients in the DEB-TACE+ICIs group had a higher objective response rate (55.0% vs. 20.0%, P=0.022), higher PFS (median, 7.2 vs. 5.7 months, P=0.036), and higher OS (median, 13.2 vs. 7.6 months, P=0.015) than those in the chemotherapy group. Multivariate analyses suggested that chemotherapy, tumor size >5cm, and multiple tumors were the independent risk factors for PFS and OS. The incidence of TRAEs was similar between the 2 groups.

Conclusion: Compared to chemotherapy, DEB-TACE plus ICIs improved survival and was well-tolerated in patients with unresectable iCCA.

Keywords: unresectable intrahepatic cholangiocarcinoma, transarterial chemoembolization, immune checkpoint inhibitor, chemotherapy, combined therapy

OPEN ACCESS

Edited by:
Yunfei Xu,
Shandong University, China

Reviewed by:
Kangshun Zhu,
The Second Affiliated Hospital of Guangzhou Medical University, China
Xiaoming Yang,
University of Washington, United States
Chuansheng Zheng,
Huazhong University of Science and Technology, China
Lujun Shen,
Sun Yat-Sen University Cancer Center (SYSUCC), China

***Correspondence:**
Xiao-Qi Huang
julianahuang@163.com

Specialty section:
This article was submitted to Cancer Immunity and Immunotherapy, a section of the journal Frontiers in Immunology

Received: *09 May 2022*
Accepted: *20 June 2022*
Published: *08 July 2022*

Citation:
Yang X-G, Sun Y-Y, Li D-S, Xu G-H and Huang X-Q (2022) Efficacy and Safety of Drug-Eluting Beads Transarterial Chemoembolization Combining Immune Checkpoint Inhibitors in Unresectable Intrahepatic Cholangiocarcinoma: A Propensity Score Matching Analysis. Front. Immunol. 13:940009. doi: 10.3389/fimmu.2022.940009

INTRODUCTION

Intrahepatic cholangiocarcinoma (iCCA) is the second most common primary liver malignancy. In the last decade, its global incidence has increased from 0.44 per, 100000 to 1.18 cases per, 100000; the mortality has increased from 1.5 per, 100000 to 2.5 cases per, 100000 in men and 1.2 per, 100000 to 1.7 cases per, 100000 in women (1, 2). The iCCA patients are often asymptomatic, the disease is usually accidentally discovered, typically by imaging, when in an advanced stage; thus, most patients have a poor prognosis. The major clinical symptoms are abdominal pain, jaundice, and weight loss (3). Considering the advanced disease stage, including vascular invasiveness and distal metastasis, most iCCA (approximately 80%) patients lose their chance to undergo surgical resection and transplantation (4, 5). Moreover, even after treatment, early recurrence and metastasis are prone to occur.

The median overall survival (OS) of untreated iCCA patients has been reported to be 3 to 6 months (6, 7). Previous study has suggested that chemotherapy (gemcitabine+cisplatin) can improve the clinical outcomes for unresectable iCCA (8). However, many patients have a chemo-refractory or discontinue chemotherapy due to severe adverse reactions associated with treatment. Thus, new treatment methods have been proposed, including loco-regional therapy, biological therapy, and targeted therapy (3, 9); yet, there is still no consensus on the best therapy for unresectable iCCA.

Over the years, there has been much interest in transarterial chemoembolization (TACE) (10). However, minimal vascularity and lower drug concentration due to leakage of loading chemotherapeutic agents are the biggest challenges when treating patients with iCCA (11). Recent studies have found that drug-eluting beads transarterial chemoembolization (DEB-TACE) can enhance intratumoral drug penetration and reduce systemic side effects compared to conventional TACE (12, 13). Moreover, the OS of unresectable iCCA patients treated with DEB-TACE was 9-10 months (14–16).

Rapid advances in cancer immunotherapy using immune checkpoint inhibitors (ICIs), such as atezolizumab combined with bevacizumab, have significantly improved outcomes in unresectable hepatocellular carcinoma (HCC) compared to sorafenib (17). Recently, China Food and Drug Administration (CFDA) approved camrelizumab combined with chemotherapy (gemcitabine+cisplatin) (Gemox) as a first-line systemic treatment for advanced biliary tract cancer based on phase II study results (18), and sintilimab plus bevacizumab biosimilar (Ibi305) as a first-line systemic therapy for middle-advanced HCC based on phase II/III study results (19).

DEB-TACE is used to achieve more extensive tumor necrosis, which can induce anti-tumor immune response in patients with unresectable iCCA; yet, it may not confer long-time anti-tumor effect. However, combining DEB-TACE with ICIs may further increase the development of tumor antigen-specific memory T cells, sustaining anti-tumor responses in unresectable iCCA patients (20). Thus, the aim of current study was to examine and compare the efficacy and safety of DEB-TACE combined with immune checkpoint inhibitors (DEB-TACE+ICIs) versus chemotherapy (gemcitabine+cisplatin) for unresectable iCCA patients.

MATERIALS AND METHODS

Patient Cohort

This retrospective study was performed in accordance with the principles of the Declaration of Helsinki and was approved by the ethical review committee of Sichuan Cancer Hospital. The requirement to obtain informed patient consent was waived. Clinical data of patients with unresectable iCCA who underwent DEB-TACE+ICIs or chemotherapy as first-line therapy at Sichuan Cancer Hospital between May, 2019 and August, 2021 were analyzed. Unresectable iCCA included multifocal tumors, extensive regional lymphadenopathy, distant metastases, non-reconstructable vascular involvement, or severe underlying liver parenchymal disease. Patients were initially treated with DEB-TACE plus ICIs because of the rejection of system chemotherapy.

The inclusion criteria were: 1) age between 18 and 80 years; 2) histologically or cytologically confirmed diagnosis of iCCA; 3) Eastern Cooperative Oncology Group performance score (ECOG PS) of ≤ 2; 4) Child-Pugh class ≤ 7. The exclusion criteria were: 1) with other malignancies; 2) previously received TACE, curative resection, ablation, hepatic arterial infusion chemotherapy (HAIC), other systemic treatment, or radiotherapy; 3) current or previous central nervous system metastasis; 4) mixed feature iCCA-HCC; 5) with current or previous severe cardiovascular disease or coagulation disorders; 6) incomplete clinical or imaging data.

Preoperative Evaluation

For research analysis, we collected the preoperative clinical data from the medical record systems: sex, age, ECOG PS, Child-Pugh class, carcinoembryonic antigen (CEA), carbohydrate antigen 199 (CA_199), tumor number, tumor size, extrahepatic metastasis, hematologic and biochemical indexes. Also, all patients underwent contrast-enhanced magnetic resonance imaging (MRI) or computed tomography (CT) scan one week before the first treatment.

Chemoembolization Procedure

CalliSpheres® (Jiangsu Hengrui Medicine Co. Ltd, Jiangsu, China) beads (100-300 μm) were loaded with doxorubicin (50 - 80 mg). The loading process (21) was: 1) the concentration of doxorubicin was 20 mg/ml; 2) the supernatant of CalliSpheres® beads was excluded, then beads and doxorubicin were mixed; 3) non-ionic contrast agent was added into the mixture (using a 1:1 ratio) for further application.

Before performing chemoembolization, celiac arteriography and superior mesenteric arteriography were implemented to evaluate the feeding arteries of the tumor. Then, microcatheters were used to catheterize the tumor-feeding arteries. The mixture of CalliSpheres® beads and non-ionic contrast agent were injected at the speed of 1 ml/min. The injection was completed if the stasis flow of the contrast agent

was observed. If one vial of CalliSpheres® beads did not complete the chemoembolization, regular Embosphere (Biosphere Medical, Roissy en France, France) with 100-300 μm was used.

DEB-TACE was repeated "on demand" in patients with no deteriorating physical status or organ function after contrast-enhanced MRI or CT detected viable tumors during follow-up.

Immune Check Inhibitors (ICIs) and Chemotherapy Administration

Administration of ICIs was first within one week after the initiated DEB-TACE. Intravenous administration of 200 mg camrelizumab (Hengrui Medical, Suzhou, China) or sintilimab (Innovent Biologics, Suzhou, China) was conducted every 3 weeks; the administration was stopped if severe toxicity, tumor progression, or death appeared. Dose interruption, but not reduction, was allowed.

In the chemotherapy group, intravenous administration of every cycle comprised cisplatin (25mg per square meter) followed by gemcitabine (1000 mg per square meter); every drug was performed on day 1 and 8 every 21 days, first for four cycles. If there was no tumor progression at four cycles, patients could continue treatment for another 12 weeks using the same regimen. However, if patients could not tolerate the adverse reaction to therapy, discontinuation or reduction of the dose was recommended and determined by oncologists with more than 10 years of experience in the field.

Postoperative Follow-Up

All patients were regularly follow-up at intervals of 3-6 weeks after the first treatment. The follow-up included physical examination, contrast-enhanced MRI or CT of the abdomen, chest CT, laboratory tests, and other examinations. The last follow-up time was January 31, 2022.

During follow-up, DEB-TACE+ICIs or chemotherapy was stopped when intolerable toxicity, disease progression, or change in the treatment regimen occurred. The choice of follow-up treatment, such as a change in chemotherapy regimen, ICIs (chemotherapy group), radiotherapy, ablation, TACE (chemotherapy group), or optimal supportive care, was performed based on discussions between our multidisciplinary liver tumor team and the patient's requirements.

Assessments

Tumor responses were assessed by 2 radiologists with 10 years of experience based on the modified Response Evaluation Criteria in Solid Tumors (mRECIST). Multiple tumors were defined as more than one tumor. Tumor responses were categorized as complete response (CR), partial response (PR), stable disease (SD), or progression disease (PD). The objective response rate (ORR) was defined as the proportion of patients achieving CR and PR. Disease control rate (DCR) was defined as the proportion of patients with complete, partial response, or stable disease. Tumor responses of all patients were confirmed no less than four weeks after the initial observation.

Progression-free survival (PFS) was defined as the time from the first day of inpatients to PD or death from any cause, whichever occurred first. OS was defined as the time from to the first day of inpatients to the time of death or the last follow-up date.

Adverse events (AEs) were recorded and evaluated based on the Common Terminology Criteria for Adverse Events Version 5.0.

Statistical Methods

Statistical analyses were carried out using the SPSS Statistics 25.0 (SPSS Inc., Chicago, IL, USA). The propensity score model included age, sex, tumor number (single or multiple), and tumor differentiation. The model provided a 1:1 match between the 2 groups, as previously described (22). Before and after propensity score matching (PSM), categorical data were expressed as frequency; quantitative data were expressed as mean ± standard deviation and median (range) for normally and non-normally distributed variables, respectively. To determine the significant differences between the 2 groups, continuity correction and Mann-Whitney U test, Chi-square, or Fisher exact test were used. Survival curves of PFS and OS were analyzed by the Kaplan–Meier method using the log-rank test. Univariate and multivariate analyses were used Cox's proportional hazards regression model to determine the prognostic factors. Variables (P<0.1) in the univariate analysis were entered into the multivariable analysis to look for predictors of efficacy. A two-sided P level less 0.05 was considered statistically significant.

RESULTS

Patient Characteristics

Totally 49 patients with unresectable iCCA were included in current study, 20 patients received DEB-TACE+ICIs and 29 patients received chemotherapy (**Figure 1**). In the DEB-TACE +ICIs group, 7 patients received camrelizumab, and 13 patients received sintilimab.

PD was seen in 2 patients after DEB-TACE+ICIs treatment; 1 patient received chemoradiotherapy and another patient received systemic chemotherapy. In addition, PD was observed in 5 patients after chemotherapy; 2 patients received a change of chemotherapy regimen, 1 patient received DEB-TACE+ICIs, and 2 patients received chemoradiotherapy.

Before PSM, patients in the chemotherapy group had a higher aspartate aminotransferase (AST)(P=0.035) and albumin (P=0.018) compared to those in the DEB-TACE group (**Table 1**). Performing PSM resulted in matched cohorts of 20 patients every group with well-balanced baseline characteristics (**Table 1**).

Tumor Response Evaluation

The PR and ORR were higher in the DEB-TACE+ICIs group than those in the chemotherapy group before PSM (PR, 50.0% vs. 13.8%, respectively, P=0.006; ORR, 55.0% vs. 13.8%, respectively, P=0.002) and after PSM (PR, 50.0% vs. 20.0%, respectively, P=0.047; ORR, 55.0% vs. 20.0%, respectively, P=0.022), and the

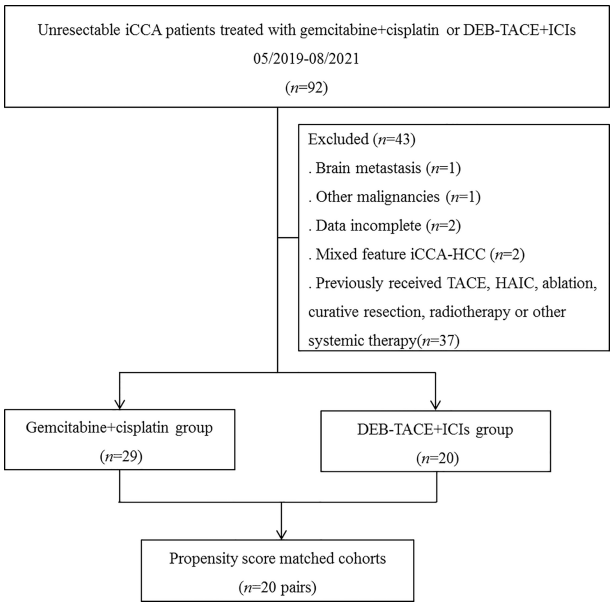

FIGURE 1 | Flow diagram of patient enrollment. iCCA, intrahepatic cholangiocarcinoma; DEB-TACE+ICIs, drug-eluting beads transarterial chemoembolization combined with immune checkpoint inhibitors; TACE, transarterial chemoembolization; HAIC, hepatic arterial infusion chemotherapy.

DCR of 2 groups before and after PSM were similar (respectively, $P>0.05$)(**Table 2**).

Survival Analysis

The median follow-up time was 7.2 months (range, 2.8-28.5 months) in this study. In addition, 55.0% (11/20) patients in the DEB-TACE group and 69% (20/29) patients in the chemotherapy group died.

Before PSM, the median PFS was higher in the DEB-TACE +ICIs group than in the chemotherapy group: 7.2 months (95% CI: 6.012–8.388) versus 5.0 months (95% CI: 2.390–7.610) (P=0.026, **Figure 2a**); the median OS was higher in the DEB-TACE+ICIs group than in the chemotherapy group: 13.2 months (95%: CI 4.977–21.423) versus 7.6 months (95% CI: 6.583–8.617) (***P***= 0.004, **Figure 2b**).

Performing PSM, the median PFS was higher in the DEB-TACE+ICIs group than in the chemotherapy group: 7.2 months (95% CI: 6.012–8.388) versus 5.7 months (95% CI: 3.056–8.344) (P=0.036, **Figure 3a**); the median OS was higher in the DEB-TACE+ICIs than in the chemotherapy group: 13.2 months (95% CI: 4.977–21.423) versus 7.6 months (95% CI: 6.317–8.883) (P=0.015, **Figure 3b**).

Prognostic Factors Analyses

The univariate and multivariate analyses results in the matched cohort were shown (**Table 3**). Cox's proportional hazard model

TABLE 1 | Baseline characteristics of patients in the two groups before and after PSM.

	Before PSM			After PSM		
Characteristics, n (%)	**DEB-TACE+ICIs (n=20)**	**Chemotherapy (n=29)**	***P***	**DEB-TAEC+ICIs (n=20)**	**Chemotherapy (n=20)**	***P***
Median age, years (range)	59 (34-76)	59 (31-78)	0.906	59 (34-76)	59 (31-74)	>0.999
≤ 60	10 (50.0)	15 (51.7)		10 (50.0)	10 (50.0)	
> 60	10 (50.0)	14 (48.3)		10 (50.0)	10 (50.0)	
Sex			0.458			0.519
Male	11 (55.0)	19 (65.5)		11 (55.0)	13 (65.0)	
Female	9 (45.0)	10 (34.5)		9 (45.0)	7 (35.0)	
ECOG PS			0.353			0.429
0	8 (40.0)	8 (27.6)		8 (40.0)	5 (25.0)	
1	10 (50.0)	20 (69.0)		10 (50.0)	14 (70.0)	
2	2 (10.0)	1 (3.4)		2 (10.0)	1 (5.0)	
Child-Pugh class			0.388			0.348
A5	13 (65.0)	22 (75.9)		13 (65.0)	16 (80.0)	
A6	3 (15.0)	5 (17.2)		3 (15.0)	3 (15.0)	
B7	4 (20.0)	2 (6.9)		4 (20.0)	1 (5.0)	
CA199, U/ml			0.938			0.723
≤ 37	6 (30.0)	9 (31.0)		6 (30.0)	5 (25.0)	
> 37	14 (70.0)	20 (69.0)		14 (70.0)	15 (75.0)	
CEA, ng/ml			0.062			0.197
≤ 5	10 (50.0)	7 (24.1)		10 (50.0)	6 (30.0)	
> 5	10 (50.0)	22 (75.9)		10 (50.0)	14 (70.0)	
AST, U/L	32.3±16.3	58.1±54.2	0.035	32.3±16.3	38.1±17.4	0.377
ALT, U/L	28 (12-75)	40 (15-175)	0.080	28 (12-75)	39.5 (19-175)	0.137
Albumin, g/dl	38.8±5.5	39.4±3.4	0.018	38.8±5.5	38.6±3.7	0.270
Bilirubin (μmol/L)	11.9 (6.8-36.1)	14.1 (4.7-95.9)	0.143	11.9 (6.8-36.1)	12.5 (4.7-95.9)	0.315
WBC ($x10^9$/L)	7.1±1.6	6.3±2.0	0.817	7.1±1.6	6.9±2.0	0.640
Neutrophile ($x10^9$/L)	5.1±1.4	4.4±1.7	0.940	5.1±1.4	4.9±1.7	0.864

(Continued)

TABLE 1 | Continued

Characteristics, n (%)	Before PSM			After PSM		
	DEB-TACE+ICIs (n=20)	Chemotherapy (n=29)	*P*	DEB-TAEC+ICIs (n=20)	Chemotherapy (n=20)	*P*
PLT (x10^9/L)	196±75	187±61	0.610	196±75	200±58	0.472
HGB (g/L)	125±18	129±18	0.870	125±18	132±17	0.897
Tumor number			0.923			0.206
Single	12 (60.0)	17 (58.6)		12 (60.0)	8 (40.0)	
Multiple	8 (40.0)	12 (41.4)		8 (40.0)	12 (60.0)	
Tumor size, cm	6.7±3.0	5.8±3.0	0.544	6.7±3.0	6.3±2.9	0.889
≤ 5	6 (30.0)	14 (48.3)		6 (30.0)	8 (40.0)	
> 5	14 (70.0)	15 (51.7)		14 (70.0)	12 (60.0)	
Tumor differentiation			0.592			0.765
II	5 (25.0)	7 (24.1)		5 (25.0)	5 (25.0)	
III	7 (35.0)	14 (48.3)		7 (35.0)	9 (45.0)	
IV	8 (40.0)	8 (27.6)		8 (40.0)	6 (30.0)	
Extrahepatic metastasis			0.945			>0.999
Yes	15 (75.0)	22 (75.9)		15 (75.0)	15 (75.0)	
No	5 (25.0)	7 (24.1)		5 (25.0)	5 (25.0)	

PSM, propensity score matching; DEB-TACE+ICIs, drug-eluting bead transarterial chemoembolization combined with immune checkpoint inhibitors; ECOG PS, Eastern Cooperative Oncology Group performance score; CA199, Carbohydrate antigen_199; AST, aspartate aminotransferase; CEA, carcinoembryonic antigen; ALT, alanine transaminase; WBC, white blood cell; PLT, platelet; HGB, Hemoglobin.

suggested that the treatment option (DEB-TACE+ICIs vs. chemotherapy)(hazard ratio [HR]=2.325, 95% CI: 1.135–4.764, *P*=0.021), tumor size (≤5cm vs. >5cm)(HR=2.749, 95% CI: 1.185-6.378, *P*=0.019), and tumor number (single vs. multiple) (HR=1.721, 95% CI: 0.452-3.120, *P*=0.045), were independent predictive factor for PFS. Furthermore, treatment option

TABLE 2 | Summary of response rates before and after PSM.

All response, n (%)	Before PSM			After PSM		
	DEB-TACE+ICIs (n=20)	Chemotherapy (n=29)	*P*	DEB-TACE+ICIs (n=20)	Chemotherapy (n=20)	*P*
CR	1(5.0)	0 (0)	0.224	1 (5.0)	0 (0)	0.311
PR	10 (50.0)	4 (13.8)	0.006	10 (50.0)	4 (20.0)	0.047
SD	7 (35.0)	20 (69.0)	0.019	7 (35.0)	13 (65.0)	0.058
PD	2 (10.0)	5 (17.2)	0.476	2 (10.0)	3 (15.0)	0.633
ORR	11 (55.0)	4 (13.8)	0.002	11 (55.0)	4 (20.0)	0.022
DCR	18 (90.0)	24 (82.8)	0.476	18 (90.0)	17 (85.0)	0.633

PSM, propensity score matching; DEB-TACE+ICIs, drug-eluting bead transarterial chemoembolization combined with immune checkpoint inhibitors; CR, complete response; PR, partial response; SD, stable disease; PD, progressive disease; ORR, objective response rate; DCR, disease control rate.

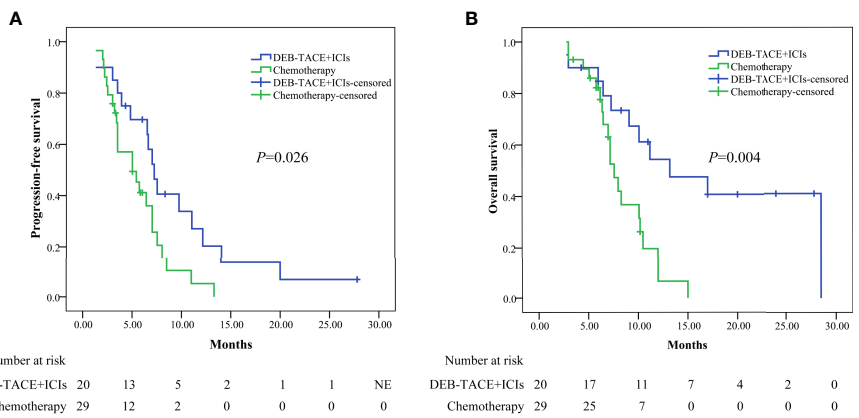

FIGURE 2 | Kaplan-Meier analyses of progression-free survival **(A)** and overall survival **(B)** in the two groups before PSM. DEB-TACE+ICIs, drug-eluting beads transarterial chemoembolization combined with immune checkpoint inhibitors; PSM, propensity score matching.

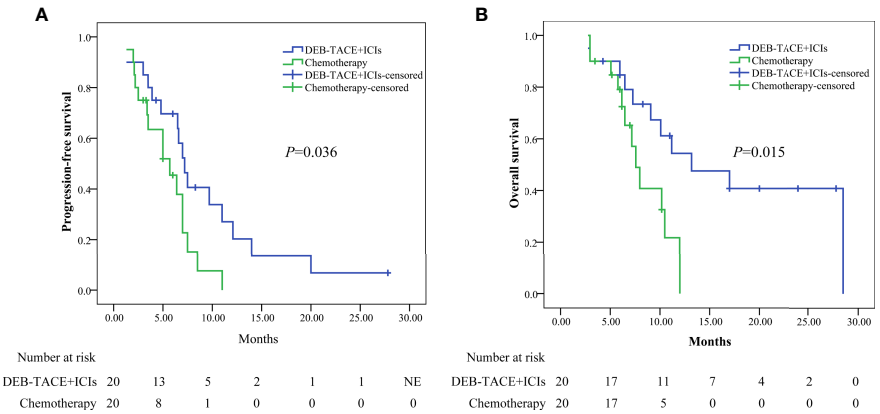

FIGURE 3 | Kaplan-Meier analyses of progression-free survival **(A)** and overall survival **(B)** in the two groups after PSM. DEB-TACE+ICIs, drug-eluting beads transarterial chemoembolization combined with immune checkpoint inhibitors; PSM, propensity score matching.

TABLE 3 | Prognostic factors associated with PFS and OS after PSM.

Variables	Progression-free survival						Overall survival					
	Univariate analysis			Multivariate analysis			Univariate analysis			Multivariate analysis		
	HR	95% CI	*P*	HR	95% CI	*P*	HR	95% CI	*P*	HR	95% CI	*P*
Age (years) ≤60/>60	1.559	0.768-3.166	0.219				1.866	0.798-4.364	0.150			
Sex Female/Male	0.686	0.339-1.388	0.295				0.911	0.401-2.070	0.823			
ECOG PS 0/1+2	1.149	0.549-2.404	0.712				1.862	0.725-4.785	0.196			
Child-Pugh class A5/A6+B7	0.809	0.468-2.645	0.809				2.021	0.775-5.273	0.150			
CA199 (u/ml) ≤37/>37	0.665	0.298-1.485	0.320				1.256	0.464-3.399	0.653			
CEA (ug/ml) ≤5/>5	1.202	0.566-2.556	0.632				1.495	0.582-3.840	0.404			
AST (U/L) ≤40/>40	1.003	0.458-2.196	0.994				1.145	0.484-2.709	0.759			
ALT (U/L) ≤35/>35	0.775	0.372-1.614	0.775				1.638	0.641-4.188	0.303			
Albumin level (g/L) ≤35/>35	0.337	0.188-1.770	0.337				0.278	0.110-1.112	0.216			
Tumor number Single/Multiple	1.379	0.678-1.805	0.035	1.721	0.452-3.120	0.045	1.204	0.525-1.762	0.061	1.452	0.567-2.148	0.032
Tumor size (cm) ≤5/>5	2.436	1.060-5.600	0.036	2.749	1.185-6.378	0.019	2.117	0.922-4.863	0.067	1.961	1.124-3.321	0.023
Tumor differentiation II/III+IV	1.189	0.531-2.662	0.674				1.623	0.551-4.781	0.379			
Extrahepatic metastasis Yes/No	0.841	0.376-1.883	0.674				0.616	0.209-1.814	0.379			
Treatment DEB-TACE+ICIs/Chemotherapy	2.170	1.020-4.619	0.044	2.481	1.150-5.354	0.021	2.906	1.174-7.194	0.006	2.882	1.153-7.203	0.024

Analyses were performed using Cox's proportional hazards regression model. PFS, progression-free survival; OS, overall survival; PSM, propensity score matching; HR, Hazard Ratio; CI, confidence interval; ECOG PS, ALT, alanine transaminase; Eastern Cooperative Oncology Group performance score; TBIL, total bilirubin; AST, aspartate transaminase; DEB-TACE+ICIs, drug-eluting bead transarterial chemoembolization combined with immune checkpoint inhibitor.

(HR=2.882, 95% CI: 1.153–7.203, *P*=0.024), tumor size (HR=1.961, 95% CI: 1.124–3.321, *P*=0.023), and tumor number (HR=1.452, 95% CI: 0.567-2.148, *P*=0.032) were identified as the independent predictive factor for OS (**Table 3**).

Safety

After PSM, the incidence of treatment-related AEs (TRAEs) in 2 groups was reported. TRAEs were observed at 92.5% (37/40), and no more than grade 4 occurred in the 2 groups (**Table 4**). ICIs-related AEs (irAEs) caused interruption of ICIs in 20% (4/20) of patients in the DEB-TACE+ICIs group. Moreover, TRAEs led to dose interruption and reduction of chemotherapy in 15.0% (3/20) and 15.0% (3/20) patients in the chemotherapy group, respectively.

The frequency of TRAEs related to hematologic toxic effects, including leukopenia (10.0% vs. 40.0%, *P*=0.028), and neutropenia (5.0% vs. 35.0%, *P*=0.018), were lower in DEB-TACE group than chemotherapy group. TRAEs related to hepatic function, including increased ALT and AST, hyperbilirubinemia, and hypoalbuminemia were no significant difference between the 2 groups (respectively, *P*>0.05). ICIs-related AEs (irAEs) mainly included hypothyroidism and reactive cutaneous capillary endothelial proliferation (RCCEP). The incidence rate of hypothyroidism was 25% (5/20), and RCCEP was 25% (5/20).

DISCUSSION

This study suggested that DEB-TACE+ICIs improved survival in unresectable iCCA patients compared to chemotherapy. The result of median OS was increased from 6.6 months to 13.2 months, which might be related to the better ORR and PFS in patients who received DEB-TACE+ICIs compared to those treated with chemotherapy. Furthermore, multivariate analyses showed that DEB-TACE+ICIs was an independent predictor for prolonged PFS and OS. Thus, DEB-TACE+ICIs may be a good choice for unresectable iCCA who refuse systemic chemotherapy.

Previous studies (14, 23–25) have assessed unresectable iCCA patients treated with DEB-TACE and reported the median PFS was 3.0-3.9 months and OS was 10.5-12.4 months. Other studies reported that the median PFS and OS was 1.4-4.0 months and 4.3-12.7 months, respectively, in advanced biliary tract cancer patients treated with ICIs alone (26–29). Moreover, Chen et al. recently reported that the median PFS and OS was 6.1 months and 11.8 months, respectively, in advanced biliary tract cancer patients treated with camrelizumab plus Gemox (18). In current study, the median PFS and OS was 7.2 months and 13.2 months, respectively, in unresectable iCCA patients treated with DEB-TACE plus ICIs, which showed that DEB-TACE+ICIs might be an appropriate treatment plan in patients with unresectable iCCA. DEB-TACE is based on the administration of drug-eluting beads intra-arterially *via* catheter, which leads to local tumor necrosis, subsequently eliciting an anti-cancer immune response that may be further boosted with ICIs (11, 20). Liao et al. examined the effect of DEB-TACE on cellular immune function and regulatory T cells in patients with HCC and found that DEB-TACE can stimulate the cytokine spectrum and increase $CD4^+$ and $CD8^+$ T cells in PBMCs of HCC patients while reducing the Treg cell population (30). Moreover, Lee et al.

TABLE 4 | Summary of TRAEs after PSM.

Event, n (%)	Chemotherapy (n=20)			DEB-TACE+ICIs (n=20)			P		
Any TRAE	**Any grade**	**Grade 1/2**	**Grade 3/4**	**Any grade**	**Grade 1/2**	**Grade 3/4**	**Any grade**	**Grade 1/2**	**Grade 3/4**
	20(100.0)	**17 (85.0)**	**8 (40.0)**	**17 (85.0)**	**16 (80.0)**	**6 (30.0)**	**0.072**	**0.677**	**0.507**
Hematologic toxic effects									
Leukopenia	8 (40.0)	6 (30.0)	2 (10.0)	2 (10.0)	1 (5.0)	0 (0)	0.028	0.037	0.147
Neutropenia	7 (35.0)	6 (30.0)	1 (5.0)	1 (5.0)	1 (5.0)	0 (0)	0.018	0.037	0.311
Reduced hemoglobin level	3 (15.0)	2 (10.0)	1 (5.0)	1 (5.0)	1 (5.0)	0 (0)	0.292	0.548	0.311
Thrombocytopenia	6 (30.0)	5 (25.0)	1 (5.0)	2 (10.0)	2 (10.0)	0 (0)	0.114	0.212	0.311
Hepatic function									
Increased AST	5 (25.0)	3(15.0)	2 (10.0)	9(45.0)	6 (30.0)	3(15.0)	0.185	0.256	0.633
Increased ALT	5 (25.0)	3 (15.0)	2 (10.0)	9 (45.0)	5 (25.0)	4 (20.0)	0.185	0.429	0.376
Hyperbilirubinemia	4 (20.0)	4 (20.0)	0 (0)	6 (30.0)	6 (30.0)	0 (0)	0.465	0.465	>0.999
Hypoalbuminemia	4 (20.0)	4 (20.0)	0 (0)	5 (25.0)	5 (25.0)	0 (0)	0.705	0.705	>0.999
Nonhematologic toxic effects									
Nausea	8 (40.0)	8 (40)	0 (0)	6 (30.0)	6 (30.0)	0 (0)	0.507	0.507	>0.999
Vomiting	9 (45.0)	7 (35.0)	2(10.0)	8 (40.0)	6 (30.0)	2 (10.0)	0.749	0.736	>0.999
Anorexia	4 (20.0)	4 (20.0)	0 (0)	2 (10.0)	2 (10.0)	0 (0)	0.376	0.376	>0.999
Fatigue	7 (35.0)	4 (20.0)	3 (15.0)	8 (40.0)	5 (25.0)	3 (15.0)	0.744	0.705	>0.999
Constipation	1 (5.0)	1 (5.0)	0 (0)	2 (10.0)	2 (10.0)	0 (0)	0.548	0.548	>0.999
Abdominal pain	3 (15.0)	3 (15.0)	0 (0)	6 (30.0)	4 (20.0)	2 (10.0)	0.256	0.677	0.147
Alopecia	3 (15.0)	2 (10.0)	1 (5.0)	2 (10.0)	2 (10.0)	0 (0)	0.633	>0.999	0.311
Rash	1 (5.0)	1 (5.0)	0 (0)	3 (15.0)	3 (15.0)	0 (0)	0.292	0.292	>0.999
Hypothyroidism	0 (0)	0 (0)	0 (0)	5 (25.0)	5 (25.0)	0 (0)	0.017	0.017	>0.999
RCCEP	0 (0)	0 (0)	0 (0)	5 (25.0)	5 (25.0)	0 (0)	0.017	0.017	>0.999

TRAEs, treatment-related adverse events; PSM, propensity score matching; TRAE, treatment-related adverse event; DEB-TACE+ICIs, drug-eluting bead transarterial chemoembolization combined with immune checkpoint inhibitors; AST, aspartate aminotransferase; ALT, alanine transaminase; RCCEP, reactive cutaneous capillary endothelial proliferation.

found that DEB-TACE can change the Th1/Th2 balance in the tumor microenvironment (TME) in patients with HCC, thus improving survival (31). To sum up, DEB-TACE+ICIs may produce synergistic antitumor activity and contribute to improved survival.

In this study, the presence of tumor size >5cm or multiple tumors was identified as an independent risk factor for PFS and OS, which was consistent with previous studies (2, 14, 15, 32). DEB-TACE can enhance intratumoral concentration and release loaded chemotherapeutic agents in a controlled manner, further enhancing necrosis and leading to increase tumor response in iCCA patients (16). In addition, multiple tumors are easier to embolize by DEB-TACE, which results in a favorable prognosis of iCCA patients (16).

There were no new or unexpected TRAEs observed in current study. All the TRAEs were well-tolerated and consistent with previous reports (7, 15, 18, 19). The incidence of chemotherapy-related AEs (hematologic toxic effects) was higher in the chemotherapy group than in the DEB-TACE+ICIs group. The irAEs showed that RCCEP (25.0%) was lower than the result in a previous study (62%) (18), and hypothyroidism was consistent with a previous study (33). After receiving thyroxine or glucocorticoid, the irAEs were recovered within 2 weeks. These results suggested that DEB-TACE+ICIs did not increase the risk of TRAEs over chemotherapy, which showed that DEB-TACE+ICIs was safe.

There were some limitations in current study. Firstly, current study was a retrospective analysis, which might be subject to the impact of selection biases. We implemented the PSM model to resolve the effect result in confounding factors. A randomized clinical trial is required to validate the findings from this study. Secondly, these variables (including subgroup analysis) were not analyzed in current study due to the small sample size. Finally, we did not evaluate programmed cell death-Ligand 1 (PD-L1), mismatch repair protein (MMR) deficiency, and microsatellite instability-high (MSI-H) status before using ICIs.

In conclusion, DEB-TACE plus ICIs improved PFS and OS compared to chemotherapy with well tolerated in patients with unresectable iCCA.

DATA AVAILABILITY STATEMENT

The raw data supporting the conclusions of this article will be made available by the authors without undue reservation.

ETHICS STATEMENT

The studies involving human participants were reviewed and approved by Sichuan Cancer Hospital. Written informed consent for participation was not required for this study in accordance with the national legislation and the institutional requirements. Written informed consent was not obtained from the individual(s) for the publication of any potentially identifiable images or data included in this article.

AUTHOR CONTRIBUTIONS

Conception and design: Huang X-Q and Xu G-H. Collection and assembly of data: Yang X-G, Sun Y-Y, and Li D-S. Data analysis and interpretation: Yang X-G. Manuscript writing: All authors. All authors contributed to the article and approved the submitted version.

FUNDING

This study was supported by the Wu Jieping Medical Fund (NO.320.6750.2020-10-122), Beijing Medical Award Fund (NO.YXJL-2020-0972-0424), and a Special Research Fund Project of Tumour Interventional (NO.2020S04).

REFERENCES

1. Bertuccio P, Malvezzi M, Carioli G, Hashim D, Boffetta P, El-Serag HB, et al. Global Trends in Mortality From Intrahepatic and Extrahepatic Cholangiocarcinoma. *J Hepatol* (2019) 71(1):104–14. doi: 10.1016/j.jhep.2019.03.013
2. Valle JW, Kelley RK, Nervi B, Oh DY, Zhu AX. Biliary Tract Cancer. *Lancet* (2021) 397(10272):428–44. doi: 10.1016/S0140-6736(21)00153-7
3. Banales JM, Marin JJG, Lamarca A, Rodrigues PM, Khan SA, Roberts LR, et al. Cholangiocarcinoma 2020: The Next Horizon in Mechanisms and Management. *Nat Rev Gastroenterol Hepatol* (2020) 17(9):557–88. doi: 10.1038/s41575-020-0310-z
4. El-Diwany R, Pawlik TM, Ejaz A. Intrahepatic Cholangiocarcinoma. *Surg Oncol Clin N Am* (2019) 28(4):587–99. doi: 10.1016/j.soc.2019.06.002
5. Ebata T, Ercolani G, Alvaro D, Ribero D, Di Tommaso L, Valle JW. Current Status on Cholangiocarcinoma and Gallbladder Cancer. *Liver Cancer* (2016) 6 (1):59–65. doi: 10.1159/000449493
6. Khan SA, Tavolari S, Brandi G. Cholangiocarcinoma: Epidemiology and Risk Factors. *Liver Int* (2019) 39 Suppl 1:19–31. doi: 10.1111/liv.14095
7. Valle J, Wasan H, Palmer DH, Cunningham D, Anthoney A, Maraveyas A, et al. Cisplatin Plus Gemcitabine Versus Gemcitabine for Biliary Tract Cancer. *N Engl J Med* (2010) 362(14):1273–81. doi: 10.1056/NEJMoa0908721
8. Lamarca A, Ross P, Wasan HS, Hubner RA, McNamara MG, Lopes A, et al. Advanced Intrahepatic Cholangiocarcinoma: *Post Hoc* Analysis of the Abc-01, -02, and -03 Clinical Trials. *J Natl Cancer Inst* (2020) 112(2):200–10. doi: 10.1093/jnci/djz071
9. Valle JW, Borbath I, Khan SA, Huguet F, Gruenberger T, Arnold D, et al. Biliary Cancer: Esmo Clinical Practice Guidelines for Diagnosis, Treatment and Follow-Up. *Ann Oncol* (2016) 27(suppl 5):v28–37. doi: 10.1093/annonc/mdw324
10. Kodali S, Shetty A, Shekhar S, Victor DW, Ghobrial RM. Management of Intrahepatic Cholangiocarcinoma. *J Clin Med* (2021) 10(11):2368. doi: 10.3390/jcm10112368
11. Chang Y, Jeong SW, Young Jang J, Jae Kim Y. Recent Updates of Transarterial Chemoembolilzation in Hepatocellular Carcinoma. *Int J Mol Sci* (2020) 21 (21):8165. doi: 10.3390/ijms21218165

12. Lammer J, Malagari K, Vogl T, Pilleul F, Denys A, Watkinson A, et al. Prospective Randomized Study of Doxorubicin-Eluting-Bead Embolization in the Treatment of Hepatocellular Carcinoma: Results of the Precision V Study. *Cardiovasc Intervent Radiol* (2010) 33(1):41–52. doi: 10.1007/s00270-009-9711-7
13. Taylor RR, Tang Y, Gonzalez MV, Stratford PW, Lewis AL. Irinotecan Drug Eluting Beads for Use in Chemoembolization: *In Vitro* and in Vivo Evaluation of Drug Release Properties. *Eur J Pharm Sci* (2007) 30(1):7–14. doi: 10.1016/j.ejps.2006.09.002
14. Zhou TY, Zhou GH, Zhang YL, Nie CH, Zhu TY, Wang HL, et al. Drug-Eluting Beads Transarterial Chemoembolization With Callispheres Microspheres for Treatment of Unresectable Intrahepatic Cholangiocarcinoma. *J Cancer* (2020) 11(15):4534–41. doi: 10.7150/jca.39410
15. Sun T, Zhang W, Chen L, Ren Y, Liu Y, Zheng C. A Comparative Study of Efficacy and Safety of Transarterial Chemoembolization With Callispheres and Conventional Transarterial Chemoembolization in Treating Unresectable Intrahepatic Cholangiocarcinoma Patients. *J Cancer* (2022) 13(4):1282–8. doi: 10.7150/jca.67523
16. Melchiorre F, Patella F, Pescatori L, Pesapane F, Fumarola E, Biondetti P, et al. Deb-Tace: A Standard Review. *Future Oncol* (2018) 14(28):2969–84. doi: 10.2217/fon-2018-0136
17. Finn RS, Qin S, Ikeda M, Galle PR, Ducreux M, Kim TY, et al. Atezolizumab Plus Bevacizumab in Unresectable Hepatocellular Carcinoma. *N Engl J Med* (2020) 382(20):1894–905. doi: 10.1056/NEJMoa1915745
18. Chen X, Wu X, Wu H, Gu Y, Shao Y, Shao Q, et al. Camrelizumab Plus Gemcitabine and Oxaliplatin (Gemox) in Patients With Advanced Biliary Tract Cancer: A Single-Arm, Open-Label, Phase Ii Trial. *J Immunother Cancer* (2020) 8(2):e001240. doi: 10.1136/jitc-2020-001240
19. Ren Z, Xu J, Bai Y, Xu A, Cang S, Du C, et al. Sintilimab Plus a Bevacizumab Biosimilar (Ibi305) Versus Sorafenib in Unresectable Hepatocellular Carcinoma (Orient-32): A Randomised, Open-Label, Phase 2-3 Study. *Lancet Oncol* (2021) 22(7):977–90. doi: 10.1016/S1470-2045(21)00252-7
20. Cheu JW, Wong CC. Mechanistic Rationales Guiding Combination Hepatocellular Carcinoma Therapies Involving Immune Checkpoint Inhibitors. *Hepatology* (2021) 74(4):2264–76. doi: 10.1002/hep.31840
21. Zhou GH, Han J, Sun JH, Zhang YL, Zhou TY, Nie CH, et al. Efficacy and Safety Profile of Drug-Eluting Beads Transarterial Chemoembolization by Callispheres(R) Beads in Chinese Hepatocellular Carcinoma Patients. *BMC Cancer* (2018) 18(1):644. doi: 10.1186/s12885-018-4566-4
22. Li S, Lyu N, Han X, Li J, Lai J, He M, et al. Hepatic Artery Infusion Chemotherapy Using Fluorouracil, Leucovorin, and Oxaliplatin Versus Transarterial Chemoembolization as Initial Treatment for Locally Advanced Hepatocellular Carcinoma: A Propensity Score-Matching Analysis. *J Vasc Interv Radiol* (2021) 32(9):1267–76.e1. doi: 10.1016/j.jvir.2021.06.008
23. Kuhlmann JB, Euringer W, Spangenberg HC, Breidert M, Blum HE, Harder J, et al. Treatment of Unresectable Cholangiocarcinoma: Conventional Transarterial Chemoembolization Compared With Drug Eluting Bead-Transarterial Chemoembolization and Systemic Chemotherapy. *Eur J Gastroenterol Hepatol* (2012) 24(4):437–43. doi: 10.1097/MEG.0b013e3283502241
24. Luo J, Zheng J, Shi C, Fang J, Peng Z, Huang J, et al. Drug-Eluting Beads Transarterial Chemoembolization by Callispheres Is Effective and Well Tolerated in Treating Intrahepatic Cholangiocarcinoma Patients: A Preliminary Result From Ctilc Study. *Med (Baltimore)* (2020) 99(12):e19276. doi: 10.1097/MD.0000000000019276
25. Hyder O, Marsh JW, Salem R, Petre EN, Kalva S, Liapi E, et al. Intra-Arterial Therapy for Advanced Intrahepatic Cholangiocarcinoma: A Multi-Institutional Analysis. *Ann Surg Oncol* (2013) 20(12):3779–86. doi: 10.1245/s10434-013-3127-y
26. Ueno M, Ikeda M, Morizane C, Kobayashi S, Ohno I, Kondo S, et al. Nivolumab Alone or in Combination With Cisplatin Plus Gemcitabine in Japanese Patients With Unresectable or Recurrent Biliary Tract Cancer: A Non-Randomised, Multicentre, Open-Label, Phase 1 Study. *Lancet Gastroenterol Hepatol* (2019) 4(8):611–21. doi: 10.1016/S2468-1253(19)30086-X
27. Yoo C, Oh DY, Choi HJ, Kudo M, Ueno M, Kondo S, et al. Phase I Study of Bintrafusp Alfa, a Bifunctional Fusion Protein Targeting Tgf-Beta and Pd-L1, in Patients With Pretreated Biliary Tract Cancer. *J Immunother Cancer* (2020) 8(1):e000564. doi: 10.1136/jitc-2020-000564
28. Piha-Paul SA, Oh DY, Ueno M, Malka D, Chung HC, Nagrial A, et al. Efficacy and Safety of Pembrolizumab for the Treatment of Advanced Biliary Cancer: Results From the Keynote-158 and Keynote-028 Studies. *Int J Cancer* (2020) 147(8):2190–8. doi: 10.1002/ijc.33013
29. Kang J, Jeong JH, Hwang HS, Lee SS, Park DH, Oh DW, et al. Efficacy and Safety of Pembrolizumab in Patients With Refractory Advanced Biliary Tract Cancer: Tumor Proportion Score as a Potential Biomarker for Response. *Cancer Res Treat* (2020) 52(2):594–603. doi: 10.4143/crt.2019.493
30. Liao J, Xiao J, Zhou Y, Liu Z, Wang C. Effect of Transcatheter Arterial Chemoembolization on Cellular Immune Function and Regulatory T Cells in Patients With Hepatocellular Carcinoma. *Mol Med Rep* (2015) 12(4):6065–71. doi: 10.3892/mmr.2015.4171
31. Lee HL, Jang JW, Lee SW, Yoo SH, Kwon JH, Nam SW, et al. Inflammatory Cytokines and Change of Th1/Th2 Balance as Prognostic Indicators for Hepatocellular Carcinoma in Patients Treated With Transarterial Chemoembolization. *Sci Rep* (2019) 9(1):3260. doi: 10.1038/s41598-019-40078-8
32. Venturini M, Sallemi C, Agostini G, Marra P, Cereda S, Reni M, et al. Chemoembolization With Drug Eluting Beads Preloaded With Irinotecan (Debiri) Vs Doxorubicin (Debdox) as a Second Line Treatment for Liver Metastases From Cholangiocarcinoma: A Preliminary Study. *Br J Radiol* (2016) 89(1067):20160247. doi: 10.1259/bjr.20160247
33. Cai M, Huang W, Huang J, Shi W, Guo Y, Liang L, et al. Transarterial Chemoembolization Combined With Lenvatinib Plus Pd-1 Inhibitor for Advanced Hepatocellular Carcinoma: A Retrospective Cohort Study. *Front Immunol* (2022) 13:848387. doi: 10.3389/fimmu.2022.848387

Conflict of Interest: The authors declare that the research was conducted in the absence of any commercial or financial relationships that could be construed as a potential conflict of interest.

frontiers | Frontiers in Immunology

ORIGINAL RESEARCH
published: 08 July 2022
doi: 10.3389/fimmu.2022.927041

A Novel Artificial Neural Network Prognostic Model Based on a Cancer-Associated Fibroblast Activation Score System in Hepatocellular Carcinoma

Yiqiao Luo[1], *Huaicheng Tan*[1,2], *Ting Yu*[3], *Jiangfang Tian*[1] *and Huashan Shi*[1,4*]

[1] Cancer Center, West China Hospital, Sichuan University, Chengdu, China, [2] West China School of Medicine, West China Hospital, Chengdu, China, [3] Department of Pathology, State Key Laboratory of Biotherapy, West China Hospital, West China School of Medicine, Sichuan University, Chengdu, China, [4] Department of Biotherapy, Cancer Center, West China Hospital, Sichuan University, Chengdu, China

OPEN ACCESS

Edited by:
Xuesong Gu,
Beth Israel Deaconess Medical Center and Harvard Medical School, United States

Reviewed by:
Shuai Wang,
University of Pittsburgh Medical Center, United States
Wenjie Huang,
Zhujiang Hospital Southern Medical University, China

***Correspondence:**
Huashan Shi
shihuashan@scu.edu.cn

Specialty section:
This article was submitted to Cancer Immunity and Immunotherapy, a section of the journal Frontiers in Immunology

Received: 23 April 2022
Accepted: 13 June 2022
Published: 08 July 2022

Citation:
Luo Y, Tan H, Yu T, Tian J and Shi H (2022) A Novel Artificial Neural Network Prognostic Model Based on a Cancer-Associated Fibroblast Activation Score System in Hepatocellular Carcinoma. Front. Immunol. 13:927041. doi: 10.3389/fimmu.2022.927041

Introduction: Hepatocellular carcinoma (HCC) ranks fourth as the most common cause of cancer-related death. It is vital to identify the mechanism of progression and predict the prognosis for patients with HCC. Previous studies have found that cancer-associated fibroblasts (CAFs) promote tumor proliferation and immune exclusion. However, the information about CAF-related genes is still elusive.

Methods: The data were obtained from The Cancer Genome Atlas, International Cancer Genome Consortium, and Gene Expression Omnibus databases. On the basis of single-cell transcriptome and ligand–receptor interaction analysis, CAF-related genes were selected. By performing Cox regression and random forest, we filtered 12 CAF-related prognostic genes for the construction of the ANN model based on the CAF activation score (CAS). Then, functional, immune, mutational, and clinical analyses were performed.

Results: We constructed a novel ANN prognostic model based on 12 CAF-related prognostic genes. Cancer-related pathways were enriched, and higher activated cell crosstalk was identified in high-CAS samples. High immune activity was observed in high-CAS samples. We detected three differentially mutated genes (*NBEA*, *RYR2*, and *FRAS1*) between high- and low-CAS samples. In clinical analyses, we constructed a nomogram to predict the prognosis of patients with HCC. 5-Fluorouracil had higher sensitivity in high-CAS samples than in low-CAS samples. Moreover, some small-molecule drugs and the immune response were predicted.

Conclusion: We constructed a novel ANN model based on CAF-related genes. We revealed information about the ANN model through functional, mutational, immune, and clinical analyses.

Keywords: cancer-associated fibroblasts, hepatocellular carcinoma, artificial neural network, single-cell transcriptome analysis, prognosis

INTRODUCTION

According to epidemiologic data, hepatocellular carcinoma (HCC) accounts for more than 80% of primary liver cancers and is the fourth most common cause of cancer-related death worldwide (1, 2). To our knowledge, the treatment options are limited for patients with advanced HCC (3). Thus, it is important to understand the mechanism of the progression of HCC and predict the survival rate and novel small-molecule drugs for patients with HCC.

In the tumor microenvironment (TME), the crosstalk between tumorigenic cells and fibroblasts may be the cause of the emergence of hyperactive fibroblasts, which are called cancer-associated fibroblasts (CAFs) (4). CAFs have been verified to be tumor-promoting components that can secrete growth factors, inflammatory ligands, and extracellular matrix (ECM) proteins to promote tumor proliferation and immune exclusion (5).

The artificial neural network (ANN), which was introduced in the 1950s, is a machine learning technique inspired by the human neuronal synapse system (6). Previous studies have verified that the ANN model has a better predictive capacity than the logistic Cox regression model (7). Thus, the ANN model has been widely applied in the biochemical and medical fields (8, 9).

In our study, we performed not only single-cell transcriptome analysis of HCC but also ligand–receptor interactions to determine CAF-related genes. Through Cox regression and random forest analyses, we filtered 12 CAF-related prognostic genes, which were recruited to construct a prognostic ANN model. We further performed functional, immune, mutational, and clinical analyses to estimate the constructed ANN model thoroughly.

METHODS

Data Preparation

The transcriptome RNA sequencing data, Illumina human methylation 450 cohort, copy number variation (CNV), and the corresponding related data of HCC were extracted from The Cancer Genome Atlas (TCGA) database (https://portal.gdc.cancer.gov/) (including 340 patients) and the International Cancer Genome Consortium (ICGC) data portal (https://dcc.icgc.org) (including 226 patients). The GSE76427 cohort was downloaded from the Gene Expression Omnibus (GEO) (https://www.ncbi.nlm.nih.gov/geo/) (including 115 patients). Patients with complete clinical information (stage, follow-up information, age, and gender) were selected for this study. Otherwise, the patients who did not meet the criteria were excluded.

Single-Cell Transcriptome Analysis

The expression profiling of single-cell RNA sequence GSE151530 (10X Genomics), which contained 46 HCC samples, was obtained from the GEO database (10). We used the R package "Seurat" to analyze the single-cell RNA sequence data. We collected 47,822 cells for further analyses. The data were normalized by using "NormalizeData" and "ScaleData" from the "Seurat" R package. We divided the cells into six subclusters based on the annotation in GSE151530. The R package "monocle" was used to perform single-cell trajectory analysis (11). The cells were filtered with the following conditions: a) num_cells_expressed ≥ 10 and b) min_expr = 0.1. Subsequently, the top 1,500 variable genes were selected to perform a single-cell trajectory analysis. The R package "monocle" was used to visualize the trajectory.

Cell Communication Analyses

The R package "Cellphonedb" was utilized to speculate the ligand–receptor pairs ($P < 0.05$) by Python. The crosstalk of ligand–receptor pairs between CAFs and other subclusters, as well as the activated pathways of cell communication, were analyzed by the R package "cellchat".

Functional Analyses

The gene annotation and analysis resource Metascape (https://metascape.org) was used for the enrichment analysis. After we obtained the differentially expressed genes, we performed gene ontology (GO) analyses by using Metascape. We used the gene enrichment analysis (GSEA) (4.1.0) application to obtain the enrichment pathways in high- and low–CAF activation score (CAS) samples. To analyze the functional enrichment of tumor-infiltrating immune cells (TICs), we calculated the relative abundance of immune cells in each sample by using the R package "cibersortR". We obtained the immune-related pathways from a previous article (12). Angiogenesis, the T effector/IFN response, checkpoint, myeloid inflammation, epithelial-mesenchymal transition (EMT), and hypoxia were identified in previously published articles (13–15). The CTA, neoantigen, and proliferation scores were obtained in a previous article (16). Then, we performed ssGSEA to assess the enrichment score of samples by using the R package "gsva".

Mutational Analyses

We extracted the mutation data of HCC from the TCGA database by the R package "TCGAbiolinks". The mutation data were further analyzed, and the mutational landscape and lollipop chart were illustrated by the R package "maftools".

Construction of a CAF-Related Prognostic ANN Model

We constructed and trained the ANN in the TCGA dataset by using the R package "survivalmodels" (https://cran.r-project.org/web/packages/survivalmodels/). The clinical data of HCC were extracted, and we performed univariate and multivariate Cox regression analyses by the R package "survival". As a result, we obtained 14 candidates. Then, we performed a random forest (ntree = 1,000) to further filter our candidates. Finally, the R package "survivalmodel" was used to construct the ANN model. Twelve CAF-related prognostic genes were selected and input into the input layer. The activation function was ReLU in three hidden layers. The loss function was the negative log partial likelihood under the Cox PH model. The dropout parameter was

used to avoid overfitting. We performed a 1,000 iteration random search using the adam optimizer utilizing "mlr3" packages to tune these hyperparameters. The CAS was calculated on the basis of Cox regression.

Validation of the Constructed CAF-Related Prognostic ANN Model

The TCGA dataset was set as the training cohort, whereas ICGC and GSE76427 were used as the testing cohorts. The concordance index (C-index) was calculated using the R package "Pec". The heatmap was illustrated by the R package "pheatmap". The area under the curve (AUC) was calculated by using the R package "timeROC". We performed Kaplan–Meier analyses in the three cohorts using the R package "survival".

Prediction of the Sensitivity of Chemotherapeutic Drugs and Exploration of Novel Small-Molecule Drugs

The Genomics of Drug Sensitivity in Cancer (GDSC) database (www.cancerRxgene.org), where we can obtain drug response data and genomic markers of sensitivity, was used to predict the sensitivity of four common chemotherapeutic drugs in the high- and low-CAS samples. We performed a ridge regression analysis to determine the half-maximal inhibitory concentration (IC50) by using the R package "pRRophetic". To predict novel small-molecule drugs, we introduced two online databases: a) the Cancer Therapeutics Response Portal (CTRP) 2.0 database (http://portals.broadinstitute.org/ctrp/), which includes sensitivity data of 481 small-molecule compounds in 860 cancer cell lines (CCLs); and b) the Profiling Relative Inhibition Simultaneously in Mixtures (PRISM) database (https://www.theprismlab.org/), with which we can screen thousands of drugs in hundreds of human CCLs. The AUC is a standard value for the evaluation of drug sensitivity. A lower AUC value represents better drug sensitivity. In addition, the differentially expressed genes between high- and low-CAS samples of HCC were potential therapeutic targets. Thus, we detected potential drugs that targeted the genes and illustrated the corresponding mechanism of action (MoA) by using the online database ConnectivityMap (cMap) (https://clue.io/).

Prediction of the Immunotherapeutic Response

We introduced the online database Tumor Immune Dysfunction and Exclusion (TIDE) (http://tide.dfci.harvard.edu) (17), which is a popular enrichment algorithm extensively used in cancer-related studies (18–20). We extracted the response to the treatment against PD-1 and CTLA4 in 47 patients (21) to predict the immunotherapeutic response between patients with HCC with high and low CAS based on subclass mapping (https://cloud.genepattern.org/gp/).

Statistical Analyses

R software (version 4.0.4) was used to analyze statistical data and construct images. We used the Wilcoxon test to analyze the differences between the two groups. The difference in proportions was analyzed by the chi-squared test. A P-value < 0.05 was considered to be statistically significant. All correlation analyses were performed by Pearson's correlation. The heatmap in our study was generated by the R package "pheatmap". Univariate and multivariate Cox regression analyses were performed by the R package "survival". The nomogram was built by using the R package "RMS". The calibration curves and AUCs were obtained by the R packages "rms" and "survivalROC". The 1-, 3-, and 5-year decision curve analysis (DCA) was performed by using the R package "rmda". *$P < 0.05$, **$P < 0.01$, and ***$P < 0.001$.

RESULTS

Single-Cell Transcriptome Analysis of HCC and the Functional Enrichment of CAF-Related Genes

Six subclusters of single cells, including malignant cells, B and T cells, tumor-associated macrophages (TAMs), tumor-associated endothelial cells (TECs), and cancer-associated fibroblasts (CAFs), were split and illustrated by performing a uniform manifold approximation and projection (UMAP) plot (**Figure 1A**). Then, we used Monocle 2 to perform pseudotime analysis, which is a great approach to study lineage specification and hierarchize molecular events (22). We noticed that CAFs, which we were most interested in, were present at the end of the differentiation trajectory (**Figure 1B**). Furthermore, we performed the ligand–receptor interaction network among six subclusters (**Figure 1C**) and extracted the number of ligand–receptor pairs between CAFs and other subclusters (**Figure 1D**). We demonstrated that CAFs and TECs had the most ligand–receptor pairs, followed by CAFs and TAMs. Subsequently, we performed ligand–receptor interactions between CAFs and other subclusters (**Figure 1E**). Genes that were significantly related to CAFs were chosen for further analysis. Functional enrichment analysis of the CAF-related genes was performed by the online enrichment analysis tool Matascape in a bar graph (**Figure 1F**) and corresponding network (**Figure 1G**). Tumor-associated pathways were enriched, such as the PI3K-Akt-mTOR signaling pathway, blood vessel development, signaling by receptor tyrosine kinases, and positive regulation of cell migration.

Twelve CAF-Related Genes Were Identified as a Predictive Model in HCC

We performed univariate Cox regression analysis to further screen CAF-related prognostic genes in the TCGA dataset. As a result, 14 genes were selected (**Figure 2A**). To further obtain the strictest model, we performed random forest analysis and filtered the candidate genes. Finally, 12 CAF-related genes with variable importance values greater than 0 were selected as a prognostic model for patients with HCC (**Figure 2B**). Then, we performed the mutational landscape of 12 CAF-related prognostic genes (**Figure 2C**). We demonstrated that *HGF* had the highest mutation (24%), followed by *CD44* (12%) and *CSF1* and *NRP1* (6%). The highest type of mutation was a missense

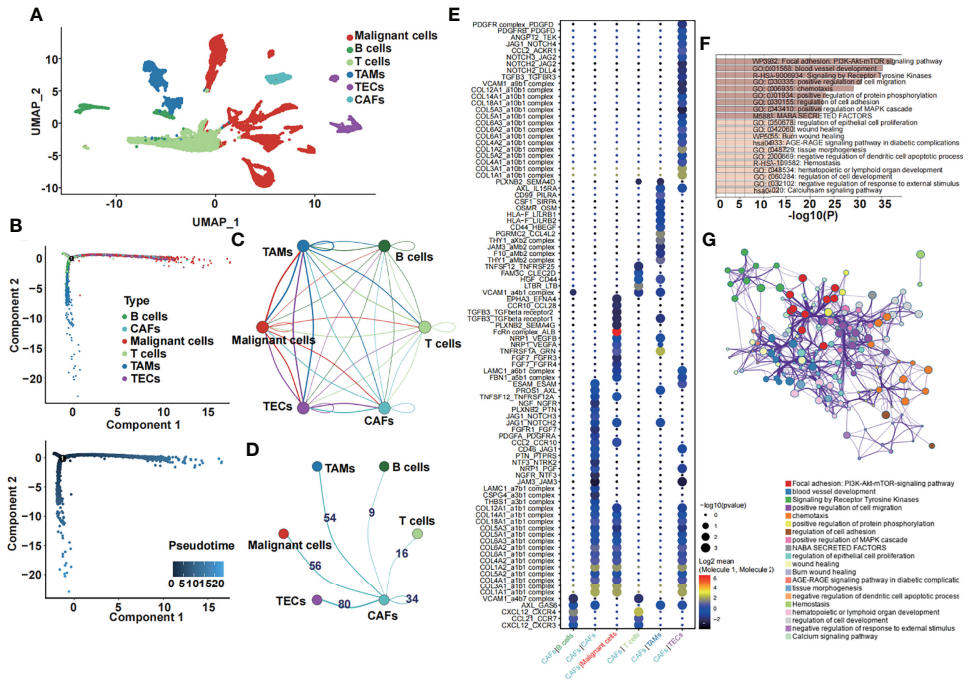

FIGURE 1 | Single-cell transcriptome analysis and the function of CAF-related genes. **(A)** The six cell subclusters are shown. **(B)** Pseudotime analysis of six cell subclusters was performed. **(C)** The ligand–receptor interaction network among six subclusters is shown. **(D)** The number of ligand–receptor pairs between CAFs and other subclusters is shown. **(E)** The specific ligand–receptor pair between CAFs and other subclusters is shown. **(F)** Enrichment analysis of the differentially expressed CAF-related genes. **(G)** The corresponding network of the enrichment analysis of the differentially expressed CAF-related genes.

mutation. Moreover, we summarized the mutation analysis results (**Figure 2D**). The most common variant and variant type were missense mutation and single-nucleotide polymorphisms (SNPs), respectively. The number of single-nucleotide variants (SNVs) showed that the cytosine (C) to adenine (A) mutation was the most frequent mutation. The median variant per sample was 1. Moreover, we listed the top 10 mutated genes for further analysis. Subsequently, we performed a CNV analysis of 12 CAF-related prognostic genes in the TCGA dataset (**Figure 2E**), and we found that *EFNA4* had the highest CNV gain mutation, whereas *CSF1* had the highest CNV loss mutation. Then, we constructed a circle plot to exhibit the correlation among 12 CAF-related prognostic genes (**Figure 2F**). The 12 CAF-related prognostic genes were all risk factors and had strong positive correlations with a P-value less than 0.0001.

An ANN Prognostic Model Was Created on the Basis of 12 CAF-Related Prognostic Genes

We constructed an ANN model based on the 12 selected CAF-related prognostic genes in the TCGA dataset. A schematic diagram is shown in **Figure 3A**. Twelve CAF-related genes were input into the input layer. The hyperparameters of the networks were as follows: a) three hidden layers; b) 35, 27, and 19 nodes in each layer; c) dropout rate = 0.286; d) learning rate = 0.4621984; and e) weight decay = 0.3156897. As a result, we obtained the output data. The output layer included one neuron and the CAS was calculated by performing Cox regression. To assess the prediction capacity, we introduced the C-index. We demonstrated that the C-index was higher in the ANN model than in the Cox model. Moreover, the C-index was satisfactory in the ICGC and GSE76427 datasets (**Figure 3B**). By performing AUC analysis, we obtained the same result that the ANN model was better than the Cox model (**Figure 3C**). Subsequently, the CAS of each sample was calculated in the TCGA dataset (**Figure 3D**), and patients with high CAS had a worse survival status, and vice versa. The result was confirmed in the ICGC and GSE76427 datasets (**Supplementary Figures 1A, B**). By performing Kaplan–Meier analysis in the TCGA dataset, we revealed that patients with HCC with high CAS had shorter overall survival (P = 0.0065) (**Figure 3E**). The result was verified in the ICGC and GSE76427 datasets (**Supplementary Figures 1C, D**), and the P-value was 0.016 in both datasets. To evaluate the accuracy of our ANN model, we performed ROC analysis in the TCGA, ICGC, and GSE76427 datasets. We illustrated that the 1-, 3-, and 5-year AUCs were more than 0.6 in the TCGA dataset (**Figure 3F**), which revealed that our ANN model was an accurate prognostic model. The result was also confirmed in the ICGC and GSE76427 datasets with an AUC less than 0.6 (**Supplementary Figures 1E, F**).

We performed univariate Cox regression subgroup analyses of the CAS in three datasets (TCGA, ICGC, and GSE76427). In the

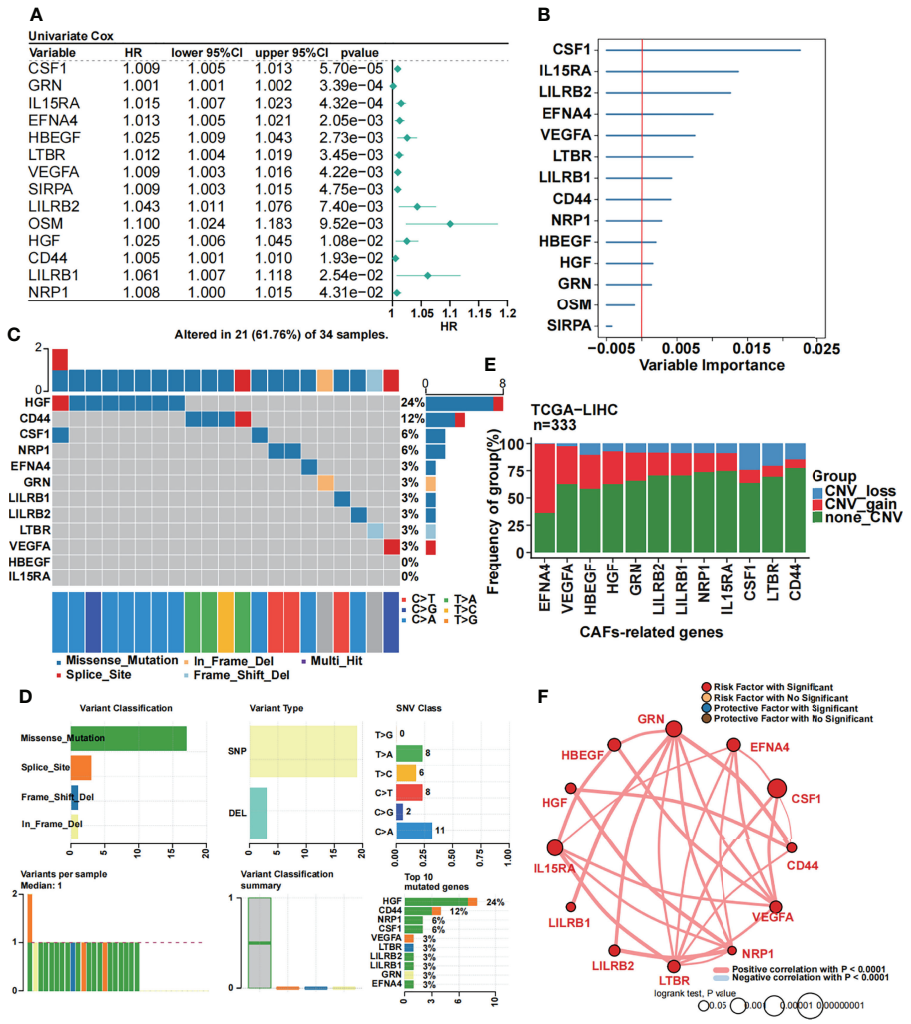

FIGURE 2 | Identification of 12 CAF-related prognostic genes. **(A)** Univariate Cox regression of CAF-related genes. **(B)** Random forest analysis of the candidate CAF-related prognostic genes. **(C)** The mutational landscape of 12 CAF-related prognostic genes. **(D)** Summary of the mutational analysis including variant classification, variant type, SNV class, variants per sample, variant classification summary, and the top 10 mutated genes. **(E)** The CNV status in 12 CAF-related prognostic genes. **(F)** Univariate Cox regression analysis and Pearson's correlation of the 12 CAF-related prognostic genes.

TCGA dataset, stage I, female, and age < 60 were considered the risk factors (**Supplementary Figure 2A**). In the ICGC dataset, stage III, stage IV, female, male, and age < 70 were regarded as the risk factors (**Supplementary Figure 2B**). In GSE76427, stage II and male were considered to be the risk factors (**Supplementary Figure 2C**).

A Nomogram Was Constructed Based on our CAF-Related ANN Model

To evaluate whether our ANN model could act as an independent prognostic marker, we performed univariate and multivariate Cox regression analyses in three cohorts (TCGA, ICGC, and GSE76427) (**Figures 4A, B**). According to the univariate and multivariate Cox regression, the CAS of our ANN model was significantly associated with low overall survival in the three cohorts, which revealed that our constructed ANN model could act as an independent prognostic marker for patients with HCC. Thus, we built a nomogram based on the CAS to predict the 1-, 3-, and 5-year overall survival for patients with HCC (**Figure 4C**). For instance, a 60-year-old (20 points) male (3 points) patient with HCC with stage III (51 points) and −5 CAS values (40 points) received a total of 114 points, and the 1-, 3-, and 5-year survival rates of this patient were approximately 69%, 42%, and 25%, respectively. Then, we built calibration curves for assessing predicted risk versus observed risk (**Figure 4D**). The 1-, 3-, and 5-year calibration curves showed a great capacity for prediction. In addition, we calculated the AUC of our nomogram (**Figure 4E**), which indicated that the nomogram had the highest AUC compared to a single parameter. Finally, we performed 1-, 3-, and 5-year DCA to assess whether our constructed model was

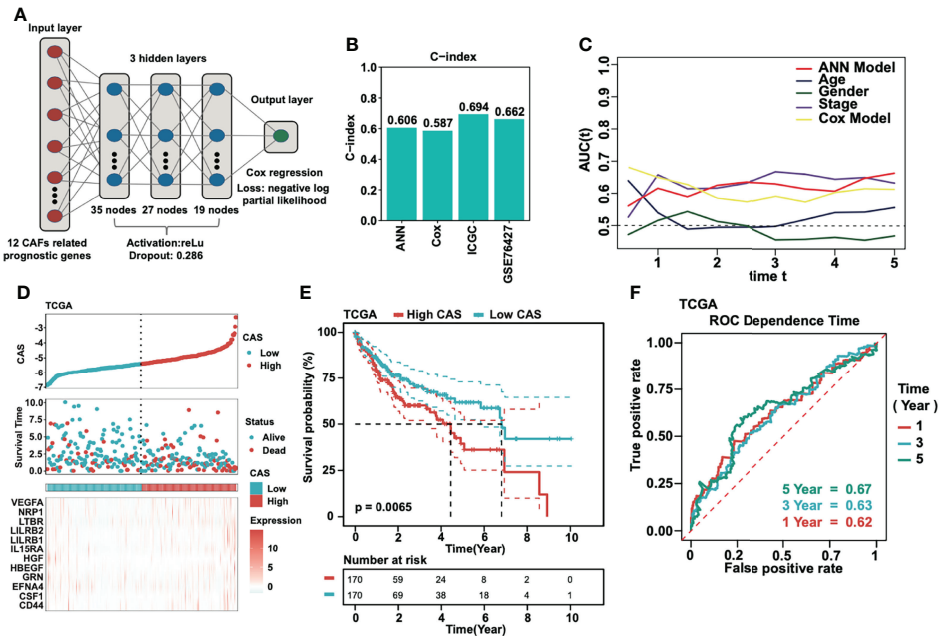

FIGURE 3 | Construction of the ANN model. **(A)** The schematic diagram of the constructed ANN model. **(B)** Detection of the C-index of the ANN, traditional Cox model, ICGC, and GSE76427. **(C)** AUC analyses of the constructed ANN model compared to the traditional Cox model and other parameters. **(D)** The CAS and corresponding survival status in each sample in the TCGA dataset. **(E)** Kaplan–Meier analysis of high- and low-CAS samples in the TCGA dataset. **(F)** ROC analysis of the ANN model in 1-, 3-, and 5-year survival prediction in the TCGA dataset.

worth utilizing (**Figure 4F**). The results illustrated that our nomogram was acceptable for patients with HCC.

Enrichment Analysis of the Constructed CAF-Related ANN Model

We obtained the differentially expressed genes between high- and low-CAS samples and input the genes into Metascape, which is the online enrichment analysis tool. The significantly enriched terms in the high-CAS group are shown (**Figure 5A**). The top five items were matrix metalloproteinases, response to hexose, regulation of membrane potential, benzene-containing compound metabolic process, and steroid catabolic process. Moreover, the significantly enriched terms in the low-CAS group are shown (**Figure 5B**). The top five items were core matrisome, ECM organization, matrisome associated, proteoglycans, and cellular response to growth factor stimulus. In addition, we performed GSEA to explore the enriched pathways in high- and low-CAS samples (**Figures 5C, D**). We observed that ABC transporters, antigen processing and presentation, natural killer cell–mediated cytotoxicity, Nod-like receptor signaling pathway, and Toll-like receptor signaling pathway were enriched in the low-CAS group, whereas calcium signaling pathway, ECM receptor interaction, Notch signaling pathway, ribosome, and Vascular endothelial growth factor (VEGF) signaling pathway were enriched in the high-CAS samples. Then, according to the median expression of CAF-related genes, we divided the samples into two subgroups (high and low groups) and determined that the high groups had higher activated cell crosstalk than the low groups (**Figure 5E**). We summarized the significant crosstalk pathways, which indicated that the high group could activate most pathways (**Figure 5F**). Furthermore, we illustrated some specific pathways. On the one hand, the high group could send the signal from the Macrophage migration inhibitory factor (MIF) signaling pathway (CD74-CXCR4) (**Supplementary Figure 3A**), VEGF signaling pathway (VEGFA-VEGFR1) (**Supplementary Figure 3B**), PROS signaling pathway (PROS1-AXL) (**Supplementary Figure 3C**), and GDF signaling pathway (GDF15-TGFBR2) (**Supplementary Figure 3D**). On the other hand, the high group could receive signals from the Epidermal growth factor (EGF) signaling pathway (HBEGF-EGFR) (**Supplementary Figure 3E**) and Tumor necrosis factor-like weak inducer of apoptosis (TWEAK) signaling pathway (TNFSF12-TNFRSF12A) (**Supplementary Figure 3F**).

In addition, we analyzed some pathways of interest (**Figure 5G**). We illustrated that T cell coinhibition, angiogenesis, and Major histocompatibility complex class I were significantly upregulated in high-CAS samples. However, the type II Interferon (IFN) response pathway was significantly enriched in low-CAS samples. Moreover, the correlation between CAS and pathways is shown in the right panel. We found that T cell coinhibition had the most significantly positive correlation with CAS.

Immune Analysis of the Constructed CAF-Related ANN Model

The 22 TICs were divided into four groups based on the risk or protective factors with or without significance, and we also performed correlation analysis (**Figure 6A**). We demonstrated that M0 macrophages and activated dendritic cells were risk factors, whereas resting memory CD4 T cells were protective

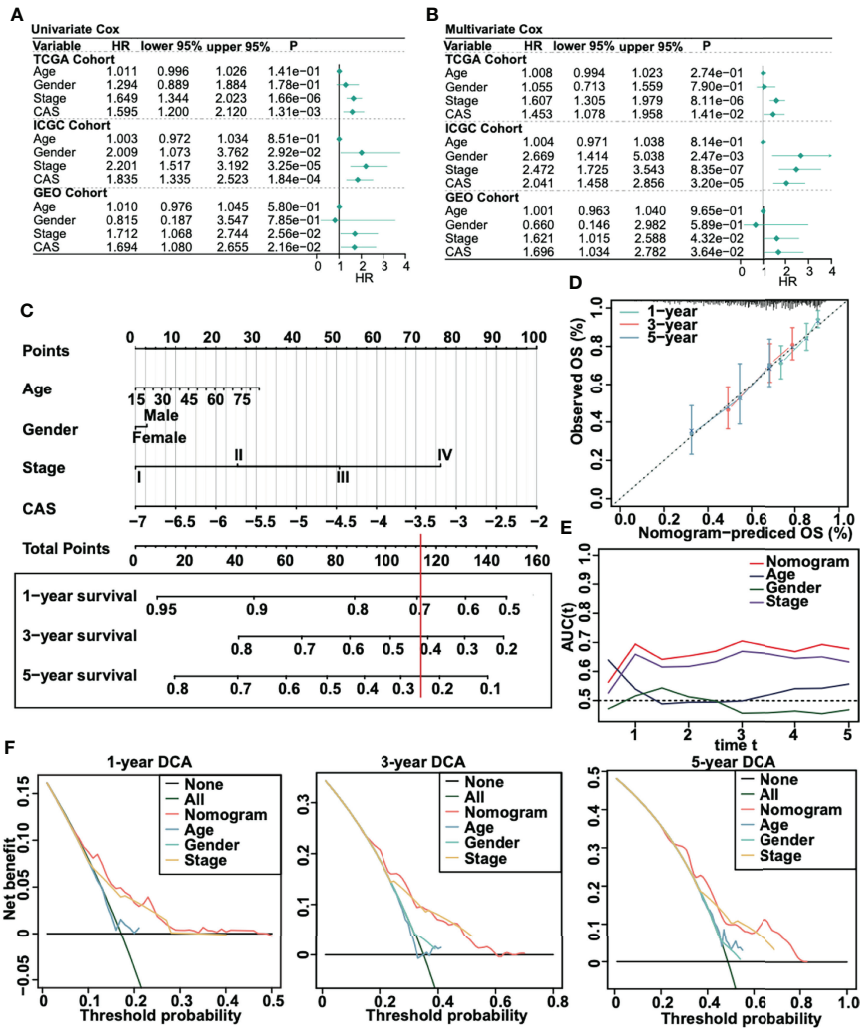

FIGURE 4 | Creation of a nomogram for patients with HCC. **(A)** Univariate Cox regression in TCGA, ICGC, and GSE75427 cohorts. **(B)** Multivariate Cox regression in TCGA, ICGC, and GSE75427 cohorts. **(C)** Constructed nomogram based on CAS. **(D)** One-, 3-, and 5-year calibration curves were generated. **(E)** AUC analysis between the constructed nomogram and parameters was performed. **(F)** One-, 3-, and 5-year DCA was performed.

factors. We detected some positive or negative correlations among 22 TICs. Then, we illustrated a heatmap to analyze the TME and tumor purity and the expression of TICs and immunocompetence (**Figure 6B**). The immune and ESTIMATE scores were significantly higher in high-CAS samples and had a positive correlation with CAS. Activated memory CD4 T cells, follicular helper T cells, and neutrophils were highly expressed in high-CAS samples, whereas regulatory T cells and resting memory CD4 T cells were highly expressed in low-CAS samples, and CD8 T cells were highly regulated in patients with low CAS. To evaluate immunocompetence, we included immune checkpoints (*CD274*, *CTLA4*, *HAVCR2*, *IDO1*, *LAG3*, and *PDCD1*) and immunocompetence (*CD8A*, *CXCL10*, *CXCL9*, *GZMA*, *GZMB*, *IFNG*, *PRF1*, *TBX2*, and *TNF*) (23, 24). We found that the checkpoints *CTLA4*, *IDO1*, and *CD274* were highly expressed in high-CAS samples, whereas *TBX2* was significantly highly expressed in low-CAS samples. Furthermore, we performed a multi-omics analysis of 75 immunomodulators between high- and low-CAS samples. We included 14 antigen presentation factors, three co-stimulators, eight co-inhibitors, 22 ligands, 19 receptors, three cell adhesion factors, and six other factors (**Figure 6C**). We detected mRNA expression, frequency of mutation, amplification, and deletion, as well as the gene expression correlated with the DNA methylation beta value between high- and low-CAS samples. Finally, we detected cancer-testis antigen (CTA) (**Figure 6D**), neoantigens (**Figure 6E**), and proliferation (**Figure 6F**) scores between high- and low-CAS samples. The CTA score can increase the speed of tumorigenesis, against apoptosis, and enhance proliferation. We uncovered that high-CAS samples had higher CTA scores, neoantigen expression, and proliferation capacity. Through correlation analysis, we demonstrated a

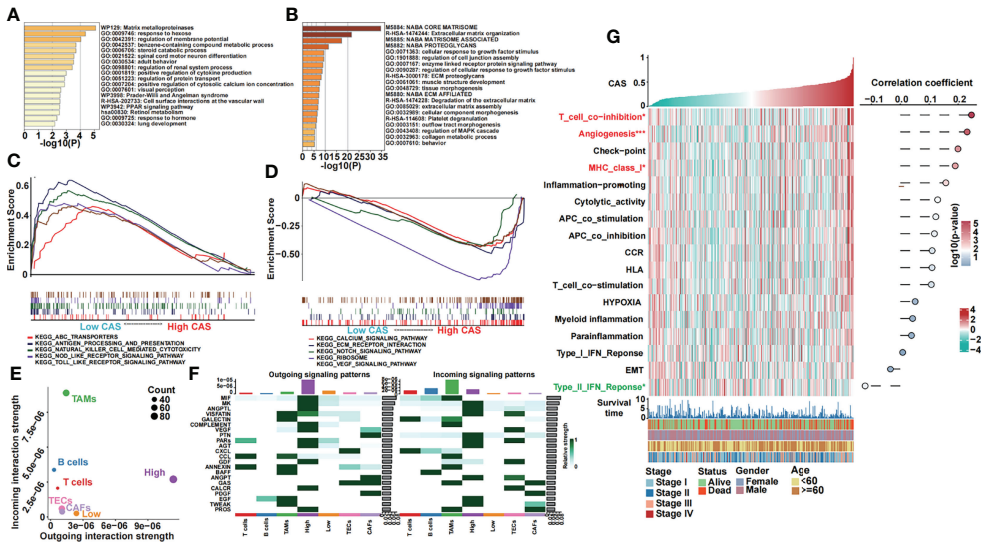

FIGURE 5 | Functional analyses of our constructed ANN model. **(A)** GO analysis of differentially expressed genes in high-CAS samples was performed in Metascape. **(B)** GO analysis of differentially expressed genes in low-CAS samples was performed in Metascape. **(C)** Five KEGG pathways were enriched in the low-CAS samples by performing GSEA. **(D)** Five KEGG pathways were enriched in high-CAS samples by performing GSEA. **(E)** Summary of the crosstalk of the subclusters. **(F)** Outgoing and incoming signaling of high- and low-CAS samples as well as other cell subclusters. **(G)** A heatmap illustrating the expression and the correlation between CAS and the pathways of interest.

significantly positive correlation between CAS and the CTA score (P = 0.03), neoantigens (P = 0.0014), and proliferation (P= 0.044).

Mutational Analysis of the Constructed CAF-Related ANN Model

We performed mutational analysis between low and high-CAS samples. First, we detected all mutation counts: non-synonymous and synonymous mutation counts (**Figure 7A**). Unfortunately, we did not detect any significance between the two groups. In addition, we filtered 26 genes whose mutation counts were more than 15 and subsequently illustrated a mutational landscape in high- and low-CAS samples (**Figure 7B**). The most frequently mutated gene in high-CAS samples was *TP53* (33%), followed by *CTNNB1* (25%) and *TTN* (24%). In comparison, the most frequently mutated gene in low-CAS samples was *CTNNB1* (25%), followed by *TTN* (25%) and *TP53* (23%). To determine differentially mutated genes between high- and low-CAS samples, we generated a forest plot (**Figure 7C**). The mutation counts of *NBEA* and *FRAS1* were higher in high-CAS samples, whereas *RYR2* had more mutation counts in low-CAS samples. Furthermore, we noticed that *TP53* had the highest percentage of mutation counts in high-CAS samples. Thus, we generated a lollipop chart of *TP53* to exhibit the mutation frequency and the types of mutation in high- and low-CAS samples (**Figure 7D**). After that, we generated a bar graph to illustrate the frequency of amplification and deletion of each arm in high- and low-CAS samples (**Figure 7E**). We demonstrated that the frequency of amplification in arms 1p, 12p, and 20q was significantly higher in high-CAS samples. However, in low-CAS samples, arms 10q and 10p showed a higher frequency of amplification. The frequency of deletion in arms 20q and 20p was significantly higher in low-CAS samples and lower in arm 1q compared to high-CAS samples. By performing correlation analysis between CAS and the frequency of amplification/deletion, unfortunately, we did not detect significance not only in the correlation but also in the frequency of mutation between high- and low-CAS samples.

The Constructed CAF-Related ANN Model Guides Clinical Treatment

To our knowledge, one of the main treatments for HCC is chemotherapy, which includes 5-fluorouracil, cisplatin, gemcitabine, and doxorubicin. Thus, we predicted the sensitivity of the chemotherapeutic drugs between high- and low-CAS samples in the TCGA dataset (**Figure 8A**). We found that three drugs (5-fluorouracil, cisplatin, and gemcitabine) had more sensitivity in high-CAS samples than in low-CAS samples (P-value = 0.00063, 0.018, and 0.00045, respectively). We also detected the estimated IC50 between high- and low-CAS samples in the ICGC and GSE76427 datasets (**Supplementary Figures 4A, B**). 5-Fluorouracil, which was confirmed in three datasets, had higher sensitivity in high-CAS samples than in low-CAS samples. In addition, we predicted small-molecule drugs by using the CTRP and PRISM databases (**Figure 8B**). Brefeldin A, SR-II-138A, CR-1-31B, BRD-K97651142, KX2-391, and tosedostat were negatively correlated with the CAS, and the estimated AUC value was lower in high-CAS samples. The results indicated that

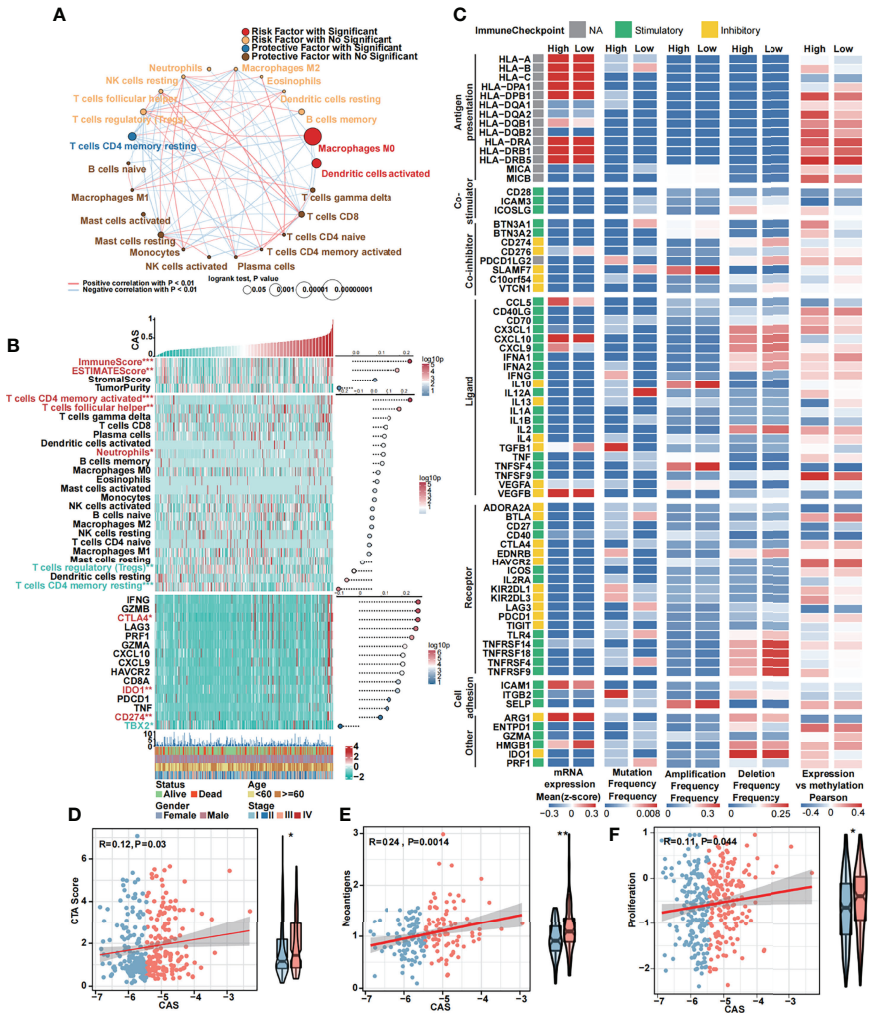

FIGURE 6 | Immune analyses of the constructed ANN model. **(A)** Cox regression and Pearson's correlation analysis of 22 TICs. **(B)** The expression and Pearson's correlation of immune, ESTIMATE, stromal score, tumor purity, TICs, checkpoints, and immunocompetences of each sample are illustrated in a heatmap. **(C)** Multi-omics analysis of 75 immunomodulators between high- and low-CAS samples. **(D)** The Pearson's correlation between the CTA score and CAS and the expression of the CTA score in high- and low-CAS samples. **(E)** The Pearson's correlation between neoantigens and CAS, and the expression of neoantigens in high- and low-CAS samples. **(F)** The Pearson's correlation between proliferation and CAS, and the expression of proliferation in high- and low-CAS samples.

the predicted small-molecule drugs had higher sensitivity in patients with high CAS. In addition, the immune response against PD1 and CTLA4 was predicted by using subclass mapping in the TCGA dataset (**Figure 8C**). We found that the immune response against PD1 was significant in patients with high CAS (P = 0.001). This result was confirmed in ICGC and GSE76427 datasets (P = 0.006 and 0.038) (**Supplementary Figures 4C, D**). Then, the total immune response was detected between high- and low-CAS samples by using the TIDE algorithm (**Figure 8D**). The results indicated that the patients with high CAS had a better immune response (P = 0.018). The result was also confirmed in the ICGC and GSE76427 datasets (**Supplementary Figures 4E, F**). Finally, other potential small molecular drugs and the corresponding mechanisms were illustrated by performing MoA analysis (**Supplementary Figure 5**).

DISCUSSION

In our study, we first identified 12 CAF-related genes by performing single-cell transcriptome, ligand–receptor interaction, Cox regression, and random forest analyses. A novel ANN model was then constructed, and the CAS of each sample was obtained. By performing functional analysis, we demonstrated that some cancer-related pathways and activated cell crosstalk pathways were enriched in high-CAS samples. In addition, we detected higher immunogenicity in high-CAS samples by performing an immune analysis. By illustrating the mutational landscape, we recovered significantly mutated genes between high- and low-CAS samples. Furthermore, a CAS-based nomogram was constructed for patients with HCC. The common chemotherapeutic drug 5-fluorouracil had been

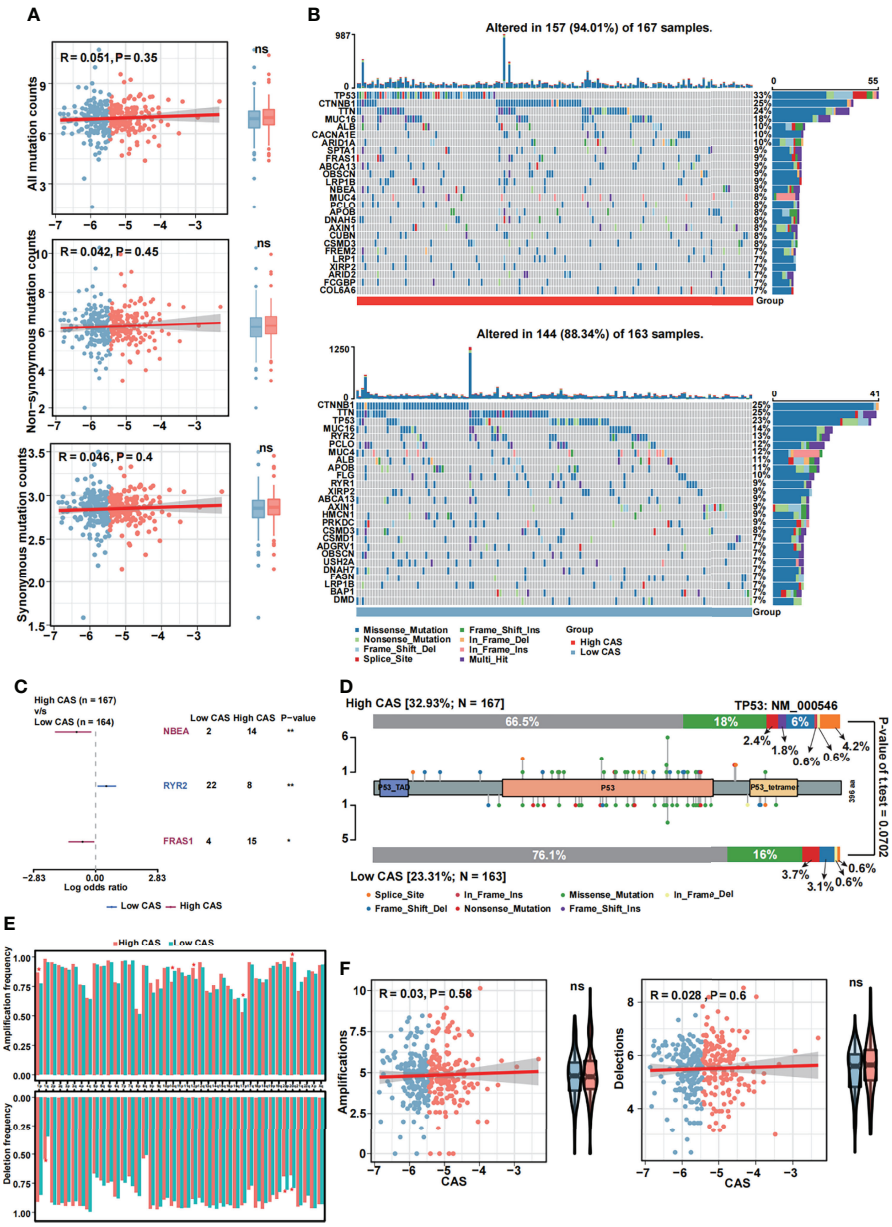

FIGURE 7 | Mutational analyses of the constructed ANN model. **(A)** The Pearson's correlation analysis between CAS and all mutation, non-synonymous mutation and synonymous mutation counts, and the counts of all mutation, non-synonymous mutation and synonymous mutation in high- and low-CAS samples. **(B)** Landscape of the 26 mutated genes that had more than 15 mutation counts in high-CAS samples (25) and low-CAS samples (lower). **(C)** Differentially mutated genes between high- and low-CAS samples. **(D)** A lollipop chart illustrates the location and the type of mutation in TP53. **(E)** The amplification and deletion frequency in each arm between high- and low-CAS samples. **(F)** The Pearson's correlation between CAFs and amplification/deletion, and the frequency of amplification/deletion in high- and low-CAS samples. *P-value < 0.05; **P-value < 0.01; NS: No Significance.

verified to have higher sensitivity in high-CAS samples in three cohorts. We also predicted some small-molecule drugs. Finally, we revealed that the immune response was better in high-CAS samples than in low-CAS samples.

We utilized the ANN model instead of the traditional Cox regression model. Here, we pointed out that the regression models have some limitations; for instance, the regression models are based on the presumption that all the data are linear, which is not always true in most biological situations (26). One of the advantages of the ANN model was that it can learn with experience and adapt to the error rate even in the situation that the validation cohorts were different from the derivation cohort, whereas the regression models can only fix within the parameters of the original derivation cohort. Another

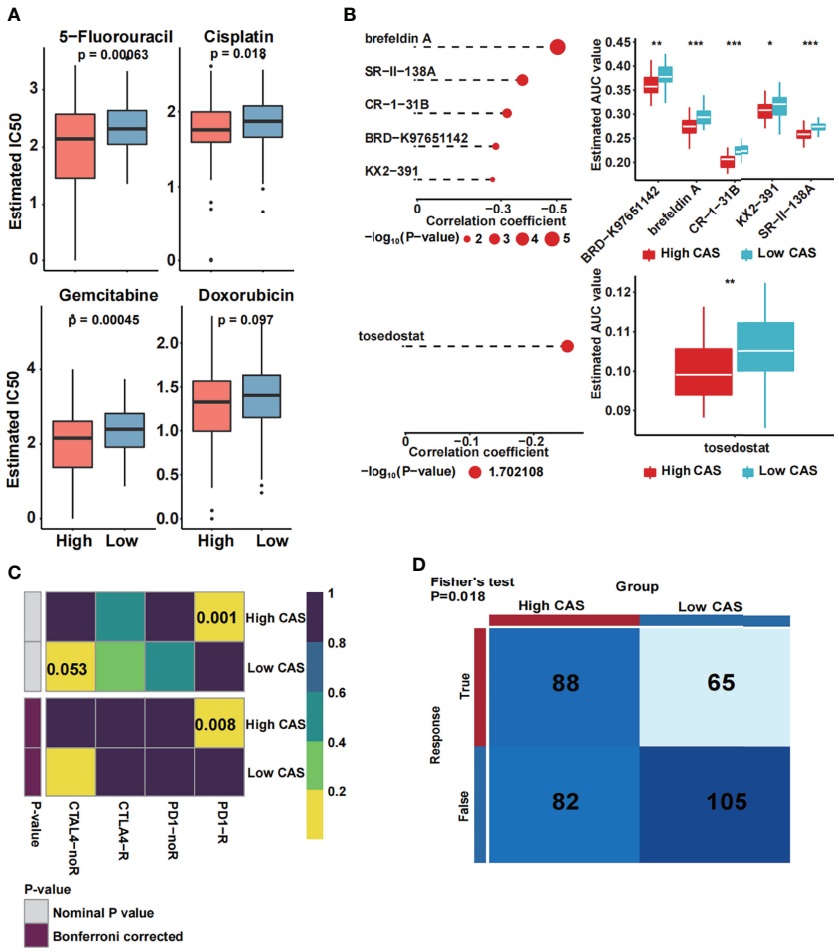

FIGURE 8 | Prediction of drug and immune response. **(A)** The estimated IC50 of four common chemotherapeutic drugs in high- and low-CAS samples. **(B)** The prediction and the estimated AUC value of small-molecule drugs in the CTRP 2.0 and PRISM databases. **(C)** The immune response against PD1 and CTLA4 in patients with high and low CAS. **(D)** The total immune response in patients with high and low CAS. *P-value < 0.05; **P-value < 0.01; ***P-value < 0.001.

advantage is that the ANN model can handle large amounts of data (7). Thus, the ANN model was suitable for predicting the prognosis of patients.

We noticed that some cancer-related pathways, including the NOTCH signaling pathway and VEGF signaling pathway, were enriched in high-CAS samples. Interestingly, VEGF signaling was also activated in the high expression group in the cell communication analysis. Furthermore, according to the heatmap of the pathways of interest, we noticed that angiogenesis was enriched in high-CAS samples and positively correlated with CAS. The results demonstrated that the constructed ANN model was positively correlated with cancer progression and aggressive angiogenesis progression. One previous study revealed that CAFs promoted angiogenesis in HCC *via* the VEGF-mediated EZH2/VASH1 pathway (27). Another study indicated that CAFs promoted cancer invasion and the key function of CAFs was to drive vasculogenesis and angiogenesis (28). Thus, anti-VEGF therapy might become a potential method for patients with HCC with high CAS. In addition, we recovered that the type II IFN (IFN-γ) response pathway was enriched in low-CAS samples. A previous study revealed that IFN-γ was a vital factor in tumor cell elimination (29), and this finding was supported by experiments using a mouse model (30).

According to the heatmap, the immune score and ESTIMATE score were significantly higher in high-CAS samples, revealing that our ANN model was associated with immune regulation. In addition, memory $CD4^+$ T cells undergo fast expansion and cause a more effective and faster immune response (31). Follicular helper T cells are a subset of $CD4^+$ cells that play a critical role in the immune and effector response functions of T cells (32). In our study, we demonstrated that activated memory $CD4^+$ T cells and follicular helper T cells were highly expressed in high-CAS samples and had a positive correlation with CAS, which indicated that high-CAS samples had a better immune response than low-CAS samples. Studies have found that neutrophils are involved in the different stages of the oncogenic process, including tumor initiation, growth,

proliferation, and metastatic spreading (33, 34). The expression of neutrophils was significantly higher in high-CAS samples, and the result was consistent with previous studies. Moreover, the immune checkpoints *CTLA4*, *IDO1*, and *CD274* were increased in the high-CAS samples. Previous studies have pointed out that checkpoints are key players in cancer development and immunotherapy (35). Thus, blocking the expression of *CTLA4*, *IDO1*, and *CD274* may be a novel target for the immune treatment of HCC. The CTA, neoantigen, and proliferation scores were positively correlated with CAS, which was consistent with our results.

By performing mutational analysis, we revealed that patients with high CAS had a higher mutational frequency of *NBEA* and *FRAS1* and a lower mutational frequency of *RYR2*. *NBEA* has been certified as a novel tumor suppressor gene, and mutation of *NBEA* can cause poor outcomes in multiple myeloma (36). Previous research found that *RYR2* mutation was significantly associated with better clinical prognosis (37) and reduced the risk of development (38) in breast cancer. In addition, the *RYR2* mutation correlated with better prognosis was involved in the immune response and enhanced antitumor immunity in esophageal adenocarcinoma (18). *FRAS1* was found to have a high mutational frequency in high-CAS samples. A previous study indicated that *FRAS1* has the ability to regulate epidermal basement membrane adhesion and cell migration (39). In addition, *FRAS1* was more frequently mutated in metastatic breast cancer than in primary breast cancer (40). Another study demonstrated that *FRAS1* mutation may be associated with an increase in the development of metastatic disease or death from prostate cancer (41). Above all, the results were coincidental with our findings. Moreover, we demonstrated that the frequency of *TP53* mutation is the highest in patients with high CAS (33%). *TP53* acts as a tumor suppressor and induces growth inhibition and apoptosis (42). Approximately, 13%–48% of liver cancers harbor *TP53* mutations (43, 44). Our findings and the results from previous studies were consistent.

We predicted some small-molecule drugs with higher sensitivity in patients with high CAS, including brefeldin A, SR-II-138A, CR-1-31B, BRD-K97651142, KX2-391, and tosedostat. Brefeldin A has been reported to markedly inhibit proliferation and induce autophagic cell death *via* the Akt/mTOR and ERK pathways when encapsulated in mixed nanomicelles (45). CR-1-31B, an inhibitor of eukaryotic translation initiation factor 4A, has been found to significantly reduce the growth and initiate the apoptosis of gallbladder cancer cells (46). In addition, one article reported that the Src/FAK pathway inhibitor KX2-391 significantly increased the sensitivity of HepG2/doxorubicin cells to doxorubicin in HCC (47). The novel metalloenzyme inhibitor tosedostat has shown promising activity for patients with acute myeloid leukemia (48). However, we have not found any reports about SR-II-138A and BRD-K97651142.

In our study, we first constructed an ANN model based on CAF-related prognostic genes in HCC. However, this study still has some limitations. To begin with, our data were obtained from the TCGA, ICGC, and GEO online databases, which need to be verified in a large sample in reality. In addition, the prognostic ANN model needs to be certified in a real clinical cohort before application.

In conclusion, we created a novel CAF-related ANN model that is suitable for individually predicting the prognosis of patients with HCC and guiding clinical treatment through functional, mutational, immune, and clinical analyses.

DATA AVAILABILITY STATEMENT

The original contributions presented in the study are included in the article/**Supplementary Material**. Further inquiries can be directed to the corresponding author.

AUTHOR CONTRIBUTIONS

YL and HT: Conception and design and writing of the manuscript. TY and JT: Development of methodology, and analysis and interpretation of the data. HS: Review and revision of the manuscript. All authors contributed to the article and approved the submitted version.

ACKNOWLEDGMENTS

We are grateful to the founders and contributors of the online databases, from which we obtained vital information. We thank the creators of the excellent R studio software, by which we can analyze the extracted data correctly.

SUPPLEMENTARY MATERIAL

The Supplementary Material for this article can be found online at: https://www.frontiersin.org/articles/10.3389/fimmu.2022.927041/full#supplementary-material

Supplementary Figure 1 | Validation of the constructed ANN model in ICGC and GSE76427. **(A)** The CAS and corresponding survival status in each sample in the ICGC dataset. **(B)** The CAS and corresponding survival status in each sample in the GSE76427 dataset. **(C)** Kaplan-Meier analysis of high and low CAS samples in the ICGC dataset. **(D)** Kaplan-Meier analysis of high and low CAS samples in the GSE76427 dataset. **(E)** ROC analysis of the ANN model in 1-, 3-, and 5-year survival prediction in the ICGC dataset. **(F)** ROC analysis of the ANN model in 1-, 3-, and 5-year survival prediction in the GSE76427 dataset.

Supplementary Figure 2 | Univariate Cox regression subgroup analyses of the CAS in three datasets. **(A)** Subgroup analysis in TCGA dataset. **(B)** Subgroup analysis in the ICGC dataset. **(C)** Subgroup analysis in the GSE76427 dataset.

Supplementary Figure 3 | The different ligand–receptor pairs between high and low CAS samples. **(A)** High CAS cells communicate with TAMs, B cells and T cells through CD74-CXCR4 in the MIF signaling pathway. **(B)** High CAS cells communicate with TECs *via* VEGFA-VEGFR1 in the VEGF signaling pathway. **(C)** High CAS cells communicate with TAMs through TNFSF12-TNFRSF12A in the TWEAK signaling pathway. **(D)** High CAS cells communicate with TAMs and CAFs through PROS1-AXL in the PROS signaling pathway. **(E)** High CAS cells

communicate with TAMs through HBEGF-EGFR in the EGF signaling pathway. **(F)** High CAS cells communicate with TECs and TAMs through GDF15-TGFBR2 in the GDF signaling pathway.

Supplementary Figure 4 | Validation of the sensitivity of the chemotherapeutic drugs and immune response. **(A)** The estimated IC50 of four common chemotherapeutic drugs in high and low CAS samples in the ICGC dataset. **(B)** The estimated IC50 of four common chemotherapeutic drugs in high and low CAS samples in GSE76427. **(C)** The immune response against PD1 and CTLA4 in high and low CAS patients in the ICGC dataset. **(D)** The immune response against PD1 and CTLA4 in high and low CAS patients in the GSE76427 dataset. **(E)** The total immune response in high and low CAS patients in the ICGC dataset. **(F)** The total immune response in high and low CAS patients in the GSE76427 dataset.

Supplementary Figure 5 | Prediction of the possible drugs and the corresponding mechanism by MoA analysis.

REFERENCES

1. El-Serag HB, Rudolph KL. Hepatocellular Carcinoma: Epidemiology and Molecular Carcinogenesis. *Gastroenterology* (2007) 132(7):2557–76. doi: 10.1053/j.gastro.2007.04.061
2. Fitzmaurice C, Allen C, Barber RM, Barregard L, Bhutta ZA, Brenner H, et al. Global, Regional, and National Cancer Incidence, Mortality, Years of Life Lost, Years Lived With Disability, and Disability-Adjusted Life-Years for 32 Cancer Groups, 1990 to 2015: A Systematic Analysis for the Global Burden of Disease Study. *JAMA Oncol* (2017) 3(4):524–48. doi: 10.1001/jamaoncol.2016.5688
3. Thomas MB, Jaffe D, Choti MM, Belghiti J, Curley S, Fong Y, et al. Hepatocellular Carcinoma: Consensus Recommendations of the National Cancer Institute Clinical Trials Planning Meeting. *J Clin Oncol Off J Am Soc Clin Oncol* (2010) 28(25):3994–4005. doi: 10.1200/JCO.2010.28.7805
4. Nurmik M, Ullmann P, Rodriguez F, Haan S, Letellier E. In Search of Definitions: Cancer-Associated Fibroblasts and Their Markers. *Int J Cancer* (2020) 146(4):895–905. doi: 10.1002/ijc.32193
5. Kalluri R. The Biology and Function of Fibroblasts in Cancer. *Nat Rev Cancer* (2016) 16(9):582–98. doi: 10.1038/nrc.2016.73
6. Lee JG, Jun S, Cho YW, Lee H, Kim GB, Seo JB, et al. Deep Learning in Medical Imaging: General Overview. *Korean J Radiol* (2017) 18(4):570–84. doi: 10.3348/kjr.2017.18.4.570
7. Ghoshal UC, Das A. Models for Prediction of Mortality From Cirrhosis With Special Reference to Artificial Neural Network: A Critical Review. *Hepatol Int* (2008) 2(1):31–8. doi: 10.1007/s12072-007-9026-1
8. Yazdani Charati J, Janbabaei G, Alipour N, Mohammadi S, Ghorbani Gholiabad S, Fendereski A. Survival Prediction of Gastric Cancer Patients by Artificial Neural Network Model. *Gastroenterol Hepatol Bed Bench* (2018) 11(2):110–7.
9. Afshar S, Afshar S, Warden E, Manochehri H, Saidijam M. Application of Artificial Neural Network in miRNA Biomarker Selection and Precise Diagnosis of Colorectal Cancer. *Iran BioMed J* (2019) 23(3):175–83. doi: 10.29252/ibj.23.3.175
10. Ma L, Wang L, Khatib SA, Chang CW, Heinrich S, Dominguez DA, et al. Single-Cell Atlas of Tumor Cell Evolution in Response to Therapy in Hepatocellular Carcinoma and Intrahepatic Cholangiocarcinoma. *J Hepatol* (2021) 75(6):1397–408. doi: 10.1016/j.jhep.2021.06.028
11. Qiu X, Mao Q, Tang Y, Wang L, Chawla R, Pliner HA, et al. Reversed Graph Embedding Resolves Complex Single-Cell Trajectories. *Nat Methods* (2017) 14(10):979–82. doi: 10.1038/nmeth.4402
12. Liang JY, Wang DS, Lin HC, Chen XX, Yang H, Zheng Y, et al. A Novel Ferroptosis-Related Gene Signature for Overall Survival Prediction in Patients With Hepatocellular Carcinoma. *Int J Biol Sci* (2020) 16(13):2430–41. doi: 10.7150/ijbs.45050
13. McDermott DF, Huseni MA, Atkins MB, Motzer RJ, Rini BI, Escudier B, et al. Clinical Activity and Molecular Correlates of Response to Atezolizumab Alone or in Combination With Bevacizumab Versus Sunitinib in Renal Cell Carcinoma. *Nat Med* (2018) 24(6):749–57. doi: 10.1038/s41591-018-0053-3
14. Gibbons DL, Creighton CJ. Pan-Cancer Survey of Epithelial-Mesenchymal Transition Markers Across the Cancer Genome Atlas. *Dev Dyn* (2018) 247 (3):555–64. doi: 10.1002/dvdy.24485
15. Liberzon A, Subramanian A, Pinchback R, Thorvaldsdóttir H, Tamayo P, Mesirov JP. Molecular Signatures Database (MSigDB) 3. *0 Bioinf (Oxford England)* (2011) 27(12):1739–40. doi: 10.1093/bioinformatics/btr260
16. Thorsson V, Gibbs DL, Brown SD, Wolf D, Bortone DS, Ou Yang TH, et al. The Immune Landscape of Cancer. *Immunity* (2018) 48(4):812–30.e14. doi: 10.1016/j.immuni.2018.03.023
17. Jiang P, Gu S, Pan D, Fu J, Sahu A, Hu X, et al. Signatures of T Cell Dysfunction and Exclusion Predict Cancer Immunotherapy Response. *Nat Med* (2018) 24(10):1550–8. doi: 10.1038/s41591-018-0136-1
18. Liu Z, Liu L, Jiao D, Guo C, Wang L, Li Z, et al. Association of RYR2 Mutation With Tumor Mutation Burden, Prognosis, and Antitumor Immunity in Patients With Esophageal Adenocarcinoma. *Front Genet* (2021) 12. doi: 10.3389/fgene.2021.669694
19. Liu Z, Lu T, Wang L, Liu L, Li L, Han X. Comprehensive Molecular Analyses of a Novel Mutational Signature Classification System With Regard to Prognosis, Genomic Alterations, and Immune Landscape in Glioma. *Front Mol Biosci* (2021) 8:682084. doi: 10.3389/fmolb.2021.682084
20. Liu Z, Lu T, Li J, Wang L, Xu K, Dang Q, et al. Clinical Significance and Inflammatory Landscape of Anovel Recurrence-Associated Immune Signature in Stage II/III Colorectal Cancer. *Front Immunol* (2021) 12. doi: 10.3389/fimmu.2021.702594
21. Roh W, Chen PL, Reuben A, Spencer CN, Prieto PA, Miller JP, et al. Integrated Molecular Analysis of Tumor Biopsies on Sequential CTLA-4 and PD-1 Blockade Reveals Markers of Response and Resistance. *Sci Transl Med* (2017) 9(379). doi: 10.1126/scitranslmed.aah3560
22. Meistermann D, Bruneau A, Loubersac S, Reignier A, Firmin J, François-Campion V, et al. Integrated Pseudotime Analysis of Human Pre-Implantation Embryo Single-Cell Transcriptomes Reveals the Dynamics of Lineage Specification. *Cell Stem Cell* (2021) 28(9):1625–40.e6. doi: 10.1016/j.stem.2021.04.027
23. Ayers M, Lunceford J, Nebozhyn M, Murphy E, Loboda A, Kaufman DR, et al. IFN-γ-Related mRNA Profile Predicts Clinical Response to PD-1 Blockade. *J Clin Invest* (2017) 127(8):2930–40. doi: 10.1172/JCI91190
24. Hugo W, Zaretsky JM, Sun L, Song C, Moreno BH, Hu-Lieskovan S, et al. Genomic and Transcriptomic Features of Response to Anti-PD-1 Therapy in Metastatic Melanoma. *Cell* (2016) 165(1):35–44. doi: 10.1016/j.cell.2016.02.065
25. Wei T, Weiler SME, Tóth M, Sticht C, Lutz T, Thomann S, et al. YAP-Dependent Induction of UHMK1 Supports Nuclear Enrichment of the Oncogene MYBL2 and Proliferation in Liver Cancer Cells. *Oncogene* (2019) 38(27):5541–50. doi: 10.1038/s41388-019-0801-y
26. Cross SS, Harrison RF, Kennedy RL. Introduction to Neural Networks. *Lancet (London England)* (1995) 346(8982):1075–9. doi: 10.1016/S0140-6736(95)91746-2
27. Huang B, Huang M, Li Q. Cancer-Associated Fibroblasts Promote Angiogenesis of Hepatocellular Carcinoma by VEGF-Mediated EZH2/VASH1 Pathway. *Technol Cancer Res Treat* (2019) 18:1533033819879905. doi: 10.1177/1533033819879905
28. Pape J, Magdeldin T, Stamati K, Nyga A, Loizidou M, Emberton M, et al. Cancer-Associated Fibroblasts Mediate Cancer Progression and Remodel the Tumouroid Stroma. *Br J Cancer* (2020) 123(7):1178–90. doi: 10.1038/s41416-020-0973-9
29. Dighe AS, Richards E, Old LJ, Schreiber RD. Enhanced *In Vivo* Growth and Resistance to Rejection of Tumor Cells Expressing Dominant Negative IFN Gamma Receptors. *Immunity* (1994) 1(6):447–56. doi: 10.1016/1074-7613(94)90087-6
30. Kaplan DH, Shankaran V, Dighe AS, Stockert E, Aguet M, Old LJ, et al. Demonstration of an Interferon Gamma-Dependent Tumor Surveillance System in Immunocompetent Mice. *Proc Natl Acad Sci USA* (1998) 95 (13):7556–61. doi: 10.1073/pnas.95.13.7556
31. Golubovskaya V, Wu L. Different Subsets of T Cells, Memory, Effector Functions, and CAR-T Immunotherapy. *Cancers* (2016) 8(3). doi: 10.3390/cancers8030036
32. Raphael I, Nalawade S, Eagar TN, Forsthuber TG. T Cell Subsets and Their Signature Cytokines in Autoimmune and Inflammatory Diseases. *Cytokine* (2015) 74(1):5–17. doi: 10.1016/j.cyto.2014.09.011

33. Swierczak A, Mouchemore KA, Hamilton JA, Anderson RL. Neutrophils: Important Contributors to Tumor Progression and Metastasis. *Cancer Metastasis Rev* (2015) 34(4):735–51. doi: 10.1007/s10555-015-9594-9
34. Coffelt SB, Wellenstein MD, de Visser KE. Neutrophils in Cancer: Neutral No More. *Nat Rev Cancer* (2016) 16(7):431–46. doi: 10.1038/nrc.2016.52
35. Lian J, Yue Y, Yu W, Zhang Y. Immunosenescence: A Key Player in Cancer Development. *J Hematol Oncol* (2020) 13(1):151. doi: 10.1186/s13045-020-00986-z
36. O'Neal J, Gao F, Hassan A, Monahan R, Barrios S, Kilimann MW, et al. Neurobeachin (NBEA) Is a Target of Recurrent Interstitial Deletions at 13q13 in Patients With MGUS and Multiple Myeloma. *Exp Hematol* (2009) 37 (2):234–44. doi: 10.1016/j.exphem.2008.10.014
37. Xu Z, Xiang L, Wang R, Xiong Y, Zhou H, Gu H, et al. Bioinformatic Analysis of Immune Significance of RYR2 Mutation in Breast Cancer. *BioMed Res Int* (2021) 2021:8072796. doi: 10.1155/2021/8072796
38. Wei Y, Wang X, Zhang Z, Zhao C, Chang Y, Bian Z, et al. Impact of NR5A2 and RYR2 3'UTR Polymorphisms on the Risk of Breast Cancer in a Chinese Han Population. *Breast Cancer Res Treat* (2020) 183(1):1–8. doi: 10.1007/s10549-020-05736-w
39. Kiyozumi D, Sugimoto N, Sekiguchi K. Breakdown of the Reciprocal Stabilization of QBRICK/Frem1, Fras1, and Frem2 at the Basement Membrane Provokes Fraser Syndrome-Like Defects. *Proc Natl Acad Sci USA* (2006) 103(32):11981–6. doi: 10.1073/pnas.0601011103
40. Lefebvre C, Bachelot T, Filleron T, Pedrero M, Campone M, Soria JC, et al. Mutational Profile of Metastatic Breast Cancers: A Retrospective Analysis. *PLoS Med* (2016) 13(12):e1002201. doi: 10.1371/journal.pmed.1002201
41. Wang V, Geybels MS, Jordahl KM, Gerke T, Hamid A, Penney KL, et al. A Polymorphism in the Promoter of FRAS1 Is a Candidate SNP Associated With Metastatic Prostate Cancer. *Prostate* (2021) 81(10):683–93. doi: 10.1002/pros.24148
42. Belinky F, Nativ N, Stelzer G, Zimmerman S, Iny Stein T, Safran M, et al. *PathCards: Multi-Source Consolidation Hum Biol Pathways Database (Oxford)* (2015) 2015. doi: 10.1093/database/bav006
43. Ahn SM, Jang SJ, Shim JH, Kim D, Hong SM, Sung CO, et al. Genomic Portrait of Resectable Hepatocellular Carcinomas: Implications of RB1 and FGF19 Aberrations for Patient Stratification. *Hepatology* (2014) 60(6):1972–82. doi: 10.1002/hep.27198
44. Takai A, Dang HT, Wang XW. Identification of Drivers From Cancer Genome Diversity in Hepatocellular Carcinoma. *Int J Mol Sci* (2014) 15 (6):11142–60. doi: 10.3390/ijms150611142
45. Zhang JM, Jiang YY, Huang QF, Lu XX, Wang GH, Shao CL, et al. Brefeldin A Delivery Nanomicelles in Hepatocellular Carcinoma Therapy: Characterization, Cytotoxic Evaluation *In Vitro*, and Antitumor Efficiency *In Vivo*. *Pharmacol Res* (2021) 172:105800. doi: 10.1016/j.phrs.2021.105800
46. Cao Y, He Y, Yang L, Luan Z. Targeting Eif4a Using Rocaglate CR−1−31B Sensitizes Gallbladder Cancer Cells to TRAIL−Mediated Apoptosis Through the Translational Downregulation of C−FLIP. *Oncol Rep* (2021) 45(1):230–8. doi: 10.1016/j.biopha.2017.09.065
47. Yu M, Zou Q, Wu X, Han G, Tong X. Connexin 32 Affects Doxorubicin Resistance in Hepatocellular Carcinoma Cells Mediated by Src/FAK Signaling Pathway. *Biomedicine Pharmacotherapy = Biomedecine pharmacotherapie* (2017) 95:1844–52. doi: 10.1016/j.biopha.2017.09.065
48. DiNardo CD, Cortes JE. Tosedostat for the Treatment of Relapsed and Refractory Acute Myeloid Leukemia. *Expert Opin Investig Drugs* (2014) 23 (2):265–72. doi: 10.1517/13543784.2014.864276

Conflict of Interest: The authors declare that the research was conducted in the absence of any commercial or financial relationships that could be construed as a potential conflict of interest.

Publisher's Note: All claims expressed in this article are solely those of the authors and do not necessarily represent those of their affiliated organizations, or those of the publisher, the editors and the reviewers. Any product that may be evaluated in this article, or claim that may be made by its manufacturer, is not guaranteed or endorsed by the publisher.

frontiers | Frontiers in Immunology

ORIGINAL RESEARCH
published: 18 July 2022
doi: 10.3389/fimmu.2022.838374

Comprehensive Analysis Identifies and Validates the Tumor Microenvironment Subtypes to Predict Anti-Tumor Therapy Efficacy in Hepatocellular Carcinoma

Haohan Zhang[1†], *Yi Yao*[1,2†], *Jie Wu*[1†], *Jin Zhou*[1], *Chen Zhao*[1], *Junju He*[1] *and Bin Xu*[1*]

[1] Cancer Center, Renmin Hospital of Wuhan University, Wuhan, China, [2] Hubei Provincial Research Center for Precision Medicine of Cancer, Wuhan, China

Objective: The objective of this study was to explore and verify the subtypes in hepatocellular carcinoma based on the immune (lymphocyte and myeloid cells), stem, and stromal cells in the tumor microenvironment and analyze the biological characteristics and potential relevance of each cluster.

Methods: We used the xCell algorithm to calculate cell scores and got subtypes by k-means clustering. In the external validation sets, we verified the conclusion stability by a neural network model. Simultaneously, we speculated the inner connection between clusters by pseudotime trajectory analysis and confirmed it by pathway enrichment, TMB, CNV, etc., analysis.

Result: According to the results of the consensus cluster, we chose k = 4 as the optimal value and got four different subtypes (C1, C2, C3, and C4) with different biological characteristics based on infiltrating levels of 48 cells in TME. In univariable Cox regression, the hazard ratio (HR) value of C3 versus C1 was 2.881 (95% CI: 1.572–5.279); in multivariable Cox regression, we corrected the age and TNM stage, and the HR value of C3 versus C1 was 2.510 (95% CI: 1.339–4.706). C1 and C2 belonged to the immune-active type, C3 and C4 related to the immune-insensitive type and the potential conversion relationships between clusters. We established a neural network model, and the area under the curves of the neural network model was 0.949 in the testing cohort; the same survival results were also observed in the external validation set. We compared the differences in cell infiltration, immune function, pathway enrichment, TMB, and CNV of four clusters and speculated that C1 and C2 were more likely to benefit from immunotherapy and C3 may benefit from FGF inhibitors.

OPEN ACCESS

Edited by:
Hongda Liu,
Nanjing Medical University, China

Reviewed by:
Pil Soo Sung,
Catholic University of Korea, South Korea
Shuai Wang,
University of Pittsburgh Medical Center, United States
Lu Zhang,
First Affiliated Hospital of Xi'an Jiaotong University, China
Long Liu,
First Affiliated Hospital of Zhengzhou University, China

***Correspondence:**
Bin Xu
xubin_oncology@whu.edu.cn

†These authors share first authorship

Specialty section:
This article was submitted to Cancer Immunity and Immunotherapy, a section of the journal Frontiers in Immunology

Received: *17 December 2021*
Accepted: *07 March 2022*
Published: *18 July 2022*

Citation:
Zhang H, Yao Y, Wu J, Zhou J, Zhao C, He J and Xu B (2022) Comprehensive Analysis Identifies and Validates the Tumor Microenvironment Subtypes to Predict Anti-Tumor Therapy Efficacy in Hepatocellular Carcinoma. Front. Immunol. 13:838374. doi: 10.3389/fimmu.2022.838374

Discussion: Our analysis provides a new approach for the identification of four tumor microenvironment clusters in patients with liver cancer and identifies the biological differences and predicts the immunotherapy efficacy between the four subtypes.

Keywords: hepatocellular carcinoma, tumor immunology, tumor microenvironment subtypes, precise treatment, immunotherapy, tumor-infiltrating lymphocytes, tumor stromal cells, stem cells

INTRODUCTION

Hepatocellular carcinoma (HCC) is one of the most lethal malignancies worldwide, with low survival rates in advanced-stage patients and minimal improvement in survival trends. The tumor microenvironment (TME) consists of many cell types, including immune infiltrates (lymphocyte and myeloid cells), cancer-associated fibroblasts (CAFs), and vascular endothelial cells. Immune cells and stromal cells, which are two major types of non-tumor cell components, play crucial roles in tumor progression and metastasis (1, 2). Previous studies have been conducted on the relationship between tumor-infiltrating immune cells and clinical outcomes (3). However, other components in the TME, such as stromal cells, also affect the therapeutic outcome (4), and the research on the comprehensive compendium of the cell landscape in TME is still lacking in LIHC.

Immunotherapy has received tremendous attention and is revolutionizing cancer treatment. Immune checkpoint inhibitors (ICIs) can reverse the immunosuppressive microenvironment by decreasing the potential of tumor immune escape, resulting in a noteworthy improvement of prognosis (5). In TME, multiple factors affect immunotherapy. The stem cells and stromal cells could suppress pro-inflammatory processes and promote the immune tolerance (6). Accordingly, not all cancer patients exhibit the same response to immunotherapy, and it is of utmost importance to identify the immunodominant population to help clinicians conduct immunotherapy or immunotherapy-based combination strategies.

In view of this situation, this study aimed at establishing the tumor microenvironment subtypes based on 48 types of cells, including immune (lymphocyte and myeloid cells), stem, and stromal cells in TME. We investigated the differences in biological characteristics among different subtypes, including infiltration of immune cells, tumor microenvironment status, tumor mutations, and the differences in prognosis and the efficacy of immunotherapy, which may refer to current research on treatment strategies for patients with LIHC.

METHODS

Data Source

RNA-seq data of LIHC patients were downloaded from The Cancer Genome Atlas (TCGA) (https://portal.gdc.cancer.gov/) and further normalized into transcripts per kilobase (TPM) for analysis. Normalized microarray gene expression data of the Hoshida Y et al. cohort (GSE10141) were available from the Gene Expression Omnibus (GEO) database (https://www.ncbi.nlm.nih.gov/geo/), and LIHC transcriptome and clinical data of the Japanese cohort were available from the International Cancer Genome Consortium (ICGC) database (https://dcc.icgc.org). TCGA dataset was used to investigate the immune subtypes of tumor microenvironment subtypes, and the Hoshida Y et al. cohort and Japanese cohort were independently used for external validation.

The enrichment scores of 64 cells in TME were inferred by the xCell algorithm, which integrated the advantages of gene-set enrichment with deconvolution approaches to remove dependencies between cell types (7). When selecting cell types, we first removed the other cell type family, which mainly included neural and sebaceous cells, in the algorithm. According to the cell p-value and the standard deviation of cell scores, we removed 8 cell types again. The tumor purity of TCGA patients was inferred by ESTIMATE (Estimation of Stromal and Immune cells in Malignant Tumors using Expression data), ABSOLUTE, LUMP (leukocyte unmethylation for purity), and CPE (consensus measurement of purity estimations) algorithms, and the immune subtypes of TCGA patients were provided in the study of Vésteinn Thorsson et al. (8). Moreover, related features, including the signature scores of tumor proliferation, wound healing, macrophage regulation, lymphocyte infiltration signature, IFN-γ response and TGF-β response, leukocyte fraction, tumor-infiltrating lymphocyte (TIL) regional fraction, and intratumor heterogeneity, were also used in our study.

Non-Supervisor Clustering and Identification of TME Subtypes

We performed the k-mean consensus cluster method to identify tumor microenvironment subtypes for TCGA patients, based on the R package "ConsensusClusterPlus". Performance of consensus matrix, empirical cumulative distribution function (CDF) plots, and relative change in area under CDF curve were considered when selecting optimal k value. The tumor microenvironment subtypes of patients in the Japanese cohort and the Hoshida Y et al. cohort were determined by a neural network model, which was trained and internally validated in TCGA dataset (the training and testing cohorts were randomly divided at a ratio of 7:3).

The neural network consisted of the input layer, hidden layers, and output layer. We set the cell matrix as the input layer and the subtype result as the output layer. The setting of the hidden layer neural nodes refers to the following formula:

$$N_h = \frac{N_s}{a*(N_i + N_o)}$$

N_i is the number of neurons in the input layer; N_o is the number of neurons in the output layer; N_s is the number of training set samples; and a could be an arbitrary variable.

We used the receiver operating characteristic (ROC) curve analysis to confirm the performance of the prognostic model.

Survival Analysis

The KM and Cox regression analyses were used to calculate the significance of differences in the overall survival (OS) for categorical variables. The statistical difference of the OS in the KM curve analysis was compared using the log-rank test, and the pairwise comparison was performed between multiple groups. For continuous variables, Cox regression was used to calculate the hazard ratio (HR) and significance of differences in the OS.

Gene Set Enrichment Analysis

R package "DESeq2" implement procedures were utilized for the differential expression analysis between any cluster and other patients (9). The genes with a false discovery rate (FDR, also known as Benjamini–Hochberg-adjusted p-values) < 0.05 and absolute log-transformed fold change (log2FC) > 1.0 were defined as differential expression genes. The gene list is then ranked by log2FC and studied using gene set enrichment analysis, which was computed by the R package "ClusterProfiler" (10). The signaling pathway information in the Molecular Signatures Database (MSigDB) (https://www.gsea-msigdb.org/gsea/msigdb/) was used. The pathway enrichment scores for each patient were calculated by the gene set variation analysis (GSVA).

Genomic Mutation and Copy Number Variants

The gene mutation data of LIHC were downloaded from TCGA database. The "Maftools" R package was applied to visualize the gene mutations and type of the mutation (11). The copy number data were recognized by GISTIC 2.0 (12).

Pseudotime Trajectory Analysis

Through inversed pseudotime trajectory analysis, we reduced the dimensions of all samples on the same plane, observed the distribution between different clusters, and explored the latent associations between clusters. Through the pseudotime ordering of each patient, we attempted to reveal the patient's possible disease development directions (13).

Evaluation of Drug Sensitivity and Patients' Response to Immunotherapy

Using the pRRophetic algorithm (14), a ridge regression model was established to predict the sensitivity value (IC50) of 51 drugs for LIHC patients of TCGA, the Japanese cohort, and the Hoshida Y et al. cohort based on the expression profile. pRRophetic is a popular enrichment algorithm, which was extensively utilized in medical studies (15–19). The potential response of patients to immunotherapy was inferred by the tumor immune dysfunction and exclusion (TIDE) score, which calculates how the expression of each gene in the tumor interacts with the level of cytotoxic T-cell infiltration to affect patient survival (20). Generally, a lower TIDE score predicts a better response to immunotherapy.

Other Statistical Analysis

Immune and stromal scores were calculated using the ESTIMATE algorithm, which was provided in the R package "estimate," and the correlation analysis was conducted based on the Spearman method. The Kruskal–Wallis test examined the statistical difference of distribution in three or more groups, and the Wilcoxon test compared that of two groups. The missing value of clinical data in our study was imputed by multiple imputation methods based on chain equitation. The FDR was calculated by the Benjamin–Hochberg method for adjusting the p-value in multiple comparisons.

RESULTS

The Association Between 48 Cells in TME and Clinical Characteristics in TCGA Patients

Based on the xCell algorithm, a total of 48 types of cells, including immune (including lymphocyte and myeloid cells), stem, and stromal cells in TME, were available for analysis in LIHC. The correlation between tumor microenvironment cells and the age of patients was calculated (**Figure 1A**). The adipocytes and macrophages M2 were significantly positively correlated with age. In contrast, the granulocyte-macrophage progenitor was negatively correlated with age. Although CD8+ T cells, CD4+ memory T cells, CD4+ naïve T cells, T helper 1 (Th1) cells, and T helper 2 (Th2) cells were positively associated with the patients' age, the associations were insignificant. The associations between age and each cell score in the TME of patients are shown in the **Supplementary Figure 1**.

Subsequently, we compared the estimated cell scores across different genders, levels of obesity, Child–Pugh grade, alcohol consumption, TNM stages, T stages, N stages, and M stages (**Figure 1B**). In comparing different levels of obesity and different Child–Pugh grades, the CD4+ T effector memory cells, immature dendritic cells, and macrophages M2 had higher scores in obese people and in the Child–Pugh grade B/C population. Maturation of dendritic cells could act as antigen-presenting cells and initiate the host anticancer immune response (21), but patients with obesity and poor liver function grading may have maturation disturbance of dendritic cells. When comparing the cell scores between TNM stages, the score of conventional dendritic cells and activated dendritic cells decreased in stage III/IV and stage T3/T4, which could activate cytotoxic T lymphocytes cross-presenting antigens (22).

We utilized the TME cell network to depict the comprehensive landscape of tumor–immune cell interactions, cell lineages, and their effects on the overall survival of patients with LIHC (**Figure 1C**, **Supplemental Table 1**). Through univariable Cox analysis, we found that only the Th 2 cell score was associated with poor prognosis in lymphoid, which was consistent with previous research conclusions (23). Many

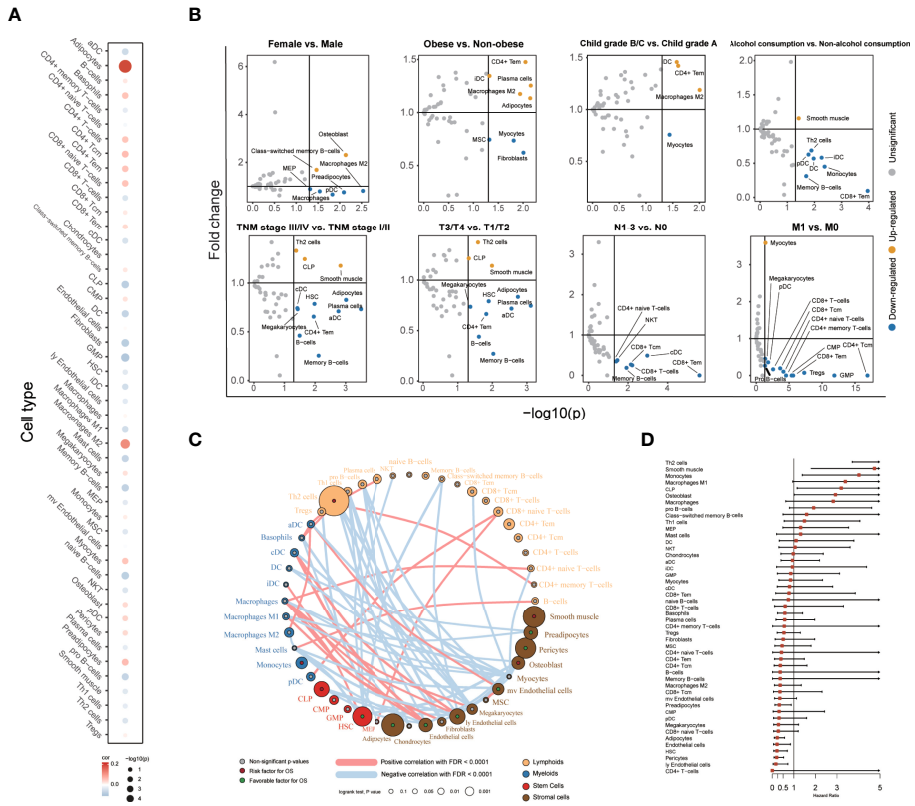

FIGURE 1 | The association between 48 cells in TME and clinical characteristics with patients. **(A)** Correlation between age and cell score. The size of each cell represented the correlation between age and cell score. Spearman correlation coefficients and the associated p-value (Spearman) were shown. **(B)** Volcano plot diagrams showed the comparison of cell infiltration levels. The significance (p-value) versus and fold change were plotted on the X-axis and T-axis. **(C)** Landscape of the TME in LIHC. Cellular interaction of the TME cell types. The lymphoid cells are marked by yellow; the myeloid cells are marked by blue; stem cells are marked by red; and stromal cells are marked by brown. The size of each cell represents the survival impact of each TME cell type, which was calculated by log10 (log-rank test p values indicated). Risk factors are indicated in red, and favorable factors for overall survival are indicated in green. The lines connecting TME cells represent cellular interactions. The thickness of the line represents the strength of correlation estimated by Spearman correlation analysis. Positive correlation is indicated in red and negative correlation in blue. **(D)** Forest plots showing multivariable Cox regression analyses of the cell score, and each score is adjusted by age and TNM stage.

cells, such as adipocytes and endothelial cells, were associated with favorable prognosis, which was usually thought to accelerate tumor metastasis (24, 25). We also calculated the HR of these cells using multivariable Cox analysis to correct the age and TNM stage (**Figure 1D**). Similar to the result of univariable Cox analysis, we found that Th 2 cells were associated with poor prognosis, and endothelial cells, etc., were associated with favorable prognosis.

Identification of Subtypes in TME of Patients With LIHC

The consensus matrix was used as the similarity matrix to define the final clusters. Sample classification robustness was analyzed by consensus clustering, which involved k-means clustering by resampling randomly selected tumor profiles (**Figure 2A**). According to the results of the consensus cluster and the areas under the curve of the consensus distribution function (CDF) plot, we chose k = 4 as the optimal value and divided 370 LIHC patients into four different subtypes (C1, C2, C3, and C4) with 57 samples in C1, 57 samples in C2, 144 samples in C3, and 112 samples in C4. In parallel, the overall survival in the TME clusters was significantly different (p of log-rank test = 0.0026, **Figure 2B**). Compared to patients of C1, those of C2 and C3 had a significantly poorer overall survival. In univariable Cox regression, the HR value of C2 versus C1 was 2.128 (95% CI: 1.087–4.165), that of C3 versus C1 was 2.881 (95% CI: 1.572–5.279), and that of C4 versus C1 was 1.413 (95% CI: 0.740–2.698). In multivariable Cox regression, the HR value of C2, C3, or C4 versus C1 was 1.983 (95% CI: 1.005–3.916), 2.510 (95% CI: 1.339–4.706), or 1.307 (95% CI: 0.677–2.525), respectively, by correcting the age and TNM stage (**Figure 2C**).

To explore the potential relationship between the four tumor microenvironment clusters, we used pseudotime ordering to analyze the development of the four subtypes (**Figure 2D**). According to the result, the patients in C1 and C3 were seated at both ends of the pseudotime ordering analysis, while the patients of C2 and C4 were in the middle of pseudotime ordering. The result of the pseudotime ordering analysis was similar to the overall survival result of each cluster. The pseudotime ordering suggested that C1 and C4 may be at a

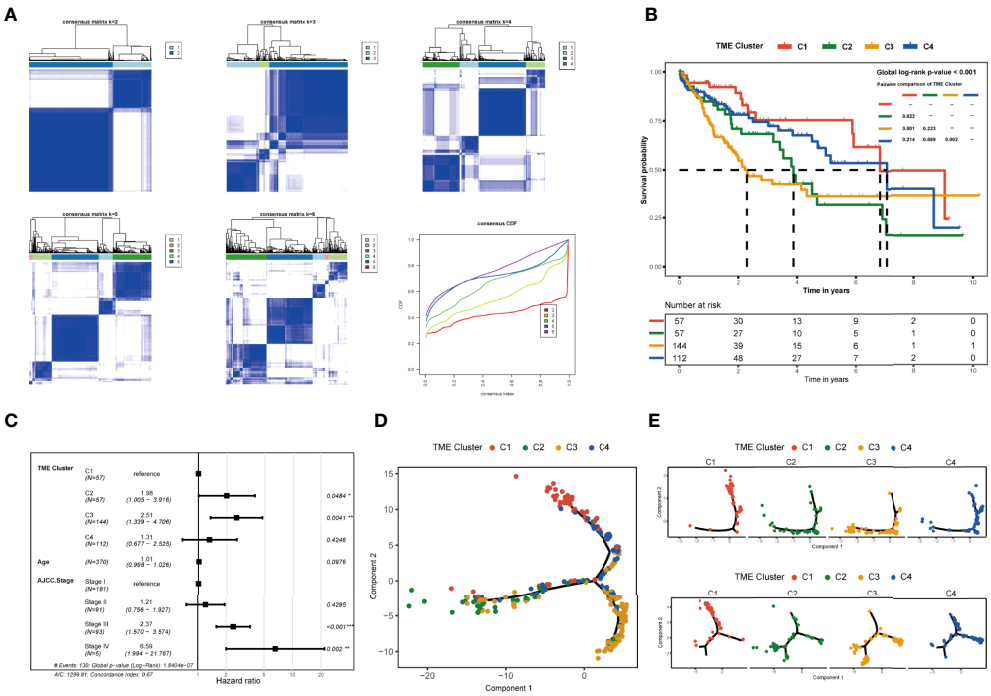

FIGURE 2 | Identification and clinical characteristics of TME subgroups. **(A)** Consensus clustering displaying the robustness of sample classification using multiple iterations (×1,000) of k-means clustering. The consensus distribution function (CDF) depicting the cumulative distribution from consensus matrices at a given cluster number (k). **(B)** Kaplan–Meier curves for overall survival of 370 patients in TCGA database showed the association between TME subtypes and overall survival (global log-rank test, p = 0.00033). **(C)** Forest plots showing multivariate Cox regression analyses of the TME class, age, and TNM stage on the overall survival of LIHC patients. **(D)** Pseudotime trajectory analysis speculated the developmental relationship of the clusters based on the differential genes. **(E)** Pseudotime trajectory analysis of 370 patients in TCGA based on the glycan biosynthesis and metabolism pathway-related genes and cellular processes (including transport and catabolism, cell growth and death, cellular community, and cell motility) pathway-related genes. *p≤ 0.05, **p≤ 0.01, ***p≤ 0.001.

similar stage in the glycan biosynthesis and metabolism pathways and cellular process pathways (including transport and catabolism, cell growth and death, cellular community, and cell motility) and have a potential timing relationship with C2 and C3 (**Figure 2E**, **Supplementary Figure 2**). In carbohydrate metabolism-, energy metabolism-, and nucleotide metabolism-related pathways and all cellular process-related pathways, we observed that C2 and C4 were on different timing stages, which may have a potential temporal evolution relationship (**Supplementary Figure 2**). We discussed the more particular biological characteristics and enrichment analysis in the next.

The Immune Characteristics in Different TME Clusters

To further characterize and understand the biological and immune differences and connections among these TME clusters, we contrasted the difference of cell scores in each TME cluster. As illustrated in **Figure 3A**, we observed a higher CD8+ T cell infiltration, including that of the CD8+ T cells, CD8+ T effector memory cells, and CD8+ T center memory cells, in C2 and C1 patients. Meanwhile, macrophages M1 and dendritic cells had higher cell scores in patients of C1 and C2. Concurrently, the other two clusters (C3 and C4) showed lower infiltration levels of CD8+ T cells, and the patients of C3 had lower endothelial cell scores.

The ESTIMATE, LUMP, IHC, and CPE scores from each TME cluster were also compared, which provided a qualitative estimation of tumor purity (**Figure 3B**). We observed that patients of C3 had higher tumor purity than other clusters. We counted the leukocyte fraction, stromal fraction, and intratumor heterogeneity in each subtype (**Figure 3C**). Notably, there was no significant difference in intratumor heterogeneity among the four subgroups, but C3 had the lowest leukocyte fraction and stromal fraction scores.

By probing the association between six identified immune subtypes and TME clusters, we found that most wound healing immune subtype patients belonged to TME C3, which means a high proliferation rate and an association with worse survival (**Figure 3D**). In contrast to wound healing, the IFN-γ-dominant subtype principally flowed to TME C2, which usually had the highest macrophages M1 and CD8+T cells. The lymphocyte-depleted subtype had minimal T helper cells and mainly flowed to TME C3 and C4. Furthermore, we discovered that C1 and C2 had higher lymphocyte infiltration and macrophage regulation scores than the other clusters, and C2 had higher macrophage regulation than others (**Figure 3E**). Simultaneously, C1 and C4 had a lower proliferation rate than C2 and C3, and C3 had the lowest

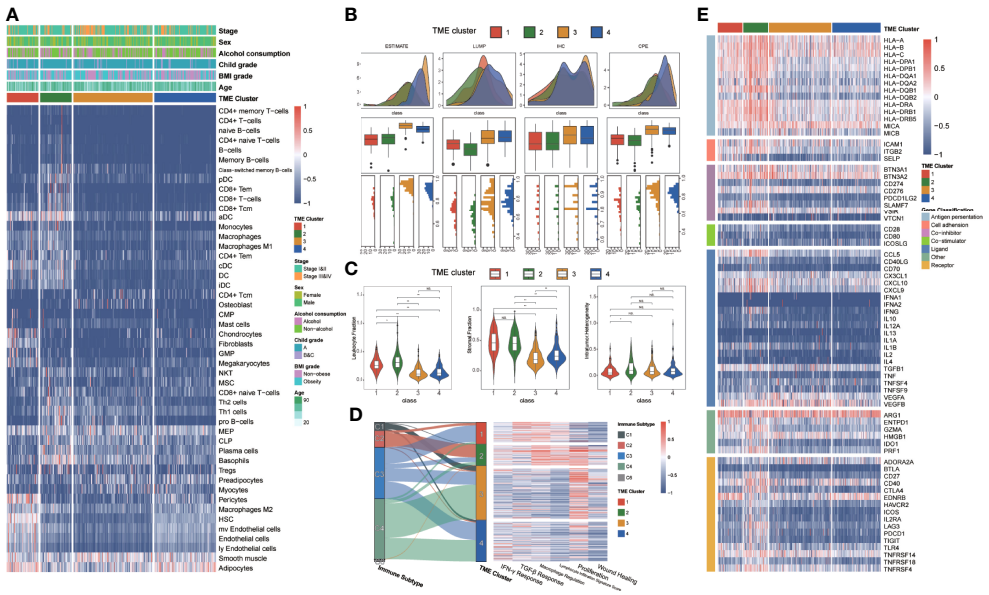

FIGURE 3 | The immune characteristics of different TME clusters. **(A)** Unsupervised clustering of TME cells for 370 patients in TCGA database. Clinical stage, sex, alcohol consumption, Child grade, BMI grade, age, and TME cluster were shown as patient annotations. **(B)** The boxplots showed the comparison of tumor purities with ESTIMATE, LUMP, IHC, and CPE, respectively. The thick line represents the median value. The bottom and top of the boxes were the 25th and 75th percentiles (interquartile range). The whiskers encompassed 1.5 times the interquartile range. The statistical difference of four groups was compared through the Kruskal–Wallis test. **(C)** Violin plots showed the comparison of immunocompetence with leukocyte fraction, stromal fraction, and intratumor heterogeneity respectively. The differences between every two groups were compared through the Kruskal–Wallis test. **(D)** Sankey diagram illustrates change between the immune subtype and TME cluster in each patient. Heatmap of IFN-γ response, TGF-β response, macrophage regulation, lymphocyte infiltration, proliferation, and wound healing in different TME clusters. **(E)** Heatmap of immune genes that were differentially expressed in patients from different TME clusters. *p≤ 0.05, **p≤ 0.01, ns: p> 0.05.

IFN-γ signature. To seek the difference of immunocompetence between each cluster, we examined the immunomodulatory gene expression in each cluster (**Figure 3D**). Almost all antigen presentation genes were highly expressed in C2 and C1, and the receptor genes had a high gene expression in C2.

The Analyses of Differentially Expressed Genes and Enriched Functions Between Different TME Clusters

We selected the top quarter with the most considerable variance from all genes to analyze the differential expression of genes in each TME cluster (**Figure 4A**, **Supplemental Table 2**). The highly altered genes involved in different TME clusters were TRARG1, CLEC4G, and GDF2 in C1; immunoglobulin lambda variable cluster family genes in C2; LGALS14, SST, and CYP11B2 in C3; and Lnc-NPVF-2, LUZP2, AQP6 in C4.

Then we used the gene sets in the MSigDB database to annotate the enriched biological functions, selected the significant enrichment pathway, and scored each patient by GSVA (**Figure 4B**). In TME C1, immune response-related pathways were highly enriched, including TGF-β signaling, complement activation, and B-cell receptor signaling pathway. The pathway enrichment of TME C2 was similar to that of C1, and those immune-related pathways were also enriched in C2. Nevertheless, IFN-α and IFN-γ response pathways and MYC target pathways were highly enriched in C2, specifically. Meanwhile, the cell cycle-related pathways were activated in TME C3, and the metabolism and decomposition-related pathways were activated in TME C4. In contrast, we found that cell cycle and cell proliferation-related pathways were the least enriched in C1, meaning that TME C1 may have the lowest cell proliferation rate. The metabolism-related and the oxidation–reduction (redox) reaction-related pathways were lowly enriched in C2 (**Figure 4C**). The downregulated pathways of C3 and C4 were highly similar, but C1 and C3 were opposite, especially in immune-related pathways (**Figures 4B, C**). Although the enrichment of immune pathways was similar in C1 and C2, the DNA replication and cell-cycle pathways were more enriched in C2. The same pattern also appeared in C3 versus C4, the metabolic-related pathways of C4 were more enriched, and the cell proliferation-related pathways were more enriched in C3 (**Supplementary Figure 3**).

Genomic Alteration Landscape of Different TME Clusters

To investigate the genomic alteration landscape of the TME cluster, we found that C3 showed a significantly higher tumor mutation burden and copy number variation than C1 (**Figure 5A**). By comparing genes with mutation rates greater than 5%, we observed that TP53, CTNNB1, OBSCN, DNAH7, CSMD1, RB1, FRAS1, and KMT2D, the most frequent alterations identified in

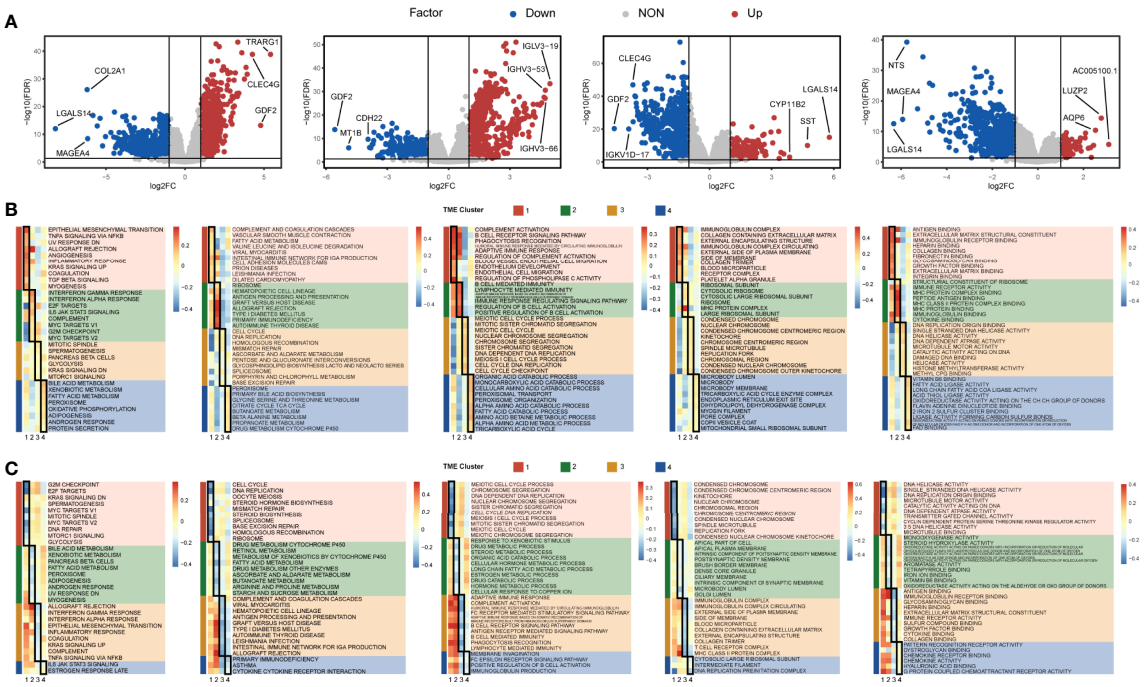

FIGURE 4 | Differentially expressed genes and enriched functions in the TME cluster. **(A)** The volcano map showed the differentially expressed genes of each cluster. Red dots represent upregulated genes, blue dots represent downregulated genes, and gray dots represent no differentially expressed genes. **(B)** The Hallmark, KEGG, Gene Ontology Biological Process (GOBP), Gene Ontology Cellular Component (GOCC), and Gene Ontology Molecular Function (GOMF) enrichment analyses were performed for upregulated genes in each cluster, respectively. **(C)** The above enrichment analyses were performed for downregulated genes in each cluster, respectively.

LIHC (**Supplemental Table 3**), had significantly different patterns between clusters. Considering that the APOBEC family members, including APOBEC3A and APOBEC3B, catalyze mutation and promote cancer growth (26, 27), we chose the APOBEC activity-related mutational signatures, SBS2 and SBS13, to investigate the differences of the immune microenvironment among clusters. We found that C3 had more mutations in APOBEC-related signatures.

Through the description of the entire cluster of CNV landscapes (**Figure 5B**) by GISTIC 2.0, we discovered that the CNV of C1 was significantly less than those of the other three clusters. Although the degree of amplification was generally higher in C2, there were more amplifications and deletions of the chromosomal locus in C3. The chromosomal specificity loci, such as 11q13.3 and 9p21.3, only had no significant amplification in C1 (**Supplemental Tables 4**-**5**).

Internal Validation and External Exploration of TME Clusters

The LIHC patients in TCGA dataset were randomly divided into the training cohort (n = 259) and the testing cohort (n = 111). We incorporated the matrix of putative cell scores into the neural network model and verified it in the validation set to determine TME clusters (**Figure 6A**). For internal validation, the accuracy of the neural network model was 0.949 in the testing cohort. In the external validation dataset, we used the neural network model to obtain the TME clusters and observed consistent survival differences between predicted TME clusters in the Japanese cohort and the Hoshida Y et al. cohort with that in TCGA dataset (**Figure 6B**).

To verify the stable interrelationship among the four subtypes, we performed pseudotime ordering analyses in the validation set with the same genes (**Figure 6C**). In all datasets, the patients in C1 and C3 were distributed at both endpoints of the hypothetical timeline and the patients of C2 and C4 were in the middle of the hypothetical timeline.

The landscape of infiltrating cells in TME was also explored (**Figures 6D, E**). Higher CD8+ T cell scores of C1 patients were observed in different validation datasets. Moreover, endothelial cells' legible low-infiltrating score could be observed in C3 patients, and the Th 1 cells had a low infiltrating score in C4. These findings in validation datasets indicate a similar pattern of infiltrating cell enrichment with that of TCGA dataset.

Therapeutic Response to Chemotherapy and Immunotherapy of Patients in Different TME Clusters

To find the response of LIHC patients to drugs in different TME clusters, we inferred the IC50 value of the 51 drugs in TCGA-LIHC, the Japanese cohort, and the Hoshida Y et al. cohort patients (**Figure 7A**). We found that patients in C1 might be more sensitive to paclitaxel, cisplatin, bortezomib, etc. The patients in C2 might be more sensitive to docetaxel,

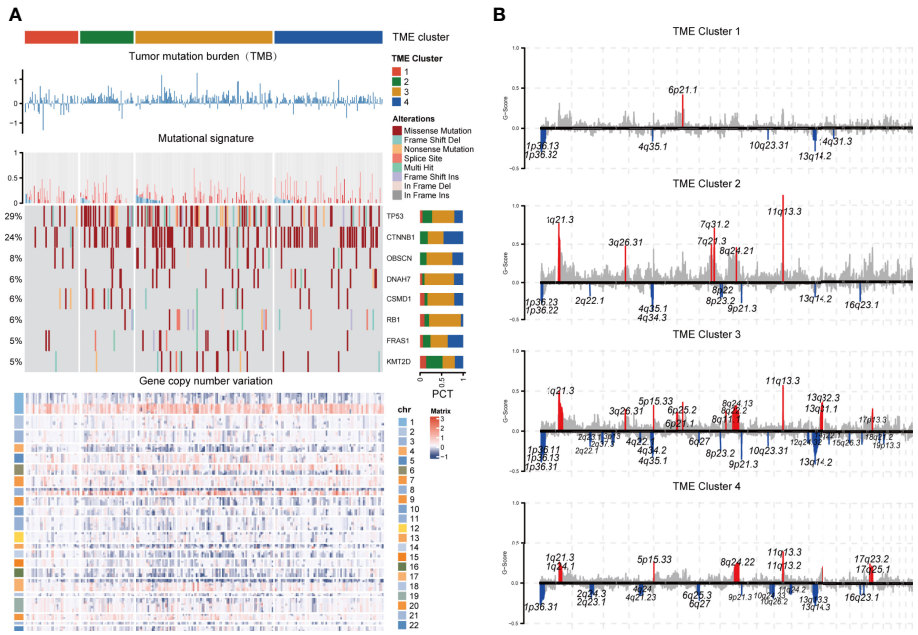

FIGURE 5 | Genomic alteration landscape of each TME cluster. **(A)** The log10TMB of each cluster, gene-level CNV mutational signature, waterfall chart of significant (>5%) and differently (Fisher's exact test $p < 0.1$) mutated genes, and heatmap of gene copy number variation were shown from the top to the bottom panels. Patients were ordered by the combined contribution of APOBEC-related mutational signatures (SBS2 + SBS13) with each cluster. **(B)** GISTIC copy number variation analysis. The amplifications and deletions of chromosomal regions were colored red and blue, respectively (FDR cutoff: 0.01).

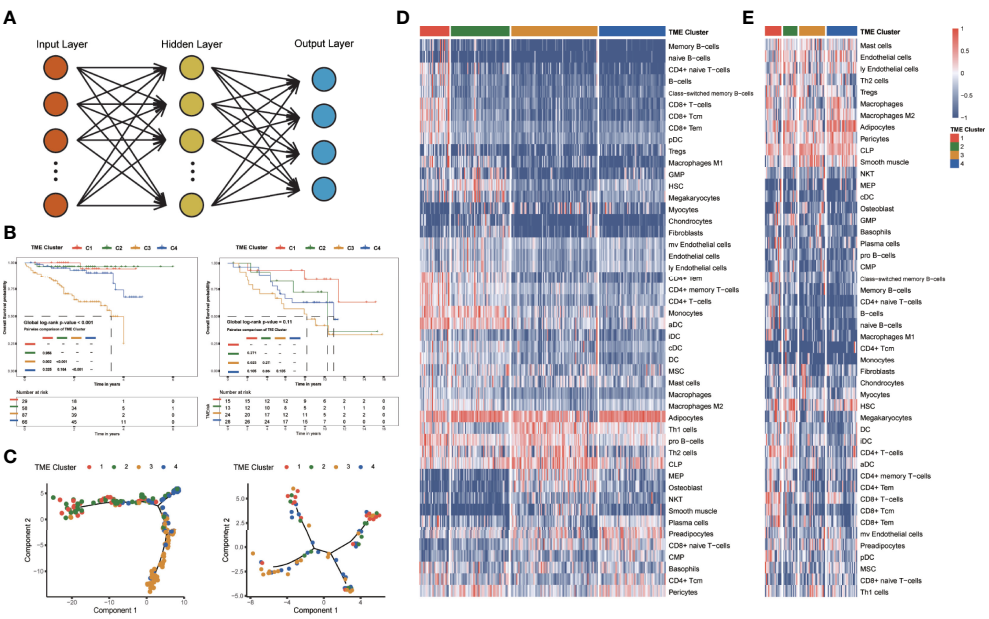

FIGURE 6 | Identification and clinical characteristics of TME clusters in the verification group. **(A)** Neural network. The cell matrix was the input layer, and the subtype result was the output layer. **(B)** Kaplan–Meier curves for overall survival of 240 patients in the Japanese cohort (global log-rank test, $p < 0.0001$), and 80 patients in the Hoshida Y et al. cohort (global log-rank test, $p = 0.11$). **(C)** Pseudotime trajectory analysis of the Japanese cohort and the Hoshida Y et al. cohort. **(D)** Unsupervised clustering of TME cells for 240 patients in the Japanese cohort. **(E)** Unsupervised clustering of TME cells for 80 patients in the Hoshida Y et al. cohort.

elesclomol, etc. The patients in C3 were less sensitive to most targeted drugs, except epothilone B and gemcitabine. Furthermore, patients in C4 might be more sensitive to metformin, vinorelbine, erlotinib, etc. The potential response of ICB therapy was estimated by the TIDE algorithm, which can evaluate the efficacy of anti-PD1 and anti-CTLA4 treatments. We discovered that C1 had the lowest TIDE score than other clusters (**Figure 7B**), which means the patients of C1 may get more benefits from immunotherapy. Comparing the scores of C2 patients in three cohorts, we speculated that C2 patients could not benefit from immunotherapy stably. Moreover, the patients of C3 and C4 may have poor immunotherapy efficacy.

DISCUSSION

We identified four tumor microenvironment subtypes based on the lymphocytes, myeloid cells, stem, and stromal cells and discussed the difference of survival, cell infiltration, tumor mutation burden, copy number variation, and functional enrichment pathways between the clusters. A neural network model was established based on the obtained cell matrix and verified in the Japanese and Hoshida Y et al. cohorts. In conclusion, the multiple signatures suggested that the long-term outcome and immunotherapy efficacy of patients may be different among four TME subtypes.

It was generally considered that the hematopoiesis becomes skewed toward myeloid and away from lymphoid lineages with age; therefore, aging negatively impacted CD8+ T cell immunity and positively connected with adipocytes (28). Similar trends may also exist in the tumor microenvironment of LIHC patients. The increase of adipocytes and the decrease of granulocyte-macrophage progenitor may indicate the transformation to the aging microenvironment, which may dramatically affect tumor progression (29). Our study suggested that macrophage M2 was increased in older LIHC patients, with obvious tumor-promoting functions (30). Tumor-associated adipocytes can promote the immunosuppressive TME and aggravate tumor progression (31). Considering the immune cell-adipocyte cross talk mentioned in single-cell studies, the growth of adipocytes may cause systemic energy imbalance in TME (32). In summary, we speculated that elderly patients might have a more immunosuppressed TME than young patients.

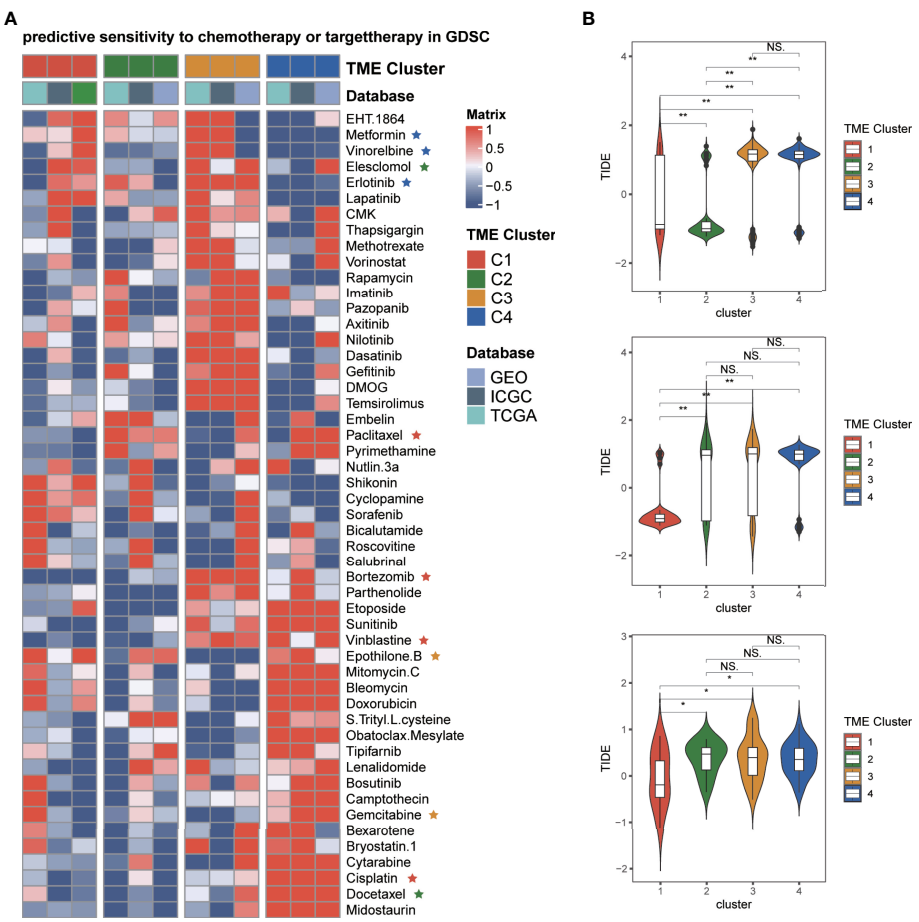

FIGURE 7 | Predicting the efficacy of each TME cluster. **(A)** Heatmap of drug sensitivity in patients of different TME clusters in TCGA, Japanese, and Hoshida Y et al. cohorts. **(B)** Violin plots showed the comparison of the TIDE score of TME clusters in TCGA, respectively. *p≤ 0.05, **p≤ 0.01, ns: p> 0.05.

Besides, most of the previous research was based on the immune microenvironment and did not analyze the types of stromal cells and stem cells. Our research explored immune and non-immune cells in the immune microenvironment of liver cancer, which makes our study more complete and closer to the real situation. The TME component of LIHC may be unique, such as the existence of endothelial cells. Highly endothelial cell infiltration was usually associated with poor survival, and the liver sinusoidal endothelial cells could not be ignored in the liver, which has vital physiological and immunological functions, including antigen presentation, and leukocyte recruitment (33). In liver cancer, a high endothelial cell score is associated with a good prognosis, and correspondingly, the patients of C3 have a lower endothelial cell score and worse prognosis. Likewise, in the non-neoplastic cirrhotic and non-cirrhotic liver, PD-L1 was expressed on Kupffer cells (macrophages that reside in hepatic sinusoids), endothelial cells, and immune cells, all of which scored lowly in C3 (34). This result is consistent with the low expression of CD274 in C3, which also indicates that immunotherapy may be less effective in C3. In addition, a single-cell sequencing study found that exhausted CD8+ T cells and regulatory T cells were preferentially enriched and potentially clonally expanded in LIHC, but the functions of CD8+ T cells were repressed (35). Although the patients of C2 had a higher CD8+ T cell score than C1, the functions of CD8+ T cells may be inhibited.

We observed that the enrichment of pathways in different types seems regular. For instance, the cell cycle and cell proliferation-related pathways had the highest enrichment in TME C3, followed by C2, C4, and C1. In immune-related pathways, the enrichment of C1 and C2 was opposite to that of C3 and C4. These results indicated that the immune phenotype of C1 may be similar to that of C2 and antagonistic to that of C3 and C4. Simultaneously, the cell proliferation-related pathways in C1 that had the lowest enrichment may indicate that the cancer cells were less malignant, which explained the better survival outcome of patients in C1. Interestingly, the patients of C1 had a relatively inactive immune microenvironment compared with patients of C2. The immune cell scores, stromal fraction, and immune pathway enrichment were similar in C1 and C2. Intriguingly, the expression of immune-related genes of C2 was even higher, but C2 did not have a better survival outcome than C1. Regarding the metabolism laws of the four subtypes, we believed that the metabolism and cell cycle of C1 were relatively inactive, and there is an evolutionary process from C1 to high-metabolome subtypes by pseudotime ordering analysis. Considering that the enrichment of immune and metabolic-related pathways in C2 was higher than that in C1, we speculated the high immune activity could not control more malignant tumors in C2, which may explain why the survival outcome of C2 was worse than that of C1. In addition, the TIDE score consisted of a dysfunction score and an exclusion score, which were associated with the average expressions of CD8A, CD8B, GZMA, GZMB, and PRF1 (20). The above cytotoxic T lymphocyte markers were expressed differently between C1and C2; therefore, the TIDE scores between C1 and C2 were different.

As for the differences of TMB in each cluster, proliferative hepatocellular carcinoma was associated with chromosomal instability and TP53 mutations, and non-proliferative tumors were a well-differentiated phenotype with CTNNB1 mutations (36). The TP53 mutation frequency was higher in C2; we speculated that the patients of C2 may belong to the proliferative hepatocellular carcinoma. Involved in CNV, although the amplified chromosomes were at the same locus, the amplified genes were not the same among clusters. Oncogenes expressed by chromosomal 11q13.3, such as CCND1 and some FGF family genes, increased the immune checkpoint signature expression, including CD274, PDCD1, BTLA, CTLA4, HAVCR2, IDO1, and LAG3 (37). We discovered that CCND1 was only amplified in C2, which may account for the high expression of immune checkpoint signatures in C2. There have been targeted drugs applicated for 11q13.3 amplification (38). However, the amplified genes were significantly different between clusters, and only patients in C3 were accompanied by amplified FGF family genes, which suggested a better response to FGF inhibitors. It is also noteworthy that FGF3 amplification may be associated with multiple lung metastases and a poorly differentiated tumor (39).

We also observed a similar situation at site 9p21.3. LIHC does not belong to the frequent 9p21 loss cancer type, but this CNV type can distinguish between subtypes with obvious deletion (C1) and no apparent deletion (C2–4), according to our study. The 9p21 loss correlates with "cold" tumor-immune phenotypes and shorter survival (40). In melanoma, the deletion of 9p21 was associated with primary resistance to anti-PD-1/PD-L1 monotherapy, suggesting that immunotherapy may not be effective in C2–4. On the other hand, we must pay attention to the high expression of CD274 in C2, suggesting that C2 patients may benefit from immunotherapy. Combined with 9p21.3 loss, the immunotherapy efficacy in these patients may be variational. Moreover, this conclusion is the same as the result calculated by TIDE in our study. In parallel, patients with deletions or mutations in CDKN2A and CDKN2B, common deletion genes in C2–4, had a significantly shorter time to progress on chemotherapy (41). In contrast, C2 and C3–4 have different genes deleted at the chromosomal 9p21. The patients of C2 had more CDKN2B and CDKN2B-AS1 deletions than C3–4. The CDKN2B-AS1 knockdown inhibited cell proliferation, migration, and invasion and induced G1 arrest and apoptosis of tumor cells (42). In short, C2 patients may have fewer metastases than C3 and 4.

In brief, the patients of C1 have lower malignancy and higher immunological activity, without 9p21.3 deletion or 11q13.3 amplification, and can achieve better curative effects in immunotherapy. C2 patients have high immunological activity and a high expression of immune checkpoint inhibitors. The malignance of the two clusters may be lower and tumor not easy to metastasize, and both of them may benefit from immunotherapy or local therapy. The patients of C3 with lower immune and stromal cell infiltration, and highest tumor purity, find it challenging to benefit from immunotherapy. They may get better curative effects from drugs that target FGF/FGFR, including lenvatinib (43). The patients of C4 may belong to immune-insensitive subtypes like C3 and develop toward C3. Considering that the cell-division M phase-related pathways, like the sister chromatid segregation pathway,

were highly enriched in C3, the vinorelbine drugs may achieve good results in C4.

Although our study confirmed four TME subtypes that potentially predicted antitumor treatment efficacy, our research still has limitations. The experimental data were lacking in our study, and the evaluation of efficacy of therapies mentioned in our study should be performed in larger-scale clinical data. In conclusion, our study laid an accurate foundation of four TME subtypes, which may provide therapeutic inspiration for patient selection for appropriate therapies in LIHC.

DATA AVAILABILITY STATEMENT

Publicly available datasets were analyzed in this study. These data can be found here: https://dcc.icgc.org https://www.ncbi.nlm.nih.gov/geo/query/acc.cgi?acc=GSE10141.

AUTHOR CONTRIBUTIONS

Research design: JW, HZ, BX, and YY. Data collection: CZ, JH, and JZ. Data analysis: HZ. Manuscript preparation: HZ and JW. Chart preparation: HZ and JW. Revisions: YY, JW, BX, and HZ. All authors confirm that they contributed to the manuscript review and critical revision for important intellectual content and read and approved the final draft for submission. All authors are also responsible for the manuscript content.

FUNDING

This work was supported by grants from the Wuhan University Medical Faculty Innovation Seed Fund Cultivation Project (grant no. TFZZ2018025), Chen Xiao-Ping Foundation for the Development of Science and Technology of Hubei Province (grant no.CXPJJH12000001-2020313), the National Natural Science Foundation of China (grant nos. 81670123 and 81670144), the Fundamental Research Funds for the Central Universities (grant no. 2042021kf0129), the Fundamental Research Funds for the Central Universities (grant no. 2042021kf0129), and the Nature Science Foundation of Hubei Province (grant no. 2021CFB086).

ACKNOWLEDGMENTS

We thank all the following physicians and Medical doctors for assistance of this article: Tianyu Lei, Jing Lin, all belonging to Renmin Hospital of Wuhan University.

SUPPLEMENTARY MATERIAL

The Supplementary Material for this article can be found online at: https://www.frontiersin.org/articles/10.3389/fimmu.2022.838374/full#supplementary-material

REFERENCES

1. Quail DF, Joyce JA. Microenvironmental Regulation of Tumor Progression and Metastasis. *Nat Med* (2013) 19(11):1423–37. doi: 10.1038/nm.3394
2. Zhou W, Zhou Y, Chen X, Ning T, Chen H, Guo Q, et al. Pancreatic Cancer-Targeting Exosomes for Enhancing Immunotherapy and Reprogramming Tumor Microenvironment. *Biomaterials* (2021) 268:120546. doi: 10.1016/j.biomaterials.2020.120546
3. Liu X, Wu S, Yang Y, Zhao M, Zhu G, Hou Z. The Prognostic Landscape of Tumor-Infiltrating Immune Cell and Immunomodulators in Lung Cancer. *Biomed Pharmacother* (2017) 95:55–61. doi: 10.1016/j.biopha.2017.08.003
4. Binnewies M, Roberts EW, Kersten K, Chan V, Fearon DF, Merad M, et al. Understanding the Tumor Immune Microenvironment (TIME) for Effective Therapy. *Nat Med* (2018) 24(5):541–50. doi: 10.1038/s41591-018-0014-x
5. Garon EB, Rizvi NA, Hui R, Leighl N, Balmanoukian AS, Eder JP, et al. Pembrolizumab for the Treatment of non-Small-Cell Lung Cancer. *N Engl J Med* (2015) 372(21):2018–28. doi: 10.1056/NEJMoa1501824
6. Börger V, Bremer M, Ferrer-Tur R, Gockeln L, Stambouli O, Becic A, et al. Mesenchymal Stem/Stromal Cell-Derived Extracellular Vesicles and Their Potential as Novel Immunomodulatory Therapeutic Agents. *Int J Mol Sci* (2017) 18(7):1450. doi: 10.3390/ijms18071450
7. Aran D, Hu Z, Butte AJ. Xcell: Digitally Portraying the Tissue Cellular Heterogeneity Landscape. *Genome Biol* (2017) 18(1):220. doi: 10.1186/s13059-017-1349-1
8. Thorsson V, Gibbs DL, Brown SD, Wolf D, Bortone DS, Ou Yang TH, et al. The Immune Landscape of Cancer. *Immunity* (2018) 48(4):812–30 e14. doi: 10.1016/j.immuni.2018.03.023
9. Anders S, Huber W. Differential Expression Analysis for Sequence Count Data. *Genome Biol* (2010) 11(10):R106. doi: 10.1186/gb-2010-11-10-r106
10. Yu G, Wang LG, Han Y, He QY. Clusterprofiler: An R Package for Comparing Biological Themes Among Gene Clusters. *Omics J Integr Biol* (2012) 16(5):284–7. doi: 10.1089/omi.2011.0118
11. Mayakonda A, Lin DC, Assenov Y, Plass C, Koeffler HP. Maftools: Efficient and Comprehensive Analysis of Somatic Variants in Cancer. *Genome Res* (2018) 28(11):1747–56. doi: 10.1101/gr.239244.118
12. Mermel CH, Schumacher SE, Hill B, Meyerson ML, Beroukhim R, Getz G. GISTIC2.0 Facilitates Sensitive and Confident Localization of the Targets of Focal Somatic Copy-Number Alteration in Human Cancers. *Genome Biol* (2011) 12(4):R41. doi: 10.1186/gb-2011-12-4-r41
13. Trapnell C, Cacchiarelli D, Grimsby J, Pokharel P, Li S, Morse M, et al. The Dynamics and Regulators of Cell Fate Decisions are Revealed by Pseudotemporal Ordering of Single Cells. *Nat Biotechnol* (2014) 32(4):381–6. doi: 10.1038/nbt.2859
14. Geeleher P, Cox N, Huang RS. Prrophetic: An R Package for Prediction of Clinical Chemotherapeutic Response From Tumor Gene Expression Levels. *PloS One* (2014) 9(9):e107468. doi: 10.1371/journal.pone.0107468
15. Liu Z, Liu L, Weng S, Guo C, Dang Q, Xu H, et al. Machine Learning-Based Integration Develops an Immune-Derived lncRNA Signature for Improving Outcomes in Colorectal Cancer. *Nat Commun* (2022) 13(1):816. doi: 10.1038/s41467-022-28421-6
16. Liu Z, Guo C, Li J, Xu H, Lu T, Wang L, et al. Somatic Mutations in Homologous Recombination Pathway Predict Favourable Prognosis After Immunotherapy Across Multiple Cancer Types. *Clin Trans Med* (2021) 11(12):e619. doi: 10.1002/ctm2.619
17. Liu Z, Guo C, Dang Q, Wang L, Liu L, Weng S, et al. Integrative Analysis From Multi-Center Studies Identities a Consensus Machine Learning-Derived lncRNA Signature for Stage II/III Colorectal Cancer. *EBioMedicine* (2022) 75:103750. doi: 10.1016/j.ebiom.2021.103750
18. Liu L, Liu Z, Meng L, Li L, Gao J, Yu S, et al. An Integrated Fibrosis Signature for Predicting Survival and Immunotherapy Efficacy of Patients With Hepatocellular Carcinoma. *Front Mol Biosci* (2021) 8:766609. doi: 10.3389/fmolb.2021.766609
19. Liu Z, Liu L, Guo C, Yu S, Meng L, Zhou X, et al. Tumor Suppressor Gene Mutations Correlate With Prognosis and Immunotherapy Benefit in

Hepatocellular Carcinoma. *Int Immunopharmacol* (2021) 101(Pt B):108340. doi: 10.1016/j.intimp.2021.108340
20. Jiang P, Gu S, Pan D, Fu J, Sahu A, Hu X, et al. Signatures of T Cell Dysfunction and Exclusion Predict Cancer Immunotherapy Response. *Nat Med* (2018) 24(10):1550–8. doi: 10.1038/s41591-018-0136-1
21. Tiberio L, Del Prete A, Schioppa T, Sozio F, Bosisio D, Sozzani S. Chemokine and Chemotactic Signals in Dendritic Cell Migration. *Cell Mol Immunol* (2018) 15(4):346–52. doi: 10.1038/s41423-018-0005-3
22. Gardner A, Ruffell B. Dendritic Cells and Cancer Immunity. *Trends Immunol* (2016) 37(12):855–65. doi: 10.1016/j.it.2016.09.006
23. Bruni D, Angell HK, Galon J. The Immune Contexture and Immunoscore in Cancer Prognosis and Therapeutic Efficacy. *Nat Rev Cancer* (2020) 20 (11):662–80. doi: 10.1038/s41568-020-0285-7
24. Maishi N, Hida K. Tumor Endothelial Cells Accelerate Tumor Metastasis. *Cancer Sci* (2017) 108(10):1921–6. doi: 10.1111/cas.13336
25. Attané C, Muller C. Drilling for Oil: Tumor-Surrounding Adipocytes Fueling Cancer. *Trends Cancer* (2020) 6(7):593–604. doi: 10.1016/j.trecan.2020.03.001
26. Law EK, Levin-Klein R, Jarvis MC, Kim H, Argyris PP, Carpenter MA, et al. APOBEC3A Catalyzes Mutation and Drives Carcinogenesis *In Vivo*. *J Exp Med* (2020) 217(12):e20200261. doi: 10.1084/jem.20200261
27. Wang D, Li X, Li J, Lu Y, Zhao S, Tang X, et al. APOBEC3B Interaction With PRC2 Modulates Microenvironment to Promote HCC Progression. *Gut* (2019) 68(10):1846–57. doi: 10.1136/gutjnl-2018-317601
28. Drijvers JM, Sharpe AH, Haigis MC. The Effects of Age and Systemic Metabolism on Anti-Tumor T Cell Responses. *eLife* (2020) 9:e62420. doi: 10.7554/eLife.62420
29. Fane M, Weeraratna AT. How the Ageing Microenvironment Influences Tumour Progression. *Nat Rev Cancer* (2020) 20(2):89–106. doi: 10.1038/s41568-019-0222-9
30. Wan S, Zhao E, Kryczek I, Vatan L, Sadovskaya A, Ludema G, et al. Tumor-Associated Macrophages Produce Interleukin 6 and Signal *via* STAT3 to Promote Expansion of Human Hepatocellular Carcinoma Stem Cells. *Gastroenterology* (2014) 147(6):1393–404. doi: 10.1053/j.gastro.2014.08.039
31. Liu Y, Tiruthani K, Wang M, Zhou X, Qiu N, Xiong Y, et al. Tumor-Targeted Gene Therapy With Lipid Nanoparticles Inhibits Tumor-Associated Adipocytes and Remodels the Immunosuppressive Tumor Microenvironment in Triple-Negative Breast Cancer. *Nanoscale Horiz* (2021) 6(4):319–29. doi: 10.1039/d0nh00588f
32. Rajbhandari P, Arneson D, Hart SK, Ahn IS, Diamante G, Santos LC, et al. Single Cell Analysis Reveals Immune Cell-Adipocyte Crosstalk Regulating the Transcription of Thermogenic Adipocytes. *eLife* (2019) 8:e49501. doi: 10.7554/eLife.49501
33. Shetty S, Lalor PF, Adams DH. Liver Sinusoidal Endothelial Cells - Gatekeepers of Hepatic Immunity. *Nat Rev Gastroenterol Hepatol* (2018) 15 (9):555–67. doi: 10.1038/s41575-018-0020-y
34. Ihling C, Naughton B, Zhang Y, Rolfe PA, Frick-Krieger E, Terracciano LM, et al. Observational Study of PD-L1, TGF-β, and Immune Cell Infiltrates in Hepatocellular Carcinoma. *Front Med* (2019) 6:15. doi: 10.3389/fmed.2019.00015
35. Zheng C, Zheng L, Yoo JK, Guo H, Zhang Y, Guo X, et al. Landscape of Infiltrating T Cells in Liver Cancer Revealed by Single-Cell Sequencing. *Cell* (2017) 169(7):1342–56.e16. doi: 10.1016/j.cell.2017.05.035
36. Calderaro J, Ziol M, Paradis V, Zucman-Rossi J. Molecular and Histological Correlations in Liver Cancer. *J Hepatol* (2019) 71(3):616–30. doi: 10.1016/j.jhep.2019.06.001
37. Chan AW, Zhang Z, Chong CC, Tin EK, Chow C, Wong N. Genomic Landscape of Lymphoepithelioma-Like Hepatocellular Carcinoma. *J Pathol* (2019) 249(2):166–72. doi: 10.1002/path.5313
38. Sawey ET, Chanrion M, Cai C, Wu G, Zhang J, Zender L, et al. Identification of a Therapeutic Strategy Targeting Amplified FGF19 in Liver Cancer by Oncogenomic Screening. *Cancer Cell* (2011) 19(3):347–58. doi: 10.1016/j.ccr.2011.01.040
39. Arao T, Ueshima K, Matsumoto K, Nagai T, Kimura H, Hagiwara S, et al. FGF3/FGF4 Amplification and Multiple Lung Metastases in Responders to Sorafenib in Hepatocellular Carcinoma. *Hepatology (Baltimore Md)* (2013) 57 (4):1407–15. doi: 10.1002/hep.25956
40. Han G, Yang G, Hao D, Lu Y, Thein K, Simpson BS, et al. 9p21 Loss Confers a Cold Tumor Immune Microenvironment and Primary Resistance to Immune Checkpoint Therapy. *Nat Commun* (2021) 12(1):5606. doi: 10.1038/s41467-021-25894-9
41. Lowery MA, Ptashkin R, Jordan E, Berger MF, Zehir A, Capanu M, et al. Comprehensive Molecular Profiling of Intrahepatic and Extrahepatic Cholangiocarcinomas: Potential Targets for Intervention. *Clin Cancer Res* (2018) 24(17):4154–61. doi: 10.1158/1078-0432.Ccr-18-0078
42. Huang Y, Xiang B, Liu Y, Wang Y, Kan H. LncRNA CDKN2B-AS1 Promotes Tumor Growth and Metastasis of Human Hepatocellular Carcinoma by Targeting Let-7c-5p/NAP1L1 Axis. *Cancer Lett* (2018) 437:56–66. doi: 10.1016/j.canlet.2018.08.024
43. Sato J, Satouchi M, Itoh S, Okuma Y, Niho S, Mizugaki H, et al. Lenvatinib in Patients With Advanced or Metastatic Thymic Carcinoma (REMORA): A Multicentre, Phase 2 Trial. *Lancet Oncol* (2020) 21(6):843–50. doi: 10.1016/s1470-2045(20)30162-5

Conflict of Interest: The authors declare that the research was conducted in the absence of any commercial or financial relationships that could be construed as a potential conflict of interest.

Publisher's Note: All claims expressed in this article are solely those of the authors and do not necessarily represent those of their affiliated organizations, or those of the publisher, the editors and the reviewers. Any product that may be evaluated in this article, or claim that may be made by its manufacturer, is not guaranteed or endorsed by the publisher.

frontiers | Frontiers in Immunology

ORIGINAL RESEARCH
published: 22 July 2022
doi: 10.3389/fimmu.2022.947712

Comparative Analysis of Mutation Status and Immune Landscape for Squamous Cell Carcinomas at Different Anatomical sites

Wenqi Ti, Tianhui Wei, Jianbo Wang and Yufeng Cheng**

Department of Radiation Oncology, Qilu Hospital, Cheeloo College of Medicine, Shandong University, Jinan, China

OPEN ACCESS

Edited by:
Xuesong Gu,
Beth Israel Deaconess Medical Center and Harvard Medical School, United States

Reviewed by:
Yang Li,
Anhui Medical University, China
Bo Xiang,
Central South University, China
Jun Liu,
Wuhan University, Wuhan, China

***Correspondence:**
Yufeng Cheng
qlcyf@sdu.edu.cn
Jianbo Wang
qlwjb2008@163.com

Specialty section:
This article was submitted to Cancer Immunity and Immunotherapy, a section of the journal Frontiers in Immunology

Received: *19 May 2022*
Accepted: *20 June 2022*
Published: *22 July 2022*

Citation:
Ti W, Wei T, Wang J and Cheng Y (2022) Comparative Analysis of Mutation Status and Immune Landscape for Squamous Cell Carcinomas at Different Anatomical sites. Front. Immunol. 13:947712. doi: 10.3389/fimmu.2022.947712

Objective: It has been controversial whether tumor mutation burden (TMB) affects the prognosis and the efficacy of immunotherapy in different tumor types. We provided a comprehensive analysis of mutation status and immune landscape of squamous cell carcinomas (SCCs) from four sites in order to investigate the relationship of TMB with prognosis and immune cell infiltration in different SCCs.

Methods: The transcriptome profiles and somatic mutation data of SCCs downloaded from the Cancer Genome Atlas (the Cancer Genome Atlas) database were analyzed and visualized. Then, TMB was calculated to analyze its correlations with prognosis and clinical features. Differentially expressed genes (DEGs) between the high and low TMB groups were screened for functional enrichment analysis. CIBERSORT algorithm was used to compare differences of immune cell infiltration between two groups in different SCCs. In addition, immune DEGs associated with prognosis were identified and risk prediction model was constructed *via* Cox regression analysis.

Results: Missense mutation was the most dominant mutation type in SCCs. The difference was that the top10 mutated genes varied widely among different SCCs. High TMB group had better prognosis in lung squamous cell carcinoma (LUSC) and cervical squamous cell carcinoma (CESC), while the result was reverse in head and neck squamous cell carcinoma (HNSCC) and esophageal squamous cell carcinoma (ESCC). In addition, patients with older age, smoking history, earlier pathological stage and no lymphatic invasion had higher TMB. The identified DEGs were mainly enriched in the regulation of immune system, muscular system and the activity of epidermal cells. The proportions of CD8+T cells, CD4+ memory T cells, follicular helper T cells, macrophages were distinct between two groups. The prognosis-related hub genes (CHGB, INHBA, LCN1 and VEGFC) screened were associated with poor prognosis.

Conclusion: This study reveals the mutation status and immune cell infiltration of SCCs at different anatomical sites. TMB is closely related to the prognosis of SCCs, and its effects on prognosis are diverse in different SCCs, which might result from the situation of

immune cell infiltration. These findings contribute to the exploration of biomarkers for predicting the efficacy of immunotherapy in SCCs and providing innovative insights for accurate application of immunotherapy.

Keywords: squamous cell carcinoma, immune cell infiltration, tumor mutation burden, prognosis, the Cancer Genome Atlas database

INTRODUCTION

Squamous cell carcinomas (SCCs) are the most common human solid tumors, arising from the epithelia of the aerodigestive and genitourinary tracts. They are frequently found in nasal cavity, oropharynx, esophagus, lung and anogenital region (1). SCCs from different parts of the body share some important properties due to their common histopathological features. They share certain common risk factors, such as smoking, excess alcohol drinking and human papillomavirus (HPV) infection (2). Cancer-related DNA hypermethylation is influenced by cell-type-specific chromatin markers or transcriptional programs, resulting in a tendency for some tumors from the same origin to aggregate common methylation data. For example, SCCs (HNSCC, ESCC, LUSC, and CESC) are strongly associated with METH2 and METH3 (3). Therefore, SCCs from different anatomical sites may have similar molecular patterns and clinical outcomes.

Chemotherapy, radiotherapy and surgery are traditional tumor treatments, which often have little effect on some metastatic, recurrent and refractory diseases (4). In recent years, studies of the anti-tumor immune response have promoted the development of therapeutic strategies, among which immunotherapy has become spotlighted in the field of cancer. Immunotherapy regulates the immune system to improve anti-tumor immune response and overcome immune escape mechanism. Because of its high clinical safety, lasting efficacy and effective improvement of survival, it has brought revolutionary innovation and has gradually become the pillar of modern cancer treatment. However, the benefits of immunotherapy remain unclear with low response rates and only a minority of people benefiting from it. A retrospective study using publicly reported cancer statistics and analyses of response rates to immune checkpoint inhibitors (ICIs) treatment found that less than 13% of patients who met immunotherapy indications responded to ICIs (5). Even among melanoma patients with the highest ICIs response rate, the rate was only 40% (6). Immunotherapy bring hope to patients, but also face many challenges in clinical application.

Since immunotherapy is still unable to achieve effectiveness for most cancer patients, there is still a huge space for development of immunotherapy in the era of precision therapy. Therefore, it is necessary to accurately screen potential beneficiaries by predictive biomarkers in order to guide the rational use of therapy in clinical practice. Cancer arises on account of accumulation of somatic mutations and other genetic changes that cause abnormal cell proliferation and ultimately tumorigenesis. With the advancement of high-throughput sequencing, we obtain detailed understanding of the cancer genome and mutational signatures. Most cancers carry between 1,000 and 20,000 somatic mutation, with few to hundreds of insertions, deletions, and rearrangements (7). Tumors induced by exposure to mutagens, such as lung cancer (tobacco) or skin cancer (ultraviolet), tend to have increased mutation rates (8, 9). With regards to this, tumor mutation load (TMB) is used to measure the degree of genetic variation in tumors. TMB is defined as the number of somatic gene non-synonymous mutations in a specific genomic region, which is generally expressed as mutations per million bases (Mut/Mb). Many explorations have revealed that higher nonsynonymous mutation may produce more neoantigens on the surface of tumor cells. These neoantigens can be detected and targeted by the immune system, triggering anti-tumor immune responses and improving the sensitivity of immunotherapy (10). Therefore, as a new biomarker, TMB has been paid more and more attention in predicting the response and prognosis of immunotherapy. In fact, TMB has been shown to be significantly associated with objective response rate to PD-1/PD-L1 inhibitors in a variety of tumors (11). SCC is one of the cancer types with the highest proportion of somatic gene mutations and HLA gene mutations (12). However, the correlation between TMB and the immune landscape in different SCCs has not been systematically studied.

In this study, we explored the mutated genomic pattern and immune cell infiltration in different SCCs. It helps explain the immune escape and limited immunotherapy response rates in SCCs, provides critical insights into common cancer-related genes and regulatory pathways across multiple anatomical sites. This is essential for the widespread use of immunotherapy in solid malignancies.

METHODS

Data Acquisition and Processing

Clinical information, transcriptome profiles and somatic mutation data of SCC were downloaded from the the Cancer Genome Atlas database (https://portal.gdc.cancer.gov), which is publicly available. We mainly discussed the following four types of SCCs: head and neck squamous cell carcinoma (HNSCC), esophageal squamous cell carcinoma (ESCC), lung squamous cell carcinoma (LUSC), and cervical squamous cell carcinoma (CESC). Clinical data was composed of age, sex, race, smoking history, human papillomavirus (HPV) infection, AJCC-TNM stages, survival time and survival status, etc. RNA-seq data were downloaded in "HTSeq-FPKM" workflow type. The mutation analysis in the Cancer Genome Atlas category "Masked Somatic Mutation" were based on the VarScan program. We visualized

the somatic mutation data using "maftools" R package, which commonly provided specific functionality in cancer genomic research.

TMB Calculation and Evaluation

TMB refers to the total amount of somatic gene coding errors, base substitutions, insertions, or deletions detected per million bases. We calculated TMB as the number of nonsynonymous somatic mutations divide by the length of exons *via* Perl scripts and classified SCC samples into high and low TMB groups based on quartile TMB. Subsequently, we combined the TMB scores with the clinical data. The survival differences between low and high TMB categories were compared using Kaplan-Meier survival analysis and the log-rank test. Wilcoxon rank-sum test and Kruskal-Wallis test were used to analyze the differences of two TMB groups among different clinical traits.

Differentially Expressed Genes and Functional Enrichment Pathways

Differentially expressed genes (DEGs) were screened by "limma" package between two groups of TMB in SCC, where FDR (false discovery rate) <0.05, and |log2FC (fold change) | >1 were adopted. The heatmap was generated by "pheatmap" package. Then, the Gene Ontology (GO) and Kyoto Encyclopedia of Genes and Genomes (KEGG) pathway analysis of DEGs were displayed with "ggplot2", "clusterProfiler" and "enrichplot" R packages. Both p-value < 0.05 and q-value < 0.05 were considered as significantly enrichment pathways.

Estimation of Immune Cell Infiltration

CIBERSORT algorithm was used to evaluate immune cell infiltrations of each sample in the Cancer Genome Atlas database. CIBERSORT, which identifies cell types by estimating relative subsets of RNA transcripts, can accurately calculate the relative content of 22 immune cell from complex tissues. Wilcoxon rank sum test was used to compare the differences of immune cell infiltration between high and low TMB groups in different squamous cells, finally shown in violin plot. When $p < 0.05$, the results of immune cell fraction inferred by CIBERSORT were statistical significance.

Identification of Immune-Related DEGs and Construction of Prognostic Model

Immune-related genes were obtained from the immune omics database (https://www.immport.org), and were found the intersection with DEGs through "VennDiagram" package. Overlapping genes were known as immune-related DEGs. Univariate and multivariate Cox regression analysis were used to identify prognostic immune-related DEGs to construct prognostic models by "survival" R package. Risk ratios (HR) and 95% confidence intervals (95% CI) for hub genes in the prognostic model were calculated. In addition, Kaplan-Meier survival analysis and log-rank test were taken to examine the differential survival between high and low expression groups of prognostic immune-related DEGs. P-value < 0.05 was considered with prognostic value. Subsequently, the risk score for each SCC patient was computed based on the prognostic model. The formula was as follows: risk score $=\Sigma$ ($\beta i \times EXPi$), where βi stemmed from the multivariate Cox analysis and EXPi represents the expression level of selected immune gene. According to median risk score, patients were divided into low-risk and high-risk groups. Survival differences between the above two groups were compared *via* Kaplan-Meier survival analysis and log-rank test. Finally, the Receiver Operating Characteristic (ROC) curve was performed to assess the predictive value of the constructed prognostic model.

Relationship Between Prognosis-Related Hub Genes Mutation and Immune Cell Infiltration

We assessed the relationship between the hub genes copy number alteration (CNA) and the level of immune cell infiltration through tumor immune estimation resource (TIMER) database "SCNA" module (https://cistrome.shinyapps.io/timer/). The Somatic Copy Number Alterations (SCNA) module contains the following four CNA: deep deletion, arm-level deletion, arm-level gain, and high amplification. P< 0.05 was considered significant.

Statistical Analysis

Overall survival (OS) refers to the time interval from the date of diagnosis to the date of death. Survival curves were constructed by Kaplan–Meier analysis, and the differences between groups were tested by log-rank test. For non-parametrical statistical hypothesis, Wilcoxon rank-sum test was run for two categories, and Kruskal-Wallis test was applied for three or more categories. The "limma" package was used for normalization and differentiation analysis. The R software (Version 4.0.1) laid the basis for all statistical analyses. All statistical tests were double-tailed, and statistical significance was set by P <0.05.

RESULTS

Landscape of Genome Mutation in SCC

Somatic mutation data of 1470 SCC samples were downloaded from the Cancer Genome Atlas database, including sample name, chromosome where the mutation occurred, starting and ending location of mutation, mutation classification, mutation type, etc. In the waterfall plot, 1383 (94.08%) SCC patients occurred somatic mutations, with mutation types represented by different color-coded annotations (**Figure 1A**). The following findings were consistent in HNSCC, ESCC, LUSC and CESC. Missense mutation was the most common variant classification, followed by nonsense mutation and frameshift deletion. In addition, single nucleotide polymorphism (SNP) was the most dominant mutation type. However, the C > T transition was the most frequent single nucleotide variants (SNV) in HNSCC, ESCC and CESC. The transition of C>A was more common in LUSC (**Figures 1B–E**). The top10 mutated genes were displayed by horizontal histogram (**Figures 1F–I**). It can be seen that the top10 mutated genes in HNSCC included TP53, TTN, FAT1, CDKN2A, MUC16, C SMD3, NOTCH1, PIK3CA, SYNE1

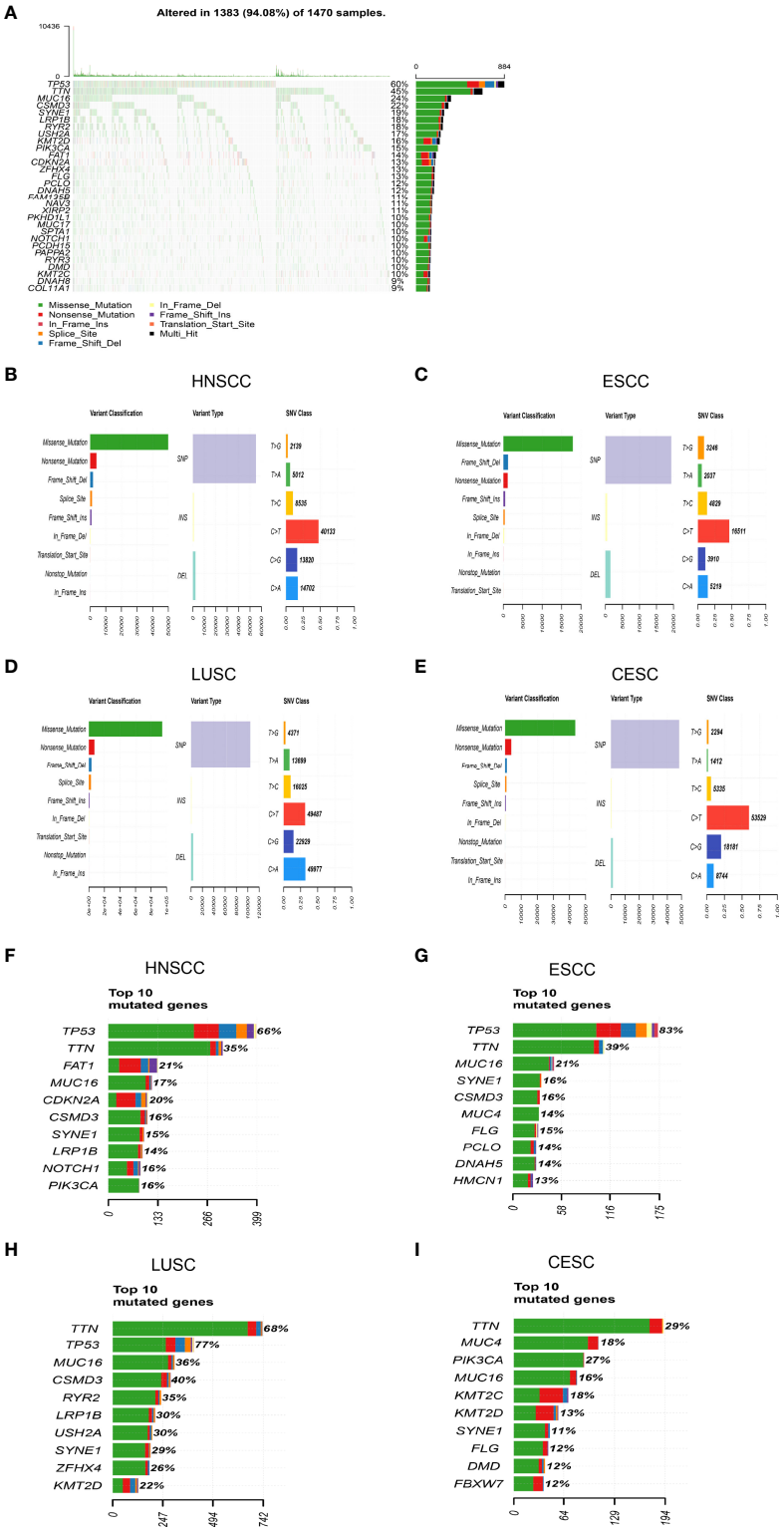

FIGURE 1 | Summary of mutational landscape in SCC patients from TCGA database **(A)** Mutation information in each SCC sample was shown in the waterfall plot, in which various colors representing different mutation types were annotated at the bottom. **(B–E)** Missense mutation was the most common variant classification, and SNP was the most dominant mutation type in SCC. The C > T transition was the most frequent SNV in HNSCC, ESCC and CESC. The transition of C>A was more common in LUSC. **(F–I)** The top10 mutated genes were displayed respectively in different SCCs.

and LRP1B. The top10 mutated genes in ESCC were TP53, TTN, MUC16, SYNE1, CSMD3, FLG, MUC4, PCLO, DNAH5 and HMCN1. The top10 mutated genes in LUSC were TP53, TTN, CSMD3, MUC16, RYR2, LRP1B, USH2A, SYNE1, ZFHX4 and KMT2D. The top10 mutated genes in CESC were TTN, PIK3CA, MUC4, KMT2C, MUC16, KMT2D, FLG, DMD, FBXW7 and SYNE1. The sequences of mutated genes in horizontal histogram were based on the total number of mutations that had occurred. The proportions of the number of samples with genetic mutations to the total number of samples were expressed as percentages. Consequently, the above two orders were slightly different.

TMB Correlated With Prognosis and Clinical Characteristics

Clinical data of SCCs downloaded from the Cancer Genome Atlas was shown in detail (**Table 1**). Kaplan-Meier survival curve showed that TMB was associated with prognosis. However, TMB was not consistent with prognosis in different SCCs (**Figure 2A**). In HNSCC and ESCC, patients with low TMB had better prognosis (p=0.023, p=0.039). But, patients with high TMB had better prognosis in LUSC and CESC (p=0.031, p=0.017). In addition, the relationship between TMB and clinical features had also been described in SCCs. The results indicated that patients with older age (p<0.001), smoking history (p<0.001), lower pathological stages (p<0.001), and no lymphatic invasion (p=0.005) generally had higher TMB (**Figures 2B, D, E, G**). However, no significant correlations were observed between TMB and gender, AJCC-T stage, and AJCC-M stage (**Figures 2C, F, H**). As we all know, HPV infection is a risk factor for HNSCC and CESC. We also analyzed the relationship between HPV status and TMB in HNSCC and CESC. But the result showed no significant association between TMB and HPV infection (**Figure 2I**). Furthermore, TMB differed considerably among the four types of SCCs, with the highest TMB in LUSC (**Figure 2J**, p<0.001).

TABLE 1 | Clinical characteristics of 1326 patients with SCC from TCGA database.

Variables	Number (%)
Vital status	
Alive	812 (61.24%)
Dead	514 (38.76%)
Age, y	60.74 ± 13.13
Gender	
Female	525 (39.59%)
Male	801 (60.41%)
HPV status	
Positive	65 (4.90%)
Negative	88 (6.63%)
Unknow	1173 (88.6%)
Smoking history	
Yes	788 (59.43%)
No	339 (25.56%)
Unknow	199 (15.01%)
Pathological stage	
Stage I & II	651 (49.10%)
Stage III & IV	461 (34.77%)
Unknow	214 (16.14%)
AJCC-T	
T1&T2	793 (59.80%)
T3&T4	417 (31.45%)
TX	116 (8.75%)
AJCC-N	
N0	792 (59.73%)
N1-3	489 (36.88%)
NX	45 (3.39%)
AJCC-M	
M0	823 (62.07%)
M1	101 (7.61%)
MX	402 (30.32%)

Differentially Expressed Genes Between Two TMB Groups and Functional Pathway Analysis

1282 DEGs with FDR <0.05 and||log (fold change) > 1| were screened by "limma" package, including 876 upregulated genes and 406 downregulated genes in high-TMB group. The expression of the top 40 DEGs in the two TMB groups was shown by heatmap (**Figure 3A**). In GO enrichment analysis, it was found that DEGs were mainly involved in muscle system process, the activity of epidermal cells and immune-related functions (**Figure 3B**). According to KEGG pathway analysis, DEGs was found in immune signal mediation, cytochrome P450, cytokine regulation and other signaling pathways (**Figure 3C**).

Comparison of Immune Cell Infiltration

CIBERSORT algorithm was used to estimate the relative proportion of 22 immune cells represented by various colors in each SCC sample (**Figure 4A**). Then, we compared the differences of immune cell infiltrations between low-TMB group and high-TMB group in these four types of SCCs. In the violin plot, low-TMB group was represented in green, while high-TMB group in red (**Figures 4B, C**). It was found that high-TMB group had more CD8 T cells in LUSC and CESC (p=0.008, p=0.012), less CD4 memory resting T cells in LUSC (p=0.004), more CD4 memory activated T cells in LUSC and CESC (p=0.014, p=0.030), more follicular helper T cells in LUSC (p=0.012), less regulatory T cells in ESCC, LUSC and CESC (p=0.024, p=0.011, p=0.025), more resting NK cells in HNSCC (p=0.047), more activated NK cells in LUSC (p=0.006), less monocytes in ESCC (p=0.044), more macrophages M1 in LUSC and CESC (p<0.001, p=0.010).

Immune-Related DEGs and Prognostic Model

1695 immune-related genes were downloaded from the immune omics database. Then, we identified 98 immune-related DEGs that overlapped between immune-related genes and DEGs through "VennDiagram" package (**Figure 5A**). Then four hub genes (CHGB, INHBA, LCN1 and VEGFC) related to prognosis were selected from 98 immune-related genes *via* univariate and multivariate cox analysis. The survival curve showed that high expression of these four genes was associated with poor prognosis (**Figures 5B–E**). To explore the significance of hub genes in assessing the prognosis of SCC patients, the following formula was used to calculate risk score for each patient: risk score= -0.0243×expression of LCN1+0.0029×expression of

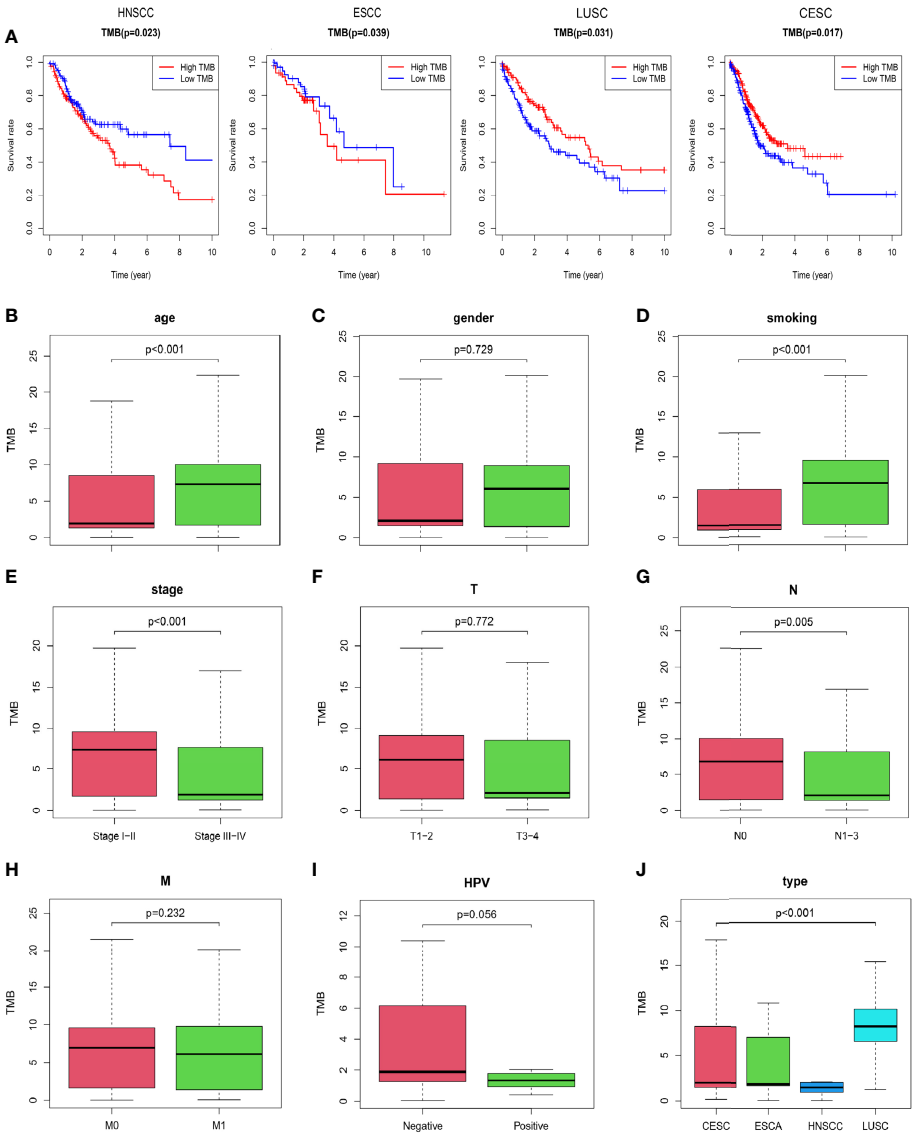

FIGURE 2 | Prognosis of TMB and association with clinical characteristics **(A)** Patients with low TMB had better prognosis In HNSCC and ESCC. Patients with high TMB had better prognosis in LUSC and CESC. **(B, D, E, G)** Patients with older age, smoking history, lower pathological stage, and no lymphatic invasion had higher TMB. **(C, F, H)** No significant correlations were observed between TMB and gender, AJCC-T stage, and AJCC-M stage. **(I)** There was no significant correlation between TMB and HPV infection. **(J)** TMB was significantly different among the four types of SCCs, with the highest TMB in LUSC.

CHGB+0.0041×expression of INHBA+0.0121×expression of VEGFC. We classified patients into high and low risk groups based on the median risk score. The results showed that the high-risk group had worse prognosis (**Figure 5F**, p<0.001). The area under the curve (AUC) was 0.613 (**Figure 5G**), which had certain predictive value.

Analysis Based on TIMER Database

We explored the relationship between copy number alteration (CNA) of prognosis-related hub genes and immune cell infiltration *via* TIMER database "SCNA" module. Comparing with diploid/normal expression of hub genes, we found that CNA of hub genes could reduce immune cell infiltration, including B cells, CD8+ T cells, CD4+ T cells, macrophages, neutrophils, and dendritic cells (**Figures 6A–D**).

DISCUSSION

Immunotherapy subverts the previous concept of anti-tumor therapy, which shifts from relying on the outside world to relying on the own immune system to kill cancer cells. However, the clinical application of immunotherapy still has significant

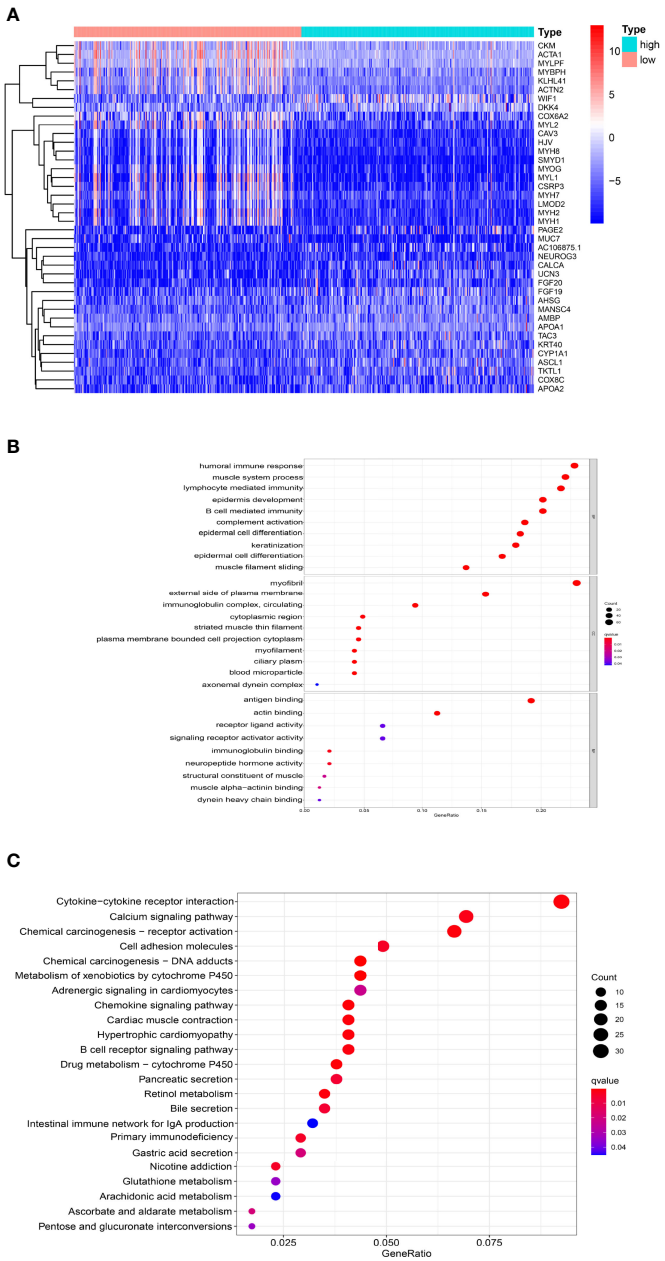

FIGURE 3 | Transcriptome analysis of high TMB and low TMB groups **(A)** The heatmap showed the top 40 DEGs between two TMB groups. **(B)** GO analysis revealed that DEGs were involved in muscle system process, the activity of epidermal cells and immune-related function. **(C)** KEGG pathway analysis of DEGs was found in immune signal mediation, cytochrome P450, cytokine regulation signaling pathways.

complexity and uncertainty, and still faces some challenges related to efficacy and safety. Although many studies are currently exploring the mechanisms of antitumor immunotherapy, the understanding of biomarkers that predicts immunotherapy sensitivity and drug resistance is still preliminary. PD-L1 expression is one of the most studied predictive markers, and several anti-tumor immunotherapy drugs based on PD-L1 protein expression have been approved for marketing (13). However, PD-L1 is not always a perfect biomarker due to the heterogeneity and instability inherent in tumors (14). Therefore, several candidate biomarkers have been extensively studied, including DNA mismatch repair defects (dMMR), microsatellite instability (MSI), tumor-infiltrating lymphocytes (TILs), tumor mutation burden (TMB), and so on.

A number of studies have shown that TMB is associated with immunotherapy efficacy in a variety of tumors. The anti-tumor

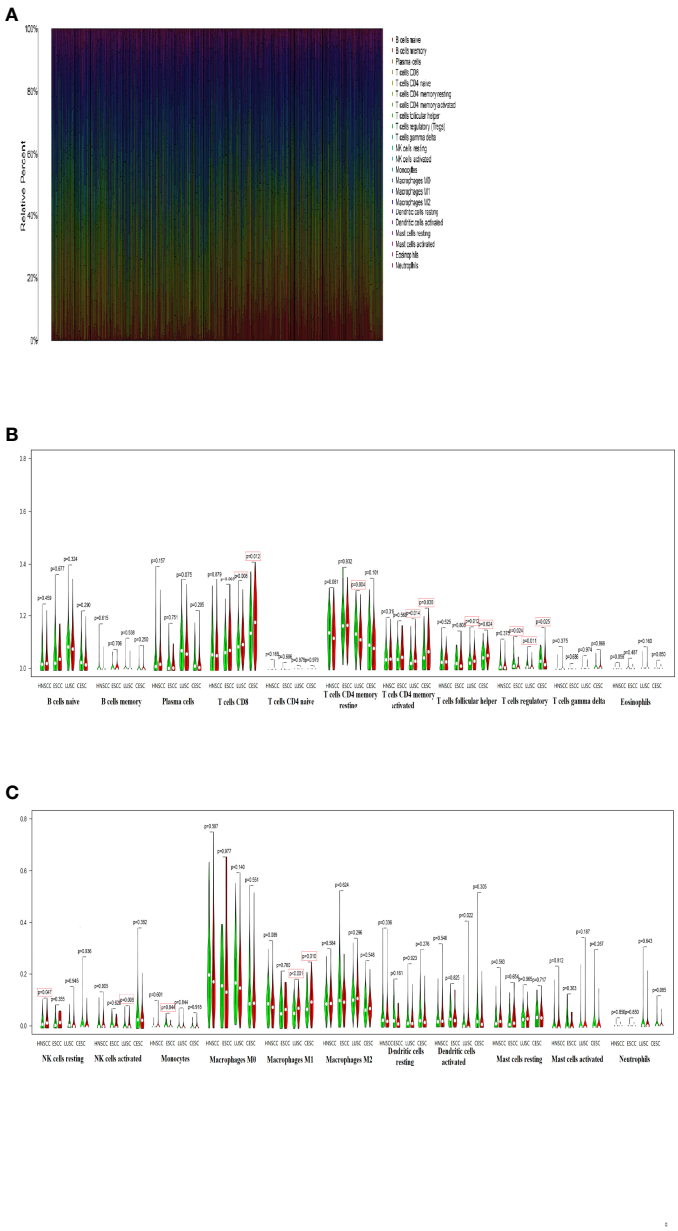

FIGURE 4 | Comparison of immune cell infiltrations in different types of SCCs **(A)** 22 immune cells proportion in each SCC sample were shown in barplot. **(B, C)** Immune cell infiltrations were different between two TMB groups in HNSCC, ESCC, LUSC and CESC.

effects of the immune system depend on its effective recognition of antigen. A few somatic mutations in tumors can produce neoantigens that can be recognized and targeted by the immune system. Importantly, not all mutations produce neoantigens. In fact, only a few mutations can produce neoantigen-containing peptides. These peptides are processed by antigen-processing mechanisms and loaded onto the major histocompatibility complex (MHC), and even fewer are recognized by T cells (15–17). Therefore, the prevailing view is that the more mutations detected, the more probable it is to generate neoantigens, and the more likely these neoantigens are to be immunogenic and trigger T-cell responses. TMB was first identified as a biomarker for immune checkpoint inhibitors in melanoma (18). Recently, the Food and Drug Administration (FDA) approved pembrolizumab for adult and pediatric patients with TMB > 10Mut/Mb. This approval was based on efficacy data from 10 refractory solid tumor cohorts participated in a multicenter, non-randomized, open-label study KEYNOTE-158 (19). The number of somatic mutations varied significantly across many tumor types, with melanoma having the highest

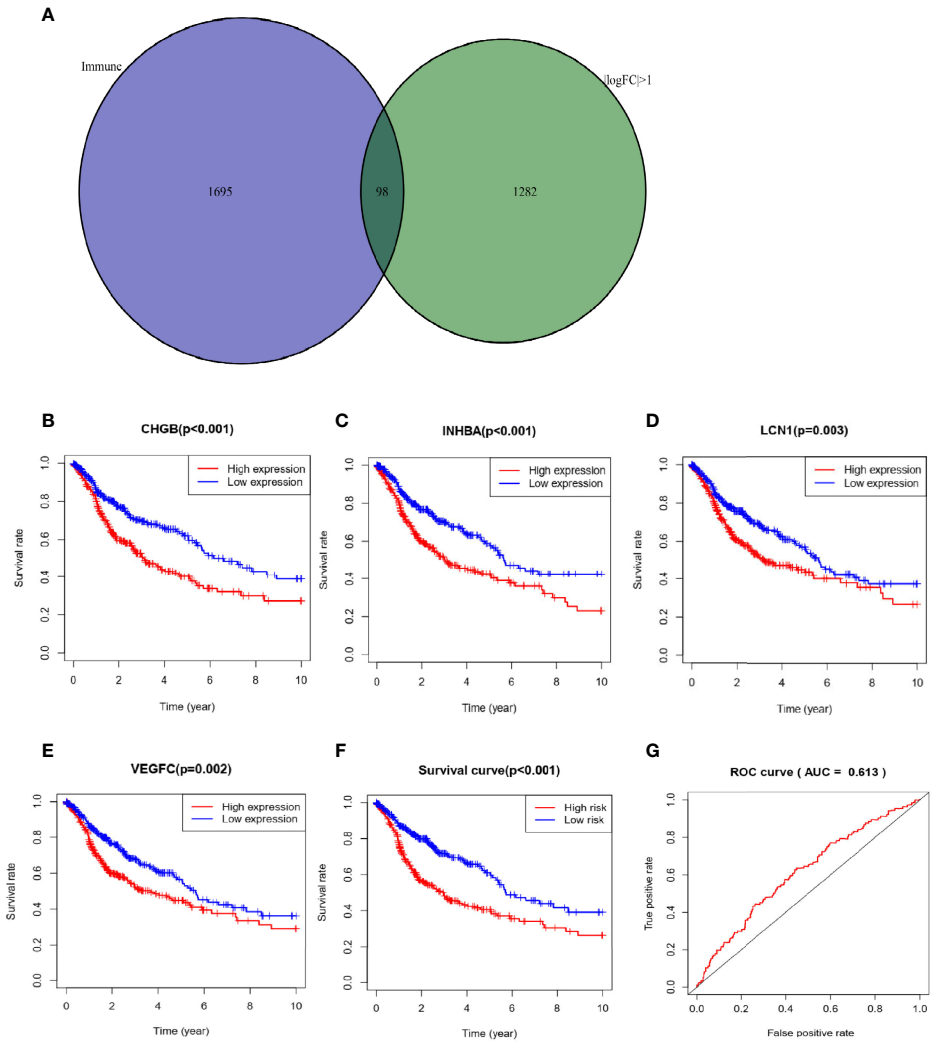

FIGURE 5 | Construction of prognostic model for SCC **(A)** Immune-related DEGs was shown in Venn plot. **(B–E)** High expression of hub genes was associated with poor prognosis. **(F)** The high-risk group had worse prognosis. **(G)** The area under the curve (AUC) was 0.613.

number of mutations, followed by non-small cell lung cancer and other squamous cancers, and leukemia and certain childhood cancers having the lowest number of mutations (20, 21). In addition, the predictive value of TMB for overall survival was inconsistent among different cancers. There are some limitations to the potential use of TMB in practice, making this approval highly controversial (22). It can be seen that TMB as a possible universal biomarker of pan-cancer has certain advantages, but also has inherent limitations.

Tumor development is closely related to genetic mutations of key molecules. Most of the mutations found in tumors are already present in normal tissue, so the accumulation and combination of these mutations may be more important than their occurrence alone (23). The types and frequency of mutations also vary widely among different typs of tumors. This study systematically analyzed mutation profiles in four common squamous cell carcinomas, which has certain clinical significance for precision immunotherapy.

First, we focused on analyzing the differences in the mutational status of four SCCs. Single nucleotide mutations are caused by the substitution of a single base. The changes are related to prediction of disease, response to drugs and tumor pathogenesis. Mutations are usually enriched in a specific local sequence situation. For instance, ultraviolet induced pyrimidine dimers, whose faulty repair results in C>T mutations of at CpC or TpC dinucleotides. The mutations associated with smoking were mainly C > A mutations (24). Certain genetic mutations appear to be more frequent or potentially specific in specific squamous cell carcinomas. The most common mutated genes were TP53 and TTN in HNSCC, ESCC and LUSC. Differently, the most common in CESC were TTN and PIK3CA. As one of the most important tumor suppressor genes, P53 plays a critical

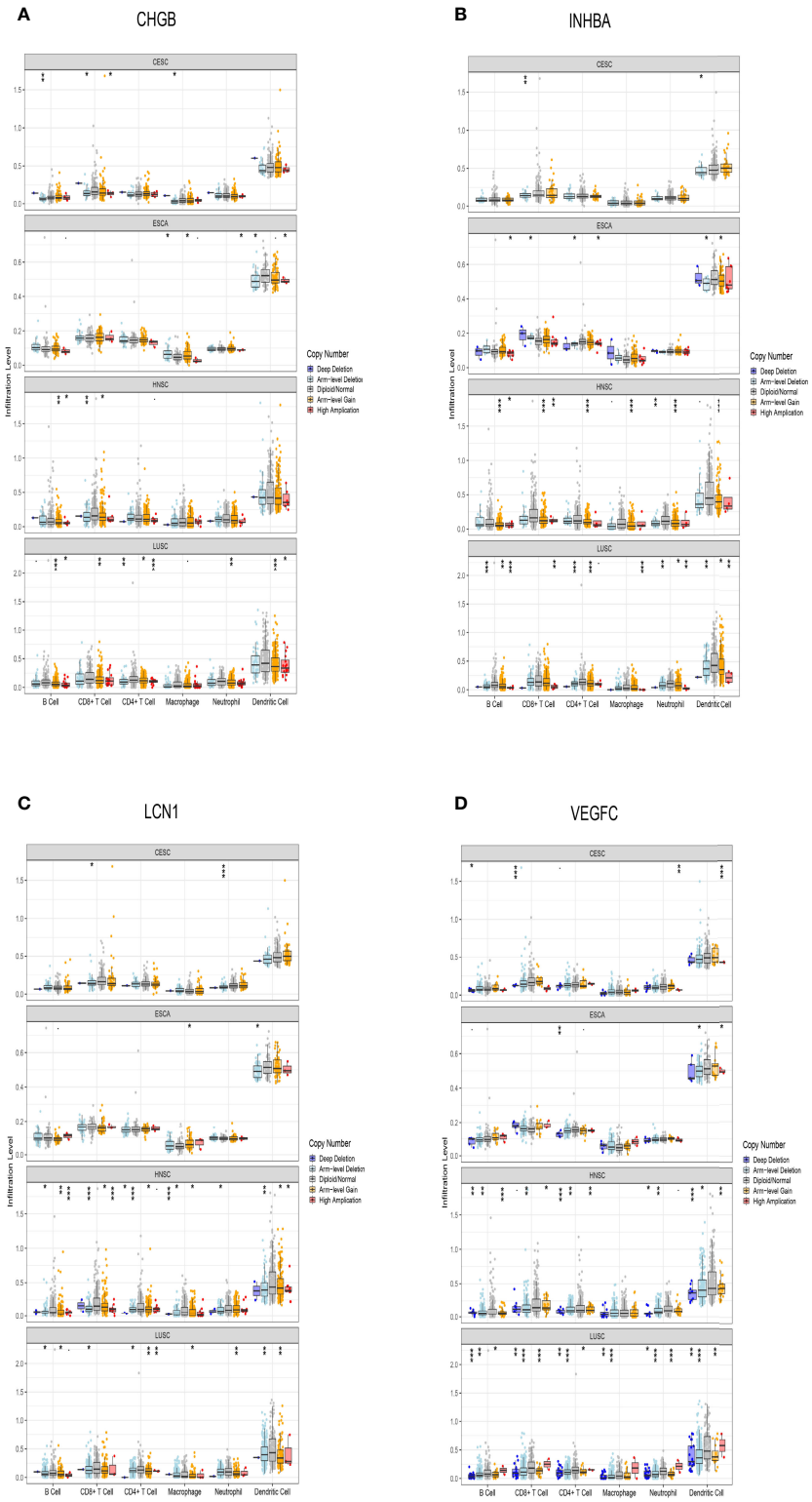

FIGURE 6 | Association between somatic copy number alteration (CNA) of prognosis-related hub genes and immune cell infiltration levels. **(A–D)** CNA of hub genes could reduce immune cell infiltration. * means p< 0.05, ** p< 0.01, *** p< 0.001.

role in tumor development because it controls cell growth, apoptosis and regulates angiogenesis. Missense mutations of TP53 lead to the expression of a conformationally altered stable protein that has negative activity against wild-type P53 and has also acquired functional carcinogenic activity. Thus, mutation of only one TP53 allele may result in a significant oncogenic phenotype (25, 26). TTN, the second most mutated gene in solid tumors, is the gene encoding the sarcomere protein, which plays a key structural, developmental and regulatory role in heart and skeletal muscle (27). TTN mutation predicts higher TMB and correlates with the response rate to immune checkpoint blockade (28). It is also found that the frequency of gene mutation is positively correlated with the length of exon. TTN is the gene with the longest exon length in the whole genome. As the second longest gene in the genome, MUC16 has a high mutation frequency, which is associated with significant tumor mutation load. This result also supports the correlation between higher mutational load and mutational status of genes with long exons (29). Previous studies have found that patients with TTN/TP53 dual mutations have better benefits in OS and DFS compared with patients with TTNWT/TP53MT status, suggesting that TTN and TP53 mutations may have synergistic effects in LUSC (). PIK3CA is the most commonly mutated gene in human papillomavirus (HPV) associated squamous cell carcinoma and is an important factor in predicting the prognosis of cervical cancer patients (31–33).

Moreover, we analyzed the correlation of TMB with prognosis and clinical traits. In our study, high TMB was associated with smoking and HPV negative. Some mutational processes can lead to high TMB, such as POLE/POLD1 mutation, mismatch repair deficiency, UV light, tobacco smoking, AID/APOBEC activation. Thus, cancers associated with chronic mutagen exposure, such as lung cancer (tobacco) and melanoma (UV), show higher TMB (25). This may be the reason why LUSC has the highest TMB in these four types of SCCs. Smoking-related mutations have been found to be associated with responses to checkpoint blockade and thus may underlie some tumor responses to PD-1 pathway blockade (10). However, TMB may have different effects on tumor immunity depending on anatomic location. In HNSCC, smoking is mainly immunosuppressive. In LUSC, it's more conducive to inflammatory response (24). After HPV infection, the E7 oncoprotein was found to cause centrosomal abnormalities that disrupt mitosis and increase the risk of chromosome misalignment and aneuploidy, while chromosome instability may lead to increased genetic mutations. In theory, HPV-positive patients should have higher TMB values (34). We also found that older patients had higher TMB. This has also been confirmed in previous studies. TMB increases significantly with age, with a 2.4-fold difference between 10 and 90 years old (35).

In addition, it was found that TMB related DEGs were enriched in the regulation of immune system and muscular system through GO and KEGG pathway analysis. We also identified four immune-related DEGs that were strongly associated with poor prognosis, including: CHGB, INHBA, LCN1 and VEGFC. CHGB was first identified in pheochromocytoma and encodes proteins that are mainly expressed in endocrine cells and neurons (36). Abnormal expression of CHGB gene has been reported in many tumor types, and its upregulated expression is highly correlated with metastasis (37, 38). INHBA, encoding a member of the TGF-beta superfamily of proteins, has been shown to be associated with poor prognosis in a variety of solid tumors39). The molecular mechanism and tumor-promoting function of INHBA remain unclear. Currently, most hypotheses focus on metastasis. Wamsley et al. suggested that activins were necessary to maintain a cancer stem cell-like phenotype and contribute to metastasis of NSCLC (40). 41 also confirmed this viewpoint in HNSCC (41). LCN1 (lipocalin-1), known as tear lipocalin, is mainly expressed in secretory glands and tissues (42). It has been reported that LCN1 overexpression is an independent predictor of poor prognosis in breast cancer (43). However, few studies have investigated its expression level in other malignant tumors. Vascular endothelial growth factor C (VEGFC), an activator of lymphangiogenesis, plays an important role in promoting lymph node metastasis and tumor progression (44).

Based on the plotted survival curve, we found that LUSC and CESC patients with high TMB were significantly associated with better survival, while HNSCC and ESCC patients with high TMB had poor prognosis. The mechanism behind this association may lie in the significant differences in immune cell invasion density and immune activity between low and high TMB subtypes of these cancers (45). We analyzed the association between TMB and immune cell infiltration in squamous cell carcinoma and found that these associations were often related to the type of cancer. It can be seen in the violin plot of immune cell infiltration, high-TMB group had more CD8 T cells and less regulatory T cells in LUSC and CESC. McGrail et al. analyzed somatic mutation data from more than 10,000 patients in the TCGA database and determined the association between predicted neoantigen load and CD8 T cells. They found that in cancers where CD8 T cell levels were positively correlated with neoantigen load, such as melanoma, lung cancer, and bladder cancer, high-TMB tumors had significantly higher ORR than low-TMB tumors (21). A retrospective study also showed that increased CD8+ T cell infiltration and increased CD8+ T cell/regulatory T cell ratio were positively associated with ICB treatment response (46).

Macrophages are important immune cells in tumor microenvironment and can be polarized into subtypes with different functions in different microenvironments, including M1 and M2 macrophages. M1 macrophages secrete cytokines such as TNF-α, which have anti-tumor, anti-angiogenesis and activation of adaptive immunity. Tumor-associated macrophages (TAMs) is an important regulator of tumorgenesis, usually manifested as M2 subtype. It inhibits Th1 immunity by promoting tumor angiogenesis and invasion and is associated with poor prognosis (47). In this study, we found that the group with high TMB had higher macrophage M1 infiltration in LUSC and CESC. This may also be one of the reasons why high TMB group has better prognosis in LUSC and CESC. In clinical trials, it could be used to stratize patients and assign the most appropriate treatment according to the type of target cell, thus increasing the chances of overall success.

Inevitably, there were also a few limitations in the investigation. This study was a retrospective analysis using public database and the results have not been validated in prospective clinical trials. Therefore, relevant conclusions need to be further studied. Although further validation is required, these results may provide new insights into the determinants of immunotherapy response to SCCs.

CONCLUSIONS

Based on TCGA database, this study systematically elaborated the effect of TMB on the prognosis and the relationship between TMB and immune cell infiltration of SCCs. We found that TMB has different effects on prognosis in SCCs at different anatomical sites, which may be related to the difference in immune cell infiltration. In addition, we identified 4 hub genes associated with prognosis and constructed a risk prognosis model. However further studies are needed to verify the clinical application of this prognostic model. Overall, new insights can be gained by regarding different SCCs as a whole.

DATA AVAILABILITY STATEMENT

The original contributions presented in the study are included in the article/supplementary material. Further inquiries can be directed to the corresponding authors.

AUTHOR CONTRIBUTIONS

YC and JW contributed to the design of the study. WT and TW collected and analyzed the TCGA data. WT was the major contributor in writing the manuscript. YC supervised the study. All authors read and approved the final version of the manuscript.

FUNDING

This work was supported by the Special fund for Taishan Scholar Project (NO. ts20190973).

REFERENCES

1. Dotto GP, Rustgi AK. Squamous Cell Cancers: A Unified Perspective on Biology and Genetics. *Cancer Cell* (2016) 29(5):622–37. doi: 10.1016/j.ccell.2016.04.004
2. Li B, Cui Y, Nambiar DK, Sunwoo JB, Li R. The Immune Subtypes and Landscape of Squamous Cell Carcinoma. *Clin Cancer Res* (2019) 25 (12):3528–37. doi: 10.1158/1078-0432.Ccr-18-4085
3. Hoadley KA, Yau C, Hinoue T, Wolf DM, Lazar AJ, Drill E, et al. Cell-Of-Origin Patterns Dominate the Molecular Classification of 10,000 Tumors From 33 Types of Cancer. *Cell* (2018) 173(2):291–304.e296. doi: 10.1016/j.cell.2018.03.022
4. Strait AA, Wang XJ. The Role of Transforming Growth Factor-Beta in Immune Suppression and Chronic Inflammation of Squamous Cell Carcinomas. *Mol Carcinog* (2020) 59(7):745–53. doi: 10.1002/mc.23196
5. Haslam A, Prasad V. Estimation of the Percentage of US Patients With Cancer Who Are Eligible for and Respond to Checkpoint Inhibitor Immunotherapy Drugs. *JAMA Netw Open* (2019) 2(5):e192535. doi: 10.1001/jamanetworkopen.2019.2535
6. Robert C, Long GV, Brady B, Dutriaux C, Maio M, Mortier L, et al. Nivolumab in Previously Untreated Melanoma Without BRAF Mutation. *N Engl J Med* (2015) 372(4):320–30. doi: 10.1056/NEJMoa1412082
7. Martincorena I, Campbell PJ. Somatic Mutation in Cancer and Normal Cells. *Science* (2015) 349(6255):1483–9. doi: 10.1126/science.aab4082
8. Lawrence MS, Stojanov P, Polak P, Kryukov GV, Cibulskis K, Sivachenko A, et al. Mutational Heterogeneity in Cancer and the Search for New Cancer-Associated Genes. *Nature* (2013) 499(7457):214–8. doi: 10.1038/nature12213
9. Vogelstein B, Papadopoulos N, Velculescu VE, Zhou S, Diaz LAJr., Kinzler KW. Cancer Genome Landscapes. *Science* (2013) 339(6127):1546–58. doi: 10.1126/science.1235122
10. Carlisle JW, Steuer CE, Owonikoko TK, Saba NF. An Update on the Immune Landscape in Lung and Head and Neck Cancers. *CA Cancer J Clin* (2020) 70 (6):505–17. doi: 10.3322/caac.21630
11. Goodman AM, Kato S, Bazhenova L, Patel SP, Frampton GM, Miller V, et al. Tumor Mutational Burden as an Independent Predictor of Response to Immunotherapy in Diverse Cancers. *Mol Cancer Ther* (2017) 16(11):2598–608. doi: 10.1158/1535-7163.Mct-17-0386
12. Gonzalez-Perez A, Perez-Llamas C, Deu-Pons J, Tamborero D, Schroeder MP, Jene-Sanz A, et al. IntOGen-Mutations Identifies Cancer Drivers Across Tumor Types. *Nat Methods* (2013) 10(11):1081–2. doi: 10.1038/nmeth.2642
13. Meric-Bernstam F, Larkin J, Tabernero J, Bonini C. Enhancing Anti-Tumour Efficacy With Immunotherapy Combinations. *Lancet* (2021) 397 (10278):1010–22. doi: 10.1016/s0140-6736(20)32598-8
14. Kim H, Chung JH. PD-L1 Testing in Non-Small Cell Lung Cancer: Past, Present, and Future. *J Pathol Transl Med* (2019) 53(4):199–206. doi: 10.4132/jptm.2019.04.24
15. Coulie PG, Van den Eynde BJ, van der Bruggen P, Boon T. Tumour Antigens Recognized by T Lymphocytes: At the Core of Cancer Immunotherapy. *Nat Rev Cancer* (2014) 14(2):135–46. doi: 10.1038/nrc3670
16. Snyder A, Chan TA. Immunogenic Peptide Discovery in Cancer Genomes. *Curr Opin Genet Dev* (2015) 30:7–16. doi: 10.1016/j.gde.2014.12.003
17. Chan TA, Yarchoan M, Jaffee E, Swanton C, Quezada SA, Stenzinger A, et al. Development of Tumor Mutation Burden as an Immunotherapy Biomarker: Utility for the Oncology Clinic. *Ann Oncol* (2019) 30(1):44–56. doi: 10.1093/annonc/mdy495
18. Chan TA, Wolchok JD, Snyder A. Genetic Basis for Clinical Response to CTLA-4 Blockade in Melanoma. *N Engl J Med* (2015) 373(20):1984. doi: 10.1056/NEJMc1508163
19. Subbiah V, Solit DB, Chan TA, Kurzrock R. The FDA Approval of Pembrolizumab for Adult and Pediatric Patients With Tumor Mutational Burden (TMB) ≥10: A Decision Centered on Empowering Patients and Their Physicians. *Ann Oncol* (2020) 31(9):1115–8. doi: 10.1016/j.annonc.2020.07.002
20. Bodor JN, Boumber Y, Borghaei H. Biomarkers for Immune Checkpoint Inhibition in Non-Small Cell Lung Cancer (NSCLC). *Cancer* (2020) 126 (2):260–70. doi: 10.1002/cncr.32468
21. McGrail DJ, Pilié PG, Rashid NU, Voorwerk L, Slagter M, Kok M, et al. High Tumor Mutation Burden Fails to Predict Immune Checkpoint Blockade Response Across All Cancer Types. *Ann Oncol* (2021) 32(5):661–72. doi: 10.1016/j.annonc.2021.02.006
22. Prasad V, Addeo A. The FDA Approval of Pembrolizumab for Patients With TMB >10 Mut/Mb: Was It a Wise Decision? No. *Ann Oncol* (2020) 31 (9):1112–4. doi: 10.1016/j.annonc.2020.07.001
23. Martincorena I, Roshan A, Gerstung M, Ellis P, Van Loo P, McLaren S, et al. Tumor Evolution. High Burden and Pervasive Positive Selection of Somatic Mutations in Normal Human Skin. *Science* (2015) 348(6237):880–6. doi: 10.1126/science.aaa6806
24. Desrichard A, Kuo F, Chowell D, Lee KW, Riaz N, Wong RJ, et al. Tobacco Smoking-Associated Alterations in the Immune Microenvironment of Squamous Cell Carcinomas. *J Natl Cancer Inst* (2018) 110(12):1386–92. doi: 10.1093/jnci/djy060

25. Alexandrov LB, Nik-Zainal S, Wedge DC, Aparicio SA, Behjati S, Biankin AV, et al. Signatures of Mutational Processes in Human Cancer. *Nature* (2013) 500 (7463):415–21. doi: 10.1038/nature12477
26. Soussi T, Wiman KG. TP53: An Oncogene in Disguise. *Cell Death Differ* (2015) 22(8):1239–49. doi: 10.1038/cdd.2015.53
27. Ware JS, Cook SA. Role of Titin in Cardiomyopathy: From DNA Variants to Patient Stratification. *Nat Rev Cardiol* (2018) 15(4):241–52. doi: 10.1038/nrcardio.2017.190
28. Jia Q, Wang J, He N, He J, Zhu B. Titin Mutation Associated With Responsiveness to Checkpoint Blockades in Solid Tumors. *JCI Insight* (2019) 4(10):1732. doi: 10.1172/jci.insight.127901
29. Li X, Pasche B, Zhang W, Chen K. Association of MUC16 Mutation With Tumor Mutation Load and Outcomes in Patients With Gastric Cancer. *JAMA Oncol* (2018) 4(12):1691–8. doi: 10.1001/jamaoncol.2018.2805
30. Cheng X, Yin H, Fu J, Chen C, An J, Guan J, et al. Aggregate Analysis Based on TCGA: TTN Missense Mutation Correlates With Favorable Prognosis in Lung Squamous Cell Carcinoma. *J Cancer Res Clin Oncol* (2019) 145(4):1027–35. doi: 10.1007/s00432-019-02861-y
31. Seiwert TY, Zuo Z, Keck MK, Khattri A, Pedamallu CS, Stricker T, et al. Integrative and Comparative Genomic Analysis of HPV-Positive and HPV-Negative Head and Neck Squamous Cell Carcinomas. *Clin Cancer Res* (2015) 21(3):632–41. doi: 10.1158/1078-0432.Ccr-13-3310
32. Beaty BT, Moon DH, Shen CJ, Amdur RJ, Weiss J, Grilley-Olson J, et al. PIK3CA Mutation in HPV-Associated OPSCC Patients Receiving Deintensified Chemoradiation. *J Natl Cancer Inst* (2020) 112(8):855–8. doi: 10.1093/jnci/djz224
33. Martell K, McIntyre JB, Kornaga EN, Chan AMY, Phan T, Köbel M, et al. PIK3CA Mutation and CNV Status and Post-Chemoradiotherapy Survival in Patients With Cervical Cancer. *Gynecol Oncol* (2020) 158(3):776–84. doi: 10.1016/j.ygyno.2020.06.506
34. Wang J, Sun H, Zeng Q, Guo XJ, Wang H, Liu HH, et al. HPV-Positive Status Associated With Inflamed Immune Microenvironment and Improved Response to Anti-PD-1 Therapy in Head and Neck Squamous Cell Carcinoma. *Sci Rep* (2019) 9(1):13404. doi: 10.1038/s41598-019-49771-0
35. Chalmers ZR, Connelly CF, Fabrizio D, Gay L, Ali SM, Ennis R, et al. Analysis of 100,000 Human Cancer Genomes Reveals the Landscape of Tumor Mutational Burden. *Genome Med* (2017) 9(1):34. doi: 10.1186/s13073-017-0424-2
36. Stenman A, Svahn F, Hojjat-Farsangi M, Zedenius J, Söderkvist P, Gimm O, et al. Molecular Profiling of Pheochromocytoma and Abdominal Paraganglioma Stratified by the PASS Algorithm Reveals Chromogranin B as Associated With Histologic Prediction of Malignant Behavior. *Am J Surg Pathol* (2019) 43(3):409–21. doi: 10.1097/pas.0000000000001190
37. Chen Z, Xiong S, Li J, Ou L, Li C, Tao J, et al. DNA Methylation Markers That Correlate With Occult Lymph Node Metastases of non-Small Cell Lung Cancer and a Preliminary Prediction Model. *Transl Lung Cancer Res* (2020) 9(2):280–7. doi: 10.21037/tlcr.2020.03.13
38. Zhang Y, Chen P, Zhou Q, Wang H, Hua Q, Wang J, et al. A Novel Immune-Related Prognostic Signature in Head and Neck Squamous Cell Carcinoma. *Front Genet* (2021) 12:570336. doi: 10.3389/fgene.2021.570336
39. Lyu S, Jiang C, Xu R, Huang Y, Yan S. INHBA Upregulation Correlates With Poorer Prognosis in Patients With Esophageal Squamous Cell Carcinoma. *Cancer Manag Res* (2018) 10:1585–96. doi: 10.2147/cmar.S160186
40. Wamsley JJ, Kumar M, Allison DF, Clift SH, Holzknecht CM, Szymura SJ, et al. Activin Upregulation by NF-κb is Required to Maintain Mesenchymal Features of Cancer Stem-Like Cells in non-Small Cell Lung Cancer. *Cancer Res* (2015) 75(2):426–35. doi: 10.1158/0008-5472.Can-13-2702
41. Chang WM, Lin YF, Su CY, Peng HY, Chang YC, Lai TC, et al. Dysregulation of RUNX2/Activin-A Axis Upon miR-376c Downregulation Promotes Lymph Node Metastasis in Head and Neck Squamous Cell Carcinoma. *Cancer Res* (2016) 76(24):7140–50. doi: 10.1158/0008-5472.Can-16-1188
42. Wojnar P, Lechner M, Redl B. Antisense Down-Regulation of Lipocalin-Interacting Membrane Receptor Expression Inhibits Cellular Internalization of Lipocalin-1 in Human NT2 Cells. *J Biol Chem* (2003) 278(18):16209–15. doi: 10.1074/jbc.M210922200
43. Zhang X, Cui Y, He M, Jiao Y, Yang Z. Lipocalin-1 Expression as a Prognosticator Marker of Survival in Breast Cancer Patients. *Breast Care (Basel)* (2020) 15(3):272–80. doi: 10.1159/000503168
44. Karaman S, Detmar M. Mechanisms of Lymphatic Metastasis. *J Clin Invest* (2014) 124(3):922–8. doi: 10.1172/jci71606
45. Wang X, Li M. Correlate Tumor Mutation Burden With Immune Signatures in Human Cancers. *BMC Immunol* (2019) 20(1):4. doi: 10.1186/s12865-018-0285-5
46. Hanna GJ, Lizotte P, Cavanaugh M, Kuo FC, Shivdasani P, Frieden A, et al. Frameshift Events Predict Anti-PD-1/L1 Response in Head and Neck Cancer. *JCI Insight* (2018) 3(4):e98811. doi: 10.1172/jci.insight.98811
47. Locati M, Curtale G, Mantovani A. Diversity, Mechanisms, and Significance of Macrophage Plasticity. *Annu Rev Pathol* (2020) 15:123–47. doi: 10.1146/annurev-pathmechdis-012418-012718

Conflict of Interest: The authors declare that the research was conducted in the absence of any commercial or financial relationships that could be construed as a potential conflict of interest.

Publisher's Note: All claims expressed in this article are solely those of the authors and do not necessarily represent those of their affiliated organizations, or those of the publisher, the editors and the reviewers. Any product that may be evaluated in this article, or claim that may be made by its manufacturer, is not guaranteed or endorsed by the publisher.

frontiers | Frontiers in Immunology

TYPE Original Research
PUBLISHED 26 July 2022
DOI 10.3389/fimmu.2022.945878

OPEN ACCESS

EDITED BY
Hongda Liu,
Nanjing Medical University, China

REVIEWED BY
Guo-Jun Yu,
Huai'an First People's Hospital, China
Shuai Wang,
University of Pittsburgh Medical Center, United States

*CORRESPONDENCE
Ming Shi
sm200@sohu.com
Junnian Zheng
jnzheng@xzhmu.edu.cn
Dan Liu
liudan_bd@sina.com

SPECIALTY SECTION
This article was submitted to Cancer Immunity and Immunotherapy, a section of the journal Frontiers in Immunology

RECEIVED 17 May 2022
ACCEPTED 04 July 2022
PUBLISHED 26 July 2022

CITATION
Su Y, Qi R, Li L, Wang X, Li S, Zhao X, Hou R, Ma W, Liu D, Zheng J and Shi M (2022) An immune-related gene prognostic risk index for pancreatic adenocarcinoma.
Front. Immunol. 13:945878.
doi: 10.3389/fimmu.2022.945878

An immune-related gene prognostic risk index for pancreatic adenocarcinoma

Yang Su[1], Ruoshan Qi[1], Lanying Li[1], Xu Wang[1], Sijin Li[1], Xuan Zhao[1], Rui Hou[2], Wen Ma[1], Dan Liu[1*], Junnian Zheng[1*] and Ming Shi[1*]

[1]Jiangsu Center for the Collaboration and Innovation of Cancer Biotherapy, Cancer Institute, Xuzhou Medical University, Xuzhou, China, [2]College of Pharmacy, Xuzhou Medical University, Xuzhou, China

Objective: Our goal is to construct an immune-related gene prognostic risk index (IRGPRI) for pancreatic adenocarcinoma (PAAD), and to clarify the immune and molecular features in IRGPRI-defined PAAD subgroups and the benefit of immune checkpoint inhibitors (ICIs) therapy.

Method: Through differential gene expression analysis, weighted gene co-expression network analysis (WGCNA), and univariate Cox regression analysis, 16 immune-related hub genes were identified using the Cancer Genome Atlas (TCGA) PAAD dataset (n = 182) and immune gene set. From these genes, we constructed an IRGPRI with the Cox regression method and the IRGPRI was verified based on the Gene Expression Omnibus (GEO) dataset (n = 45). Then, we analyzed the immune and molecular features and the benefit of ICI therapy in IRGPRI-defined subgroups.

Results: Five genes, including *S100A16*, *CD40*, *VCAM1*, *TNFRSF4* and *TRAF1* were used to construct IRGPRI. As with the results of the GEO cohort, the overall survival (OS) was more favorable in low IRGPRI patients versus high IRGPRI patients. The composite results pointed out that low IRGPRI was associated with immune response-related pathways, high level of CTLA4, low KRAS and TP53 mutation rate, more infiltration of activated memory $CD4^+$ T cells, $CD8^+$ T cells, and more benefits from ICIs therapy. In comparison, high IRGPRI was associated with cancer-related pathways, low expression of CTLA4, high KRAS and TP53 mutation rate, more infiltration of M2 macrophages, and less benefit from ICIs therapies.

Conclusion: This IRGPRI is an encouraging biomarker to define the prognosis, immune and molecular features, and benefits from ICIs treatments in PAAD.

KEYWORDS

pancreatic adenocarcinoma, immune gene, prognosis, immunotherapy, CTLA4

Introduction

Pancreatic adenocarcinoma (PAAD) is a high-graded neoplasm of digestive system, with a 5-year survival rate of lower than 10% (1). PAAD is predicted to become the second-leading cause of cancer death by 2030 (2, 3). Owing to lifestyle changes, the global incidence of PAAD is expected to increase (4). In clinical practice, histological grading, tumor staging and molecular classification may be employed to assess in the prognosis of PAAD patients. However, these clinicopathological features generally cannot provide accurate prognostic information for patients (5). Some inflammatory molecules are involved in the prognosis of PAAD patients; however, their sensitivity and specificity are not robust enough (6). Currently, some researches pay attention to the immune-related gene signatures in the prognosis of PAAD (7–9). For example, Zhang Q's team built a prognostic model of PAAD using 3 lncRNA pairs (10). Bu F and his colleagues construct a prognostic model of PAAD using 18 immune-related gene pairs (11). Nevertheless, few studies tried to build the prognostic model of PAAD based on the immune-related central genes. Here, we screened immune-related central genes associated with the patient prognosis through weighted gene co-expression network analysis (WGCNA). Meanwhile, few studies pay attention to immune features and immunotherapy of PAAD at the same time.

The treatment of PAAD remains a major challenge, and surgery is an option of the highest priority. However, only 15~20% patients are suitable for resection, and 80% of those who undergo surgery will recur (12). Radiotherapy and chemotherapy have been shown to benefit patients with PAAD and improve the overall survival; however, the survival rate remains low (13). There is no therapeutic drug that can provide nonsurgical candidates with long-term benefits (13). Immunotherapy is an exciting new anticancer therapy that activates the immune system to identify tumor-specific antigens (14, 15). Clinical trials of PAAD have showed that immunotherapy has a good application prospect in the treatment of PAAD (16). In addition, resistant individuals are better candidates for immunotherapy (17). Immune checkpoint inhibitor (ICI) therapy, such as those targeting cytotoxic T lymphocyte-associated protein 4 (CTLA4), programmed death-ligand 1 (PD-L1) and programmed death 1 (PD1), have been shown to be significantly beneficial for the survival versus traditional therapies (1–5). For PAAD, anti-CTLA4 therapy leads to an enhanced anti-tumor immune response (18, 19). However, a variety of factors may affect the effectiveness of immunotherapy, such as the tumor microenvironment (TME), and few immunogene-based biomarkers are good predictors of the patient prognosis. Identifying potential prognostic markers associated with treatment benefits is conducive to the individualize immunotherapy of PAAD patients. Therefore, it is urgent to identify indicators that can predict the prognosis and immunotherapeutic effect of PAAD.

Here, we aimed to explore prognostic markers for PAAD that could predict the results of traditional therapy and suggest the value of immunotherapy. By focusing on all immune-related genes (IRGs) in PAAD transcriptome data, the present study was designed to screen IRGs associated with the patient prognosis through WGCNA, and construct the IRGPRI. Subsequently, we described the molecular and immunological characteristics of IRGPRI and detected its ability to predict the patient prognosis and ICI therapy efficacy. The results suggest that IRGPRI is an encouraging prognostic biomarker.

Methods

Datasets and patients

The RNA sequence data (RNA-seq data) and clinicopathological information of 182 PAAD samples (178 cancer samples vs. 4 para-cancer samples) were obtained from the TCGA database (https://portal.gdc.cancer.gov/). Additionally, RNA-seq data of 45 PAAD samples (GSE28735) and their survival information were obtained from the GEO database. Expression data in human renal cell carcinoma samples (GSE67501) and metastatic melanoma (GSE115821) from patients who did or did not respond to ICI therapy were also obtained from the GEO database. The IRG list was derived from the ImmPort (https://www.immport.org/shared/home) databases and InnateDB (https://www.innatedb.ca/).

Identification of immune-related hub genes

According to the RNA-seq data of PAAD samples (178 cancer samples vs. 4 para-cancer samples) derived from TCGA, lists of genes in different expressions ($p < 0.05$, $|\log2FC| > 1$) were determined with the limma package of R. From InnateDB and ImmPort, we obtained the immune-related gene lists. IRGs in different expressions were obtained and analyzed with Gene Ontology (GO) and Kyoto Encyclopedia of Genes and Genomes (KEGG) analyses by using the clusterProfiler package of R.

Then, hub genes were determined by WGCNA. First, calculated the Pearson correlation coefficient between two genes, according to the expression data to design the similarity matrix, and then using a network type of a signed and soft threshold $\beta = 6$ to convert into an adjacency matrix, followed by transformation into a topological matrix by using the topological overlap measure (TOM) indicating the degree of correlation between genes. 1-TOM was selected as the distance to cluster the genes, and then a dynamic pruning tree was constructed to determine the modules. In the end, three modules were identified by assigning the merging threshold function as 0.3. Based on the genes of notably related modules (the turquoise

and blue modules), the network was constructed by between-gene edges at the weight of more than 0.3. The genes in turquoise modules were used for subsequent analyses, of which 16 significantly survival-associated IRGs were used for further analyses ($p < 0.05$, log-rank test).

Construction and verification of the IRGPRI

Among 16 immune-related hub genes, based on multivariate Cox regression analysis, the five genes that had a significant effect on OS were employed to construct an IRGPRI. In the Cox model, we calculated the IRGPRI of each sample as per the formula: IRGPRI = [Expression level (certain genes) × gene coefficient]. The prognostic ability of the IRGPRI was assessed by K-M survival curve and log-rank test with both GEO and TCGA cohorts. Univariate and multivariate Cox regression analyses were performed to verify the independent prognostic value of IRGPRI.

Thorough assessment of molecular and immunologic features and ICI therapy in high IRGPRI and low IRGPRI groups

For signaling pathway analysis, limma package of R was used for analyzing low IRGPRI (n = 89) and high IRGPRI (n = 88) samples by differential expression analysis of all genes. The clusterProfiler package of R ($p < 0.05$) was used to preform gene set enrichment analysis (GSEA) method on GO and HALLMARK gene sets, in order to identify the signaling pathways where genes in different expressions were implicated. GSVA package of R was utilized for single sample GSEA (ssGSEA) analysis of several typical gene sets. For gene mutation analysis, genetic alteration data were downloaded from the TCGA database. Then, we performed correlation analyses to analyze the correlation between IRGPRI and the expression of CTLA4 and PD-L1 (CD274).

To determine immune features of PAAD samples, their expressions were input into CIBERSORT (https://cibersort.stanford.edu/) with 1,000 iterations to calculate the relative percentage of 22 classes of immune cells. Next, we made a comparison of the obtained percentage and clinicopathological factors between two IRGPRI subgroups, and assessed the results by means of a landscape map.

Statistical analysis

Using an independent t-test, we carried out comparison of continuous variables between high IRGPRI and low IRGPRI groups. Categorical data were analyzed by the chi-square test. Beyond that, univariate survival analysis was completed by Kaplan-Meier survival analysis and the log-rank test. Multivariate survival analysis was conducted in the Cox regression model. A two-sided p-value < 0.05 was accepted as statistically significant differences.

Results

Immune-related hub genes

By differential expression analysis (178 cancer samples vs. 4 normal samples), 1672 genes in different expressions were obtained (Figure S1A). Through intersection of these genes with IRGs from InnateDB and ImmPort, 245 IRGs in different expressions were identified (Figure S1B). There was a remarkable association of 245 genes in different expressions with 1058 GO terms and 67 KEGG pathways, as indicated by functional enrichment analysis (Table S1). Top 8 GO terms and KEGG pathways are provided in Figure S1C and S1D.

To determine the immune-related hub genes, we performed WGCNA analysis on the candidate genes (n = 245). A negative correlation was observed between the logarithm log(k) of the node with connectivity K and the logarithm log (P (k)) of the probability of the node. According to the scale-free network, the best soft-thresholding power was 6 (Figure S2). According to the best soft-thresholding power and the average linkage hierarchical clustering, 3 modules were identified (Figures 1A, B), to which 245 genes were assigned. Based on the Pierson correlation coefficient between the module and sample characteristics of each module, turquoise and blue modules were strongly associated with PAAD. There were 24 edges and 20 genes for the blue module, 1489 edges and 88 genes for the turquoise module of the networks with a threshold weight of more than 0.3 (Figures 1C, D). Thus, the genes in the turquoise module were used for further analyses. We obtained all 116 genes in the turquoise module. We determined that the expression level of 16 immune-related hub genes of them was strongly correlated with OS of PAAD patients, as shown in Figure 2 and Figure 3A.

Survival outcomes in different IRGPRI groups

The prognostic index was constructed for each cancer sample calculated by the coefficient in Table S2.

In univariate Cox regression analysis, IRGPRI, grade, and age were notably associated with the prognosis of PAAD (Figure 3B). Later, IRGPRI was proven to be an independent prognostic factor by multivariate Cox regression analysis, (Figure 3C and Table S3).

With the cutoff value of the median IRGPRI, low IRGPRI patients achieved better OS than high IRGPRI patients based on the TCGA dataset ($p < 0.001$, log-rank test) (Figure 3D). The

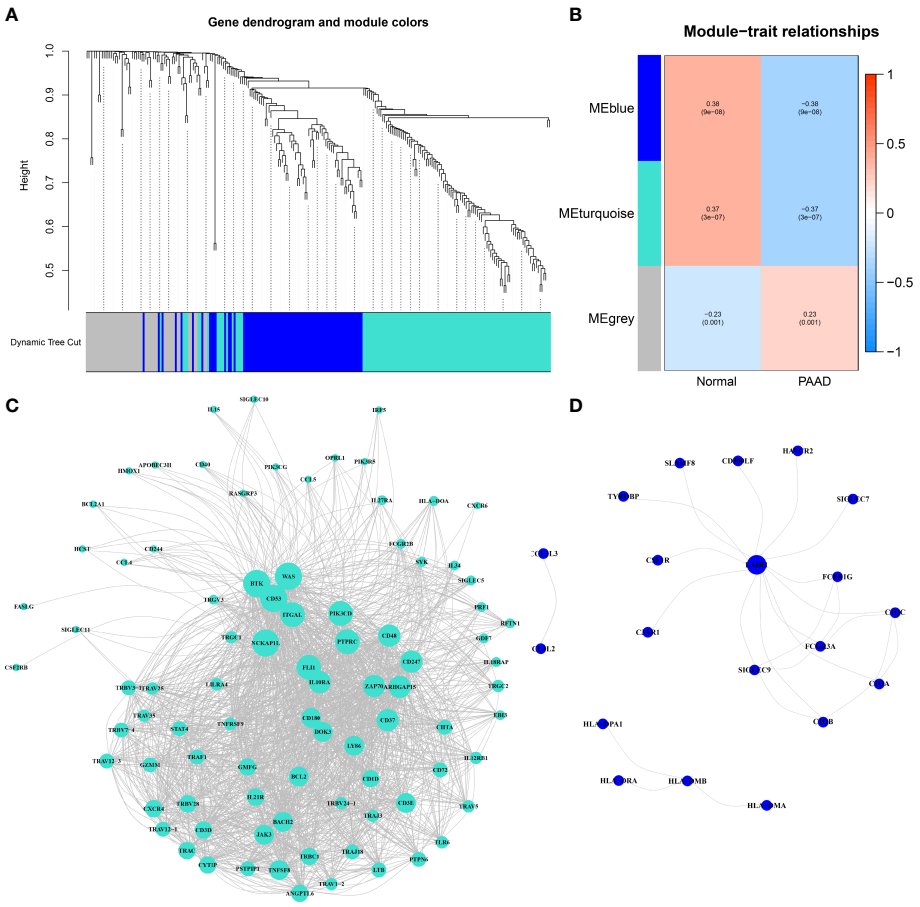

FIGURE 1
Immune-related hub genes. **(A)** Weighted gene coexpression network analysis (WGCNA) of immune-related differentially expressed genes with a soft threshold β = 6. **(B)** Gene modules related to PAAD obtained by WGCNA. **(C)** The network of the genes in the turquoise module (weight of edge > 0.3). **(D)** The network of the genes in the blue module (weight of edge > 0.3).

roles of IRGPRI were then validated by the GSE28735 PAAD dataset (n = 45). In Figure 3E, patients in the low IRGPRI subgroup achieved a notably favorable prognosis versus high IRGPRI subgroup (p = 0.010, log-rank test).

Molecular features in different IRGPRI subgroups

Enriched gene sets in different IRGPRI subgroups were determined by GSEA. Some cancer-related pathways were observed in high IRGPRI samples (Figure 4A), while enriched gene sets of low IRGPRI samples were identified in some immune response-related pathways (Figure 4B).

Next, gene mutation analysis was performed to obtain further biological information on the immunological nature of the IRGPRI subgroups. Missense variation was identified as the most common mutation, followed by nonsense and frameshift insertion. Top 20 genes with the greatest mutation rate were then determined in the IRGPRI subgroups. In both groups, the mutation rates of KRAS, TP53, CDKN2A, and SMAD4 were all greater than 15%. The high IRGPRI subgroup showed more mutations of KRAS, TP53, and MUC16 genes (Figure 4C), while the low IRGPRI subgroup had more mutation of RNF43 genes (Figure 4D).

Subsequently, the association of IRGPRI score with CTLA4 expression and PD-L1 was explored. We found that the IRGPRI score was negatively correlated with CTLA4 (r = -0.34, p < 0.001), as shown in Figures 5A–D. Meanwhile, the association of IRGPRI score with marker genes of cell proliferation and migration was explored. We found that the IRGPRI score was positively correlated with PCNA (r = 0.25, p < 0.001), MKI67 (r = 0.38, p < 0.001) and MMP14 (r = 0.27, p < 0.001), as shown in Figures S3A–F.

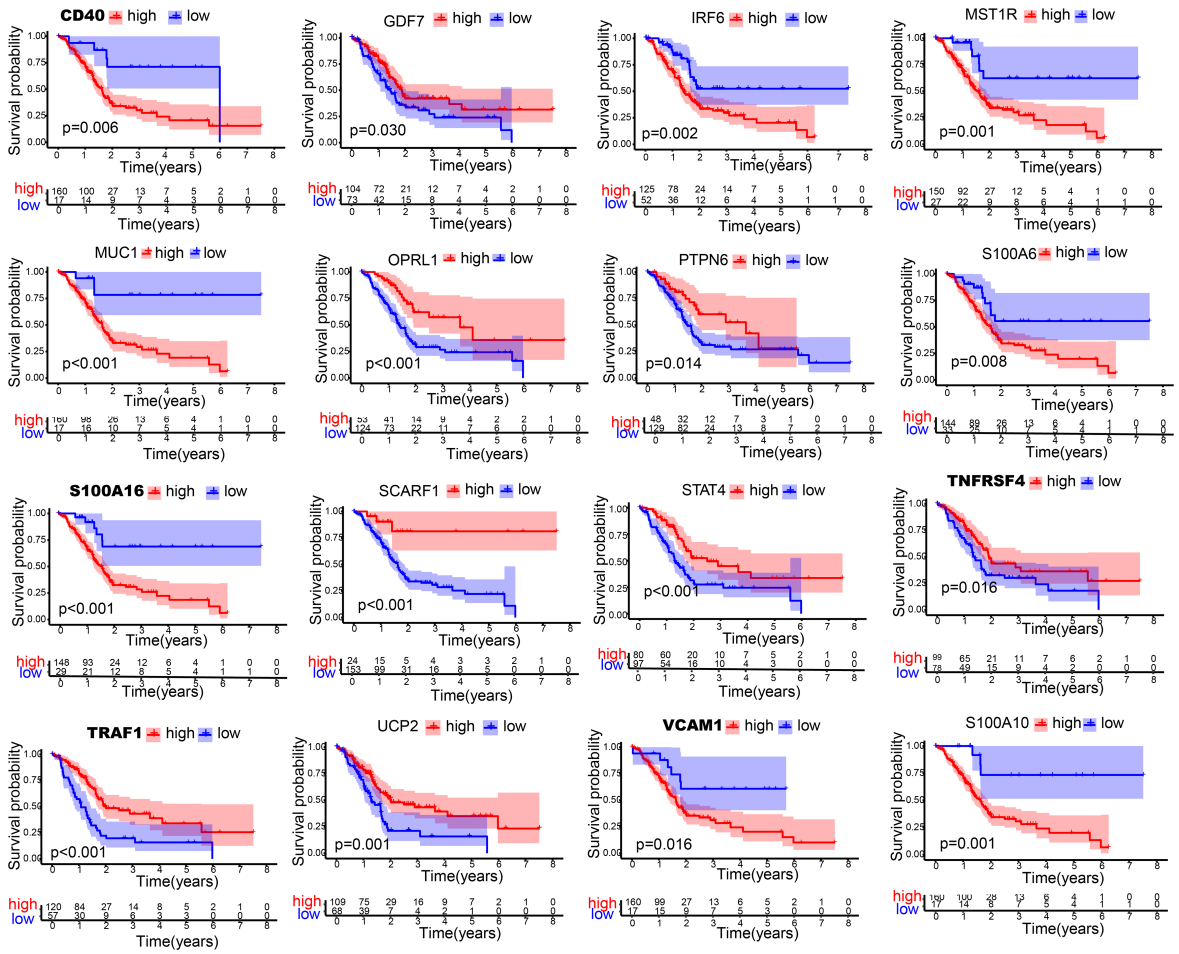

FIGURE 2
Kaplan-Meier curves of 16 immune-related hub genes. Kaplan-Meier survival analysis of 16 immune-related genes in TCGA cohort.

Immune cell infiltration and function in different IRGPRI subgroups

To detect the constituents of immune cells in the IRGPRI subgroups, Wilcoxon test was performed to compare the distribution of immune cells in high- and low- IRGPRI subgroups. We found more abundant activated memory CD4+ T cells, B cell native and Tregs in the low IRGPRI subgroup, and more M2 macrophages, Mast cells resting and activated NK cells in the high IRGPRI subgroup (Figure 6A). Figure 6B displayed the features related to the immune landscape of different IRGPRI subgroups, including the clinicopathological features.

Then, we defined the molecular and immune function between different IRGPRI subgroups by certain gene signatures. There were more CD8+ T cells, checkpoints, T cell co-stimulation in the low IRGPRI subgroup (Figure 6C).

Relationship between IRGPRI grouping and clinical and immune subtypes

We could find from Figure 7A and Figure S4 that the proportion of the TNM stage was almost equally distributed between low- and high- IRGPRI groups, but there were more Grade 1 samples and fewer Grade 3/4 samples in the low IRGPRI group versus the high IRGPRI group ($p = 0.033$, chi-square test). In Figure 7B, more C1 immune subtypes were found in the high IRGPRI group and more C3 immune subtype were found in the low IRGPRI group ($p = 0.001$, chi-square test).

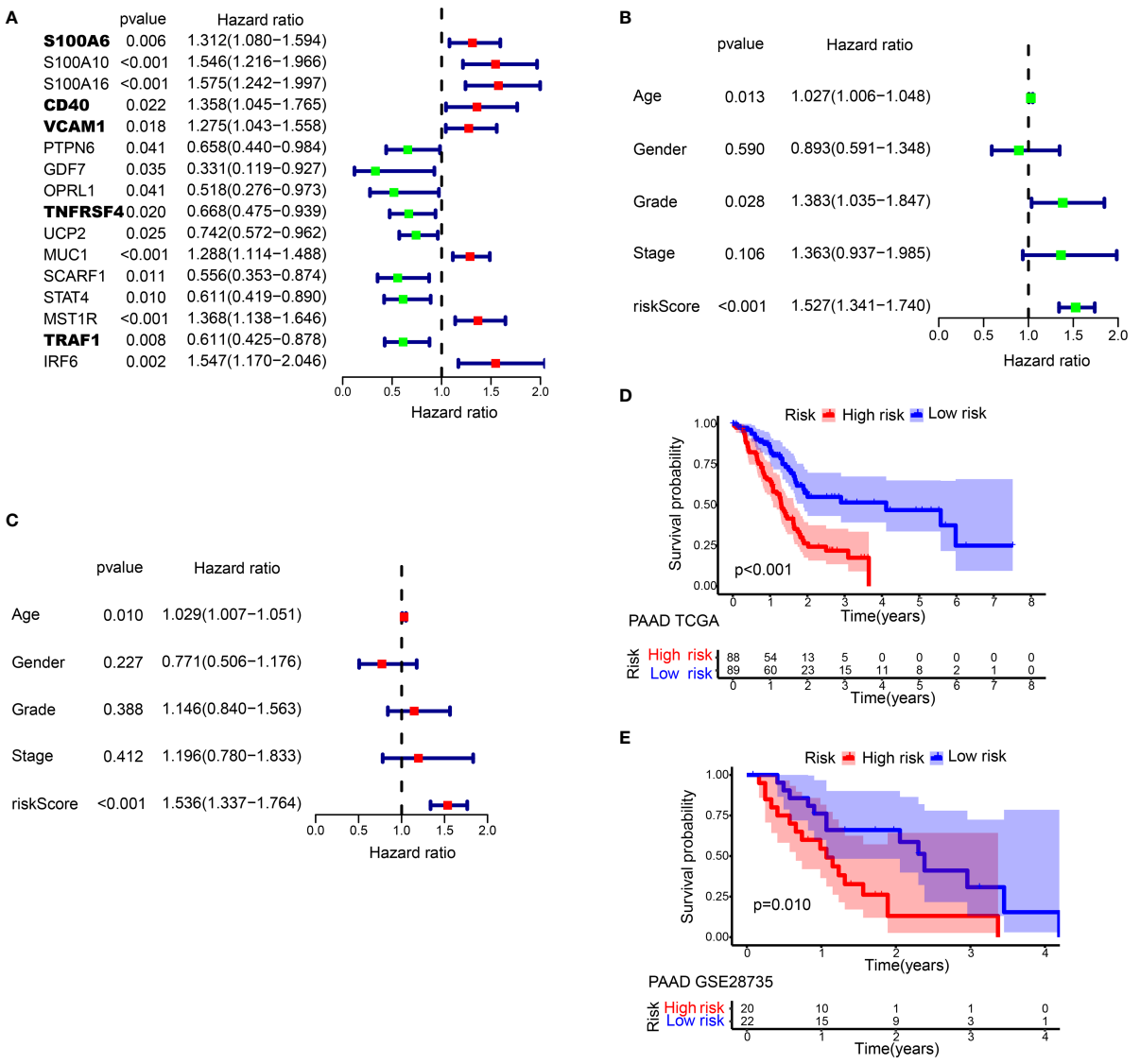

FIGURE 3
Prognostic analysis of different IRGPRI subgroups. **(A)** Univariate Cox analysis of 16 immune-related hub genes. **(B)** Univariate Cox analysis of clinicopathological factors and the IRGPRI score. **(C)** Multivariate Cox analysis. **(D)** Kaplan-Meier survival analysis of the IRGPRI subgroups in the TCGA cohort. **(E)** Kaplan-Meier survival analysis of the IRGPRI subgroups in the GEO cohort (GSE28735).

Relationship between IRGPRI grouping and immunotherapy

Due to the lack of public data on PAAD immunotherapy, we can only select other tumor immunotherapy data to verify the predictive role of IRGPRI model. In order to further explore the predictive role of IRGPRI model in immunotherapy, we analyzed the expression data in samples from human renal cell carcinoma patients who did or did not respond to anti-PD-1 immunotherapy (GSE67501). The results showed that the risk score in patients who did not respond to anti-PD-1 immunotherapy (stable disease or progressive disease) was higher than it in patients who responded to anti-PD-1 immunotherapy (complete response or partial response) (Figure 8A). Moreover, we performed receiver operating characteristic (ROC) analysis to determine the diagnostic value of risk score in ICI therapy efficacy, and the area under the ROC curve is 0.857 (Figure 8B). Then we analyzed the expression data in metastatic melanoma samples from patients who did or did not respond to ICI therapy (GSE115821). The results also showed that the risk score in patients who did not respond to ICI therapy was higher than it in patients who responded to ICI therapy (Figure 8C). And the area under the

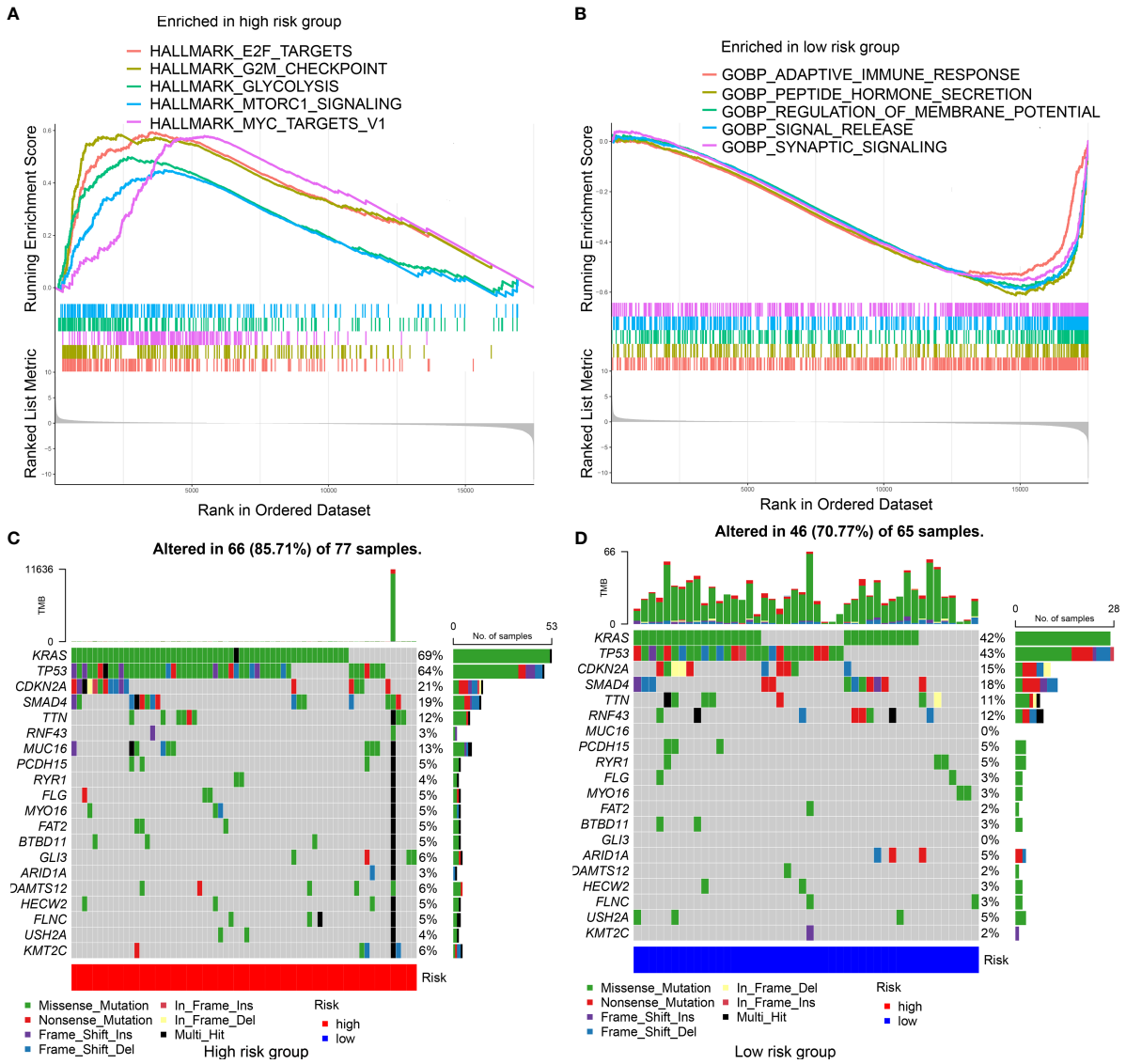

FIGURE 4
Molecular characteristics of different IRGPRI subgroups. **(A)** Gene sets enriched in IRGPRI-high group. **(B)** Gene sets enriched in IRGPRI-low group. **(C, D)** Significantly mutated genes in the mutated PAAD samples of IRGPRI-high group **(C)** and IRGPRI-low group **(D)**. Mutated genes (rows) are ordered by mutation rate; samples (columns) are arranged to emphasize mutual exclusivity among mutations. The right shows mutation percentage, and the top shows the overall number of mutations. The color-coding indicates the mutation type.

ROC curve is 0.784 (Figure 8D). The above results suggest that IRGPRI may be a potential prediction model for predicting the efficacy of immunotherapy. The graphical abstract of our research is shown in the Figure S5.

Discussion

The role of immune cells that constitute the TME in tumor progression has been recognized (20). Increasing evidence indicates that immune gene characteristics may be prognostic or predictive factors of PAAD (21, 22). Immunotherapy has been confirmed as an effective option for PAAD patients (23–25). Given that the immunosuppressive microenvironment of PAAD can affect the efficacy of immunotherapy (26–28), it is crucial to determine which patients will benefit most from these treatments. Although different prognostic markers for PAAD have been evaluated for multiple years, we still cannot find an effective biomarker to predict the prognostic outcomes of PAAD patients and the suitability for immunotherapy. This highlights

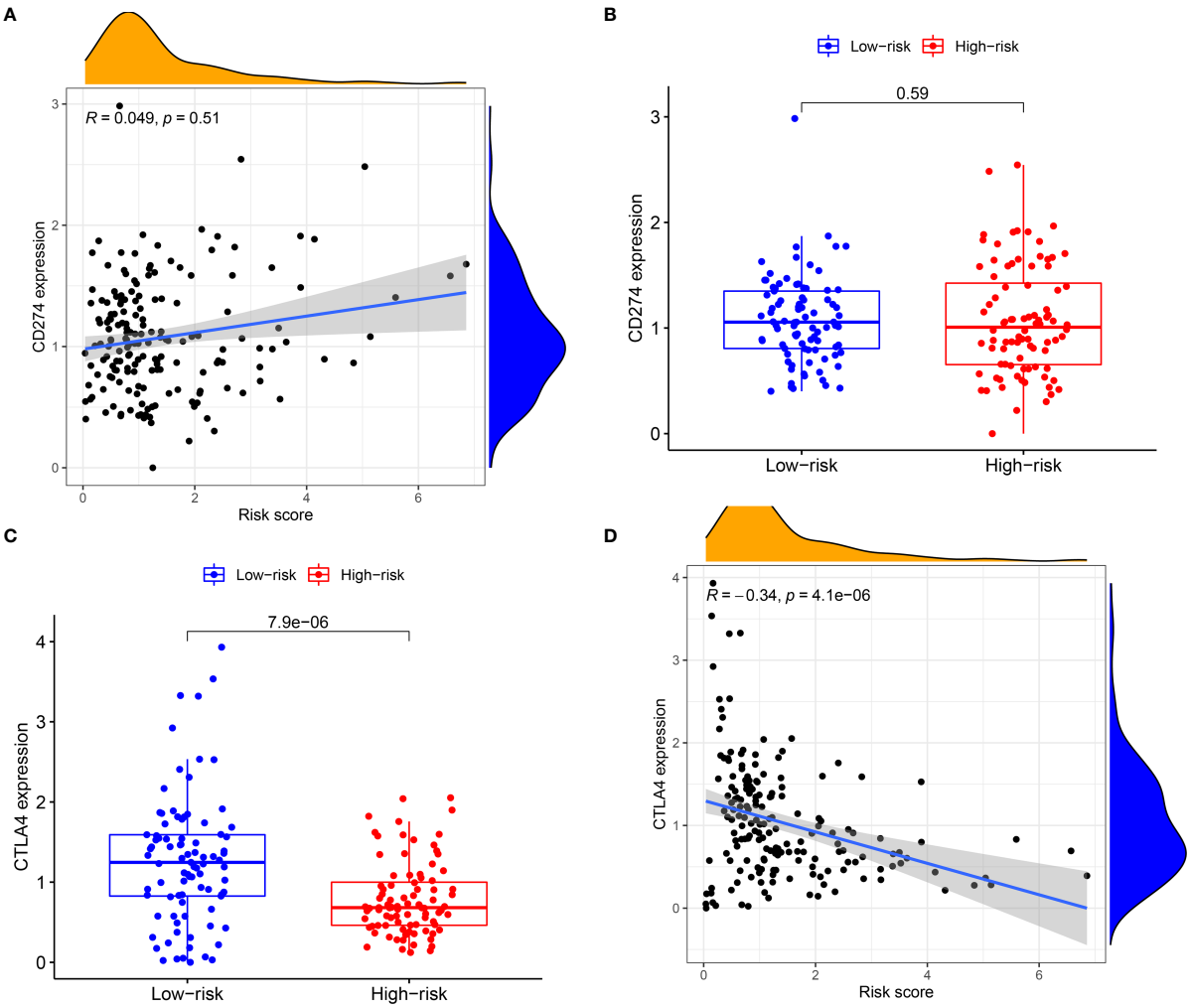

FIGURE 5
The relationship between IRGPRI score and the expression levels of PD-L1 or CTLA4. **(A)** Correlation analysis between IRGPRI and PD-L1. **(B)** PD-L1 in different IRGPRI subgroups. **(C)** CTLA4 expression in different IRGPRI subgroups. **(D)** Correlation analysis between IRGPRI and CTLA4 expression.

the need to identify biomarkers for the PAAD prognosis and the efficacy of immunotherapy.

WGCNA is a virtual approach to assisting in identifying potential therapeutic targets or immune-related biomarkers. In this study, based on the PAAD immune gene dataset, WGCNA was used to determine 16 immune-related central genes that affected the OS of patients; and based on S100A16, CD40, VCAM1, TNFRSF4 and TRAF1 that were independent prognostic factors of OS, IRGPRI was constructed. IRGPRI has been proven to be an effective immune-related biomarker for the prognosis of PAAD. In TCGA and GEO arrays, the survival rate was lower in patients with high IRGPRI and higher in those with low IRGPRI.

IRGPRI is composed of five genomes: S100A16, CD40, VCAM1, TNFRSF4 and TRAF1. S100A16 has been shown to be associated with obese, type 2 diabetes mellitus and inflammation *via* calcium-dependent mechanism (29). Moreover, it has also been found that S100A16 is correlated with the occurrence and progression of many tumors (30–34). S100A16 enhances the progression and metastasis of PAAD *via* FGF19 mediated AKT and ERK1/2 pathway (30). The study of Gangping Tu, et al. showed that in comparison with the normal pancreas, S100A16 was highly expressed in tissues with PAAD, and the increase of its expression level may be correlated with an unfavorable prognosis of PAAD patients (35). CD40 is a cell surface member of the tumor necrosis factor (TNF) receptor superfamily. An active CD40 is closely related to the tumor immunity (36). VCAM1 expression is associated with the tumorigenesis and unfavorable prognosis of high-grade serous ovarian cancer (37). TNFRSF4 may be a promising

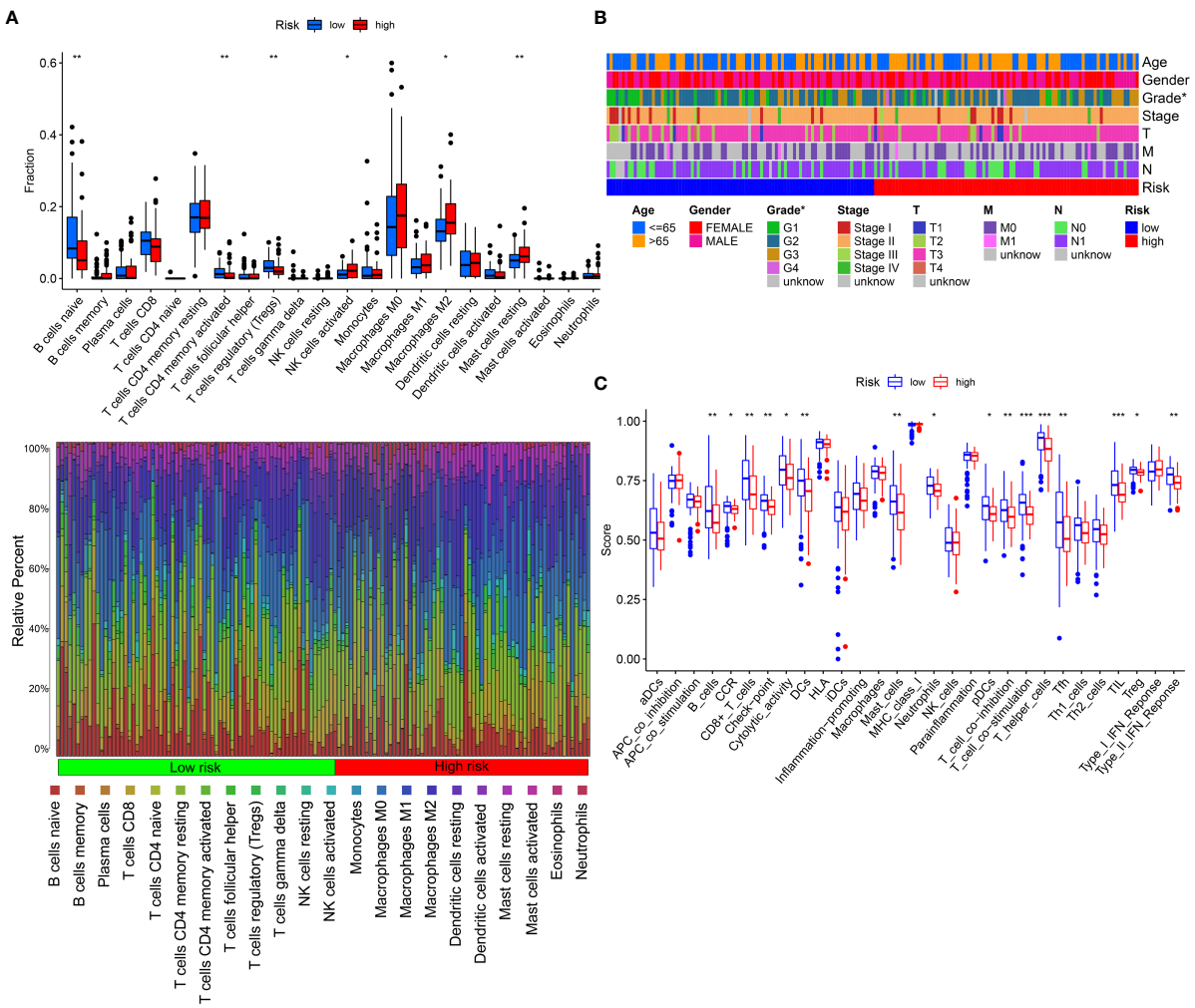

FIGURE 6
The landscape of the TME in PAAD and the characteristics of different IRGPRI subgroups. **(A)** The proportions of TME cells in different IRGPRI subgroups. **(B)** The IRGPRI grouping and proportions of TME cells for PAAD patients in the TCGA cohort. Age, Gender, Grade, Tumor stage, T, N, and survival M are shown as patient annotations. **(C)** The molecular and immune-related function of different IRGPRI subgroup. (*p < 0.05, **p< 0.01, ***p < 0.001).

immunotherapy target and prognostic biomarker for liver cancer (38). TRAF1 is important in the maintenance of immune function of CD8+T cells (39). In the computation formula of IRGPRI, the coefficient of S100A16, CD40 and VCAM1 is a positive number, while the coefficient of TNFRSF4 and TRAF1 is a negative number. Therefore, IRGPRI is negatively correlated with TNFRSF4 and TRAF1, while IRGPRI is positively correlated with S100A16, CD40 and VCAM1. In conclusion, IRGPRI is a biomarker that is associated with prognosis and tumor immunity.

We investigated gene mutations in different IRGPRI subgroups to further understand the immunological properties of IRGPRI subgroup. KRAS and TP53 mutations are more common in the high IRGPRI samples than those in the low IRGPRI samples. KRAS mutation is correlated with high circulating regulatory T cell levels, both of which indicate poorer prognosis in advanced PAAD patients (40). In addition, TP53 mutation is associated with more aggressive diseases and worse patient prognosis in various cancers (41, 42). KRAS, TP53, SMAD4 and CDKN2A are considered as the major drivers for the occurrence of PAAD. Among 71 patients who received adjuvant chemotherapy and radical surgery, those with less mutations in the four driver genes tended to obtain better outcomes (43). Therefore, as with our survival results, high IRGPRI group with high TP53 and KRAS mutations have a worse prognosis than low IRGPRI group with low TP53 and KRAS mutations.

Then, we will explore the correlation of IRGPRI with known predictive markers for immunotherapy, such as PD-L1 and

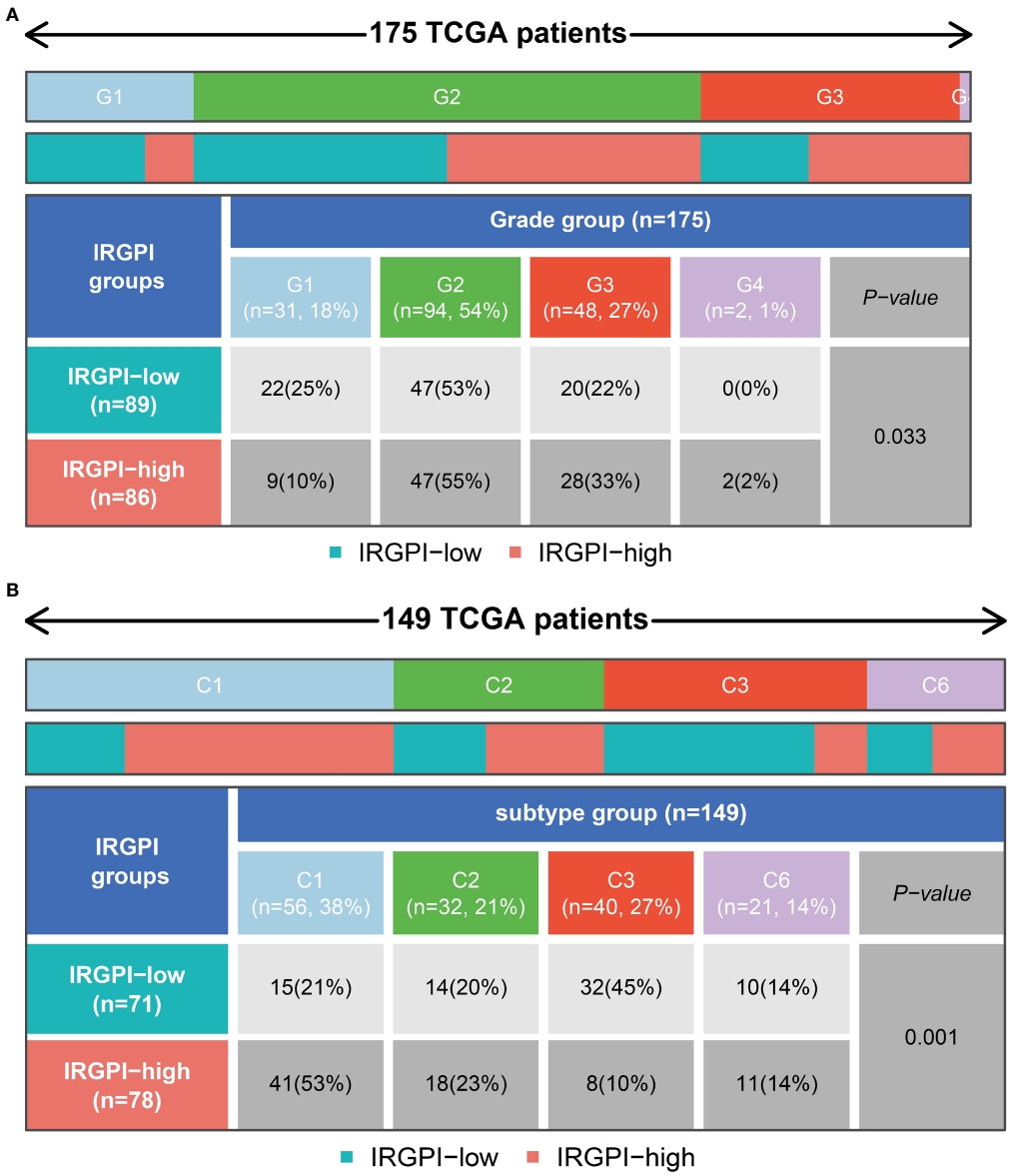

FIGURE 7
Relationship between IRGPRI grouping and clinical and immune subtypes.**(A)** Heat map and table showing the distribution of PAAD grade (G1, G2, G3 and G4) between the IRGPRI subgroups. **(B)** Heat map and table showing the distribution of PAAD immune subtypes (C1, C2, C3 and C6) between the IRGPRI subgroups.

CTLA4. In general, PD-L1+ and CTLA4+ tumors tend to respond better to immune checkpoint inhibitor therapy than negative tumors (44–46). Similar results were observed in PAAD, although IRGPRI scores were not strongly associated with PD-L1. However, we found a significant correlation between IRGPRI score and CTLA4, suggesting that CTLA4 may help explain why IRGPRI affected the prognosis of immunotherapy to a certain extent.

Understanding the TME may help find new methods for the treatment of PAAD, or modifying the TME may improve the effectiveness of immunotherapy. In the two IRGPRI subpopulations, there are differences in the constituent of certain immune cells and the activity of immune functions. CD8+ T cells, checkpoints, T cell co-stimulation are more active in the low IRGPRI group, while M2 macrophages are more common in the high IRGPRI group. Many studies have uncovered that intensive infiltration of T cells, especially cytotoxic CD8+ T cells, indicates a good prognosis (47–49). M2 macrophage is a major subtype of macrophages in most tumors, that promotes aggressive phenotype formation and

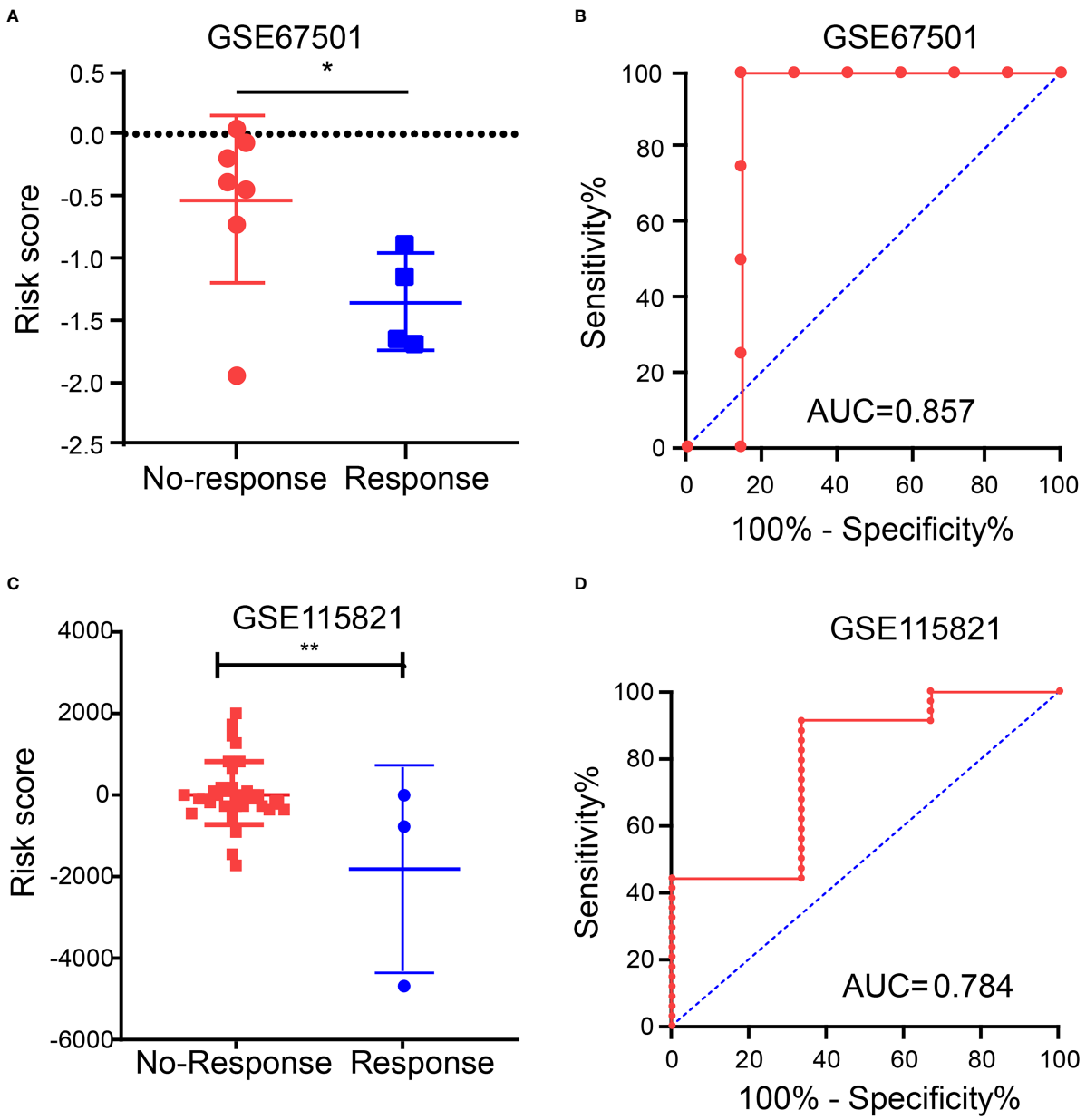

FIGURE 8
Immunotherapy efficacy in different IRGPRI subgroups. **(A)** The risk score in patients who did or did not respond to anti-PD-1 immunotherapy. **(B)** Diagnostic value of risk score by ROC curve in GSE67501. **(C)** The risk score in patients who did or did not respond to ICI therapy. **(D)** Diagnostic value of risk score by ROC curve in GSE115821. (*p < 0.05 and **p< 0.01).

tumor growth, and is associated with a poor prognosis of PAAD (50, 51). Meanwhile, there were more C1 immune subtypes in the high IRGPRI group and more C3 immune subtype in the low IRGPRI group. TCGA tumors can be clustered into six immune subtypes. C3 had the best prognosis, while C1 had less favorable outcomes (52). These conclusions also were supported by our study results. This implies that the high IRGPRI group has immunosuppressive characteristics, while the low IRGPRI group has better tumor immunity potential.

In order to further explore the predictive role of IRGPRI model in immunotherapy, we analyzed immunotherapy sequencing data. Since no sequencing cohort was found for the efficacy of PAAD immunotherapy, we analyzed renal cell carcinoma immunotherapy cohort (GSE67501) and metastatic melanoma immunotherapy cohort (GSE115821). The results showed that the risk score in patients who did not respond to ICI therapy was significantly higher than the risk score in patients who responded to ICI therapy. These results mean

that IRGPRI may be a potential prediction model for predicting the efficacy of immunotherapy.

However, there are still some limitations in our study. First, a PAAD immunotherapy cohort is needed to verify the predictive role of IRGPRI in immunotherapy. Second, a prospective cohort study is needed to confirm the prognostic value of this model.

In conclusion, IRGPRI is an encouraging immune-related prognostic marker. IRGPRI may help identify molecular and immune features and predict the prognosis of PAAD patients. Additionally, IRGPRI may have predictive implication for immunotherapy, which should be further verified in further studies.

Data availability statement

The datasets presented in this study can be found in online repositories. The names of the repository/repositories and accession number(s) can be found in the article/supplementary material.

Author contributions

MS and YS made important contributions to the study conception and design. YS and RQ conducted data analysis and interpretation. All authors participated in the drafting and revision of the manuscript. All authors read, revised and approved this manuscript and agreed to be responsible for all aspects of the research to ensure the data accuracy and integrity of this work.

Funding

This research was supported by Natural Science Research Plan of Huaian (No. HAB202022), National Natural Science Foundation of China (No. 81972719, 82003164), National science research in Universities of Jiangsu Province (No. 21KJA320008, 20KJB320032, 21KJB320021), Jiangsu Province Natural Science Foundation (No. BK20210910, BK20201012, BK20210913), Innovative and Entrepreneurial Doctor Project of Jiangsu Province (JSSCBS20211256), Key Research & Developement Plan of Xuzhou (No. KC18102), Science and Technology Project of Xuzhou (No. KC20126), Scientific Research Foundation of Xuzhou Medical University (No. D2019050).

Conflict of interest

The authors declare that the research was conducted in the absence of any commercial or financial relationships that could be construed as a potential conflict of interest.

Publisher's note

All claims expressed in this article are solely those of the authors and do not necessarily represent those of their affiliated organizations, or those of the publisher, the editors and the reviewers. Any product that may be evaluated in this article, or claim that may be made by its manufacturer, is not guaranteed or endorsed by the publisher.

Supplementary material

The Supplementary Material for this article can be found online at: https://www.frontiersin.org/articles/10.3389/fimmu.2022.945878/full#supplementary-material

SUPPLEMENTARY FIGURE 1
Differentially expressed immune-related genes in PAAD. **(A)** Heatmap displaying all differentially expressed genes (DEGs) between PAAD samples (red) and para-cancer samples (blue) ($p < 0.05$, $|log2FC| > 1$). **(B)** Heatmap displaying immune-related DEGs between PAAD samples (red) and para-cancer samples (blue). **(C)** Gene Ontology (GO) enrichment analysis of the immune-related DEGs ($p < 0.05$). **(D)** Kyoto Encyclopedia of Genes and Genomes (KEGG) pathway analysis of the immune-related DEGs ($p < 0.05$).

SUPPLEMENTARY FIGURE 2
Determination of the soft-thresholding power in the WGCNA analysis. As seen from the graph, the optimal soft threshold for WGCNA was 6.

SUPPLEMENTARY FIGURE 3
The relationship between IRGPRI score and the expression levels of PCNA, MKI67 or MMP14. **(A)** PCNA in different IRGPRI subgroups. **(B)** Correlation analysis between IRGPRI and PCNA. **(C)** MKI67 expression in different IRGPRI subgroups. **(D)** Correlation analysis between IRGPRI and MKI67 expression. **(E)** MMP14 expression in different IRGPRI subgroups. **(F)** Correlation analysis between IRGPRI and MMP14 expression.

SUPPLEMENTARY FIGURE 4
Distribution of TNM stage subtypes in different IRGPRI subgroups. Heat map and table showing the distribution of PAAD stage (Stage 1, Stage 2, Stage 3 and Stage 4) between the IRGPRI subgroups.

SUPPLEMENTARY FIGURE 5
Graphical Abstract.

References

1. Siegel RL, Miller KD, Fuchs HE, Jemal A. Cancer statistics, 2021. *CA Cancer J Clin* (2021) 71(1):7–33. doi: 10.3322/caac.21654

2. Rahib L, Smith BD, Aizenberg R, Rosenzweig AB, Fleshman JM, Matrisian LM. Projecting cancer incidence and deaths to 2030: the unexpected burden of thyroid, liver, and pancreas cancers in the united states. *Cancer Res* (2014) 74 (11):2913–21. doi: 10.1158/0008-5472.CAN-14-0155

3. Park W, Chawla A, O'Reilly EM. Pancreatic cancer: A review. *JAMA* (2021) 326(9):851–62. doi: 10.1001/jama.2021.13027

4. Chen X, Zeh HJ, Kang R, Kroemer G, Tang D. Cell death in pancreatic cancer: from pathogenesis to therapy. *Nat Rev Gastroenterol Hepatol* (2021) 18 (11):804–23. doi: 10.1038/s41575-021-00486-6

5. Luo G, Fan Z, Gong Y, Jin K, Yang C, Cheng H, et al. Characteristics and outcomes of pancreatic cancer by histological subtypes. *Pancreas* (2019) 48(6):817–22. doi: 10.1097/MPA.0000000000001338

6. Yako YY, Kruger D, Smith M, Brand M. Cytokines as biomarkers of pancreatic ductal adenocarcinoma: A systematic review. *PloS One* (2016) 11(5): e0154016. doi: 10.1371/journal.pone.0154016

7. Chen B, Hu C, Jiang L, Xiang Z, Zuo Z, Lin Y, et al. Exploring the significance of novel immune-related gene signatures in the prognosis and immune features of pancreatic adenocarcinoma. *Int Immunopharmacol* (2021) 92:107359. doi: 10.1016/j.intimp.2020.107359

8. Wang W, Yan L, Guan X, Dong B, Zhao M, Wu J, et al. Identification of an immune-related signature for predicting prognosis in patients with pancreatic ductal adenocarcinoma. *Front Oncol* (2020) 10:618215. doi: 10.3389/fonc.2020.618215

9. Zhang X, Li X, Xie J, Zhu Q, Yuan Y. A novel immune-related prognostic signature predicting survival in patients with pancreatic adenocarcinoma. *J Oncol* (2022) 2022:8909631. doi: 10.1155/2022/8909631

10. Zhang Q, Wang Z, Yu X, Zhang M, Zheng Q, He Y, et al. Immune subtypes based on immune-related lncRNA: Differential prognostic mechanism of pancreatic cancer. *Front Cell Dev Biol* (2021) 9:698296. doi: 10.3389/fcell.2021.698296

11. Bu F, Nie H, Zhu X, Wu T, Lin K, Zhao J, et al. A signature of 18 immune-related gene pairs to predict the prognosis of pancreatic cancer patients. *Immun Inflammation Dis* (2020) 8(4):713–26. doi: 10.1002/iid3.363

12. Conroy T, Bachet JB, Ayav A, Huguet F, Lambert A, Caramella C, et al. Current standards and new innovative approaches for treatment of pancreatic cancer. *Eur J Cancer* (2016) 57:10–22. doi: 10.1016/j.ejca.2015.12.026

13. Kotteas E, Saif MW, Syrigos K. Immunotherapy for pancreatic cancer. *J Cancer Res Clin Oncol* (2016) 142(8):1795–805. doi: 10.1007/s00432-016-2119-2

14. Gu S, Qian L, Zhang Y, Chen K, Li Y, Wang J, et al. Significance of intratumoral infiltration of b cells in cancer immunotherapy: From a single cell perspective. *Biochim Biophys Acta Rev Cancer* (2021) 1876(2):188632. doi: 10.1016/j.bbcan.2021.188632

15. Yang Z, Ma Y, Zhao H, Yuan Y, Kim BYS. Nanotechnology platforms for cancer immunotherapy. *Wiley Interdiscip Rev Nanomed Nanobiotechnol* (2020) 12 (2):e1590. doi: 10.1002/wnan.1590

16. Wang J, Reiss KA, Khatri R, Jaffee E, Laheru D. Immune therapy in GI malignancies: A review. *J Clin Oncol* (2015) 33(16):1745–53. doi: 10.1200/JCO.2015.60.7879

17. Laheru D, Lutz E, Burke J, Biedrzycki B, Solt S, Onners B, et al. Allogeneic granulocyte macrophage colony-stimulating factor-secreting tumor immunotherapy alone or in sequence with cyclophosphamide for metastatic pancreatic cancer: a pilot study of safety, feasibility, and immune activation. *Clin Cancer Res* (2008) 14(5):1455–63. doi: 10.1158/1078-0432.CCR-07-0371

18. Yamamoto K, Venida A, Yano J, Biancur DE, Kakiuchi M, Gupta S, et al. Autophagy promotes immune evasion of pancreatic cancer by degrading MHC-I. *Nature* (2020) 581(7806):100–5. doi: 10.1038/s41586-020-2229-5

19. Sandin LC, Eriksson F, Ellmark P, Loskog AS, Totterman TH, Mangsbo SM. Local CTLA4 blockade effectively restrains experimental pancreatic adenocarcinoma growth *in vivo*. *Oncoimmunology* (2014) 3(1):e27614. doi: 10.4161/onci.27614

20. Kwon MJ. Emerging immune gene signatures as prognostic or predictive biomarkers in breast cancer. *Arch Pharm Res* (2019) 42(11):947–61. doi: 10.1007/s12272-019-01189-y

21. Lei Y, Tang R, Xu J, Zhang B, Liu J, Liang C, et al. Construction of a novel risk model based on the random forest algorithm to distinguish pancreatic cancers with different prognoses and immune microenvironment features. *Bioengineered* (2021) 12(1):3593–602. doi: 10.1080/21655979.2021.1951527

22. Li Y, Yao P, Zhao K, Ye Z, Zhang H, Cao J, et al. Individualized prognostic signature for pancreatic carcinoma validated by integrating immune-related gene pairs (IRGPs). *Bioengineered* (2021) 12(1):88–95. doi: 10.1080/21655979.2020.1860493

23. Liu X, Li Z, Wang Y. Advances in targeted therapy and immunotherapy for pancreatic cancer. *Adv Biol (Weinh)* (2021) 5(3):e1900236. doi: 10.1002/adbi.201900236

24. Cao D, Song Q, Li J, Jiang Y, Wang Z, Lu S. Opportunities and challenges in targeted therapy and immunotherapy for pancreatic cancer. *Expert Rev Mol Med* (2021) 23:e21. doi: 10.1017/erm.2021.26

25. Ye Y, Zheng S. Successful immunotherapy for pancreatic cancer in a patient with TSC2 and SMAD4 mutations: A case report. *Front Immunol* (2021) 12:785400. doi: 10.3389/fimmu.2021.785400

26. Wu J, Cai J. Dilemma and challenge of immunotherapy for pancreatic cancer. *Dig Dis Sci* (2021) 66(2):359–68. doi: 10.1007/s10620-020-06183-9

27. Vitiello GA, Cohen DJ, Miller G. Harnessing the microbiome for pancreatic cancer immunotherapy. *Trends Cancer* (2019) 5(11):670–6. doi: 10.1016/j.trecan.2019.10.005

28. Yu Q, Tang X, Zhao W, Qiu Y, He J, Wan D, et al. Mild hyperthermia promotes immune checkpoint blockade-based immunotherapy against metastatic pancreatic cancer using size-adjustable nanoparticles. *Acta Biomater* (2021) 133:244–56. doi: 10.1016/j.actbio.2021.05.002

29. Gonzalez LL, Garrie K, Turner MD. Role of S100 proteins in health and disease. *Biochim Biophys Acta Mol Cell Res* (2020) 1867(6):118677. doi: 10.1016/j.bbamcr.2020.118677

30. Fang D, Zhang C, Xu P, Liu Y, Mo X, Sun Q, et al. S100A16 promotes metastasis and progression of pancreatic cancer through FGF19-mediated AKT and ERK1/2 pathways. *Cell Biol Toxicol* (2021) 37(4):555–71. doi: 10.1007/s10565-020-09574-w

31. Li T, Ren T, Huang C, Li Y, Yang P, Che G, et al. S100A16 induces epithelial-mesenchymal transition in human PDAC cells and is a new therapeutic target for pancreatic cancer treatment that synergizes with gemcitabine. *Biochem Pharmacol* (2021) 189:114396. doi: 10.1016/j.bcp.2020.114396

32. Ou S, Liao Y, Shi J, Tang J, Ye Y, Wu F, et al. S100A16 suppresses the proliferation, migration and invasion of colorectal cancer cells in part *via* the JNK/p38 MAPK pathway. *Mol Med Rep* (2021) 23(2):164. doi: 10.3892/mmr.2020.11803

33. Xu ZH, Miao ZW, Jiang QZ, Gan DX, Wei XG, Xue XZ, et al. Brain microvascular endothelial cell exosome-mediated S100A16 up-regulation confers small-cell lung cancer cell survival in brain. *FASEB J* (2019) 33(2):1742–57. doi: 10.1096/fj.201800428R

34. Sun X, Wang T, Zhang C, Ning K, Guan ZR, Chen SX, et al. S100A16 is a prognostic marker for colorectal cancer. *J Surg Oncol* (2018) 117(2):275–83. doi: 10.1002/jso.24822

35. Tu G, Gao W, Li Y, Dian Y, Xue B, Niu L, et al. Expressional and prognostic value of S100A16 in pancreatic cancer *Via* integrated bioinformatics analyses. *Front Cell Dev Biol* (2021) 9:645641. doi: 10.3389/fcell.2021.645641

36. Vonderheide RH. CD40 agonist antibodies in cancer immunotherapy. *Annu Rev Med* (2020) 71:47–58. doi: 10.1146/annurev-med-062518-045435

37. Huang J, Zhang J, Li H, Lu Z, Shan W, Mercado-Uribe I, et al. VCAM1 expression correlated with tumorigenesis and poor prognosis in high grade serous ovarian cancer. *Am J Transl Res* (2013) 5(3):336–46.

38. Cai Q, Zhu M, Duan J, Wang H, Chen J, Xiao Y, et al. Comprehensive analysis of immune-related prognosis of TK1 in hepatocellular carcinoma. *Front Oncol* (2021) 11:786873. doi: 10.3389/fonc.2021.786873

39. Wang C, McPherson AJ, Jones RB, Kawamura KS, Lin GH, Lang PA, et al. Loss of the signaling adaptor TRAF1 causes CD8+ T cell dysregulation during human and murine chronic infection. *J Exp Med* (2012) 209(1):77–91. doi: 10.1084/jem.20110675

40. Cheng H, Luo G, Jin K, Fan Z, Huang Q, Gong Y, et al. Kras mutation correlating with circulating regulatory T cells predicts the prognosis of advanced pancreatic cancer patients. *Cancer Med* (2020) 9(6):2153–9. doi: 10.1002/cam4.2895

41. Zhang Z, Hao R, Guo Q, Zhang S, Wang X. TP53 mutation infers a poor prognosis and is correlated to immunocytes infiltration in breast cancer. *Front Cell Dev Biol* (2021) 9:759154. doi: 10.3389/fcell.2021.759154

42. Lizhi L, Rongdong H, Shaohua H, Yingquan K, Huihuang X, Shan L, et al. Association between TP53 mutation and prognosis in wilms tumor: A meta-analysis. *Fetal Pediatr Pathol* (2021) 40(6):653–62. doi: 10.1080/15513815.2020.1725937

43. Hayashi H, Kohno T, Ueno H, Hiraoka N, Kondo S, Saito M, et al. Utility of assessing the number of mutated KRAS, CDKN2A, TP53, and SMAD4 genes using a targeted deep sequencing assay as a prognostic biomarker for pancreatic cancer. *Pancreas* (2017) 46(3):335–40. doi: 10.1097/MPA.0000000000000760

44. Hansen AR, Siu LL. PD-L1 testing in cancer: Challenges in companion diagnostic development. *JAMA Oncol* (2016) 2(1):15–6. doi: 10.1001/jamaoncol.2015.4685

45. Oliva M, Spreafico A, Taberna M, Alemany L, Coburn B, Mesia R, et al. Immune biomarkers of response to immune-checkpoint inhibitors in head and neck squamous cell carcinoma. *Ann Oncol* (2019) 30(1):57–67. doi: 10.1093/annonc/mdy507

46. Pai CS, Simons DM, Lu X, Evans M, Wei J, Wang YH, et al. Tumor-conditional anti-CTLA4 uncouples antitumor efficacy from immunotherapy-related toxicity. *J Clin Invest* (2019) 129(1):349–63. doi: 10.1172/JCI123391

47. Bindea G, Mlecnik B, Tosolini M, Kirilovsky A, Waldner M, Obenauf AC, et al. Spatiotemporal dynamics of intratumoral immune cells reveal the immune landscape in human cancer. *Immunity* (2013) 39(4):782–95. doi: 10.1016/j.immuni.2013.10.003

48. Fridman WH, Zitvogel L, Sautes-Fridman C, Kroemer G. The immune contexture in cancer prognosis and treatment. *Nat Rev Clin Oncol* (2017) 14 (12):717–34. doi: 10.1038/nrclinonc.2017.101

49. Zhuang H, Zhang C, Hou B. FAM83H overexpression predicts worse prognosis and correlates with less CD8(+) T cells infiltration and ras-PI3K-Akt-mTOR signaling pathway in pancreatic cancer. *Clin Transl Oncol* (2020) 22 (12):2244–52. doi: 10.1007/s12094-020-02365-z

50. Han BW, Ye H, Wei PP, He B, Han C, Chen ZH, et al. Global identification and characterization of lncRNAs that control inflammation in malignant cholangiocytes. *BMC Genomics* (2018) 19(1):735. doi: 10.1186/s12864-018-5133-8

51. Liu CY, Xu JY, Shi XY, Huang W, Ruan TY, Xie P, et al. M2-polarized tumor-associated macrophages promoted epithelial-mesenchymal transition in pancreatic cancer cells, partially through TLR4/IL-10 signaling pathway. *Lab Invest* (2013) 93(7):844–54. doi: 10.1038/labinvest.2013.69

52. Thorsson V, Gibbs DL, Brown SD, Wolf D, Bortone DS, Ou Yang TH, et al. The immune landscape of cancer. *Immunity* (2018) 48(4):812–30.e14. doi: 10.1016/j.immuni.2018.03.023

frontiers | Frontiers in Immunology

TYPE Systematic Review
PUBLISHED 17 August 2022
DOI 10.3389/fimmu.2022.956533

OPEN ACCESS

EDITED BY
Yunfei Xu,
Shandong University, China

REVIEWED BY
Giovanni Brandi,
University of Bologna, Italy
Jie-ying Liang,
Sun Yat-sen University Cancer Center (SYSUCC), China
Dawei Deng,
Dalian Medical University, China

*CORRESPONDENCE
Wenhong Deng
wenhongdeng@whu.edu.cn
Weixing Wang
wangwx@whu.edu.cn

†These authors have contributed equally to this work

SPECIALTY SECTION
This article was submitted to Cancer Immunity and Immunotherapy, a section of the journal Frontiers in Immunology

RECEIVED 30 May 2022
ACCEPTED 02 August 2022
PUBLISHED 17 August 2022

CITATION
Zhang L, Chen C, Chai D, Li C, Guan Y, Liu L, Kuang T, Deng W and Wang W (2022) The association between antibiotic use and outcomes of HCC patients treated with immune checkpoint inhibitors.
Front. Immunol. 13:956533.
doi: 10.3389/fimmu.2022.956533

The association between antibiotic use and outcomes of HCC patients treated with immune checkpoint inhibitors

Lilong Zhang[1,2†], Chen Chen[1†], Dongqi Chai[1,2], Chunlei Li[1,2], Yongjun Guan[1,2], Li Liu[1,2], Tianrui Kuang[1,2], Wenhong Deng[1*] and Weixing Wang[1*]

[1]Department of General Surgery, Renmin Hospital of Wuhan University, Wuhan, China, [2]Hubei Key Laboratory of Digestive System Disease, Wuhan, China

Objective: Recently, immune checkpoint inhibitor (ICI) treatment has shown encouraging performance in improving the prognosis of hepatocellular carcinoma (HCC) patients. The gut microbiome plays a vital role in altering the efficacy of ICIs, which may be impacted by antibiotics. The aim of the meta-analysis is to estimate the influence of antibiotic use on the survival of HCC patients treated with ICIs.

Methods: The literature review was conducted using databases like PubMed, EMBASE, Cochrane Library, CNKI, WANFANG DATA, VIP, Google Scholar, and ClinicalTrials.gov before May 15, 2022. The primary endpoints were overall survival (OS), progression-free survival (PFS), objective response rate (ORR), and disease control rate (DCR).

Results: A total of six retrospective studies met the inclusion criteria. 1056 patients were included in the study, of which 352 (33.33%) received antibiotic treatment. The meta-analysis results revealed antibiotic use did not affect the OS (HR: 1.41, 95% CI: 0.96-2.08, P = 0.088) and PFS (HR: 1.21, 95% CI: 0.73-2.00, P = 0.459) in HCC patients treated with ICIs. Besides, the use of antibiotics did not reduce the ORR (OR: 1.06, 95% CI: 0.69-1.64, P = 0.784) and DCR (OR: 0.42, 95% CI: 0.09-2.06, P = 0.286) in HCC patients treated with ICIs.

Conclusion: Current evidence reveals that antibiotic use does alter the therapeutic efficacy of ICIs in HCC patients.

Systematic Review Registration: https://www.crd.york.ac.uk/, identifier CRD42022311948.

KEYWORDS

immune checkpoint inhibitors, antibiotic, hepatocellular carcinoma, prognosis, meta-analysis

Introduction

Primary liver cancer is the sixth most common type of cancer worldwide and ranks third in cancer-related deaths globally, amongst which hepatocellular carcinoma (HCC) accounts for 75-85% of all liver cancer cases (1). The prognosis of HCC is poor since most patients are diagnosed at an advanced stage or have limited liver reserve because of cirrhosis. This makes curative treatments, such as resection or ablative therapy, and liver transplantation difficult. In recent years, there has been significant development in advanced HCC therapeutics (2, 3); however, the effectiveness of systemic treatment like sorafenib is still suboptimal (4). Newer treatments, like multi-kinase inhibitors (regorafenib and cabozantinib) and monoclonal antibodies (ramucirumab), have a low overall survival (OS) of just 8.5-10.6 months (5).

Immune checkpoint inhibitors (ICIs), such as anti-programmed cell death 1 (anti-PD-1)/programmed cell death ligand 1 (PD-L1) and anti-cytotoxic T-lymphocyte-associated protein 4 (CTLA-4) antibodies, are novel and promising therapies that have been effective in prolonging survival in advanced HCC patients (6–9). The advanced HCC treated with nivolumab had an objective response rate (ORR) of 14% and a median OS of 15.1 months (6). More recently, the combination of nivolumab and ipilimumab has shown a manageable safety profile, with an ORR as high as 32% and durable responses (9). According to the promising results of early phase clinical trials, levatinib plus pembrolizumab is considered to have the potential to represent a novel treatment option for HCC patients (10). Despite the favorable outcomes, not all advanced HCC patients respond to ICI treatment. Patients who do not respond to ICI therapy often experience tumor progression and may even suffer severe immune adverse effects, such as pneumonia, myocarditis, and hepatitis, all of which can be fatal (11, 12). Therefore, the search for potential factors influencing its efficacy is extremely necessary for a more targeted selection of treatment populations in clinical practice (13).

In 2015, a heavyweight study correlating the effect of intestinal microbiomes on the efficacy of ICI treatment was published for the first time in Science (14). Next, it has been reported that intestinal microbiomes can influence the anti-PD-1 treatment response in HCC patients, with responders having higher taxonomic richness and more gene counts than non-responders (15, 16). It is well known that antibiotics are the most common clinical cause of alterations in gut flora. Recently, two studies published in the same issue of "liver cancer" have come to opposite conclusions regarding the effect of antibiotics on the efficacy of ICI treatment in HCC (17, 18). Besides, some similar studies have been undertaken throughout the world, but there has been no consensus established. To address these clinical problems, the first meta-analysis was conducted by our team to investigate whether the antibiotics influence the efficacy of ICI therapy in HCC patients. This will provide evidence-based results for the clinical application of antibiotics in HCC patients undergoing ICI treatment, thereby maximizing the clinical benefit for patients.

Methods

Literature search strategies

The Preferred Reporting Items for Systematic Reviews and Meta-Analyses (PRISMA) guidelines were strictly followed while conducting the meta-analysis (19). The protocol for the meta-analysis is available on PROSPERO (CRD42022311948). The literature review was conducted using databases like PubMed (https://pubmed.ncbi.nlm.nih.gov/), EMBASE (https://www.embase.com/), Cochrane Library (https://www.cochranelibrary.com/), CNKI (https://www.cnki.net/), WANFANG DATA (https://www.wanfangdata.com.cn/), and VIP (http://www.cqvip.com/) before May 15, 2022. "Anti-Bacterial Agents"[Mesh], "Immune Checkpoint Inhibitors"[Mesh], "Liver Neoplasms"[Mesh], "Carcinoma, Hepatocellular "[Mesh], and their entry terms were searched in [All Fields]. Detailed search strategies are presented in Table S1. A gray literature search was performed using Google Scholar to find reports that were not indexed in the previously mentioned databases, such as conference abstracts, presentations, and unpublished trial data. The Clinical Trial Registration Platform, like ClinicalTrials.gov (https://clinicaltrials.gov/), was utilized to search for ongoing trials. Besides, we also manually searched the reference lists of eligible papers.

Study selection criteria

Full-text articles and conference abstracts were included based on the inclusion criteria, which are as follows: (1) patients diagnosed with HCC; (2) patients treated with ICIs; (3) patients divided into the non-antibiotic group and antibiotic group based on the history of antibiotic use; (4) provided at least one of the outcomes of interest [OS, progression-free survival (PFS), ORR, and disease control rate (DCR)]. Articles that failed to report information about subjects, such as sample size and other basic information, were discarded. When studies reported

overlapping patient populations, only the article with the most complete data and rigorous methodology was selected.

Data extraction and quality assessment

Data extraction mainly focused on the author, publication year, study type, period, and region, the number of patients, types of ICI treatment, treatment-related outcomes (OS, PFS, ORR, and DCR), covariates of multivariate analysis for OS and PFS, the reason for antibiotic use, types and timing of antibiotic use, and antibiotic (median) duration. If both univariate and multivariate analyses were used to calculate the hazard ratio (HR), the latter was preferred because the result was adjusted for confounding factors and was more accurate. Authors were contacted if the relevant data was not immediately accessible from published abstracts or articles. The Newcastle-Ottawa Scale (NOS) score was applied to estimate the quality of the selected literature 42. Literature with a score ≥ 7 was regarded as high-quality ones. All the above steps were independently cross-checked by two authors (Zhang Lilong and Chen Chen), and all differences were addressed by the senior author (Deng Wenhong and Wang Weixing).

Statistical methods

Statistical analysis was conducted using Stata SE15.0. The relationship between the efficacy of ICI therapy and antibiotic usage was reported as an odds ratio (OR) with a 95% confidence interval (95% CI). The effect of antibiotic use on the risk of survival in HCC patients was calculated using the HR and 95% CI. The chi-square test was applied to determine the statistical heterogeneity among the studies. $P > 0.1$ and $I^2 < 50\%$ revealed low heterogeneity where a fixed-effect model was adopted; otherwise, the random-effect model was utilized. The subgroup analysis was carried out to minimize the impact of heterogeneity on the meta-analysis. Publication bias was measured using Begg's and Egger's tests. Sensitivity analysis by the leave-one-out method was used to assess the stability of the results. All P values were two-sided, and the statistical significance was set at $P < 0.05$.

Results

Studies retrieved and characteristics

467 eligible records were screened for their titles and abstracts to check for their eligibility. After a detailed analysis of 14 full-text records, we found that six studies met the inclusion criteria (17, 18, 20–23). The articles by Ren *et al.* (24) and Jun *et al.* (25) were excluded from the meta-analysis due to insufficient data and duplicate publication, respectively. The flow diagram of identifying eligible studies is shown in Figure 1. The baseline characteristics and the scores of the quality assessment are shown in Table 1. The score for four articles was 7 or 8 points, and the articles were

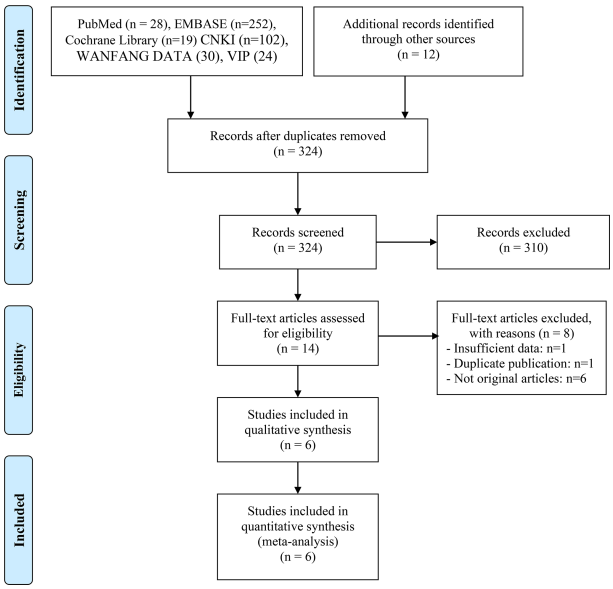

FIGURE 1
The flow diagram of identifying eligible studies.

TABLE 1 Baseline characteristics of included studies.

Author	Year	Study type	Study period	Study region	Number of antibiotic	Number of non- antibiotic	Types of ICI treatment	Outcomes	Quality (NOS Score)
Fessas et al.	2021	Retrospective	2017-2019	Europe, America, Asia	170	279	Anti-PD(L)-1 and/or Anti-CTLA-4	OS, PFS, ORR, DCB	8
Spahn et al.	2020	Retrospective	08/2015-12/2019	Germany, Austria, Switzerland	21	78	Anti-PD(L)-1 (nivolumab, pembrolizumab)	OS, PFS	7
Cheung et al.	2021	Retrospective	01/2014-12/2019	China (Hong Kong)	109	286	Anti-PD(L)-1 (nivolumab, pembrolizumab) and/or CTLA-4 (ipilimumab)	OS	7
Alshammari et al.	2021	Retrospective	–	Saudi Arabia	20	39	Anti-PD(L)-1 (nivolumab)	OS, ORR	5
Chen_xj et al.	2021	Retrospective	09/2018-06/2020	Chian (Nanchang)	18	22	Anti-PD(L)-1 (camrelizumab, tislelizumab, sintilimab, toriplimab, pembrolizumab)	OS, PFS, ORR, DCB	7
Chen_q et al.	2018	Retrospective	05/2016-12/2017	Chian (Fujian)	14	19	Anti-PD(L)-1 (nivolumab, pembrolumab)	OS, PFS, ORR, DCB	6

ICI, Immune checkpoint inhibitors; PD-1, programmed cell death 1; PDL-1, programmed cell death ligand 1; CTLA4, cytotoxic T-lymphocyte-associated protein 4; OS, overall survival; PFS, progression-free survival; ORR, objective response rate; DCR, disease control rate; NOS, Newcastle-Ottawa Scale.

deemed high-quality. The remaining two studies received 5 and 6 points and were deemed moderate-quality. The information from the survival analysis and antibiotic use was also listed in Table S2.

Overall survival

Five studies (18, 20–23) reported median OS, with a mean median OS of 8.275 months, ranging from 3.3 to 15.3 months in

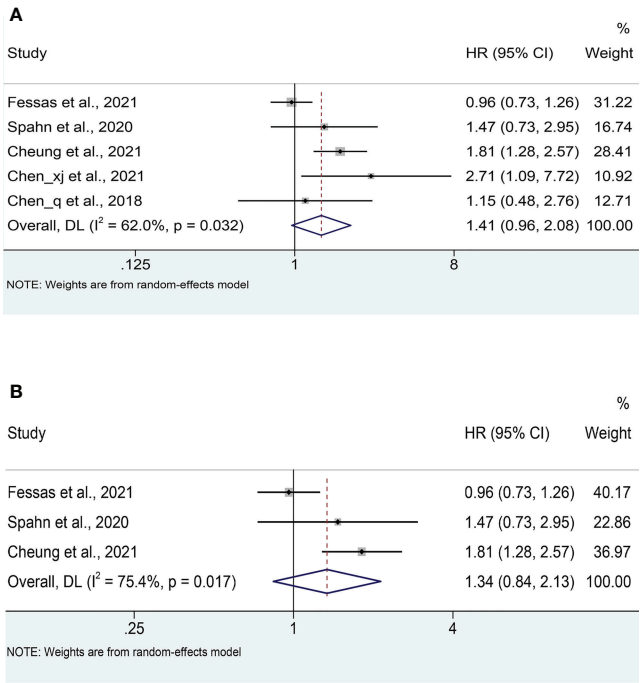

FIGURE 2
(A) Meta-analysis of the overall OS. **(B)** Meta-analysis of OS after excluding Chinese literature. OS: overall survival; HR: hazard ratio; CI: confidence interval.

the antibiotic group; while the mean median OS in the non-antibiotic group was 12.62 months, ranging from 4 to 17.4 months (Figure S1A). The meta-analysis for OS was performed using survival data from 5 studies (17, 18, 21–23), which included 1016 participants (332 with antibiotics versus 684 with non-antibiotics). As illustrated in Figure 2A, significant heterogeneity was observed in the studies (I^2 = 62.0%, P = 0.032), therefore a random-effects model was applied. The results revealed that antibiotic use did not shorten OS in HCC patients treated with ICIs (HR: 1.41, 95% CI: 0.96-2.08, P = 0.088). Begg's and Egger's tests indicated no significant publication bias (Begg's test P = 0.906; Egger's test P = 0.940). To estimate the influence of each study on the overall meta-analysis, we conducted a sensitivity analysis using the leave-one-out method. The results showed that no single study significantly impacted the pooled HR of OS (Figure 3A). Besides, two Chinese articles were excluded from the analysis to investigate the reliability of the results further. As shown in Figure 2B, excluding the two articles did not change the results (HR: 1.34, 95% CI: 0.84-2.13, P = 0.222). Thus, it would be safe to assume that the meta-analysis results were relatively stable and reliable.

Progression-free survival

Four cohort studies (18, 21–23) reported median PFS with a mean of 4.95 months ranging from 2 to 6.7 months in the antibiotic group and 5.975 months ranging from 3.7 to 8.9 months in the non-antibiotic group (Figure S1B). Pooled data from 4 studies (18, 21–23) with a total of 621 patients (223 with antibiotics versus 398 with non-antibiotics) was used to assess the association between antibiotic usage and PFS. Due to significant heterogeneity, a random-effects model was used (I^2 = 72.7%, P = 0.012). The results revealed no effect of the use of antibiotics on the PFS of HCC patients (HR: 1.21, 95% CI: 0.73-2.00, P = 0.459, Figure 4A). Begg's test shows no publication bias in the results (P = 0.308), while Egger's test shows publication bias (P = 0.034). Therefore, the "trim and fill" method was further used to verify the effect of publication bias on the meta-analysis results. We found that the trend of PFS remained unchanged following the correction by the "trim and fill" method. The sensitivity analysis results also confirmed that no single study could substantially affect the pooled HR of PFS (Figure 3B). After excluding the two Chinese articles, the results were still consistent (Figure 4B, I^2 = 61.4%, P = 0.107; HR: 0.89, 95% CI: 0.57-1.39, P = 0.608), thereby confirming the reliability of our conclusion.

Objective response rate and disease control rate

Four studies (18, 20–22) with a total of 581 patients (222 with antibiotics versus 359 with non-antibiotics) were included in the meta-analysis of ORR. No significant heterogeneity was included in the studies (I^2 = 0%, P = 0.408), and a fix-effects model was applied. We found that antibiotic usage did not reduce ORR in HCC patients treated with ICIs (OR: 1.06, 95% CI: 0.69-1.64, P = 0.784, Figure 5A). No remarkable publication

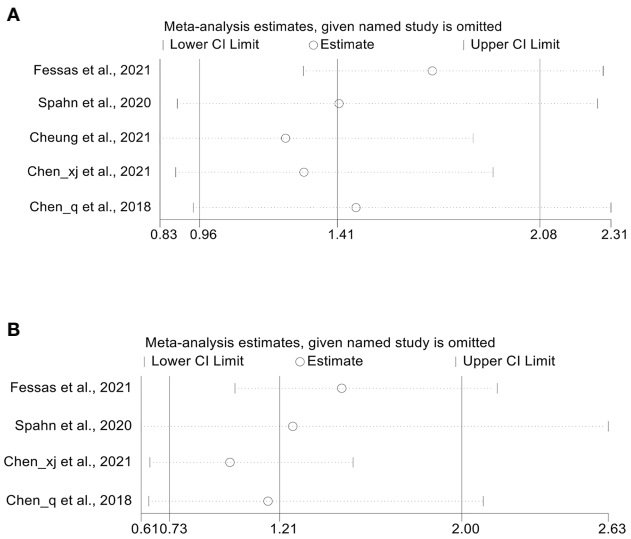

FIGURE 3
(A) Sensitivity analysis of the overall OS. **(B)** Sensitivity analysis of the overall PFS. OS, overall survival; PFS, progression-free survival; CI, confidence interval.

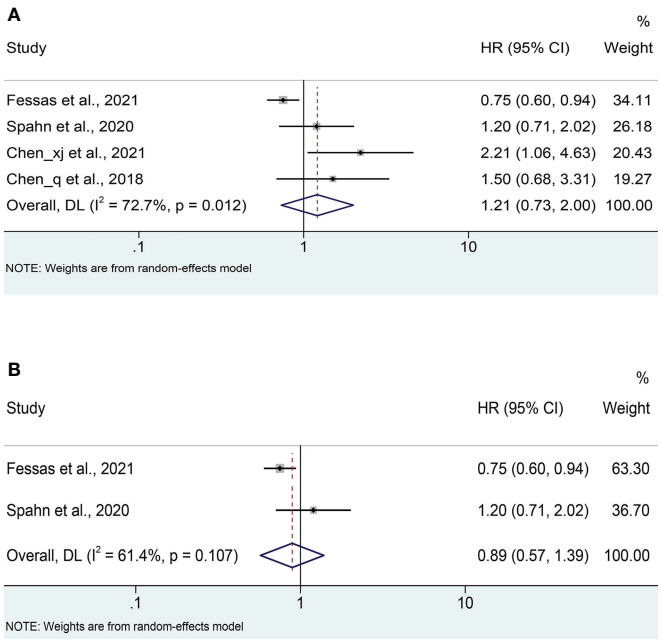

FIGURE 4
(A) Meta-analysis of the overall PFS. **(B)** Meta-analysis of PFS after excluding Chinese literature. PFS, progression-free survival; HR, hazard ratio; CI, confidence interval.

biases were observed using the Begg's (P = 1.000) and Egger's tests (P = 0.153).

The DCR meta-analysis included 3 cohort studies (18, 21, 22) with a total of 522 patients (202 with antibiotics versus 320 with non-antibiotics). Since significant heterogeneity was observed in the included studies (I^2 = 82.3%, P = 0.003), a random-effects model was performed. The results revealed no significant difference in DCR between antibiotic and non-antibiotic groups (OR: 0.42, 95% CI: 0.09-2.06, P = 0.286, Figure 5B). Similarly, no remarkable publication biases were observed using the Begg's (P = 0.296) and Egger's tests (P = 0.126).

In addition, we also found that the use of antibiotics did not affect the complete response rate (Figure S2A, I^2 = 0.0%, P = 0.968; OR: 0.406, 95% CI: 0.040-4.089, P = 0.444) and partial response rate (Figure S2B, I^2 = 0.0%, P = 0.532; OR: 0.610, 95% CI: 0.172-2.162, P = 0.444) in the HCC patients with ICI therapy.

Discussion

With the increased use of ICIs in cancer therapeutics, tremendous effort has been made to uncover possible factors that impact its efficacy. Among the identified factors, a growing body of evidence has indicated a crucial role for the intestinal microbiome (26). Frequent use of antibiotics interferes with intestinal flora, and its effect on the efficacy of ICIs has recently sparked an intense debate (27). Currently, several meta-analyses have revealed that antibiotic administration may be related to poor prognosis in tumor patients receiving ICIs (28–31). However, these studies are focused on lung, melanoma, bladder, and kidney cancers, and no studies on liver cancer have been conducted. To the best of our knowledge, this is the first meta-analysis that investigated the relationship between antibiotics and ICI efficacy in the treatment of HCC. We present all the available evidence to confirm that antibiotic use does not impact the prognosis and response in HCC patients treated with ICIs. Publication bias and sensitivity analyses further confirmed the dependability of our results.

It has been established that in patients with chronic liver disease, intestinal barrier dysfunction allows for increased intestinal bacterial translocation (32). Long-term exposure to lipopolysaccharide from intestinal microbiomes is crucial to the development of cirrhosis and HCC by activating the TGF-β pathway, which is an important molecular driver for anti-apoptotic and proliferative signaling in hepatocyte (33, 34). Once HCC is established, the gut-liver axis keeps up to affect the anti-tumor immune response and perturbation of the intestinal bacteria, in which antibiotics have a direct impact on the tumor microenvironment (35). The general deleterious effect on the outcomes of antibiotic use in malignancy is

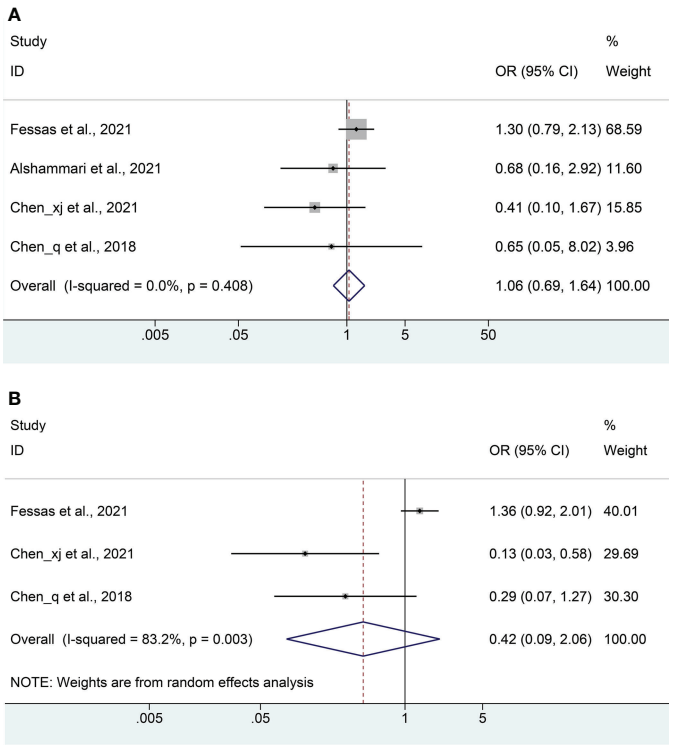

FIGURE 5
Meta-analysis of the objective response rate **(A)** and disease control rate **(B)**. OR, odds ratio; CI, confidence interval.

considered to be related to the detrimental impact of antibiotics on decreasing the diversity and taxonomy of the gut microbiome, causing a reduction in *Bifidobacteria*, *Ruminococcus*, and *Akkermansia*, while favoring the growth of other specific bacteria, such as *Bacteroides* (16, 36). Such bacteria can induce immunosuppression by promoting myeloid-derived suppressor cells, $FOXP3^+$ and $CD4^+$ $CD25^+$ T-regulatory (Treg) cells, and by producing prostaglandins, which negatively correlate with the ICI response (37).

HCC differs from other cancers in that it develops in the context of cirrhosis, a pathological state already linked to immunosuppressive microbiota (38). Cirrhosis is accompanied by a dysbiosis of intestinal microbiota, with an increase in immunosuppressive bacteria and a decrease in beneficial bacteria. Studies in mouse models show a decrease in *Bifidobacterium* and an increase in gram-negative bacteria, such as *Bacteroides* and *Escherichia Coli*, presumably contributing to the progression of HCC (39). Thus, disrupting this immunosuppressive interaction by antibiotics may be a plausible explanation for the no effect of antibiotics on the poor prognosis of HCC patients treated with ICIs. Unlike lung and melanoma cancers, HCC has a distinct immunosuppressive tumor microenvironment (40), due to the abundant recruitment of myeloid suppressor cells and macrophages, which directly suppress cytotoxic T cells and produce chemokines, such as CCL17, CCL18, and CCL22, which further attract Treg cells. Interestingly, Han *et al.* recently demonstrated that antibiotic-induced microbiota dysbiosis enhances the anti-tumor efficacy of gamma delta T cells during immunotherapy in a mouse model (41). To sum up, the impact of antibiotics on ICI therapy in HCC patients is inconclusive. In the comprehensive meta-analysis of six studies, we found that antibiotic use had no effect on the outcomes of ICI treatment in patients with HCC.

Notably, some inherent limitations do exist in this study. To begin with, we present a meta-analysis that depends on the published articles. The lack of enough data prevented us from conducting subgroup analyses based on the type of antibiotic used, route of administration, duration of use, etc. In addition, the study included mainly Asians, and the total number of patients analyzed was relatively small. Finally, we were unable to examine the association between antibiotic use and ICI-induced adverse events, which should be highlighted in our follow-up work. Therefore, future larger, multi-institutional studies with standardized prospective data collection are needed to further confirm our findings above.

Conclusion

Current evidence reveals that, unlike other oncological indications, antibiotic use does not affect the efficacy of ICI treatment in HCC patients.

Data availability statement

The original contributions presented in the study are included in the article/Supplementary Material. Further inquiries can be directed to the corresponding authors.

Author contributions

LZ, CC, WD, and WW conceived and designed the study. LZ, DC, CC, YG, LL, and CL were responsible for the collection and assembly of data, data analysis, and interpretation. LZ, DC, and CC were involved in writing the manuscript. LZ, CC, TK, and WW revised the manuscript. All the work was performed under WD and WW instruction. All authors contributed to the article and approved the submitted version.

Funding

This work was supported by grants from the Natural Science Foundation of China (No. 82172855, 81870442) and the Natural Science Foundation of Hubei Province, China (No. 220171530).

Conflict of interest

The authors declare that the research was conducted in the absence of any commercial or financial relationships that could be construed as a potential conflict of interest.

Publisher's note

Supplementary material

The Supplementary Material for this article can be found online at: https://www.frontiersin.org/articles/10.3389/fimmu.2022.956533/full#supplementary-material

SUPPLEMENTARY FIGURE 1
The median overall survival (A) and median progression-free survival (B) for included studies.

SUPPLEMENTARY FIGURE 2
Meta-analysis of the complete response rate (A) and partial response rate (B). OR: odds ratio; CI: confidence interval

References

1. Sung H, Ferlay J, Siegel RL, Laversanne M, Soerjomataram I, Jemal A, et al. Global cancer statistics 2020: GLOBOCAN estimates of incidence and mortality worldwide for 36 cancers in 185 countries. *CA Cancer J Clin* (2021) 71(3):209–49. doi: 10.3322/caac.21660

2. De Lorenzo S, Tovoli F, Barbera MA, Garuti F, Palloni A, Frega G, et al. Metronomic capecitabine vs. best supportive care in child-pugh b hepatocellular carcinoma: a proof of concept. *Sci Rep* (2018) 8(1):9997. doi: 10.1038/s41598-018-28337-6

3. Dhanasekaran R, Limaye A, Cabrera R. Hepatocellular carcinoma: current trends in worldwide epidemiology, risk factors, diagnosis, and therapeutics. *Hepat Med* (2012) 4:19–37. doi: 10.2147/HMER.S16316

4. Lim H, Ramjeesingh R, Liu D, Tam VC, Knox JJ, Card PB, et al. Optimizing survival and the changing landscape of targeted therapy for intermediate and advanced hepatocellular carcinoma: A systematic review. *J Natl Cancer Inst* (2021) 113(2):123–36. doi: 10.1093/jnci/djaa119

5. Ko KL, Mak LY, Cheung KS, Yuen MF. Hepatocellular carcinoma: recent advances and emerging medical therapies. *F1000Res* (2020) 9: F1000 Faculty Rev7–620. doi: 10.12688/f1000research.24543.1

6. El-Khoueiry AB, Sangro B, Yau T, Crocenzi TS, Kudo M, Hsu C, et al. Nivolumab in patients with advanced hepatocellular carcinoma (CheckMate 040): an open-label, non-comparative, phase 1/2 dose escalation and expansion trial. *Lancet* (2017) 389(10088):2492–502. doi: 10.1016/S0140-6736(17)31046-2

7. Finn RS, Qin S, Ikeda M, Galle PR, Ducreux M, Kim TY, et al. Atezolizumab plus bevacizumab in unresectable hepatocellular carcinoma. *N Engl J Med* (2020) 382(20):1894–905. doi: 10.1056/NEJMoa1915745

8. Nakano S, Eso Y, Okada H, Takai A, Takahashi K, Seno H. Recent advances in immunotherapy for hepatocellular carcinoma. *Cancers (Basel)* (2020) 12(4): 775. doi: 10.3390/cancers12040775

9. Yau T, Kang YK, Kim TY, El-Khoueiry AB, Santoro A, Sangro B, et al. Efficacy and safety of nivolumab plus ipilimumab in patients with advanced hepatocellular carcinoma previously treated with sorafenib: The CheckMate 040 randomized clinical trial. *JAMA Oncol* (2020) 6(11):e204564. doi: 10.1001/jamaoncol.2020.4564

10. Rizzo A, Dadduzio V, Ricci AD, Massari F, Di Federico A, Gadaleta-Caldarola G, et al. Lenvatinib plus pembrolizumab: the next frontier for the treatment of hepatocellular carcinoma? *Expert Opin Investig Drugs* (2022) 31 (4):371–8. doi: 10.1080/13543784.2021.1948532

11. de La Rochefoucauld J, Noël N, Lambotte O. Management of immune-related adverse events associated with immune checkpoint inhibitors in cancer patients: a patient-centred approach. *Intern Emerg Med* (2020) 15(4):587–98. doi: 10.1007/s11739-020-02295-2

12. Puzanov I, Diab A, Abdallah K, Bingham CO3rd, Brogdon C, Dadu R, et al. Managing toxicities associated with immune checkpoint inhibitors: consensus recommendations from the society for immunotherapy of cancer (SITC) toxicity management working group. *J Immunother Cancer* (2017) 5(1):95. doi: 10.1186/s40425-017-0300-z

13. Rizzo A, Ricci AD. PD-L1, TMB, and other potential predictors of response to immunotherapy for hepatocellular carcinoma: how can they assist drug clinical trials? *Expert Opin Investig Drugs* (2022) 31(4):415–23. doi: 10.1080/13543784.2021.1972969

14. Sivan A, Corrales L, Hubert N, Williams JB, Aquino-Michaels K, Earley ZM, et al. Commensal bifidobacterium promotes antitumor immunity and facilitates

anti-PD-L1 efficacy. *Science* (2015) 350(6264):1084–9. doi: 10.1126/science.aac4255

15. Mao J, Wang D, Long J, Yang X, Lin J, Song Y, et al. Gut microbiome is associated with the clinical response to anti-PD-1 based immunotherapy in hepatobiliary cancers. *J Immunother Cancer* (2021) 9(12):e003334. doi: 10.1136/jitc-2021-003334

16. Zheng Y, Wang T, Tu X, Huang Y, Zhang H, Tan D, et al. Gut microbiome affects the response to anti-PD-1 immunotherapy in patients with hepatocellular carcinoma. *J Immunother Cancer* (2019) 7(1):193. doi: 10.1186/s40425-019-0650-9

17. Cheung KS, Lam LK, Seto WK, Leung WK. Use of antibiotics during immune checkpoint inhibitor treatment is associated with lower survival in hepatocellular carcinoma. *Liver Cancer* (2021) 10(6):606–14. doi: 10.1159/000518090

18. Fessas P, Naeem M, Pinter M, Marron TU, Szafron D, Balcar L, et al. Early antibiotic exposure is not detrimental to therapeutic effect from immunotherapy in hepatocellular carcinoma. *Liver Cancer* (2021) 10(6):583–92. doi: 10.1159/000519108

19. Page MJ, McKenzie JE, Bossuyt PM, Boutron I, Hoffmann TC, Mulrow CD, et al. The PRISMA 2020 statement: an updated guideline for reporting systematic reviews. *BMJ* (2021) 372:n71. doi: 10.1136/bmj.n71

20. Alshammari K, Alsugheir F, Aldawoud M, Alolayan A, Algarni MA, Sabatin F, et al. Association between antibiotic exposure and survival in patients with hepatocellular carcinoma treated with nivolumab. *J Clin Oncol* (2021) 39(15 SUPPL). doi: 10.1200/JCO.2021.39.15_suppl.e16186

21. Chen Q. The impact of antibiotics on efficacy of anti-PD-1 therapy in solid tumors. *Fujian Med Univ* (2018).

22. Chen XJ. Relationship between the efficacy of primary liver cancer and antibiotic applicants for immune checkpoint inhibitors. *Zhengzhou University* (2021).

23. Spahn S, Roessler D, Pompilia R, Gabernet G, Gladstone BP, Horger M, et al. Clinical and genetic tumor characteristics of responding and non-responding patients to PD-1 inhibition in hepatocellular carcinoma. *Cancers (Basel)* (2020) 12 (12):3830. doi: 10.3390/cancers12123830

24. Ren ZG, Gao Y, Wei C, Li X, Liu S, Zhang J, et al. Association between use of antibiotics (ATB) and clinical outcomes with tislelizumab (tisle) monotherapy. *Ann Oncol* (2021) 32:S835. doi: 10.1016/j.annonc.2021.08.1353

25. Jun T, Ozbek U, Dharmapuri S, Hardy-Abeloos C, Zhu H, Lin JY, et al. Antacid exposure and immunotherapy outcomes among patients with advanced hepatocellular carcinoma. *Ther Adv Med Oncol* (2021) 13:17588359211010937. doi: 10.1177/17588359211010937

26. Christofi T, Baritaki S, Falzone L, Libra M, Zaravinos A. Current perspectives in cancer immunotherapy. *Cancers (Basel)* (2019) 11(10):1472. doi: 10.3390/cancers11101472

27. Yu Y, Zheng P, Gao L, Li H, Tao P, Wang D, et al. Effects of antibiotic use on outcomes in cancer patients treated using immune checkpoint inhibitors: A systematic review and meta-analysis. *J Immunother* (2021) 44(2):76–85. doi: 10.1097/CJI.0000000000000346

28. Wilson BE, Routy B, Nagrial A, Chin VT. The effect of antibiotics on clinical outcomes in immune-checkpoint blockade: a systematic review and meta-analysis of observational studies. *Cancer Immunol Immunother* (2020) 69(3):343–54. doi: 10.1007/s00262-019-02453-2

29. Wu Q, Liu J, Wu S, Xie X. The impact of antibiotics on efficacy of immune checkpoint inhibitors in malignancies: A study based on 44 cohorts. *Int Immunopharmacol* (2021) 92:107303. doi: 10.1016/j.intimp.2020.107303

30. Xu H, Xu X, Wang H, Ge W, Cao D. The association between antibiotics use and outcome of cancer patients treated with immune checkpoint inhibitors: A systematic review and meta-analysis. *Crit Rev Oncol Hematol* (2020) 149:102909. doi: 10.1016/j.critrevonc.2020.102909

31. Yang M, Wang Y, Yuan M, Tao M, Kong C, Li H, et al. Antibiotic administration shortly before or after immunotherapy initiation is correlated with poor prognosis in solid cancer patients: An up-to-date systematic review and meta-analysis. *Int Immunopharmacol* (2020) 88:106876. doi: 10.1016/j.intimp.2020.106876

32. Lin RS, Lee FY, Lee SD, Tsai YT, Lin HC, Lu RH, et al. Endotoxemia in patients with chronic liver diseases: relationship to severity of liver diseases, presence of esophageal varices, and hyperdynamic circulation. *J Hepatol* (1995) 22(2):165–72. doi: 10.1016/0168-8278(95)80424-2

33. Dapito DH, Mencin A, Gwak GY, Pradere JP, Jang MK, Mederacke I, et al. Promotion of hepatocellular carcinoma by the intestinal microbiota and TLR4. *Cancer Cell* (2012) 21(4):504–16. doi: 10.1016/j.ccr.2012.02.007

34. Seki E, De Minicis S, Osterreicher CH, Kluwe J, Osawa Y, Brenner DA, et al. TLR4 enhances TGF-beta signaling and hepatic fibrosis. *Nat Med* (2007) 13 (11):1324–32. doi: 10.1038/nm1663

35. Ma C, Han M, Heinrich B, Fu Q, Zhang Q, Sandhu M, et al. Gut microbiome-mediated bile acid metabolism regulates liver cancer *via* NKT cells. *Science* (2018) 360(6391). doi: 10.1126/science.aan5931

36. Gopalakrishnan V, Spencer CN, Nezi L, Reuben A, Andrews MC, Karpinets TV, et al. Gut microbiome modulates response to anti-PD-1 immunotherapy in melanoma patients. *Science* (2018) 359(6371):97–103. doi: 10.1126/science.aan4236

37. Spakowicz D, Hoyd R, Muniak M, Husain M, Bassett JS, Wang L, et al. Inferring the role of the microbiome on survival in patients treated with immune checkpoint inhibitors: causal modeling, timing, and classes of concomitant medications. *BMC Cancer* (2020) 20(1):383. doi: 10.1186/s12885-020-06882-6

38. Herbst DA, Reddy KR. Risk factors for hepatocellular carcinoma. *Clin Liver Dis (Hoboken)* (2012) 1(6):180–2. doi: 10.1002/cld.111

39. Ponziani FR, Nicoletti A, Gasbarrini A, Pompili M. Diagnostic and therapeutic potential of the gut microbiota in patients with early hepatocellular carcinoma. *Ther Adv Med Oncol* (2019) 11:1758835919848184. doi: 10.1177/1758835919848184

40. Levitsky J. Does the liver provide immunosuppressive advantage? *Clin Liver Dis (Hoboken)* (2019) 13(6):180–3. doi: 10.1002/cld.817

41. Han J, Zhang S, Xu Y, Pang Y, Zhang X, Hu Y, et al. Beneficial effect of antibiotics and microbial metabolites on expanded Vδ2Vγ9 T cells in hepatocellular carcinoma immunotherapy. *Front Immunol* (2020) 11:1380. doi: 10.3389/fimmu.2020.01380

42. Wells G, Shea B, O'Connell D. *The Newcastle-Ottawa scale (NOS) for assessing the quality if nonrandomizes studies in meta-analyses*. Available at: http://www.ohri.ca/programs/clinical_epidemiology/oxford.asp (Accessed 29 December 2019).

frontiers | Frontiers in Immunology

TYPE Original Research
PUBLISHED 25 August 2022
DOI 10.3389/fimmu.2022.898498

OPEN ACCESS

EDITED BY
Xuesong Gu,
Beth Israel Deaconess Medical Center and Harvard Medical School, United States

REVIEWED BY
Mélanie Bruchard,
INSERM U1231 Lipides, Nutrition, Cancer (LNC), France
Constantinos Zambirinis,
The State University of New Jersey, United States
Pierpaolo Correale,
Azienda ospedaliera 'Bianchi-Melacrino-Morelli', Italy

*CORRESPONDENCE
Casper H. J. van Eijck
c.vaneijck@erasmusmc.nl

SPECIALTY SECTION
This article was submitted to Cancer Immunity and Immunotherapy, a section of the journal Frontiers in Immunology

RECEIVED 18 March 2022
ACCEPTED 26 July 2022
PUBLISHED 25 August 2022

CITATION
van der Sijde F, Dik WA, Mustafa DAM, Vietsch EE, Besselink MG, Debets R, Koerkamp BG, Haberkorn BCM, Homs MYV, Janssen QP, Luelmo SAC, Mekenkamp LJM, Oostvogels AAM, Smits-te Nijenhuis MAW, Wilmink JW, van Eijck CHJ and the Dutch Pancreatic Cancer Group (2022) Serum cytokine levels are associated with tumor progression during FOLFIRINOX chemotherapy and overall survival in pancreatic cancer patients.
Front. Immunol. 13:898498.
doi: 10.3389/fimmu.2022.898498

Serum cytokine levels are associated with tumor progression during FOLFIRINOX chemotherapy and overall survival in pancreatic cancer patients

Fleur van der Sijde[1], Willem A. Dik[2], Dana A. M. Mustafa[3], Eveline E. Vietsch[1], Marc G. Besselink[4], Reno Debets[5], Bas Groot Koerkamp[1], Brigitte C. M. Haberkorn[6], Marjolein Y. V. Homs[7], Quisette P. Janssen[1], Saskia A. C. Luelmo[8], Leonie J. M. Mekenkamp[9], Astrid A. M. Oostvogels[5], Marja A. W. Smits-te Nijenhuis[2], Johanna W. Wilmink[10], Casper H. J. van Eijck[1]* and the Dutch Pancreatic Cancer Group

[1]Erasmus MC Cancer Institute, Department of Surgery, University Medical Center Rotterdam, Rotterdam, Netherlands, [2]Laboratory of Medical Immunology, Department of Immunology, Erasmus MC, University Medical Center Rotterdam, Rotterdam, Netherlands, [3]Tumor Immuno-Pathology Laboratory, Department of Pathology, Erasmus MC, University Medical Center Rotterdam, Rotterdam, Netherlands, [4]Cancer Center Amsterdam, Department of Surgery, Amsterdam UMC, University of Amsterdam, Amsterdam, Netherlands, [5]Laboratory of Tumor Immunology, Department of Medical Oncology, Erasmus MC, University Medical Center Rotterdam, Rotterdam, Netherlands, [6]Department of Medical Oncology, Maasstad Hospital, Rotterdam, Netherlands, [7]Department of Medical Oncology, Erasmus MC, University Medical Center Rotterdam, Rotterdam, Netherlands, [8]Department of Medical Oncology, Leiden University Medical Center, Leiden, Netherlands, [9]Department of Medical Oncology, Medisch Spectrum Twente, Enschede, Netherlands, [10]Cancer Center Amsterdam, Department of Medical Oncology, Amsterdam UMC, University of Amsterdam, Amsterdam, Netherlands

Background: Biomarkers predicting treatment response may be used to stratify patients with pancreatic ductal adenocarcinoma (PDAC) for available therapies. The aim of this study was to evaluate the association of circulating cytokines with FOLFIRINOX response and with overall survival (OS).

Methods: Serum samples were collected before start and after the first cycle of FOLFIRINOX from patients with PDAC (n=83) of all disease stages. Overall, 34 circulating cytokines were analyzed with a multiplex immunoassay. In addition, changes in peripheral blood immune cell counts were determined by flow cytometry to correlate with differences in cytokine levels. Chemotherapy response was determined by CT scans with the RECIST 1.1 criteria, as disease control (n=64) or progressive disease (n=19) within eight cycles of FOLFIRINOX.

Results: Patients with high serum IL-1RA concentrations after one cycle of chemotherapy were less likely to have tumor progression during FOLFIRINOX (OR 0.25, *P*=0.040). Increase of circulating IL-1RA concentrations correlated with increase of total, classical (CD14+CD16-), and non-classical monocytes (CD14-CD16+), and dendritic cells. In multivariable cox regression, including the variables chemotherapy response outcome and baseline CA19-9 level, serum concentrations of IL-7 (HR 2.14, *P*=0.010), IL-18 (HR 2.00, *P*=0.020), and MIP-1β (HR 0.51, *P*=0.025) after one cycle of FOLFIRINOX showed correlations with OS.

Conclusions: Circulating IL-1RA, IL-7, IL-18, and MIP-1β concentrations are biomarkers associated with FOLFIRINOX response in PDAC patients, suggesting an important role for specific immune cells in chemotherapy response and PDAC progression. Cytokine-based treatment might improve patient outcome and should be evaluated in future studies.

KEYWORDS

pancreatic cancer, biomarker, treatment response, cytokine, IL-1RA

Introduction

FOLFIRINOX is a combined chemotherapy regimen, including fluorouracil, leucovorin, irinotecan and oxaliplatin. It is currently the standard first-line treatment for locally advanced (LAPC) and metastatic pancreatic ductal adenocarcinoma (PDAC). Although the survival of patients with PDAC has improved with the implementation of this chemotherapy combination, the overall prognosis remains poor. Patients with LAPC have a median overall survival (OS) of approximately two years (1), whereas metastatic disease patients a median OS of 11 months after FOLFIRINOX treatment (2). Meanwhile, 60-70% of these patients will experience FOLFIRINOX-induced toxicity (1–3), affecting their quality of life. Therefore, biomarkers with the ability to predict treatment response or with prognostic properties are urgently needed to personalize treatment and to avoid unnecessary toxicity (4).

Prognostic biomarkers are biomarkers that can be used to identify the likelihood of a clinical event, recurrence of disease or disease progression. Predictive biomarkers can be used to identify individuals that will experience a favorable or unfavorable effect from exposure to a medical product (e.g. chemotherapy) compared to patients without this biomarker (5). The predictive value of a biomarker needs to be confirmed in a study including at least two treatment groups, preferably a randomized controlled trial, to prove its treatment-specific effect and exclude prognostic effects (6). For this patient population it could mean that patients not responding to FOLFIRINOX might benefit from other types of chemotherapy, such as gemcitabine with nab-paclitaxel.

Cancer cells display pro-inflammatory properties, inducing a tumor-promoting environment (7). PDAC is thought to be an inflammation-driven cancer; the tumor microenvironment includes predominantly pro-inflammatory instead of tumor-suppressive immune cells, supporting cancer progression (8). Several systemic inflammation markers, such as the systemic immune-inflammation index (9), neutrophil-to-lymphocyte ratio (10), or Glasgow prognostic score (11) are of prognostic significance and alterations can be detected even prior to PDAC diagnosis (12, 13).

The stromal microenvironment of PDAC is a complex structure of extracellular matrix, fibroblasts, and inflammatory cells (14). These inflammatory cells produce a variety of growth factors, cytokines, and chemokines (14, 15). Cytokines are signaling molecules that play an important role in the interaction and function of cells. Cytokines are mainly produced by immune cells, but also normal epithelial cells, stromal cells, fibroblasts, and cancer cells can produce both pro-inflammatory and anti-inflammatory cytokines (10). High levels of circulating immunosuppressive, tumor-promoting cytokines, such as transforming growth factor-beta (TGF-β), interleukin (IL)- 1β, IL-6, IL-8, and tumor necrosis factor-alpha (TNF-α), and lower levels of tumor-suppressive cytokines, e.g. IL-11, IL-12, and interferon-gamma (IFN-γ), have been found to correlate with poor prognosis in PDAC patients (16–21). Circulating cytokine concentrations might reflect tumor aggressiveness and immune status associated with tumor progression (22). Whether circulating cytokine levels can also predict the response to FOLFIRINOX is yet unknown. We hypothesized that dysregulation of the immune system, demonstrated by an

increase of pro-inflammatory and decrease of anti-inflammatory cytokines, is prone to FOLFIRINOX non-response.

In this study, we evaluated the levels of circulating cytokine concentrations before and after one cycle of FOLFIRINOX, and assessed differences between patients with and without progressive disease at chemotherapy response evaluation CT scans. In addition, peripheral blood immune cell subsets were measured and correlations with changes in cytokine concentrations were determined in order to affirm the origin of these cytokines. Also, the association with early tumor progression during FOLFIRINOX and prognostic value for OS of individual cytokine markers was assessed.

Materials and methods

This article was written according to the Reporting recommendations for tumor marker prognostic studies (REMARK) guidelines (23).

Study design

Patients were selected from the local pancreatic biobank at the Erasmus MC, Rotterdam (MEC-2015-085) and participated in two multicenter, prospective trials conducted in the Netherlands. Patients with resectable or borderline resectable PDAC participated in the randomized clinical trial PREOPANC-2 (Dutch trial register NL7094, MEC-2018-004) comparing neoadjuvant FOLFIRINOX chemotherapy to neoadjuvant gemcitabine-based chemoradiotherapy, followed by surgical resection of the primary tumor (24). Patients with LAPC or metastatic PDAC participated in the iKnowIT study (Dutch trial register NL7522, MEC-2018-087), a prospective cohort study investigating the predictive value of circulating biomarkers. All trials were approved by the ethics committees of all participating centers: Erasmus MC, University Medical Center (Rotterdam, the Netherlands), Amsterdam UMC (Amsterdam, the Netherlands), Maasstad Hospital (Rotterdam, the Netherlands), and Medisch Spectrum Twente (Enschede, the Netherlands), and conducted in accordance with the declaration of Helsinki.

Patient selection

All patients had histologically confirmed PDAC and were treated with first-line FOLFIRINOX between February 2015 and October 2019. Patients with resectable, borderline resectable, or locally advanced disease were scheduled for eight cycles of FOLFIRINOX and patients with metastatic disease for maximum twelve cycles of FOLFIRINOX, according to the PREOPANC-2 study protocol (resectable or borderline resectable disease) or the current standard of care in the Netherlands (LAPC and metastatic disease). Exclusion criteria were: age <18 years, co-medication with other chemotherapeutics, and previous treatment with FOLFIRINOX chemotherapy. A CT scan was performed before start of treatment and after each fourth cycle of chemotherapy to evaluate treatment response, based on the Response Evaluation Criteria in Solid Tumours (RECIST) 1.1 criteria, as part of standard clinical practice. Differences in circulating cytokine levels were tested between patients with disease control patients, including those with stable disease, partial response or complete response to FOLFIRINOX, and progressive disease patients, if CT evaluation showed progression within eight cycles of FOLFIRINOX.

Patient characteristics, such as age, sex, stage of disease, laboratory results, CT scan evaluations, and follow-up data were retrieved from medical records by a medical doctor. Follow-up ended upon the death of the patient. Due to the explorative character of this study, no formal sample size calculation was performed.

Sample collection

Peripheral venous blood samples were collected before the start of chemotherapy and before the start of the second cycle of FOLFIRINOX, approximately two weeks later. Blood was collected in 10 mL serum tubes (Becton Dickinson, Franklin Lakes, NJ, USA) and 10 mL EDTA tubes (Becton Dickinson, Franklin Lakes, NJ, USA). Serum tubes were centrifuged at room temperature for 10 minutes at 1000g. Serum was then divided in aliquots and stored at -80°C until further use. Freshly obtained whole blood from EDTA tubes was used within 24 hours to enumerate immune cell populations.

Cytokine detection

All serum samples were first analyzed with the ProcartaPlex Cytokine & Chemokine Convenience 34-Plex Human Panel 1A immunoassay (Invitrogen, Carlsbad, CA, USA, for detail see Supplementary Table 1), and measured using the Luminex MAGPIX system (Luminex, Austin TX, USA). Only cytokines detected in at least 70% of samples were used for further analyses. The cytokines IL-1β, IL-1RA, IL-2, and IL-18 were also measured using (high sensitivity) immunoassays from a different supplier (R&D systems, Minneapolis, MN, USA, Supplementary Table 1). In addition, soluble IL-2 receptor (sIL-2R) was quantified with enzyme-linked immunosorbent assay (ELISA; Diaclone, Besançon, France) as a sensitive marker for T-lymphocyte activation and regulator of IL-2-dependent cell function (25, 26).

Serum samples were subjected to a maximum of three freeze-thaw cycles and thawed on ice prior to use. Supernatants were loaded on Luminex or ELISA plates at the

recommended dilutions with standard protein controls, according to the manufacturer's instructions. For Luminex assays, cytokines were quantified by the analysis of raw data using xPONENT 4.2 software (Luminex, Austin, TX, USA). For the ELISA assay, standard curves were constructed and used to quantify sIL-2R. Further technical details are shown in Supplementary Table 1.

Immune cell enumeration

Flow cytometry was performed to quantify main granulocyte, monocyte, and lymphocyte subsets (Supplementary Table 2). Peripheral blood samples for immunophenotyping were available for 50/83 patients (60.2%). Whole blood was stained with monoclonal antibodies (MoAb) and after lysis of red blood cells analyzed by multi-color FCM on a BD 3-laser Celesta flow cytometer using FACSDiva 8.x software (Becton Dickinson, Franklin Lakes, NJ, USA). An overview of the monoclonal antibodies used is available in Supplementary Table 3. Absolute cell counts were determined using Flow-Count Fluorospheres (Beckman Coulter, Brea, CA, USA). The MoAb panel has been optimized, and compensated using Fluorescence minus one (FMO) controls (27). Data were gated and analyzed using FlowJo software (Tree Star, San Carlos, CA, USA). The gating strategy is presented in Supplementary Figure 1.

Statistical analysis

Detection rates of cytokines were compared between disease control and progressive disease patients using Fisher's exact tests, and with Chi-squared test for the comparison between the different stages of disease. Absolute circulating cytokine concentrations and immune cell counts, and the percentage increase of cytokine concentrations and immune cell numbers between disease control and progressive disease patients were compared with Mann-Whitney U tests. The comparison of cytokine concentrations between patients with resectable, LAPC, and metastatic disease was calculated with Kruskal-Wallis tests. Correlations between alterations in cytokine concentrations and immune cell numbers were determined with Pearson's correlation coefficient.

Univariable and multivariable binary logistic regression was performed to analyze the predictive value of circulating cytokine levels for tumor progression during FOLFIRINOX chemotherapy, including patient characteristics with known association with treatment outcome: stage of disease and baseline CA19-9 levels. Cytokine levels were dichotomized based on the median concentration for each individual cytokine per time point of measurement.

Overall survival (OS) was calculated as the time between the start of FOLFIRINOX and death. The prognostic value of circulating cytokine levels was tested with univariable and multivariable Cox regression analysis, including known prognostic factors: age, stage of disease, chemotherapy response, and baseline CA19-9 levels. Differences in median OS were derived from Kaplan-Meier curves whereby groups of patients with cytokine levels below or above the median concentration were compared using log-rank tests.

Only two-sided tests were used and *P*-values <0.05 were considered statistically significant. Data were analyzed using SPSS Statistics for Windows (version 25.0; IBM, Armonk, NY, USA).

Results

Patient characteristics

In total, cytokine data obtained from 166 samples from 83 PDAC patients were available for analysis. Patient characteristics are presented in Table 1. The cohort consisted of patients from all disease stages: 34% was diagnosed with resectable or borderline resectable disease, 42% with LAPC, and 24% with metastatic disease. In this cohort, 19 (23%) patients showed progressive disease during FOLFIRINOX.

Cytokine detection rates and treatment response outcome

Supplementary Table 4 gives an overview of the 34 cytokines and chemokines measured using a multiplex panel, showing their detection rate, mean concentrations with standard deviation, and median concentrations with interquartile range. GM-CSF, GRO-α, IL-5, IL-12p70, IL-23, IL-31, and TNF-β were not detected in any of the samples. Eotaxin, IP-10, MIP-1β, RANTES, SDF-1α were detected in all serum samples. Comparisons of cytokine detection rates between patients with disease control and patients with progressive disease during FOLFIRINOX are presented in Table 2. Before the start of FOLFIRINOX, IL-1β (28% vs 5%) and IL-2 (18% vs 0%) were more often detected in samples from disease control patients then in samples from progressive disease patients (both *P*=0.059). After one cycle of FOLFIRINOX, IL-1RA was more often detected in patients with disease control (48%) compared to patients with progressive disease (21%, *P*=0.038).

To improve the detection rates of IL-1β, IL-1RA, IL-2, and IL-18, these cytokines were re-analyzed with high sensitivity singleplex or duplex immunoassay from a different manufacturer (Supplementary Table 1). Eotaxin, IL-7, IP-10, MCP-1, MIP-1β, RANTES, and SDF-1α all met the inclusion criteria of detection in >70% of samples and were selected for further analyses. Together with the sIL-2R, a total of eleven cytokines were used to create predictive and prognostic models.

TABLE 1 Patient characteristics.

	All patients, *n*=83 (%)
Age (years), median (IQR)	64 (58-70)
Sex, male	47 (57)
Stage of disease	
Resectable or borderline resectable	28 (34)
Locally advanced	35 (42)
Metastatic	20 (24)
Response[a] to FOLFIRINOX	
Stable disease	54 (65)
Partial response	10 (12)
Progressive disease	19 (23)
Response[a] to FOLFIRINOX, dichotomized	
Disease control	64 (77)
Progressive disease	19 (23)
Time point of CT evaluation progressive disease* (n=19)	
After cycle 1	1 (5)
After cycle 2	3 (16)
After cycle 3	2 (11)
After cycle 4	9 (47)
After cycle 6	1 (5)
After cycle 8	3 (16)
Number of cycles of FOLFIRINOX received, median (IQR)	8 (4-8)
Baseline CA19-9 (kU/L), median (IQR)	320 (60-1296)

CA19-9, carbohydrate antigen 19-9; IQR, interquartile range. [a]According to the RECIST 1.1 criteria.

Cytokine concentrations and treatment response outcome

In Supplementary Table 5 we show the comparisons between cytokine detection rates and cytokine concentrations between patients with resectable, LAPC, and metastatic disease both before and after one cycle of FOLFIRINOX. There were no statistically significant differences between the different stages of disease and we did not perform additional analyses for the individual disease stage groups, also because of the limited number of patients per disease stage.

IL-1β and IL-2 results were only available for 88 samples (*n*=44 patients). The other samples could not be used due to absence of detectable bead signals. With individual assays, IL-1β, IL-1RA, IL-18 and sIL-2R were detected in all available samples. IL-2 was detected in only 28% of samples and results of this cytokine will therefore not be further discussed.

There were no significant differences in median concentrations of any of the eleven cytokines (Eotaxin, IL-1β, IL-1RA, sIL-2R, IL-7, IL-18, IP-10, MCP-1, MIP-1β, RANTES, SDF-1α) between disease control and progressive disease patients in samples drawn before the start or after one cycle of FOLFIRINOX. However, pro-inflammatory/tumor-promoting cytokines (eotaxin, IL-1β, IL-18) seemed to be found in higher concentrations in progressive disease patients, while disease control patients showed higher levels of anti-inflammatory/tumor-suppressive cytokines (IL-1RA, sIL-2R, IL-7), as presented in Figure 1A.

In patients with disease control, IL-18 showed a larger increase during FOLFIRINOX (median increase 89%; IQR 46-142%) compared to patients with progressive disease (median increase 44%; IQR 11-81%), *P*=0.007), visualized in Figure 1B. An overview of cytokine concentrations during treatment for all cytokines investigated is included in Supplementary Figure 2.

Cytokine concentrations in a predictive model

To investigate the value of individual cytokine concentrations to predict early tumor progression during FOLFIRINOX, a binary logistic regression model was created. Early tumor progression was defined as progression of disease during or immediately after FOLFIRINOX treatment, established on CT scans using the RECIST 1.1 criteria. From univariable analyses, the variables IL-1RA concentration after one cycle of FOLFIRINOX (OR 0.19, 95% CI 0.06-0.63), IL-18 before the start of FOLFIRINOX (OR 2.62, 95% CI 0.88-7.74), an increase of IL-18 (OR 0.33, 95% CI 0.11-0.94), and an increase of MIP-1β (OR 0.37, 95% CI 0.13-1.08) were selected for multivariable analyses. In this patient cohort, stage of disease and baseline CA19-9 level did not predict early tumor progression. The results of the univariable and multivariable analyses are presented in Table 3. In multivariable analysis, only IL-1RA concentration after one cycle of FOLFIRINOX remained an independent predictor of FOLFIRINOX response (OR 0.25; 95% CI 0.07-0.094, *P*=0.040). Patients with IL-1RA concentrations above the median of the measurements showed a lower risk of early tumor progression during FOLFIRINOX.

Correlation between cytokines and immune cells

IL-1RA, IL-18, and MIP-1β, predictors of early tumor progression in univariable analysis, are cytokines produced by monocytes (28–30). Therefore a correlation matrix was made between the percentage increase of serum concentrations of these cytokines and the percentage increase of monocyte cell numbers, based on results available from 50 patients (Figure 2). The increase of circulating IL-1RA concentrations correlated significantly with total monocytes (Pearson's r=0.69, *P*<0.001), classical monocytes (r=0.63, *P*<0.001), non-classical monocytes,

TABLE 2 Comparison of detection rates of cytokines and chemokines between patients with disease control and patients with progressive disease during FOLFIRINOX, measured with a multiplex Luminex panel.

Before start of FOLFIRINOX

Cytokine/chemokine	Detection rate disease control (%), *n*=64	Detection rate progressive disease (%), *n*=19	*P*
IFN-γ	4 (6)	1 (5)	1.000
IL-1α	12 (19)	4 (21)	1.000
IL-1β	18 (28)	1 (5)	0.059
IL-1RA	2 (3)	1 (5)	0.547
IL-2	12 (19)	0 (0)	0.059
IL-6	1 (2)	1 (5)	0.408
IL-7	45 (70)	14 (74)	1.000
IL-10	2 (3)	0 (0)	1.000
IL-15	6 (9)	0 (0)	0.328
IL-17A	13 (20)	1 (5)	0.172
IL-18	29 (45)	6 (32)	0.428
IL-21	6 (9)	1 (5)	1.000
IL-22	5 ()	0 (0)	0.584
IL-27	5 (78)	0 (0)	0.584
MCP-1	62 (97)	18 (95)	0.547
MIP-1α	18 (28)	5 (26)	1.000
TNF-α	10 (16)	0 (0)	0.107
After 1 cycle of FOLFIRINOX			
Cytokine/chemokine	**Detection rate disease control (%), *n*=64**	**Detection rate progressive disease (%), *n*=19**	***P***
IFN-γ	6 (9)	1 (5)	1.000
IL-1α	11 (17)	3 (16)	1.000
IL-1β	14 (21)	4 (21)	1.000
IL-1RA	31 (48)	4 (21)	0.038[a]
IL-2	10 (16)	0 (0)	0.107
IL-6	4 (6)	2 (11)	0.616
IL-7	45 (70)	13 (68)	1.000
IL-10	3 (5)	0 (0)	1.000
IL-15	4 (6)	0 (0)	0.569
IL-17A	14 (22)	2 (11)	0.340
IL-18	44 (69)	11 (58)	0.416
IL-21	4 (6)	2 (11)	0.616
IL-22	4 (6)	1 (5)	1.000
IL-27	5 (8)	0 (0)	0.584
MCP-1	62 (97)	17 (90)	0.223
MIP-1α	13 (20)	4 (21)	1.000
TNF-α	8 (13)	1 (5)	0.677

IFN, interferon; IL, interleukin; IL-1RA, interleukin-1 receptor antagonist; IP-10, interferon gamma-induced protein 10; MCP, monocyte chemoattractant protein; MIP, macrophage inflammatory protein; TNF, tumor necrosis factor. [a]Significant P-value.
P-values are calculated by Fisher's exact tests.

and dendritic cell (r=0.41, *P*=0.011) increase in the peripheral blood (r=0.66, *P*<0.001). IL-18 correlated with total monocytes (r=0.39, *P*=0.015), and classical monocytes (r=0.40, *P*=0.014). MIP-1β correlated with dendritic cells (r=0.45, *P*=0.004), and classical monocytes (r=0.33, *P*=0.046). Also, the cytokines in this correlation plot were correlated to the other cytokines as well (Pearson's correlation between IL-1RA - IL-18 r=0.52, IL-1RA - MIP-1β r=0.50, IL-18 - MIP-1β r=0.39, all P<0.001), meaning that an increase after FOLFIRINOX for one cytokine is accompanied by the increase of the other cytokine concentrations.

Overall, an increase in all determined immune cell types was observed after one cycle of FOLFIRINOX (Supplementary Figure 3). There were no statistically significant differences in cell numbers before the start of FOLFIRINOX, after one cycle of FOLFIRINOX or in increase over time between disease control and progressive patients. However, we could detect a trend

10.3389/fimmu.2022.898498

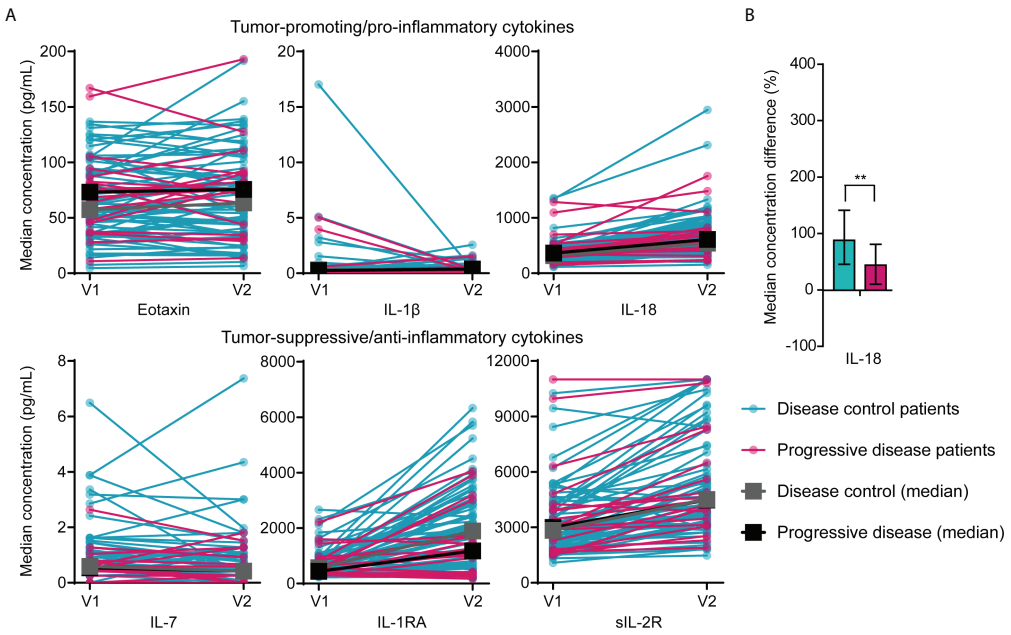

FIGURE 1
Differences in circulating cytokine concentrations between patients with disease control and patients with progressive disease during FOLFIRINOX treatment. **(A)** Concentrations of pro-inflammatory (eotaxin, IL-1β, and IL-18) and anti-inflammatory cytokines (IL-7, IL-1RA, sIL-2R) in serum of individual patients with disease control (n=64) and patients with progressive disease (n=19) before start of FOLFIRINOX (V1) and after one cycle of FOLFIRINOX (V2) and the median concentration over time for the two response groups. Median concentrations before or after one cycle did not show statistical significant differences between the two groups. **(B)** Percentage increase of serum IL-18 concentrations after one cycle of FOLFIRINOX in patients with disease control and progressive disease. $^{**}P < 0.01$, calculated with Mann-Whitney U test.

towards a stronger increase of tumor-suppressive cells (e.g. neutrophils, B cells, NK cells, and monocytes) in disease control patients, together with a slight increase of immunosuppressive cells (e.g. γδ T cells) in progressive disease patients, as shown in Figure 3. However, there was also an increasing trend in T cells visible, including T helper cells and/or regulatory T cells (CD4+) and cytotoxic T cells (CD8+), in progressive disease patients.

TABLE 3 Univariable and multivariable binary logistic regression model for the prediction of early tumor progression during FOLFIRINOX.

Variable	Univariable		Multivariable	
	OR for progressive disease(95% CI)	*P*	OR for progressive disease(95% CI)	*P*
IL-1RA after 1 cycle of FOLFIRINOX				
<median	Ref		Ref	
>median	0.19 (0.06-0.63)	0.007[a]	0.25 (0.07-0.94)	0.040[a]
IL-18 before start of FOLFIRINOX				
<median	Ref		Ref	
>median	2.62 (0.88-7.74)	0.083	2.08 (0.63-6.92)	0.231
IL-18 increase during 1 cycle of FOLFIRINOX				
≤50%	Ref		Ref	
>50%	0.33 (0.11-0.94)	0.038[a]	0.66 (0.119-2.27)	0.506
MIP-1β increase during 1 cycle of FOLFIRINOX				
No	Ref		Ref	
Yes	0.37 (0.13-1.08)	0.069	0.73 (0.21-2.48)	0.729

CI, confidence interval; IL, interleukin; IL-1RA, interleukin-1 receptor antagonist; MIP, macrophage inflammatory protein; OR, odds ratio; Ref, reference. [a]Significant P-value.

10.3389/fimmu.2022.898498

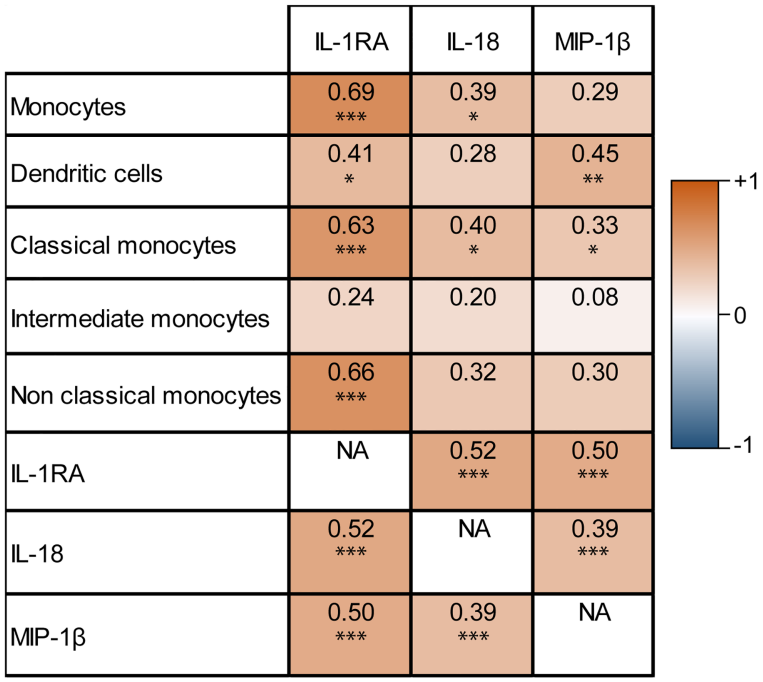

FIGURE 2
Correlation matrix of monocyte-related serum cytokine concentration increase and circulating monocyte cell number increase after one cycle of FOLFIRINOX. Increasing IL-1RA, IL-18, and MIP-1β concentrations after one cycle of FOLFIRINOX showed significant correlations with the increase of several subsets of monocytes. *$P < 0.05$, **$P < 0.01$, ***$P < 0.001$, calculated with Pearson's correlation. NA = 'not applicable' in the correlation matrix.

Cytokines associated with overall survival

The median follow-up time was 16.5 months for patients alive at last follow-up. Median OS for the total cohort was 12.5 months. Median OS was different for patients of the three disease stages; resectable disease 13.2 months, LAPC 15.7 months, and metastatic disease 9.0 months (P=0.008). In univariable analyses, IL-1RA concentration after FOLFIRINOX (HR 0.64 for concentrations above the median of measurements), sIL-2R before the start of FOLFIRINOX (HR 1.55), IL-7 after FOLFIRINOX (HR 1.57), IL-18 before (HR 1.56) and after FOLFIRINOX (HR 1.57), and MIP-1β after FOLFIRINOX (HR 0.63) were statistically significant predictors for OS, as shown in Supplementary Table 6. In multivariable analysis, including the variables baseline CA19-9 and RECIST treatment response outcome, IL-7 (HR 2.14; 95% CI 1.20-3.80, P=0.010), IL-18 (HR 2.00; 95% CI 1.11-3.60, P=0.020), and MIP-1β (HR 0.51; 95% CI 0.28-0.92, P=0.025) concentrations measured after one cycle of FOLFIRINOX remained significant prognostic factors for OS after FOLFIRINOX treatment. Patients with a high level of IL-7 and IL-18, and low level of MIP-1β were at risk for shorter OS. Stage of disease was not a prognostic variable in our Cox proportional hazards model (LAPC HR 0.61, P=0.113, metastatic disease HR 1.63, P=0.139). In Supplementary Figure 4 Kaplan-Meier curves are shown for overall survival in patients with cytokine levels below or above the median cytokine concentration in this cohort for IL-1RA, IL-7, IL-18, and MIP-1β. High IL-1RA and MIP-1β and low IL-7 concentrations after one cycle of FOLFIRINOX show a trend of better overall survival after FOLFIRINOX treatment, though not statistically significant (respectively P=0.095, P=0.074, and P=0.087). IL-18 levels after FOLFIRINOX do not influence overall survival in these Kaplan-Meier curves (P=0.789).

Discussion

In this multicenter study, we investigated serum cytokine concentrations in PDAC patients treated with FOLFIRINOX and the correlations of these cytokines with treatment response and prognosis. We found that most cytokines showed increasing concentrations after one cycle of FOLFIRINOX compared to baseline. However, IL-18 showed a stronger increase in patients responding to treatment. Low IL-1RA serum concentrations after one cycle of FOLFIRINOX were associated with an increased risk of early tumor progression during FOLFIRINOX. In addition, high IL-18 and IL-7, and low MIP-1β concentrations after one cycle of FOLFIRINOX were poor prognostic factors for OS. Our results support the hypothesis

10.3389/fimmu.2022.898498

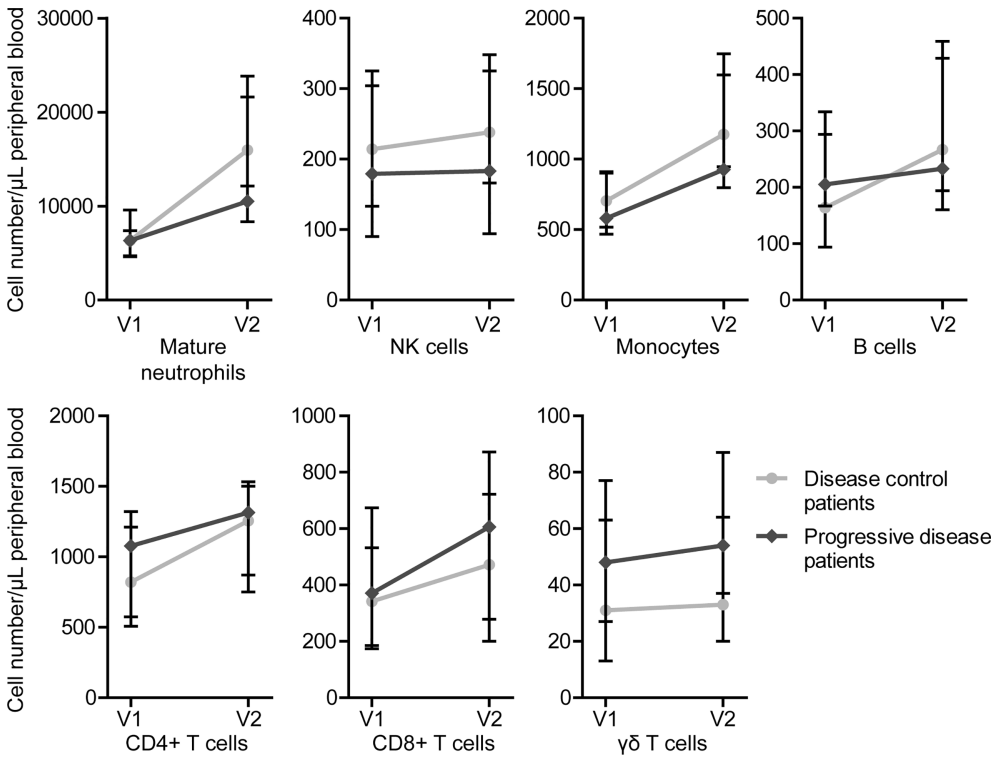

FIGURE 3
Circulating immune cell numbers in patients with disease control and patients with progressive disease before start of FOLFIRINOX (V1) and after one cycle of FOLFIRINOX (V2). Circulating cell numbers of mature neutrophils, NK cells, monocytes, B cells, and CD4+ T cells showed a larger increase in patients with disease control, CD8+ and γδ T cells in patients with progressive disease. Data is presented as median cell numbers with interquartile ranges.

that prognosis in PDAC patients is at least partially determined by the activation level of the immune system and its response to cancer cells (7). We found a clear serum cytokine pattern in patients with disease control and patients with progressive disease during FOLFIRINOX. Favorable, anti-inflammatory cytokines, such as IL-1RA, IL-7, and MIP-1β were detected in higher concentrations in responding patients, while pro-inflammatory, tumor-promoting cytokines, such as IL-18 and IL-1β, were higher in patients with early progressive disease.

The correlation we observed between IL-1RA, IL-18 and MIP-1β with different monocyte subsets might indicate that differences in cytokine concentrations are related to differences in the immune environment and cellular response to chemotherapy. Though, the strong increase of T cells, including cytotoxic T cells (CD8+) and CD4+ cells including both T helper cells as well as regulatory T cells, in progressive disease patients, was unexpected. However, it is not clear whether the increase of all the investigated cell types might be explained by the increased cell proliferation in reaction to chemotherapy-induced cell death, by the administration of granulocyte colony-stimulating factor (G-CSF) after every chemotherapy cycle, or as a result of the proliferative effect on immune cells of FOLFIRINOX (31). Furthermore, we did not investigate the functional status and exhaustion rate of CD4+ and CD8+ cell populations, which is crucial in further studies.

The results found in this study are affirmed by existing literature on circulating cytokine levels and outcome in PDAC patients. Circulating IL-18 levels were previously found to increase during treatment with gemcitabine in combination with 5-FU or oxaliplatin, and higher IL-18 levels were associated with shorter OS (32). IL-1β is thought to facilitate tumor growth, angiogenesis, and metastasis in PDAC and may therefore negatively influence patient prognosis (17, 19). Both IL-18 and IL-1β are associated with objective gemcitabine-based chemotherapy response (19, 33). Also, MIP-1β and RANTES have been shown to associate with PDAC patient outcome (34, 35).

An interesting finding is that most cytokines with prognostic value in our study relate to the nuclear factor-κB (NF-κB) pathway, which plays a crucial role in the regulation of a plethora of inflammatory genes (36). The NF-κB signaling cascade is usually activated by pathogens, damaged tissue, and necrotic cells, and it includes a negative feedback loop, regulating its own activity (37). In cancer environments the NF-κB

signaling pathway is continuously activated, resulting in constant production of large amounts of pro-inflammatory cytokines. Activation of the NF-κB pathway promotes all hallmarks of cancer: tumor cell proliferation and survival, angiogenesis, metastasis, and immune suppression (36, 38). IL-1β, which was found in higher concentrations in patients with poor prognosis, is a known activator of the NF-κB pathway (39). Also, several DNA mutations can activate the pathway (39, 40), including *KRAS* and *TP53* mutations which are found in almost all PDAC tumors (41). IL-1RA, the natural antagonist of IL-1, may regulate activation of the NF-κB pathway, thus reducing the negative effects of the pathway and improving patient prognosis (40).

Other cytokines which are also controlled by NF-κB were not or only in a limited number of patient samples detected. For example, TNF-α, IL-6, and IL-8, cytokines that have been shown to be upregulated in PDAC patients (17, 19, 42), were only detected in a limited number of samples. The relatively low serum cytokine concentrations and therefore lack of detection, is probably the most important limitation of this study. The cytokine concentrations measured in our study seem to be low in comparison to other studies with PDAC patients (17, 19, 35). This may be related to the immunoassay used to detect the cytokines. We chose to start our pilot project with a broad multiplex panel to screen for 34 different cytokines. Only small serum volumes were needed, which was an advantage because of the limited availability of serum from our patients, included in large multicenter, prospective studies. However, the small sample volumes in the discovery panel might explain the low detection rate of cytokines and increased sensitivity with the individual cytokine assays using larger serum volumes.

In this pilot study, the sample size was relatively small and cytokine concentrations and immune cell numbers varied widely between patients, also resulting in wide interquartile ranges for the median IL-1RA concentration. Most of our findings did therefore not reach statistical significance and we could only highlight some trends in cytokine and cell count differences between treatment response groups. The number of variables analyzed in this study might have led to a type I error. Though, we deliberately did not correct our raw data for multiple testing since this could result in type II errors, which are acceptable in exploratory studies such as this one. Unfortunately, subgroup analyses for the individual disease stages could not be performed due to the limited number of patients. Though, we did not find differences in cytokine detection rates or concentrations between patients of different disease stages.

In this study, we focus on responders and non-responders to FOLFIRINOX. In our dataset, the objective response rate (ORR) was 12% and the disease control rate 77%. Especially the ORR is lower than reported outcomes from other FOLFIRINOX clinical trials with ORR varying between 16-40% for metastatic patients (3, 43) and 17-30% for LAPC patients (41, 44, 45). The benefit of treatment, however, is often overestimated due to exclusion of patients with poor prognosis in clinical trials and are therefore not comparable to real-world data.

In the future, the predictive and prognostic value of IL-1RA must be confirmed in a large clinical trial including two different treatment arms, preferably a randomized clinical trial comparing FOLFIRINOX to gemcitabine with nab-paclitaxel outcomes. The future clinical implications of this study should include the evaluation of the additive effects of cytokine-based therapy on chemotherapy response and survival in PDAC patients. Studies with mouse models have already shown promising results of treatment with anakinra, an FDA-approved human IL-1RA protein drug used for rheumatoid arthritis. Anakinra inhibits IL-1 and by that the NF-κB pathway, reducing proliferation, migration, and invasion of PDAC cells, and IL-1 neutralization sensitizes cancer cells for immunotherapy and chemotherapy (40, 46). At this moment, two clinical trials are investigating the benefit of anakinra in addition to FOLFIRINOX (ClinicalTrials.gov identifier: NCT02021422) or gemcitabine chemotherapy (NCT02550327) in PDAC patients. Restoring the imbalance of tumor-promoting and tumor-suppressing components of the immune system might be the future of PDAC treatment.

Conclusion

Low circulating IL-1RA cytokine concentrations are associated with an increased risk of early tumor progression during FOLFIRINOX. High IL-18 and IL-7, and low MIP-1β levels are poor prognostic factors for OS in PDAC patients. This indicates that activation and changes in the systemic immune response might play an important role in chemotherapy response and PDAC progression. Cytokine-based treatment might improve patient outcome and should be evaluated in future studies.

Data availability statement

The raw data supporting the conclusions of this article will be made available by the authors, without undue reservation.

Ethics statement

The studies involving human participants were reviewed and approved by the Ethics Committee of Erasmus MC, University Medical Center Rotterdam. The patients/participants provided their written informed consent to participate in this study.

Author contributions

CE, EV, and WD supervised the project. FS, CE, DM, MB, BK, BH, MH, QJ, SL, LM, and JW provided the resources for the project. FS, MS-t, AO, and RD were responsible for the investigation. FS analyzed and visualized the data and wrote the original draft. All other authors reviewed and edited the manuscript before submission.

Funding

This research was funded in part by the Support Casper foundation and by the Eurostars project (project number ESTAR17104).

Acknowledgments

The authors would like to thank all patients for donating blood and participating in our study. Moreover, we thank J. Dumas for processing and storage of the blood samples, and M. Moskie, S. Snapper, E. Pijnappel, A. Stam, and J. Hans-Adema for their help with the collection of patient samples.

Conflict of interest

The authors declare that the research was conducted in the absence of any commercial or financial relationships that could be construed as a potential conflict of interest.

Publisher's note

All claims expressed in this article are solely those of the authors and do not necessarily represent those of their affiliated organizations, or those of the publisher, the editors and the reviewers. Any product that may be evaluated in this article, or claim that may be made by its manufacturer, is not guaranteed or endorsed by the publisher.

Supplementary material

The Supplementary Material for this article can be found online at: https://www.frontiersin.org/articles/10.3389/fimmu.2022.898498/full#supplementary-material

References

1. Suker M, Beumer BR, Sadot E, Marthey L, Faris JE, Mellon EA, et al. FOLFIRINOX for locally advanced pancreatic cancer: a systematic review and patient-level meta-analysis. *Lancet Oncol* (2016) 17(6):801–10. doi: 10.1016/S1470-2045(16)00172-8

2. Conroy T, Desseigne F, Ychou M, Bouché O, Guimbaud R, Bécouarn Y, et al. FOLFIRINOX versus gemcitabine for metastatic pancreatic cancer. *N Engl J Med* (2011) 364(19):1817–25. doi: 10.1056/NEJMoa1011923

3. Thibodeau S, Voutsadakis IA. FOLFIRINOX chemotherapy in metastatic pancreatic cancer: A systematic review and meta-analysis of retrospective and phase II studies. *J Clin Med* (2018) 7(1):7. doi: 10.3390/jcm7010007

4. van der Sijde F, Vietsch EE, Mustafa DAM, Besselink MG, Groot Koerkamp B, van Eijck CHJ. Circulating biomarkers for prediction of objective response to chemotherapy in pancreatic cancer patients. *Cancers (Basel)* (2019) 11(1):93. doi: 10.3390/cancers11010093

5. Group F-NBW. *BEST (Biomarkers, EndpointS, and other Tools) Resource. Silver Spring (MD), Bethesda (MD): Food and Drug Administration (US), National Institutes of Health (US).* (2016).

6. Ballman KV. Biomarker: Predictive or prognostic? *J Clin Oncol* (2015) 33 (33):3968–71. doi: 10.1200/JCO.2015.63.3651

7. Elinav E, Nowarski R, Thaiss CA, Hu B, Jin C, Flavell RA. Inflammation-induced cancer: crosstalk between tumours, immune cells and microorganisms. *Nat Rev Cancer* (2013) 13(11):759–71. doi: 10.1038/nrc3611

8. Bonaventura P, Shekarian T, Alcazer V, Valladeau-Guilemond J, Valsesia-Wittmann S, Amigorena S, et al. Cold tumors: A therapeutic challenge for immunotherapy. *Front Immunol* (2019) 10:168. doi: 10.3389/fimmu.2019.00168

9. Aziz MH, Sideras K, Aziz NA, Mauff K, Haen R, Roos D, et al. The systemic-immune-inflammation index independently predicts survival and recurrence in resectable pancreatic cancer and its prognostic value depends on bilirubin levels: A retrospective multicenter cohort study. *Ann Surg* (2019) 270(1):139–46. doi: 10.1097/SLA.0000000000002660

10. Mei Z, Shi L, Wang B, Yang J, Xiao Z, Du P, et al. Prognostic role of pretreatment blood neutrophil-to-lymphocyte ratio in advanced cancer survivors: A systematic review and meta-analysis of 66 cohort studies. *Cancer Treat Rev* (2017) 58:1–13. doi: 10.1016/j.ctrv.2017.05.005

11. Fu W, Wang K, Yan S, Wang X, Tang B, Chang J, et al. Prognostic significance of the modified Glasgow prognostic score in patients with pancreatic cancer: A meta-analysis. *Dose Response* (2020) 18(3):1559325820942065. doi: 10.1177/1559325820942065

12. Fest J, Ruiter R, Mulder M, Groot Koerkamp B, Ikram MA, Stricker BH, et al. The systemic immune-inflammation index is associated with an increased risk of incident cancer-a population-based cohort study. *Int J Cancer* (2020) 146 (3):692–8. doi: 10.1002/ijc.32303

13. Piro G, Simionato F, Carbone C, Frizziero M, Malleo G, Zanini S, et al. A circulating T(H)2 cytokines profile predicts survival in patients with resectable pancreatic adenocarcinoma. *Oncoimmunology* (2017) 6(9):e1322242. doi: 10.1080/2162402X.2017.1322242

14. Neesse A, Michl P, Frese KK, Feig C, Cook N, Jacobetz MA, et al. Stromal biology and therapy in pancreatic cancer. *Gut* (2011) 60(6):861–8. doi: 10.1136/gut.2010.226092

15. Yako YY, Kruger D, Smith M, Brand M. Cytokines as biomarkers of pancreatic ductal adenocarcinoma: A systematic review. *PloS One* (2016) 11(5): e0154016. doi: 10.1371/journal.pone.0154016

16. Bellone G, Novarino A, Vizio B, Brondino G, Addeo A, Prati A, et al. Impact of surgery and chemotherapy on cellular immunity in pancreatic carcinoma patients in view of an integration of standard cancer treatment with immunotherapy. *Int J Oncol* (2009) 34(6):1701–15. doi: 10.3892/ijo_00000301

17. Dima SO, Tanase C, Albulescu R, Herlea V, Chivu-Economescu M, Purnichescu-Purtan R, et al. An exploratory study of inflammatory cytokines as prognostic biomarkers in patients with ductal pancreatic adenocarcinoma. *Pancreas* (2012) 41(7):1001–7. doi: 10.1097/MPA.0b013e3182546e13

18. Farren MR, Mace TA, Geyer S, Mikhail S, Wu C, Ciombor K, et al. Systemic immune activity predicts overall survival in treatment-naïve patients with metastatic pancreatic cancer. *Clin Cancer Res* (2016) 22(10):2565–74. doi: 10.1158/1078-0432.CCR-15-1732

19. Mitsunaga S, Ikeda M, Shimizu S, Ohno I, Furuse J, Inagaki M, et al. Serum levels of IL-6 and IL-1β can predict the efficacy of gemcitabine in patients with advanced pancreatic cancer. *Br J Cancer* (2013) 108(10):2063–9. doi: 10.1038/bjc.2013.174

20. Ren C, Chen Y, Han C, Fu D, Chen H. Plasma interleukin-11 (IL-11) levels have diagnostic and prognostic roles in patients with pancreatic cancer. *Tumour Biol* (2014) 35(11):11467–72. doi: 10.1007/s13277-014-2459-y

21. Vizio B, Novarino A, Giacobino A, Cristiano C, Prati A, Ciuffreda L, et al. Potential plasticity of T regulatory cells in pancreatic carcinoma in relation to disease progression and outcome. *Exp Ther Med* (2012) 4(1):70–8. doi: 10.3892/etm.2012.553

22. Setrerrahmane S, Xu H. Tumor-related interleukins: old validated targets for new anti-cancer drug development. *Mol Cancer* (2017) 16(1):153. doi: 10.1186/s12943-017-0721-9

23. McShane LM, Altman DG, Sauerbrei W, Taube SE, Gion M, Clark GM, et al. REporting recommendations for tumour MARKer prognostic studies (REMARK). *Br J Cancer* (2005) 93(4):387–91. doi: 10.1038/sj.bjc.6602678

24. Janssen QP, van Dam JL, Bonsing BA, Bos H, Bosscha KP, Coene P, et al. Total neoadjuvant FOLFIRINOX versus neoadjuvant gemcitabine-based chemoradiotherapy and adjuvant gemcitabine for resectable and borderline resectable pancreatic cancer (PREOPANC-2 trial): study protocol for a nationwide multicenter randomized controlled trial. *BMC Cancer* (2021) 21(1):300. doi: 10.1186/s12885-021-08031-z

25. Dik WA, Heron M. Clinical significance of soluble interleukin-2 receptor measurement in immune-mediated diseases. *Neth J Med* (2020) 78(5):220–31.

26. Eurelings LEM, Miedema JR, Dalm V, van Daele PLA, van Hagen PM, van Laar JAM, et al. Sensitivity and specificity of serum soluble interleukin-2 receptor for diagnosing sarcoidosis in a population of patients suspected of sarcoidosis. *PloS One* (2019) 14(10):e0223897. doi: 10.1371/journal.pone.0223897

27. Kunert A, Basak EA, Hurkmans DP, Balcioglu HE, Klaver Y, van Brakel M, et al. CD45RA(+)CCR7(-) CD8 T cells lacking co-stimulatory receptors demonstrate enhanced frequency in peripheral blood of NSCLC patients responding to nivolumab. *J Immunother Cancer* (2019) 7(1):149. doi: 10.1186/s40425-019-0608-y

28. Pue CA, Mortensen RF, Marsh CB, Pope HA, Wewers MD. Acute phase levels of c-reactive protein enhance IL-1 beta and IL-1ra production by human blood monocytes but inhibit IL-1 beta and IL-1ra production by alveolar macrophages. *J Immunol* (1996) 156(4):1594–600.

29. Dinarello CA, Novick D, Kim S, Kaplanski G. Interleukin-18 and IL-18 binding protein. *Front Immunol* (2013) 4:289. doi: 10.3389/fimmu.2013.00289

30. Maurer M, von Stebut E. Macrophage inflammatory protein-1. *Int J Biochem Cell Biol* (2004) 36(10):1882–6. doi: 10.1016/j.biocel.2003.10.019

31. Zitvogel L, Apetoh L, Ghiringhelli F, Kroemer G. Immunological aspects of cancer chemotherapy. *Nat Rev Immunol* (2008) 8(1):59–73. doi: 10.1038/nri2216

32. Carbone A, Vizio B, Novarino A, Mauri FA, Geuna M, Robino C, et al. IL-18 paradox in pancreatic carcinoma: elevated serum levels of free IL-18 are correlated with poor survival. *J Immunother* (2009) 32(9):920–31. doi: 10.1097/CJI.0b013e3181b29168

33. Usul Afsar Ç, Karabulut M, Karabulut S, Alis H, Gonenc M, Dagoglu N, et al. Circulating interleukin-18 (IL-18) is a predictor of response to gemcitabine based chemotherapy in patients with pancreatic adenocarcinoma. *J Infect Chemother* (2017) 23(4):196–200. doi: 10.1016/j.jiac.2016.12.003

34. Romero JM, Grünwald B, Jang GH, Bavi PP, Jhaveri A, Masoomian M, et al. A four-chemokine signature is associated with a T-cell-Inflamed phenotype in primary and metastatic pancreatic cancer. *Clin Cancer Res* (2020) 26(8):1997–2010. doi: 10.1158/1078-0432.CCR-19-2803

35. Willenbrock F, Cox CM, Parkes EE, Wilhelm-Benartzi CS, Abraham AG, Owens R, et al. Circulating biomarkers and outcomes from a randomised phase 2 trial of gemcitabine versus capecitabine-based chemoradiotherapy for pancreatic cancer. *Br J Cancer* (2021) 124(3):581–6. doi: 10.1038/s41416-020-01120-z

36. Liu T, Zhang L, Joo D, Sun SC. NF-κB signaling in inflammation. *Signal Transduct Target Ther* (2017) 2:17023–. doi: 10.1038/sigtrans.2017.23

37. Nelson DE, Ihekwaba AE, Elliott M, Johnson JR, Gibney CA, Foreman BE, et al. Oscillations in NF-kappaB signaling control the dynamics of gene expression. *Science* (2004) 306(5696):704–8. doi: 10.1126/science.1099962

38. Taniguchi K, Karin M. NF-κB, inflammation, immunity and cancer: coming of age. *Nat Rev Immunol* (2018) 18(5):309–24. doi: 10.1038/nri.2017.142

39. Xia Y, Shen S, Verma IM. NF-κB, an active player in human cancers. *Cancer Immunol Res* (2014) 2(9):823–30. doi: 10.1158/2326-6066.CIR-14-0112

40. Zhuang Z, Ju HQ, Aguilar M, Gocho T, Li H, Iida T, et al. IL1 receptor antagonist inhibits pancreatic cancer growth by abrogating NF-κB activation. *Clin Cancer Res* (2016) 22(6):1432–44. doi: 10.1158/1078-0432.CCR-14-3382

41. Biankin AV, Waddell N, Kassahn KS, Gingras MC, Muthuswamy LB, Johns AL, et al. Pancreatic cancer genomes reveal aberrations in axon guidance pathway genes. *Nature* (2012) 491(7424):399–405. doi: 10.1038/nature11547

42. Padoan A, Plebani M, Basso D. Inflammation and pancreatic cancer: Focus on metabolism, cytokines, and immunity. *Int J Mol Sci* (2019) 20(3):676. doi: 10.3390/ijms20030676

43. Stein SM, James ES, Deng Y, Cong X, Kortmansky JS, Li J, et al. Final analysis of a phase II study of modified FOLFIRINOX in locally advanced and metastatic pancreatic cancer. *Br J Cancer* (2016) 114(7):737–43. doi: 10.1038/bjc.2016.45

44. Chen Z, Lv Y, Li H, Diao R, Zhou J, Yu T. Meta-analysis of FOLFIRINOX-based neoadjuvant therapy for locally advanced pancreatic cancer. *Med (Baltimore)* (2021) 100(3):e24068. doi: 10.1097/MD.0000000000024068

45. Auclin E, Marthey L, Abdallah R, Mas L, Francois E, Saint A, et al. Role of FOLFIRINOX and chemoradiotherapy in locally advanced and borderline resectable pancreatic adenocarcinoma: update of the AGEO cohort. *Br J Cancer* (2021) 124(12):1941–8. doi: 10.1038/s41416-021-01341-w

46. Das S, Shapiro B, Vucic EA, Vogt S, Bar-Sagi D. Tumor cell-derived IL1β promotes desmoplasia and immune suppression in pancreatic cancer. *Cancer Res* (2020) 80(5):1088–101. doi: 10.1158/0008-5472.CAN-19-2080

frontiers | Frontiers in Oncology

TYPE Original Research
PUBLISHED 26 August 2022
DOI 10.3389/fonc.2022.877817

OPEN ACCESS

EDITED BY
Hongda Liu,
Nanjing Medical University, China

REVIEWED BY
Maarit Tiirikainen,
University of Hawaii at Manoa, United States
Shuai Wang,
University of Pittsburgh Medical Center, United States

*CORRESPONDENCE
Hong Ren
renh_med@163.com
Boxiang Zhang
zhangboxiang@xjtufh.edu.cn

†These authors have contributed equally to this work

SPECIALTY SECTION
This article was submitted to Cancer Immunity and Immunotherapy, a section of the journal Frontiers in Oncology

RECEIVED 17 February 2022
ACCEPTED 18 July 2022
PUBLISHED 26 August 2022

CITATION
Song D, Zhou Z, Wu J, Wei T, Zhao G, Ren H and Zhang B (2022) DNA methylation regulators-related molecular patterns and tumor immune landscape in hepatocellular carcinoma.
Front. Oncol. 12:877817.
doi: 10.3389/fonc.2022.877817

DNA methylation regulators-related molecular patterns and tumor immune landscape in hepatocellular carcinoma

Dingli Song[1†], Zhenyu Zhou[2†], Jie Wu[1], Tao Wei[3], Guang Zhao[1], Hong Ren[1*] and Boxiang Zhang[1*]

[1]Department of Thoracic Surgery, The First Affiliated Hospital of Xi'an Jiaotong University, Xi'an, China, [2]Department of Hepatobiliary Surgery, Sun Yat-Sen Memorial Hospital, Sun Yat-Sen University, Guangzhou, China, [3]Department of Hepatobiliary and Pancreatic Surgery, School of Medicine, The First Affiliated Hospital of Zhejiang University, Hangzhou, China

Increasing evidence showed that the dysregulation of DNA methylation regulators is a decisive feature of almost all cancer types and affects tumor progressions. However, few studies focused on the underlying influences of DNA methylation regulators-related genes (DMRegs) in immune cell-infiltration characteristics, tumor microenvironment (TME) and immunotherapy in HCC patients. In our study, the alterations of DNA methylation regulators modification patterns (DMRPs) were clustered from hepatocellular carcinoma (HCC) samples based on the expression of DNA methylation regulators as well as genetic and transcriptional features. In addition, based on molecular identification of three distinct molecular subtypes, we found that different DMRPs alterations were related to different clinicopathological characteristics, prognosis, and immune cells infiltration features. Moreover, we constructed and validated a DNA methylation regulators-related genes score (DMRegs_score) to predict the survival of HCC patients. A high DMRegs _score, which was characterized by more TP53 wild mutation, high expression of PD-1, CTLA-4, and remarkable immunity activation, was indicative of poor prognosis. Furthermore, we validated the expression of eight genes which were used for the prognostic signature in this risk score by RT-qPCR using tissues from our center. More importantly, DMRegs_score was highly correlated with targeted drug sensitivity. Additionally, we developed a highly accurate scoring system that could be used to improve the clinical applicability of DMRegs _score. In conclusion, these findings may contribute to a better understanding of DNA methylation regulators and provide new strategies for evaluating prognosis and developing more effective combination therapy for HCC patients.

KEYWORDS

hepatocellular cancer, DNA methylation regulators, classification, immune infiltration, signature

Introduction

Liver cancer, more specifically hepatocellular carcinoma (HCC), is the main leading cause of cancer-related death worldwide in 2020 (1, 2). At present, surgery is still the most effective treatment for HCC. However, due to the occult onset and rapid progress of HCC, patients often have lost the best opportunity for surgical treatment at the time of diagnosis. What's more, the patients with HCC have poor prognosis because of high metastasis and recurrence rate (3). Therefore, exploring the molecular mechanism of HCC development and finding new early diagnosis and treatment targets are the focus of HCC research.

Epigenetic modifications, such as DNA methylation, play a crucial role in altering gene expression and contributing to disease development in mammals (4). According to present reports, methylation of the fifth carbon of the DNA cytosine within CpG dinucleotides is the most mechanistically understood form of DNA methylation (5). DNA methylation modification is a dynamic and vary process which is modulated by DNA methylation regulators, including DNA methyltransferases, DNA demethylases and DNA binding proteins (6–8). In addition, a growing body of evidence had demonstrated that dysregulation of DNA methylation regulators is a hallmark of almost all cancer types and affects tumor microenvironment (TME) or immunotherapy (7, 9, 10).

Co-inhibitory receptors Cytotoxic T-lymphocyte antigen 4 (CTLA4), programmed cell death protein 1 (PD-1), and programmed cell death ligand 1 (PD-L1) is expressed in the tumor microenvironment. Immunotherapy such as immune-checkpoint inhibitors (ICIs) that target these biomarkers activated the properties of effector T cells which can be able to kill cancer cells. Importantly, ICIs have radically reversed cancer therapy (11). Cancer immunotherapy targeting CTLA4, PD-L1, or PD-1 has become a widely used method of treating various types of cancer (12–14). Recently, anti-CTLA-4 was reported a survival benefit of HCC patients with sorafenib resistance (15). However, these immunotherapies were responding differently with patient to patient, and less than 20% of immune checkpoint blockade therapy was effective (16–18). It has been reported that the expression of PD-L1 and the status of tumor mutation burden (TMB) may be used as biomarkers to assess the effectiveness of immunotherapy (19–21). Interestingly, a recent study has revealed the characteristics of DNA methylation modification patterns of gastric cancer and explored the link between TME and DNA methylation modification, which indicated that DNA methylation may be a new predictor for immunotherapy (8). Moreover, DNA methylation regulators distinguish early HCC stages from chronic liver hepatitis B and C as well as healthy controls, intensify as the disease progresses, and is highly enriched in immune function-related genes such as PD-1 (22). These all suggest that DNA methylation regulators are closely related to immunotherapy and maybe predict the response to immunotherapy. However, it is still unclear how DNA methylation regulators affect tumors, especially cancer immunotherapy in HCC. Therefore, further elucidation of DNA methylation regulators could provide an attractive perspective on cancer immunotherapy.

In this study, we integrated patients from TCGA-LIHC cohort and ICGC LIRI-JP cohort to comprehensively evaluate the correlation between the DNA methylation modification patterns (DMRPs) and tumor immune landscape. First, we explored the expression of 20 DNA methylation regulators between normal and carcinoma tissues, and then identified 3 distinct DMRPs which were tightly correlated with immune cells infiltration and prognosis. In addition, we investigated the functional annotation to distinguish cancer associated signaling pathways to the three patterns. Moreover, we continued to quantify the DMRPs of individual HCC patients and assessed the clinical responses to immunotherapy based on DNA methylation regulators-related genes score (DMRegs_score). In conclusion, our novel DMRegs_score provides a reliable insight by which to identify and feature immune landscape of HCC, and the results suggest the DMRegs_score may be a biomarker for survival and precision treatment.

Materials and method

Data collection and preprocessing of public database

HCC patients with RNA-seq, genetic mutations (VarScan) and clinical information (included age, sex, TNM stage, follow-up time, and survival status) were obtained from the Cancer Genome Atlas (TCGA) data portal (TCGA-LIHC cohort, n=374) (http://portal.gdc.cancer.gov/). The copy number variant profiles (CNV) were downloaded from the UCSC xena (http://xenabrowser.net). The normalized data from another HCC cohort were downloaded from the International Cancer Genome Consortium (ICGC) database (ICGC LIRI-JP, n=231) (http://daco.icgc.org). GSE76427 (n=167) array was downloaded from Gene Expression Omnibus (GEO) database (https://www.ncbi.nlm.nih.gov/geo/). The 20 DNA methylation regulators were extracted from previous study (8). The TCGA and ICGC RNA sequence data (fragments per kilobase million, FPKM value) were transformed into TPM (transcripts per kilobase million) format. We excluded patients without complete clinical information and the survival time of 0, thus, a total of 685 HCC patients were further analyzed in this study. These detailed clinical information about 685 patients with HCC was presented in Tables S1, S2.

Tissue samples and real-time PCR and immunohistochemical staining

Forty-one pairs HCC and nearby non-tumor tissues were collected from HCC patients who underwent hepatic resection in Sun Yat-Sen Memorial hospital between Nov 2020 and Mar 2021. Liquid nitrogen was used to store these samples until further analysis could be completed. The patients' clinical data were also collected (Table S3). The study protocol was approved by the Ethics Committee of Sun Yat-Sen Memorial hospital and informed consent was obtained from each patient. We extracted the RNA from the tissues with Trizol (Takara, China), and performed reverse transcription using Prime Script RTase (Takara, China), according to the manufacturer's protocol, respectively. According to the manufacturer's instructions, real-time PCR was used to measure mRNA expression levels using SYBR green (Takara, China). A list of the primers used for real-time PCR is provided for Table S4. Immunohistochemical (IHC) staining was performed as described previously (23) using the following antibodies: Anti- CDCA3, Anti-CDC20, Anti-YWHAQ, Anti-ADH4, Anti-TRNP1, Anti-CYP2C9, Anti-CALU, Anti-APOC1. All antibodies used in the study are shown in Table S5. Quantitative evaluation of protein expression of IHC tissues was measured by ImageJ software. The number of stained cells was identified by trainable Weka segmentation.

Interaction among DNA methylation regulators, copy number variant (CNV) analysis and gene mutation analysis

The crosstalk network diagram of multiple DNA methylation regulators was constructed by using "igraph" package, and presented the categories "Writers", "Erasers" and "Readers" of these genes. The "RCircos" R package was used to visualize the location of 20 DNA methylation regulators in human chromosomes and the gain or loss status of copy number. The "maftools" R package was applied to evaluate the mutation status of 20 DNA methylation regulators and drawn the waterfall plots in HCC.

Molecular subgroups-based clustering analysis for DNA methylation regulators

We performed the consensus clustering with Euclidean squared distance metric and the K-means clustering algorithm to identify distinct DMRPs based on the expression of 20 DNA methylation regulators by using the "ConsensusClusterPlus" R package. HCC samples were classified into k clusters with k=2 to k=9. Based on the consistent cumulative distribution function (CDF) and delta region graphs, an optimal number of clusters was determined (24). What's more, we compared the relationships between molecular subgroups, clinical characteristics, and prognosis using the "survival" and "survminer" R packages. The clinicopathologies including age, gender, TNM stage.

Function annotation based on gene set variant analysis (GSVA)

To identify the difference between the biological process of DMRPs, the "GSVA" package in R was utilized to performe GSVA enrichment analysis. GSVA, a nonparametric and unsupervised algorithm, can quantify the gene enrichment results in the sample of a gene expression dataset (25). In addition, we employed the "limma" R package to screen the significant variance in KEGG pathways and Hallmark pathways. The well-defined gene sets of "h.all.v7.4.symbols", and "c2.cp.kegg.v7.2.symbols" were downloaded from MSigDB database.

Identification of differentially expressed genes (DEGs) between DNA methylation regulators modification patterns

The previous consensus clustering analysis had classified patients into three distinct DMRPs based on 20 DNA methylation regulators, and we identified DNA methylation regulators modification-related differentially expressed genes (DMRegs) among different DMRPs. The Bayesian method of "limma" package was used to statistical analysis, and "venndiagram" R package was applied to visualize the DMRegs. The DMRegs with adjusted $p<0.05$ and $|logFC|=0.5$ were considered as screening criterion. To explore the potential functions of DMRegs, the "clusterprofler" package in R software was utilized for Gene Ontology (GO) and Kyoto Encyclopedia of Genes and Genomes (KEGG) enrichment analysis with adjusted P values < 0.05. What's more, we further explored the gene cluster based on the expression profiles of DMRegs using unsupervised clustering methods.

Construction of the DNA methylation regulators-related gene signature

We constructed a set of scoring system to quantify the DMRPs of individual patient with HCC by using the method of LASSO cox regression, and we termed the score as DMRegs_score. The DMRegs_score was developed as follows. Univariate cox regression analysis was performed to identify overlapping DMRegs related to survival with P-values <0.05. Then "glmnet" R package was employed to establish the DMRegs_score based on the expression of significant

prognosis of DMRegs among gene clusters. Finally, the DMRegs_score was defined using a formula method like previous study: DMRegs_score = Σ (Expi * coefi), where Coefi and Expi represented the risk coefficient and expression of each gene, respectively. The Kaplan-Meier survival curve, the area under the curve (AUC) of the time-dependent receiver operating characteristics (ROC) curve were implemented to evaluate the predictive ability of the risk model. Combining clinical data with univariate and multivariate cox analysis were done to determine if the risk score was an independent feature.

Estimation the relationship between DMRegs_score and TME, PD-1, PD-L1, and CTLA4

The ESTIMATE algorithm was used to calculate the tumor microenvironment (TME) scores, including stromal scores, immune scores, and estimate scores, which represented the infiltration of immune cells and stromal cells in TME (26). Moreover, based on the transcriptome profiles, we used "GSVA" R package to perform single sample gene set enrichment analysis (ssGSEA) to quantify the relative abundance of 23 immune cell types in the TME among different DMRPs (27). The marker genes of 23 immune cell types were acquired from a previous study, including activated B cell, MDSC, macrophage, regulatory T cell and so on (Table S6). Furthermore, we analyzed the relationship between the DMRegs_score and the expression of PD-1, PD-L1, CTLA4, and antigen presentation (HLA family).

Characteristics of mutation burden and drug sensitivity analysis

By using "maftools" R package, the mutation annotation format (MAF) from the TCGA database was used to explore whether the mutations status of HCC patients was associated with high- or low-risk group. The tumor mutation burden score (TMB) was also calculated for each patient with HCC in both groups. Using the "pRRophetic" package, we analyzed the IC50 of several chemotherapeutic drugs which were commonly used to treat HCC in both groups.

Validation the DMRegs_score and establishment of a nomogram assessing system

The reliability and predictive ability of this DMRegs_score was validated based on data from GEO dataset using same methods above mentioned. Furthermore, to expand the role of DMRegs_score in clinical practice, we used "rms" package to develop a nomogram predicting the prognosis of HCC patients, which combined the clinical features and DMRegs_score. The time-dependent ROC curves and calibration were performed to describe the predictive value of 1-, 2- and 3-year, respectively.

Statistics analysis

The statistical analysis tools-R software (version 4.0.3, R Foundation for Statistical Computing, Vienna, Austria) was used in this study. Kruskal-Wallis tests or one-way ANOVA were used as nonparametric or parametric methods for comparisons of three groups, respectively using GraphPad Prism 8. And the results of RT-qPCR and IHC were conducted statistical analysis using pair t test. The forest plot and partial violin plots were generated by Sanger Box online tool. The hazard ratio (HR) and 95% confidence intervals (CI) were calculated. All statistical results with a P-value of <0.05 were considered significant.

Results

The landscape of DNA methylation regulators in HCC

A total of 20 DNA methylation regulators were identified in this study, including three writers (DNMT1, DNMT3A, and DNMT3B), three erasers (TET1, TET2 and TET3) and fourteen readers (MBD1, MBD2, MBD3, MBD4, ZBTB33, ZBTB38, ZBTB4, UHRF1, UHRF2, MECP2, UNG, TDG, NTHL1 and SMUG1). Based on a summary analysis of the incidence of somatic mutations in these 20 DNA methylation regulators, there was a low mutation rate for the patients with HCC from TCGA cohort (Figure 1A). Thirty-four patients can be found genetic mutation in available samples, and the mutation frequency of 20 DNA methylation regulators range from 1%-2%. The TET1 had the highest number of mutations of all the DNA methylation regulators (2%). The exploration of copy number variation (CNV) alteration frequency indicated common CNV alteration in the 20 DNA methylation regulators. DNMT1, UHRF1, TET2, MBD1/2/3 and ZBTB4 were focused on copy number deletion, while MECP2, DNMT3A, ZBTB33/38, NTHL1, UHRF2 and UNG had widespread frequency of CNV amplification (Figure 1B). In addition, the locations of the CNV alterations in the 20 DNA methylation regulators on chromosomes were presented in Figure 1C. The status of CNV alterations indicated that CNV might regulate the mRNA expression of DNA methylation regulators. Further analysis revealed that 19 out of 20 DNA methylation regulators were upregulated in tumor samples except TET2, although the expression of TET2 in tumor tissues is higher than in normal liver tissues (Figure 1D). These data suggest the 20 DNA methylation regulators may play important roles in HCC development.

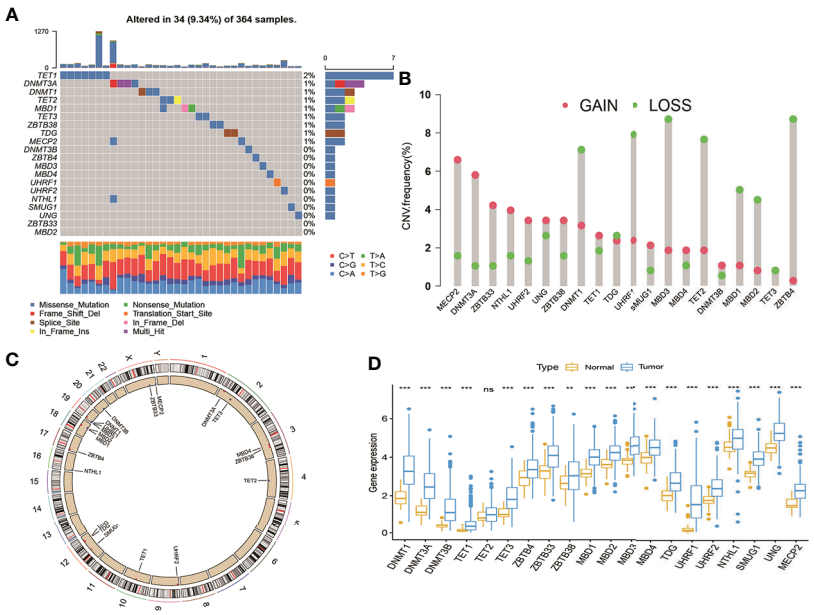

FIGURE 1
Landscape of genetic variations and transcriptional expression of DNA methylation regulators in HCC from TCGA cohort. **(A)** 34 of the 364 patients occurred genetic variations of 20 DNA methylation regulators with 9.34% mutation frequencies. **(B)** The frequency of CNV gain or loss among DNA methylation regulators. **(C)** The locations of CNV variations in DMRs on 23 chromosomes. **(D)** The expression level of 20 DNA methylation regulators between normal and HCC tissues. HCC, hepatocellular carcinoma; TCGA, The Cancer Genome Atlas; CNV, copy number variant.

Identification of DNA methylation regulators-related modification patterns in HCC

From above results, we speculated that DNA methylation regulators regulated deep-seated regulatory mechanism, which promotes us to further to investigate their potential functional in HCC. First, we gathered 570 patients from two HCC cohorts (TCGA-HCC and ICGC-LIRC) to explore the expression patterns of DNA methylation regulators involved in tumorigenesis. Spearman correlation analysis was utilized to assess mutual regulation among these DNA methylation regulators (Figure 2A). The results revealed MBD2, ZBTB33 and TET2 had a significant positive correlation with other DNA methylation regulators. Next, Cox regression and Kaplan-Meier analysis were performed to classify the prognostic relationship of these regulators with the HCC patients. Forest plot revealed that DNMT1/3A//3B, TET1/3, MBD1/2/3, TDG, UHRF1, SMUG1 and UNG were significantly associated with shorter overall survival and were considered as risk factors in HCC patients (Figure 2B). The crosstalk network showed the interaction and the prognostic value among 20 DNA methylation regulators in patients with HCC (Figure 2C). In addition, to better understand the role of DNA methylation regulators in tumor immunity, we explored the correlation between the 20 DNA methylation regulators and TME-infiltration immune cells using Spearman correlation analysis, and we found a significant negative relationship between most of these regulators and immune cells interaction (Figure 2D). Among them, DNMT1, ZBTB4 and MBD2 presented a strong positive correlation with most types of immune cells, such as activated CD4+ T cells, immature dendritic cells, and regulatory T cells. These results revealed that DNA methylation regulators regulated tumor microenvironment, which might provide strategies for immunotherapy. To understand the heterogeneity of DNA methylation regulators in HCC patients, we then performed unsupervised clustering analysis to classify patients based on the expression profiles of 20 DNA methylation regulators (Figures S1A–I). These results indicated that k=3 could achieve the best cluster efficacy. Therefore, the patients were categorized into three different DMRPs, including pattern A (n=199), pattern B (n=206) and pattern C (n=165) (Figure 2E). The Kaplan-Meier curves revealed that the pattern C had the poorer prognosis than pattern A and pattern B (Figure 2F). PCA analysis suggested three clusters were apparently discernible dimensions in the 20 DNA methylation regulators transcription profiles (Figure 2G).

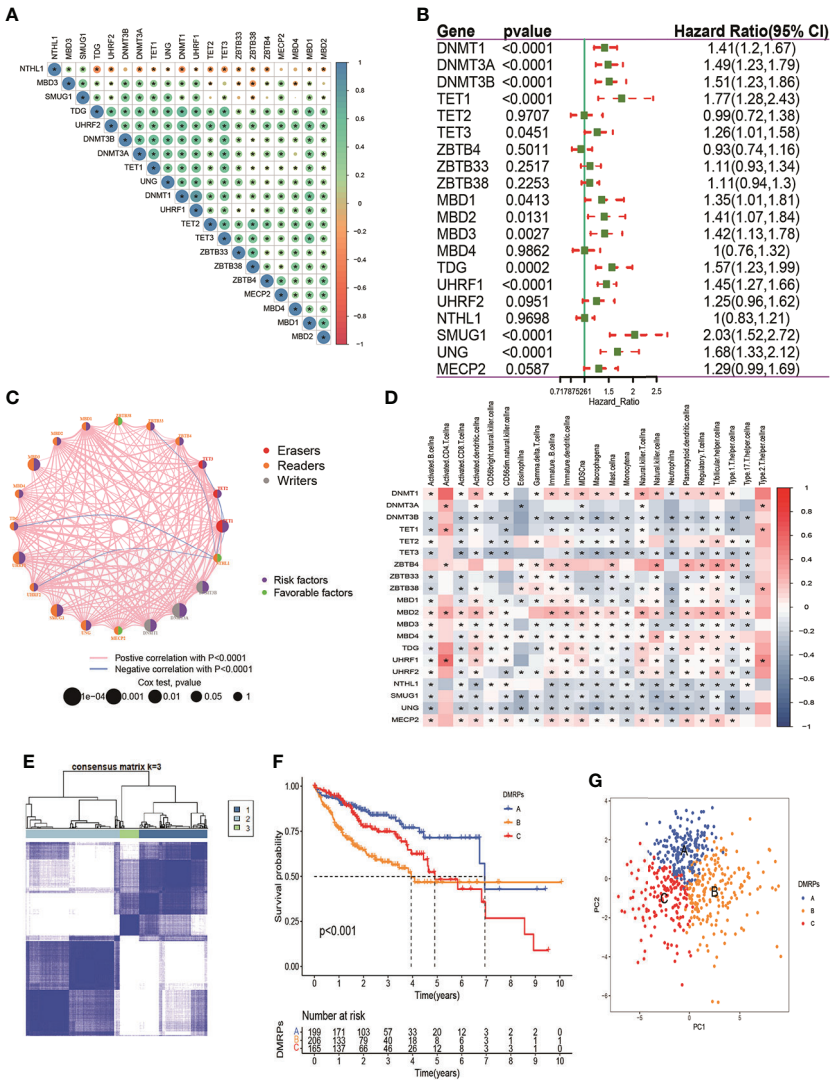

FIGURE 2
Prognosis of DNA methylation regulators and patterns of DNA methylation regulators modification. **(A)** The correlation of 20 DNA methylation regulators in HCC patients. **(B)** The prognosis of 20 DNA methylation regulators in HCC patients. **(C)** The interaction among 20 DNA methylation regulators in HCC. The pink and blue line represents positive and negative correlation. The size of the circle represents the p value of the log-rank test. Green points represent favorable factors for OS. Purple points represent risk factors for OS. **(D)** The correlation between 20 DNA methylation regulators and 23 types of immune cells. **(E)** The consensus cluster matrix for patients with HCC. **(F)** The survival analysis for different patterns of patients. **(G)** PCA analysis indicated significant separation among three patterns. * $p < 0.05$.

Distinct DMRPs and function pathways analysis

What's more, we found most of these DNA methylation regulators were highly expressed in pattern B. Pattern A was presented high expression levels of ZBTB4/33/38. Only NTHL1 was relatively highly expressed in pattern C (Figure 3A). These data indicated that three DMRPs had distinct characteristics in the DNA methylation regulators modification. Furthermore, as shown in the heatmap, we explored the association between the various clinicopathological characteristics and three patterns based on 20 DNA methylation regulators expression of the metadata set (Figure 3B). And we found pattern B was related to female patients and patients younger than 60 years old ($p<0.05$), and the number of deaths were higher than the other two patterns ($p<0.001$). Hence, the patients in pattern B had poorer prognosis than other two patterns. The comprehensive comparisons of the clinical features of the three DMRPs suggested most of these DNA methylation regulators played potential roles on oncogenesis. To investigate the underlying molecular mechanism and signal pathways to each DMRP, the GSVA enrichment analysis based on KEGG and Hallmark gene

10.3389/fonc.2022.877817

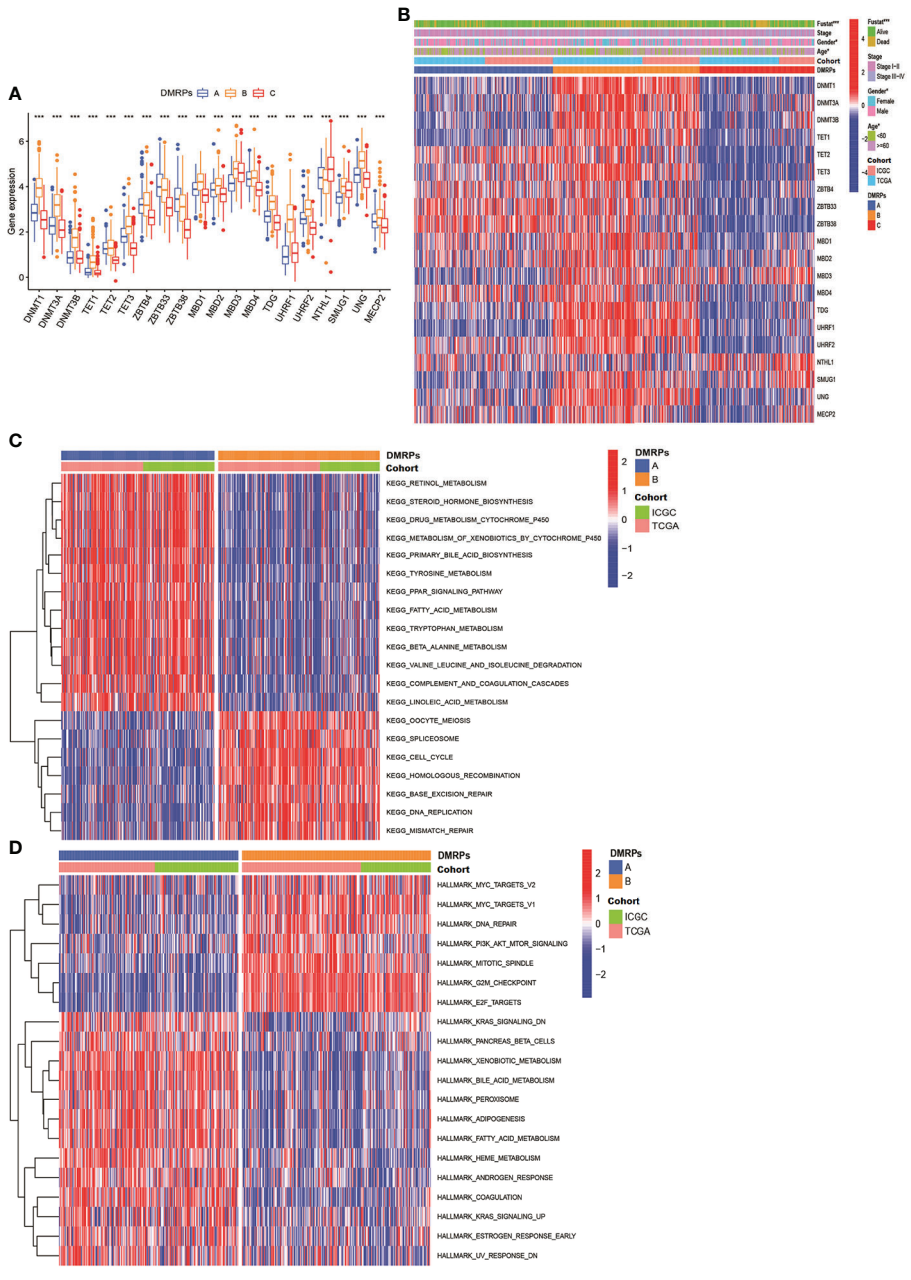

FIGURE 3
The clinical features of different DNA methylation regulator-related patterns and relevant function mechanism. **(A)** The expression of 20 DNA methylation regulators among three DNA methylation regulator-related patterns. **(B)** The heatmap of the differences between the expression of 20 DNA methylation regulators and clinicopathological factors. **(C, D)** GSVA showed the results of KEGG and Hallmark pathways in distinct DNA methylation regulators related modification patterns, respectively. * P < 0.05, ** P < 0.01, *** P < 0.001, **** P < 0.0001.

sets were conducted. As presented in Figures 3C, D, the results indicated significant difference between three patterns. The pattern B was significantly enriched in cell cycle and cancer-associated pathways, including DNA replication, PI3K/AKT/mTOR signaling. The pattern A was highly enriched in processes of metabolism and some carcinogenic activation pathways, such as retinol metabolism, Wnt pathway, mTOR pathway, and TGF-β signaling pathway (Figure 3C and Figures S2A, B, Table S7). However, the pattern C mainly presented enrichment metabolism in tyrosine and drug (Figures S2C, D). Thus, our results identified each DMRP is associated with its specific clinicopathological features and signaling pathways. Some

previous studies had reported that PI3K/mTOR signaling pathway played a critical regulatory role in the tumor microenvironment. In immunology, mTOR was becoming as a key regulator of immune responses, which played an essential regulatory role in the differentiation and function of both innate and adaptive immune cells (28).What's more, the previous results revealed that most of DNA methylation regulators were associated with multiple immune cells. Consequently, it's essential to explore the correlation between DMRPs and tumor immune cells infiltration.

Characteristics of the TME immune cell infiltration in distinct DMRPs

Previous studies had reported DNA methylation played a crucial role on tumor immune microenvironment (29, 30). Hence, we evaluated the relationship between three DMRPs and 23 types of immune cell subsets of every HCC sample using ssGSEA. The heatmap displayed significant differences in 23 immune cells infiltrations among these DMRPs with various clinicopathological features (Figure 4A). We found that natural

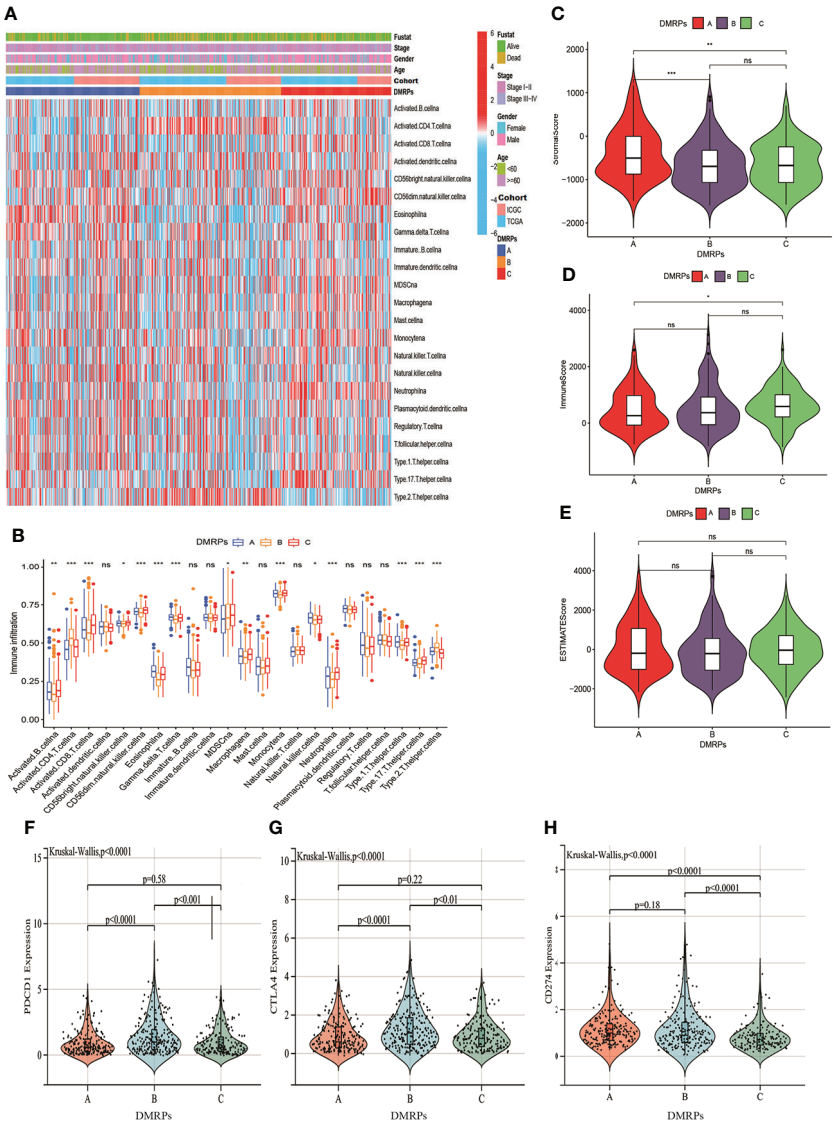

FIGURE 4
Characteristics of the TME immune cells infiltration in distinct DNA methylation regulators related modification patterns. **(A)** The heatmap of immune cell infiltration in three patterns. **(B)** The distribution of immune cells among three patterns. **(C–E)** The differences of TME score (stromal score, immune score and estimate score) among three patterns. **(F–H)** The expression levels of three important immune checkpoint in the three DMRPs. DMRPs: DNA methylation regulators related modification patterns; TME: tumor microenvironment. * P < 0.05, ** P < 0.01, *** P < 0.001, **** P < 0.0001. ns, no significance.

killer T cells, eosinophils, gamma T cells and type 1T helper cells had a higher proportion in pattern A than pattern B and C. The infiltration level of activated B cells, activated CD8 T cells, CD56bright natural killer cells, CD56dim natural killer cells, MDSCs, macrophages, monocytes, neutrophils, and type 17 T helper cells were higher in pattern C, while activated CD4 T cells and type 2 T helper cells had significantly higher infiltration in pattern B (Figure 4B). The immune landscape stated clearly that the significant differences of the relative expression of multiple immune infiltration cells among three DMRPs. To explore the influence of DNA methylation regulators on the TME of HCC, further analysis of TME scores (immune score, stromal score and estimate score) were evaluated by using the ESTIMATE algorithm. These results showed that the stromal score was the highest in pattern A than other two patterns, but there was no statistical significance between pattern B and pattern C (Figure 4C), and the highest immune score was found in pattern C (Figure 4D). However, there weren't any significant differences in estimate scores among the three patterns (Figure 4E). In addition, blocking therapy against immune checkpoints was believed to increase the aggressiveness of the host immune system against tumor cells. Hence, we further assessed the expression levels of PD-1, PD-L1 and CTLA4 among three DMRPs. The analysis of immune checkpoints suggested that pattern B exited the highest expression of PD-1compared to pattern A and pattern C (Figure 4F). Similarly, the pattern B had a higher expression level of CTLA4 than pattern A and pattern C (Figure 4G). We also compared the PD-L1 expression levels in different DMRPs and found a significant upregulation in pattern A (Figure 4H). Based on these results, we identified that HCC patients with specific DMRPs were associated with different immune infiltration characteristics, which might influence the development and progression of HCC. What's more, potential immunotherapy could be selected according to the expression of immune checkpoints in patients with different DNA methylation regulators modification.

DMRPs-related DEGs and gene clusters in HCC

To investigate the potential genetic alterations and expression perturbations affected by the three DMRPs in HCC, we screened a total of 151 DMRegs from three DMRPs using "limma" R package based on the metadata set (Figure S3A). Function annotation for these genes showed that some DMRegs were significantly correlated with metabolism in biological processes (Figure 5A), while material metabolism, glycolysis, and cell cycle were mainly pathways in KEGG analysis (Figure 5B). When we used univariate cox regression analysis to explore their relationship with the OS status of the HCC patients, and 112 DMRegs with significant prognostic value were selected to further identify (Table S8). Based on the expression profiles of these significant genes, we performed consensus clustering analysis and obtained three genomic clusters, namely gene Cluster A-C (Figure 5C and Figures S3B–I). The heatmap displayed the distinct characteristics of three phenotypes on the expression of prognostic DMRegs, and clinical analysis showed geneCluster C tended to relate to the advance TNM stage (Figure 5D). Additionally, the survival analysis demonstrated geneCluster C had a poorer survival rate (Figure 5E). Obviously, the expressions of DNA methylation regulators were significantly different among three gene clusters in the metadata set (Figure 5F). Most of these DNA methylation regulators (15/20) were presented higher expression levels in geneCluster C, such as DNMT1/3A/3B, TET1/3, ZBTB4, MBD1/2/3, TDG, UHRF1/2, SMUG1, UNG and MECP2. However, there was no significant difference between the expression of TET2, MBD4 and three gene clusters. Above all, these results illustrated the existence of specific clusters of genes in different DMRPs, which further supported the important roles of the three DMRPs in HCC.

Generation of DMRegs_score in HCC

In order to more understand the impact of these DNA methylation regulators on patients on HCC patients and better apply the research results to clinical practice, we constructed a DMRegs_score based on 112 prognostic DMRegs. As displayed in Figures 6A, B, we performed LASSO cox analysis to build prognostic risk score based on optimal λ. According to the results, we obtained 8 genes (CDCA3, CDC20, YWHAQ, ADH4, TRNP1, CYP2C9, CALU and APOC1) in the signature, including five high-risk genes (CDCA3, CDC20, YWHAQ, TRNP1, and CALU) and three low-risk genes (ADH4, CYP2C9, and APOC1) (Figure S4A). We therefore chose these 8 genes to establish the DMRegs_score using following: DMRegs_score = (0.1507*expression of CDCA3) + (0.1259*expression of CDC20) + (0.0408*expression of YWHAQ) + (0.0220*expression of TRNP1) + (0.0443 * expression of CALU) + (-0.0189*expression of CYP2C9) + (-0.0096 * expression of APOC1) + (-0.0055 * expression of ADH4). With an optimal survival cut-point value of 3.75, we divided the patients into high-risk group (n=139) and low-risk group (n=431) (Table S9). A significant worse prognosis was observed for the patients in the high-risk group compared to the low-risk group (Figure 6C). The differential expressions of eight genes between high- and low-risk group were presented in Figures S4B–J.

Three genes (ADH4, APOC1 and CYP2C9) were highly expressed in low-risk group, and the expression levels of five genes (CDCA3, CDC20, YWHAQ, TRNP1, and CALU) were higher in high-risk group. We also explored the relationship between eight genes expression and clinicopathological factors (Figure S5A). These results revealed advanced stage and death patients had higher expression level of high-risk genes. The mutated frequency of these genes was drawn using "maftool"

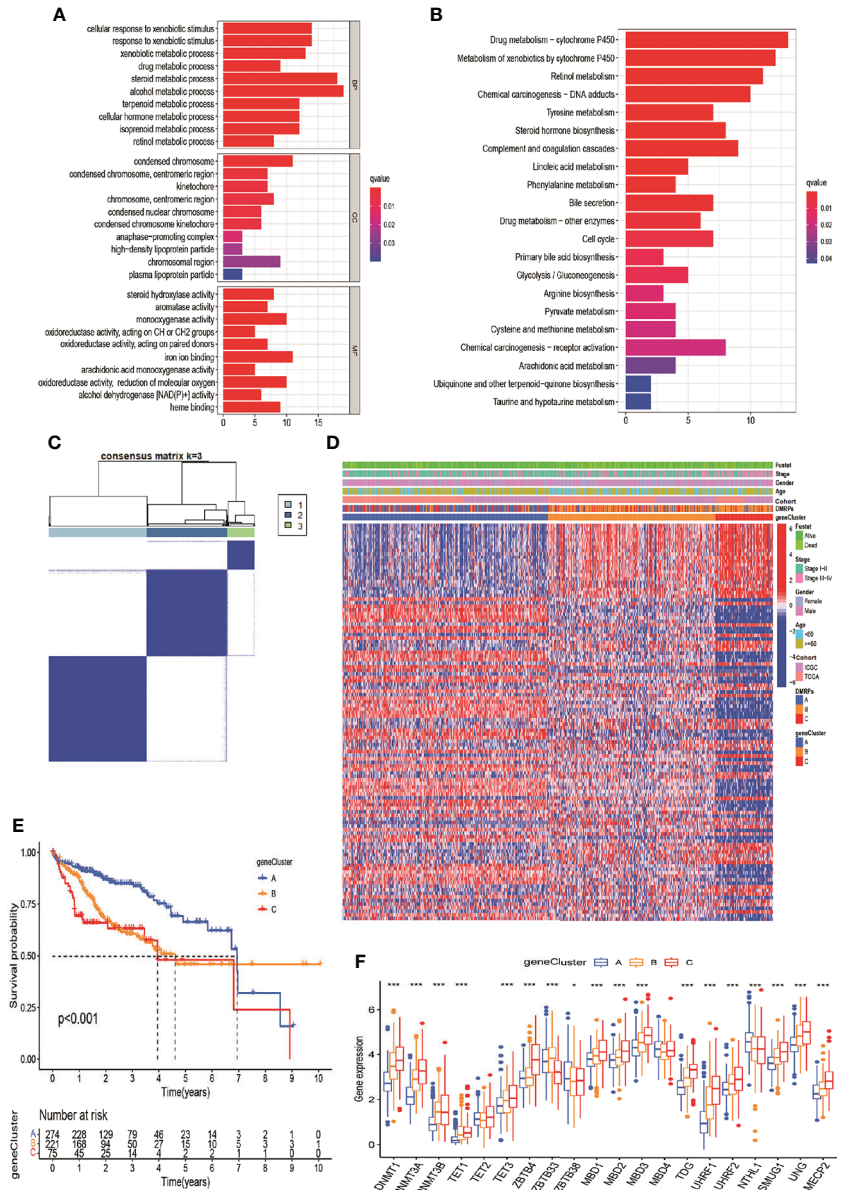

FIGURE 5
DNA modification pattern-related DEGs and gene clusters in HCC. **(A, B)** GO and KEGG enrichment analysis for DEGs of DMRPs. **(C)** Consensus cluster matrix of 570 patients for k = 3. **(D)** The relationship of clinical characteristics and unsupervised clustering of DEGs. **(E)** Kaplan-Meier curves of three gene clusters. **(F)** The expression levels of 20 DNA methylation regulators among three gene clusters. * P < 0.05, ** P < 0.01, *** P < 0.001, **** P < 0.0001.

package, and we found the few alterations happened in eight genes based on all HCC patients from TCGA (Figure S5B). The loop graph presented the chromosome locations and the gain or loss status of CNV among these risk genes (Figures S5C, D). The mutated frequency and CNV results indicated that these eight genes were epigenetically regulated by DNA methylation rather than DNA mutation or genomic alteration. What's more, the 1-, 2-, and 3-year survival rate of DMRegs_score were illustrated by AUC values of ROC curves, 0.751, 0.724 and 0.710, respectively (Figure 6D). In addition, we discovered significant differences in DMRegs_score between three DMRPs and three gene clusters (Figures 6E, F). The DMRegs_score was highest in pattern B, while that of pattern A was lowest. Differently, the gene cluster C had the highest DMRegs_score than the other two phenotypes. The Sankey diagram showed the distribution of patients in three DMRPs, three gene clusters, DMRegs_score and survival status (Figure 6G). In addition, the correlation strength among these genes in DMRegs_score was presented in Figure 6H.

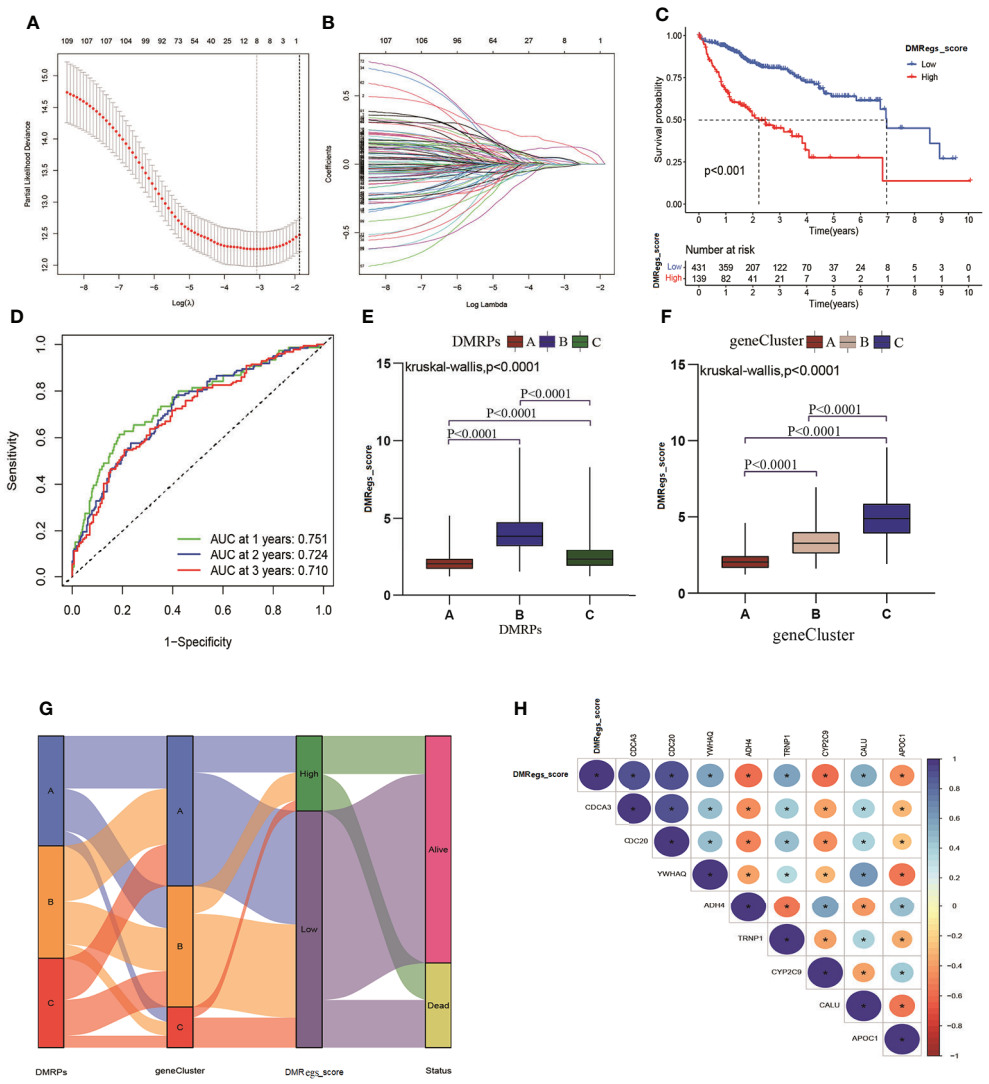

FIGURE 6
Generation of DMRegs_score. **(A, B)** The screen of candidate prognostic genes through LASSO cox regression analysis. **(C)** Survival analysis of the OS between different risk groups. **(D)** The predictive value of DMRs score. **(E, F)** The differences of DMRegs_score among DMRPs and gene clusters, respectively. **(G)** Sankey diagram of the DNA patterns, gene clusters, DMRegs_score and survival status. **(H)** The correlation between DMRegs and DMRegs_score. * P < 0.05, ** P < 0.01, *** P < 0.001, **** P < 0.0001.

Assessment of TME, immune-infiltrating cells and immune checkpoint between different risk group

In order to clearly understand the relationships between DMRegs_score, TME and immune infiltrating cells, firstly, we evaluated the differences of TME scores between high- and low-risk groups. Figure 7A illustrated the low-risk group had higher stromal score than high-risk group. However, no significant differences of immune score and estimate score were observed between two risk groups. As represented in Figure 7B, the correlation of DMRegs_score and 23 immune-infiltrating cells illustrated DMRegs_score was positively correlated with actively CD4 T cells, MDSC, immune dendritic cells, natural killer T cells and type 2 T helper cells, while was negatively correlated with eosinophil, monocytes, neutrophil, regulatory T cells, and type 1T helper cells. And the heatmap displayed the abundance of 23 types of immune cell infiltration in patients with different clinical features (Figure 7C). Notably, we found the DMRegs_score was associated with T cells, so we further

10.3389/fonc.2022.877817

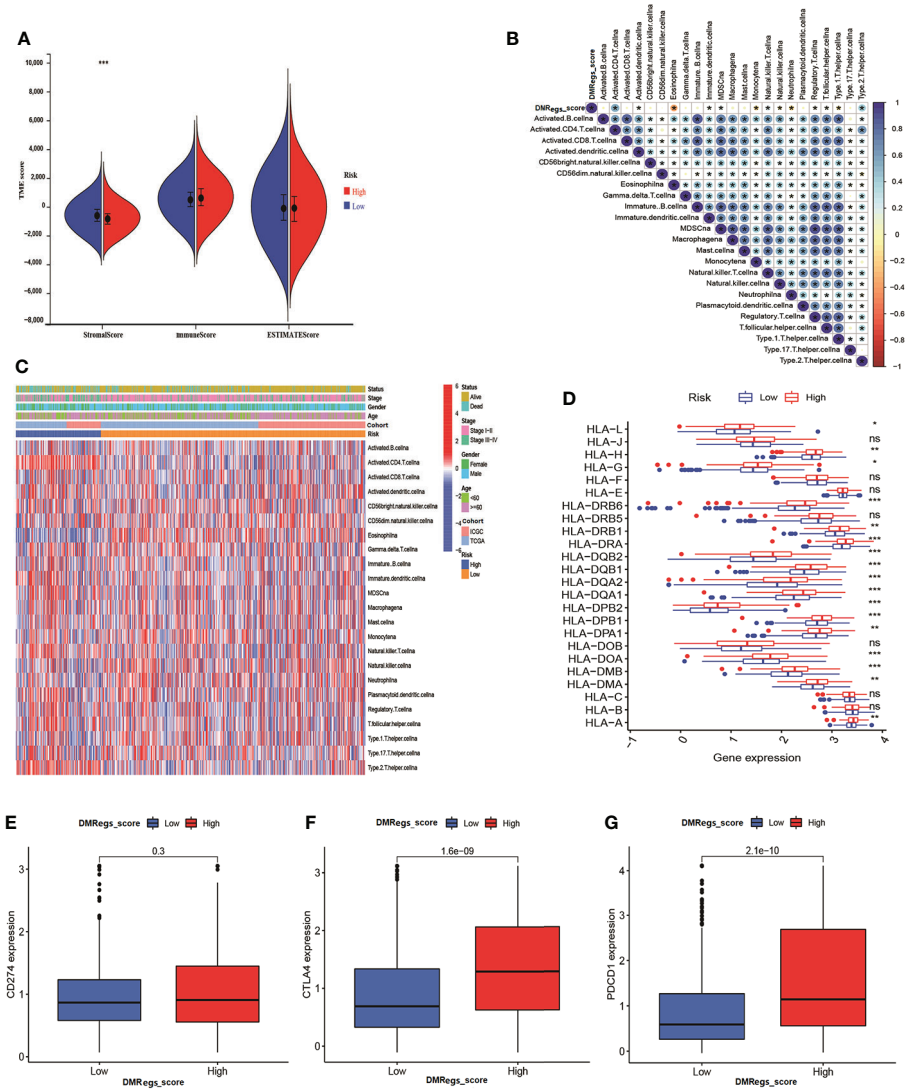

FIGURE 7
The immune cell infiltration characteristics of DMRegs_score in HCC patients. **(A)** The differences of TME score in the two risk groups. **(B)** The relationship of DMRegs_score and 23 types of immune cells infiltration. **(C)** The landscape of immune cells infiltration of DMRegs_score in patients with different clinicopathological features. **(D)** The expression differences of HLA-related genes between two risk group. **(E–G)** The expression level of CD274, CTLA4 and PDCD1 in two risk groups. * P < 0.05, ** P < 0.01, *** P < 0.001, **** P < 0.0001. ns, no significance.

explored the expression of human leukocyte antigen (HLA) related genes in different risk groups (Figure 7D). Most of the HLA-related genes presented higher expression level in high-risk group. Similarly, analysis of three important immune checkpoints revealed higher expression of PD-1 and CTLA4 in high -risk group, while the expression of PD-L1(CD274) between different risk groups was no significant difference (Figures 7E–G). These results suggested a strong correlation between DMRegs and TME of HCC patients. We guested that the DMRegs played crucial roles on the development of HCC through influenced the immune status of HCC patients.

Evaluation of the relationship between DMRegs_score and clinical characteristics

To investigate the effect of the DMRegs_score on clinical characteristics, we performed univariate and multivariate cox regression to identify whether the DMRegs_score can be an independent predicator to predict the prognosis of HCC patients. The forest plot showed the DMRegs_score could function as an independent prognostic indicator for overall survival in the multivariate analysis (Figure 8A). The clinical heat map showed

10.3389/fonc.2022.877817

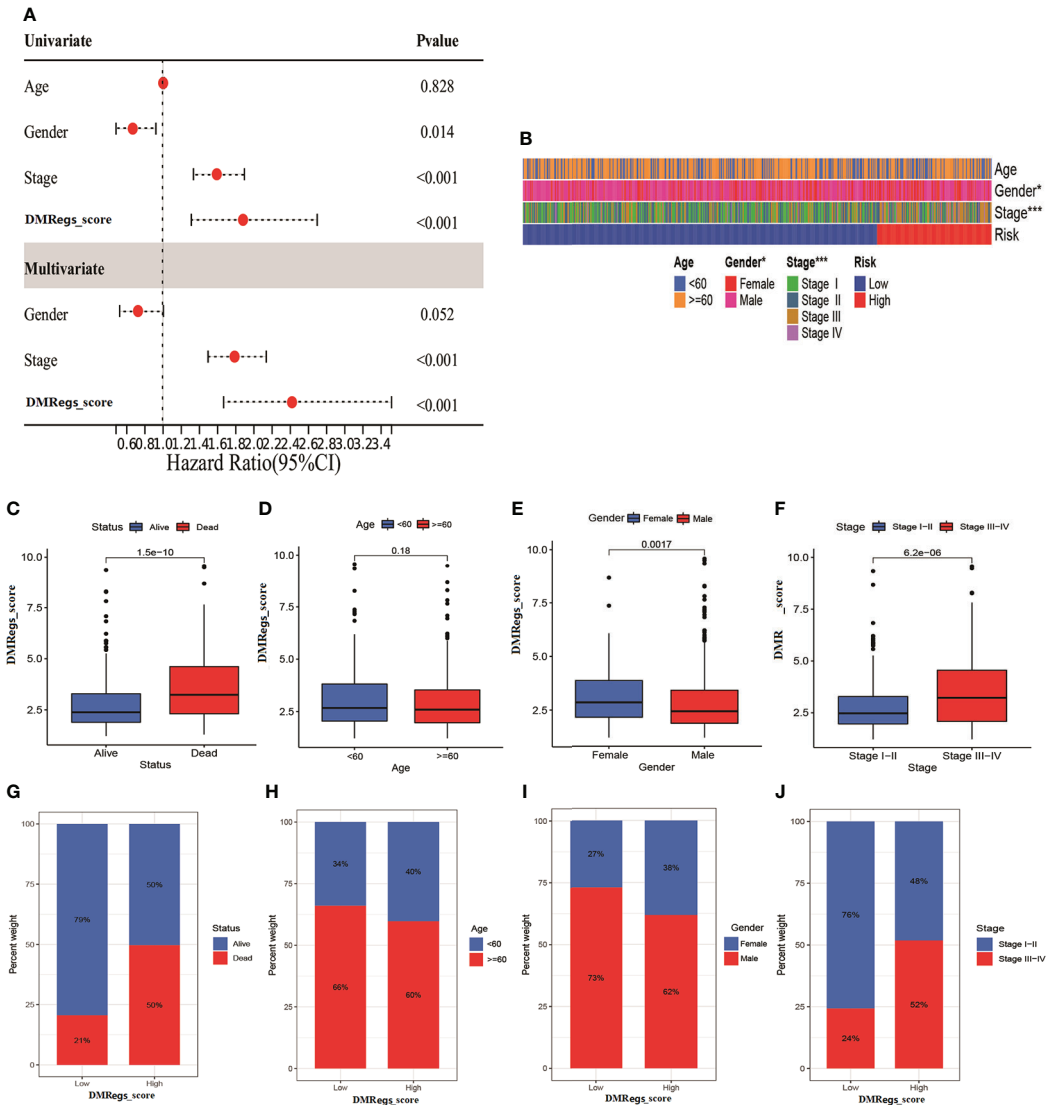

FIGURE 8
The clinical features of DMRegs_score in HCC patients. **(A)** The forest plot of univariate and multivariate cox analysis for independent prognostic factor. **(B)** The correlation heatmap of two risk groups with different clinical features. **(C–F)**. The correlation between DMRegs_score and survival status, age, gender and TNM stage. **(G–J)** The percentile of patients with different clinical features in two risk group. * P < 0.05, ** P < 0.01, *** P < 0.001, **** P < 0.0001.

more advanced stage patients gathered in high-risk group (Figure 8B). The DMRegs_score was significantly higher in death, female, and advanced stage patients, while no statistical difference was observed in age (<60 or >=60) (Figures 8C–F). What's more, we also explored the proportion of patients with different clinical characteristics in two risk groups (Figures 8G–J). The Kaplan-Meier curves suggested that, whatever the age, gender and TNM stage, the patients in high-risk group had poorer survival rate than patients in low-risk group (Figure S6).

Function enrichment, tumor mutation burden and drug sensitivity analysis

To evaluate the potential molecular mechanism of this signature, we applied GSEA based on KEGG and Hallmark gene set. The function enrichment analysis demonstrated that cell cycle, glycolysis and cancer-associated pathways were mainly enriched in high-risk group (Figures 9A, B). These results were consistent with previous DMRPs and gene-related

10.3389/fonc.2022.877817

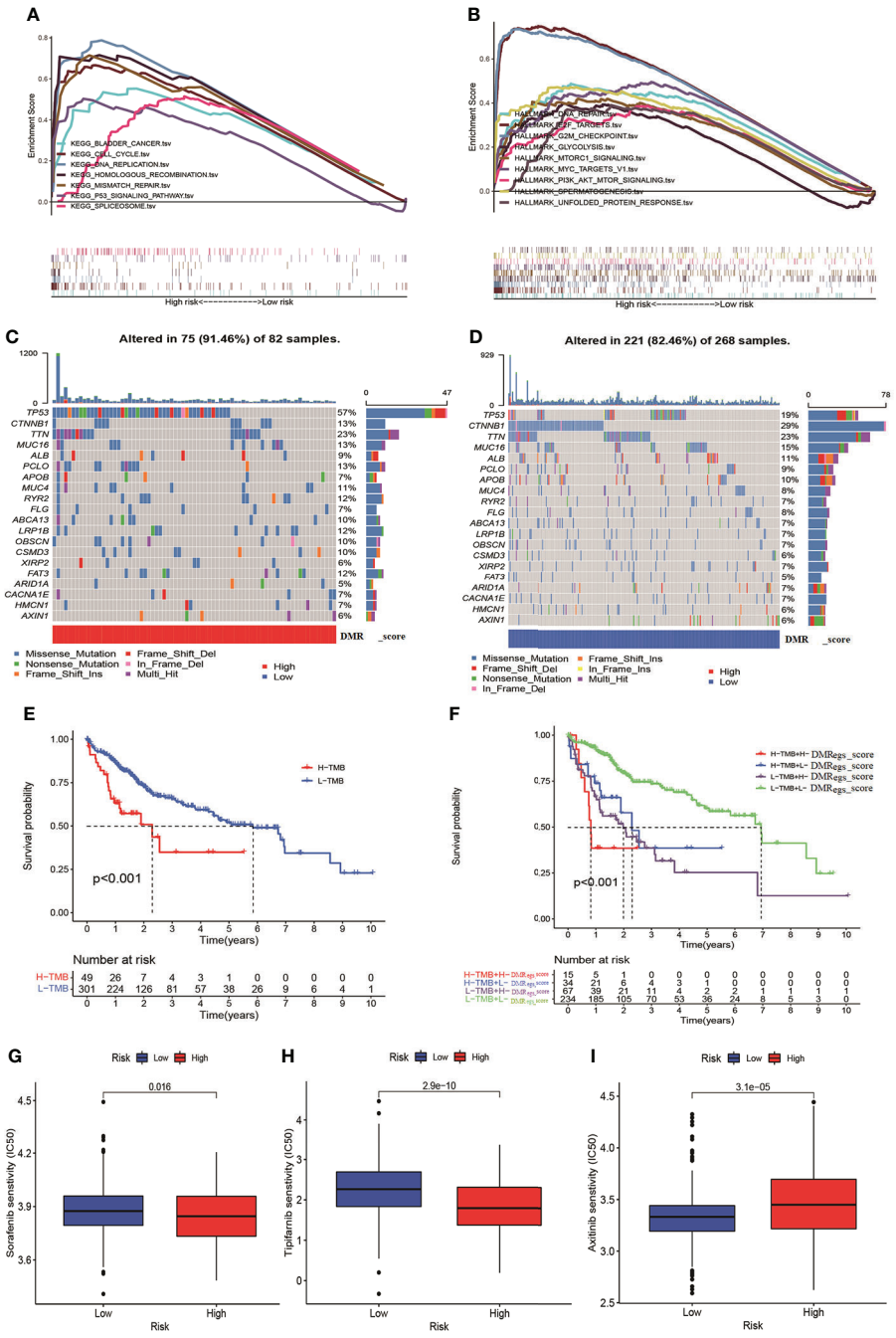

FIGURE 9
The TMB and drug sensitivity analysis for patients with different risk score. **(A, B)** The GSEA analysis in different risk groups. **(C, D)** The characteristics of tumor genetic alterations in two risk groups. **(E)** The survival analysis of patients with different TMB. **(F)** The survival analysis among four patient groups stratified by both TMB and DMRegs_score. (**G–I**) The drug sensitivity analysis of patients with different risk score. TMB: tumor mutation burden.

phenotypes. In previous studies reported TMB played a crucial role in cancer progress and immunotherapy. Therefore, we also assessed the mutational feature between two risk groups based on TCGA-LIHC cohort. The high-risk group had a higher mutation frequency (91.46%) in 82 patients, while the alteration frequency in the low-risk group was 82.46% (Figures 9C, D). The top ten mutated genes in the high- risk group were TP53, CTNNB1, TTN, MUC16, LRP1B, PCLO, APOB, MUC4, RYR2, and FAT3, and the most common type of mutation was missense mutation. Moreover, the Kaplan-

Meier curves showed that patients with lower level of TMB had a more favorable survival rate than high-TMB (Figure 9E). Combined TMB with the DMRegs_score to assess the prognosis of HCC patients, we found patients with both high-TMB and high DMRegs_score had the poorest prognosis (Figure 9F). We further screened target therapeutic drugs for the treatment of HCC patients to assess the sensitivity in different risk groups. Importantly, we observed that patients in high-risk group had lower IC50 value for sorafenib (VEGFR inhibitor), tipifarnib (farnesyltransferase inhibitor), A.443654 (AKT inhibitor), veliparib (PARP inhibitor), olaparib (PARP inhibitor), IPA-3 (PAK inhibitor), GSK-650394 (SGK inhibitor) and CCT018159 (Hsp90 inhibitor) (Figures 9G, H, Figure S7), while the IC50 values of axitinib (VEGFR inhibitor), motesanib (VEGFR), CCT007093 (PPM1D inhibitor), and lesteurtinib (JAK inhibitor) were higher in patients with high DMRegs_score (Figure 9I, Figure S7). In a word, DMRegs_score was significantly correlated with TMB and patients' clinical response to targeted therapy.

Verification the DMRegs_score and development a nomogram to predict prognosis

To validate the reliability of the DMRegs_score, we used GSE76427 as external validation group. Patients were categorized into high- and low-risk groups. The multivariate cox analysis revealed the DMRegs_score could be an independent prognostic factor (Figure S8). Survival analysis indicated the high DMRegs_score had bad survival rate (Figure 10A). And the ROC curves showed the DMRegs_score still had accurate AUC values, 1-year for 0.733, 2-year for 0.789 and 3-year for 0.823 (Figure 10B). We further established a nomogram based on the risk data of DMRegs_score and the patients' clinical features from metadata set. The nomogram composed of DMRegs_score, gender and TNM stage (Figure 10C). The AUC value of nomogram for 1-year, 2-year, and 3-year were 0.768,0.728, and 0.757, respectively (Figure 10D). In addition, we used calibration curves to confirm this nomogram prediction model (Figure 10E). However, compared with the AUC value of DMRegs_score, the nomogram scoring system had a slightly weaker predictive ability.

Validation of the expression levels of the eight risk genes which are used for the prognostic signature

Forty-one HCC tissues and adjacent normal tissues were used to detect the mRNA and protein expression of eight genes in this risk score by qRT-PCR and IHC. As presented in Figure 11, the mRNA expression level of ADH4, APOC1, and CYP2C9 were downregulated while those of CALU, CDC20, CDC3A, TRNP1, and YWHAQ were elevated in HCC tissues compared to the levels in the paired normal tissues. The results of IHC staining showed the same result as qRT-PCR, and almost genes expressed in cytoplasmic except TRNP1 expressed in nucleus (Figure 12).

Discussion

DNA methylation is closely related to carcinogenesis, tumor progression and metastasis (31, 32). In addition, by impacting multiple oncogenic pathways and tumor suppressor genes, DNA methylation regulators contribute to carcinogenesis in a broad range of tissue histologist (33, 34). In our study, based on expression levels of 20 DNA methylation regulators, we identified three DMRPs, and each DMRP correlated with different prognosis and signal pathway. Furthermore, Pattern B had the poorer prognosis and enriched in cell cycle and cancer-associated pathways, while the other two patterns mainly enriched in processes of metabolism. Besides, in order to confirm the efficacy of this regulatory mechanism, we applied consensus clustering analysis and found that genes cluster C was closely associated with more advanced TNM stage and poorer prognosis. Therefore, our study elucidates that the involvement of DNA methylation regulators in tumor development from a horizontal perspective, and provides new insights into the molecular networks involved in the regulation of DNA methylation regulators.

DNA methylation regulators can also impact the activation, differentiation, and functional fate of immune cells, which serve as a surveillance system against cancer (9, 35). For example, DNA demethylase TET2 promotes melanoma progression by maintaining the immunosuppressive function of myeloid cells and enhances anti-tumor immunity by governing G-MDSCs and CD8 + T-cell numbers (36, 37). The vast majority of studies, however, focused on a single DNA methylation regulator and its effect on altering TME (38–40). The immune cells infiltration characteristics, which are mediated by multiple synergistic DNA methylation regulator, have remained poorly understood. In this study, the DMRPs and TME immune infiltrating cells were closely related to each other. In addition, the immune scores and immune infiltrating cell types were significantly different in three DMRPs. More importantly, Based on DNA methylation regulators features found in individual tumors, we developed an effective DMRegs_score model and demonstrated its predictive ability. The clinicopathological features, prognosis and stromal score of high- and low-risk score were significantly distinct. Moreover, DMRegs_score was positively correlated with actively CD4+ T cells, MDSC, immune dendritic cells, natural killer T cells and type 2 T helper cells. Previous studies have indicated that more CD4+ T cells suggest a better prognosis (41, 42). However, our study found the tumor stage

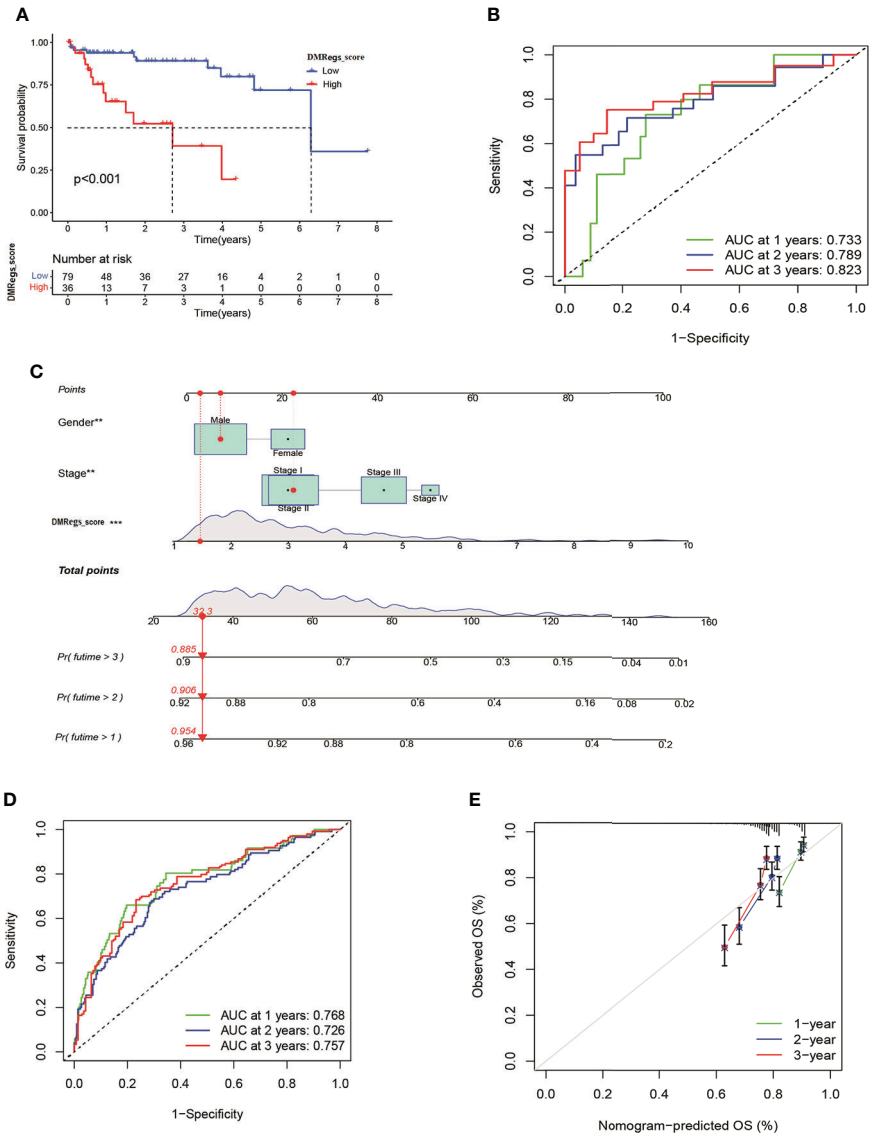

FIGURE 10
Validation of DMRegs_score in GSE76427 set and construction of nomogram. **(A)** The Kaplan- Meier curves of the OS between the two groups. **(B)** The predictive value of DMRegs_score was presented by ROC curves. **(C)** Nomogram to predict the 1-, 2- and 3-year OS of HCC patients in training set. **(D, E)** ROC and calibration curves of Nomogram for predicting of 1-, 2-, and 3-year OS in training set. ROC: receiver operating characteristic.

was more advanced in the population with high-risk group and more CD4+ T cells, and this group had better efficacy with drugs such as sorafenib and higher expression of PD-1 and CTLA-4, suggesting that the group may have a better outcome with combination therapy despite their late staging. In addition, other cancer immunotherapies in clinical trials, including dendritic cell vaccines and oncolytic viruses are also associated with TME immune infiltrating cells, such as T cells and dendritic cells (43, 44). During tumor growth, the stromal component is powerfully constricting to the immune cells, which can both be present in the tumor capsule and throughout the tumor tissue in order to prevent them from exerting anti-tumor effects (45). This is also supported by the evidence of strong stromal activation in DMRP C, where the activation of immune cells was inhibited by the AKT/mTOR pathway.

ICIs have been found to be effective in combinatorial strategies in advanced HCC patients (46). However, there is no effective biomarker for assessing the response to ICIs therapy and the prognosis of patients with HCC (47). Our detailed analyses indicated that the DMRegs_score signature probably is

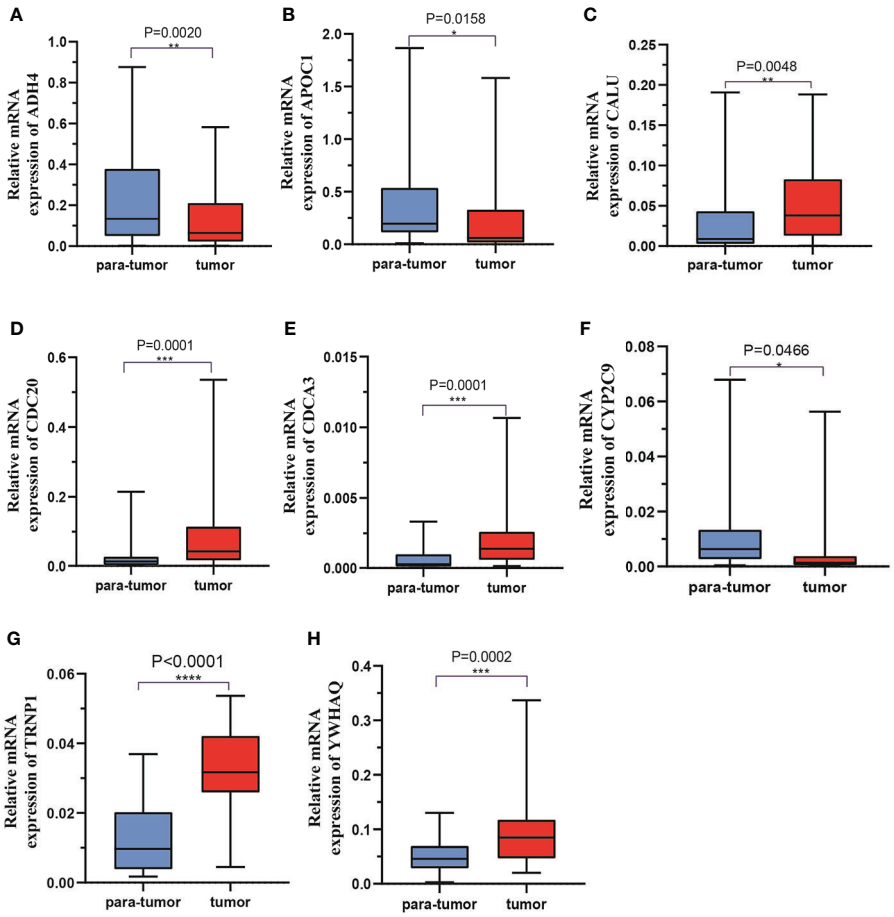

FIGURE 11
The mRNA expression levels of 8 DMRegs of prognostic signature in hepatocellular carcinoma tissues and corresponding normal tissues by RT-qPCR.

a robust and reliable biomarker to assess HCC patients' responses to ICIs and TKIs. Patients with high DMRegs_score displayed higher expression of PD-1 and CTLA-4 compared with patients with lower DMRegs_score. Previous studies indicated that higher expression of PD-1, CTLA-4 and TMB might be inclined to respond to ICIs (48, 49). Thus, we concluded that patients with high DMRegs_score, which have high TMB, high expression of PD-1, and CTLA-4 might be more suitable to ICIs. Furthermore, for advanced hepatocellular carcinoma (HCC), tyrosine kinase inhibitors (TKIs) are effective therapeutic strategies. High DMRegs_score group had lower IC50 value for some types of TKIs, such as sorafenib, tipifarnib, veliparib, olaparib, which suggested that the DMRegs_score may be predictive of TKIs and ICIs combination therapy for HCC.

In comparison to existing studies of prognostic signatures of HCC, this study has some notable advantages and limitations. First, the global DNA methylation regulators landscape was modeled in order to systematically examine the effects of DNA methylation regulators on TME in HCC patients, which have not been clarified before. Furthermore, we examined the possible role of DNA methylation regulators-related status in predicting the clinical response to immunotherapy in HCC. Our data give rules about how DNA methylation regulators influenced the multiplicity of TME. Secondly, all analyses and samples were obtained primarily based on bioinformatics analysis, and although we did some clinical validation, it is indispensable to conduct prospective studies to further validate the efficacy of DMRegs_score. Besides, a few important clinical variables like surgery and chemoradiotherapy were missing, which could have affected the prognosis of DNA methylation regulators status and the immune response.

In summary, in our comprehensive research on DNA methylation regulators, we uncovered a broad range of regulatory mechanisms in HCC through which they affected clinicopathological features, TME, and prognosis. Additionally, we investigated the therapeutic effects of DNA methylation regulators in targeted therapy and immunotherapy in HCC.

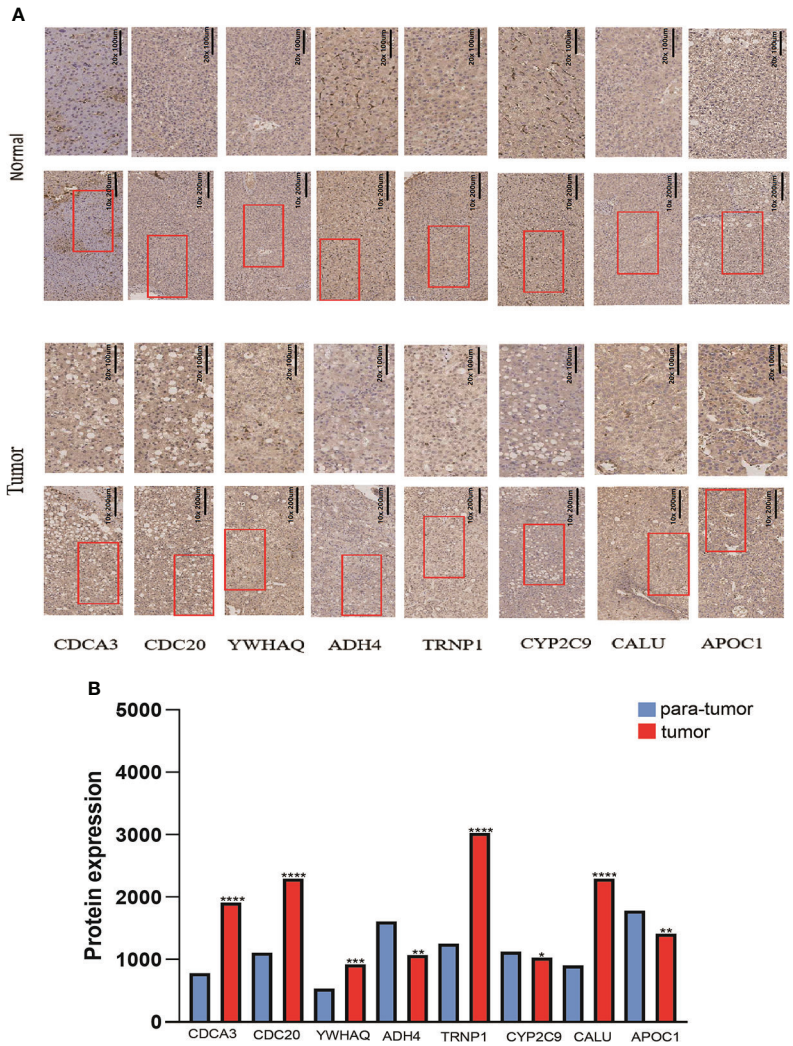

FIGURE 12
The protein expression levels of 8 DMRegs of prognostic signature in hepatocellular carcinoma tissues and corresponding normal tissues by IHC.

Our study emphasized the important clinical implications of DNA methylation regulators and provide new insights into how to personalize immunotherapy for patients with HCC.

Data availability statement

The original contributions presented in the study are included in the article/Supplementary Material. Further inquiries can be directed to the corresponding authors.

Ethics statement

The studies involving human participants were reviewed and approved by the institutional review committee of the First Affiliated Hospital of Xi'an Jiaotong University, Shaanxi Province, Xi'an, China. The patients/participants provided their written informed consent to participate in this study. Written informed consent was obtained from the individual(s) for the publication of any potentially identifiable images or data included in this article.

Author contributions

All authors listed have made a substantial, direct, and intellectual contribution to the work, and approved it for publication.

Funding

This work was supported by the National Natural Science Foundation of China under Granted (number 82102801& number 81902413); and Key Research and Development Program of Shaanxi under Granted number 2019SF-044 & number.2019SF-129.

Acknowledgments

We would like to thank all teammates for contributing this work.

Conflict of interest

The authors declare that the research was conducted in the absence of any commercial or financial relationships that could be construed as a potential conflict of interest.

Publisher's note

All claims expressed in this article are solely those of the authors and do not necessarily represent those of their affiliated organizations, or those of the publisher, the editors and the reviewers. Any product that may be evaluated in this article, or claim that may be made by its manufacturer, is not guaranteed or endorsed by the publisher.

Supplementary material

The Supplementary Material for this article can be found online at: https://www.frontiersin.org/articles/10.3389/fonc.2022.877817/full#supplementary-material

SUPPLEMENTARY FIGURE 1
The unsupervised clustering of DNA methylation regulators and consensus matrix heatmaps. **(A)** Cumulative distribution function (CDF) curve. **(B)** CDF Delta area curve, which indicates the relative change in the area under the CDF curve for each category number k compared with k-1. **(C)** The consensus matrix heatmaps for k = 2, and k = 4-9.

SUPPLEMENTARY FIGURE 2
The GSVA analysis of DNA methylaiton regulators-related patterns between pattern **(A–C)** and pattern **(B, C)**.

SUPPLEMENTARY FIGURE 3
The unsupervised clustering of DNA methylation regulators-related DEGs and consensus matrix heatmaps. **(A)** Venn diagram of DEGs among three DNA methylation regulators-related patterns. **(B)** CDF Delta area curve. **(C)** The consensus matrix heatmaps for k = 2, and k = 4-9.

SUPPLEMENTARY FIGURE 4
Characteristics of eight genes in the risk model. **(A)** The prognosis of eight genes in HCC patients. **(B–I)** The expression differences of eight genes in two risk groups.

SUPPLEMENTARY FIGURE 5
Landscape of genetic variations and transcriptional expression of eight genes. **(A)** The expression level of eight genes between different risk groups with clinical features. **(B)** 7 of the 364 patients occurred genetic variations of eight genes with 1.92% mutation frequencies. **(C)** The locations of CNV variations in eight genes on 23 chromosomes. **(D)** The frequency of CNV gain or loss among eight genes.

SUPPLEMENTARY FIGURE 6
Stratification analysis of the DMRegs_score in HCC. **(A, B)** Age (age ≤ 60 and age > 60 years old). **(C, D)** Gender (female and male). **(E, F)** Tumor stage (I-II or III-IV).

SUPPLEMENTARY FIGURE 7
The relationship between DMRegs_score and therapeutic sensitivity.

SUPPLEMENTARY FIGURE 8
The univariate and multivariate cox analysis of DMRegs_score in validating set.

References

1. Sung H, Ferlay J, Siegel RL, Laversanne M, Soerjomataram I, Jemal A, et al. Global cancer statistics 2020: GLOBOCAN estimates of incidence and mortality worldwide for 36 cancers in 185 countries. *CA Cancer J Clin* (2021) 71(3):209–49. doi: 10.3322/caac.21660

2. Llovet JM, Kelley RK, Villanueva A, Singal AG, Pikarsky E, Roayaie S, et al. Hepatocellular carcinoma. *Nat Rev Dis Primers* (2021) 7(1):6. doi: 10.1038/s41572-020-00240-3

3. Forner A, Reig M, Bruix J. Hepatocellular carcinoma. *Lancet* (2018) 391 (10127):1301–14. doi: 10.1016/S0140-6736(18)30010-2

4. Li E, Zhang Y. DNA Methylation in mammals. *Cold Spring Harb Perspect Biol* (2014) 6(5):a019133. doi: 10.1101/cshperspect.a019133

5. Smith ZD, Meissner A. DNA Methylation: roles in mammalian development. *Nat Rev Genet* (2013) 14(3):204–20. doi: 10.1038/nrg3354

6. Biswas S, Rao CM. Epigenetic tools (The writers, the readers and the erasers) and their implications in cancer therapy. *Eur J Pharmacol* (2018) 837:8–24. doi: 10.1016/j.ejphar.2018.08.021

7. Greenberg MVC, Bourc'his D. The diverse roles of DNA methylation in mammalian development and disease. *Nat Rev Mol Cell Biol* (2019) 20(10):590–607. doi: 10.1038/s41580-019-0159-6

8. Meng Q, Lu YX, Ruan DY, Yu K, Chen YX, Xiao M, et al. DNA Methylation regulator-mediated modification patterns and tumor microenvironment characterization in gastric cancer. *Mol Ther Nucleic Acids* (2021) 24:695–710. doi: 10.1016/j.omtn.2021.03.023

9. Jones PA, Ohtani H, Chakravarthy A, De Carvalho DD. Epigenetic therapy in immune-oncology. *Nat Rev Cancer* (2019) 19(3):151–61. doi: 10.1038/s41568-019-0109-9

10. Dunn J, Rao S. Epigenetics and immunotherapy: The current state of play. *Mol Immunol* (2017) 87:227–39. doi: 10.1016/j.molimm.2017.04.012

11. Wei G, Zhang H, Zhao H, Wang J, Wu N, Li L, et al. Emerging immune checkpoints in the tumor microenvironment: Implications for cancer immunotherapy. *Cancer Lett* (2021) 511:68–76. doi: 10.1016/j.canlet.2021.04.021

12. Herbst RS, Baas P, Perez-Gracia JL, Felip E, Kim DW, Han JY, et al. Use of archival versus newly collected tumor samples for assessing PD-L1 expression and overall survival: an updated analysis of KEYNOTE-010 trial. *Ann Oncol* (2019) 30 (2):281–9. doi: 10.1093/annonc/mdy545

13. Sacco AG, Chen R, Worden FP, Wong DJL, Adkins D, Swiecicki P, et al. Pembrolizumab plus cetuximab in patients with recurrent or metastatic head and neck squamous cell carcinoma: an open-label, multi-arm, non-randomised, multicentre, phase 2 trial. *Lancet Oncol* (2021) 22(6):883–892. doi: 10.1016/S1470-2045(21)00136-4

14. Pires da Silva I, Ahmed T, Reijers ILM, Weppler AM, Betof Warner A, Patrinely JR, et al. Ipilimumab alone or ipilimumab plus anti-PD-1 therapy in patients with metastatic melanoma resistant to anti-PD-(L)1 monotherapy: a multicentre, retrospective, cohort study. *Lancet Oncol* (2021) 22(6):836–847. doi: 10.1016/S1470-2045(21)00097-8

15. Sangro B, Gomez-Martin C, de la Mata M, Iñarrairaegui M, Garralda E, Barrera P, et al. A clinical trial of CTLA-4 blockade with tremelimumab in patients with hepatocellular carcinoma and chronic hepatitis c. *J Hepatol* (2013) 59(1):81–8. doi: 10.1016/j.jhep.2013.02.022

16. Yau T, Zagonel V, Santoro A, Acosta-Rivera M, Choo SP, Matilla A, et al. Nivolumab (NIVO) plus ipilimumab (IPI) plus cabozantinib (CABO) combination therapy in patients (pts) with advanced hepatocellular carcinoma (aHCC): Results from CheckMate 040. *J Clin Oncol* (2020) 38(4). doi: 10.1200/JCO.2020.38.4_suppl.478

17. Lee M, Ryoo BY, Hsu CH, Numata K, Stein S, Verret W, et al. Randomised efficacy and safety results for atezolizumab (Atezo) plus bevacizumab (Bev) in patients (pts) with previously untreated, unresectable hepatocellular carcinoma (HCC). *Ann Oncol* (2019) 30:875–5. doi: 10.1093/annonc/mdz394.030

18. Zhu AX, Finn RS, Edeline J, Cattan S, Ogasawara S, Palmer D, et al. Pembrolizumab in patients with advanced hepatocellular carcinoma previously treated with sorafenib (KEYNOTE-224): a non-randomised, open-label phase 2 trial. *Lancet Oncol* (2018) 19(7):940–52. doi: 10.1016/S1470-2045(18)30351-6

19. Samstein RM, Lee CH, Shoushtari AN, Hellmann MD, Shen R, Janjigian YY, et al. Tumor mutational load predicts survival after immunotherapy across multiple cancer types. *Nat Genet* (2019) 51(2):202–6. doi: 10.1038/s41588-018-0312-8

20. Schumacher TN, Kesmir C, van Buuren MM. Biomarkers in cancer immunotherapy. *Cancer Cell* (2015) 27(1):12–4. doi: 10.1016/j.ccell.2014.12.004

21. Roszik J, Haydu LE, Hess KR, Oba J, Joon AY, Siroy AE, et al. Novel algorithmic approach predicts tumor mutation load and correlates with immunotherapy clinical outcomes using a defined gene mutation set. *BMC Med* (2016) 14(1):168. doi: 10.1186/s12916-016-0705-4

22. Jung H, Kim HS, Kim JY, Sun JM, Ahn JS, Ahn MJ, et al. DNA Methylation loss promotes immune evasion of tumours with high mutation and copy number load. *Nat Commun* (2019) 10(1):4278. doi: 10.1038/s41467-019-12159-9

23. Zhang B, Yang C, Wang R, Wu J, Zhang Y, Liu D, et al. OTUD7B suppresses smac mimetic-induced lung cancer cell invasion and migration *via* deubiquitinating TRAF3. *J Exp Clin Cancer Res* (2020) 39(1):244. doi: 10.1186/s13046-020-01751-3

24. Wilkerson MD, Hayes DN. ConsensusClusterPlus: a class discovery tool with confidence assessments and item tracking. *Bioinformatics* (2010) 26 (12):1572–3. doi: 10.1093/bioinformatics/btq170

25. Hänzelmann S, Castelo R, Guinney J. GSVA: gene set variation analysis for microarray and RNA-seq data. *BMC Bioinf* (2013) 14:7. doi: 10.1186/1471-2105-14-7

26. Yoshihara K, Shahmoradgoli M, Martínez E, Vegesna R, Kim H, Torres-Garcia W, et al. Inferring tumour purity and stromal and immune cell admixture from expression data. *Nat Commun* (2013) 4:2612. doi: 10.1038/ncomms3612

27. Charoentong P, Finotello F, Angelova M, Mayer C, Efremova M, Rieder D, et al. Pan-cancer immunogenomic analyses reveal genotype-immunophenotype relationships and predictors of response to checkpoint blockade. *Cell Rep* (2017) 18 (1):248–62. doi: 10.1016/j.celrep.2016.12.019

28. Mafi S, Mansoori B, Taeb S, Sadeghi H, Abbasi R, Cho WC, et al. mTOR-mediated regulation of immune responses in cancer and tumor microenvironment. *Front Immunol* (2021) 12:774103. doi: 10.3389/fimmu.2021.774103

29. Wu HX, Chen YX, Wang ZX, Zhao Q, He MM, Wang YN, et al. Alteration in TET1 as potential biomarker for immune checkpoint blockade in multiple cancers. *J Immunother Cancer* (2019) 7(1):264. doi: 10.1186/s40425-019-0737-3

30. Xu YP, Lv L, Liu Y, Smith MD, Li WC, Tan XM, et al. Tumor suppressor TET2 promotes cancer immunity and immunotherapy efficacy. *J Clin Invest* (2019) 129(10):4316–31. doi: 10.1172/JCI129317

31. Koch A, Joosten SC, Feng Z, de Ruijter TC, Draht MX, Melotte V, et al. Analysis of DNA methylation in cancer: location revisited. *Nat Rev Clin Oncol* (2018) 15(7):459–66. doi: 10.1038/s41571-018-0004-4

32. Dawson MA, Kouzarides T. Cancer epigenetics: from mechanism to therapy. *Cell* (2012) 150(1):12–27. doi: 10.1016/j.cell.2012.06.013

33. Wang J, Yang J, Li D, Li J. Technologies for targeting DNA methylation modifications: Basic mechanism and potential application in cancer. *Biochim Biophys Acta Rev Cancer* (2021) 1875(1):188454. doi: 10.1016/j.bbcan.2020.188454

34. Jones PA, Issa JP, Baylin S. Targeting the cancer epigenome for therapy. *Nat Rev Genet* (2016) 17(10):630–41. doi: 10.1038/nrg.2016.93

35. Hogg SJ, Beavis PA, Dawson MA, Johnstone RW. Targeting the epigenetic regulation of antitumour immunity. *Nat Rev Drug Discovery* (2020) 19(11):776–800. doi: 10.1038/s41573-020-0077-5

36. Pan W, Zhu S, Qu K, Meeth K, Cheng J, He K, et al. The DNA methylcytosine dioxygenase Tet2 sustains immunosuppressive function of tumor-infiltrating myeloid cells to promote melanoma progression. *Immunity* (2017) 47(2):284–297.e5. doi: 10.1016/j.immuni.2017.07.020

37. Li S, Feng J, Wu F, Cai J, Zhang X, Wang H, et al. TET2 promotes anti-tumor immunity by governing G-MDSCs and CD8(+) T-cell numbers. *EMBO Rep* (2020) 21(10):e49425. doi: 10.15252/embr.201949425

38. Zhang B, Wu Q, Li B, Wang D, Wang L, Zhou YL. m(6)A regulator-mediated methylation modification patterns and tumor microenvironment infiltration characterization in gastric cancer. *Mol Cancer* (2020) 19(1):53. doi: 10.1186/s12943-020-01170-0

39. Klümper N, Ralser DJ, Bawden EG, Landsberg J, Zarbl R, Kristiansen G, et al. LAG3 (LAG-3, CD223) DNA methylation correlates with LAG3 expression by tumor and immune cells, immune cell infiltration, and overall survival in clear cell renal cell carcinoma. *J Immunother Cancer* (2020) 8(1):e000552. doi: 10.1136/jitc-2020-000552

40. Zheng Y, Wang Z, Wei S, Liu Z, Chen G. Epigenetic silencing of chemokine CCL2 represses macrophage infiltration to potentiate tumor development in small cell lung cancer. *Cancer Lett* (2021) 499:148–63. doi: 10.1016/j.canlet.2020.11.034

41. Fu J, Zhang Z, Zhou L, Qi Z, Xing S, Lv J, et al. Impairment of CD4+ cytotoxic T cells predicts poor survival and high recurrence rates in patients with hepatocellular carcinoma. *Hepatology* (2013) 58(1):139–49. doi: 10.1002/hep.26054

42. Zhu J, Feng A, Sun J, Jiang Z, Zhang G, Wang K, et al. Increased CD4(+) CD69(+) CD25(-) T cells in patients with hepatocellular carcinoma are associated with tumor progression. *J Gastroenterol Hepatol* (2011) 26(10):1519–26. doi: 10.1111/j.1440-1746.2011.06765.x

43. Lurje I, Hammerich L, Tacke F. Dendritic cell and T cell crosstalk in liver fibrogenesis and hepatocarcinogenesis: Implications for prevention and therapy of liver cancer. *Int J Mol Sci* (2020) 21(19):7378. doi: 10.3390/ijms21197378

44. Zongyi Y, Xiaowu L. Immunotherapy for hepatocellular carcinoma. *Cancer Lett* (2020) 470:8–17. doi: 10.1016/j.canlet.2019.12.002

45. Kaymak I, Williams KS, Cantor JR, Jones RG. Immunometabolic interplay in the tumor microenvironment. *Cancer Cell* (2021) 39(1):28–37. doi: 10.1016/j.ccell.2020.09.004

46. Cheng AL, Hsu C, Chan SL, Choo SP, Kudo M. Challenges of combination therapy with immune checkpoint inhibitors for hepatocellular carcinoma. *J Hepatol* (2020) 72(2):307–19. doi: 10.1016/j.jhep.2019.09.025

47. Dong Y, Wong JSL, Sugimura R, Lam KO, Li B, Kwok GGW, et al. Recent advances and future prospects in immune checkpoint (ICI)-based combination therapy for advanced HCC. *Cancers (Basel)* (2021) 13(8):1949. doi: 10.3390/cancers13081949

48. Tang B, Zhu J, Zhao Z, Lu C, Liu S, Fang S, et al. Diagnosis and prognosis models for hepatocellular carcinoma patient's management based on tumor mutation burden. *J Adv Res* (2021) 33:153–65. doi: 10.1016/j.jare.2021.01.018

49. Hong WF, Gu YJ, Wang N, Xia J, Zhou HY, Zhan K, et al. Integrative characterization of immune-relevant genes in hepatocellular carcinoma. *J Clin Transl Hepatol* (2021) 9(3):301–14. doi: 10.14218/JCTH.2020.00132

frontiers | Frontiers in Immunology

TYPE Original Research
PUBLISHED 06 September 2022
DOI 10.3389/fimmu.2022.944898

OPEN ACCESS

EDITED BY
Zheng Gong,
Jackson Laboratory, United States

REVIEWED BY
Faten Limaiem,
Hôpital Mongi Slim, Tunisia
Lincan Duan,
Third Affiliated Hospital of Kunming Medical University, China

*CORRESPONDENCE
Jianbing Wu,
Ndefy93008@ncu.edu.cn

SPECIALTY SECTION
This article was submitted to Cancer Immunity and Immunotherapy, a section of the journal Frontiers in Immunology

RECEIVED 16 May 2022
ACCEPTED 15 August 2022
PUBLISHED 06 September 2022

CITATION
Huang S, Sun L, Hou P, Liu K and Wu J (2022) A comprehensively prognostic and immunological analysis of actin-related protein 2/3 complex subunit 5 in pan-cancer and identification in hepatocellular carcinoma. *Front. Immunol.* 13:944898. doi: 10.3389/fimmu.2022.944898

A comprehensively prognostic and immunological analysis of actin-related protein 2/3 complex subunit 5 in pan-cancer and identification in hepatocellular carcinoma

Shenglan Huang[1,2], Liying Sun[1,2], Ping Hou[3], Kan Liu[1,2] and Jianbing Wu[1,2]*

[1]Department of Oncology, The Second Affiliated Hospital of Nanchang University, Nanchang, China, [2]Jiangxi Key Laboratory of Clinical and Translational Cancer Research, The Second Affiliated Hospital of Nanchang University, Nanchang, China, [3]Department of Hepatobiliary Surgery, The Second Affiliated Hospital of Nanchang University, Nanchang, China

Background: Actin-related protein 2/3 complex subunit 5 (ARPC5) is one of the members of actin-related protein 2/3 complex and plays an important role in cell migration and invasion. However, little is known about the expression pattern, prognosis value, and biological function of ARPC5 in pan-cancer. Thus, we focus on ARPC5 as cut point to explore a novel prognostic and immunological biomarker for cancers.

Methods: The public databases, including TCGA, GTEx, and UCEC, were used to analyze ARPC5 expression in pan-cancer. The Human Protein Atlas website was applied to obtain the expression of ARPC5 in different tissues, cell lines, and single-cell types. Univariate Cox regression analysis and Kaplan–Meier analysis were used to explore the prognosis value of ARPC5 in various cancers. Spearman's correlation analysis was performed to investigate the association between ARPC5 expression and tumor microenvironment scores, immune cell infiltration, immune-related genes, TMB, MSI, RNA modification genes, DNA methyltransferases, and tumor stemness. Moreover, qPCR, Western blot, and immunohistochemistry were carried out to examine the differential expression of ARPC5 in HCC tissues and cell lines. CCK8, EdU, flow cytometry, wound-healing assays, and transwell assays were conducted to explore its role in tumor proliferation, apoptosis, migration, and invasion among HCC cells.

Results: ARPC5 expression was upregulated in most cancer types and significantly associated with worse prognosis in KIRC, KIRP, LGG, and LIHC. mRNA expression of ARPC5 showed low tissue and cell specificity in normal tissues, cell lines, and single-cell types. ARPC5 expression was positively correlated with the tumor microenvironment scores, immune infiltrating cells, immune checkpoint–related genes in most cancers. ARPC5 in STAD and BRCA was positively associated with TMB, MSI, and neoantigens. We also

discovered that ARPC5 was correlated with the expression of m1A-related genes, m5C-related genes, m6A-related genes, and DNA methyltransferases. In experiment analyses, we found that ARPC5 was significantly highly expressed in HCC tissues and HCC cells. Functionally, silencing ARPC5 dramatically decreased proliferation, migration, and invasion ability of HCC cells.

Conclusions: ARPC5 expression affects the prognosis of multiple tumors and is closely correlated to tumor immune infiltration and immunotherapy. Furthermore, ARPC5 may function as an oncogene and promote tumor progression in HCC.

KEYWORDS

ARPC5, prognosis, biomarker, immune, pan-cancer, hepatocellular carcinoma

Introduction

Actin-related protein 2/3 complex (Arp2/3) is one of the major molecules that promotes the nucleation of new microfilaments and generates branched actin networks in the process of actin protein assembling into microfilaments (1). Arp2/3 complex is composed of seven conserved subunits: two actin-like subunits (Arp2 and Arp3) and four structural subunits (ARPC1/p40, ARPC2/p34, ARPC3/p21, ARPC4/p20, and ARPC5/p16) (2). The conformation of these subunits is changed by regulatory activators and inhibitory proteins; the activated Arp2/3 complex contributes to the actin-branched junction and, thus, cross-links the polymerizing actin filaments (1). As an inseparable element in the context of the actin cytoskeleton, Arp2/3 complex has been proved involving in many essential functions, including cell division, adhesion, migration, and endocytosis (3). The invasion and metastasis of cancer cells are mainly relied on actin-related pseudopodia, microfilaments, and associated proteins. The overactivation of the Arp2/3 complex generally increases the formation of invasive pseudopodia and, thus, promotes cancer migration and metastasis (4). Previous studies found that Arp2/3 subunits are highly expressed in a variety of cancers and promote the tumorigenesis and development, including pancreatic cancer (5, 6), breast cancer (7–9), lung squamous cell carcinoma (10), prostate cancer (11), gastric cancer (12), colorectal cancer (2), and bladder cancer (4). Despite the vital role of Arp2/3 complex in an extensive range of cellular processes, studies on the specific functions and mechanisms of some subunits in the complex are relatively scarce, including ARPC5.

ARPC5 is a core component of actin-related protein 2/3 (Arp2/3) complex, which is essential for activating Arp2/3 complex-mediated actin nucleation. The abnormal expression of ARPC5 likely causes functional aberrations of the whole complex. Several studies demonstrated that ARPC5 contributes to tumor growth or metastasis, including head and neck squamous cell carcinoma (13), lung squamous cell carcinoma (10), and melanoma (14). Moreover, bioinformatics analyses have suggested that ARPC5 expression is significantly increased in multiple myeloma (MM) cells compared with normal plasma cells, and high expression of ARPC5 is associated with poor overall survival (OS) in patients with MM. Our previous study also suggested that the higher ARPC5 expression has significantly poor OS and acts as an independent factor in predicting poor prognosis of hepatocellular carcinoma (HCC) patients (15). Nevertheless, the expression pattern, prognosis values, and biological roles of ARPC5 in most types of cancer have seldomly been analyzed systematically. Thus, it is essential to explore the roles of ARPC5 in pan-cancer from a novel and comprehensive perspective.

In this study, we conducted pan-cancer analyses of ARPC5 among 33 human cancer types using the Cancer Genome Atlas (TCGA) datasets, Genotype-Tissue Expression (GTEx) datasets, and some online bioinformatic analysis websites. We first investigated the expression pattern of ARPC5 in pan-cancer and discussed the associations of ARPC5 expression with pan-cancer prognosis and clinicopathological parameters. We also explored the correlation between ARPC5 and tumor microenvironment (TME) scores, immune cell infiltration, and immune subtypes. Moreover, the association between ARPC5 and tumor immunotherapy response was unveiled. In addition, a series of experiments were conducted to confirm the differential expression of APRC5 in HCC cell lines and HCC tissues and explore its potential biological functions in HCC cells. Our study preliminarily revealed the latent application of the ARPC5 as a predictive biomarker of prognosis and immunotherapy response in pan-cancer, which deserves further research.

Materials and methods

Clinical samples and ethnics approval

A total of 40 paired pathologically diagnosed HCC specimens and adjacent normal liver tissues were obtained after liver resection at the Second Affiliated Hospital of Nanchang University (Nanchang, China) from November 2020 to November 2021. One part of the specimens was fixed with 10% formalin, others were frozen with liquid nitrogen and stored in −80°C freezer until further processing. This study was prior approved by The Second Affiliated Hospital of Nanchang University Medical Research Ethics Committee, and written informed consent was provided by each patient enrolled in this study in accordance with the Declaration of Helsinki. Clinical and pathological characteristics of each patient were collected and shown in Table 1. We also obtained the postsurgical Disease-Free Survival (DFS) data of all participants until July 2022 (last follow-up visit).

TABLE 1 Clinical and pathological features of HCC patients.

Characteristics	Number of cases (%)
Age	
≤60	27 (67.5)
>60	13 (32.5)
Gender	
Male	36 (90)
Female	4 (10)
HBsAg	
Negative	9 (22.5)
Positive	31 (77.5)
Child-Pugh classification	
A	21 (52.5)
B	19 (27.5)
AFP	
≤400 ng/ml	25 (62.5)
>400 ng/ml	15 (37.5)
Liver cirrhosis	
Absent	9 (22.5)
Present	31 (77.5)
Tumor number	
Single	30 (75)
Multiple	10 (25)
Lymph nodes metastasis	
N0	37 (92.5)
N1	3 (7.5)
Distant metastasis	
M0	40 (100)
M1	0 (0)
Edmondson–Steiner grades	
I	3 (7.5)
II	20 (50)
III	19 (47.5)
IV	0 (0)

Acquisition and processing public sequencing data of pan-cancer

The RNA-sequencing data of pan-cancer (33 cancer types) were downloaded from the UCEC database (http://xena.ucsc.edu/), which integrated TCGA database and GETx Project. The datasets were normalized and batched to the $\log_2$ (Fregments Per Kilobase per Million [FPKM]+1). Five cancers with less than three samples were eliminated, and the remaining 28 cancer types were involved in the gene differential analysis. Wilcoxon Rank Sum Test was used to evaluate the ARPC5 expression level between tumor tissues and the unpaired or paired normal tissues using the "ggplot2"and "reshape2" package of R 4.0.5 software (http:///www.r-project.org/), a value of $p < 0.05$ was considered to be statistically significant. Afterward, mRNA expression of ARPC5 in different tissues, cell lines, and single-cell types were directly obtained from the Human Protein Atlas website (https://www.proteinatlas.org/).

Genetic mutation analysis of ARPC5 in pan-cancer

The web-accessible database cBioPortal (https://www.cbioportal.org/) was utilized to analyze the gene mutation characteristics of ARPC5, including the alteration frequency, mutation type, and copy number alteration in pan-cancer. The results were presented by pressing "quick search," entering ARPC5, and selecting"Cancer Types Summary" model. Then, to further explore the correlation between ARPC5 expression and genomic variation, first, we downloaded copy number variation (CNV) datasets of the levels 4 processed by GISTIC software from TCGA database and integrated the CNV data with gene expression data. Next, Wilcoxon Rank Sum Test or Kruskal–Wallis Rank Sum Test was conducted to investigate the ARPC5 differential expression in different CNV subgroups of the pan-cancer. p-values of less than 0.05 ($p < 0.05$) were considered significant.

The correlation analysis of ARPC5 with prognosis and clinical characteristics in pan-cancer

First, the clinical information and prognosis data were acquired from the UCEC database (http://xena.ucsc.edu/), which derived from a TCGA prognosis study (16), including

OS, progression-free interval (PFI), and disease-specific survival (DSS). Then, univariate Cox regression models and Kaplan–Meier analysis were conducted to explore the relationship between ARPC5 expression and prognosis in pan-cancer *via* using "survival" and "survminer" R package. The significance was obtained *via* Log-rank statistical test between the high- and low-expression subgroups. The statistical significance was defined as $p < 0.05$. Thereafter, TISIDB (http://cis.hku.hk/TISIDB/index.php) (17), which is a web portal for tumor and immune system interaction and contains numerous heterogeneous data types from TCGA database, was used to explore the correlation between ARPC5 expression and pan-cancer clinical stages, histologic grades, and tumor molecular subtypes. Correlations were assessed using Spearman's correlation analysis and presented as rank coefficient (rho) and *p*-value. The results were exhibited when *p*-values were < 0.05.

The correlation of ARPC5 expression and TME and tumor immunity

The TME significantly influences the progression and metastasis of tumors, in which immune and stromal cells are two major non-tumor components (18). The Immune and Stromal scores were calculated by ESTIMATE algorithm using the "estimate" R package, which respectively represent the proportion of immune cells and stromal cells in the TME of tumor samples. Then, we performed the Spearman's correlation analysis to evaluate the association between ARPC5 expression and the Immune/Stromal scores.

Thereafter, Tumor Immune Evaluation Resource (TIMER) (http://timer.comp-genomics.org/), a web server for comprehensive analysis of tumor-infiltrating immune cells, was used to calculate the infiltration scores of B cell, CD4 T cell, CD8 T cell, neutrophil, macrophage, and dendritic cells (DCs) in each sample. We selected the "Gene" module in TIMER and applied Spearman's correlation analysis to assess the correlation between the expression of ARPC5 and immune cell infiltration. A p value < 0.05 was considered statistically significant. The results were presented with heatmap, and the top five cancer types with the strongest correlations were displayed with scatterplots.

Immune subtypes can effectively characterize intra-tumoral immune states, including six immune subtypes: C1 (wound healing), C2 (IFN-gamma dominant), C3 (inflammatory), C4 (lymphocyte depleted), C5 (immunological quiet), and C6 (TGF-beta dominant) (19). Different tumor types varied substantially in their proportion of immune subtypes. To identify the relationship between the expression of ARPC5 and immune subtypes in different cancer types, we applied online TISIDB web portal and the Kruskal–Wallis Test to conduct the differential expression analysis of ARPC5 in different immune subtypes of pan-cancer. Significance for the results was established and displayed when *p*-values were < 0.05.

The relationship between the ARPC5 expression and immunotherapy

Immunotherapy is a validated and critically important approach for treating patients with cancer (20). In recent years, immune checkpoint inhibitors (ICIs) have shown remarkable potential in several types of cancer (21). The expression profiling of immune checkpoint–related genes on tumor cells or immune cells might effectively predict clinical benefit to checkpoint inhibitor strategies (22). Moreover, numerous studies have proved that tumor mutation burden (TMB), microsatellite instability (MSI), and neoantigens produced by somatic mutations were primary drivers of tumor immune responses, and mutational or neoantigen burden has also been studied as a predictive biomarker in patients given checkpoint inhibitors (22, 23). In this study, we first acquired the gene mutation data of 33 cancer types possessed with "varscan 2" method from TCGA database and calculated the TMB of each cancer sample with Perl 5.30.0 software (https://www.perl.org/). Meanwhile, we obtained summarized MSI data of pan-cancer from previous studies (24, 25). Then, we probed the association between ARPC5 expression with 47 immune checkpoint–related genes, TMB, and MSI with Spearman's correlation method. Moreover, Sangerbox website (http://sangerbox.com) was utilized to investigate the correlation between ARPC5 expression and neoantigens *via* "Tool" module and Spearman's correlation test. All the results were visualized as heatmaps or radar plots.

Correlation analysis of ARPC5 expression with RNA modification, DNA methylation, and tumor stemness

Increasing evidences indicated that RNA modification pathways are misregulated in human cancers and closely connected to cancer pathogenesis. Of those, the common and characterized RNA modification are the methylation of adenosine at position 6 to give N6methyladenosine (m6A), RNA 5methylcytosine (m5C), and methylation of adenosine at position 1 to give N1methyladenosine (m1A) (26). Thus, we performed Spearman's correlation analysis to explore the relationship of ARPC5 expression with the three types of RNA modification related genes, including 10 m1A-related genes (TRMT61A, TRMT61B, TRMT10C, TRMT6, YTHDF2, YTHDF3, YTHDF1, YTHDC1, ALKBH1, and ALKBH3), 13 m5C-related genes (TRDMT1, NSUN3, NSUN4, NSUN5, NSUN7, DNMT3A, NSUN2, DNMT1, NSUN6, NOP2, DNMT3B, TET2, and ALYREF), and 21 m6A-related genes

(VIRMA,WTAP, METTL14, CBLL1, RBM15, METTL3, RBM15B, ZC3H13, ALKBH5, FTO, IGF2BP1, LRPPRC, FMR1, YTHDC1, YTHDC2, HNRNPC, YTHDF2, YTHDF3, YTHDF1, HNRNPA2B1, and ELAVL1).

DNA methylation is an important epigenetic modification regulating gene expression, and deregulation of DNA methylation is strongly associated with the tumor occurrence and development (27). The process of DNA methylation is regulated by different DNA methyltransferase enzymes. In our study, we analyzed the relationship between ARPC5 and DNA methylation process by evaluating the co-expression association of five methyltransferases (DNMT1, TRDMT1, DNMT3A, DNMT3B, and DNMT3L) and ARPC5.

Cancer progression involves in gradual loss of differentiated phenotype and acquisition of stem cell–like features. A great number of genomic, epigenomic, transcriptomic, and proteomic signatures have been associated with cancer stemness (23). In this study, we obtained tumor stemness scores (DNAss and RNAss) calculated by DNA methylation signature and mRNA expression from previous study (28) and integrated transcription expression data with two stemness scores to perform the Spearman's correlation test. The online website Sangerbox was used to explore the correlation between ARPC5 expression and stemness indexes of pan-cancer.

Cell lines and RNA interference

The HCC cell lines MHCC 97-H, Huh7, HCC-LM3, and HepG2 were purchased from Procell (Wuhan, China). The normal liver cell L-02 was obtained from the Chinese Academy of Science. These cells were maintained in Dulbecco's modified Eagle's medium (DMEM; Solaibio, Beijing, China) supplementing with 10% fetal bovine serum (FBS) (Gibco, Grand Island, NY, USA), 100 μg/ml streptomycin and 100 U/ml penicillin sodium (Biotechnology, Beijing, China) at 37°C.

Three different small-interfering RNA (siRNA) sequences, targeted to ARPC5 and negative control siRNA, were designed and synthesized by GenePhram Gene (A09001, Shanghai, China). The siRNA fragments were transfected with TransIntroTM EL Transfection Reagent (TransGen Biotech, Beijing, China) in accordance with the manufacturer's protocol. Transfected cells were cultured in DMEM medium without FBS and replaced with complete medium after 4–6 h. Subsequent experiments were conducted after transfection for 48 h. The sequences of siRNA-targeted ARPC5 were listed as follows: si-ARPC5#1 sense 5′-GUGGAUGAAUAUGACGAGATT-3′ and antisense 5′-UCUCGUCAUAUUCAUCCACTT-3′; si-ARPC5#2 sense 5′-GGCAUU CCAUCACAGGAAATT -3′ and antisense 5′-UUUCCUGUGA UGGAAUGCCTT -3′; si-ARPC5#3 sense 5′-GCAGUGCUAUGUUACU GCATT-3′ and antisense 5′-UGCAGUAACAUAGCACUGCT-3′; negative control: sense 5′- UUCUCCGAACGUGUCACGUTT-3′ and antisense 5′-ACGUGACACGUUCGGAGAATT-3′.

Quantitative real-time PCR

Total RNA was extracted using Trizol Reagent (Invitrogen, Carlsbad, CA, USA) according to the manufacturer's instructions. Next, the RNA was reversely transcribed to first-strand cDNA *via* the EasyScript® One-Step gDNA Removal and cDNA Synthesis SuperMix (AE311-03, TransGen Biotech, Beijing, China). Then, quantitative real-time polymerase chain reaction (qPCR) was conducted with TB Green® Premix Ex Taq™ II (RR820A, TaKaRa, China), taking Glyceraldehyde 3-phosphate dehydrogenase (GAPDH) as the endogenous control. The relative mRNA expression of HCC cells was calculated using the $2^{-\Delta\Delta CT}$ method, and the relative mRNA expression of HCC tissues was reckoned by $2^{-\Delta CT}$. The gene primers were presented as follows: ARPC5 Forward: 5′-TGGTGTGGAT CTCCTAATGAAGT-3′; Reverse: 5′-CACGAACAATGG ACC CTACTC-3′; GAPDH Forward: 5′- GGAGCGAGA TCCCTCCAAAAT-3′; Reverse: 5′- GGCTGTTGTCATA CTTCTCATGG-3′.

Western blotting analysis

The total protein was extracted from the HCC cells and HCC tissues with radioimmunoprecipitation assay (RIPA) lysis buffer and protease inhibitor (Beyotime, Shanghai, China). Protein concentration was assessed by BCA assay kit (Beyotime, Shanghai, China). Proteins were separated in a 10% SDS-polyacrylamide gel electrophoresis (SDS-PAGE) and transferred to a PVDF membrane. The membrane was blocked with 5% nonfat milk for 2 h at room temperature and incubated with diluted primary antibody overnight at 4°C. The primary antibodies anti-ARPC5 was purchased from Abmart (1:2000, T553316S, Shanghai, China), and primary antibodies against GAPDH (1:5000, 60004-1-Ig), E-cadherin (1:5000, 20874-1-AP), N-cadherin (1:2000, 22018-1-AP), snail (1:1000,13099-1-AP), and vimentin (1:5000, 10366-1-AP) were purchased from Proteintech (Wuhan, China). Then, the membrane was treated with horseradish peroxidase (HRP)–labeled goat anti-rabbit or anti-mouse IgG antibodies (SA00001-1/SA00001-2, Proteintech, diluted at 1:10000) at room temperature for 1 h. The protein bands were detected using the chemiluminescence ELC (Beyotime, Shanghai, China) and Bio-Rad (Hercules, CA, USA) gel scanning. ImageJ software (ImageJ 1.8.0, NIH,

Bethesda, MD) was used to quantitatively analyze the relative protein content.

Immunohistochemistry staining

The 40-paired fresh HCC tissues and adjacent normal liver tissues were collected immediately after resection from the Second Affiliated Hospital of Nanchang University, formalin-fixed, paraffin-embedded, planked on a glass slide, and baked at 60°C for 2 h. This was followed with standard xylene dewaxed procedure, hydrated with the gradient ethanol, and blocked the endogenous peroxidases with 0.3% H_2O_2. After the antigen retrieval, the rabbit anti-human ARPC5(1:500, T553316S, Abmart) primary antibody was applied to the slides and incubated at 4°C overnight and followed by the secondary anti–horseradish peroxide for 30 min. Next, the slides were stained with DAB chromogenic reagent and hematoxylin. Finally, slides were dehydrated, transparent and sealed. Microscopic images were observed by light microscopy. Representative results were presented. The Image-pro plus 6.0 software (Media Cybernetics, Inc., Rockville, MD, USA) was used to calculate cumulative optical density (IOD) and pixel area of tissue, and the immunohistochemical results were expressed as mean optical density.

Cell proliferation assays

CCK8 assays and 5-ethynyl-2′-deoxyuridine (EdU) staining assays were used to detect the proliferation ability of HCC cells. For the CCK8 assay, a total of 2×10^3 transfected cells were uniformly seeded in 96-well plates and cultured for 12, 24, 48, and 72 h. CCK8 reagent (10 µl) was added into each well for 2-h incubation. The absorbance at a wavelength of 450 nm was detected on an enzyme immune-assay analyzer (Bio-Rad, Hercules, CA, USA). EdU assay was performed using YF 555 Click-iT EdU kit (C6016L, US Everbright® Inc., China) according to the manufacturer's instructions. The transfected HCC cells were planted in the 96-well plate, incubated for 24 h, and labeled with EdU reagent. After fixation and permeabilization, the cells were stained with EdU fluorescence staining kit. The images were observed and photographed by fluorescence microscopy, and ImageJ software was used to calculate the percentage of proliferation cells.

Flow cytometry

After 48 h of transfection, cell apoptosis was detected with FITC-Annexin V/PI apoptosis detection kit (F6012, US Everbright® Inc., China). According to the product instruction, first, the cells were digested with EDTA-free trypsin, centrifuged at 1,000 rpm/min for 5 min, washed three times with phosphate-buffered saline (PBS), and resuspended the cells with 100 µl of mixed buffer. Then, the cell samples were stained with 5 µl of PI and 5 µl of FITC-Annexin V. After incubating at 4°C for 15 min protected from light, another 400 µl of binding buffer was added to the flow samples and mixed well. At last, flow cytometer (FACSCalibur flow cytometer; BD Biosciences, San Jose, CA, USA) was used to detect the apoptotic cells, and the apoptosis percentage was calculated, including early apoptosis (Annexin V^+/PI^-) and late apoptosis (Annexin V^+/PI^+).

Cell migration and invasion assays

The migration ability of HCC cells was detected by Scratch assays. First, the transfected HCC cells were evenly plated and incubated in 6-well until 100% confluence. Then, a sterile 100-µl pipette tip was used to scratch the cell monolayer and produce a clear wound. The cells were washed with PBS to remove floating cells and cultured with fresh serum containing medium for 48 h. The cells images were acquired with an optical microscope system at 0, 24, and 48 h. The scratch area was measured with ImageJ software, and cell mobility was determined with the following formula: Cell migration rate (%) = (1 − scratch area/original scratch area) × 100%.

The invasion ability of HCC cells was analyzed by the Transwell chamber assay. The upper chamber was pre-covered with a layer of Matrigel gel (YB356234, BD Biosciences, USA), placed into a 24-well plate and dried overnight. Then, the transfected cells (2×10^4) were suspended with 200 µl of serum-free medium and seeded in the upper chamber, cell medium with 10% FBS was added to the lower chamber. After incubation for 48 h, the cells were fixed with 4% formaldehyde and stained with 0.1% crystal violet staining solution. The number of invading cells was counted using a light microscope at ×200 magnification.

Statistical analysis

R software (https://www.r-project.org/version 4.0.4) was used to perform bioinformatic analyses. Wilcoxon Rank Sum Test or Kruskal–Wallis Rank Sum Test was applied to evaluate the differences between groups. Kaplan–Meier method and Cox regression analysis were used for survival analysis. Spearman's correlation analyses were performed to clarify the correlations between groups. The experimental data were analyzed with GraphPad Prism 9.0 software. All experiments were repeated in triplicates. The results were reported as the $M \pm SD$. The differences between groups were analyzed by using Student's t-test or one-way analysis of variance (ANOVA). All statistical tests were two-sided, and statistical significance was set at $p < 0.05$.

Results

The expression analysis of ARPC5 in pan-cancer

In our study, we first downloaded the RNA-sequencing data of 33 cancer types from UCSC database basing on TCGA datasets and GETx datasets. After removing the cancer types with less than three samples, 22 cancer types of TCGA data (N = 8886) and 28 cancer types in TCGA target GTEx data (N = 16962) were enrolled in gene differential analysis. Then, the differential expression of ARPC5 between tumor and normal tissues of pan-cancer was assessed using Wilcoxon Rank Sum Test. Figure 1A showed the analysis of TCGA dataset, the mRNA expression of ARPC5 in tumor tissues of GBM, CESC, BRCA, ESCA, KIRP, STAD, HNSC, KIRC, LIHC, BLCA, and CHOL was higher than the corresponding normal tissues. While significant downregulation of ARPC5 was observed in LUAD, COAD, PRAD, LUSC, THCA, and KICH. After integrating the TCGA data with GTEx datasets, we discovered that the ARPC5 was upregulated in other 10 cancer types, including LGG, COAD, PRAD, LUSC, WT, SKCM, THCA, OV, PAAD, and TGCT. ARPC5 was downregulated in UCS, ALL, and KICH (Figure 1B). In addition, paired sample analysis was performed in the 18 cancer types based on TCGA datasets, ARPC5 expression was found to be upregulated in tumor tissues of BRCA, BLCA, CHOL, ESCA, HNSC, KIRC, KIRP, LIHC, LUSC, and STAD, while downregulated in KICH and THCA. (Figure 1C). The results indicated that the expression of ARPC5 was upregulated in most cancer types.

Furthermore, Human Protein Atlas website was applied to assess the APRC5 expression in different tissues and cell lines. As shown in Figures 1D–F, the ARPC5 expressed in all normal tissues and cell lines, showing low RNA tissue and cell specificity in human normal tissues, tumor cell lines, and single cell types. The mRNA expression levels of ARPC5 were relatively higher in lymph nodes, appendix, and blood and immune cells whereas lower in brain tissues and neuronal cells.

Genetic alteration status of ARPC5 in pan-cancer

The online platform cBioPortal was used to analyze the gene alteration frequency and mutation type of ARPC5 in pan-cancer. The results indicated the most common alteration types was gene "Amplification," followed by "Mutation," "Deep Deletion," and "Structural Variant." The highest alteration frequency of ARPC5 was observed in cholangiocarcinoma, in which three of 32 cases (8.33%) happened gene "Amplification." The gene alteration frequency was 7.56% in invasive breast carcinoma and 7.26% in HCC; the alteration frequency of other cancer types was less than 5% (Figure 2A). Moreover, we further explored the relationship between genomic variation and ARPC5 expression in pan-cancer *via* integrating CNV and gene expression data. Wilcoxon Rank Sum Tests or Kruskal–Wallis Rank Sum Test was used to compare the expression levels of ARPC5 in different variation status of each cancer. The results were shown in Figure 2B, remarkable difference of ARPC5 expression was found among gain variation, loss variation, and no variation groups in 14 cancer types, such as GBM, CESC, BRCA, ESCA, SARC, STAD, PRAD, HNSC, LUSC, LIHC, PAAD, OV, UCS, and BLCA. Taking LIHC as an example, neutral group showed higher ARPC5 expression than gain and loss variation groups. That indicating ARPC5 expression was closely associated with the mutation type in multiple cancer types.

The correlation of ARPC5 expression with prognosis and clinicopathology features in pan-cancer

We had clarified that ARPC5 was significantly differentially expressed among 22 cancer types in above analysis. To further investigate the correlation between the expression of ARPC5 and cancer prognosis (including OS, PFI, and DSS), single-variate Cox regression method and Kaplan–Meier analysis were conducted in 22 cancers. For univariate Cox regression analysis (Figures 3A–C), the results demonstrated that the higher ARPC5 expression was associated with worse OS in KICH, KIRC, KIRP, LGG, and LIHC, whereas the opposite results were observed in patients with OV and SKCM. The results of PFI showed higher ARPC5 expression related to shorter PFI in HNSC, KIRC, KIRP, LGG, LIHC, and PRAD. Moreover, the expression level of ARPC5 was negatively linked with DSS in KICH, KIRP, KIRC, LGG, and LIHC, whereas positive association was found in OV and SKCM. Kaplan–Meier analysis and Log-rank test further proved that high ARPC5 expression was correlated to worse OS in ESCA, HNSC, KIRC, KIRP, LGG, and LIHC, whereas the opposite results were observed in OV and SKCM (Figures 4A–H). The PFI results of Log-rank test indicated that expression of ARPC5 was negatively correlated with PFS in patients with BLCA, HNSC, KIRC, KIRP, LGG, LIHC, and PRAD (Supplementary Figure S1). The DSS results of Kaplan–Meier analysis manifested that ARPC5 expression adverse to DSS in patients with BLCA, KIRC, KIRP, LCC, and LIHC, whereas positively correlated to DSS of LUSC, OV, SKCM, and STAD (Supplementary Figure S2). In brief, these results suggested the ARPC5 can serve as an effective prognosis predictor in multiple cancers.

We further explored the relationship between expression of ARPC5 and clinicopathology features in pan-cancer, including the clinical stage, histologic grade, and tumor molecular subtype. The results with significant association were selected for display and analysis (Figure 5). The results indicated the increased

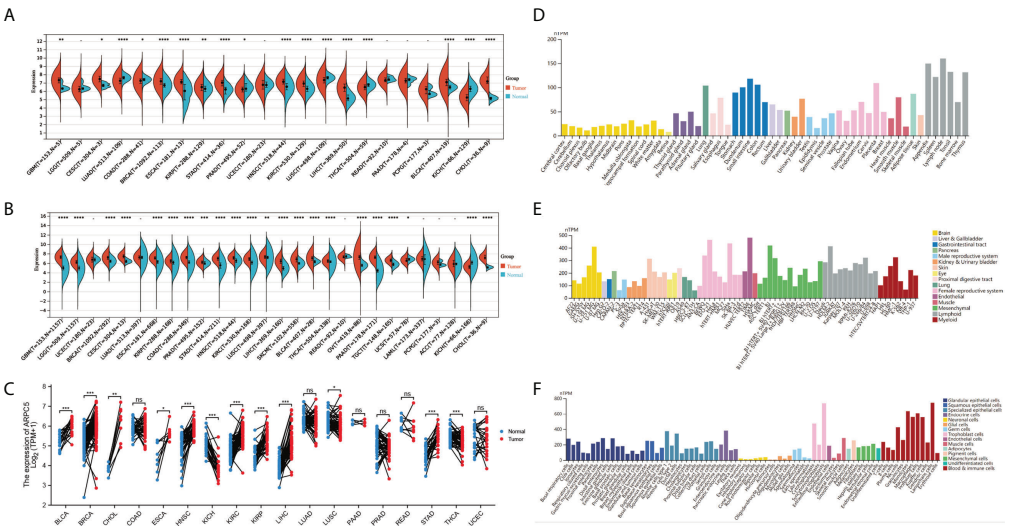

FIGURE 1
The expression levels of APRC5 in different cancers, normal tissues, and cells. **(A)** The differential expression of ARPC5 in pan-cancer tissues from TCGA datasets. **(B)** The differential expression of ARPC5 in pan-cancer tissues based on TCGA and GTEx datasets. **(C)** ARPC5 expression in paired cancer tissues and adjacent normal tissues from TCGA datasets. **(D)** The mRNA expression levels of ARPC5 in different normal tissues from HPA database. **(E)** The mRNA expression of ARPC5 in cancer cell lines from HPA database. **(F)** ARPC5 mRNA expression in different single cell types from HPA database. ns: no significance; *$p < 0.05$; **$p < 0.01$; ***$p < 0.001$; ****$p < 0.0001$.

expression of ARPC5 was positively correlated to tumor stage of KIRC (ρ = 0.311, p = 2.46e-13) and KIRP (ρ = 0.206, p = 8.51e-04) (Figures 5A–C). Similarly, there was a positive correlation between ARPC5 expression and histologic grade of KIRC (ρ = 0.268, p = 4.58e-10), LGG (ρ = 0.251, p = 7.79e-09), LIHC (ρ = 0.123, p = 0.0186), and UCEC (ρ = 0.185, p = 1,77e-05) (Figures 5D–H). It, therefore, can be concluded that ARPC5 may associate with tumorigenesis and cancer progression. As for tumor molecular subtype, we found that the expression level of ARPC5 varied among different molecular subtypes of ACC (p = 1.47e-03), BRCA (p = 1.13e-41), LGG (p = 4.81e-20), HNSC (p = 3.71e-03), KIRP (p = 5.18e-04), OV (p = 2.16e-03), LUSC (p = 2.88e-02), PCPG (p = 2.86e-03), STAD (p = 2.51e-05), and UCEC (p = 2.36e-03) (Figures 5I–R).

APRC5 expression is correlated with TME scores and immune infiltration levels in multiple cancers

In above analyses, we discovered the mRNA expression level of ARPC5 were relatively higher in immune cells. Thus, to further elucidate the potential impact of ARPC5 on the tumor immunity, we first applied the ESTIMATE algorithm to assess Immune and Stromal scores for 33 cancer types and analyzed the association between ARPC5 expression and Immune/Stromal scores using Spearman's correlation method. As shown in Table 2, the expression of ARPC5 was evidently positively related to Immune scores in 22 cancer types, including BLCA, BRCA, COAD, GBM, HNSC, KICH, KIRC, KIRP, LAML, LGG, LUAD, LUSC, OV, PCPG, PRAD, SARC, SKCM, STAD, TGCT, THCA, THYM, and UCS. No significant differences were detected in other cancer types. The Stomal scores in 15 out of 33 cancers showed significantly positive correlation with ARPC5 expression, including BLCA, GBM, KICH, KIRC, KIRP, LAML, LGG, LUAD, LUSC, OV, PCPG, PRAD, SKCM, TGCT, and THCA. ARPC5 expression was negatively correlated with Stromal scores in THYM.

Moreover, TIMER database was used to explore the correlation of ARPC5 expression with infiltration levels of B cell, $CD4^+$ T cell, $CD8^+$ T cell, neutrophil cell, macrophage cell, and DC cell in pan-cancer. The results of the Spearman's correlation analysis suggested that ARPC5 were positively associated with immune infiltration cells in most tumors. ARPC5 expression was significantly positively related to B cell in 22 cancer types, and negatively related to B cell in ESCA. The expression of ARPC5 was significantly associated with $CD4^+$ T cell in 20 cancers, $CD8^+$ T cell in 25 cancers, neutrophil cell in 32 cancers, macrophage cell in 27 cancers, and DC cell in 29 cancer types (Figure 6A). Among them, ARPC5 expression in KIRC, LGG, PRAD, THCA, and THYM was most closely related immune cells infiltration, the results were presented in Figure 6B. In KIRC, the expression of ARPC5 positively corresponded with the infiltration levels of B cell (r = 0.55, p = 5.0e-43), $CD4^+$ T cell (r = 0.46, p = 2.9e-29), $CD8^+$ T cell (r = 0.54, p = 1.5e-41), neutrophil cell (r = 0.71, p = 6.3e-81),

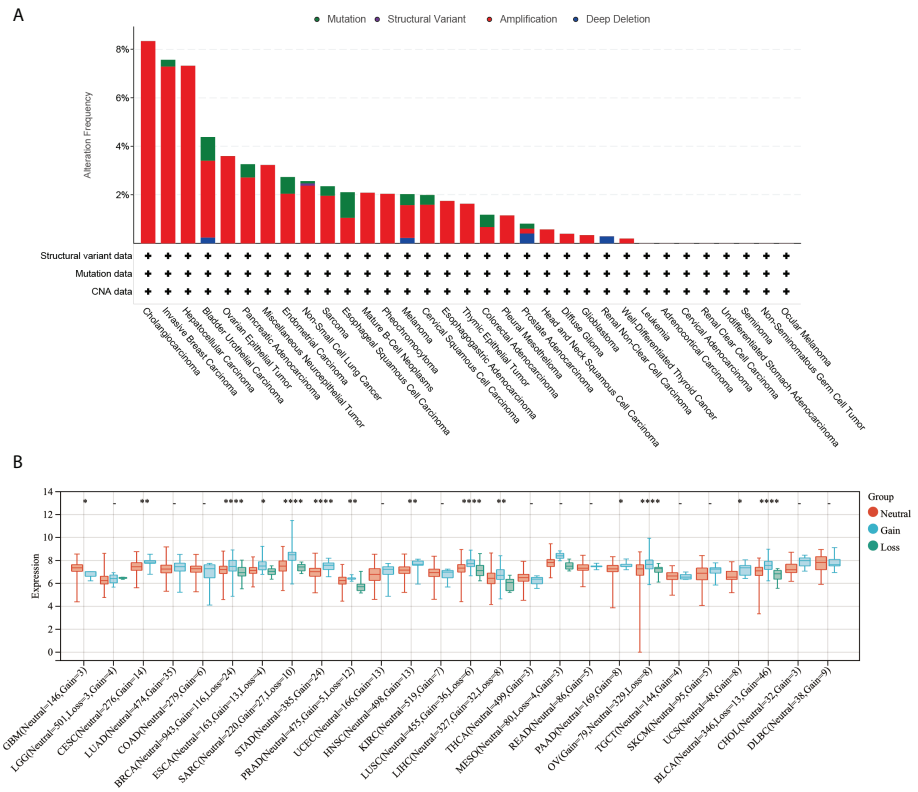

FIGURE 2
Genetic alteration of ARPC5 in pan-cancer. **(A)** Mutation type and mutation frequency of ARPC5 obtained from the cBioPortal website. **(B)** The expression levels of ARPC5 in various CNV status of pan-cancer, CNV, copy number variations; *p < 0 . 0 5 ; * *p < 0.01; ****p < 0.0001.

macrophage cell (r = 0.7, p = 2.3e-78), and DC cell (r = 0.77, p = 8.2e-103). In LGG, ARPC5 expression had a positive correlation with the proportion of B cell (r = 0.54, p = 0.9e-40), $CD4^+$ T cell (r = 0.41, p = 5.8e-22), $CD8^+$ T cell (r = 0.27, p = 1.3e-09), Neutrophil cell (r = 0.64, p = 1.9e-58), macrophage cell (r = 0.59, p = 1.5e-48), and DC cell (r = 0.62, p=7.5e-56). In PRAD, the infiltrating levels of B cell (r = 0.63, p = 1.2e-56), $CD4^+$ T cell (r = 0.38, p = 1.3e-18), $CD8^+$ T cell (r = 0.57, p = 7.5e-45), neutrophil cell (r = 0.69, p = 8.0e-70), macrophage cell (r = 0.64, p = 2.1e-57), and DC cell (r = 0.65, p = 1.4e-61) were positively related to the expression of ARPC5. Similarly, ARPC5 expression had a positive association with the infiltration levels of B cell (r = 0.43, p = 6.4e-24), $CD8^+$ T cell (r = 0.47, p = 5.1e-29), neutrophil cell (r = 0.56, p = 2.2e-43), macrophage cell (r = 0.51, p = 2.3e-34),

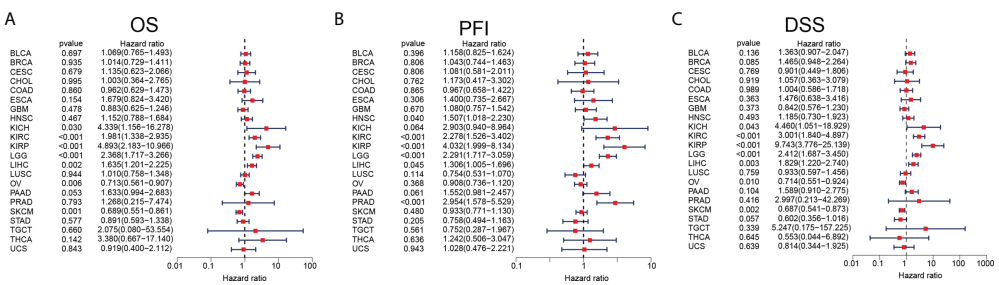

FIGURE 3
Prognosis analyses of ARPC5 in pan-cancer based on univariate Cox regression method. **(A)** The correlation between ARPC5 expression and OS. **(B)** The correlation between ARPC5 expression and PFI. **(C)** The correlation between ARPC5 expression and DSS. OS: overall survival; PFI: progression-free interval; DSS: disease-specific survival.

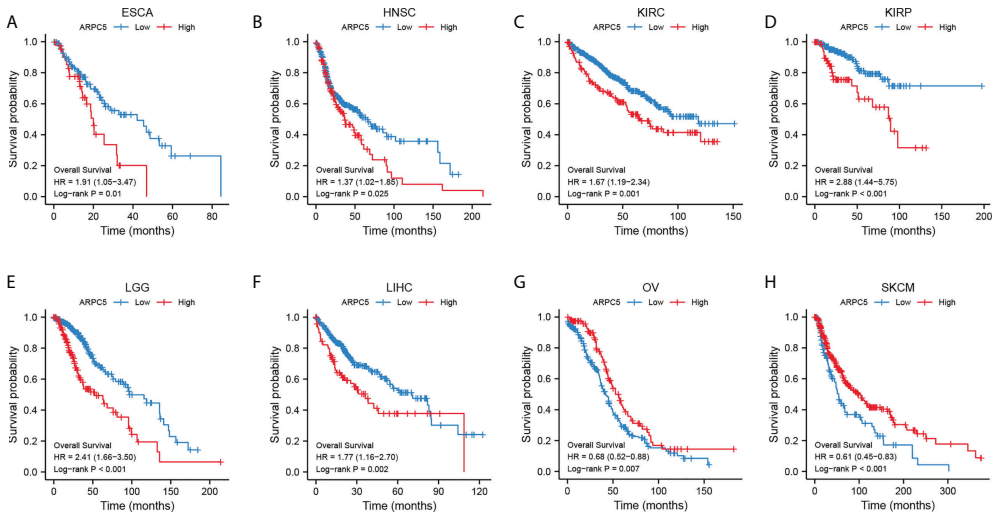

FIGURE 4
ARPC5 expression significantly correlated with OS based on Kaplan–Meier analysis. **(A)** The correlation in ESCA. **(B)** The correlation in HNSC. **(C)** The correlation in KIRC. **(D)** The correlation in KIRP. **(E)** The correlation in LIHC. **(F)** The correlation in LGG. **(G)** The correlation in OV. **(H)** The correlation in SKCM. The optimal cutoff of ARPC5 expression were used to divide patients into high- and low-expression groups.

and DC cell ($r = 0.46$, $p = 2.8e\text{-}28$) in THCA. In addition, ARPC5 positively related to the content of B cell ($r = 0.7$, $p = 1.8e\text{-}18$), $CD4^+$ T cell ($r = 0.36$, $p = 6.9e\text{-}5$), $CD8^+$ T cell ($r = 0.48$, $p = 3.8e\text{-}8$), neutrophil cell ($r = 0.31$, $p = 5.8e\text{-}4$), and DC cell ($r = 0.64$, $p = 5.1e\text{-}15$) in THYM.

In addition, we further probed into the relevance of ARPC5 expression with different immune subtypes of pan-cancer. The results revealed that ARPC5 expression was prominently related to immune subtypes in a number of cancers(Figures 7A–T), which included BLCA ($p = 3.38e\text{-}05$), BRCA ($p = 3.49e\text{-}21$), CESC ($p = 1.31e\text{-}02$), KICH ($p = 4.49e\text{-}02$), KIRC ($p = 2.79e\text{-}09$), LGG ($p = 2.42e\text{-}19$), LIHC ($p = 2e\text{-}02$), LUAD ($p = 5.6e\text{-}07$), PAAD ($p = 2.19e\text{-}03$), OV ($p = 4.67e\text{-}03$), PCPG ($p = 5.04e\text{-}03$), PRAD ($p = 8.91e\text{-}07$), READ ($p = 1.34e\text{-}02$), SARC ($p = 5.72e\text{-}03$), SKCM ($p = 1.15e\text{-}02$), STAD ($p = 1.08e\text{-}08$), TGCT ($p = 3.52e\text{-}02$), THCA ($p = 1.97e\text{-}02$), UCS ($p = 1.44e\text{-}03$), and UCEC ($p = 7.99e\text{-}05$). ARPC5 expression was generally low in C3 subtype, except for KICH, PCPG, TGCT, and ARPC5 was widely highly expressed in C2 subtype of 11 cancer types except CESC, KICH, LGG, and READ. Therefore, we speculated that ARPC5 might be more participant in IFN-gamma dominant immune processes but less involved inflammatory processes.

The association between ARPC5 expression and immune-checkmate inhibitors biomarkers

Previous studies have proved that ICIs-related genes, TMB, MSI, and tumor neoantigens can be used as effective predictors of ICIs. Thus, we discussed the correlations of ARPC5 expression with these ICIs biomarkers. First, Gene co-expression and Spearman's coefficient analyses were conducted to investigate the association between ARPC5 expression and 47 ICIs-related genes in 33 cancer types. We discovered ARPC5 was closely related to the expression of ICIs-related genes in most types of cancer, such as PRAD, TGCT, KIRC, LIHC, KIRC, THCA, LGG, KICH, PCPG, and so on. However, there was less association between ARPC5 and ICIs-related genes in CESC, SARC, MESO, and UCS (Figure 8A). In LIHC, ARPC5 exhibited significant positive correlation with most ICIs-related genes. That indicated that the ARPC5 may act as a new biomarker for ICIs in LIHC or other certain cancers.

Then, we performed an exploration to analyze the relationship of ARPC5 with TMB and MSI by integrating gene expression data and TMB and MSI data. The results of Spearman analysis showed that the expression level of ARPC5 was positively related to TMB in ACC, UCEC, STAD, SKCM, SARC, PAAD, LUAD, LGG, BRCA, and BLCA, whereas reverse correlation was presented in THYM, TGCT, and LAML (Figure 8B). We also found that the expression of ARPC5 was significantly related to MSI in 12 types of cancer. Of those, positive correlations were detected in BRCA, UCEC, STAD, READ, and HNSC; negative relations were observed in TGCT, SKCM, SARC, OV, LUSC, LUAD, and LGG (Figure 8C).

In addition, tumor neoantigens are abundantly expressed in tumor cells with strong immunogenicity and tumor heterogeneity (22). Therefore, we further measured the correlation between ARPC5 expression and tumor neoantigens. As shown in Figure 8D, the tumor neoantigens in

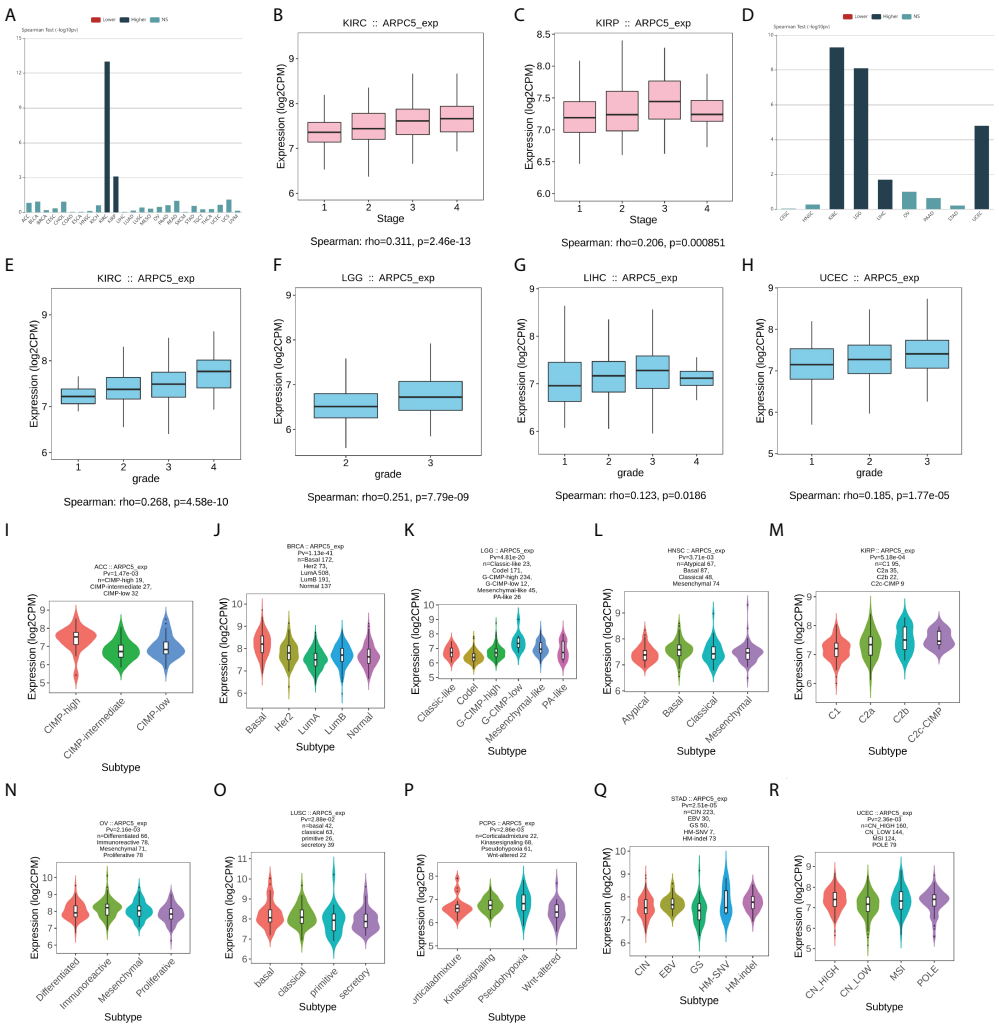

FIGURE 5
The correlation between ARPC5 expression and clinical stage, histologic grade, and tumor molecular subtypes in various cancers based on Spearman's correlation analysis (the correlation with $p < 0.05$ were displayed). **(A)** The correlation between ARPC5 expression and clinical stage in pan-cancer. **(B–C)** The expression levels of ARPC5 in different clinical stages of KIRC **(B)** and KIRP **(C)**. **(D)** The correlation between ARPC2 expression and histologic grade in pan-cancer. **(E–H)** The expression levels of ARPC5 in different histologic grades of KIRC **(E)**, LGG **(F)**, LIHC **(G)**, and UCEC **(H)**. **(I–R)** The correlation between ARPC5 expression and molecular subtypes in ACC **(I)**, BRCA **(J)**, LGG **(K)**, HNSC **(L)**, KIRP **(M)**, OV **(N)**, LUSC **(O)**, PCPG **(P)**, STAD **(Q)**, UCEC **(R)**. rho; rank coefficient of Spearman. Pv; *p*-value. NS, no significance.

five of 19 cancers showed significant positive correlation with APRC5 expression, including OV ($p = 0.003$), BRCA ($p = 0.011$), STAD ($p = 2.2e-05$), SKCM ($p = 0.025$), and PRAD ($p = 0.049$).

ARPC5 correlated with RNA modification-related genes, DNA methyltransferases, and tumor stemness scores

The RNA modification had been proved to affect mRNA stability, splicing, and translation and has important oncogenic role or tumor suppressor in different cancer types (26). The association between ARPC5 expression with RNA modification-related genes was showed in Figures 9A–C. We found that the expression level of ARPC5 in LGG, LIHC, SKCM, and UVM was significantly related to 10 m1A-related genes, whereas less correlation was observed in ACC, BLCA, CESC, ESCA, KICH, MESO, and SARC; no correlation was detected in DBLC and UCS (Figure 9A). Similarly, we examined the co-expression relations between ARPC5 and 13 m5C-related genes expression using Spearman's coefficient analysis; the results demonstrated that the expression of ARPC5 was associated with most m5C-related genes in LGG, LICH, SKCM, and

10.3389/fimmu.2022.944898

TABLE 2 The correlation between ARPC5 expression and immune scores and stromal scores of tumor microenvironments in pan-cancer.

Cancer types	Immune score		Stromal score	
	R	*p*-value	R	*p*-value
ACC	0.11	3.48E-01	0.15	1.73E-01
BLCA	0.23	**2.24E-06**	0.16	**1.34E-03**
BRCA	0.22	**2.50E-13**	0.026	3.95E-01
CESC	0.082	1.54E-01	0.037	5.15E-01
CHOL	0.083	6.29E-01	0.11	5.14E-01
COAD	0.13	**5.07E-03**	0.087	6.05E-02
DLBC	0.23	1.22E-01	0.25	8.98E-02
ESCA	0.013	8.70E-01	0.016	8.37E-01
GBM	0.48	**6.27E-11**	0.48	**9.12E-11**
HNSC	0.1	**1.97E-02**	-0.06	1.72E-01
KICH	0.56	**1.94E-06**	0.62	**7.97E-08**
KIRC	0.55	**<2.2E-16**	0.52	**<2.2E-16**
KIRP	0.42	**4.19E-14**	0.4	**1.38E-12**
LAML	0.57	**<2.2E-16**	0.65	**<2.2E-16**
LGG	0.6	**<2.2E-16**	0.56	**<2.2E-16**
LIHC	0.045	3.85E-01	0.0038	9.41E-01
LUAD	0.23	**1.31E-07**	0.24	**1.57E-08**
LUSC	0.24	**8.32E-08**	0.16	**3.72E-04**
MESO	-0.079	4.67E-01	-0.12	2.61E-01
OV	0.18	**3.20E-04**	0.19	**2.52E-04**
PAAD	0.092	2.24E-01	0.083	2.71E-01
PCPG	0.29	**9.05E-05**	0.4	**2.31E-08**
PRAD	0.43	**<2.2E-16**	0.39	**<2.2E-16**
READ	0.043	5.82E-01	0.081	3.01E-01
SARC	0.26	**2.08E-05**	0.12	5.64E-02
SKCM	0.19	**4.05E-05**	0.13	**5.93E-03**
STAD	0.11	**3.30E-02**	-0.031	5.48E-01
TGCT	0.54	**<2.2E-16**	0.41	**9.87E-08**
THCA	0.38	**<2.2E-16**	0.36	**<2.2E-16**
THYM	0.5	**1.15E-08**	-0.22	**1.62E-02**
UCEC	0.004	9.17E-01	-0.027	5.24E-01
UCS	0.4	**2.40E-03**	0.12	3.84E-01
UVM	0.059	6.04E-01	0.037	7.45E-01

R represents the coefficient correlation of Spearman analysis. Boldness indicates p-value less than 0.05.

UVM, whereas the correlation in CHOL, DLBC, ESCA, MESO, and UCS were relatively small (Figure 9B). In addition, we found that a great majority of m6A genes in COAD, LGG, LIHC, SKCM, and UVM co-expressed with ARPC5. Less significant connection, even no association between ARPC5 expression and m6A-related genes, was found in CESC, DBLC, ESCA, MESO, and UCS (Figure 9C). The above results suggested that ARPC5 may participate in RNA modification and thereby contribute to tumor development in certain cancers.

DNA methylation plays an important regulatory role in the growth, development, gene expression pattern, and genome stability, which is dynamically regulated by DNA methyltransferase and DNA demethylase activities. In our analyses, we discovered that ARPC5 expression was correlated with the expression of four methyltransferases (DNMT1, TRDMT1, DNMT3A, and DNMT3B) in multiple tumors, such as BRCA, LGG, KICH, LIHC, SKCM, THYM, and UVM (Figure 9D), whereas DNMT3L was evidently correlated with ARPC5 expression only in five cancer types: BRCA, LGG, LIHC, TGCT, and THCA.

We also analyzed the association of ARPC5 expression with tumor stemness scores (DNAss and RNAss) in 33 cancer types. The results indicated that the ARPC5 was significantly positively correlated with DNAss in PRAD and LGG ($p < 0.05$). In contrast, the expression of ARPC5 in THYM, TGCT, SARS, and LUSC was

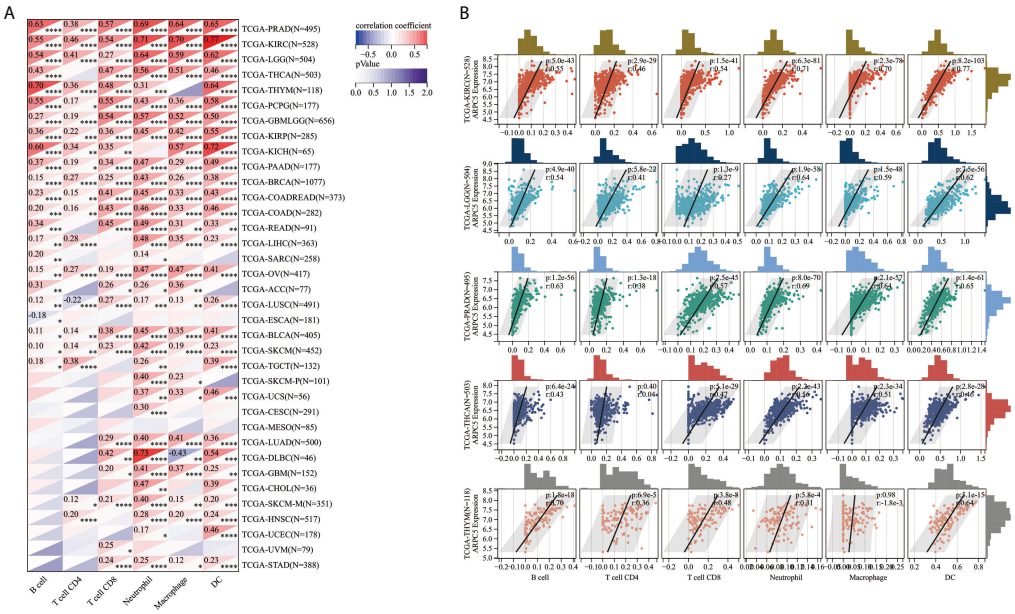

FIGURE 6
The correlation between ARPC5 and immune infiltration cells in pan-cancer based on TIMER algorithm. **(A)** Heatmap displayed the correlation between ARPC5 expression and the proportions of B cell, $CD4^+$ T cell, $CD8^+$ T cell, neutrophil, macrophage, and DC cell. **(B)** The top five cancer types (including KIRC, LGG, PRAD, THCA, and THYM) with most significant correlation between ARPC5 and immune infiltration cells were displayed with scatterplots. *$p < 0.05$; **$p < 0.01$; ***$p < 0.001$; ****$p < 0.0001$.

negatively associated with DNAss ($p < 0.05$) (Figure 9E). As for the stem cell score (RNAss), we found the expression level of ARPC5 was prominently positively related to the STAD and BRCA stem cell scores (RNAss) whereas negatively correlated with RNAss in multiple cancer types ($p < 0.05$), such as TGCT, KICH, LGG, THCA, COAD, KIRP, GBM, LAML, LIHC, OV, PRAD, CESC, and KIRC (Figure 9F).

ARPC5 is highly expressed in HCC cells and tissues

In the above expression analysis of bioinformatics method, we found that ARPC5 was significantly upregulated in multiple types of cancer, including LIHC. To further identify the results of bioinformatics analysis, the expression of ARPC5 in HCC cell lines (including MHCC97-H, Huh-7, HCC-LM3, and HepG2) and 40 paired HCC tissues was detected *via* qPCR. The results indicated that the mRNA expression level of ARPC5 was significant higher in three HCC cell lines (MHCC97-H, Huh-7, and HCC-LM3) (Figure 10A) and HCC tissues (Figure 10D) compared with that in normal liver cell line L-02 and paired adjacent liver tissues, respectively. The results of our experiments were consistent with the results of bioinformatics analysis.

Next, the protein expression level of ARPC5 in HCC cells and HCC tissues were analyzed with Western blot and immunohistochemical staining. We found that the protein expression of ARPC5 in MHCC97-H, Huh-7, HCC-LM3, and HepG2 was significantly higher than in normal live cell line (Figures 10B, C). Moreover, ARPC5 was relatively higher in HCC-LM3 and MHCC97-H, which were selected for subsequent functional experiments. Then, 10 of 40 paired HCC tissues were randomly selected for Western blot analysis; the results showed that the ARPC5 expression in most HCC tissues was upregulated compared with the adjacent normal tissues (Figure 10E). Furthermore, immunohistochemistry for ARPC5 was conducted in 40 paired HCC samples to verify the results; we found that immunohistochemical staining of ARPC5 was obviously observed in the cytoplasm of HCC cancer tissues, whereas no or weak staining was found in adjacent non-cancerous tissues. The average optical density value of ARPC5 immunohistochemical staining in cancer tissues was higher than adjacent normal liver tissues (Figures 10F, G), indicating that the ARPC5 expression was higher in tumor tissues than adjacent normal liver tissues, which cohered with the results of Western blot. Then, the patients were divided into high- and low-expression groups based on the median mRNA expression level of ARPC5, and we further conducted Kaplan–Meier survival analysis to explore the correlation between ARPC5 expression and DFS of HCC patients. The result was showed in Figure 10H; we found that high ARPC5 expression was significantly related to a poor DFS in HCC patients (HR =

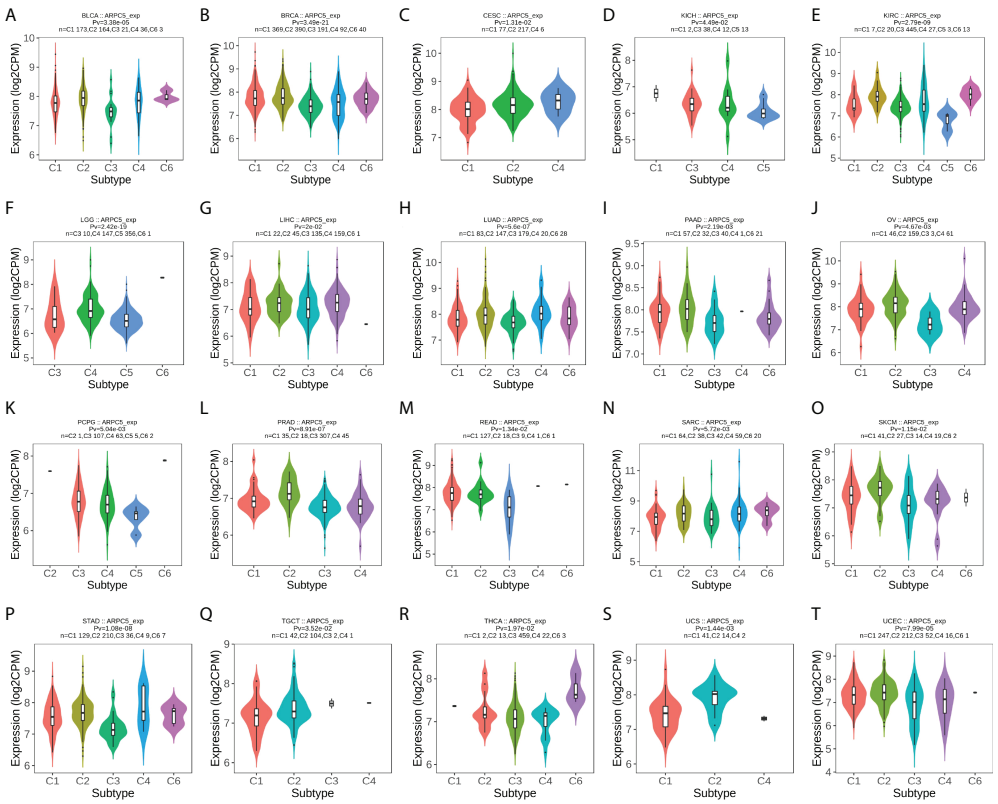

FIGURE 7
The correlation between ARPC5 expression and immune subtypes in pan-cancer using TISIDB. The cancers with significant correlation were displayed. **(A)** In BLCA. **(B)** In BRCA. **(C)** In CESC. **(D)** In KICH. **(E)** In KIRC. **(F)** In LGG. **(G)** In LIHC. **(H)** In LUAD. **(I)** In PAAD. **(J)** In OV. **(K)** PCPG. **(L)** PRAD. **(M)** In READ. (**N**) In SARC. **(O)** In SKCM. **(P)** In STAD. **(Q)** In TGCT. **(R)** In THCA. **(S)** In UCS. **(T)** In UCEC. Pv; *p*-value. C1, wound healing; C2, IFN-gamma dominant; C3, inflammatory; C4, lymphocyte depleted; C5, immunologically quiet; C6, TGF-b dominant.

2.22; 95% CI: 0.97, 5.09; p = 0.023). The median DFS of low ARPC5 expression was 47.2 months, and that of high ARPC5 expression group was 34.5 months.

Downregulation ARPC5 significantly inhibits proliferation and promotes apoptosis of HCC cells

In our previous study, we discovered that ARPC5 in HCC mainly participates in MAPK signaling pathway and WNT signaling pathway basing on KEGG enrichment analysis (15). To investigate the potential functions of ARPC5 in HCC cells, we downregulated the expressions of APRC5 and examined the effects of ARPC5 knockdown on cell proliferation and apoptosis. First, qPCR assays and Western blot were performed to verify the transfection efficiency of ARPC5 in both HCC-LM3 and MHCC 97-H cells. The results showed that ARPC5 can be effectively interfered by si-ARPC5#1 and si-ARPC5#3 (Figures 11A, B). We selected si-ARPC5#1 for subsequent function experiments. Then, we discussed the effect of ARPC5 on HCC cells proliferation using CCK8 assays and EdU staining assays. The results of EdU assays demonstrated that the silence of ARPC5 distinctly suppressed the proliferative capacity of HCC cells compared with controls (Figures 11C, D). The growth curves from CCK-8 assays suggested that proliferation of HCC cells transfected with si-ARPC5 were significantly inhibited compared with that transfected with si-NC (Figures 11E, F). Flow cytometry analysis was used to detect the apoptosis of HCC cells transfected with si-ARPC5#1; the results showed the percentage of early and late apoptotic cells significantly increased in HCC-LM3 and MHCC 97-H cells with ARPC5 downregulation (Figures 11G, H).

Knockdown of ARPC5 suppresses the invasion, migration, and epithelial-mesenchymal transition of HCC cells

The potential role of APRC5 in the cell migration and invasion was estimated by a scratch wound healing assay and transwell assays. The migration rates of HCC-LM3 and MHCC97-H cells transfected

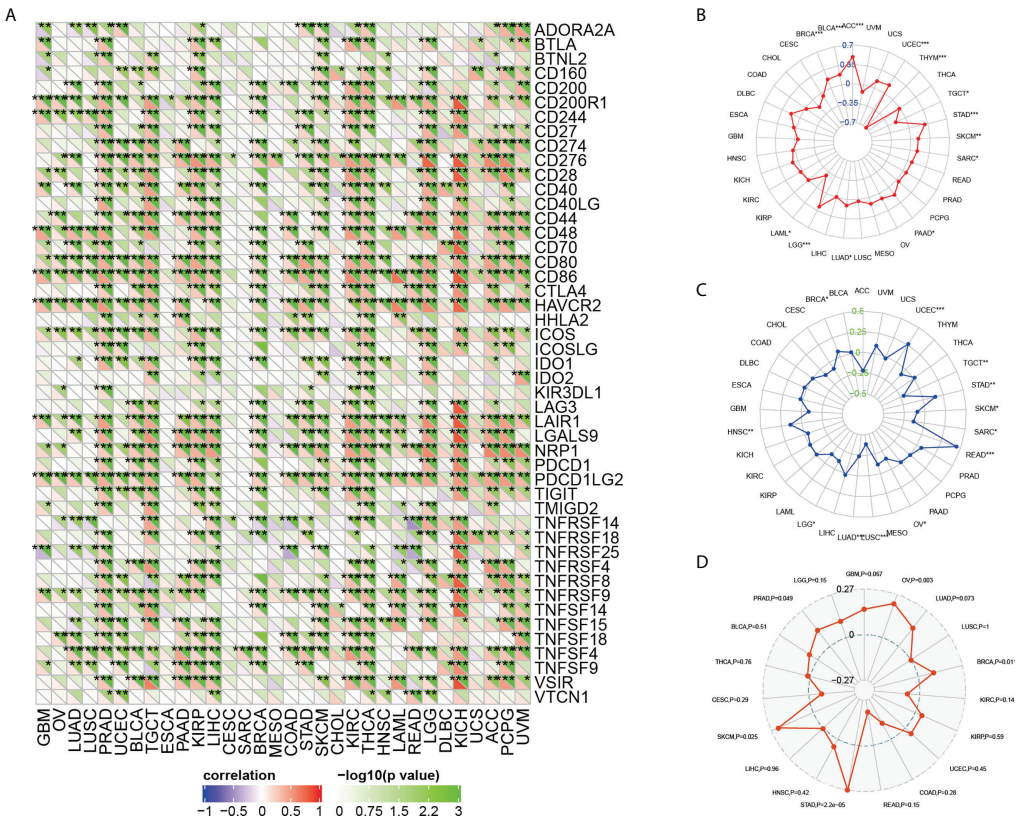

FIGURE 8
The relationship between ARPC5 and immune-checkmate inhibitors biomarkers in pan-cancer. **(A)** The heatmap showing the co-expression relationship between ARPC5 and 47 immune checkpoint–related genes. **(B)** Radar plot showing the relationship between ARPC5 and tumor mutation burden (TMB). **(C)** Radar plot showing the correlation of ARPC5 with microsatellite instability (MSI). **(D)** Radar plot showing the correlation of ARPC5 with neoantigens. The number in radar plot represents Spearman's correlation coefficient. *$p < 0.05$; **$p < 0.01$; ***$p < 0.001$.

with si-ARPC5 were evidently induced compared with those transfected with si-NC after the scratches were performed for 24 and 48 h (Figures 12A–D). Moreover, the number of invasion cells was significantly decreased following ARPC5 knockdown in HCC cells (Figures 12E, F). Epithelial-mesenchymal transition (EMT) had been reported as a critical process for tumor invasion and metastasis. We thus further examined the EMT markers (E-cadherin, N-cadherin, vimentin, and snail) by Western blot to investigate whether ARPC5 could affect EMT in HCC cells, the results showed that knockdown of ARPC5 reduced the expression of N-cadherin, Vimentin, and Snail whereas increased E-cadherin expression in HCC-LM3 and MHCC 97-H cells (Figure 12G). These results suggested that silencing ARPC5 inhibited HCC cell migration and invasion by suppressing the EMT.

Discussion

Transcriptomic gene expression analysis offers an optimal opportunity to explore the heterogeneity and complexity of different cancers and to seek new prognostic and therapeutic biomarkers. Several evidence reveals that ARPC5 is associated with tumor progression, metastasis, and prognosis, indicating that ARPC5 may represent a promising biomarker and therapeutic target. Therefore, it is critical to systematically investigate the role of ARPC5 in different types of cancer. In this study, we comprehensively analyzed the expression level of ARPC5 in multiple cancers basing on several different databases. We found that ARPC5 was significantly expressed in 22 tumor tissues compared with corresponding normal tissues and the expression levels was associated with tumor prognosis in multiple cancers. Meanwhile, we also explored the relationship of ARPC5 expression with gene mutation, gene modification, TME, tumor immune infiltration cells, ICIs response, and tumor stemness scores. Notably, we perform a series of experiments to identify the differential expression of ARPC5 in HCC tissues and HCC cells and further revealed that ARPC5 had a cancer-promoting effect in HCC cells and enhanced HCC progression for the first time.

In the present study, we found that ARPC5 expression was significantly upregulated in most cancer types basing on the TCGA

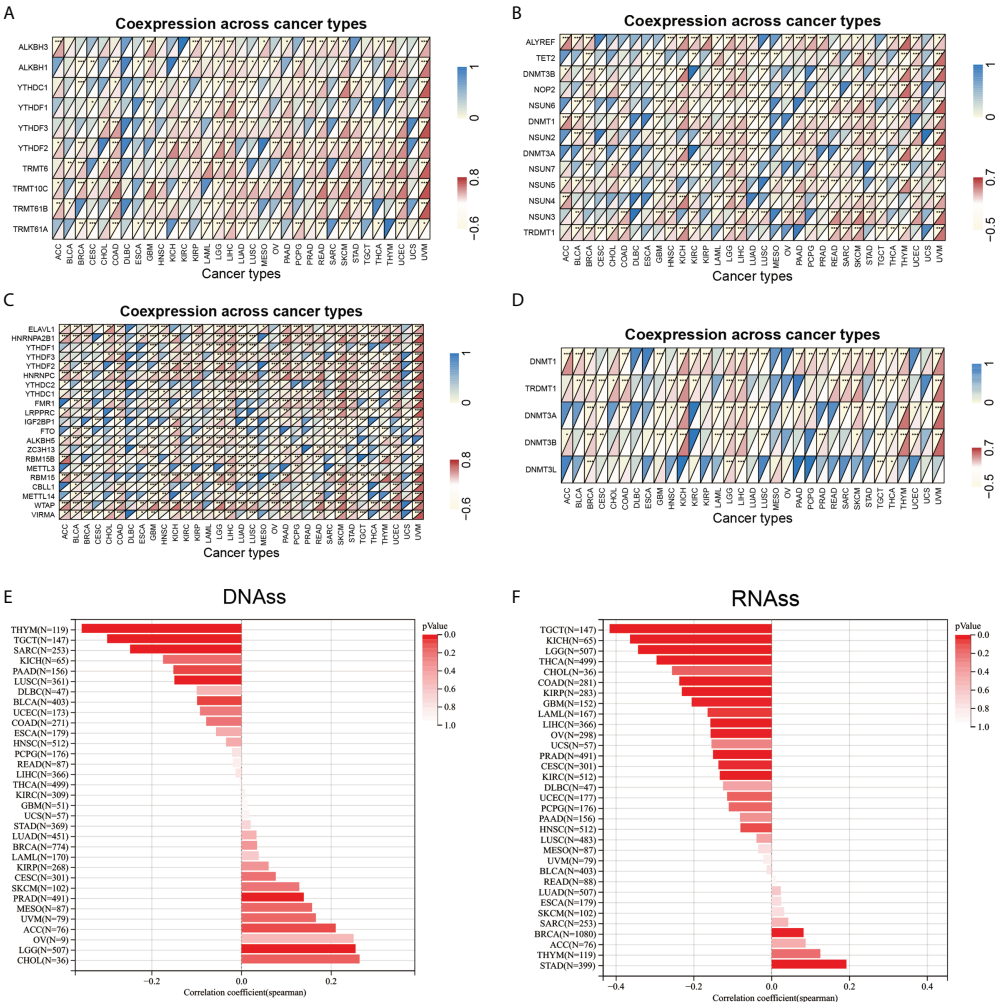

FIGURE 9
Correlation analysis between ARPC5 expression and RNA modification-related genes, DNA methyltransferases, and tumor stemness score in 33 cancer types. **(A)** Co-expression of ARPC5 with m1A-related genes. **(B)** Co-expression of ARPC5 with m5C-related genes. **(C)** Co-expression of ARPC5 with m6A-related genes. **(D)** Co-expression of ARPC5 with DNA methyltransferases. **(E)** The correlation between ARPC5 expression and Tumor Stemness score (DNAss). **(F)** The correlation between ARPC5 expression and Tumor Stemness score (RNAss). *$p < 0.05$; **$p < 0.01$; ***$p < 0.001$.

datasets integrating with GTEx datasets, including GBM, LGG, BRCA, CESC, ESCA, KIRP, COAD, PRAD, STAD, HNSC, KIRC, LUSC, LIHC, SKCM, BLCA, THCA, OV, PAAD, TGCT, and CHOL. While ARPC5 in UCS and KICH showed lower expression when compared with normal samples. It was reported that the expression of ARPC5 was significantly higher in HNSCC tissues than in non-cancer tissues, and ARPC5 was also significantly increased in invasive cancer cells (13). ARPC5 expression was significantly elevated in tumor tissues of lung squamous cell carcinoma (10). These findings were consistent with our results. To validate the results of bioinformatic analyses, we examined the expression levels of ARPC5 in 40 paired HCC tissues and HCC cell lines. The results manifested the expression of ARPC5 was higher in HCC tissues and HCC cells when compared with correspond adjacent normal liver tissues or normal liver cell both in mRNA and protein levels. The bioinformatic analyses were corroborated by experimental findings.

The prognosis value of ARPC5 was analyzed in 22 cancers in which ARPC5 expression varied significantly between cancer and normal tissues. The survival analysis revealed that ARPC5 was closely associated with survival indicators such as OS, PFS, and DSS. We found that the high expression of ARPC5 was closely linked with poor OS in ESCA, HNSC, KIRC, KIRP, LGG, LIHC, and THCA, with exception for OV and SKCM. Moreover, there were significant negative correlations between ARPC5 expression and PFS in BLCA, HNSC, KIRC, KIRP, LGG, LIHC, and PRAD, whereas positive correlation was observed in LUSC and SKCM. The association of ARPC5 with DSS presented similar results. We

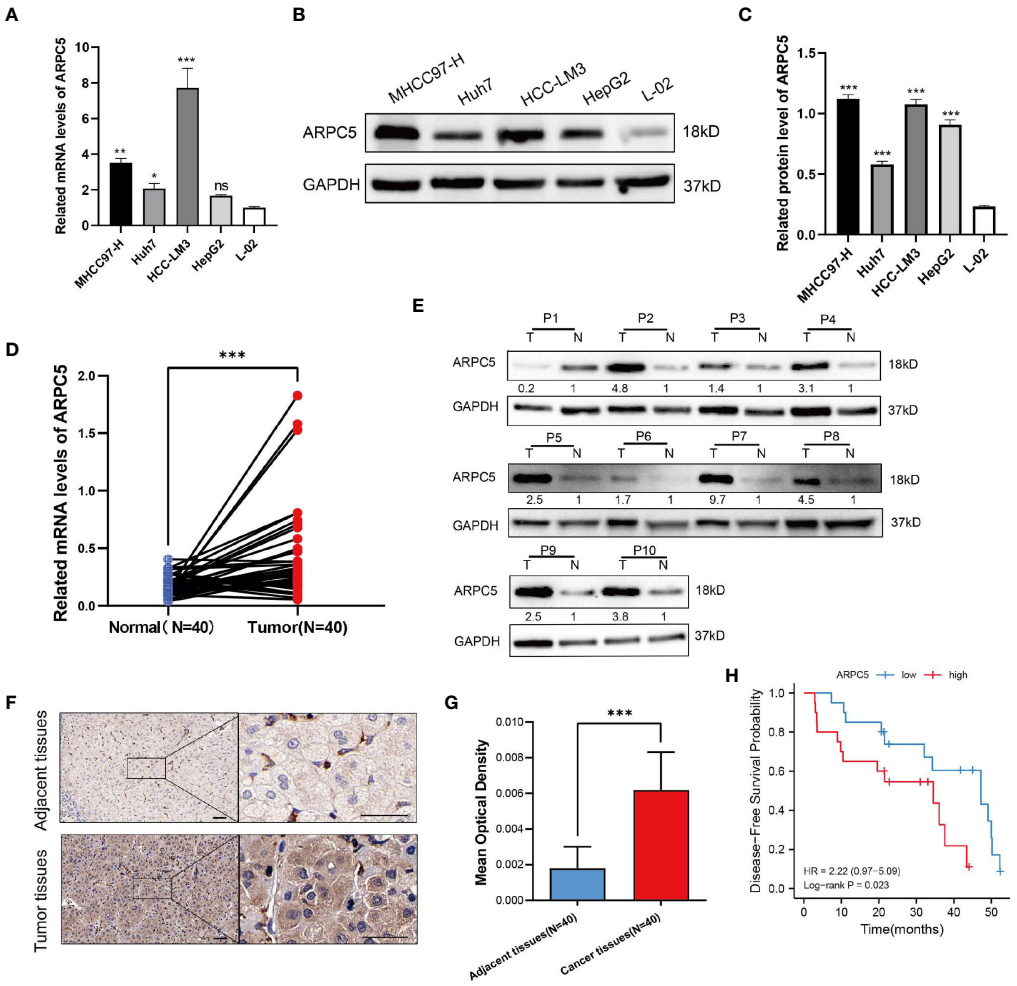

FIGURE 10
ARPC5 is upregulated in HCC cells and primary HCC tissues. **(A)** qPCR analysis of ARPC5 mRNA expression in four HCC cell lines (MHCC97-H, Huh7, HCC-LM3, and HepG2) and normal liver cell line (LO2). GAPDH was used as an internal control error bars represent *M* ± SEM (triplicate experiments). **(B, C)** The protein expression of ARPC5 was detected in four HCC cell lines and normal liver cell line with Western blot analysis. Error bars represent *M* ± SD of triplicate measurements. **(D)** The mRNA expression of ARPC5 in 40 pairs HCC tissues and adjacent para-carcinoma tissues was evaluated using qPCR. **(E)** Western blot analysis of ARPC5 protein expression in 10 paired HCC tissues and adjacent normal tissues. The number presented the relative protein expression levels of ARPC5. **(F)** Representative images of ARPC5 immunohistochemical staining analysis in the HCC tissue and adjacent normal liver tissue, original magnifications: ×40 and ×200. Scale bars, 50 μm. **(G)** Quantitative analysis of ARPC5 expression in HCC tissues based on mean optical density of immunohistochemical staining. Error bars represent the *M* ± SD of multiple tissues. **(H)** Kaplan–Meier curves showed that higher expression of ARPC5 was associated with poor DFS in HCC patients. **p* < 0.05; ***p* < 0.01; ****p* < 0.001. ns, no significance.

found a higher level of ARPC5 expression in KIRC, KIRP, LGG, and LIHC lead to unfavorable prognosis, including OS, PFS, and DSS, whereas ARPC5 in SKCM displayed the opposite results. In addition, we also proved that high expression of ARPC5 was unfavorable for DFS of patients with HCC following curative resection. Previous studies in MM and HCC reported that the high expression of ARPC5 was associated with poor OS and acted as an independent prognostic factor for MM and HCC patients (29, 30). Our current results are in harmony with these previous observations. These results indicating that ARPC5 may functions as an oncogene and represent a new prognostic biomarker for some cancer types. In this study, we found ARPC5 expression was closely correlated with tumor stage, histologic grade, and tumor molecular subtype in pan-cancer analyses. The higher the expression of ARPC5, the more advanced tumor stage for the patients with KIRC and KIRP. The similar results were presented in the correlation between ARPC5 expression and histologic grades in KIRC, LGG, LIHC, and USEC, indicating that ARPC5 can promote tumor progression and facilitate tumor malignancy. Silencing of ARPC5 inhibited cancer cell proliferation in lung squamous cell carcinoma, suggesting that ARPC5 might contribute to lung squamous cell carcinoma development (10). ARPC5 acted

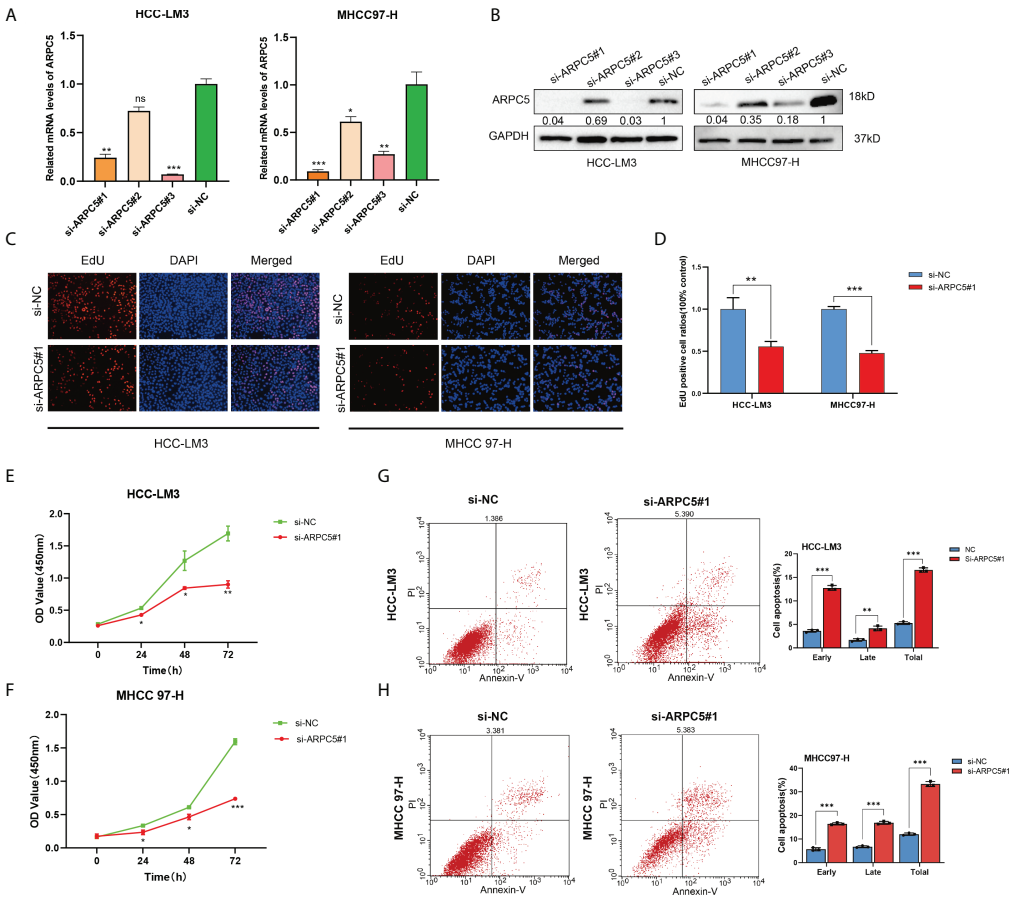

FIGURE 11
Silencing of ARPC5 inhibits cell proliferation and promotes cell apoptosis of HCC. **(A)** The knockdown efficiency of siRNA–ARPC5 was examined in HCC-LM3 and MHCC97-H cells with qPCR. **(B)** The knockdown efficiency of siRNA-ARPC5 was examined in HCC-LM3 and MHCC97-H cells with Western blot. The number presented as relative protein expression levels of ARPC5. (**C–D**) EdU assays for HCC-LM3 and MHCC 97-H were performed to evaluate cell proliferation ability after transfecting siRNA-ARPC5#1. Representative images **(C)** and the number of proliferative cells were calculated **(D)**; original magnification, ×200. **(E–F)** Cellular growth curves were evaluated by CCK-8 assays in HCC-LM3 and MHCC97-H cells. **(G–H)** Flow cytometry was applied to test the apoptosis of HCC cells transfected with si-ARPC5 #1 in HCC-LM3 and MHCC 97-H cells. All data are presented as the $M \pm SD$ of three independent experiments. $^*p < 0.05$; $^{**}p < 0.01$; $^{***}p < 0.001$. ns, no significance.

as a candidate target of miR-133a in HNSCC, knockdown ARPC5 significant reduced cell migration and invasion of HNSCC cell lines (13). In melanoma, YAP drives ARPC5 expression to enhance cell migration, invasion, and focal adhesions (14). In our study, we conducted a series of functional experiment in HCC cells and discovered downregulation ARPC5 significantly inhibits cell proliferation, migration, invasion, and EMT and promotes cell apoptosis in HCC. To our knowledge, this is the first study focus on the biological functions of ARPC5 in HCC. Nevertheless, the associated mechanisms require further elucidation.

Genetic alternation occurred in the coding region of genes leading to various disease, including tumors. Tumor heterogeneity caused by somatic mutations plays a crucial role in tumor growth and metastasis (31). The frequency of different mutational processes varies among different cancer types. In our analyses, we found that the most frequent mutation type of ARPC5 was "Amplification" mutation and the frequency of "Amplification" was varied among different cancer types, which was most commonly observed in cholangiocarcinoma, invasive breast carcinoma, and HCC. Cancer genomes mutations may be affected by intrinsic DNA replication machinery, mutation exposures, defective DNA repair, and enzymatic modifications of DNA (32). It is widely known that the epigenetic alternation caused by DNA methylation promotes the cancer susceptibility and progression. DNA hypomethylation leads to carcinogenesis and development mainly through transcriptional activation, MSI, and overexpression of oncogenes and loss of imprinting (33, 34). Thus, we further conducted co-expression analysis to explore the correlation between ARPC5 and five DNA methyltransferases (including DNMT1, TRDMT1, DNMT3A, DNMT3B, and DNMT3L). We found that ARPC5 expression was closely correlated with the expression of methyltransferases in most cancer types, especially in KICH and UVM. We speculated that

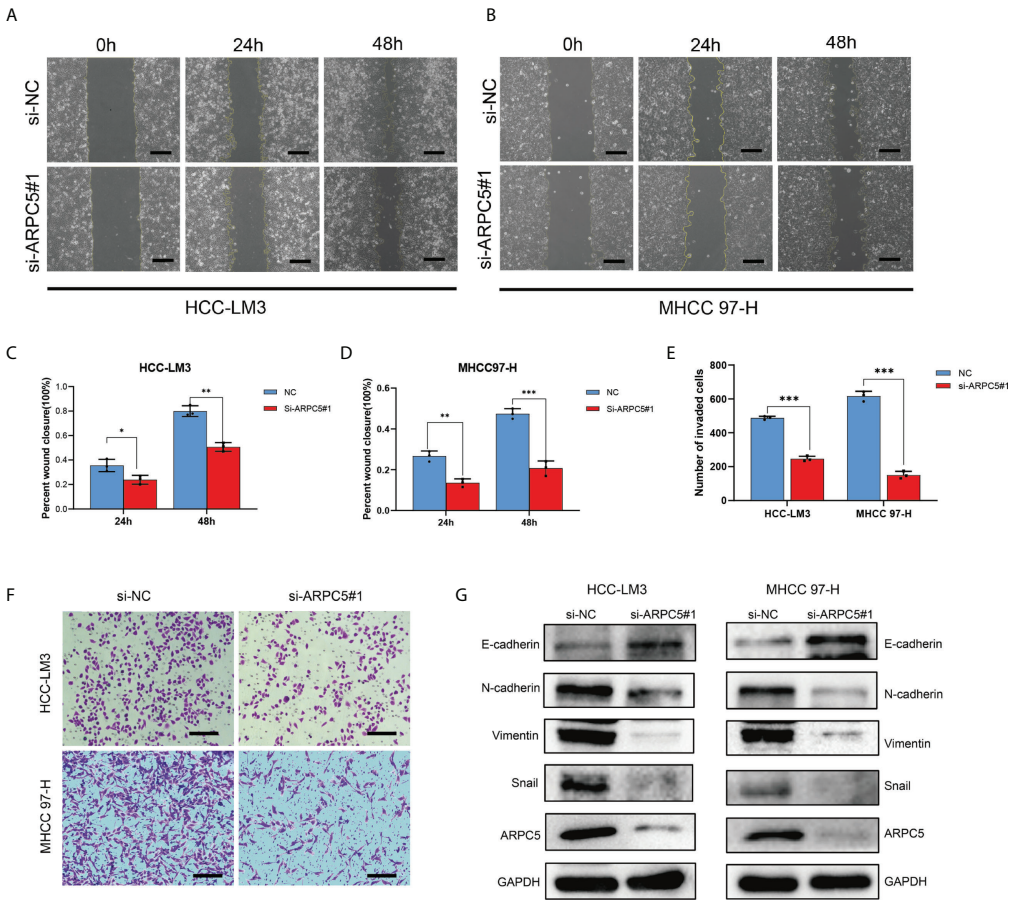

FIGURE 12
Role of ARPC5 inhibition on migration, invasion, and epithelial–mesenchymal transition (EMT) of HCC cells. **(A–D)** Migration ability was assessed by scratch wound healing assay, representative images **(A, B)** were shown (original magnification, ×200; scale bars, 50 μm), and wound healing areas were calculated **(C, D)**. **(E, F)** Transwell assay was applied to examine the invasion ability, representative images **(F)** were shown (original magnification, ×200; scale bars, 50 μm), and the histogram showed the number of invasion cells **(E)**. **(G)** Western blot showed the changes of EMT proteins in HCC-LM3 and MHCC97-H cells transfected with si-ARPC5#1. *p < 0.05; **p < 0.01; ***p < 0.001.

ARPC5 might contribute to cancer progression through influencing the genes stability.

The bidirectional interaction between cancer cells and TME is responsible for tumor development, progression, and drug resistance (35). The TME primarily consists of tumor-infiltrating cells, vasculature, extracellular matrix (ECM), as well as other matrix-associated molecules and have proved to play a significant role in clinical outcomes and response to therapy (36, 37). Immune cells in TME are especially dependent on the proper functioning of the cytoskeletal proteins, for example, Arp2/3 complex (38). Arp2/3 complex plays an essential role in cell migration of T cells, neutrophils and platelets, as well as for CTL assembly (38). The patients with ARPC1B-deficient exhibited a decrease in the number of $CD8^+$ T cell and characterized by dysfunctional T cells (39). However, the role of ARPC5 expression in TME, immune cells, and different immune subtypes still remains to be elucidated. Thus, we first explored the correlation of ARPC5 with TME with immune scores and stromal scores calculated by the ESTIMATE algorithms, which can facilitate the quantification of the immune and stromal components in each tumor sample. We found that ARPC5 was evidently positively associated with Immune scores in 22 cancers, and related to Stromal scores in 15 cancer types, suggesting ARPC5 might be a critical driver of immune cells and stromal cells. Then, we performed a more in-depth study to explore which classes of immune cells were associated with ARPC5 expression with TIMER algorithms. The results suggested that the expression of ARPC5 was positively associated with the infiltration level of B cell, $CD4^+$ T cell, $CD8^+$ T cell, neutrophil cell, macrophage cell, and DC cell in most cancer types, especially for KIRC, LGG, PRAD, THCA, and THYM. In addition, we discovered that ARPC5 was expressed inconsistently in different immune subtypes; ARPC5 was widely highly expressed in C2 subtype and lowly expressed in C3 subtype. These results prompted that ARPC5 have stronger association with certain immune cells involving in IFN-gamma dominant but less relating to inflammatory processes.

In recent years, immune checkpoint inhibitors (ICIs) have revolutionized treatment paradigms and improved survival

outcomes of many solid tumors (40). Nevertheless, only a minority of patients can benefit from ICIs with the overall response rates (RRs) no more than 20% (41). In addition, ICIs also come with a unique and sometimes devastating immune-related toxicities. Thus, there is an urgent need to explore biomarkers to accurately predict response and improve treatment selection of ICIs. The PD-L1 expression profiles in cancers have been extensively studied in the past decade. The role of PD-L1 as an effectively predictive biomarker largely based on the results of the KEYNOTE 024 trial study in non-small cell lung cancer, which showed superior outcomes in patients with PD-L1 expression greater than 50% treated with pembrolizumab as the first-line method (42). However, PD-L1 expression was discorded between resected tissues and biopsy specimens, and the expression level varied significantly among different tumor types (43). Currently, effectiveness of PD-L1 detection as an anti-tumor immune response index is still controversial. Recently numerous studies have established the major role of neo-epitopes antigens, resulting from genomic instability status on tumor cells, on cancer immune recognition and specific T-cell activation (44). Tumor with higher TMB, MSI, and neoantigens closely correlates with more T-cell recognition and better clinical outcomes (45, 46). Nevertheless, TMB is independent of PD-L1 status in most cancer types; the combination of TMB, PD-L1, and MSI-H has the better predictive performance of ICIs responsiveness than each alone (41). The present study performed a comprehensive analysis of ARPC5 with existing biomarkers of ICIs including TMB, MSI, neoantigens, and immune checkpoint–related genes in various cancer types. We detected that APRC5 expression was significantly correlated with most of the 47 immune checkpoint–related genes in most cancers, such PRAD, TGCT, KIRC, LIHC, KIRC, THCA, LGG, KICH, and PCPG. In LIHC, ARPC5 was positively related to 39 ICIs-related genes, including PD-1(PDCD1), PD-L1(CD274), PD-L2 (PDCD1LG2), and CTLA4. Moreover, ARPC5 had a correlation with TMB in 12 cancers, MSI in 12 cancers, and neoantigens in five cancers. Interestingly, ARPC5 expression in STAD and BRCA was positively associated with TMB, MSI, and neoantigens. These findings suggested that the ARPC5 can be used as a new biomarker to predict ICIs response for certain cancers.

In summary, comprehensive analyses were conducted in our study to explore the expression patterns and prognostic values of ARPC5 in pan-cancer using multiple databases. We discovered that the expression of ARPC5 was upregulated in most cancer types and high-expressed ARPC5 was associated with poor survival outcomes and tumor progression in some cancers. In addition, we found that ARPC5 was closely related to TME, tumor infiltration immune cells, immune subtypes, and biomarkers of ICIs, which might provide a new insight of ARPC5 with tumor immunity and would be favorable for mining novel therapeutic target and predictive biomarker for immunotherapy. Moreover, this study was the first to validate the differential expression of ARPC5 in HCC tissues and explore the role of ARPC5 in the proliferation, apoptosis, and invasion of HCC cells, which provided a preliminary foundation for the development of biomarker-targeting therapies in HCC.

Data availability statement

The original contributions presented in the study are included in the article/Supplementary Material. Further inquiries can be directed to the corresponding author.

Ethics statement

The studies involving human participants were reviewed and approved by The Second Affiliated Hospital of Nanchang University Medical Research Ethics Committee. The patients/participants provided their written informed consent to participate in this study.

Author contributions

JW and SH contributed to conception and design of the study. SH, LS, and PH organized the database. SH and KL performed the statistical analysis. SH wrote the first draft of the manuscript. LS, PH, and KL wrote sections of the manuscript. All authors contributed to manuscript revision, read, and approved the submitted version.

Funding

This research was supported by the National Natural Science Foundation of China (NO. 82060435).

Conflict of interest

The authors declare that the research was conducted in the absence of any commercial or financial relationships that could be construed as a potential conflict of interest.

Publisher's note

Supplementary material

The Supplementary Material for this article can be found online at: https://www.frontiersin.org/articles/10.3389/fimmu.2022.944898/full#supplementary-material

References

1. Molinie N, Gautreau A. The Arp2/3 regulatory system and its deregulation in cancer. *Physiol Rev* (2018) 98(1):215–38. doi: 10.1152/physrev.00006.2017

2. Su X, Wang S, Huo Y, Yang C. Short interfering RNA-mediated silencing of actin-related protein 2/3 complex subunit 4 inhibits the migration of SW620 human colorectal cancer cells. *Oncol Lett* (2018) 15(3):2847–54. doi: 10.3892/ol.2017.7642

3. Izdebska M, Zielińska W, Hałas-Wiśniewska M, Grzanka A. Involvement of actin and actin-binding proteins in carcinogenesis. *Cells* (2020) 9(10):2245-64. doi: 10.3390/cells9102245

4. Xu N, Qu GY, Wu YP, Lin YZ, Chen DN, Li XD, et al. ARPC4 promotes bladder cancer cell invasion and is associated with lymph node metastasis. *J Cell Biochem* (2020) 121(1):231–43. doi: 10.1002/jcb.29136

5. Laurila E, Savinainen K, Kuuselo R, Karhu R, Kallioniemi A. Characterization of the 7q21-q22 amplicon identifies ARPC1A, a subunit of the Arp2/3 complex, as a regulator of cell migration and invasion in pancreatic cancer. *Genes Chromosomes Cancer* (2009) 48(4):330–9. doi: 10.1002/gcc.20643

6. Rauhala HE, Teppo S, Niemelä S, Kallioniemi A. Silencing of the ARP2/3 complex disturbs pancreatic cancer cell migration. *Anticancer Res* (2013) 33(1):45–52.

7. Chen P, Yue X, Xiong H, Lu X, Ji Z. RBM3 upregulates ARPC2 by binding the 3'UTR and contributes to breast cancer progression. *Int J Oncol* (2019) 54(4):1387–97. doi: 10.3892/ijo.2019.4698

8. Dombkowski AA, Sultana Z, Craig DB, Jamil H. In silico analysis of combinatorial microRNA activity reveals target genes and pathways associated with breast cancer metastasis. *Cancer Inform* (2011) 10:13–29. doi: 10.4137/CIN.S6631

9. Cheng Z, Wei W, Wu Z, Wang J, Ding X, Sheng Y, et al. ARPC2 promotes breast cancer proliferation and metastasis. *Oncol Rep* (2019) 41(6):3189–200. doi: 10.3892/or.2019.7113

10. Moriya Y, Nohata N, Kinoshita T, Mutallip M, Okamoto T, Yoshida S, et al. Tumor suppressive microRNA-133a regulates novel molecular networks in lung squamous cell carcinoma. *J Hum Genet* (2012) 57(1):38–45. doi: 10.1038/jhg.2011.126

11. Liu C, Liu R, Zhang D, Deng Q, Liu B, Chao HP, et al. MicroRNA-141 suppresses prostate cancer stem cells and metastasis by targeting a cohort of pro-metastasis genes. *Nat Commun* (2017) 8:14270. doi: 10.1038/ncomms14270

12. Zhang J, Liu Y, Yu CJ, Dai F, Xiong J, Li HJ, et al. Role of ARPC2 in human gastric cancer. *Mediators Inflammation* (2017) 2017:5432818. doi: 10.1155/2017/5432818

13. Kinoshita T, Nohata N, Watanabe-Takano H, Yoshino H, Hidaka H, Fujimura L, et al. Actin-related protein 2/3 complex subunit 5 (ARPC5) contributes to cell migration and invasion and is directly regulated by tumor-suppressive microRNA-133a in head and neck squamous cell carcinoma. *Int J Oncol* (2012) 40(6):1770–8. doi: 10.3892/ijo.2012.1390

14. Lui JW, Moore SPG, Huang L, Ogomori K, Li Y, Lang D. YAP facilitates melanoma migration through regulation of actin-related protein 2/3 complex subunit 5 (ARPC5). *Pigment Cell Melanoma Res* (2022) 35(1):52–65. doi: 10.1111/pcmr.13013

15. Huang S, Li D, Zhuang L, Sun L, Wu J. Identification of Arp2/3 complex subunits as prognostic biomarkers for hepatocellular carcinoma. *Front Mol Biosci* (2021) 8:690151. doi: 10.3389/fmolb.2021.690151

16. Liu J, Lichtenberg T, Hoadley KA, Poisson LM, Lazar AJ, Cherniack AD, et al. An integrated TCGA pan-cancer clinical data resource to drive high-quality survival outcome analytics. *Cell* (2018) 173(2):400–16.e11. doi: 10.1016/j.cell.2018.02.052

17. Ru B, Wong CN, Tong Y, Zhong JY, Zhong SSW, Wu WC, et al. TISIDB: an integrated repository portal for tumor-immune system interactions. *Bioinformatics* (2019) 35(20):4200–2. doi: 10.1093/bioinformatics/btz210

18. Kurebayashi Y, Ojima H, Tsujikawa H, Kubota N, Maehara J, Abe Y, et al. Landscape of immune microenvironment in hepatocellular carcinoma and its additional impact on histological and molecular classification. *Hepatology* (2018) 68(3):1025–41. doi: 10.1002/hep.29904

19. Thorsson V, Gibbs DL, Brown SD, Wolf D, Bortone DS, Ou Yang TH, et al. The immune landscape of cancer. *Immunity* (2018) 48(4):812–30.e14. doi: 10.1016/j.immuni.2018.03.023

20. Hegde PS, Chen DS. Top 10 challenges in cancer immunotherapy. *Immunity* (2020) 52(1):17–35. doi: 10.1016/j.immuni.2019.12.011

21. Henriksen A, Dyhl-Polk A, Chen I, Nielsen D. Checkpoint inhibitors in pancreatic cancer. *Cancer Treat Rev* (2019) 78:17–30. doi: 10.1016/j.ctrv.2019.06.005

22. Gibney GT, Weiner LM, Atkins MB. Predictive biomarkers for checkpoint inhibitor-based immunotherapy. *Lancet Oncol* (2016) 17(12):e542–e51. doi: 10.1016/S1470-2045(16)30406-5

23. Matsushita H, Vesely MD, Koboldt DC, Rickert CG, Uppaluri R, Magrini VJ, et al. Cancer exome analysis reveals a T-cell-dependent mechanism of cancer immunoediting. *Nature* (2012) 482(7385):400–4. doi: 10.1038/nature10755

24. Hause RJ, Pritchard CC, Shendure J, Salipante SJ. Classification and characterization of microsatellite instability across 18 cancer types. *Nat Med* (2016) 22(11):1342–50. doi: 10.1038/nm.4191

25. Yang G, Zheng RY, Jin ZS. Correlations between microsatellite instability and the biological behaviour of tumours. *J Cancer Res Clin Oncol* (2019) 145 (12):2891–9. doi: 10.1007/s00432-019-03053-4

26. Barbieri I, Kouzarides T. Role of RNA modifications in cancer. *Nat Rev Cancer* (2020) 20(6):303–22. doi: 10.1038/s41568-020-0253-2

27. Martisova A, Holcakova J, Izadi N, Sebuyoya R, Hrstka R, Bartosik M. DNA Methylation in solid tumors: Functions and methods of detection. *Int J Mol Sci* (2021) 22(8):4247-68. doi: 10.3390/ijms22084247

28. Malta TM, Sokolov A, Gentles AJ, Burzykowski T, Poisson L, Weinstein JN, et al. Machine learning identifies stemness features associated with oncogenic dedifferentiation. *Cell* (2018) 173(2):338–54.e15. doi: 10.1016/j.cell.2018.03.034

29. Xiong T, Luo Z. The expression of actin-related protein 2/3 complex subunit 5 (ARPC5) expression in multiple myeloma and its prognostic significance. *Med Sci Monit* (2018) 24:6340–8. doi: 10.12659/MSM.908944

30. Huang S, Li D, Zhuang L, Sun L, Wu J. Identification of Arp2/3 complex subunits as prognostic biomarkers for hepatocellular carcinoma. *Front Mol Biosci* (2021) 8(612). doi: 10.3389/fmolb.2021.690151

31. Paul P, Malakar AK, Chakraborty S. The significance of gene mutations across eight major cancer types. *Mutat Res Rev Mutat Res* (2019) 781:88–99. doi: 10.1016/j.mrrev.2019.04.004

32. Alexandrov LB, Nik-Zainal S, Wedge DC, Aparicio SA, Behjati S, Biankin AV, et al. Signatures of mutational processes in human cancer. *Nature* (2013) 500 (7463):415–21. doi: 10.1038/nature12477

33. Ehrlich M. DNA Hypomethylation in cancer cells. *Epigenomics* (2009) 1 (2):239–59. doi: 10.2217/epi.09.33

34. Yu J, Hua R, Zhang Y, Tao R, Wang Q, Ni Q. DNA Hypomethylation promotes invasion and metastasis of gastric cancer cells by regulating the binding of SP1 to the CDCA3 promoter. *J Cell Biochem* (2020) 121(1):142–51. doi: 10.1002/jcb.28993

35. Belli C, Trapani D, Viale G, D'Amico P, Duso BA, Della Vigna P, et al. Targeting the microenvironment in solid tumors. *Cancer Treat Rev* (2018) 65:22–32. doi: 10.1016/j.ctrv.2018.02.004

36. Bagaev A, Kotlov N, Nomie K, Svekolkin V, Gafurov A, Isaeva O, et al. Conserved pan-cancer microenvironment subtypes predict response to immunotherapy. *Cancer Cell* (2021) 39(6):845–65.e7. doi: 10.1016/j.ccell.2021.04.014

37. Bai YP, Shang K, Chen H, Ding F, Wang Z, Liang C, et al. FGF-1/-3/FGFR4 signaling in cancer-associated fibroblasts promotes tumor progression in colon cancer through erk and MMP-7. *Cancer Sci* (2015) 106(10):1278–87. doi: 10.1111/cas.12745

38. Tur-Gracia S, Martinez-Quiles N. Emerging functions of cytoskeletal proteins in immune diseases. *J Cell Sci* (2021) 134(3):jcs253534. doi: 10.1242/jcs.253534

39. Randzavola LO, Strege K, Juzans M, Asano Y, Stinchcombe JC, Gawden-Bone CM, et al. Loss of ARPC1B impairs cytotoxic T lymphocyte maintenance and cytolytic activity. *J Clin Invest* (2019) 129(12):5600–14. doi: 10.1172/JCI129388

40. Hiam-Galvez KJ, Allen BM, Spitzer MH. Systemic immunity in cancer. *Nat Rev Cancer* (2021) 21(6):345–59. doi: 10.1038/s41568-021-00347-z

41. Jardim DL, Goodman A, de Melo Gagliato D, Kurzrock R. The challenges of tumor mutational burden as an immunotherapy biomarker. *Cancer Cell* (2021) 39 (2):154–73. doi: 10.1016/j.ccell.2020.10.001

42. Reck M, Rodriguez-Abreu D, Robinson AG, Hui R, Csoszi T, Fulop A, et al. Pembrolizumab versus chemotherapy for PD-L1-Positive non-Small-Cell lung cancer. *N Engl J Med* (2016) 375(19):1823–33. doi: 10.1056/NEJMoa1606774

43. Burdett N, Desai J. New biomarkers for checkpoint inhibitor therapy. *ESMO Open* (2020) 5(Suppl 1):e000597. doi: 10.1136/esmoopen-2019-000597

44. Gavrielatou N, Doumas S, Economopoulou P, Foukas PG, Psyrri A. Biomarkers for immunotherapy response in head and neck cancer. *Cancer Treat Rev* (2020) 84:101977. doi: 10.1016/j.ctrv.2020.101977

45. Brown SD, Warren RL, Gibb EA, Martin SD, Spinelli JJ, Nelson BH, et al. Neo-antigens predicted by tumor genome meta-analysis correlate with increased patient survival. *Genome Res* (2014) 24(5):743–50. doi: 10.1101/gr.165985.113

46. Chang L, Chang M, Chang HM, Chang F. Microsatellite instability: A predictive biomarker for cancer immunotherapy. *Appl Immunohistochem Mol Morphol* (2018) 26(2):e15–21. doi: 10.1097/PAI.0000000000000575

10.3389/fimmu.2022.944898

Glossary

ARPC5	actin-related protein 2/3 complex subunit 5
Arp2/3	actin-related protein 2/3
TCGA	the Cancer Genome Atlas database
GTEx	Genotype-Tissue Expression database
TIMER	Tumor Immune Evaluation Resource
FPKM	Fragments Per Kilobase per Million
CNV	copy number variations
TMB	tumor mutation burden
MSI	microsatellite instability;
MMRs	mismatch repairs
HCC	hepatocellular carcinoma
OS	overall survival
DSS	disease-specific survival
PFI	progression-free interval
DFS	disease-free survival
TME	tumor microenvironment
ICIs	immune checkpoint inhibitors
m6A	N6methyladenosine
m5C	RNA5methylcytosine
m1A	N1methyladenosine
qPCR	quantitative real-time polymerase chain reaction
siRNA	small-interfering RNA
EdU	5-ethynyl-2′-deoxyuridine
ACC	adrenocortical carcinoma
BLCA	bladder urothelial carcinoma
BRCA	breast invasive carcinoma
CESC	cervical squamous cell carcinoma and endocervical adenocarcinoma
CHOL	cholangiocarcinoma
COAD	colon adenocarcinoma
DLBC	lymphoid neoplasm diffuse large B cell lymphoma
ESCA	esophageal carcinoma
GBM	glioblastoma multiforme
HNSC	head and neck squamous cell carcinoma
KICH	kidney chromophobe
KIRC	kidney renal clear cell carcinoma
KIRP	kidney renal papillary cell carcinoma
LAML	acute myeloid leukemia;
LGG	brain lower grade glioma
LIHC	liver hepatocellular carcinoma;
LUAD	lung adenocarcinoma
LUSC	lung squamous cell carcinoma;
MESO	mesothelioma
OV	ovarian serous cystadenocarcinoma
PAAD	pancreatic adenocarcinoma
PCPG	pheochromocytoma and paraganglioma
PRAD	prostate adenocarcinoma
READ	rectum adenocarcinoma
SARC	sarcoma
SKCM	skin cutaneous melanoma;
STAD	stomach adenocarcinoma
TGCT	testicular germ cell tumors;
THCA	thyroid carcinoma
THYM	Thymoma
UCEC	uterine corpus endometrial carcinoma
UCS	uterine carcinosarcoma
UVM	uveal melanoma

(Continued)

Frontiers in Immunology

Explores novel approaches and diagnoses to treat immune disorders.

The official journal of the International Union of Immunological Societies (IUIS) and the most cited in its field, leading the way for research across basic, translational and clinical immunology.

Discover the latest Research Topics

See more →

Frontiers

Avenue du Tribunal-Fédéral 34
1005 Lausanne, Switzerland
frontiersin.org

Contact us

+41 (0)21 510 17 00
frontiersin.org/about/contact